American Society of Biomechanics

28th Annual Conference

LEGACY Health System

Biomechanics Laboratory

OHSU Oregon Health & Science University

Program

Portland, Oregon, September 8-11, 2004

www.biomechresearch.org

Welcome

FROM THE ASB PRESIDENT

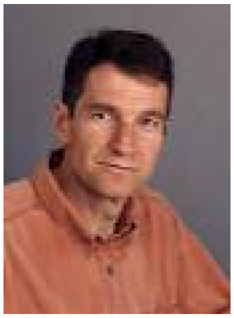

Dear ASB participants,

I would like to welcome you to beautiful Portland on behalf of the American Society of Biomechanics. Like any scientific gathering, the meeting of the American Society of Biomechanics is about the exchange of scientific information. However, it is much more than that. It is about meeting old friends and colleagues. It is about discussing new research ideas in an informal environment, and about exposing students and newcomers to the exciting field of biomechanics. Students have always been an important aspect of this conference. They compete for the New Investigator's Award in a pre-doctoral and post-doctoral category, they are exposed to a student mentoring program, and their attendance is supported by the ASB and local organizers so that costs can be kept at a minimum.

Michael Bottlang, the local organizer, and Steve Robinovitch, the program chair, have put together an exciting conference in a beautiful setting. Let's take full advantage of this meeting and the social program, for interaction, mentoring, advising, and fun.

A special aspect of this year's program will be the Jim Hay Award with a designated session in the area of Sports Biomechanics and Exercise Science. This award was instigated at the suggestion of students and friends of Jim Hay and the ASB executive board. The purpose was to honor the memory of the late Jim Hay, a pioneer in biomechanics, a founding member of the ASB, a dedicated scientist, scholar and educator whose commitment to excellence in science and to student education was unparalleled, but most of all to a friend who we miss very much.

Welcome to Portland! I wish you an enjoyable and exciting conference that you may remember for a long time, and that might give you inspiration and strength for your future research endeavors.

Walter Herzog, President ASB

FROM THE LOCAL HOST

Welcome to Portland for the 28th meeting of the American Society of Biomechanics! The ASB conference has always been my personal favorite, and it is a great honor and pleasure for us to be your host in Portland. The ASB conference provides a unique blend of science over the wide range of disciplines in biomechanics. Its character is not intimidating but stimulating for students and seasoned scientists alike. It is an ideal place to learn, to get inspired, and to establish collaborations.

You contributed a record 365 abstracts, and Steve Robinovitch assembled an exciting program. Equally impressive has been the diligence and enthusiasm with which the members of the local organizing committee have prepared this conference. All that's left to do is to enjoy the conference, meet old and new friends, and become inspired.

After an exciting scientific program, you can enjoy Portland, the city of roses, bridges, and micro-brews. Access to the ocean and lush green mountains offers a wealth of outdoor opportunities that will entice you to stay an extra day.

Michael Bottlang, Meeting Chair

Conference Committee:

Program Chair:	Steve Robinovitch, Ph.D., Department of Kinesiology, Simon Fraser University, Burnaby, B.C.
Conference Chair:	Michael Bottlang, Ph.D., Biomechanics Laboratory, Legacy Research Center, Portland, OR
Conference Co-Chair:	Steven M. Madey, M.D., Legacy Health System, Portland, OR
Organizing Committee:	Mark Sommers, MS, Biomechanics Laboratory, Legacy Research Center
	Larry Ehmke, MS, Biomechanics Laboratory, Legacy Research Center
	Marcus Mohr, MS, Biomechanics Laboratory, Legacy Research Center
	Tanja Augustin, Biomechanics Laboratory, Legacy Research Center
	Marie Shea, MS, Biomechanics Laboratory, Oregon Health & Science University, Portland, OR
	Julianne Abendroth-Smith, Exercise Science, Willamette University, Salem, OR
	Sean J. Kirkpatrick, OGI School of Science and Engineering, Portland, OR
	Brian K. Bay, Mechanical Engineering, Oregon State University, Corvallis, OR
	Dan Fitzpatrick, Orthopedic Healthcare Northwest, Eugene, OR
	Andy Karduna, Exercise and Movement Science, University of Oregon, Eugene, OR

Table of Contents

General Information

Conference

The 28th Annual Meeting of the American Society of Biomechanics provides a forum for exchange of information among the multiple disciplines in biomechanics, including biomechanical engineering, exercise science, and health sciences. Objectives of this meeting are to promote the exchange of ideas, to encourage interdisciplinary collaboration, and to foster emerging scientists in bioengineering careers.

Conference Location

The Doubletree Lloyd Center Hotel, 1000 NE Multnomah, Portland, OR 97232 is the designated Conference Hotel. All meeting events, presentations and poster exhibits will take place on the main floor of the hotel. The Doubletree Hotel provides all necessary amenities in one location to ensure an effective Annual Meeting: two restaurants, one bar, an outside swimming pool, and a complimentary fitness center. You will enjoy the convenience of staying at the hotel, meeting your colleagues for breakfast and strolling along the exhibits and posters to the sessions. Next to the hotel is a MAX light-rail stop. Max is free within downtown Portland and provides convenient transportation to many local attractions and to the ASB Banquet at the Chinese Garden.

Program

Lab Tours	Wednesday, Sept. 8	12:30 pm - 3:30 pm	NIKE, Legacy Research Center
	Thursday, Friday, Sept. 10, 11	12:40 pm - 2:00 pm	NSI, Legacy, other tours upon request
Workshops	Wednesday, Sept. 8	4:00 pm - 5.30 pm	2 concurrent workshops
Podiums	Thursday, Sept. 9	9:20 am - 12:30 pm	2 concurrent sessions
	Friday, Sept. 10	9:20 am - 12:30 pm	2 concurrent sessions
	Saturday, Sept. 11	9:20 am - 10:30 pm	2 concurrent sessions
Posters	Thursday, Sept. 9	3:30 pm - 5:00 pm	Poster Session I
	Friday, Sept. 10	3.30 pm - 5:00 pm	Poster Session II
	All posters will be displayed Wednesday through Saturday without rotation to allow maximum exposure.		
Keynotes	Thursday, Sept. 9	8:00 am - 9:00 am	Steven Vogel
	Friday, Sept. 10	8:00 am - 9:00 am	Wilson C (Toby) Hayes
	Friday, Sept. 10	2:00 am - 3:00 am	Andrew Schwartz
	Saturday, Sept. 11	8:00 am - 9:00 am	Farshid Guilak
Awards	Thursday, Sept. 9	2:00 pm - 3:30 pm	Award Session I
	Friday, Sept. 10	4:30 pm - 6:00 pm	Award Session II
	Saturday, Sept. 11	11:00 am - 12:30 pm	Award Session III / Borelli Lecture
Reception	Wednesday, Sept 8	6:30 pm	At outdoor pool area / poster area B
Banquet	Friday, Sept 10.	6.30 pm	Classical Chinese Garden
Student Luncheon (see also page10)			
	Thursday, Sept. 9	12.30 pm - 1.30 pm	Mt St. Helens Room, 2nd floor
ASB General Meeting			
	Thursday, Sept. 9	5:00 pm - 6:00 pm	Session Rooms A/B
ASB Executive Board			
	Wednesday, Sept. 8	12:30 pm - 1:30 pm	1st meeting, Halsey Room
	Saturday, Sept. 11	12:30 pm - 1:30 pm	2nd meeting, Halsey Room

Conference Hotel

Doubletree Lloyd Center Hotel, 1000 NE Multnomah, Portland. OR 97232, phone: 1-800-222 8733

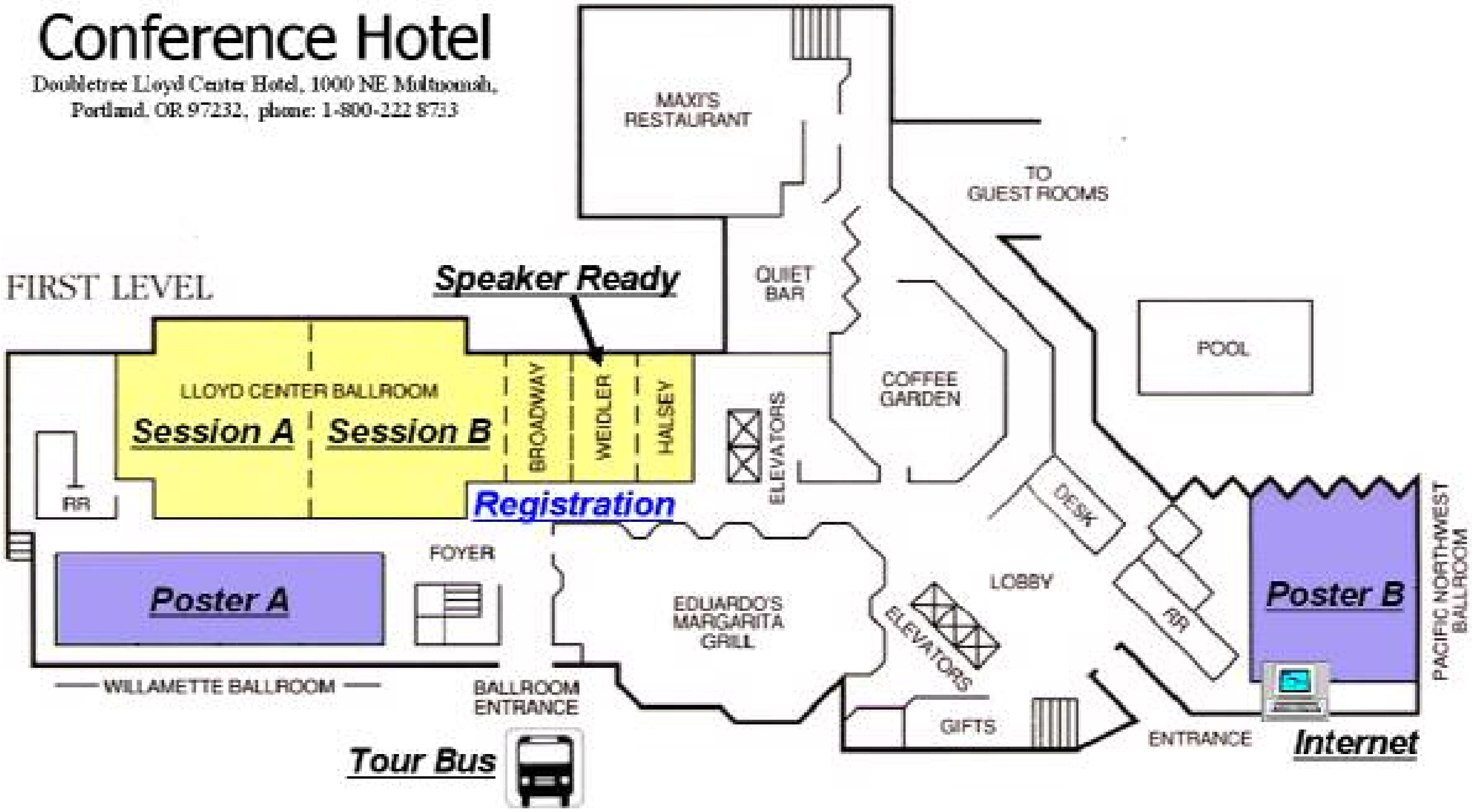

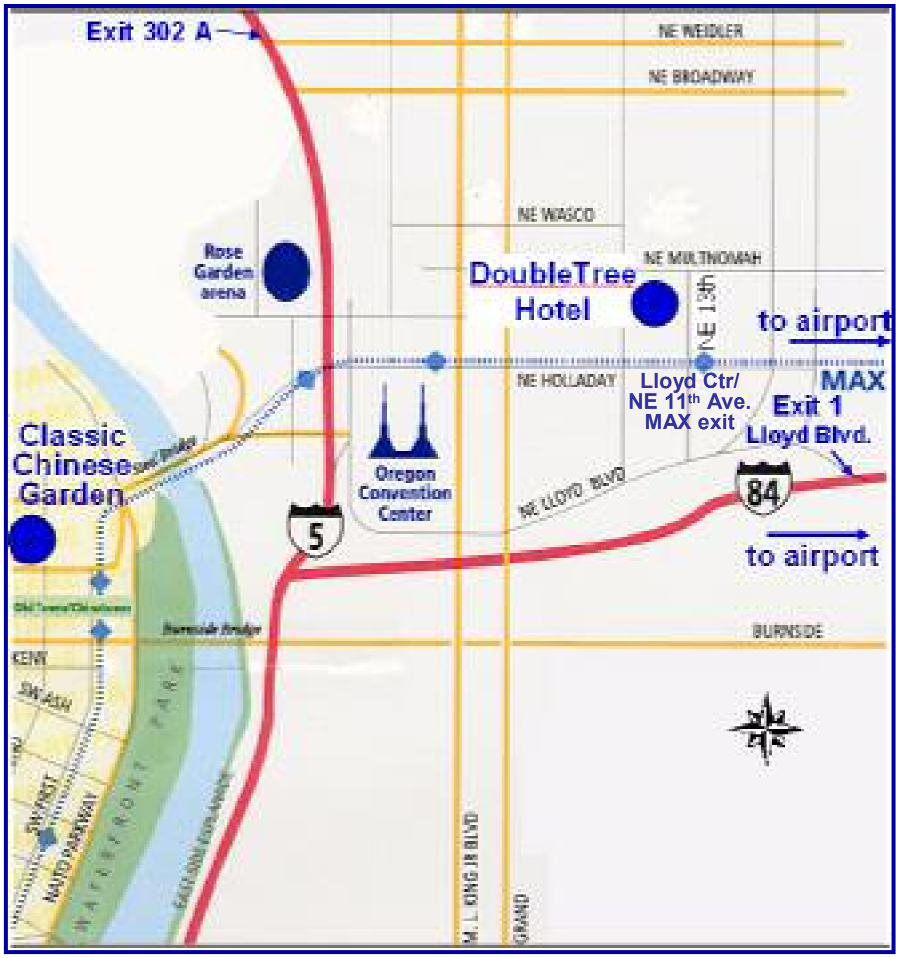

ASB Banquet

Friday, Sept 10, 6:30 pm

sponsored by Legacy and OHSU

LEGACY Health System

OHSU

Exhibits

Exhibits are conveniently located adjacent to both poster session areas. Over 15 exhibitors will be on display throughout the meeting. Be sure to visit the exhibitor displays. See page 15 for a complete list of exhibitor information.

Registration

The registration desk will be located in the conference hotel foyer. Registration desk hours are

Wednesday, Sept. 8	11:00 am - 7:00 pm
Thursday, Friday; Sept. 9,10	7.00 am - 5:00 pm
Saturday, Sept. 11	7:00 am - 12:00 pm

If you have any questions or require assistance, please drop by the registration desk for help.

Information for Presenters

Podium Presentations will be 10 minute long PowerPoint presentations followed by a 5 minute question & answer period. A Windows compatible PC, projector, and laser pointer will be provided in each conference room. Speakers must provide PowerPoint presentations on a CD. If movies are embedded, please provide the movie files on the same CD. We will copy the presentations from CD to the presentation computer and re-link all movie files.
All speakers are required to check into the Speaker Ready Room and turn in their CD the day before their presentation.
For questions, special requirements, or advance file submission, please contact Marcus Mohr (503 413 5487).

Speaker Ready Room is in the Weidler room, and will be open at the same times as the registration desk (see above).

Poster Presentations will be displayed throughout the entire conference without rotation to maximize exposure. Posters will be ordered by subjects, as indicated on page 29.

- Poster dimensions must be no larger than 46” x 46”.
- Push pins are available at the registration desk.
- Feel free to attach copies of your poster or abstract on your poster board for general distribution.
- *Presenters of odd-numbered posters attend their poster for the first half of each session.*
  (i.e., 3:30 pm – 4:15 pm on Thursday and 3:30 pm - 4:00 pm on Friday)
  Presenters of the even-numbered posters attend their posters for the second half of each session.
  (i.e., 4:15 pm – 5:00 pm on Thursday and 4:00 pm - 4:00 pm on Friday).

Poster setup:	Wednesday, Sept. 8	11:00 am - 6:00 pm
Poster dismantle:	Saturday, Sept. 11	7:00 am - noon

Chairpersons for Podium Presentations should be at the presentation room at least 15 minutes before the session start to be acquainted with the presenters and the projectionist. Session chairs should introduce the presenters, their affiliation and the titles of the presentations. It is the responsibility of the session chair to keep the presentations on schedule by maintaining presentation start time, end time, and question period.

ASB Reception — sponsored by SYNTHES USA

On the first night of the ASB meeting, you will be welcomed with a free buffet and Northwest wine to gather with colleagues around the pool and the poster exhibits. This informal reception will be held on Wednesday, September 8, at 6:00 pm at the outdoor pool area of the hotel adjacent to poster area B.

ASB Banquet — jointly sponsored by Legacy and OHSU

What can be more inspiring than to stroll with your colleagues through pavilions, waterfalls, ponds, bridges, and buffets at the Portland Classical Chinese Garden. Designed and hand-crafted by artists from Suzhou, this authentic Ming Dynasty garden will leave you with a memorable impression of the ASB meeting in Portland. You can enjoy an assortment of delectable food options, including Northwest regional cuisine featuring fresh salmon and Pan-Asian fare with an on-site wokery. A Chinese Lion Dance and live music will complete the cultural experience. The ASB banquet will be on Friday, September 10, starting at 6.30 pm. From the hotel, take the blue or red line MAX west towards Hillsboro or City Center. Exit after three MAX stops at the “Old Town/Chinatown” stop. Walk ½ block back (north) on 1st Avenue to Everett Street. Make a left (west) on Everett and head 2 blocks towards 3rd Avenue. The Classical Chinese Garden is located on the corner of SW 3rd & Everett.

General Information

Housing

The Doubletree Lloyd Center Hotel, 1000 NE Multnomah, Portland, OR 97232 is the designated Conference Hotel. All meeting events, presentations and poster exhibits will take place on the main floor of the hotel. For reservations, call 1-503-281-6111 or 1-800-222 8733 and request the ASB discount rate.

Transportation

To Conference Hotel:

- *From the airport (PDX),* take the MAX light rail (red line) to the Lloyd Center/NE 11th Ave stop, located at the conference hotel. The red line MAX leaves every 15 minutes and costs less than $2. In case you choose to drive from the airport, follow Airport Way to I-205 South, take I-84 <u>West</u> to Portland, go 5 miles and take exit 1 Lloyd Blvd. Go to the second light after the exit and take a right onto NE 13th Ave. Turn left onto NE Multnomah St.
- *From I-5 North*: Take Rose Quarter-City Center exit 302A. Take a left at the second light on Weidler. Go to 9th Avenue and take a right. Go to the second light and the hotel is on the left.
- *From I-5 south*: Take Rose Quarter-City Center exit 302A. At the first light, take a right on Weidler. Go to 9th Avenue and take a right. Go to the second light and the hotel is on the left.

In Portland: A MAX light rail stop is located at the hotel (Lloyd Center/NE 11th Ave stop). MAX will take you past many local attractions, including the Classical Chinese Garden, Powell's Book Store and the Oregon Zoo, many of which are within its fare-free zone. It runs every 15 minutes between 6 am and 1 am.

To Banquet at the Classical Chinese Garden: Take the blue or red line MAX west towards city center. Exit after three MAX stops at the "Old Town/Chinatown" stop. Walk ½ block back (north) on 1st Avenue to Everett Street. Make a left (west) on Everett and head 2 blocks towards 3rd Avenue. The Classical Chinese Garden is located on the corner of SW 3rd & Everett.

Rental Cars can be obtained directly in the hotel lobby at Guest Services (503-281-6111). Cars from Enterprise are available between $32 and $45/day and will be delivered to the hotel.

Internet Service

Computers with internet access for conference attendees will be located near the Pacific Northwest Ballroom / poster area B.

Shopping, Events

For tax-free shopping, the Lloyd Center mall is located right across the street from the Doubletree hotel. The mall houses an ice skating rink as well as a cinema multiplex.

ADA Accommodations

The conference hotel, the Banquet site, and transportation to the Banquet (MAX) are accessible to wheelchairs and scooters. All events at the conference center will be conveniently accessible on the first level floor (except the student luncheon). To arrange wheelchair accessible transportation to Laboratory tours, please contact Mark Sommers (503 413 5487) or stop by at the registration desk.

Disclaimer

No reproduction of any kind, including audiotapes and videotapes, may be made of the presentations at the ABS conference. Materials presented at the 28th ASB conference have been made available by the ASB for educational purpose only. The ASB disclaims any and all liability for injury and other damages to any individual attending the meeting and for all claims which may result from the use of techniques demonstrated therein.

Two concurrent workshops will be offered on Wednesday, September 8, starting at 4:00 pm.

Workshop A Wednesday, Sept 8 4:00 pm - 5:30 pm Room A

THE USE OF MOLECULAR BIOLOGY IN BIOMECHANICS

The scientific community has experienced a virtual explosion in applications of molecular biological methods to the fields of medicine, technology, computing and engineering. All of the highest scientific impact papers from 1996 used molecular biology to understand transduction of information by cells. These papers could justifiably be considered within the purview of biomechanics. In this tutorial, the basic tenets of molecular biology will be presented including basic cell structure and the flow of information from DNA to RNA to proteins. The most common methods used to study cells and tissues will be reviewed including gene cloning, sequencing, blotting methods and the use of reverse transcription (RT) and the polymerase chain reaction (PCR). Finally, application of these methods will be illustrated using examples of vascular, muscle and ligament cell response to mechanical signals provided by applications of exercise, strain fields and temperature. The thesis of this presentation is that molecular biological methods provide powerful tools for studying tissue response, but the careful mechanical characterization of cells, receptors and even isolated proteins remains within the area of expertise we know as biomechanics.

Organizer: Richard L. Lieber, Ph.D.
Professor of Orthopaedics and Bioengineering
UCSD and VA Medical Centers
La Jolla, CA 92093-9151
Phone: (858) 552-8585 x7016
FAX: (858) 552-4381
Laboratory Web page: www.muscle.ucsd.edu
email: rlieber@ucsd.edu

Workshop B Wednesday, Sept 8 4:00 pm - 5:30 pm Room B

MUSCLE MECHANICS

This muscle tutorial will examine recent advances (since the Hill and sliding filament model) in our understanding of muscle contraction. Topics will include:
1. Historical background on the mechanisms of contraction.
2. Hill's experiment on heat production and the Hill model
3. H. Huxley's and AF Huxley's proposal of sliding filaments (1953 and 1954, respectively)
4. The classic cross-bridge model (AF Huxley 1957)
5. The swinging cross-bridge model (H Huxley, 1969)
6. The multiple attachment cross-bridge model (AF Huxley and Simmons, 1971)
7. Cross-bridge structure and proposed interaction with actin (Rayment et al., 1994)
8. Current thinking on cross-bridge mechanics and energetics
9. Applications and transfer of these molecular concepts to whole muscle mechanics
10. Remaining Questions and problems

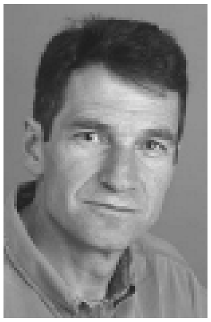

Organizer: Walter Herzog, Ph.D.
Professor, Faculty of Kinesiology
Canada Research Chair in Molecular and Cellular Biomechanics
Associate Dean Research, Kinesiology
Phone: 403-220-8525
Fax: 403-284-3553
email: walter@kin.ucalgary.ca

Keynote 1 | Thursday, Sept 9 | 8:00 am - 9:00 am | Rooms A,B

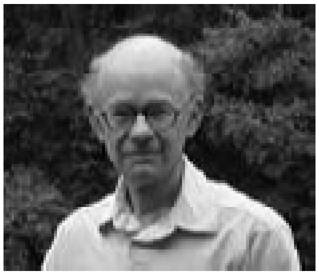

Steven Vogel is James B. Duke Professor of Biology at Duke University. He is the author of *Vital Circuits, Cats' Paws and Catapults* and *Life in Moving Fluids* and the prize-winning *Life's Devices*.

svogel@duke.edu

MUSCEL POWER: THE BIOMECHANICS BEHIND HISTORY

Until we had combustion engines, electric motors, cheap metals, and synthetics, humans mainly relied on muscle and natural materials. Thus significant historical questions need biomechanical insight. Why did the ancient Egyptians build the great pyramid of two-ton blocks? Why did Greek triremes perform so much better than the later Venetian galleys? Did the arrival of projectile weaponry tilt the balance away from Neanderthals and toward early modern humans? What can we say about the efficacy—relative to both force and power—of the various forms of ancient muscle-powered weaponry? How have we persuaded muscle, a linear engine, to drive rotary machinery? And why have equids only recently joined bovids as effective traction engines? Biomechanics may have driven technology at least as much as technology has driven history.

Keynote 2 | Friday, Sept 10 | 8:00 am - 9:00 am | Rooms A,B

Wilson C. "Toby" Hayes, Ph.D. is President of Hayes & Associates, Inc. a consulting firm providing expert testimony in injury biomechanics. Until May 1998, Dr. Hayes was director of the Orthopedic Biomechanics Laboratory at Harvard's Beth Israel Deaconess Medical Center and the Maurice E. Mueller Professor of Biomechanics at Harvard Medical School. Dr. Hayes has received a number of awards, including the Borelli Award.

wch@hayesassoc.com

SO YOU WANT TO BE AN EXPERT? LESSONS FROM FORENSIC INJURY BIOMECHANICS

A construction worker is struck by a falling cement block wall; a child's arm is amputated in a washing machine; an elderly female's neck is broken in a rollover motor vehicle accident; a railroad worker claims work-related wrist injury; a welder is killed in a refinery explosion. The parties are in court seeking compensation, with demands that sometimes seem to outstrip the claimed injuries or to have little prospect of covering the costs of lifetime care. How can a way be found through the often-conflicting stories and competing claims of personal injury, wrongful death and criminal cases to arrive at an understanding of the mechanisms of injury and a determination of who was at fault? How can scientific opinions based on injury biomechanics be used most effectively? To address these questions, this overview introduces: 1) How injury scaling can be used to describe injury severity; 2) How injury risk functions can be used to estimate the probability of injury; and 3) How injury events can be measured against tolerance criteria. Examples are drawn from motor vehicle accidents; slips, trips and falls; occupational and recreational injuries; child abuse, wrongful death and criminal cases. Litigation offers multiple roles to the expert, along with many scientific, ethical and personal challenges. If these are clearly understood and confronted, the effective expert can play a crucial role in the search for truth. In many cases, forensic injury biomechanics can provide the objective evidence that can be the deciding factor in personal injury, products and premises liability, and wrongful death and criminal cases.

Keynote 3 | Friday, Sept 10 | 2:00 pm - 3:00 pm | Rooms A,B

Andrew B. Schwartz, Ph.D.
Professor, Neurobiology
University of Pittsburgh

abs21@pitt.edu

USEFUL SIGNALS FROM THE MOTOR CORTEX

Over the years, we have shown that detailed predictive information of the arm's trajectory can be extracted from populations composed of single unit recordings from motor cortex. This high-fidelity extraction can be used to identify different components of the process that underlies volitional movement. By developing techniques to record these populations and process the signal in real-time, we have also been successful in demonstrating the efficacy of these recordings as a control signal for intended movements in 3D space. Having shown that closed-loop control of a cortical prosthesis can produce very good brain-controlled movements in virtual reality, we have been extending this work to robot control. By introducing an anthropomorphic robot arm into our closed-loop system, we have shown that a monkey can easily control the robot's movement with direct brain-control while watching the movement in virtual-reality. The animal learned this rapidly and produced good movements in 3D space. The next step was to have the animal visualize and move the arm directly without the VR display. This was much more difficult for the animal to learn, as it seemed to have difficulty understanding that the robot was to act as a tool. After the animal was trained, it was able to use the robot to reach for hand-held (by the investigator) targets. We are now developing hardware and software, as well as training monkeys to reach out for food targets at different locations in space, to retrieve them so they can be eaten.

Keynote 4 | Saturday, Sept 11 | 8:00 am - 9:00 am | Rooms A,B

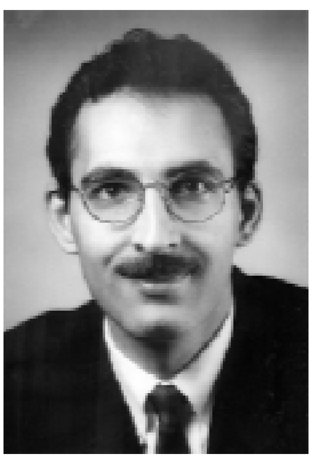

Farshid Guilak, Ph.D., is the director of the orthopaedic bioengineering laboratory at Duke University Medical Center. He has received numerous awards, including the William Harris Award, and recently became Editor-in-Chief of the Journal of Biomechanics.

Guilak@Duke.edu

BIOMECHANICS FACTORS IN OSTEOARTHRITIS:
FROM ORGANISM TO ORGANELLE

Osteoarthritis is a painful and debilitating disease of the joints which is characterized by progressive degeneration of the articular cartilage, the tissue that lines the ends of bones. The etiology of osteoarthritis is poorly understood, although it is now well accepted that mechanical factors can play an important role in the onset and progression of this disease. The goal of our studies has been to determine the effects of normal and abnormal mechanical stress on the articular cartilage using in vivo and in vitro model systems, and to characterize specific biomechanical and biochemical signaling pathways involved in chondrocyte mechanotransduction. Our studies have used in vitro explant models of articular cartilage to study the effects of controlled mechanical stress on matrix metabolism and the production of small-molecule mediators of pain and joint degeneration. To investigate the relationship between the stress-strain and fluid-flow environments at the tissue level in relation to that of the cell, multiscale finite element models were developed for single cells within articular cartilage and compared to experimental measures of cellular and subcellular deformation in situ. These models incorporate the physical properties of pericellular, cellular and subcellular structures, which were measured directly using micromechanical testing methods such as micropipette aspiration and nanoindentation. These techniques were also used to probe the physiologic response of cells to controlled mechanical and osmotic stimuli using single-cell fluorescence imaging of ion mobilization and cytoskeletal remodeling. These findings provide new insights on the ability of biophysical to initiate intracellular signaling. The long-term goal of these studies is to better understand the mechanisms through which mechanical factors influence cartilage maintenance and to develop new physical and pharmacologic therapies for the prevention or treatment of joint disease.

Student Luncheon | Thursday, Sept 9 | 12:45 pm - 1:45 pm | Mt St Helens

Student Business Meeting and Biomechanics Industry Panel Discussion

- **Pick up your lunch box**
- **Go to MT St Helens:** take the stairs across from the registration desk, and St. Helens is to your left.
- **Meet Industry representatives**
- **Discuss career goals**

The purpose of the student luncheon is to inform students about current ASB student related business, vote on current issues and elect the 2004-2005 student representative. This brief meeting will be followed by a panel discussion where scientists will provide their current perspectives on what it takes to succeed in the biomechanics industry. The panel will be composed of established biomechanists from the various industrial disciplines. Questions will be posed to the panel on topics related to what it takes to get a job in the industry, how much education is necessary, are publications essential, where jobs are located, lifestyle in the industry, etc. Additionally, the panel will take questions from ASB students attending the panel discussion. This is a great opportunity for students to see what life is like as a biomechanist in the industry and hear perspectives on how these scientist have succeeded in biomechanics.

For further information, please contact the ASB student representative Max Kurz, mkurz@mail.unomaha.edu

Women in Science Breakfast | Thursday, Sept 9 | 7:00 am - 7:45 am | Halsey

Creating a new tradition, the "Women in Science Breakfast" will be an integral part of the 2004 ASB program. The breakfast will take place on Thursday, September 9th, from 7-7:45 a.m. in the Halsey Room of the Double Tree Hotel. At this breakfast, experienced female scientists will provide their perspective on how women are making a difference in the biomechanics field. The informal setting will allow female students to extend their professional network and address questions about how to succeed in biomechanics. This breakfast will prove to be an exciting and informative venue for female students.

1st Annual Mentoring Program

This year we will initiate the first annual ASB Mentoring Program. The goal of the program is to increase the educational and professional experiences of the students attending the conference. How does it work? Any student who will attend the annual meeting can request to be matched with a senior scientist. The ASB executive board will do its best to find a suitable mentor match.

Mentoring includes:
1) introducing the student to his/her colleagues to help establish a professional network,
2) spending time with the student discussing research, education and vocational goals,
3) sharing his/her career experiences, and
4) providing constructive feedback on the student's presentation.

Please submit mentoring requests to Max Kurz (mkurz@mail.unomaha.edu), and include your contact information, one paragraph describing your research interest, your career stage and any special requests.

Did you know… that Mt St Helens lost 1,314 of its 9,677 feet during its eruption in 1980 and covered Portland with ash?

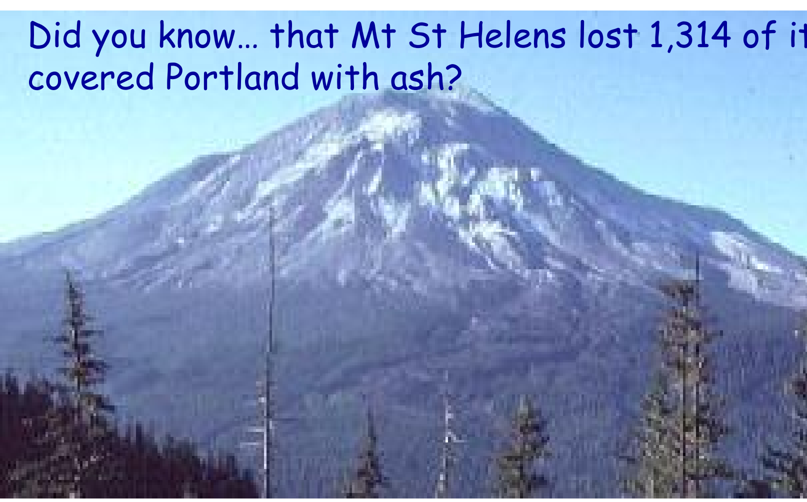

Award Session I Thursday, Sept 9 2:00 pm - 3:30 pm Rooms A/B

Young Scientist Awards

These awards recognize achievements by promising young scientists. They are awarded annually to one pre-doctoral student and one post-doctoral scientist. Nominees for these awards must be current or pending members of the ASB at the time of submission. Candidates may be self-nominated or nominated by an ASB member. The pre-doctoral award nominee must be a doctoral student at the time of the deadline for abstract submissions to the 2004 ASB meeting. The post-doctoral award nominee must have received his/her doctorate prior to April 1, 2004 and is someone who, at the time of this deadline, is within 5 years of their graduation. These awards consist of an engraved plaque, a check for $500 (USD), and a waiver of the annual meeting registration fees.

2004 Pre-Doctoral Award: **Silvia Salinas Blemker**, Stanford University, Stanford, CA

"Rectus Femoris Fiber Excursions Predicted By A 3D Model Of Muscle"

2004 Post-Doctoral Award: **Seth W. Donahue, Ph.D.,** Dept. of Biomedical Engineering, Michigan Technological University, Houghton, MI

"Bone Strength Is Not Compromised With Aging In Black Bears (Ursus americanus) Despite Annual Periods of Disuse (Hibernation)"

Jim Hay Award Inauguration

This annual award in "Biomechanics of Sports and Exercise Science" will be given for the first time at the 2004 ASB conference in honor of the late Jim Hay and his enormous contributions to the ASB specifically and biomechanics in general. With this award, the ASB will celebrate a great teacher, educator and scientist. Jim was a president and founding member of the ASB, and also served as the president of the International Society of Biomechanics. He has trained numerous students, and is best known for his textbooks on the Biomechanics of Sports Techniques. His approach to science through deterministic modeling was unique, and his love for scientific investigation unparalleled. Aside from honoring Jim in this particular way, the award is intended to stimulate young people in the areas of Biomechanics of Sports and Exercise to attend and contribute to the ASB and its annual meeting. The founding fathers of the ASB came almost exclusively from a sport and exercise background, and for a variety of reasons, this field of scientific investigation is not as strongly represented at the ASB as in previous years. Hopefully, this award will encourage increased participation from researchers in exercise and sport sciences. The Jim Hay award winner will be identified from the submitted abstracts and will receive a plaque and $500.

Award Session II | Friday, Sept 10 | 4:30 pm - 6:00 pm | Rooms A/B

Award candidates in this session have been selected from the top 20th percentile of submitted abstracts. From this pool, two finalists for each award have been selected by the ASB Awards Committee, and each of these finalists will present their work. The winner of each award will be selected by the ASB Awards Committee after this session.

Clinical Biomechanics Award

This award recognizes outstanding new biomechanics research targeting a contemporary clinical problem, and is sponsored by Elsevier Science, Ltd., publishers of Clinical Biomechanics. Candidates must be an ASB member and must be first author on an abstract with special relevance for clinical applications submitted to the 2004 ASB meeting. The winner will receive an engraved plaque and US $500.

2004 Finalists:

Allison Arnold, Ph.D., Stanford University, Stanford, CA

Muscle-Tendon Lengths and Velocities of the Hamstrings After Surgical Lengthening to Correct Crouch Gait

Dawn C. Mackey, M.S., Simon Fraser University, Burnaby, BC, Canada

Postural Steadiness During Quiet Stance Does Not Associate With Ability to Recover Balance in Older Women

Journal of Biomechanics Award

This award, sponsored by Elsevier Science, Ltd., publishers of the Journal of Biomechanics, recognizes substantive and conceptually novel mechanics approaches explaining how biological systems function. Candidates must be ASB members and must be first author of an abstract submitted to the 2004 ASB meeting. The winner will receive an engraved plaque and US $500.

2004 Finalists:

Carina Bender, M.S., University of California, Davis

Quantitative Characterization of Lateral Force Transmission in Passive Skeletal Muscle

Marie Shea, M.S., Oregon Health & Science University, Portland, OR

Influence of Sex and Genotype on Skeletal Fragility

Award Session III | Saturday, Sept 11 | 11:00 am - 12:30 pm | Rooms A/B

Borelli Award Lecture

This most prestigious honor given by the ASB, recognizes outstanding career accomplishments and is awarded annually to an investigator who has conducted exemplary research in any area of biomechanics. The award is open to all scientists, including non-ASB members, but excluding ASB officers and members of the Awards Committee. Candidates may be nominated by themselves or by others. Selection is based on originality, quality and depth of the research and its relevance to the field of biomechanics. The award consists of an engraved plaque and US $1,500.

'04 Borelli Award Recipient: **Thomas P. Andriacchi, Ph.D.**, Stanford University, Department of Mechanical Engineering
"Presentation title to be announced"

ASB President's Award

This award recognizes meritorious research involving highly innovative use of experimental or theoretical methods in any field of biomechanics that is presented as a poster at the annual ASB meeting. Candidates must be first author. The winner will be selected by the ASB Awards Committee after the final poster session. The award includes an engraved plaque and US $500 .

Laboratory Tours

Laboratory tours will be offered Wednesday afternoon and Thursday, Friday during lunch break. On Wednesday, tour buses to NIKE and Legacy will leave at the 'Ballroom' entrance of the Hotel approximately every 30 minutes, starting at 12:30 pm. The last tour bus will depart at 3:30 pm. Only tours departing before 2:00 pm will return in time for the workshops.

Wednesday, Sept. 8	12:30 pm - 5:30 pm **(last tour bus departs at 3:30 pm)**	NIKE, Legacy Research Center
Thursday, Friday, Sept. 10, 11	12:40 pm - 2:00 pm	NSI, Legacy Research Center (additional tours at OHSU, NSI, OGI upon request at the registration desk)

NIKE Sport Research Lab

Mario Lafortune, Ph.D., is the research director of the world-renown NIKE Sport Research Laboratory and will offer tours of his state-of-the-art facilities. Its missing is to provide the basic and applied research necessary to create and develop innovative products. Research is conducted in the fields of biomechanics, physiology and sensory/perception to further our understanding of the performance, protection and comfort needs of all active people.

LEGACY
Health System

Biomechanics
Laboratory

Legacy Research & Technology Center

Legacy Research & Technology Center is a full service, state-of-the-art 'hybrid' research park. Its research agenda is structured to bring the most advanced health care treatment modalities and cutting edge technologies quickly on-line, where they can be applied to the benefit of patients. The Center opened in July 1997 and contains 65,000 square feet of state-of-the-art laboratories, clinics, and an extensive support matrix, including a 9500 square foot Clinical Research Center dedicated to out-patient studies. Research is supported by Legacy, and by extramural funding sources (NIH, NSF, CDC, and NASA). The Center houses research programs in Biomechanics (Legacy Biomechanics Laboratory), Cancer, Diabetes, Neurobiology, Neurotology, Ophthalmology, Minimally Invasive Surgery, and Organ Transplantation.

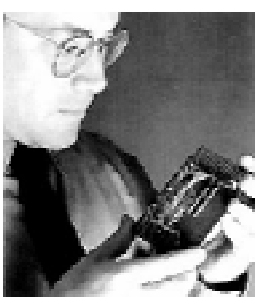

Neurological Sciences Institute / OHSU

The mission of the Neurological Sciences Institute of OHSU is to advance our understanding of the brain and neurological disorders. It houses the *Balance Disorders and Spatial Orientation Laboratories* of long-time collaborators, Dr. Fay Horak and Dr. Robert Peterka.

Dr. Horak's *Balance Disorder's Laboratory* focuses on studies of sensorimotor control of posture and movement. The role of central motor structures such as the basal ganglia and cerebellum and of peripheral sensory information such as the vestibular and somatosensory systems are studied by examining changes in motor control strategies in patients with specific neurological disorders. This understanding is applied to the development of scientifically based approaches to rehabilitation of balance disorders in neurologic patients and the elderly.

Dr. Peterka's *Spatial Orientation Laboratory* is focused on how the brain uses various sources of sensory information to provide an accurate sense of orientation. He studies vestibular related eye movement control and the interaction of vestibular, visual, and proprioceptive system information used for the control of balance and orientation in humans. He is particularly interested in the application of research results to the development of new clinical balance function tests.

Become a Member

The American Society of Biomechanics (ASB) was founded in October 1977. The purpose of the Society is to provide a forum for the exchange of information and ideas among researchers in biomechanics. The term biomechanics refers to the study of the structure and function of biological systems using the methods of mechanics.

Membership benefits include reduced registration fees at the annual meeting and a subscription to the Journal of Biomechanics. There are two types of Membership in the Society, REGULAR and STUDENT: REGULAR Membership requires 1) expertise in the field of biomechanics (i.e., publication of scientific articles) and 2) contributions to the Society (e.g., attendance at biomechanics conferences). STUDENT applicants must provide a letter from their advisor certifying student status. Attendance at the annual meeting of the American Society of Biomechanics is not required for Student Members. Applications for membership are considered quarterly by the Membership Committee. If you would like to APPLY for membership, please obtain an application form at www.asb-biomech.org or directly from the membership chair:

Julianne Abendroth-Smith
Willamette University
Phone: (503)-370-6423
E-mail: jabendro@willamette.edu

ASB General Meeting
Thursday, Sept. 9
5:00 pm - 6:00 pm
Session Room A/B

ASB Executive Board 2004

President	**Walter Herzog**, University of Calgary, (403) 220-3438, walter@kin.ucalgary.ca
Past President	**Joan Bechtold,** Medical Research Foundation, MS (612) 336-6609, bechto1@attglobal.net
President-Elect	**J. J. Trey Crisco**, Brown University, (401) 444-4231, joseph_crisco@brown.edu
Secretary/Treasurer	**Ted Gross**, University of Washington, (206) 341-5604, tgross@u.washington.edu
Secretary/Treasurer-Elect	**Don Anderson**, University of Iowa, Iowa City, IA, (319) 335-8135, don-anderson@uiowa.edu
Meeting Chair	**Michael Bottlang**, Legacy Research Center, Portland, OR, (503) 413 5457, mbottlan@lhs.org
Program Chair	**Steve Robinovitch**, Simon Fraser University, (604) 291-3566, stever@sfu.ca
Program Chair-Elect	**Art Kuo**, University of Michigan, (734) 647-2505, artkuo@umich.edu
Membership Chair	**Julianne Abendroth-Smith**, Willamette University, (503) 370-6423, jabendro@willamette.edu
Education Committee Chair	**Steve McCaw**, Illinois State University, (309) 438-3804, smccaw@ilstu.edu
Communications Chair	**Kathy Simpson**, University of Georgia, (706) 542-4385, ksimpson@coe.uga.edu
Newsletter Editor	**Andy Karduna**, University of Oregon, Eugene, OR, (541) 346-0438, karduna@uoregon.edu
Student Representative	**Max Kurz**, University of Nebraska, Omaha, mkurz@mail.unomaha.edu

The ASB Executive Board is pleased to announce that next year's 29th Annual Meeting of the American Society of Biomechanics will be held August 1-5, 2005, in Cleveland, Ohio. This meeting will be in conjunction with the 20th Congress of the International Society of Biomechanics, organized by Brian Davis and Ton van den Bogert of the Cleveland Clinic. The venue will be Cleveland State University, conveniently located downtown. This combined meeting will attract a much larger number of participants than the usual ASB Annual Meetings, and promises to have an exceptional scientific program.

Exhibitors

Exhibits are conveniently located adjacent to both poster session areas. Over 15 exhibitors will be present. Be sure to visit the exhibitor displays. Exhibit hours are:

Thursday, Sept. 9	8:00 am – 5:00 pm
Friday, Sept. 10	8:00 am – 5:00 pm
Saturday, Sept. 11	8:00 am – 11:00 pm

National Center for Injury Prevention and Control
4770 Buford Highway NE
Atlanta, GA 30341-3724

www.cdc.gov/ncipc/

ohcinfo@cdc.gov

Kistler Instrument Corp.
75 John Glenn Drive
Amherst, NY 14228-2171, USA

www.kistler.com

sales.us@kistler.com

Innovision Systems Corporation
3717 Peters Rd.
Columbiaville, MI 48421-9304, USA

www.innovision-systems.com

sales@innovision-systems.com

Motion Analysis Corporation 3617
Westwind Blvd.
Santa Rosa, California 95403

www.motionanalysis.com

biomechanics@motionanalysis.com

Tekscan, Inc.
307 West First Street
South Boston, MA 02127-1309, USA

www.tekscan.com

marketing@tekscan.com

RSscan International
Lammerdries 27
B-2250 Olen, Belgium

www.rsscan.com

info@rsscan.com

Peak Performance Technologies, Inc.
7388 S. Revere Parkway, Suite 901
Centennial, CO 80112, USA

www.peakperform.com

info@peakperform.com

Noraxon U.S.A. Inc.
13430 N. Scottsdale Road, Suite 104
Scottsdale, Arizona 85254, USA

www.noraxon.com

info@noraxon.com

Vision Research, Inc.
190 Parish Drive
Wayne, New Jersey 07470, USA

www.visiblesolutions.com

phantom@visiblesolutions.com

EnduraTEC
5610 Rowland Road
Minnetonka, MN 55343, USA

www.enduratec.com

electroforce@EnduraTEC.com

zFlo, Inc.
67 Federal Avenue
Quincy, MA 02169, USA

www.zflo.com

info@zflomotion.com

Motion Imaging Corporation
15 McCoy Place
Simi Valley, CA 93065, USA

www.mi-as.com

sales@mi-as.com

Innovative Sports Training, Inc.
3711 North Ravenswood, Suite 150
Chicago, IL 60613, USA

www.innsport.com

sales@innsport.com

Novel, Inc.

964 Grand Avenue
St. Paul, MN, 55105

www.novel.de/

novelinc@novel.de

Vicon Motion Systems Inc - US
9 Spectrum Pointe
Lake Forest, CA 92630

www.vicon.com

moveme@vicon.com

my schedule

Wednesday, 12:30 pm___

Wednesday, 3:30 pm___

Wednesday, 4:00 pm___

Wednesday, 6:30 pm___

Thursday, 7:45 pm ___

Thursday, 9:20 am___

Thursday, 11:00 am___

Thursday, 12.30 pm___

Thursday, 2:00 pm ___

Thursday, 3:30 pm___

Thursday, 5:00 pm___

Friday, 7:45 am___

Friday, 9.20 am___

Friday, 11:00 am___

Friday, 12.30 pm___

Friday, 2:00 pm ___

Friday, 3:30 pm___

Friday, 4:30 pm___

Friday, 6:30 pm___

Saturday, 7:45 am___

Saturday, 9:20 am___

Saturday, 11.00 am___

Saturday, 12.30 pm ___

Podium Presentations

	Session A	Session B
Thursday, Sept. 9 9:20 am - 10.50 am 11:00 am - 12:30 pm	Joint Neuromechanics Sports Biomechanics	Gait & Movement I: Basic Science Orthopaedics I: Basic Science
Friday, Sept. 10 9:20 am - 10.50 am 11:00 am - 12:30 pm	Cell & Tissue Biomechanics Balance & Falls	Gait & Movement II: Clinical & Methods Orthopaedics II: Clinical
Saturday, Sept. 11 9:20 am - 10.50 am	Biomechanics Modeling	Muscle & Reflex

9:20 am - 10:50 am Symposium I: Joint Neuromechanics **Room A**

Chair: Francisco Valero-Cuevas

9:20 - 9:30 **Introduction to Joint Neuromechanics Symposium**
Francisco J. Valero-Cuevas, Neuromuscular Biomechanics Laboratory, Cornell University, Ithaca, NY, USA.

9:30 - 9:50 **THE ROLE OF RECIPROCAL EXCITATION IN THE REGULATION OF STIFFNESS OF THE FELINE ANKLE**
T. Richard Nichols
Department of Physiology, Emory University, Atlanta, GA 30322.

9.50 - 10:10 **ROLE OF SKIN MATERIAL PROPERTIES IN DETERMINING THE SENSITIVITY OF STRETCH-SENSITIVE CUTANEOUS MECHANORECEPTORS**
Peter Grigg
Department of Physiology, University of Massachusetts Medical School, Worcester, MA 01609, USA.

10:10 - 10:30 **NEURO-SENSORY ROLE OF JOINT PERIARTICULAR TISSUE AFFERENTS: A HUMAN KNEE MODEL**
Yasin Dhaher
Sensory Motor Performance Program, The Rehabilitation Institute of Chicago and Department of Physical Medicine and Rehabilitation, Northwestern University, Chicago, IL 60611 USA.

10:30 - 10:50 **ARE NEUROLOGIC FACTORS IMPORTANT IN DEGENERATIVE ARTHRITIS?**
Paul T. Salo
Department of Surgery, University of Calgary, Calgary, AB, Canada

9:20 am - 10:50 am | Gait and Movement I: Basic Science | Room B

Chairs: Jonathan Dingwell (University of Texas), Lena Ting (Georgia Tech/Emory University)

9.20 - 9:35 **LOCAL DYNAMIC STABILITY IMPROVES AT SLOWER WALKING SPEEDS**
Laura C. Marin[1,2] and Jonathan B. Dingwell[1,2]
[1]Nonlinear Biodynamics Lab, Dept. of Kinesiology, University of Texas, Austin, TX, USA.
[2]Dept. of Biomedical Engineering, University of Texas, Austin, TX, USA.

9.35 - 9:50 **INDIVIDUAL CONTRIBUTIONS OF WEIGHT AND MASS TO THE METABOLIC COST OF WALKING**
Alena Grabowski, Claire T. Farley, and Rodger Kram
Locomotion Laboratory, Dept. of Integrative Physiology, University of Colorado, Boulder, USA.

9.50 - 10:05 **WHAT CAUSES A CROSS-OVER STEP WHEN WALKING ON UNEVEN GROUND? A STUDY IN HEALTHY YOUNG WOMEN**
Sibylle B. Thies and James A. Ashton-Miller
[1] Biomechanics Research Laboratory, Dept. of Biomedical Engineering, University of Michigan, Ann Arbor, MI, USA.

10:05 - 10:20 **MODULATION OF MUSCLE SYNERGIES OVER TIME DURING POSTURAL RESPONSES**
Gelsy Torres-Oviedo[1], Jane M. Macpherson[2] and Lena H. Ting[1]
[1]Department of Biomedical Engineering, Georgia Tech/Emory University, Atlanta, GA, USA.
[2]Neurological Sciences Institute, Oregon Health & Science University, Beaverton OR, USA.

10.20 - 10:35 **POSTURAL STEADINESS DURING QUIET STANCE DOES NOT ASSOCIATE WITH ABILITY TO RECOVER BALANCE IN OLDER WOMEN**
Dawn C. Mackey and Stephen N. Robinovitch
Injury Prevention and Mobility Laboratory, School of Kinesiology, Simon Fraser University, Burnaby, BC, Canada.

10:35 - 10:50 **POSTURAL SWAY RESPONSES TO PREDICTABLE AND UNPREDICTABLE MOVING VISUAL SCENES**
Mark Musolino[1,2,4], Patrick Loughlin[1,2,3] and Mark Redfern[1,2,4]
[1]Human Movement and Balance Laboratory. [2]Dept. of Bioengineering,
[3]Dept. of Electrical Engineering, and [4]Dept. of Otolaryngology, University of Pittsburgh, Pittsburgh, PA, USA.

11:00 am - 12:30 pm Sports Biomechanics **Room A**

Chairs: Mario Lafurtune (Nike Sport Research Laboratory), Darren J. Stefanyshyn (University of Calgary)

11:00-11:15 **FOOTWEAR THAT ALLOWS RELATIVE HORIZONTAL MOVEMENT BETWEEN THE FOOT AND OUTSOLE REDUCES KNEE JOINT MOMENTS DURING RUNNING**

Darren J. Stefanyshyn, Jay T. Worobets and Brady Anderson
Human Performance Laboratory, University of Calgary, Calgary AB, Canada.

11:15-11:30 **KINEMATIC STUDY OF LEFT ARM DURING GOLF SWING**

Koon Kiat Teu[1], Wangdo Kim[1],*, Franz Konstantin Fuss[1] and John Tan[2]
[1]School of Mechanical & Production Engineering, Nanyang Technological University, Singapore;
[2]Physical Education & Sports Science, National Institute of Education, Singapore.

11:30-11:45 **OPTIMAL CONTROL SIMULATIONS OF STANDING LONG JUMPS WITH FREE AND RESTRICTED ARM MOVEMENT**

Blake M. Ashby[1] and Scott L. Delp[1,2]
[1]Neuromuscular Biomechanics Laboratory, Mechanical Engineering Department, Stanford University, Stanford, CA, USA.
[2]Bioengineering Department, Stanford University, Stanford, CA, USA.

11:45 - 12:00 **PREDICTING THE ANTERIOR-POSTERIOR COMPONENT OF GROUND REACTION FORCE FROM WEARABLE INSTRUMENTATION**

Dan C. Billing[1,2], Jason P. Hayes[1,2], John Baker[3], Romesh C. Nagarajah[1]
[1]IRIS, Swinburne University of Technology, Hawthorn, Melbourne, Australia.
[2]CRC for microTechnology, Hawthorn, Melbourne, Australia.
[3]Australian Institute of Sport, Belconnen, Canberra, Australia.

12:00 - 12:15 **PROSPECTIVE STUDY OF STRUCTURAL AND BIOMECHANICAL FACTORS ASSOCIATED WITH THE DEVELOPMENT OF PLANTAR FASCIITIS IN FEMALE RUNNERS**

Irene S. Davis[1,2], Clare E. Milner[1], and Joseph Hamill[3],
[1]Department of Physical Therapy, University of Delaware, Newark, DE.
[2]Joyner Sportsmedicine Institute, Lexington, KY. [3]Department of Exercise Science, University of Massachusetts, Amherst, MA.

12:15 - 12:30 **MEASURING REAL TIME HEAD ACCELERATIONS IN COLLEGIATE FOOTBALL PLAYERS**

Stefan Duma[1], Sarah Manoogian[1], Gunnar Brolinson[2,3], Mike Goforth[3], Jesse Donnenwerth[3], Richard Greenwald[4], Jeffrey Chu[4], Bill Bussone[1], Joel Stitzel[1], Joseph Crisco[5]
[1]Virginia Tech – Wake Forest Center for Injury Biomechanics.
[2]Edward Via Virginia College of Osteopathic Medicine.
[3]Virginia Tech Sports Medicine. [4]Simbex. [5]Brown Medical School.

11:00 am - 12:30 pm Orthopaedics I: Basic Science **Room B**

Chairs: Marie Shea (Oregon Health & Science University), Andrew Karduna (University of Oregon)

11:00 - 11:15 **KNEE KINEMATICS DURING ACTIVITY IN ACL DEFICIENT PATIENTS ARE LESS AFFECTED IN THOSE WHO COPE WELL WITH THE INJURY**
Peter J. Barrance[1], Glenn N. Williams[2], Thomas S. Buchanan[1]
[1]Center for Biomedical Engineering Research, University of Delaware, Newark, DE.
[2]Graduate Program in P.T. & Rehabilitation Science, The University of Iowa, Iowa City, IA.

11:15-11:30 **PREDICTION OF RELAXATION FROM CREEP IN LIGAMENTS**
Ashish L. Oza[1], Roderic S. Lakes[2,3] and Ray Vanderby[1,2,3]
[1]Orthopedic Research Laboratories, Department of Orthopedics and Rehabilitation University of Wisconsin, Madison, WI.
[2]Department of Biomedical Engineering, University of Wisconsin, Madison, WI.
[3]Department of Engineering Physics, University of Wisconsin, Madison, WI.

11:30-11:45 **AN MRI IMAGE-BASED METHOD FOR QUANTIFYING MENISCUS STRAINS**
Qunli Sun[1, 2], Robert T. Burks[2], Patrick E. Greis[2], and Jeffrey A. Weiss[1, 2]
[1]Department of Bioengineering, University of Utah, Salt Lake City, UT, USA.
[2]Dept. of Orthopedics, University of Utah, Salt Lake City, UT, USA.

11:45 - 12:00 **CARPAL BONE SCALING IS ISOMETRIC AND NOT GENDER SPECIFIC**
James C. Coburn[1], Joseph J. Crisco[1,2], Douglas C. Moore[1], M. Anwar Upal[2]
[1]Dept. of Orthopaedics, Brown Medical School & Rhode Island Hospital, Providence, RI.
[2]Div. of Engineering, Brown University, Providence, RI.

12:00 - 12:15 **INFLUENCE OF SEX AND GENOTYPE ON SKELETAL FRAGILITY**
Marie Shea[1], Brenden L. Hansen[1], Dawn A. Olson[2], Denise Dinulescu[2], Ben Orwoll[2], John K. Belknap[2], Eric S. Orwoll[2], and Robert F. Klein[2]
[1]Orthopaedic Biomechanics Laboratory, Oregon Health & Science University, Portland, OR, USA.
[2]Bone and Mineral Unit, Oregon Health & Science University, Portland, OR, USA.

12:15 - 12:30 **HETEROGENEOUS ADAPTATION OF THE PATELLOFEMORAL JOINT TO SHORT- AND LONG-TERM ANTERIOR CRUCIATE LIGAMENT DEFICIENCY**
Andrea Clark[1], Walter Herzog[1], John Matyas[2], Leona Barclay[2] and Tim Leonard[1].
[1]The Human Performance Lab, Faculty of Kinesiology, University of Calgary, AB, Canada.
[2]McCaig Centre for Joint Injury and Arthritis Research, University of Calgary, AB, Canada.

9:20 am - 10:50 am Symposium II: Cell and Tissue Biomechanics **Room A**

Chair: Walter Herzog (University of Calgary)

9:20 - 9:35 **Introduction to Cell and Tissue Biomechanics Symposium**
Walter Herzog, Faculty of Kinesiology, University of Calgary

9:35 - 10:00 **TITIN AND MUSCLE**
Henk Granzier, Veterinary Comparative Anatomy, Pharmacology & Physiology, Washington State University

10:00 - 10:25 **CELLULAR MECHANOTRANSDUCTION IN BONE**
Christopher Jacobs, Department of Mechanical Engineering and Department of Functional Restoration, Stanford University, and Rehabilitation Research and Development Center, VA Palo Alto Health Care Systems

10:25 - 10:50 **LIGAMENTS AND TENDONS**
Albert J. Banes, Department of Orthopaedics, UNC School of Medicine Chapel Hill, NC

9:20 am - 10:50 am Gait and Movement II: Clinical/Methods **Room B**

Chairs: Li-Shan Chou (University of Oregon), Nicholas Stergiou (University of Nebraska at Omaha)

9.20 - 9:35 **IN VIVO SHOULDER KINEMATICS: A COMPARISON OF MEASUREMENT METHODS**
Duane A. Morrow, Diana K. Hansen, Denny J. Padgett, Kai-Nan An, Kenton R. Kaufman
Motion Analysis Laboratory, Division of Orthopedic Research, Mayo College of Medicine, Rochester, MN, USA

9.35 - 9:50 **ESTIMATION OF THE ACCURACY OF A SHAPE-FROM-SILHOUETTE MARKERLESS MOTION CAPTURE SYSTEM**
Lars Mündermann[1], Ajit Chaudhari[1], Gene Alexander[1], Thomas P. Andriacchi[1,2,3]
[1]Division of Biomechanical Engineering, Stanford University, Stanford, CA.
[2]Bone and Joint Center, Palo Alto VA, Palo Alto, CA.
[3]Department of Orthopedic Surgery, Stanford University Medical Center, Stanford, CA.

9.50 - 10:05 **DOES FOOTWEAR INFLUENCE THE STRUCTURE OF CHAOTIC GAIT PATTERNS?**
Max J. Kurz, Nicholas Stergiou and Daniel Blanke
HPER Biomechanics Laboratory, University of Nebraska at Omaha, Omaha, NE.

10:05 - 10:20 **COMPARING MOMENTUM AND STABILITY TRADEOFFS DURING BIDIRECTIONAL GAIT INITIATION IN OLDER ADULTS AND PARKINSONISM**
Chris J. Hass[1,2], Dwight E. Waddell[1], Steve L. Wolf[3], Jorge L. Juncos[2], Robert J.Gregor[1]
[1]Center for Human Movement Studies, Georgia Institute of Technology, Atlanta, GA, USA.
[2]Department of Neurology, Emory University, Atlanta, GA, USA.
[3]Department of Rehabilitation Medicine, Emory University, Atlanta, GA, USA.

10.20 - 10:35 **MUSCLE-TENDON LENGTHS AND VELOCITIES OF THE HAMSTRINGS AFTER SURGICAL LENGTHENING TO CORRECT CROUCH GAIT**
Allison Arnold[1], May Liu[1], Michael Schwartz[3], Sylvia Õunpuu[4], Luciano Dias[5], Scott Delp[1,2]
[1]Depts. of Mechanical Engineering and [2]Bioengineering, Stanford University, Stanford, CA.
[3]Motion Analysis Laboratory, Gillette Children's Specialty Healthcare, St. Paul, MN.
[4]Center for Motion Analysis, Connecticut Children's Medical Center, Hartford, CT.
[5]Motion Analysis Center, Children's Memorial Medical Center, Chicago, IL.

10:35 - 10:50 **GAIT EFFECIENCY: CENTER OF MASS MOTION, VO_2 AND WALKING SPEED**
Michael S. Orendurff, Ava D. Segal, Jocelyn S. Berge, Kevin C. Flick and Glenn K. Klute
Motion Analysis Laboratory, Rehabilitation Research and Development, Seattle, Washington.

11:00 am - 12:30 pm Balance and Falls Room A

Chairs: Darryl G. Thelen (University of Wisconsin-Madison), Elizabeth T. Hsiao-Wecksler (University of Illinois at Urbana-Champaign)

11:00 - 11:30	**MULTIDIRECTIONAL POSTURAL INSTABILITY IN PARKINSON'S DISEASE** Fay B. Horak, PhD, PT Balance Disorders Laboratory, Dept of Neurology, Physiology & Pharmacology and Biomedical Engineering, Neurological Sciences Institute, Oregon Health & Science University. **INVITED LECTURE**
11:30 - 11:45	**THE EFFECT OF HAND POSITION ON WRIST KINEMATICS AT LANDING FROM A FORWARD FALL FROM A KNEELING POSITION** Karen L. Troy, Courtney D. Gavin, Mark D. Grabiner University of Illinois at Chicago, Chicago, IL
11:45 - 12:00	**SAFE LANDING DURING A FALL: EFFECT OF RESPONSE TIME ON ABILITY TO AVOID HIP IMPACT DURING SIDEWAYS FALLS** Fabio Feldman and Stephen N. Robinovitch Injury Prevention and Mobility Laboratory, School of Kinesiology, Simon Fraser University, Burnaby, BC, Canada.
12:00 - 12:15	**SIMULATION OF FORWARD FALLS: EFFECT OF LOWER EXTREMITY CONTROL STRATEGY ON INJURY RISK** Jia-Hsuan Lo and James Ashton-Miller Biomechanics Research Laboratory, Department of Mechanical Engineering, University of Michigan, Ann Arbor, MI, USA.
12:15 - 12:30	**EFFECTS OF BLURRING VISION ON M/L BALANCE DURING STEPPING UP OR DOWN TO A NEW LEVEL IN THE ELDERLY** [1]John G Buckley, [1]Karen Heasley, [2]Andy Scally and [1]David B Elliott. [1]Vision and Mobility Research Laboratory, Department of Optometry. [2]Institute of Health Research, School of Health, University of Bradford, Bradford, UK.

11:00 am - 12:30 pm Orthopaedics II: Clinical Room B

Chairs: Steven M. Madey (Legacy Health System), Sean S. Kohles (Kohles Bioengineering)

11:00-11:15 **OPTIMIZATION OF BONE ALIGNMENT TO REPRODUCE PLANTAR PRESSURES IN A SUBJECT-SPECIFIC FINITE ELEMENT FOOT MODEL**

Ahmet Erdemir[1], Marc Petre[1,2], Sachin Budhabhatti[1,3] and Peter R. Cavanagh[1]
[1]Dept. of Biomedical Engineering, Cleveland Clinic Foundation, Cleveland, OH, USA.
[2]Dept. of Biomedical Engineering, Case Western Reserve University, Cleveland, OH, USA
[3]Dept. of Chemical & Biomedical Engineering, Cleveland State University, Cleveland, OH, USA.

11:15-11:30 **THE EFFECTS OF SKELETAL METASTASIS ON BONE TISSUE PROPERTIES**

Ara Nazarian[1,5], Jae Y Rho[3], Marc Grynpas[4], David Zurakowski[2], Ralph Müller[5] and Brian D. Snyder[1, 2]
[1]Orthopedic Biomechanics Laboratory, Beth Israel Deaconess Medical Center and Harvard Medical School, Boston, MA. [2]Dept. of Orthopaedic Surgery, The Children's Hospital, Boston, MA.
[3]Dept. of Biomed. Eng., University of Memphis, Memphis, TN.
[4]Institute for Biomat. and Biomedical Engineering, University of Toronto, Toronto, Canada.
[5]Institute for Biomedical Engineering, Swiss Federal Institute of Technology, Zürich, CH.

11:30-11:45 **METHODS TO DETERMINE *IN VIVO* CARTILAGE STRESS IN THE PATELLOFEMORAL JOINT FROM WEIGHT-BEARING MRI**

Thor Besier[1], Garry Gold[2], Christine Draper[1], Chris Powers[3], Scott Delp[1,4], and Gary Beaupré[4]
Departments of Mechanical Engineering[1], Bioengineering[1], and Radiology[2], Stanford University, Stanford. CA.
[3]Department of Biokinesiology and Physical Therapy, University of Southern California, LA.
[4]VA Palo Alto Rehabilitation R&D Center, Palo Alto, CA.

11:45 - 12:00 **DO THE MECHANICAL PROPERTIES OF INTERVERTEBRAL DISCS MATCH THOSE OF ADJACENT VERTEBRAE?**

Daniel Skrzypiec, Phill Pollintine, Michael A. Adams
Department of Anatomy, University of Bristol, Bristol BS2 8EJ, UK.

12:00 - 12:15 **INTERVERTEBRAL NECK INJURY CRITERION FOR SIMULATED FRONTAL IMPACTS**

Paul C. Ivancic, Shigeki Ito, Manohar M. Panjabi, Adam M. Pearson, Yasuhiro Tominaga, Jaw-Lin Wang, S. Elena Gimenez
Biomechanics Research Laboratory, Yale University School of Medicine, New Haven, CT, USA.

12:15 - 12:30 **OBLIQUE IMPACT TESTING OF BICYCLE HELMETS**

Steven M. Madey, Larry W. Ehmke, Mark B. Sommers, and Michael Bottlang
Biomechanics Laboratory, Legacy Research & Technology Center, Portland, OR

9:20 am - 10:50 am Biomechanical Modeling **Room A**

Chairs: Rahman Davoodi (University of Southern California), Ahmet Erdemir (The Cleveland Clinic Foundation)

9.20 - 9:35	**USING COMPUTED MUSCLE CONTROL TO GENERATE FORWARD DYNAMIC SIMULATIONS OF GAIT FROM EXPERIMENTAL DATA** Darryl G. Thelen[1] and Frank C. Anderson[2] [1]Dept. of Mechanical Engineering, University of Wisconsin-Madison, Madison, WI, USA. [2]Dept. of Mechanical Engineering, Stanford University, Stanford, CA, USA.
9.35 - 9:50	**COMPUTATION OF MOTION PATTERNS OF THE COCHLEAR PARTITION** Hongxue Cai, Brett Shoelson, and Richard S. Chadwick Section on Auditory Mechanics, NIDCD/NIH, Bethesda, MD 20892
9.50 - 10:05	**INVESTIGATING CHRONIC STRESS EXPOSURE FOLLOWING INTRAARTICULAR FRACTURE USING A FINITE ELEMENT MODEL OF THE ANKLE** Donald D. Anderson, Nicole M. Grosland, and Thomas D. Brown Department of Orthopaedics and Rehabilitation, The University of Iowa, Iowa City, IA, USA.
10:05 - 10:20	**CLINICIAN-FRIENDLY SOFTWARE FOR BIOMECHANICAL MODELING AND CONTROL OF MOVEMENT** Rahman Davoodi, Chet Urata, Emanuel Todorov, and Gerald E. Loeb A.E. Mann Institute and Biomedical Engineering Department, University of Southern California Los Angeles, CA, USA.
10.20 - 10:35	**MINIMAL ACTUATION REQUIREMENTS FOR POWERING THE PASSIVE WALKING MODEL WITH KNEES** Jesse C. Dean[1] and Arthur D. Kuo[1,2] [1]Dept. of Biomedical Engineering, [2]Dept. of Mechanical Engineering University of Michigan, Ann Arbor, MI.
10:35 - 10:50	**STATIC FORCE PRODUCTION IN A THREE-DIMENSIONAL MUSCULOSKELETAL MODEL OF THE CAT HINDLIMB** Lale Korkmaz[1], Thomas J. Burkholder[2] and Lena H. Ting[3] [1]Woodruff School of Mechanical Engineering, Georgia Institute of Technology, Atlanta, GA. [2]School of Applied Physiology, Georgia Institute of Technology, Atlanta, GA. [3]Coulter Department of Biomedical Engineering, Georgia Tech/Emory University, Atlanta, GA.

9:20 am - 10:50 am Muscle and Reflex **Room B**

Chairs: David A Hawkins (University of California - Davis), Kevin P. Granata (Virginia Tech)

9.20 - 9:35 **MAGNETIC RESONANCE ELASTOGRAPHY FOR THE ASSESSMENT OF MUSCLES IN HYPERTHYROIDISM**
Stacie I. Ringleb[1], Laurel Littrell[2], Qingshan Chen[1], Sabine Bensamoun[1], Michael D. Brennan[3], Kenton R. Kaufman[4], Richard L. Ehman[2], Kai-Nan An[1]
[1]Orthopedics Biomechanics Laboratory, Mayo Clinic College of Medicine, Rochester, MN.
[2]MRI Research Laboratory, Mayo Clinic College of Medicine, Rochester, MN.
[3]Dept. of Endocrinology, Mayo Clinic, Rochester, MN. [4]Motion Analysis Laboratory, Mayo Clinic College of Medicine, Rochester, MN.

9.35 - 9:50 **SMALL CHANGES IN THE TIMING OF ACTIVATION AFFECTS FIBER LENGTHS AND SERIAL SARCOMERE NUMBER ADAPTATIONS IN RABBIT TIBIALIS ANTERIOR EXPOSED TO ECCENTRIC EXERCISE**
Timothy A Butterfield, Walter Herzog.
Human Performance Laboratory, University of Calgary, Calgary, Alberta, Canada.

9.50 - 10:05 **STRESS-DEPENDENT AND STRESS-INDEPENDENT GENE EXPRESSION IN RAT SKELETAL MUSCLE AFTER A SINGLE BOUT OF "EXERCISE"**
Eric Hentzen[1], Michelle Lahey[1], Liby Mathew[1], David Peters[1], Ilona A. Barash[1], Jan Fridén[2] and Richard L. Lieber[1]
[1]Departments of Orthopaedic Surgery and Bioengineering, University of California, San Diego, Veterans Affairs Medical Center, San Diego.
[2]Department of Hand Surgery, Sahlgrenska University Hospital, Göteborg, Sweden.

10:05 - 10:20 **EFFECTS OF STATIC FLEXION-RELAXATION ON PARASPINAL REFLEX BEHAVIOR**
Ellen Rogers, Kevin Moorhouse, and Kevin Granata[1]
Musculoskeletal Biomechanics Laboratory, Virginia Polytechnic Institute, Blacksburg, VA, USA.

10.20 - 10:35 **FORCE TRANSMISSION VIA MYOFASCIAL PATHWAYS IN DYNAMIC CONDITIONS OF A SINGLE HEAD OF MULTI-TENDONED RAT EDL MUSCLE**
Huub Maas[1], and Peter A. Huijing[2,3]
[1]School of Applied Physiology, Georgia Institute of Technology, Atlanta, GA, USA.
[2]Faculty of Human Movement Sciences, Vrije Universiteit Amsterdam, The Netherlands.
[3]Institute for Biomedical Technology, Universiteit Twente, Enschede, The Netherlands.

10:35 - 10:50 **QUANTITATIVE CHARACTERIZATION OF LATERAL FORCE TRANSMISSION IN PASSIVE SKELETAL MUSCLE**
Carina J. Bender, M.S. and David A. Hawkins, Ph.D.
Human Performance Laboratory, Exercise Science Graduate Group, University of California, Davis.

Posters

Poster Presentations will be displayed throughout the entire conference without rotation to maximize exposure. Posters will be ordered by subjects, as indicated below, and displayed in poster area A (Willamette Ballroom) and poster area B (Pacific Northwest Ballroom).

Presenters of odd-numbered posters are encouraged to attend their poster during the first half of each poster session, (i.e. 3:30-4:15 pm on Thursday, 3:30 pm - 4:00 and Friday) and Presenters of even-numbered posters are encouraged to attend their poster during the second half of each poster session. (i.e., 4:15 pm – 5:00 pm on Thursday and 4:00 - 4:30 on Friday).

Poster setup:	Wednesday, Sept. 8	11:00 am - 6:00 pm
Poster dismantle:	Saturday, Sept. 11	7:00 am - noon

Subject	Poster #'s	Poster Area
Bone	100-111	A
Cartilage/Tendon/Ligament	112-137	A
Lower Extremity	138-180	A
Upper Extremity	181-203	A
Spine	204-226	A
Methods	227-241	B
Muscle	242-271	B
Posture and Balance	272-282	B
Rehabilitation Engineering	283-288	B
Gait and Movement	289-314	B
Aging	315-325	B
Cardiovascular	326-330	B
Sport Science	331-341	B

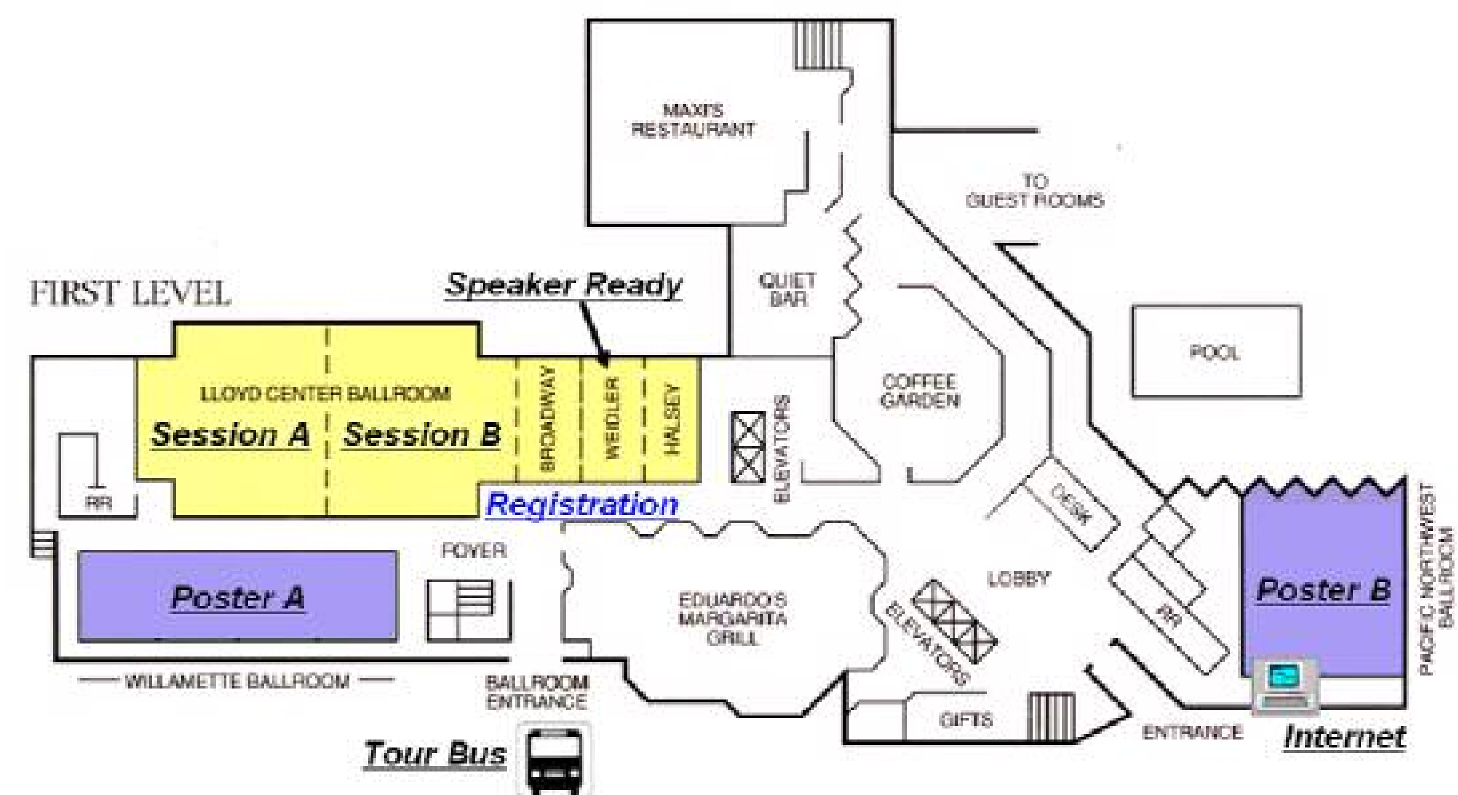

 # 100 DISPLACED OLECRANON FRACTURES IN CHILREN: A BIOMECHANICAL ANALYSIS OF FIXATION METHODS

Stefan Parent[1], Michelle Wedemeyer[1], Megan Anderson[2], Fran Faro[2], Andrew Mahar[1,2],Francois Lalonde[1], Peter Newton[1,2]
[1]Department of Orthopedics,Children's Hospital, San Diego San Diego, CA, USA; [2]Department of Orthopaedic Surgery, University of California, San Diego,San Diego, CA, USA.

 # 101 VISCOELASTIC EFFECTS AT THE BONE-SCREW INTERFACE

Serkan İnceoğlu[1], Atilla Akbay[1], and Robert F. McLain[2]
[1]Spine Research Laboratory, Spine Institute, The Cleveland Clinic Foundation, Cleveland, OH, USA
[2]Dept. of Orthopeadic Surgery, Spine Institute, The Cleveland Clinic Foundation, Cleveland, OH, USA

 # 102 BIOMECHANICAL EVALUATION OF VERTEBRAL AUGMENTATION WITH CALCIUM SULFATE CEMENT IN CADAVERIC OSTEOPOROTIC VERTEBRAL COMPRESSION FRACTURES

Andrew Mahar[1,2] , Andrew Perry[1], Noemi Arrieta[1], Steven Garfin[1], Jennifer Massie[1], Choll Kim[1]
[1]Department of Orthopaedics University of California, San Diego, San Diego, CA; [2]Department of Orthopedics Children's Hospital, San Diego, San Diego, CA.

 # 103 QUANTIFYING FRACTURE ENERGY IN A CLINICAL SERIES OF TIBIAL PILON FRACTURE CASES

Donald D. Anderson, Valerie L. Muehling, J. Lawrence Marsh, and Thomas D. Brown
Department of Orthopaedics and Rehabilitation, The University of Iowa, Iowa City, IA, USA

 # 104 EFFECT OF FLOOR STIFFNESS ON IMPACT FORCES DURING FALLS ON THE HIP

Andrew C.T. Laing, Iman Tootoonchi, Stephen N. Robinovitch
Injury Prevention and Mobility Laboratory, School of Kinesiology, Simon Fraser University, Burnaby, BC, Canada.

 # 105 FURTHER EVIDENCE THAT BONE MINERAL DENSITY AND SOFT TISSUES INFLUENCE PELVIC FRACTURE IN OLDER WOMEN DURING LATERAL IMPACT

Brandon S. Etheridge[1], David P. Beason[1], Jorge E. Alonso[2], Robert Lopez[3], *Alan W. Eberhardt[1]
[1]Dept. of Biomedical Engineering, [2]Division of Orthopaedic Surgery, [3]Department of Radiology University of Alabama at Birmingham, Birmingham, Alabama, USA.

 # 106 THREE-DIMENSIONAL FINITE ELEMENT BONE DAMAGE SIMULATIONS USING QUASI-CONTINUUM DAMAGE MECHANICS

Victor Kosmopoulos[1] and Tony S. Keller[2]
[1]Department of Mechanical Engineering, School of Engineering, The College of New Jersey, Ewing, NJ, United States;
[2]Department of Mechanical Engineering, College of Engineering and Mathematics, The University of Vermont, Burlington, VT, United States.

 # 107 ANALYSIS OF FATIGUE DAMAGE IN BOVINE TRABECULAR BONE

Partha Ganguly[1], Tara L. A. Moore[2], and Lorna J. Gibson[3]
[1]Schlumberger-Doll Research Cambridge, MA, USA; [2]Exponent, Inc., Philadelphia, PA, USA
[3]Department of Materials Science and Engineering, Massachusetts Institute of Technology, Cambridge, MA, USA.

 # 108 BONE STRENGTH IS NOT COMPROMISED WITH AGING IN BLACK BEARS (URSUS AMERICANUS) DESPITE ANNUAL PERIODS OF DISUSE (HIBERNATION)

Seth W. Donahue[1, 2] and Kristin B. Harvey[1]
Departments of [1]Mechanical Engineering - Engineering Mechanics and [2]Biomedical Engineering, Michigan Technological University, Houghton, MI

 # 109 CHARACTERIZATION OF A HUMAN VERTEBRAL BODY COLLAPSE USING A 6-DOF ROBOTIC SYSTEM

Wafa Tawackoli, Kay Sun, Michael A.K. Liebschner
Department of Bioengineering, Rice University, Houston, TX, USA.

 # 110 PERMEABILITY & MICROARCHITECTURAL MEASUREMENTS IN CALCANEUS

S. Solomon Praveen, Craig J. Bennetts, Kimerly A. Powell, and Brian L. Davis
Orthopaedic Research Center, The Cleveland Clinic Foundation, Cleveland, OH, USA

 # 111 COMPARISON OF THREE DIFFERENT HYDROXYAPATITE COATINGS IN AN UNLOADED IMPLANT MODEL-EXPERIMENTAL CANINE STUDY

[1]Daugaard, H; 1Elmengaard, B; [2]Bechtold, J E, 1Jensen T B, 1Søballe, K
[1]Orthopaedic Research Laboratory, Aarhus University Hospital, Denmark; [2]Midwest Orthopaedic and Minneapolis Medical Research Foundation

Cartilage Tendon Ligaments

 # 112 DYNAMIC BENDING MECHANICS OF THE DEVELOPING SPINE

David J. Nuckley, Richard M. Harrington, and Randal P. Ching
Applied Biomechanics Laboratory, Mechanical Engineering Department, University of Washington, Seattle, WA, USA.

 # 113 TRACKING NON-UNIFORM STRAIN OF THE AORTIC VALVE

Todd C. Doehring[1] and Ivan Vesely[2]
[1] Department of Biomedical Engineering, Lerner Research Institute, Cleveland Clinic Foundation, Cleveland, OH, USA,
[2] Saban Research Institute, Los Angeles, CA, USA

 # 114 LIGAMENTOUS VERSUS PHYSEAL FAILURE IN MURINE MEDIAL COLLATERAL LIGAMENT BIOMECHANICAL TESTING

Hossam B. El- Zawawy; Matt J. Silva; Linda J. Sandell; Rick W. Wright
Department of Orthopaedic Surgery, Washington University School of Medicine at Barnes Jewish Hospital, St. Louis, MO.

 # 115 VISCOELASTIC CHARACTERIZATION OF CERVICAL SPINAL LIGAMENTS

Scott R. Lucas[1], Cameron R. Bass[1], Robert S. Salzar[1], James B. Folk[1], Lucy E. Donnellan[1], Glenn Paskoff[2], and Barry S. Shender[2]
[1]Center for Applied Biomechanics, University of Virginia; [2]NAVAIR, Patuxent River.

 # 116 RESPONSE SURFACE ANALYSIS OF FLEXURAL AND MEMBRANE STRESSES TO CHARACTERIZE FLEXIBLE BIOLOGIC MATERIALS

Sean S. Kohles[1]
[1]Kohles Bioengineering, Portland State University, and Oregon Health & Science University, Portland, OR.

 # 117 SERUM COMP CONCENTRATION IS RELATED TO LOAD DISTRIBUTION AT THE KNEE DURING WALKING IN HEALTHY ADULTS

Anne Mündermann[1,2], Karen B. King[3], Chris O. Dyrby[1,2], Thomas P. Andriacchi[1,2,4]
[1]Division of Biomechanical Engineering, Stanford University, Stanford, CA; [2]Bone and Joint Center, Palo Alto VA, Palo Alto, CA; [3]Department of Medicine, University of California San Francisco, San Francisco, CA; [4]Department of Orthopedic Surgery, Stanford University Medical Center, Stanford, CA.

 # 118 A MICRO-MECHANICAL COMPOSITE ANALYSIS OF ENGINEERED CARTILAGE

Sean S. Kohles[1], Christopher G. Wilson[2], and Lawrence J. Bonassar[3]
[1]Kohles Bioengineering, Portland State University, and Oregon Health & Science University, Portland, OR; [2]Wallace H. Coulter Department of Biomedical Engineering, Georgia Institute of Technology; Atlanta, GA;[3]Sibley School of Mechanical and Aerospace Engineering, Cornell University, Ithaca, NY.

 # 119 CHARACTERIZATION OF PLANTAR TISSUES UNDER THE METATARSAL HEADS

Andrew R. Fauth[1,2] and Neil A. Sharkey[1,2,3]
[1]Center for Locomotion Studies, The Pennsylvania State University, University Park, PA; [2]Dept. of Kinesiology, The Pennsylvania State University, University Park, PA; [3]Dept. of Orthopaedics and Rehabilitation, The Pennsylvania State University, Hershey, PA.
These data describe the *in vitro* material properties of the plantar soft tissues beneath the first and second metatarsal heads and can be used in detailed hyperelastic numerical models of the soft tissues on the plantar surface of the foot.

 # 120 HYPERELASTIC PROPERTIES OF NORMAL AND DIABETIC HEEL PADS FROM AN INVERSE FINITE ELEMENT MODEL OF INDENTATION

Ahmet Erdemir[1], Meredith L. Viverios[2], Jan S. Ulbrecht[3], and Peter R. Cavanagh[1]
[1] Department of Biomedical Engineering, Cleveland Clinic Foundation, Cleveland, OH, USA; [2] Instron Corporation Headquarters, Canton, MA, USA; [3] Depts of Biobehavioral Health and Medicine, Penn State University, University Park, PA, USA.

 # 121 FACTORS INFLUENCING THE ACCURACY OF ARTICULAR CARTILAGE THICKNESS MEASUREMENT FROM MRI

Seungbum Koo[1], Peter Kornaat[2], Garry Gold[2] and Thomas P. Andriacchi[1,3]
[1]Biomotion Laboratory, Stanford University, Stanford, CA, USA; [2]Department of Radiology, Stanford University, Stanford, CA, USA; [3]Department of Orthopaedic Surgery, Stanford University, Stanford, CA, USA

 # 122 LIGAMENTOUS INJURY DURING SIMULATED FRONTAL IMPACT

Manohar M. Panjabi, Adam M. Pearson, Shigeki Ito, Paul C. Ivancic, S. Elena Gimenez, Yasuhiro Tominaga
Biomechanics Research Laboratory, Yale University School of Medicine, New Haven, CT, USA

 # 123 FE ANALSIS OF THE MECHANICAL BEHAVIOR OF CHONDROCYTES

S.K.Han1, S. Federico[1], A. Grillo[2], F. Musumeci2, G. Giaquinta[2], and W. Herzog[1]
[1]Human Performance Laboratory, the University of Calgary, Canada; [2]Dept of Physical and Chemical Methodologies for Engineering, University of Catania, Italy.

 # 124 SHEAR-STRESS-INDUCED CHONDROCYTE DEATH IS REDUCED BY ANTIOXIDANT TREATMENT

James A. Martin, Anneliese D. Heiner, Benjamin R. Beecher, and Thomas D. Brown
Department of Orthopaedics and Rehabilitation, The University of Iowa, Iowa City, Iowa

 # 125 SPEED EFFECTS ON KNEE ADDUCTION MOMENTS USING INTERVENTION FOOTWEAR: IMPLICATION FOR THE TREATMENT OF KNEE OSTEOARTHRITIS

David Fisher[1], Anne Mündermann[1,2], and Thomas Andriacchi[1,2]
[1]Stanford Biomotion Laboratory, Biomechanical Engineering Division, Mechanical Engineering Department, Stanford, CA, USA; [2] Department of Veterans Affairs, VA Palo Alto Health Care System Rehabilitation R&D Center, Palo Alto, CA, USA.

 # 126 NORMAL VIBRATION FREQUENCIES OF THE VOCAL LIGAMENT

Ingo R. Titze[1,2] and Eric J. Hunter[1]
[1]National Center for Voice and Speech, A division of Denver Center for the Performing Arts, Denver, CO, USA; [2]Department of Speech Pathology and Audiology, The University of Iowa, Iowa City, IA, USA.

 # 127 LUMBAR FACET JOINT CAPSULE CREEP DURING STATIC FLEXION

Jesse S. Little[1] and Partap S. Khalsa[1]
[1]Dept. of Biomedical Engineering, State University of New York at Stony Brook, Stony Brook, NY, USA;

 # 128 BIOMECHANICAL COMPARISON OF AN INTRA- CORTICAL FIXATION ANCHOR VERSUS STANDARD ANCHOR FIXATION FOR ROTATOR CUFF REPAIR

Andrew Mahar[1,2], Darin Allred[2], Gaurav Abbi[2], Michelle Wedemeyer[1], Robert Pedowitz[2]
[1]Department of Orthopedics Children's Hospital, San Diego San Diego, CA; [2]Department of Orthopaedics University of California, San Diego, San Diego, CA

 # 129 CAPSULE REPRESENTATION IN A TOTAL HIP DISLOCATION FINITE ELEMENT MODEL

Kristofer J. Stewart[1], Douglas R. Pedersen[1,2], John J. Callaghan[1,2], and Thomas D. Brown[1,2]
[1]Department of Orthopaedics and Rehabilitation, University of Iowa, Iowa City, IA, USA; [2]Department of Biomedical Engineering, University of Iowa, Iowa City, IA

 # 130 INFLUENCE OF VASTI ORIENTATION ON THE PATELLAR LIGAMENT FORCE/ QUADRICEPS FORCE RATIO DURING KNEE EXTENSION

Sam Chen[1], Irving Scher[2], Christopher Powers[1], and Thay Lee[3]
[1]Musculoskeletal Biomechanics Research Laboratory, Department of Biokinesiology and Physical Therapy, University of Southern California, Los Angeles, CA, USA; [2]Exponent, Failure Analysis Associates, Los Angeles, CA, USA; [3]Orthopedic Biomechanics Laboratory, Long Beach VA Heathcare System, Long Beach, CA.

 # 131 PATELLOFEMORAL LESIONS INCREASE PRESSURE APPLIED TO SURROUNDING CARTILAGE

John J. Elias[1], Derek R. Bratton[1], David M. Weinstein[1], Andrew J. Cosgarea[2]
[1]Medical Education and Research Institute of Colorado, Colorado Springs, CO; [2]Department of Orthopaedic Surgery, Johns Hopkins University, Baltimore, MD.

 # 132 IN VIVO QUANTIFICATION OF ACHILLES TENDON DYNAMIC CREEP

Russell Dunning, B.S. and David A. Hawkins, Ph.D.
Human Performance Laboratory, Biomedical Engineering Graduate Group University of California, Davis

133 NON-LINEAR, VISCOELASTIC PROPERTIES OF THE HUMAN LUMBAR FACET JOINT CAPSULE

Jesse S. Little[1] and Partap S. Khalsa[1]
[1]Dept. of Biomedical Engineering, State University of New York at Stony Brook, Stony Brook, NY USA

134 HUMAN LUMBAR FACET JOINT CAPSULE STRAINS DURING AXIAL ROTATIONS

Allyson Ianuzzi[1] and Partap S. Khalsa[1]
[1]Dept. of Biomedical Engineering, Stony Brook University, Stony Brook, NY, USA

135 POSTERIOR CRUCIATE LIGAMENT RESPONSE TO PROXIMAL TIBIA IMPACTS

Adam J. Bartsch[1,2], Alan S. Litsky[1,3,4], Joseph R. Leith[4], Rod G. Herriott[1,5] and Joseph D. McFadden[1,6]
[1]Biotrauma Laboratory; [2]Department of Mechanical Engineering; [3]Biomedical Engineering Center and [4]Department of Orthopaedics, The Ohio State University, Columbus, OH, USA; [5]Transportation Research Center, East Liberty, OH, USA; [6]National Highway Traffic Safety Administration, East Liberty, OH, USA.

136 MICROMOTION OF MULTI-STRAND FREE TENDON GRAFTS SECURED WITH INTERFERENCE FIXATION

Douglas J. Adams, Matthew W. Wheeler, and Carl W. Nissen
Department of Orthopaedic Surgery, University of Connecticut Health Center, Farmington, CT

137 QUANTITATIVE PREDICTION OF ARTICULAR CARTILAGE DEGENERATION FOLLOWING INCONGRUOUS INTRA-ARTICULAR FRACTURE REDUCTION

Yang Dai[2], Thomas D. Brown[1, 2], J. Lawrence Marsh[1]
[1]Department of Orthopaedics and Rehabilitation, University of Iowa, Iowa City, IA, USA; [2] Department of Biomedical Engineering, University of Iowa, Iowa City, IA.

Lower Extremity

138 THE EFFECTS OF ADDED LEG MASS ON THE BIOMECHANICS AND ENERGETICS OF WALKING

Raymond C. Browning[1], Jesse Modica[1], Rodger Kram[1] and Ambarish Goswami[2]
[1]Locomotion Laboratory, Department of Integrative Physiology, University of Colorado, Boulder, CO, USA. [2]Honda Research and Development, San Jose, CA.

139 DOES SUSTAINING A LOWER EXTREMITY STRESS FRACTURE ALTER LOWER EXTREMITY MECHANICS IN RUNNERS?

Clare E. Milner[1], Irene S. Davis[1,2] and Joseph Hamill[3]
[1]Department of Physical Therapy, University of Delaware, Newark, DE, USA; [2]Joyner Sportsmedicine Institute, Lexington, KY, USA; [3]Department of Exercise Science, University of Massachusetts, Amherst, MA, USA.

140 CORONAL KNEE MOTION IN CHILDREN PERFORMING DROP LANDINGS IS NOT INFLUENCED BY GENDER

Jeremy J. Bauer, Michael J. Pavol, Wilson C. Hayes, Christine M. Snow
Bone Research Laboratory and Biomechanics Laboratory, Dept. of Exercise & Sport Science, Oregon State University, Corvallis, OR, USA.

141 CHARACTERIZING KINEMATICS OF 3-D HUMAN MOVEMENTS USING QUATERNIONS

Laurie Held[1], Jill L. McNitt-Gray [1,2,3], and Henryk Flashner[3,4]
Biomechanics Research Lab, Departments of Biomedical Engineering[1]; Kinesiology[2]; Biological Sciences[3], and Aerospace and Mechanical Engineering[4] University of Southern California, Los Angeles, CA.

142 CLASSIFICATION TREE ANALYSIS OF FOOT TYPES USING 3-D MEASURES

Eric S. Rohr[1], William R. Ledoux[1,2,3], Jane B. Shofer[1], Randal P. Ching[1,2,3], and Bruce J. Sangeorzan[1,2]
[1]RR&D Center of Excellence for Limb Loss Prevention and Prosthetic Engineering, VA Puget Sound Health Care System, Seattle, WA; Departments of [2]Orthopaedics and Sports Medicine and [3]Mechanical Engineering, University of Washington, Seattle, WA.

143 THE INFLUENCE OF DIFFERENT MIDSOLE HARDNESS ON KNEE JOINT LOADS DURING RUNNING

Katja J. Michel[1,2] Frank I. Kleindienst[1] Alex Stacoff[2] Berthold Krabbe[1] and Edgar Stüssi[2]
[1]Biomechanical Lab, adidas Innovation Team, adidas-Salomon AG, Scheinfeld, Germany; [2]Biomechanical Laboratory, Department of Materials, Swiss Federal Institute of Technology, Zürich, Switzerland.

 # 144 EFFECT OF DYNAMIC ANKLE JOINT STIFFNESS ON JOINT MECHANICS DURING GAIT

Prism S. Schneider[1], James M. Wakeling[2] and Ronald F. Zernicke[1]
[1]Human Performance Laboratory, University of Calgary, Calgary, Canada; [2]Department of Basic Veterinary Sciences, Royal Veterinary College, London, UK

 # 145 DIFFERENCES IN FRONTAL PLANE MECHANICS DURING WALKING BETWEEN PATIENTS WITH MEDIAL AND LATERAL KNEE OSTEOARTHRITIS

Robert J. Butler[1], Irene S. Davis[1,2], Todd Royer[3], Stephanie Crenshaw[3] and Emily Mika[1]
[1]Department of Physical Therapy, University of Delaware, Newark, DE, USA; [2]Joyner Sportsmedicine Institute, Harrisburg, PA USA; [3]Department of Health and Exercise Science, University of Delaware, Newark, DE USA.

 # 146 COMPUTATIONAL ASSESSMENT OF CONSTRAINT IN POSTERIOR-STABILIZED TOTAL KNEE REPLACEMENTS

Matthew F. Moran[1,2], Safia Bhimji[5], Joseph Racanelli[5] and Stephen J. Piazza[1,2,3,4]
[1]Center for Locomotion Studies and Departments of [2]Kinesiology, [3]Mechanical Engineering, and [4]Orthopaedics and Rehabilitation, The Pennsylvania State University, University Park, PA; 5Stryker Orthopedics, Mahwah, NJ.

 # 147 DIRECTION-DEPENDENCE OF POLYETHYLENE WEAR FOR METAL COUNTERFACE SCRATCH TRAVERSE

Matthew C. Paul[2,1], Liam Glennon[2,1], Thomas E. Baer[1], Thomas D. Brown[1,2]
[1]Dept. of Orthopaedics and Rehabilitation; [2]Dept. of Biomedical Engineering, Univ. of Iowa

 # 148 MODELING THE EFFECT OF HALLUX LIMITUS ON FIRST RAY PLANTAR PRESSURE DISTRIBUTIONS

Marc Petre[1,2], Ahmet Erdemir[1], Sachin Budhabhatti[1,3] and Peter R. Cavanagh[1]
[1]Dept. of Biomedical Engineering, Cleveland Clinic Foundation, Cleveland, OH, USA; [2]Dept. of Biomedical Engineering, Case Western Reserve University, Cleveland, OH, USA [3]Dept. of Chemical & Biomedical Engineering, Cleveland State University, Cleveland, OH, USA.

 # 149 THE EFFECT OF FOOT TYPE ON PLANTAR PRESSURE

William R. Ledoux[1,2,3], Eric S. Rohr[1], Charles Harp[1,3], Randal P. Ching[1,3], and Bruce J. Sangeorzan[1,2]
[1]RR&D Center of Excellence for Limb Loss Prevention and Prosthetic Engineering, VA Puget Sound Health Care System, Seattle, WA; Departments of [2]Orthopaedics and Sports Medicine and [3]Mechanical Engineering, University of Washington, Seattle, WA.

 # 150 EFFECT OF GENDER ON LANDING STRATEGY IN PREADOLESCENT CHILDREN

Michelle Sabick, Ph.D., Jeanie Sutter, M.S., Ronald Pfeiffer, Ed.D. A.T.C., Kevin Shea, M.D.
Center for Orthopaedic and Biomechanics Research, Boise State University, Boise, Idaho, USA

 # 151 FIXATION STRENGTH EVALUATION OF HIP IMPLANTS UNDER BIAXIAL ROCKING MOTION

Larry W. Ehmke[1], James C. Krieg[1], Daniel C. Fitzpatrick[2], and Michael Bottlang[1]
[1]Biomechanics Laboratory, Legacy Clinical Research & Technology Center, Portland, OR; [2]Orthopedic Healthcare Northwest, Springfield, OR;

 # 152 LOWER EXTREMITY JOINT COUPLING IN RUNNERS WHO DEVELOPED PATELLOFEMORAL PAIN SYNDROME

Tracy A. Dierks[1], Irene S. Davis[1,2], and Joseph Hamill[3]
[1]Department of Physical Therapy, University of Delaware, Newark, DE, USA; [2]Joyner Sportsmedicine Institute, Mechanicsburg, PA, USA; [3]Department of Exercise Science, University of Massachusetts, Amherst, MA, USA.

 # 153 KNEE MOMENTS WHILST CARRYING A LOAD DURING WALKING

Richard Jones[1], Lei Ren[1,2], Jim Richards[1], and David Howard[1,2]
[1]Centre for Rehabilitation and Human Performance Research, University of Salford, UK; [2]School of Computing, Science and Engineering, University of Salford, UK.

 # 154 AGE AND GENDER DIFFERENCES IN ARCH HEIGHT AND ARCH STIFFNESS

Rebecca Avrin Zifchock[1] and Irene Davis[1,2]
[1]Motion Analysis Laboratory, University of Delaware, Newark, DE, USA; [2]Joyner Sportsmedicine Institute, Mechanicsburg, PA, USA.

 # 155 THE ROLE OF SELECT BIARTICULAR MUSCLES DURING SLOPE WALKING

Andrea N. Lay[1], Chris J. Hass[2], Robert J. Gregor[3]
[1]School of Mechanical Engineering, Bioengineering Program, Georgia Tech, Atlanta, GA, USA; [2]Dept of Biobehavioral Sciences, Teachers College, Columbia University, New York, NY, USA; [3]School of Applied Physiology, Georgia Tech, Atlanta, GA, USA.

 # 156 JOINT MECHANICAL CONTRIBUTIONS VARY WITH SQUATTING DEPTHS

Joo-Eun Song[1], and George J. Salem[1]
[1]Musculoskeletal Biomechanics Research Laboratory, Dept. of Physical Therapy and Biokinesiology, University of Southern California, Los Angeles, CA, USA.

 # 157 DYNAMIC CADAVERIC GAIT SIMULATION: STEPS INTO THE FUTURE

Andrew H. Hoskins[1,2], Andrew R. Fauth[1,3], and Neil A. Sharkey[1,3,4]
[1]Center for Locomotion Studies; [2]Dept. of Mechanical and Nuclear Engineering, and [3]Dept. of Kinesiology, Pennsylvania State University, University Park, PA, USA; [4]Dept. of Orthopaedics and Rehabilitation, Pennsylvania State University, Hershey, PA, USA.

 # 158 PLANTAR PRESSURE REDUCTION BY FOOTWEAR: A FINITE ELEMENT MODEL

Sachin Budhabhatti[1,2], Ahmet Erdemir[1], Marc Petre[1,3], and Peter R. Cavanagh[1]
[1]Dept. of Biomedical Engineering, Cleveland Clinic Foundation, Cleveland, OH, USA; [2]Dept. of Chemical & Biomedical Engineering, Cleveland State University, Cleveland, OH, USA; [3]Dept. of Biomedical Engineering, Case Western Reserve University, Cleveland, OH, USA.

 # 159 CHARACTERIZING HOW THE ASSUMED QUADRICEPS FORCE DISTRIBUTION INFLUENCES THE PATELLOFEMORAL PRESSURE DISTRIBUTION

John J. Elias
Medical Education and Research Institute of Colorado, Colorado Springs, CO.

 # 160 COMPARISON OF KNEE JOINT MOMENTS REPORTED IN DIFFERENT SEGMENTAL REFERENCE FRAMES

Kristian M. O'Connor, Sarika K. Monteiro, and Jennifer E. Earl
Department of Human Movement Sciences, University of Wisconsin Milwaukee, WI, USA

 # 161 DYNAMICS AND MULTIJOINT CONTROL DURING SINGLE LEG SQUAT WITH AND WITHOUT ACTIVATION OF ABDOMINAL OBLIQUE MUSCLES

Roongtiwa Vachalathiti[1], Jill L. McNitt-Gray[2,3,4], Witaya Mathiyakom[2,5], Heather Boni[2]
[1]Faculty of Physical Therapy and Applied Movement Science, Mahidol University, Bangkok, Thailand; [2]Departments of Kinesiology, [3]Biomedical Engineering, [4]Biological Sciences, [5]Gerontology, University of Southern California, Los Angeles, CA, USA.

 # 162 QUANTIFICATION OF MUSCULAR CHALLENGE DURING OBSTACLE CROSSING IN THE ELDERLY: EMG vs. JOINT MOMENT

Li-Shan Chou, Heng-Ju Lee, and Michael E. Hahn
Motion Analysis Laboratory, Department of Exercise and Movement Science University of Oregon, Eugene, Oregon, U.S.A.

 # 163 HORIZONTAL IMPULSE GENERATION CHARACTERISTICS DURING THE SPRINT START ARE INFLUENCED BY SHANK SEGMENT CONTROL

Kathleen E. Costa[1] and Jill L. McNitt-Gray[2]
[1]Coaching & Sport Sciences, United States Olympic Committee, Chula Vista, CA; [2]Biomechanics Laboratory, Dept. of Kinesiology, Biomedical Engineering, Biological Sciences University of Southern California, Los Angeles, CA, USA.

 # 164 MODELING THE INFLUENCE OF FLIGHT PHASE CONTROL ON CENTER OF MASS TRAJECTORY AND REACTION FORCES DURING LANDING

J. L. McNitt-Gray[1,2,3], P. S. Requejo[1], H. Flashner[3,4], and L. Held[2]
Biomechanics Research Laboratory Departments of [1]Kinesiology, [2]Biomedical Engineering, [3]Biological Sciences, and [4]Aerospace and Mechanical Engineering University of Southern California, Los Angeles, CA 90089, USA.

 # 165 DAILY ACTIVITY PROFILE OF TOTAL KNEE REPLACEMENT PATIENTS

William Nechtow[1,2], Thorsten Schwenke[1], Kirsten Moisio[1], and Markus Wimmer[1,2]
[1]Department of Orthopedic Surgery, RUSH University Medical Center Chicago, IL, USA; [2]Department of Bioengineering, University of Illinois at Chicago, Chicago, IL, USA

 # 166 FACTORS PRODUCING A "SOFT" LANDING IN TERMS OF BOTH FORCE AND SOUND

Sara C. Novotny and Richard N. Hinrichs
Department of Kinesiology, Arizona State University, Tempe, AZ, USA.

 # 167 ANTERIOR CRUCIATE LIGAMENT INJURY AND PATELLAR LIGAMENT INSERTION ANGLE

Choongsoo S. Shin[1], Chris O. Dyrby[1], Brenna K. Hearn[1], Ajit M. Chaudhari[1], and Thomas P. Andriacchi[1,2]
[1]Department of Mechanical Engineering, Stanford University, Stanford, CA, USA; [2]Veterans Administration Palo Alto RR&D Center, Palo Alto, CA,

 # 168 ANKLE BIOMECHANICS DURING A SPIN TURN

Ava D. Segal[1,2], Michael S. Orendurff[1], Kevin C. Flick[1], Jocelyn S. Berge[1], Glenn K. Klute[1,2]
[1]Rehab. Research and Development Center, Department of Veteran Affairs, Seattle, WA USA; [2]Dept. of Mechanical Engineering, University of Washington, Seattle, WA USA.

 # 169 EFFECT OF INTERNAL AND EXTERNAL KNEE ROTATION ON HOOP STRAIN IN THE MEDIAL MENISCUS

Kurt Bormann[1], Oliver Kessler[2], Savas E. Lacatusu[3], Tanja Augustin[3], Mark B. Sommers[3], and Michael Bottlang[3]
[1]University of Iowa, Iowa City, IA, USA; [2]Stryker Europe, Thalwil, Switzerland; [3]Legacy Biomechanics Laboratory, Portland, OR, USA,

 # 170 EFFECT OF POSITIVE POSTERIOR HEEL FLARE ON LOWER EXTREMITY KINEMATICS DURING RUNNING GAIT

Robin M. Queen[1,4] Michael T. Gross[2,4] and Bing Yu[1,2,3,4]
[1]Department of Biomedical Engineering, [2]Division of Physical Therapy, [3]Department of Orthopedics, [4]Center for Human Movement Science, The University of North Carolina at Chapel Hill, Chapel Hill, NC, USA.

 # 171 EFFECTS OF AGE GROUP ON LANDING MECHANICS IN THE ADOLESCENT FEMALE BASKETBALL PLAYER

Thomas Kernozek[1], Hanni Cowley[1], and David Carney[1]
[1]Biomechanics Laboratory, Department of Health Professions, University of Wisconsin–La Crosse, La Crosse, WI, USA.

 # 172 OBJECTIVE QUANTIFICATION OF FOOT ARCH BY CURVATURE MAPS

Xiang Liu[1], Wangdo Kim[1] and Burkhard Drerup[2]
[1]School of Mechanical & Production Engineering, Nanyang Technological University, Singapore
[2]Klinik und Poliklinik für Technische Orthopädie und Rehabilitation, Universtätsklinikum, Münster, Germany.

 # 173 EFFECTIVENESS OF TWO KNEE BRACES ON MEDIAL COMPARTMENT OSTEOARTHRITIS

Richard Jones[1], Jim Richards[1], and Jordi Sanchez-Ballester[2]
[1]Centre for Rehabilitation and Human Performance Research, University of Salford, UK; [2]Specialist Registrar Orthopaedics, Stepping Hill Hospital, Stockport, UK.

 # 174 A PARAMETRIC FINITE ELEMENT STUDY OF CONSTRAINED ACETABULAR LINERS

Suzanne M. Bouchard[2], Kristofer J. Stewart[1], Douglas R. Pedersen[1], John J. Callaghan[1], Thomas D. Brown[1,2]
[1]Department of Orthopaedics and Rehabilitation, University of Iowa, Iowa City, IA, USA; [2]Department of Biomedical Engineering, University of Iowa, Iowa City, IA.

 # 175 DROP LANDING EXERCISE DOES NOT INCREASE MAXIMUM JUMP HEIGHT IN CHILDREN

Allison T. Lulay, Jeremy J. Bauer, Christine M. Snow, and Michael J. Pavol
Department of Exercise and Sport Science, Oregon State University, Corvallis, OR, USA

 # 176 CLINICAL QUANTIFICATION OF FRONTAL PLANE KNEE ANGLE: CORRELATION OF 2D AND 3D MOTION ANALYSIS

John D. Willson[1] and Irene Davis[1,2]
[1]Department of Physical Therapy, University of Delaware, Newark, DE, USA; [2]Joyner Sportsmedicine Institute, Mechanicsburg, PA, USA.

 # 177 THE ROLE OF THE VASTUS MEDIALIS AND VASTUS LATERALIS IN MEDIAL-LATERAL KNEE JOINT STABILITY

Alex E. Albertini[1] and Yasin Y. Dhaher[2]
[1]Biomedical Engineering, Northwestern University, Evanston, IL, USA; [2]Sensory Motor Performance Program, Rehabilitation Institute of Chicago, Chicago, IL, USA.

 # 178 INITIAL HORIZONTAL MOMENTUM ALTERS CONTROL OF THE REACTION FORCE RELATIVE TO THE CENTER OF MASS

Witaya Mathiyakom[1,5], Jill McNitt-Gray[1,2,3] and Rand Wilcox[4]
Departments of [1]Kinesiology, [2]Biomedical Engineering, [3]Biological Sciences, [4]Psychology, and [5]Gerontology University of Southern California, Los Angeles, CA.

 # 179 A DYNAMIC MODEL FOR ASSESSMENT OF MICROMOTION AND MIGRATION IN KNEE ARTHROPLASTIES

Marcus Mohr[1], Mark B. Sommers[1], Patrick Dawson[2], Scott Steffensmeier[3], and Michael Bottlang[1]
[1]Biomechanics Laboratory, Legacy Research & Technology Center, Portland, OR; [2]Oregon Health & Science University, Portland, OR; [3]Zimmer, Inc., Warsaw, IN.

 # 180 PROBLEMATIC SITES OF THIRD BODY EMBEDMENT IN POLYETHYLENE FOR WEAR ACCELERATION IN TOTAL HIP ARTHROPLASTY

Hannah J. Lundberg[2], Kristofer J. Stewart[1], Douglas R. Pedersen[1], Thomas D. Brown[1,2]
[1]Department of Orthopaedics and Rehabilitation, University of Iowa, Iowa City, IA, USA; [2]Department of Biomedical Engineering, University of Iowa, Iowa City, IA.

Upper Extremity

 # 181 REALISTIC TESTING OF RIOT HELMET PROTECTION AGAINST PROJECTILES

Cathie L. Kessler, Jean-Philippe Dionne, Doug Bueley, Aris Makris
Med-Eng Systems Inc., Ottawa, Ontario, Canada.

 # 182 VARIATION IN MUSCLE MOMENT ARMS WITH INDEX FINGER POSTURE

Derek G. Kamper[1,2,] Erik Cruz[2], Heidi Waldinger[2]
[1]Department of Physical Medicine and Rehabilitation, Northwestern University Feinberg School of Medicine, Chicago, IL, USA; [2]Sensory Motor Performance Program, Rehabilitation Institute of Chicago, Chicago, IL, USA

 # 183 A MUSCULOSKELETAL MODEL OF THE UPPER EXTREMITY FOR SURGICAL SIMULATION AND NEUROCONTROL APPLICATIONS

Katherine R. S. Holzbaur, MS[1], Wendy M. Murray, PhD[2], Scott L. Delp, PhD[1,2,3]
[1]Mechanical Engineering Department, Stanford University, Stanford, CA; [2]VA Palo Alto HCS Bone and Joint Center, Palo Alto, CA; [3]Bioengineering Department, Stanford University, Stanford, CA.

 # 184 CONTROL OF FINGER FORCE VECTOR IN THE FLEXION-EXTENSION PLANE

Fan Gao[1], Vladimir M. Zatsiorsky[1] and Mark L. Latash[2]
[1]Biomechanics Laboratory, Department of Kinesiology, the Pennsylvania State University, UP, State College, PA, USA [2]Motor Control Laboratory, Department of Kinesiology, the Pennsylvania State University, UP, State College, PA, USA.

 # 185 MEASUREMENT FORCES DURING MANIPULATION IN NON-HUMAN PRIMATES

Warren G. Darling[1], James Herrick[2], David McNeal[2], Kimberly Stilwell-Morecraft[2], Robert J. Morecraft[2]
[1]Department of Exercise Science, The University of Iowa, Iowa City, IA 52242; [2]Division of Basic Biomedical Sciences, The University of South Dakota, Vermillion, SD 57069.

 # 186 THE EFFECT OF HAND POSITION ON GROUND REACTION FORCES WHEN FALLING FORWARD FROM KNEELING HEIGHT

Courtney D. Gavin[1], Karen L. Troy[1], and Mark D. Grabiner[1]
[1]Musculoskeletal Biomechanics Laboratory, University of Illinois at Chicago, Chicago, IL USA.

 # 187 WHAT EFFECT DOES THE FLEXOR CARPI RADIALIS HAVE ON SCAPHOID MOTION?

Kristin D. Zhao; Jinrok Oh, MD; Steven L. Moran, MD; Maile Ceridon; Ronald L. Linscheid, MD; Kai-Nan An, PhD
Biomechanics Laboratory, Department of Orthopedic Research, Mayo Clinic, Rochester, Minnesota, USA

 # 188 THUMB KINEMATICS WITH NON-ORTHOGONAL AND NON-INTERSECTING AXES OF ROTATION MAY BE NECESSARY TO PREDICT REALISTIC ISOMETRIC THUMBTIP FORCES IN MULTIPLE DIRECTIONS

Veronica J. Santos[1] and Francisco J. Valero-Cuevas[1,2]
[1]Neuromuscular Biomechanics Laboratory, Cornell University, Ithaca, NY, U.S.A.; [2]The Hospital for Special Surgery, New York, NY, USA

 # 189 FINGER COORDINATION DURING MOMENT PRODUCTION ON A MECHANICALLY FIXED OBJECT

Jae Kun Shim[1,2] Mark L. Latash[2] and Vladimir M. Zatsiorsky[2]
[1]Biomechanics Laboratory and [2]Motor Control Laboratory, Department of Kinesiology, The Pennsylvania State University, State College, PA, USA.

 # 190 A CONCENTRIC AND ECCENTRIC LOADING REGIME FOR SHOULDER REHABILITATION

Karen P. Norton[1] and Sean S. Kohles[2]
[1]U.S. Army Natick Soldier Center, Natick, MA; [2]Kohles Bioengineering, Portland State University, and Oregon Health & Science University, Portland, OR.

 # 191 INTERNAL AND EXTERNAL ROTATION OF THE SHOULDER: EFFECTS OF PLANE, END RANGE DETERMINATION, AND SCAPULAR MOTION

Sean P. McCully[1], Naveen Kumar[2], Mark D. Lazarus[3], and Andrew R. Karduna[1]
[1]Orthopaedic Biomechanics Laboratory, Department of Exercise and Movement Science, University of Oregon, Eugene, OR, USA; [2]Drexel University School of Medicine, Philadelphia, PA, USA [3]Department of Orthopaedic Surgery, Thomas Jefferson University, Philadelphia, PA, USA.

 # 192 CARPAL TUNNEL SYNDROME AFFECTS FINGER FORCE PRODUCTION

Shouchen Dun, Robert J. Goitz, Zong-Ming Li
Hand Research Laboratory, Departments of Orthopaedic Surgery and Bioengineering University of Pittsburgh, Pittsburgh, PA, USA.

 # 193 A ROBOT-ASSISTED MEASURE OF FINGER JOINT STIFFNESS

Gregg Davis, Shouchen Dun, and Zong-Ming Li
Hand Research Laboratory, Departments of Orthopaedic Surgery and Bioengineering University of Pittsburgh, PA, USA.

 # 194 THE EFFECT OF PECTORALIS MINOR RESTING LENGTH VARIABILITY ON SCAPULAR KINEMATICS

John D. Borstad[1] and Paul M. Ludewig[2]
[1]Physical Therapy Division, The Ohio State University, Columbus, OH, USA. [2]Department of Physical Therapy, University of Minnesota, Minneapolis, MN, USA

 # 195 FLUOROSCOPIC ASSESSMENT OF THE EFFECTS OF ROTATOR CUFF FATIGUE ON GLENOHUMERAL KINEMATICS IN SHOULDER IMPINGEMENT SYNDROME

Philip J. Royer[1], Edward J. Kane[1], Kyle E. Parks[1], Jacob C. Morrow[1], Richard R. Moravec[1], Douglas S. Christie[1], Deydre S. Teyhen[1,2]
[1]Physical Therapy Research Center, U.S. Army-Baylor University Graduate Program in Physical Therapy, Fort Sam Houston, TX, USA; [2]Department of Kinesiology & Health Education, The University of Texas, Austin, TX, USA.

 # 196 RELIABILITY OF A KINEMATIC MODEL OF THE UPPER EXTREMITY

Kristof Kipp, B.S., Michelle Sabick, Ph.D., Mark DeBeliso, Ph.D.
Center for Orthopedic and Biomechanics Research, Boise State University, Boise, Idaho, USA

 # 197 QUANTIFICATION OF UPPER EXTREMITY MOTION DURING A TRIP-INDUCED FALL IN OLDER ADULTS

Courtney D. Gavin[1], Karen L. Troy[1], and Mark D. Grabiner[1]
[1]Musculoskeletal Biomechanics Laboratory, University of Illinois at Chicago, Chicago, IL USA

 # 198 WRIST POSITION INFLUENCES RANGE OF MOTION

Laurel Kuxhaus[1], Jesse A. Fisk[2], Thomas H. Christophel[1], and Zong-Ming Li[1]
[1]Hand Research Laboratory, Departments of Orthopaedic Surgery and Bioengineering;
[2]Musculoskeletal Research Center, Department of Bioengineering, University of Pittsburgh, Pittsburgh, PA, USA.

 # 199 DIRECTIONAL FORCE CONTROL OF THE THUMB

Laurel Kuxhaus, Daniel A. Harkness, and Zong-Ming Li
Hand Research Laboratory, Departments of Orthopaedic Surgery and Bioengineering University of Pittsburgh, Pittsburgh, PA, USA.

 # 200 RELATIVE TIMING OF MUSCLE FATIGUE AND COORDINATION CHANGES DURING REPETITIVE DUMBBELL LIFTING

Kyle R. Voge, B.S. and Jonathan B. Dingwell, Ph.D.
Nonlinear Biodynamics Lab, Dept. of Kinesiology, University of Texas, Austin, TX, USA

 # 201 UPPER EXTREMITY JOINT STRESSES ASSOCIATED WITH WALKER-ASSISTED AMBULATION IN POST-SURGICAL PATIENTS

Margaret A. Finley[1,2] and Kevin J. McQuade[1,2]
[1] Rehabilitation Research and Development Service, Baltimore Veterans Administration Medical Center, Baltimore, MD, USA; [2] University of Maryland School of Medicine, Dept of Physical Therapy and Rehabilitation Science, Baltimore, MD, USA

 # 202 EFFECT OF WEARING A WRIST SPLINT ON SHOULDER POSTURE WHEN PICKING AN OBJECT FROM A BOX

Amy G. Mell and Richard E. Hughes
Department of Orthopaedic Surgery, University of Michigan, Ann Arbor, MI USA.

 # 203 IS THE THUMB A FIFTH FINGER?

Halla Bjorg Olafsdottir[1], Mark L. Latash[1], and Vladimir M. Zatsisorsky[2]
[1]Motor Control Laboratory and [2]Biomechanics Laboratory, Department of Kinesiology, The Pennsylvania State University, State College, PA.

Spine

 # 204 POSITIONAL STABILITY TESTING OF A PROSTHETIC DISC NUCLEUS DEVICE

Joseph E. Hale[1], Britt K. Norton[1], Laura J. Bauer[1], Sara E. Ross[1], and William C. Hutton[2]
[1]Raymedica, Inc., Minneapolis, MN; [2]Department of Orthopaedics, Emory University School of Medicine, Atlanta, GA.

 # 205 SPINAL INSTABILITY DUE TO SIMULATED FRONTAL IMPACTS

Adam M. Pearson, Manohar M. Panjabi, Paul C. Ivancic, Shigeki Ito, Bryan W. Cunningham, Wolfgang Rubin, S. Elena Gimenez
Biomechanics Research Laboratory, Yale University School of Medicine, New Haven, CT, USA

 # 206 BIOMECHANICAL RESPONSE OF ENTIRE LUMBAR SPINE TO LARGE COMPRESSION –A FINITE ELEMENT MODEL STUDY

Tim Brown[1], Raghu N. Natarajan[2] and Gunnar B.J. Andersson[2]
[1]Bioengineering Department, University of Illinois at Chicago, Chicago, IL, USA; [2]Department of Orthopedic Surgery, Rush University Medical Center, Chicago, IL.

 # 207 OCCUPATIONAL VIBRATION AND POSITION SENSE

Sara E. Wilson and Feng Zhang[1]
[1] Human Motion Control Laboratory, Mechanical Engineering, University of Kansas, Lawrence, KS, USA

 # 208 EFFECT OF LOADING RATE ON COMPRESSIVE FAILURE MECHANICS OF THE PEDIATRIC CERVICAL SPINE

Paul Z. Elias, David J. Nuckley, and Randal P. Ching
Applied Biomechanics Laboratory, Dept. of Mechanical Engineering, University of Washington, Seattle, WA, USA.

 # 209 ANALYSIS OF THE 360 DEGREE MOTION ENVELOPE OF HUMAN LUMBOSACRAL JOINTS

Wafa Tawackoli and Michael A.K. Liebschner
Department of Bioengineering, Rice University, Houston, TX, USA.

 # 210 DIGITAL FLUOROSCOPIC VIDEO ASSESSMENT OF SAGITTAL PLANE LUMBAR SPINE FLEXION

Deydre S. Teyhen[1,2] Lawrence D. Abraham[1] and Timothy W. Flynn[3]
[1]Department of Kinesiology & Health Education, The University of Texas, Austin, TX, USA; [2]U.S. Army-Baylor Graduate Program in Physical Therapy, Fort Sam Houston, TX, USA; [3]Department of Physical Therapy, Regis University, Denver, Colorado, USA.

 # 211 STABILIZATION OF INTERVERTEBRAL DISCS BY TISSUE ENGINEERED NUCLEUS REPLACEMENT: A BIOMECHANICAL FEASIBILITY STUDY

Frank Heuer, Cornelia Neidlinger-Wilke, Lutz Claes and Hans-Joachim Wilke
Institute of Orthopaedic Research and Biomechanics University of Ulm, Germany.

 # 212 IN VITRO BIOMECHANICS OF LUMBAR DISC ARTHROPLASTY WITH THE PRODISC TOTAL DISC IMPLANT

Denis J. DiAngelo[ab], Kevin T. Foley[ba], Brian Morrow[a], Jung Song[a], and Tom Mroz[b]
[a]Department of Biomedical Engineering, The University of Tennessee, Memphis, TN; [b]Department of Neurosurgery, The University of Tennessee, Memphis, TN.

 # 213 FINITE ELEMENT ANALYSIS OF HUMAN FACET JOINT CAPSULE DURING PHYSIOLOGICAL MOTIONS FOR TWO LUMBAR MOTION SEGMENTS

Anita C. Saldanha[1], Yi-Xian Qin[1], Vijay K. Goel[2], Partap S. Khalsa[1]
[1]Biomedical Engineering Department, Stony Brook University, Stony Brook, NY, 11794 USA; Bioengineering Department, University of Toledo, Toledo, OH, USA.

 # 214 STRUCTURAL BEHAVIOUR OF THORACIC SPINAL UNIT; THE ROLE OF THE POSTERIOR ARTICULAR FACETS IN SPINAL DEFORMITY

Behnam Heidari[1], David FitzPatrick[1], Keith Synnott[2] and Damien McCormack[2]
[1]Department of Mechanical Engineering, University College Dublin, Dublin, Ireland; [2]Spinal Unit Research Group (SURG), National

 # 215 CERVICAL SPINE TOLERANCE TO DYNAMIC TENSILE LOADING

Eno M. Yliniemi[1], Joseph A. Pellettiere[2], Erica J. Doczy[3], David J. Nuckley[1], and Randal P. Ching[1]
[1]Applied Biomechanics Laboratory, Department of Mechanical Engineering, University of Washington, Seattle, WA, USA; [2]Biomechanics Branch, Air Force Research Laboratory, Wright-Patterson AFB, Dayton, OH, USA; [3]General Dynamics, Dayton, OH, USA.

 # 216 CAN A PENDULUM BE USED TO STUDY DYNAMIC PROPERTIES OF THE SPINE?

Lindsey Fujita[1], Joseph J. Crisco[1,2], David B. Spenciner[2]
[1]Department of Orthopaedics, Brown Medical School and Rhode Island Hospital, Providence, RI; [2]Division of Engineering, Brown University, Providence, RI.

 # 217 AN ERGONOMICS INTERVENTION WITH CONSTRUCTION CONCRETE LABORERS TO DECREASE LOW BACK INJURY RISK

Jennifer A Hess[1] Steven Hecker[1] Marc Weinstein[2] and Mindy Lunger[3]
[1]Labor Education and Research Center, University of Oregon; [2]Lillis Business College, University of Oregon; [3]Student Health Center, University of Oregon.

 # 218 COMPARISON OF THE PASSIVE STABILIZATION PROVIDED TO THE HUMAN CERVICAL SPINE BY THREE DIFFERENT CERVICAL BRACES

Karthik Balasubramanian[1], Naomi Hawkins[1], Sorin Siegler[1]
[1]Biomechanics Laboratory, Drexel University, Philadelphia, PA, USA.

 # 219 COMPRESSIVE STRENGTH EVALUATION OF OSTEOPOROSIS VERTEBRA BY FINITE-ELEMENT ANALYSIS BASED ON PATIENT-SPECIFIC MODELS

Jiro Sakamoto[1], Yasuhide Kanazawa[1], Daisuke Tawara[1], Juhachi Oda[1], Serina Awamori[2], Hideki Murkami[2], Norio Kawahara[2], and Katsuro Tomita[2]
[1]Graduate School of Natural Science, Kanazawa University, Ishikawa, JAPAN; [2]Graduate School of Medical Science, Kanazawa University, Ishikawa, JAPAN.

 # 220 EFFICACY AND KINEMATIC CHARACTERISTICS OF TWO NEW CERVICAL ORTHOSES

Songning Zhang[1], Michael Wortley[1], Kurt Clowers[1] and John H. Krusenklaus[2]
[1]Biomechanics/Sports Medicine Laboratory, The University of Tennessee, Knoxville, TN, USA; [2]Tennessee Sports Medicine Group, Knoxville, TN, USA.

 # 221 A VIRTUAL MODEL OF THE HUMAN CERVICAL SPINE FOR PHYSICS-BASED SIMULATION

Hyung S. Ahn and Denis J. DiAngelo
Department of Biomedical Engineering, The University of Tennessee Health Science Center, Memphis, Tennessee, USA.

 # 222 DYNAMIC FIXATION SYSTEMS COMPARED TO THE RIGID SPINAL INSTRUMENTATION-A FINITE ELEMENT INVESTIGATION

Sri Lakshmi Vishnubhotla[1], Vijay K. Goel[1], Sasidhar Vadapalli[1], Akiyoshi Masuda[1], Ashutosh Khandha[1], Miranda N. Shaw[1], Jared Walkenhorst[2], Larry Boyd[3]
[1]Spine Research Center, University of Toledo, and Medical College of Ohio, Toledo, OH; [2]Spine Wave Inc., CT;[3]Department of Biomedical Engineering, Duke University, Durham, NC.

 # 223 THE THREE-DIMENSIONAL LUMBAR SPINE KINEMATICS OF TRANSFEMORAL AMPUTEES WITH AND WITHOUT BACK PAIN WHILE WALKING

Joseph M. Czerniecki[1,2], Ava D. Segal[1], Ali Shakir[3], Michael S. Orendurff[1]
[1]Rehab Research and Development, Department of Veterans Affairs, Seattle, WA USA; [2]Dept. of Rehabilitation Medicine, University of Washington, Seattle, WA USA; [3]Buffalo Spine and Sports Medicine, PC, Buffalo, NY USA.

 # 224 BIOMECHANICAL EXAMINATION OF INTERVERTEBRAL DISCS SUBSEQUENT TO BURST FRACTURE

Suneil R. Ramchandani[1], Manohar M. Panjabi[1], Peter A. Cripton[1], and Tyler J. VanderWeele[2]
[1]Biomechanics Research Laboratory, Yale Univ. School of Medicine, New Haven, CT, USA; [2]Department of Biostatistics, Harvard School of Public Health, Boston, MA, USA.

 # 225 TRUNK MUSCLE ACTIVATION PATTERNS IN INDIVIDUALS WITH DEGENERATIVE DISC DISEASE: A COMPARISON OF SUBJECTS WITH AND WITHOUT LOW BACK PAIN

Sheri P. Silfies[1] and Andrew Karduna[2]
[1]Rehabilitation Sciences Biomechanics Laboratory, Drexel University, Philadelphia, PA, USA; [2]Department of Exercise and Movement Science, University of Oregon, Eugene, OR, USA.

 # 226 EVALUATION OF 3D RECONSTRUCTION OF THE RIB CAGE FROM BIPLANAR RADIOGRAPHY

David Mitton[1], Maxime Chauvet[1,2], Sébastien Laporte[1], Chao Yang[2], Samuel Bertrand[1], Kristin Zhao[2], Chunfeng Zhao[2], Kai-Nan. An[2] and Wafa Skalli[1]
[1]Laboratory of Biomechanics ENSAM-CNRS UMR 8005, Paris, FRANCE; [2]Biomechanics Laboratory, MAYO Clinic, Rochester, MN, USA.

Methods

 # 227 A MULITIVARIATE LOGISTICAL MODEL DESCRIBING COMPRESSIVE SENSITIVITY OF TACTILE RECEPTORS

Sean S. Kohles[1], Sam Bradshaw[2], and Fred J. Looft[3]
[1]Kohles Bioengineering, Portland State University, and Oregon Health & Science University, Portland, OR;
[2]Azul Systems, Inc., Sacramento, CA; [3]Department of Electrical & Computer Engineering, Worcester Polytechnic Institute, Worcester, MA.

 # 228 COMPUTATIONAL SIMULATION OF CORNEAL APPLANATION

T.-H. Kwon[1], D. A. Pecknold[1], J. Ghaboussi[1], S. Sayegh[2], and Y. M. Hashash[1]
[1]Dept. of Civil and Env. Engineering, Univ. of Illinois at Urbana-Champaign, IL 61801; [2]Medical Director, The EYE Center, Champaign, IL 61820.

 # 229 TIME-EVENT CROSS CORRELATION: A NEW TECHNIQUE FOR TIME SERIES COMPARISON APPLIED TO SHOULDER JOINT KINETICS DURING WALKER ASSISTED AMBULATION

Liu Wei[1] and McQuade Kevin[2]
[1]Department of Physical Therapy and Rehabilitation Science, School of Medicine, University of Maryland, USA.
[2]Biomechanics Laboratory, Rehabilitation Research and Development Service, Baltimore Veterans Administration Medical Center, USA.

 # 230 FACTORS AFFECTING THE ACCURACY OF 2D-DLT CALIBRATION

Scott P. McLean[1], Peter F. Vint[2], Richard N. Hinrichs[3], John K. DeWitt[4], Bryan Morrison[3], and Jason Mitchell[1]
[1]Biomechanics Laboratory, Kinesiology Dept., Southwestern University, Georgetown, TX, USA; [2]Research Integrations, Inc., Tempe, AZ, USA; [3]Biomechanics Laboratory, Kinesiology Dept., Arizona State University, Tempe, AZ, USA; [4]Exercise Physiology Laboratory, NASA-Johnson Space Center, Houston, TX, USA.

 # 231 EFFECT OF VARIATIONS IN CORNEA CHARACTERISTICS ON MEASURED INTRAOCULAR PRESSURE

T.-H. Kwon[1], D. A. Pecknold[1], and J. Ghaboussi[1]
[1]Dept. of Civil and Env. Engrg., Univ. of Illinois at Urbana-Champaign, IL 61801.

 # 232 PREDICTING OUT-OF-PLANE POINT LOCATIONS USING THE 2D-DLT

Richard N. Hinrichs[1], Bryan Morrison[1], Peter F. Vint[2], John K. DeWitt[3], Jason Mitchell[4] and Scott P. McLean[4]
[1]Biomechanics Laboratory, Kinesiology Dept., Arizona State University, Tempe, AZ, USA [2]Research Integrations, Inc., Tempe, AZ, USA; [3]Exercise Physiology Laboratory, NASA-Johnson Space Center, Houston, TX, USA; [4]Biomechanics Laboratory, Kinesiology Dept., Southwestern University, Georgetown, TX, USA.

 # 233 LARGE DEFORMATION AND FLUID MODELING IN THE ANTERIOR CHAMBER IN IMPACTS TO THE HUMAN EYE

Joel Stitzel[1] Stefan Duma[1] and Joseph Cormier[2]
[1]Virginia Tech - Wake Forest University Center for Injury Biomechanics USA; [2]Biodynamics Research Corporation, USA.

 # 234 RELIABILITY OF A TECHNIQUE FOR DETERMINING SAGITTAL KNEE GEOMETRY FROM LATERAL KNEE RADIOGRAPHS

John W. Chow, Soo-An Park, Jeff T. Wight and Mark D. Tillman
Center for Exercise Science, University of Florida, Gainesville, FL, USA.

 # 235 SOFT TISSUE MODELING AND MECHANICS

Amy E. Kerdok[1,2], Simona Socrate[1,3], Robert D. Howe[1,2]
[1]Harvard/MIT Division of Health Sciences and Technology, Cambridge, MA; [2]Biorobotics Laboratory, Harvard University Division of Engineering and Applied Sciences, Cambridge, MA; [3] Massachusetts Institute of Technology Dept. of Mechanical Engineering, Cambridge, MA.

 # 236 QUANTITATIVE SHEAR WAVE MAGNETIC RESONANCE ELASTOGRAPHY: COMPARISON TO A DYNAMIC SHEAR MATERIAL TEST

Stacie I. Ringleb[1], Qingshan Chen[1], Armando Manduca[2], Richard L. Ehman[2], Kai-Nan An[1]
[1]Orthopedics Biomechanics Laboratory, Mayo Clinic College of Medicine, Rochester, MN; [2]MRI Research Laboratory, Mayo Clinic College of Medicine, Rochester, MN.

 # 237 TIME-LAG RADIOGRAPHIC ASSESSMENT OF BRAIN DISTORTION DURING HEAD IMPACT SIMULATION

Jan F. Schöbel, Mark B. Sommers, and Michael Bottlang
Biomechanics Laboratory, Legacy Research & Technology Center, Portland, OR.

 # 238 LASER SPECKLE MEASUREMENTS FOR SKIN MECHANICS AND DIAGNOSTICS

Sean J. Kirkpatrick
Department of Biomedical Engineering, Oregon Health & Science University, 20000 NW Walker Rd., Beaverton, OR 97006, USA.

 # 239 A NOVEL DEVICE FOR CALIBRATING SHEET ARRAY PRESSURE SENSORS AND FOR MONITORING THEIR PERFORMANCE

Thomas E. Baer[1], Douglas R. Pedersen[1,2], M. James Rudert[1], Nicole A.Vos[2], Nicole M. Grosland[1,2], Thomas D. Brown[1,2]
[1]Department of Orthopaedics and Rehabilitation, [2]Department of Biomedical Engineering, University of Iowa.

 # 240 CAPSTONE DESIGN OF A CRANIAL VASCULAR MECHANICAL MODEL

Ryan Mangan[2], Sean S. Kohles[1], Nedzib Biberic[2], Nick Leech[2], Trenton J. McKinney[3], Edward Stan[3], Mihaela L. Surdu[3], Cathy Biber[2], and James McNames[3]
[1]Kohles Bioengineering, Portland State University, and Oregon Health & Science University, Portland, OR; [2]Department of Mechanical and Materials Engineering, Portland State University, Portland, OR; [3]Department of Electrical and Computer Engineering, Portland State University, Portland, OR.

 # 241 CEREBRAL MECHANICS DURING TRAUMATIC BRAIN INJURY

[1]Binu Oommen[a], David Nicholson[a], Ted Conway[a], Alexandra SchÄonning[b], Irina Ionescu[c]
[a]Mechanical Engineering, University of Central Florida, Orlando, FL, USA; [b]Mechanical Engineering, University of North Florida, Jacksonville, FL, USA; [c]Super Computing Institute, University of Utah, Salt Lake City, UT.

Muscle

 # 242 DYNAMIC TRUNK KINEMATIC STIFFNESS DURING FLEXION AND EXTENSION

P.J. Lee[1], K.M. Moorhouse[2], and K.P. Granata[2]
[1]Musculoskeletal Biomechanics Lab, ME, Virginia Tech, Blacksburg, VA, USA; [2]Musculoskeletal Biomechanics Lab, ESM, Virginia Tech, Blacksburg, VA, USA.

 # 243 MUSCLE CONTRIBUTIONS TO FORWARD PROGRESSION DURING WALKING

May Q. Liu[1], Frank C. Anderson[1], Marcus G. Pandy[3], and Scott L. Delp[1,2]
Departments of [1]Mechanical Engineering and [2]Bioengineering, Stanford University, Stanford, CA, USA; [3]Department of Biomedical Engineering, University of Texas at Austin, Austin, TX, USA.

 # 244 DENSITY AND HYDRATION OF FIXED HUMAN MUSCLE TISSUE

Samuel R. Ward and Richard L. Lieber
Departments of Bioengineering and Orthopaedic Surgery, University of California San Diego and VA Medical Center San Diego, CA, USA.

 # 245 BIOMECHANICAL & MUSCULAR DIFFERENCES IN THREE JUMP CONDITIONS

Jennifer M. Neugebauer and Keith R. Williams
Exercise Science Graduate Group, University of California, Davis, USA.

 # 246 RECTUS FEMORIS FIBER EXCURSIONS PREDICTED BY A 3D MODEL OF MUSCLE

Silvia S. Blemker[1] and Scott L. Delp1,[2]
Departments of [1]Mechanical Engineering and [2]Bioengineering. Stanford University.

 # 247 A BIOMECHANICAL METHOD TO IMPROVE INDIVIDUAL PLANNING AND CONTROLLING OF TRAINING

Markus Tilp, Martin Sust and Sigrid Thaller
Institute of Sport Sciences, Karl-Franzens-University Graz, Austria, Europe.

 # 248 MORPHOLOGY, ARCHITECTURE AND BIOMECHANICS OF HUMAN CERVICAL MULTIFIDUS MUSCLES

Jess S. Anderson[1], Andrew W. Hsu[1], and Anita N. Vasavada[1,2]
[1]Department of Veterinary and Comparative Anatomy, Pharmacology and Physiology; [2]Program in Bioengineering, Washington State University, Pullman, WA USA.

 # 249 SHORTENING AND LENGTHENING FORCE-VELOCITY PROPERTIES OF HUMAN SINGLE MUSCLE FIBERS

David C. Lin[1,2] and Kasey Schertenleib[2]
[1]Programs in Bioengineering and Neuroscience and [2]Dept. of Veterinary and Comparative Anatomy, Pharmacology and Physiology, Washington State Univ., Pullman, WA, USA.

 # 250 MRI-BASED GEOMETRY OF NECK MUSCLES FOR BIOMECHANICAL MODELS

Richard Lasher[1], Travis Meyer[1], Kyle Kraemer[1], Patrick Gavin[2], Anita Vasavada[1]
[1]Program in Bioengineering, [2]Department of Veterinary Clinical Sciences (Radiology) Washington State University, Pullman, WA USA.

 # 251 MUSCLE-TENDON ULTRASOUND: QUANTITATIVE CONSIDERATIONS

Lisa Coughlin and David Hawkins
Human Performance Laboratory, Biomedical Engineering Graduate Group, University of California, Davis, CA USA

 # 252 PASSIVE AND ACTIVE SARCOMERE LENGTH NON-UNIFORMITY IN SKELETAL MUSCLE

Jolene L. Lepp[1], Dilson E. Rassier[1], Gerald H. Pollack[2], Walter Herzog[1]
[1]Human Performance Laboratory, University of Calgary, Calgary, AB, Canada; [2]Dept. of Bioengineering, University of Washington, Seattle, WA,

 # 253 A THREE-DIMENSIONAL MODEL OF VOCAL FOLD ABDUCTION/ADDUCTION

Eric J. Hunter[1] and Ingo R. Titze[1,2]
[1]National Center for Voice and Speech, A division of Denver Center for the Performing Arts, Denver, CO, USA; [2]Department of Speech Pathology and Audiology, The University of Iowa, Iowa City, IA, USA.

 # 254 MUSCLE WEAKNESS AND FORCE SHARING IN THE CAT HINDLIMB

Karyn M.A. Weiss-Bundy[1], Tim R. Leonard[2] and Walter Herzog[2]
[1]Human Performance Laboratory, Dept. of Mechanical Engineering, University of Calgary, Calgary, AB, Canada. [2]Human Performance Laboratory, Dept. of Kinesiology, University of Calgary, Calgary, AB, Canada.

 # 255 SARCOMERE NON-UNIFORMITY ASSOCIATED WITH STABILITY OF SKELETAL MUSCLE MYOFIBRILS

Dilson E. Rassier, Timothy Leonard and Walter Herzog
Human Performance Laboratory, Faculty of Kinesiology University of Calgary (AB), Canada

 # 256 TEMPERATURE DEPENDENCE OF CROSSBRIDGE KINETICS IN SLOW AND FAST SKELETAL MUSCLE FIBERS: CROSSBRIDGE MODELING

Sampath K. Gollapudi[1] and David C. Lin[1,2,3]
[1]Dept. of Mechanical and Materials Engineering; [2]Programs in Bioengineering and Neuroscience; [3]Dept. of Veterinary and Comparative Anatomy, Pharmacology and Physiology, Washington State Univ., Pullman, WA, USA.

 # 257 THUMB FORCE DEFICIT AFTER LOWER MEDIAN NERVE BLOCK

Zong-Ming Li, Daniel A. Harkness, Robert J. Goitz
Hand Research Laboratory, Departments of Orthopaedic Surgery and Bioengineering University of Pittsburgh, PA 15213.

 # 258 KNEE JOINT KINETICS AND LOWER EXTREMITY MUSCLE ACTIVATION DURING FRONT AND BACK SQUATS

Mark D. Tillman, Jon C. Gullett, Gregory M. Gutierrez, and John W. Chow
Center for Exercise Science, University of Florida, Gainesville, Florida.

259 DEVELOPING AND TESTING OF AN EMG DRIVEN MODEL TO ESTIMATE ANKLE MOMENTS AND MUSCLE FORCES

Shay Cohen and Thomas S. Buchanan
Center for Biomedical Engineering Research, University of Delaware, Newark, DE 19716.

260 ANGULAR ACCELERATION OF THE HEAD/NECK SYSTEM INDUCED BY STERNOCLEIDOMASTOID

Prasanna Krithivasan[1] and Anita Vasavada[1,2]
[1]Department of Mechanical and Materials Engineering, [2]Program in Bioengineering Washington State University, Pullman, WA USA.

261 AMPLIFICATION OF MUSCLE FIBER LENGTH CHANGES IN THE HUMAN SOLEUS MUSCLE-TENDON COMPLEX

John A. Hodgson[2], Ron Roiz[1], Taija Finni[4], Hae-Dong Lee[3], V. Reggie Edgerton[2] and Shantanu Sinha[3]
Departments of [1]Cybernetics, [2]Physiological & [3]Radiological Sciences, UCLA, Los Angeles, CA 90095 and [4]Department of Health Sciences, University of Jyväskylä, 40014 Jyväskylän, Finland.

262 MUSCLE FUNCTION IN THE GENERATION OF PROPULSIVE AND BRAKING FORCES DURING RUNNING

Adam R. Gaines[1], Richard N. Hinrichs[1], and Philip E. Martin[2]
[1] Department of Kinesiology, Arizona State University, Tempe, AZ 85287-0404 USA; [2] Department of Kinesiology, The Pennsylvania State University, College Park, PA 16802 USA.

263 STRAIN DISTRIBUTION IN *IN-VIVO* HUMAN TRICEPS SURAE DURING PASSIVE AND ACTIVE DYNAMIC MOVEMENTS

Hae-Dong Lee[1,2], Taija Finni[3], John A. Hodgson[2], V. Reggie Edgerton[2], and Shantanu Sinha[1]
Departments of [1]Radiological and [2]Physiological Sciences, UCLA, CA 90095, USA and [3]Department of Health Sciences, University of Jyväskylä, 40014 Jyväskylän, Finland.

264 EXPERIMENTAL VALIDATION OF A SURFACE EMG MODEL

David A. Gabriel
Raymond Nelson Reid Biomechanics Laboratory, Brock University, St. Catharines, ON, Canada L2S 3A1.

265 SURFACE ELECTROMYOGRAPHIC SPIKE ACTIVITY AND MOTOR UNIT FIRING RATES AT DIFFERENT LEVELS OF MAXIMUM CONTRACTION

David Gabriel[1], Scott Rubinstein[2], Anita Christie[2], J. Greig Inglis[1], and Gary Kamen[2]
[1]Raymond Nelson Reid Biomechanics Laboratory, Brock University, St. Catharines, ON, CA; [2]Motor Control Laboratory, University of Massachusetts at Amherst, Amherst, MA, USA.

266 EFFECT OF POSITIVE POSTERIOR HEEL FLARE ON KINETICS AND TIBIALIS ANTERIOR MUSCLE ACTIVATION DURING RUNNING GAIT

Robin M. Queen[1,4] Michael T. Gross[2,4] and Bing Yu[1,2,3,4]
[1]Department of Biomedical Engineering, [2]Division of Physical Therapy, [3]Department of Orthopedics, [4]Center for Human Movement Science, The University of North Carolina at Chapel Hill, Chapel Hill, NC, USA.

267 A NOVEL METHOD FOR THE ASSESSMENT OF MEASURED ISOMETRIC FORCE-TIME FUNCTIONS

Sigrid Thaller and Markus Tilp
Institute of Sports Sciences, Karl-Franzens-University Graz, Graz, Austria, Europe.

268 EFFECTIVENESS OF A COLLAGEN HYDROLYSATE-BASED NUTRITIONAL SUPPLEMENT ON THE LEVEL OF JOINT PAIN, RANGE OF MOTION AND MUSCLE FUNCTION IN INDIVIDUALS WITH MILD OSTEOARTHRITIS OF THE KNEE: A RANDOMIZED CLINICAL TRIAL

Carpenter MR, McCarthy S, Kline G, Angelopoulos TJ, Rippe JM.
Rippe Health Assessment, Celebration Hospital, Orlando, FL USA.

269 RELATIONSHIP OF MUSCLE FIBER PENNATION ANGLE TO EMG AND JOINT MOMENT DURING GRADED ISOMETRIC CONTRACTIONS USING ULTRASOUND IMAGING

Dustyn P. Roberts and Thomas S. Buchanan
Center for Biomedical Engineering Research, University of Delaware, Newark, DE.

270 MUSCLE ACTIVATION PATTERNS IN MALES AND FEMALES DURING DROP LANDINGS ONTO THE HEELS

Rhonda L. Boros[1] and John H. Challis[2]
[1]Applied Biodynamics Laboratory, Boston University, Boston, MA, USA; [2]The Biomechanics Laboratory, The Pennsylvania State University, University Park, PA, USA.

 # 271 **ON THE ANATOMY OF THE EXTENSOR MECHANISM AND WHY COCONTRACTION IS NECESSARY FOR VERSATILE STATIC FINGERTIP FORCES**

Francisco J. Valero-Cuevas
Neuromuscular Biomechanics Laboratory, Cornell University, Ithaca, NY, USA

Posture & Balance

 # 272 **AUDIO BIOFEEDBACK OF TRUNK ACCELERATIONS IMPROVES BALANCE IN SUBJECTS WITH BILATERAL VESTIBULAR LOSS**

Marco Dozza [1 2], Fay Horak [2], and Lorenzo Chiari[1]
[1] DEIS - Dept. of Electronics, Computer Science, and Systems – University of Bologna, Italy;
[2] Neurological Science Institute – Oregon Health and Sciences University, Portland, OR, USA

 # 273 **EFFECTS OF PREPARATION ON POSTURAL STABILITY WHILE ACCEPTING A WEIGHT IN THE OUTSTRETCHED HANDS**

[1]Jennifer Rattenbury, [2]Ted Milner, [1]Stephen N. Robinovitch,
[1]Injury Prevention and Mobility Laboratory, [2]Biomechanics Laboratory; School of Kinesiology, Simon Fraser University, Burnaby, British Columbia, Canada.

 # 274 **THE EFFECTS OF SOLDIER LOADS ON FOOT PLACEMENT DURING QUIET STANCE**

Jeffrey M. Schiffman, Leif Hasselquist, Karen P. Norton, Carolyn K. Bensel
Center for Military Biomechanics Research, Natick Soldier Center, Natick MA, USA.

 # 275 **DETECTING A LOSS OF BALANCE IN YOUNG ADULTS PERFORMING A MAXIMAL FORWARD REACH**

Alaa A. Ahmed[1], M.S. and James A. Ashton-Miller[1,2], PhD.
Biomechanics Research Laboratory, Depts. of [1]Biomedical & [2]Mechanical Engineering University of Michigan, Ann Arbor, MI, U.S.A.

 # 276 **PREDICTION OF MUSCLE ACTIVATION PATTERNS FOR POSTURAL CONTROL USING A LINEAR FEEDBACK MODEL**

Daniel B. Lockhart[1] and Lena H. Ting[2]
[1]Woodruff School of Mechanical Engineering, Georgia Institute of Technology, Atlanta, GA; [2]Coulter Department of Biomedical Engineering, Georgia Tech/Emory University, Atlanta, GA.

 # 277 **HOW DOES ABILITY TO RECOVER BALANCE DEPEND ON THE TIME REQUIRED TO EXECUTE A STEP?**

Elmine H. Postma, Dawn C. Mackey and Stephen N. Robinovitch.
Injury Prevention and Mobility Laboratory, School of Kinesiology, Simon Fraser University, Burnaby, BC, Canada.

 # 278 **NONLINEAR ANALYSIS OF POSTURAL CONTROL IN DIFFERENT POSITIONS**

Georgios Korellis, Clinton J. Wutzke, Max J. Kurz, and Nicholas Stergiou
HPER Biomechanics Lab, University of Nebraska at Omaha, Omaha, NE, USA.

 # 279 **EFFECTS OF SUPPORT SURFACE ML COMPLIANCE ON STEPPING BEHAVIOR OF HEALTHY ADULTS: AGE AND GENDER DIFFERENCES**

Bing-Shiang Yang[1] and James A. Ashton-Miller
Biomechanics Research Laboratory, Department of Mechanical Engineering, University of Michigan, Ann Arbor, Michigan.

 # 280 **THE EFFECT OF HIGH INTENSITY STRENGTH TRAINING ON ANKLE INVERSE DYNAMICS IN BALANCE IMPAIRED OLDER ADULTS**

Jennifer A. Hess
Department of Exercise and Movement Science, University of Oregon, Eugene, OR.

 # 281 **TAI CHI AND STANCE WIDTH EFFECTS ON POSTURAL SWAY AND KNEE FLEXION**

Arun K. Ramachandran[1], Yang Yang[2], Karl S. Rosengren[2], and Elizabeth T. Hsiao-Wecksler[1]
[1]Department of Mechanical & Industrial Engineering; [2]Dept. of Kinesiology University of Illinois at Urbana-Champaign, Urbana, IL.

 # 282 **MINIMAL FORWARD STEP LENGTH NEEDED FOR BALANCE RECOVERY OF HUMAN BODY AFTER PERTURBATIONS**

Ming Wu[12], Linhong Ji[3], Dewen Jin[3] and Yi-chung Pai [4]
[1]Sensory Motor Performance Program, Rehabilitation Institute of Chicago, Chicago, IL, USA; [2]Northwestern University Medical School, Chicago, IL, USA; [3]Department of Precision Instrument, Tsinghua University, Beijing, PR China; [4]Department of Physical Therapy, University of Illinois at Chicago, Chicago, USA.

Rehabilitation Engineering

 # 283 EMG ACTIVITY OF TRUNK MUSCLES DURING WHEELCHAIR PROPULSION

Yusheng Yang[1], Alicia Koontz[1], Michael L. Boninger[1] Ronald Triolo[2], Rory A. Cooper[1]
[1]Human Engineering Research Laboratories, VA Medical Center, Pittsburgh, PA, USA; [2]Cleveland FES Center, Case Western Reserve University, Cleveland, OH.

 # 284 VARIABLE STIFFNESS PROSTHESIS FOR TRANSTIBIAL AMPUTEES

Glenn K. Klute[1,2], Joel C. Perry[1,2], Joseph M. Czernicki[1,3]
[1]Dept. of Veteran Affairs, Seattle, WA USA; [2]Dept. of Mechanical Engineering, University of Washington, Seattle, WA USA; [3]Dept. of Rehabilitation Medicine, University of Washington, Seattle, WA USA.

 # 285 TRUNK MOVEMENT PATTERNS AND PROPULSION EFFICIENCY IN WHEELCHAIR USERS WITH AND WITHOUT SCI

Alicia M. Koontz, Michael L. Boninger, Ian Rice, Yusheng Yang, Rory A. Cooper
Human Engineering Research Laboratories, VA Medical Center, Pittsburgh, PA, USA University of Pittsburgh, Dept. of Rehabilitation Science and Technology, Pittsburgh, PA

 # 286 PARAMETERS AFFECTING AXIAL STIFFNESS OF TIBIAL FIXATION IN AN ILIZAROV ANKLE DISTRACTOR

Jonathan K. Nielsen[2], Charles L. Saltzman[1,2], Thomas D. Brown[1,2]
[1]Department of Orthopaedics and Rehabilitation, University of Iowa, Iowa City, IA, USA; [2]Department of Biomedical Engineering, University of Iowa, Iowa City, IA.

 # 287 BIOMECHANICAL ANALYSIS OF A WHEELCHAIR WHEELIE IN PERSONS WITH SCI

Nethravathi Tharakeshwarappa[1,2], Alicia Koontz[1,2], Rory Cooper[1,2], and Michael Boninger[1,2]
[1]Dept. of Rehab. Science and Technology, University of Pittsburgh, Pittsburgh, PA 15261; [2]Human Engineering Research Laboratories, Highland Drive VA Medical Center, Pittsburgh, PA.

 # 288 DRAG FORCE NORMALIZED WHEELCHAIR PROPULSION FORCES

W. Mark Richter, Russell Rodriguez, Kevin R. Woods, and Peter W. Axelson
BioMobility Laboratory, Beneficial Designs, Nashville, TN USA.

Gait and Movement

 # 289 GAIT DEVIATIONS IN A VIRTUAL REALITY ENVIRONMENT

John H. Hollman[1] Robert H. Brey[2] Richard A. Robb[3] Tami Bang[4] and Kenton R. Kaufman[4]
[1]Program in Physical Therapy, Mayo Clinic College of Medicine, Rochester, MN; [2]Department of Otorhino-laryngology, Mayo Clinic College of Medicine, Rochester, MN; [3]Biomedical Imaging Resource, Mayo Clinic College of Medicine, Rochester, MN; [4]Department of Orthopedics, Mayo Clinic College of Medicine, Rochester, MN.

 # 290 PREDICTED HIP JOINT REACTION FORCES DURING PRONE HIP EXTENSION WITH VARYING CONTRIBUTION FROM THE GLUTEAL MUSCLES

Cara L. Lewis[1], Shirley A. Sahrmann[2], and Daniel W. Moran[3]
[1]Movement Science Program; [2]Program in Physical Therapy, School of Medicine; [3]Department of Biomedical Engineering Washington University in St. Louis, St. Louis, MO, USA.

 # 291 TRADE-OFFS IN THE DETERMINATION OF OPTIMUM STEP LENGTH IN HUMAN WALKING

Arthur D. Kuo[1], Jiro Doke[1], and J. Maxwell Donelan[2]
[1]Dept. of Mechanical Engineering, University of Michigan, Ann Arbor, MI [2]University of Alberta, Edmonton, Canada.

 # 292 AN ARTIFICIAL NEURAL NETWORK THAT UTILIZES A CHAOTIC CONTROL SCHEME FOR STABLE LOCOMOTION

Max J. Kurz and Nicholas Stergiou
HPER Biomechanics Laboratory, University of Nebraska at Omaha, Omaha, NE.

 # 293 ASSESSMENT OF BACKPACK INTERFACE LOADING USING A WHOLE BODY GAIT MODEL

Lei Ren[1,2], Richard Jones[2], David Howard[1,2] and Jim Richards[2]
[1]School of Computing, Science & Engineering; [2]Centre for Rehabilitation & Human Performance Research Salford University, UK.

 # 294 FULL BODY INVERSE DYNAMICS SOLUTIONS: AN ERROR ANALYSIS AND A HYBRID APPROACH

Raziel Riemer, Sang-Wook Lee, and Xudong Zhang
Biomechanics and Ergonomics Lab, Department of Mechanical and Industrial Engineering University of Illinois at Urbana-Champaign, Urbana, IL 61801, USA.

 # 295 EFFECTS OF GAIT VELOCITY ON COP SYMMETRY MEASURES IN INDIVIDUALS WITH STROKE

Mary M. Rodgers, Larry Forrester, Christopher Mizelle, Michelle Harris-Love
Department of Physical Therapy and Rehabilitation Science, University of Maryland School of Medicine, Baltimore, MD, USA.

 # 296 THE EFFECTS OF MUSCLE TRAINING ON GAIT CHARACTERISTICS IN CHILDREN WITH DOWN SYNDROME

Bee-Oh Lim[1], Dong-Ki Han[2] and Young-Hoo Kwon[1]
[1]Biomechanics Laboratory, Texas Woman's University, Denton, TX; [2]Adapted Physical Activity Laboratory, Dept. of Physical Education, Seoul National University, Seoul, Korea.

 # 297 THE ROLE OF HEAD STABILIZATION IN NECK AND TRUNK MOVEMENT DURING FOUR DIFFERENT LOCOMOTION TASKS

Gail F Forrest[1] and Ronita Cromwell[2]
[1]Kessler Medical Rehabilitation Research and Education Corporation, West Orange, NJ, USA; [2]Department of Physical Therapy, Center for Rehabilitation Sciences, and Sealy Center on Aging, The University of Texas, Medical Branch Galveston.

 # 298 TIBIOFEMORAL LOAD DISTRIBUTION DURING GAIT OF NORMAL SUBJECTS

Rose F. Riemer[1,2,] Tammy Haut Donahue[2], and Kenton R. Kaufman[1]
[1]Motion Analysis Laboratory, Mayo Clinic, Rochester, MN, USA; [2]Mechanical Engineering, Michigan Technological University, Houghton, MI, USA.

 # 299 NEUROMUSCULAR RESPONSE TO UNEXPECTED GAIT PERTURBATIONS IN ANTERIOR CRUCIATE LIGAMENT INJURED NON-COPERS

Reed Ferber[1] Janet L. Ronsky[1] Vincent von Tscharner[1] and Louis R. Osternig[2]
[1]Human Performance Laboratory, Faculty of Kinesiology, University of Calgary, AB, Canada; [2]Department of Exercise and Movement Science, University of Oregon, Eugene, OR, USA.

 # 300 ACCELERATION DURING WALKING: THE EFFECT OF ANKLE KINETICS ON CENTER OF MASS POSITION AND VELOCITY

Michael S. Orendurff, Ava D. Segal, Jocelyn S. Berge, Kevin C. Flick and Glenn K. Klute
Motion Analysis Laboratory, Rehabilitation Research and Development, Seattle, WA. USA

 # 301 EFFECT OF EXTERNALLY-CUED STRIDE FREQUENCY SELECTION ON TEMPERO-SPATIAL PARAMETERS OF GAIT

Michael P. Hanlon and Ross Anderson
Physical Education and Sport Sciences Department, University of Limerick, Limerick, Ireland

 # 302 EFFECTS OF CHANGING PROTOCOL, GRADE, AND DIRECTION ON THE PREFERRED GAIT TRANSITION SPEED DURING HUMAN LOCOMOTION

Alan Hreljac, Rodney Imamura, W. Brent Edwards, and Escamilla, R. F.
Kinesiology and Health Science Department, California State University, Sacramento

 # 303 JOINT LOADING AND BONE MINERAL DENSITY IN PERSONS WITH UNILATERAL, TRANS-TIBIAL AMPUTATION

Todd D. Royer and Michael Koenig
Dept of Health, Nutrition and Exercise Sciences, University of Delaware, Newark, Delaware, USA

 # 304 EVALUATING SYMMETRY OF THE SWING LEG DURING RUNNING WITH VELOCITY-VELOCITY PROFILES

Ryan A. Jorden[1], Gary D. Heise[2], Kendall Mallory[3], and Dan Packard[3]
[1]Department of Kinesiology, Westmont College, Santa Barbara, CA 93108; [2]Sport and Exercise Science, [3]Physics, University of Northern Colorado, Greeley, CO.

 # 305 EMOTION RECOGNITION FROM BODY MOVEMENT KINEMATICS

M. Melissa Gross[1], Geoffrey E. Gerstner[2], Daniel E. Koditschek[3], Barbara L. Fredrickson[4] and Elizabeth A. Crane[1]
[1]Department of Movement Science; [2]Department of Biologic and Materials Science; [3]Department of Electrical Engineering and Computer Science, and [4]Department of Psychology University of Michigan, Ann Arbor, MI, USA.

 # 306 STIFFNESS DURING WALKING: A COMPARISON BETWEEN CHILDREN WITH AND WITHOUT SPASTICITY

Robin D. Dorociak[1], Molly P. Nichols[1], Susan Sienko Thomas[2], and Cathleen E. Buckon[2]
[1]Motion Analysis Laboratory and [2]Clinical Research, Shriners Hospitals for Children Portland, Portland, OR, USA.

 # 307 FOOT ORTHOSES ALTER MUSCLE ACTIVITY PATTERNS IN RUNNERS DIAGNOSED WITH PATELLOFEMORAL PAIN SYNDROME

Yukiko Toyoda[1], Benno Nigg[1], Preston Wiley[2] and Neil Humble[3]
[1]Human Performance Lab, Faculty of Kinesiology, University of Calgary, Calgary, Canada; [2]Sport Medicine Center, Faculty of Kinesiology, University of Calgary, Calgary, Canada; [3]Department Surgery, University of Calgary, Canada.

 # 308 EXTERNAL LOAD AFFECTS GROUND REACTION FORCE PARAMETERS NONUNIFORMLY DURING RUNNING IN WEIGHTLESSNESS

John K. DeWitt[1], Grant Schaffner[2], Mitzi S. Laughlin[2], James A. Loehr[2] and R. Donald Hagan[3]
[1]Bergaila Engineering Services, Houston, TX, USA; [2]Wyle Life Sciences, Houston, TX, USA; [3]NASA Johnson Space Center, Houston, TX, USA.

 # 309 DIRECTLY COMPARING STANDING AND WALKING STABILITIES

Hyun Gu Kang[1] and Jonathan B. Dingwell[1,2]
[1]Nonlinear Biodynamics Lab, Dept. of Kinesiology, University of Texas, Austin, TX, USA; [2]Dept. of Biomedical Engineering, University of Texas, Austin, TX, USA.

 # 310 ARM CONSTRAINT AND INTER-LIMB COORDINATION DURING WALKING IN HEALTHY ADULTS

Matthew P. Ford PT, PhD[1], Robert C. Wagenaar PhD[2], Karl M. Newell, PhD[3]
[1]Department of Physical Therapy, The University of Alabama at Birmingham, Birmingham, AL; [2]Department of Rehabilitation Sciences, Boston University, Boston, MA; [3]Department of Kinesiology, The Pennsylvania State University, University Park, PA.

 # 311 VALIDATION OF A THREE-DIMENSIONAL WHOLE BODY MULTISEGMENT MODEL FOR LOAD CARRIAGE STUDIES

Lei Ren[1,2], Richard Jones[2], David Howard[1,2] and Jim Richards[2]
[1]School of Computing, Science & Engineering; [2]Centre for Rehabilitation and Human Performance Research Salford University, UK.

 # 312 THE USE OF CENTER OF MASS ANALYSIS FOR GAIT ASSESSMENT IN CHILDREN WITH CEREBRAL PALSY

Bradford C. Bennett, Adam Wolovick, Tim Franklin, Paul E. Allaire, & Mark F. Abel
Motion Analysis and Motor Performance Laboratory, University of Virginia.

 # 313 INITIAL CONDITION VARIABLES AND AGE GROUP AS DETERMINANTS OF SLIP SEVERITY

Brian E. Moyer[1], April J. Chambers, Mark S. Redfern, and Rakié Cham
Human Movement and Balance Laboratory, Bioengineering Department, University of Pittsburgh, Pittsburgh, PA, USA.

 # 314 INSTRUMENTATION SYSTEM FOR BIOMECHANICAL ANALYSIS OF FACTORS AFFECTING BACKPACK USER COMFORT

Jennifer L. Springer, B.S. and David A. Hawkins, Ph.D.
Human Performance Laboratory, Biomedical Engineering Graduate Group, University of California, Davis, CA.

 # 315 THE PRESENCE OF AN OBSTACLE INFLUENCES THE STEPPING RESPONSE DURING SIMULATED AND REAL TRIPS

Karen L. Troy[1] and Mark D. Grabiner[1]
[1]Musculoskeletal Biomechanics Laboratory, University of Illinois at Chicago, Chicago, IL, USA

 # 316 STEPPING UP TO A NEW LEVEL. EFFECTS OF BLURRING VISION IN THE ELDERLY

[1]Karen Heasley, [1]John G Buckley, [2]Andy Scally, [3]Pete Twigg, and [1]David B. Elliott
[1]Vision and Mobility Research Laboratory, Department of Optometry; [2]Institute of Health Research, School of Health, and [3]School of Engineering, Design and Technology, University of Bradford.

 # 317 EFFECT OF INITIAL VELOCITY ON THE THRESHOLD OF BALANCE RECOVERY PRELIMINARY RESULTS

Kodjo E. Moglo, Marc-André Cyr and Cécile Smeesters
Research Centre on Aging, Sherbrooke Geriatric University Institute, Sherbrooke, QC, Canada;
Department of Mechanical Engineering, Université de Sherbrooke, Sherbrooke, QC, Canada

 # 318 INFLUENCE OF PASSIVE ELASTIC JOINT MOMENTS ON THE METABOLIC ENERGY CONSUMPTION OF MUSCLES DURING GAIT

Darryl G. Thelen
Dept. of Mechanical Engineering, University of Wisconsin-Madison, Madison, WI, USA

 # 319 A BIOMECHANICAL MODEL FOR TISSUE INJURY IN PELVIC ORGAN PROLAPSE

Amanda Clark[1], Qi Liu[2], and Marie Shea[2]
[1]Division of Urogynecology and Reconstructive Pelvic Surgery; [2]Orthopaedic Biomechanics Laboratory, Oregon Health & Science University, Portland, OR, USA.

 # 320 AGE INDUCED MECHANICAL PLASTICITY IN LOCOMOTION

Paul DeVita, Joe Helseth, Brandon Noyes, Michelle Pullen, Doug Powell & Tibor Hortobagyi
Biomechanics Laboratory, Dept. of Exercise and Sport Science, East Carolina University,Greenville, NC, USA

 # 321 AGE-RELATED DIFFERENCES IN PEAK JOINT VELOCITIES DURING SINGLE STEP RECOVERY FROM A FORWARD FALL

Michael L. Madigan and Emily M. Lloyd
Musculoskeletal Biomechanics Laboratory, Virginia Tech, Blacksburg, VA, USA

 # 322 THE RELATIONS BETWEEN MUSCLE STRENGTH AND MOVEMENT OF CENTER OF MASS OF THE BODY DURING OBSTACLE NEGOTIATION IN THE COMMUNITY-DWELLING OLDER ADULTS

Hsiu-Chen Lin[1], Shu-Ya Chen[1], Hong-Wen Wu[1], Ching-Sheng Li[1], Hui-Fen Pan[1], Horng-Chaung Hsu[2]
[1]School of Physical Therapy, China Medical University, Taichung, Taiwan; [2]Department of Orthopedics, China Medical University Hospital, Taichung, Taiwan.

 # 323 THE ALTERATIONS TRAJECTORY OF CENTER OF MASS WHEN NEGOTIATING OBSTACLES WITH DIFFERENT HEIGHTS IN THE OLDER ADULTS

Shu-Ya Chen[1], Hsiu-Chen Lin[1], Hong-WenWu[1], Hui-Fen Pan[1], Ching-Sheng Li[1], Horng-Chaung Hsu[2]
[1]School of Physical Therapy, China Medical University, Taichung, Taiwan; [2]Department of Orthopedics, China Medical University Hospital, Taichung, Taiwan.

 # 324 SAGITTAL AND FRONTAL SWAY ANGLES DURING LOCOMOTION IN THE ELDERLY

Heng-Ju Lee and Li-Shan Chou
Motion Analysis Laboratory, Department of Exercise and Movement Science, University of Oregon, Eugene, Oregon, U.S.A.

 # 325 QUIET STANDING AND STABILITY LIMITS: EFFECT OF WORK EXPERIENCE AND AGE

Steven R. Torgerud[1], Shirley Rietdyk[1], James D. McGlothlin[2] and Mark J. Knezovich[2]
[1]Biomechanics Laboratory, [2]School of Health Sciences, Purdue University, IN, USA.

Cardiovascular

 # 326 EFFECT OF CONSTRICTION SHAPE ON FLOWS IN STENOSED CHANNELS

Xiaohong Yu and Allen T. Chwang
Department of Mechanical Engineering, The University of Hong Kong, HK.

 # 327 THE EFFECT OF ANTI-HYPERTENSIVE DRUGS ON CAROTID HAEMODYNAMICS

Fadi P. Glor[1,2], Ben Ariff[3], Alun D. Hughes[3], Lindsey A. Crowe[4], Pascal R. Verdonck[1], Simon A.McG. Thom[3], David N. Firmin[4], X. Yun Xu[2]
[1]Cardiovascular Mechanics and Biofluid Dynamics Research Unit, Ghent University, Belgium; [2]Department of Chemical Engineering & Chemical Technology, Imperial College London, UK; [3]Clinical Pharmacology and Therapeutics, St. Mary's Hospital, Imperial College London, UK; [4]Cardiovascular Magnetic Resonance Unit, R. Brompton and Harefield NHS Trust, London, UK.

 # 328 IMAGE-BASED COMPUTATIONAL FLUID DYNAMICS FOR CAROTID ARTERIES: A COMPARISON BETWEEN IMAGING TECHNIQUES

Fadi P. Glor[1,2], Ben Ariff [3], Alun D. Hughes[3], Lindsey A. Crowe[4], Pascal R. Verdonck[1], Dean C. Barratt[5], Simon A.McG. Thom[3], David N. Firmin[4], X. Yun Xu[2]
[1]Cardiovascular Mechanics and Biofluid Dynamics Research Unit, Ghent University, Belgium; [2]Department of Chemical Engineering & Chemical Technology, Imperial College London, UK; [3]Clinical Pharmacology and Therapeutics, St. Mary's Hospital, Imperial College London, UK; [4]Cardiovascular Magnetic Resonance Unit, R. Brompton and Harefield NHS Trust, London, UK; [5]Computational Imaging Sciences Group, Imaging Sciences, Guy's Hospital, London, UK.

 # 329 CONSTITUTIVE MODELING OF VASCULAR CONSTRUCTS: A MODIFIED BURST PRESSURE METHOD

Kathryn A. Lagerquist[1,2] , Samuel Jensen-Segal[1], Sean J. Kirkpatrick[2], Monica T. Hinds[2], and Kenton W. Gregory[1]
[1]Oregon Medical Laser Center, Portland, OR, USA; [2]Dept. of Biomedical Engineering, Oregon Health & Science University, Portland, OR, USA.

 # 330 LONGITUDINAL TENSILE PROPERTIES OF ELASTIN, CURED ELASTIN, AND NATIVE CAROTID ARTERY

Ping-Cheng Wu, Ann Bazar, and Kenton W. Gregory
Oregon Medical Laser Center, Providence St. Vincent Medical Center, Portland, OR.

Sport Science

 # 331 ANGULAR MOMENTUM TRANSFER DURING A POWER TENNIS SERVE

Brian J. Gordon and Jesús Dapena
Biomechanics Laboratory, Dept. of Kinesiology, Indiana University, Bloomington, IN, USA.

 # 332 BICYCLE SEAT INTERFACE PRESSURE: RELIABILITY, VALIDITY, AND INFLUENCE OF HAND POSITION AND WORKLOAD

Eadric Bressel[1], John Cronin[2], and Alicia Exeter[1]
[1]Biomechanics Laboratory, Utah State University, Logan UT, USA; [2]Sport Performance Centre, Auckland University of Technology, Auckland, New Zealand.

 # 333 THE USE OF A WIRELESS NETWORK TO PROVIDE REAL-TIME AUGMENTED FEEDBACK FOR ON-WATER ROWING

DJ Collins[1,2], Dr Ross Anderson[1] & Dr Derek T. O'Keeffe
[1] Department of PE and Sport Science, University of Limerick, Limerick, Ireland; [2] Biomedical Electronics Laboratory, Department of Electronic and Computer Engineering, University of Limerick, Ireland.

 # 334 FOOT AND ANKLE PRESSURE MEASUREMENT DURING FORWARD SKATING

David J. Pearsall, Curt Dewan, René Turcotte, and David L. Montgomery
Department of Kinesiology and Physical Education, Montréal, Québec, Canada

 # 335 3D COMPUTER SIMULATION OF ROUNDHOUSE KICK IN TAEKWONDO

Young-Kwan Kim[1], Gary T. Yamaguchi[2], and Richard N. Hinrichs[1]
[1]Department of Kinesiology, Arizona State University, Tempe, AZ, USA; [2]Exponent®, Inc., Phoenix, AZ, USA

 # 336 LOWER TRUNK KINEMATICS AND MUSCLE ACTIVITY DURING DIFFERENT TYPES OF TENNIS SERVES

John W. Chow, Soo-An Park, Mark D. Tillman and Guy B. Grover
Center for Exercise Science, University of Florida, Gainesville, FL, USA.

 # 337 INFLUENCE OF TORSO ROTATION AND ARM COCKING STYLES ON ELBOW VARUS TORQUE IN BASEBALL PITCHING

Jeff T. Wight[1], Guy B. Grover[1], John W. Chow[1], James G. Richards[2], and Mark D. Tillman[1]
[1]Center for Exercise Science, University of Florida, Gainesville, FL, USA; [2]Dept. of Health, Nutrition, and Exercise Sciences, U. of Delaware, Newark, DE, USA.

 # 338 RELATIONSHIPS BETWEEN EMG FREQUENCY SPECTRUM AND RATE OF FORCE DEVELOPMENT CHANGES

Loren Z.F. Chiu[1], Andrew C. Fry[2], Brian K. Schilling[2], and Lawrence W. Weiss[2]
[1]Musculoskeletal Biomechanics Research Laboratory, Biokinesiology & Physical Therapy, University of Southern California, Los Angeles, CA, USA; [2]Musculoskeletal Dynamics Laboratory, Human Movement Sciences & Education, The University of Memphis, Memphis, TN, USA.

 # 339 THE EFFECTS OF ALTERED CYCLING POSTURE AND CADENCE ON SUBSEQUENT RUNNING MECHANICS

Rachel D. Durham and Julianne Abendroth-Smith, Ed.D.
Willamette University, Salem OR.

 # 340 AMPLITUDES OF MUSCLE ACTIVITY DURING EARLY PRACTICE TRIALS COMPARED WITH THOSE OF A WELL-LEARNED SKILL

Gary D. Heise and Cory Christiansen
School of Sport and Exercise Science, University of Northern Colorado, Greeley, CO, USA.

 # 341 GASTROC-SOLEUS MUSCLE ACTIVATION AND ITS ASSOCIATION TO ANKLE AND KNEE MOMENTS DURING EXPECTED AND UNEXPECTED SIDE STEP CUT TASKS

Jeff R. Houck [1], Sara Bigham [1], Patty Cruz [1], Megan Vanderhoof [1], Luke McCann [1], Cheri Ward [1],Kenneth De Haven [2], Andrew Duncan [2]
[1]Ithaca College- Rochester, 300 East River Road, Rochester, NY, [2]University of Rochester Medical Center, Rochester, NY

 # 342 A COMPARISON OF VERTICAL GROUND REACTION FORCES BETWEEN ONE AND TWO-LEG DROP LANDINGS

Steven T. McCaw, Saori Hanaki, Meredith A. Olson, and Joshua J. Kauten
School of Kinesiology and Recreation, Illinois State University, Normal, IL, USA

Poster Session I: Thursday, 3:30 pm - 5:00 pm:

Poster Session II: Friday, 3:30 pm - 4:30 pm:

notes

Explore Portland

Check out the Portland favorites of the Legacy Biomechanics Lab Team:

Michael's Favorite:
Fernando's Hideaway offers authentic cuisine of Spain at its best, with 'tapas' and a great wine selection. After a dinner in the quite and elegant restaurant, venture upstairs to Portland's hottest Salsa Club or join a free Salsa lesson at 9 pm. You will not regret it!
(503) 248 4709; 824 SW 1st Ave.; take MAX westbound red or blue to to exit 'Morrison/SW 3rd Ave' .

Tanja's Favorite:
The Hawthorne district between 32nd and 39th of Hawthorne street is a fun place to explore. You will find plenty of charming coffee shops and interesting stores. Nice restaurants and bars will come into your sight as you walk along. The "Cold Stone" will make your ice cream dreams come true. A short cab ride will get you there.
Alternatively, you can explore the more upscale Pearl District, with its ever growing variety of restaurants and shops. Combine it with a visit to Powells, the worlds largest independent book store!
Take westbound red- or blue line MAX (free) to Galleria, then switch to northbound Streetcar (free) to 10th & Couch.

Larry's Favorite:
Bike Portland! Rent a bike and head out to the largest urban park in the U.S. for a few hours of mountain biking. The Fat Tire Farm in NW Portland will set you up with a bike for $20/2hr or $40/day (Cruisers for $25/day). When you're tired of single track, ride into downtown Portland and explore it on your bike!
(503) 223 2182; 2714 NW Thurman; *www.fattirefarm.com/trails/trail_forestpark.html*
Grab a bite to eat afterwards at Portland's best Thai Restaurant: Beau Thai - 730 NW 21st Ave.

Mark's Family Favorite:
It doesn't matter how old of a kid you are or have at the Oregon Museum of Science and Industry (OMSI) every age will be able to discover new things related to science and technology in a most enjoyable way. A museum for the kid in each of us!
(503) 797-OMSI (6674); 1945 SE Water Avenue; MAX downtown, then bus Route 83 to OMSI

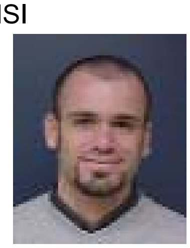

Marcus' Favorite:
Want to get a taste of fine northwestern microbrews? Bridgeport Brew Pub is Oregon's oldest craft brewery, serving award winning beers in a century old brick stone building. Tip: Try their cask-conditioned IPA!
1313 NW Marshall St.; Take westbound red- or blue line MAX (free) to Galleria, then switch to northbound Streetcar ($1.30) to 14th & Northrup. Walk one block south.

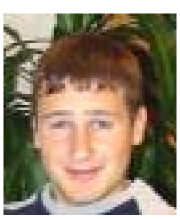

Matt's Favorite:
Head up through trendy Hawthorne blvd to the landmark McMenamins Bagdad theater and pub for dinner and a movie. Beer, Pizza, and $3.00 2nd-run movies are a great bargain for a night on the town. Plus, it's located in the heart of Hawthorne District, an oasis of alternative restaurants, bars, and eclectic stores.
(503) 225-5555; 3702 SE Hawthorne Blvd at the corner of 37th Ave. A short cab-ride from hotel.

Savas' Favorite:
The Portland City Grill. Enjoy spectacular views from the 36th floor at one of Portland's most popular restaurant, offering USDA Prime steaks, fresh Hawaiian, Pacific Coast and Alaskan seafood prepared with classic, Northwest, island, and Asian influences. While the restaurant is rather spendy, its bar attracts crowds with plenty of affordable appetizers, live piano, and stunning view on downtown and the cascade mountains.
(503) 450 0030; 111 SW Fifth Avenue; a short cab-ride from the hotel.

Brochure sponsored by adidas

Sponsors

The American Society of Biomechanics gratefully acknowledges the following sponsors. Their generous support was crucial to realize the 28th Annual Meeting of the Society.

PLATINUM Sponsors (≥ $5,000)

LEGACY Health System

OHSU Oregon Health & Science University

The Whitaker Foundation

NIAMS National Institute of Arthritis and Musculoskeletal and Skin Diseases

SYNTHES®

GOLD Sponsors (≥ $2,000)

NIKE®

adidas

OGI School of Science & Engineering Department of Biomedical Engineering

zimmer

stryker® Europe

TIME	Wednesday, 9/8/04	Thursday, 9/9/04	Friday, 9/10/04	Saturday, 9/11/04
7:45		**Welcome Remarks** Michael Bottlang (meeting chair) Steve Robinovitch (program chair)	**Welcome Remarks** Steve Madey (meeting co-chair) Tony Melaragno, MD (Legacy Chief of Research)	**Welcome Remarks** Marie Shea (OHSU Biomechanics) Stephen Hanson (OGI Dean of BME)
8:00		**Keynote** Steven Vogel, Ph.D. *Comparative Biomechanics: Life's Physical World*	**Keynote** Wilson C (Toby) Hayes, Ph.D. *Lessons on Forensic Injury Biomechanics*	**Keynote** Farshid Guliak, Ph.D.: *Biomechanics & Arthritis: From Organism to Organell*
9:00		**Break**	**Break**	**Break**
9:20		**A Parallel Session B** A: Symposium I *Joint Neuromechanics* B: Gait and Movement I: *Basic Science*	**A Parallel Session B** A: Symposium II *Cell & Tissue Biomechanics* B: Gait and Movement II: *Clinical & Methods*	**A Parallel Session B** A: Biomechanical Modeling B: Muscle & Reflex
10:50		**Break**	**Break**	**Break**
11:00	*Registration opens*	**A Parallel Session B** A: Sport Biomechanics B: Orthopaedics I: *Basic Science*	**A Parallel Session B** A: Balance & Fall B: Orthopaedics II: *Clinical*	**Award Session III** *BORELLI Lecture & Award Announcements* Closing Remarks: Michael Bottlang
12:30	**Laboratory Tours:** NIKE, Legacy *Tour buses leave every 1/2 h from 12:30 - 3:30. Tours leaving after 2:00 will no return in time for workshops.* ASB: Executive Meeting I (Halsey)	**Lunch** Lab Tours: Legacy, NSI Student Luncheon: Mt St. Helens	**Lunch** Lab Tours: Legacy, NSI	ASB: Executive Meeting II (Halsey)
2:00		**Award Session I** Young Scientist Awards Jim Hay Award Inauguration	**Keynote** Andrew Schwartz, Ph.D.: *Usful signal s from motor cortex*	
3:30		**Poster Session I**	**Poster Session II**	
4:00	**A Parallel Workshops B** A: Richard Lieber, Ph.D. *Molecular Biology in Biomechanics* B: Walter Herzog, Ph.D. *Muscle Mechanics*	Willamette Ballroom *(refreshments served)* Pacific NW Ballroom	Willamette Ballroom *(refreshments served)* Pacific NW Ballroom	ENJOY OREGON!
5:00		**ASB General Meeting**	**Award Session II** (4:30 - 6:00) Clinical Biomech., ASB Microstrain, J. Biomech. Awards	
6:30	***Welcome Reception***		**Banquet** *Classical Chinese Garden*	

POSTER Category	Poster #	Area
Bone	100-111	A
Cartilage/Tendon/Ligament	112-137	A
Lower Extremity	138-180	A
Upper Extremity	181-203	A
Spine	204-226	A
Methods	227-241	B
Muscle	242-271	B
Posture and Balance	272-282	B
Rehabilitation Engineering	283-288	B
Gait and Movement	289-314	B
Aging	315-325	B
Cardiovascular	326-330	B
Sport Science	331-341	B

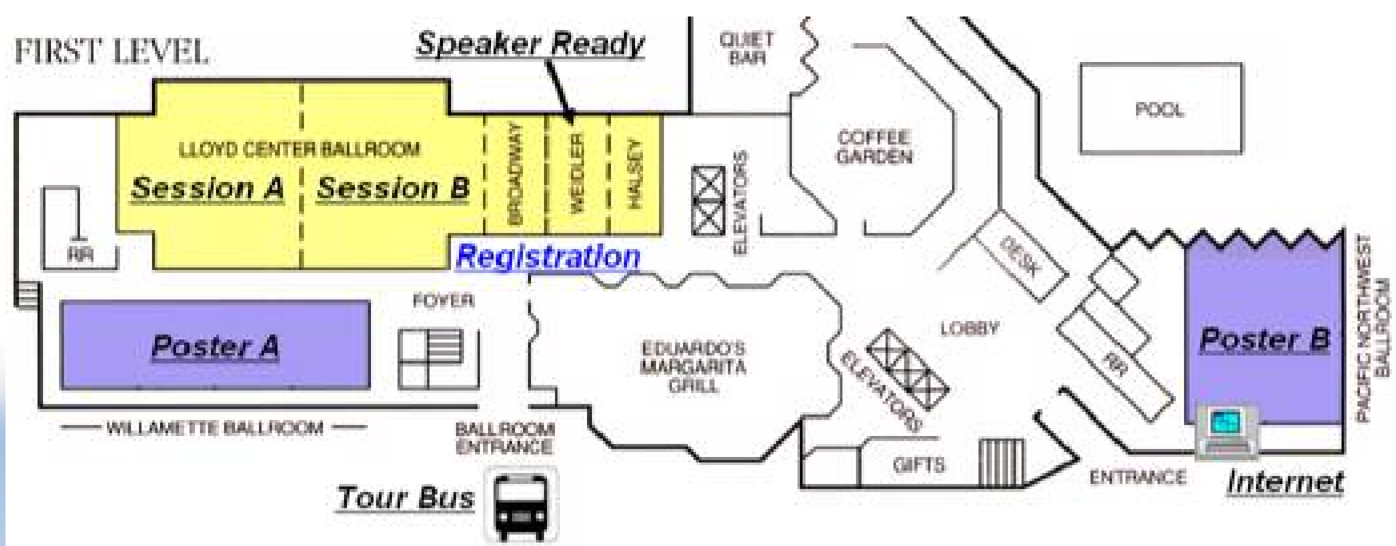

QUANTIFYING FRACTURE ENERGY IN A CLINICAL SERIES OF TIBIAL PILON FRACTURE CASES

Donald D. Anderson, Valerie L. Muehling, J. Lawrence Marsh, and Thomas D. Brown

Department of Orthopaedics and Rehabilitation, The University of Iowa, Iowa City, IA, USA
e-mail: don-anderson@uiowa.edu web: poppy.obrl.uiowa.edu/OBL_Lab_Website

INTRODUCTION

One of the first qualitative judgments an orthopaedic surgeon makes in fracture treatment involves looking at the injured limb and its radiographs to assess injury severity. Particularly for severe, highly comminuted fractures, important treatment decisions hinge on this judgment, including the timing and type of treatment. This in turn influences the risk for limb-threatening complications and the patient's prognosis for healing and the potential for post-traumatic osteoarthritis.

Surgeon judgments currently rely primarily upon radiographic fracture classification, identifying (using plain radiographs or CT scans) characteristic features shown to correlate with clinical prognosis. The features can be subtle, making the process highly susceptible to error and very sensitive to the level of experience of the grader. Not surprisingly, classification of comminuted intra-articular fractures has proven very problematic, with no single ordinal scale able to reliably and reproducibly provide agreement among different clinicians as to injury severity (Swiontkowski et al., 1997). This presents a problem because it limits the compilation of a collective body of literature to guide the evolution of clinical care of these patients.

We have developed and piloted a CT-based technique that has the potential to quantify the assessment of injury severity in complex fractures in a way not previously possible (Anderson et al., 2003). The technique exploits the fundamental principle that mechanical energy is required to create new free surface area in a brittle solid (bone), and that the amount of energy required is directly related to the amount of *de novo* surface area.

In this study, fracture energy measures were used to quantify injury severity in a series of clinical fracture cases, and these measures were compared to the clinical judgment of an experienced orthopaedic surgeon.

METHODS

Injury severity was quantified in a series of eleven tibial pilon fracture cases seen between 8/2001 and 5/2003. The patients (9 male, 2 female) ranged in age from 20 to 64 years. Comminution severity ranged from minimal to extensive.

CT studies obtained during standard clinical care were analyzed. Contralateral limb scans provided intact endosteal and periosteal bone surface areas over a comparable distal segment of the patient's tibia, for taring purposes. Bone free surface area measurements were extracted from CT datasets using validated digital image analysis routines (Beardsley et al., 2002). The *de novo* surface area liberated during fracture was estimated based on the difference between free surface areas measured on fractured and intact tibias of each patient. Local bone densities, extrapolated from CT Hounsfield units, were incorporated into a formal fracture energy measure. The clinical cases were rank ordered by an experienced orthopaedic traumatologist in terms of lowest to highest injury severity, based on subjective appearance of A-P and lateral plain radiographs of the cases. A Spearman rank order analysis was performed to compare the fracture energy measures with the clinical rank ordering.

RESULTS AND DISCUSSION

Bone free surface areas measured in intact tibias ranged from 8577 to 25,059 mm^2. Among fractured tibias, surface areas ranged from 8722 to 30,826 mm^2, yielding net liberated surface areas ranging from 2 to 75% of the intact side. (Of note, between matched intact tibias in two publicly available CT datasets, there was a less than 1.2% side-to-side variation in measured surface area.) When plotted alongside scout images of the distal tibia (Figure 1), these differences in measured bone surface areas show variation in the degree of proximal to distal fragmentation, and reflect the proximity of a given fracture to the distal tibia articular surface. The Spearman analysis comparing clinical rank ordering with the fracture-liberated surface area ranking yielded an R value of 0.72, showing good agreement. Incorporating local bone densities into a fracture energy measure increased the correlation to an R = 0.90.

SUMMARY

We have developed estimates of the liberated bone surface area associated with a series of clinical pilon fractures. Our previous work has shown that this parameter correlates closely with fragmentation energy. Because mechanical fracture toughness is bone density-dependent, we have incorporated local material variability, available in the form of CT Hounsfield densities, into a formal fracture energy measure. The energy measures here calculated agree favorably with the clinical impression of the treating surgeon, in terms of a rank ordering of injury severity.

REFERENCES

Anderson, D.D. et al. (2003). *Proceedings of 27th ASB Meeting,* Paper #81.

Beardsley, C.L. et al. (2002). *J Biomech,* **35**, 331-338.

Swiontkowski, M.F. et al. (1997). *J Orthop Trauma*, **11**, 467-470.

ACKNOWLEDGEMENTS

Funded by the Arthritis Foundation, the Orthopaedic Research and Education Foundation, and the NIH (AR46601 and AR048939).

Figure 1: A plot of bone surface areas along two fractured distal tibias shows the unique traits of different fractures.

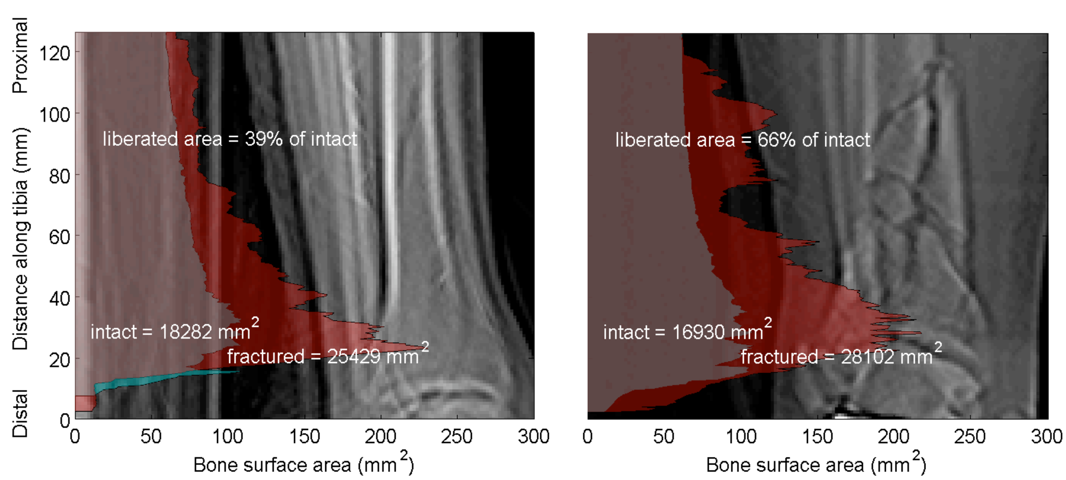

NON-LINEAR, VISCOELASTIC PROPERTIES OF THE HUMAN LUMBAR FACET JOINT CAPSULE

Jesse S. Little [1] and Partap S. Khalsa [1]

[1] Dept. of Biomedical Engineering, State University of New York at Stony Brook, Stony Brook, NY USA; E-mail: partap.khalsa@sunysb.edu

INTRODUCTION

The facet joint capsule (FJC) is innervated with mechanically sensitive neurons and is a source of low back pain (LBP) (Cavanaugh, 1995). An approach to studying the lumbar spine and its components contributing to LBP is to develop computational models (e.g., FEM). However, existing FE models (Gilbertson et al., 1995) of the human lumbar spine have not used realistic geometry and material properties of lumbar FJC, modeling it as uniaxial springs rather than as an anisotropic, viscoelastic 3D material. The purpose of this study was to determine the material properties of the FJC, both parallel and perpendicular to the dominant orientation of the collagen fibers.

METHODS

Intact, unembalmed lumbar spines (n = 8) were procured using an institutionally approved protocol. Specimens were dissected and the laminae of the superior and inferior facets were transected to free the intact joint and capsule from the spine. The sides of the capsules were trimmed, allowing the facet joint to be opened flat. The geometry of the specimens was controlled to produce specimens with the collagen fiber orientation aligned either "parallel" or "perpendicular" to the axis of loading (n = 25 and n = 10, respectively).

Capsules were tested using a uniaxial ramp-hold (R-H) protocol (15% strain/s to 10-50% strain with a 300 s hold) or a haversine displacement protocol (10-50% strain at 0.2, 1.0, and 2.0 Hz; parallel only). During R-H trials, a viscous stress calculation was made at the peak force, and an elastic stress was taken from the average of force values during the last 5 s of the hold, after relaxation occurred. Eulerian plane strain was measured optically (Little et al., 2003).

A secant modulus was defined for comparison of the viscous (E_V) & elastic (E_E) R-H data. A tangent modulus (E) was computed to define the linear portion of the R-H trials. For "parallel" specimens, the storage (E'), loss (E") and complex (E*) moduli were found from the phase lag between stress & strain during the dynamic trials.

RESULTS AND DISCUSSION

During R-H trials, the stress-strain relationship parallel to fiber orientation was exponential in form. The "parallel" E_V was significantly larger than E_E for all strains (Fig. 1; Wilcoxon, $p < 0.001$, for all). E_V was similar in magnitude to values previously reported for the cervical spine. The perpendicular E was linear in nature, reaching a mean value of ~ 2 MPa from 20-50% strain. The perpendicular E_V was larger than E_E at all strains, but statistical significance was not detected (Wilcoxon, $p > 0.05$). The parallel E was larger compared to the perpendicular E at 50% strain (Mann-Whitney, $p < 0.001$).

During dynamic trials, the mean stress-strain

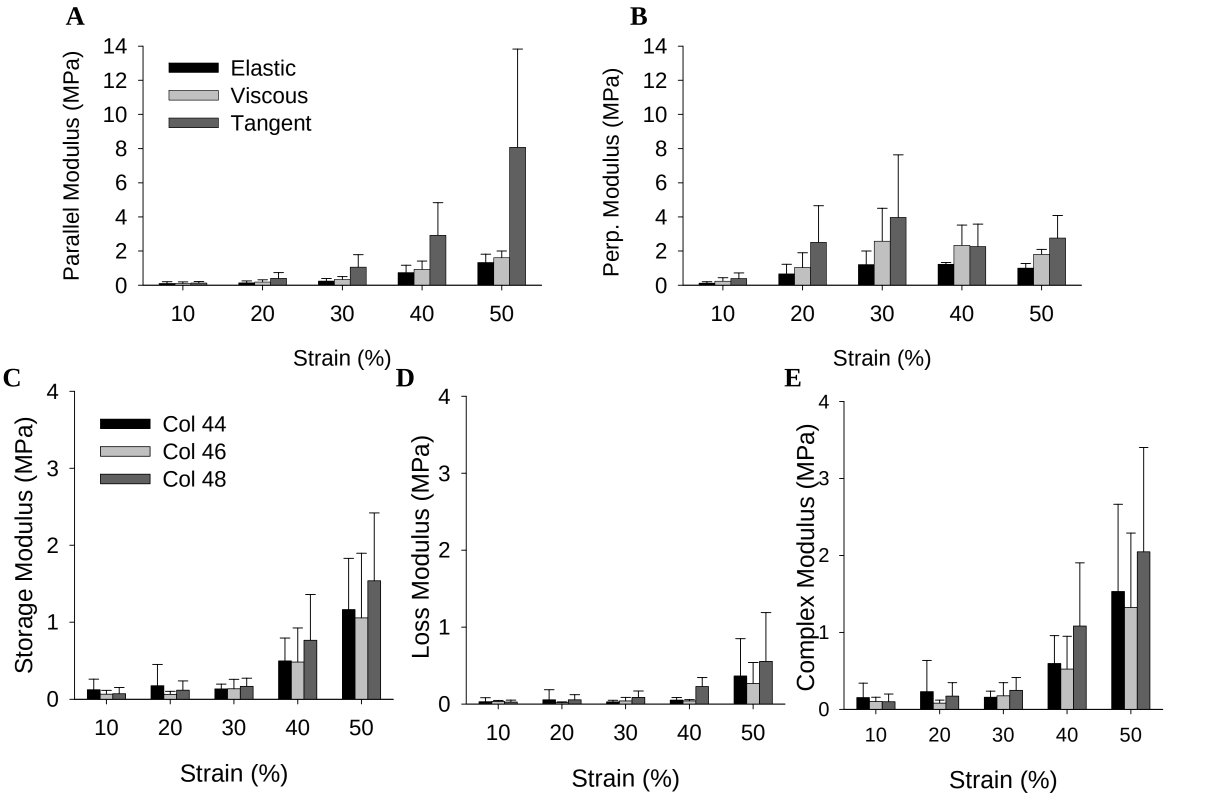

Figure 1. The “Viscous” and “Elastic” secant modulus and the “Tangent” modulus were found for the FJC during Ramp-Hold trials, both parallel (A) and perpendicular (Perp., B) to the collagen fiber orientation. (C-D) Dynamic moduli were found for the FJC parallel to the collagen fibers during cyclic loading trials at 0.2, 1.0, and 2.0 Hz.

relationship was also exponential in form. E*, E” and E’ were unaffected by changes in cycling frequency, but did significantly increase with increasing haversine strain (2F-RM ANOVA, $p > 0.05$ and $p < 0.001$, respectively). E*, E” and E’ were maximum at 50% haversine strain and were similar to E_V, E_E, and (E_V - E_E), respectively.

Lumbar facet joint capsules exhibited stress relaxation (SR). Perpendicular capsules had an SR rate independent of peak strain magnitude, typical of linear viscoelastic materials. Parallel capsules had a non-linear SR rate, as it was dependent upon the peak strain magnitude.

SUMMARY

The mechanical behavior of the FJC was non-linear, viscoelastic and anisotropic, and was consistent with the anatomical data of the dominant orientation of collagen fibers in the FJC perpendicular to the long axis of the spine. The data supports the concept that in order to fully elucidate the FJC’s role in LBP, it should be modeled as a 3D material with appropriate characteristics.

REFERENCES

Cavanaugh J.M. (1995). *Spine*, **20**, 1804-09.

Gilbertson L.G. et al. (1995). *Crit. Rev. Biomed. Eng*. **23**, 411-473.

Little J.S. et al. (2003). *Transactions of the BMES’03*, 31:11.P5.20.

ACKNOWLEDGEMENTS

PHS Grant # AT001701-01 (Khalsa)

COMPARISON OF THE PASSIVE STABILIZATION PROVIDED TO THE HUMAN CERVICAL SPINE BY THREE DIFFERENT CERVICAL BRACES

Karthik Balasubramanian[1], Naomi Hawkins[1], Sorin Siegler[1]

[1]Biomechanics Laboratory, Drexel University, Philadelphia, PA, USA kb55@drexel.edu

Introduction

Cervical collars play an important role in stabilization of the cervical spine, both in emergent situations, as well as in long-term rehabilitative care (Alaranta, 1994).
Quantifying the support characteristics of each collar becomes imperative, then, in identifying the appropriate collar to use under given circumstances. Present biomechanical studies focus nearly exclusively upon identifying range of motion (ROM) for different collars using goniometers (Alaranta, 1994, Beavis, 1989) or radiological techniques (Fisher, 1977). However, range of motion (ROM) can be considered a subjective technique, as the range of motion may vary depending upon the amount of torque applied to the neck. In addition, the cervical spine needs to be supported within this range of motion, so flexibility becomes a significant objective measure of collar efficacy.

Methods

Ten healthy volunteers (5 male, 5 female), ranging in age from 21-60, with no history of cervical spine trauma or other disorders were selected for this study. The testing was performed in an unconstrained six-degree of freedom testing apparatus, using the methods of McClure (1998). Each subject was fitted and tested sequentially with three collars manufactured by the Philadelphia Collar Company; the NecLoc®,Flat-2-Piece®, and the C-Loc®, and then was tested without a collar, to serve as a control. The testing was performed passively by an operator, and motion in each direction (left and right lateral bending, flexion, extension, and left and right axial rotation) was repeated five times. The resulting ROM and flexibility data was then subjected to a repeated measures ANOVA (RMANOVA) test, followed by a Fisher's PLSD post-hoc test to determine statistical significance (P-value <0.05).

Results and Discussion

Lateral bending: All three cervical collars produced either statistically significant reduction in range of motion or statistically significant passive support (decreased flexibility). There were no statistically significant differences between the braces in these functions. However, the Flat-2-Piece collar provided the most reduction in ROM as well as the most passive support.

Flexion: All three collars produced statistically significant reduction in range of motion without providing statistically significant support to the cervical spine. The C-Loc brace provided the most ROM reduction as well as passive support, with no statistically significant passive stabilization differences between braces.

Extension: None of the braces limited range of motion in a statistically significant way or provided statistically significant passive support in this direction. However, the 2-Piece collar did provide the most ROM reduction as well as passive support.

Axial rotation: All cervical collars limited range of motion and provided passive support in a statistically significant way. There were no statistically significant differences between the braces, with the Flat-2-piece and NecLoc collars providing more passive stabilization than the C-Loc collar.

Summary

Many previous studies, examined only the limitation in range of motion provided by cervical collars (Lee, 1998,Lunsford, 1994), in this study, both the limitation in range of motion and the amount of passive support provided by the cervical collar were quantified. The study revealed that some cervical collars significantly limit range of motion and increase passive support to the cervical spine. However, there are significant differences between collars and it is therefore recommended that these features be seriously considered by clinicians when prescribing cervical collars to their patients. This is particularly important when collars are used as a preventative measure, rather than as a “reminder” that the patient needs to protect their neck.

References

Alaranta, H., et al. (1994). *Scand J. Rehabil Med*, **26**
Beavis, A. (1989), *Prosthet Orthot Int.***6**
Fisher S.V., et al. (1977). *Arch Phys Med Rehabil*, **58**
Lee, T.T., et al. (1998) *Spine*, **18**
Lunsford, et al.(1994) *J Prosthetics and Orthotics*, **6**
McClure, P., et al. (1998). *Spine*, **23**

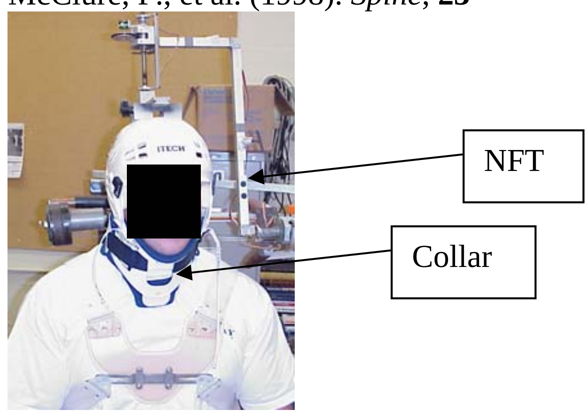

Figure 1: Photograph of a subject wearing a cervical collar and situated in the NFT.

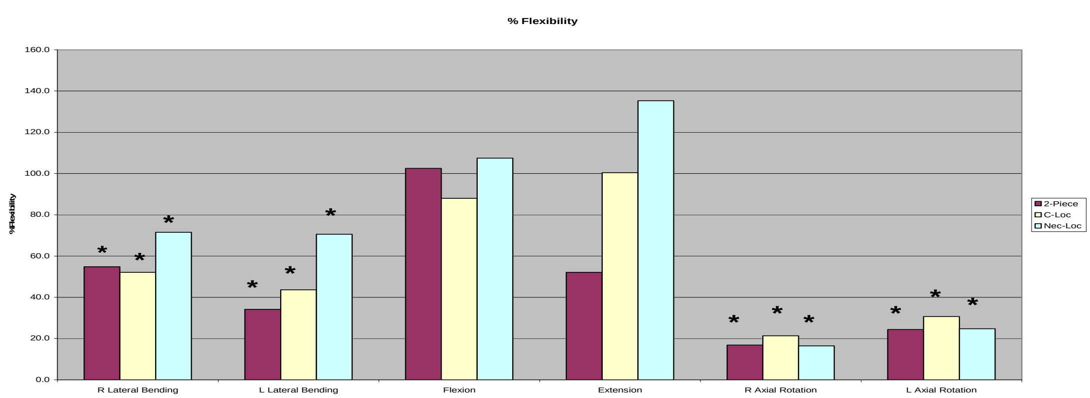

Figure 2 – Comparison between the braces in terms of percentage of unbraced flexibility (* indicates statistical significance)

RELIABILITY OF A KINEMATIC MODEL OF THE UPPER EXTREMITY

Kristof Kipp, B.S., Michelle Sabick, Ph.D., Mark DeBeliso, Ph.D.

Center for Orthopedic and Biomechanics Research, Boise State University,
Boise, Idaho, USA
E-mail: MSabick@boisestate.edu Web: http://coen.boisestate.edu/cobr

INTRODUCTION

In an effort to expedite comparison and exchange of upper extremity motion data, the Standardization and Terminology Committee of the International Society of Biomechanics (ISB) has put forth recommendations for the use of standardized Joint Coordinate Systems for the shoulder, elbow, and wrist (van der Helm et al, in press). The purpose of this study was to establish the reliability of joint angle measurements using a simplified version of the standardized JCS adapted for automated motion capture using surface markers. Measurements of isolated joint motions determined using both manual goniometry and the simplified JCS (sJCS) were compared to determine if the sJCS would produce joint angle measurements similar to those commonly obtained clinically.

METHODS

Five subjects performed isolated upper extremity joint movements in the cardinal planes of the body. Each subject performed twelve different movements corresponding to individual upper extremity joint rotational degrees of freedom. Each motion was performed twice. Total joint range of motion in each trial was measured using two techniques: (1) manually with a goniometer in accordance with the American Academy of Orthopedic Surgeon's guidelines (Greene and Heckman, 1994), and (2), calculated using the sJCS from the positions of retroreflective markers on the upper extremity tracked with an infrared motion capture system (Vicon Motion Systems, Lake Forest, CA).

The standardized JCS was adapted for automated motion capture by placing retroreflective markers on easily identifiable surface landmarks (Fig. 1). The originally proposed model was simplified by using the acromion process to estimate the location of the center of the humeral head. All other landmarks coincide with the standardized JCS and represent points that are used to estimate joint centers. Euler angles based on the sequences described in the standardized JCS were used to compute shoulder, elbow, and wrist joint angles for each movement.

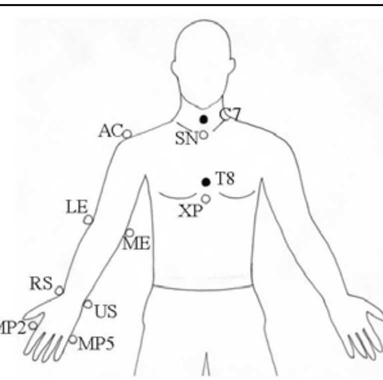

Figure 1. Surface marker locations.

The two sets of joint angle data were analyzed for repeatability and agreement using the methods of Bland and Altman (1986). The aim of the study was to determine if the sJCS angle measurements using surface markers would produce similar results to the clinical standard, goniometry.

RESULTS AND DISCUSSION

Goniometry: The intra-observer interclass reliability coefficient for all joints was r≥0.99. The mean and standard deviation (SD) of the intra-observer differences for all joints were -0.23± 3.3°. 93% of the intra-observer differences were within ± 2 SD of the mean difference.

sJCS: The interclass reliability coefficient for all joints was r≥0.99. The mean and SD of the differences for all joints was -1.8± 3.4°. 94% of the differences were within ± 2 SD of the mean difference.

Goniometry vs. sJCS: The interclass reliability coefficient between the two measurement techniques was r=0.95 (Fig. 2). The mean and SD of the technique differences for all joints was 13.6± 12.1°. 98% of the technique differences were within ± 2 SD of the mean difference.

These results show a high agreement between the two joint measurement techniques and suggest that the sJCS is suitable for the measurement of human upper extremity motion.

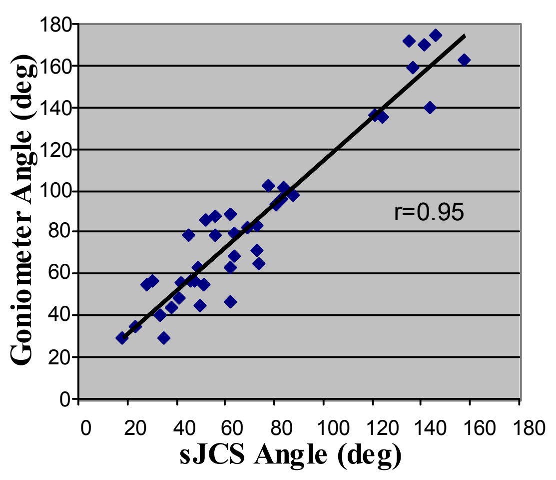

Figure 2. Correlation between goniometer and sJCS measurements of joint angle for all 13 upper extremity motions.

The goniometer generally produced greater range of motion values than did the sJCS method. The one exception was internal rotation of the humerus, where the sJCS measurements were greater. The maximum difference between techniques was 38° for shoulder abduction and the minimum difference was 1° for ulnar deviation.

Even though the acromion process was used to estimate the glenohumeral joint center, the shoulder angle measurements calculated using the sJCS were still significantly related to the goniometer measurements. For many applications, this simplification may be sufficiently accurate. Refining the methods for locating the shoulder joint center is a focus of our ongoing research.

SUMMARY

The simplified ISB Joint Coordinate System shows promise for use in upper extremity motion capture using surface markers. The landmarks used are prominent, easy to identify, and yield highly repeatable measures. A better method for identifying the shoulder joint center is still needed as the calculations using the acromion process to approximate the humeral head produced the greatest measurement variability.

REFERENCES

van der Helm, F.T.C. et al. (in press). *J. Biomechanics*

Greene, W.B., Heckman, J.D. (1994). The clinical measurement of joint motion. Amer. Acad. of Orthopaedic Surgeons.

Bland, J. M., Altman, D. G. (1986). *Lancet,* **1**, 307-310.

ACKNOWLEDGEMENTS

The authors would like to thank Kristin Bovey for her invaluable support.

EMG ACTIVITY OF LOWER LIMB MUSCLES DURING A MAXIMAL CYCLING TEST

Dimitris Katsavelis, Kris Berg, and Nick Stergiou
HPER Biomechanics Laboratory, University of Nebraska at Omaha
Email: nstergiou@mail.unomaha.edu Web: www.unocoe.unomaha.edu/hper.htm

INTRODUCTION

Electromyography (EMG) is a useful tool to analyze muscle activation patterns. It has recently received extensive attention investigating both dysfunctional and functional muscle activity related to cycling (Gregor et al., 1991).

Missiuro et al. (1962) suggested peripheral and central mechanisms of fatigue produced by intense exertion and low-intensity work, respectively. The same group of scientists showed that integrated electromyography (iEMG) from biceps and triceps grew steadily during intense physical exertion. On the other hand, Sacco et al. (1997) showed that both iEMG and power output decline during a cycling trial as result of the reduced recruitment of fatigued muscle. A fatigued muscle was also associated with reduced recruitment of synergistic muscles. In another study Takaishi et al. (1994) found that recruitment patterns were cadence dependent. Thus, different muscles were used at different cadences.

The purpose of the present study was to determine the contribution of vastus lateralis and rectus femoris during a maximal cycling test. It was hypothesized that iEMG will have declined until the last minute followed by an increase during the last minute, when the athletes will have forced themselves towards the end of the race.

METHODS

Five healthy competitive cyclists (4 males, and 1 female) participated. Subjects underwent a simulated five-minute race on a cycling ergometer (Figure 1). EMG data were collected using bipolar surface electrodes placed over two major muscles, the vastus lateralis and the rectus femoris. EMG activity was recorded at 600 Hz and analyzed by using a mathematical integration method. Subjects were also allowed to adjust their cadence and resistance throughout the five-minute test as they would while racing.

Figure 1: Cycle ergometer

RESULTS AND DISCUSSION

The results showed that even though the rectus femoris appeared to increase its activation during the test (table 1), a one-way ANOVA analysis of the iEMG activity revealed that activation in both muscles did not vary significantly in each of the five minutes of the test ($p \geq .05$). Additionally, the vastus lateralis was found to have more than twice the activation of the rectus femoris throughout the test.

Another finding of this study was that the number of bursts – or RPM - followed the pattern of the anticipated EMG activity. Indeed, the number of bursts (RPM) during the first minute was significantly higher ($p < .05$) than the rest of the minutes.

IEMG activity did not significantly alter as was anticipated. Therefore, no evidence of central fatigue was observed. The lack of significance change in iEMG might occured because subjects attempted to pace themselves throughout the test. The cadence and resistance adjustments were part of the strategy of each subject that resulted in high inter-subject variability. Moreover, the fact that the test was not performed in a competition setting may have also altered the behavior of the subject from a motivation perspective. A further explanation that might cause high inter-subject variability is the measurement of EMG itself, which is accompanied by subjectivity (Hunter et al., 2002).

SUMMARY

Competitive cyclists appeared to pace themselves in order to avoid early fatigue that might have inhibited their performance. Therefore, they maintained their effort as well as their output of muscle action potentials throughout the race. Vastus lateralis contributed more than rectus femoris during the race, however, an examination of all the knee extensors may reveal results that are more meaningful.

A further normalization of the EMG signal may also help to decrease inter-subject variability. More research is needed to describe the variation in cadence and resistance manipulation during high-intensity cycling.

REFERENCES

Gregor, R.J. et al. (1991). *Exerc. Sport Sci. Rev.* **19**, 127-169.
Hunter, A.M. et al. (2002). *Med. Sci. Sports Exerc.* **34**, 857-861.
Missiuro, W. et al. (1962). *Acta Physiol. Polon.* **13**, 11-23.
Sacco, P. et al. (1997). *Muscle Nerve*, **7**, 710-717.
Takaishi, T. et al. (1994). *Eur. J. Appl. Physiol.* **69**, 154-158.

Table 1: Group means of iEMG activity and RPM (SD).

	1st minute	2nd minute	3rd minute	4th minute	5th minute
Vastus Lateralis	30.40(±12.0)	29.85(±10.4)	28.08(±10.7)	29.52(±12.1)	30.09(±12.1)
Rectus Femoris	11.71(±7.8)	10.84(±6.5)	10.70(±8.1)	14.47(±16.7)	14.34(±16.9)
RPM	123(±12.0)	112(±12.0)	107(±12.0)	101(±12.0)	111(±12.0)

INDIVIDUAL CONTRIBUTIONS OF WEIGHT AND MASS TO THE METABOLIC COST OF WALKING

Alena Grabowski, Claire T. Farley, and Rodger Kram

Locomotion Laboratory, Dept. of Integrative Physiology, University of Colorado, Boulder, USA
E-mail: alena.grabowski@colorado.edu

INTRODUCTION

Three major mechanical factors affect the metabolic cost of walking: generating force to support body weight (Griffin et al. 2003) performing work to accelerate and redirect the center of mass from step-to-step (Donelan et al. 2002), and swinging the limbs. Previous walking studies have measured changes in metabolic cost attributable to mechanical manipulations such as reduced gravity, added load, and aiding propulsive force (Farley and McMahon 1992; Griffin et al. 2003; Gottschall and Kram 2003). However, it remains unclear how much *each* mechanical factor contributes to the overall metabolic cost of walking. In this study we examined how force and work contribute to the metabolic cost of walking by *independently* manipulating weight and mass. We used different combinations of simulated reduced gravity and added mass, while controlling leg swing. We hypothesized that body weight support and the work required to redirect and accelerate body mass *each* incur a substantial metabolic cost.

METHODS / PROTOCOL

Ten healthy adults volunteered to participate (5 male, 5 female, mass: 68.65 +/- 8.1kg, weight: 673.5 +/- 79.3N; mean +/- S.D.). Subjects performed a standing trial and 8 walking trials at 1.25 m/s on a motorized treadmill. Subjects walked normally (1.0M & 1.0BW; M=mass, BW=body weight), at three levels of simulated reduced gravity (1.0M & 0.75BW, 0.50BW, 0.25BW), and with two added loads (1.25M & 1.25BW, 1.50M & 1.50BW). Then, by combining reduced gravity and loading (1.25M & 1.0BW, 1.50M & 1.0BW) subjects walked at normal body weight with added mass. Trials were 7 minutes with 5 minutes of rest given between.

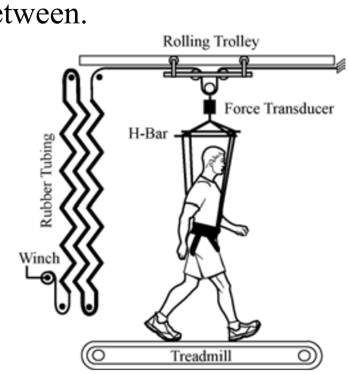

Figure 1: Reduced gravity apparatus.

We reduced body weight by applying a nearly constant upward force to the pelvis near the whole body center of mass (Fig. 1) as described by Griffin et al. (Griffin et al. 1999). We added loads by securing strips of lead symmetrically to a wide, well-padded belt that wrapped tightly around the subject's hips.

We measured oxygen consumption and carbon dioxide production rates for minutes 4-6 of each trial using an open-circuit respirometry system (Physio-Dyne Instrument, Quogue, NY), and calculated metabolic rates (Brockway 1987). Net metabolic rate was determined by subtracting standing metabolic rate from walking metabolic rates.

We compared metabolic rates across all conditions using a single factor repeated measures design (ANOVA). We used Newman-Keuls post hoc tests to determine statistical significance ($p \leq 0.05$).

RESULTS

Reducing only body weight resulted in a moderate, and less than proportional decrease in net metabolic rate (Fig. 2). Reducing weight by 25%, 50% and 75% decreased net metabolic rate by 3%, 11%, and 21%, respectively.

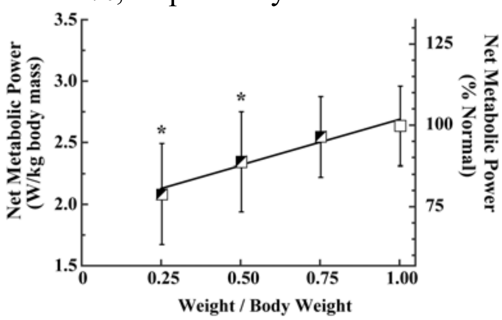

Figure 2: Net metabolic power walking normally (open) and in simulated reduced gravity (half-filled). Asterisk indicates significantly different from normal ($p \leq 0.05$).

Adding mass *and* weight resulted in a substantial and more than proportional increase in net metabolic rate (Fig. 3). Added loads equal to 25% and 50% of body weight and mass increased net metabolic rate by 39% and 98%, respectively. Adding mass *without* changing body weight resulted in a nearly proportional increase in net metabolic rate (Fig. 3). Added loads equal to 25% and 50% of body mass alone increased net metabolic rate by 18% and 48%, respectively.

DISCUSSION

We retain our hypothesis that body weight support and the work needed to redirect and accelerate body mass *each* incur a substantial metabolic cost. Our results from reduced gravity, and from added weight and mass are similar to previous studies. However, by separating the affects of weight and mass, we were able to distinguish the individual contributions of each. We found that the change in cost due to reduced weight is less than the change in cost due to added mass. Further, our results suggest that body weight support comprises approximately 28%, whereas center of mass work comprises approximately 49% of the net metabolic cost of walking.

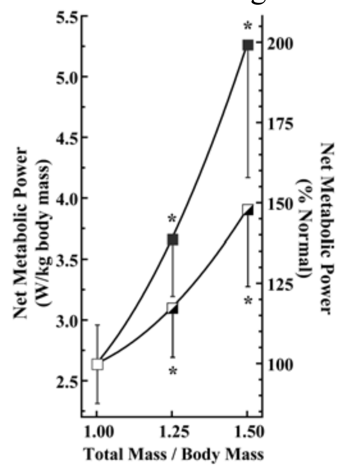

Figure 3: Net metabolic power walking normally (open), with added mass at normal body weight (half-filled), and with added mass and weight (filled). Asterisk indicates significantly different from normal ($p \leq 0.05$).

REFERENCES

Brockway, J.M. (1987). *Human Nutrition - Clinical Nutrition,* **41**(6): 463-71.

Donelan, J.M. (2002). *Journal of Exp. Biology,* **205**: 3717-27.

Farley, C.T. and T.A. McMahon (1992). - *Journal of Appl. Phys.,* **73**(6): 2709-12.

Gottschall, J.S. and R. Kram (2003). *Journal of Appl. Phys.,* **94**(5): 1766-72.

Griffin, T.M. et al. (2003). *Journal of Appl. Phys.,* **95**(1): 172-83.

Griffin, T.M. et al. (1999). *Journal of Appl. Phys.,* **86**(1): 383-90.

ACKNOWLEDGEMENTS

The National Institute of Arthritis and Musculoskeletal and Skin Diseases Grant AR-44688 supported this work.

RATE OF CHANGE OF CENTROIDAL ANGULAR MOMENTUM QUANTIFIES POSTURAL INSTABILITY

Ambarish Goswami
Honda Research Institute, Mountain View, CA 94041
E-mail: agoswami@honda-ri.com

ABSTRACT

Despite recent advances, the modeling, analysis, prediction and control of human postural stability remain a subject of much research interest. At the most fundamental level postural balance refers to the rotational stability of the overall human body. Based on the mechanics of multi-body systems, this paper suggests the use of $\dot{\boldsymbol{H}}_G$, the rate of change of centroidal angular momentum as a quantity for the general analysis of postural balance.

INTRODUCTION

Maintenance of stability is of central importance to the coordination of all human movements and interactions. Stability is a concept that appears to be easily understood but hard to define[2, 5]. Two extreme cases are easily identifiable: the static upright configuration which is solidly stable and an irreversible topple to the ground which is unquestionably unstable. Characterization of other cases, and especially ones involving non-ground interaction forces, are less straightforward.

To determine the stability one needs the joint positions, velocities and torques of the subject. Also needed are the frictional property of the foot/ground surface and the interaction forces from the environment. Given the large number of variables involved, efforts are often directed towards identifying a simple parameter that reflects the overall state of postural stability. This parameter then either becomes a measure of balance, or may play the role of a control parameter for balance maintenance system.

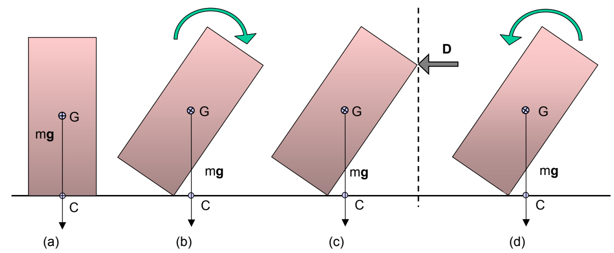

Figure 1: Stability evaluation based solely on the GCoM may lead to misleading results.

BACKGROUND

A static posture is said to be balanced[3] if the GCoM, the point on the ground through which the gravity line from the center of mass (CoM) passes, falls within the convex hull of the foot support area. Using this criterion, the block in Fig. 1a is stable and that in Fig. 1b is unstable.

Since GCoM depends only on the body configuration and not the velocity or forces, stability analysis based uniquely on the GCoM can often be misleading. As an example both the cases shown in Fig. 1c and 1b are characterized unstable, while in reality for 1c this characterization is incorrect and for 1d it is incomplete.

Center of pressure (CoP) rectifies the limitation of the GCoM point. However since CoP can never exit the support polygon, it does not provide any information about the degree of *instability*. The foot rotation indicator (FRI) point, which can leave the support polygon, extends the CoP concept in that it can additionally perform the role of an instability measure[1]. The FRI point, however, is defined only during the single support phase. Stability analysis based on $\dot{\boldsymbol{H}}_G$ does not suffer from the limitations of GCoM, CoP, and FRI point.

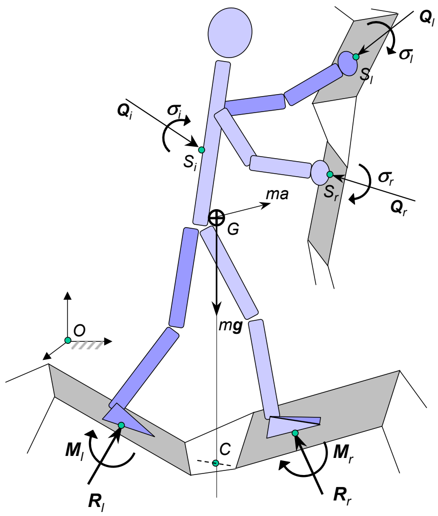

Figure 2: A general human/environment interaction scneario for postural stability. The person's feet are subjected to individual force/moment pairs $\boldsymbol{F}_l/\boldsymbol{M}_l$ (left foot) and $\boldsymbol{F}_r/\boldsymbol{M}_r$ (right foot). Interaction with the environment happens through force/moments $\boldsymbol{Q}_l/\boldsymbol{\sigma}_l$ at left hand and $\boldsymbol{Q}_r/\boldsymbol{\sigma}_r$ at right hand. There are other interaction force/torque $\boldsymbol{Q}_i/\boldsymbol{\sigma}_i$ active at any arbitrary point on the body. CoP is not well-defined, nor is GCoM in this case.

ANGULAR MOMENTUM

The equation for translational dynamic equilibrium can be written as:

$$\boldsymbol{R} + m\boldsymbol{g} + \boldsymbol{Q} = m\boldsymbol{a} \tag{1}$$

where $\boldsymbol{R} = \boldsymbol{R}_l + \boldsymbol{R}_r$, $m = \sum m_i$ is the total mass of the subject located at CoM, $\boldsymbol{Q} = \sum \boldsymbol{Q}_i$ is the resultant of all the external non-ground forces and $\boldsymbol{a}$ is the acceleration of the CoM. Eq. 1 can be solved for the magnitude and direction of $\boldsymbol{R}$ but not the location of its line of action. For that we need to solve the moment equation.
Taking moments about an arbitrary inertial point O, we have

$$\boldsymbol{M} + \boldsymbol{OP}_l \times \boldsymbol{R}_l + \boldsymbol{OP}_r \times \boldsymbol{R}_r + \boldsymbol{\sigma} + \sum \boldsymbol{OS}_i \times \boldsymbol{Q}_i + \boldsymbol{OG} \times m\boldsymbol{g} = \dot{\boldsymbol{H}}_G + \boldsymbol{OG} \times m\boldsymbol{a} \tag{2}$$

where $\dot{\boldsymbol{H}}_G$ is the overall centroidal angular momentum of the subject, $\boldsymbol{M} = \boldsymbol{M}_l + \boldsymbol{M}_r$, $\boldsymbol{\sigma} = \sum \boldsymbol{\sigma}_i$ and $\dot{\boldsymbol{H}}_G = \sum \dot{\boldsymbol{H}}_{Gi} + \sum \boldsymbol{GG}_i \times m_i \boldsymbol{a}_i$.

Taking moments about the CoM G, we have the simpler equation

$$\boldsymbol{M} + \boldsymbol{GP}_l \times \boldsymbol{R}_l + \boldsymbol{GP}_r \times \boldsymbol{R}_r + \boldsymbol{\sigma} + \sum \boldsymbol{GS}_i \times \boldsymbol{Q}_i = \dot{\boldsymbol{H}}_G \tag{3}$$

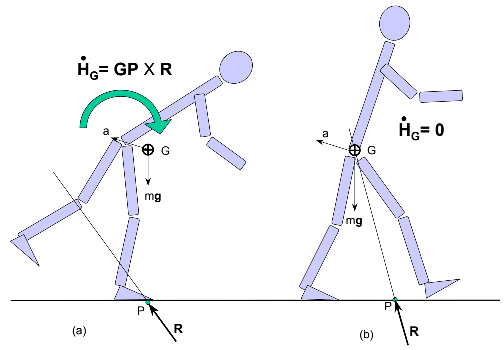

Figure 3: This figure describes the essence of stability analysis based on $\dot{\boldsymbol{H}}_G$. In Fig. 3a the resultant GRF, denoted by $\boldsymbol{R}$ passes through the CoM, denoted by G. This results in a zero $\dot{\boldsymbol{H}}_G$ and the person is rotationally stable. In Fig. 3b the GRF generates a net moment around the CoM and $\dot{\boldsymbol{H}}_G = \boldsymbol{GP} \times \boldsymbol{R}$. This non-zero $\dot{\boldsymbol{H}}_G$ signifies a tendency to tip-over.

which forms the basis of analysis and control of balance in human.

According to a fundamental principle of mechanics $\dot{\boldsymbol{H}}_G$ is equal to the resultant centroidal moment. A net zero centroidal moment implies rotational stability. Conversely, rotational instability implies a non-zero $\dot{\boldsymbol{H}}_G$ that occurs when the external forces and moments result in a non-zero centroidal moment. Fig. 3 schematically explains the essence of our approach when interaction forces arise only from the ground. Others have used angular momentum information to control motion of humanoid robots [4].

References

[1] A. Goswami. Postural stability of biped robots and the foot rotation indicator (FRI) point. *International Journal of Robotics Research*, 18(6):523–533, 1999.

[2] J. H. Jhoun. *Studies of human standing, stepping and gait initiation*. PhD thesis, Northwestern University, Evanston, IL, 1997.

[3] A. Patla, J. Frank, and D. Winter. Assessment of balance control in the elderly: Major issues. *Canadian Physiotherapy*, 42:89–97, 1990.

[4] A. Sano and J. Furusho. Realization of natural dynamic walking using the angular momentum information. In *IEEE International Conference on Robotics and Automation*, volume 3, pages 1476–1481, 1990, Cincinnati, OH.

[5] H. van der Kooij. *Human balance control in standing and walking*. PhD thesis, Universiteit Twente, Netherlands, 2000.

AGE-RELATED DIFFERENCES IN PEAK JOINT VELOCITIES DURING SINGLE STEP RECOVERY FROM A FORWARD FALL

Michael L. Madigan and Emily M. Lloyd

Musculoskeletal Biomechanics Laboratory, Virginia Tech, Blacksburg, VA, USA
E-mail: mlm@vt.edu   Web: www.biomechanics.esm.vt.edu

INTRODUCTION

Falls are among the most common and debilitating medical problems experienced by older adults. Previous research has shown that the ability to recover from a forward fall with a single step depends largely on maximum stepping speed. Wojcik et al. (1999), for example, reported a strong correlation between stepping speed and the ability to recover from a forward fall. Thelen et al. (1997) suggested that the maximum stepping speed is lower in older adults compared to young, and this lower stepping speed limits the ability of older adults to recover from falls. An age-related reduction in maximum stepping speed could potentially be caused by a localized reduction in peak joint velocity at an individual joint (i.e. hip, knee, or ankle), and/or in a specific movement direction (i.e. flexion or extension). Knowing this may allow training and rehabilitation routines aimed at fall prevention to focus on joints and/or movements most critical to fall recovery, and may improve their efficacy. Therefore, the purpose of this study was to evaluate age-related differences in peak joint velocities of the stepping limb during single step recovery from a forward fall.

METHODS

A total of twenty male subjects participated, including 10 young (19-23 years, mean 20.6 years) and 10 older (65-83 years, mean 74 years) adults. The tripping protocol was adapted from Thelen et al. (1997). Subjects were released from a forward-leaning posture and asked to recover their balance using a single step of the right leg. Upon successful recovery, the lean was increased and the process repeated until subjects failed twice at a single lean. Failure criteria are described in Wojcik et al. (1999). Lean magnitude was quantified by measuring the tension in a cable used to hold the subjects in the forward-leaning posture. This tension was measured as percent body weight (BW). The initial lean angle was 12% BW and increments were 4% BW.

During recoveries, body position data were sampled at 200Hz using an OPTOTRAK 3020 motion analysis system (NDI, Waterloo, Ontario). Forceplate data was also collected for other analyses. Using the body position data, sagittal plane joint velocities were calculated in flexion and extension at the hip, knee, and ankle of the stepping leg. Peak velocities in each of these movements were determined for the time interval between release to the instant that the stepping leg contacted the floor.

To determine if peak joint velocities vary with age and lean magnitude, a multiple regression analysis was used. Independent variables included lean, lean^2, AGE (a dummy variable equal to 0 for young subjects and 1 for older subjects), and AGE*lean. Regression coefficients significantly different from zero ($p<0.05$) indicated which independent variables made a significant contribution to the prediction of peak joint velocity. Independent *t*-tests were used to determine if peak joint velocities used during recovery from each subject's largest achieved lean magnitude differed between age groups.

RESULTS AND DISCUSSION

Representative joint velocities during a typical recovery are shown in Figure 1. General observations of the data indicate peak joint velocities during single step recoveries were highest at the knee (in both flexion and extension), followed by hip flexion and ankle plantar flexion. Peak joint velocities in ankle dorsiflexion and hip extension were similar. Peak joint velocities exhibited a significant increase as lean magnitude increased, with the exception of peak ankle dorsiflexion velocity and peak hip extension velocity. No 'AGE' coefficients in the multiple regression equations were significant, indicating there were no age-related differences in peak joint velocities between age groups while holding lean magnitude constant. However, during recovery from each subject's largest achieved lean magnitude, older adults exhibited slower peak hip flexion velocity, peak knee flexion velocity, peak knee extension velocity, and peak ankle plantar flexor velocity (Table 1).

These differences imply that the maximum speed at which older adults can flex their hips, flex their knees, extend their knees, and plantarflex their ankles is lower than

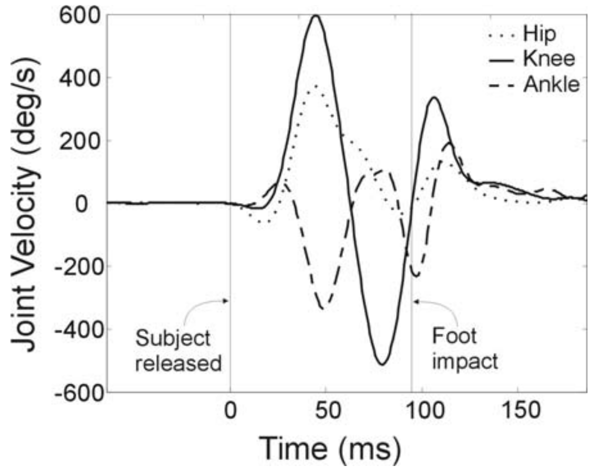

Figure 1: Representative joint velocities during a single step recovery. Positive values correspond to flexion (d-flexion).

young adults. Furthermore, these smaller velocities may be causally-related to the lower maximum lean achieved by older subjects.

SUMMARY

Our results suggest the previously reported age-related reduction in stepping speed results from an age-related reduction in peak hip flexion velocity, knee flexion and extension velocity, and ankle plantar flexion velocity.

REFERENCES

Thelen, D.G. et al. (1997). *J. Gerontol Med Sci.*, **52A**, M8-M13.

Wojcik, L.A. et al. (1999). *J. Gerontol Med Sci.*, **54A**, M44-M50

Table 1. Peak Joint Velocities at Maximum Leans

	Young	Older	
Peak Hip Flexion Velocity (deg/s)	475.2 (72.0)	348.7 (53.2)	*
Peak Hip Extension Velocity (deg/s)	104.6 (51.9)	106.6 (37.3)	
Peak Knee Flexion Velocity (deg/s)	698.3 (43.9)	488.0 (99.7)	*
Peak Knee Extension Velocity (deg/s)	713.5 (80.0)	534.9 (134.0)	†
Peak Ankle D-flexion Velocity (deg/s)	96.6 (48.0)	107.1 (33.4)	
Peak Ankle P-flexion Velocity (deg/s)	354.4 (56.4)	256.0 (35.7)	*

Notes: Values are means (standard deviation). * p<0.001 † p=0.002

A NOVEL DEVICE FOR CALIBRATING SHEET ARRAY PRESSURE SENSORS AND FOR MONITORING THEIR PERFORMANCE

Thomas E. Baer[1], Douglas R. Pedersen[1,2], M. James Rudert[1], Nicole A.Vos[2], Nicole M. Grosland[1,2], Thomas D. Brown[1,2]
[1]Department of Orthopaedics and Rehabilitation, [2]Department of Biomedical Engineering, University of Iowa
Email: thomas-baer@uiowa.edu

INTRODUCTION

Sheet array pressure sensors are used widely in biomechanical research, as well as in a variety of industrial settings, to measure interfacial contact stress in real time and with relatively high spatial resolution.

Sensors of this class generally consist of an array of electrical junctions between two sheets of thin, flexible plastic. Pressure on the sheets changes the electrical characteristics (*e.g.,* piezoresistivity, in the case of Tekscan®) of each junction, which is then interpreted according to a user-generated calibration curve and reported as an instantaneous contact stress value.

Accurate calibration of such sensors has often been problematic, however, due to the inherent difficulty of applying a suitably well-prescribed force distribution over the sensing area. Furthermore, applying enough force to load the entire sensor surface suitably into the functional regime for calibration purposes is impractical (*e.g.,* roughly 40 KN to reach 50% of the functional range in the case of the Tekscan® K-Scan knee sensor). Adding to the complexity of the problem is significant variation within the array on any given sensor and, by extension, from sensor to sensor. Further, during a typical experimental protocol, this variability may be exacerbated by functionally induced changes in the responses of individual elements.

THE DEVICE

To meet these challenges, a novel "wringer" device (**Fig. 1**) was built to transiently apply a known force to sequential rows of junctions as the sensor is passed between a pair of rollers.

Figure 1. Sheet Array Sensor Calibrator

A Shore 75D polyurethane rubber was identified as a material suitable to distribute the load over multiple rows of junctions, while being rigid enough to load the center row of the contact patch with enough force to achieve stresses substantially spanning the physically expected range.

The rollers were compressed against one another by an air cylinder. They were linked by gears so that they rotated at the same rate (but in opposite directions) to minimize shear stress on the surface of the sensor.

CALIBRATION PROCEDURE

Data Capture

The sensor is positioned between the rollers and a given load applied. The sensor is drawn slowly through the rollers and raw data are captured. The process is repeated for a range of roller compression loads.

The Computation

To convert raw values to calibrated pressures requires a computation of stress at each individual junction. A finite element model of the two parallel cylinders in contact was used to determine the load borne by the junctions in rows about the center of the contact patch.

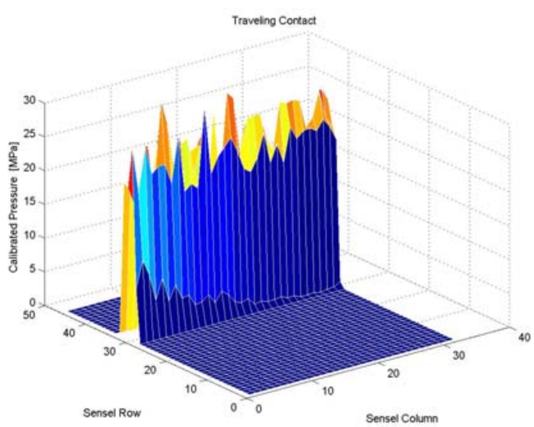

Figure 2. Transient response signal during roller loading

Each capture was post-processed using Matlab®. In an iterative process, the applied roller load was initially assumed to follow the FEA distribution for each level of roller load. These data were used to fit provisional power-law calibration curves. This in turn provided "traveling" waves of contact stress (**Fig. 2**), which could be integrated and compared with the applied roller force. This comparison generated an error signal, by means of which the fitted calibration coefficients could be iteratively adjusted so as to return an integrated load asymptotically closer to the applied roller force. The end result was an array of location-specific calibration curves of algebraically consistent form (**Fig. 3**). Sensor sites departing appreciably from these calibration norms were flagged as performing aberrantly (*e.g.,* due to local damage), a basis for not including their readings in the functional data stream.

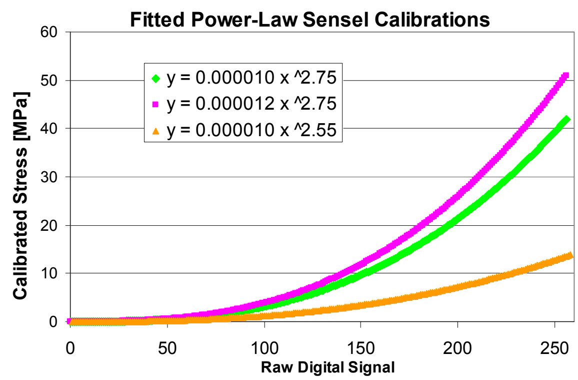

Figure 3. Iterated Power-Law Calibration curves for 3 specific sensor junctions

MONITORING

The device was designed so that the sensor can be removed from an experimental environment (*e.g.,* a cadaveric joint), passed between the rollers for evaluation, and returned to the experimental setting quickly and with a minimum of disturbance of the test setup. Logging the response of each junction to known loads over the course of the experiment makes it possible to accurately correct the data for both global and localized changes in sensor performance.

CONCLUSION

A new device and method are shown to be applicable to sheet array pressure sensors. The device both calibrates and monitors the performance of each individual sensing element in the array.

ACKNOWLEDGEMENTS

Financial support provided by:
NIH grant 5 P50 AR048939
CDC grant R49 CCR721745

EFFECT OF WEARING A WRIST SPLINT ON SHOULDER POSTURE WHEN PICKING AN OBJECT FROM A BOX

Amy G. Mell and Richard E. Hughes

Department of Orthopaedic Surgery
University of Michigan, Ann Arbor, MI USA
E-mail: rehughes@umich.edu

INTRODUCTION

Reducing wrist motion may affect shoulder motion because of the kinematic interdependence of the joints of the upper extremity. Previous reports have suggested that wearing a wrist splint can affect shoulder posture during activities of daily living (Adams et al., 2003). Many occupational tasks require reaching into boxes to retrieve objects. Understanding whether wearing a wrist splint affects shoulder posture is clinically important because patients being conservatively treated for hand/wrist disorders often return with shoulder disorders. A scientific analysis of the interrelationship between wrist splint use and risk factors for shoulder disorders is necessary to assist in determining whether the shoulder pain may be caused by the conservative treatment of the hand/wrist disorder.

The objective of this study was to test the hypothesis that wearing a flexible wrist splint while picking an object from a box increases known postural risk factors for shoulder disorders. A secondary hypothesis was that the height of the front of the box modulated the effect of wearing a wrist splint on shoulder kinematics.

MATERIALS AND METHODS

Ten healthy volunteers participated in the study. Each study participant was asked to grasp a plastic ball in a box (figure 1) and move it to a tube that returned the ball to its original position. This task was completed five time for each test condition. A wooden dowel was placed at four heights at the front of the box (2.5, 5, and 7.5 cm) to experimentally control the front barrier height. One test condition did not have any dowel at all. Two splint conditions were tested (wearing a large Donjoy Orthopaedics wrist splint and not wearing a splint). Therefore, there were eight experimental conditions, and each study participant completed each test condition. The order of test conditions was randomized for each study participant.

Figure 1. Study participant reaching into box while wearing wrist splint. Kinematics were measured using MotionStar tracking system.

Data were collected using a MotionStar electromagnetic tracking system using MotionMonitor data acquisition software. Sampling rate was 100 Hz. Data were smoothed using a two-way low-pass fourth order Butterworth filter with an 8 Hz cutoff frequency. Digitized landmarks were used to construct anatomic coordinate systems, and these were represented in the local coordinate systems of each electromagnetic sensor. The anatomic coordinate systems used were those proposed by van der Helm and Pronk (1995). At each point in time, the anatomic coordinate systems were rotated using the rotation matrices of the electromagnetic sensors. Euler angles were computed using the sequences proposed by van der Helm and Pronk (1995).

A repeated measures two-way ANOVA model was used to test for the effect of wearing a wrist splint and barrier height on minimum (and maximum) humeral elevation, plane of elevation, and axial rotation.

RESULTS

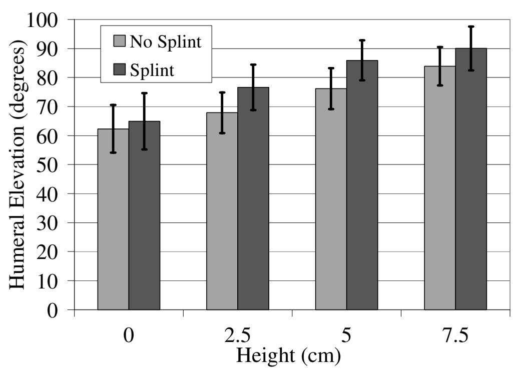

Figure 2. Mean (S.D.) humeral elevation angles with and without a wrist splint for four barrier heights.

Wearing a wrist splint increased the maximum humeral elevation angle ($p<0.001$), and the height of the barrier also increased the maximum humeral elevation angle ($p<0.001$). The mean maximum humeral elevation angle was lowest for the no splint and no barrier condition (62.3 ^{o}), and it was highest when reaching over the highest barrier with a splint (90.0 ^{o}) (figure 2). The average difference in maximum humeral elevation between the splint and no splint conditions was 6.8^o. No statistically significant interaction between wrist splint and barrier height was found ($p=0.463$). No statistically significant effects were found for minimum elevation angle.

Wearing a wrist splint also increased maximum axial rotation ($p<0.001$), and higher barriers caused increased maximum axial rotation ($p<0.001$). Maximum plane of elevation, which represents how far forward the humerus is, was decreased by both wearing a splint ($p<0.001$) and height of the barrier ($p<0.001$). In contrast to the other two measures, the minimum of the plane of elevation was also reduced by wearing a splint ($p<0.001$) and decreased with increasing barrier height ($p=0.028$).

DISCUSSION

Our data suggest that wearing a wrist splint while reaching into a box may increase the likelihood of shoulder injury. Epidemiological studies have shown that elevated arm postures is a risk factors for shoulder pain, including rotator cuff pathology. Punnett et al. (2000) showed, for example, that elevated humeral postures were associated with shoulder disorders in automobile assembly work. Therefore, an increase in humeral elevation, which was produced by wearing a wrist splint, increases the risk of a shoulder disorder. Unfortunately, however, the epidemiological data is unclear about how much increase in risk results from the magnitude of elevation increase found in our study.

REFERENCES

Adams, B.D. et al. (2003) *J. Hand Surg*. 28A, 898-903.
Punnett, L. et al. (2000) *Scand. J. Work, Env. & Health*, 26, 283-291.
van der Helm, F.C.T. and Pronk, G.M. (1995) *J. Biomech. Eng.*, **117**, 27-40.

TEMPERATURE DEPENDENCE OF CROSSBRIDGE KINETICS IN SLOW AND FAST SKELETAL MUSCLE FIBERS: CROSSBRIDGE MODELING

Sampath K. Gollapudi[1] and David C. Lin[1,2,3]

[1]Dept. of Mechanical and Materials Engineering, [2]Programs in Bioengineering and Neuroscience, [3]Dept. of Veterinary and Comparative Anatomy, Pharmacology and Physiology, Washington State Univ., Pullman, WA, USA
Email: sampath@vetmed.wsu.edu

INTRODUCTION

Temperature dependence of crossbridge kinetics in skeletal muscle fibers has long been of interest to biophysics researchers. Depending on the type of the muscle fiber, *i.e.*, slow or fast, the biochemical and mechanical properties of the fibers are influenced by the changes in temperature in a different way (Zhao and Kawai, 1994; Wang and Kawai, 2001; Ranatunga, 1996; Ranatunga *et al*., 2001). Namely, the Q_{10} for slow fibers is usually greater than for fast fibers. These studies have established that these differences are due to variations in the chemical kinetics of the crossbridge cycle. This information can bridge the vast amount of single fiber data (usually done at lower temperatures) to *in vivo* function (> 35 ^{0}C). However, all these studies employed complex multi-state crossbridge models for analysis, mostly in the isometric condition. These models are difficult to implement for more macroscopic applications, especially for shortening and lengthening contractions.

This study aims to model the temperature dependent mechanical properties of slow and fast-twitch fibers based on the current available biophysical data from skeletal muscle fibers. One such potential model is Huxley's two-state crossbridge muscle model with the Distribution-Moment (DM) approximation (Zahalak, 1981). Ultimately, this research will determine whether a simplified crossbridge model can be used to study the mechanical properties of single fibers at *in vivo* temperatures by using the experimental data from distinct fiber types obtained at lower temperatures.

METHODS

The DM approximation of the crossbridge model was employed to estimate the bond distribution function, $n(x, t)$, where n is the fraction of attached crossbridges, x is crossbridge extension, and t is time. The DM model parameters represent the biophysical processes of muscle contraction, namely the attachment rate, $f(x)$, and the detachment rate, $g(x)$, of the crossbridges. In the case of an isometric contraction, the crossbridge distribution function reduces to: $n = f / (f+g)$ and therefore the isometric force, F_0 ($\propto n$) can be directly estimated. The effect of temperature on the parameter f is quite significant, whereas the parameter g is temperature independent (Zhao and Kawai, 1994). Table 1 provides the list of Q_{10} and g values considered for the fast (rabbit Psoas) fibers obtained from the literature. The values of Q_{10} and g used for slow (rabbit Soleus) fibers are 3 and 2 s^{-1} respectively.

Table 1. Parameters for Psoas Fibers

	Temperature Range, (^{0}C)	Q_{10} for f	g (s^{-1})
Model 1	7 - 32	3.0	10
Model 2	5 - 30	3.3	15
Model 3	5 - 20	8.0	15
	20 - 30	3.3	15

RESULTS AND DISCUSSION

The normalized isometric force as a function of temperature for rabbit Psoas and Soleus fibers are shown in figures 1 and 2. The simulated force response and the experimental data for rabbit Psoas (figure 1) and Soleus (figure 2) fibers were all superimposed on the same plot to validate the setting of DM model parameters. From the figure 1 (rabbit Psoas), it is evident that the simulated response of Model 2 closely approximates the experimental curve provided by Zhao and Kawai, whereas the simulated response of Model 3 closely replicates the one provided by Ranatunga. These simulations revealed that this approach can reasonably well predict the isometric force generating properties over a wide range of temperatures. The results shown here pertain to the isometric condition, but the same approach will be extended to study the crossbridge kinetics in shortening contractions. Specifically, the experimental data of ATPase kinetics and

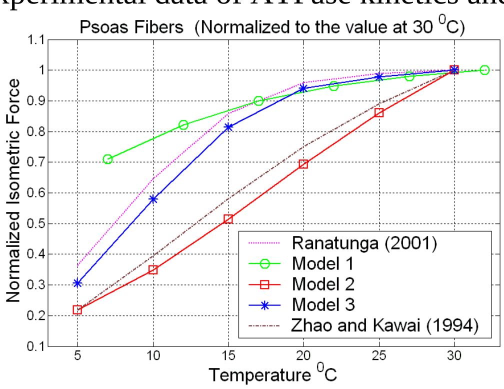

Figure 1. Normalized force vs. temperature curves for Psoas fibers

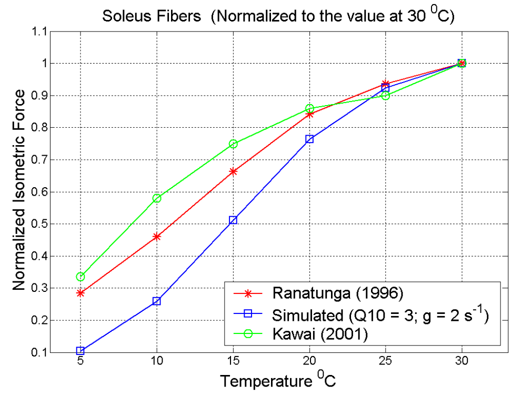

Figure 2. Normalized force vs. temperature curves for Soleus fibers

force-velocity changes with temperature will be used to estimate and confirm detachment kinetics for negatively strained crossbridges.

SUMMARY

A simplified crossbridge model with distribution moment approximation was employed to tie the biophysical experimental data to macroscopic force predictions. Correspondence of simulations to data in the literature was obtained to justify the crossbridge model.

REFERENCES

Zhao, Y. and Kawai, M. (1994), *Biophys. J.* **67**(4): p. 1655-1668.

Wang, G. and Kawai, M. (2001), *J Physiol (Lond)*, **531**(1): p. 219-234.

Coupland, M.E., Puchert. E., and Ranatunga, K.W. (2001), *J Physiol (Lond)*, **536**(3): p. 879-891.

Ranatunga, K. (1996), *Biophys. J.*, **71**(4): p. 1905-1913.

Zahalak, G. I. (1981), *Mathematical Biosciences*. **55**: p. 89-114

ACKNOWLEDGEMENTS

Support provided by the Whitaker Foundation

NEUROMUSCULAR RESPONSE TO UNEXPECTED GAIT PERTURBATIONS IN ANTERIOR CRUCIATE LIGAMENT INJURED NON-COPERS

Reed Ferber,[1] Janet L. Ronsky,[1] Vincent von Tscharner,[1] and Louis R. Osternig [2]

[1] Human Performance Laboratory, Faculty of Kinesiology, University of Calgary, AB, Canada
[2] Department of Exercise and Movement Science, University of Oregon, Eugene, OR, USA
E-mail: rferber@kin.ucalgary.ca Web: www.kin.ucalgary.ca/hpl

INTRODUCTION

Anterior cruciate ligament deficient (ACLD) patients who achieve only low to moderate levels of functional recovery after ACL rupture and experience knee instability are referred to as non-copers (Fitzgerald et al., 2000). The inability to react to gait perturbations and stabilize their injured knee through muscle activation may be the result of neuromuscular reprogramming following ACL injury. Few studies have investigated how ACLD non-copers react to unexpected perturbations while walking (Ferber et al, 2002). It was reported that ACLD non-copers exhibit potentially injurious lower extremity joint moments to stabilize their knee in response to the perturbation. However, the muscle electromyographic (EMG) patterns which produced these joint moments were not reported.

Changes in EMG intensity and frequency have been shown to correspond with slow and fast motor unit activation when analyzed using a wavelet analysis technique (Wakeling et al., 2001). This technique may provide insight as to why ACLD non-copers exhibit knee instability during unexpected gait perturbations. Therefore, the purpose of this study was to examine the EMG response patterns of ACLD non-copers in response to unexpected gait perturbations using a wavelet analysis technique compared to non-injured controls

METHODS

Ten (5 males and 5 females) ACLD non-copers were compared with 10 (5 males and 5 females) non-injured, age and gender-matched control (CON) adult subjects. The ACLD subjects had sustained an isolated unilateral ACL injury more than 2 years prior to testing (5.7 ± 5.1 yr) which was confirmed by an orthopedic surgeon. All ACLD subjects exhibited at least one episode of knee joint instability (“giving way”) and were thus classified as non-copers (Fitzgerald et al., 2000).

Subjects walked along a 5 m wooden walkway in which a force plate, capable of translational movement, was embedded. The force plate moved forward or backwards a distance of 10 cm at a velocity of 40 cm/s upon heel contact. A total of 36 trials were collected consisting of 12 forward perturbations (FP), 12 non-perturbation, and 12 backward perturbation trials. The backward and non-perturbation trials, along with the random order of trials, were used to help prevent possible accommodation and anticipation of the FP condition.

EMG data were collected using bipolar surface electrodes (DE-02, Delsys, Boston, MA, USA). The electrodes were placed on the skin overlying the muscle belly of the biceps femoris (BF) and vastus lateralis (VL). EMG signals were resolved into time-frequency space using wavelet analysis (von

Tscharner, 2000) and then averaged across the 12 trials for the FP condition. A set of 13 wavelets were used with a center frequency ranging from 7 Hz (wavelet 0) to 542 Hz (wavelet 12). These data were pooled into high (180-220 Hz: wavelet 6-8: fast motor units) and low (25-60 Hz: wavelet 2-3: slow motor units) frequency bands.

RESULTS AND DISCUSSION

The CON subjects exhibited a typical slow-to-fast motor unit recruitment pattern and a primary slow twitch response in magnitude for both the BF (Fig 1) and VL. The ACLD non-copers demonstrated a similar slow-to-fast motor unit response for the VL muscle but exhibited a very atypical pattern of VL activation. Similar to CON, the initial ACLD VL response was 200 msec after heel strike but was significantly reduced in magnitude compared to the control group. In addition, the primary quadriceps response for the ACLD non-copers was observed significantly later in stance (300 msec after heel strike) and a third reactive response was observed 400 msec after heel strike.

The ACLD non coper BF response was even more distinct from the CON group in that a graded motor unit response pattern was not observed but a significantly greater fast motor unit response in magnitude around 150 msec after heel strike (Fig 1). A second BF muscle activation burst at 250 msec was required possibly for additional neuromuscular control. Several additional bursts of BF activation for both slow and fast motor units were also observed following the initial burst for the ACLD group whereas the CON group exhibited a single reactive BF activation (Fig 1).

SUMMARY

The ACLD non-copers did not exhibit 1) a graded response pattern for the slow and fast motor units, 2) a primary slow motor unit response of the BF muscle, or 3) a co-activation response in either timing or magnitude for the BF or VL muscles as compared to CON. The response pattern exhibited by the ACLD non-copers may be a mechanism that partially explains why they are unable to sufficiently stabilize their knee.

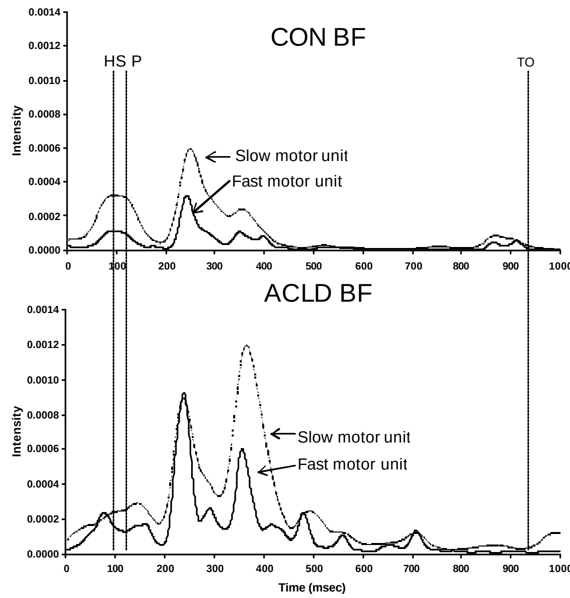

Figure 1: Biceps femoris fast and slow motor unit activation patterns for the CON and ACLD group. The vertical lines indicate heel strike (HS), onset of the perturbation (P), and toe off (TO).

REFERENCES

Ferber, R, et al. (2002). *Clin Biomech* **18**(2), 132-141.

Fitzgerald, G.K. et al. (2000). *Knee Surg Sports Traum*, **8**, 76-82.

von Tscharner, V. (2000). *J. Electromyogr. Kinesiol*. **10**, 433-445.

Wakeling, J.M. (2001). *Eur J App Phys*, **86**, 40-47.

ACKNOWLEDGEMENTS

This study has been supported, in part, by the ISB, the NATA REF (399-I007), and the Eugene Evonuk Foundation.

NEUROMUSCULAR RESPONSE TO UNEXPECTED GAIT PERTURBATIONS IN ANTERIOR CRUCIATE LIGAMENT INJURED NON-COPERS

Reed Ferber,[1] Janet L. Ronsky,[1] Vincent von Tscharner,[1] and Louis R. Osternig [2]

[1] Human Performance Laboratory, Faculty of Kinesiology, University of Calgary, AB, Canada
[2] Department of Exercise and Movement Science, University of Oregon, Eugene, OR, USA
E-mail: rferber@kin.ucalgary.ca Web: www.kin.ucalgary.ca/hpl

INTRODUCTION

Anterior cruciate ligament deficient (ACLD) patients who achieve only low to moderate levels of functional recovery after ACL rupture and experience knee instability are referred to as non-copers (Fitzgerald et al., 2000). The inability to react to gait perturbations and stabilize their injured knee through muscle activation may be the result of neuromuscular reprogramming following ACL injury. Few studies have investigated how ACLD non-copers react to unexpected perturbations while walking (Ferber et al, 2002). It was reported that ACLD non-copers exhibit potentially injurious lower extremity joint moments to stabilize their knee in response to the perturbation. However, the muscle electromyographic (EMG) patterns which produced these joint moments were not reported.

Changes in EMG intensity and frequency have been shown to correspond with slow and fast motor unit activation when analyzed using a wavelet analysis technique (Wakeling et al., 2001). This technique may provide insight as to why ACLD non-copers exhibit knee instability during unexpected gait perturbations. Therefore, the purpose of this study was to examine the EMG response patterns of ACLD non-copers in response to unexpected gait perturbations using a wavelet analysis technique compared to non-injured controls

METHODS

Ten (5 males and 5 females) ACLD non-copers were compared with 10 (5 males and 5 females) non-injured, age and gender-matched control (CON) adult subjects. The ACLD subjects had sustained an isolated unilateral ACL injury more than 2 years prior to testing (5.7 ± 5.1 yr) which was confirmed by an orthopedic surgeon. All ACLD subjects exhibited at least one episode of knee joint instability (“giving way”) and were thus classified as non-copers (Fitzgerald et al., 2000).

Subjects walked along a 5 m wooden walkway in which a force plate, capable of translational movement, was embedded. The force plate moved forward or backwards a distance of 10 cm at a velocity of 40 cm/s upon heel contact. A total of 36 trials were collected consisting of 12 forward perturbations (FP), 12 non-perturbation, and 12 backward perturbation trials. The backward and non-perturbation trials, along with the random order of trials, were used to help prevent possible accommodation and anticipation of the FP condition.

EMG data were collected using bipolar surface electrodes (DE-02, Delsys, Boston, MA, USA). The electrodes were placed on the skin overlying the muscle belly of the biceps femoris (BF) and vastus lateralis (VL). EMG signals were resolved into time-frequency space using wavelet analysis (von

Tscharner, 2000) and then averaged across the 12 trials for the FP condition. A set of 13 wavelets were used with a center frequency ranging from 7 Hz (wavelet 0) to 542 Hz (wavelet 12). These data were pooled into high (180-220 Hz: wavelet 6-8: fast motor units) and low (25-60 Hz: wavelet 2-3: slow motor units) frequency bands.

RESULTS AND DISCUSSION

The CON subjects exhibited a typical slow-to-fast motor unit recruitment pattern and a primary slow twitch response in magnitude for both the BF (Fig 1) and VL. The ACLD non-copers demonstrated a similar slow-to-fast motor unit response for the VL muscle but exhibited a very atypical pattern of VL activation. Similar to CON, the initial ACLD VL response was 200 msec after heel strike but was significantly reduced in magnitude compared to the control group. In addition, the primary quadriceps response for the ACLD non-copers was observed significantly later in stance (300 msec after heel strike) and a third reactive response was observed 400 msec after heel strike.

The ACLD non coper BF response was even more distinct from the CON group in that a graded motor unit response pattern was not observed but a significantly greater fast motor unit response in magnitude around 150 msec after heel strike (Fig 1). A second BF muscle activation burst at 250 msec was required possibly for additional neuromuscular control. Several additional bursts of BF activation for both slow and fast motor units were also observed following the initial burst for the ACLD group whereas the CON group exhibited a single reactive BF activation (Fig 1).

SUMMARY

The ACLD non-copers did not exhibit 1) a graded response pattern for the slow and fast motor units, 2) a primary slow motor unit response of the BF muscle, or 3) a co-activation response in either timing or magnitude for the BF or VL muscles as compared to CON. The response pattern exhibited by the ACLD non-copers may be a mechanism that partially explains why they are unable to sufficiently stabilize their knee.

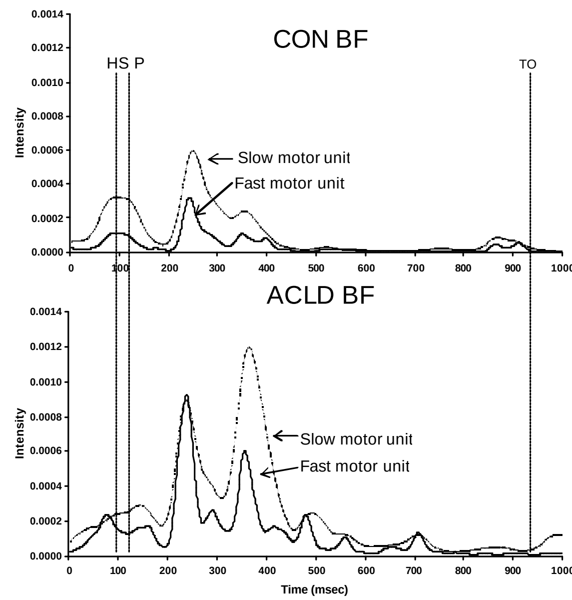

Figure 1: Biceps femoris fast and slow motor unit activation patterns for the CON and ACLD group. The vertical lines indicate heel strike (HS), onset of the perturbation (P), and toe off (TO).

REFERENCES

Ferber, R, et al. (2002). *Clin Biomech* **18**(2), 132-141.

Fitzgerald, G.K. et al. (2000). *Knee Surg Sports Traum*, **8**, 76-82.

von Tscharner, V. (2000). *J. Electromyogr. Kinesiol*. **10**, 433-445.

Wakeling, J.M. (2001). *Eur J App Phys*, **86**, 40-47.

ACKNOWLEDGEMENTS

This study has been supported, in part, by the ISB, the NATA REF (399-I007), and the Eugene Evonuk Foundation.

IMPACT ATTENUATION AND KINETIC CHARACTERISTICS OF CROSS-TRAINING SHOES IN LANDING ACTIVITIES

Songning Zhang, Kurt Clowers and Charles Kohstall

Biomechanics/Sports Medicine Laboratory, The University of Tennessee, Knoxville, TN, USA
E-mail: szhang@utk.edu

INTRODUCTION

Most footwear studies have concentrated on shoes used in running (De Clerq, et al., 1994; Nigg, 1995). Only a few studies in the literature (Dufek and Bates, 1991) have examined the footwear used in other sports. No specific studies have been found in the literature on the biomechanical characteristics of cross-training footwear. Cross-training footwear is designed to meet needs of a variety of sports and sport training environment. Key features of training shoes include generating power for performance and attenuating impacts for injury prevention. These shoes should be able to withstand rigors of different surface conditions. In addition, athletes must feel comfortable wearing these shoes in different activities and on different surfaces. Therefore, the purpose of this study was to examine kinetic characteristics of impact attenuation in landing in different training shoes.

METHODS

Ten healthy recreational male athletes (age: 21.5±2.5 yrs, body mass: 83.3±9.0 kg, height: 1.80±0.1 m) with no impairments to their lower extremities at the testing time participated in the study. A digital video camera (120 Hz) was used to obtain right sagittal kinematic data; a force platform (AMTI) for ground reaction forces (GRF) and two miniature accelerometers (Piezotronics, Inc.) for forehead and the distal tibia accelerations (ACC) were sampled at 1200 Hz for 1.5 sec.

The subjects were instructed to perform five step-off landing trials and five maximum vertical jumping trials in each of the four training shoes (Shoe A – D, successful models from three leading companies) in eight test conditions (landing and jumping in 4 shoes). The landing height was determined individually based upon an amount of potential energy of a "mid-size" person (80 kg) landing from a 60 cm height. In addition, a pair of shoes from each model was also selected for material testing. Only landing data were presented in this abstract.

At the end of testing, subjects filled out a survey form about their perception on cushion and comfort characteristics of the training footwear using 5-point Likert scale. A two-way 3×3 (joint $\times$ height) repeated measures ANOVA and post-hoc comparisons ($p<0.05$) were performed on selected kinematic variables; a one-way ANOVA was used to detect difference for j selected GRF and ACC variables.

RESULTS AND DISCUSSION

The results demonstrated that Shoes A and B had significantly lesser F1 values than C and D (Table 1). Shoe A and B also showed lower F1 loading rate (LrateF1) than the two other shoes. Shoe A also displayed significantly lower LrateF1 than B. Other GRF variables did not show any significant changes.

Table 1. Selected GRF variables in the landing activity

Shoe	F1	F2	LrateF1
A	23.2±7.8	63.0±13.3	2274.0±772.9
B	25.6±7.4	63.2±15.0	2630.5±863.9 [1]
C	29.2±8.6 [1,2]	62.9±17.2	3316.6±1048.0 [1,2]
D	28.0±8.6 [1,2]	61.5±13.3	3336.6± 1069.5[1,2]

[1]: significantly different from Shoe A.
[2]: significantly different from Shoe B.
[3]: significantly different from Shoe C.
F1: first maximum GRF (N/kg).
F2: second maximum GRF (N/kg).
LrateF1: loading rate of F1 (N/kg/s).

The accelerometer data indicated that the peak leg acceleration for the Shoe C was significantly greater than Shoe A (Table 2). On the other hand, the LMax for Shoe B was significantly greater than the Shoe D. The shock attenuation index for Shoe C was significantly greater than that for the Shoe D. The average scores obtained from the survey for the cushion are provided in Figure 1.The lowest score indicated the better cushion. The results indicated that the subjects favored the Shoe B slightly better than the other three shoes in the cushion category. In addition, the impact material testing results showed lower forefoot bending stiffness for Shoe A and B (29.4 and 37.9 N/mm) compared to Shoe C and D (60.3 and 59.8 N/mm) obtained in a modified ASTM test for forefoot flexibility.

Table 2. Selected ACC variables

Shoe	Hmax	LMax	AttnIndex
A	3.3±1.2	33.3±15.2	88.9±4.6
B	3.2±1.2	35.0±17.6	89.6±4.7
C	3.5±1.8	40.4±19.7 [1]	90.3±4.1
D	3.6±1.7	31.7±13.9 [2]	88.0±4.7 [3]

[1]: significantly different from Shoe A.
[2]: significantly different from Shoe B.
[3]: significantly different from Shoe C.
HMax: maximum head acceleration (g).
LMax: maximum leg (tibia) acceleration (g).
AttnIndex: shock attenuation index (%).

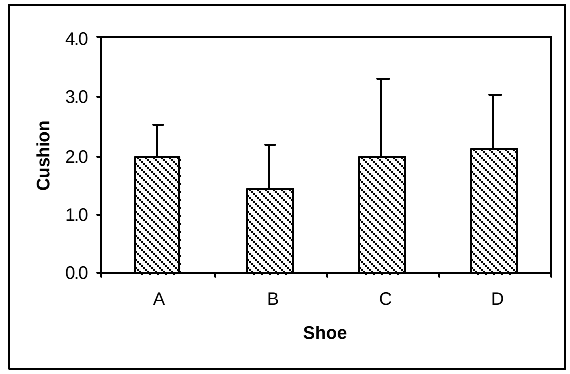

Figure 1. Mean values of cushion characteristics from the survey (1-best and 5 – worst).

The first peak GRF and the forefoot stiffness favored Shoes A and B suggesting possibility of better impact attenuating properties in the forefoot region. The Shoe C demonstrated a higher peak leg shock than the Shoe A. On the other hand, there were trends of greater peak knee contact angular velocity (not presented due to limited space) for the Shoes C and D compared to the Shoe A (significant) and B. These kinematic results also seemed to favor Shoe A and B.

SUMMARY

The results from this study suggest that the training shoe A and B showed slightly better impact attenuation properties, especially at the forefoot region.

REFERENCES

De Clerq, D., et al. (1994). *J. Biomech.*, **27**, 1213-1222.

Dufek, J. S. and Bates, B. T. (1991). *Med. Sci. Sports Exerc.*, **23**, 1062-1067.

Nigg, B.C., GK; Bruggemann, G.P. (1995). *J. App. Biomch.*, **11**, 407-432.

ACKNOWLEDGEMENTS

This study was supported by a grant from Adidas America, Inc.

BIOMECHANICAL CHARACTERISTICS AND POWER GENERATION OF JUMPING ACTIVITIES IN CROSS-TRAINING SHOES

Kurt Clowers, Songning Zhang and Charles Kostall

Biomechanics/Sports Medicine Laboratory, The University of Tennessee, Knoxville, TN, USA
E-mail: kclowers@utk.edu

INTRODUCTION

Most footwear studies have concentrated on shoes used in running (De Cleq, et al., 1994; Nigg, 1995). There are few studies that have investigated footwear used in jumping (Stefanyshyn and Nigg, 2000). No specific studies have been found in the literature on the biomechanical characteristics of cross-training footwear. Cross-training footwear is designed to meet the needs of a variety of sports and sport training environment. Key features of training shoes include generating power for performance and attenuating impacts for injury prevention. These shoes should be able to withstand the rigors of different surface conditions. In addition, athletes must feel comfortable wearing these shoes in different activities and on different surfaces. Therefore, the purpose of this study was to examine biomechanical characteristics and power generation for jumping in different training shoes.

METHODS

Ten healthy recreational male athletes (age: 21.5 ±2.5 yrs, body mass: 83.3±9.0 kg, height: 1.80±0.1 m) with no impairments to their lower extremities at the testing time participated in the study. A digital video camera (120 Hz) was used to obtain right sagittal kinematic data; a force platform (AMTI) for ground reaction forces (GRF) and two miniature accelerometers (Piezotronics, Inc. for forehead and the distal tibia accelerations (ACC) were sampled at 1200 Hz for 1.5 sec.

The subjects were instructed to perform five step-off landing trials and five maximum vertical jumping trials in each of the four training shoes (Shoe A – D, successful models from three leading companies) in eight test conditions (landing and jumping in 4 shoes). The landing height was determined individually based upon an amount of potential energy of a “mid-size” person (80 kg) landing from a 60 cm height. GRF data were normalized by multiplying respective jump height to control the effect of the different jump heights achieved by individuals. In addition, a pair of shoes from each model was also selected for material testing. Only jumping data were presented in this abstract.

At the end of the testing session, subjects filled out a survey form about their perception on cushion and comfort characteristics of the training footwear using 5-point Likert scale. A two-way 3 x 3 joint x height) repeated measures ANOVA and post-hoc comparisons were performed on selected kinematic variables; a one-way ANOVA was used to detect difference for jump height and selected GRF and ACC variables. The significance level was set at $p<0.05$.

RESULTS AND DISCUSSION

Kinematic differences among shoes were seen mainly in the ankle angular kinematics (Table 1). Shoes A and B demonstrated greater maximum dorsiflexion angles than

Shoe C. The plantarflexion angle at takeoff was greater for Shoe D than for Shoe A and C. The range of motion and maximum plantar flexion velocity was greater for Shoe C than for A and D.

For the lower extremity joints (not presented due to limited space), significant differences were observed between the knee and hip joint from the ankle joint kinematic variables. The hip joint had greater ROM and lesser peak plantarflexion angle than the knee and ankle joints.

Table 1. Selected ankle angular kinematic variables

Shoe	Amax	ATO	ROM	Vext
A	27.6 ±6	-31.9 ±6	59.4 ±5	-571 ±53
B	28.0 ±6	-32.6 ±6	60.2 ±5	-572 ±75
C	30.3 ±5[1,2]	-31.6 ±6	61.9±5[1]	-597 ±79[2]
D	28.7 ±5	-30.1 ±6[1,3]	58.9 ±5[3]	-564 ±68[3]

Note:
[1]: significantly different from Shoe A
[2]: significantly different from Shoe B
[3]: significantly different from Shoe C
Amax: maximumangle (degree)
ATO: takeoff angle (degree)
ROM: range of motion (degree)
Vext: maximum plantarflexion angular velocity (degree/s)

The GRF variables for jumping did not show significant changes across shoes except for differences of the minimum vertical GRF between A and D before the normalization was applied. However, significant differences were observed after applying the normalizing procedure to selected GRF variables (Table 2). Shoe C had significantly greater maximum vertical GRF than shoe A. Both shoe C and D had greater maximum power than shoe A.

The material testing results indicated that Shoe A and B had the smallest bending stiffness values (29.4 and 37.9 N/mm) compared to Shoe C and D (60.3 and 59.8 N/mm) obtained in a forefoot flexibility test. On the other hand, energy loss for Shoe A and B (41% and 43%) were greater than Shoe C and D (33 and 35%). These results were consistent with the maximum power results and were in agreement with the findings of a previous study on forefoot stiffness (Stefanyshyn and Nigg, 2000). However, the perception scores (shown in a different abstract) suggested that Shoe C and D had harder perceived heel cushioning that may pose a potential threat to the body.

Table 2. Selected GRF variables

Shoe	FJmin	FJmax	PWmax
A	2.6±1.0	15.3±2.1	48.3±17.2
B	2.5±1.2	15.8±2.4	49.1±17.8
C	2.4±0.9	15.9±2.4	49.8±16.3[1]
D	2.3±1.2[1]	16.2±2.5[1]	50.8±17.8[1]

Note:
[1]: significantly different from Shoe A
[2]: significantly different from Shoe B
[3]: significantly different from Shoe C
FJmin: minimum vertical GRF (Nm/kg)
FJmax: maximum vertical GRF (Nm/kg)
PWmax: maximum power (Wm/kg)

SUMMARY

The initial absences of significance in the jumping GRF data might be due to the jump heights were not the same for all subjects thus disguising the true differences among the shoes. After normalization Shoe D and C seemed to show better performance in the maximum power compared to Shoe A. Better performance may, however, come at a price, decreased comfort and cushioning.

REFERENCES

De Clerq, D., et al. (1994). *J. Biomech.*, **27,** 1213-1222.
Nigg, B.C., GK; Bruggemann, GP. (1995). *J. App. Biomch.*, **11**, 407-432.
Stefanyshyn, D.J. and Nigg, B.M. (2000). *Med Sci Sports Exerc*, **32**, 471-476.

ACKNOWLEDGEMENTS

This study was supported by a grant from Adidas America, Inc.

BICYCLE SEAT INTERFACE PRESSURE: RELIABILITY, VALIDITY, AND INFLUENCE OF HAND POSITION AND WORKLOAD

Eadric Bressel [1], John Cronin [2], and Alicia Exeter [1]

[1] Biomechanics Laboratory, Utah State University, Logan UT, USA
[2] Sport Performance Centre, Auckland University of Technology, Auckland, New Zealand
E-mail: ebressel@cc.usu.edu

INTRODUCTION

Bicycle seat discomfort and perineal (i.e., crotch) pathologies such as saddle sores and pudendal neuropathy are reported to influence between 35-81% of bicyclists following short and long distance rides (e.g., Schrader et al., 2002). Bicycle seat pressure is thought to be a major extrinsic risk factor for seat injuries (e.g., Schwarzer et al., 2002) and while a few researchers have examined solutions for reducing seat pressure through variations in saddle design (Spears et al., 2003) and riding position (Schrader et al., 2002), the reliability, and validity of the pressure measurements have not been reported. The purpose of this study was to examine the validity and reliability of bicycle seat interface pressure measurements using a commercially available pressure-sensing mat designed for bicycle seats. A second objective was to establish baseline pressure measurements for females and males during stationary bicycling under different workload and hand position conditions.

METHODS

Nineteen recreational cyclists (9 female, 10 male) completed two separate identical bicycle ergometer trials at 118 W in the top and drop handlebar positions and at 300 ± 82.4 W in top handlebar position (Figure 1). Seat pressures were sampled at 5 Hz via a computer interface module connected to a pressure-sensing mat designed for bicycle seats (FSA, Vista Medical Ltd). The pressure mat was 1.0 mm thick and consisted of a 27.9 x 34.3 cm flexible lycra material that contained a matrix of 768 piezoresistive sensors. Mean pressures were calculated as the average of all sensor values and peak pressures as the highest individual sensor value recorded for each condition. Pressure values were calculated over the total, anterior, posterior, left, and right side of the pressure-sensing matrix. A grid on the pressure-sensing mat was used to position the horizontal and vertical midlines of the mat over the horizontal and vertical midlines of the seat (Figure. 1).

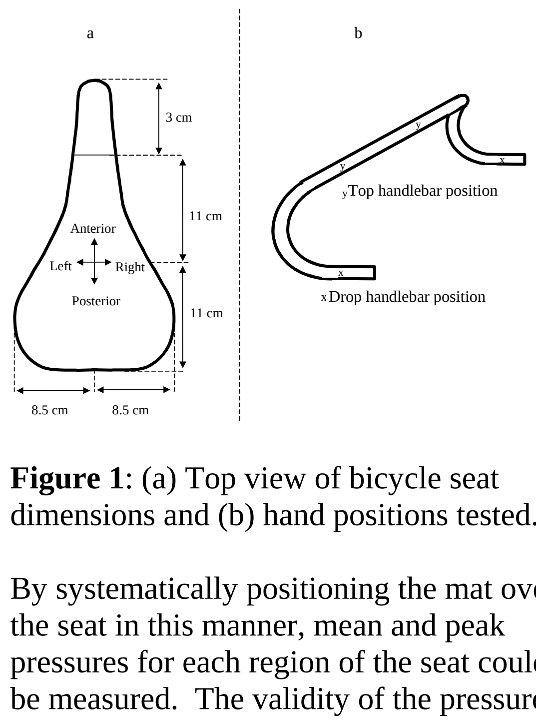

Figure 1: (a) Top view of bicycle seat dimensions and (b) hand positions tested.

By systematically positioning the mat over the seat in this manner, mean and peak pressures for each region of the seat could be measured. The validity of the pressure system was examined through the relationship (Pearson *r*) between known static seat loads and the sum of seat pressures. Within and between trial reliability was examined with Intraclass correlation coefficients (ICC). Main effects and interactions for average mean and peak pressures were examined with a two-factor condition (high workrate top, low workrate top and drop handlebar position) by gender (male and female) ANOVA with repeated measures and follow-up comparisons on the condition factor. The probability of a Type I error set at 0.05.

RESULTS AND DISCUSSION

The relationship (*r*) between seat loads and the sum of seat pressures was 0.97 ($p = 0.001$). Within trial ICC ranged between 0.90 and 0.99 and the between trial ICC values ranged between 0.78 and 0.96. Because univariate analyses revealed similar results for all seat regions, only mean pressures for the total seat region are reported (Table 1). Mean pressures were on average 24% greater in the 118 W top than 300 W top handlebar condition, and in comparison to the 118 W drop handlebar condition, mean pressures were 9% greater. Mean pressures for the 118 W drop condition were 16% greater than values for the 300 W top handlebar condition. The gender comparison revealed that male pressure values were greater (18%), and a significant interaction ($p = 0.02$) revealed that female values were not influenced by hand position (Table 1).

It can be observed from Table 1 that when participants moved from a top to drop handlebar position, seat pressure decreased and when participants pedaled at a higher workrate, seat pressure decreased. Weight shifts from the seat to handlebars and pedals, respectively, may account for the pressure changes observed (Stone & Hull, 1995). It may be that a lower center of gravity in females, however, decreases their capacity to shift weight to the handlebars, thereby reducing their capacity to decrease seat pressures. In conclusion, pressure measurements were found to be reliable during pedaling and valid statically. Additionally, the results indicated that workrate and hand position were factors influencing seat pressure and that males and females responded differently to adjustments of these factors.

REFERENCES

Schrader, S.M. et al. (2002). *J Androl*, ***23***, *927-934*.

Schwarzer, U. et al. (2002). *J Urol*, ***41***, *139-143*.

Spears, I.R. et al. (2003). *Med Sci Sports Exerc*, ***35***, *11620-1625*.

Stone, C., Hull, M.L. (1995). *J Biomech*, **28**, 365-375.

ACKNOWLEDGMENTS

Utah State University Gardner Travel Award.

Table 1: Mean seat pressures (mean ± SD; kPa) for males (n = 9) and females (n = 10) riding at two different workloads and handpositions

Variable	Tops 118 W	Drops 118 W	Tops 300 W
Male [c]	19.3 (2.2)	17.2 (1.4)	14.6 (3.0)
Female	15.3 (1.7)	14.4 (1.7)	12.0 (1.8)
All subjects	17.4 (2.8) [a]	15.9 (2.0) [b]	13.3 (2.8)

[a] $p < 0.05$. Significantly greater than 118 W drop and 300 W top handlebar conditions. [b] $p < 0.05$. Significantly greater than 300 W condition. [c] $p < 0.05$. Mean of all values is significantly greater than female values

EXTERNAL LOAD AFFECTS GROUND REACTION FORCE PARAMETERS NON-UNIFORMLY DURING RUNNING IN WEIGHTLESSNESS

John K. DeWitt[1], Grant Schaffner[2], Mitzi S. Laughlin[2], James A. Loehr[2] and R. Donald Hagan[3]

[1] Bergaila Engineering Services, Houston, TX, USA; [2] Wyle Life Sciences, Houston, TX, USA; [3] NASA Johnson Space Center, Houston, TX, USA

E-mail: john.k.dewitt1@jsc.nasa.gov

INTRODUCTION

Long-term exposure to microgravity induces detriments to the musculoskeletal system (Schneider et al., 1995; LeBlanc et al., 2000). Treadmill exercise is used onboard the International Space Station as an exercise countermeasure to musculoskeletal deconditioning due to spaceflight.

During locomotive exercise in weightlessness (0G), crewmembers wear a harness attached to an external loading mechanism (EL). The EL pulls the crewmember toward the treadmill, and provides resistive load during the impact and propulsive phases of gait. The resulting forces may be important in stimulating bone maintenance (Turner, 1998). The EL can be applied via a bungee and carabineer clip configuration attached to the harness and can be manipulated to create varying amounts of load levels during exercise.

Ground-based research performed using a vertically mounted treadmill found that peak ground reaction forces (GRF) during running at an EL of less than one body weight (BW) are less than those that occur during running in normal gravity (1G) (Davis et al., 1996). However, it is not known how the GRF are affected by the EL in a true 0G environment. Locomotion while suspended may result in biomechanics that differ from free running. The purpose of this investigation was to determine how EL affects peak impact force, peak propulsive force, loading rate, and impulse of the GRF during running in 0G. It was hypothesized that increasing EL would result in increases in each GRF parameter.

METHODS

Four subjects (2M/2F; 172.75 ± 11.14 cm; 73.18 ± 14.03 kg) ran at 3.13 m/s (7 mph) during 0G onboard NASA's KC-135 airplane and on the ground (1G). Vertical GRF data were collected at 250 Hz for 25 sec during multiple trials with a GRF-measuring treadmill (Kistler Gaitway, Amherst, NY).

During 0G trials, the subjects wore a harness attached to an EL. EL was provided by one or two bungees in series with one to five carabineer clips. EL was adjusted between trials by placing clips in series with the bungees. The bungee/clip setups were attached on each side of the harness at hip height. Bilateral dynamic loading forces were measured at 120 Hz with load cells (ELPS-T3E-500L, Entran Devices, Inc, Fairfield, NJ) placed inline with the EL configuration. The mean dynamic EL for each trial was calculated throughout the entire trial. During 1G trials, subjects ran without the harness and EL configuration.

Eight consecutive footfalls (4 left and 4 right) were processed from each trial. The eight footfalls were chosen from the middle of the trial when it could be assured that the subject had achieved the 3.13 m/s running speed. Forty-four trials were used in the analysis. All GRF data were conditioned at 40 Hz using a Butterworth filter to remove any artifact. Peak impact force, peak propulsive force, loading rate (peak impact force/time to peak impact force) and impulse were determined for each footfall. Trial means for all eight footfalls were computed for each GRF variable. All variables were normalized to subject body weight (BW).

Correlation analysis and standard linear regression were performed to assess the relationship of each GRF parameter to EL. An alpha level of $p<.05$ was chosen to denote significance. The regression equations were used to predict the EL necessary to replicate 1G mean values.

RESULTS AND DISCUSSION

The mean dynamic EL magnitude ranged from .53 to 1.24 BW and was significantly correlated to all GRF parameters (see Table 1). The r^2 values reflect that the EL accounts for only part of the variance, suggesting that additional factors may affect the GRF.

During running in 0G, GRF increased with increases in EL; however, their responses were highly varied. For example, peak impact force increases almost twice as fast as peak propulsive force (regression coefficients 1.29 vs. .67) with increasing EL. No single EL during 0G running sufficiently replicates GRF generated in 1G. For example, a .91 BW EL would replicate the mean peak impact force in 1G, but an EL of 1.72 would be required to replicate 1G peak propulsive forces.

SUMMARY

When an EL is applied to a subject during running in 0G via a bungee system, GRF parameters increase as the load level increases. It also appears that the EL affect upon the GRF is not uniform – increasing EL does not increase each GRF parameter at the same rate. EL levels that create 1G-like GRF based on one parameter may over- or under-load the body based on another parameter. Studies that examine the kinematics of locomotion in 0G may explain why these effects occur. It is possible that different methods of applying EL during 0G running must be developed to better replicate 1G-like GRF.

REFERENCES

Schneider, V. et al. (1995). *Acta Astronautica,* 36(8-12):463-466.

LeBlanc, A. et al. (2000). *J Appl Physiol,* 89:2158-2164.

Davis, B.L. et al. (1996). *Aviat Space Environ Med,* 67(3):235-242.

Turner, C.H. (1998). *Bone,* 23(5):399-407.

Table 1: Correlations and regression coefficients relating mean dynamic EL (BW) to GRF parameters. All coefficients and correlations were significant ($p<.05$).

Variable	r^2	**Regression Coefficient, B**	**Intercept**	**Mean 1G Value**	**Predicted EL for 1G Replication**
Peak Impact Force (BW)	0.42	1.29	.66	1.84	.91 BW
Peak Propulsive Force (BW)	0.37	.67	1.22	2.37	1.72 BW
Loading Rate (BW/s)	0.41	51.97	11.80	46.38	.67 BW
Impulse (BW*msec)	0.54	164.14	163.79	372.57	1.27 BW

THE EFFECTS OF SOLDIER LOADS ON FOOT PLACEMENT DURING QUIET STANCE

Jeffrey M. Schiffman, Leif Hasselquist, Karen P. Norton, Carolyn K. Bensel

Center for Military Biomechanics Research, Natick Soldier Center, Natick MA, USA
E-mail: Jeffrey.Schiffman@Natick.army.mil

INTRODUCTION

Predetermined foot positions are often used in the testing of balance control. However, as McIlroy and Maki (1997) pointed out, constraining the feet outside the subject's preferred stance position could affect the postural responses under study. McIlroy and Maki recommended a stance width and angle based on the mean of measurements made on young and old adults, both male and female, who were instructed to assume a comfortable foot position while standing unshod. These authors did not address the possibility that an experimental manipulation applied to the subject could alter the subject's preferred foot position. We investigated the effects that placing external loads on the body have on preferred stance. The conditions studied included three load weights and five different center of mass locations of a load carried in a backpack (a Modular Lightweight Load Carrying Equipment (MOLLE) backpack).

Table 1: Means (SD) of Volunteer Characteristics

Age (yr)	19.57 (2.31)
Height*(m)	1.75 (0.07)
Weight (kg)	74.11 (5.98)
Time in Service (mos)	7.57 (2.24)

*11 of 14 volunteers measured for height

METHODS

Fourteen Army enlisted men participated in the study (Table 1). Informed consent was obtained and the study was conducted in accordance with Army Regulation 70-25 (Use of Volunteers as Subjects in Research).

Load Conditions

We tested the soldiers under three load weight configurations comprised of Army clothing and equipment: unloaded (6 kg), fighting load (16 kg), and march load (40 kg). In all configurations, the soldiers carried a rifle at the ready position. The unloaded configuration consisted of combat boots, socks, T-shirt, and shorts. The fighting load consisted of the unloaded outfit plus a helmet, an armor vest, and a cloth vest with pouches on the front (a MOLLE Fighting Load Carrier). The pouches contained a canteen, grenades, and ammunition. The march load consisted of the fighting load plus the backpack and a 20-kg steel weight. The weight, held in place by foam blocks, was placed in one of five positions within the pack, resulting in five distinct mass center locations (Figure 1).

Experimental Measures

To establish a foot placement position for each of the seven load conditions, the volunteer stood on a sheet of paper (0.76 m x 0.46 m) with eyes focused straight ahead and weight evenly distributed on both feet. The volunteer assumed a relaxed standing posture with feet placed in a comfortable position. Stance width and stance angle were measured as described by McIlroy and Maki (1997), with the exception that the measurements were taken on shod feet. Volunteers were first tested unloaded and then with the fighting load. For the five march load conditions, the order of testing was based on three 5X5 Latin Squares. Separate one-way repeated measures ANOVAs (seven load conditions, $p<.05$) were performed on stance width and angle.

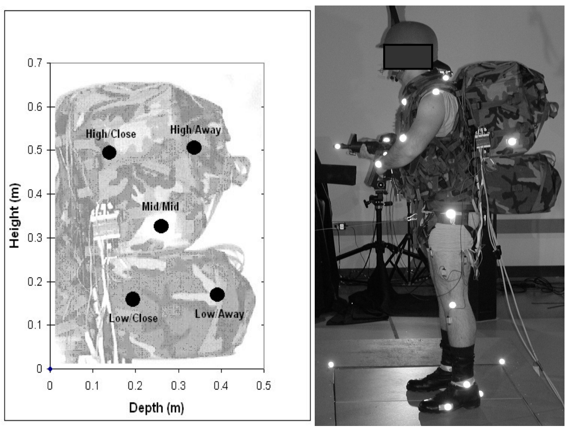

Figure 1: Five backpack mass center locations relative to the back and a soldier with the march load.

RESULTS AND DISCUSSION

No significant differences were found in the ANOVAs for stance width or angle. Load condition means are in Table 2. Depending upon condition, the standard deviations were as high as 22% and 55% of the mean stance width and angle, respectively. McIlroy and Maki (1997) also found large inter-subject variability on these measures.

The volunteers had greater stance widths and angles compared to past findings. McIlroy and Maki (1997) reported an average stance width of 0.18 m and an average stance angle of 11.6º for young adults, men and women combined. In our study, the average values were 0.26 m and 23.95º, respectively. McIlroy and Maki's subjects were unshod; the soldiers in this study wore military boots. Use of footwear or the characteristics of the boots worn in this study may have influenced the foot position chosen, resulting in greater stance widths and angles than those obtained by McIlroy and Maki.

In considering why differences in the external load on the body as great as 34 kg were not reflected in preferred foot position, the influence of the volunteers' military training should be noted. Soldiers are taught to adopt a wide stance when engaging in combat maneuvers with a rifle (Department of the Army, 2001). They are also taught to stand with feet 10 in. apart (or 0.25 m, a value that approximates the mean stance width obtained under each load condition) when adopting a rest position during marching drills. In assuming a comfortable stance in the study, the volunteers may have drawn on their training and adopted a military stance.

Table 2: Mean (SD) Stance Width and Angle

Load	Stance Width (m)	Stance Angle (º)
Unloaded	0.26 (0.05)	25.68 (10.56)
Fighting	0.25 (0.05)	25.93 (14.17)
March, Low & Away	0.27 (0.06)	23.21 (11.54)
March, Low & Close	0.25 (0.04)	23.89 (12.50)
March, Mid & Mid	0.26 (0.05)	23.07 (11.64)
March, High & Away	0.26 (0.05)	24.36 (11.59)
March, High & Close	0.27 (0.05)	21.39 (10.23)

SUMMARY

No differences in stance width or angle were found as load weight carried increased or weight position changed. Future studies that test balance in soldiers may choose to adopt as a standardized foot position a stance width of 0.26 m and a stance angle of 23.95º, the average values obtained in the present study.

REFERENCES

Department of the Army (2001). *IET Soldiers Handbook* (TRADOC Pamphlet 600-4). Fort Monroe, VA: Author

McIlroy, W. E., & Maki, B. E. (1997). Preferred placement of the feet during quiet stance: Development of a standardized foot placement for balance testing. *Clinical Biomechanics,* **12***,* 66-70.

LOWER EXTREMITY JOINT COUPLING IN RUNNERS WHO DEVELOPED PATELLOFEMORAL PAIN SYNDROME

Tracy A. Dierks[1], Irene S. Davis[1,2], and Joseph Hamill[3]

[1]Department of Physical Therapy, University of Delaware, Newark, DE, USA
[2]Joyner Sportsmedicine Institute, Mechanicsburg, PA, USA
[3]Department of Exercise Science, University of Massachusetts, Amherst, MA, USA
E-mail: tdierks@udel.edu Web: http://www.udel.edu/PT/davis/index.htm

INTRODUCTION

Patellofemoral Pain Syndrome (PFPS) is one of the most prevalent running overuse injuries, yet the mechanisms of PFPS are still not well understood. Most PFPS studies have examined joint motions in isolation. However, it has been suggested that abnormalities in joint coupling between the foot, shank, and thigh may be related to running injuries (Bates et al. 1978). To evaluate joint coupling, various methods have been used (Table 1). Timing differences assess coupling at distinct points during stance. The continuous relative phase (CRP) and vector coding methods examine coupling throughout all of stance. Few studies have used these methods in an injured population. To date, there are no prospective studies comparing joint coupling in runners who develop PFPS and uninjured runners, which may lend insight into causative mechanisms. Therefore, the purpose of this study was to compare, prospectively, joint coupling in female runners who later develop PFPS to uninjured runners who did not develop PFPS. It was hypothesized that PFPS coupling would be less synchronous and more out-of-phase.

METHODS

All data are part of an ongoing prospective running injury study of female competitive distance runners. To date, 15 have developed PFPS. Data were collected prior to developing PFPS and were compared to 15 mileage matched runners from the same study who have not developed an injury to date. Subjects ran along a 25m runway at a speed of 3.65m/s (±5%). Ground reaction force (GRF) data (960 Hz) and kinematic data (120 Hz, filtered at 8 Hz) were collected. For each subject, coupling variables from the 4 methods (Table 1) were computed for 8 individual trials and averaged. Group means and standard deviations were then calculated. The CRP was derived from the angles and velocities of two joint motions, with a CRP value of 0^o meaning the two joint motions were in-phase (Hamill et al. 1999). Vector coding was derived from angle-angle plots, with coupling angles of 45^o relating to equal movement between the two joint motions (Heiderscheit et al. 2002). Both CRP and vector coding were assessed during 4 periods of stance, which were based on events of the vertical GRF. One-tailed independent t-tests were used with $p \leq 0.10$, due to the preliminary nature of the data.

RESULTS AND DISCUSSION

Table 1: Definition of terms and joint coupling relationships.

Movement Terms (plane and reference)	
EV	Rearfoot eversion. (Frontal, Calcaneus to Tibia.)
TIR	Tibial internal rotation. (Transverse, Calcaneus to Tibia.)
KF	Knee flexion. (Sagittal, Tibia to Femur.)
KIR	Knee internal rotation. (Transverse, Tibia to Femur.)
KADD	Knee adduction. (Frontal, Tibia to femur.)
Timing Differences (measure of synchrony)	
EV-TIR	Time to peak EV minus time to peak TIR.
EV-KF	Time to peak EV minus time to peak KF.
EV-KIR	Time to peak EV minus time to peak KIR.
EV-KADD	Time to peak EV minus time to peak KADD.
TIR-KF	Time to peak TIR minus time to peak KF.
TIR-KIR	Time to peak TIR minus time to peak KIR.
CRP (phasing relationship) & Vector Coding (continuous excursion ratio)	
$RF_{(ev/in)}$-$K_{(f/e)}$	Rearfoot EV & inversion coupled with KF & knee extension.
$RF_{(ev/in)}$-$K_{(rot)}$	Rearfoot EV & inversion coupled with KIR & knee external rotation.
$RF_{(ev/in)}$-$T_{(rot)}$	Rearfoot EV & inversion coupled with TIR & tibial external rotation.
$RF_{(ev/in)}$-$K_{(ad/ab)}$	Rearfoot EV & inversion coupled with KADD & knee abduction.
$T_{(rot)}$-$K_{(f/e)}$	TIR & tibial external rotation coupled with KF & knee extension.
$T_{(rot)}$-$K_{(rot)}$	TIR & tibial external rotation coupled with KIR & knee external rotation.

In general, PFPS runners displayed greater time between peaks, suggesting less synchrony (Table 2). PFPS runners were significantly less synchronous for TIR-KF, due to TIR reaching its peak before KF. PFPS runners were significantly more synchronous for EV-KADD, due to uninjured runners reaching peak KADD sooner. The delay in the KADD reversal and the earlier reversal in TIR may result in a malalignment of the patella, which may predispose a runner to PFPS. In general, CRP results suggested that PFPS runners were more out-of-phase. CRP relationships involving tibial rotation resulted in PFPS runners displaying significantly more out-of-phase coupling during period 3 (Figure 1). Period 3 typically follows, and may include, maximum loading and joint reversals. This out-of-phase coupling may be a result of an earlier TIR reversal (noted in timing differences), which may affect load distributions. For $RF_{(ev/in)}$-$K_{(ad/ab)}$, periods 1 and 3 were more in-phase for PFPS runners while period 2 was more out-of-phase (Figure 1). This is most likely a result of the later KADD reversal in PFPS runners. For $RF_{(ev/in)}$-$K_{(f/e)}$, PFPS runners were significantly more out-of-phase during periods 1 and 2. Overall, vector coding results were similar. However, the relationships involving tibial rotation suggested that PFPS runners displayed less relative tibial external rotation during period 4 (Figure 2). In contrast, PFPS runners displayed greater relative tibial rotation during period 3 for $T_{(rot)}$-$K_{(f/e)}$.

Table 2: Timing differences & standard deviations (). A negative value indicates that the proximal motion reached its peak first. *p≤0.10. Values are % of stance.

	EV-TIR		EV-KF		EV-KIR	
Uninjured	5.0	(8.0)	5.5	(5.1)	-6.5	(9.5)
PFPS	8.6	(10.8)	3.7	(4.7)	-7.7	(10.8)
	EV-KADD*		**TIR-KF***		**TIR-KIR**	
Uninjured	14.2	(14.0)	0.5	(7.8)	-11.5	(11.1)
PFPS	5.2	(17.4)	-4.9	(11.3)	-16.1	(14.0)

SUMMARY

The preliminary results of this study suggest that, prior to the development of PFPS, female runners display differences in joint coupling when compared to those that do not develop PFPS. These differences appear to occur in coupling relationships involving tibial rotation or knee adduction/abduction.

REFERENCES

Bates, B.T. et al. (1978). *Running*, Fall, 24-30.
Hamill, J. et al. (1999). *Clin. Biomech.*, 14, 297-308.
Heiderscheit, B.C. et al. (2002). *J.A B.*, 18, 110-121.

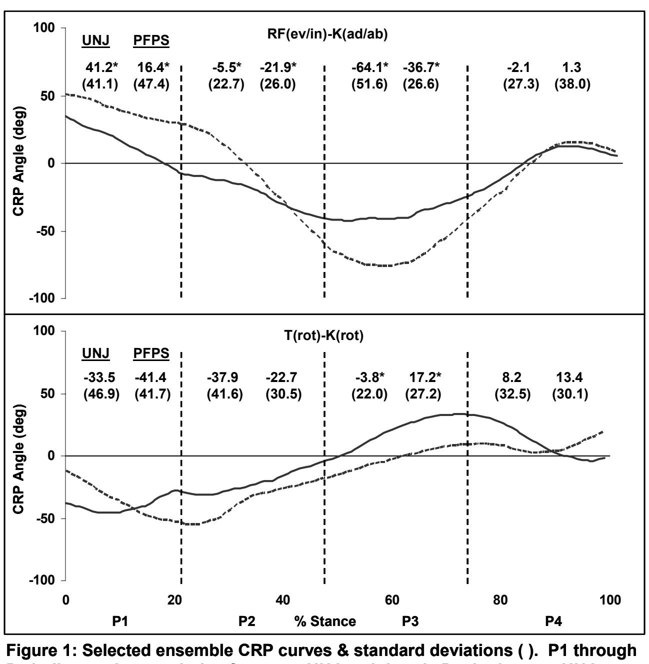

Figure 1: Selected ensemble CRP curves & standard deviations ( ). P1 through P4 indicates the 4 periods of stance. UNJ=uninjured. Dashed curve=UNJ, Solid curve=PFPS. *p≤0.10.

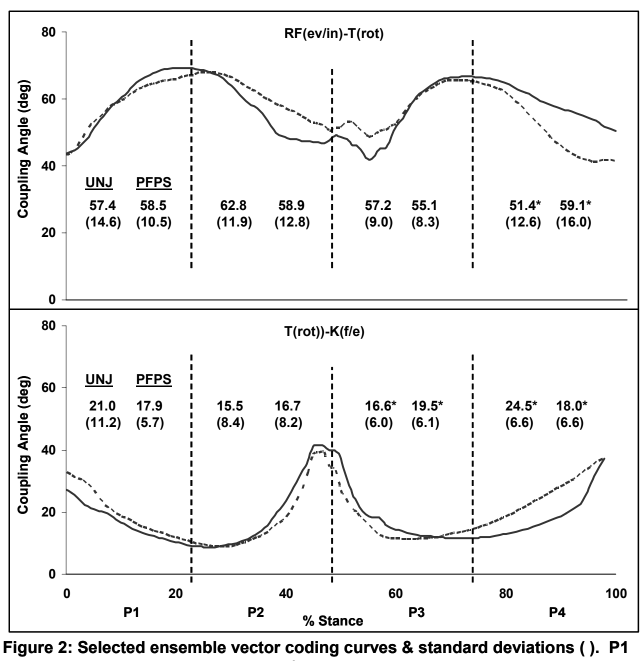

Figure 2: Selected ensemble vector coding curves & standard deviations ( ). P1 through P4 indicates the 4 periods of stance. UNJ=uninjured. Dashed curve=UNJ, Solid curve=PFPS. *p<0.10.

TRACKING SLOW-TIME-SCALE CHANGES IN MOVEMENT COORDINATION

Jonathan B. Dingwell [1,2] and David Chelidze [3]

[1] Nonlinear Biodynamics Lab, Dept. of Kinesiology, University of Texas, Austin, TX, USA
[2] Dept. of Biomedical Engineering, University of Texas, Austin, TX, USA
[3] Dept. of Mechanical Engineering, University of Rhode Island, Kingston, RI, USA
E-mail: jdingwell@mail.utexas.edu Web: http://www.edb.utexas.edu/faculty/dingwell/

INTRODUCTION

Slowly developing chronic diseases will become more prevalent as world populations age (Santos-Eggimann, 2002). Diseases like peripheral neuropathy and/or osteoarthritis lead to changes in coordination that develop slowly over time. Tracking the progression of these disease processes is very important, but it is also very difficult. By comparison, changes in movement coordination patterns are relatively easily accessible.

Our goal is to develop new methods to track changes in underlying (i.e. "hidden") disease states from biomechanical data. Here, we demonstrate that methods for tracking hidden damage mechanics in mechanical systems (Chaterjee et al., 2002; Chelidze et al., 2002) can also track slow-time-scale changes in movement coordination.

METHODS

We assume our system can be modeled as a hierarchical dynamic system of the form:

$$\dot{x} = f(x, m(f)), \quad \dot{f} = e\, g(f, x) \qquad \text{(1a, 1b)}$$

where x = the *observable* states of the fast-time-scale system, f = the *hidden* slowly-varying dynamics, $0 < e << 1$, and $m(f)$ = the parameters in Eq. 1a (i.e. if $e = 0$ exactly, these parameters would be constant).

In most biological contexts, we do not know the governing differential equations. Given a single measured time series, $x(r)$, however,

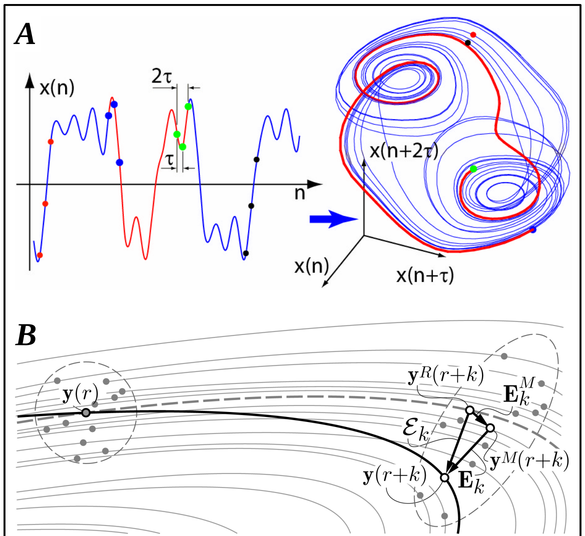

Figure 1. ***A:*** State space reconstruction. The original 1-dimensional time series is "embedded" in a multi-dimensional vector space defining equivalent states of the system. ***B:*** Tracking function estimation. (—) is the current trajectory. (– –) is the corresponding model trajectory. $\mathbf{E}_k$ is the estimated error, $\mathbf{E}_k^M$ is the modeling error, and e_k is the true error, or drift in the system.

we can form a topologically equivalent state space using delay reconstruction (Fig. 1A):

$$y(r) = [x(r), x(r+t), \ldots, x(r+(d-1)t)] \qquad (2)$$

where t is a suitable time delay and d is the appropriate embedding dimension (Sauer et al., 1991). Data from the unperturbed system are then used to construct a locally linear model of the system behavior (Fig. 1B). Drift in f leads to "errors" ($\mathbf{E}_k$) between the actual and predicted system behavior. If our model is good, then the model error ($\mathbf{E}_k^M$) will be small and $\mathbf{E}_k \approx e_k \equiv$ the true error or drift in the system dynamics. $\mathbf{E}_k$ can then be used to define the following *tracking metric*:

$$j = \langle F \| \mathbf{E}_k(y(r), f) \| \rangle \approx \langle \| e_k(y(r), f) \| \rangle \quad (3)$$

where $\langle \cdot \rangle \equiv$ the RMS over the index r and F is an appropriate filter (Chelidze et al., 2002). Thus, this metric essentially tracks the average error, over time, in the predicted fast-time-scale dynamics that is introduced by the slow-time-scale dynamics.

To test whether this algorithm could track "hidden" physiological processes (e.g. injury or disease) from accessible kinematic data, we asked one healthy subject to walk on a motorized treadmill at their self-selected pace. The treadmill incline was increased from 0° to +8° slowly over 15 minutes (Fig. 2A). Kinematic data were recorded (Vicon-612, Oxford Metrics, Oxford, UK) from markers placed on the treadmill frame and on the subject's hip, knee and ankle joints. The knee joint kinematics defined $x(r)$, the fast-time-scale dynamics. These data were subjected to the tracking analysis to see how well the algorithm could track the slowly changing treadmill inclination.

RESULTS AND DISCUSSION

The basic kinematics of knee joint motions remained largely unchanged across the duration of the trial (Fig. 2B). The tracking metric (Eq. 3), computed from the knee joint data, gave a reasonable approximation to the treadmill angle (Fig. 2C). Although the prediction was not perfect, it should be noted that the algorithm was applied "blindly" (i.e. no attempt was made to optimize or alter the original code in any way). It is anticipated that by accounting for additional features particular to biological systems (e.g. noise, multiple time scales, etc.), much better results can be obtained.

Valid damage tracking metrics could be defined from first-principles models of a dynamic system and the damage process, but defining such models for biological

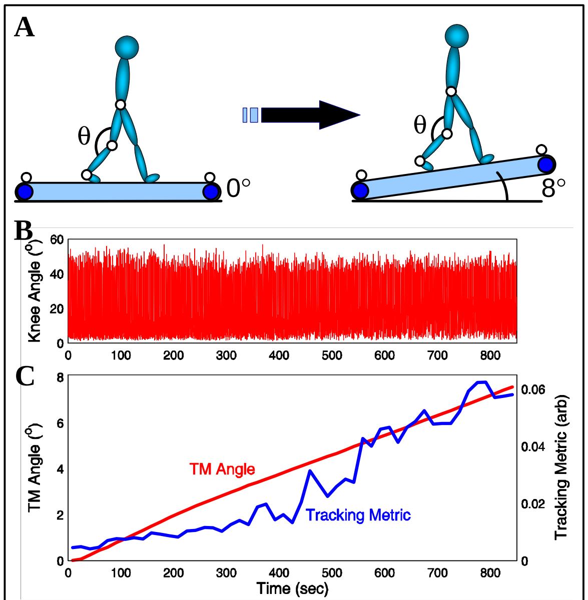

Figure 2: ***A:*** Marker arrangement used in treadmill data collection. ***B:*** Recorded knee joint angle over the entire trial showed little variation. ***C:*** Treadmill angle and tracking metric. The algorithm tracked the treadmill angle from the knee joint data fairly well.

systems is usually prohibitively difficult. One could experimentally derive various metrics from intuition, etc. However, one cannot predict *a priori* if any such metric will work or be valid. By using a state space formulation, the proposed method yields a valid measure of the slow-time-scale dynamics, without the need for highly detailed models of system dynamics (Chelidze et al., 2002). We anticipate this approach (with some modifications) can also be used to track other "hidden" biological processes like muscle fatigue, repetitive strain injury, or disease progression.

REFERENCES

Chatterjee, A. et al. (2002). *J. Sound & Vibration*, **250** (5): 877-901.
Chelidze, D. et al. (2002). *J. Vibration & Acoustics*, **124** (2): 250-264.
Santos-Eggimann, B. (2002). *Aging Clin Exp. Res.*, **14** (4): 287-292.
Sauer, T. (1991). *J. Statistical Physics*, **65** (3-4): 579-616.

LOCAL DYNAMIC STABILITY IMPROVES AT SLOWER WALKING SPEEDS

Laura C. Marin [1,2] and Jonathan B. Dingwell [1,2]

[1] Nonlinear Biodynamics Lab, Dept. of Kinesiology, University of Texas, Austin, TX, USA
[2] Dept. of Biomedical Engineering, University of Texas, Austin, TX, USA
E-mail: jdingwell@mail.utexas.edu Web: http://www.edb.utexas.edu/faculty/dingwell/

INTRODUCTION

Increased walking variability has been found in numerous patient populations known to be at increased risks of falls. It is assumed this increased variability implies increased instability and greater risk of falls. These more variable populations also walk slower, suggesting they are trying to *improve* their stability and prevent falls. However, slower speeds in young healthy subjects lead to greater variability (Winter, 1983, Öberg et al., 1993). Thus, there is a paradox here: patients at risk of falling slow down to attain better stability, but slowing down leads to greater variability, which is supposed to indicate greater *in*stability. This study seeks to resolve this paradox.

We quantified local dynamic stability in young, healthy adults walking at various speeds using established techniques and compared the trends found to trends in variability. Our results show that local dynamic stability exhibits very different trends than variability. This provides further evidence that equating instability with increased variability may not be appropriate.

METHODS

Eleven healthy subjects (age: 21-34 yr, 5 female) participated after giving informed consent. After preferred walking speed (PWS) was determined, each subject performed three treadmill trials at each of five walking speeds: PWS, PWS ±20%, and PWS ± 40%. Three-dimensional kinematic data of a single marker on the first thoracic vertebrae were collected at 60 Hz using a six-camera Vicon motion analysis system (Oxford Metrics, Oxford, UK). Because subjects tended to "wander" on the treadmill, 3D velocities were computed and analyzed, as these time series were more stationary.

Multi-dimensional state spaces were reconstructed from each time series and its time-delayed copies (Sauer et al., 1991). An embedding dimension of $d_E = 5$ was used (Dingwell & Cusumano, 2000).

Dynamic stability was quantified by estimating maximum finite-time Lyapunov exponents (λ*) from these state space data (Rosenstein et al., 1993; Dingwell & Cusumano, 2000). These λ* exponents directly quantify the sensitivity of a system to small local perturbations in state space, and are thus a direct measure of intrinsic local dynamic stability. Estimates of λ* were calculated over two time scales. Short-term exponents were computed between 0 and 1 stride while long-term exponents were computed between 4 and 10 strides.

Stride to stride variability was assessed by time-normalizing the data for each stride then computing the mean of the standard deviations (SD) at each time increment.

RESULTS AND DISCUSSION

When subjects walked faster or slower than their PWS, they exhibited greater variability

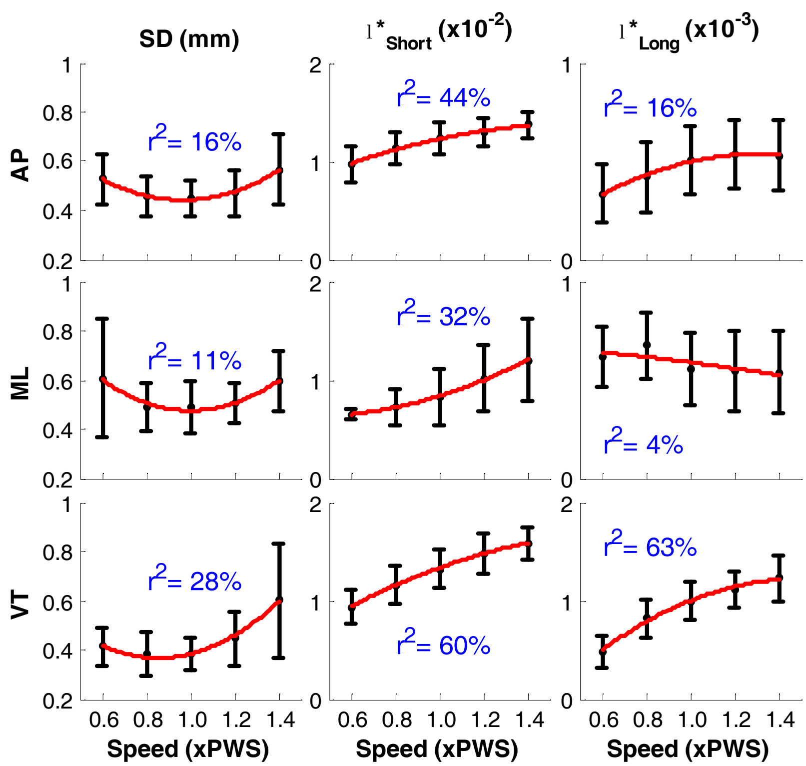

Figure 1: Variability and local dynamic stability measures as a function of walking speed. In the first column, the black dots with error bars show the means and standard deviation (±SD) for each direction: anterior-posterior (AP), medial-lateral (ML), and vertical (VT). The second and third columns show the mean (±SD) short-term and long-term λ* (λ^*_{Short} and λ^*_{Long}). The red trend lines represent quadratic curve fits to all data sets. For each set of data, the r^2 values indicate the proportion of the variance in the data explained by the quadratic fit.

(Fig 1, column 1). In all three directions, significant differences in variability with speed were found ($p<0.001$).

However, neither short-term nor long-term λ* exponents exhibited these parabolic trends. The short-term λ* exponents (Fig 1, column 2) in all directions increased with increasing speed, indicating greater instability. Two directions of long-term λ* exponents (Fig 1, column 3) also increased with speed. The medial-lateral long-term λ* showed a slight decreasing trend, but with an adjusted r^2 of only 4%. Significant differences in each of the six λ* exponents with speed were found ($p\leq 0.002$).

SUMMARY

In agreement with previously published research (Winter, 1983, Öberg et al., 1993), variability increased with walking speed below and above the preferred speed. However, the increased local dynamic stability exhibited by these young, healthy subjects suggests an explanation for the paradox presented above. Slower walking may indeed by a valid strategy for improving stability and reducing the risk of falling despite the resulting increases in variability.

REFERENCES

Dingwell, J.B. and Cusumano, J.P. (2000) Chaos, **10** (4): 848-63.

Öberg, T., et al., (1993). *J. Rehabil. Research & Dev.*, **30**: 210-223.

Rosenstein, M.T., J. J. Collins, et al. (1993). *Physica D*, **65**: 117-134.

Sauer, T. et al. (1991). *J. Stat. Phys.* **65**(3/4): 579-616.

Winter, D.A. (1983). *J. Motor Behavior*, **15**: 302-330.

ACKNOWLEDGEMENTS

Funding for this project was provided by a Biomedical Engineering Research Grant from the Whitaker Foundation.

BIOMECHANICAL RESPONSE OF ENTIRE LUMBAR SPINE TO LARGE COMPRESSION –A FINITE ELEMENT MODEL STUDY

Tim Brown [1] , Raghu N. Natarajan [2] and Gunnar B.J. Andersson [2]
[1]Bioengineering Department, University of Illinois at Chicago, Chicago, IL, USA
[2] Department of Orthopedic Surgery, Rush University Medical Center, Chicago, IL, USA
E-mail: Raghu_Natarajan@Rush.edu Web: www.ortho.rush.edu/CADlab/

INTRODUCTION

During normal daily activities and in the workplace, the lumbar spine is exposed to very large and complex loading conditions. The mechanisms by which the lumbar spine supports standing postures with and without external loads are complex and not well understood. In vivo studies give insight into the loading conditions prevalent during normal and intense activities, but they are still limited in scope and detail in describing the total biomechanical response to the postural loading the lumbar spine is subject to. A compressive "follower" load (1200 N) has been successfully applied in-vitro (1) to the whole lumbar spine to mimic the mechanical behavior of the musculature. Finite element models have tried to mimic the mechanics of the musculature by using optimal stabilizing moments at each motion segment level, pelvic rotation, or a variation of the follower load technique (2). These studies provide few details of the biomechanical behavior of each segment under the large compressive load. The current study with the help of a validated 3-D, non-linear, finite element model created from CT images will address this issue. The "follower" load technique was used to apply large, axial compressive loading of 2000 N to the model and ensured that the compressive load vector was perpendicular to the midplane of each intervertebral disc, mimicking the mechanical behavior of the musculature and minimizing motion artifacts that are inherent when applying a large, axial compressive load.

The goal of this study was to investigate the complete biomechanical response of the intervertebral discs and the facet joints to large compressive loads. The findings of this study will help better understand the effect of large compressive loading of the lumbar spine and its potential consequences in terms of location of lumbar disc component failure.

METHODS

The finite element representation of L1-S1 included six vertebrae with posterior elements, five discs, 6 ligaments per level and pairs of facet joints at each level. The cortical bone, cancellous bone, posterior elements, endplates, facet cartilage, annulus and nucleus were modeled as 8-node, three-dimensional, isoparametric elements. The left and right superior and inferior articulating surfaces of the facet cartilage were modeled by 4-node, quadrilateral, moving frictionless contact surfaces. The annular fibers of the intervertebral discs were assembled in a criss-cross fashion at an angle of approximately 30°. The ligaments and annular fibers were modeled as 2-node, non-linear truss elements with cross-sectional area and reacted to axial tension only. Excellent agreement was found between the finite element validation results and the in vitro study (3) at all motion segment levels for all loading modes. "Follower" rods and guides through which the vertebra move were then developed bilaterally that followed the lordotic curve of the lumbar spine in the sagittal plane such that when the compressive load was applied, its vector was perpendicular to the mid-plane of each disc.

RESULTS AND DISCUSSION

Successful application of the "follower" load should result in a minimization of the segmental rotations at each level. In the frontal and transverse planes, the current finite element model with the "follower" rod and guide system produced rotations at each level that were less than one degree for the compressive load of 2000 N.

The force-disc compression response was nonlinear at all levels. The model predicted a total axial compression of 10.6 mm, with 2.0 mm at L1-L2, 2.6 mm at L2-L3 mm, 3.0 mm at L3-L4, 2.7 mm at L4-L5, and 3.1 mm at L5-S1. Berkson et al. (4) measured the compression in single motion segments from L1-L2 to L5-S1 in vitro and reported an average value of 0.51 mm of disc compression for a 400 N axial compressive load. The finite element model values at 400 N of axial compression was in agreement with these values.

The results from the finite element study suggest that failure would occur in the endplates at all levels. Maximum von Mises stress varied from 8 MPa to 13 MPa in the endplates. The location of the failure was on the periphery of the endplate at the trabecular interface at each level.

The response of the annular fibers to applied load exhibited nonlinear behavior at all levels. The outer and middle layers at all levels had an average maximum von Mises stress below 5 MPa. For the inner layer, all levels were at or above 10 MPa with L1-L2 having the highest value of 28 MPa. Overall, the current finite element model showed that the annular fiber failure occurs near the inner surface of the annulus, which compares well with the published results.

The highest value of annular matrix von Mises stress of 10 MPa occurred at L1-L2 and the lowest value of 6 MPa occurred at L4-L5. The values of the maximum average von Mises stress occurred in the posterior quadrant at L1-L2 and at the inner posterior quadrant at L2-L3 to L5-S1. The maximum average von Mises stress in the nucleus ranged from 5.5 MPa at L1-L2 to 8.0 MPa at L5-S1.

At all of the segment levels, facet forces exhibited non-linear behavior with load. The right lateral facets showed the highest contact forces at the L1-L2 to L3-L4 levels and the left lateral facets showed the highest contact forces at the L4-L5 to L5-S1 levels. The maximum contact force generated from the 2000 N compressive load was at L4-L5 (613 N) and the smallest was at L5-S1 (184 N).

SUMMARY

A 3-D finite element model of the entire lumbar spine was developed and using the "follower" load concept was able to apply large compressive loads that are seen in vivo and reported in the literature. Detailed biomechanical behavior of the whole lumber spine under large compressive load is presented here. Current model predictions of disc compression values, locations of both endplate failure and annular fiber failure and the load supported by facet joints all agree with those reported in literature.

REFERENCES

(1) Patwardhan et al., (2002). J. of Orthopedic Research 21:540-546.
(2) Shirazi-Adl A. and Parnianpour M. (2000) Clinical Biomechanics 15:718-725.
(3) Panjabi M.M., et al., (1994) J. of Bone and Joint Surgery 76-A:413-424, 1994.
(4) Berkson M.H., et al., (1979) J. of Biomechanical Engineering 101:53-57.

AN MRI IMAGE-BASED METHOD FOR QUANTIFYING MENISCUS STRAINS

Qunli Sun [1, 2], Robert T. Burks [2], Patrick E. Greis [2], and Jeffrey A. Weiss [1, 2]

[1] Department of Bioengineering, University of Utah, Salt Lake City, UT, USA
[2] Department of Orthopedics, University of Utah, Salt Lake City, UT, USA
E-mail: Qunli.Sun@utah.edu Web: www.bioen.utah.edu

INTRODUCTION

The important role of menisci in the knee joint is demonstrated by the deleterious effects of injury or menisectomy on the articular cartilage. The strain distribution in menisci reflects the load transfer and contact stress in the knee joint. In vitro measurement of meniscus strain is difficult, while in vivo strain measurement is impossible. Further, direct numerical simulation of the meniscus mechanics is complicated by the fact that the boundary conditions and material properties are difficult to determine. The objective of this study was to develop a noninvasive technique for quantifying deformations and strains of the meniscus based on magnetic resonance (MR) images.

METHODS

A fresh-frozen left cadaveric knee (male, 64 years old) was prepared and mounted on a customer-built MR-compatible loading device. Volumetric MR images of the knee at full extension (256×256 matrix, 140 mm FOV, 232 slices of 1 mm thickness) were acquired using a short TE double echo 3D spoiled acquisition technique (Kim et al. 2003), on a 1.5 T scanner (GE Signa Horizon, Milwaukee, WI). The first set of the images (template) was collected in the unloaded configuration; while the second set (target) was collected while an axial compressive load of 200 lb was applied to the knee (about 1x body weight). The MR scans were performed with a TMJ coil and spanned from the medial to the lateral extremes of the knee. The femur, tibia, articular cartilages and menisci were segmented manually in the template images to construct their geometries that were used to generate their finite element (FE) mesh.

A technique termed Hyperelastic Warping (Rabbitt, et al. 1995 and Weiss, et al. 1998) was used to extract the deformations and strains in menisci from the template and target images. Briefly speaking, the template domain is modeled as a deformable continuum. An image-based energy is formed to introduce the intensity difference between the template and target images into the energy functional of the system. By minimizing the energy functional, a spatially varying force from the image intensity difference is produced to deform the template images into alignment with the target images. The hyperelastic constitutive model is used to regularize the problem to ensure a 1-to-1 mapping between the template and target images. The nonlinear optimization problem is solved using FE method for deformations and strains.

It is difficult to validate Warping analysis using experimental measurements. So an indirect method was employed to validate Warping method for predicting meniscus strains from MR images. First, an FE model of a knee was constructed from the template images with appropriate material properties, proper boundary conditions, and an axial compressive force. A nonlinear FE analysis was performed to provide a “forward FE” solution. By applying the deformation map from the forward FE solution to the template images, a set of synthetic target images was generated. Then, using the template and synthetic target images, the validation warping analysis was performed to predict the deformations and strains in medial meniscus. By comparing the forward FE and validation warping solutions, Warping method was validated for measuring the meniscus strains from MR images.

RESULTS AND DISCUSSION

Validation Analysis: The validation of Warping was performed by quantitatively comparing displacements and hoop stretches in meniscus between the forward FE and validation warping solutions (Fig.1 and 2). As we can see, Warping can reproduce the displacement and stretch distributions obtained from the forward FE analysis with an overall relative error of 6.31% and 0.69%, respectively. That means that Warping is accurate to predict meniscus strain distribution from MR images.

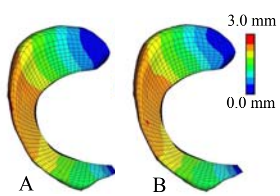

Figure 1: Comparison between forward FE and Warping displacements. A) Forward FE solution. B) Warping solution.

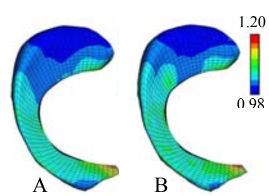

Figure 2: Comparison between forward FE and Warping hoop stretches. A) Forward FE solution. B) Warping solution.

Warping Analysis: The warping analysis was then performed to measure strains in medial meniscus using the template and target images. After warping, the geometry of the deformed template matched that of the target very well (Fig. 3). And the intensity difference of template and target images decreased dramatically and became uniform (Fig. 4). These indicate that the geometric registration was accomplished very well. The hoop strain was plotted (Fig. 5). Compared to the published experimental data (Jones et al. 1996), the Warping prediction had similar distribution trend of the peripheral hoop strains to the

Figure 3: Comparison of target (solid) and deformed template (mesh).

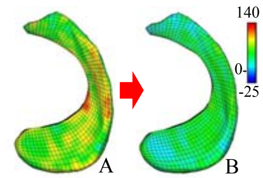

Figure 4: Intensity difference of template and target images. A) Before warping. B) After warping.

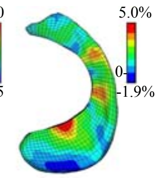

Figure 5: Hoop strain distribution.

experimental measurement, which showed significantly less strain in the posterior portion compared to the anterior and middle portions. The values are also very close if we converted the experimental load to 1x body weight (Table 1).

Table 1: Comparison of peripheral hoop strains between Warping and experimental measurements.

	Anterior	Middle	Posterior
Warping results (1xbody weight)	0.98%	1.22%	0.49%
Jones et al.'s data (Converted to 1xbody weight)	0.95%	0.88%	0.51%

SUMMARY

This research demonstrated the feasibility of noninvasive strain measurement in menisci using Hyperelastic Warping and MR images. The method is a true 3D method and does not require exact material properties and boundary conditions. It allows determining meniscus strains under a variety of loading conditions, both in cadaveric tissue *in vitro* or to patients *in vivo*.

REFERENCES

Kim, S. E. et al. (2003). *Proceedings of ISMRM 13th Annual Mtg*, P.1533.

Rabbitt, R. D. et al. (1995). *SPIE,* **2573**, 252-265.

Weiss, J. A. et al. (1998). *SPIE,* **3254**, 477-484,

Jones, R. S. et al. (1996). *Clin. Biomech*., **11**, 295-300.

ACKNOWLEDGEMENTS

The research was supported by NSF (#BES-0134503). The contributions of N. Phatak, Dr. S. E. Kim, and J. L. McCann in image acquisition are gratefully recognized.

BIOMECHANICAL & MUSCULAR DIFFERENCES IN THREE JUMP CONDITIONS

Jennifer M. Neugebauer and Keith R. Williams

Exercise Science Graduate Group, University of California, Davis, USA
Email: jmneugebauer@yahoo.com
Website: http://www.dbs.ucdavis.edu/grad/exs_sci_gg/default.html

INTRODUCTION

Vertical jumps are performed in many athletic situations with maximizing the height jumped a common goal. Most jumps involve a countermovement (CMJ), which includes a stretch-shortening cycle (SSC) movement. At the beginning of the upward phase of movement in a CMJ, the muscles have been activated due to the SSC resulting in substantially higher ground reaction forces compared to a NCMJ. The increase in force in a preloaded condition (CMJ) compared to a non-preloaded condition (NCMJ) is referred to here as force potentiation. Contractile potentiation, elastic energy storage and return, and increased muscular activation have all previously been identified as contributing to force potentiation[1,2]. Contractile potentiation is considered here to be an increase in force resulting from the contractile mechanisms for a given level of muscular activation, which is assumed to result from an alteration of the number of cross-bridges formed and/or the force generated per cross-bridge.

Previous studies[3] have varied the type of preload in non-jumping movements to identify the performance benefit (i.e. increased torque or increased work), but studies have not varied the type of preload specifically in a jumping motion in which the subject initiates the jump from the ground (i.e. not a drop jump). Additionally, recent improvements in the use of ultrasound to monitor muscle and tendon behavior provide a useful technique for identifying how the muscle-tendon unit functions during different types of jumps.

The purpose of this study was to investigate the effect of pre-activation on force and contractile potentiation during three jump conditions through the analysis of gastrocnemius (gastroc) length and activation behavior, ankle kinematics, and ground reaction forces.

METHODS

Nine female collegiate club volleyball players performed three modified jumps that involved ankle plantarflexion only on an inclined sled positioned at 29.2° relative to the ground. The three jumps were a NCMJ, a CMJ, and an isometric preload jump (IPJ). During the three jumps, electromyography (EMG) of the gastroc, soleus, and tibialis anterior (TA) were acquired to determine activation patterns, along with kinematic data to measure ankle movement, ground reaction forces to assess externally applied forces, and ultrasound images of the medial gastroc to monitor muscle fascicle length. The IPJs were designed such that the force at the beginning of the upward phase of the jump (T3) was comparable to that in CMJs at T3, but without the use of the SSC to attain that force.

RESULTS AND DISCUSSION

CMJs and IPJs had greater jump heights than NCMJs, as expected. The foot reaction force along the direction of the jump ($F_{z'}$) at the beginning of the upward phase of both CMJs and IPJs was comparable (1124.7 N and 1071.6 N, respectively) (Figure 1).

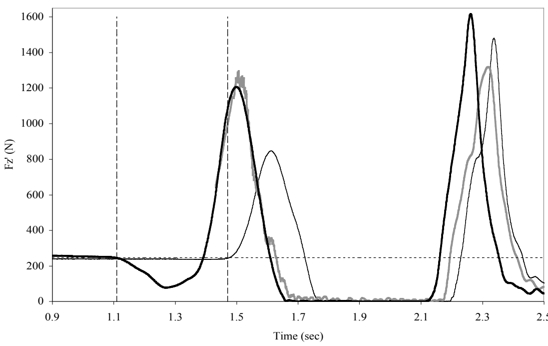

Figure 1. Average (n=3) force ($F_{z'}$)-time plot for NCMJ (thin line), CMJ (thick line), and IPJ for a representative subject

EMG activity of the gastrocnemius, soleus, and tibialis anterior did not differ significantly in any of the three jump conditions. Gastroc fascicle lengths at the beginning of the upward phase of movement were shortest in CMJs, and comparable in IPJs and NCMJs (Figure 2). Ankle angle comparisons suggested that muscle-tendon unit (MTU) lengths were comparable in all three jumps at the time of upward movement, indicating longer tendon lengths in CMJs compared to both NCMJs and IPJs.

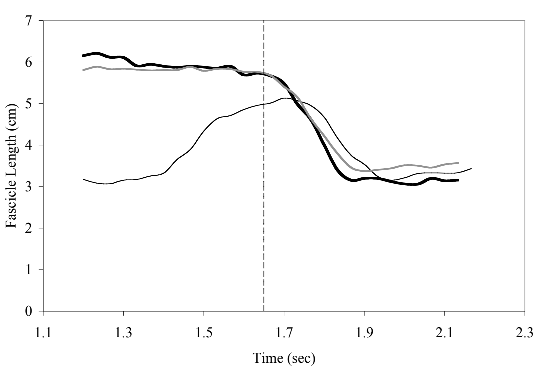

Figure 2. Average (n=3) muscle fascicle lengths for a representative subject during NCMJ (gray line), CMJ (thin black line), and IPJ (thick black line).

Force potentiation was similar in both the CMJs and the IPJs as indicated by the comparable forces ($F_{z'}$) at the beginning of the upward phase of movement for the CMJs and IPJs and lower forces for the NCMJs. Additionally, at T3, contractile potentiation occurred in IPJs and CMJs compared to NCMJs based on the observation of comparable EMG activation of the gastrocnemius, soleus, and TA in all three jumps combined with greater reaction forces in the CMJs and IPJs.

SUMMARY

As expected, CMJ and IPJ jump heights were greater than NCMJ jump heights, and these differences could be attributed to force and contractile potentiation at the start of the upward movement. While trends in the data showed CMJ jump heights to be slightly greater on average than IPJs, the differences were not statistically significant. Differences in pre-activation force levels of IPJs and CMJs were minimal and did not influence jump height. The non-significant results suggest that SSC contributions in the CMJs did not provide an overall increase in jump height compared to the IPJ condition, perhaps indicating that mechanisms such as contributions from elastic energy were not greater in the CMJ jump as might have been expected.

REFERENCES

1. Finni, T., *et al*. (2000). *European Journal of Applied Physiology*. 83: 416-426.
2. Komi, P.V., and C. Bosco. (1978). *Medicine and Science in Sports and Exercise*. 10(4): 261-265.
3. Walshe, A.D., *et al*. (1998). *Journal of Applied Physiology*. 84(1): 97-106.

DYNAMIC TRUNK KINEMATIC STIFFNESS DURING FLEXION AND EXTENSION

P.J. Lee[1], K.M. Moorhouse[2], and K.P. Granata[2]

[1]Musculoskeletal Biomechanics Lab, ME, Virginia Tech, Blacksburg, VA, USA
[2]Musculoskeletal Biomechanics Lab, ESM, Virginia Tech, Blacksburg, VA, USA
Email: palee2@vt.edu Web: http://www.biomechanics.esm.vt.edu/msbiolab/

INTRODUCTION

Spinal stability is related to active stiffness of trunk musculature but accurate measurements of trunk stiffness and dynamics are currently unavailable (Cholewicki et al, 2000). Active stiffness of the trunk may significantly vary as different muscles within the trunk are activated for various dynamic tasks. The purpose of this study was to quantify the role of flexor muscles versus extensor muscles on active trunk stiffness. This will provide a better understanding into trunk stiffness and stability.

Active trunk stiffness can be calculated using standard deconvolution techniques and second order parametric analysis (Moorhouse, Granata, 2004). We hypothesize that trunk stiffness will be higher when the trunk is preloaded with an external flexion moment compared to when it is preloaded with an equivalent external extension moment

METHODS

Seven females and eight males with no history of LBDs and with an average weight and stature of 69.9 ± 22.9 kg and 173.9 ± 10.2 cm respectively participated in the study. Before participation, all subjects signed informed consent approved by the Virginia Tech human subjects review board.

A harness and cable system attached the subject to a servomotor (Pacific Scientific, Rockford, IL) such that cable tension applied external loads at the T10 level of the trunk. The motor was programmed to provide three levels of isotonic load, 100 N, 135 N, and 170 N while the subjects stood upright with their pelvis and legs strapped to a rigid support. Superimposed on the preload were force perturbations of ± 30 N applied in a pseudo-random stochastic fashion with a flat bandwidth from 0-50 Hz. Pseudorandom stochastic inputs were chosen to avoid problems with voluntary responses due to predictable stimuli (Kearny, Hunter, 1990).

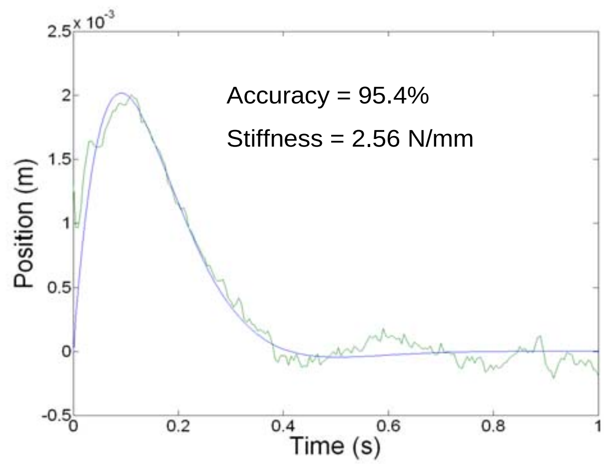

Figure 1: Typical impulse Response and Parametric model estimate.

The applied forces were measured by a force transducer attached to the motor sampled at 1000 Hz (Omega, Stamford, CT). The small amplitude dynamic trunk movement was recorded using IRED motion analyses at 200 Hz. Three pseudorandom perturbation trials of ten seconds were performed at each load level presented in random order. The protocol was performed with the isotonic loads applied to invoke both flexor and extensor muscle groups for a total of eighteen trials.

Using standard deconvolution techniques and 2nd order parametric analyses, trunk stiffness, damping, and inertia were calculated from the transfer function describing the relation between input force and output trunk movement (Moorhouse, Granata, 2004). Quality if model was determined by comparing estimated and observed motion variance accounted for (VAF).

RESULTS AND DISCUSSION

Nonparametric transfer functions indicated that dynamics of the trunk disturbed by random force impulse could accurately be represented by an underdamped 2nd order system (Figure 1). Mean VAF was 90.3% indicating the model accurately represented active trunk kinematic response.

Trunk flexor and extensor muscles functions demonstrate significantly different biomechanics (Table 1). Trunk stiffness was significantly higher during activation of extensor muscle groups than flexor muscle groups. The mean stiffness value for activation of flexor muscles was 3.06 N/mm compared to 3.62 N/mm for extensor muscles. Trunk stiffness increased significantly with load level. There was no significant with respect to gender. Additionally, there was a significant interaction between trunk flexor/extensor muscle group and load level (Figure 2).

Table 1: Stiffness was significantly higher during activation of extensor muscles than flexor muscles

Flexor/extensor	**$p<.05$**
load level	**$p<.01$**
gender	$p=.226$
flexion/extension x load level	**$p<.05$**

SUMMARY

Stability analyses must consider the fact that trunk flexor and extensor muscles demonstrate significantly different biomechanics. Past research has associated increased levels of trunk stiffness with increased stability of the trunk. Interaction between trunk flexor/extensor muscle activation and load level suggest stability of the spine might be higher during activation of extensor muscles at higher load levels.

On going work includes development of a theoretical model to help explain the significant biomechanical difference between flexor and extensor muscle witnessed experimentally. This will provide insight into stability of the spine for dynamic tasks that activate flexor and/or extensor muscle.

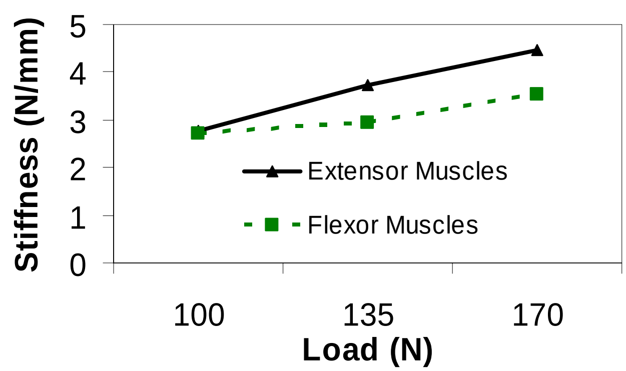

Figure 2: Interaction between flexor/extensor activation and load level was significant.

REFERENCES

Cholewicki, Simons, Radebold. *J.Biomechanics* 2000;33:1377-85.
Moorhouse, Granata. *International Society of Electrophysiology & Kinesiology*. 2004
Kearny, Hunter. *Crit.Rev.Biomed.Eng.* 1990;18:55-87.

ACKNOWLEDGEMENTS

This research was funded by a grant R01 AR49923-01 from NIOSH of the CDC

TIME-EVENT CROSS CORRELATION: A NEW TECHNIQUE FOR TIME SERIES COMPARISON APPLIED TO SHOULDER JOINT KINETICS DURING WALKER ASSISTED AMBULATION

INTRODUCTION

Comparison of two time series signals of kinematics or kinetic variables of human motion is a common method of analysis in biomechanical studies. Classical comparison analysis looks at a single variable based on discrete timing event, such as time-to-peak. One approach, called cross correlation, has been used in biomechanics for different purposes, such as EMG pattern detection (Li and Caldwell, 1999). However, this approach does not provide information about possible correlations based on a continuous time event. The purpose of this study was to compare and demonstrate how time-event cross correlation analysis (TEC) can be a useful alternative tool with the advantage of being able to combine the correlation and continuous time-event domains to look at biomechanical variables.

To demonstrate the utility of this technique shoulder kinetics during gait with a walker was evaluated in patients ambulating with an instrumented walker following total hip and total knee surgery. These Patients were recruited as part of a larger study on upper-extremity joint loads associated with walker use (McQuade, Finley, Liu, In-press JRRD).

METHODS

Kinematic data were collected using three active infra-red cameras (Optotrack®, Northern Digital Inc., Waterloo, Ontario). Kinetic data were collected using a standard four-point walker instrumented with strain gauge force transducers (AMTI, Watertown, MA, USA). Three-dimensional kinematics and hand contact force of both upper extremities were collected at 100 Hz.

Inverse dynamics was used to calculate shoulder joint moments. Shoulder flexion and extension moment of surgical and non-surgical side was ensemble averaged for 20 subjects from 0 to 100% of walker gait cycle which was defined beginning of positive vertical hand transducer force loading in the walker handles through pick up of the walker to next initial loading (contact-swing-contact).

Time-event cross correlation of shoulder moment (surgical side vs non-surgical side) was computed by using moving short time windowing (10% of walker gait cycle) technique (Equation, 1 and Liu, McQuade, In-press JBM), which is modified from cross correlation (Equation, 2). The cross correlation coefficient, time lag, and walker gait cycle were constructed as 3-D surface plot by using MatLab (Mathworks, Natick, MA).

$$R_{xy}(n,k) = \frac{C_{xy}(k+n+m)w(m)}{\sqrt{C_{xx}(0)C_{yy}(0)}} \qquad \text{Equation 1}$$

$$R_{xy}(k) = \frac{C_{xy}(k)}{\sqrt{C_{xx}(0)C_{yy}(0)}} \qquad \text{Equation 2}$$

RESULTS AND DISCUSSION

There is no significant different in terms of peak amplitude of shoulder flexion and extension moment within walker gait cycle compared surgical side with non-surgical side by using classical method (Figure, 1). This single discrete timing event comparison cannot provide the details of correlation between surgical side and non-surgical side shoulder moment during walker gait cycle.

The result from time-event cross correlation (Figure, 2) revealed the different distribution pattern of cross correlation coefficient along the time lag and walker gait cycle, which can not be assessed from figure 1.

SUMMARY

This study provides the alternative tool to describe subtle changes based on time-event cross correlation analysis, which in turn allows us to gain more information on comparison of biomechanical variable during cyclical motion.

REFERENCES

Li, L., Caldwell, G.E. (1999). *J. Electromyography and Kinesiology,* **9**, 385-389.
McQuade, K., Finley, M., Liu, W., *J Rehabilitation Research & Development* (In Press), 2004
Liu, W., McQuade, K., *J Biomechanics* (In Press), 2004

ACKNOWLEDGEMENTS

The authors thank Margaret Finely and Shih Chiao Tseng for their assistance with data collection. This work was supported by Rehabilitation Research and Development Service, Baltimore Veterans Administration Medical Center.

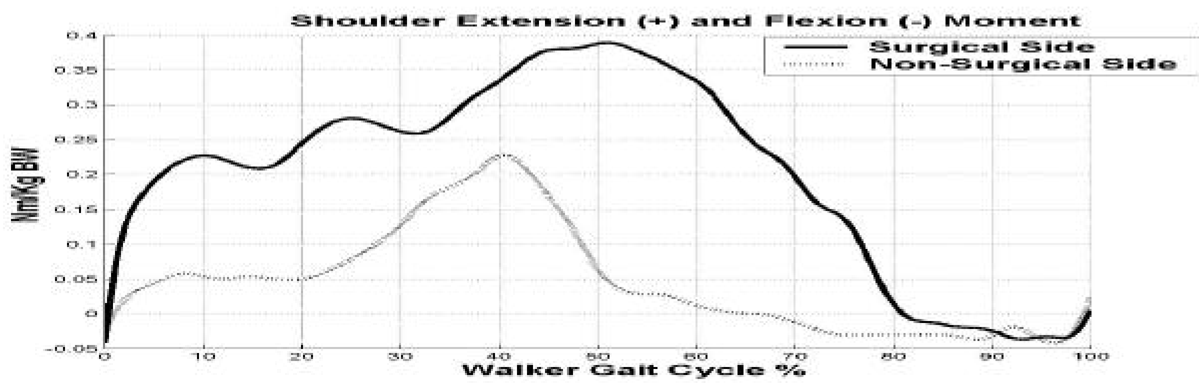

Figure 1: This figure illustrates shoulder flexion and extension moment (surgical vs non-surgical side).

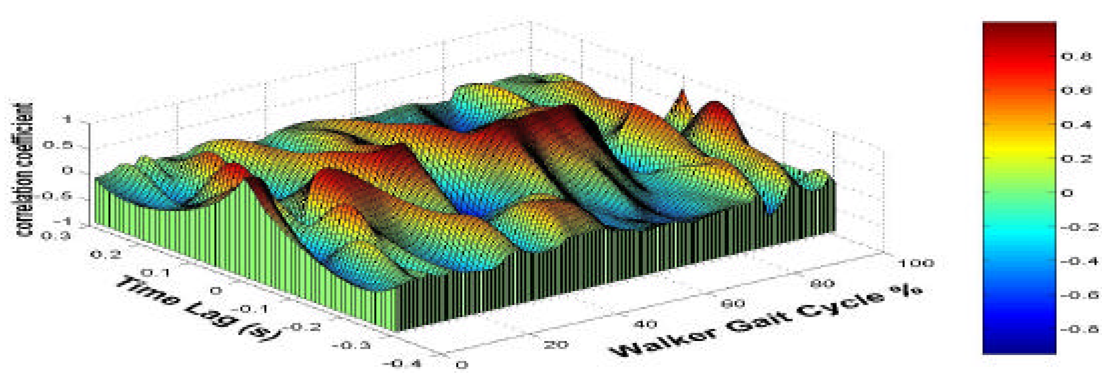

Figure 2: This figure illustrates time-event cross correlation of shoulder flexion and extension moment (surgical vs non-surgical side). Color indicates that darker red is greater correlation of while blue indicates less correlation as illustrated in reference of the percent walker gait cycle.

HETEROGENEOUS ADAPTATION OF THE PATELLOFEMORAL JOINT TO SHORT- AND LONG-TERM ANTERIOR CRUCIATE LIGAMENT DEFICIENCY

Andrea Clark[1], Walter Herzog[1], John Matyas[2], Leona Barclay[2] and Tim Leonard[1]

[1] The Human Performance Lab, Faculty of Kinesiology, University of Calgary, AB, Canada
[2] McCaig Centre for Joint Injury and Arthritis Research, University of Calgary, AB, Canada.

E-mail: walter@kin.ucalgary.ca

INTRODUCTION

Focal chondral or osteochondral defects occur at an earlier age, are more severe and cover a larger portion of the cartilage surface on the patella compared to the femoral groove in the human patellofemoral joint (Meachim and Emery, 1974, Hjelle et al., 2002). The majority of research investigating the etiology of patellofemoral cartilage defects has focused on joint biomechanics. Less attention has been given to other possible factors such as the different material properties and/or histological architecture of the cartilages (Froimson et al., 1997). We have shown that differences exist between healthy feline patellar and femoral groove cartilages in tissue thickness, chondrocyte shape and chondrocyte volumetric fraction in both magnitude and depth distribution (Clark et al., 2003). Furthermore, under identical applied loads, changes to all of these parameters differ in magnitude and depth distribution. We hypothesized that these differential histological parameters may result in predisposing one of the surfaces to altered biosynthetic activity and/or structural damage compared to the other.

The purpose of this study was to investigate if the cartilages of the feline patellofemoral joint adapt differently to anterior cruciate ligament (ACL)-deficiency, and to elucidate where, throughout the depth of the cartilage, this adaptation begins. We wanted to systematically quantify feline patellofemoral histology in short- (4 months) and long-term (67 months) ACL-deficient knees.

METHODS

Unilateral ACL-transection was carried out on twelve skeletally mature male cats. The animals were then allowed free movement until sacrifice either 4 (n=6) or 67 (n=6) months post surgery. The experimental femur and patella were dissected free and histologically fixed using a ruthenium hexammine trichloride fixative solution (Hunziker et al., 1982). Full thickness osteochondral blocks (3mm x 1mm) were harvested from the same anatomical sites in experimental specimens. 0.5µm thick sections were cut and stained with toluidine blue for light microscopy. Cartilage thickness and chondrocyte shape, clustering, size and volumetric fraction were quantified.

RESULTS

Feline patellofemoral cartilages adapted differently to ACL-deficiency: the cartilage of the femoral grooves had little microscopic pathology compared to the patellae (Figure 1).

4 months after surgery the patellar articular cartilage from the experimental joints was thicker, contained larger chondrocytes more frequently arranged in clusters and had a larger volumetric fraction of chondrocytes compared to normal controls (Figure 1). Interestingly, the majority of these changes were only observed in the middle layer (Figure 1).

At 67 months post surgery we found significant differences in patellae cartilage compared to normal controls including increased thickness, rounded and clustered

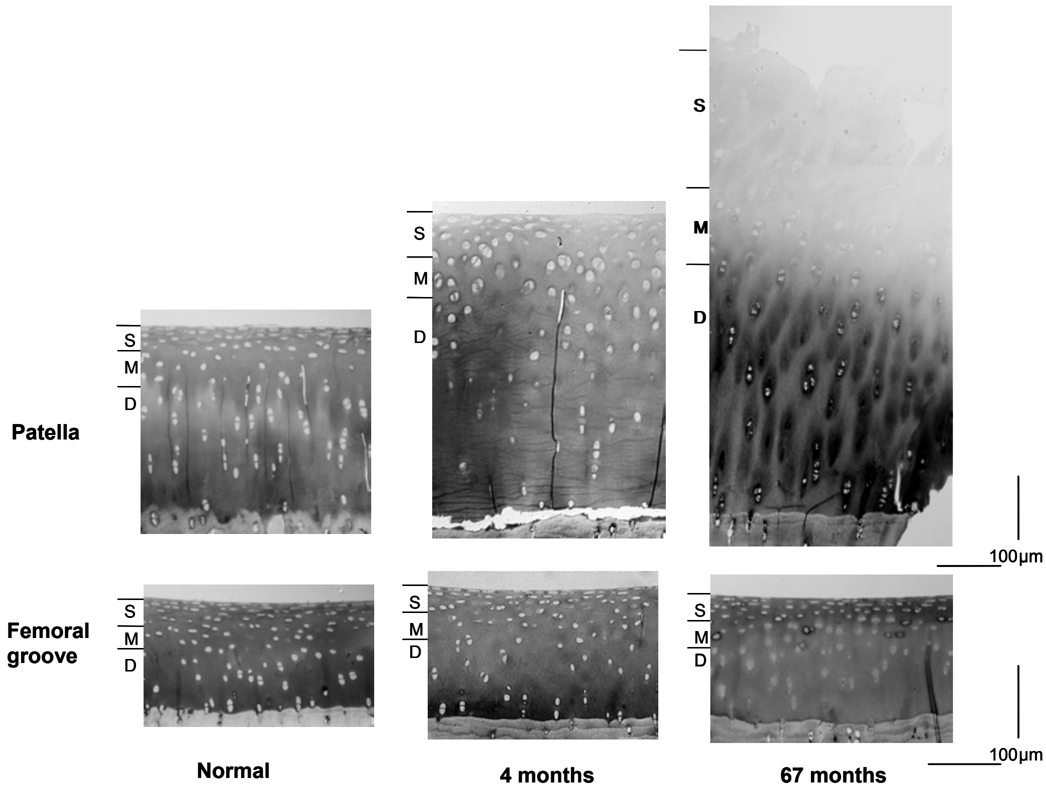

Figure 1: Comparison of normal, 4 or 67 months post ACL- transection articular cartilage. The superficial (S), middle (M) and deep (D) histological layers are indicated for each section. Sections taken from the feline patella and femoral groove, 0.5µm thick, stained with toluidine blue and photographed at 100x magnification.

superficial layer chondrocytes, a fibrillated and fissured cartilage surface and uneven proteoglycan staining throughout cartilage depth (Figure 1). These changes were most apparent in the middle and superficial layers (Figure 1).

DISCUSSION

Cartilage adaptation to ACL-deficiency was heterogeneous within the patellofemoral joint: the femoral groove cartilage had little pathology compared to the patellae. We hypothesize that this is due, in part, to the differential histological parameters (see intro) of the surfaces in healthy cartilage. Furthermore, patellar cartilage adaptation was first apparent in the middle layer 4 months after surgery. We have shown that the largest tissue strains and changes to chondrocyte volume and shape occur in the middle layer of healthy patellar tissue under static load (Clark et al., 2003). Furthermore, the middle layer of patellar cartilage contains the largest and most spherical chondrocytes throughout tissue depth. We speculate that these properties of middle layer patellar tissue may enable it mechanically and/or biologically to respond most quickly to changes that occur in the patellofemoral joint with ACL-deficiency.

REFERENCES

Clark A et al. (2003) *J. Biomech.* 36, 553.
Froimson M et al. (1997) *OA. Cart.* 5, 377.
Hjelle K et al. (2002) *J. Arthro. Surg.* 18, 730.
Hunziker E et al. (1982) *J. Ultrastructure Res.* 81, 1.
Meachim G and Emery I (1974) *Ann. Rheum. Dis.* 33, 39.

ACKNOWLEDGEMENTS

CIHR, AHFMR and The Arthritis Society

THE PRESENCE OF AN OBSTACLE INFLUENCES THE STEPPING RESPONSE DURING SIMULATED AND REAL TRIPS

Karen L. Troy[1] and Mark D. Grabiner[1]

[1]Musculoskeletal Biomechanics Laboratory, University of Illinois at Chicago, Chicago, IL, USA email: klreed@tigger.uic.edu

INTRODUCTION Falling is a frequent cause of serious injury in the older adult population and trips are a dominant cause of falls. Although there are few laboratory protocols that induce actual trips, there are many studies that utilize surrogate tasks. Performance of surrogate tasks require similar biomechanical characteristic stepping responses, but unlike a trip, these tasks do not involve an obstacle.

Recovery from a trip over a previously unseen obstacle requires safe and rapid negotiation of an obstacle for which limited information has been acquired, followed by restoration of dynamic equilibrium. We hypothesized that the stepping kinematics following an actual trip would be significantly different than those of surrogate tasks having similar rapid execution requisites but that did not involve an obstacle. Specifically, we expected that steps following a trip would be higher and faster than those of the surrogates.

METHODS Thirteen subjects each participated in three different protocols, performed on three separate days. During the experiments the participants were protected from a fall to the ground by a safety harness attached to an instrumented dynamic rope. The first task was a trip that was induced during locomotion (Pavol et al. 1999). No information about the means by which the trip would be induced was provided. The trip was induced during mid- to late-swing by a pneumatically-powered obstacle that was part of the laboratory floor and was not visible to the subject at any time. After being remotely triggered, it rose to a height of 5 cm in about 150 ms. Data from only one trip per subject was collected.

The second task used a motorized treadmill to induce a rapid forward-directed postural disturbance (Owings et al, 2000). Initially the subject stood quietly on the belt of the treadmill (Series 1800, Marquette Electronics, Milwaukee, WI, USA) which, when activated, accelerated to the designated velocity in approximately 150 ms. The subjects were instructed to recover their balance and then continue walking. A maximum of 11 trials were performed by each subject and the fastest treadmill speed was 1.12 m/s (2.5 mph). In the present analysis, only data from the first successful recovery at this speed were used.

In the third task, subjects were released from a static forward leaning position and instructed to recover with a single step (Owings et al, 2000). The subject was positioned at the initial static lean angle with their arms folded across their chest, feet aligned forward with their heels on the ground, shoulder width apart. The lean angle was increased until the maximum recoverable lean angle was determined. Data from the first trial at the maximum recoverable lean angle were used in the present study.

Maximum step height, step length of the leading and trailing limbs (in the leaning task there was no trailing limb data), and peak vertical and peak horizontal velocity of the leading and trailing feet were derived from the kinematics of the reflective markers placed bilaterally over the lateral malleoli.

RESULTS AND DISCUSSION The trajectories of the leading and trailing limbs following the trip were higher and faster than those during the treadmill recovery (Figure 1). MANOVA revealed a significant effect of task ($p<0.001$). The between-task differences in maximum step height, step length, and peak vertical velocity were all significant ($p<0.001$). Maximum step height and peak vertical velocity of the leading and trailing limbs were significantly larger during recovery from the trip compared to the treadmill recovery ($p<0.01$). The step heights of the leading and trailing legs were 12.8±7.3 and 19.0±6.9 cm higher following the trip than

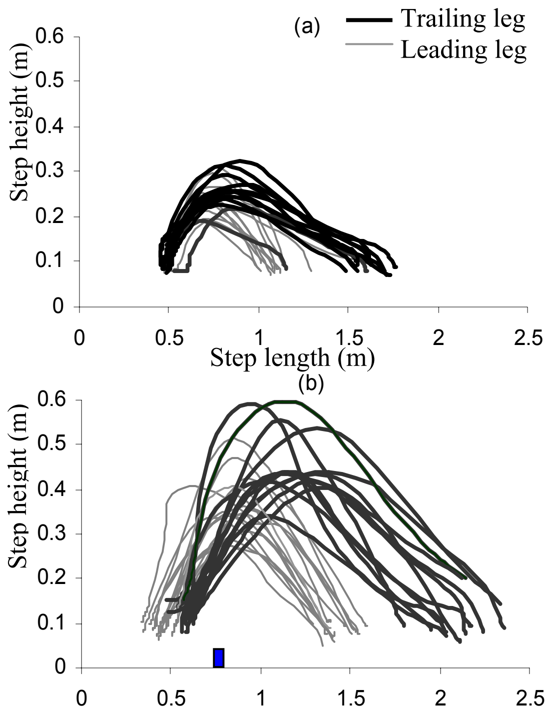

Figure 1: Ankle trajectories from (a) treadmill and (b) tripping activities in the sagittal plane, from left to right. In (b) the obstacle location is marked

following the treadmill perturbation, respectively. Similarly, peak vertical velocities for the leading and trailing legs after the trip were 0.79±0.77 and 0.93±0.55 m/s faster than after the treadmill.

Foot state variables of the leading limb during the leaning task were not different than those measured during the treadmill task although they were significantly different compared to those of the trip (Table 1). Between-task comparisons of all three activities were limited to the leading limb variables in a subset of subjects (7 total), all of whom had the same maximum recoverable lean angle. MANOVA revealed that compared to the leaning task, tripping resulted in significantly larger leading leg step height, step length, and vertical velocity ($p<0.013$ for each measure). These variables were not significantly different between leaning and treadmill tasks.

These results demonstrate important differences in stepping kinematics resulting from a trip compared to surrogate tasks. The state variables associated with recovery from a trip are considerably different than those associated with recovery from a lean or treadmill task, both of which have been implied as surrogates to study recovery from a forward-directed trip (Schillings et al, 1996; Schillings et al, 2000; Owings et al, 2000).

Although the onset of the disturbance was difficult to predict for the leaning and treadmill tasks, the tasks share similarities such as the unambiguous nature of the postural disturbance. During the leaning and treadmill tasks it was obvious to the participants that the floor/treadmill belt was devoid of objects that might obstruct the stepping responses. We believe that these features enhance pre-planning of the recovery task execution, including the specification of a smaller safety factor in terms of maximum step height.

The results of the present study strongly suggest the presence of important differences between the surrogate tasks for forward-directed trips examined here and actual trips. Further, these important differences appear to be related to the presence of an obstacle. If task-specific training is a plausible approach to reducing the incidence of falls and fall-related injuries, then the extent to which the training task resembles the actual task is a key design consideration.

REFERENCES

Owings et al (2000). *J Am Geriatr Soc* **48**:42-50
Pavol et al. (1999) *J Gerontol* **54**:M583-590
Schillings et al. (1996) *J Neurosc Meth* **67**:11-17
Schillings et al. (2000) *J Neurophysiol* **83**:2093

Table 1: *Post hoc* comparisons of recovery leg variables from tripping, treadmill, and leaning tasks, for the reduced data set (7 subjects, all with the same maximum recoverable lean angle).

	Trip	Treadmill	Lean	p (trip vs. lean)	p (trip vs. tread.)	p (tread. vs. lean)
max height (m)	0.327	0.232	0.216	<0.001	<0.001	0.271
step length (m)	0.935	0.599	0.605	<0.001	<0.001	0.816
peak vertical velocity (m/s)	2.167	1.28	1.16	0.013	0.002	0.285
peak horizontal velocity (m/s)	4.976	3.851	3.563	0.033	0.081	0.185

DIRECTLY COMPARING STANDING AND WALKING STABILITIES

Hyun Gu Kang [1] and Jonathan B. Dingwell [1,2]

[1] Nonlinear Biodynamics Lab, Dept. of Kinesiology, University of Texas, Austin, TX, USA
[2] Dept. of Biomedical Engineering, University of Texas, Austin, TX, USA
E-mail: jdingwell@mail.utexas.edu Web: http://www.edb.utexas.edu/faculty/dingwell/

INTRODUCTION

Falls are one of the primary causes of accidental deaths for those over age 65. Clinical assessment of fall risk in the elderly is typically based on measures obtained from standing balance tests. However, most falls occur during walking and these measures do not predict these falls well (Niino et al., 2000, Owings et al., 2000).

Several methods have also been proposed to quantify stability during walking. But due to inherent differences in task dynamics and definitions of stability measures, it has not been possible to directly compare stability between standing and walking. This study proposes a new dynamically and biomechanically rigorous metric for quantifying upper body stability that allows direct comparisons between walking and standing.

THEORY AND METHODS

The dynamics of a system can be evaluated by examining the trajectories of its state space. For a rigid body with mass, its inherent 6 degrees of freedom $[x\ y\ z\ q\ f\ y]$, plus their time derivatives $[\dot{x}\ \dot{y}\ \dot{z}\ \dot{q}\ \dot{f}\ \dot{y}]$ fully describe the dynamics of this 2nd order system. The local stability of such a system can then be described by quantifying the rate of divergence of neighboring state trajectories measured as a natural log of the Euclidian distance over time (Rosenstein et al 1993; Dingwell and Cusumano, 2000). A larger mean log divergence <ln *D*> indicates greater local dynamic instability.

One healthy male subject age 33 participated with IRB approved consent. He walked on a level treadmill (Woodway USA, Waukesha, WI) at his self-selected speed of 1.2 m/s for 3 trials of 5 minutes, resting at least 2 minutes between trials. He then stood on a 6-DOF force plate (Bertec, Columbus OH) at a comfortable stance for 3 trials of 5 minutes. A large curved fabric screen was placed 2 m in front of the subject to control the visual environment. The subject wore a safety harness attached to a rigid structure to prevent any falls. The 3D motions of the torso were sampled at 60 Hz from reflective markers on left and right scapulae, and T1 and T10 vertebrae, using a 6-camera motion capture system (Vicon-612, Oxford Metrics, Oxford, UK). During standing trials, force plate data were also sampled at 1080 Hz.

A 12-dimensional state space, $S(t) \in \Re^{12}$, for the torso was defined from the XYZ excursions of the T1 marker, the torso rotations in pitch, roll, and yaw, and their time derivatives. All states were demeaned and normalized to unit variance to prevent large values in any one state from dominating the state space trajectories. Mean log divergence over time of the nearest neighbor trajectories was calculated using a published algorithm (Rosenstein et al 1993) that was modified to use the state space trajectories defined above. To parameterize the mean log divergence curves, the following double exponential curve fit was used:

$$\langle \ln D \rangle = A - Be^{-t/t_1} - Ce^{-t/t_2} \qquad (1)$$

where t_1 and t_2 represent the time constants that describe how quickly <ln *D*> will saturate to *A*. All Calculations were done in MATLAB (Mathworks, Natick MA).

Thus, upper body motions were defined in the same sense for both standing and walking trials. This then allows the fundamental stability properties of these standing and walking movements, as observed within these state spaces, to be compared directly.

RESULTS AND DISCUSSION

The mean log divergences (Fig. 1) do not show a distinct linear region indicative of exponential dynamics (i.e. chaos). Both dynamics show a similar asymptotic behavior that occurs over two different time scales (Eq. 1). All curve fits achieved $r^2 > 0.98$. The Standing divergences show smaller time constants compared to the walking trials indicative of faster divergence (Table 1). This was unexpected since walking appears to be a more 'dynamic' task than standing.

Table 1: Standing and Walking Time Constants [seconds].

	Standing		Walking	
Trial	t_1	t_2	t_1	t_2
1	0.5047	0.0022	1.4549	0.0377
2	0.7268	0.0004	0.8500	0.0299
3	0.7620	2×10^{-8}	0.9070	0.0267

SUMMARY

This new proposed stability metric allows a direct comparison that reveals differences between the stability characteristics of standing and walking. Future work will determine if the two dynamics are correlated, or how they interact to influence fall risk.

Because our proposed metric is defined in a dynamically rigorous way, it could also be used to compare the dynamic stability of a wide range of movements and tasks that could not otherwise be compared directly.

Standing:

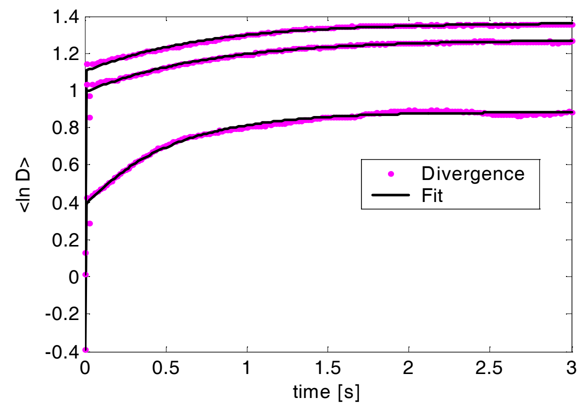

Walking:

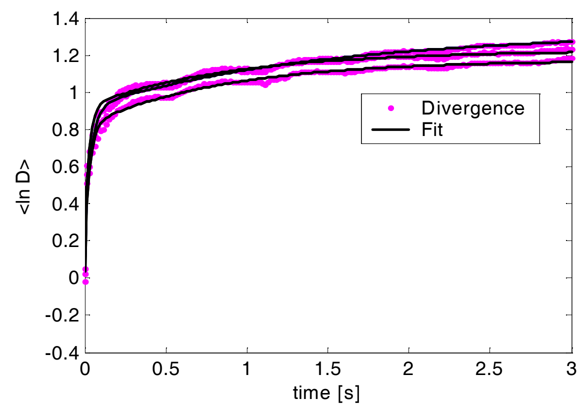

Figure 1: Mean log divergences and their curve fits. Both show a similar behavior: a steep initial rise and a slower saturation.

REFERENCES

Dingwell, J.B. and Cusumano, J.P. (2000) Chaos, **10** (4): 848-63.
Niino N, et al. (2000). *J. Epidemiol*, **10**, S90-S4.
Owings, T.M. et al (2000). *J Gerontol A Biol. Sci. Med. Sci.*, **55**, M469-M76.
Rosenstein, M.T. et al (1993). *Physica D*, **65**, 117-134.

ACKNOWLEDGEMENTS

This study was funded by a Biomedical Engineering Research Grant from the Whitaker Foundation.

Capstone Design of a Cranial Vascular Mechanical Model

Ryan Mangan[2], Sean S. Kohles[1], Nedzib Biberic[2], Nick Leech[2], Trenton J. McKinney[3], Edward Stan[3], Mihaela L. Surdu[3], Cathy Biber[2], and James McNames[3]
[1] Kohles Bioengineering, Portland State University, and Oregon Health & Science University, Portland, OR;
[2] Department of Mechanical and Materials Engineering, Portland State University, Portland, OR;
[3] Department of Electrical and Computer Engineering, Portland State University, Portland, OR
Email: ssk@kohlesbioengineering.com Web: www.kohlesbioengineering.com

INTRODUCTION

Traumatic brain injury (TBI) is an acquired injury to the brain caused by an external physical force resulting in impairments such as cognition, language, memory, etc. [Rosner, 1993]. TBI is a leading cause of death and disability in children. One of the largest dangers confronting patients with severe TBI is elevated intracranial pressure. As the brain swells due to the original injury, the pressure within the calvarium increases and can cause regional ischemia. This secondary injury, in turn, causes cell death and potentially permanent impairment.

Few diagnostic devices or physiologic models are available to mechanically assess the cranial vascular state. It is proposed that a mechanical model representing the cranial environment would serve as an enabling platform with objectives: 1) to evaluate pressure and compliance monitoring devices; 2) to complement emerging mathematical models describing cerebral autoregulation and mass transport; and 3) to educate clinicians and bioengineers studying TBI. The mechanical performance specifications used to design a proof-of-concept model were based on human physiology, cerebral vascular tissue properties, and transport phenomena [Rowell, 1986; Rosner, 1993; Miller and Chinzei, 1997; Humphrey, 2002; Monson et al., 2003].

METHODOLOGY

This project was completed by a team of ME and ECE undergraduates as a Senior Capstone requirement. The ME students were primarily responsible for designing and implementing a physical model of the cranium that includes engineered versions of the major cerebral vascular dynamics components, including the cranium, brain tissue with ventricles, arteries, capillaries, veins, blood, and cerebrospinal fluid (CSF). The ECE students were primarily responsible for the computer-based control of a pulsatile pump that mimics blood flow, control of the arteriole dilation/contraction, and application of pressure sensors in several locations within the model. The computer interface and analog input/output were implemented with LabWindows.

RESULTS AND DISCUSSION

A single pathway, vascular mechanics model has been developed for the following cranial subsystems (with selected properties based on physiologic constraints):

Heart and Blood: A computer controlled, peristaltic (flexible-tube) pump maintains pulsatile pressure (mean arterial pressure = 100 mmHg) drives a corn syrup, blood analog (Newtonian, dynamic viscosity, μ = $12x10^{-3}$ Ns/m^2 with 10:4.1 syrup:water volume ratio) through the vascular system (volumetric flow = 650 ml/min).

Vascular Tissue: Length segments consisting of synthetic materials functioning as rigid arteries, contractable-distensible arterioles, porous media capillaries, collapsible venules, and rigid veins simulates the intracranial vascular pressure drop from 100 to 5 mmHg. The mechanism to simulate vasoconstriction consists of closed-loop of wire rope transferring a decreasing diameter to a flexible tube via lengthwise rigid plates (Figure 1).

Figure 1: Vasoconstriction mechanism (wire fixed to cranial wall on left with tension applied by motor on the right).

<u>Cranium, Brain Tissue and Cerebrospinal Fluid</u>: A compressible gel (bulk modulus, K = 1300 MPa) surrounds the vascular system and both transfers pressure to the cranial vault (via pneumatic brain injury balloon) as well as mechanically responds to volume changes from vasoconstriction. The CSF ($\mu = 1\text{x}10^{-3}$ Ns/m^2) shifts as pressure develops between the brain tissue and the cranial shell (rigid, plastic cylinder), transferring perivascular pressure to the venous system.

Pressure and flow along the length of each vascular segment have indicated targets for the designed system (Figure 2).

SUMMARY

The cylindrical, proof-of-concept design has provided an initial means to clarify ICP mechanisms during TBI (Figure 3). Future efforts will convert the system into a spherical cranial analog for continued study.

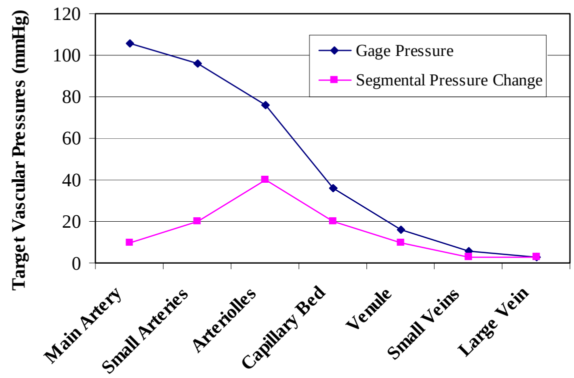

Figure 2: Vascular design target pressures.

REFERENCES

Humphrey, J.D. (2002) *Cardiovascular Solid Mechanics*, Springer.

Miller, K., Chinzei, K. (1997) *J Biomech*, **30**:1115-1121.

Monson, K.L. et al. (2003) *J Biomech Eng*, **125**:288-294,.

Rosner, M.J. (1993) In: *Neurosurgical Intensive Care*, McGraw-Hill.

Rowell, L.B. (1986) *Human Circulation and Regulation During Physical Stress*, Oxford Univ Press.

ACKNOWLEDGMENTS

Partial funding for this project was provided by a grant from the Thrasher Foundation. The authors thank Drs. B Goldstein and W Wakeland.

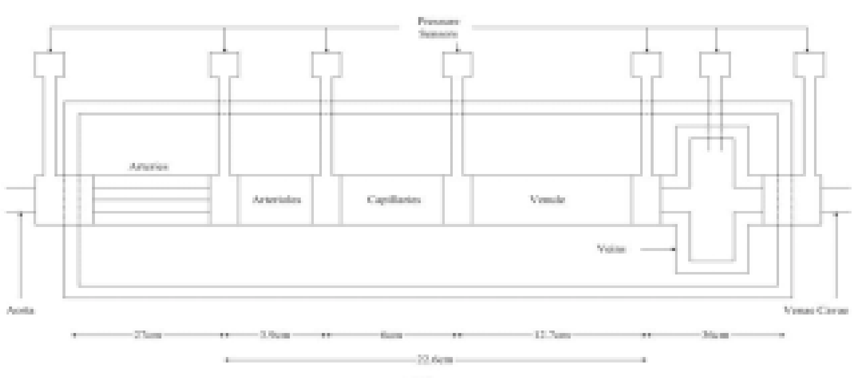

Figure 3: Schematic (left) of cranial system and pressure measurement ports.

THE EFFECT OF HAND POSITION ON WRIST KINEMATICS AT LANDING FROM A FORWARD FALL FROM A KNEELING POSITION

Karen L. Troy[1], Courtney D. Gavin[1], Mark D. Grabiner[1]
[1]University of Illinois at Chicago, Chicago, IL email: klreed@tigger.uic.edu

INTRODUCTION

In the United States, distal radius fractures are the most common upper extremity fracture in adults over the age of 65 years. The incidence has been reported as 8-10 fractures per 1000 person-years (Vogt et al. 2002). An estimated 15% of women sustain such fractures by age 80 (Nordin et al. 1980).

Several groups have examined the impact forces acting at the wrist resulting from a fall (Chiu and Robinovitch 1998; Hsiao and Robinovitch 1998; Robinovitch and Chiu 1998; Chou et al. 2001; DeGoede and Ashton-Miller 2003). Most of these experiments have measured ground reactions at landing after a forward fall from a kneeling position in which the subject lands with both hands on a force plate. However, kinematics such as wrist flexion angle, ulnar deviation, and hand position relative to the body have not been previously reported.

Wrist kinematics during impact affect the manner in which bones are loaded. Such data is important and necessary for developing models of distal radius fractures. Therefore, we measured wrist dorsiflexion, ulnar deviation, and angular dorsiflexion velocity from forward falls initiated from a kneeling position. Multiple hand-torso positions were evaluated.

METHODS

8 healthy adults (aged 23 to 53) participated in this study. The key upper extremity markers were placed bilaterally on the third metacarpal, midway between the radial and ulnar heads, the lateral humeral epicondyles and the acromion processes. Kinematics were recorded with an 8-camera motion capture system (Motion Analysis, Santa Rosa, CA) operating at 60 Hz. Ground reaction forces were collected with two AMTI force plates at 2400 Hz.

Each subject kneeled in front of the two force plates so that when they leaned forward their hands could each contact one plate and their nose would line up with a place marker. Four targets were marked with numbered Xs on each plate (Figure 1). The Xs were positioned so that the hands were either placed high (ear-level) or low (armpit-level), and spaced wide or narrow. Each subject leaned forward from a kneeling position and targeted a set of Xs for three consecutive trials. In addition to the four targets, three trials in which no target was specified were also recorded, for a total of 15 trials per subject. Subjects were allowed to flex the elbows as necessary when landing, and to rest between trials. Target order was randomized between subjects.

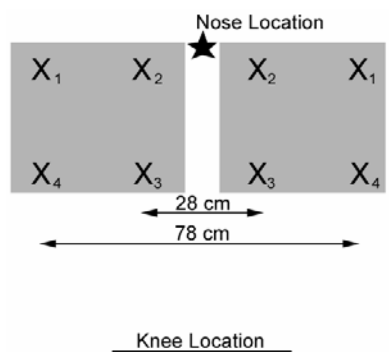

Figure 1 Target location and force plate setup

For each trial the instant of hand contact and the instant of peak resultant force was determined from the force plate recordings. Initial contact was defined as the time when the resultant force exceeded 1% of subject body weight. Ulnar deviation and wrist dorsiflexion were averaged for each hand and hand position during the 67 ms following hand contact with the force plate (peak resultant force occurred 25 to 40 ms after initial contact for all trials). Average wrist angular velocity for the 67 ms interval was calculated by dividing the change in dorsiflexion angle by the elapsed time. Repeated measures ANOVA was used to compare the three outcome variables. Where indicated, paired t-tests with Bonferroni corrections were used to conduct *post hoc* multiple comparisons.

RESULTS

Hand position significantly affected wrist flexion, ulnar deviation, and angular velocity at impact ($p<0.001$). When the hands were low on the body and narrowly spaced the average ulnar deviation was 9°±4° and the average wrist dorsiflexion angle was 38° ±7°. In contrast, when the hands were high on the body and widely spaced, ulnar deviation was 6° ±6° and wrist dorsiflexion was 30° ±6° ($p=0.003$).

Although low hand positions resulted in less dorsiflexion than high hand positions ($p<0.001$), low hand positions were associated with faster dorsiflexion velocities (350°/sec vs. 321°/sec, $p=0.009$). This is likely a result of subjects preparing for low hand position landings by dorsiflexing their wrists before ground contact. Low hand positions also had significantly larger ulnar deviation angles than high positions ($p=.0034$).

Narrowly spaced hand positions resulted in higher flexion angles ($p=0.003$), however ulnar deviation was not significantly greater ($p=0.061$)

The self-selected (non-specified) hand position had the highest dorsiflexion velocity (374°/sec) and the lowest ulnar deviation (5.0°) of all the positions tested. Although selected individual comparisons between specified and self-selected positions achieved significance, none of the measures were significantly different from all four specified positions.

DISCUSSION

Ground reaction forces for simulated forward falls have been reported in the past, but to date, the kinematics of the wrist during the impact phase do not appear to have been reported. This kinematic information is particularly important in the wrist where numerous ligaments provide passive restraint against excessive motion. Specifically, the high dorsiflexion velocity measured in the present study probably increases the overall stiffness of both the passive and active restraints during impact. In rapid loading situations such as those investigated here, the internal joint forces may be on the order of multiple body weights.

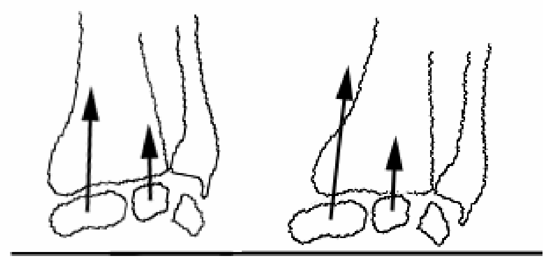

(a) **(b)**

Figure 2 Forces transmitted from the scaphoid and lunate to the radius of the right hand with (a) neutral wrist position (b) 10° ulnar deviation

Since there is an interest in reducing the number of distal radius fractures resulting from forward falls, complete understanding of both the kinematic and kinetic behavior of the wrist during impact, both of which influence loading of the radius, is important (Figure 2). This data, combined with the accompanying ground reaction data, will be useful as boundary conditions for a finite element model.

REFERENCES

Chiu J. et al. (1998) *J Biomech* **31**(12)
Chou PH et al. (2001. *Clin Biomech* **16**(10)
DeGoede KM et al (2003) *J Biomech* **36**(3)
Nordin BE et al. (1980) *Clin Endocr Metab* **9**(1)
Robinovitch SN.et al. (1998) *J Orthop Res* **16**(3)
Vogt MT et al. (2002) *J Am Geriatr Soc* **50**(1)

PARAMETER ROLES FOR A NONLINEAR MATHEMATICAL MUSCLE MODEL

Laura A Frey Law and Richard K. Shields

Graduate Program in Physical Therapy and Rehabilitation Science, Carver College of Medicine,
The University of Iowa, Iowa City, IA E-mail: richard-shields@uiowa.edu

INTRODUCTION

A highly published model incorporating two differential equations with six constant parameters, can predict non-fatigued, isometric contractions in submaximally activated, able-bodied, quadriceps muscle (Ding, et al., 1998, 2002). This model has not yet been validated for muscles with different force time characteristics, such as slow or paralyzed muscles. Diverse muscle conditions may require alterations to the model parameters.

The purpose of this study was to evaluate the role and sensitivity of each parameter to promote its use for a variety of muscle conditions. This model has undergone several evolutions, with the addition and subtraction of parameters and equations. Ultimately, future applications of this model will benefit from the knowledge of each parameter's role in the model.

METHODS

The model consists of two, non-linear, differential equations (eqs 1 and 2), with two state variables (C_N and F) and six constant parameters (A, τ_1, τ_2, τ_c, km, and Ro) (Ding, et al., 1998, 2002). Eq 1 represents the calcium kinetics and the formation of the Ca^{2+} - troponin complex, where C_N (dimensionless) represents this rate-limiting step of muscle force production (Ding, et al., 1998). Eq 1 contains two constant parameters, τ_c (ms), the time constant controlling the calcium dynamics (C_N) and Ro (dimensionless), a scaling factor for C_N to model the catch-like property of muscle (Ding, et al., 2000). Eq 2 contains four constant parameters, A, τ_1, τ_2, and km, and both state variables, C_N and F, to model force output.

$$\frac{dC_N}{dt} = \frac{1}{\tau_c}\sum_{i=1}^{n} R_i \exp(-\frac{t-t_i}{\tau_c}) - \frac{C_N}{\tau_c} \quad (1)$$

$$where: R_i = 1 + (R_0 - 1)\exp(-\frac{t_i - t_{i-1}}{\tau_c})$$

$$\frac{dF}{dt} = A\frac{C_N}{k_m + C_N} - \frac{F}{\tau_1 + \tau_2 \frac{C_N}{k_m + C_N}} \quad (2)$$

$$C_N = \sum_{i=1}^{n} R_i \frac{t-t_i}{\tau_c}\exp(-\frac{t-t_i}{\tau_c}) \quad (3)$$

Parameter A (N/ms) has been described as a force-scaling factor and a scaling factor for the muscle shortening velocity (Ding, et al., 2002). The time constant, τ_1 (ms), controls force decay when C_N is zero i.e. no strongly bound cross-bridges exist (Ding, et al., 1998). A second time constant, τ_2 (ms), controls force relaxation in the presence of C_N, which has been described as the force decay due to "extra friction between actin and myosin resulting from the presence of strongly bound cross-bridges" (Ding, et al., 2002). The most recent parameter addition to the model, k_m, controls the sigmoidal relationship between calcium release (i.e. strongly-bound cross-bridges) and force production in Eq 2 (Ding, et al., 1998).

The model was solved using Matlab (R 12, The Mathworks, Inc., USA), for 11 different inputs: a twitch (Tw), a doublet (Dblt), and nine 12-pulse trains (5, 10, and 20 Hz) using three patterns each - constant frequency

(CT), doublet at start (DT) and dual doublet, at start and mid-train (DDT)). The sensitivity and role of each parameter was determined by incrementally changing one parameter through a range of 10 values while keeping the remaining five parameters constant (baseline value) for all 11 inputs. Parameter values tested (Table 1) were determined based on previously reported values (Ding, et al., 1998; Ding, et al., 2000; 2002). The effect of each parameter on selected force outputs (peak force (PF), force time integral (FTI), time to peak (TTP), half relaxation time (HRT), fusion index (FI), and doublet PF difference) was determined.

Table 1: Model parameter values tested.

	baseline	**increment**	**range**
A	5.0	1.0	1-10
$\boldsymbol{\tau_1}$	50	10.0	20-110
$\boldsymbol{\tau_2}$	200	100.0	100-1000
$\boldsymbol{\tau_c}$	20	5.0	10-55
$\mathbf{k_m}$	0.5	0.1	0.1-1.0
Ro	2.0	0.5	0.5-5.0

RESULTS AND DISCUSSION

The six constant parameters of the model, A, τ_1, τ_2, τ_c, k_m, and R_o, exhibited several redundant characteristics, but also had unique individual effects on the muscle model. The overall levels of influence of each parameter on selected force characteristics are located in Table 2.

Several parameters had redundant roles in this model. Parameters A, τ_c, and R_o had the greatest influence on the characteristics selected, followed closely by τ_1 and k_m. Tau$_2$ had little specific effect on the model, despite the large increment size used.

SUMMARY

Parameter redundancy is clearly depicted, however several parameters play more critical roles in determining force magnitude and force time characteristics than do others. This sensitivity analysis enables future advancements of this mathematical model to proceed more systematically for diverse applications.

REFERENCES

Ding, J., et al. (1998). *J. Applied Physiology* **85,** 2176-89.
Ding, J., et al. (2000). *J. Applied Physiology* **88,** 917-25.
Ding, J., et al. (2002). *Muscle & Nerve* **26,** 477-85.

ACKNOWLEDGEMENTS

We would like to acknowledge support provided by NIH (RKS) and The Foundation for Physical Therapy (LAFL).

Table 2: Summary of parameter influence. The first and second (if present) parameters listed in each column are the primary influences; the rest have minimal but measurable effects.

Influence Level	PF	FTI	TTP	HRT	Fusion Index	Dblt-Tw PF
strong	A	A	τ_c	τ_c	τ_c	Ro
↑	km*	τ_c		τ_1	τ_1	km
	τ_c	km*	km*			
↓	τ_2	τ_1, τ_2	τ_1, τ_2	τ_2, km	τ_2, km*	τ_1, τ_2, τ_c
weak	τ_1, Ro	Ro	Ro†			

* Inverse relationship †For doublet inputs only

PERMEABILITY & MICROARCHITECTURAL MEASUREMENTS IN CALCANEUS

S. Solomon Praveen, Craig J. Bennetts, Kimerly A. Powell, and Brian L. Davis

Orthopaedic Research Center, The Cleveland Clinic Foundation, Cleveland, OH, USA
E-mail: praveens@bme.ri.ccf.org

INTRODUCTION

The calcaneus comprises a large volume of cancellous bone surrounded by a thin cortical shell. In addition, it houses a large volume of bone marrow in its inter trabecular spaces. During physiological loading, the calcaneus experiences both tension and compression strains that can be related to the forces applied to the foot. These features make the calcaneus an ideal site to study marrow - bone interactions and their possible role in bone growth or maintenance.

Permeability is one of the essential parameters needed to study any fluid - solid interaction. Specific permeability is the parameter that measures the contribution of the porous medium to the conductivity and is independent of the permeating fluid properties and flow mechanisms. Permeability values were calculated using Darcy's law and is given by

$$Q = \left(\frac{kA}{\mu}\right)\left(\frac{\Delta p}{L}\right)$$

Where Q - Volumetric flow rate (m^3/s), A - normal cross sectional area of the specimen (m^2), μ - Dynamic fluid viscosity (Pa s), L - Length of bone core (m), Δp - Pressure drop across the specimen and k - specific or intrinsic permeability (m^2).

There is one study available in the literature that measured permeability of mediolateral bone cores in the calcaneus (Grimm and Williams, 1997). As the calcaneus experiences complex forces during physiological loading, we hypothesized that the permeability will be different at different locations. The aim of this study is to measure the permeability of the calcaneus in different locations and compare permeability values with microarchitectural measurements.

METHODS

Bone cores from eighteen calcaneal specimens in the age range of 36 - 91 years were used. Bone cores (length: 1- 4 cm, diameter 8.4 mm) were harvested from each calcaneus in three different locations (Figure1) and imaged using micro CT method. Bone marrow from the cores was removed using trichloroethylene - ultrasound treatment (Sharp *et al*, 1990). Permeability was then measured using a custom-made permeability measurement device and microsyringe pump at various flow velocities (5 ml/h - 400 ml/h). Corn oil was used as a permeant to measure bone permeability at room temperature. Permeability values from different locations were compared using Wilcoxon matched pairs test. Permeability values were also compared with the micro-architectural measurements.

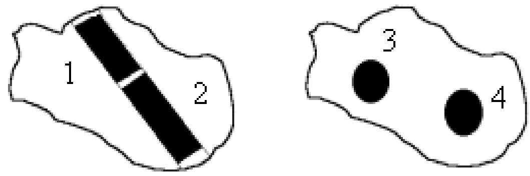

Figure 1. Location of bone cores.

RESULTS AND DISCUSSION

Darcy flow condition can be verified if the relationship between the flow velocity and pressure drop is linear with a zero intercept (Nauman *et al*, 2000). With a few exceptions of very osteoporotic bone cores, all other bone cores verified this condition. Permeability in the calcaneus was dependent on the location of bone cores (Figure 2). In the tuber calcaneus, the mediolateral bone cores offered the highest resistance to fluid flow. Comparing the micro-architectural measurements with permeability values revealed that the permeability was dependent on the presence of rods and plates (Figure 3). Using logarithmic regression analysis, permeability was found to be dependent on surface area (Figure 4).

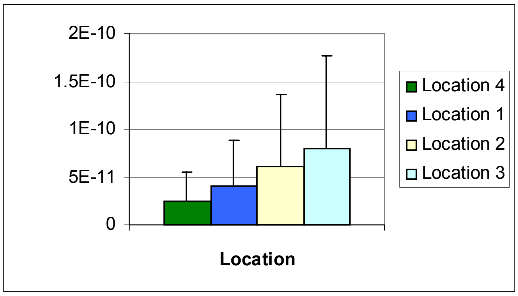

Figure 2. Permeability of calcaneus at different locations. The permeability values were significantly different at all locations (p value < 0.05).

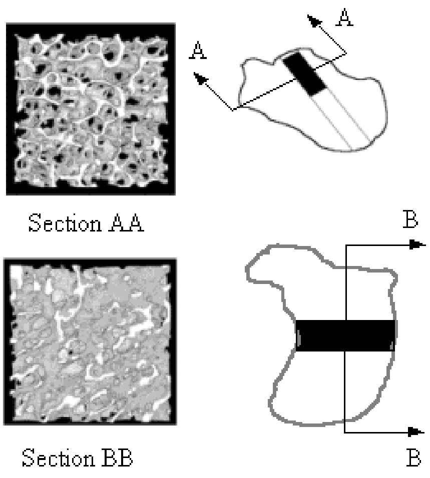

Figure 3. The presence of plates and rods with respect to fluid flow direction.

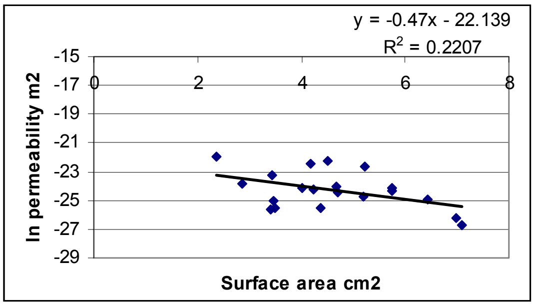

Figure 4. Intertrabecular permeability from all bone core locations vs surface area using logarithmic regression analysis (p value < 0.05).

SUMMARY

A more extensive micro-architectural study with age and gender matched controls, will provide information regarding the effects of aging on bone permeability and its subsequent effect on bone remodeling. The results from this study along with pressure, strain, viscosity, and micro-architectural measurements will help us understand the marrow-matrix interaction in the calcaneus during normal activities of daily living.

REFERENCES

1. Grimm MJ, Williams JL (1997). *J Biomech*. **30**: 743-745.
2. Sharp DJ, Tanner KE, Bonfield W. (1990). *J Biomech*. **23**: 853-857.
3. Nauman EA, Fong KE, Keaveny TM. (1999). *Ann Biomed Eng*. **27**: 517-524.

ACKNOWLEDGEMENTS

We would like to thank the pathology department for providing tissue samples.

IMAGE-BASED COMPUTATIONAL FLUID DYNAMICS FOR CAROTID ARTERIES: A COMPARISON BETWEEN IMAGING TECHNIQUES

Fadi P. Glor[1,2], Ben Ariff[3], Alun D. Hughes[3], Lindsey A. Crowe[4], Pascal R. Verdonck[1], Dean C. Barratt[5], Simon A.McG. Thom[3], David N. Firmin[4], X. Yun Xu[2]

[1] Cardiovascular Mechanics and Biofluid Dynamics Research Unit, Ghent University, Belgium
[2] Department of Chemical Engineering & Chemical Technology, Imperial College London, UK
[3] Clinical Pharmacology and Therapeutics, St. Mary's Hospital, Imperial College London, UK
[4] Cardiovascular Magnetic Resonance Unit, R. Brompton and Harefield NHS Trust, London, UK
[5] Computational Imaging Sciences Group, Imaging Sciences, Guy's Hospital, London, UK
E-mail: fadi@navier.UGent.be Web: http://navier.ugent.be/public/biomed/

INTRODUCTION

Estimation of *in vivo* WSS has been of considerable interest due to the high mortality rate related to cardiovascular failure and strong link between wall shear stress (WSS) and the initiation and progression of atherosclerotic plaque. Methods by which WSS is evaluated from *in vivo* velocity measurement have proved less reliable than methods based on computational fluid dynamic (CFD) simulations. Both Magnetic Resonance Imaging (MRI) and 3D ultrasound (3DUS) are capable of providing the anatomical and flow data required for subject-specific CFD simulations. This study compares predicted 3D flow patterns based on black blood (BB) MRI and 3DUS, and relates the differences to the expected variability within each imaging technique.

METHODS

Nine healthy volunteers (8 males and 1 female, aged between 24 and 56), were scanned using both imaging modalities. BB MR images, acquired on a Siemens Magnetom Sonata 1.5 T scanner, were segmented semi-automatically using the *region growing method* described by Long et al. (1998) for Time-Of-Flight MR images followed by the *Snake Method* which deforms and smoothes the contour of the preliminary region.

An ultrasound scanner (ATL-Philips Medical Systems, WA) equipped with a conventional 5 to 12 MHz broadband linear array transducer (HDI 5000, ATL-Philips Medical Systems) was used to image ECG gated 2D transverse cross-sections of the carotid bifurcation. Simultaneously, an electromagnetic position and orientation measurement (EPOM) device (Ascension Technology Inc, Vermont) mounted on the probe recorded the position and orientation of the probe in 3D space. Acquired images were segmented using purpose-built software. In combination with the information from the EPOM device, the data allowed reconstruction of a smooth 3D geometry of the carotid bifurcation. The US device and reconstruction of the carotid artery bifurcation from 3DUS images have been described in detail by Barratt (2002).

Computational meshes were fitted using an enhanced in-house purpose-built mesh generator. The partial differential equations describing the movement of the fluid were solved numerically using the Quadratic Upwind Interpolation for Convective Kinematics differencing scheme implemented in CFX-4.4 (AEATechnology, 1999). Two cardiac cycles of 80 equally spaced time-steps were simulated. Blood density was 1176 kg/m^3 and the Quemada-model was used to model blood viscosity.

Table 1: Summary of the root mean square error (RMSE). Between brackets, the percent RMSE, i.e. 100 x RMSE/(average value). For comparison, results from two separate MRI reproducibility studies are quoted.

Artery	WSS [N/m^2]	OSI [-]	WSSGs [N/m^3]	WSSGt [$N/(s.m^2)$]	WSSAG [rad/m]
CCA	0.314 (45.9%)	0.0658 (104%)	56.1 (35.3%)	1.80 (24.8%)	96.2 (78.0%)
ICA	0.534 (44.0%)	0.0416 (123%)	164 (54.5%)	3.34 (36.6%)	74.5 (91.6%)
ECA	0.397 (40.0%)	0.0420 (193%)	149 (52.8%)	2.11 (28.1%)	90.4 (88.4%)
mean	0.411 (42.7%)	0.0481 (166%)	150 (55.4%)	2.29 (29.1%)	87.6 (86.3%)
Thomas et al. (2003)	0.44 (32%)	0.021 (109%)	38 (55%)	-	61 (73%)
Glor et al. (2003)	0.43 (27.3%)	0.025 (106%)	214 (65.7%)	2.35 (19.5%)	68.1 (79.8%)

RESULTS AND DISCUSSION

There was no significant difference in areas measured by 3DUS and BB-MRI, although areas measured by BB-MRI tended to be greater. The differences between image modalities found in this study were greater than the uncertainty reported in the reproducibility studies of each of the techniques separately (Glor, 2004; Thomas et al., 2003), but lower than the variability found in the comparative study of MRI and US on a carotid phantom (Frayne et al., 1993).

The root-mean-square error (RMSE) for a number of haemodynamic parameters is reported in Table 1, together with the RMSE reported in separate MRI reproducibility studies (Glor et al., 2003; Thomas et al., 2003). The concerned haemodynamic parameters are defined and discussed by Longest (2002). The RMSE for the haemodynamic wall parameters fell in the range of the expected variability of either imaging technique, except for the OSI.

CONCLUSION

MRI and 3DUS are comparable for combining with CFD for carotid flow prediction. Because of relative high cost of MRI, ultrasound is expected to replace MRI in future haemodynamic studies of superficial arteries.

REFERENCES

AEATechnology (1999). *CFX-4.4 Programming and Operating Manual*.

Barratt D.C. (2002). *Quantification of carotid disease using Three-Dimensional Ultrasound Imaging*. Ph.D. thesis, London University.

Frayne R., et al. (1993). *Med. Phys.*, **20**, 415–425.

Glor F.P. (2004). *Integrating medical imaging and computational fluid dynamics for measuring blood flow in carotid arteries*. Ph.D. thesis, Universiteit Gent.

Glor F.P., et al. (2003). *Annals of Biomedical Engineering*, **31**, 142–151.

Long Q., et al. (1998). *Comput. Meth. Programs Biomed.*, **56**, 249–259.

Longest P.W. (2002). *Computational Analyses of Transient Particle Hemodynamics with Applications to Femoral Bypass Graft Designs*. Ph.D. thesis, NC State University, Raleigh, NC.

Thomas J.B., et al. (2003). *Annals of Biomedical Engineering*, **31**, 132–141.

ACKNOWLEDGMENTS

Support was provided by Pfizer UK, the Ghent University (BOF 01102403) and the British Heart Foundation.

A Micro-Mechanical Composite Analysis of Engineered Cartilage

Sean S. Kohles[1], Christopher G. Wilson [2], and Lawrence J. Bonassar [3]
[1] Kohles Bioengineering, Portland State University, and Oregon Health & Science University, Portland, OR;
[2] Wallace H. Coulter Department of Biomedical Engineering, Georgia Institute of Technology; Atlanta, GA;
[3] Sibley School of Mechanical and Aerospace Engineering, Cornell University, Ithaca, NY.
Email: ssk@kohlesbioengineering.com Web: www.kohlesbioengineering.com

INTRODUCTION

In the design of engineered tissues, the processes of biomaterial degeneration and neotissue synthesis combine to affect the mechanical state of the multi-phase composite. Cell-polymer constructs as used in engineered cartilage, may consist of chondrocytes seeded on scaffolds of biodegradable polymers [Wilson et al., 2002]. Synthetic scaffolds degrade passively in culture, as the cells proliferate and assemble an extracellular matrix (ECM) composed primarily of glycosaminoglycan (GAG) and collagen [Saha et al., 2004]. During construct development, the presence of cells, polymer scaffold, and ECM can be modeled at a unit-cell level to predict the contributions of the constituents toward the effective elastic properties (Figure 1).

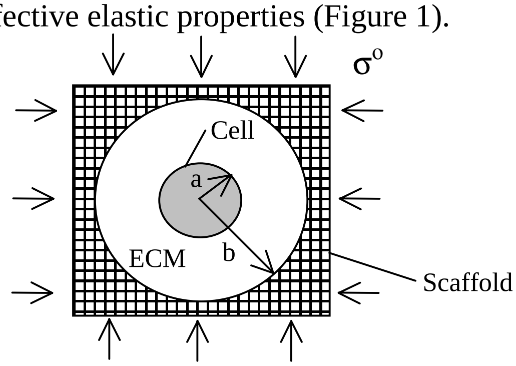

Figure 1: Composite spheres model of a single cell, surrounded by synthesized ECM, and supported within a homogeneous scaffold mesh during a confined, compression stress state (σ^o).

METHODOLOGY

Three-Phase Model

The effective bulk modulus (K) for a spherical cell (r = a), surrounded by a layer of ECM (r = b), within a homogeneous scaffold matrix, can be analyzed as a three-phase model. Applying Eshelby's formula to evaluate the strain energy stored during confined compression, the nondilute solution (high concentration of interactive cells) becomes [Christensen, 1991]:

$$K = K_s + \frac{(K_{c\text{-}m} - K_s)c}{1 + [(1-c)(K_{c\text{-}m} - K_s)/(K_s + \frac{4}{3}\mu_s)]}$$

where the cell-ECM volume fraction, $c = (a/b)^3$, produces a dynamic cell-ECM inclusion (c-m) within a scaffold of bulk (K_s) and shear (μ_s) moduli. During cellular proliferation, the volumetric concentration of the cell-ECM inclusion within the scaffold may be described by: $\zeta = 1\text{-}e^{-\Gamma}$ for $\Gamma = 0$ to ∞ (0 to 100% concentration) [Wu et al., 1999]. Isotropic relations also provide input for constituent properties: $\mu = E/2(1+\nu)$ and $K = E/3(1\text{-}2\nu)$, from the elastic modulus (E) and Poisson's ratio (ν). Volume fractions of constituents (c) and elastic properties (K, K_s, μ_s) were incorporated from the following biochemical and biomechanical experiments, respectively, as a means to determine $K_{c\text{-}m}$.

Cartilage Composite Culture

Cell-polymer-ECM composite constructs were prepared as previously described [Wilson et al., 2002]. Briefly, bovine articular chondrocytes were harvested from the femoral chondyles and tibial plateau of a ~2 month-old calf, within 6 hours of slaughter. Cells were liberated via a 0.3% collagenase digestion overnight at 37°C on a horizontal shaker, counted, and stored in culture media at 37°C for less than 48 hours. Polymeric scaffolds were made from a nonwoven polyglycolic acid (PGA) fleece. A 12.7 mm punch was used to cut circular patches approximately 1 mm thick. The patches were immersed in a 1% w/v poly-L-lactic acid (PLLA) solution in methylene chloride for 10 sec and allowed to dry for at least 10 min (resulting in 27% PLLA to PGA by mass). The scaffolds were then sterilized in ethanol for 30 min, allowed to dry in a desiccator for 24 hours, and prewet in culture media at 37°C for 6 hours prior to seeding. At seeding, the scaffolds were incubated with a suspension of $2.5x10^6$ cells in 1.0 mL of culture media for 12 hours at 37°C on a horizontal shaker. Once seeded, the initial constructs were transferred to 12-well plates for culture in 3 mL of media, with media changes every 2 to 3 days.

Composite Harvest

Engineered cartilage composite constructs were then harvested at 2, 5, 8, 14, 35, or 47 days (n = 4 per time point). At each time point, 6 mm diameter samples were extracted along the center axis of each disk using a biopsy punch. The samples were rinsed in phosphate buffered saline and used for mechanical testing within 3 hours of harvest. The remaining pieces were weighed, lyophilized, reweighed, and stored at –20 °C for biochemical analyses.

Biomechanical Testing

The disks were tested in confined compression using a mechanical testing device. The disks were equilibrated in 0.15 M PBS at pH 7.4 and subjected to sequential steps of 0.5 to 5% strain up to 30% total strain. After stress relaxation, the equilibrium stress at each static strain level was recorded. A best fit linear regression curve of the equilibrium stress to applied strain was fit to determine the equilibrium modulus for the constructs. In addition, mechanical evaluation of degrading scaffolds (without cultured cells) was conducted.

Biochemical Assays

Construct fragments reserved for biochemical analysis (and volume fraction determination) were digested in papain (0.125 mg/mL) overnight at 60 °C. Sulfated-GAG content was measured via the dimethylmethylene blue spectrophotometric method. Collagen content was measured indirectly through a spectrophotometric assay for hydroxyproline using a Hy-pro:collagen ratio of 1:10.

RESULTS AND DISCUSSION

Bulk modulus results indicate the dynamic influence of proliferating cell density, ECM synthesis, and scaffold degradation over time (Figure 2)

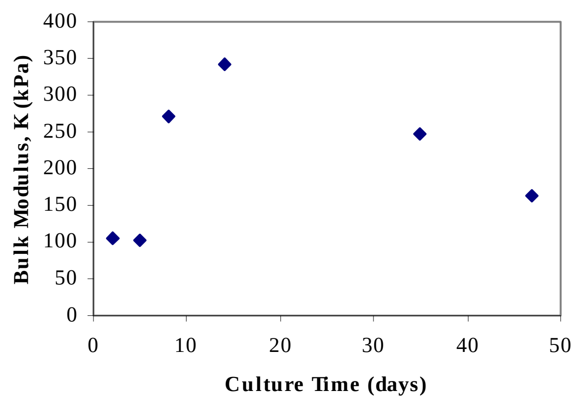

Figure 2: Dynamic engineered cartilage moduli based on a composite spheres model.

SUMMARY

This approach has been previously validated in native cartilage studies [Wu et al., 1999; Federico et al., 2004] and may provide insight toward engineered tissue dynamics.

REFERENCES

Christensen, R.M (1991) *Mechanics of Composite Materials*, Krieger Publ.

Federico, S. et al. (2004) *JBiomech*, **37(3)**:401-404.

Saha, A.K. et al. (2004) *AnnBiomedEng*, **32(6)**:650-660.

Wilson, C.G. et al. (2002) *ArchBiochem Biophys*, **408(2)**:246-254.

Wu, J.Z. et al., (1999) *JBiomech*, **32(6)**:563-572.

ACKNOWLEDGMENT

This work was supported by the National Institutes of Health (NIDCR grant DE14288).

COMPUTATIONAL ANALYSIS OF THE MECHANICAL BEHAVIOR OF LIGAMENTS

Naira H. Campbell-Kyureghyan and William S. Marras

Biodynamics Laboratory, Dept. of Industrial and Systems Eng., Ohio State University, Columbus, OH, USA
E-mail: kyureghyan.1@osu.edu Web: osuergo.eng.ohio-state.edu

INTRODUCTION

Ligaments play a variety of roles in the behavior of the lumbar spine as well as other joints. They limit movement, store energy, and provide stability to the joint. As a result, any computational biomechanical model that attempts to explain injury pathway(s) in the lumbar spine must use an accurate depiction of the ligament behavior if it is to describe the spinal loads reliably. For biomechanical models, the material properties are the parameters that have the greatest effect on the behavior.

The inherent variability of biological tissue leads to a range of properties, not a single, known or estimated value. Moreover, the limited existing material property data varies widely from study to study. To present, no study has systematically investigated the effect of varying the material properties within their feasible range. The goal of this presentation is to show the effect of the material property variations and strain rate on the cyclic behavior of ligaments, as well as their importance in biomechanical modeling.

METHODS

A nonlinear Kelvin-Voight model was developed in this study to represent the hysteretic ligament behavior. The spring and dashpot behavior is strain dependent and is governed by

$$E = \{1.0 + \tanh(\psi\,[\varepsilon - \varepsilon_0])\}\,E_{active}/2$$

where E is the current spring or dashpot coefficient, E_{active} is the coefficient when the ligament is fully active, ψ is a parameter defining the shape of the transition between the active and inactive states, ε is the current strain, and ε_0 is the strain at center of the modulus transition zone (activation strain).

Experimental data from different loading cycles (Tkaczuk, 1968) and at different strain rates (Solomonow, 2004) were considered a starting point for an investigation into the effect of loading rate and the material properties of the ligament on the behavior. An analysis of each parameter has been performed to determine their influence on the model output. Hysteretic energy dissipation is used as a damage measure in many areas of mechanics, and is calculated herein for both the first and third cycles of a testing sequence.

RESULTS AND DISCUSSION

The maximum stress was calculated for a wide range of strain rate, activation strain, and viscous coefficient. The activation strain was found to have a considerable effect on the overall ligament behavior, and faster rates of load application were associated with the higher stress levels, with the effect being more pronounced in the first loading cycles. Increasing strain rate from 25 to 100%/sec resulted in the maximum stress increasing by 31%. The maximum stress decreased by 19.5% as the activation strain varied from 2.5% to 15%. Experimental results also indicate increased stiffness and earlier activation with cycling.

Energy dissipation exhibited a nonlinear dependence on the viscoelastic parameters and increased as much as five-fold with strain rates from 12.5%/sec to 100%/sec. Conversely, larger activation strains (from 5% to 15%) lead to a 60% decrease in the energy dissipation. These effects were present at a smaller scale, but were no less important, at the third and later cycles, as seen in Figure 1.

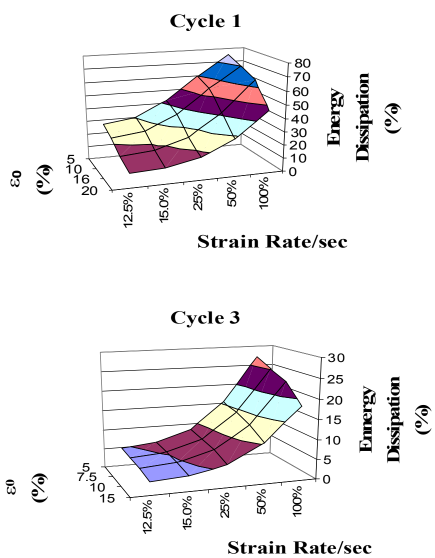

Figure 1: Energy dissipation at first and third cycle as a function of ε_0 and strain rate.

An examination of the results indicates that faster movement rates lead to higher tensile stresses and more energy dissipation in the ligaments. This fact, coupled with the rapid decrease in energy dissipation from the first to later cycles, reinforces commonly held beliefs about injury prevention. The results suggest that one strategy for reducing the risk of injury to the spine due to repetitive loading is to start slowly with smaller loads, and to increase the load and loading rate gradually to the desired level.

CONCLUSIONS

In conclusion, this study showed that small variations in even a single parameter can result in large changes in the ligament behavior. The results underline the importance of understanding the relationship between the work environment, material testing, and modeling on the prediction of injury. In order to be truly useful, the parameters for biomechanical models must come from both the real world and the laboratory, and the material testing must be performed under realistic conditions.

REFERENCES

Solomonow M. (2004). *J. EMG & Kin.*, **14**, 49-60.

Tkaczuk, H. (1968). *ACTA Orthopaedica Scandinavica Supplementum*, **115**, 1-69.

ANALYSIS OF FATIGUE DAMAGE IN BOVINE TRABECULAR BONE

Partha Ganguly[1], Tara L. A. Moore[2], and Lorna J. Gibson[3]
[1]Schlumberger-Doll Research, Cambridge, MA, USA
[2]Exponent, Inc., Philadelphia, PA, USA
[3]Department of Materials Science and Engineering, Massachusetts Institute of Technology, Cambridge, MA, USA
E-mail: ljgibson@mit.edu

INTRODUCTION

Cyclic loading of trabecular bone can lead to fatigue damage and increased risk of fracture in both young and the elderly populations. Fatigue damage processes in trabecular bone include reduction of elastic modulus and accumulation of residual strain. Development of models relating the above effects to the loading variables (stress, strain) is essential for a predictive understanding of the process. This study analyzes the effect of stress and strain variation on fatigue damage processes in bovine trabecular bone, and develops a model relating fatigue life to the stress level.

METHODS

Bovine trabecular bone specimens were tested under monotonic and cyclic compression loadings (Moore, 2002, 2003). For monotonic tests, the initial modulus (E_0) for each specimen was determined by fitting a linear curve to the initial portion (ε = 0.001 to 0.004) of the compressive stress-strain curve. The secant moduli (E_{sec}) of the specimens at higher strains were calculated and normalized by the initial modulus. For cyclic compression tests, the initial modulus (E_0) was measured by taking the slope of the best linear fit of the final preconditioning loading cycle (ε = 0.001 to 0.003). The cyclic stress-strain curves were divided into 4 ranges of maximum normalized stress ($\Delta\sigma/E_{sec}$), (0.005-0.006), (0.006-0.007), (0.007-0.008) and (0.008-0.009). The curves were analyzed to determine (a) the reduction in secant modulus with increasing compressive strain, and (b) the accumulation of residual strain with increasing number of cycles.

DATA ANALYSIS

The decrease in secant modulus with increasing strain for bovine trabecular bone was similar under monotonic and cyclic compression tests. The secant modulus decrease was relatively independent of the loading characteristics. This similarity in the secant modulus decrease under the two loadings suggests a strain-based failure criterion for trabecular bone. Residual strain accumulation with increasing number of cycles was divided into primary and secondary phases. The primary phase involved the initial cycles (~1-5) of cyclic loading. The primary residual strain was similar for cyclic compression tests at different normalized stresses. For a given specimen, the secondary residual strain accumulation rate (i.e. accumulation per cycle) was approximately constant and was less than that in the primary phase.

NUMERICAL MODEL

For any given cycle in the cyclic compression test, the maximum strain (ε_{max}) measured during that cycle is the sum of the residual strain at the beginning of the cycle (ε_{res}) and the strain increment during the cycle ($\Delta\sigma/E_{sec}$, where $\Delta\sigma$ is the maximum stress in the cycle, and E_{sec} is the secant modulus). The residual strain can be divided into a primary ($\varepsilon_{res}{}^{pr}$) and a secondary ($\varepsilon_{res}{}^{sec}$) component,

$$\varepsilon_{\max} = \left(\varepsilon_{res}^{pr} + N^{\sec} \frac{d\varepsilon_{res}^{\sec}}{dN} \right) + \frac{\Delta\sigma}{E_{\sec}} \quad (1)$$

where N^{sec} is the number of cycles in the secondary phase and $d\varepsilon_{res}^{sec}/dN$ is the secondary residual strain accumulation rate. $d\varepsilon_{res}^{sec}/dN$ was a function of the maximum normalized stress, while E_{sec}/E_0 was a function of the maximum strain (ε_{max}). Incorporating $\varepsilon_{max}=f_1^{-1}(E_{sec}/E_0)$, $d\varepsilon_{res}^{sec}/dN= f_2(\Delta\sigma/E_0)$ in Eq. (1),

$$f_1^{-1}(E_{sec}/E_0)=\left\{\varepsilon_{res}^{pr}+(N-N^{pr})f_2(\Delta\sigma/E_0)\right\}+\frac{(\Delta\sigma/E_0)}{(E_{sec}/E_0)} \quad (2)$$

where, $N = N^{pr} + N^{sec}$, and N^{pr} is the number of cycles in the primary phase.

The functions f_1 and f_2 varied from specimen to specimen. Upper and lower bounds for the normalized secant modulus (E_{sec}/E_0) vs. N variation could be estimated by evaluating Eq. (2) for suitable bounds of functions f_1 and f_2. Bounding functions for f_1 were estimated using upper and lower bounds of the normalized secant modulus reduction with increasing strain during monotonic loading. For each of the four stress ranges, the upper and lower bounds of the f_2 function were estimated from experimentally determined residual strain accumulation rates. Given the bounds of f_1 and f_2, the bounding curves for the normalized secant modulus variation with increasing number of cycles were determined using Eq. (2).

RESULTS

The model predicts the bovine trabecular bone S-N curve, i.e. the number of cycles corresponding to a given loss of secant modulus at different normalized stresses. From Eq. (2):

$$N=\frac{f_1^{-1}(E_{sec}/E_0)-\varepsilon_{res}^{pr}-\left(\dfrac{\Delta\sigma/E_0}{E_{sec}/E_0}\right)}{f_2(\Delta\sigma/E_0)}+N^{pr} \quad (3)$$

f_1, ε_{res}^{pr} and N^{pr} were relatively insensitive to changes in normalized stress. The variation of secondary residual strain accumulation rate with normalized stress (f_2) was estimated from experimental data, and the number of cycles (N) at each normalized stress, corresponding to a 10% loss in secant modulus, was determined using Eq. (3). The upper and lower bounds of the S-N curves were determined using the bounds of f_1 and f_2. The bounds compared well with experimentally observed S-N data (**Figure 1**). The predicted endurance limit for bovine trabecular bone at 10^6 cycles fell between $\Delta\tilde{\sigma}/E_0$ values of 0.0032 and 0.0024.

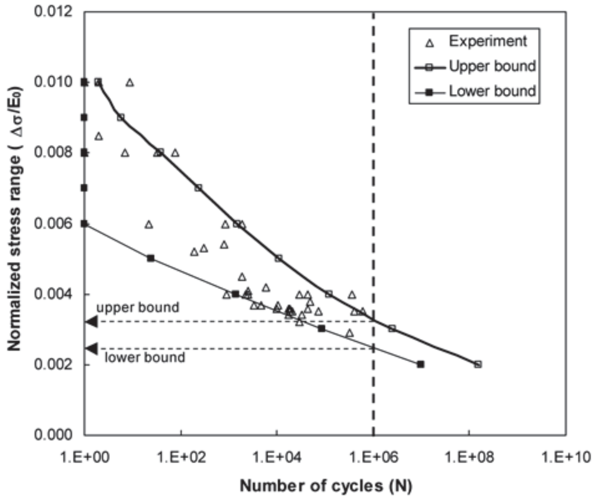

Figure 1: Comparison of model bounds and experimental S-N data for bovine trabecular bone. The upper and lower values of the endurance limit are shown.

DISCUSSION

The experimentally determined E_{sec}/E_0 vs. N variation for different trabecular bone specimens were observed to lie within the bounds defined by the model. Considering that the inputs to the numerical model were (a) bounds of the f_1 function (determined from monotonic loadings), and (b) bounds of the f_2 function for each $\Delta\sigma/E_0$ range, the model suggests the possibility of effective estimation of E_{sec}/E_0 vs. N plots based on a small number of cyclic tests, complimented by more economical monotonic compression tests, and reduces the need for long-term fatigue tests.

REFERENCES

Moore, T.L.A., Gibson, L.J. (2003). *J. Biomech. Eng,* **125**, 769-776.
Moore, T.L.A., Gibson, L.J. (2002). *J. Biomech. Eng,* **124**, 63-71.

ACKNOWLEDGEMENTS

The authors wish to thank the Ford Foundation, Alberta Heritage Scholarship Fund, NSERC (Canada), Cambridge-MIT Institute, and the Matoula S. Salapatas Chair in Materials Science and Engineering at MIT for financial assistance.

THE EFFECT OF ANTI-HYPERTENSIVE DRUGS ON CAROTID HAEMODYNAMICS

Fadi P. Glor[1,2], Ben Ariff[3], Alun D. Hughes[3], Lindsey A. Crowe[4], Pascal R. Verdonck[1], Simon A.McG. Thom[3], David N. Firmin[4], X. Yun Xu[2]

[1] Cardiovascular Mechanics and Biofluid Dynamics Research Unit, Ghent University, Belgium
[2] Department of Chemical Engineering & Chemical Technology, Imperial College London, UK
[3] Clinical Pharmacology and Therapeutics, St. Mary's Hospital, Imperial College London, UK
[4] Cardiovascular Magnetic Resonance Unit, R. Brompton and Harefield NHS Trust, London, UK
E-mail: fadi@navier.UGent.be Web: http://navier.ugent.be/public/biomed/

INTRODUCTION

Recent studies (Stanton et al., 2001) have illustrated that the effect of sustained anti-hypertensive treatments using a particular calcium-blocker (CB) or ACE-inhibitor (AI) have a different impact on carotid morphology despite the same pressure drop. Patients on AI treatment show a decrease in lumen diameter (LD) and intima-media thickness (IMT), whereas CB maintains LD and lowers IMT even more.

The reason for these morphological changes is unknown. A pressure drop is typically followed by a drop in LD, in analogy with the deflation of a balloon. Furthermore, the smaller pressures and anti-hypertrophic effects of the drug induce a decrease in IMT. This explains the long-term effects of AI. For the CB treatment, it was hypothesised that the changes could be mediated by the local shear stresses. In this hypothesis, the AI treatment would show elevated shear stresses, which would increase LD (Powell, 2003) and stretch the IMT in the circumferential direction.

The aim of this study was therefore to investigate the acute effects of the administration of CB or AI on the carotid shear stresses. This was done using image-based computational fluid dynamics (CFD).

METHODS

Ten subjects were submitted to a double-blind, placebo controlled, randomised, 3 way cross over clinical trial. The protocol involved one week of treatment with CB, AI or placebo, followed by a wash-out period. Pressure, geometry, flow and vessel wall parameters were assessed after every treatment. Of the 10 subjects, 8 subjects were scanned using magnetic resonance imaging (MRI) and 2 claustrophobic subjects were assessed with 3D ultrasound (3DUS).

Time-Of-Flight MR images acquired on a Siemens Magnetom Sonata 1.5T scanner were segmented semi-automatically using the *region growing method* described by Long et al. (1998) followed by the *Snake Method* which deforms and smoothes the contour of the preliminary region.

An ultrasound scanner (ATL-Philips Medical Systems, WA) equipped with a conventional 5 to 12 MHz broadband linear array transducer (HDI 5000, ATL-Philips Medical Systems) was used to image ECG gated 2D transverse cross-sections of the carotid bifurcation. Simultaneously, an electromagnetic position and orientation measurement (EPOM) device (Ascension Technology Inc, Vermont) mounted on the probe recorded the position and orientation of the probe in 3D space. Acquired images were segmented using purpose-built software. In combination with the information from the EPOM device, the data allowed reconstruction of a smooth 3D geometry of the carotid bifurcation. The US device and reconstruction of the carotid artery bifurcation from 3DUS images have been described in detail by Barratt (2002).

Computational meshes were fitted using an enhanced in-house purpose-built mesh generator. The partial differential equations describing the movement of the fluid were solved numerically using the Quadratic Upwind Interpolation for Convective Kinematics differencing scheme implemented in CFX-4.4 (AEATechnology, 1999). Two cardiac cycles of 80 equally spaced time-steps were simulated. Blood density was 1176 kg/m^3 and the Quemada-model was used to model blood viscosity.

RESULTS AND DISCUSSION

Figure 1 shows the time-averaged wall shear stress (WSS) distribution for three subjects WSS was higher after the CB- than after the AI-intake on all segments of the carotid wall (p¡0.1). This increase was mainly due to an increased flow and heart rate with the CB treatment, rather than to changes in carotid geometry. This result confirms the hypothesis made at the start: the increased LD and decreased IMT for patients on CB treatment are due to a raise in local WSS.

CONCLUSION

In the present work, image-based CFD has been applied successfully in a clinical study. It showed that the studied calcium-blocker (CB) raised the shear stresses in the carotid artery in comparison with the ACE-inhibitor (AI). This explained the long-term effects of CB or AI intake.

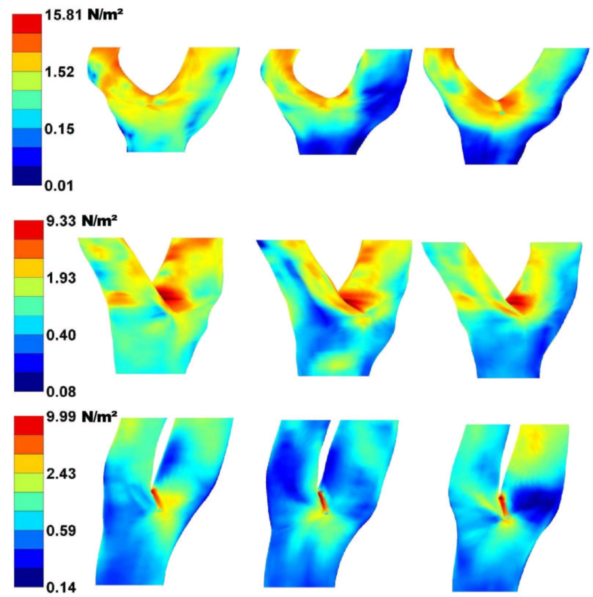

Figure 1: The time-averaged wall shear stress distribution for three subjects (rows) after CB (left), placebo (middle) and AI (right) intake.

REFERENCES

AEATechnology (1999). *CFX-4.4 Programming and Operating Manual*.

Barratt D.C. (2002). *Quantification of carotid disease using Three-Dimensional Ultrasound Imaging*. Ph.D. thesis, London University.

Long Q., et al. (1998). *Comput. Meth. Programs Biomed.*, **56**, 249–259.

Powell J. (2003). J.W. Hallett, J.J. Earnshaw, J.A. Reekers, eds., *Comprehensive Vascular and Endovascular Surgery*, Mosby, 728.

Stanton A.V., et al. (2001). *Clinical Science*, **101**, 455–464.

ACKNOWLEDGMENTS

Support was provided by Pfizer UK, the Ghent University (BOF 01102403) and the British Heart Foundation.

IN VITRO BIOMECHANICS OF LUMBAR DISC ARTHROPLASTY WITH THE PRODISC TOTAL DISC IMPLANT

Denis J. DiAngelo [ab], Kevin T. Foley [ba], Brian Morrow [a], Jung Song [a], and Tom Mroz [b]
[a] Department of Biomedical Engineering, The University of Tennessee, Memphis, TN
[b] Department of Neurosurgery, The University of Tennessee, Memphis, TN
Email: ddiangelo@utmem.edu Web: http://memphis.mecca.org/bme

INTRODUCTION

An alternative approach to lumbar fusion surgery is to restore motion to the diseased segment with a disc prosthesis. The goal of the disc prosthesis is to replace the diseased disc while preserving and/or restoring the motion at the operated spinal level. The purpose of this study was to determine the ability of the PRODISC® (Spine Solutions Inc., Paoli, PA) disc prosthesis to restore lumbar spine motion and compare this motion to that of the harvested and fused spines.

METHODS

Six fresh human cadaveric lumbar spines (L1-Sacrum) were procured and screened with anteroposterior (AP) and lateral radiographs to exclude those with osteopenia. The specimens were mounted in a programmable testing apparatus and tested in flexion, extension, lateral bending, and axial rotation under displacement control. Three different conditions were evaluated: the harvested spine, spine with L5-S1 lumbar disc replacement using the PRODISC, and L5-S1 pedicle screw fixation (Synthes Spine). The instrumented spine underwent an anterior discectomy at L5-S1 and insertion of the disc prosthesis as per manufacturer´s instructions. The appropriate implant size and lordotic angle were determined using trial spacers inserted into the interbody space and confirmed using fluoroscopy. The appropriate-sized implant was gently impacted into the L5-S1 interspace by the spine surgeon; proper placement was confirmed visually and fluoroscopically. Following disc spine testing, the pedicle screw fixation hardware was inserted by the spine surgeon under fluoroscopic guidance, as per manufacturer´s instructions. A previously developed in vitro testing protocol was adopted; i.e., a target moment of 8Nm with limit checks of 25 degrees total spine rotation, maximum bending moment of 10Nm, or 200 N actuator load. For axial rotational tests, a 100 N compressive load was applied to the spinal construct. Measurements included individual vertebral motions, total spine rotation, and applied loads. Motion patterns were analyzed by comparing the percent contribution of the rotation at the implanted level (L5-S1) relative to overall total rotation (L1-Sacrum) for the disc, fused, and harvested conditions at a common end limit of global (L1-Sacrum) moment (8Nm). Motion and flexibility data were analyzed with a one-way ANOVA and S-N-K test were used with significance set at $p = 0.05$.

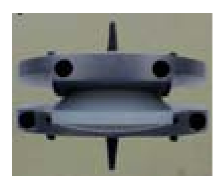

Figure 1: PRODISC Lumar Spine Prosthesis. The implant consists of two forged cobalt-chrome alloy endplates and an ultra-high molecular weight polyethylene inlay element.

RESULTS

The normalized motion data are shown in Figure 2. There were no significant differences in the normalized motion responses at the implanted level for the PRODISC spines compared to the harvested spines, except for left axial rotation and extension, although the PRODISC did provide up to 72% ± 17% of the harvested limit in extension. Significant differences existed between the fused condition and both the harvested and disc spine conditions for all modes of loading. The mean relative MSU rotations for the three different spine conditions are shown in Figure 3 for flexion and extension loading. Application of the fusion hardware reduced the motion at the operated level as illustrated in Figure 3.

DISCUSSION

In contrast to the spines with pedicle fixation, the PRODISC implants maintained a natural range of lumbar mobility and stability during flexion, extension and lateral bending, and adequate motion in combined (left+right) axial rotation (66% of harvested). Use of a prosthetic total disc replacement device, such as the PRODISC, to treat symptomatic degenerative lumbar disc disease may minimize or alleviate the adjacent segment disease associated with pedicle fixation.

REFERENCES

DiAngelo DJ, et al. (2002). *J Neurosurg*, Nov;97(4 Suppl):447-55.

AKNOWLEDGEMENTS

Research funds from Spine Solutions, Inc. and tissue from the Medical Education Research Institute, Memphis, TN.

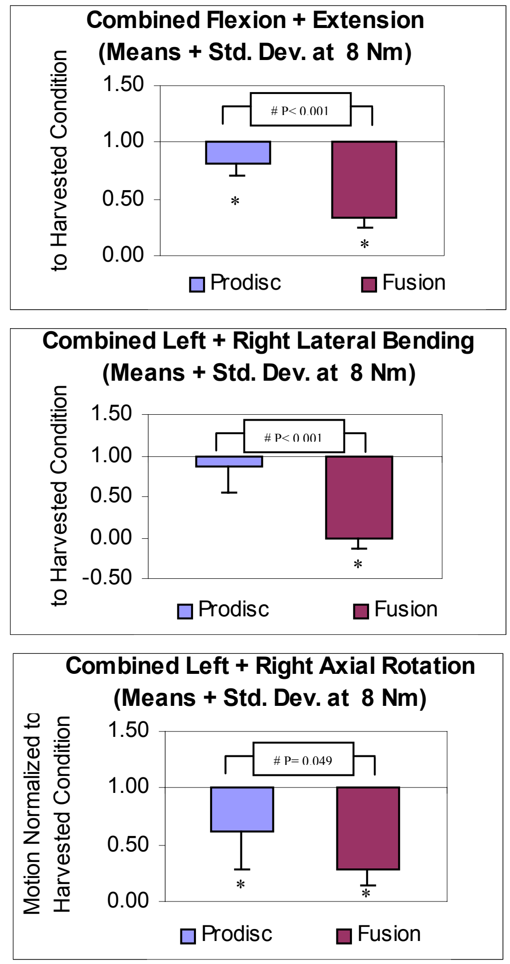

Figure 2: Normalized motion.
* Signifies significant difference with harvested condition and
# signifies significant difference between PRODISC and fusion.

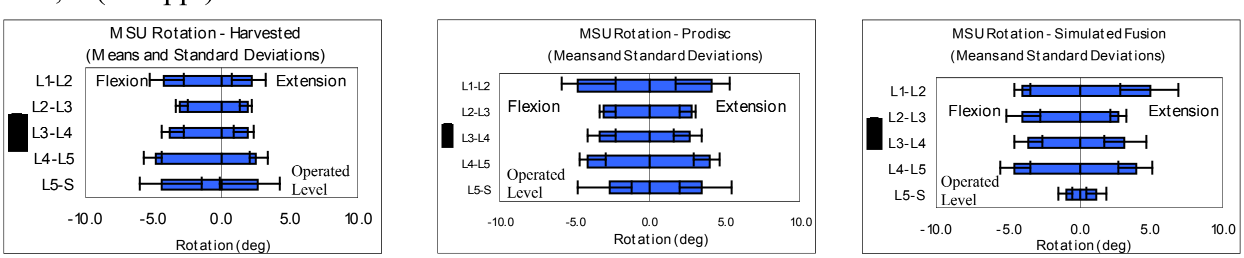

Figure:3: Relative Motion Segment Unit (MSU) Rotations. For the harvested, PROISC, and fused spine conditions during flexion and extension.

ARM CONSTRAINT AND INTER-LIMB COORDINATION DURING WALKING IN HEALTHY ADULTS

Matthew P. Ford PT, PhD[1], Robert C. Wagenaar PhD[2], Karl M. Newell, PhD[3]

[1]Department of Physical Therapy, The University of Alabama at Birmingham, Birmingham, AL
[2]Department of Rehabilitation Sciences, Boston University, Boston, MA
[3]Department of Kinesiology, The Pennsylvania State University, University Park, PA
E-mail: mford@uab.edu

INTRODUCTION

Human walking is a complex skill involving the coordination between upper and lower body motion. As walking velocity increases there is increased counter-rotation between the thorax and pelvis, along with increased arm swing and hip excursion. The arm and contralateral leg move more in-phase, while the arm and ipsilateral leg demonstrate a more out of phase pattern with increased walking velocity. Furthermore, torso and pelvic rotation becomes tightly coupled, while arm movement frequency synchronizes more with stride frequency at higher walking velocities (Wageenaar & Beek, 1992; Wagenaar & van Emmerik, 2000).

Published findings have shown that reduced arm movement amplitude during over-ground walking, leads to adaptive decreases in transverse rotation of the trunk, hip excursion, stride length, and walking velocity (Jackson et al., 1983; Eke-Okoro et al., 1997; Sigg et al., 1997). However, the question remains as to how reduced arm movement amplitude impacts arm motion on the opposite side, and the phasing, and frequency relations between arm and leg movements.

METHODS

Ten healthy (ages 21 to 24) healthy subjects were recruited. Subjects walked on a treadmill while systematically increasing the belt velocity (0.22, 0.40, 0.63, 0.85, 1.10, 1.30, 1.52 m/s) and then decreasing it (same increments) under three different conditions: 1. no arm constraint 2. right arm constrained 3. left arm constrained. The arm was constrained by placing the arm in a sling and securing it to the thorax.

3D kinematic data were collected through a Skill Technologies® 6D Research System. The total range of movement amplitudes for arms, thorax, pelvis, and legs was calculated by subtracting the minimal angular displacement from the maximal angular displacement. The shoulder and hip angle time-series data were used to compute the point estimates of relative (PERP) phase between ipsilateral and contralateral limb pairs. We determined if the power in arm movement frequency was higher at stride or step frequency during walking. Movement frequencies and corresponding power in shoulder and hip angle were estimated by calculating the power spectral density function of the shoulder and hip angle time series.

$$\mathrm{RPI} = \frac{P_1 - P_2}{P_1 + P_2}$$

P_1 represents the power (from power spectral analysis) of arm movement frequency at stride frequency, while P_2 represents the power of arm movement frequency at step frequency.

Statistical analysis revealed no significant differences in dependent measures between same ascending and descending velocity levels. Therefore, data from the decreasing velocity levels was combined with the increasing velocity levels. The effects of systematically varying walking velocity and arm constraint were evaluated by a within-group analysis of variance with repeated measures. A Bonferonni Test with a 0.01 significance level was used for post-hoc comparisons.

RESULTS

The constrained arm movement amplitude was significantly ($p < .0001$) decreased as compared to non-constrained arm motion, and did not significantly increase with walking velocity. When one arm was constrained, the non-constrained arm movement amplitude was significantly greater above 1.10 m/s ($p < .000001$), as compared to arm swing during walking with no constraint.

As walking velocity increased the non-constrained arm movement frequency was more strongly synchronized with the stride frequency ($p < .0001$; Figure 1). However, with a significant reduction in arm movement amplitude the constrained arm was unable to synchronize with the stride frequency as walking velocity increased.

Arm constraint also led to significant ($p < .0001$) decreases in transverse rotation of the torso and pelvis. Moreover, subjects increased hip excursion, but decreased stride frequency as they attempted to maintain the spatial temporal relations when walking at a constant velocity.

DISCUSSION

In sum, the results from the present study demonstrate flexibility of the coordination dynamics of walking to meet constraints

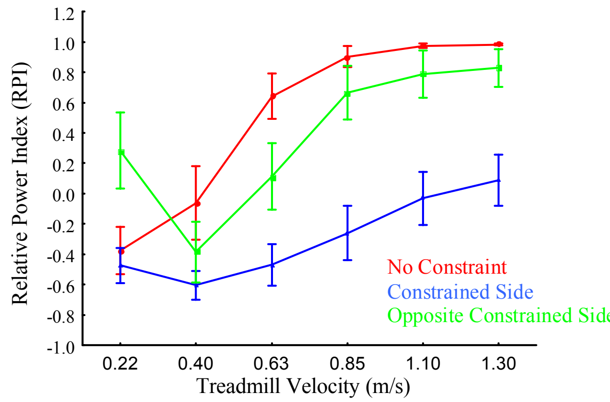

Figure 1: demonstrates the synchronization between arm movement frequency and stride frequency as treadmill velocity increases. A RPI value of 1 indicates that arm movement frequency was strongly synchronized with stride frequency.

imposed on the movements of body segments. However, the data suggest that the ability to modify arm movement amplitude, along with frequency, is necessary for synchronization with the stride frequency at higher walking velocity. Considering, slower walking velocity in patients with severe upper extremity dysfunction (e.g., stroke) may be due to inability to alter coordination patterns at higher walking velocities. Future studies should investigate the underlying dynamics of arm dysfunction and adaptations during treadmill and over-ground walking.

REFERENCES

Eke-Okoro et al. (1997). *Clinical Biomechanics*, **12**, 516-521.

Jackson et al. (1983). *Electromyography and Clinical Neurophysiology*, **23**, 435-446.

Sigg et al. (1997). *Clinical Kinesiology*, **51**, 33-36.

Wagenaar & Beek (1992). *J. Biomechanics*, **25**, 1007-1015.

Wagenaar & van Emmerik (2000). *J. Biomechanics*, **33**, 853-861.

IN VITRO TESTING OF MULTILEVEL ANTERIOR LUMBAR INTERBODY FUSION (ALIF): EFFECTS OF UNILATERAL AND BILATERAL PEDICLE FIXATION

Denis J. DiAngelo[ab], Kevin T. Foley[ba], Bobby J. McVay[a], and Jeff Scifert[c]
[a] Department of Biomedical Engineering, The University of Tennessee, Memphis, TN, USA
[b] Department of Neurosurgery, The University of Tennessee, Memphis, TN, USA
[c] Medtronic Sofamor Danek, Memphis, TN, USA
Email: ddiangelo@utmem.edu Web: http://memphis.mecca.org/bme

INTRODUCTION

Multi-level, stand-alone anterior lumbar interbody fusion (ALIF) has a lower fusion rate than single-level ALIF. Pedicle screw fixation can be used for supplemental stabilization in order to increase the fusion rate. The objective of this study was to determine the biomechanical influence of unilateral and bilateral pedicle screw fixation on two-level ALIF in vitro. It was hypothesised that both unilateral and bilateral pedicle fixation increased the stability of a two-level ALIF.

METHODS

between unilateral 3-screw, bilateral 4-screw, and bilateral 6-screw constructs Seven fresh human cadaveric lumbar spines (L1-S1) were harvested, mounted in a programmable testing apparatus, and biomechanically tested in flexion/extension, right/left lateral bending, and right/left axial rotation (DiAngelo, 2002). Five spine conditions were evaluated: harvested spine(H), bilateral anterior interbody cages alone at L4-L5 and L5-S1 (CAGE), CAGE and three unilateral pedicle screws and rod fixation at L4-L5-S1 (UPF), CAGE and 4 bilateral pedicle screws and rod fixation at L4-L5-S1 (BPF6), and CAGE with six bilateral pedicle screws and rod fixation at L4 and S1 bodies, skipping the L5 screws (BPF4). Measurements included vertebral motion, applied load, and bending/rotational moments. Global moment and rotation data were combined to calculate flexibility. Flexibility and motion data were normalized to the harvested state and compared at end limits using a one-way ANOVA and S-N-K test with significance at $p = 0.05$.

A) Inter Fix-RP Cage B) Sextant Pedicle Screw Fixation System.

Figure 1: Spinal Instrumentation (Medtronic Sofamor Danek).

RESULTS

The normalized motion data are shown in Figure 2. A significant decrease in the normalized motion occurred between the harvested condition and all instrumented conditions in flexion, extension, and lateral bending. Both bilateral pedicle fixation techniques resulted in a significant reduction in motion in flexion and extension compared to cages alone. There was also a trend in reduced motion in flexion and a significant reduction in extension between UPF and CAGE. There were no significant differences between the unilateral and bilateral fixation techniques. Addition of all posterior instrumentation conditions produced a significant reduction in flexibility in lateral bending and a trend in flexibility reduction in flexion and extension.

DISCUSSION

Pedicle fixation provided additional stabilization to two-level anterior lumbar interbody cages in flexion and extension. There were no biomechanical differences between unilateral 3-screw, bilateral 4-screw, and bilateral 6-screw constructs.

CONCLUSIONS

This study is the first to report the in vitro effects of unilateral versus bilateral pedicle screw fixation on multilevel ALIF. All modes of posterior instrumentation provided additional stabilization to two-level anterior lumbar cages in flexion and extension. Interestly, unilateral pedicle fixation functioned similarly to bilateral fixation.

REFERENCES

DiAngelo DJ, et al. (2002). *J Neurosurg*, Nov;97(4 Suppl):447-55.

ACKNOWLEDGEMENTS

Research funds from Medtronic Sofamor Danek and tissue from the Medical Education Research Institute, Memphis, TN.

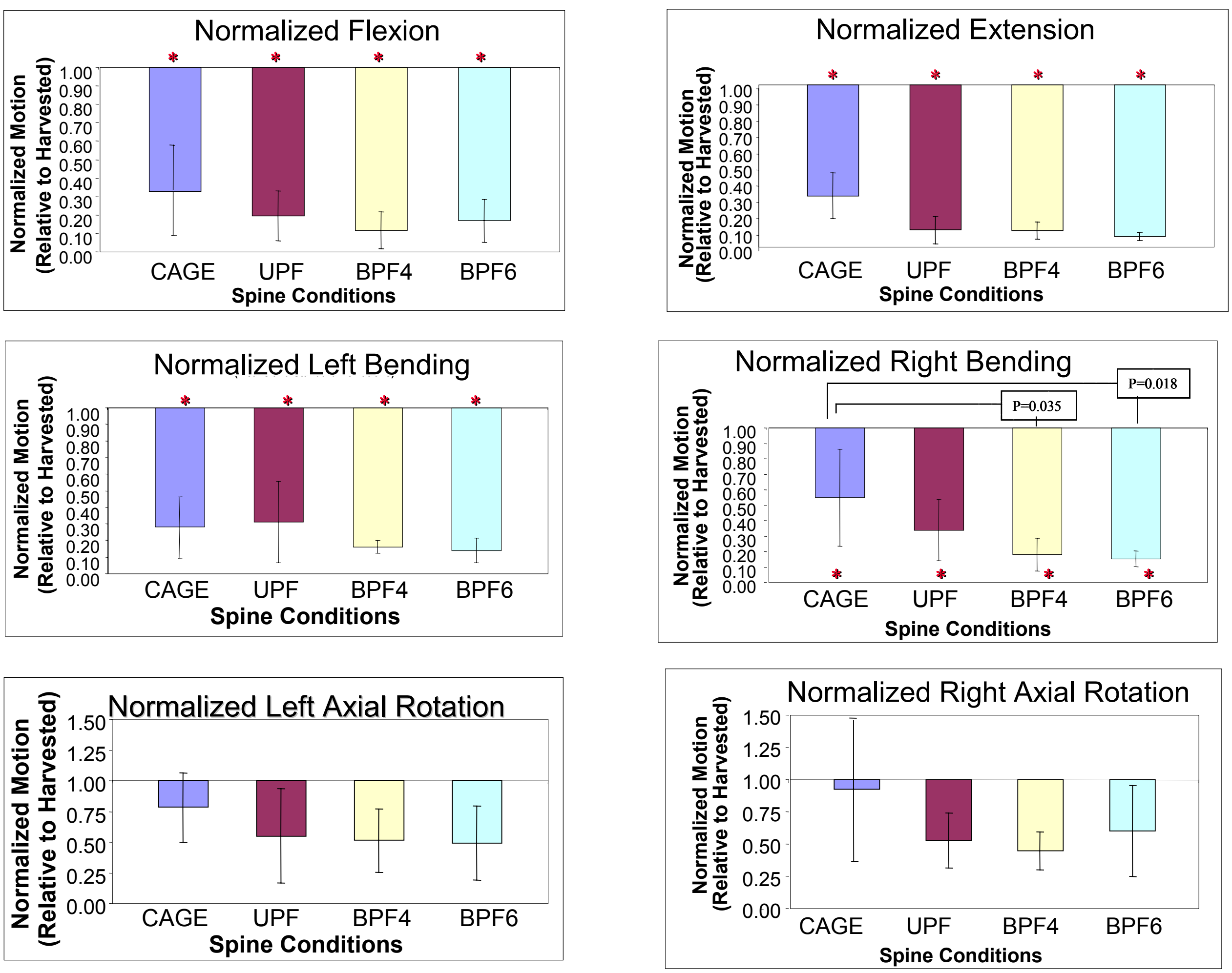

Figure 2: Normalized Motion. Motion at operated region of instrumented spine normalized to harvested spine for flexion, extension, right and left lateral bending, and right and left axial rotation.

MOTION COMPENSATION ASSOCIATED WITH SINGLE-LEVEL CERVICAL FUSION: WHERE DOES THE LOST MOTION GO?

Denis J. DiAngelo[ab], Kevin T. Foley[ba], and John S. Schwab[a]

[a] Department of Biomedical Engineering, The University of Tennessee Health Science Center, Memphis, TN, USA
[b] Department of Neurosurgery, The University of Tennessee Health Science Center, Memphis, TN, USA
Email: ddiangelo@utmem.edu Web: http://memphis.mecca.org/bme

INTRODUCTION

Anterior cervical discectomy and fusion, a commonly performed surgical procedure, has a high rate of clinical success. However, there is a reported incidence of subsequently symptomatic degenerative disc disease of 3 percent per year at adjacent spinal levels. The motion lost through fusion is thought to be transferred to the adjacent motion segment units (MSUs). This increased motion may contribute to the development and advancement of disc degeneration, segmental instability, osteoarthritis, or stenosis. The objective of this study was to determine the influence of single-level cervical fusion on vertebral kinematics and biomechanical stability for different levels of cervical fusion.

MATERIALS AND METHODS

Seven fresh adult human cadaveric cervical spines (C2-T1) were harvested and radiographed to exclude those with degenerative diseases. The spines were mounted in a programmable testing apparatus and tested in flexion, extension, right and left lateral bending, and right and left axial rotation. The spines were tested in seven different conditions: the harvested condition and six independent single-level fused conditions (i.e., C2-C3, C3-C4, C4-C5, C5-C6, C6-C7, C7-T1). Fusion was simulated by attaching custom-designed clamps to pairs of adjacent spinal bodies (see Figure 1). The clamps could be removed and reattached to create the same alignment at each vertebral level. A previously developed *in vitro* testing protocol was adopted, i.e., incremental loading up to a target moment at T1 between 2 to 3Nm with limit checks of 35 degrees total spine rotation, maximum bending moment of 5Nm, and applied actuator load of 75N (DiAngelo and Foley, 2003). Motion of the individual spinal bodies was measured with an optical tracking system. Additional measurements included applied load and moment. Data for the motion segment unit (MSU) rotations and global stiffnesses were normalized to the harvested condition and compared using a one-way ANOVA and S-N-K test with significance set at P = 0.05.

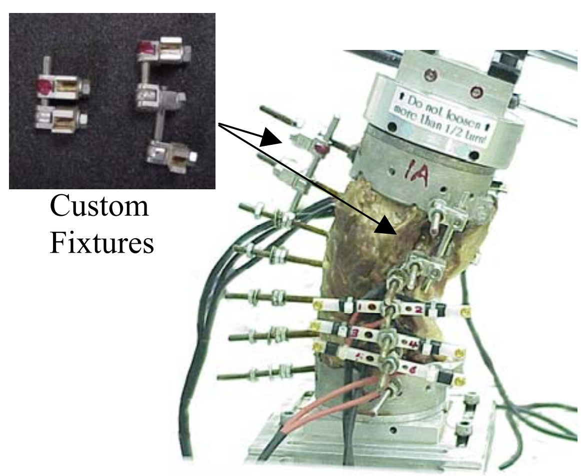

Figure 1: Custom fixtures were used to simulate single-level fusion.

RESULTS

The relative changes in the rotations of each MSU for the different fused conditions relative to their contribution in the harvested condition are shown in Figure 2 for flexion. A significant reduction in motion occurred at all fused MSU levels for flexion and extension ($P<0.05$). There were no significant differences in the rotational changes at the other levels compared to the harvested condition. The motion compensation occurred primarily at the adjacent segments. Similar results in the motion compensation occurred in lateral bending and axial rotation. When the relative rotations at the superior, fused, and inferior MSUs were analyzed with respect to the overall rotation of those three MSUs, the motion compensation at the adjacent levels was significant. Significant differences occurred at the level above the fusion site for the C3-C4 & C4-C5 fusion in both flexion and extension. The opposite occurred at C5-C6 and C6-C7; a significant increase in motion compensation occurred at the MSU below the C6-C7 fusion and the C5-C6 fusion in extension.

DISCUSSION

Questions still remain about what causes the degeneration and progression of disease at segments adjacent to a fused level. It was hypothesized that the adjacent segments carry an increased load due to the fusion that results in increased motion compensation at those segments. Such a hypothesis was supported by the results of this study. Vertebral rotations at the segments immediately adjacent to a fused level were larger than the rotations of the other levels of the spine and the compensation, when examining the fused level and the two adjacent segments, was significant. The results from this study further suggest that there is increased motion at the segment below a fusion in the lower cervical spine (C5-C6, C6-C7) or at the segment above an upper cervical fusion (C3-C4, C4-C5). This information may help to better understand the effects of single-level fusion on the advancement of degenerative disc disease and subsequent treatment plans.

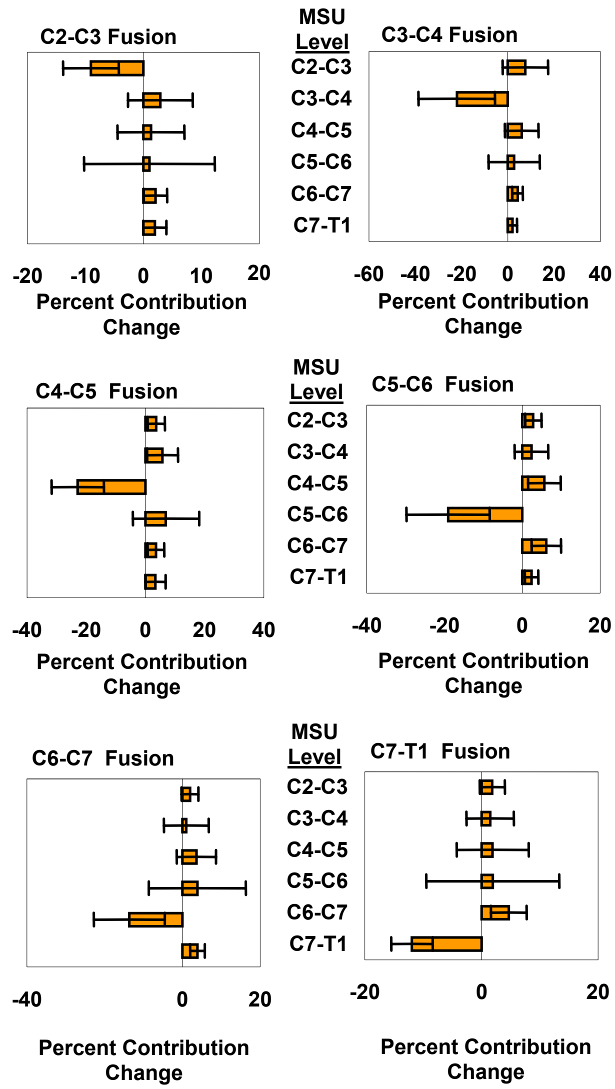

Figure 2: MSU Rotations. Percent Change in MSU Rotation of Fused Levels Normalized to Harvested Contribution For Flexion Loading. Decrease rotation to the left and increased rotation to the right.

REFERENCES

DiAngelo DJ, Foley KT (2003). *Spinal Implants: Are We Evaluating Them Appropriately?,* ASTM STP1431, 155-172.

PROBLEMATIC SITES OF THIRD BODY EMBEDMENT IN POLYETHYLENE FOR WEAR ACCELERATION IN TOTAL HIP ARTHROPLASTY

Hannah J. Lundberg [2], Kristofer J. Stewart [1], Douglas R. Pedersen [1], Thomas D. Brown [1,2]

[1] Department of Orthopaedics and Rehabilitation, University of Iowa, Iowa City, IA, USA
[2] Department of Biomedical Engineering, University of Iowa, Iowa City, IA, USA
E-mail: hannah-lundberg@uiowa.edu Web: mnypt.obrl.uiowa.edu/OBL_Lab_Website

INTRODUCTION

Total hip arthroplasty (THA) wear is highly variable within patient cohorts and can be accelerated by counterface roughening due to third body ingress. Scratching from third body debris, embedded in the polyethylene liner, is the primary means whereby femoral head roughening occurs. In this study, we identified acetabular sites most problematic for particle embedment, in terms of scratching kinetically critical regions of the femoral head. Gait-cycle traverse loci were calculated for acetabular sites corresponding to previously identified regions of femoral head roughening. Instantaneous local contact stress and sliding distance were included as factors influencing the severity of femoral head scratching for a given embedment site.

METHODS

Gait-cycle acetabular traverse loci were calculated for 284 femoral reference points equally spaced over the femoral head. These points were determined from wear simulations using a sliding-distance-coupled finite element model for THA wear (Maxian et al., 1996), and corresponded to locations of putative femoral counterface roughening.

Femoral reference points (P_{Fem}) were defined in an anatomical anterior-lateral-superior coordinate system. Loci of acetabular points over-passing these reference points were calculated by transforming the points using rotation matrices corresponding to flexion, abduction, and external rotation angles (α, β, and ψ, respectively) of the gait cycle, per Equation 1. Sixteen rotation increments for each motion were used, taken from experimental data for the stance portion of one gait cycle (Pedersen et al., 1998). This resulted in 16 segments that defined each locus of P_{Fem} on the acetabulum. Each locus corresponded to a path on the acetabulum traversed by points overpassing the femoral regions.

$$P_{Loc} = [R_{Ext}]^T [R_{Abd}]^T [R_{Flx}]^T * P_{Fem} \quad (1)$$

$$R_{Flx} = \begin{bmatrix} \cos\alpha & \sin\alpha & 0 \\ -\sin\alpha & \cos\alpha & 0 \\ 0 & 0 & 1 \end{bmatrix},\ R_{Abd} = \begin{bmatrix} 1 & 0 & 0 \\ 0 & \cos\beta & \sin\beta \\ 0 & -\sin\beta & \cos\beta \end{bmatrix},\ R_{Ext} = \begin{bmatrix} \cos\psi & 0 & -\sin\psi \\ 0 & 1 & 0 \\ \sin\psi & 0 & \cos\psi \end{bmatrix}$$

To determine the most problematic areas for polyethylene embedment, a damage propensity index (DPI) was identified. Increased scratching severity from a third body embedded in the polyethylene would plausibly occur in proportion to contact stress and sliding distance at the site of embedment, so the index considered contributions from both factors. Instantaneous local contact stress, σ, was taken from previous finite element data. Contact stress data were available for each femoral reference point at 24 serial time points (41667-cycle intervals of habitual activities within each 1-million cycle wear simulation). Sliding distance, d, was calculated incrementally from the gait rotation angles. A weight factor (wf), based on the volumetric wear that resulted from the corresponding 1-million cycle wear simulation, was also incorporated into the index. All variables were normalized from 0 to 1 based on the maximum value from each group.

To take into account the total effect of the variables throughout a 1-million cycle wear simulation, the product of the variables was taken for each femoral reference point for each of the 24 time increments (see Equation 2). The incremental index was then summed over all 24 increments to arrive at the total damage index at each femoral reference point. Because some femoral reference points resulted in loci points that intersected other such points, a final summation was performed to obtain a total damage propensity at each acetabular location. The resulting index identified areas of the acetabulum most problematic for debris embedment.

$$DPI = \sum \sigma * d * wf \qquad (2)$$

RESULTS AND DISCUSSION

Example traverse loci are displayed in Figure 1. Figure 2 shows the problematic acetabular areas. Areas of the acetabulum most critical for increased wear due to debris embedment (per the above DPI criterion) were concentrated on the supero-lateral aspect of the bearing surface.

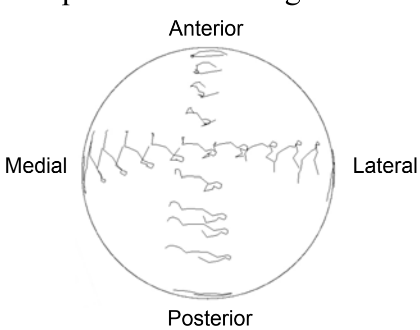

Figure 1. Gait-cycle P_{Fem} traverse loci on the acetabular cup for normal level walking.

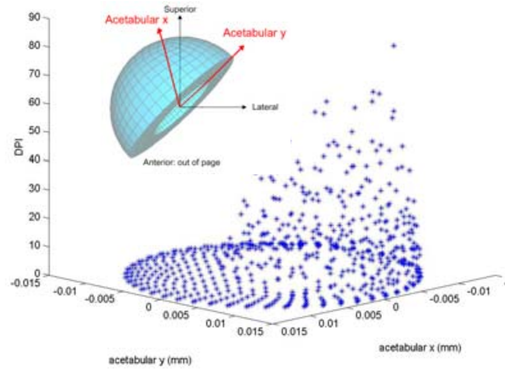

Figure 2. Plot of the DPI over a projection of the acetabular surface. Problematic acetabular areas for debris embedment are on the supero-lateral-most aspect of the cup. Anatomical axes are shown on an example acetabular cup.

SUMMARY

A new analytical tool has been introduced to evaluate the relative damage propensity associated with various sites of third body embedment in polyethylene. Gait-traverse loci of femoral points on the acetabulum throughout the stance portion of a gait cycle have been calculated. The data show that the supero-lateral aspect of the acetabular cup is by far the most problematic area for debris embedment.

REFERENCES

Maxian, T.A. et al. (1996). *J. Biomechanics*, **29**, 687-692.
Pedersen, D.R. et al. (1998). *Iowa Orthopaedic J.*, **18**, 43-53.

ACKNOWLEDGEMENTS

Supported by grants from the NIH (AR44106, AR47653), DePuy, Inc., and an NSF graduate research fellowship (HJL). Helpful suggestions by Dr. John J. Callaghan were also appreciated.

QUANTITATIVE CHARACTERIZATION OF LATERAL FORCE TRANSMISSION IN PASSIVE SKELETAL MUSCLE

Carina J. Bender, M.S. and David A. Hawkins, Ph.D.

Human Performance Laboratory, Exercise Science Graduate Group
University of California, Davis
E-mail: dahawkins@ucdavis.edu Web: http://www.exb.ucdavis.edu/faculty/hawkins/index.htm

INTRODUCTION

Muscle-tendon research is critical for advancing preventative, surgical and rehabilitative techniques in orthopedic and sports medicine. Depending on architectural arrangements within individual muscles and between adjacent structures, a number of force transmission pathways are available. Traditionally, the myotendinous pathway is considered the exclusive means for muscular force transmission, but alternate pathways may employ intramuscular and inter-muscular connective tissues to transmit force laterally (lateral force transmission, LFT) (Huijing, et. al., 1998). Lateral force transmission was investigated in normal and partially compromised passive skeletal muscle systems in order to identify contributing factors and to quantify the fraction of total system force that can be transferred laterally.

METHODS

Tensile tests were performed for simulated tenotomy and fasciotomy conditions. The peroneus longus (PL) and middle gastrocnemius (MG) muscles of the chicken were selected for their similar architecture and the intermuscular fascial interface connecting the muscles along 50-80% of their lengths. The muscle system was mounted to a testing fixture (Figure 1) that allowed removal and reattachment of the distal end of the muscles to simulate tenotomy. The distal clamps were connected to a modified Cambridge

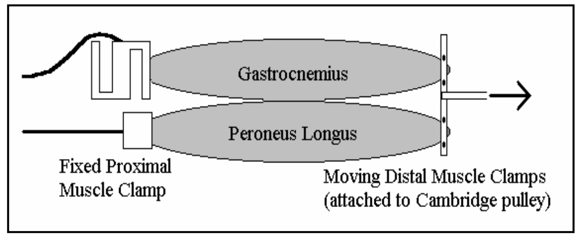

Figure 1. Diagram of testing setup.

Technology Model 300B Lever System. The proximal end of MG was clamped to a 222-N force transducer (Omega Engineering). A computer with analog to digital converter and custom LabVIEW software (National Instruments) controlled the Cambridge system to produce 20% strain in the muscle(s) at 1% strain per second while recording displacement and force data at 10 Hz and digital images of the muscle deformation at 1 Hz.

Tests were conducted under three levels of tenotomy (both muscles attached, only PL attached, only MG attached) and three levels of fasciotomy (100% intact, 33% transected distally, 66% transected distally). Release of the distal end of one muscle (unattached) followed by deformation of the distal end of the other (attached) muscle allowed the magnitude of LFT (F_{LFT}) to be quantified, defined as the force transmitted via the intermuscular fascia from the distally attached muscle to the proximal end of the distally unattached muscle. F_{LFT} was normalized to total force measured at the distal end (F_{Total}) to determine the fraction of total force that was transmitted laterally (F_{LFT}/F_{Total}).

The elastic moduli (slope of the linear portion of the force-deformation curve) for each muscle and the fascia were determined. The elastic modulus of the fascia was determined using system and individual muscle moduli. The ratio of the modulus of the muscle receiving force divided by the modulus of the muscle transmitting force (E_R/E_T) provided the relative stiffness of the two muscles. The ratio of elastic moduli of the fascia and transmitting muscle (E_F/E_T) provided a measure of the relative stiffness of these two components.

The influences of three covariates (fraction of initial fascia intact (*"Fascia"*), ratio of elastic moduli of the muscles (E_R/E_T), and ratio of elastic moduli of the fascia and transmitting muscle (E_F/E_T)) were evaluated by ANCOVA to determine their relative importance to the occurrence of LFT.

RESULTS AND DISCUSSION

The magnitude of lateral force transmission was affected by the extent of fascia and the relative properties of the muscles and fascia. With the fascia intact, 16% to 32% of the force applied distally to one muscle was transferred laterally to the other muscle. The relative amount of force transmitted laterally (F_{LFT}/F_{Total}) decreased with increased fasciotomy (Figure 2) and depended on which muscle was attached.

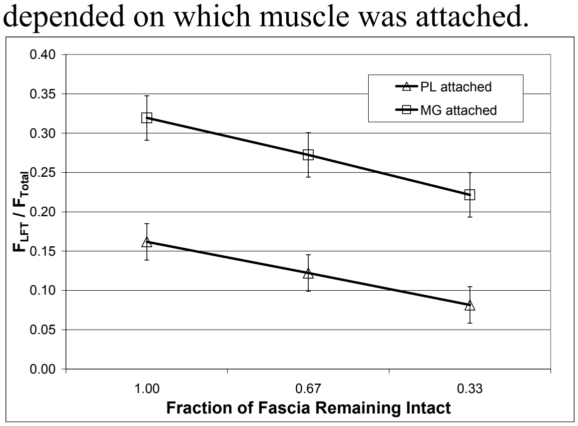

Figure 2. Relative lateral force transmission with progressive fascia removal.

There was no clear relationship between LFT and the relative stiffness of the two muscles. However, the relative stiffness of the fascia was important. As the elastic modulus of the fascia increased relative to that of the transmitting muscle, the fraction of the total force transmitted through the interface increased. The relationship between relative F_{LFT} and E_F/E_T was statistically significant ($p < 0.001$), with 21-95% of the variability in F_{LFT}/F_{Total} accounted for by variability in E_F/E_T.

Analysis of the effects of relative tissue properties and interface quantity by ANCOVA revealed the relative importance of each of these factors. F_{LFT}/F_{Total} can be expressed as a function of these significant contributors ($R^2 = 0.83$) as:

$$F_{LFT}/F_{Total} = 0.024 + (0.156 \bullet Fascia) - \left(0.014 \bullet E_R/E_T\right) + \left(0.032 \bullet E_F/E_T\right)$$

SUMMARY

Lateral force transmission between the muscles tested was sizeable and showed directionality (32% of the force applied distally to the gastrocnemius muscle was transferred laterally to the peroneus longus muscle while only 16% of the force applied distally to the peroneus longus was transferred laterally to the gastrocnemius). There was poor correlation between LFT and the relative stiffness of muscles transmitting and receiving force. Results suggest that contact area and fascia stiffness were the greatest contributors to LFT and that the architectural arrangement of fascia and muscle may play an important role.

REFERENCES

Huijing, P.A., et al. (1998). *J Exp Bio*, **201**, 682-691.

Monti, R.J., et al. (1999) *J Biomech*, **32**, 371-380.

GAIT EFFECIENCY: CENTER OF MASS MOTION, VO_2 AND WALKING SPEED

Michael S. Orendurff, Ava D. Segal, Jocelyn S. Berge, Kevin C. Flick and Glenn K. Klute

Motion Analysis Laboratory, Rehabilitation Research and Development, Seattle, Washington
michael.orendurff@med.va.gov www.seattlerehabresearch.org

INTRODUCTION

Metabolic measurement while walking at increasing speeds shows a predictable increase in oxygen consumption (ml/kg/min) for normal individuals (figure 1a). However, when calculating the metabolic cost per meter traveled (ml/kg/m) a more parabolic curve emerges suggesting that gait is most efficient near 1.3 m/s and becomes less efficient at slower and faster walking speeds (figure 1b). The decrease in efficiency at faster speeds is supported by mechanical calculations[1,2,3] but the cause of the decrease in efficiency at slow walking speeds has not been elucidated.

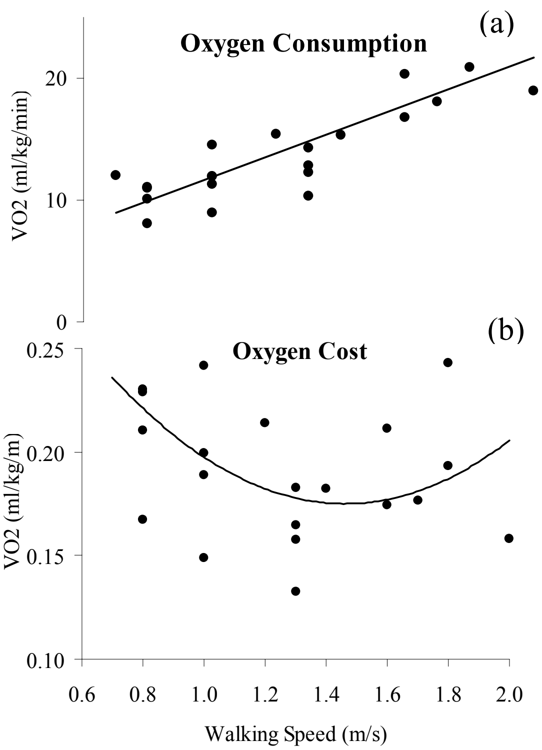

Figure 1. VO_2 at several walking speeds for 5 normal adults.

While a variety of mechanical and energy transfer mechanisms may be less efficient at slow walking speeds, increasing step width has been shown to increase the metabolic and mechanical cost of ambulation by approximately 50%[1]. The purpose of this experiment was to evaluate vertical and mediolateral center of mass (COM) displacement to determine if this could explain some of the observed decrease in gait efficiency at slower walking speeds.

METHODS

Ten adults who were free from gait abnormalities gave informed consent to participate in this IRB-approved protocol. A sensormedics VmaxST portable metabolic device measured oxygen consumption while subjects (n = 6) walked overground at four speeds from 0.6 to 2.0 m/s. Speed was measured and controlled by a cart pushed by an investigator next to the subject. Metabolic data was monitored in real time and was collected for a minimum of two minutes after a steady state of oxygen consumption was achieved. Subjects rested until steady state in a chair between each walking speed. Following O_2 measurements, gait measurements were made using a 10-camera Vicon 612 system. Thirty-eight reflective markers were placed on each subject (n = 10) according to Vicon's full-body Plug-In-Gait model. Subjects walked at four speeds from 0.7 m/s to 1.6 m/s, with five trials at each speed. Data was collected at 120 Hz, smoothed using a quintic spline at 20 MSE, labeled and modeled using Vicon Workstation software. Segmental analysis was used to calculate the COM of each segment and then for the whole body. COM displacement in the vertical (Z) and mediolateral (X) directions were compared across walking speeds using mixed effects ANOVAs with linear contrasts post hoc. The *p*-value was set at 0.05 *a priori*.

RESULTS

The data show that vertical (Z) COM displacement was at a minimum at the slowest walking speed and increased with speed ($p < 0.05$). Mediolateral (X) COM was at a minimum at the fastest walking speeds and increased as walking speed decreased ($p < 0.05$).

Speed (m/s)	COM Z disp (cm)	COM X disp (cm)
0.7	2.74 ± 0.52	6.99 ± 1.34
1.0	3.61 ± 0.66*	5.96 ± 1.68*
1.2	4.06 ± 0.72*	4.41 ± 1.23*
1.6	4.83 ± 0.92*	3.85 ± 1.41
SS	4.89 ± 1.03†	3.29 ± 1.29†

Mean ± SD * indicates statistically significant difference from speed directly above ($p < 0.05$).
† indicates statistically significant difference from speed two values above ($p < 0.05$)
SS = Self-selected walking speed: 1.61 ± 0.22 m/s

The vertical COM displacement is consistent with other work[4], but this is the first time that mediolateral COM data has been reported across walking speeds. These data suggest that the mediolateral movement of the COM may be associated with the observed decrease in gait efficiency observed at very slow walking speeds. Although the vertical COM displacement did increase as walking speed increased, it did not disturb gait efficiency until walking speeds exceeded 1.6 m/s. At this speed individuals were as efficient per meter traveled as they were at 1.0 m/s, but the faster speed presumably cut transit time substantially. It may be that these normal subjects picked the fastest walking speed where gait efficiency could be maintained in order to traverse a short distance. In the vertical direction COM displacement may allow a potential to kinetic energy exchange, so that even if the vertical excursion is great some energy transfer may reduce metabolic cost. However, the increase in mediolateral COM displacement at slow walking speeds may be more costly since the COM must be reversed at both ends of the range, requiring additional energy, which is reflected in the metabolic costs at slow speeds[2]. This effect may play a role in choosing a self-selected walking speed, although other factors may also be important. Individuals with gait pathology often choose a slow walking speed, possibly for reasons other than efficiency. Fear of falling, reduced sensation or motor control and weakness may all play a role in determine walking speed. Nevertheless walking slowly is much less efficient than walking near 1.2 m/s where efficiency appears maximized and COM displacement in the vertical and mediolateral directions are nearly equal.

REFERENCES

1. Donelan, J.M., Kram, R., Kuo, A.D. (2001) *Proc. R. Soc. Lond. B* 268, 1985-92.
2. Tesio, L., Lanzi, D., Detrembleur, C. (1998) *Clin Biomech* 13, 77-82.
3. Donelan, J.M., Kram, R., Kuo, A.D. (2002) *J. Exp Biol.* 205, 3717-3727.
4. Lee, C.R., Farley, C.T. (1998) *J Exp Biol.* 201, 2935-44.

ACKNOWLEDGEMENT

This work was supported by Department of Veteran Affairs grant # A2661C.

AN ELECTROMYOGRAPHIC ANALYSIS OF COMMERCIAL AND COMMON ABDOMINAL EXERCISES

Rafael F. Escamilla[1], Michael McTaggart[2], Ethan Fricklas[2], and Alan Hreljac[3]
[1]Department of Physical Therapy, California State University, Sacramento, CA, USA
[2]Department of Biomedical Engineering, Duke University, Durham, NC, USA
[3]Department of Kinesiology & Health Science, California State University,Sacramento,CA, USA
Email: rescamil@csus.edu Web: http://www.hhs.csus.edu/pt

INTRODUCTION

There are numerous commercial abdominal machines on the market that claim to target abdominal muscular and minimize lower back stress, but there is only a sparsity of data to support these claims. The purpose of this study was to test the effectiveness of seven popular commercial abdominal machines (Ab Slide, Ab Twister, Ab Rocker, Ab Roller, Ab Doer, Torso Track, and SAM) and two common abdominal exercises (Crunch and Bent-Knee Sit-up) on activating abdominal and extraneous musculature.

MATERIALS AND METHODS

Twelve healthy male and female subjects participated in this study. Surface electrodes were positioned in pairs on the subject's dominant side over the upper and lower rectus abdominis, external obliques, long head of the triceps brachii, rectus femoris, pectoralis major, and lower erector spinae. EMG data were collected from a Noraxon 8-channel telemetry EMG system during five repetitions for each exercise. Each repetition was performed in a slow and controlled manner, taking approximately 3-4 s to complete. EMG exercise data were normalized by maximum voluntary isometric contractions. Differences in muscle activity were assessed by a one-way repeated measures Analysis of Variance ($p < 0.01$).

RESULTS AND DISCUSSION

Mean EMG data among the abdominal exercises are shown in Table 1. Compared to all exercises: 1) upper and lower rectus abdominis activity was significantly greater in the Ab Slide, Torso Track, Crunch, and Bent-Knee Sit-up; 2) external oblique activity was significantly greater in the Bent-Knee Sit-up and Ab Slide; 3) rectus femoris activity was significantly greater in the Bent-Knee Sit-up, Ab Twister, and Ab Rocker; 4) triceps brachii and pectoralis major activity were significantly greater in the Ab Slide and Torso Track; and 5) erector spinae activity was significantly greater in the Ab Doer.

Both the Torso Track and Ab Slide activated abdominal musculature by resisting trunk extension rather than by actively flexing the trunk. Hence, these exercises may be effective for individuals who want to avoid trunk flexion but still activate the abdominals. In contrast, the crunch or sit-up may is better suited for individuals who want to activate the abdominals without trunk extension. The Ab Twister, Ab Rocker, Bent-Knee Sit-up, and Ad Doer had the greatest hip flexor and back activity, which may be problematic for individuals with low back problems due to the tendency of these muscles to increase lumbar lordosis and anterior pelvic tilt.

SUMMARY

The Ab Slide, Torso Track, Crunch, and Bent-Knee Sit-up were the best exercises for activating the abdominal and oblique muscles. The Ab Slide and Torso Track were also effective in activating upper extremity muscles while minimizing lower back and hip flexion activity.

Table 1. Mean EMG±SD ($p < 0.01$) for each muscle and exercise expressed as a percent of each muscle's maximum isometric voluntary contraction.

Exercise	Upper Rectus Abdominis	Lower Rectus Abdominis	External Obliques	Rectus Femoris	Triceps Brachii	Erector Spinae	Pectoralis Major
Ab Slide	44±19[a]	46±18[e]	47±33[h]	8±11	21±12[k]	6±6	14±7[m]
Torso Track	41±20[c]	46±18[e]	36±31	4±4	26±21[k]	5±6	15±11[m]
Crunch	30±9[b]	31±9[f]	18±15	4±7	2±3	1±1	7±11
Bent Knee Sit-up	27±13[b]	35±14[f]	56±30[h]	41±25[i]	2±3	4±2	7±6
Super Abdominal Machine (SAM)	26±17[d]	28±11[g]	25±25	17±17	7±7	6±3	12±8
Ab Roller	24±15[d]	23±14[g]	17±15	2±2	4±4	3±3	4±3
Ab Twister	8±5	11±6	19±17	33±31[j]	4±3	2±2	6±6
Ab Rocker	7±3	8±4	29±25	28±21[j]	5±3	4±3	6±7
Ab Doer	12±6	13±8	11±5	10±12	1±1	14±7[l]	4±4
Pairwise Comparisons	a, b, c, d	e, f, g	h	i, j	k	l	m

Pairwise Comparisons ($p < 0.01$) in EMG activity Between Abdominal Exercises

a) Upper abdominal: Ab Slide > all other abdominal exercises except Torso Track
b) Upper abdominal: Ab Slide, Crunch, Bent Knee Sit-ups > Ab Doer, Ab Rocker, & Ab Twister
c) Upper abdominal: Torso Track > Ab Doer, Ab Rocker, Ab Twister, & Ab Roller
d) Upper abdominal: SAM & Ab Roller > Ab Doer, Ab Rocker, & Ab Twister
e) Lower abdominal: Torso Track & Ab Slide > all other abdominal exercises
f) Lower abdominal: Bent Knee Sit-ups & Crunch > Ab Doer, Ab Rocker, & Ab Twister
g) Lower abdominal: SAM, Crunch, & Ab Roller > Ab Doer & Ab Rocker
h) External oblique: Bent Knee Sit-up & Ab Slide > Ab Roller, Crunch, Ab Twister, & Ab Doer
i) Rectus femoris: Bent knee Sit-up > Ab Roller, Ab Slide, Torso Track, Crunch, SAM, Ab Doer
j) Rectus femoris: Ab Twister & Ab Rocker > Ab Roller, Ab Slide, Torso Track, & Crunch
k) Triceps brachii: Torso Track & Ab Slide > all other abdominal exercises
l) Erector spinae: Ab Doer > all other abdominal exercises
m) Pectoralis major: Torso Track & Ab Slide > Ab Roller & Ab Doer

ACCELERATION DURING WALKING: THE EFFECT OF ANKLE KINETICS ON CENTER OF MASS POSITION AND VELOCITY

Michael S. Orendurff, Ava D. Segal, Jocelyn S. Berge, Kevin C. Flick and Glenn K. Klute

Motion Analysis Laboratory, Rehabilitation Research and Development, Seattle, WA. USA
michael.orendurff@med.va.gov   www.seattlerehabresearch.org

INTRODUCTION

Most gait analysis is conducted at constant walking speed. But human gait involves increases in walking speed to navigate obstacles or meet timing deadlines. Hurrying to avoid an approaching car in a crosswalk, catching a closing elevator door, or rushing toward a hissing teapot involves an increase in walking speed. Theoretical experiments using induced acceleration analysis (Lohmann, 2004) and energy transfer modeling (Meinders, 1998) have attempted to explain the contribution of limb segments and individual joints to the body's center of mass (COM) acceleration during constant speed walking, but to date no work has focused on the joint mechanisms used to increase walking speed. Understanding individual joint contributions used in accelerating gait may improve prosthetic designs for amputees. The purpose of this experiment was to compare the differences in COM position, COM velocity and ankle kinetics during accelerating and constant speed walking.

METHODS

Seven adults who were free from gait abnormalities gave informed consent to participate in this IRB-approved protocol. Gait measurements were made using a 10-camera Vicon 612 system (Lake Forest, CA). Thirty-eight reflective markers were placed on each subject according to Vicon's full-body Plug-In-Gait model. Subjects completed six trials across an embedded forceplate (Kistler, Wintethur, CH) at their self-selected walking speed (SSWS) and were then instructed to walk at their self-selected speed to the forceplate and then accelerate as quickly as possible until the end of the walk way (Accel). Kinematic data was collected at 120 Hz, smoothed using a quintic spline at 20 MSE, labeled and modeled using Vicon Workstation software. Segmental analysis was used to calculate the COM of each segment and then for the whole body. COM forward (Y) velocity, sagittal ankle moments and sagittal ankle powers were compared across walking speeds using repeated measures ANOVAs and Scheffe's tests post hoc($p < 0.05$)

RESULTS and DISCUSSION

Self-selected walking speed was 1.5 ± 0.2 m/s. Subjects were able to increase their COM speed from 1.4 ± 0.2 to 2.2 ± 0.3 m/s during the acceleration task ($p > 0.05$). The onset of COM acceleration often coincided with a drop in COM position (see figure 1). The maximum ankle plantarflexor moment at 25% of the gait cycle was significantly lower in the acceleration trials than during constant speed walking (0.1 ± 0.2 VS 0.3 ± 0.1 Nm/kg; $p < 0.05$; see figure 2), suggesting that reduced support from the ankle was influencing the vertical position of the COM. This may be an indication that a potential-to-kinetic energy exchange was utilized to accelerate the COM forward at a faster rate during midstance. In late stance the peak plantarflexion moment was greater during acceleration than constant speed walking (1.7 ± 0.2 VS 1.4 ± 0.1 Nm/kg; $p < 0.05$). The peak ankle power in pre-swing was also increased during accelerating gait (5.3 ± 2.7 VS 3.9 ± 1.1 W/kg; $p = 0.05$; see figure 3), suggesting that the ankle is an important joint for increasing walking speed.

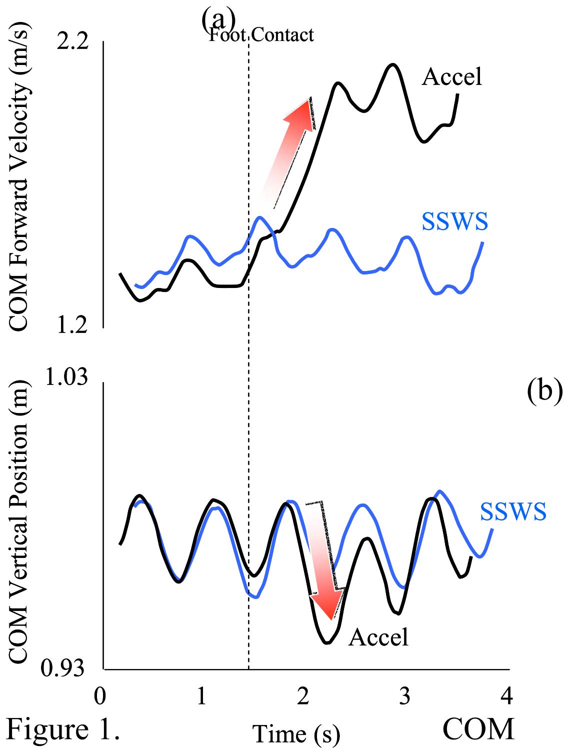

Figure 1. COM forward velocity (a) and vertical position (b) shown as a subject accelerates from 1.3 to 1.8 m/s.

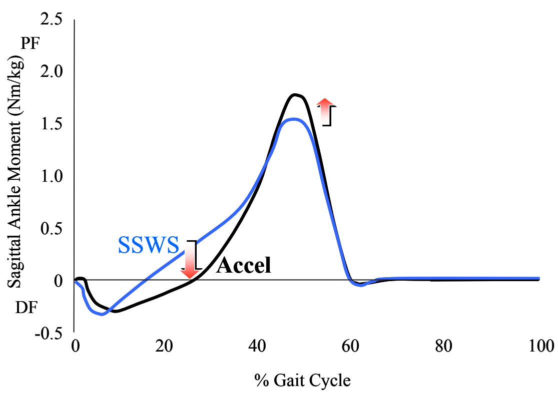

Figure 2. Ankle plantarflexor moments were reduced in midstance and increased in pre-swing during acceleration trials.

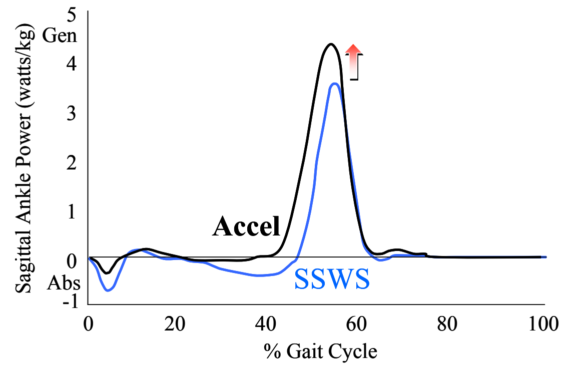

Figure 3. Sagittal Ankle power increased in late stance during acceleration trials.

SUMMARY

Increasing walking speed appears to involve both potential-to-kinetic energy exchanges and increased joint power output at the ankle. The function of the ankle may permit acceleration by altering support moments and propulsive moments. Further work is needed to understand the contribution of other joints to increasing walking speed. Amputees who lack a sound ankle joint face unique challenges in gait acceleration which must be overcome by compensation at other joints. Understanding how amputees increase their walking speed may assist is defining design parameters for novel lower extremity prostheses. Improving the ability of amputees to meet the demands of changing walking speed may improve their mobility.

REFERENCES

Lohan Siegel, K., Kepple, T.M., & Stanhope, S.J. (2004) *Gait Posture.* 19, 69-75.

Meinders, M., Gitter, A., & Czerniecki, J.M. (1998) *Scand J Rehab Med.* 30, 39-46.

ACKNOWLEDGEMENT

Funded by Department. of Veteran Affairs grant #A2661C.

DESIGN OF A PRE-CLINICAL TEST FOR PROSTHETIC ANKLE IMPLANTS

Nick J. Byrne[1], Heidi Ploeg[2], Daren Deffenbaugh[3]
[1]Department Biomedical Engineering, University of Wisconsin, Madison, WI, USA
[2]Department Mechanical Engineering, University of Wisconsin, Madison, WI, USA
[3]DePuy, Inc. a Johnson & Johnson company, Warsaw, IN, USA
E-mail: njbyrne@wisc.edu Web: http://www.engr.wisc.edu/groups/BM/

INTRODUCTION

Component loosening, migration, and subsidence are the biggest concerns to implant designers and orthopedic surgeons when faced with the challenge of providing adequate total ankle replacements (TAR). It is commonly known in the biomaterials and orthopedics communities that excessive wear debris in orthopedic implants can lead to osteolysis, resulting in these adverse effects (Ratner 1996). Many wear tests have been done on hip and knee replacements (Calonius 2002), however wear simulation has not been done on TAR's. Various static and dynamic tests have been performed on TAR components (Greenwald 2000 and Valderrabano 2003), however these were performed under a wide range of conditions and examined a variety of results. Therefore it would be prudent to examine TAR strength and wear characteristics under physiological loading.

The purpose of this project is to design a test that will simulate the long-term mechanical loading for any TAR design under standard, physiological loads and ranges of motion. The test should quantify component wear and strength, and allow for a direct comparison between various TAR designs. The focus of this project, however, will be the AGILITY Ankle by DePuy, Inc.

METHODS

The development of the test design presented here began with research of current ankle testing being performed, results of those tests, and post-operative performance of various TAR's (Pyevich 1998). Clinical retrievals of TAR's were obtained from DePuy, photographed, and catalogued to serve as clinical validation of this test. A finite element analysis of the implanted Agility ankle (Galik 2002) was obtained to serve as computational validation.

The test will examine two loading regimes, that of the healthy person, referred to as normal, and that of the post-operative TAR recipient. The normal load scheme will be examined since the ultimate goal of orthopaedic manufacturers is to return normal function to TAR recipients. Post-operative loads and ranges of motion will also be examined in order to be able to compare these test results with the clinical retrievals.

Figure 1: AMTI knee wear simulator

The tibial and talar components of the AGILITY Ankle will first be fixed in a polyurethane bone substitute following actual surgical procedure. The components will then be mounted in an AMTI knee wear simulator similar to the one shown in Figure 1. The testing environment will be a bovine serum at 37° C.

For the post-operative load cycle, a maximum axial load, F_{max}, of 3.3 times body weight (750 N), that is 2475 N, will be applied sinusoidally at a load ratio (F_{min}/F_{max}) of 0.1 to the tibial component by an axial actuator, which will simultaneously rotate to provide a cyclic torsional load from 40 kg-cm external down to -25 kg-cm internal torque. This loading will be synchronized with rotation of the talar component in the sagittal plane about the medial-lateral axis of the talar component. The range of motion will be 10 degrees of dorsiflexion and 14 degrees of plantarflexion (Stauffer 1977), and will be applied via an auxiliary rotary actuator. Also, a shear force of 0.4 times body weight, that is 300 N, will be applied in the anterior-posterior (a-p) direction via a horizontal actuator. The simulation of the normal load case will have the same load pattern as the post-operative case described above, with magnitudes of: F_{max} equal to 5.2 times body weight, that is 3900 N, torque from 49 kg-cm to –32 kg-cm, and a-p shear of 0.8 times body weight, that is 600 N (Seireg 1975).

This combination of loading and range of motion will closely simulate a normal and post-operative gait cycle. Load frequency, test duration, and Agility component size (1-6) will also be investigated according to physiological conditions, testing capabilities, and test duration.

SUMMARY

A concept for a standardized test for prosthetic ankle implants has been developed. Normal and post-operative axial, torsional, and shear loads will be applied in physiological magnitudes and ranges of motion, mimicking a physiological gait cycle. This test will allow for direct quantitative analysis of and comparison between various implants. Testing will be conducted in the summer of 2004 at DePuy, Inc. in Warsaw, IN.

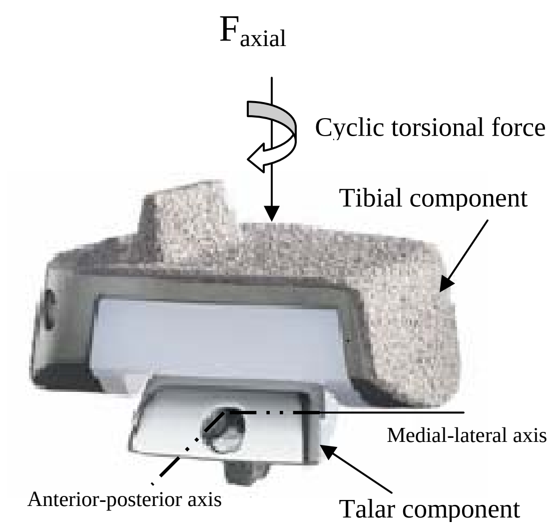

Figure 2: AGILITY Ankle prosthetic ankle implant by DePuy, Inc.

REFERENCES.

Ratner, B. et al (1996). *Biomaterials Science: An Introduction to Materials in Medicine*, Academic Press.
Calonius, O., Saikko, V., (2002). *Clinical Orthopedics*, 399, 219-230.
Greenwald, A. et al (2000). (www.orlinc.com).
Valderrabano, V. et al (2003). *Foot and Ankle International*, **24(**12), 881-900.
Pyevich, M. et al (1998). *JBJS*, **80A**, 1410-1420.
Stauffer, R. et al (1977*).* *Clin Orthop*, **127**, 189-196.
Seireg, A., Arvikar (1975). *Biomech*, **8**(2), 89-102.
Galik, K. (2002). U. of Pitt., PhD thesis.

ACKNOWLEDGEMENTS

Funding for this project was provided by DePuy, Inc., a Johnson & Johnson company. Laboratory facilities and research staff assistance were also generously provided.

EFFECTIVENESS OF A LATERALLY WEDGED INSOLE ON KNEE JOINT VARUS MOMENT IN NORMAL HEALTHY ELDERS; A MOTION ANALYTIC STUDY

Wataru KAKIHANA,[1] Masami AKAI,[1] Kimitaka NAKAZAWA,[1]
Kenji NAITO,[2] Suguru TORII [2]

[1] Department of Rehabilitation for Movement Functions, Research Institute of National Rehabilitation Center for Persons with Disabilities, Tokorozawa, Saitama, Japan
[2] Graduate School of Human Sciences, Waseda University, Tokorozawa, Saitama, Japan
E-mail: kaki@rehab.go.jp

INTRODUCTION

In 1987, the effect of wearing a laterally wedged insole in osteoarthritic patients with a varus deformity of the knee (OA patients) was first reported,[1] and, since then, kinematic and kinetic analyses concerning this condition have mainly focused on a static standing position. Yasuda and Sasaki[1] reported that wearing a laterally wedged insole reduced the load in the medial compartment of the knee, which was effective for the treatment in OA patients. Recently, Kerrigan et al.[2] found that, in dynamic gait conditions, wearing a laterally wedged insole reduced the knee joint varus moment in OA patients, which suggested an effective mechanism for the treatment in OA patients. However, it was not show how the evidence resulted in the reduction in the knee joint varus moment with a laterally wedged insole.

Our previous srtudy[3] found that the healthy young adults wearing a laterally wedged insole had both changes of knee joint varus moment and subtalar joint valgus moment during gait via the more laterally shifted location of the center of pressure. The objective of this study was to assess the kinematic and kinetic effects of wearing a laterally wedged insole on the knee joint moment during gait, specifically in the frontal plane, in normal healthy elders.

METHODS

Twenty elderly females (age: 68.2±5.7 yr, height: 149.9±5.2 cm, weight: 55.7±7.4 kg) participated in this experiment. The anteroposteriol radiographs of bilateral whole-legs including the hip, knee, and ankle were taken with standing and knee full extension position with barefoot in each side. With these weight-bearing radiographs, the femorotibial angles of right leg (174.6±4.6 °) were measured as the static alignment of the lower extremity.

Three-dimensional gait analyses were conducted with a motion analysis system (VICON) operating at 60 Hz with 12 infrared cameras and 8 force platforms (KISTLER) operating at 60 Hz. The laterally wedged insoles used in this study were made of Ethylene Vinyl Acetate (EVA 8200), which has a coefficient of elasticity of 100-300 kg/mm^2. Two different laterally wedged insoles were tested: no wedge (N) and a wedge with a 6 ° lateral angle (W) along the full length of the insole from the hindfoot to the forefoot. They were attached to the bare feet of the subjects using adhesive tapes after ethanol swab.

Subjects were asked to walk at a controlled cadence of 95 steps/minute while listening to a metronome along the walkway. Angles and moments at the knee and subtalar joints in the frontal plane, and ground reaction forces and center of pressure during the stance phase of the gait were measured.

RESULTS AND DISCUSSION

The knee joint varus moment was significantly smaller for insole W compared with insole N (a 10.4% reduction, P <.001), whereas the subtalar joint valgus moment was significantly greater for insole W compared with insole N (a 33.3% increase, P <.001) (Figure 1). The angles at the knee and subtalar joints did not show any changes between the two insole conditions. No obvious differences in the insole conditions were found for the mediolateral and vertical GRFs during the stance phase; however, this was not true for the moment arm of the subtalar joint valgus moment. The distance for insole W was significantly greater compared with insole N (a 41.1% increase, $P <.001$). The location of the center of pressure parallel to the subtalar joint axis was more laterally shifted for insole W, and, hence, it had a significantly smaller knee joint varus moment than insole N.

Regression analysis was used to examine the association between the femorotibial angle and the knee joint varus moment during gait with insole N. There was a highly correlation between pairs of variables ($r^2=0.80$, $P <.001$). Our next research will be to show how the beneficial effects of wearing a laterally wedged insole is found in age matched OA patients.

SUMMARY

In comparison with insole N, insole W significantly reduced the knee joint varus moment and increased the subtalar joint valgus moment during gait. This finding was correlated with a more laterally shifted location of the center of pressure during the stance phase of the gait with insole W. These results show that wearing a laterally wedged insole reveals its dynamic effect during gait biomechanically.

REFERENCES

1) Yasuda K., Sasaki T. (1987). *Clin Orthop,* **215**,162-172.

2) Kerrigan CK et al. (2002). *Arch Phys Med Rehabil*, **83**, 889-893.

3) Kakihana et al. (2004). *Am J Phys Med Rehabil*, **83**, 273-278.

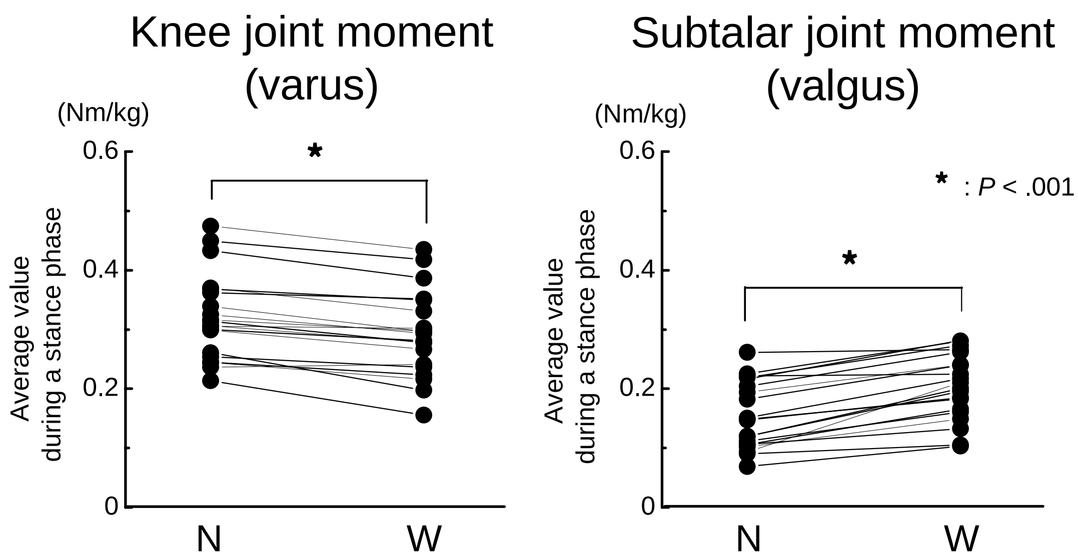

Figure 1: Differences between the knee joint varus moment and the subtalar joint valgus momentwhen the subjects walked with insoles no wedged (*N*) and high wedge with 6 ° lateral (*W*). Each symbol indicates the subjects (n=20). * indicated *P*<.001.

DIFFERENCES IN FRONTAL PLANE MECHANICS DURING WALKING BETWEEN PATIENTS WITH MEDIAL AND LATERAL KNEE OSTEOARTHRITIS

Robert J. Butler[1], Irene S. Davis[1,2], Todd Royer[3], Stephanie Crenshaw[3] and Emily Mika[1]

[1] Department of Physical Therapy, University of Delaware, Newark, DE, USA
[2]Joyner Sportsmedicine Institute, Harrisburg, PA USA
[3] Department of Health and Exercise Science, University of Delaware, Newark, DE USA
Email: rbutler@udel.edu Web: http://www.udel.edu/PT/davis/index.htm

INTRODUCTION

Knee osteoarthritis is a disease affecting a large population of older adults. While knee osteoarthritis is most common in the medial compartment, it also occurs in the lateral compartment. A number of biomechanical studies have evaluated walking mechanics in patients with medial knee osteoarthritis. It has been reported that patients with medial knee osteoarthritis exhibit increased frontal plane moments at the knee. However, there are no studies examining the walking mechanics in patients with lateral knee osteoarthritis. As well, there is little information on what occurs at the rearfoot and hip joints as a result of changes in knee joint mechanics in patients with knee osteoarthritis.

Therefore, the purpose of this study is to evaluate the differences in frontal plane mechanics of the rearfoot, knee and hip in patients with medial and lateral knee osteoarthritis during walking. It is hypothesized that patients with lateral knee OA would have decreased abduction moments and increased abduction angles during walking. Associated with the increased knee valgus, greater peak eversion angle and inversion moment were expected in the patients with lateral knee osteoarthritis. As well, hip adduction was expected to increase leading to an increased abduction moment.

METHODS

This is an ongoing study of which seven subjects (5 women and 2 men) with lateral knee osteoarthritis have been recruited. 7 subjects with medial knee osteoarthritis and matched for gender, Kellgren-Lawrence grade, BMI, and age were used for comparison. Subjects were included after being radiographically diagnosed with a Kellgren-Lawrence grade of 2-4 on an anterior-posterior flexed knee radiograph. A VICON motion analysis system and Bertec force platform were used to collect three dimensional motion analysis data.

The variables of interest included the first peak knee external abduction moment, second peak knee external abduction moment, and peak knee adduction angle. Peak eversion and inversion moment in the rearfoot along with peak adduction and the first and second peak hip external adduction moment were also evaluated in order to examine changes in mechanics at adjacent joints. Statistical analyses were performed using t-tests with an alpha level of 0.05. Directional t-tests were used for the hypotheses at the knee and bi-directional t-tests were used for the hip and rearfoot since there is no data to support hypotheses at these joints.

RESULTS AND DISCUSSION

Results are reported in Table 1 and Figures 1-3.

Table 1. Mean values for variables of interest

		Lat	Med	p
Knee				
	1st Pk Ab Mom	-0.15	-0.42	0.00
	2nd Pk Ab Mom	-0.15	-0.27	0.01
	Pk Ad Angle	-6.7	5.0	0.00
Hip				
	1st Pk Ab Mom	-0.62	-0.61	0.77
	2nd Pk Ab Mom	-0.60	-0.53	0.19
	Pk Ad Angle	6.6	5.4	0.57
Ankle				
	Pk Inv Mom	-0.05	-0.04	0.45
	Pk Eversion	1.7	6.2	0.02

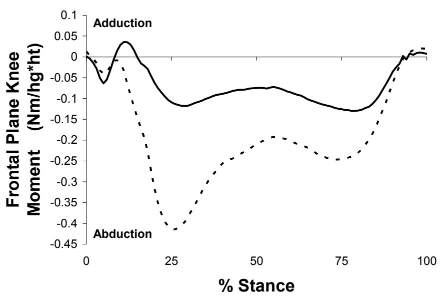

Figure 1. Frontal Plane Knee Moment in patients with lateral (solid) and medial (dashed) knee osteoarthritis

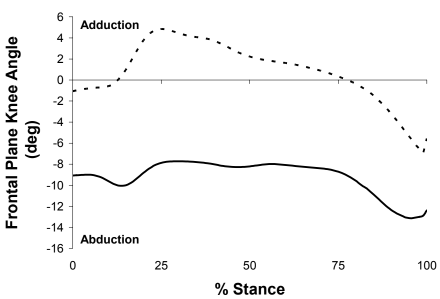

Figure 2. Frontal Plane Knee Angle in patients with lateral (solid) and medial (dashed) knee osteoarthritis

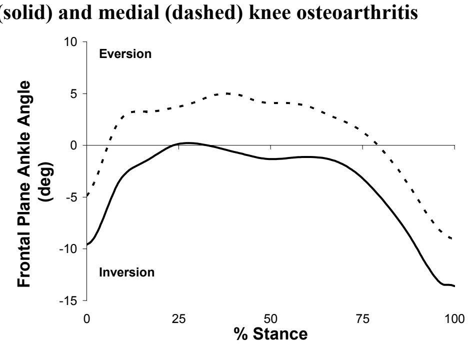

Figure 3. Rearfoot Angle in patients with lateral (solid) and medial (dashed) knee osteoarthritis

Therefore it appears that patients with lateral knee osteoarthritis have different frontal plane lower extremity mechanics during walking compared to patients with medial knee osteoarthritis. As hypothesized, knee abduction moments and adduction motion were reduced in the lateral population. Also in support of our hypothesis, there was a trend toward an increase in the second abduction peak at the hip in the patients with lateral knee osteoarthritis. This suggests increased forces at the hip during propulsion which may lead to a more rapid joint deterioration. Also surprisingly, it was observed that patients with lateral knee osteoarthritis had approximately 5 deg less eversion in the rearfoot throughout stance. While increased eversion is often associated with genu valgus, this may be evidence of a compensation mechanism to maintain a plantigrade foot. Therefore the potential for increased foot injuries may exist.

SUMMARY

The results of this study suggest that patients with medial and lateral knee osteoarthritis exhibit different walking mechanics at the knee, hip and rearfoot. These differences should be taken into account when seeking interventions to slow down the progression of knee osteoarthritis in the lateral compartment.

ACKNOWLEDGEMENTS

This study has been supported by NIH grant# P20 RR16458.

KINEMATIC STUDY OF LEFT ARM DURING GOLF SWING

Koon Kiat Teu[1], Wangdo Kim[1,#], Franz Konstantin Fuss[1] and John Tan [2]

[1] School of Mechanical & Production Engineering, Nanyang Technological University, Singapore
[2] Physical Education & Sports Science, National Institute of Education, Singapore
E-mail: MWDKim@ntu.edu.sg

INTRODUCTION

The knowledge of how golfer uses the different segmental motion to strike the ball may provide valuable information. The objective of this study is to ascertain the contribution of the segmental rotations to the club head speed of a golf swing.

METHODS

The method involved utilizing electrogoniometer (biometrics, UK) to obtain the joint angles of the left arm (shoulder, elbow, forearm and wrist) throughout the motion. The golf swing in this study was depicted as a five-segment model. Orthogonal Cartesian frame was attached to each segment (Figure 1): the glenohumeral joint, elbow joint, wrist joint, end of the grip and center of the club head. The directions of the three axes of each frame were constructed so as to approximate the different axes of rotation for each segment and the origin was located at the center of each relevant joint. The directions of the three axes of each frame were constructed so as to approximate the different axes of rotation for each segment and the origin was located at the center of each relevant joint.

The Dual Euler angles method (Ying and Kim, 2002), based on dual number method (Fisher, 1999), was used. The screw motion sequence Zy'x'' was observed in this study.

The dual velocity of the end point (club head) is given:

$$ {}^5\hat{V}^5_{30} = {}^5_3\hat{M}\,({}^3\hat{V}^3_{10} + {}^3\hat{V}^3_{21} + {}^3\hat{V}^3_{32}) $$

where ${}^R\hat{V}^p_{ij}$ = dual velocity at a point P of body i relative to body j in terms of the unit vectors of frame {R}. The forward velocity of the club head can be defined as the y-component of the dual component of ${}^5\hat{V}^5_{30}$ which is normal to the club head (Figure 1).

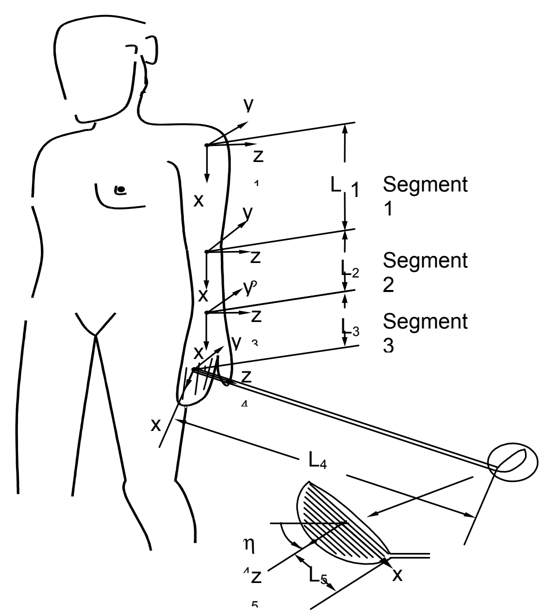

Figure1: The anatomical position and positions of frames on the subject and the club head.

RESULTS AND DISCUSSION

To test the algorithm, calculated velocity of the club head is compared to the measured velocity of the club head. The calculated velocity is derived using the algorithm while the measured velocity is derived using the Video Analysis (Peak Technology, 200Hz). The closeness of the 2 curves in Figure 2 indicates the workability of the proposed method.

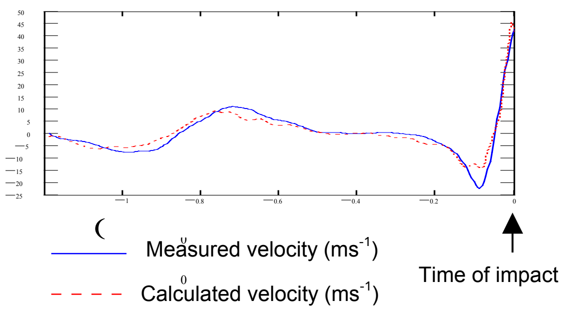

Figure 2: Comparison between the calculated and measured club head velocity.

Table 1 shows the individual contributions of the different segment to the final forward velocity. For this particular golfer, the forearm supination, upper arm abduction and external rotation and hand extension contributed significantly (about 80%) to the final club head velocity. The contribution of the hand extension together with ulnar deviation, commonly known as the hand "cocking" movement, shows good agreement with many simulations and experiments done by Sprigings and Neal (2000). This study also uncovers the importance of external rotation of upper arm and supination of the forearm in golf swing. These two rotations along the longitudinal axes are neglected with use of the traditional 2-dimensional approaches. Details of such joint actions were detected with the present three-dimensional segmental analysis.

SUMMARY

The method provides an efficient approach of assessing the effectiveness of the arm segment rotations in producing club head speed. This method can be easily applied to other actions to describe and assess the contribution of segmental rotations to performance. In general, the method provides convenient access to movement recording and analyses. This method of analysis provides detailed information which may be omitted with other approaches.

Table 1: Individual contribution to the resultant velocity at the impact.

	Angular velocity (Rad/sec)	*Individual Linear velocity (m/sec)(%)*
Resultant club-head velocity	39	32 (100%)
Upper arm: retroversion+ / anteversion–	-1.1	0 (0%)
Upper arm: adduction + / abduction–	-4	6 (19%)
Upper arm: internal + / external rotation–	-10	6 (19%)
Forearm: extension+/ flexion-	4	4 (13%)
Forearm: pronation+ / supination–	-8	5 (16%)
Hand: extension + / flexion –	12	8 (25%)
Hand: ulnar +/ radial abduction-	5	3 (9%)

REFERENCES

Fischer,IS.(1999). *Dual-number methods in kinematics, statics, and dynamics*. Boca Raton, CRC Press.
Sprigings, E. J. and Neal, R. J. (2000) *J.Applied Biomechanics*, **16**, 356-365.
Ying, N. and Kim. W. (2002), *J.Biomechanics* **35,** 1647-1657

EFFECTS OF SINGLE-LEVEL FUSION ON THE INSTANT AXIS OF ROTATION PATTERNS IN AN IN-VITRO MULTI-LEVEL CERVICAL SPINE MODEL

John S. Schwab[1], Denis J. DiAngelo[1,2], and Kevin T. Foley[2,1]

[1] Department of Biomedical Engineering, The University of Tennessee Health Science Center, Memphis, TN, USA
[2] Department of Neurosurgery, The University of Tennessee Health Science Center, Memphis, TN, USA
Email: ddiangelo@utmem.edu Web: http://memphis.mecca.org/bme

INTRODUCTION

Anterior cervical discectomy and fusion is an accepted surgical treatment for degenerative disc diseases. However, there is a reported 3% incidence of subsequent symptomatic degenerative disc disease in 25% of patients ten years postoperatively. It is thought that the motion segment units (MSUs) adjacent to a fusion may alter the instantaneous axis of rotation (IAR) patterns, which may contribute to the advancement of disc degeneration. The objective of this study was to determine the influence of single-level cervical fusion on adjacent segment IAR patterns.

MATERIALS AND METHODS

Seven fresh adult human cadaveric cervical spines (C2-T1) were procured and mounted in a programmable testing apparatus and tested in flexion and extension. The spines were tested in seven different conditions: the harvested condition and six independent single-level fused conditions (i.e., C2-C3, C3-C4, C4-C5, C5-C6, C6-C7, C7-T1). Custom-designed clamps were attached to pairs of adjacent spinal bodies to induce fusion (Figure 1). The clamps could be removed and reattached to create the same alignment at each vertebral level. A previously developed *in vitro* testing protocol was used that induced a physiologic motion response across the cervical spine (DiAngelo and Foley, 2003). Measurements included applied load and moment and individual spinal bodies kinematics. MSU rotations and translations were used to calculate the IAR locations and paths. The data were overlaid onto the respective specimen's lateral radiograph. Mean values of the IAR locations were grouped into six different quadrants of the MSU, as shown in Figure 2, and expressed as combinations of anterior or posterior and caudal, disc, or cranial locations.

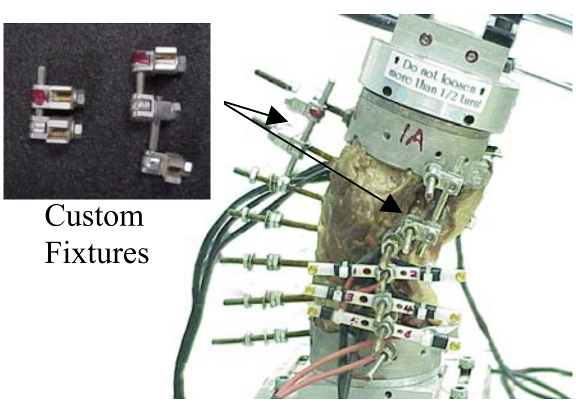

Figure 1: Custom fixtures were used to simulate single-level fusion.

Figure 2: Compartmental Method for Determining Locus of the IAR.

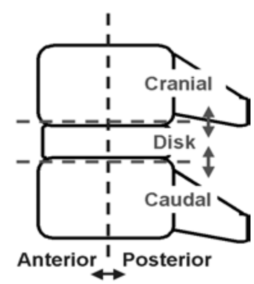

RESULTS

The percent distribution of the mean IAR locations in the different regions is shown in

Table 1 for the different spine conditions. The mean values of the IAR locations for the harvested and fused spine conditions are shown in Figures 3 and 4.

Table 1: IAR Locations By Region

Spine Conditions		Percent IAR Location				
		Ant	Post	Cran	Disc	Caud
Harvested:	Flex	81	19	19	35	46
	Ext	35	65	15	53	32
Fused:						
Superior MSU	Flex	52	48	22	19	59
	Ext	31	69	17	31	52
Inferior MSU	Flex	47	53	28	34	38
	Ext	21	79	32	29	39

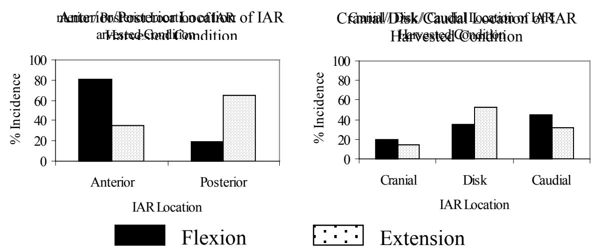

Figure 3: Harvested mean IAR locations.

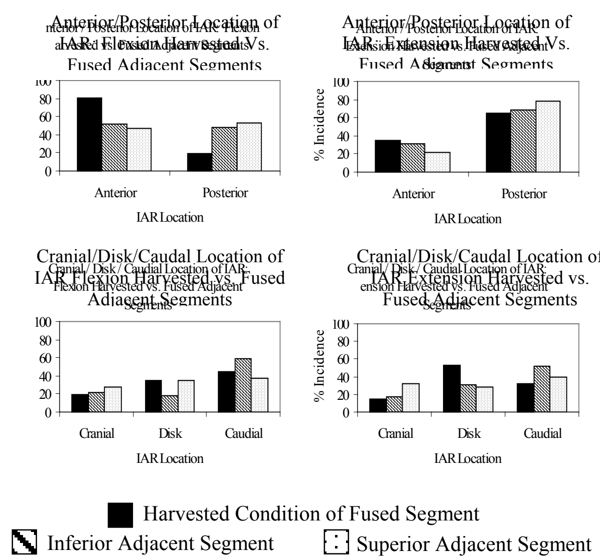

Figure 4: Fused segment adjacent mean IAR locations.

DISCUSSION

Questions still remain about what causes the disc degeneration and progression of disease at segments adjacent to a fused level. It was hypothesized that fusion causes altered loading patterns in adjacent segments that in turn, causes changes in the motion patterns i.e. IAR patterns of the adjacent joint.

For the superior and inferior segments adjacent to the single level fusion, the location of the IAR during flexion shifted posteriorly. During flexion, the superior adjacent segment IAR location shifted downward, and the inferior adjacent segment IAR location shifted upward. During extension, however, the mean IAR location remained at the posterior location. In extension, like in flexion, the superior adjacent segment IAR location shifted downward and the inferior adjacent segment IAR shifted upward. These shifts indicate changes in motion pattern, possibly loading the joints in such a way to induce increased strain.

The increased shifts in the mean IAR location at the adjacent levels are indications that fusion may cause increased strain, and/or changes in motion at levels adjacent to fusion. Whether these changes are solely responsible for the increased incidence of adjacent level disease seen clinically is still being debated. These results support the notion that single level fusion contributes to adjacent level disease.

REFERENCES

DiAngelo DJ, Foley KT (2003). *Spinal Implants: Are We Evaluating Them Appropriately?,* ASTM STP1431, 155-172.

ACKOWLEDGEMENTS

Research funds from Methodist LeBonheur Healthcare Foundation and Cervical Spine Research Society. Tissue from the Medical Education Research Institute, Memphis, TN.

MUSCLE CONTRIBUTIONS TO FORWARD PROGRESSION DURING WALKING

May Q. Liu[1], Frank C. Anderson[1], Marcus G. Pandy[3], and Scott L. Delp[1,2]

Departments of [1]Mechanical Engineering and [2]Bioengineering, Stanford University, Stanford, CA, USA
[3]Department of Biomedical Engineering, University of Texas at Austin, Austin, TX, USA
E-mail: MQL@stanford.edu Web: nmbl.stanford.edu

INTRODUCTION

Diminished walking speed limits mobility in many patients with neuromuscular disorders. Understanding which muscles contribute to forward progression during normal walking may facilitate the development of treatments to increase walking speed. Although the plantarflexors have been identified as important contributors to forward progression during the preswing phase of the gait cycle (Neptune et al. 2001), the roles of other muscles during walking are not well understood. The purpose of this study was to determine 1) which muscles contribute to forward progression of the body center of mass during normal walking and 2) when during the gait cycle are these contributions the greatest.

METHODS

The dynamic optimization solution for normal gait obtained by Anderson and Pandy (2001) was used as the basis of our analysis. The body was modeled as a 10-segment, 23-degree-of-freedom articulated linkage actuated by 54 Hill-type muscles. The interaction between the foot and the ground was modeled using five stiff spring-damper units distributed under the sole of the foot. The joint angular displacements, ground reaction forces, and muscle excitation patterns predicted by the dynamic optimization solution were similar to those obtained from five healthy subjects who walked at an average speed of 1.35 m/s (Anderson and Pandy 2001).

The contribution of a muscle to forward progression was quantified by the muscle's contribution to the forward acceleration of the body center of mass throughout the gait cycle (a_m). We performed a perturbation analysis of the muscle forces to compute a_m using the following approximation:

$$a_m\big|_t \approx \frac{2F_m\left[x(F_m + dF_m)\big|_{t+\Delta t} - x(F_m)\big|_{t+\Delta t}\right]}{\Delta t^2 dF_m}$$

where F_m is a muscle's unperturbed force, dF_m is the magnitude of force perturbation (1.0 N), $x(F_m)$ is the position of the body center of mass in the direction of progression, and Δt is the duration of the perturbation window (0.03 s). This expression was evaluated every 0.02 s during the simulation for each muscle.

We integrated a_m for all muscles over each phase of the gait cycle to estimate each muscle's contribution to the change in forward velocity of the body. We then summed and ranked the magnitudes of these contributions. The a_m for muscles whose velocity contributions comprised at least 75% of the summed velocity magnitudes are presented. Only data from the stance phase are reported because muscle contributions to forward acceleration were much larger during stance than during swing.

RESULTS AND DISCUSSION

Stance limb muscles decelerate the body during the loading response (Fig. 1), when the ground reaction force is directed posteriorly. The net negative muscle influence is primarily due to hip and knee extensors (GMX and VAS, respectively). The dorsiflexors (DF) switch roles during this phase; they decelerate the body until foot-flat (~6% of the gait cycle), after which they produce a small forward acceleration.

The deceleration due to vasti dominates the first half of single limb support. Near the end of single limb support, the plantarflexors accelerate the body, although GAS begins to do so earlier than SOL. There are also smaller contributions from GMDA and GMDP.

The largest muscle contributions to forward progression occur during preswing, when the ground reaction force is directed anteriorly. GAS and SOL together account for the majority of the acceleration from muscles. In agreement with Neptune et al. (2001), the peak acceleration due to SOL is nearly twice that of GAS.

SUMMARY

Using a perturbation analysis, we analyzed muscle contributions to forward progression during normal walking. Our findings suggest that overactivity of the hip and knee extensors during the loading response or weak plantarflexors could limit walking speed in some patient populations.

REFERENCES

Anderson, F.C., Pandy, M.G. (2001). *J. Biomech. Eng*, **123**, 381-390.

Neptune. R.R. et al. (2001). *J. Biomech.,* **34**, 1387-1398.

ACKNOWLEDGEMENTS

NIH, Whitaker Foundation, Department of Veterans Affairs

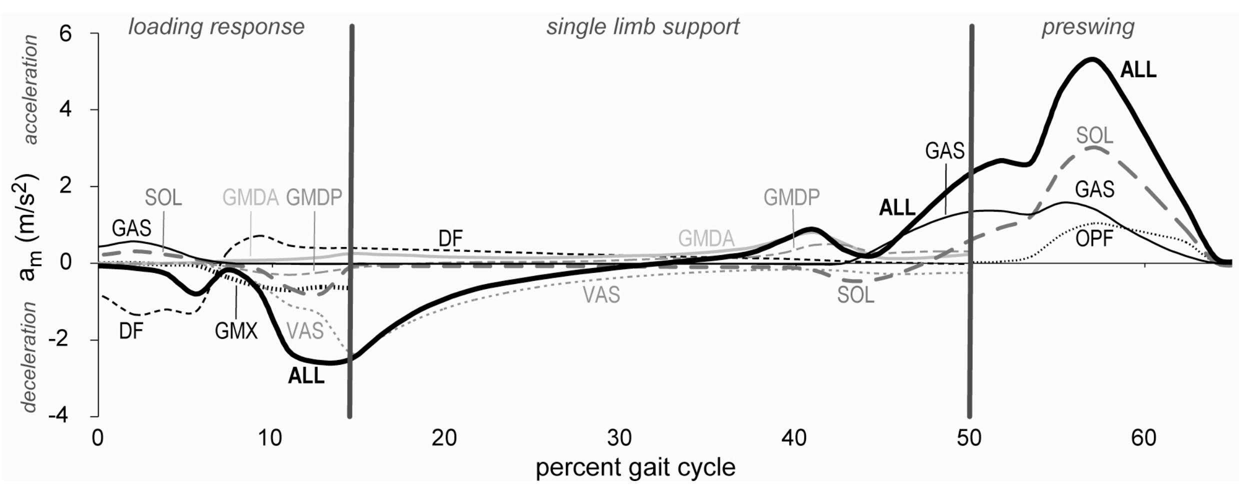

Figure 1: Muscle contributions to forward acceleration of the body center of mass. ALL: combined contributions from all stance-side muscles; SOL: soleus; GAS: gastrocnemius; GMDA: anterior portion of gluteus medius; GMDP: posterior portion of gluteus medius; DF: dorsiflexors; GMX: gluteus maximus; VAS: vasti; OPF: other plantarflexors besides GAS and SOL.

USING COMPUTED MUSCLE CONTROL TO GENERATE FORWARD DYNAMIC SIMULATIONS OF GAIT FROM EXPERIMENTAL DATA

Darryl G. Thelen [1] and Frank C. Anderson [2]

[1] Dept. of Mechanical Engineering, University of Wisconsin-Madison, Madison, WI, USA
[2] Dept. of Mechanical Engineering, Stanford University, Stanford, CA, USA
E-mail: thelen@engr.wisc.edu Web: www.cae.wisc.edu/~thelen

INTRODUCTION

Forward dynamic simulation offers a powerful framework for investigating how the elements of the neuromusculoskeletal system interact to generate movement. Unfortunately, using dynamic optimization to compute muscle excitations that produce coordinated movement, especially for complex activities like gait, can require weeks or even months of computer time (Anderson and Pandy, 2001). Furthermore, numerical difficulties are often endemic to this approach (Neptune, 1999). Computed Muscle Control (CMC), which has been used successfully to simulate pedaling, can generate muscle-actuated simulations of movement orders of magnitude faster than dynamic optimization approaches (Thelen et al., 2003). The objective of this study was to adapt CMC to generate subject-specific simulations of human gait.

METHODS

The body was modeled as an 8-segment, 21-degree-of-freedom articulated linkage actuated by 64 Hill-type muscle-tendon units (Zajac, 1989). The coupling of muscle activation to excitation was modeled as a first-order process with rise and decay times of 10 ms and 40 ms, respectively. Foot-floor forces were prescribed to experimental values ($\vec{f}_{exp}$), with variations determined by translational and rotational spring-dampers applied at the ground reaction center-of-pressure under each foot.

Prior to applying the CMC algorithm, the experimental data were pre-processed to ensure dynamic consistency between the measured kinematics and ground reaction forces. Specifically, using the unaltered ground reaction forces as input, the model equations of motion (EOM) were solved for the translational accelerations of the pelvis and the angular accelerations of the back joint that would eliminate all residual forces and moments. These accelerations were then integrated to produce new trajectories for the back angles and pelvis position. Nonlinear optimization was used to solve for the initial values of the back and pelvis trajectories (i.e., the integration constants) that minimized deviation from the measured kinematics. The resulting joint angles ($\vec{q}_{exp}$) and corresponding actuator lengths were fit with 7th order splines (Woltring, 1986).

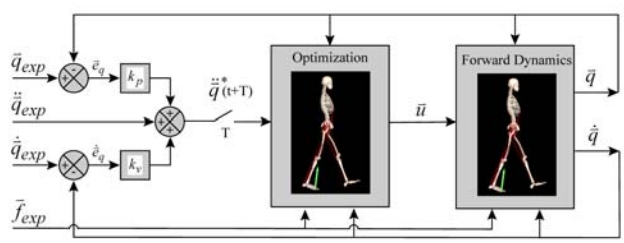

Fig. 1: Computed Muscle Control Algorithm.

CMC was then used to compute muscle excitations that would drive a forward dynamic simulation to track $\vec{q}_{exp}$ (Fig. 1). At a time *t* in the simulation, the tracking errors ($\vec{e}_q, \dot{\vec{e}}_q$) between the model and experimental kinematics were used to compute a set of desired joint angular accelerations ($\ddot{\vec{q}}^*$) that should be achieved a short interval (*T=0.01 s*) later to track $\vec{q}_{exp}$. Muscle activation and contraction dynamics were integrated forward for a range of muscle excitations ($\vec{0} < \vec{u} < \vec{1}$) to estimate the range of muscle-tendon forces that could be generated at *t+T*. Static optimization was used to compute a set of muscle excitations that would produce forces within this range ($\vec{F}_{\min} \le \vec{F}^* \le \vec{F}_{\max}$) and generate the desired accelerations ($\ddot{\vec{q}}^*$) while minimizing a performance criterion ($J = \sum V_i a_i^2$, where V_i and a_i are the volume and activation of muscle *i*). Muscle excitations were held constant during integration of the system state equations from *t* to *t+T*. This process was repeated every *T* seconds until the simulation was completed. We report the results for generating simulations of the half gait cycles of 10 young adults who walked at comfortable speeds.

RESULTS

Pre-processing introduced only small changes in the measured kinematics (e.g., less than ~1 cm for pelvis translations). The CMC algorithm tracked experimental joint angles with mean rms errors ranging from 0.4 to 1.1 deg. Deviations in the ground reaction forces were also small (Table 1). The computed muscle activations corresponded closely to EMG activities of the major lower extremity muscles (Fig. 2). Only about 20 minutes of computer time were needed to generate each simulation.

Table 1. Mean (±sd) rms errors between simulated and experimental quantities

Ground Forces (N)		Sagittal Angle (deg)	
A-P	1.7 ±0.5	Hip	0.5 ±0.1
M-L	1.4 ±0.4	Knee	1.1 ±0.2
Vertical	11.3 ±2.9	Ankle	0.4 ±0.1

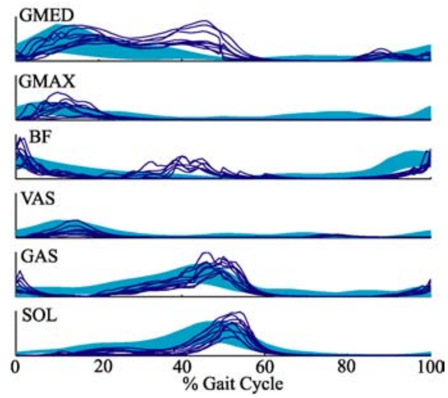

Fig. 2: Computed muscle activations (solid) and normalized EMG signals (shaded, Winter 1991).

DISCUSSION AND SUMMARY

Forward dynamic simulation permits lines of investigation not available to inverse dynamic techniques (Zajac et al., 2003). In this study, we used CMC to generate 10 subject-specific simulations of normal gait. The speed and accuracy of our new approach will allow forward dynamic simulation to be used to greater extents than it has been previously. Future applications include using CMC to generate subject-specific simulations of gait for individuals with movement disorders. Such simulations may prove to be valuable in identifying the underlying causes of a movement disorder and in planning treatment.

REFERENCES

Anderson, F.C. and Pandy, M.G. (2001). *J. Biomech. Eng.* **123**, 381-390.
Neptune, R. (1999). *J. Biomech. Eng.* **121**, 249-252.
Thelen, D. G., et al. (2003). *J. Biomech.* **36**, 321-328.
Winter, D.A. (1991). The *Biomechanics and Motor Control of Human Gait*, Waterloo Biomechanics.
Woltring, H. (1986). *Adv. Eng. Software* **8**, 104-113.
Zajac, F.E. (1989). *Crit Rev Biomed Eng* **17**, 359-411.
Zajac, F.E., et al. (2003). *Gait & Posture* **17**, 1-17.

ACKNOWLEDGEMENTS

NIH R41 HD45109-01; Center for Motion Analysis, Connecticut Children's Medical Center.

THUMB FORCE DEFICIT AFTER LOWER MEDIAN NERVE BLOCK

Zong-Ming Li, Daniel A. Harkness, Robert J. Goitz

Hand Research Laboratory, Departments of Orthopaedic Surgery and Bioengineering
University of Pittsburgh, PA 15213. Email: zmli@pitt.edu

INTRODUCTION

Disorders resulting from traumatic injuries to and various diseases of peripheral nerves are common in clinical practice. Clinical manifestations of hand dysfunction are distinct depending on the nerve involved. The purpose of this study was to investigate the effects of a lower median nerve lesion on thumb motor function. The lesion was simulated by performing median nerve block at the wrist using an anesthetic.

METHODS

Six healthy young male subjects participated in this study. We injected 4 mL of 0.5% bupivacaine hydrochloride (Astra Pharmaceuticals, Westborough, MA, USA) into the carpal tunnel. An experimental apparatus was designed to measure maximum voluntary contraction (MVC) forces of the thumb (Figure 1). A six degree-of-freedom force transducer, together with a thumb ring, was used to measure thumb forces in the transverse plane at the middle of the proximal phalanx of the thumb.

Each subject was tested both before and after median nerve block. Post-block testing started after we verified complete median nerve block, approximately 40 minutes after the injection. Subjects grasped a vertical dowel with the forearm stabilized in a midprone position. Each subject performed 15 circumferential MVC trials with randomized starting directions. The subject was given 15 s to complete each circumferential trial and 60 s of rest between each trial. Data was collected from each subject at 100 samples per second. A force envelope was constructed based on the 15-trials. The area enclosed by the force envelope was divided into extension, abduction, flexion, and adduction quadrants. One- and two-factor Repeated Measures ANOVAs were used to analyze outcome measures.

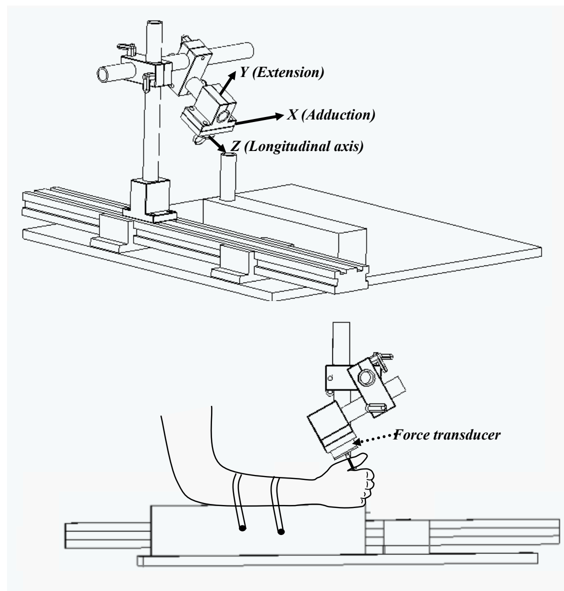

Figure 1. Schematic of experimental setup to measure thumb force production.

RESULTS

Force magnitudes were significantly reduced after nerve block ($p < 0.001$) resulting in significantly smaller force envelopes (Figure 2). The average decrease across all directions was 27.9%. A maximum decrease of 42.4% occurred at 199°, corresponding to a combined direction of abduction and slight flexion, while a minimum decrease of 10.5% occurred at 328° corresponding to a combined direction of adduction and slight flexion. Relative decreases at 0° (adduction), 90° (extension), 180° (abduction), and 270° (flexion) directions were 17.3%, 21.2%, 41.2% and 33.5%, respectively. Areas enclosed by the post-block envelopes were significantly smaller than the pre-block envelopes ($p<0.001$). Post-block force envelope area, 10700 ± 4474 N^2, was 51.9% of pre-block force envelope area, 20628 ± 7747 N^2. Quadrant area decreased significantly ($p < 0.001$), with a maximal percentage decrease of 60.9% in the abduction quadrant, followed by a 52.3% area decrease in the flexion quadrant.

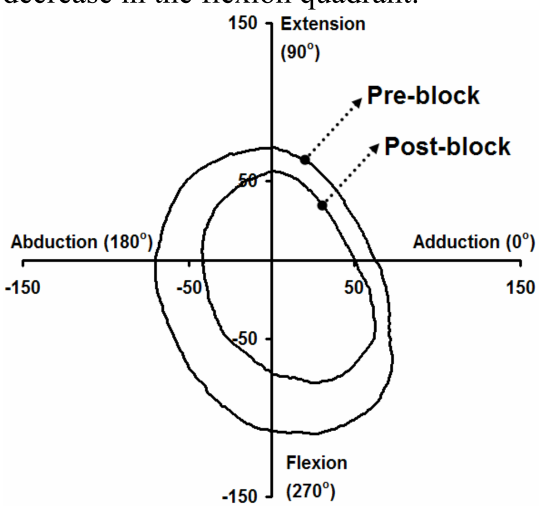

Figure 1. Average force envelopes produced by the thumb before and after median nerve block. Unit in N.

DISCUSSION

Preferential force weakening in the quadrants of abduction and flexion after median nerve block agrees with known anatomical and neuromuscular features of the thumb. The median nerve innervates the abductor pollicis brevis, the opponens pollicis and the superficial head of the flexor pollicis brevis, all of which contribute to the abduction and flexion of the thumb (Smutz *et al.*, 1998); therefore, denervation of these muscles after median nerve block would cause the greatest force deficit related to median nerve function (Kaufman *et al.*, 1999). Additionally, as force application moved towards adduction, the force deficit decreased as neuromuscular control shifted from the median nerve to the ulnar nerve via the first dorsal interosseous and adductor pollicis brevis. Force deficit in extension was also comparably small as extension forces are mainly produced by the extensors pollicis brevis and longus originating in the forearm.

Our reported force decreases following median nerve block (40.9% in abduction, 34.1% in flexion) were smaller than those reported in the literature (Boatright and Kiebzak, 1997; Kozin *et al.*, 1999; Kaufman *et al.*, 1999). The discrepancy may be due to the different testing methods. The methods of strength testing may also help explain the different magnitudes of strength deficit after the nerve block. In addition, all previous results were based on forces obtained in discrete direction(s) and focused exertions. The current study utilized a method of force production in a continuous, circumferential and dynamic manner, which may use different muscle coordination patterns to produce forces in the same directions.

REFERENCES

Boatright JR, Kiebzak GM (1997) J Hand Surg [Am] 22: 849-852

Kaufman KR, *et al.* (1999) Clin Biomech 14: 141-150

Kozin SH, *et al.* (1999) J Hand Surg [Am] 24: 64-72

Smutz WP, *et al.* (1998) J Biomech 31: 565-570

ACKNOWLEDGEMENTS

The Aircast Foundation and Whitaker Foundation.

A BIOMECHANICAL METHOD TO IMPROVE INDIVIDUAL PLANNING AND CONTROLLING OF TRAINING

Markus Tilp, Martin Sust and Sigrid Thaller

Institute of Sport Sciences, Karl-Franzens-University Graz, Austria, Europe
E-mail: markus.tilp@uni-graz.at Web: http://www-gewi.kfunigraz.ac.at/sw

INTRODUCTION

The most important influence factors on sport performance can be found by trainer experience, by statistical methods or by appropriate modelling. It is very effective to describe the connection between performance determining factors (PDF) and sport performance mathematically. We want to suggest a method which allows finding the essential factors for the sport performance, getting them individually and estimating the possible performance development of an athlete by simulation. The focus of this work is kept on the method but not on the complexity of the used model.

METHODS

To achieve the mentioned aims, one has to create an appropriate model of the sport movement. Then one has to develop measuring methods to determine the model parameters individually to be able to simulate the movement under different conditions. We describe this method for the simple movement of a squat jump (SJ) with maximum voluntary effort (MVE). For this work we define the jumping height as sport performance.

From classical mechanics we know that during a SJ the movement of the centre of mass is determined by the ground reaction forces. These forces can be divided into forces caused by muscles forces F_M and non-muscle forces F_{NM} (weight of athlete) which are constant during an attempt.

$$(1)\ F_{Ground\,Reaction} = F_M + F_{NM}$$

A geometry function G allows to describe the transfer of muscle force f_M and contraction velocity v_M from inside the body (model muscle of the quadriceps femoris) to the outside (F_M,V), considering the muscle position and the length of bones individually.

$$(2)\quad F_M = G \cdot f_M$$

$$(3)\quad V = \frac{1}{G} \cdot v_M$$

The measurement of the 5 anthropometric parameters needed is described in Sust et al. (1997a).

To express the forces produced by the muscle during contraction we use a modified Hill model, extended by an activation function S(t) (see Sust et al. (1997b)).

$$(4)\quad f_M(t) = S(t) \cdot \left(\frac{c}{v_M(t) + b} - a \right) \quad \text{with}$$

$$(5)\quad S(t) = 1 - e^{At}$$

The Hill parameters a, b, and c can easily be transformed to well defined terms like maximal isometric force (fiso), maximal possible contraction velocity (vmax) and maximal possible power (pmax) (Sust 1978). Together with the parameter “A” for the activation we call these the muscle properties (MP). The whole model is described by a differential equation with 10 parameters (mass, 5 anthropometrical parameters, 3 parameters derived from Hill´s equation, 1 activation parameter) of which 6 can be measured directly, whereas the MPs have to be determined by nonlinear regression.

The measurement system at the Institute of Sport Sciences in Graz, Austria, consists of an adjustable inclined plane on which a subject sits and moves a slide by extending the legs. Position and velocity of the slide as well as the forces developed on the slide are measured simultaneously. After 2 series of 3 different measurements (Fig. 1) a nonlinear regression (Opfermann, 2000) determines the free parameters (=MP) in such a way that ONE set of constant parameters describes 6 different curves.

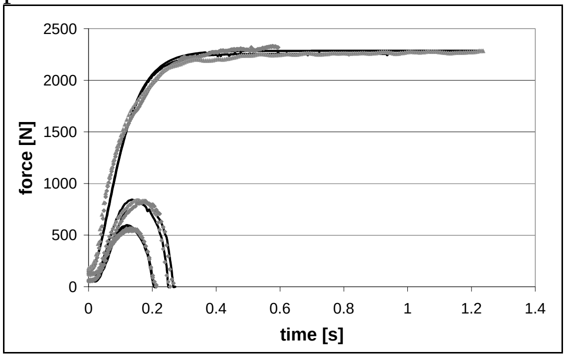

Figure 1: Experiment (grey dotted) and fitted model curves (black) from 2 isometric and 4 concentric leg extensions

This procedure is only possible if the subject executes the movement with MVE because otherwise the muscle activation cannot be described by equation (5).

RESULTS

Most simulations with (often complex) mathematical models known to the authors are using average muscle parameters from literature (e.g. Forcinito et al. 1998, Nigg/Herzog, 1999). The individual measurement of muscle properties enables simulating movements individually. In a testing group of sport students (n=31) we could determine an average value for fiso/a=0.24 which fits perfectly with literature (Nigg/Herzog, 1999: 0.25, Enoka, 2002: 0.15 -0.25) but the individual values ranged from 0.1 – 0.54. We conclude that the use of average values in biomechanical models cannot be adequate for individual simulations.

Although the model seems to be quite simple (e.g. no elasticity, just one model muscle), it is possible to show several effects observed in reality, like e.g. the optimal starting position or why in some cases the increase of the maximal force by training may not lead to an increased performance.

Comparisons of simulations with MP from different individuals also showed that the fictitious increase of one muscle property leads to totally different performance changes. This encourages the demand for the individualization of training.

SUMMARY

A biomechanical method is shown which helps to determine the most important PDFs for jumping height in squat jumping individually. A measurement system similar to a leg press supplies the position, velocity and force data as function from time of several leg extension movements. A modified Hill type model uses this as input data. A data fitting algorithm determines the unknown muscle properties which are parameters of the model. This knowledge helps planning and controlling the training process. Furthermore it is possible to estimate performance development by simulation.

REFERENCES

Enoka, R.M. (2002). *Neuromechanics of human movement.* Human Kinetics

Forcinito, M. et al. (1998). *Journal of Biomechanics*, **31**, 1093 – 1099

Nigg, B.M., Herzog, W. (1999). *Biomechanics of the musculo-skeletal system*. Wiley

Opfermann, J. (2000). *Programmpaket für nichtlineare Anpassungen,* Selb 2000

Sust, M. (1978). *Theorie und Praxis der Körperkultur*, **27**, 763 - 768

Sust, M. et al. (1997a). *Human Movement Science*, **16**, 533 -546

Sust, M. et al. (1997b). *Intern. J. Neuroscience*, **92**(1-2), 103 -118

A NOVEL METHOD FOR THE ASSESSMENT OF MEASURED ISOMETRIC FORCE-TIME FUNCTIONS

Sigrid Thaller and Markus Tilp

Institute of Sports Sciences, Karl-Franzens-University Graz, Graz, Austria, Europe
E-mail: sigrid.thaller@uni-graz.at

INTRODUCTION AND THEORETICAL BACKGROUND

There are many methods to assess the isometrically measured force-time function described in literature (e.g., Bobbert & van Zandwijk 1999; Hatze 1981; Sust, Schmalz et.al. 1997; van Soest & Bobbert 1993; Zatsiorsky 1995). Many authors use

(1) $$F(t) = F_{\max}\left(1 - e^{-At}\right)$$

for modelling the force development over time with maximum voluntary contraction (MVC). Here $F_{\max}$ denotes the peak force and A is a parameter describing the activation rate. The values of $F_{\max}$ and A are found by nonlinear parameter identification, i.e., by minimizing the distance between the measured function and the calculated function (1) in the least-square-sense.

Measured force functions normally are not as smooth as described by formula (1). There are parts of the curve where the subject does not perform the movement with MVC or where elastic components influence the measurement. Therefore, the parameter identification does not yield to reliable results.

We suggest a method where only the "good" parts of the measurement are used. To recognise the "good" parts we consider the following function:

(2) $$s(t) = \ln \frac{1}{F_{\max}}[F_{\max} - F(t)].$$

Inserting equation (1) into (2) leads to $s(t) = -At$, i.e., the function $s(t)$ is a straight line with slope $-A$.

Analoguously to equation (2) we define

(3) $$s(t_i) = \ln \frac{1}{F_{\max}}[F_{\max} - F_m(t_i)],$$

where $F_m(t_i)$ denotes the measured isometric force at time t_i and $F_{\max}$ denotes the peak force, i.e., the maximum of all measured $F_m(t_i)$ plus some constant (e.g., +2%), such that $F_{\max}$ is always greater than $F_m(t_i)$ and (3) is well defined.

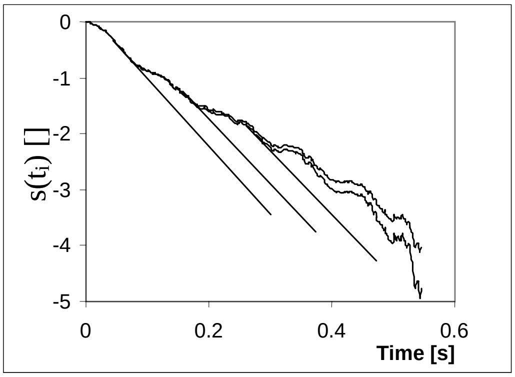

Figure 1: Two functions $s(t_i)$ with different values of $F_{\max}$. The slopes of the linear parts are nearly the same.

The shape of function (3) depends on the estimated value of $F_{\max}$ (see Figure 1). The linear parts of (3) are the time intervals where the force development corresponds with equation (1). The slopes of these parts lead to the parameter A in (1) regarding only the time intervals where the movement is actually performed with MVC (Figure 2).

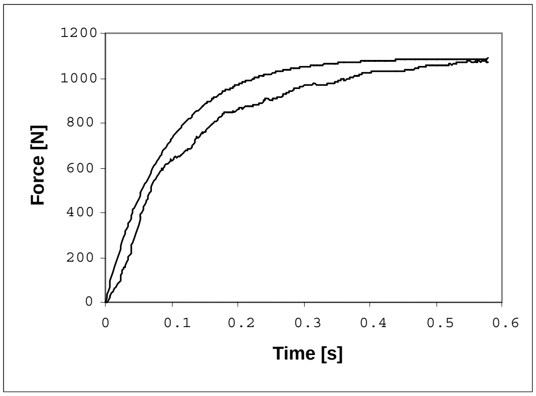

Figure 2: Measured force development and force development with MVC.

METHODS

14 subjects (mass 71.6 ± 7.5 kg, height 1.78 ± 0.10 m, age 24.9 ± 3.7 y) performed isometric contractions on an inclined leg press. The force was measured with a Kistler platform (500 Hz). The measurements were repeated after three weeks. For applying the suggested new method for identifying the parameter A we set F_{max} the maximum of the measured forces increased by 2%. The slopes over each 20 measurement points in equation (3) were calculated with linear regression and we chose the second minimum over all so found slopes as parameter A, because the beginning of the force-time curve is not correctly described by (1) and the end of the curve is too much influenced by the choice of F_{max}.

RESULTS AND DISCUSSION

For the mean value of the parameter A calculated with the standard method we got 7.95 ± 2.03 s^{-1} and 7.96 ± 2.16 s^{-1} for the first and second measurement resp. The correlation coefficient rating the reliability was $r = 0.75$. The new method led to $A = 9.15 \pm 2.75\ s^{-1}$ and $A = 8.98 \pm 2.57\ s^{-1}$and a correlation coefficient of $r = 0.91$.
The choice of calculating the linear regression over 20 points depends on the frequency of the force measurements. If we use too many points the correlation coefficients of the linear regressions will be smaller. If the time interval is too short, oscillations in the force-time curve will influence the result. As the linear parts in equation (3) correspond with the MVC, the total length of all linear parts helps to assess the isometrically measured force development.

SUMMARY

We introduce a novel method for determining a parameter describing the activation rate with maximum voluntary contraction. The comparison with a customary method of nonlinear parameter estimation shows a better reliability of our method. So it is even possible to determine this parameter using isometric force measurements of not quite maximal voluntary contraction and to rate the subjective effort.

REFERENCES

Bobbert, M.F., van Zandwijk, J.P. (1999). *Biol. Cybern.* **81**, 101-108.

Hatze, H. (1981). *Myocybernetic contol models of skeletal muscle.* University of South Africa, Pretoria.

Sust, M., Schmalz, T. et.al. (1997). *Intern. J. Neuroscience*, **92**, 103-118.

Van Soest, A.J., Bobbert, M.F. (1993). *Biol. Cybern.* **69**, 195-204.

Zatsiorsky, V.M. (1995). *Science and practice of strength training*. Human Kinetics.

OBJECTIVE QUANTIFICATION OF FOOT ARCH BY CURVATURE MAPS

Xiang Liu [1], Wangdo Kim [1] and Burkhard Drerup [2]

[1] School of Mechanical & Production Engineering, Nanyang Technological University, Singapore
[2] Klinik und Poliklinik für Technische Orthopädie und Rehabilitation, Universtätsklinikum, Münster, Germany
E-mail: mwdkim@ntu.edu.sg

INTRODUCTION

Measurement and categorization of different foot arches can help to design proper sole insert, improve athlete performance as well as reducing the possibility of injuries in sports. Various techniques such as palpation, X-ray and footprint parameters (Chu, et al., 1995, McCrory, et al., 1997, Staheli, et al., 1987) have been proposed to measure different arch types but each technique has its own drawback. In this paper, we try to measure the arch height directly by a non-invasive, direct and objective method: curvature maps. The foot's underside scanned by a three-dimensional laser scanner and the anatomical landmarks are extracted from the curvature maps. The curvature calculation is performed again on a specific area selected for the arch surface fitting. The arch types are clearly categorized by our own defined arch index.

METHODS

Subjects in this study included 5 men and a woman. All subjects had no history of foot surgery and did not show significant pain and discomfort in normal weight-bearing activities. Two subjects have flatfoot and others are normal. The unloading feet were scanned when the subjects were sitting comfortably with their feet elevated by another chair. The smoothed surface was exported in the form of scattered points to MATLAB for further processing.

By minimizing the difference between the scattered points and the surface represented by a six-coefficient polynomial with weighted least square method and normal equations, the Koenderink shape index (Fig. 1) could be derived (Koenderink and van Doorn, 1992, Frobin and Hierholzer, 1982, 1985).

From the map of Koenderink shape index, the convex regions are examined. Possible candidates should be those obvious convex regions repeated on all of the foot's maps and easy to be distinguished from their neighbours. According to this standard, three anatomical landmarks (A, B and C) are selected as shown in Fig. 1. They are the centers of gravity of 100 points on the site of the landmarks with Koenderink shape index exceeding a certain threshold which varies from landmark to landmark. A and C are the regions around the heads of the first and fourth metatarsal, respectively. B is the most convex part of the heel. The lines (AB and BC) span a plane which works as a reference plane. Then along the line AB, the point with maximum distance (DH) to the plane ABC is located (point D in Fig. 2). At the same time, the points within 10mm to the line AB on the plane ABC are chosen for the surface fitting (indicated with a blue rectangle region in Fig. 2.). With D as the center, a whole surface is fitted to the blue region. Two principle curvatures are extracted. The one in the direction of AB reflecting how curved the medial arch is, is taken as the arch index after normalized by the length AB.

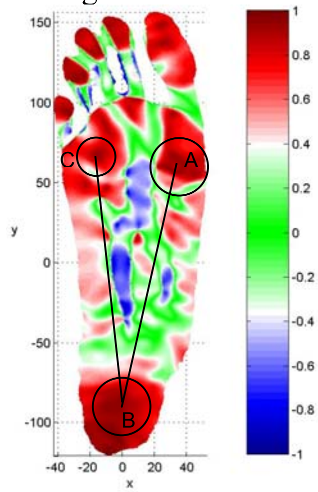

Figure 1. The map of Koenderink shape index of the foot's underside. Red: convex, green: saddle-shaped, blue: concave, white: transitions between these three different shapes.

RESULTS AND DISCUSSION

Table 1: The mean arch index of each subject's arch from 10 measures.

Subjects	Mean arch index	σ
1	0.3412	0.0402
2	0.3777	0.0370
3	0.5115	0.0699
4	0.6260	0.0732
5	0.5747	0.0402

The first two subject's feet are medically certified as flatfoot. The others' are normal. From our method, the flatfoot is distinguished by their small arch index values. The other normal feet have a mean value of 0.5707, which is much larger than that of flatfoot. The standard deviation is an order of magnitude less than the mean value, which shows the good repeatability of this method.

SUMMARY

We have provided an objective way to determine foot arch types by curvature maps. More subjects would be required to form a statistical pool in order to classify them into 3 categories (flatfoot, normal, high arch).

REFERENCES

Chu, W.C. et al. (1995). *IEEE Transactions on Biomedical Engineering*, 42, 11, 1088-1093.

Frobin, W., Hierholzer, E. (1982). *Journal of Biomechanics*, 15, 379-390.

Frobin, W., Hierholzer, E. (1985). *Proceedings of SPIE Biostereometrics '85*, 602; 109-115.

Koenderink, J., van Doorn, A. (1992). *Image and Vision Computing*, 10, 8, 557-565.

McCrory, J.L. et al. (1997). *Foot*, 7, 79-81.

Rodgers, M.M. (1987). *Journal of Biomechanics*, 20, 547-551.

Staheli, L.T. et al. (1987). *The Journal of Bone and Joint Surgery*, 69, 3, 426-428.

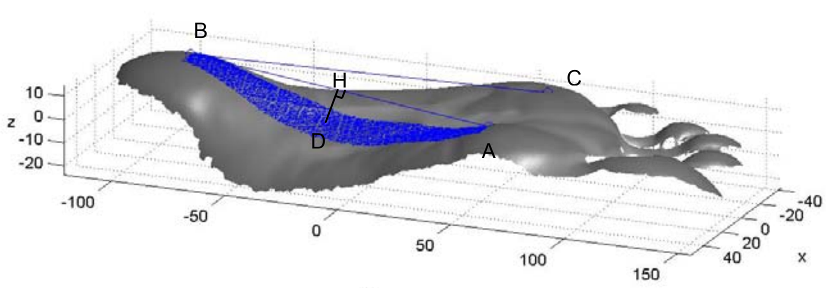

Figure 2: The illustration of the method to extract the index of foot arch.

HYPOTHETICAL DESIGN FOR ANKLE-SUBTALAR JOINT PROSTHESIS

Wong Yue Shuen [1] , Ning Ying [2] and Wangdo Kim [2]

[1] Department of Orthopedic Surgery, Alexandra Hospital, Singapore
[2] School of Mechanical & Production Engineering, Nanyang Technological University, Singapore, 639798
E-mail: mwdkim@ntu.edu.sg

INTRODUCTION

The ankle and subtalar joints together form the most distal principal joint complex of the lower limb. Proper function of these joints is essential for normal gait. Disease or injuries of these joints leads to pain, stiffness or abnormal motion (degenerative arthritis). Thus far, there are two common surgical approaches to the treatment of degenerative arthritis in the foot and ankle. The joint can be either be fused, or it can be replaced by an artificial prosthesis of some sort. In recent years, success has been achieved in developing various ankle prostheses for the treatment of ankle arthritis. Fairly normal function can be now been achieved for patients with isolated ankle arthritis by using these prostheses.

However, there has been as yet been very little work done on the subtalar joint due to its complex joint surfaces and limited understanding of the kinematics. The objective of this study is to design a prosthesis that has similar design consideration and dimensions as the present successful generation of ankle prostheses, but that also allow some degree of motion along the axis approximating that of the subtalar joint. The approach has several potential advantages owing to that prosthesis design and implantation technique is similar to presently available implants, which should translate into less difficulty in learning the technique (for the surgeon), less complication and a lower rate of morbidity.

METHODS

As part of the process of designing the prosthesis, a cadaveric analysis of ankle-subtalar kinematic was performed. The aim of the experiments was to a) validate previous description of hindfoot kinematics; b) determine various parameters which would help us to design the prosthesis; c) provide a benchmark for comparison after design and implementation of a prospective implant.

The ‘Flock of Bird’ (FOB) electromagnetic measuring system (Ascension Technology Corporation, Burlington, VT, USA) was used to measure and track the kinematic data. In order to passively generate plntarflexion-dorsiflexion and eversion-inversion movement in the ankle-subtalar joint complex, a custom designed rig was built. (Fig. 1). Because the measurement system would be affected by distortion to an electromagnetic field, all components of the rig were built of non-metallic materials.

Total ten trans-knee amputation cadaver specimen was tested. Each specimen was thawed for 24 hours prior to the experiment. Each specimen was then prepared. A 9mm drill was used to create a pilot hole in the articular surface of the tibial plateau and the shank rod threaded in. The three receiver fixtures were then inserted into the tibia, talus and calcaneus. In the neutral position, each of the four landmarks was then digitized five times using the pen device attached to the last FOB receiver. At the same time, data from the other three receivers was simultaneously collected. This procedure allowed us to create a reference for the three receivers with respect tot the anatomical coordinate system.

As both the ankle and subtalar joints have been previously shown to have both transnational and rotational movement, it was decided that the Dual Euler Angle method would ne used to describe the kinematics.

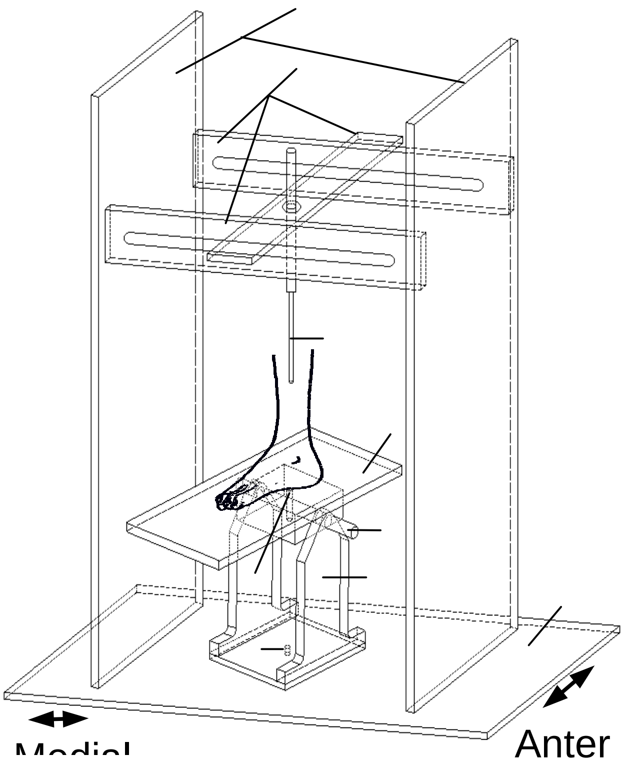

Fig. 1: Experimental Rig for vitro experiment on foot/shank specimen

RESULTS AND DISCUSSION

The results indicate that during the dorsiflexion-plantarflexion, at maximum plantarflexion of the foot, 29.2° of plantarflexion of the calcaneus with respect to the tibia is associated with 27° of plantarflexion at the ankle joint and with 2.1° of plantarflexion at the subtalar joint. At maximum of dorsiflexion of the foot, 18.6° of dorsiflexion of the calcaneus relative to the tibia is associated with 19.1° of dorsiflexion at the ankle joint and with 0.6° plantarflexion at the subtalar joint. The data correlates well with previously published kinematic description of the ankle subtalar joint complex. Both the ankle and subtalar joint show 6 degree of freedom motion an multiaxial characteristics.

SUMMARY

The end results of this study are the fabrication of two prostheses milled out of aluminum. The final products could be used as real implants, and have not been validated even for kinematics in cadaveric experiments. However, this study does review pertinent literature and knowledge, which leave open the possibility that a novel solution may be available for the treatment of plantar arthritis. Factors that predict for success in prosthesis design in the ankle include minimal bone cuts, semi-constrained articulation, non-cemented bone interface, and preservation of the malleoli and collateral ligaments. In addition, it is unlikely that a successful anatomical prosthesis will ever be found for treatment of subtalar arthritis. Because of the close proximity of the ankle and subtalar joints, a single prosthesis that can support rotations along the both axes may not be achievable.

REFERENCES

Ying, N. et al. (2002). *J. Biomechanics,* 35,1647-1657.
Ying, N. et al. (2004). *Clinical Biomechanics*, 19,153-160.

KINEMATIC ESTIMATION OF THE ROTATION CENTER OF THE GLENOHUMERAL JOINT FOR A DIGITAL MANIKIN

Kei Aoki[1,2], Masaaki Mochimaru[1,2] and Makiko Kouchi[1,2]

[1] Digital Human Research Center, National Institute of Advanced Industrial Science and Technology, Tokyo, Japan
[2] CREST, Japan Science and Technology Agency (JST), Kyoto, Japan
E-mail: aoki-kei@aist.go.jp Web: www.dh.aist.go.jp

INTRODUCTION

"Digital manikin" is software used for designing automobile or workspace. The reach envelope of a digital manikin differs from that of an actual human even if they have the same posture and body proportion. The main cause is the difference of the anatomical structure around the shoulder between the two. In order to improve the shoulder structure of a digital manikin, it is important to know the motion of the rotation center of the glenohumeral (GH) joint. This study aims to propose a simple estimation method of the rotation center (GH center).

METHODS

Various methods have been proposed (e.g. Meskers et al., 1998; Veeger, 2000; Stokdijk et al., 2000) to estimate the GH center. However, these methods need to measure the surface landmarks on the scapula, which is difficult to find. On the other hand, Bao and Willems (1999) developed an estimation method under the geometric constraints of the segment model around the shoulder complex. This model is suitable for a digital manikin because of their similarity. Referring to them, we developed a simple method, using pre-established "positioning motion" and three or more markers. This is, so to speak, a dynamic calibration of the GH center.

In developing the estimation method, three conditions are assumed for the positioning motion. They are (1) Torso movement is negligible. (2) Skin movements are negligible. (3) Arm moves without a displacement of the scapula. Thus, the range of motion of the arm is limited.

Under these conditions, the GH center can be estimated by following two kinematic solutions. (a) The GH center is fixed to a point in the absolute coordinate system during a very short time even if the arm is moving. Therefore, the GH center is calculated by solving a linear formula which is composed of the condition that the distance between the GH center and each of three markers does not change during a very short time. (b) The GH center in the upper arm coordinate system is fixed in the head of humerus. Namely, if the posture of the upper arm can be measured, the GH center is calculated using the matrix of the coordinate transformation from a standard posture. The constant position vector of the GH center from the marker set is optimized by minimizing the difference between these two solutions during the positioning motion. Using this marker set and the estimated position vector, the GH center in the absolute coordinate system can be estimated easily.

SIMULATION

In order to decide the optimal positioning motion, effect of the skin movements was simulated using a virtual model shown in Figure 1. The random errors (maximum 5

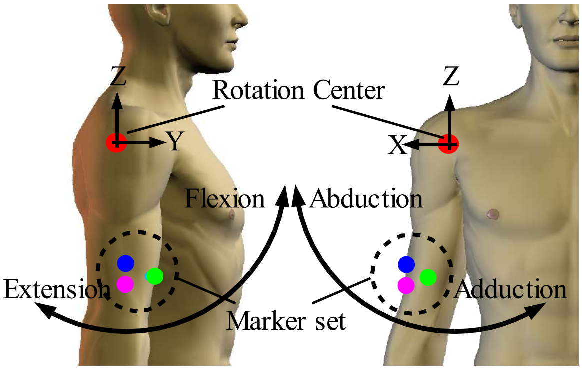

Figure 1: Virtual human upper arm model The range of motion around the GH joint was established at 120° flexure and abduction, and 40° extension and adduction.

mm for each direction) were given to the three markers to represent the displacement due to skin movements. The GH center was estimated as the model moved its upper arm within a limited range of motion (condition 3). We found (1) The error in vertical direction (Z) became large when the range of motion was too small. (2) The error in sagittal direction (Y) was canceled out by flexion and extension. (3) The error in horizontal direction (X) was canceled out by abduction and adduction. From these results, the optimal positioning motion was determined as the compound motion of 60° flexion, 10° extension, 90° abduction, and 30° adduction as shown in Figure 2. When this motion was given to the virtual model, the error in the GH center (X, Y, Z) was (2.9, 2.4, 1.8) [mm].

VALIDATION AND DISCUSSION

For the purpose of verifying this method, an actual subject (age 22, male) was measured. The location of the head of humerus and three markers were measured using an MRI system. The estimated GH center during the positioning motion was found in the head of humerus as Figure 3. Consequently, it is concluded that this method is useful to estimate the GH center accurately and easily. In addition, this method is applicable to

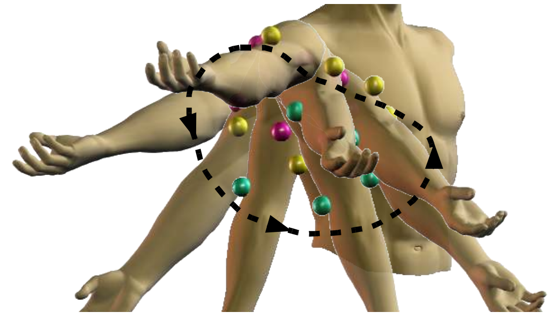

Figure 2: The optimal positioning motion Four basic motions are combined.

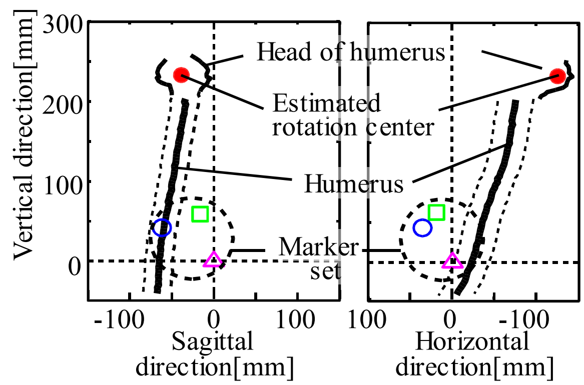

Figure 3: Estimated rotation center for an actual subject

other 3-D joints, because this method is independent of shoulder structure.

SUMMARY

This study proposed an estimation method of the rotation center of the glenohumeral joint that is applicable to a digital manikin. Using this method, the GH center fixed in the upper arm coordinate system can be estimated.

REFERENCES

Meskers, C.G. et al. (1998). *J. Biomech.*, **31**, 93-96

Veeger, H.E.J. (2000). *J. Biomech.*, **33**, 1711-1715

Stokdijk, M. et al. (2000). *J. Biomech.*, **33**, 1629-1636

Bao, H., Willems, P.Y. (1999). *J. Biomech.,* **32**, 943-950

EFFECT OF CONSTRICTION SHAPE ON FLOWS IN STENOSED CHANNELS

Xiaohong Yu and Allen T. Chwang

Department of Mechanical Engineering, The University of Hong Kong, HK
E-mail: yuxh@hkusua.hku.hk Web: hkumea.hku.hk

INTRODUCTION

The partial occlusion of arteries due to stenotic obstruction is one of the most frequently occurring abnormalities in men and women. Many researchers have devoted themselves to study the blood flow in arteries, especially in stenosed arteries. However, they used different stenosed models in experiments or in calculations. Tutty (1992) used a part of the circle as the constriction shape of the channel, Liu and Yamaguchi (2001) used a combination curves, Young and Tsai (1973) used a cosine curve as the generatrix for axisymmetric constriction in tubes, and Long et al. (2001) used a similar curve combination as Liu and Yamaguchi (2001) for the generatrix. As to the Nonsymmetric models, they were constructed by subtracting the uniform tubes by circular cylinders (Young and Tsai, 1973) or some other shaped cylinders (Long et al., 2001). Furthermore, different investigators used different fluids in the simulation or different methods to deal with the data. Therefore, the effects of the constriction shape on flows were not obvious.

The present study will make some effort to investigate the effect of constriction shape on steady or unsteady flows in stenosed channels.

METHODS

In order to make meaningful comparisons, the constriction shapes used in the present study are similar to those of previous works: the circle constriction (M1) as used by Tutty (1992), the cosine constriction (M2) by Young and Tsai (1973), and the combination curves constriction (M3) by Liu and Yamaguchi (2001). Figure 1 gives the basic constriction shapes M1, M2 and M3, where D is the unperturbed channel width.

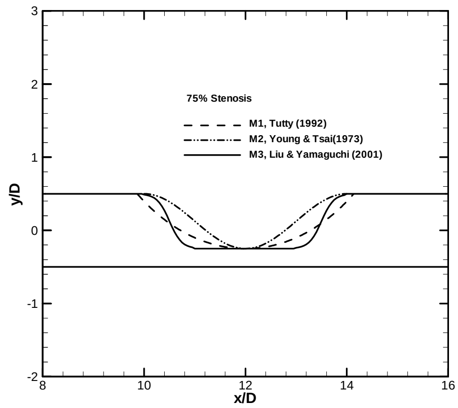

Figure 1: Basic constriction shapes

Steady or unsteady flows in these channels are simulated numerically in the present study. The governing equations are the incompressible, unsteady Navier-Stokes equations in an integral form. The fluid is assumed to be homogeneous, incompressible and Newtonian, and the wall to be rigid. Structured grid is utilized in the calculation, and the equations are solved by cell-vertex based finite volume method.

RESULTS AND DISCUSSION

A study of the constriction shape effect on the pressure drop and the shear stress distribution across the constriction, is first conducted at a moderate Reynolds number (Re = 750) for steady flow. The fully developed flow is used at the inlet of the channels.

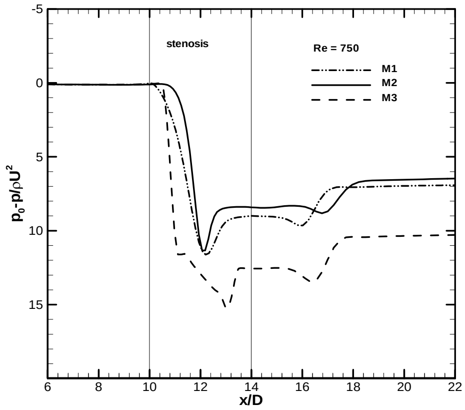

Figure 2: Pressure variation across the constrictions

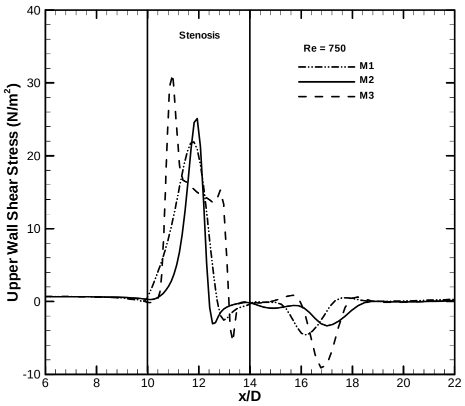

Figure 3: Wall shear stress distribution

Figure 2 shows that M3 gives higher pressure drop than M1 and M2, and from Figure 3, M3 has a different shear stress distribution from the other two models. This is primarily due to the fact that M3 has a longer length of the smallest section. Although the pressure or the shear stress has some difference among three models, the trend is similar for all. At the poststenotic part, the wall shear stress distribution is low and oscillating for all models, which causes the stenosis to grow.

The pulsatility is a major property of the blood flow. Therefore, the present study also considers the different phenomena induced by the pulsatile flow in three models. According to Tutty (1992) and Liu and Yamaguchi (2001), realistic nonsinusoidal waveform is used in the calculation for Re = 750 and $St = D^2 / QT$ =0.035, where Q is the peak volumetric flow rate per unit depth of the channel, D the unperturbed width of the channel, and T the time taken for a complete cycle of the flow.

Under the above situations, M3 has the stronger and more extensive eddies for relatively low frequency unsteady flow than the other two models at the same instant. This is mainly caused by the more abrupt area changes of M3. It still produces different pressure variation and wall shear stress distribution as in the steady case, but the trend is similar as in the other two models at any given time.

SUMMARY

Three different shapes are used to study the effect of constriction shape on steady or unsteady flows in stenosed channels. It is found that the constriction shape has little effect on the pressure and wall shear stress distribution in the stenosed channels. Although the models used in the present study are two-dimensional, the results should be qualitatively valid for three-dimensional stenosed pipes.

REFERENCES

Liu, H., Yamaguchi, T. (2001). *J. Biomech. Eng.,* **123**, 88-96.

Long, Q. et al. (2001). *J. Biomechanics,* **34,** 1229-1242.

Tutty, O.R. (1992). *J. Biomech. Eng.,***114**, 50-54.

Young, D.F., Tsai, F.Y. (1973). *J. Biomechanics,* **6,** 395-410.

Compressive Strength Evaluation of Osteoporosis Vertebra by Finite-Element Analysis Based on Patient-Specific Models

Jiro SAKAMOTO[1], Yasuhide KANAZAWA[1], Daisuke TAWARA[1], Juhachi ODA[1], Serina AWAMORI[2], Hideki MURAKAMI[2], Norio KAWAHARA[2], and Katsuro TOMITA[2]

[1]Graduate School of Natural Science, Kanazawa University, Ishikawa, JAPAN
[2]Graduate School of Medical Science, Kanazawa University, Ishikawa, JAPAN
E-mail: sakamoto@t.kanazawa-u.ac.jp Web: http://www.hm.t.kanazawa-u.ac.jp/bionic/

INTRODUCTION

In almost every cases of diagnosis for vertebral osteoporosis, quantitative value of bone is measured two-dimensionally, such as, bone mineral density is measured by DXA or bone mass density is measured by ultrasound. That kind of diagnosis is not sufficient to evaluate risk of compression fracture of vertebrae, because it dose not evaluate mechanical strength of vertebrae directly. Mechanical strength of vertebra depends on its shape, cortical bone thickness, density distribution of cancellous bone, material properties of bone tissue, and so on. All of the factors related to mechanical strength of vertebra are inherently individual. Patient-specific mechanical analysis is required to evaluate vertebral fracture risk in clinic. Computational models of vertebrae were constructed by using CT images of osteoporosis patients and finite-element analyses of the individual vertebra models were carried out in this study. Several models of female lumber vertebra were constructed for different ages. Ultimate fracture load obtained by finite-element analyses with compressive loading condition were compared each other, and influence of vertebra strength due to osteoporosis was considered.

MATERIALS AND METHOD

X ray CT images were taken from three osteoporosis patients who visited to the orthopedic clinic of the university hospital and a healthy volunteer. All of the patients are Japanese female. Their age and bone mineral density of L1 vertebra measured by DXA are shown in table 1 with condition of the disease. L1 vertebra was focused on, because it was located near the inflection point of spine and favorite site of osteoporosis fracture. Interval of CT section of L1 vertebra was set as 1mm. Mechanical Finder (RCCM Co.) is computer software for bone strength analysis considering individual bone shape, cortical thickness and bone density distribution. Patient-specific finite-element models of L1 based on CT images were obtained by using this software as shown in figure 1. Thin shell elements were used to

Table 1 Age, BMD of L1, and condition of osteoporosis of the patients.

Sign	Age	BMD[g/cm^2]	Condition
A	**59**	**1.043**	**Normal**
B	**84**	**0.865**	**Slight Osteoporosis**
C	**64**	**0.667**	**Osteoporosis**
D	**71**	**0.435**	**Severe Osteoporosis**

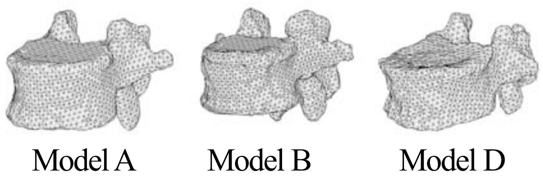

Fig.1 Patient-specific finite-element models of L1

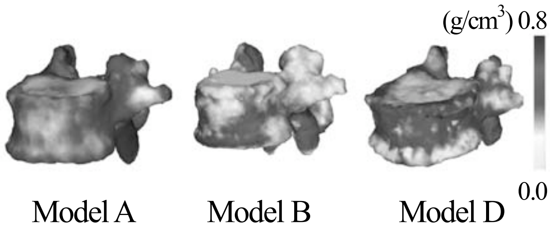

Fig.2 Bone density distribution of the patient-specific FE models except for cortical shell elements.

represent thin cortical bone on the surface. Figure 2 shows bone density distribution of the models except for the cortical shell elements. Young's modulus and strength of each solid element is given one by one calculating from bone mass density and CT value. Relationship between the mechanical properties and bone mass density obtained by past studies (e.g., Carter 1977) was used in the calculation. Simple compressive loading was considered in the analyses, that is, bottom surface was fixed and uniform pressure was applied to upper surface of vertebra. Non-linear finite-element analyses considering bone fracture process were carried out with incremental loading condition. If principal stress over the local strength of an element, constitutive equation of the element is changed considering a crack initiated along orthogonal direction to the principal stress (e.g. Kwak 1990).

RESULTS AND DISCUSSION

An example of crack propagation process on the cortical surface is shown in figure 3 for the case of model C (osteoporosis). In cortical bone surface, crack was initiated at anterior midpoint of the vertebra, and the crack was propagated widely around anterior surface. Small fracture of cancellous bone arose from anterior side at lower load, and the fracture part grew to posterior side with increasing of load, then breakdown of the vertebra occurred when the fracture extended over circumference. Ultimate fracture load is defined as load at last increment just before breakdown, because finite-element analysis is not able to continue after breakdown. Figure 4 shows ultimate compressive fracture load of the models versus bone mineral density (BMD) measured by DXA. Positive correlation is observed between BMD and the ultimate fracture load. BMD obtained by DXA seems effective index for osteoporosis diagnosis in mechanical viewpoint, even though it is not mechanical property and measured two-dimensionally.

SUMMARY

Compressive strength of osteoporosis vertebrae was analyzed by finite-element method for patient-specific models based on CT images, in this paper. Ultimate fracture load obtained by the analyses decrease depending on bone mineral density measured by DXA.

REFFERENCES

Dennis R.Carter and Wilson C.Hayes (1977), *The Compressive Behavior of Bone as a Two-Phase Porous Structure, Journal of bone and joint surgery*, **59A No.7**, 954-962

H.G. Kwak and F.C. Filippou (1990), *Finite Element Analysis of Reinforced Concrete Structures Under Monotonic Loads, Structural Engineering Mechanics and Materials, UCB/SEMM,* **90/14**, 32-34

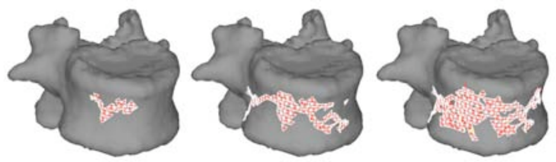

F=450N F=550N F=600N

Fig.3 Crack propagation process on the cortical surface in bone fracture analysis of model C. Fractured finite-elements are shown with total load F.

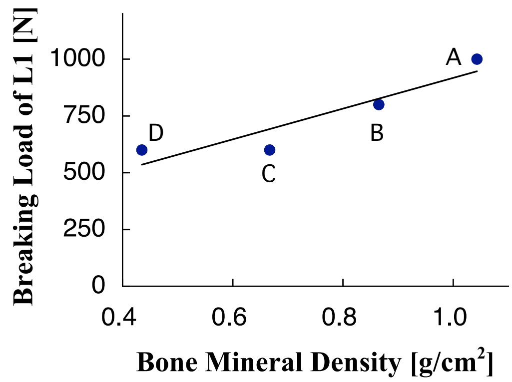

Fig.4 Ultimate compressive fracture load of the models versus bone mineral density measured by DXA

EFFECT OF EXTERNALLY-CUED STRIDE FREQUENCY SELECTION ON TEMPERO-SPATIAL PARAMETERS OF GAIT

Michael P. Hanlon and Ross Anderson

Physical Education and Sport Sciences Department, University of Limerick, Limerick, Ireland
E-mail: michael.hanlon@ul.ie   Web: www.ul.ie/~pess

INTRODUCTION

Walking speed in humans is determined by the product of stride length (StrL) and stride frequency (StrF). These two components are usually involuntarily chosen by the walker to produce some voluntarily chosen walking speed (e.g. moderate or fast). The length-frequency relationship over a range of walking speeds has been analysed in literature both directly and indirectly. Sekiya and Nagasaki (1998), concluded that walk ratio (StrL/StrF) is invariant over speeds ranging from very slow to very fast in males and also invariant in females from the preferred to very fast speeds. From this, it can be assumed that if an individual increases their walking speed, they do so by increasing both their StrL and StrF in a proportionate manner. This relatively consistent walk ratio means that for each StrF, humans have a typical StrL that they match with it. This theory holds true in natural gait when the individual is free to pick their own StrF and StrL.

This study examines the effect that imposing particular stride frequencies has on individual's tempero-spatial characteristics of gait. This is of importance as metronome-controlled gait is used to analyse gait characteristics at different stride frequencies (Winter, 1983) and rhythmic training has been proposed as a training modality for gait rehabilitation in patients with neurological disorders (e.g. hemiparesis and Parkinson's disease).

METHODS

Twenty healthy adults volunteered for this study, 13 women and 7 men (age: 27.5±7.7 years; height: 1.71±0.07 m). Subjects gave informed consent to participate. Subjects were instructed to walk along a 20-m walkway at a constant speed. Firstly, they performed five walks at their normal walking speed (NV), then 5 at their slow walking speed (SV) and finally 5 at their fast walking speed (FV). A wireless infrared timing system (Brower Speedtrap 2, Utah, USA) measured the speed of the subject over the middle 10 m of the walkway. A video capture system consisting of a digital camera linked to a laptop captured video footage over the middle 5 m of the walkway.

After completing five trials at each walking speed the three trials with least speed variability in each condition were analyzed using the captured video to calculate the mean step frequency for each condition. A metronome (Aquapacer Solo, Inverurie, UK) was programmed with a frequency called NF, equalling the mean step frequency used by the subject in NV. Subjects were then instructed to walk with the beat such that each heel strike coincided with a beep from the metronome. The subjects walked ~40 m for rhythm familiarization before completing 5 trials on the 20-m walkway following the NF rhythm. With the same procedure, subjects carried out 5 walks at the cadence that matched their slow walking cadence (SF) and 5 walks at the cadence that matched their fast walking cadence (FF).

StrL was calculated as walk speed*stride time, where walking speed was calculated using the time taken to walk 10 m between photogates and stride time was calculated in the free walking condition using the captured video and in the cadence-controlled situation it was assumed to match the metronome. StrL was then normalized by dividing by height. A two-way repeated measured ANOVA was used to assess the effect of StrF and type of walking (free walking or cadence control) on StrL. Statistical significance assumed at $p<0.05$.

RESULTS AND DISCUSSION

Mean speeds chosen in each condition (NV, SV and FV) were similar to previous data (Sekiya and Nagasaki, 1998). One subject's data was removed as an outlier as their SV selection was more than three standard deviations from the group mean. The two-way repeated measures ANOVA illustrated that StrF had a significant effect on StrL. This agrees with the previously mentioned research. An interaction effect exists between StrF and type of walking (free or cadence control) showing that the effect of StrF on StrL was significantly different at the slow ($p=0.000$) and fast frequencies ($p=0.000$) dependent on whether it was free walking or cadence control.

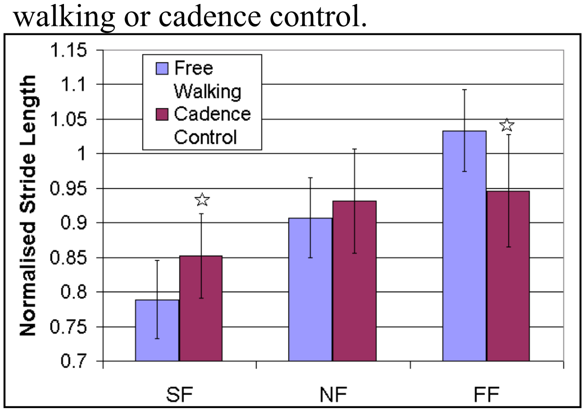

Figure 1: Normalised StrL employed when walking at three different StrF (slow, normal and fast) in two different conditions. Stars indicate significant difference of StrL between conditions ($p<0.05$).

When forced to walk with their SF the group walked faster than when they used this same slow step frequency as part of free walking (9.2±7.3 m/s faster) and when forced to walk with their FF they walked slower than when using this same fast step frequency as part of free walking (16.1±13.8 m/s slower).

Figure 1 shows that the StrL chosen by the subjects to match with both slow and fast stride frequencies differed significantly dependent on whether this was done as part of free walking or in a cadence controlled setting. These initial results are of great importance to researcher's who may assume that a subject's spatial gait characteristics will be the same if the StrF is the same regardless of whether this StrF is chosen freely or forced using a metronome. Our data would refute this assumption and indicate that gait data recorded at a metronome-controlled stride frequency should not be used to illustrate 'normal' gait characteristics for that stride frequency, especially at the slower and faster frequencies.

SUMMARY

Controlling cadence results in altered spatial gait parameters at slow and fast frequencies compared to free walking at these same frequencies.

REFERENCES

Sekiya, N., Nagasaki, H. (1998). *Gait and Posture*, **7**, 225-227.

Winter, D.A. (1983). *J Motor Behavior*, **15**, 302-330.

ACKNOWLEDGEMENTS

Funding for this research is provided by the Irish Research Council for Science, Engineering and Technology: funded by the National Development Plan.

A GENERALIZED APPROACH TO THREE-DIMENSIONAL KINEMATIC AND KINETIC ANALYSIS OF OPEN-LOOP MULTI-SEGMENT SYSTEMS

Lei Ren and David Howard
Centre for Rehabilitation and Human Performance Research &
School of Computing, Science and Engineering, Salford University, United Kingdom
E-mail: d.howard@salford.ac.uk

INTRODUCTION

Three-dimensional kinematic and kinetic analysis using photogrammetric techniques has been increasingly used in biomechanical studies of human movement (Allard, et al., 1995), as more complex morphology can be investigated than with simple 2D analyses. However, most 3D applications only focus on specific parts of the body, such as the lower limbs, where the structure of the multi-segment model is relatively simple, and the kinetic analysis is only conducted from distal to proximal segments sequentially.

Real biomechanical systems are more complex as human and animal skeletons are composed of interconnected articulated links with hundreds of degree of freedom (DOF) and complicated topologies; moreover the environmental constraints are various. This paper presents a methodology for 3D kinematic and kinetic analysis of general open-loop multi-body systems, which can be used for a large range of biomechanical systems, whether human or animal. The proposed methodology is being implemented in a software package, SMAS (Salford Motion Analysis System), which is now almost complete.

METHODS

The biomechanical system is modelled as a set of rigid segments, connected by generic joints with up to six independent DOF. Three templates are employed to define the biomechanical system: the body template, marker template and force template. All definitions are generic, so that any open-loop multi-body system can be described.

The body template represents the topology of the multi-body system, which includes the definitions of body segments, their adjacent segments, and interconnecting joints.

The marker template defines two marker sets: technical markers and anatomical landmarks. Technical markers are attached to body segments to record their changing positions and orientations, and are associated with technical frames. Anatomical (or bony) landmarks are used to define bone-embedded local frames for each body segment.

The force template describes the properties of the external force systems acting on the biomechanical system. For each force system (3 forces and 3 moments), an application segment, application positions and force evaluation functions are defined. These external forces can be set as known (e.g. measured by force plates) or as unknown.

For kinematic analysis, a least squares method (Challis, 1995) is used to estimate the position and orientation of body segments from the technical marker coordinates. The CAST protocol (Cappozzo et al., 1995) is employed, based on a set of calibration procedures, to establish the mapping between the technical and anatomical frames. The calibration procedure allows for the use of different landmark identification techniques (e.g. markers and/or wands). The joint centers can be identified using a functional method (Cappozzo, 1984) or directly from anatomical landmarks. The anatomical landmarks (derived or real) are then used to define anatomical frames and the orientations of body segments. Thereafter the joint kinematics can be described based on the topology defined in the body template. The anatomical landmarks and frames allow the measured motions to be described by reference to skeletal geometry. However, this methodology can also be used in cases where only technical markers are involved.

For kinetic analysis, the inverse dynamics method is employed. However, this differs from the conventional approach where the calculations proceed sequentially, from distal to proximal segments. In SMAS, the calculation sequence depends on the system topology and the environmental constraints defined in the body and force templates. The algorithm starts from all solvable segments, calculates the forces and moments at their adjacent joints, then runs iteratively until no solvable segment remains. Different approaches are used to derive joint forces and moments according to the determinacy of the system. In the under-determined case, inverse dynamics is used to derive all the solvable joint forces and moments, whereas, in the determinate case, all joint forces and moments can be calculated. If redundancy exists, a least squares method (Kuo, 1998) is employed to improve the accuracy of the calculated joint kinetics.

RESULTS AND DISCUSSION

The methodology is being implemented as a MATLAB based software package, SMAS, which is now almost complete. Figure 1 shows a 3D whole-body SMAS model. The polygons represent the body segments with anatomical landmarks at their vertices.

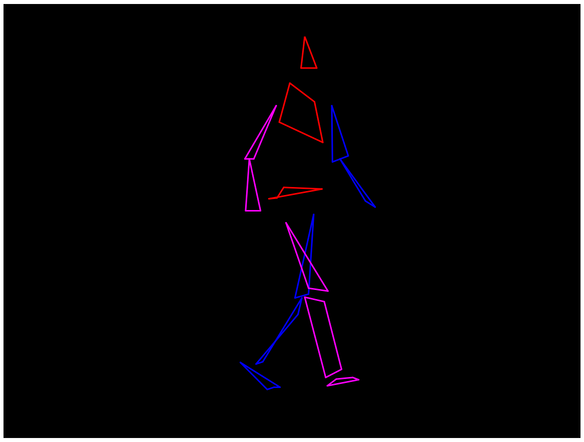

Figure 1: A SMAS 3D animation of walking

The SMAS methodology applies to general open-loop multi-segment systems, and makes best use of the available kinematic information. Moreover, unknown external forces and moments can be derived, as well as the internal joint forces and moments.

REFERENCES

Allard, P. et al. (1995). *Three-dimensional analysis of human movement*. Human Kinetics Press.

Cappozzo, A. et al. 1995. *Clin. Biomech.*, **10**, 171–178.

Cappozzo, A. 1984. *Hum. Mov. Sci.*, **3**, 27–54

Challis, J. H. 1995. *J. Biomech.*, **28**, 733–737

Kuo, A. D. 1998 *J. Biomech. Eng.* **120**, 148–159

ACKNOWLEDGEMENTS

Funding for this work has been provided by the UK Ministry of Defence

ASSESSMENT OF BACKPACK INTERFACE LOADING USING A WHOLE BODY GAIT MODEL

Lei Ren [1,2], Richard Jones [2], David Howard [1,2] and Jim Richards [2]

[1] School of Computing, Science and Engineering
[2] Centre for Rehabilitation and Human Performance Research
Salford University, United Kingdom
E-mail: d.howard@salford.ac.uk

INTRODUCTION

Backpacks are well known devices that enable people to increase their load carriage capability, but when heavily loaded may lead to excessive joint loadings, muscle fatigue or even impairment (Myles, 1979; Knapik et al. 1996). The interface pressure distribution between the pack and the bearer can be measured using pressure sensor arrays to assess comfort and the potential for tissue damage (Holewijn, 1990; Martin and Hooper, 2000). However, it is difficult to measure the resultant pack interface forces directly, as the interface properties are very complex.

This paper presents a method for assessing the interface forces between the backpack and the bearer. A multi-camera system was used to record the three-dimensional motions of all the major body segments during walking with a backpack. A validated whole body multi-segment model was employed to derive the dynamic pack interface forces, which can be used in the biomechanical assessment of different load carriage systems.

METHODS

In order to obtain the kinematic data, whole body gait measurements with a loaded backpack were conducted. Four healthy male subjects were selected from a population of postgraduate students. Prior to participation, the subjects provided informed consent. The subjects walked along an indoor walkway at a self-selected speed. The rucksack was loaded at two different weights, 11.75 Kg and 23.5 Kg. A six camera Qualisys motion analysis system was used to capture motion data. Two Kistler force plates were used to record ground reaction forces.

A set of specially designed plastic plates for whole body gait measurement (Ren et al, 2004), each carrying four reflective markers, was employed to record the motions of all the major body segments. The locations of the marker clusters permits carriage of a backpack without obscuring markers. The positions of the anatomical landmarks, used for local frame definitions for each body segment, were determined by a set of calibration procedures.

In this study, a validated three-dimensional whole body multi-segment model based on inverse dynamics algorithms (Ren et al, 2004) was employed to derive the interface pack forces acting on the bearer’s truck. The raw marker data processing and the pack force calculations were conducted using a MATLAB software package SMAS (Ren and Howard, 2004), which has been developed for three-dimensional kinematic and kinetic analysis of general articulated multi-body systems.

Missing markers are dealt with by a fill-gap procedure and the maximum allowable gap is 15 consecutive frames. After fill-gap processing, the data were filtered using a low pass fourth-order Butterworth digital filter with a cut-off frequency of 6 Hz. Based on the filtered marker data and the calibration data, the joint center positions, and angular and mass centre accelerations of each body segment were then calculated.

Using the calculated motion data and the recorded ground reaction forces on both force plates, the dynamic pack forces acting on the bearer's trunk were then derived using the SMAS software package. The calculation starts from the measured ground reactions, solves the inverse dynamics (segment by segment), and finally derives the pack interface forces.

RESULTS AND DISCUSSION

Figure 1 shows typical results for the calculated pack forces over a walking cycle at two pack weights. It can be seen that the anterior-posterior and lateral pack forces acting on the bearer's torso are relatively small. The average values of these forces over a walking cycle are around zero. The vertical pack force fluctuates around the loaded pack weight with two peak values, which is similar in form to the trajectory of the trunk mass center (Rose and Gamble, 1994).

This preliminary investigation indicates that increasing pack load has no particular effect on the anterior-posterior and lateral pack forces, while the peak vertical pack force increases with increasing pack load. Future studies will include higher loads and the effect of walking velocity on the dynamic pack interface forces.

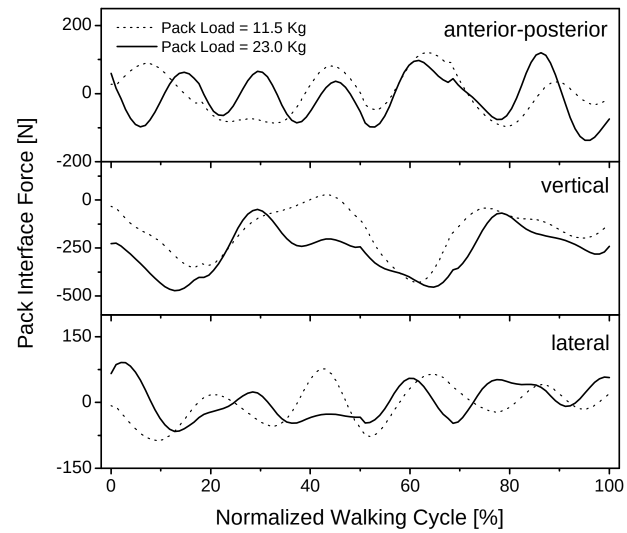

Figure 1: Calculated pack interface forces over a walking cycle for two pack weights (11.75 Kg and 23.5 Kg)

REFERENCES

Holewijn, M. (1990). *Eur. J. Appl. Physiol.*, 61, 237–245

Knapik, J., Harman, E. and Reynolds, K. (1996). *Appl. Ergon.*, 27, 207–215

Martin, J. and Hooper, R. (2000). *Proceedings of NATO RTO Meeting 56*, Kingston, Canada

Myles, W.S. and Saunders, P.L. (1979). *Eur. J. Appl. Physiol.* 42, 125–131

Ren, L. and Howard, D. (2004). *Proceedings of ASB 2004*, Oregon, USA.

Ren, L., Jones, R., Howard, D. and Richards, J. (2004). *Proceedings of ASB 2004*, Oregon, USA

Rose, J. Gamble, J. G. (1994). *Human Walking. 2nd Edition*. Willliams & Wilins.

ACKNOWLEDGEMENTS

Funding for this work has been provided by the UK Ministry of Defence

VALIDATION OF A THREE-DIMENSIONAL WHOLE BODY MULTI-SEGMENT MODEL FOR LOAD CARRIAGE STUDIES

Lei Ren [1,2], Richard Jones [2], David Howard [1,2] and Jim Richards [2]

[1] School of Computing, Science and Engineering
[2] Centre for Rehabilitation and Human Performance Research
Salford University, United Kingdom
E-mail: d.howard@salford.ac.uk

INTRODUCTION

In the biomechanical analysis of human movement, multi-segment models have often been used to assess the forces, moments and powers generated at joints. Many researchers have represented only part of the body, however some have used whole body models for activities involving both lower extremities and the upper body, such as whole body balance control (MacKinnon and Winter, 1993) and weight lifting (Kingma, et al., 1996). However, none of these models were used or validated for dynamic walking conditions.

This paper describes the development and validation of a three-dimensional whole body multi-segment model for load carriage studies. A set of marker clusters were designed to record the motions of all major body segments during walking. The model was validated by comparing the measured and calculated ground reaction forces in all three planes of motion.

METHODS

In this study, the human body was modeled as a rigid articulated multi-segment system, which includes 13 body segments: the head, torso, pelvis, right and left forearms, right and left humerii, and both legs (thighs, shanks and feet). Anthropometric data for each body segment are based on de Leva, 1996, but modified for the forearm and torso segments because of the different segment definitions used in this study.

Four healthy male subjects participated in the experiments. The subjects walked in trainers along a walkway at two speeds, normal and fast. The motion data was collected at 100Hz using a 6-camera Qualisys motion analysis system. Two Kistler force plates were used to record ground reaction forces. Each test condition was repeated six times.

Plastic plates, each carrying four reflective markers, were attached to each body segment. The plastic plates eliminate the relative motion between the markers, thus increasing the accuracy of the recorded motion data.

Anatomical landmarks and bone-embedded anatomical reference systems were defined for each major body segment based mainly on Cappozzo et al., 1995, and Van der Helm and Pronk, 1995. Before the walking trials, a set of calibration procedures was conducted to locate the anatomical landmarks using the CAST technique (Cappozzo et al., 1995). In this study, the shoulder joint centre is defined to be the functional humerothoracic joint centre, which is the effective centre of rotation between the upper arm and the trunk. A functional approach (Gamage and Lasenby, 2002) has been used to locate the humerothoracic joint centre, as well as the hip joint centre. The positions of other joint centres were determined directly from anatomical landmarks.

The raw marker data was processed by a MATLAB software package SMAS (Salford Motion Analysis Software), which was developed for three-dimensional kinematic and kinetic analysis of general articulated multi-body systems. The joint center positions were derived from the dynamic marker data and the calibration data. The segments' angular and mass center accelerations were then calculated.

Using the motion equations of the multi-segment system, the ground reaction forces can be completely determined from the segments' inertial properties and motions (Winter, 1990). The whole body model was validated by comparing the calculated with the measured ground reaction forces.

RESULTS AND DISCUSSION

The validation of the model was conducted for all subjects at both walking velocities. The estimated ground reaction forces were determined from the vector summation of mass times mass center acceleration minus weight for all body segments. The measured ground reaction forces were obtained by adding the values from both force plates. The results show that the calculated ground reaction forces are in good agreement with the measured values. Figure 1 shows a typical result for one subject (36 yrs, 90 Kg).

This model has been used for load carriage studies. Since backpack interface forces are difficult to measure, the validity of the model was investigated for unloaded conditions. The validated whole body model was then used to assess joint kinetics and locomotion energetics during load carriage.

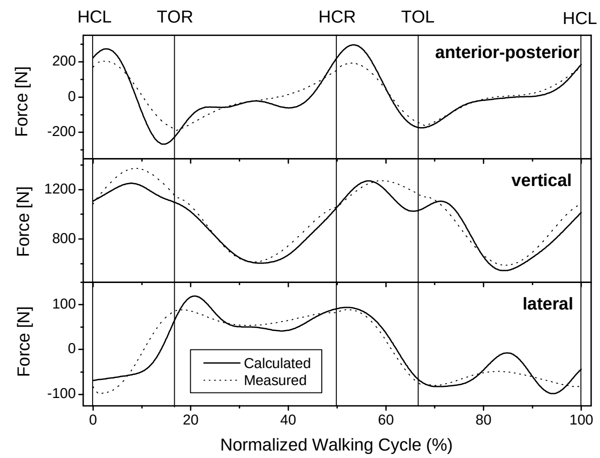

Figure 1: Calculated and measured ground reaction forces over a complete gait cycle (walking velocity: 1.43 m/s)

REFERENCES

Cappozzo, A. et al. (1995). *Clin. Biomech.*, **10**, 171–178.

Gamage, S. S. H. U. and Lasenby J., 2002. *J. Biomech.*, 35, 87–93.

Kingma, I. et al. (1996). *Hum. Mov. Sci.*, **15**, 833-860.

de Leva, P. (1996). *J. Biomech.*, **29**, 1223–1230.

MacKinnon, C.D., Winter, D.A. (1993). *J. Biomech.*, **26**, 633-644.

Van der Helm, F. C. T. and Pronk, G.M., (1995). *J. Biomech. Eng.*, **177**, 27–40.

Winter, D. A., 1990. *The Biomechanics and Motor Control of Human Movement (2nd Editon)*. John Wiley and Sons Ltd.

ACKNOWLEDGEMENTS

Funding for this work has been provided by the UK Ministry of Defence

EFFECTIVENESS OF TWO KNEE BRACES ON MEDIAL COMPARTMENT OSTEOARTHRITIS

Richard Jones[1], Jim Richards[1], and Jordi Sanchez-Ballester[2]
[1]Centre for Rehabilitation Human Performance Research, University of Salford, UK
[2] Specialist registrar orthopaedics, Stepping Hill Hospital, Stockport UK
r.k.jones@salford.ac.uk www.healthcare.salford.ac.uk/crhpr

INTRODUCTION

Osteoarthritis (OA) of the knee joint is a common occurrence in the worldwide population affecting approximately 80% of individuals by the age of 55 (Altman 1987). It is widely known that knee OA is more prevalent in the medial compartment of the knee joint than the lateral compartment (Huch et al. 1997) and has been estimated that during normal gait approximately 60-80% of the load across the knee joint is transmitted to the medial compartment (Prodromos et al,.1985).

An increase in the adduction moment of the knee has been shown to correlate with a decrease function and an increase in pain, the principal complaints of knee OA sufferers (Kim et al. 2004). Treatment options such as high tibial osteotomy and unicompartmental arthroplasty are available to the sufferer are aimed to minimise the adduction moment and therefore reducing the load on the medial compartment of the knee. However surgery may be inappropriate for some populations. Conservative management techniques to reduce the adduction moment at the knee have been introduced which include valgus bracing of the knee. Several studies investigated the use of valgus knee braces for medial compartment OA, and have reported that patients experience significant pain relief and an improvement in physical function (Hewett et al. (1998); Matsumo et al. (1997)) and also a reduction in medial compartment load (Pollo et al. 2002). However the efficacy of knee bracing is still questioned as being a placebo effect giving the wearer perceived confidence in the stability of the limb.

This current study investigates the effect of two types of knee brace, a simple hinged knee brace with no direct valgus support and a custom cast valgus knee brace with direct valgus support. Both the perceived benefits of brace wearing and the changes in biomechanical function of the supported and unsupported knee in medial compartment OA are investigated.

METHODS

12 subjects with radiological confirmed medial compartment osteoarthritis were recruited for the study.

Kinematic and kinetic analyses were performed on each subject whilst wearing no brace. Each subject was then randomly selected either a cast valgus brace or an off-the-shelf simple hinged brace. Both braces were fitted by the same orthotist and the subjects were instructed on how to self-fit. Each subject wore the brace for a period of six months when kinematic and kinetic gait analysis was repeated. Under a cross-over design, the subjects wore the second brace for a period of six months where kinematic and kinetic gait analysis was repeated.
Patients were also assessed clinically using: visual analogue pain scores for resting, standing, walking and climbing stairs, and Hospital for Special Surgery activity questionnaires and analgesia consumption was also recorded. The above measures were taken at the initial (0 Month) and then at the crossover point of the two braces, at 6 and 12 months. One-way ANOVA tests were performed with post hoc pairwise comparison for the kinematic, kinetic and questionnaire data.

RESULTS AND DISCUSSION

Questionnaire results

Table One HSS mean score

Condition	HSS Score
Initial	49.3
Simple Brace	53.5
Valgus Brace	65.7*

Table Two VAS mean scores

Con	Rest	Walk	Stand	Stairs
Initial	4.9	8.0	6.0	8.5
Simple brace	3.6	7.4	6.3	7.9
Valgus brace	2.9*	5.4*	4.8	5.9*

* denotes significance at $p<0.05$

From the questionnaires it was found that significant improvement in both the symptoms and function were found with the valgus brace. No significant improvement was found for the simple brace but an improvement was seen.

The kinematic data did not show any significant improvements for any of the braces, however, a reduction in knee flexion during swing was found in the valgus brace. The mean difference was 6 degrees which as well as being statistically significant it is also clinically significant; the simple brace had no such restriction.

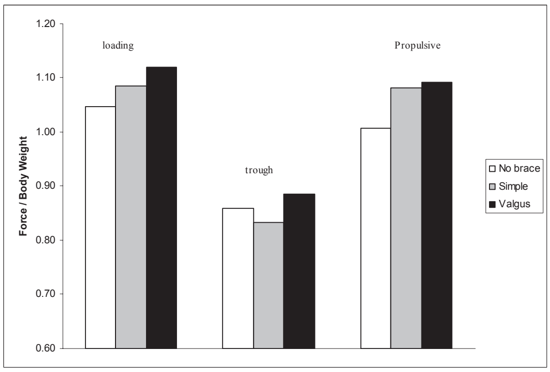

Figure One. Vertical ground reaction forces (normalised to bodyweight)

The force platform data showed that the valgus brace produced significantly greater loading forces in the vertical and posterior direction, and a significant increase in the propulsive vertical forces. These data reflect an increased confidence during loading and an improvement in the ability to push off vertically. The simple brace showed improvements in the vertical and posterior loading but not to the same extent as the valgus brace.

These increases in forces may not be viewed as a positive outcome as this would suggest more load is being transferred to the knee joint, in particular the medial compartment. However, as significant improvements were also found for the pain scores and function questionnaires.

It can therefore be suggested that the valgus brace is having a supportive role and allowing the subject to have a greater loading and push off forces which are being supported by the brace, therefore reducing pain and functional impairment.

SUMMARY

Both braced conditions gave the subjects more confidence, with the valgus brace showing greater biomechanical and perceived functional improvement during gait, although a restriction during swing phase was seen. This would support the view that the perceived improvements gained by using the valgus knee brace are due to biomechanical changes and not due to a placebo effect.

REFERENCES

Altman, R (1987) *Am J Med*, **83**, 65-69

Huch, K, Kuettner, K. Dieppe, P. (1997) *Arthritis Rheum*, **26**, 667-674.

Prodromos, C et al, (1985) *J Bone Joint Surg*, **67A**, 1188-194

Kim, W et al. (2004) *Knee,* In press

Hewett et al. (1998) *Orthopedics*, **21** 131-8.

Pollo et al. (2002) *Am J Sports Med*, **30** 414-421.

Matsumo, H., Kadowaki, K and Tsuji, H. (1997) Arch Phys Med, **78**, 745-749.

KNEE MOMENTS WHILST CARRYING A LOAD DURING WALKING

Richard Jones[1], Lei Ren[1,2], Jim Richards[1], and David Howard[1,2]
[1]Centre for Rehabilitation and Human Performance Research, University of Salford
[2] School of Computing, Science and Engineering, University of Salford, UK
r.k.jones@salford.ac.uk www.healthcare.salford.ac.uk/crhpr

INTRODUCTION

Military personnel are required to carry increasingly heavy loads. It is important to understand, from a military 'duty of care' point of view, the increased risks of such load carriage.

The magnitude of loads that act on the lower limbs during walking is increased with the addition of a backpack which can be sometimes up to 70% of bodyweight (Knapik, et al. (1996). In considering that a soldier can cover around 11 km in one day, the added effect of such a load over time can have a serious effect on the injuries sustained. In trained personnel, load carriage was particularly implicated in injuries. Many trained personnel suffer injuries to the lower-limb and back region accounting for 80% of all injuries (Neely, 1998).

The knee joint is a commonly injured site in both training and serving personnel. Knee pain is an increasingly debilitating condition which can put an individual out of action for up to 14 days (Knapik et al. 1992). Given the increased loads and distances a soldier is required to cover, the exposure to such loads will only be increased with added stresses on the knee joint. Han et al. (1993) found an increased external flexion moment when increasing loads. Any increase in these moments would put an increase in load on the knee joint structures and therefore could cause an increased pain and injury. Many studies have been performed on load carriage but there is a dearth of literature on biomechanical studies of carrying a load and its effect on specific joints. This current study investigates the changes in the adduction and flexion moments acting on the knee joint under different load carriage conditions during walking.

METHODS

Eight, healthy, male subjects took part in the study. 3-Dimensional motion analysis (Proreflex, Qualisys, Sweden) was performed capturing at 100 Hz with simultaneous bilateral Kistler (UK) force platforms sampling at 200 Hz. Subjects wore t-shirts and shorts and their own comfortable footwear.

Markers were places over the following anatomical landmarks, lateral and medial malleolus, 1st and 5th metatarsal heads, calcaneus, lateral and medial epicondyle, and greater trochanter on both limbs. Rigid cluster plates were placed on the thigh and shank sections using the CAST technique (Cappozzo et al. 1995).

The subjects undertook three walking conditions: Walk with no pack, 90 Pattern Bergen Load 1 (12 kg), 90 Pattern Bergen Load 2 (24 kg). Six trials of each condition were performed at the subjects' self-selected pace.

Data were digitised and exported as a C3D file into Visual 3D (USA). The peak knee adduction moment and the peak flexion moment during loading were recorded from both limbs. Data were normalised to subjects' mass.

A one-way repeated measures analysis of variance was performed for each limb. Post-hoc pairwise comparisons with Bonferroni corrections identified any differences ($P<0.05$).

RESULTS AND DISCUSSION

Knee adduction moment

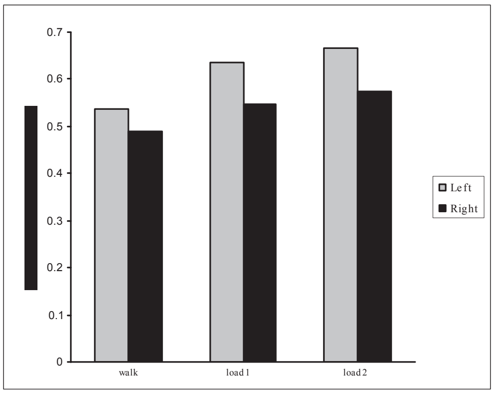

Figure One: Knee adduction moment during load carriage. (normalised to mass)

There were no significant differences in the knee adduction moment during the loading for left and right sides. However, there were increases of 19 and 25% for the 2 loads respectively.

Knee flexion moments

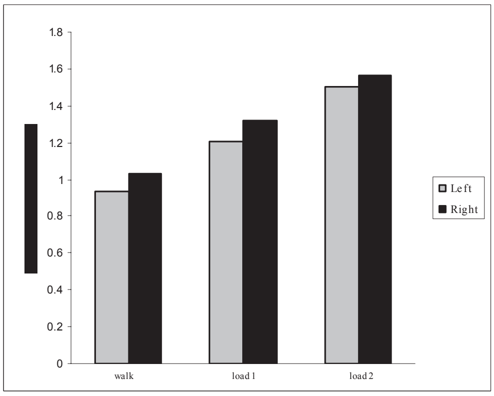

Figure Two: Knee flexion moments during load carriage. (Normalised to mass)

There were no significant differences in the peak knee flexion moment during loading between walking without a backpack and walking with the backpack with the 12 kg load for the two sides. A significant difference was seen in the peak knee flexion moment during loading between walking without a backpack and with the backpack with the 24 kg load.

Although the 12 kg load did not show any significant increase, an increase in the mean showed a 29% increase in the moment and a 60% increase with the 24 kg load. This is in agreement with the study performed by Han et al, 1993). This indicates a linear but disproportionate increase in loading on the structures of the knee compared with the actual load carried.

Larger loads were not tested due to ethical constraints on this study.

SUMMARY

Military load carriage can be much larger typically upwards of 50% body weight, and if the relationship between knee flexion moment and load carriage is linear this implies a 100% increase in the knee flexion moment compared with unloaded walking. This disproportionate increase in loading on the structures of the knee could have a clinically significant effect and cause breakdown and pathology in the knee.

REFERENCES

Cappozzo, A. et al. (1995) *Clin Biomech* **10**, 171-178.
Neely, F.G. (1998) *Sports Med* **26** 253-263.
Knapik, J., Harman, E and Reynolds, K. (1996) *Appl Ergon* **27,** 207-216.
Han, K.H. et al. (1993) *J Biomech* **26**, 354.
Knapik J. et al. (1992) *Milit Med* **157** 64-7.

ACKNOWLEDGEMENT

This work was funded by the UK Ministry of Defence.

POSITIONAL STABILITY TESTING OF A PROSTHETIC DISC NUCLEUS DEVICE

Joseph E. Hale [1], Britt K. Norton [1], Laura J. Bauer [1], Sara E. Ross [1], and William C. Hutton [2]

[1] Raymedica, Inc., Minneapolis, MN
[2] Department of Orthopaedics, Emory University School of Medicine, Atlanta, GA
E-mail: j.hale@raymedica.com

INTRODUCTION

Intervertebral disc nucleus replacement is quickly emerging as a viable alternative to fusion in the early treatment of degenerative disc disease. Unlike fusion, disc nucleus replacement has the ability to restore normal disc height without impairing mobility. Current designs rely on the surrounding annulus to retain nucleus replacement devices within the disc cavity. The purpose of this study is to evaluate the positional stability of a hydrogel-based prosthetic disc nucleus device in human cadaveric motion segments.

METHODS

An in vitro biomechanical study was carried out using cadaveric lumbar motion segments, each implanted with a prosthetic disc nucleus device. A total of 11 cadaveric lumbar motion segments (age 33-69 years) were each denucleated and then implanted with a single, fully-hydrated prosthetic disc nucleus device (PDN-SOLO®, Raymedica, Inc.). All devices were appropriately sized to the disc space height and their position within the disc cavity was verified radiographically (Figure 1). Fully-hydrated devices were implanted in this study to assess the intended functional state of the device in vivo. Clinically, the device is implanted in a dehydrated state and becomes fully hydrated over a period of time.

Two experiments were conducted. In the first experiment (n=6), the force required to extract the device from the intervertebral disc space was determined using methods similar to those employed for intervertebral fusion devices [ASTM F2077-03]. With a 500 N axial compressive load applied to the motion segment, the device was pulled-out through the standard surgical opening created in the posterior annulus to implant a dehydrated device.

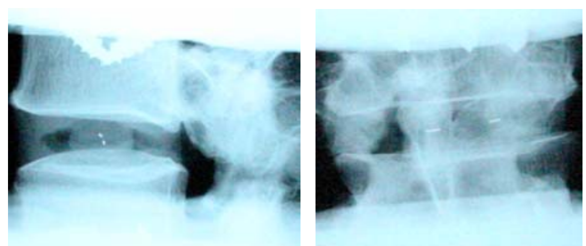

Figure 1. Lateral (left) and A/P (right) radiographs of an implanted motion segment. Device position is verified by visualization of platinum-iridium markers imbedded in the hydrogel core.

In the second experiment (n=5), motion segments were subjected to a loading protocol designed to produce disc prolapse [Adams & Hutton, 1982; 1985]. With the specimens fully flexed to maximize stretching of the posterolateral annulus in the vicinity of the opening made to implant the device, cyclic compressive loads of 500-1500 N, 500-2500 N and 500-4000 N were applied (3600 cycles total, 1 Hz). Specimens were then hyperflexed 4-5 degrees beyond the limit of flexion and monotonically loaded to failure at a rate of 500 N/sec. Each specimen was carefully monitored during testing to detect any device movement and subsequently dissected to determine the final position of the device.

RESULTS AND DISCUSSION

In the first experiment, the mean maximum force needed to pull a single PDN device out of the disc cavity was 364.5 N (Table 1), approximately 44% more than was required for the paired PDN device design in a previous study [Hale et al., 2003]. A considerable difference in maximum pull-out force was observed as a function of the lumbar spine level implanted; however, the small sample size and relatively large standard deviation for the two groups made further statistical analysis impractical.

Table 1. Pullout Test Results

Specimen #	Max. Pullout Force [N]	
	L2-L3	**L4-L5**
1		375
2	298	
3		409
4	183	
5		541
6	381	
Mean (St Dev)	287.3 (99.4)	441.7 (87.7)
	364.5 (119.1)	

In the second experiment, the imposed loading conditions correspond to physiological extremes of load magnitude and flexion and thus, represent a "worst-case" scenario. Failure of the specimen generally occurred in the range of about 5500 - 7000 N. In every case, the device remained in the disc cavity, with little or no apparent movement relative to pre-test radiographs observed at dissection. Further examination of the dissected motion segment typically revealed that one or both endplates were fractured (Figure 2).

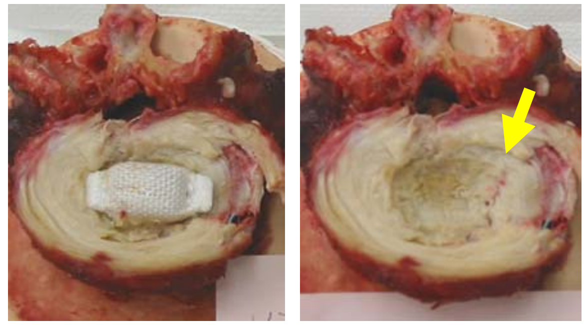

Figure 2. Dissected motion segment with PDN device in place (left) and endplate fracture (right; arrow) after device removal.

SUMMARY

In the absence of any formal test standards for spinal arthroplasty devices, the methods employed in this study provide a reasonable and quantitative means by which to evaluate the positional stability of such devices. Although the results of this in vitro study cannot be used to predict clinical outcomes, they do demonstrate positional stability of the PDN-SOLO prosthetic disc nucleus device and reflect the positive clinical experience to date with this device. Additional testing, utilizing the methods developed in this study, is needed to assess the positional stability of other device designs.

REFERENCES

Adams & Hutton (1982) *Spine* **7(3)**:184-91

Adams & Hutton (1985) *Spine* **10(6)**:524-31

ASTM (2003) F2077: Test Methods for Intervertebral Fusion Devices, vol. 13.01

Hale et al. (2003) *Proceedings of American Society of Biomechanics.*

ACKNOWLEDGEMENTS

Financial support for this study was provided by Raymedica, Inc.

DOES SUSTAINING A LOWER EXTREMITY STRESS FRACTURE ALTER LOWER EXTREMITY MECHANICS IN RUNNERS?

Clare E. Milner[1], Irene S. Davis[1,2] and Joseph Hamill[3]

[1] Department of Physical Therapy, University of Delaware, Newark, DE, USA
[2] Joyner Sportsmedicine Institute, Lexington, KY, USA
[3] Department of Exercise Science, University of Massachusetts, Amherst, MA, USA
E-mail: milner@udel.edu Web: http://www.udel.edu/PT/davis/Lab.htm

INTRODUCTION

Stress fractures are common in runners, particularly in females who sustain approximately twice as many as males. A stress fracture is one of the most serious running injuries, requiring six to eight weeks rest from running, and the risk of reinjury is high. The risk of reinjury may be up to 36%, compared to between 1% and 21% risk of initial stress fracture (Hauret et al., 2001). There is some evidence that stress fractures are related to running gait mechanics. In cross-sectional studies, runners who had sustained a stress fracture had higher instantaneous loading rate (ILRZ) and peak tibial shock (PPA) and reduced knee flexion excursion (KEXC). The effect of a previous stress fracture on running mechanics is unknown and could be a factor in the high rate of reinjury in this group.

The aim of this study was to determine whether pre-injury running mechanics are altered following the occurrence and recovery from a lower extremity stress fracture. In addition, impact peak (IPEAK) and braking load rates (ILRY, ALRY) will be examined, as they may also be linked to injury in runners. It was expected that the magnitudes of ILRZ, PPA and KEXC that have been related to stress fracture would be present prior to the injury, and that they would remain the same post injury.

METHODS

These data are part of an ongoing prospective study of female distance runners. Currently uninjured adult female runners, typically running at least 20 miles per week, are recruited into a two year longitudinal study. An instrumented gait analysis is performed on entry into the study. Subjects run overground at 3.7m/s in standard laboratory running shoes. Five trials are recorded using a six camera motion capture system at 120 Hz and a force platform and accelerometer at 960 Hz. Three-dimensional kinematics and kinetics are calculated for both lower extremities.

Subjects are then followed monthly for two years. Running mileage and injuries are tracked. All participants who sustain a stress fracture of the lower extremity are asked to return to the laboratory for a second instrumented gait analysis. The post-injury analysis is performed when they have recovered from injury and returned to at least 50% of their pre-injury mileage.

To date, six runners (30±13 y, 24±12 mpw) have sustained a lower extremity stress fracture or tibial stress reaction. A tibial stress reaction is operationally defined as bone pain and tenderness located over a diffuse area of several centimeters. The pain is alleviated by rest and worsens with continued running. Essentially this is the early stage of development of a full stress fracture and will likely progress to fracture if the training load is not removed (Batt et al., 1998). We have included stress reaction in this group as it indicates susceptibility to stress fracture. A control group of 6 uninjured runners matched for age and mileage (23± 8 y, 26±1 mpw) was also included. Comparisons were made between controls and injured runners' pre- and post-injury data. Statistical analyses were not conducted due to the small sample size.

RESULTS AND DISCUSSION

Using a 15% change as being clinically relevant, several variables showed a notable increase following stress fracture in these runners (Table 1). ILRZ and PPA were higher in the stress fracture group compared to controls prior to injury. In addition, ILRZ and PPA became notably higher post-injury in the fracture group. Since stress fractures are essentially fatigue fractures of the bone, their occurrence relates to the load per cycle and the number of cycles. Increasing either of these factors increases the risk of exceeding the fatigue limit of the tissue. ILRZ and PPA indicate the magnitude of compression loading per cycle, therefore higher values indicate increased risk.

Table 1: Changes in selected variables following a lower extremity stress fracture or reaction in female runners (mean ± SD).

	CTRL	PRE	POST
ILRZ (BW/s)	97.7	120.20#	146.19*
PPA (g)	5.22	9.10#	10.88*
KEXC (º)	35.5	34.4	32.1
IPEAK (BW)	1.55	1.87#	1.96
ILRY (BW/s)	34.00	39.13#	50.74*
ALRY (BW/s)	7.10	7.04	11.13*

Greater than 15% difference between control and pre-injury.* Greater than 15% change pre- to post-injury.

These data suggest that runners who sustain a stress fracture have a more risky gait prior to injury and are adopting an even more risky gait following recovery from stress fracture. This finding may explain the high incidence of reinjury following a lower extremity stress fracture in runners.

Of the additional variables studied, both ILRY and ALRY increased notably following recovery from stress fracture. ILRY was also increased compared to controls in the fracture group prior to injury. These shear loading rates indicate the magnitude of bending loads that the lower extremity is subject to, in addition to the compressive loading that occurs during initial weight acceptance in stance. It has been shown that anterior-posterior bending strength is related to the risk of tibial stress fracture (Milgrom et al., 1989). Therefore, the magnitude of anterior-posterior loading rates may be directly related to stress fracture. The secondary planes of ground reaction force are often overlooked in gait analyses, but these substantial changes indicate that they are worthy of further investigation in relation to stress fracture injuries in runners.

SUMMARY

Runners who sustain a lower extremity stress fracture have higher lower extremity load rates and shock prior to injury in comparison with controls. Post-injury subjects adopted a more risky gait, with further increases in lower extremity load rates and shock.
These preliminary data suggest that interventions to reduce loading post fracture need to be developed.

REFERENCES

Batt, M.E. et al. (1998). *Med. Sci. Sports Exerc.*, **30**, 1564-1571.
Hauret, K.G. et al. (2001). *Military Med.*, **166**, 820-826.
Milgrom, C. et al. (1989). *J. Biomechanics*, **22**, 1243-1248.

ACKNOWLEDGEMENTS

Supported by Dept of Defense grant DAMD17-00-1-0515.

THE RELATIONS BETWEEN MUSCLE STRENGTH AND MOVEMENT OF CENTER OF MASS OF THE BODY DURING OBSTACLE NEGOTIATION IN THE COMMUNITY-DWELLING OLDER ADULTS

Hsiu-Chen Lin[1], Shu-Ya Chen[1], Hong-Wen Wu[1], Ching-Sheng Li[1], Hui-Fen Pan[1], Horng-Chaung Hsu[2]

[1] School of Physical Therapy, China Medical University, Taichung, Taiwan
[2] Department of Orthopedics, China Medical University Hospital, Taichung, Taiwan
E-mail: hclin@mail.cmu.edu.tw

INTRODUCTION

Tripping by an obstacle is an activity that causes highly incidence of falls in the elderly. Muscle strength of lower extremity has been proved as an index to predict the risk of falling (Daubney, 1999). The improved muscle strength can enhance the performance in obstructed gait for the community-living older adults (Lamoureux, 2003). However, limited studies established the relationships between the muscle strength and the controlled movements of the body. The purpose of this study was to investigate the relationships of the maximal muscle strength of the body and the movements of center of mass (COM) of the body during crossing the obstacles withdifferent heights in the community-dwelling older adults.

METHODS

Twenty community-dwelling older adults aged over 65 (77.58±5.92 yrs) were recruited with informed consent. The maximal voluntary isometric contractions (MVIC) of trunk flexor and extensor, knee flexors and extensors, ankle dorsiflexors and plantarflexors were measured by a Nicholas hand-held dynamometer. Thirty-nine reflective markers were then placed on head, trunk, upper extremities, pelvis, and lower limbs to define the movements of each segment. A seven-camera motion analysis system (VICON 370, Oxford Metrics, UK) was used to collect 3D kinemetic data of the body, and a 15-linkage human model was used to calculate the trajectory of whole body's COM. An adjustable obstacle was positioned in the middle of the 10-meter walkway. The subjects were then asked to walk with their self-selected paces and perform stepping over the obstacles with four different heights (0, 10, 20, 30 percent of leg length). At least 3 trials of the movement data for each limb and each condition were collected. Maximum movement ranges, velocities, and accelerations of the body's COM trajectories in medial-lateral and up-down directions were extracted as dependent variables for the regression analysis with the maximal muscle strengths.

RESULTS AND DISCUSSION

The significant correlation with the maximum movement ranges and maximal velocities of the body COM were found mostly in the ankle muscles of the leading leg for the 10% condition. When crossing the higher obstacles, more muscles around the knee and trunk were found to be required (Fig. 1). These results implied that more muscle groups were recruited to control the movements of the body COM while crossing the higher obstacles.

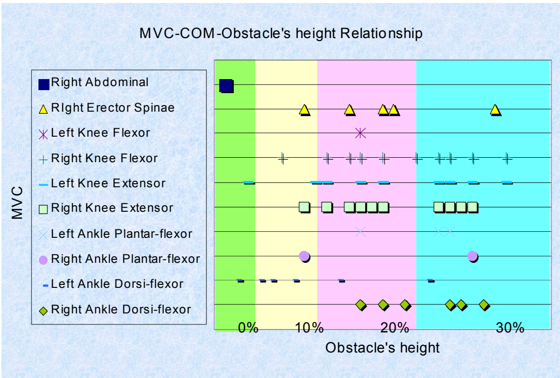

Figure 1: The significant correlations of the MVICs of the muscles in the lower body and the variables of body COM when crossing the obstacles with different heights.

We also noticed that the significant correlations were most likely occurred between MVIC of the leading leg and the maximal velocities of the body COM, rather than maximal displacements or accelerations, during crossing the obstacles (Fig. 2). It indicated that the adjustments and adaptations of the obstacle-walking came from the muscles mainly changed, accordingly to the obstacle heights, the velocities of the body's movement to successfully complete the tasks.

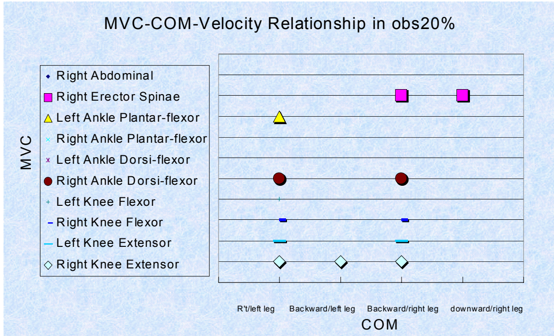

Figure 2: The correlation of MVICs and the velocities of body COM during crossing the obstacles with 20%LL height.

SUMMARY

The results suggested that more muscles were required to control the movements of the body COM while crossing the higher obstacles. The muscle strength can affect the performance of the challenging tasks. Clinical professionals should pay more attention for the deficits of muscle strength in obstacle negotiation for older adults.

REFERENCES

Daubney M.E., Culham E.G., (1999). *Phys Ther*, **79**, 1177-1185.

Lamoureux E., et al. (2003) *Gait & Posture*, **17**, 276-283.

ACKNOWLEDGEMENTS

The authors would like to thank for the financial support from National Science Council of Taiwan.

COMPARING NORMAL GAIT ANALYSES USING CONVENTIONAL AND LEAST SQUARES, SIX DEGREE-OF-FREEDOM MODELS

Frank L. Buczek, Ph.D., Michael J. Rainbow, B.S., Kevin M. Cooney, P.T., Matthew R. Walker, M.Sc., James O. Sanders, M.D.

Motion Analysis Laboratory, Shriners Hospitals for Children, Erie, PA, USA
E-mail: fbuczek@shrinenet.org

INTRODUCTION

The conventional gait model (HH) is widely used in clinical settings, and reflects several models common since the early 1980s (Baker and Rhodda, 2003). Principle weaknesses in this approach include the use of markers on one segment to define virtual markers that track adjacent segments in a mathematically exact solution, and the use of a simple vector to represent the foot. In contrast, a least squares, six degree-of-freedom (LS-6DOF) approach uses an over-determined set of physical markers to track individual segments while accounting for measurement error (Cappozzo, 1991; Spoor and Veldpaus, 1980). A least squares approach may also have benefits in muscle modeling (Kuo, 1998; Thelen, 2003). The purpose for this IRB approved study was to compare 20 gait analysis variables across HH and two LS-6DOF models in normal subjects. We hypothesized that these latter approaches would provide data similar to HH in the sagittal plane, and different from HH in the coronal and transverse planes.

METHODS

All biomechanical models were created in Visual3D (C-Motion, Inc., Rockville MD, USA). The HH approach was implemented using the Helen Hayes option for the lower extremities and pelvis. The first LS-6DOF approach (6H) began with the HH model, but tracked segments using a minimum of four physical markers on each body segment. The second LS-6DOF approach (OPT) began with 6H, but added upper body segments, and changed the definition for the hip and ankle centers. (The hip was located medially one proximal thigh radius from the greater trochanter, and the ankle was located distal to the midpoint of the malleoli as in Buczek, et al., 1994.) A hybrid marker configuration allowed a single stride to be analyzed using HH, 6H, and OPT models in each of 25 normal subjects. Marker trajectories were collected at 120 Hz using a ten-camera Vicon 612 system (Oxford Metrics Group, Oxford, England), with cubic-spline interpolation and low-pass filtering (6 Hz cutoff) accomplished in Visual3D. Ground reaction forces were collected at 1560 Hz using three strain-gauge force plates (OR6-7, Advanced Mechanical Technology, Inc., Watertown MA, USA) and were analog low-pass filtered at 1050 Hz. Twenty gait analysis variables were compared across the three models. Dependent t-tests were used to detect differences in these hip, knee, and ankle angles, moments, and powers, in two families of comparisons: HH vs. 6H, and HH vs. OPT. A Bonferroni-adjusted alpha of 0.0025 (that is, 0.05/20) maintained the family-wise Type I error rate at $p \leq 0.05$.

RESULTS AND DISCUSSION

Due to space restrictions, tabular results of statistics will not be presented. Instead, results will be discussed in general terms, with a few sample figures illustrating noteworthy trends.

Comparison of HH and 6H models demonstrated changes due to the method of tracking body segments. Most differences were attributed to the higher fidelity foot model in 6H, and to a more anterior position of the knee center when tracked by a shank cluster in 6H rather than a lateral knee marker in HH. (This marker moved posterior to the femoral epicondyles when the knee was flexed.) Twelve of 20 comparisons were significantly different, but sagittal plane differences were not always appreciated in graphical data. For example, ankle plantarflexion at push-off was significantly greater for 6H than HH (-19.5 ± 8.8 vs. -14.6 ± 6.3 deg), as were maximum plantarflexion moment (1.40 ± 0.247 vs. 1.37 ± 0.019 Nm/kg) and maximum power generation (3.66 ± 1.22 vs. 3.03 ± 1.03 W/kg), yet little clinical difference could be discerned in the moment data (Figure, panels a - c). In general, coronal and transverse plane angles differed graphically but not statistically (due to increased variability), while moment and power data differed significantly for some variables. The OPT model resulted in a hip center generally more posterior to that for HH, and an ankle center more inferior. Eleven of 20 comparisons were significantly different for HH vs. OPT, and some of these compensated for differences due to tracking alone (6H). Additional interpretations are too numerous to be listed here.

SUMMARY

Our hypotheses were partially supported, with significant differences found in all three anatomical planes, some of which were not appreciated graphically. Future work will focus on accuracy assessments, and the effects of LS-6DOF kinematics on muscle modeling.

REFERENCES

Baker R., Rhodda J. (2003) *Proc. of the GCMAS*, Wilmington DE, May 7.

Buczek F.L., et al. (1994) *J. Biomechanics*, **27**(12), 1447-1457.

Cappozzo A. (1991) *Human Movement Science*, **10**, 589-602.

Kuo A.D. (1998) *J. Biomechanical Engineering*, **120**(1): 148-159.

Spoor C.W., Veldpaus F.E. (1980) *J. Biomechanics*, **13**, 391-393.

Thelen D.G. (2003) *Proc. Amer. Soc. Biomechanics*, Toledo OH, Sep 26.

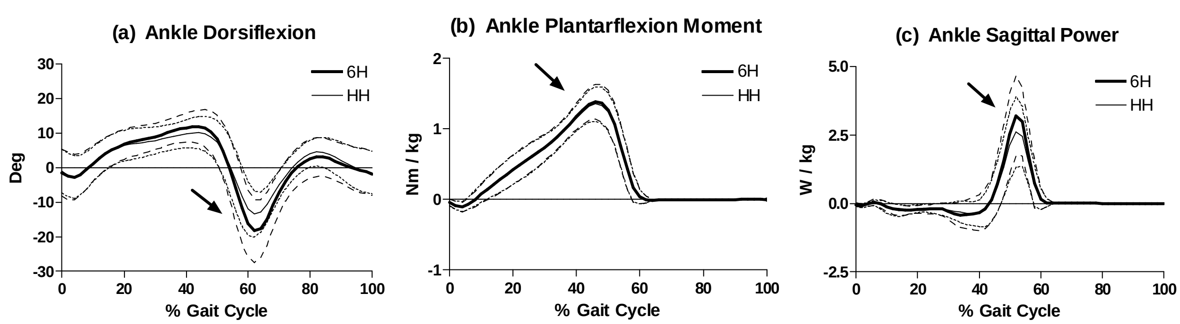

Figure. Ensemble average ankle data (n = 25), with means (solid lines) plus or minus one standard deviation (dashed lines). Panels (a) – (c) report HH vs. 6H comparisons for sagittal plane ankle angle, intrinsic moment, and power, respectively. Arrows indicate areas where significant differences were obtained via dependent t-tests. These were graphically (and clinically) less obvious for the peak plantarflexion moment, panel (b).

EFFICACY AND KINEMATIC CHARACTERISTICS OF TWO NEW CERVICAL ORTHOSES

Songning Zhang [1], Michael Wortley [1], Kurt Clowers [1] and John H. Krusenklaus [2]

[1]Biomechanics/Sports Medicine Laboratory, The University of Tennessee, Knoxville, TN, USA
[2]Tennessee Sports Medicine Group, Knoxville, TN, USA
E-mail: szhang@utk.edu

INTRODUCTION

Physicians often prescribed cervical collars for extrication stabilization of trauma patients and as a treatment option for injuries to the cervical spine. Miami J, Aspen and Philadelphia cervical orthoses are among the most studied collars in the literature (Askins and Eismont, 1997; Sandler, et al., 1996). However, effectiveness of cervical collars in the literature is often shown with large variation in ROM values. Moreover, studies do not commonly provide sufficient information about control of experiment, randomization of test conditions, numbers of trials per test condition, and experimental setup. These may be related to inconsistent results in cervical orthoses literature. Therefore, the main purpose of this study was to examine and compare the efficacy of two new cervical collars with two established collars in restricting range of motion in cervical spine movements with emphasis on experimental controls.

METHODS

Twenty healthy subjects (age: 24.0 ± 2.4 yrs) with no impairments to their spine at the testing time and no history of major spinal pathology participated in the study with ten males and ten females. A three-dimensional (3D) analysis system (120 Hz, Vicon) was used to obtain 3D kinematic data. Three spherical retroreflective markers were placed on the anterior maxilla (CHN), the forehead (FRHD), and the top of the head (CRN) with the FRHD and CRN markers placed on the corresponding positions on a plastic helmet that was affixed to the head of using a rubber band to ensure a stable helmet attachment to the head. The 3D angular kinematic data were computed using an adapted method (Areblad, et al., 1990).

Four cervical collars were tested: two new cervical orthoses, C-Breeze® (CB) and XTW (Philadelphia Cervical Collar Company, Thorofare, New Jersey) and two established orthoses, Miami J® (MJ) (Jerome Medical, Moorestown, New Jersey) and Aspen® (AS) (Aspen Medical Products, Long Beach, California). The same investigator applied all cervical collars to all subjects according to the instruction manual provided by the manufacturers. In the test session, kinematic data was collected with subjects wearing no collar (unbraced) and the four collars performing three different head/neck movements: flexion-extension, left-right lateral flexion, and left-right axial rotation, in 15 test (randomized) conditions. Each collar was discarded after single use to maintain material integrity. Gender and collar differences on selected ROM variables were examined using a one-way repeated measures ANOVA with post hoc comparisons ($p < 0.05$).

RESULTS AND DISCUSSION

The post hoc comparisons indicated that all four braces had significantly reduced ROMs in all movements compared to the unbraced conditions (Table 1). The XTW showed less restriction in flexion than the MJ and CB. All these three collars had less ROM in extension compared to the MJ. For the same movement, the XTW performed better than the CB and AS. Furthermore, the CB showed less ROM than the MJ in lateral bending (flexion). In addition, the CB, AS and XTW all had less ROM in axial rotation than the MJ.

Table 1. Average ROM (deg) during the cervical movements: mean ± SD.

Brace	Flex	Extend	L. Flex
Unbraced	56.0±7	68.6±13	83.5±11
MJ	8.5±8 [a]	31.1±17 [a]	51.5±15 [a]
CB	9.6±7 [a]	27.2±16 [a,b]	46.3±15 [a,b]
AS	11.6±11 [a]	26.2±16 [a,b]	46.6±15 [a]
XTW	12.5±9 [a,b,c]	23.0±14 [a,b,c,d]	45.3±15 [a]

[a] – significantly different from unbraced; [b] – significantly different from MJ; [c] – significantly different from CB; [d] – significantly different from AS

The MJ and CB showed significantly greater percent reduction on flexion ROM than the XTW collar (Table 2). For extension and lateral flexion, all these three collars showed greater percent ROM reduction than the MJ. The XTW also showed greater reduction than the CB and Aspen in extension. Finally, only the CB showed a significantly greater reduction in axial rotation than the MJ.

Table 2. Average percent ROM reduction compared to the unbraced movements: mean ± SD.

Brace	Flex	Extend	L. Flex	Rot
MJ	84.8±14	55.5±20	37.9±17	65.4±15
CB	82.9±13	60.8±20 [1]	44.6±16 [1]	69.6±12 [1]
AS	79.7±18	62.5±19 [1]	44.0±16 [1]	67.4±15
XTW	77.9±16 [1,2]	67.0±17 [1,2,3]	45.5±17 [1]	68.1±14

[1] – significantly different from MJ; [2] – significantly different from CB; [3] – significantly different from AS

The raw and percent ROM values from this study are within the ranges of ROM data reported in previous studies (Askins and Eismont, 1997; Sandler, et al., 1996).

Further analyses suggested that the CB collar demonstrated more superior immobilization in extension, lateral bending and axial rotation than the MJ. The XTW and AS collars also showed greater restriction than the MJ in extension and lateral bending. On the other hand, the MJ and CB orthoses showed greater ROM reduction in flexion than the XTW. The XTW collar showed better capacity in restricting ROM than all other three collars in lateral bending. An analysis on the materials and design of the four collars showed some improved features for the CB and/or XTW compared to the MJ and/or AS, which include greater fastener strap surface area, stiffer and lighter plastic body, improved comfort, and better sizing selection.

SUMMARY

The results suggested that the two new cervical orthoses, C-Breeze and XTW collars, along with the two widely used Miami J and Aspen, are effective in restricting ROMs in the cervical spine. The performance of the C-Breeze and XTW cervical orthoses are comparable or better than what was reported in previous studies for the Miami J and Aspen collars (Askins and Eismont, 1997; Sandler, et al., 1996).

REFERENCES

Areblad, M., et al. (1990). *J Biomech*, **23**, 933-940.

Askins, V. and Eismont, F. J. (1997). *Spine*, **22**, 1193-1198.

Sandler, A. J., et al. (1996). *Spine*, **21**, 1624-1629.

ACKNOWLEDGEMENTS

Sponsored by DeRoyal Industries, Inc.

KNEE JOINT KINETICS AND LOWER EXTREMITY MUSCLE ACTIVATION DURING FRONT AND BACK SQUATS

Mark D. Tillman, Jon C. Gullett, Gregory M. Gutierrez, and John W. Chow

Center for Exercise Science, University of Florida, Gainesville, Florida
Email: mtillman@hhp.ufl.edu

INTRODUCTION

Most activities of daily living require the coordinated contraction of several muscle groups simultaneously. Squats require this type of synchronization and are considered one of the most functional and efficient weight-bearing exercises whether an individual's goals are sport specific or are for an increased quality of life (Lutz et al., 1993). Because a strong and stable knee is extremely important to an athlete's or patient's success, an understanding of knee biomechanics while performing the squat is helpful to therapists, trainers, and athletes alike (Escamilla, 2001).

Two forms of the squat lift are the back squat and the front squat. Strength and conditioning professionals have recognized the similarities between the lifts, but feel that these variations can be used to protect and isolate different muscle groups. It is believed that the front squat requires lower muscular force in the low back and may also isolate the quadriceps more than back squats. These beliefs are not supported by empirical evidence. The two primary purposes of this study were to determine which squat variation places the least force and torque on the knee and to examine the effects of front and back squats on primary as well as secondary muscle groups. More specifically, we compared the compressive forces, shear forces, and moments applied to the tibiofemoral joint, and lower extremity muscle activity as well.

METHODS

Nine healthy males and six healthy females (22.1 ± 3.6 yr, 171.2 ± 6.4 cm, 69.7 ± 6.2 kg) who were experienced at performing both front and back squats participated in this study. All subjects were free from orthopedic injuries that would have limited their ability to perform. To assess the electromyographic (EMG) activity of selected muscles [Rectus Femoris (RF), Vastus Lateralis (VL), Vastus Medialis (VM), Biceps Femoris (BF), Semitendinosis (ST), and lumbar Erector Spinae (ES)], six pairs of surface electrodes were attached to the right side of the body. The amplified EMG signals were sampled at 900 Hz using a Peak Motus® 2000 system. Three genlocked video cameras collecting at 60 Hz and a force plate collecting at 900 Hz were used to collect data for knee kinetics calculations. Subjects performed one of two variations of the squat exercise, chosen randomly, with their right foot on the force plate. For each trial, the subjects squatted a load of 70% of their pre-determined 1 repetition maximum lift. Subjects lifted nearly 90% of their body weight during the back squat and almost 70% of their body weight during the front squat. Two trials consisting of three repetitions each were performed for each squat variation being tested. The second repetition of each trial was used for subsequent analyses. Joint reaction forces and moments were calculated for the knee using an inverse dynamic analysis that combined the anthropometric, kinematic, and ground reaction force data. In order to calculate the average normalized EMG values, the raw EMG signals were full-wave rectified and divided by the corresponding maximum EMG value for that muscle. All EMG data were partitioned into ascending and descending phases.

In order to identify any potential differences between the front and back squat for the kinetic variables, separate paired t-tests with Bonferroni corrections were performed. EMG data for each of the six muscles tested were analyzed using a 2 x 2 (bar position x phase) repeated measures MANOVA with $\alpha = 0.05$.

RESULTS AND DISCUSSION

The back squat resulted in higher compressive forces on the knee (10.8 ± 2.1 N/kg) than the front squat (9.2 ± 1.5 N/kg) ($t_{14} = 3.661$, $P = 0.003$). Shear forces at the knee did not vary between the back and front squat ($t_{14} = -1.243$, $P = 0.234$). Extension moments at the knee did not vary between the two types of squats ($t_{14} = 1.284$, $P = 0.220$). Bar position did not influence muscle activity. Univariate tests indicated that all six muscles were more active ($P \leq 0.003$) during the ascent phase of the exercise (Figure 1). By decreasing the compressive force encountered while performing squats, the risk of osteoarthritis and pain may be reduced. Since the muscles monitored were equally active during the front squat while lifting a lighter load, it is presumable that the same workout can be achieved with less compressive forces on the knee. This information suggests that front squats could be advantageous for people with knee problems such as ligament and meniscus tears, and for general long-term joint health.

SUMMARY

The front squat was shown to be just as effective as the back squat in terms of overall muscle recruitment, with significantly less compressive forces on the knee. This suggests that front squats may be more beneficial for certain individuals.

REFERENCES

Escamilla (2001). *Med Sci Sports Exercise*, 33(1), 127-141.

Lutz et al. (1993). *J Bone Joint Surg Am*, (75), 732-739.

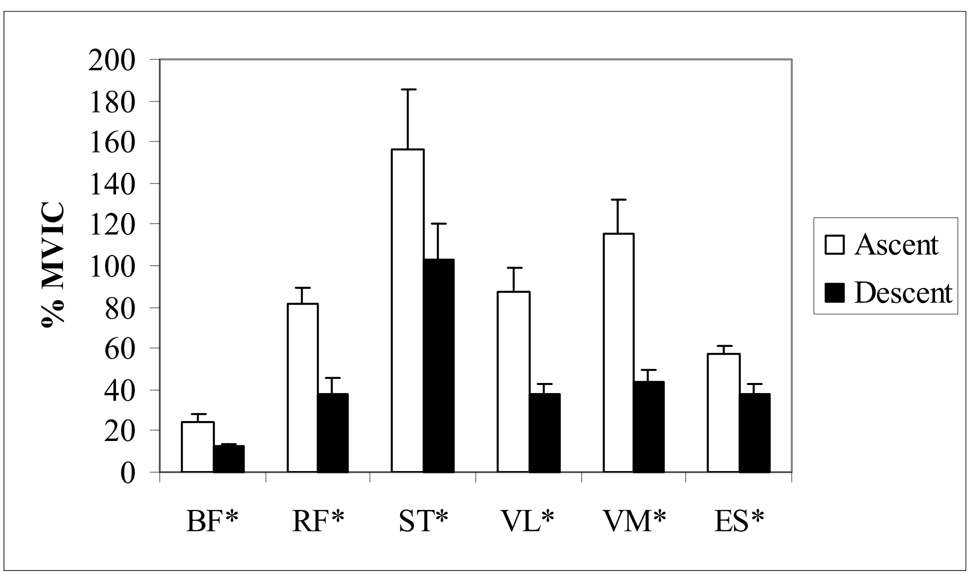

Figure 1. Average muscle activity during the ascending and descending phases of the squat as a percentage of maximal voluntary isometric contraction (%MVIC). *Significant difference between phases (p<0.05).

DISPLACED OLECRANON FRACTURES IN CHILREN: A BIOMECHANICAL ANALYSIS OF FIXATION METHODS

Stefan Parent[1], Michelle Wedemeyer[1], Megan Anderson[2], Fran Faro[2], Andrew Mahar[1,2], Francois Lalonde[1], Peter Newton[1,2]
amahar@chsd.org

[1] Department of Orthopedics
Children's Hospital, San Diego
San Diego, CA, USA

[2] Department of Orthopaedic Surgery
University of California, San Diego
San Diego, CA, USA

INTRODUCTION

Olecranon fractures (Figure 1) represent about 5% of all pediatric elbow fractures, yet complications may result from the injury or the surgical approach.

Figure 1: Displaced olecranon fracture.

Several methods of fixation have been proposed for treating these fractures including metallic wire tension bands or use of a lag screw with or without metallic wire. In children, a lag screw across the open physis may cause growth arrest so surgeons utilize a physis-sparing technique using dual smooth Kirschner wire insertion with tension band wiring. With this technique, the fracture is first reduced with two Kirschner wires. A wire is passed transversely through a hole drilled in the posterior aspect of the ulna distal to the fracture site. The wire is then tightened around the projecting heads of the Kirshner wires as a tension band. (Figure 2)
While this surgical technique has proven clinically efficacious, a second surgery is

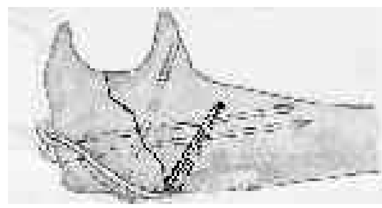

Figure 2: Tension band technique

required for wire removal due to its subcutaneous position. The use of resorbable suture material as the tension band has been previously proposed to obviate the second surgery and is currently in use at this facility. Despite casting, muscular contractions are still possible and may cause loss of fracture reduction. Thus, questions remain regarding the ability of two materials to apply articular compression and the ability of these materials to resist deformation during low and high muscle loads. Therefore, the purpose of this study is to (1) determine differences in intraoperative compression during fracture reduction, and (2) determine differences in fracture stabilization following cyclic physiologic loading during two load levels.

METHODS

To evaluate intra-articular compression, ten synthetic ulnas were randomly assigned to either wire or suture tension band groups. Identical olecranon fractures were created using a custom cutting jig. A compression only load cell was then inserted at the fracture surface prior to stabilization. Compression force (N) data were sampled at 5Hz for the duration of wire insertion as well as wire/suture knot tightening. The maximum compression and residual compression (amount of compression following surgical completion) were compared with a one-way ANOVA ($p<0.05$)

To evaluate biomechanical stability, nineteen fractured synthetic ulna models were randomly assigned to either wire (18 gauge stainless steel) or suture (#2 Vicryl) tension band constructs. These were further divided between low and high load groups. All repairs were completed by the same orthopedic surgeon using standard techniques Each repair was placed in a custom loading rig inside a mechanical testing machine (Figure 3).

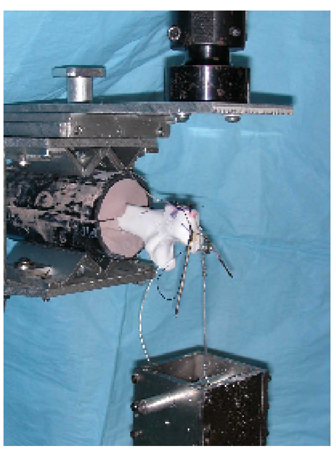

Figure 3: Test setup

Loads were delivered to the olecranon via a wire simulating the triceps brachii muscle. Fracture separation was measured using a linear voltage displacement transducer placed across the dorsal aspect of the fracture site. The low load group cycled loading from 0-10N for 100 cycles followed by a failure test at 0.5mm/sec. The high load group experienced cycled loading from 0-100N for 100 cycles followed by a failure test at 0.5mm/sec. Data for fracture separation (mm) and load (N) were sampled at 5Hz during each test. Displacement due to cyclic loading (mm) and failure load (N) were statistically compared using a two-way ANOVA ($p<0.05$) with a Tukey's *post-hoc* correction test.

RESULTS

Maximum compression achieved using a wire tension band (208±35N) was significantly greater ($p<0.025$) than the maximum compression achieved using suture (134±48N). The residual force was statistically greater ($p<0.004$) for the wire group (60±13N) compared to the suture group (28±11N). There was no difference in fracture displacement between groups during low physiologic loads with both displacements less than 0.1mm. However, the suture group (1.4±0.8mm) had significantly greater ($p<0.001$) displacement compared to the wire group (0.07±.2mm) during high load tests. Failure loads were significantly greater ($p<0.001$) for the wire group for both load settings. (Figure 4)

Figure 4: Failure loads

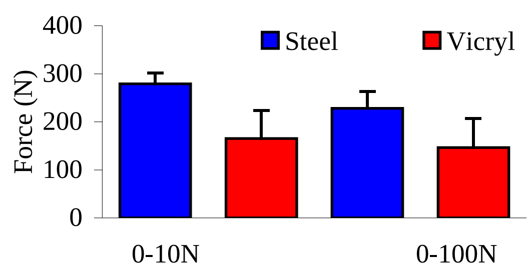

DISCUSSION

The suture tension band had lower ultimate failure loads and produced less compression at the fracture site. However, if low loads are expected or if the fracture is reduced easily, the suture tension band may be an appropriate alternative to the wire method.

ACKNOWLEDGEMENTS
This study was funded in part by the Children's Hospital Orthopedic Research and Education Fund.

IS THE THUMB A FIFTH FINGER?

Halla Bjorg Olafsdottir [1], Mark L. Latash [1], and Vladimir M. Zatsisorsky [2]

[1] Motor Control Laboratory and [2]Biomechanics Laboratory, Department of Kinesiology,
The Pennsylvania State University, State College, PA, 16802 USA
E-mail: hbo101@psu.edu, Web: www.personal.psu.edu/faculty/m/l/mll11/index.htm

INTRODUCTION

Previous studies of finger interaction during maximal (MVC) and submaximal force production tasks (Li et al. 1998a,b; Zatsiorsky et al. 1998, 2000) revealed three characteristics of finger interaction: (1) Sharing (total force is shared among the fingers in a stable way); (2) Force deficit (FD, peak force produced by a finger in a multi-finger task is smaller than its peak force in a similar single-finger task, see also Ohtsuki, 1981; Kinoshita et al. 1995) and (3) Enslaving (voluntary force production by a finger leads to involuntary force production by other fingers of the hand, see also Kilbreath and Gandevia, 1994).

The thumb is special among human hand digits. Its muscular apparatus does not involve multi-digit, multi-tendon muscles. Its mobility is different: It can act in parallel or in opposition to the fingers. In this study we investigated whether indices of digit interaction between the thumb and the fingers differ from those that describe interaction of the fingers among themselves, and whether these indices depended on the thumb position with respect to the fingers.

METHODS

Apparatus:: Six unidirectional piezoelectric force sensors (208C02, PCB Piezotronics, Depew, NY) were attached to a horizontal wooden board. Four sensors (for the index, middle, ring and little fingers) were positioned on the top of the board such that each finger could rest comfortably on a sensor. Two sensors were used to measure thumb force when it acted in parallel and in opposition to the fingers. During its action in parallel to the fingers, the thumb was abducted 45°. During its action in opposition, the thumb sensor was placed at the bottom of the board aligned with the middle finger.

Experimental Procedure: Subjects (n=12; 6 males and 6 females, all right-handed) sat on a chair, resting the right forearm on a foam pad attached to the armrest of the chair. The wrist was supported, and the proximal part of the palm rested on a wooden bar attached to the board. The upper arm was at 30° abduction and 10° of flexion, the elbow was at 120° flexion, the wrist was at 20° extension, the metacarpophalangeal joints were in a neutral position while the interphalangeal joints were at 20° of flexion. Subjects were instructed to produce maximal voluntary force (MVC) by pressing on the force sensors with subsets of digits. For each thumb position, 21 digit combinations were used. EMG was used to check for possible muscle co-contraction.

RESULTS AND DISCUSSION

The thumb produced much higher peak force when it acted in opposition to the fingers and showed a dramatic increase in its share of the total force in the five-digit test (Fig 1). The other digits also produced somewhat higher forces when the thumb acted in opposition. In the five-digit task, the fingers decreased their shares when the thumb acted in opposition but showed unchanged sharing between the two thumb positions in the four-finger task.

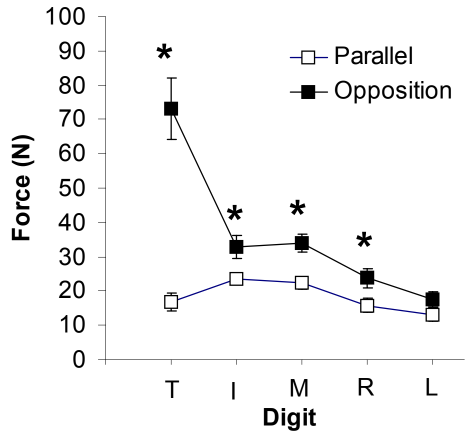

Figure 1. MVC in a five-digit task.

Enslaving during multi-digit tasks increased significantly when the thumb acted in opposition, however, these effects were not seen in single-digit tasks. FD was high when the thumb acted in parallel and showed an increase with the number of task digits up to four but dropped in the five-digit task (Fig 2). FD was very small when the thumb acted in opposition. For both thumb positions, the indices of digit interaction showed no differences between groups of digits that did or did not include the thumb.

The fact that including or not including the thumb in a task, had no effect on the indices of digit interaction, indicates that for a given configuration of the hand the central nervous system treats the thumb as a fifth finger. These results provide strong support for the central (neural) origin of interactions among digits of the human hand. We modeled the data using a force mode approach (Danion et al. 2003). The model showed a small error (2.1 N) for the data when the thumb acted in parallel to the fingers, but a large error (over 6 N) when the thumb acted in opposition.

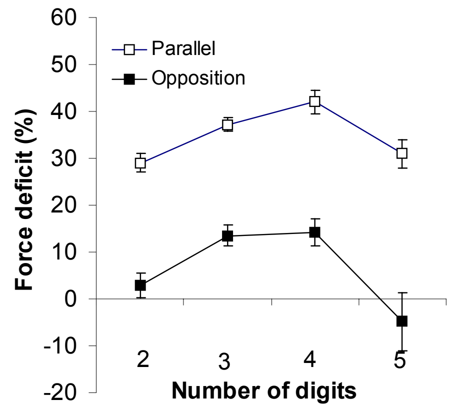

Fig.2. Force deficit in multi digit tasks.

REFERENCES

Danion, F. et al. (2003). *Biol Cybern*, **88**, 91-98.

Kilbreath S.L. et al (1994). *J Physiol,* **47,** 487- 497.

Kinoshita, H. et al. (1995). *Ergonomics.* **38,** 1212-1230.

Li Z-M. et al. (1998). *Exp Brain Res,* **119,** 276-286.

Li Z-M. et al. (1998). *Exp Brain Res,* **122,** 71-78.

Zatsiorsky V.M. et al. (1998). *Biol Cybern,* **79,** 139-150.

Zatsiorsky V.M. et al. (2000). *Exp Brain Res,* **131,** 187-195.

ACKNOWLEDGEMENTS

AR-048563, AG-018751 and NS-35032 from NIH.

BIOMECHANICAL COMPARISON OF AN INTRA- CORTICAL FIXATION ANCHOR VERSUS STANDARD ANCHOR FIXATION FOR ROTATOR CUFF REPAIR

Andrew Mahar[1,2], Darin Allred[2], Gaurav Abbi[2], Michelle Wedemeyer[1], Robert Pedowitz[2]

[1] Department of Orthopedics
Children's Hospital, San Diego
San Diego, CA

[2] Department of Orthopaedics
University of California, San Diego
San Diego, CA

INTRODUCTION

The integrity of the rotator cuff after repair is a major determinant of a good functional result. Clinical studies have demonstrated that greater than fifty percent of repairs involving more than just the supraspinatus tendon have been left with residual deficiencies.

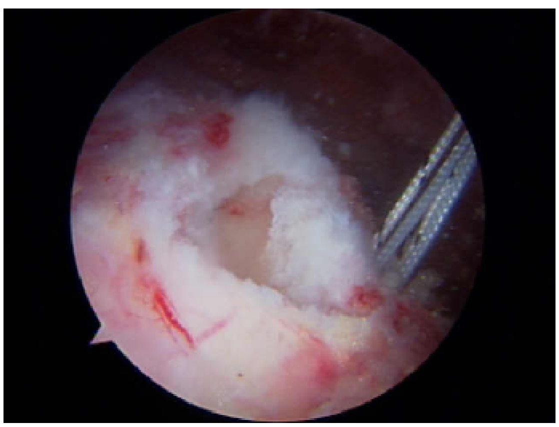

Figure 1: Arthroscopic view of partial thickness rotator cuff tear.

Many different modes of failure of suture anchors have been identified. Failure may occur by anchor displacement or pullout, suture breakage, knot slippage, or suture pulling though the tendon. New devices and suture material are under development to eliminate the clinical problems mentioned above. This study compares the fixation strength of an anchor designed for intra-cortical fixation to the fixation strength of standard anchors used for rotator cuff repair.

METHODS

Four types of suture anchors (n = 8 per group) were inserted into human cadaveric humeri in random order: the Arthrex FT (cortical fixation anchor), Mitek Fastin RC, Linvatec Super Revo and Smith and Nephew Twin Fix Ti 5.0. Anchors were placed in the human cadaver supraspinatus footprint to the manufacturer's recommended depth. After preconditioning to 10N, each construct was cycled between 10N and 60N for a maximum of 500 cycles at 0.5 Hz using a materials testing machine. If still intact, constructs were loaded at 0.5 mm/sec to failure. (Figure 1)

Figure 1: Example of test setup.

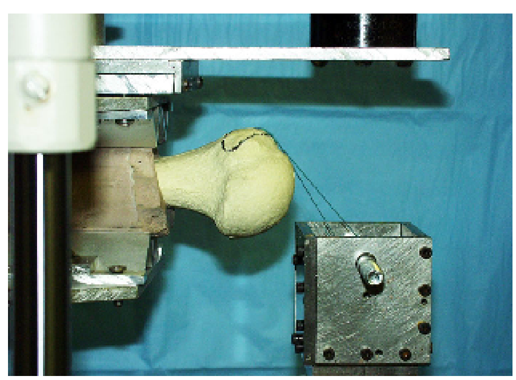

Force (N) and displacement (mm) were recorded throughout the experiment. The number of cycles, mode, magnitude, and location of failure was recorded for each specimen. The rotation (degrees) and displacement (mm) of the anchor within the bone was measured with image intensified fluoroscopy employing a radio-opaque device for image calibration. All mechanical and fluoroscopic data was analyzed using a one-way ANOVA ($p<0.05$) with a Tukey's *post-hoc* correction for multiple comparisons.

RESULTS

The intra-cortical fixation anchor had the greatest number of cycles to 3mm of failure (380±160). This was not significantly different than the Smith and Nephew anchor (331±190), however both values were significantly greater than both the Linvatec (114±47) and Mitek (54±53) anchors ($p<0.002$).

The intra-cortical fixation anchor (Arthrex FT) had a statistically significant greater failure load (140N±23) than the other devices ($p<0.02$). (Figure 2) There was no significant difference in failure load between the other three anchors.

Figure 2: Failure Loads

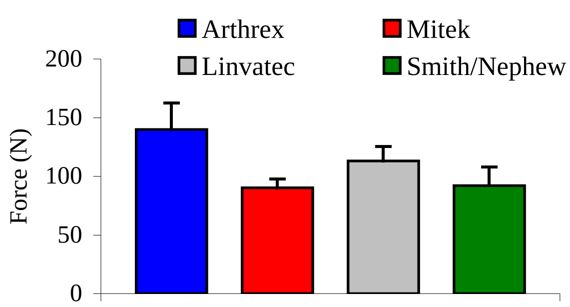

For the rotation calculated from fluoroscopy, there was no statistically significant difference between the anchors tested. The anchors exhibited a wide variability in angular change with a range from 1 to 70 degree change. Overall, the combined angular change for anchors was 16.6±17.8 degrees.

There was no statistically significant difference between the anchors tested for total displacement change with a range of 1.24mm to 2.48mm. Overall the average displacement across anchors was 1.7±1.6mm.

All anchors except the Arthrex anchors failed at the knot or the suture eyelet interface. The Arthrex anchors all failed by pulling out of the bone but employed a different type of suture material in their construct.

DISCUSSION

Intra-cortical fixation performed well compared to sub-chondral fixation in human cadaver bone. This anchor incorporates a recessed suture eyelet loop, which allows anchor placement flush with the cortical surface. Most previous studies utilize straight pull-out loads to test anchor fixation, however physiologic suture loads are oblique to the direction of anchor placement. In the present study, a clinically-relevant oblique cyclic loading protocol resulted in significant angular displacement as well as anchor translation with all of the anchors tested. This observation could explain some cases of early gap formation after rotator cuff repair.

ACKNOWLEDGEMENTS

This study was funded in part by a unrestricted research grant from Arthrex.

Age and Gender Differences in Arch Height and Arch Stiffness

Rebecca Avrin Zifchock[1] and Irene Davis[1,2]
[1]Motion Analysis Laboratory, University of Delaware, Newark, DE, USA
[2]Joyner Sportsmedicine Institute, Mechanicsburg, PA, USA
email: beckyaz@udel.edu web: http://www.udel.edu/PT/davis/Lab.htm

INTRODUCTION

The foot is a complex structure that is often difficult to classify. One common way to categorize the foot is using arch structure. Several methods have been used to classify the arch, including radiographs and footprints (Kanatli et al., 2001). Williams, et al. (Williams et al., 2000) proposed using Arch Height Index (AHI), a measure of arch height normalized to foot length. The method was shown to validly and reliably assess arch structure, however the study did not examine differences between males and females or among different age groups.

It has been previously shown that females have a greater tendency toward knee valgus during active loading (Ferber et al., 2003). An everted, or low-arched, foot may be linked to changes in alignment up the chain, which could internally rotate the knee, placing it into greater valgus (James et al., 1978). Therefore, females may also have lower, more everted arches. Females have also been shown to have increased ligament laxity (Wilkerson et al., 2000). This may be reflected in a decreased stiffness in the arches of females as compared to males.

A second factor that may be linked with arch structure is age. Arches are commonly thought to "fall" with age. Prince, et al., have suggested that physiological changes that occur with aging that may affect the structure and properties (such as stiffness) of the joints (Prince et al., 1997).

To date, there are no studies examining the difference in arch structure between males and females and among age groups. Understanding such differences could lend insight as to why injury biases exist.

Therefore, the purpose of this study is to identify whether there is a significant difference in the arch height and arch stiffness between genders and among age groups. It was hypothesized that females would have lower, less stiff arches and that arch height would decrease and arch stiffness would increase with age.

METHODS

This is an ongoing study of which sixty-nine subjects, 37 male and 32 female, between the ages of 20 and 59 gave consent to participate in this study, see Table 1.

Table 1: Age distribution of subjects

Age, yrs	20-29	30-39	40-49	50-59
males	10	9	8	10
females	10	8	7	8

Potential subjects with a history of neuromuscular conditions or diseases, gross foot deformities, or surgery that would affect the alignment of their feet were excluded from the study.

Portable platforms that raised the subject's feet 19mm off the floor were positioned to support each foot under the heel and metatarsal heads only. This eliminated the "floor effect" and allowed the arch to drop as much as the foot anatomy permitted. Total foot length and truncated foot length (the most posterior point on the foot to the 1st metatarsal head) was measured while seated. Dorsum height at ½ total foot length was measured while seated and standing. The arch height index (AHI), as described by Williams, et al. (Williams et al., 2000) was used to obtain a normalized value of arch height, in a dimensionless unit we call AHI units, for comparison between subjects:

AHI = dorsum height/truncated foot length

AHI was measured in a seated and standing condition to obtain a measure of arch stiffness (AS) in BW/AHI units:

$AS = \Delta$ load/ Δ AHI

where: Δ load = 50% BW – 10% BW

10% BW = weight of the leg

All comparisons were made using the data obtained for the dominant foot. Statistical comparisons between males and females were made using three independent t-tests: (1) Male versus Female standing AHI, (2) Male versus Female seated AHI, (3) Male versus Female AS. Comparisons among age groups were made using two one-way ANOVAs: (4) AHI among age groups as divided into decades, and (5) AS among age groups as divided into decades. All analyses were performed at $\alpha = 0.05$.

RESULTS AND DISCUSSION

Female's arches were significantly less stiff than those of males ($p = 0.001$). This finding is consistent with previous findings that report greater ligament laxity in females as compared to males (Wilkerson et al., 2000). AHI was not different between genders in either the seated or standing conditions.

Neither AHI nor AS were different among age groups. However, it is interesting to note that, in both the seated and standing condition, there is an apparent step-wise decrease AHI from the 30-39 to 40-49 to 50-59 age groups (see Figure 1). There is also an obvious drop in AS in the 50-59 age group. This is another surprising outcome, as stiffness is typically thought to increase with age.

SUMMARY

This study showed a significant gender difference is arch stiffness. However, no gender differences were found in arch height, and no differences (arch height or arch stiffness) were found among age groups. These data are part of an ongoing study, and it is possible that these results will change as subjects are added.

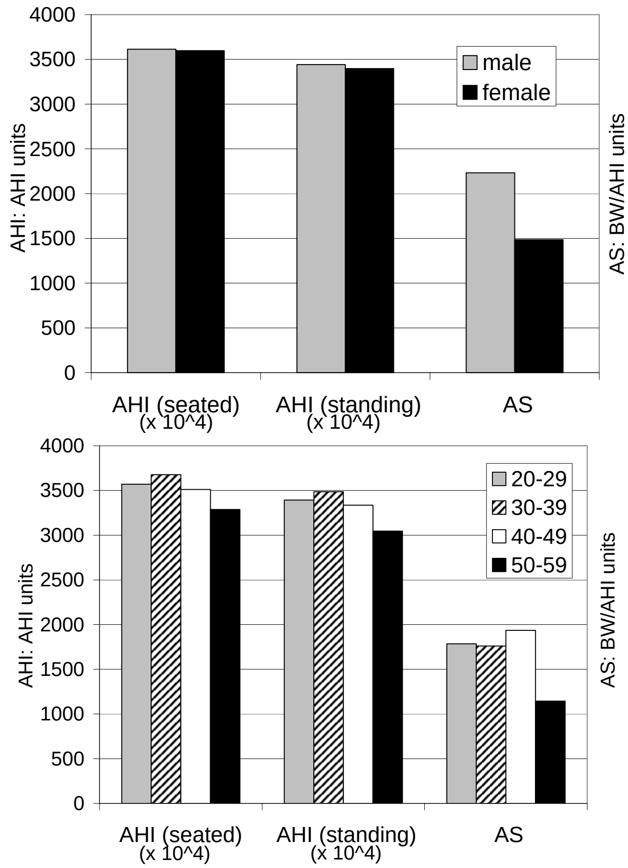

Figure 1: Gender and age comparisons of Arch Height Index and Arch Stiffness

REFERENCES

Ferber, R., et al., 2003. Clin Biomech 18(4), 350-357.

James, S. L., et al., 1978. Am J Sports Med 6(2), 40-50.

Kanatli, U., et al., 2001. J Ped Orth 21(2), 225-228.

Prince, F., et al., 1997. Gait Posture 5, 128-135.

Rozzi, S. L., et al., 1999. Am J Sports Med 27(3), 312-319.

Wilkerson, R. D. and M. A. Mason. 2000. Iowa Orthop J 20, 46-48.

Williams, D. S. and I. S. McClay. 2000. Phys Ther 80(9), 864-871.

ACKNOWLEDGEMENTS

The authors would like to thank John Willson for his help with data collection.

VARIABILITY IN THE GOLF SWING AND ITS EFFECT ON PERFORMANCE ACCURACY

Keith D.J. Fitzpatrick & Dr. Ross Anderson

Dept of Physical Education and Sport Science, University of Limerick, Limerick, Ireland.
E-mail: Keith.Fitzpatrick@ul.ie Web: www.ul.ie/~pess/

INTRODUCTION

A golf swing and its successful execution depends on the performance of a complex sequential action involving the feet and knees, rotation of the hips, trunk and shoulders and movement of the arms, wrists and hands (Richards *et al*., 1985). With the complexity of the motor skill there is a large scope for variability in the golf swing. Many journals have reported variability in various aspects or components of the swing for example; the timing of the golf swing angle of hip rotation and shoulder rotation throughout the swing (Burden *et al*., 1998), weight transfer patterns during the swing (Richards *et al*., 1985) and the speed of clubhead (Watanabe *et al*., 1998). Sanders and Owens (1992) showed variability in the position of the hub (the focal point of the clubhead during the swing).

Many researchers have found that the degree of kinematic variability (KV) is reduced in lower handicap golfers (Sanders & Owens 1992; Richards *et al*., 1985). This may indicate that a reduction in KV may be key to an improvement in performance. Many studies in the past have been limited to indoor research where the flight of the ball is restricted by the size of the laboratory (Egret *et al*., 2003) and as such the effect of this variability on the performance outcome remains unknown. The aim of this study is to investigate the correlation between KV of certain angular kinematic parameters and the performance variability (PV – i.e. the landing location of the ball) in golf.

METHODS

22 male national level golfers (mean handicap 7.5 ± 0.7; mean age of 14.9 ± 0.7) participated in the study; each hit 30 balls off a synthetic grass surface at a flag 120 meters away. The flag was indicative of the required direction as opposed to distance. During the trial each golfer was videoed on 4 genlocked 50Hz SVHS cameras. The subjects were familiarised with the experimental procedure and all possible risks before providing written consent to participate as approved by the University of Limerick Research Ethics Committee.

The PV of each shot was determined by the landing location of the ball for each of the 30 shots. The landing location was recorded as an x-y coordinate; the coordinate system is defined as follows: origin – the location of the tee; y-axis – the line joining the origin and flag; x-axis – located at the origin perpendicular to the y axis.

A 95% confidence ellipsoid was created; the x-axis of the ellipsoid was equal to the 1.96 of the standard deviation of the x coordinates (n=30), the y-axis was equal to the 1.96 of the standard deviation of the y coordinates (n=30), the centre of the ellipsoid was located at the mean x and y coordinate. The area of the ellipsoid was then calculated; the area of the ellipsoid is indicative of PV. All 30 shots for each subject were digitised for all four camera views. The raw data was filtered prior to scaling by application of a Jackson Knee optimised Butterworth filter, calculation of the angular kinematic parameters was carried out; trail knee angle (TKA), lead knee angle (LKA), angle between the hip and shoulders (HSA), trail elbow angle (TEA) and lead elbow angle (LEA).

RESULTS AND DISCUSSION

Initial results based on the data of two of the golfers found variability in each of the angles studied at the moment of contact between the clubhead and the golf ball; TKA: $137.7^0 \pm 8.2^0$; LKA: $147.3^0 \pm 15.5^0$; TEA $136^0 \pm 15.2^0$; LEA: $134^0 \pm 13.4^0$; HAS: $32.5^0 \pm 16.4^0$.

Initial findings, based on case study analysis, show that TKA correlated with PV. As can be observed in Figure 1, as the TKA for this golfer, approached 146^0 the shots became more accurate in the X direction. The TKA also influenced the distance in the Y direction of the flight of the balls; as the TKA reduced in magnitude the distance increased.

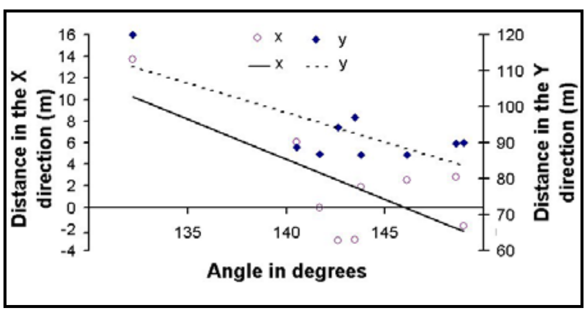

Figure 1: Relationship between the TKA and the PV of the ball in the X and Y direction for one of the volunteer.

Figure 2, based on a separate case study analysis, demonstrates that as TEA decreased in this particular golfer, he hit the balls further. Once more as the TEA correlated with the accuracy in the Y direction. Initial results suggest that a specific angle of approximately 138^0 correlates best with accuracy, for this golfer.

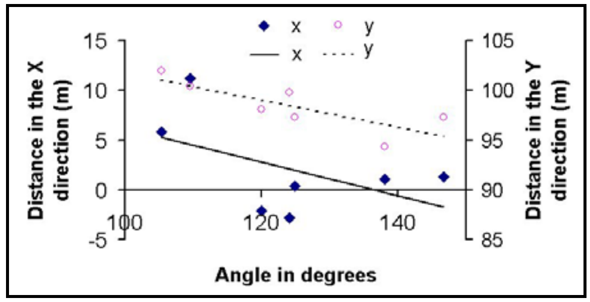

Figure 2: Relationship between the TEA and the PV of the ball in the X and Y direction for one of the volunteer.

SUMMARY

Preliminary results suggest that certain kinematic variability effects the accuracy of a golf shot. A trade off between accuracy and distance hit may cause this variability. The KV of certain joints is of more influence over PV than others and furthermore the specific joint with greatest influence over the PV can fluctuate between golfers. Additional analysis is required to establish if this variability is significant with respect to the accuracy of the golf shot.

REFERENCE

Burden, A. M., *et al*. (1998). *Journal of Sports Sciences* (16): 165-176.
Egret, C. I., *et al*. (2003). *International Journal of Sports Medicine* **24**: 465-469.
Richards, J., *et al*. (1985). *Res Q Exerc Sport* **56**(4): 361-365.
Sanders, R. and P. Owens (1992). *International Journal of Sports Biomechanics* **8**: 320-330.
Watanabe K., *et al*. (1998). *World Scientific Congress of Golf,* St. Andrews, Scotland., Human Kinetics.

ACKNOWLEDGEMENTS

Funding for this research is provided by the Irish Research Council for Science, Engineering and Technology: funded by the National Development

THE USE OF A WIRELESS NETWORK TO PROVIDE REAL-TIME AUGMENTED FEEDBACK FOR ON-WATER ROWING

DJ Collins[1&2], Dr Ross Anderson[1] & Dr Derek T. O'Keeffe

[1] Department of PE and Sport Science, University of Limerick, Limerick, Ireland
[2] Biomedical Electronics Laboratory, Department of Electronic and Computer Engineering, University of Limerick, Ireland
E-mail: d.j.collins@ul.ie Web: www.ul.ie/~pess/

INTRODUCTION

All elite athletes today have concentrated training programmes, enabling them to maximise their preparation time for competition. These demanding programmes require next to instant feedback of the performance. Existing techniques to achieve this include data loggers, EMG monitoring and motion analysis systems. However, the majority of these systems are lab based, depend on a physical link between the athlete and the monitoring system and do not provide real-time augmented feedback (rAF). This presents a acute problem when considering on-water rowing where races are held over courses of 2000m.

Commercially available telemetry systems may offer a solution to this problem, however the cost of the majority of these systems (>$15 000) is outwith the budget of the typical athlete, coach and sport biomechanist. A limited amount of research has been carried out in the area of rAF for rowing (Hawkins 2000; Anderson 2002) and the use of telemetry systems for rowing (McBride & Elliott 1999; Smith & Loschner 2002). These systems illustrate the requirement for a rAF telemetry system, however each of these systems has disadvantages; namely the lab based nature and/or one-way communication.

With recent advancements in wireless technology in the IT sector, new low cost communication technologies suitable for telemetry have become available; one such technology is the IEEE 802.11b. It is the incorporation of these communication technologies with existing sensors (accelerometers, potentiometers etc.), software and hardware that will lead the way for low-cost two-way wireless communication to be established between the rower and coach.

The aim of this research is to investigate the suitability, from a range and throughput perspective, of 802.11b as a suitable base technology for rAF in rowing.

METHOD

To test the suitability of the 802.11b technology, a test network was constructed. Two Dell Latitude laptops, equipped with LabVIEW 7 and a LinkSYS Wireless 802.11b adapter card, were used to simulate the transmitter (L1) and the receiver (L2) The testing was seperated into three separate sections; indoor, outdoor and continuous. Indoor and outdoor testing involved simulating a typical telemetry system by transmitting files of different sizes. The files (2kb to 100kb) were made up of random data. The files were transmitted from L1 to L2 using a LabVIEW coded program. The program recorded the transmission time for each file, to ms accuracy. This procedure was repeated for varying distances, up to 30m for the indoor testing and 150m for the outdoor testing. The final section of the testing simulated the transmission of a continuous stream of data. An NI-6024E data acquisition card in L1 was connected to a function generator. The function generator produced a continuous data, based on a 200Hz sine wave. A second LabVIEW coded program acquired this data and simultaneously sent this data over the 802.11b network to L2. The latency between acquiring the data at L1 and receiving the data at L2 was calculated.

RESULTS AND DISCUSSION

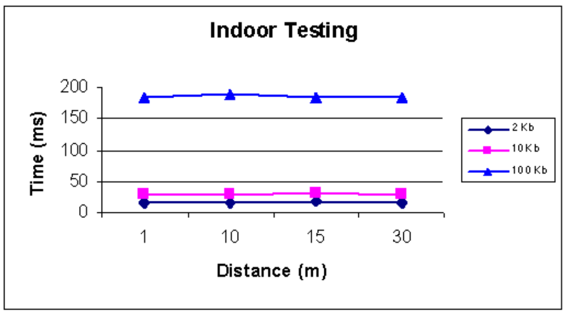

Figure 1: Transmission time Vs Distance for different file sizes; indoor testing.

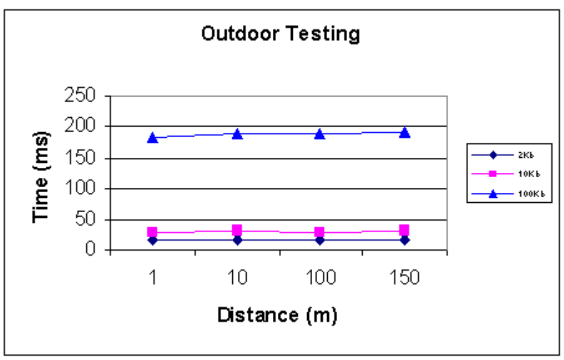

Figure 1: Transmission time Vs Distance for different file sizes; outdoor testing.

As can be seen from Figure 1 and Figure 2 the distance between the transmitter and receiver does not affect the time taken to send data over the 802.11b network. However, it does illustrate that the file size is the determining factor when considering transmission time; the 100Kb file was transmitted in under at just under 200ms. When the continuous data signal was transmitted across the 802.11b network the time lag was in the region of 200 to 300ms. These transmission times are relatively small, and for rAF in rowing, are inconsequential and may be considered real-time.

SUMMARY

From the results obtained, the possibility of developing a low-cost real-time augmented feedback telemetry communications system for on-water rowing is possible. This would provide a mechanism for rowers, coaches and sport biomechanists to gain valuable biomechanical and kinematical data of a rower's performance as it is occurring. More specifically, as IEEE 802.11 offers a solution regardless of required range or sampling rate. It is on this technology that the developmental drive should be focused as it may offer an all-encompassing solution to both stationary sports (e.g. archery) and ambulatory sports (e.g. rowing). Development of such a real-time augmented feedback system will certainly assist those elite athletes with highly concentrated training programmes.

REFERENCES

Anderson R, Harrison AJ & Lyons G (2002), In: *The Engineering of Sport 4*, eds S Ujihashi, SJ Haake,
Blackwell Science, Oxford, UK, 803 – 809
Hawkins D (2000). Journal of Biomechanics **33**(2): 241-245
McBrid ME & BC Elliott (1999) ISBS Symposium XV11, Perth, Australia.
Smith RM & C Loschner (2002) Journal of Sports Science **20**(10): 783-791

ACKNOWLEDGEMENTS

This research has been supported, in part, by National Instruments.

EXPERIMENTAL VALIDATION OF A SURFACE EMG MODEL

David A. Gabriel

Raymond Nelson Reid Biomechanics Laboratory, Brock University, St. Catharines, ON, Canada L2S 3A1
E-mail: dgabriel@arnie.pec.brocku.ca

INTRODUCTION

An earlier model (Gabriel, 2003) of surface electromyographic (SEMG) activity has been revised to include muscle fiber lengths and muscle-tendon end-effects. Motor unit action potential (MUAP) shape due to electrode location along (x-direction) and above (y-direction) the muscle fibers was also included.

The model will be used to simulate SEMG with known motor unit (MU) firing patterns to validate inferences made about MU firing based on interference pattern (IP) analysis.

METHODS

Model Description: The intracellular action potential (IAP) was divided into three phases: rising, rapidly falling, and a slowly falling after potential. The total duration of these phases were taken from Dimitru et al. (1999) and were dependent on muscle fiber semi-lengths. Fiber semi-lengths ranged from 40 to 60 mm, with a total IAP duration of 34.4 to 43.8 msec, respectively. From Dimitrov and Dimitrova (1998), the basic shape of the rising and rapidly falling phases of the IAP was given by:

$$\varphi(t) = A_1 \, t^{A_2} \exp(-A_3 t) \qquad \text{eq. 1}$$

with coefficients A_1=21242; A_2=48133; A_3=14.033. A cubic spline was used to construct the slowly falling after potential. The first derivative ($d\varphi(t)/dt$) was convolved with impulse response (IR) function of the anisotropic (an) volume conductor, $1/r_{an}(t)$, which was the sum of two dipoles that were opposite in direction but located at the same position relative to the motor end-plate (ep). For each dipole, the distance from the observation point $P(x_0,y_0)$ to the current of the IAP profile was:

$$r_{an} = \sqrt{(x_0 - x_{ep} - vt)^2 + K_{an}(y_0)^2} \qquad \text{eq. 2}$$

where v (4 m/sec) was muscle fiber conduction velocity, and K_{an} was the anisotropy ratio (σ_x/σ_y), between conductivities in the longitudinal and transverse directions, respectively. The conductivities were σ_x=0.5 $(\Omega m)^{-1}$ and σ_y=0.1 $(\Omega m)^{-1}$. $P(x_0,y_0)$ was located at the mid-point between the end-plate the muscle fiber end. To calculate the SFAP:

$$\varphi(t, x_0, y_0) = C_{an} \cdot \frac{\partial \varphi(t)}{\partial t} * \frac{1}{v} IR(t) \qquad \text{eq. 3}$$

The source strength was $C_{an}=d^2K_{an}\sigma_i/12\sigma_{an}$. Fiber diameter (d) was 55 µm. Axoplasmic conductivity was σ_i=1.01 $(\Omega m)^{-1}$and tissue conductivity was $\sigma_{an}=(\sigma_x \cdot \sigma_y)^{1/2}$.

There were 250 muscle fibers per motor unit and 50 MUs. The firing frequency was normally distributed with a mean of 20±5 Hz. The MUAPs were then inserted at normally distributed intervals corresponding to ±20% of firing frequency. The MUAP trains were summated to generate the synthetic IP. The result was then passed through a transfer function that accounted for the filtering properties of bipolar surface electrodes:

$$\Psi(\omega) = \sin^2\left(\frac{\omega d}{2v}\right) \qquad \text{eq. 4}$$

where ω was angular frequency, v (4.0 m/sec) was muscle fiber conduction velocity, d (1.0 cm) was the inter-electrode distance.

Experimental Validation: Thirteen subjects performed 5 maximal voluntary contractions (MVCs) of the elbow flexors. The MVCs were 5 seconds in duration at 3-minute rest intervals. Force was measured with the JR3 load cell (JR3 Inc., Woodland, CA). Biceps SEMG was monitored with DE-2.1 (Delsys Inc., Boston, MA) electrodes. The SEMG signals were amplified (10,000×) and band-passed filtered (20-450 Hz) using the BAGNOLI-4 (Delsys Inc.) bioamplifier, before A/D conversion at 2 kHz (CODAS, DATAQ Instruments Inc., Akron, OH) on a Pentium III IBM-PC. Data reduction and analysis were performed on a 1-sec stationary portion of the signal in MATLAB (The Math Works, Natick, MA).

RESULTS AND DISCUSSION

The average mean power frequency (MPF) for the sample was 90 ± 11 Hz. These values are nearly identical to the 89 ± 13.3 Hz to 123 ± 23.5 Hz reported by Moritani and Muro (1987) for ramp isometric contractions of the elbow flexors.

Figure 1 illustrates a representative power spectrum from one subject, and for a synthetic biceps SEMG signal. Since the strongest contributor to the power spectrum was MUAP duration, which was determined by muscle fiber semi-lengths. Tuning the model for the sample involved skewing the semi-lengths within the physiologic range towards a limit of 60 mm. All other variables were held constant. The resulting synthetic SEMG signals had an average MPF of 90 ± 6 Hz. The average median frequency (MDF) was 79 ± 7 Hz. The average MDF for the experimental data was 77 ± 9 Hz. Clearly, the MPF and MDF values are remarkably close to the experimental data. Thus, the power spectra from synthetic SEMG suggests that the model was able to faithfully generate synthetic SEMG signals.

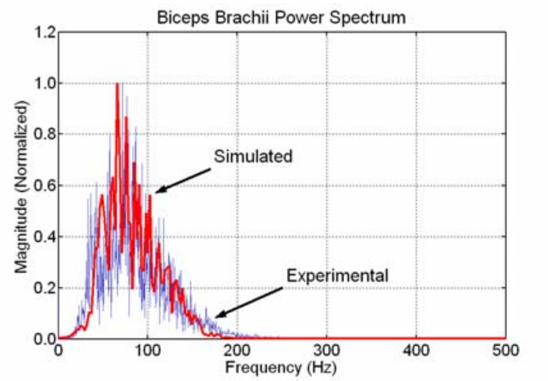

Figure 1: Power spectrum from one subject (blue) and from simulated SEMG (red).

SUMMARY

An SEMG model based on muscle fibers of finite length can produce realistic power spectra for the biceps brachii.

REFERENCES

Dimitrov, GV, Dimitrova, NA (1989). *Med. Eng. & Phys.*, **20**, 371-381.

Dumitru, D. et al. (1999). *Clin. Neurophysiol.*, **110**, 1876-1882.

Gabriel, DA (2003). *Conference Proceedings: Twenty-Seventh Annual Meeting of the American Society of Biomechanics*.

Moritani, T., Muro, M. (1987). *Eur. J. Appl. Physiol.*, **56**, 260-265.

ACKNOWLEDGEMENTS

This work was funded by the NSERC of Canada.

Effects of Static Flexion-Relaxation on Paraspinal Reflex Behavior

Ellen Rogers, Kevin Moorhouse, and Kevin Granata[1]

Musculoskeletal Biomechanics Laboratory, Virginia Polytechnic Institute, Blacksburg, VA, USA
[1]E-mail: Granata@vt.edu

INTRODUCTION

Static trunk flexion working postures and disturbed trunk muscle reflexes are related to the risk of low back pain (Marras et al., 1993; Radebold et al., 2000). Animal studies conclude that these factors may be related in that passive tissue strain in spinal ligaments causes subsequent short-term changes in reflex (Solomonow et al., 2003). There are no studies that document paraspinal reflex behavior following a period of static flexion-relaxation loading in humans.

Flexion-relaxation occurs during extreme lumbar flexion when the trunk muscles are deactivated and passive tissues in the spine provide full resistance against a flexion load. Flexion loading of the viscoelastic tissues of the spine causes inter-vertebral laxity and tissue creep (McGill and Brown, 1992). Laxity or creep in these tissues from prolonged ligament strain causes mechanoreceptors to become desensitized and therefore unable to reflexively initiate muscular forces necessary to control destabilizing motion.

The objective of this study was to develop a method to quantify paraspinal reflex gain in human subjects and determine the change in reflex gain following a period of flexion-relaxation.

METHODS

Eighteen subjects maintained static lumbar flexion for fifteen minutes. Flexion-relaxation was assured by monitoring paraspinal EMG activity throughout the flexion period. Paraspinal muscle reflexes were elicited both before and after flexion using force perturbations and recorded from active surface EMG electrodes.

A harness and cable system attached the subject to a servomotor (Pacific Scientific, Rockford, IL) such that cable tension applied flexion loads at the T10 level of the trunk. The motor was programmed to provide three levels of isotonic load, 100 N, 135 N, and 170 N. Superimposed on the preload were force perturbations of ±75 N applied in a pseudo-random stochastic fashion with a flat bandwidth from 0-50 Hz.

To quantify paraspinal reflex dynamics, the EMG response to a force perturbation was modeled as the closed loop transfer function of the system. Reflex gain was identified as the peak value of the impulse response function relating input force to EMG response using time-domain deconvolution analyses (Hunter and Kearney, 1983). A typical impulse response function is shown in Figure 1.

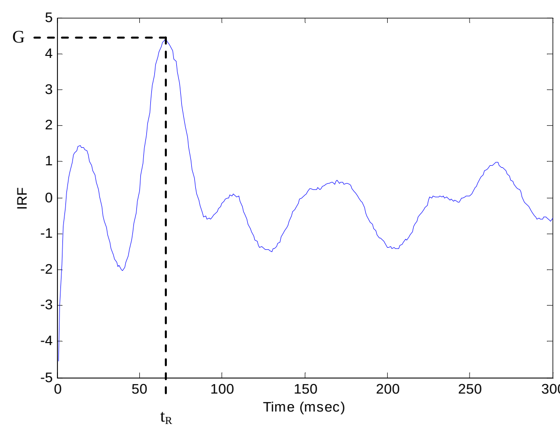

Figure 1. Typical Impulse Response function, showing peak reflex gain, G and latency, t_R.

Statistical repeated measures analyses were performed to determine the effect of flexion-relaxation, gender and preload on paraspinal reflex dynamics.

RESULTS AND DISCUSSION

Three primary effects were observed in the results, shown in Table 1. First, reflexes showed a trend toward increased gain after the period of flexion-relaxation ($p<0.054$). Second, reflexes increased with trunk extension exertion ($p<0.02$). Finally, there was a significant effect of gender in reflex gain, with females having larger reflex gain than males ($p<0.01$).

Reflex latency showed no significant effects for gender, preload level, or flexion-relaxation.

Table 1. Mean (standard deviation) of peak reflex gain and latency

	Men	Women
G_R	1.054 (0.420)*	1.529 (0.802)*
t_R (ms)	68.62 (15.84)	65.81 (9.89)
Before Flexion		
G_R	1.070 (0.469)	1.333 (0.635) ¹
t_R (ms)	69.39 (15.83)	65.36 (8.28)
After Flexion		
G_R	1.038 (0.369) *	1.724 (0.905) * ¹
t_R (ms)	67.86 (15.97)	66.26 (11.33)
100 N preload		
G_R	0.987 (0.375) *²	1.476 (0.846) *²
t_R (ms)	70.70 (17.71)	68.36 (12.07)
135 N preload		
G_R	1.032 (0.465) *	1.467 (0.735) *
t_R (ms)	68.46 (15.93)	65.45 (7.59)
170 N preload		
G_R	1.112 (0.418) *²	1.644 (0.834) *²
t_R (ms)	66.71 (13.85)	63.62 (9.17)

* indicates significance due to gender p<0.05
¹ indicates significance due to flexion-relaxation p<0.05
² indicates significance due to preload p<0.05

SUMMARY

Paraspinal reflex gain was increased immediately following 15 minutes of static flexion-relaxation posture. The change in reflex response following the flexion-relaxation protocol was attributed to creep of the viscoelastic tissues within the spine. Creep of the spinal tissues has been well documented in humans during static flexion.

These results agree with animal models wherein a hyperexcitable reflex response is observed following prolonged ligament stretch (Solomonow et al., 2003). It is noteworthy that those feline models demonstrate that the period of hyperexcitability is transient and is followed by a period of prolonged reflex depression lasting up to 7 hours. We suspect this same reflex gain depression following the period of hyperexcitability might be similarly observed in humans and must be investigated in future research.

Systems theory representation of spine biomechanics indicates that reduced feedback gain may adversely influence spinal stability and risk of injury. Likewise, patients with LBP demonstrate reduced and slowed reflexes compared to asymptomatic control subjects, but it remains unclear whether this neuromuscular effect is a compensatory result of low back pain or a contributing cause. Nonetheless, it has been proposed that changes in paraspinal muscle response following flexed posture work may contribute to LBP risk.

REFERENCES

Hunter IW and Kearney RE (1983) *Med.Biol.Eng Comput.* 21, 203-9.
Marras W.S., et.al. (1993) *Spine* 18, 617-28.
McGill S.M. and Brown S. (1992) *Clin Biomech* 7, 43-6.
Radebold A., et al. (2000) *Spine* 25, 947-54.
Solomonow M. et al. (2003). *Journal of Electromyography and Kinesiology*. 13, 381-396.

ACKNOWLEDGEMENTS

This study was supported in part by a grant AR46111 from NIAMS of the National Institutes of Health.

HUMAN LUMBAR FACET JOINT CAPSULE STRAINS DURING AXIAL ROTATIONS

Allyson Ianuzzi[1] and Partap S. Khalsa[1]

[1] Dept. of Biomedical Engineering, Stony Brook University, Stony Brook, NY, USA
Email: partap.khalsa@stonybrook.edu

INTRODUCTION

The lumbar facet joint capsule (FJC) is innervated with mechanically-sensitive neurons, and it is a known cause of low back pain (LBP) (Cavanaugh, 1995). In order to understand mechanisms of LBP, FJC strains during physiological motions (extension, flexion, lateral bending) have been examined in cadaveric studies (Ianuzzi et al., 2004). These data have been used to validate finite element models (FEM) of the lumbar spine. However, FJC strain magnitudes during axial rotations are unknown. The purpose of this study was to quantify FJC strains in human lumbar spine specimens during axial rotation.

METHODS

Unembalmed, human lumbar spines (n = 6, T_{12}-sacrum) were dissected free of all superficial tissue to expose the FJC. The sacrum was fixed to the testing surface. At T_{12}, the spine was connected to a rotatory actuator that was suspended over the specimen. As the spine was axially rotated, the applied torque was measured using a torque sensor. A given trial consisted of 15 cycles to 20º left & right axial rotation (LAR & RAR, respectively) at speeds of 2, 6, 20, 65, 100, and 125 deg/s.

Plane strains (LaGrangian large strain formulation) were measured in the left FJCs (L_3 – sacrum) by optically tracking markers attached to capsule surfaces and organized as maximum & minimum ($\overline{E}_1$ & $\overline{E}_2$, respectively). L_3, L_4, and L_5 vertebral kinematics were measured (6 degrees of freedom) by optically tracking markers attached to transverse processes. Given the high variability and the small sample size, significant differences in torque, vertebral motion, and FJC strain across speed were assessed using Friedman's test (FT) with post hoc Student-Newman-Keuls test (SNK, $\alpha = 0.05$ both). Median and 75th percentiles were reported.

RESULTS AND DISCUSSION

Median torque during LAR & RAR were similar in absolute magnitude. During LAR, torque increased in absolute magnitude with increasing speed (Fig.1;FT, $p<0.001$); torque during LAR was significantly larger at the faster speeds (65, 100, 125, 120 deg/s) vs. the slower speeds (2, 6, 20 deg/s; SNK $p<0.05$).

Speed did not have a significant effect on vertebral rotation during LAR or RAR (FT, $p>0.05$; Fig. 2A, LAR shown). X- and Z-axis vertebral rotations at L_3 were generally larger in absolute magnitude versus L_4 and L_5. At

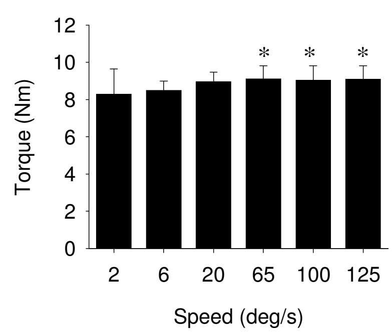

Fig. 1 Median torque (at T_{12}) during left axial rotation increased significantly with increasing speed (n=6, error bars show 75th percentile). *Significantly larger than 2, 6, & 20 deg/sec

L_4, Y-axis rotations were larger than those about the other two axes. L_5 rotations were highly variable and without clear pattern.

Speed did not have a significant effect on FJC strain (Fig. 2B; FT, p>0.07). $\bar{E}_1$ FJC strains at $L_{3\text{-}4}$ and $L_{4\text{-}5}$ were similar in magnitude during LAR and RAR, while L_5-S_1 FJC strains were larger during LAR versus RAR. $\bar{E}_2$ FJC strains were similar in magnitude at $L_{3\text{-}4}$ during LAR and RAR, while at $L_{4\text{-}5}$ and L_5-S_1, $\bar{E}_2$ strains were larger in magnitude during RAR versus LAR.

FJC strain magnitudes during axial rotation were smaller than those that occurred during flexion in prior studies (Ianuzzi et al., 2004; 5% versus up to 20%, respectively). The difference in strain magnitude was probably due to the difference in the biomechanics of the motions. During flexion, intervertebral (IV) motions are primarily restricted by the posterior soft tissues, while during axial rotation, the facets restrict IV motions.

SUMMARY

FJC strain in the lumbar spine developed during axial rotation were smaller in magnitude than in other motions for the same torque limit. The biomechanical data from the current study will be used to validate a FEM of the lumbar spine, currently under development in our lab. The model will be used to simulate spine motions to investigate potential mechanisms for LBP.

ACKNOWLEDGEMENT

Funding provided by AT001701-05 (Khalsa).

REFERENCES

Cavanaugh JM (1995) Spine, **20**(16), 1804-1809.

Ianuzzi A, et al. (2004) Spine J, **4**(2), 141-52.

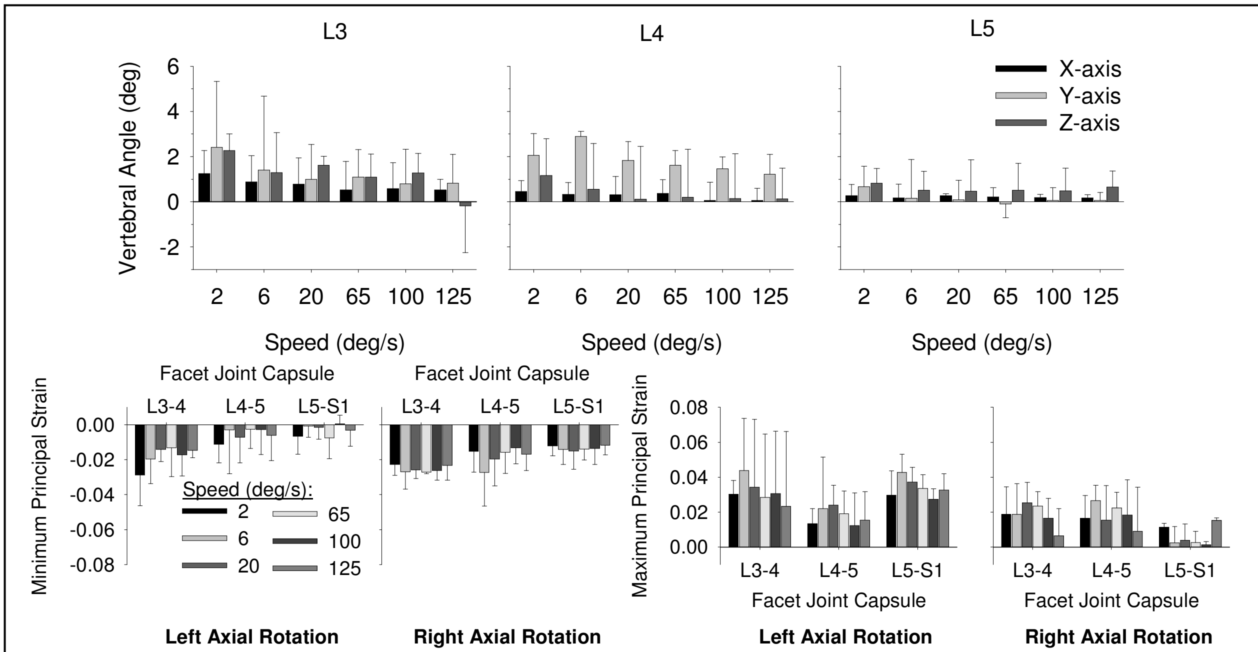

Fig. 2 **Top)** During left axial rotation, loading speed did not have a significant effect on vertebral angle (Friedman's Test, p>0.05). **Bottom)** Min. (left) and max. (right) FJC strains on the left side of the lumbar spine during axial rotation varied in absolute magnitude according to the direction of the applied load (i.e., left axial rotation versus right axial rotation).

A PARAMETRIC FINITE ELEMENT STUDY OF CONSTRAINED ACETABULAR LINERS

Suzanne M. Bouchard[2], Kristofer J. Stewart[1], Douglas R. Pedersen[1], John J. Callaghan[1], Thomas D. Brown[1,2]

[1] Department of Orthopaedics and Rehabilitation, University of Iowa, Iowa City, IA, USA
[2] Department of Biomedical Engineering, University of Iowa, Iowa City, IA, USA
E-mail: Suzanne-bouchard@uiowa.edu Web: mnypt.obrl.uiowa.edu/OBL_Lab_Website

INTRODUCTION

Dislocation is the second leading cause of failure in total hip replacements, with roughly 2-11% of cases dislocating after the primary surgery. Of revision surgeries for recurrent dislocation, as many as 50% are unsuccessful at preventing further dislocation (Shapiro 2003). Because of the problematic nature of recurrent dislocation, several constrained acetabular cup designs have recently been developed for use as a last-best-effort to maintain stability.

Unfortunately, the clinical outcomes for constrained liners are highly variable. This investigation is a step toward fully characterizing constrained acetabular cups, using a finite element model to explore the design of these devices. Finite element nonlinearity challenges included (1) the interference fit between the femoral head and the cup during intra-operative assembly, (2) appropriate material and kinematic definitions, and (3) cup-to-constraining ring contact. A formulation was developed to vary cup features parametrically. The model was utilized to study both the intra-operative assembly process, and lever-out dislocation.

METHODS

A three-dimensional finite element mesh of a constrained acetabular cup system was developed using PATRAN's pre-processing software. The geometry was tailored to capture the salient design features of constrained acetabular cups from three manufacturers. The baseline model for parametric testing used a 28mm diameter head, with a cup opening radius of 13.75mm. The liner was 8mm thick until just below the equatorial plane, where the thickness was reduced to 6mm to accommodate the metal constraining ring. The articular radius of the cup was 14.5 mm and the inside corner of the lip had a fillet radius of 1.0 mm. Beyond the fillet, the cup receded at a 45º angle (Figure 1, A).

The finite element model contained 31,971 elements with 101,877 degrees of freedom. The femoral component was modeled as a rigid body using triangular facets (Figure 1, B). The metal constraining ring was modeled as titanium with a linear material definition (E = 110 GPa, $\nu = 0.3$), and the UHMWPE cup was given a nonlinear elastic/plastic material definition (Cripton

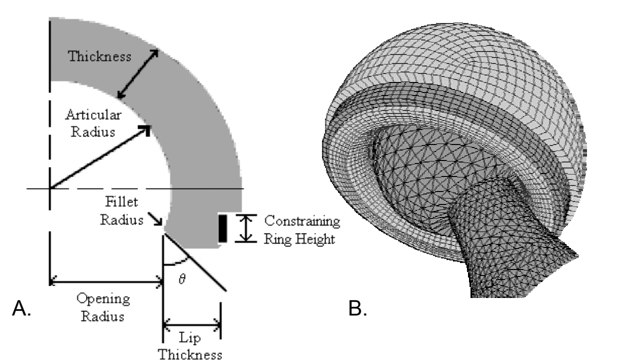

Figure 1: A) Cross-sectional view of the base model. B) Finite element model of the constrained acetabular cup with constraining ring and femoral head and neck, just prior to impingement.

1993). The nodes on the back of the cup above the hemispheric plane were constrained, simulating rigid bony bed support.

The opening radius, lip thickness, and head size were varied parametrically, and simulations of the assembly process and lever-out dislocation were executed for each series using ABAQUS standard finite element code. The key output metric for the assembly process was the force required to insert the head into the cup. For lever-out, the metrics of primary interest were peak resisting moment about the head center, polyethylene Von Mises stress, and rotation angle at dislocation.

RESULTS AND DISCUSSION

As expected, the opening radius had a significant effect on the force required to push the femoral head into the cup. For a series of five cups with increasing opening radii from 13.6 to 13.9 mm, the reaction force ranged linearly from 39.3 to 545.5 N (R^2 = 0.966). The moment about the center of the head as the femoral component rotated out of the cup decreased monotonically (Figure 2).

For a series of six liners with varied lip thickness from 4.5 to 7 mm, the relationship with assembly force also increased linearly with a range of 222.8 to 282.3 N (R^2=0.97). The maximum moment resisting rotation of the head was much less affected in this series, but decreased from 4.79 N-m to 4.63 N-m as the lip thickness increased.

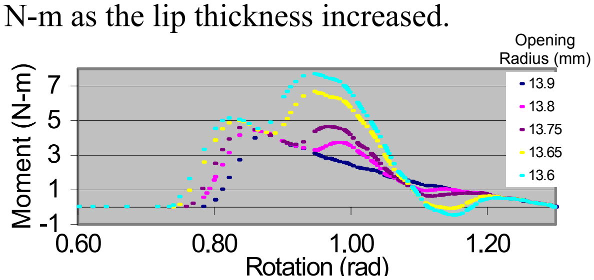

Figure 2: Moment about head center as the head rotated out of the cup

Unlike the relationships seen for assembly force in the previous two series, there was no linear correlation between head size and assembly force (Table 1). As expected, the range of motion increased with head size (Figure 3), although the peak resisting moment did not follow this trend.

Table 1: Effect of head size on assembly force

Head Size (mm)	22	26	28	32	36	40
Force (N)	469	266	240	313	341	250

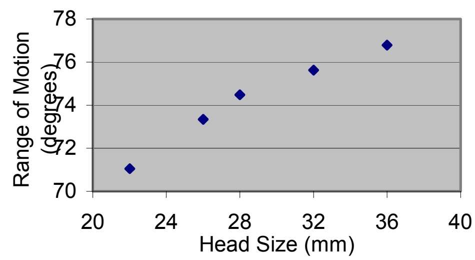

Figure 3: Angle of rotation at dislocation

CONCLUSION

When the lip thickness is reduced the constraining ring plays a greater role in the liner's resisting moment, but the stress in the UHMWPE at the motion limit is also increased. Increasing head size alone increases the motion, but not the peak resisting moment. Because the interactions between design parameters can be complex, finite element modeling is very beneficial for exploring design alternatives.

REFERENCES

Shapiro, G.S., et al. (2003). *The Use of a Constrained Acetabular Component for Recurrent Dislocation. J. Arthroplasty*, **18**, 250-258.

Cripton, P.A., (1993) Thesis. Queen's University.

ACKNOWLEDGEMENTS

Funding source: DePuy Orthopaedics Inc.

THE ALTERATIONS TRAJECTORY OF CENTER OF MASS WHEN NEGOTIATING OBSTACLES WITH DIFFERENT HEIGHTS IN THE OLDER ADULTS

Shu-Ya Chen[1], Hsiu-Chen Lin[1], Hong-Wen Wu[1], Hui-Fen Pan[1], Ching-Sheng Li[1], Horng-Chaung Hsu[2]

[1] School of Physical Therapy, China Medical University, Taichung, Taiwan
[2] Department of Orthopedics, China Medical University Hospital, Taichung, Taiwan
E-mail: sychen@mail.cmu.edu.tw

INTRODUCTION

Over 20 percent of people over 65 years old and living in the community fall each year. The age-related changes in postural control and falls in the older adults remain unclear. Tripping by an obstacle is one of the activities that cause falls most frequently in the elderly (Lin, 2002). A better knowledge in the alterations of the postural performance in the elderly is important for studying the falling problems. The trajectory of center of mass (COM) of the body has been used to represent the capability of the human's static or dynamic postural control (Chou, 2001). The aim of this study was to investigate the strategy on the adjustment of the body COM when negotiating the obstacles with different heights in the elderly.

METHODS

Twenty-two community-dwelling elders aged over 65 (77.58±5.92 years old) were recruited with informed consent. Thirty-nine reflective markers were then placed on the body for each subject. A seven-camera motion analysis system was used to collect the kinemetic data, and a 15-linkage human model was used to calculate the trajectory of whole body's COM. The subjects were then asked to walk with their self-selected paces and perform stepping over the obstacles with four different heights (0, 10, 20, 30 % of leg length). Maximum movement ranges, velocities, and accelerations of the body's COM trajectories were extracted as dependent variables. Repeated ANOVA was used to compare the variables between heights with significance level of 0.05.

RESULTS AND DISCUSSION

The sway of body COM in medial-lateral (ML) and up-down (UD) directions increased with the obstacle heights. The results agreed with Latughton's study that suggested the larger ranges of motion in the swing leg increased the body sway. The forward (F) maximal velocity had not significantly trend with the obstacle conditions, it might mostly depend on the subject preferred pace. The maximum velocities in UD directions increased significantly with obstacle heights while in backward (B) direction, meaning minimum forward velocity decreased with the obstacle heights (Fig. 1). These results suggested that the elder subjects would slow down the progression significantly to accommodate the higher obstacle conditions.

Corresponding results were found in the maximal acceleration in the FB and UD directions, which increased with the heights to achieve the changes in maximal velocities. The alterations of maximum velocities seemed revealing the strategy when cope with the obstacles. The maximum acceleration demonstrated a high level of changes in COM trajectory, implied the rapid response of postural control were required during obstacle-crossing.

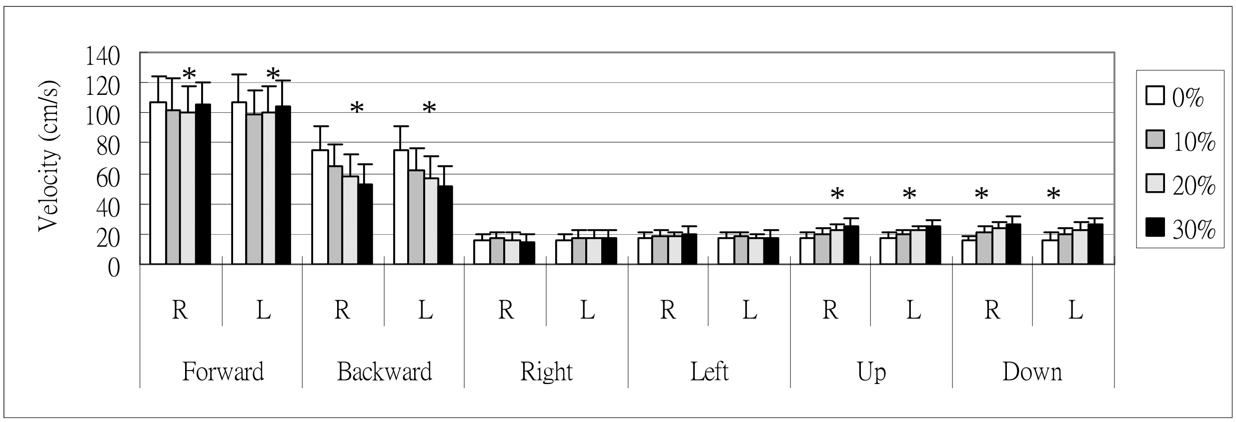

Figure 1: The maximum velocities in six different directions when crossing the obstacles with different heights in the elderly. (R: right leg leading, L: left leg leading)

SUMMARY

The older adults had a raised and rapid changed COM trajectory adopting with the higher obstacle, resulting a more unstable condition and increased the risks of fall. To cope with this challenging but frequent activity, the elderly should be suggested to increase their muscle strength of lower extremities and dynamic motor control.

REFERENCES

Chou, L.S., et al. (2001). *Gait and Posture*, **13**, 17-26.

Daubney, M.E., Culham, E.G. (1999). *Phys Ther*, **79**, 1177-1185.

Laughton CA, et al. (2003). *Gait and Posture*, **18**, 101-108.

Lin, M.R., et al. (2002). *Taiwan Journal of Public Health*, **21**, 73-82.

ACKNOWLEDGEMENTS

The authors would like to thank for the financial support from National Science Council of Taiwan.

FULL BODY INVERSE DYNAMICS SOLUTIONS: AN ERROR ANALYSIS AND A HYBRID APPROACH

Raziel Riemer, Sang-Wook Lee, and Xudong Zhang
Biomechanics and Ergonomics Lab, Department of Mechanical and Industrial Engineering
University of Illinois at Urbana-Champaign, Urbana, IL 61801, USA
E-mail: xudong@uiuc.edu

INTRODUCTION

Inverse dynamics is a powerful tool for biomechanical analysis of human movement (Winter 1990), but is subject to various sources of inaccuracy. Otimization-based methods have been developed to improve the precision of inverse dynamics computations (e.g., Kuo 1998; Cahouët et al. 2002). While the efficacy of these methods have been tested using simulated data (Kuo 1998) and real data of symmetric planar motions (Cahouët et al. 2002), they have not been applied to analysis of full-body, asymmetric motions where additional constraints or residual errors may arise. Further, these current methods only consider a partial list of error-contributing factors (e.g., noise-polluted acceleration and force plate data). Many other inverse dynamics input variables such as segmental angle and mass properties can also be subject to significant errors or uncertainties (Desjardins et al.1998; Holden et al. 1997).

In this work, we explore a new approach to inverse dynamics computations applicable for full-body asymmetric movements. Our approach incorporates both motion and ground reaction force measurements, and optimally weighs the top-down and bottom-up solutions based on an analysis of the uncertainties in all possible variables contained in the equations of motion.

METHODS

The entire human body is represented by a 13-segment linkage consisting of the forearms (including the hands), upper-arms, torso, upper-legs, lower-legs, feet, and two weightless links connecting the bi-lateral shoulder and hip joints. The torso segment inter-connects the mid-points of above two links.

Two separate models meeting at the bottom of the torso are constructed. They serve as the bases for two sets of Newton-Euler equations for inverse dynamics solutions, one for the upper body, and one for the lower body which incorporates the ground reaction force measurements. Consequently, there are two different torque estimates at the bottom of the torso, resulting respectively from the "conventional" top-down and bottom-up inverse dynamics solutions. One key constraint in our approach is that the discrepancy between the two estimates should be nullified; i.e., the two torque estimates must be adjusted to a common value. This adjustment leads to a "chain reaction" of changes in the remaining joint torque estimates such that the sum of weighted changes is minimal in a least-squares sense. Additional constraints on the residual errors at the top-most or bottom-most segments are also enforced.

The weights are quantified by the uncertainties in the joint torques: the greater the uncertainty, the greater the amount of adjustment made to the original estimates. Here the uncertainties are determined using an error analysis method (Doeblin 1966):

$$E = \sqrt{\left(\frac{d\tau}{dx_1}\Delta x_1\right)^2 + \left(\frac{d\tau}{dx_2}\Delta x_2\right)^2 + \ldots\ldots + \left(\frac{d\tau}{dx_n}\Delta x_n\right)^2} \qquad (1)$$

where τ is the torque at a given joint; Δx_i are estimated errors associated with the input variables in the equation of motion; and E is the statistical representation of uncertainty ($\pm 3\sigma$) in the torque value. The error magnitudes (Δx_i) are synthesized from literature data (Kingma et al. 1996; Schmiedmayer & Kastner 2000; Ganley & Powers 2004) and our own experimental results. The new torque at the bottom of torso is adjusted according to following rule:

$$\tau' = \tau_B + \frac{\tau_T - \tau_B}{E_T^2 + E_B^2} E_B^2 \tag{2}$$

where τ' is the new torque; τ_T and τ_B are torque estimates resulting from the top-down and bottom-up solutions, respectively; E_T and E_B are the uncertainty estimates obtained from the error analysis. The τ' thus determined is a least-squares solution that minimizes the weighted total of torque changes $\sum \Delta\tau_i^2 / E_i^2$.

To demonstrate the efficacy of the proposed approach, we conducted an experiments in which three males (weight: $82.2 \pm 7.3kg$; height: $180.2 \pm 0.08m$) walked at natural speed with the right foot landing on a force plate (AMTI BP600900). A six-camera Vicon system recorded their movements.

RESULTS AND DISCUSSION

The magnitudes of uncertainties change over time particularly the top-down solution τ_T (Fig. 1). Also revealed is the error-accumulation in the bottom-up direction. Therefore, it is important to weigh the adjustments and do so in a frame-by-frame manner. The grand-average (over time and across subjects) for the discrepancy $\|\tau_T - \tau_B\|$ (Fig. 2) is 9.2 Nm, and for the uncertainty $(E_T^2 + E_B^2)^{1/2}$ as assessed by the error analysis is 15.4 Nm. Both are in the same order of magnitude as error values previously reported (Plamondon et al. 1996), which lends credence to the error analysis performed in this work.

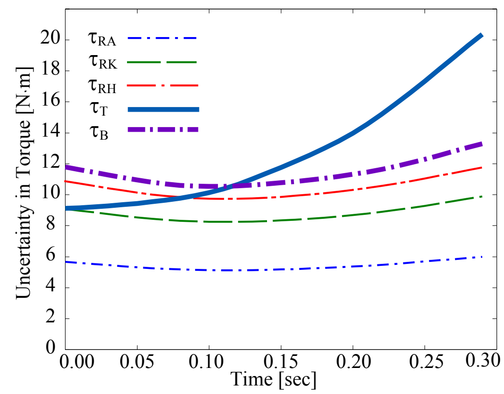

Figure 1: Sample profiles of uncertainties in joint torques during the left-leg-swing phase.

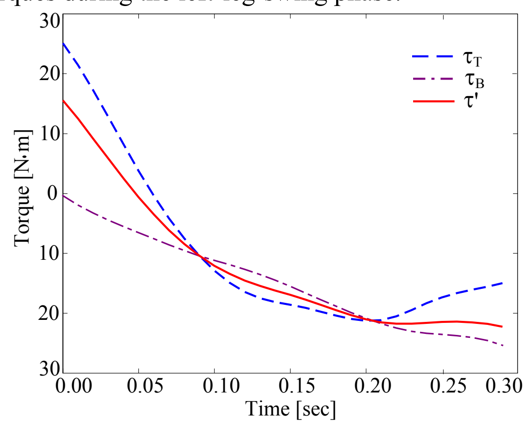

Figure 2: Torques at the bottom of the torso resulting from the top-down, bottom-up, and new approaches.

REFERENCES

Cahouët, V. et al. (2002). *J. Biomech.,* **35**, 1507-1513.

Desjardins, P.A. et al. (1998). *Med. Eng. & Phys.,* **20**, 153-158.

Doeblin, O.E. (1966). *Measurement Systems: Application and Design*. McGraw Hill.

Ganley, J.K. & Powers, M.C. (2004). *Clinical Biomech.*, **19**, 50-56.

Holden, P.J. et al. (1997). *Gait & Posture*, **5**, 217-227.

Kingma, I.T. et al. (1996). *J. Biomech.,* **29**, 693-704.

Kuo, D.A. (1998). *J. Biomech. Eng.,* **120,** 148-159.

Plamondon, A. et al. (1996). *Clinical Biomech.*, **11** (2), 101-110.

Schmiedmayer, H.B. & Kastner, J. (2000). *J. Biomech. Eng.,* **122**, 523-527.

Winter, D.A. (1990). *Biomechanics and Motor Control of Human Movement*. John Wiley & Sons.

ACKNOWLEDGEMENTS

This work is funded by ONR (N00014-03-0260) and CDC (K01OH007838). We also thank Dr. Elizabeth Hsiao-Wecksler and Mr. Matthew Major for their help with the experiment.

EFFECT OF INITIAL VELOCITY ON THE THRESHOLD OF BALANCE RECOVERY PRELIMINARY RESULTS

Kodjo E. Moglo, Marc-André Cyr and Cécile Smeesters

Research Centre on Aging, Sherbrooke Geriatric University Institute, Sherbrooke, QC, Canada
Department of Mechanical Engineering, Université de Sherbrooke, Sherbrooke, QC, Canada
E-mail: Cecile.Smeesters@USherbrooke.ca Web: www.cdrv.ca

INTRODUCTION

It is only recently that studies have focused on postural disturbances at the threshold of balance recovery, i.e., postural disturbances large enough that balance recovery is not always possible and a fall can occur. The knowledge at the threshold of balance recovery is thus very limited. In particular, the effect of initial velocity on the threshold of balance recovery has not been quantified, despite experimental (Berg et al., 1997; Pavol et al., 2001) and theoretical (Maki and McIlroy, 1999; Pai and Patton, 1997; van den Bogert et al., 2002) qualitative evidence of its importance.

The purpose of this study is to quantify the effect of initial velocity on the threshold of balance recovery using both experiments and theoretical modeling. Furthermore, a method will be developed to compare experiments with different initial velocities, regardless of the postural disturbance.

EXPERIMENTAL METHODS

The maximum forward pull force that healthy young adults could sustain and still recover balance using a single step was determined for different walking velocities (1) and different initial lean angles (2) (Figures 1 and 2). The maximum forward lean angle that healthy young adults could be released from and still recover balance using a single step was also determined (3). The pull forces and lean angles were sequentially increased until the subjects failed twice at a given force or angle. Body segment kinematics and forces were recorded using an optoelectronic motion measurement system and force sensors. In particular, the equivalent disturbance angular positions and velocities were measured, i.e., the angular positions and velocities in the sagittal plane from the vertical to the line connecting the stance ankle and the center of mass at the time when the subject activated joint torques to attempt balance recovery.

THEORETICHAL METHODS

Since one initially falls nearly as straight as a rigid link, the initial part of a fall, prior to joint torque activation, was simulated using an inverted pendulum model. The mass, length, initial angular position, initial angular velocity and pull force of the model were representative of our subjects and each of our experimental postural disturbances.

RESULTS

Both the experiments and the theoretical model showed (Figures 1 and 2) that:

- The maximum forward pull force that subjects could sustain decreased as initial walking velocity increased.
- The maximum forward pull force (in effect adding initial velocity), that

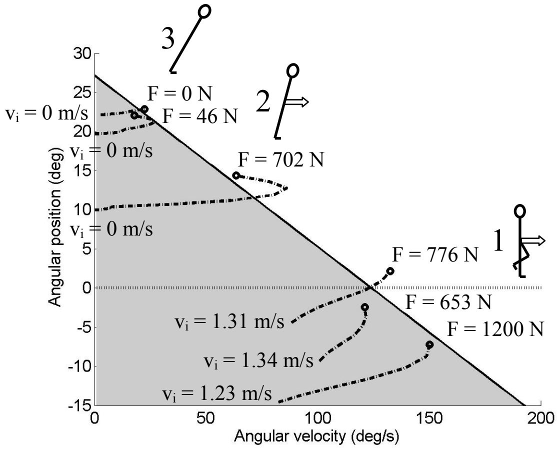

Figure 1: Experimental results

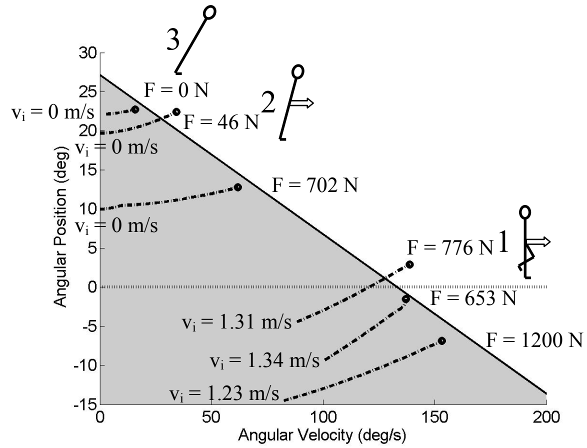

Figure 2: Theoretical model results

subjects could sustain increased as the initial lean angle decreased.

- The equivalent disturbance angular position and velocity points, for both the maximum forward pull and lean trials, formed a disturbance threshold line.

DISCUSSION

Preliminary results have shown that an increase in initial velocity, whether it is produced by walking or artificially added by pulling, decreased the postural perturbation one could sustain. More importantly, the disturbance threshold line thus formed separated falls from recoveries, regardless of the postural disturbance. If the postural perturbation generated an equivalent disturbance angular position and velocity point below the disturbance threshold line (grey area), balance recovery was possible. If the postural perturbation generated an equivalent disturbance angular position and velocity point above the disturbance threshold line (white area), balance recovery was not possible and a fall occurred.

SUMMARY

Further human experiments are needed but preliminary results have shown that initial velocity had a detrimental effect on the threshold of balance recovery. Moreover, the disturbance threshold line method to compare experiments with different initial velocities shows substantial promise, especially when you consider how different the three postural disturbances were. It even suggests that results from experiments with no initial velocity can predict results of experiments with initial velocity.

REFERENCES

Berg, W.P. et al. (1997). *Age Ageing*, **26**(4), 261-268.

Pavol, M.J. et al. (2001). *J. Geront.*, **56A**(7), M428-437.

Maki, B.E., McIlroy, W.E. (1999). *IEEE Trans. Rehabil. Eng.*, **7**(1), 80-90.

Pai, Y.C., Patton, J. (1997). *J. Biomech.*, **30**(4), 347-54.

van den Bogert, A.J. et al. (2002). *J. Biomech.*, **35**(2), 199-205.

ACKNOWLEDGEMENTS

We gratefully acknowledge the assistance of Véronic Francoeur-Castilloux, Gabrielle Gaudreault-Malépart, Jean-Sébastien Gosselin, Mathieu Hamel, Simon Héroux, Michel Morin, Grégoire Poirier Richer, Étienne Poulin, Dominique Régnier and Yves Roy, along with the support of grant RG-02-0585 from the Whitaker Foundation.

EFFECT OF DISC DEGENERATION ON BIOMECHANICAL RESPONSE OF LUMBAR DISCS SUBJECTED TO CYCLIC LOADING

Jamie Ryan Williams, Raghu N. Natarajan and Gunnar B. J. Andersson
Department of Orthopedic Surgery, Rush University Medical Center, Chicago, IL, USA
E-mail: Jamie_Williams@rush.edu

INTRODUCTION

Extensive clinical as well as experimental research had demonstrated that injuries such as disc herniations and fissure formation in the endplates, are often accompanied with changes in the elastic and poroelastic material properties of the annulus, nucleus and endplates. Studies have shown that the stiffness of the motion segment increases with mild to moderate degeneration and stiffness decreases as the degeneration becomes more severe [1,2]. The purpose of this study was to understand how disc degeneration affects the biomechanical characteristics of a lumbar motion segment subjected to cyclic loading. This was achieved with the help of finite element models by comparing biomechanical characteristics of a healthy motion segment (Grade I) with those of a degenerated lumbar disc (Grade IV) at the end of four hours of cyclic loading.

METHODS

Degeneration is classified into five grades according to Thompson's criterion using T2-weighted sagittal MRIs. Grade I indicates normal and Grade V indicates the most advanced degeneration with each grade denoting specific changes that can be observed on the MRIs. The nucleus and to a lesser extent the annulus undergo dramatic morphological and compositional changes with age and degeneration. The compositional changes include significant loss of hydration and decreases in the concentration of proteoglycans within these tissues [3-5].

A three-dimensional finite element model of the L4-L5 motion segment, which was validated for circadian loading conditions [6], was used to represent the normal, healthy Grade I disc. The Grade IV model was created by modifying the material properties of the inner and outer annulus and the nucleus using values taken from the literature.

The finite element models were loaded at a frequency of one cycle per minute. The load varied from F_{max} to 40 % of F_{max} . F_{max} was applied over 1.5 seconds and reduced to 40% of F_{max} over 1.5 seconds. The reduced load (40% F_{max}) was held constant over 57 seconds. The disc height loss when the maximum load reached 10^{th} cycle as well as when the maximum load reached 240^{th} cycle was compared.

RESULTS

Figure 1 compares the disc height loss as a function of maximum applied load as predicted by finite element models representing Grade I and Grade IV discs. Results are presented at the maximum load during 10^{th} cycle as well as at the 240^{th} cycle. The plots illustrate how disc degeneration affects the biomechanical properties both during early stages of cyclic loading as well as after considerable number of cyclic loadings.

The disc height loss was larger during 240th cycle of loading both in normal disc (Grade I) as well as in degenerated disc (Grade IV) as compared to the height loss during early stages of the cyclic loading. Cyclic loading also showed that Grade I discs are much more flexible than Grade IV discs as evident from the result that the disc height loss for all loading values in Grade IV discs were less than those seen in healthy discs.

At peak 2000N load, Grade I disc deformation increased from 2.5 mm at 10th loading cycle to 4.5 mm at 240th load cycle. The corresponding increase in deformation was 1.0 mm to 1.8 mm in a degenerated disc. Stiffness of a healthy disc with 2000 N peak load decreased from 800 N/mm at 10th cycle load to 444 N/mm at 240th cycle loading indicating that stiffness decreased as load cycle increased.

When subjected to large compressive loads (3000N), the healthy discs had an increase in height loss of 48% during 240th cycle of loading as compared to height loss during 10th cycle of loading. In the case of degenerated discs the corresponding increase in height loss was 40% during 240th cycle. At smaller compressive loads (1000N), healthy discs showed an increase in disc height of 110% at 240th cycle of loading as compared to disc height loss at the 10th cycle of loading. However, at these smaller compressive loads, there was no change in disc height loss in degenerated discs as the number of load cycles increased.

DISCUSSION

In response to four hours of cyclic loading, healthy discs showed that as the number of loading cycles increased, disc height loss at peak load also increased due to larger amount of fluid continuously moving out of the disc which may be attributed to not enough time was provided for the disc to completely relax. Disc height loss at peak load during early stages of the cyclic loading as well after 240 cycles of loading in healthy discs were larger than the corresponding loss of height in degenerated discs indicating that the fluid flow in and out of the disc is large in healthy discs. At large peak loads, disc height loss was also large in healthy disc, which may in part be due to deformation of the solid matrix. This increased deformation of the solid matrix may result in further injury of the disc. In both healthy and degenerated discs for a particular peak load, as the number of load cycles increased, stiffness decreased.

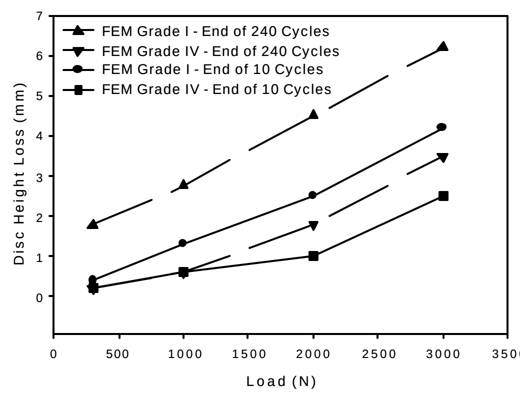

Figure 1: Effect of disc degeneration on biomechanical response of lumbar discs subjected to cyclic loading

REFERENCES

[1] Fujiwara, et al., (2000) Spine 25(23):3036-3044. [2] Nachemson, A and Schultz, A, (1979) *Spine*, 4(1): 1-8, [3] Urban JPG, et al. (1988) *Spine*, 10: 494-507, [4] Iatridis J, et al., (1997) *J. Orthop Research*, 15: 318-322, [5] Iatridis J, et al., (1998) *J. Biomechanics*, 31: 535-544, [6] Williams JR, et al., (2004) Proceedings of the 50th Annual Meeting of the Orthopedic Research Society

ACKNOWLEDGEMENTS

NIH: AR48152-02

MODULATION OF MUSCLE SYNERGIES OVER TIME DURING POSTURAL RESPONSES

Gelsy Torres-Oviedo [1], Jane M. Macpherson [2] and Lena H. Ting [1]

[1] Department of Biomedical Engineering, Georgia Tech/Emory University, Atlanta, GA, USA
[2] Neurological Sciences Institute, Oregon Health & Science University, Beaverton OR, USA
E-mail: gelsy@neuro.gatech.edu Web: http://users.ece.gatech.edu/~gelsy/

INTRODUCTION

In both cats and humans, postural responses to support surface translations are characterized by different EMG patterns for each direction of perturbation (Macpherson 1988, Henry et al. 1998). It has been shown that complex EMG patterns of the initial automatic postural response (APR) can be composed of a limited set of muscle synergies (Ting and Macpherson 2002). We investigated whether muscle synergies can characterize the variability in muscle activation for the entire postural response including background, transient, automatic, and voluntary activity. We also tested synergies robustness when reconstructing postural responses at different stance configurations.

METHODS

3 freely standing cats were translated in 12 directions while standing with the paws at 62 to 135.5% of preferred anterior-posterior stance distance. EMG activity in 14 left hindlimb muscles was recorded before, during, and after perturbations. EMGs were binned every 10 ms over a 1 s duration.

Each synergy was represented as a vector of constant positive-valued components indicating the relative activity level of each muscle within that synergy (Tresch et al. 1999). A synergy is thus defined as a group of muscles whose relative activity level is fixed. Synergies are scaled independently by synergy coefficients. Varying synergy coefficients provides the flexibility needed to reconstruct muscle patterns.

The synergies and coefficients that best reconstructed EMG responses over time were computed using a nonnegative matrix factorization algorithm (Lee and Seung 2001). Synergy vectors extracted from EMG at the shortest stance distance were used to reconstruct EMG data at all other stances.

RESULTS AND DISCUSSION

In all cats, only 5 synergies were required to reproduce > 96% of the muscle activity at the shortest distance (Figure 1).

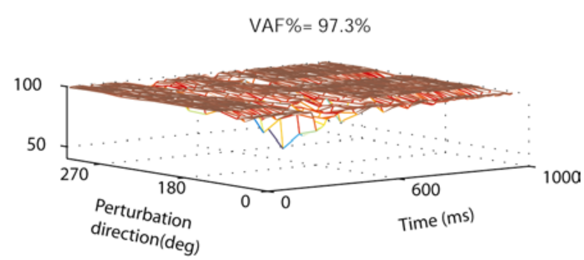

Figure 1: Percent EMG variability accounted for by 5 synergies over time and perturbations in cat Ru.

Therefore, synergy vectors can reconstruct not only the initial APR (EMG activity from 60 to 140 ms after perturbation onset) but also background, early, and late activity, which could have voluntary components. Synergies were very similar to those extracted from the initial APR ($0.6 < r^2 < 0.98$).

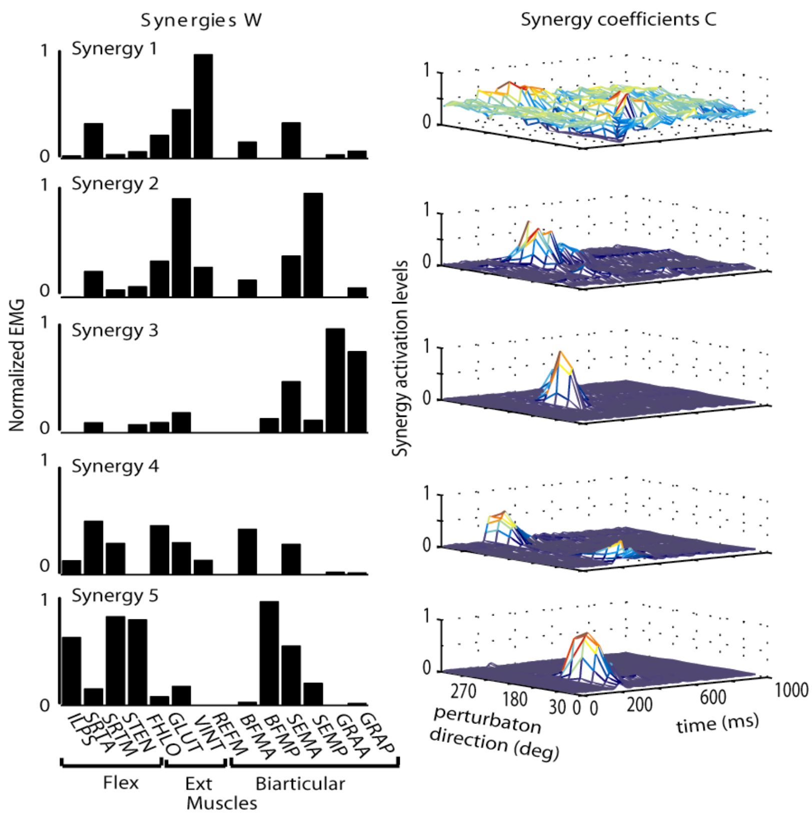

Figure 2: Muscle synergies and synergy activation levels versus perturbation direction and time.

Two synergies were dominated by either flexor or extensor muscles, another synergy by adductors, and two synergies by biarticular muscles. Each synergy vector responds to a preferred range of perturbation directions 60 – 300 ms following perturbation onset (Figure 2). However, only the 'extensor synergy' (synergy 1) was active in the background period of 0 to 120 ms. This synergy was also activated during 180 to 360° perturbations and was inhibited during 0 to 180° perturbations, when the 'flexor synergy' (synergy 5) was active. Finally, at the end of platform displacement only the extensor synergy was active again.

Moreover, the same 5 synergies reproduced >91% of the muscles EMGs at all stance distances (4 postures x 14 muscles x 12 directions x 100 time bins).

ACKNOWLEDGEMENTS
Funded by NIH HD46922.

SUMMARY

The muscle activity before, during, and after postural perturbations can be accounted for by 5 muscle synergies even at different stance distances. This robustness suggests that synergies can characterize not only the initial automatic postural response, but also EMG patterns during quiet standing, early reflex response, and voluntary behaviors.

REFERENCES

Henry, S. M. et al.(1998). *J. Neurophysiol.* 80, 1939-1950.
Lee, D. D. and Seung, H. S. (2001). *Adv. Neural Info. Proc. Syst.,* 13, 556-562.
Macpherson, J. M. (1988) *J. Neurophysiol.* 60, 218-231.
Macpherson, J. M. (1994). *J. Neurophysiol.* 71, 931-940.
Ting and Macpherson (2002) *Proc IV World Congress Biomechanics.*
Tresch, M. C. et al. (1999). *Nat. Neuroscience,* 2, 162-167.

MORPHOLOGY, ARCHITECTURE AND BIOMECHANICS OF HUMAN CERVICAL MULTIFIDUS MUSCLES

Jess S. Anderson[1], Andrew W. Hsu[1], and Anita N. Vasavada[1,2]

[1]Department of Veterinary and Comparative Anatomy, Pharmacology and Physiology
[2]Program in Bioengineering, Washington State University, Pullman, WA USA
E-mail: vasavada@wsu.edu Web: www.bioengineering.wsu.edu\alias\?AnitaVasavada

INTRODUCTION

Multifidus is a deep spinal muscle which may play a critical role in spinal stability, proprioception, injury and pain. The morphology of lumbar multifidus has been reported (Macintosh *et al.*, 1986), but little is known about cervical multifidus. The objectives of this study were (1) to describe the fascicular attachment pattern of cervical multifidus; (2) to quantify the muscle's architecture parameters and (3) to model its moment-generating capacity.

METHODS

We studied cervical multifidus in nine cadaveric specimens (6F, 3M). Fascicles of multifidus with common cranial and caudal attachments were isolated and are referred to here as *fascicular subgroups*. After harvesting and digestion of connective tissue, the mass and musculotendon, fascicle and sarcomere lengths were measured. Fascicle length was normalized by optimal sarcomere length (2.8 µ) to calculate optimal fascicle length. Physiological cross sectional area (PCSA) was calculated by dividing mass by density and optimal fascicle length. The data were incorporated into a biomechanical model of the neck (Vasavada *et al.*, 1998) developed in Software for Interactive Musculoskeletal Modeling (Musculographics, Santa Rosa, CA). Each fascicular subgroup was modeled as a distinct muscle, and moment arms, force- and moment-generating capacity were calculated for extension, axial rotation and lateral bending.

RESULTS AND DISCUSSION

Cervical multifidus can be divided into two layers (Figure 1). The superficial layer consists of three bands of fascicles originating from the facet capsules of C4/C5 through C6/C7, which all insert on the spinous process of C2. A deeper layer of fascicles originates more posteromedially on the facet capsules and inserts on superior laminae. Fascicles originating from C4/C5 insert on C2, those from C5/C6 on C3, and those from C6/C7 on C4. The two layers of multifidus are also seen in the thoracic and lumbar spine; however, fascicles arise from transverse processes in the thoracic spine (unpublished observations) and mamillary processes in the lumbar spine (Macintosh et al, 1986) instead of facet capsules.

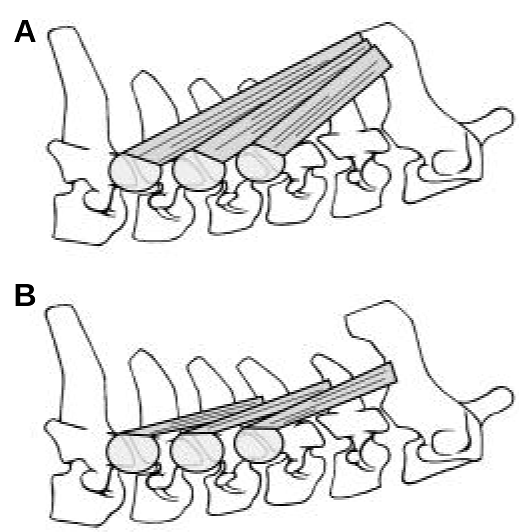

Figure 1. Schematic of multifidus attachment patterns in the cervical region (C2-C7). (A) Superficial layer. (B) Deep layer.

The mass of individual fascicular subgroups ranges from 0.1 to 2.7 g, and the total mass of multifidus averages 5.8 g (± 2.2 g), with the superficial layer comprising 61% (± 11.5%) of the total. On average, fascicle length is approximately half the total musculotendon length. For subgroups that cross the same number of segments, musculotendon lengths are shorter in the deep layer. Average sarcomere length is 2.5 μ, which is shorter than optimal length. If it is assumed that all cadavers went into rigor in a neutral spine posture, this implies that sarcomeres would be at optimal length in a slightly flexed posture.

Table 1: Architecture parameters of cervical multifidus.

	Mass (g)	PCSA (cm^2)	MT length (cm)	Optimal fascicle length (cm)
Superficial				
C4/C5-C2	0.9 (0.6)	0.4 (0.2)	3.7 (0.4)	1.9
C5/C6-C2	1.5 (0.8)	0.6 (0.3)	5.0 (1.0)	2.6
C6/C7-C2	1.4 (0.7)	0.5 (0.2)	5.6 (1.5)	2.9
Deep				
C4/C5-C2	0.4 (0.2)	0.2 (0.1)	3.4 (0.8)	1.9
C5/C6-C3	0.8 (0.5)	0.4 (0.2)	3.1 (1.1)	2.0
C6/C7-C4	1.1 (0.4)	0.5 (0.1)	3.4 (0.5)	2.0
Total	5.8 (2.2)	2.3 (0.6)		

In the neutral position, multifidus has equal moment-generating capacity for extension and lateral bending. The total moment-generating capacity of multifidus is less than 1 Nm in any plane of motion. Extension moment-generating capacity decreases beyond 40° extension due to decreases in both moment arm and force. Extension moment-generating capacity increases with flexed postures due to increases in force. Axial rotation moment-generating capacity is greater in ipsilateral rotated postures (due to increases in both moment arm and force) and lower in contralateral rotated postures (due to decreases in moment arm). Lateral bending moment-generating capacity increases in ipsilateral bent postures primarily because of increases in moment arm, and in contralateral bent postures because of increases in force.

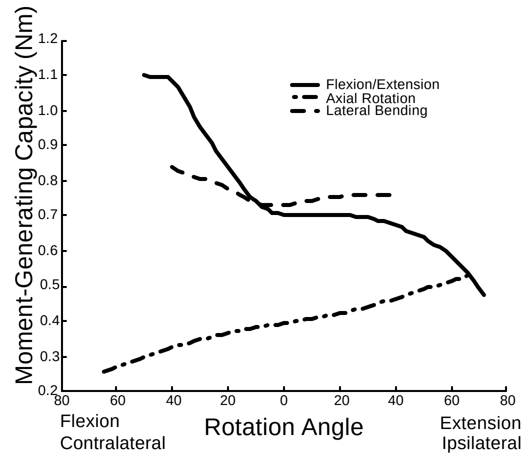

Figure 2: Maximum moment-generating capcity of cervical multifidus (sum of all fascicular subgroups).

SUMMARY

We have described the fascicular attachment patterns, quantified architecture parameters, and calculated biomechanical properties of cervical multifidus. Further, we confirmed that multifidus has direct attachment onto the cervical facet capsule, corroborating its hypothesized role in neck pain and injury (e.g., Winkelstein *et al.*, 2000). Although multifidus is capable of generating only small forces and moments, its ability to control motions at specific intervertebral joints may make it an important contributor to the control of head and neck posture.

REFERENCES

Macintosh *et al.* (1986). *Clin Biomech*, **1**:196-204.
Vasavada *et al.* (1998). *Spine*, **23**: 412-421.
Winkelstein *et al.* (2000). *Spine* **25**: 1238-1246.

ACKNOWLEDGEMENTS

We would like to thank the George W. Bagby foundation for financial support. Specimens were obtained from National Disease Research Interchange.

CAPSULE REPRESENTATION IN A TOTAL HIP DISLOCATION FINITE ELEMENT MODEL

Kristofer J. Stewart [1], Douglas R. Pedersen [1,2], John J. Callaghan [1,2], and Thomas D. Brown [1,2]

[1] Department of Orthopaedics and Rehabilitation, University of Iowa, Iowa City, IA, USA
[2] Department of Biomedical Engineering, University of Iowa, Iowa City, IA, USA
E-mail: kristofer-stewart@uiowa.edu Web: mnypt.obrl.uiowa.edu/OBL_Lab_Website

INTRODUCTION

Nonlinear finite element (FE) analysis of total hip dislocation has opened exciting new avenues for minimizing this poorly understood but all-too-common major complication of total hip arthroplasty (THA). Factors affecting the propensity for dislocation include mechanical design of the implant, inappropriate implant placement, untoward hip joint motions by the patient, bony impingement, and compromise of periarticular soft tissue integrity due to surgical technique. Capsule deficit due to prior hip surgery is one of the major risk factors for dislocation. Previously validated FE models (Scifert, 1998; Nadzadi, 2003), which investigated how several total hip component design and surgical placement variables contribute to resisting the propensity for dislocation when subjected to at-risk hip joint motions, have now been enhanced with the incorporation of experimentally based hip capsule representation and anatomic bone structures.

METHODS

For purposes of incorporating the entire hip capsule into the existing computational model (Fig. 1A), it was important to include the full circumferential mapping of material properties, and to unambiguously define a number of discrete geometric sectors. Eight individual capsule sectors were defined, as a compromise between mapping a relatively large number of distinct circumferential locations, versus having tissue samples large enough to reliably test.

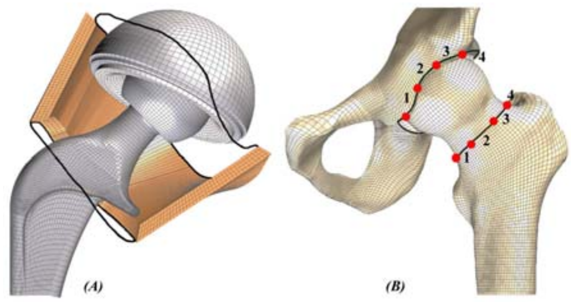

Figure 1: (A) Computational FE model enhanced with capsule representation (anterior capsule removed for viewing), (B) anterior view of capsule sector definitions.

These eight capsule sectors were incorporated into the whole-joint finite element model at anatomically appropriate insertion points, using rigid body renditions of the femur and hemi-pelvis (Fig. 1B). Detailed anatomic features of these bony structures were extracted from CT data, using edge-detection methods operating on 1-mm serial sections. Triangulated surfaces were fitted to the resulting point cloud data for the femur and hemi-pelvis. These surfaces, which were zoned with a three-dimensional, all-quadrilateral rigid body finite element mesh using TrueGrid's (v2.1,XYZ Scientific Applications, Inc., Livermore, CA) mesh generator, provide quantitative spatial basis for establishing capsule attachment sites (solid black line, Figs. 1A, 1B). Accurate registration of each capsule sector into this computational model was achieved using common reference points and initial geometric measurements obtained from previous experimental work (Stewart, 2002). Each capsule sector was meshed entirely with hexahedral continuum elements having experimentally-based hyperelastic material characteristics (Yeoh, 1990).

To highlight the capsule's contribution to stability, kinematics and kinetics were input for the most dislocation-prone maneuver identified by Nadzadi et al. (2003): the low sit-to-stand maneuver. ABAQUS/Explicit V6.3-1 (ABAQUS, INC., Pawtucket, RI) provided an effective method for solving complex contact problems introduced with the inclusion of hip capsule representation.

RESULTS AND DISCUSSION

Resisting moment development (Fig. 2) as a function of angular motion input served as the key output metric for this study.

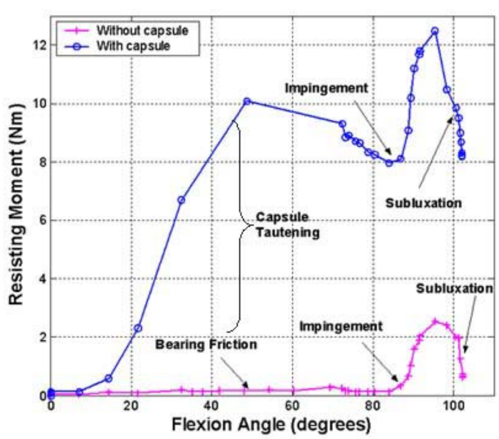

Figure 2: Femoral resisting moment comparison between hardware-only and capsule-enhanced models.

In the capsule-enhanced model, the angular motion input was met with substantial resistance due to progressive tautening of the capsule even from the initiation of flexion. This tautening resistance resulted in a dramatic increase in the resisting moment developed throughout the low sit-to-stand maneuver. These preliminary results show that capsule representation provides approximately a 3.6-fold increase in construct stability, compared to an otherwise identical hardware-only construct.

For this particular extreme maneuver, the capsule was stressed (Fig. 3C) to about 70% of its failure strength (Stewart, 2002). Since this tautened tissue lies appreciably eccentric to the neck-liner impingement fulcrum (Figs. 3A, 3B), it works efficiently "in parallel" with the implant itself to resist the tendency for dislocation, reducing the peak polyethylene stresses at the impingement site and at the head egress site by typically 27% and 50%, respectively, relative to the hardware-only case.

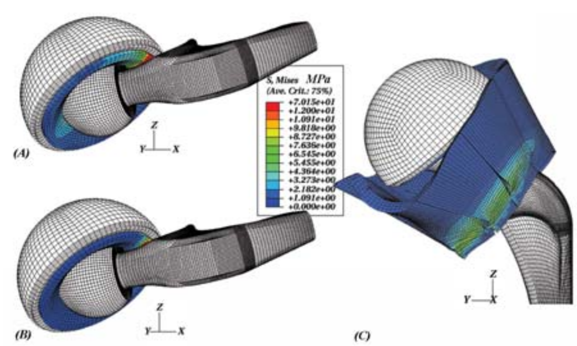

Figure 3: (A) Component-only model well into impingement, (B) capsule-enhanced model at same instant, and (C) posterior view of capsule stress contours.

REFERENCES

Scifert, C.F., et al. (1998). *Clinical Orthopaedics,* **335**, 152-162.

Nadzadi, M.E., et al. (2003). *J Biomech,* **36**, 577-591.

Stewart, K.J., et al. (2002). *J Biomech,* **35**, 1491-1498.

Yeoh, O.H. (1990). *Rubber Chemistry and Technology,* **63**, 792-805.

ACKNOWLEDGEMENTS

Study supported in part by AR NIH 46601

SURFACE ELECTROMYOGRAPHIC SPIKE ACTIVITY AND MOTOR UNIT FIRING RATES AT DIFFERENT LEVELS OF MAXIMUM CONTRACTION

David Gabriel[1], Scott Rubinstein[2], Anita Christie[2], J. Greig Inglis[1], and Gary Kamen[2]

[1]Raymond Nelson Reid Biomechanics Laboratory, Brock University, St. Catharines, ON, CA
[2]Motor Control Laboratory, University of Massachusetts at Amherst, Amherst, MA, USA
E-mail: dgabriel@arnie.pec.brocku.ca

INTRODUCTION

A form of surface electromyographic (SEMG) interference pattern (IP) analysis has been advanced as a means to monitor motor unit (MU) firing. A correlational link has been made with power spectral analysis (Gabriel et al., 2001) but the technique has yet to be validated using simultaneous recordings from both surface and indwelling electrodes. This study monitored both surface and indwelling muscle activity to validate a form of IP analysis.

METHODS

Thirteen subjects reported to the University of Massachusetts (Amherst) Motor Control Laboratory for a single test session. Subjects sat in a testing chair with their lower leg secured in a jig designed to isolate the action of the dorsiflexors during an isometric contraction (see Figure 1). After a brief familiarization period, subjects completed two isometric contractions of the dorsiflexors at 40, 60, 80, and 100% of maximal voluntary contraction (MVC). Contractions were limited to 10 seconds and occurred at 3 minute intervals. Visual feedback was provided to participants through a video monitor.

Force was monitored using the MB-250 strain gauge force transducer (Interface, Inc., Scottsdale, AZ), mounted beneath the footplate. The force signal was sampled at 50 Hz. The SEMG activity of tibialis anterior (TA) was recorded with Ag/AgCl electrodes (Therapeutics Unlimited Inc., Iowa City, IA). The signal was amplified (2000x), band-passed (20-500 Hz) filtered and sampled at 2.5 kHz. The MU activity was monitored with a 25-gauge quadrifilar needle electrode placed near the surface electrodes (Patten and Kamen, 2000). The MU recordings were bandpassed (1 kHz-10kHz) filtered and sampled at 25.6 kHz (Dantec Counterpoint, Dantec Electronic Medicinsk, Skorlunde, Denmark).

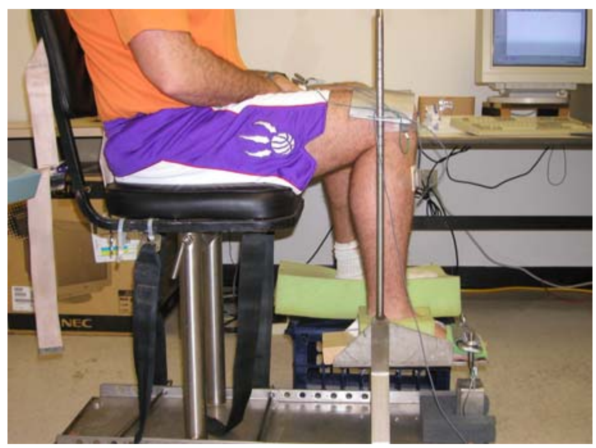

Figure 1: The chair and lower-leg testing unit designed for isometric dorsiflexion contractions.

Analysis of force and SEMG was conducted on a stationary segment of data 1-sec in duration (see Figure 2). Mean spike frequency (MSF), mean power frequency (MPF), mean spike amplitude (MSA), and root-mean-square (RMS) amplitude were calculated in MATLAB (The Math Works, Natick, MA). Firing rates were obtained during a stable portion of the contraction.

The data were subjected to a one-way repeated measures analysis of variance, with orthogonal polynomials for statistical trend testing across the levels of percent MVC. Pearson correlation coefficients were calculated for MSF and MPF and for MSA and RMS amplitude.

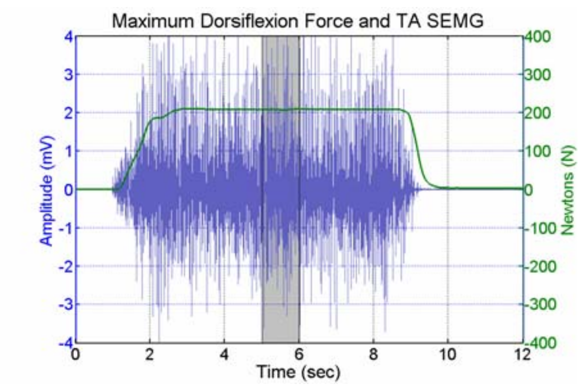

Figure 1: Force (green) and SEMG (blue) from one subject at 100% MVC.

RESULTS AND DISCUSSION

Maximum dorsiflexion strength for the sample was 245±63 N. MSF was 150±22 Hz and MPF was 141±22 Hz at 100 % MVC. Likewise, RMS amplitude was 311±22 μV and MSA was 659±270 μV. The frequency and amplitude content of the SEMG signal exhibited a quadratic increase (P<0.01) while MU firing rates rose linearly from 16±3 to 34±6 pulses per second across the four levels of force (P<0.01). There was a high correlation between MSF and MPF (0.95; P<0.01) and between MSA and RMS amplitude (0.99; P<0.01).

The force, SEMG and firing rate data are all consistent with values reported in the literature (Broman et al., 1985; Patten and Kamen, 2000; Van Cutsem et al., 1997; Moritani and Muro, 1987). Both linear and non-linear increases in MPF with percent MVC been observed, and it is muscle dependent. Whether the increase in MPF is linear or nonlinear, it is has been linked with an increase in MU firing rate, as the percent MVC increases. The MPF is not a pure indicator of MU firing rate, as it is affected by conduction velocity of the newly recruited MUs and the correlation of firing between MUs (Broman et al., 1985). The MPF frequency is nevertheless sensitive to changes in firing rate (Moritani and Muro, 1987). This study also demonstrated that MSF was equivalent to MPF, and that MSF was sensitive to firing rate, thus, adding to the validity of this measure. The same was true for MSA and RMS amplitude.

SUMMARY

MSF and MSA were equivalent to the traditional measures of MPF and RMS amplitude. A linear increase in firing rates across the four force levels was associated with a quadratic increase in the mean frequency content of the signal. Thus, MSF and MSA were sensitive to changes in MU firing rate as percent MVC increased.

REFERENCES

Broman, H., et al. (1985). *Journal of Applied Physiology*, 58, 1428-1437.
Gabriel, D.A., et al. (2001). *Journal of Electromyography and Kinesiology*, 11, 123-129.
Patten, C., Kamen, G. (2000). *European Journal of Applied Physiology*, 83, 128-143.
Van Cutsem, M., et al. (1997). *Candian Journal of Applied*, 22, 585-597.
Moritani, T., Muro, M. (1987). *European Journal of Applied Physiology*, 56, 260-265.

ACKNOWLEDGEMENTS

Funded by NSERC of Canada, the NIH, the ASB Travel Fellowship, and matching funds from the FAHS of Brock University.

CORONAL KNEE MOTION IN CHILDREN PERFORMING DROP LANDINGS IS NOT INFLUENCED BY GENDER

Jeremy J. Bauer, Michael J. Pavol, Wilson C. Hayes, Christine M. Snow

Bone Research Laboratory and Biomechanics Laboratory, Dept. of Exercise & Sport Science,
Oregon State University, Corvallis, OR, USA
E-mail: bauerje@onid.orst.edu

INTRODUCTION

The incidence of knee ligament injuries is reported to be over 4-fold greater in women than in men (Arendt and Randall, 1995; Hewett, 1999). However, researchers to date have not conclusively determined why women are more likely to experience these debilitating injuries compared to men.

Currently, theories explaining the increased knee injury prevalence in women are based on differences in anatomy, hormones and biomechanics/neuromuscular control (Ford, 2003). While there are obvious differences in bony anatomy and hormones between men and women, knee injuries ultimately result from a failure of the supporting knee structures to withstand the applied forces that arise from the kinematics and kinetics of a task.

A majority of knee injuries occur from non-contact events such as landing or pivoting. Differences in knee kinematics have been reported between men and women performing landing activities. Specifically, valgus-directed bilateral knee motion measured in the coronal plane has been reported to be 2.0 and 3.7 cm greater in women compared to men when performing drop jumps from 31 cm and rebounds, respectively (Ford, 2003; Myer, 2002). Modifying landing biomechanics has been reported to decrease the incidence of knee injury 3.6-fold, eliminating gender differences in knee injury incidence (Hewett, 1999).

Pre-pubertal children provide an opportunity to study gender differences in knee joint kinematics independent of hormonal effects. While gender differences in sagittal-plane knee kinematics have been reported in adults performing drop jumps from three different heights, no gender differences were reported in sagittal-plane knee kinematics in pre-pubertal children performing drop landings from 61 cm (Huston, 2001; Owings, 2002). However, no studies have examined gender differences in coronal knee motion in pre-pubertal children.

Our aim was to determine whether gender differences in coronal knee motion during drop landings exist in pre-pubertal children. We hypothesized that pre-pubertal boys and girls would have similar coronal knee kinematics.

METHODS

Sixteen pre-pubertal children (8 girls, age = 8.2 ± 1.1 yrs, mass = 34.7 ± 8.4 kg; 8 boys, age = 8.4 ± 0.8 yrs, mass = 30.5 ± 3.1 kg; mean ± SD), untrained in drop landings, were instructed to step off of a 61 cm high platform and to land with one foot on each of two 40 x 60 cm force platforms (Bertec, Columbus, OH) mounted 5 mm apart. Ground reaction forces (GRF) were sampled at 1080 Hz. A six-camera motion capture system (Vicon Motion Systems, Lake

Forest, CA) sampling at 120 Hz and synchronized with the force platforms, recorded the position of two reflective markers placed on the lateral aspect of the left and right knee joint centers of each child, respectively.

The coronal (varus/valgus) motion of the knee during landing was quantified by the change in the coronal-plane inter-knee distance between two time points (TP): TP1) 3 frames (0.025s) before ground contact as determined from GRF data, and TP2) maximum inter-knee distance in cases of initial varus motion after ground contact or minimum inter-knee distance in cases of initial valgus knee motion. Coronal knee motion was calculated by subtracting the distance at TP2 from that at TP1. Therefore, varus motion is negative and valgus motion is positive. The mean of 10 trials was treated as the datum for each subject.

A two-tailed t-test assuming equal variance was used to determine whether gender differences in coronal knee motion were equal to 0. Statistical significance was set at $p < 0.01$ due to the small subject sample size.

RESULTS AND DISCUSSION

Coronal knee motion during landing did not differ between boys and girls ($p = 0.17$). Knee motion in boys and girls was 2.0 ± 3.3 cm and -1.0 ± 5.0 cm respectively. Mean knee motion of each girl ranged from -9.1 to 6.5 cm. Mean knee motion of each boy ranged from -2.9 to 7.3 cm. The lack of difference in coronal knee motion supports an earlier claim that gender differences in knee kinematics upon landing develop with age (Owings, 2002). However, it does appear as though there may be more variance in the pre-pubertal population compared to the high-school population. A strength of this study is the inclusion of 10 trials for each subject where previous studies in adults used the mean from only 3 trials. In addition, this study is unique in assessing gender differences in pre-pubertal children. The small subject sample size (n=16) is a limitation to the study.

SUMMARY

Knee kinematics upon landing do not appear to be gender specific in pre-pubertal children, suggesting that the neuromuscular control of the limbs also does not differ. Neuromuscular training has been shown to eliminate gender differences in knee injury incidence in a young high-school population (Hewett, 1999). Therefore, neuromuscular training of girls before and during puberty might potentially prevent the development of any gender differences in mechanics that place women at greater risk of knee injury.

REFERENCES

Arendt, E., Randall, D. (1995). *Am. J. Sports Med.*, **23**, 694-701.
Ford, K.R. et al. (2003). *Med. Sci. Sports Exerc.*, **35**, 1745-1750.
Hewett, T.E. et al. (1999). *Am.J. Sports Med.*, **27**, 699-705.
Huston, L.J. et al. (2001). *Am.J. Knee Surg.*, **14**, 215-219.
Myer, G.D. et al. (2002). *Med. Sci. Sports Exerc.*, **34**, S247.
Owings, T.M. et al. (2002). *Med. Sci. Sports Exerc.*, **34**, S85.

ACKNOWLEDGEMENTS

Supported by NIH AR 45655-01.

INFLUENCE OF VASTI ORIENTATION ON THE PATELLAR LIGAMENT FORCE/ QUADRICEPS FORCE RATIO DURING KNEE EXTENSION

Sam Chen[1], Irving Scher[2], Christopher Powers[1], and Thay Lee[3]

[1] Musculoskeletal Biomechanics Research Laboratory, Department of Biokinesiology and Physical Therapy, University of Southern California, Los Angeles, CA, USA
[2] Exponent, Failure Analysis Associates, Los Angeles, CA, USA
[3]Orthopedic Biomechanics Laboratory, Long Beach VA Heathcare System, Long Beach, CA, USA
E-mail: powers@usc.edu Web: asb-biomech.org

INTRODUCTION

Early biomechanical descriptions of the patellofemoral joint characterized this articulation as a frictionless pulley system in which the patellar ligament force was equal to the force applied by quadriceps tendon. However, more recent studies have revealed that the patella also acts as a lever; a force differential between the patellar ligament and quadriceps tendon results from a moving contact point of the patella on the femur (Yamaguchi et al.; van Eidjen et al.). Previous cadaveric studies have shown that the ratio of patellar ligament force to quadriceps force can range from 0.64 at 70 degrees to 1.16 at 10 degrees of knee flexion (Buff et al., Huberti et al.).

A limitation of previous cadaveric studies in this area is that the loading of the extensor mechanism was accomplished through the central quadriceps tendon (i.e., anterior and parallel to the femoral axis). Given that the vasti originate from the linea aspera, which runs along the posterior aspect of the femur, it is unlikely that the application of the quadriceps force along the axis of the femur is representative of the actual extensor resultant force.

The purpose of this preliminary study was to compare the effects of an axial loading condition (central quadriceps tendon loading parallel to the femur) and an anatomically based, multi-plane loading condition (individual vasti loaded, taking into consideration physiologic muscle fiber orientation) on the ratio of quadriceps force to patellar ligament force at various knee flexion angles. Such information is important to better characterize the biomechanics of the extensor mechanism for more accurate models of the patellofemoral joint.

METHODS

Two fresh frozen cadaver knees without severe arthrosis were dissected, keeping the retinaculum and quadriceps tendons intact, and placed onto a rigid jig. The jig held the tibia distal to the tibial tuberosity, and the femur at mid-diaphysis. The jig was capable of holding the knee in flexion (up to 90 degrees), and allowed the cut rectus femoris and vasti tendons to be loaded in physiologic directions.

The knees were placed into a neutral position at four varying degrees of flexion. Jig settings were recorded while loads were applied to the rectus femoris and vasti tendons in each position. On one specimen (knee 1 – a patella alta), the tibial plateau was excised, and all ligaments were removed except the patellar ligament. This allowed the tibio-femoral joint reaction force to be eliminated while maintaining patello-femoral kinematics.

A buckle transducer (NK Biotechnical Corp., “S” transducer, 670N range, 1N resolution) was placed on the patellar ligament near the tibial attachment. A six-axis load cell on the jig measured the force and torque applied to the femur by the patella. A complete set of data included the magnitude and direction of each applied force, the 6-axis loading on the femur, and the patellar ligament force.

Measurements were taken while weights were used to pull the proximal end of the cut rectus femoris superiorly with 157N of force. Additional measurements were taken with weights pulling the central, medial vasti, and lateral vasti tendons in physiologic directions; the loads for the three groups were calculated to produce a resultant force of 157N. Vastus intermedius was not distinguished from rectus femoris in this experiment.

RESULTS AND DISCUSSION

The F_{PL}/F_Q ratio was different for loading the rectus femoris with and without the vasti (Table 1). This difference was most pronounced at the extremes of the flexion angles.

Table 1: F_{PL}/F_Q ratio for rectus femoris loading with and without vasti.

	Knee 1		Knee 2	
Knee flexion	Central tendon	Cental and vasti tendons	Central tendon	Cental and vasti tendons
0°	1.03	1.69	1.15	1.54
20°	1.07	1.14	1.15	1.02
40°	1.04	1.04	0.96	0.86
60°	0.77	0.54	0.86	0.72

Previous authors have determined the F_{PL}/F_Q ratio while loading only along or slightly posterior to the long axis of the femur. Our ratios for rectus-only loading were similar to those reported by Buff et al. and Huberti, et al. However, when loading in more physiologic directions using the vasti, the F_{PL}/F_Q ratio increased substantially at 0 degrees flexion and decreased substantially at higher degrees of knee flexion.

At low flexion angles, the additional force required by loading the vasti was transmitted to the patellar ligament. Thus the F_{PL}/F_Q ratio at low angles may be under-predicted in the models used previously. At higher flexion angles, this alters the effective moment arm of the quadriceps, resulting in a decrease in the patellar ligament force and an increase in the patella-femoral joint reaction force.

SUMMARY

The vasti affect the F_{PL}/F_Q ratio by changing the direction of the quadriceps’ resultant force on the patella. The previously reported range of F_{PL}/F_Q ratios were underestimated for low flexion angles and overestimated for high flexion angles.

REFERENCES

Buff, H, et al. (1988). *J Biomech*, **21**, 17-23.

Huberti, et al. (1984). *J. Orthop Res.,* **2**(1), 49-54.

van Eijden, TM, et al. (1985). *J Biomech*, **18**(10), 803-809.

Yamaguchi, GT, Zajac, FE. (1989). *J Biomech*, **22**(1), 1-10.

ACKNOWLEDGEMENTS

This work was supported by the Whitaker Foundation.

THE EFFECT OF HAND POSITION ON GROUND REACTION FORCES WHEN FALLING FORWARD FROM KNEELING HEIGHT

Courtney D. Gavin[1], Karen L. Troy[1], and Mark D. Grabiner[1]
[1] Musculoskeletal Biomechanics Laboratory, University of Illinois at Chicago
Chicago, IL USA E-mail: cgavin1@uic.edu

INTRODUCTION Forward falls are the dominant cause of upper extremity injuries (Oskam, et al 1998). Since a large percentage of these falls are unavoidable, focusing on strategies to reduce the incidence of injury resulting from such falls is important.

Several groups have examined the ground reaction forces that result from forward falls (Kim and Ashton-Miller 2003; DeGoede and Ashton-Miller 2002). The primary focus of such studies has been to identify strategies that fallers could employ to reduce the peak resulting force from a fall. However, these studies have not reported or controlled for hand position relative to the torso. It is likely that peak ground reaction force varies with varying hand-torso position.

Therefore, we hypothesized that falls in which the hands are widely spaced would result in larger lateral shear forces, while falls in which the hands are placed high relative to the torso would result in increased anterior shear force. Overall, we hypothesized that there exists a hand-torso position in which resultant ground reaction force is minimized.

The purpose of the study was to determine how varying hand-torso position affects ground reaction forces, as well as to determine whether a hand-torso position exists that can minimize ground reaction forces during impact from a fall initiated from a kneeling position.

METHODS Eight healthy adults (three males, five females) aged 22 to 53 years old participated in the study. Each subject was instructed to kneel in front of two side by side force plates (ATMI) so that by falling forward, each hand would contact one plate and their nose would line up with a place marker located between the plates (Figure 1). Ground reaction data was recorded at 2400 Hz. For a given trial, the subject leaned forward from a kneeling position and targeted one of four specified hand positions (marked with numbered Xs). These positions included placing the hands wide or keeping them a narrow distance apart and having them high relative to the torso (approximately shoulder height) or low relative to the torso (near the axilla). Each specified location was targeted for three consecutive trials. In addition to the four specific locations, each subject performed three trials in which hand position was self-selected. This resulted in a total of fifteen trials per subject. Subjects were instructed to flex the elbows as necessary and were allowed a rest in between trials. The order in which targets were specified was randomized.

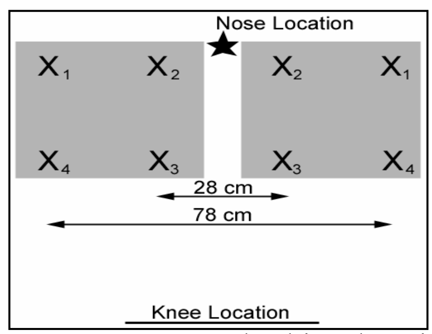

Figure 1: Target and subject location.

A repeated measures ANOVA was done to compare hand positions. *Post hoc* paired t-tests with Bonferroni adjustments were done to identify significant differences between hand positions, as well as differences between the right and left hands.

RESULTS AND DISCUSSION Ground reaction forces varied significantly with hand-torso position, both within and between subjects ($p=0.001$). For example, the average resultant ground reaction force when the hands were low and narrow was 65±14% bodyweight, whereas the average resultant ground reaction force when the hands were high and wide was 79±29% bodyweight (Figure 2, p=0.001).

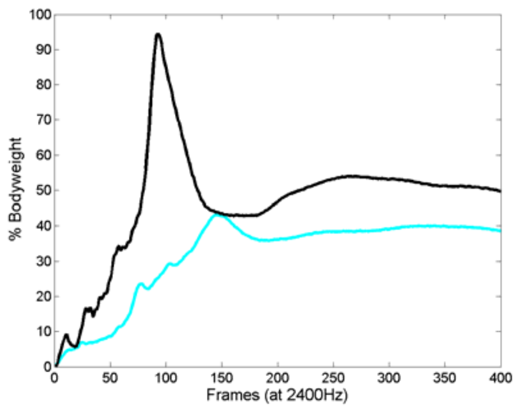

Figure 2: Typical resultant ground reaction force for a subject in two positions: low and narrow (cyan) and high and wide (black).

Similar to other study's results (Chiu and Robinovitch 1998), the initial peak of impact force was greater than the second force peak. There was not a significant difference between the left and right hand within subjects (p=0.894).

The *post hoc* comparisons of hand positions revealed significant differences between the three components of the resultant ground reaction force produced and the factors of hand position (Table 1). The two widely-spaced hand positions had significantly larger lateral shear components than the narrow hand positions (p<0.01). The high hand-torso positions resulted in larger anterior shear forces than the low positions (p<0.01). The high position also produced a significantly larger vertical component to the ground reaction force (p<0.01) than the low positions. Overall, the high positions produced a significantly larger resultant ground reaction force than did the low positions (p<0.01).

When the resultant ground reaction forces produced from a kneeling height were scaled up to forces from a standing height, the forces were 159.3% higher, an increase from the already high forces produced by each subject. This may be important in future studies involving modeling of falls from standing height, as well as in creating fall arrest strategies to minimize serious injury.

In conclusion, it is apparent that varying hand position when contacting the ground after a minor fall can affect the ground reaction force produced. Specifically, placing the hands high relative to the torso produces the greatest resultant force, where placing the hand low and a narrow width apart produces the smallest resultant force. These results are the first of their kind that examine specific positions the hands can be placed in when contacting the ground after a fall. Furthermore, these results will be useful as boundary conditions for finite element models of wrist fractures.

REFERENCES

Chiu, J. and Robinovitch, S.N. (1998). *J. Biomech*, **31**, 1169-1176.

DeGoede, K.M. and Ashton-Miller, J.A. (2003). *J. Biomech*, **36**, 413-420.

Kim, K-J. and Ashton-Miller, J.A. (2003). *Clin. Biomech*, **18**, 311-318.

Oskam, J., et al. (1998). *Injury*, **29**, 353-355.

Table1: Ground reaction force components in percent bodyweight. Negative medial shear force represents lateral force.

	medial	anterior	vertical	resultant
low, narrow	4 ± 8	13 ± 6	64 ± 13	65 ± 14
low, wide	-0.7 ± 6	13 ± 7	71 ± 20	72 ± 20
high, narrow	6 ± 6	22 ± 10	78 ± 28	80 ± 29
high, wide	-5 ± 6	15 ± 8	78 ± 28	79 ± 29
self-selected	2 ± 6	13 ± 7	68 ± 17	69 ± 17

QUANTIFICATION OF UPPER EXTREMITY MOTION DURING A TRIP-INDUCED FALL IN OLDER ADULTS

Courtney D. Gavin[1], Karen L. Troy[1], and Mark D. Grabiner[1]
[1] Musculoskeletal Biomechanics Laboratory, University of Illinois at Chicago
Chicago, IL USA E-mail: cgavin1@uic.edu

INTRODUCTION Falls become more common in adults as they age and often result in serious injuries such as fractures. Distal radius, or Colles' fractures are the most common type of upper extremity fall-related fracture (Donaldson, et al. 1990). Even after they are healed, Colles' fractures can continue to compromise normal function and activities of daily living (Madhok and Bhopal 1992).

Using the upper extremities to safely arrest the momentum of the body during a fall to the ground is a time-critical and complex motor event, the difficulty of which may be exacerbated by age. A primary research focus of experiments that simulate forward falls has been the quantification of upper extremity impact forces and reduction of these forces by manipulating landing biomechanics (DeGoede, Ashton-Miller et al. 2002). Experimental simulations of forwards falls onto the hands have been designed to safely circumvent many hazards of subjecting young and older subjects to upper extremity impacts. However, the availability of ample time to consider and pre-plan the motor task may influence execution of the motor task. It is possible that the motion of the upper extremities immediately following a postural disturbance that results in a forward fall may depart from the expected synchronous and symmetrical motions observed during these simulated falls.

Therefore, the aim of this study was to quantify the symmetry and synchronicity between the upper extremities, as well as to examine the overall motion of the arms relative to the torso during the descent phase of a fall resulting from an unexpected trip.

METHODS Eight adults aged 65 years and older were evaluated in this study. A six camera system (Motion Analysis, Santa Rosa, CA) was used to record kinematic motion of 19 passively reflective markers used to create a 13-segment model of the body. Subjects walked at a self selected velocity and were protected from all fall to the ground by a safety harness system. They were informed they would be tripped during one of a series of walking trials, but they were not informed during which trial this would occur or the means by which the trip would be induced. The trip was induced during mid swing by a concealed, pneumatically driven obstacle that rose to a height of 5 cm in about 150 ms from the floor; the presence of which the subjects were previously unaware. A rope held by an investigator, plainly visible across the pathway, was used as a decoy.

Upper extremity kinematics (elbow flexion, shoulder flexion, and shoulder abduction) were analyzed from the instant of the trip up to, and including, the last data point available in the recording. The data was further divided into two time periods, based on trunk flexion angle. Time segment one (T_1) included kinematic data from the instant the trip occurred until the trunk reached 50% of its maximum flexion angle. Time segment two (T_2) included kinematic data from this point until the last point of data collection.

The cross-correlation (xcorr) between the right and left extremities for T_1 and T_2 of each arm motion was calculated (MATLAB). For between-subject comparisons the maximum xcorr was extracted from the cross correlation function and normalized using the equation:

$$\mathbf{XCORR_{max}} = \frac{\mathbf{max\ (xcorr_{xy})^2}}{\mathbf{(xcorr_{xx} * xcorr_{yy})}}$$

This calculation was used as a general metric of the similarities of the time series for each arm motion. The phase shift, tau (τ), at the point in time when the maximum cross correlation value occurred was also extracted from the cross correlation function. The $XCORR_{max}$ represented symmetry and the phase shift represented synchronicity.

A summary representation of upper extremity position was also computed. Position of the limbs relative to the torso was examined at three time points: the instant of the trip, the point dividing T_1 and T_2, and the last point of the data series. The difference in flexion between right and left limbs was calculated for the overall data set (Figure 1).

The $XCORR_{max}$ values and phase shift for each of the three motions analyzed were compared between T_1 and T_2 using repeated measures ANOVA and *post hoc* paired t-tests with Bonferroni corrections. The right and left upper extremity summary positions at the three points were compared using paired t-tests (SPSS version 12.0).

RESULTS AND DISCUSSION Upper extremity motion becomes more symmetric over the course of the fall. In other words, $XCORR_{max}$ for T_2 was larger than T_1 (p=0.021). On average, $XCORR_{max}$ for shoulder flexion increased significantly from 0.34 to 0.84 (p=0.002). Elbow flexion $XCORR_{max}$ increased from 0.77 to 0.90 and shoulder abduction $XCORR_{max}$ decreased from 0.92 to 0.88. For both elbow flexion and shoulder abduction there was not a significant change in the $XCORR_{max}$, but throughout the motion they were both close to 1.0, representing very strong symmetry.

The differences in phase shift between upper extremity motion during T_1 and T_2 were not significant (p=0.147). However, a *post hoc* power analysis revealed that the statistical power was low (0.363). When the data of one subject, a clear outlier, was removed, the phase shift significantly decreased from T_1 to T_2 (p=0.040) and the statistical power increased to 0.678.

The motion of the upper extremities relative to the torso changed throughout the fall. The flexion of the upper extremities significantly increased from time point 1 to 2 (p=0.014) and between time points 1 and 3 (p=0.004), but not between time points 2 and 3 (p=0.727).

Figure 1 suggests that towards the end of the fall all individuals exhibit little difference in flexion of their arms. In addition, the three time points analyzed demonstrated both arms were positioned approximately 38º relative to the torso in the beginning of the fall and progressed to 95º out in front of their torso. This configuration allows for preparation in minimizing injury at impact.

The purpose of this study was to investigate the symmetry and synchronicity of the upper extremities, as well as overall arm motion during a trip-induced fall. The results indicate that during the initial phase of the fall, the upper extremities were generally less symmetric and synchronous. However, as ground contact becomes imminent, the upper extremities' motions became significantly more symmetric. There was also a trend for the phase shift (τ) between the right and left arms to decrease over the course of the fall.

The present data suggest that available preplanning time inherent in experimental protocols to safely investigate the use of the upper extremities to arrest body momentum during a fall are reasonable surrogates. By increasing the understanding of the limits of upper extremity function, it may be possible to improve fall arrest strategies and decrease the incidence of fall-related injuries in older adults.

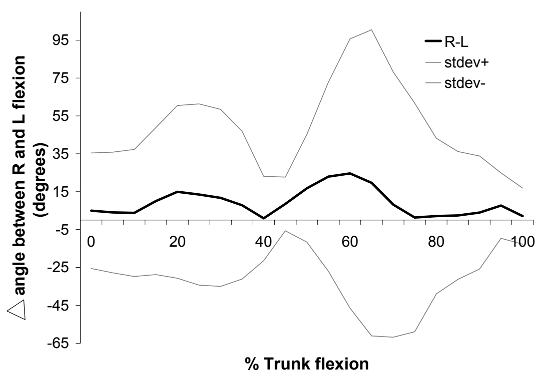

Figure 1: Difference between right and left flexion angles of all subjects during entire fall.

REFERENCES

DeGoede, K.M., et al. (2002). *J. Biomech Eng,* **124**, 107-112.
Donaldson, L.J., et al. (1990). *J. Epidemiol Commun H*, **44**, 241-245.
Madhok, R. and Bhopal, R.S. (1992). *Public Health*, **106**, 19-28.

WRIST POSITION INFLUENCES RANGE OF MOTION

Laurel Kuxhaus[1], Jesse A. Fisk[2], Thomas H. Christophel[1], and Zong-Ming Li[1]

[1] Hand Research Laboratory, Departments of Orthopaedic Surgery and Bioengineering
[2] Musculoskeletal Research Center, Department of Bioengineering
University of Pittsburgh, Pittsburgh, PA, USA
E-mail: zmli@pitt.edu

INTRODUCTION

The unique motion capabilities of the human wrist are critical to our daily lives. Wrist kinematics have been studied at the individual carpal bone and entire wrist complex levels. Motion of the wrist complex has two degrees of freedom: flexion/extension (FE) and radial/ulnar deviation (RUD). Pronation/supination is insignificant (Volz *et al.,* 1980 and Youm *et al.,* 1978). Clinically, wrist range of motion (ROM) assesses wrist function, yet little is known about the coupling between position in one direction and range of motion in the others. The purpose of this study was to quantify how FE ROM is affected by RUD and vice versa.

METHODS

Ten self-reported right-handed male subjects, aged 28.3±4.9 years (mean ± SD) and free of upper extremity trauma and neuropathies volunteered to participate in this study and indicated their consent via a form approved by the University of Pittsburgh's Institutional Review Board. We attached four light-reflective markers (∅=5mm) to the hand and three to the wrist (Figure 1). Subjects rested their flexed elbows on a table and continuously circumducted their hand in a clockwise direction at a self-selected speed while holding a 2.5cm cylinder. We recorded the marker positions with a six-camera motion analysis system (VICON 460, Oxford, UK) for 30 seconds at 120 samples-per-second. To gain familiarity with our task, subjects performed one practice trial.

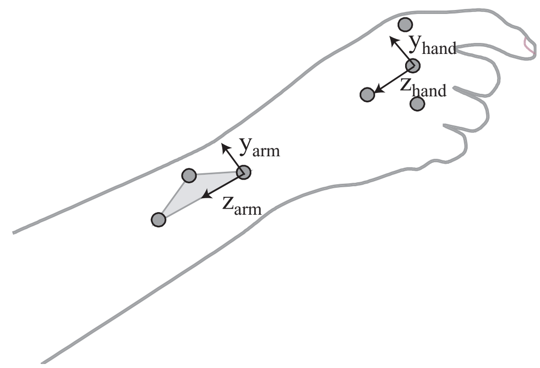

Figure 1: Schematic of markers with local hand and forearm coordinate systems.

Subsequent analyses were conducted with custom MATLAB (The MathWorks, Natick, MA) software. We defined coordinate systems on the hand and forearm (Figure 1) and calculated the YXZ Euler angles of the hand relative to the forearm: a FE, RUD, and pronation/supination rotation sequence. As we focused on the interaction between FE and RUD in this study, we computed the 2D convex hull (envelope) of the angle-angle data for each subject in these directions.

RESULTS AND DISCUSSION

One subject's motion and convex hull (envelope) are shown in Figure 2. The calculated individual and average ROM-position relationships are shown in Figure 3.

The maximum FE ROM was 99.5°±19.5° (mean±SD) at 1.9°±5.0° of radial deviation. The maximum RUD ROM was 51.0°±7.8° at 8.1°±10.2° of extension. This agrees with our intuitive sense that maximal RUD ROM in the FE plane occurs with the wrist in a slightly extended position.

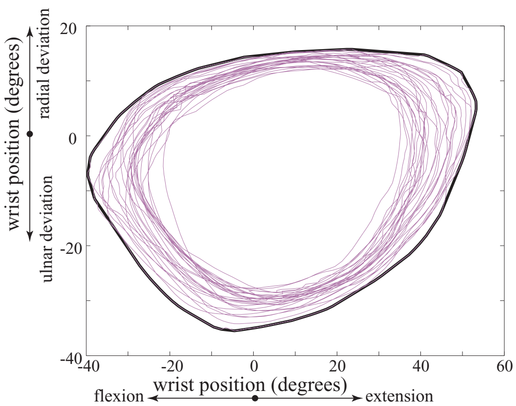

Figure 2: Wrist motion data and envelope for one representative subject.

Our wrist ROM-position coupling curves (Figure 3) are parabolic. Wrist position in one direction strongly influences the ROM in the other direction. Maximum ROM in FE (or RUD) occurs when the wrist is near the neutral position of RUD (or FE). The ROM in one direction diminishes quickly as the wrist moves away from the neutral position. We note that a few of the individual curves seem distinct from the rest. While this may reflect true inter-subject variability or motivation levels, similar trends were observed across all subjects.

We quantified wrist motion coupling between two directions during circumduction. Future work will investigate how the ROM coupling is altered by injury and other pathologies. Given the strong interdependence of FE and RUD found in these control subjects, we recommend wrist position be specified when ROM data are reported. Similarly, clinical assessments of

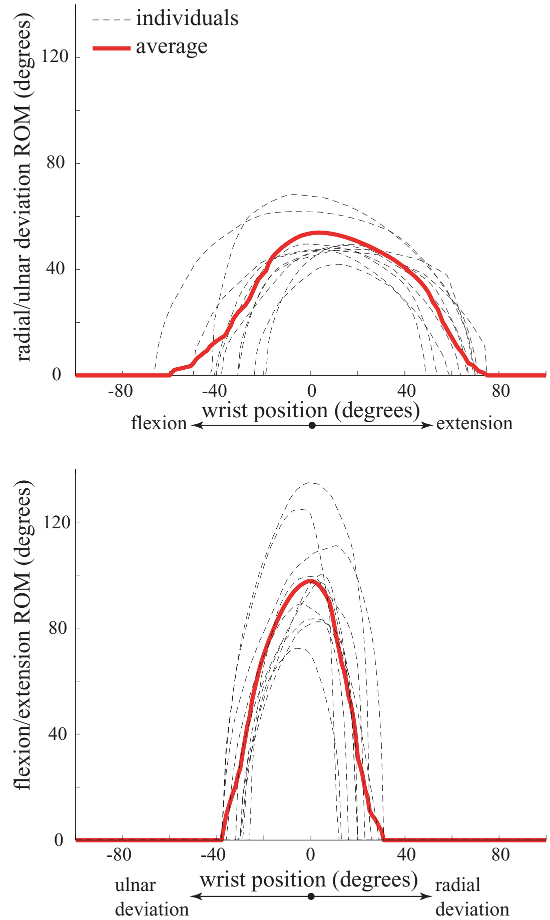

Figure 3: Relationship between RUD ROM and extension position (top) and vice-versa (bottom).

unidirectional wrist ROM should standardize wrist position in the others.

REFERENCES

Volz, R.G. *et al.* (1980). *Clin Orthop,* 112-117.

Youm, Y. *et al.* (1978). *J Bone Joint Surg [Am],* **60**, 423-431.

ACKNOWLEDGEMENTS

This material is based upon work supported under a National Science Foundation Graduate Research Fellowship (LK) and the Whitaker Foundation (ZML).

FOOT AND ANKLE PRESSURE MEASUREMENT DURING FORWARD SKATING

David J. Pearsall, Curt Dewan, René Turcotte, and David L. Montgomery
Department of Kinesiology and Physical Education, Montréal, Québec, Canada
E-mail: david.pearsall@mcgill.ca Web: www.mcgill.ca

INTRODUCTION

Insole pressure measurement systems have been used extensively to investigate the dynamics of footwear with regards to the plantar surface of the foot (Hennig et al., 1996). Though substantial pressures occur at the plantar foot surface, other considerable pressures may occur elsewhere within the boot, particularly during agility tasks involving changes in direction, starts and stops (Schaff, 1987). Hence measures about the foot and ankle within footwear are required for the full dynamic interaction between the two components to be understood. This is particularly relevant in skate design. Hence, the purpose of this study was to evaluate the pressure at the skate boot-to-foot/ankle surface during forward skating.

METHODS

Sixteen flexible piezo-resistive sensors (1.2 cm x 1.8 cm x 0.2 cm thick, FSA Verg Inc.,Canada) were taped to discrete surface anatomical sites (see Fig 1,2)

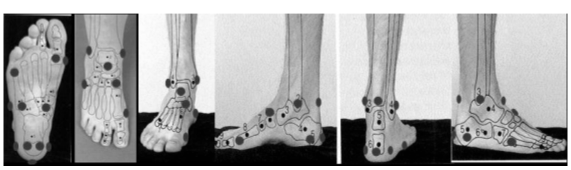

Figure 1:
Sensor placement around the foot and ankle

Prior to adhering the sensors to the foot /ankle, all sensors were calibrated by utilizing an air bladder (Tekscan Inc;, West Boston, MA, USA) that applied uniform pressures to each sensor for 10 steps from 0 to 100 PSI (690 KPa) in both ascending and descending (i.e. loading and unloading) directions. This calibration process also permitted correction factors of creep and hysteresis to be determined. The linearity of the sensors to both rising and falling pressures over a 10 second loading period was high ($r > 0.95$).

Sensor signals were recorded by a data logger contained within a waist pack worn by the subject. Sensor measures were sampled at 100 Hz.

Bauer Vapor XX model skates (size 8.5) and athletic socks were worn by each of five subjects. The subject was allowed to select his own lacing tension deemed sufficient for proper fit. Pressures were measured during standing and at constant velocity (26 kph) forward skating.

After skating, the data for 30 skating strides were downloaded by interfacing the data logger to a computer, via a Ethernet cable. Subsequently, data were processed within MatLab™ modules to describe parameters within normalized stride cycles.

RESULTS AND DISCUSSION

Average pressure estimates surrounding the foot/ankle varied substantially between and within regions during the skating stride (Fig 2). In most instances, the dynamic pressure measures straddled the static standing reference pressures. As well, positive pressures around the foot /ankle existed throughout the skating stride, even during the swing phase. On the plantar foot surface, maximum pressures were observed at the I MT head (281 KPa), heel (126.9 to 153.8 KPa) and lateral arch (104.1 KPa). On the medial aspect, similar pressure magnitudes were observed e.g. medial malleolus (243.4 KPa) and I MT head (142.7 KPa). Lateral pressures were less but still substantial e.g. lateral malleolus (124.1 KPa) as were dorsal pressures e.g. dorsalis pedis (161.3 KPa) and navicular (86.9 KPa). The least pressures were observed posteriorly e.g. both calcaneous and Achilles tendon (11.7 KPa).

The variances associated with the above measures were considerable i.e. coefficient of variations of 27% to 89% for plantar measures and greater (46% to 111%) for the other regions. In part, this may be attributed to anthropometric and skating technique differences between subjects, as well as subtle alteration in sensor placements due to skin-to-bone movement that may produce great changes in point contact pressure, particularly at highly contoured surface bone features.

SUMMARY

In summary, the results demonstrate the feasibility of adopting this protocol and technology to estimate the dynamic interface pressures between the body and surrounding footwear that, in turn, may be applied to a variety of other work or sport contexts. Future studies will need to control for factors affecting the variance. With regards to skating, other various tasks (e.g. tight turns, cross overs, starts / stop, etc.) will be similarly examined, as well as the potential relationships between fit, comfort and performance.

REFERENCES

Hennig E, Valiant GA, Liu Q. (1996) *J Appl Biomech* 1996; 12: 143-150.
Schaff et al. (1987) *Sportvertletz Sprotschaden*, 1(3):118-29

ACKNOWLEDGEMENTS

NSERC Canada
Bauer-Nike Hockey Inc.

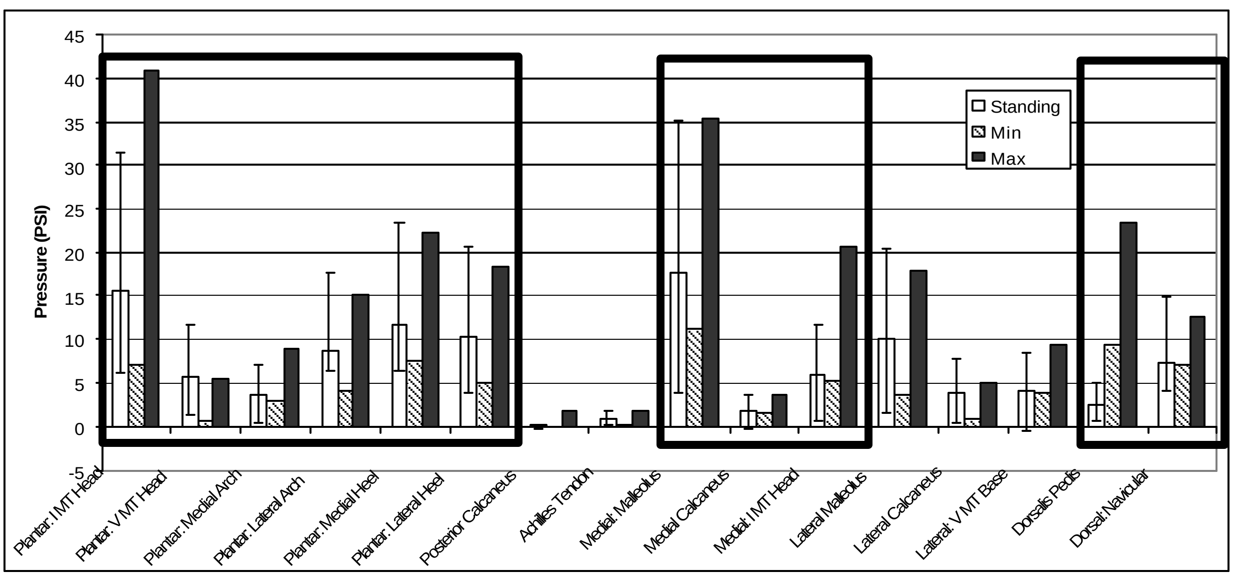

Figure 2:
Average Pressure Measurements (± SD) during Standing and Skating (minimum and maximum)

EVALUATION OF 3D RECONSTRUCTION OF THE RIB CAGE FROM BIPLANAR RADIOGRAPHY

David Mitton[1], Maxime Chauvet[1,2], Sébastien Laporte[1], Chao Yang[2], Samuel Bertrand[1], Kristin Zhao[2], Chunfeng Zhao[2], Kai-Nan. An[2] and Wafa Skalli[1]

[1] Laboratory of Biomechanics ENSAM-CNRS UMR 8005, Paris, FRANCE
[2] Biomechanics Laboratory, MAYO Clinic, Rochester, MN, USA

INTRODUCTION

A three-dimensional personalized geometrical model of the rib cage is essential for clinical evaluation or for personalized biomechanical finite element modelling (Le Borgne et al. 1998). The 3D information could be obtained by CT-Scan but with a high irradiation dose for the patient. In the specific case of the rib cage, a method based on two antero-posterior views at 20° from each other was previously developed (Dansereau and Stokes 1988). 3D reconstructions based on frontal and lateral radiographs have been applied to the spine (Mitton et al. 2000) and knee (Laporte et al. 2003). The method for the knee is based on contour identification in the X-rays and is called NSCC (Non Stereo Corresponding Contours). More recently, this method was also applied to the rib cage (Laporte et al. 2004).
The purpose of this study was to evaluate the accuracy of this method when applied to the rib cage as compared to CT-scan reconstructions.

METHODS

One fresh cadaveric spine, from vertebrae T3 to L4, was removed of soft tissue and organs. The rib cage, with ligaments and muscles intact, was harvested. T3 and L4 were mounted and fixed to a custom designed stereoradiography apparatus via bone cement. Lateral and frontal radiographs were obtained. The rib cages were then scanned in a CT-scan device (GE Medical System, USA) at Mayo Clinic (Rochester, MN, USA) with 1.3 mm consecutive slices. The 3D reconstruction was performed using the SliceOmatic® software. The accuracy of this technique was evaluated to ± 1mm (Landry et al. 1997).

Eighteen ribs were reconstructed using a method based on biplanar X-rays (frontal and lateral views) with the following steps :

1) calibration of the biplanar radiographic environment (Dumas et al 2003).
2) 3D reconstruction of the whole spine (Pomero et al. 2004).
3) identification of 2D contours in the X-rays.
4) 3D reconstruction using NSCC method (Laporte et al. 2004).

3D reconstructions were performed with a custom software package developed in collaboration between the *Laboratoire de recherche en imagerie et orthopédie,* (ETS - CRCHUM, Montréal, Canada) and the *Laboratoire de biomécanique* (CNRS-ENSAM, Paris, France).

The reconstructions obtained from the frontal and lateral X-rays were compared to the gold standard ,CT-scan results (semi-automatic reconstruction).
The comparison between the two modalities was based on parameters computation. For example, the chord length and the maximal

width were computed from biplanar X-rays and CT-scan for each rib.

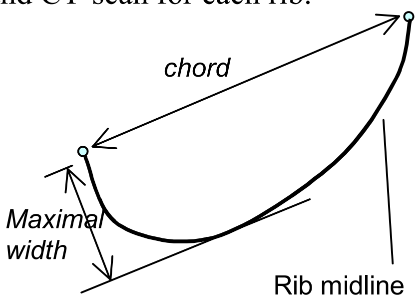

Figure 1: Rib parameters evaluated on both 3D reconstructions

RESULTS AND DISCUSSION

The reconstruction from biplanar X-rays is given as an example (Figure 1).
The comparison results are given for the chord length and the maximal width (Table 1).

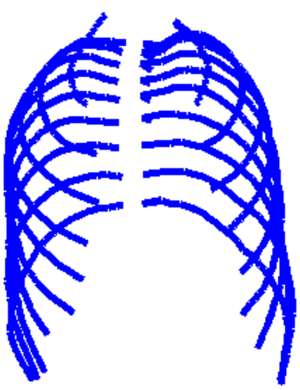

Figure 1: 3D reconstruction obtained from frontal and lateral X-rays.

Table 1: Differences between biplanar radiographic reconstructions and CT-scan ones.

	Mean (SD) mm	Relative errors %
Chord length	2.9 (3.6)	5
Maximal width	6.5 (5.5)	3

The personalized rib cage geometry can accurately be obtained from frontal and lateral X-rays. Because radiographs are commonly obtained in the clinic, the patient would not need to be subjected to the additional radiation exposure with CT-scan evaluations.

SUMMARY

Personalized bone geometry is important both for developing successful clinical interventions and developing accurate finite element models. This study evaluated the accuracy of a method to obtain 3D personalized geometry of the rib cage using frontal and lateral X-rays. Results from the biplanar radiographs are similar to those from CT-scan semi-automatic reconstruction using millimetric slices (difference in chord length and maximal width are lower than 5%). This method has the added advantage of a lower radiation dose for the patient.

REFERENCES

Dansereau J. and Stokes I.A. (1988) *J. Biomech,* **21**, 893-901

Dumas R, Skalli W. et al. (2003) *J. Biomech,* **36**, 827-34.

Mitton D., de Guise J.A. et al. (2000) *Med Biol Eng Comput,* **38**, 133-139

Landry C., de Guise J.A. et al. (1997) *Ann Chir*, **51**, 868-874

Laporte S., Mitton D. et al. (2003) *Comput Methods Biomech Biomed Engin,* **6**, 1-6

Laporte S., Mitton D. et al. (2004) *Proceedings of the CARS*

Le Borgne P. Lavaste F. et al.. (1998), *Proceedings of 4th IRSSD, Vermont, USA*

Pomero V., Skalli W. et al. (2004) *Clin Biomech*, **19**, 240-247

ACKNOWLEDGEMENTS

The authors wish to acknowledge M. Martinet for his important technical support.

EFFECTIVENESS OF A COLLAGEN HYDROLYSATE-BASED NUTRITIONAL SUPPLEMENT ON THE LEVEL OF JOINT PAIN, RANGE OF MOTION AND MUSCLE FUNCTION IN INDIVIDUALS WITH MILD OSTEOARTHRITIS OF THE KNEE: A RANDOMIZED CLINICAL TRIAL

Carpenter MR, McCarthy S, Kline G, Angelopoulos TJ, Rippe JM.
Rippe Health Assessment, Celebration Hospital, Orlando, FL USA
E-mail: tangelop@rippelifestyle.com

INTRODUCTION

Insoluble collagen makes up a majority of articular cartilage, and it has been theorized that new treatments should focus on improving the health of this existing joint collagen. Since collagen hydrolysate contains an abundance of the amino acids that play a role in the synthesis of collagen, which is one of the two major protein components of cartilage matrix, it may help maintain joint health. For this reason, collagen hydrolysate, a natural component of gelatine, has been suggested as a mode of treatment with minimal side effects. Therefore the purpose of this study was to evaluate the effectiveness of a collagen hydrosylate-based nutritional supplement on the level of joint pain, range of motion, and muscle function in individuals with mild arthritis of the knee.

METHODS

Study population. 250 patients with symptoms of mild OA of the knee based on criteria from the American College of Rheumatology (ACR) were randomized into the study, 126 into the collagen hydrolysate-supplemented (CH) therapy group and 124 into the placebo therapy group. Of the 250 patients 190 patients completed the study; 88 patients in the (CH) group and 102 patients in the placebo group. These 190 patients build the intention-to-treat (ITT) population for which the statistical analysis was carried out. The rate of drop outs in the CH group is about 30%

RESULTS AND DISCUSSION

The comparisons of pain and mobility with the two questionnaires of the Knee Pain Scale, WOMAC score section B, Lequesne-Index, 50-Foot Walk Test and 6-Minute Walk Test show no differences between the therapy groups. Changes in the range of motion were evaluated with a goniometer. No significant changes were observed between groups. Muscle function was assessed with numerous measures of isokinetic leg strength, measured on a Biodex 2000 (Biodex, NY; test-retest reliability has been studied). Significant between group differences are depicted in Table 1. While these data show that CH supplementation does not impact subjective measures of pain more than placebo over a 14-week rehabilitation program, significantly greater improvements are seen in various more objective measures of joint function. Therefore further studies investigating the benefits of CH or other nutritional supplements during joint rehabilitation may have to also evaluate more objective measures of joint and muscle function in addition to evaluation of joint pain, mobility and range of motion.

ACKNOWLEDGEMENTS

This work was supported by Gelita Health Initiative, Inc.

Table 1. Isokinetic Leg Strength (mean ± SD)

Variable	Baseline	Week 14	Diff. basel.-week14	p*
Peak Torque/BW for Extension at 60°/sec				
CH Group	46±16.2 (n=85)	48±15.9 (n=81)	-1.8±7.0 (n=81)	0.0229
Placebo Group	48±14.5(n=101)	47±14.1 (n=92)	0.9±6.1 (n=92)	
Peak Torque/BW for Flexion at 60°/sec				
CH Group	25±9.8 (n=85)	26±9.9 (n=81)	-1.2±5.2 (n=81)	0.0266
Placebo Group	25±8.3 (n=101)	25±7.4 (n=92)	0.3±4.6 (n=92)	
Work/BW for Extension at 60°/sec				
CH Group	56±21.0 (n=85)	59±20.9 (n=81)	-3.0±8.0 (n=81)	0.0288
Placebo Group	58±19.0(n=101)	58±18.6 (n=91)	0.5±9.0 (n=91)	
Power for Extension at 60°/sec				
CH Group	74±35.6 (n=85)	79±36.6 (n=81)	-4.7±15.7 (n=81)	0.0162
Placebo Group	75±31.5 (n=101)	77±31.8 (n=91)	-0.4±11.9 (n=91)	
Power for Flexion at 180°/sec				
CH Group	61±32.3 (n=86)	69±35.8 (n=82)	-7.6±17.1 (n=82)	0.0341
Placebo Group	64±32.3 (n=101)	67±30.4 (n=92)	-2.8±13.9 (n=92)	

*Mann-Whitney-U-Test (α=0.05, two-sided) for difference between the therapy group

RECTUS FEMORIS FIBER EXCURSIONS PREDICTED BY A 3D MODEL OF MUSCLE

Silvia S. Blemker[1] and Scott L. Delp[1,2]

Departments of [1]Mechanical Engineering and [2]Bioengineering. Stanford University
E-mail: ssblemker@stanford.edu Web: http://www.stanford.edu/group/nmbl

INTRODUCTION

Computer models of the musculoskeletal system frequently represent the force-length behavior of muscle with a lumped-parameter model (Zajac, 1989). Lumped-parameter models assume that muscle fibers have a simple two-dimensional arrangement and that all fibers undergo the same change in length (or “excursion”). These simplifications may misrepresent muscle fiber excursions and the resulting force-length behavior, especially for muscles with complex architecture. Herzog and ter Keurs (1988) have demonstrated that lumped-parameter models do not accurately predict the *in vivo* force-length behavior of the rectus femoris, a bipennate muscle of the lower limb. In this study, we created a three-dimensional (3D) model of the rectus femoris to determine how a more accurate representation of the fiber arrangement affects the predictions of muscle fiber excursions.

METHODS

3D models of the rectus femoris and the vasti muscles (Fig. 1B) were generated from magnetic resonance (MR) images (Fig. 1A). A representation of the muscle fiber geometry (Fig. 1C) was created by morphing a template fiber geometry to the 3D model. We studied the muscle’s action at the knee by prescribing the motion of the tibia relative to the femur according to published kinematic data (Walker et al., 1988). The motions of the patella, the patellar tendon, and the muscles were calculated via simulations performed with NIKE3D, an implicit finite-element solver (Puso et al., 2002). In the simulation, a transversely-isotropic, incompressible, hyperelastic constitutive model was used to describe the stress-strain relationship in the muscle and tendon tissue (Blemker et al., 2004), the bones were assumed to be rigid, and a penalty formulation was used to resolve muscle-bone, muscle-muscle, and bone-bone contact. The simulation results were analyzed in a graphics-based musculoskeletal modeling environment, and the lengths of individual fibers in the rectus femoris were calculated.

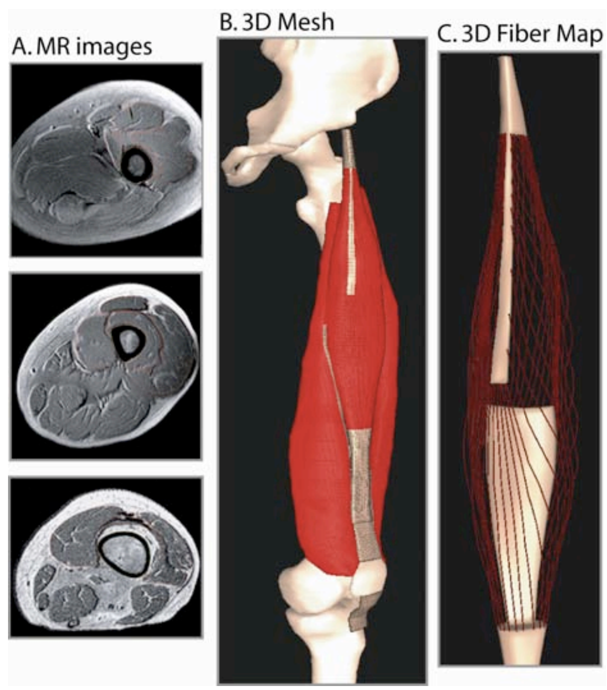

Figure 1: Muscles and bones were outlined in several MR images (A), 3D finite-element models (B) of the quadriceps were generated from the outlines, and 3D representations for the fibers of the rectus femoris (C) and other muscles were created.

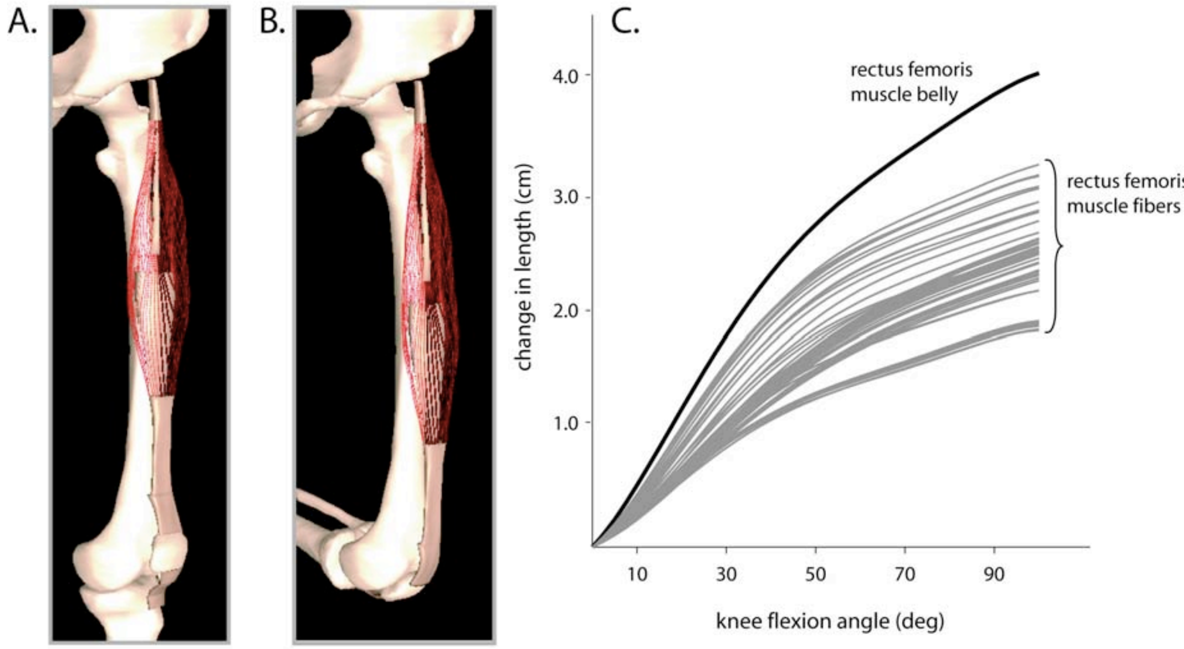

Figure 2: Rectus femoris fiber geometry with the knee extended (A) and flexed (B), and changes in length (C) vs. knee flexion angle predicted by the 3D model.

RESULTS AND DISCUSSION

The 3D model predicted rectus femoris changes in length and moment arms that are consistent with experimental measurements (Buford et al., 1997). The excursions of the rectus femoris muscle fibers varied significantly. Some fibers changed length by 50% less than the muscle belly. By contrast, a lumped-parameter model of this muscle would predict that all fibers excursions are equal and similar in magnitude to the excursions of the muscle belly.

These results indicate that the rectus femoris fiber excursions may be overestimated in lumped-parameter models of muscle. This difference may explain the errors in force-length estimates from lumped-parameter models. More realistic representations of muscle are needed to deepen our understanding of *in vivo* muscle function.

REFERENCES

Blemker et al. (2004) *J Biomech*, in review.

Buford et al. (1997) *IEEE Trans Rehab Eng*, **5**, 367-379.

Herzog and ter Keurs (1988) *Pflugers Arch*, **411**, 642-647.

Puso et al. (2002) *Lawrence Livermore National Labs Technical Report*, UCRL-MA-105268.

Walker et al. (1988) *J Biomech*, **21**, 965-974.

Zajac (1989) *Critical Reviews in Biomedical Engineering*, **17**, 359-411.

.

ACKNOWLEDGEMENTS

Peter Pinsky, Jeff Weiss, the Lawrence Livermore National Labs, the Stanford Bio-X Program, the NSF, and the NIH.

BIOMECHANICAL ANALYSIS OF A WHEELCHAIR WHEELIE IN PERSONS WITH SCI

Nethravathi Tharakeshwarappa[1,2], Alicia Koontz[1,2], Rory Cooper[1,2], and Michael Boninger[1,2]
[1]Dept. of Rehab. Science and Technology, University of Pittsburgh, Pittsburgh, PA 15261
[2]Human Engineering Research Laboratories, Highland Drive VA Medical Center, Pittsburgh, PA
net5@pitt.edu web:www.herlpitt.org

INTRODUCTION

A wheelie is an acquired skill that involves elevating the front castors and balancing on the rear wheels. A wheelie makes it easier to overcome daily life physical barriers, such as rough surfaces, curbs, bumps and door thresholds. Bonaparte et al. (2001) studied wheelie proactive/reactive strategies and Lin et al. (2002) studied the relationship between wheelchair pitch angle and pushrim force. Both studies were conducted with unimpaired individuals as the test subjects. The purpose of this study was to investigate trunk motion, applied pushrim forces, and pitch angles during the initiation and balance phases of a wheelie to better understand the strategies used by wheelchair users with spinal cord injuries.

METHODS

Four men and one woman (mean age 37.6 ± 6 years, height 1.8 ± 0.1meters and weight 65.4 ± 11 kg) with a spinal cord injury ranging from T4 to C7 provided informed consent to participate in the study. Subjects had to be able to perform a wheelie and balance on the rear wheels for one minute to be included in the study. An OPTOTRAK (Northern Digital, Inc.) motion analysis system was used to record motion of the body and the wheelchair at a sampling rate of 60Hz. A SMART^{Wheel} (Three Rivers Holdings, Mesa, AZ) was used to record the 3D dynamic forces and moments imparted to the pushrim at a rate of 240 Hz, and two AMTI force plates were used to record ground reaction force data at 360Hz. SMART^{Wheels} were installed on the subject's own wheelchair and infrared markers were placed on thirteen salient points on the right upper extremity and trunk as well as the wheelchair frame. The subject started with the wheelchair centered on the force plates. Marker coordinates, force plate, and pushrim forces and moments, were recorded for 10 seconds during which time the subject popped a wheelie and maintained the wheelie position until given a verbal cue after 9 seconds to land the front casters. The pitch angle was defined as the angle between the line connecting two markers on the wheelchair frame with respect to their locations at the beginning of the trial when all four wheels were on the ground (Figure1). Trunk angle was defined as angle between the thigh and trunk.

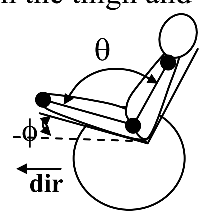

Figure 1. Pitch (ϕ) and trunk (θ) angle

Pushrim resultant force magnitude and direction with respect to the wheelchair, instantaneous direction (**dir**) was calculated as given in Equations 2 and 3. Unlike the previously mentioned studies, wheelchair motion was not assumed to be along a Cartesian axis.

$$\mathbf{dir} = \frac{(\mathbf{H}-\mathbf{L})\times(\mathbf{R}-\mathbf{L})}{\|(\mathbf{H}-\mathbf{L})\times(\mathbf{R}-\mathbf{L})\|} \;(1); \quad F_{mag} = \|\mathbf{F}\| \;(2); \quad F_{dir} = \mathbf{F} \bullet \mathbf{dir}\,(3)$$

The **dir** is a unit vector along the wheelchair's instantaneous forward direction and is calculated using Equation 1 where **H** is the 3D coordinates of the marker on the hub, and **L** and **R**, are the left and right contact points on the force plate respectively. F_{dir} in Equation 3 indicates the component of the resultant push rim force

(**F**) along the instantaneous direction (**dir**). If F_{dir} is positive, it implies that **F** acts along **dir,** and if F_{dir} is negative, it implies that **F** acts opposite to **dir**.

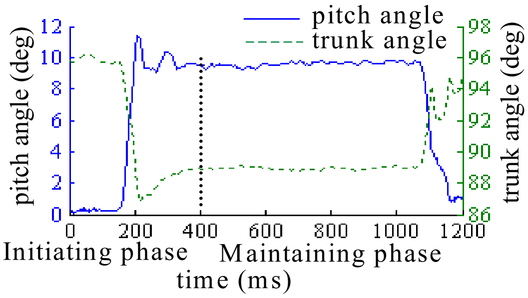

Figure2: Pitch and trunk angle (ensemble average of all five subjects)

The plot of pitch and trunk angle was visually inspected to discern the initial lift off of the casters and wheelie balance. (Figure 2). Maximum pitch angle, minimum trunk angle, trunk range of motion (ROM), and Maximum force (normalized to body weight), were determined for the initiation phase. Pitch angle, trunk angle, and normalized force were averaged over the middle five seconds of the maintaining phase.

RESULTS AND DISCUSSION

In all the subjects, the pitch angle was higher in the initiation phase than in the maintaining phase indicating that they tended to overshoot their balance point upon initial elevation of the castors. Conversely, the trunk angle is higher in maintaining phase than in initiating phase indicating that subjects used greater trunk flexion to elevate the castors than to balance in the wheelie. In the initiation phase, the maximum pitch angle occurred at the point when the trunk was maximally flexed (Figure 2). A forward flexed trunk causes the body's center of mass to move forward and thus the wheelchair must then be tipped further backward to keep the combined body/wheelchair center of mass over the rear wheels. The two subjects with cervical level injuries were noted to have the smallest trunk ranges of motion during the initiation phase and one of them applied forces almost 30% his body weight to lift the castors off the ground. As expected, subjects needed to exert more force to initiate the wheelie versus maintaining the wheelie.

SUMMARY

This study provides insight into the relationships between pitch angle, trunk angle, and pushrim force for a wheelie maneuver. The body's center of mass with respect to the rear axles also influences wheelie performance. Future studies that involve a larger sample of wheelchair users and an investigation of axle position location on wheelie performance are warranted.

REFERENCES

Bonaparte JP et al. (2001). *Arch Phys Med Rehabil*, **82**, 475-9.

Lin PC et al. (2002*). Proceedings of American Society of Biomechanics*

ACKNOWLEDGEMENTS

PVA, EPVA and NIDRR H133A011107

Table 1. Kinetic and kinematic data in wheelie initiating and maintaining phases

Subjects	Initiating phase				Maintaining phase (5 sec)		
	Max. pitch angle (deg)	Min. trunk angle (deg)	Max. pushrim force / body weight(%)	Trunk ROM (deg)	Mean Pitch angle (deg)	Mean Trunk angle (deg)	Pushrim force / body weight(%)
1(C7)	9.3	82.8	5.05	11.7	6.1	87.4	1.57
2(C7/C8)	12.3	88.8	29.34	9.7	11.0	90.0	2.55
3(T7/8)	12.3	78.6	6.57	28.1	10.7	90.4	0.95
4(T12-L1)	16.8	86.7	6.65	15.8	11.6	89.4	2.12
5(T4)	12.1	75.6	18.87	22.1	8.0	84.4	7.25
Mean(SD)	12.6(2.7)	82.5(5.4)	13.3(10.55)	17.5(7.6)	9.5 (2.3)	88.3 (2.5)	2.9(2.5)

THE EFFECT OF PECTORALIS MINOR RESTING LENGTH VARIABILITY ON SCAPULAR KINEMATICS

John D. Borstad [1] and Paul M. Ludewig [2]

[1] Physical Therapy Division, The Ohio State University, Columbus, OH, USA
e-mail: borstad.1@osu.edu
[2] Department of Physical Therapy, University of Minnesota, Minneapolis, MN, USA

Background: Subacromial impingement is a common pathology of the shoulder. Scapular kinematic alterations have been identified in individuals with subacromial impingement including decreased posterior tipping, increased internal rotation and decreased upward rotation. Mechanisms of altered scapular kinematics should be identified to assist in treating persons with impingement.

One proposed mechanism is pectoralis minor adaptive tightness. A tight pectoralis minor would limit full scapular motion by increases in passive tension at shorter muscle lengths. The purpose of this study was to examine the effect of altered pectoralis minor lengths on scapular kinematics.

Method: Both in vitro and in vivo analyses were performed in this study. In both components, an electromagnetic motion system captured scapular orientation relative to the trunk during arm elevation. For the in vitro analysis, surgical bone pins secured sensors to the scapula, humerus, and sternum of eleven fresh cadavers. Cadaver arms were passively elevated in the coronal and scapular planes independently under five pectoralis minor conditions: intact, intact plus dissected, shortened ten percent, maximally shortened, and cut. The cut ends of the muscle were overlapped and sutured to shorten the muscle. Analysis of the subacromial space during unique scapular rotations was performed by calculating the vector distance between the anterior-lateral acromion and the greater tubercle of the humerus.

For the in vivo analysis, fifty subjects were separated by normalized pectoralis minor resting length into long and short groups of 25 each. Motion sensors were taped over the sternum and scapula, while a third sensor was secured by a plastic cuff to the humerus.

Data were collected during active flexion, abduction, and scapular plane elevation.

Analysis: In vitro, scapular orientations relative to the trunk were analyzed at 30°, 60°, 90°, and 120° humeral elevation with a two-way repeated measures (pectoralis minor condition by angle) ANOVA. In vivo, scapular orientations were analyzed between groups at the same elevation angles with a mixed model ANOVA. For both components, significant interactions were further analyzed for significant simple effects at each elevation angle. Subacromial space estimates were compared at the extremes of scapular rotation.

Results: During in vitro abduction, there was a statistically significant interaction effect for both scapular internal rotation and tipping. For tipping, the maximum shortened pectoralis minor condition was further anteriorly tipped than the intact condition at all elevation angles. IR was not significant at separate angles. Tipping was a statistically significant main effect during elevation in both planes with maximum shortened more anterior than intact, intact plus dissected, and cut in scapular plane. The subacromial space was demonstrated to decrease with maximum scapular anterior tipping and internal rotation. In vivo, significant interactions between group and elevation angle were present in all planes for tipping and during abduction only for internal rotation. In all planes, the short group lacked posterior tipping at both 90° and 120° of elevation. The short group demonstrated increased internal rotation at 30°, 60°, and 90° during abduction. Group was also a significant main effect for both internal rotation and tipping during all motions with the short group less posteriorly tipped and more internally rotated.

Conclusions: A relatively short pectoralis minor resulted in altered scapular motions during arm elevation both in vitro and in vivo. The shorter pectoralis minor restricted full scapular posterior tipping and external rotation. These normal scapular motions are necessary to clear the acromion from the elevating humerus. In vitro scapular rotations demonstrated that limitations in posterior tipping and external rotation will minimize the subacromial space. The combination of scapular motion limitations and a reduced subacromial space will increase the likelihood of impingement in individuals with a short pectoralis minor.

DEVELOPING AND TESTING OF AN EMG DRIVEN MODEL TO ESTIMATE ANKLE MOMENTS AND MUSCLE FORCES

Shay Cohen and Thomas S. Buchanan

Center for Biomedical Engineering Research, University of Delaware, Newark, DE 19716

INTRODUCTION

Estimation of individual muscle force and its contribution to a joint moment has an important role in understanding injuries and disease. In previous work, we have developed EMG-driven models to estimate isometric forces in muscles about the elbow (Manal et al., 2002). Similarly, Lloyd and Besier (2003) used EMG-driven models to predict dynamic flexion and extension knee moments for a varied range of tasks. This approach has the advantage of estimating muscle force *in vivo* using EMG signals and an anatomical muscle model as input, and thereby relies on a person's particular neural control strategy rather than an assumed cost function. Developing the anatomical model is a fundamental step towards good force prediction. The more detailed the model, the more it is able to predict a variety of muscle contractions. Practical limitations, such as the ability to get EMG signals from all muscles, generally leads to a simplification of the model.

The purpose of this work is to develop and test an EMG driven model to predict dynamic muscle forces in the ankle joint. This model will be used in future studies to examine ankle muscle contributions to gait in patients with neuromuscular impairments.

METHODS

We modeled the ankle as a one degree of freedom hinge, with rotation allowed only in the sagital plane. The model includes four primary muscles: soleus and two heads of gastrocnemious as plantar flexors, and tibialis anterior as the dorsiflexor. Hill-type muscle models were used to account for each muscle's force-length and force-velocity relations. The transformation of EMG to muscle activation was calculated using the Lloyd and Besier (2003) EMG to activation model in combination with the terms introduced by the Manal & Buchanan (2003) model for the neural to muscle activation step. Delp et al,'s (1990) SIMM modeling software and the associated lower extremity model were used to calculate the muscle-tendon lengths and moment arms. As an initial step, optimal fiber length, pennation angle and tendon slack length were set to the default values specified in the SIMM lower limb model.

EMG signals were collected from healthy subjects, then rectified, filtered, and normalized relative to maximum EMGs. The tasks included: dynamometer trials and walking trials, where for the later, inverse dynamics was used to calculate ankle joint moments. Range of motion for the dynamometer trials was 5^o to 20^o, dorsiflexion to plantar flexion, which is the average range during gait.

Calibration of the model was accomplished by simulated annealing. Upper and lower bounds for the optimization process were set to keep the muscle parameters within the physiological range. Passive moments that were measured during passive trials were used to constrain passives forces in muscles.

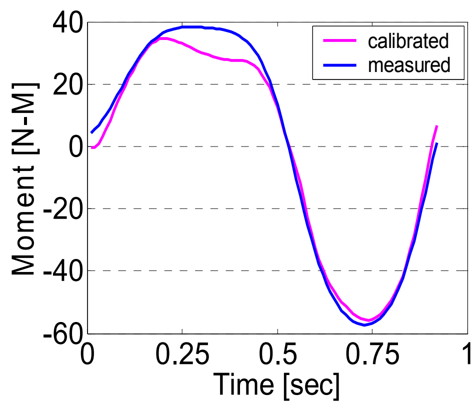

Figure 1: The model was calibrated by adjusting parameters until the estimated (calibrated) joint moments best matched the measured moments.

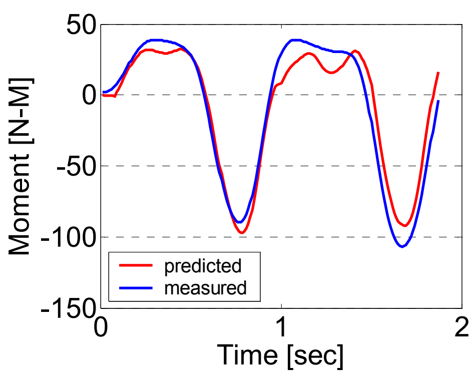

Figure 2: Prediction of ankle moments for a novel trial following calibration on the trial shown in Figure 1.

RESULTS AND DISCUSSION

Calibration of the model on a dynamometer trial is shown in Figure 1 (RMS error is 4.5 N-m and R^2=0.99). Figure 2 shows predicted moment on another dynamometer trial (RMS error is 12 N-m, R^2=0.95).

The maximum isometric muscles forces estimated by the model were much higher values than those in SIMM, with an average increase of about 200%. This is because our subjects had greater maximal joint moments when measured using the dynamometer and because we modeled the ankle using a subset of the muscles instead of the full thirteen muscles in the SIMM model.

The ankle muscles tested are characterized by relatively high pennation angles, for which values vary widely in the literature. We suggest *in vivo* measurement of the pennation angles for the specific subjects. For example, using ultrasound we found that the pennation angle for the tibialis anterior was 10^o, compare to the 5^o we used based on the model in SIMM.

Finally, only four muscles were used in this model to represent the ankle joint musculature. This simplification may require the use of “muscles” with slightly different parameters to compensate for the excluded muscles.

SUMMARY

The model presented has demonstrated its ability to estimate ankle muscle moments in static and dynamic trials. With better subject specific muscle parameters we expect more accurate predictions that will allow us to use this to better understand muscle control in people with neuromuscular impairments.

REFERENCES

Delp, S. L., et al. (1990). *IEEE Trans Biomed Eng* **37:** 757-67

Lloyd, D. G. and T. F. Besier (2003). *J Biomech* **36:** 765-76

Manal, K. et al. (2002), *Comp Biol Med* **32:** 25-36

Manal, K. and T. S. Buchanan (2003). *J Biomech* **36:** 1197-202

ACKNOWLEDGEMENTS

This work was supported, in part, by NIH R01 HD38582.

IN VIVO TESTING PROTOCOL FOR DETERMINING THE PULLOUT STRENGTH OF A POLYAXIAL SCREW BY USING A CANINE MODEL

Zeferino Damián-Noriega [1] , José Antonio Cuellar-Puente [2], Rodolfo Pérez-Madrigal [3] ,

[1] Departamento de Energía, División de Ciencias Básicas e Ingeniería, Universidad Autónoma Metropolitana Unidad Azcapotzalco, Ciudad de México, México.
E-mail: zdn@correo.azc.uam.mx Web: fenix.uam.mx/mecanica/ABINDICE.htm
[2] Departamentos de Neurocirugía y [3] Bioterio, Instituto Nacional de Neurología y Neurocirugía, Ciudad de México, México.

INTRODUCTION

Bilateral longitudinal plates or rods and polyaxial screws (PAS) are used for cranio-vertebral arthrodesis (CVA) as orthopedic treatment of cervical spine disorders, and it is necessary to assure the CVA biomechanical stability because of the high degree of mobility afforded by the upper cervical spine (Puttlitz et al., 2004). In this case the mineral density of occipital bone plate and vertebral lateral masses is an important factor which contributes to that stability and therefore to clinical success, so the screw-bone interface has been evaluated by means of pullout or insertional torque tests and up-to-date fresh-frozen human cadaver bone has been used (Yamagata et al., 1992; Zdeblick et al., 1993). These kind of tests demands a lot of expensive hardware, so we propose in this work, a novel testing protocol for determining in vivo the pullout yield torque of a PAS and by this way to calculate its pullout strength. We think this protocol will be more economical and it would let us know the actual PAS pullout strength.

METHODS

At the beginning of our work we had thought to perform the PAS pullout tests as many researchers have done with pedicle screws (Yamagata, Zdeblick). A 3.5 mm-diameter and 7 mm-long polyaxial screw, used for fixing craniovertebral longitudinal plates, was fully inserted in the occipital bone plate of an anaesthetized Rottweiler young adult dog (3 years old). After this first step, we asked ourselves: “Why do we not perform the test in vivo?” Having this in mind, a pullout mechanical device (PMD) was designed (figure 1) and it will be machined in stainless steel. In the next step the PAS will be extracted for attaching the PMD to the screw head. The PAS will be inserted again and then a tightening torque will be applied with an adjustable torque wrench (ATW) and using an open end wrench as opposite wrench.

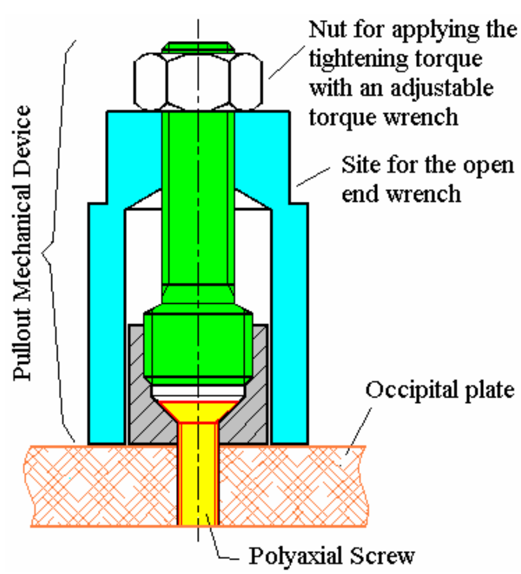

Figure 1: Cross-section of the Pullout Mechanical Device for determining the pullout strength in vivo of a polyaxial screw, by applying a tightening torque.

The tightening torque will pull out the PAS and the yield torque will be the maximum tightening torque we obtain, after which we think the torque value will decrease. The torque wrench will be adjusted in steps of 1 in-lb until the yield torque is obtained, which will be registered for calculating the pullout yield force by using the following equation (Shigley J.E. and Mischke C.R., 1990):

$$F_{poy} = T / K.d$$

Where:

F_{poy} = Pullout yield force
T = Maximum tightening torque
K = Torsion coefficient
d = Basic diameter of the nut inserted to the ATW drive socket

The first pullout test will be performed after April 2nd, at the Instituto Nacional de Neurología y Neurocirugía, México City, México.

RESULTS AND DISCUSSION

We anticipate sending you the pullout test results in April. We are sure that the PMD will accomplish our objective of evaluating in vivo the pullout strength of a PAS by using a canine model, avoiding the use of expensive hardware. This testing protocol will also save unnecessary deaths of laboratory animals.

SUMMARY

The screw-bone interface has been evaluated by means of pullout or insertional torque tests and up-to-date human cadaver bone has been used. We now propose an in vivo testing protocol to determine the pullout strength of a polyaxial screw, by using a canine model, a pullout mechanical device that we have designed, an adjustable torque wrench and an open end wrench as opposite wrench.

REFERENCES

Puttlitz C.M. et al. (2004). *J Bone Joint Surg, 86-A (3):561-568.*
Yamagata M. et al (1992). *Spine* Vol. 17 No. 3S.
Zdeblick T.A. et al. (1993). *Spine* Vol. 18 (12), 1673-1676.
Shigley, J.E. and Mischke C.R. (1990). *Diseño en Ingeniería Mecánica (cuarta edición en español)*. McGraw Hill Interamericana de México.

ACKNOWLEDGEMENTS

Support for this study was provided by the Mexican Orthopedic Surgical Instruments Company.

A TENDON SLACK LENGTH CALCULATION FROM MUSCULOTENDON EXCURSION

Miloslav Vilimek

Laboratory of Biomechanics, Dept. of Mechanics, Faculty of Mechanical Engineering, Czech Technical University in Prague, Czech Republic

E-mail: vilimek@biomed.fsid.cvut.cz Web: asb-biomech.org

INTRODUCTION

Many researchers and biomedical engineers dealt with developing of a general method for musculotendon actuator force calculation. In the equation, which express dynamic conditions of muscle and tendon loading, are some input parameters, which are difficult to measured or simply obtain otherwise. One of these input parameters is tendon slack length. From relationships between maximum and minimum length of musculotendon, pennation angle, normalized muscle and tendon slack length has been deduced relation for tendon slack length calculation. The values from this finding are close to experimentally measured and published data.

METHODS

A problem of muscle forces calculation of the elbow during flex/ext movements has been gone before this investigation. We have created simple model of elbow with seven MT actuators, four flexors and three extensors. Each MT actuator was represent as a three element Hill-type muscle in series with tendon, and from experimental collected kinematic and EMG data, …, also from net joint moment calculated from inverse dynamics, were studied behavior of several optimization criteria, EMG-driven and hybrid (EMG-driven with optimization) models. One of the input parameters for tendon dynamic expression is tendon slack length L_s^T.

The muscle force-length property has a limited range of fiber lengths over which a muscle can operate effectively. For representing of this property we use in terms normalized force $(\tilde{F}^M = F^M / F_0^M)$ and normalized muscle length $(\tilde{L}^M = L^M / L_0^M)$ (Zajac, 1989), L_0^M represent optimal muscle-fiber length, and peak isometric force is F_0^M. The effective operating range of muscle begins at roughly $0.5L_0^M$ and ends at $1.5L_0^M$ muscle cannot generate active force beyond these lengths.
Calculation of the length tension is in this case based on next statement: "When tendon slack length is large, muscle-fiber length is small; thus, muscle excursion will be small. Conversely, when tendon slack length is small, muscle-fiber length is large, and muscle excursion will be large. The relationship between optimal muscle-fiber length and MT excursion has been shown to vary widely among muscles, and it cannot be used to definethe value of L_0^M precisely (Garner & Pandy, 2003; Brand et al., 1988)". The muscle excursion is defined as the difference between the maximum physiological length $L_{\max}^{MT}$ and the minimum physiological length $L_{\min}^{MT}$ of the muscle. So, the relation between optimal muscle-fiber

length and MT excursion is the value of tendon slack length L_s^T. We use for expression of L_0^M and L_s^T in terms two quantities, $\tilde{L}_{\min}^M$ and $\tilde{L}_{\max}^M$, represented the minimum and maximum physiological muscle lengths normalized by L_0^M (as well as Garner & Pandy, 2003).
From the relationship between minimum and maximum MT length, *α/α₀* is pennation angle/optimal pennation angle, equations (1) and (2), and the facts, the values of $\tilde{L}_{\min}^M = 0.5$ and $\tilde{L}_{\max}^M = 1.5$ are known, we can deduced finding (3), relationship between tendon slack length and minimal and maximal MT length.

$$\tilde{L}_{\min}^{MT} = L_S^T + L_0^M \tilde{L}_{\min}^M \cos(\alpha) \quad (1)$$

$$\tilde{L}_{\max}^{MT} = L_S^T + L_0^M \tilde{L}_{\max}^M \cos(\alpha) \quad (2)$$

$$L_S^T = 1.5L_{\min}^{MT} - 0.5L_{\max}^{MT} \quad (3)$$

RESULTS AND DISCUSSION

The equation (3), can be used for tendon slack length calculation. We used it for seven muscles about elbow, the range of elbow angle was between 0° and 145°. The values are shown in table 1. with optimized values (Garner & Pandy, 2003) and measured data (Winters, 1988). Calculated values are only from one specimen. We can discussed, the tendon slack length value must be grater than zero, equation (4),

$$L_S^T = 1.5L_{\min}^{MT} - 0.5L_{\max}^{MT} \geq 0 \quad (4)$$

and obtained condition is (5):

$$\Rightarrow 3L_{\min}^{MT} \geq L_{\max}^{MT} \quad (5)$$

This condition (5) correspond with maximal and minimal sarcomere length, maximum of sarcomere lengths equal 3x minimum sarcomere length (see for example Gordon et al., 1966).

SUMMARY

We have equation for easily tendon slack length calculation. This method should be used for first approach, and can help investigators, who can not directly measure this value. The values from this finding are close to published data.

REFERENCES

Garner, B.A., Pandy, M.G., (2003): *Estimation of Musculotendon Properties in the Human Upper Limb*. Annals of Biomedical Engineering, **31**, 207-220.
Zajac, F.E., (1989): *Muscle and tendon: properties, models, scaling, and application to biomechanics and motor control.* Critical Reviews in Biomedical engineering **17**, 359-411.
Brand, P. W. et al. (1988): *Relative tension and potential excursion of muscles in the forearm and hand.* J. Hand Surgery **6**, 209–219.
Gordon,A.M., Huxley,A.F. (1966): *The The variation in isometric tension with sarcomere length in vertebrae muscle fibers.* J.of Physiology **184**, 170-192.

ACKNOWLEDGEMENTS

This investigation has been supported by the research project No.: MSM 210000012.

Table 1: calculated values of L_s^T $[cm]$ from eq.(3) and published data.

Muscle:	**Brachoradialis**	**Brachialis**	**Biceps brachii**	**Triceps brachii**
Equation (3):	8.24	4.10	22.45	17.71
Garner & Pandy:	6.04	1.75	22.98	19.05
Winters:	7.00	3.00	20.50	19.33

EMG ACTIVITY OF TRUNK MUSCLES DURING WHEELCHAIR PROPULSION

Yusheng Yang[1], Alicia Koontz[1], Michael L. Boninger[1] Ronald Triolo[2], Rory A. Cooper[1]
[1]Human Engineering Research Laboratories, VA Medical Center, Pittsburgh, PA, USA
[2] Cleveland FES Center, Case Western Reserve University, Cleveland, OH, USA
E-mail: yuy7@pitt.edu Web: www.herlpitt.org

INTRODUCTION

Paralysis of the core trunk musculature likely contributes to propulsion inefficiency (Koontz et al., 2004). Researchers have been looking into the use of functional electrical stimulation (FES) to improve trunk control, balance and posture in persons with spinal cord injury (SCI). Preliminary findings show that reaching ability can be improved with stimulation of the abdominal and back muscles (Kukke et al., 2002). In order to study the effect of FES on wheelchair propulsion, an understanding of trunk muscle activity during propulsion is needed. This information is necessary to determine the intensity and temporal information for synchronizing the stimulation signals with the propulsion cycle in a future study. Therefore, the purpose of this study was to determine the intensity and timing of trunk muscle activity during the propulsion and recovery phases of propulsion and to observe the corresponding trunk movements.

METHODS

Subjects: One male unimpaired subject provided informed consent prior to participation in the study. He was 24 years old, 58 kilograms and 1.71 meters tall.

Experimental protocol: Bipolar, surface electrodes (Noraxon Inc., Scottsdale, AZ) were placed over three abdominal muscles (rectus abdominis — RA, external oblique — EO and internal oblique — IO), and three back muscles (longissimus thoracis — LT, iliocostalis lumborum — IL, and multifidus — MU). Ten seconds of electromyography (EMG) data were collected with the subject laying supine on the mat at rest to determine the baseline activity levels. In addition, ten seconds of maximum voluntary contraction (MVC) EMG data during maximal effort manual muscle tests were recorded. A test wheelchair was fitted bilaterally with SMART^{Wheel} (Three Rivers Holdings, Inc., Mesa, AZ), force and torque sensing pushrims, and secured to a computer-controlled dynamometer with a four-point tie down system. Infrared emitting diode (IRED) markers were placed on the subject's acromion process and hip to record trunk position in a global reference frame via a three-dimensional motion analysis (Northern Digital Inc., Ontario, Canada). Subjects were instructed to propel at a steady-state speed of 0.9, and 1.8 m/s at a resistance that simulated propulsion up a ramp for one minute before collecting twenty seconds of data.

Data analysis: The EMG data were sampled at 1000 Hz, full wave rectified and smoothed with a 10-Hz low pass filter. The EMG voltages during propulsion were normalized by the highest value attained during the manual muscle tests for each muscle (%MVC). Significant EMG activity was defined as activity with an intensity of at least 3 standard deviations of the mean EMG activity at baseline.

SMART^{Wheel} data were collected at 240 Hz and filtered with an 8th order Butterworth low-pass filter, zero lag and 20 Hz cut-off frequency. Afterwards, the EMG and kinetic data were linearly interpolated for synchronization with the kinematic data collected at a rate of 60 Hz. Trunk flexion angle was calculated based on trunk position during the propulsion trials relative to trunk position in the resting position. Data from all ten continuous strokes on the right side were averaged together to provide a single value for the trial and normalized as percentage of the whole propulsion cycle. The start and end of push phase was determined as the presence/absence of forces detected by SMART^{Wheel} .

RESULTS AND DISCUSSION

In the beginning of the push phase, abdominal muscles (RA, EO and IO) had low levels of activity (Figure 1A), while the back muscles (LT, IL, and MU) showed higher levels of activity (Figure 1B) for both slow and fast speed conditions (Table 1). The trunk was continuously leaning forward from 7 to 11 degrees (slow speed), and 25 to 36 degrees (fast speed) condition during the push phase (Figure 1C). While delivering forces to the rim, the back muscles contracted eccentrically to provide trunk stability and hold the trunk in a flexed position. A forward flexed trunk may help manual wheelchair users transfer their power from their upper extremities to the pushrim thereby improving mechanical efficiency. In early recovery, back muscles acted concentrically to bring the trunk and upper limbs back. Abdominal muscles showed peak activity in late recovery phase (85% to 86 % of the cycle), and contracted concentrically to bring the trunk forward to prepare for the next stroke.

SUMMARY

We are currently extending this study to recruit more subjects. With these data, we plan to develop a stimulation pattern specific for wheelchair propulsion for individuals with SCI who have a functional electrical stimulation neuroprotheses.

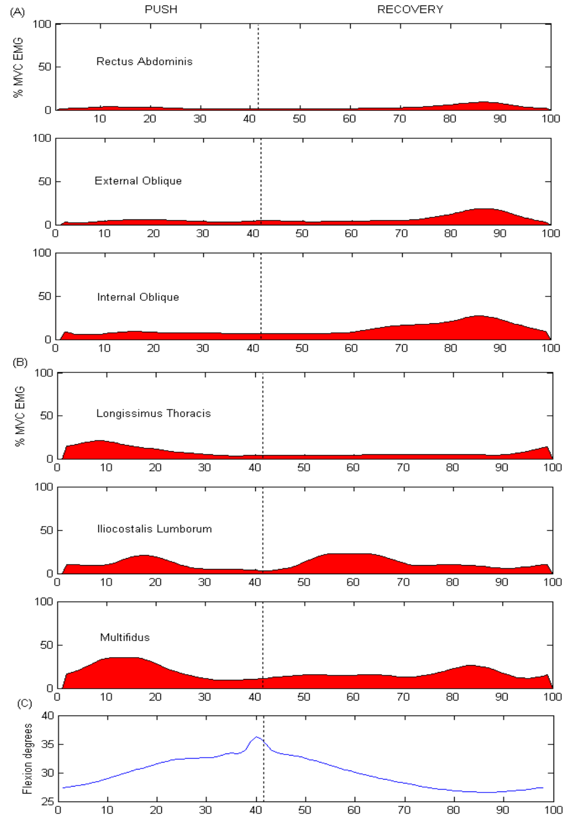

Figure 1. Mean EMG profile of abdominal muscles (A), and back muscles during a stroke cycle at speed of 1.8 m/sec (B). Trunk flexion angle during the stroke cycle(C).

REFERENCES

Koontz et al (2004). *Proceedings of ASB'2004* , in review.
Kukke et al. (2002). *J of Spinal Cord Med,* **25**, S21.

ACKNOWLEDGEMENTS

NIDRR (H133A011107), and VA Rehab R&D (B3043-C).

		0.9 m/sec						1.8 m/sec					
	Muscle	RA	EO	IO	LT	IL	MU	RA	EO	IO	LT	IL	MU
Push Phase	Duration % cycle	Not active	0-10	0-45	5-38	7-24	0-45	Always active					
	Peak intensity % MVC	Not active	3.6	3.9	9.1	8.7	19.9	3.4	5.8	9.5	20.6	19.9	30.5
Recovery Phase	Duration % cycle	Not active	78-100	46-100	66-100	70-91	46-100	Always active					
	Peak intensity % MVC	Not active	3.6	4.8	7.7	3.8	8.4	8.9	19.0	27.8	14.1	24.6	25.5

Table1. The average timing of EMG activity under two different speeds. The push phase ended at 45% cycle at 0.9m/sec, and 43 % cycle at 1.8m/sec.

DO THE MECHANICAL PROPERTIES OF INTERVERTEBRAL DISCS MATCH THOSE OF ADJACENT VERTEBRAE?

Daniel Skrzypiec, Phill Pollintine, Michael A. Adams

Department of Anatomy, University of Bristol, Bristol BS2 8EJ, UK
E-mail: D.Skrzypiec@bristol.ac.uk

INTRODUCTION

Many spinal disorders are related to mechanical failure of either the vertebral body or intervertebral disc. These two structures must act together to resist the high axial (compressive) forces which are habitually applied to the spine by gravity and muscle action (Pollintine et al. 2004). Compressive forces acting on the vertebral body generate tensile forces in the transverse plane of the disc's annulus fibrosus.

The vertebral body has a rich blood supply and can strengthen or weaken rapidly in response to changes in prevailing mechanical loading. It's strength falls markedly following hormonal changes at the menopause. Intervertebral discs, on the other hand, are the largest avascular structures in the body, have a low cell density, and adapt slowly (if at all) to changes in their environment. A miss-match in adaptive potential between discs and vertebrae could possibly lead to injury and degenerative changes in either tissue (Adams and Dolan 1997).

We hypothesize that the (tensile) properties of the annulus fibrosus are able to adapt to match the (compressive) properties of adjacent vertebral bodies.

METHODS

Twenty one human thoraco-lumbar motion segments aged 64-90 yrs (mean 77 yrs) were compressed to failure while positioned in moderate flexion. Failure always occurred in the vertebral body, and the compressive strength of each was measured at the elastic limit. Immediately after testing, the intervertebral disc were removed from each motion segment, wrapped in cling film, sealed in a plastic bag and stored at -20º C.

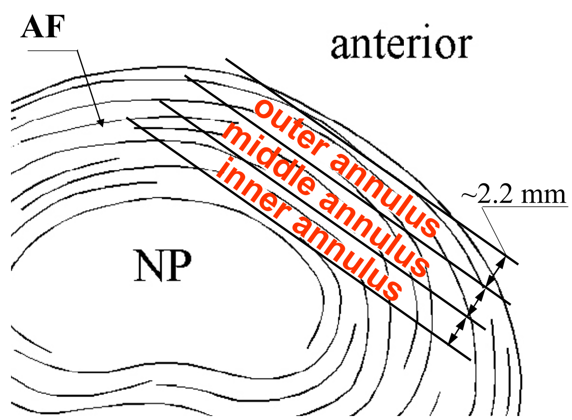

Figure 1: Tangential specimens obtained from the outer, middle, and inner annulus.

On the day of testing, a device incorporating several razor blades was used to obtain tangential specimens from the antero-lateral region of the annulus fibrosus while it was still frozen (Figure 1). Specimens were approximately 2.2 mm thick. Another razor device was used to make dumbbell-shaped annulus specimens. Each end of these was secured with cyanoacrylate adhesive to the smooth inner surface of folded sand paper. The outer (rough) surfaces of the sand paper were gripped in the clamps of a miniature materials testing machine (Minimat 2000). Average free length was 6.5 mm.

Four preconditioning tensile tests were used to bring specimens to a steady state. They were then loaded to failure at 1 mm/s.

Ultimate tensile stress of the annulus specimens (MPa) was compared with the compressive strength (MPa) of the adjacent vertebrae, using linear regression.

RESULTS AND DISCUSSION

The ultimate tensile stress of annulus specimens decreased from an average of 8.2 MPa in the outer annulus to 1.0 MPa in the inner annulus. Radial differences were significant according to a single factor ANOVA ($P< 0.001$) and were greater than those reported previously for non-degenerated specimens (Ebara et al. 1996).

The ultimate tensile stress of the annulus decreased with age in the outer, middle and inner annulus ($P= 0.03$, $P< 0.001$, and $P= 0.001$ respectively).

The ultimate tensile stress of the outer and middle annulus was proportional to the compressive strength of adjacent vertebrae in male specimens ($P = 0.01$ and $P= 0.04$ respectively). However, no such relationship was noted for female or inner annulus specimens.

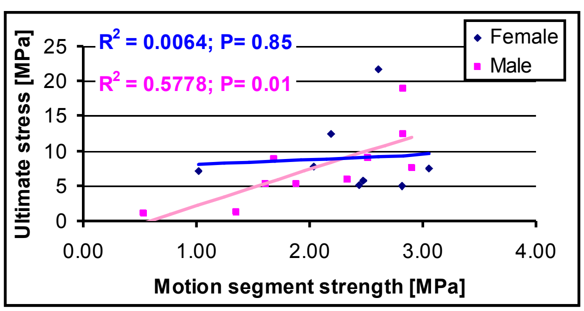

Figure 2: Ultimate tensile stress of outer annulus compared to compressive strength of adjacent vertebrae ("motion segment").

In multiple regression analyses, age was a better predictor of annulus strength than was vertebral strength. Age and vertebral strength predicted up to 70% of the variance in annulus ultimate tensile stress (Table 1).

Table 1: Multiple regression results

Annulus	R^2	P
Outer	0.32	0.05
Middle	0.62	0.01
Inner	0.70	0.01

CONCLUSIONS

Tensile strength of the annulus fibrosus decreases with age, especially in the middle and inner annulus. This may be attributable to structural disruption in old discs.

Tensile strength of the outer and middle annulus is proportional to the compressive strength of adjacent vertebrae, but only in male specimens. This may be attributable to greater compressive loading of male spines.

Annulus fibrosus has a limited ability to adapt to prevailing mechanical loading.

REFERENCES

Adams, M.A., Dolan, P. (1997). *The Lancet,* **350**, 734-5.
Pollintine, P. et al. (2004). *J. Biomech,* **37**, 197-204.
Ebara, S. et al. (1996). *Spine,* **21**, 452-61.

ACKNOWLEDGEMENTS

Research supported by "DISCS", London. We thank Dr Fengdong Zhao for assisting in these experiments.

THE EFFECTS OF ALTERED CYCLING POSTURE AND CADENCE ON SUBSEQUENT RUNNING MECHANICS

Rachel D. Durham and Julianne Abendroth-Smith, Ed.D.

Willamette University, Salem OR

INTRODUCTION

Many triathletes complain of experiencing difficulties while running following cycling, but these difficulties are usually only felt in about the first kilometer of the run (Millet and Vleck, 2000). To improve performance in the run portion of a triathlon, it would be beneficial to minimize the negative effects from cycling. The purpose of this study was to compare the effects of two cycling positions, sitting up and spinning at the end of the cycling portion versus staying in the tucked riding position, on subsequent running mechanics.

Many studies have been done on the kinematic and physiological changes which occur during running following a bout of cycling (Quigley and Richards, 1996; Hue, et al., 2001; Hausswirth, et al., 1997), but no studies have examined a practical way to minimize the difficulties. The task of cycling is much different than running; one reason being that cycling is a non-weight bearing activity and running is a weight bearing activity in which the body experiences a large increase in impact forces. Another reason athletes may experience difficulties is because of blood flow redistribution time. The primary muscles used in cycling are different than the muscles primarily used in running; as the athlete transitions from one event to the other, there may be a delay in which the blood flow is being redirected to the working muscles (Anderson, 2003). A technique that is used by some triathletes to minimize the negative effects is to sit up and spin in a lighter gear towards the end of the bike portion of a triathlon. This may aid the athlete in the run portion of the triathlon, and examining this technique is beneficial because athletes can possibly utilize it to minimize the effects of the transition.

METHODS

Four college-age volunteers, who train by running and cycling, were used in this study. Informed consents were obtained, with approval from the University IRB.
Two tests were conducted for each subject in a random order. A 5-minute warm up run was performed prior to each test. The subjects rode their own bike, mounted to a CycleOps Fluid II stationary trainer, for a 40-minute period, and then transitioned into a 5-minute run at a 5K pace; each subject rode and ran at their own chosen cadence. For the control (C), the subjects remained in the crouched position for the entire 40-minute ride with no change in posture, gear, or cadence on the bike before transitioning into the run. For the treatment (T), during the last 5-minutes of the cycle portion, the subjects sat in a more upright position and pedaled at a faster cadence in a lighter gear before transitioning into the run. Data was collected and analyzed during the first and last portion of each run (labeled C1, C2, T1, T2); for each condition, 4 trials were collected for each subject, over about a 100 m stretch (four cameras set at 20 m distances). Maximum stride length (defined as right heel to left heel displacement), average trunk angle (absolute angle from the right horizontal), and thigh-knee angle (absolute thigh angle from right horizontal and relative thigh to shank angle) were measured for each trial.

A 2D motion measurement system was used for digitizing (60Hz); data was low-passed filtered (6 Hz, Butterworth), and analyzed for the above variables.

RESULTS

Means and SDs across all subjects are seen in Table one. The maximum stride length between all conditions was found to be statistically significantly different (F = 5.79, df = 3, p = .001). Post hoc comparisons showed only C1 to be statistically larger from the other conditions.

Table 1. Average Stride Lengths and Trunk Angles Across Subjects.

	Stride Length		Trunk Angle	
	mean	SD	mean	SD
Control1	1.02	0.14	78.49	2.08
Control2	0.97	0.07	78.39	2.36
Treat1	0.97	0.11	78.90	2.35
Treat2	0.97	0.11	78.69	2.15

Average trunk angles showed no significant differences. However, a trend in C1 and C2 was seen with a more forward leaning posture, while the angle during T1 and T2 was more erect.

The high-knee angle diagrams demonstrated differences within each subject. Averaged across subjects, the T2 diagram showed greater hip flexion over the other conditions (Figure 1), indicating a greater range of motion of the hip. For C1, FS occurred on average with less hip flexion, but similar hip extension and knee motion to the other conditions.

DISCUSSION AND CONCLUSIONS

The statistically significant difference of C1 when compared to the rest of the conditions shows that there was a change in the running step length after cycling, while the run during T1 was much more similar to the latter runs of C2 and T2. It is apparent that there is a possibility of the treatment influencing the subsequent run due to the similarities of step length. It is inconclusive whether each subject likely reached a steady state by the end of both conditions, though the similar step length of C2, T1 and T2 gives some indication of this.

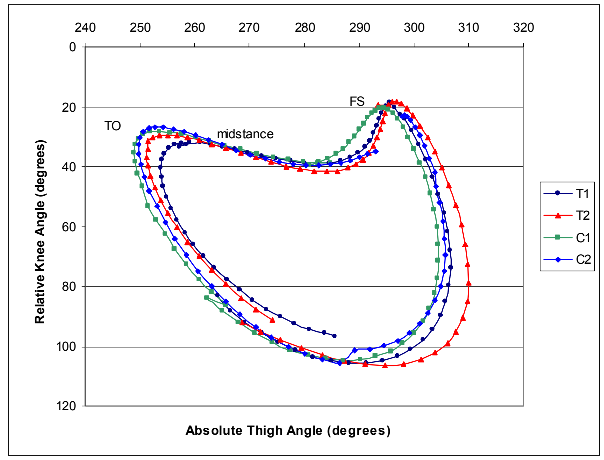

Figure 1. Angle-angle diagram averaged across subjects.

For C1, as a subject remains in the crouched position for the entire 40-minutes, the body appears to take longer to adapt to the transition of running. Sitting up and spinning in the saddle allows for a more upright posture (more similar to running), making the beginning of the run comparable to the end of the run, overall causing the athlete to be more consistent with their running mechanics. However, the greater range of motion of T2 seen in the angle-angle diagram indicates not all changes are taken into account with the alteration in riding position.

REFERENCES

Anderson (2003) Peak Performance. www.pponline.co.uk/encyc/0624b.htm

Hausswirth ,et al. (1997) *Int J of Sports Medicine,* 18, 330-339.

Hue, et al. (2001) *J Sports Med & Ph Fit*, 41, 300-305

Millet & Vleck (2000). *Brit J Sport Med*, 34, 384-390.

POSTERIOR CRUCIATE LIGAMENT RESPONSE TO PROXIMAL TIBIA IMPACTS

Adam J. Bartsch [1,2], Alan S. Litsky [1,3,4], Joseph R. Leith [4],
Rod G. Herriott [1,5] and Joseph D. McFadden [1,6]

[1] Biotrauma Laboratory, [2] Department of Mechanical Engineering, [3] Biomedical Engineering Center and [4] Department of Orthopaedics, The Ohio State University, Columbus, OH, USA
[5] Transportation Research Center, East Liberty, OH, USA
[6] National Highway Traffic Safety Administration, East Liberty, OH, USA
E-mail: bartsch.3@osu.edu

INTRODUCTION

Shearing and flexion of the knee joint are recognized as two important injury mechanisms associated with frontal automobile impacts. In a frontal collision, the automobile is decelerated over a short period of time. Due to inertia the occupant's lower extremities travel until arrested by safety belts, air bags or the knee bolster/steering column. In frontal crashes dynamic loading of the flexed lower extremity by the knee bolster/steering column causes the posterior cruciate ligament (PCL) to be the most frequently injured structure.

There is currently no acceptable injury threshold for PCL injuries in frontal crash testing. Kuppa et al.[a] defined 15 mm of knee slider displacement (tibia subluxation) as the current 50% probability of injury to the midsize male anthropomorphic test device (ATD).

Crash tests were conducted with Hybrid III (HIII) ATD's to determine impact testing input parameters. Impact testing was then carried out on flexed HIII lower extremities and flexed post mortem human subject (PMHS) lower extremities. A comparison was made in an effort to relate PMHS tibia subluxation and PCL injury timing to HIII knee slider displacement.

METHODS

An impact protocol to determine PCL response of PMHS lower limbs was developed from a series of 10 frontal ATD crash tests conducted at the Transportation Research Center in East Liberty, Ohio. This protocol was then used in proximal tibia impacts to both HIII ATD and PMHS lower limbs for comparison of tibia subluxation and PCL injury timing.

Ten (10) PMHS lower extremities were tested at the Biotrauma Laboratories at The Ohio State University. Eight (8) lower extremities were tested dynamically with a pneumatic impactor striking the tibial tuberosity normal to the surface at impact energy ranging from 110 J to 434 J (3.1 m/sec to 6.2 m/sec). Two (2) lower extremities were tested quasistatically [Bionix, MTS Systems, Eden Prairie, MN] to verify instrumentation technique and determine knee stiffness.

RESULTS AND DISCUSSION

From eight (8) dynamic impacts (Figure 1) it was determined that the 50% likelihood of AIS 2+ (moderate to severe) injury to the lower extremity occurred at an impact energy of approximately 125 J with a 22.75 kg impactor. This energy corresponded to a knee slider displacement of roughly 10 mm in the HIII midsize male ATD under the same impact scenario.

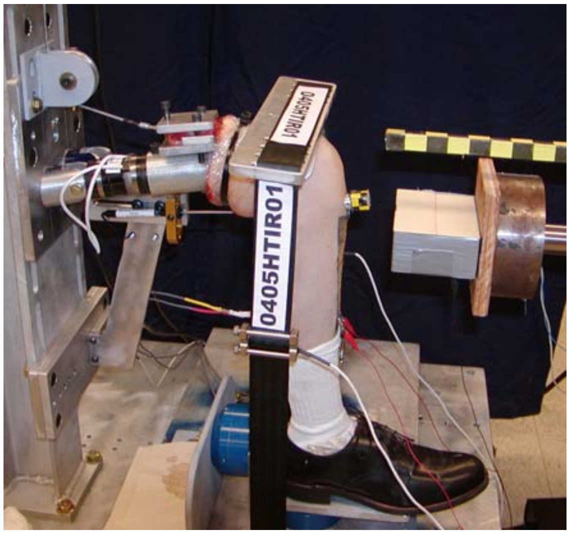

Figure 1: Experimental set-up for PMHS lower extremity impact testing

Additionally, two (2) quasistatic tibia posterior displacement tests were performed and the average stiffness of the knee joint complex was found to be approximately 2100 N/cm. The current stiffness value for the midsize male ATD knee slider was found by Viano et al.[b] to be 1490 N/cm.

SUMMARY

The current 50% probability of injury to the midsize male ATD is 15 mm of knee slider displacement. The results of the eight dynamic impacts indicated that this value might not be conservative enough to prevent injury. Additionally, the quasistatic knee stiffness (at 0.5 mm/sec) value was shown to be higher than that obtained in previous work (Figure 2).

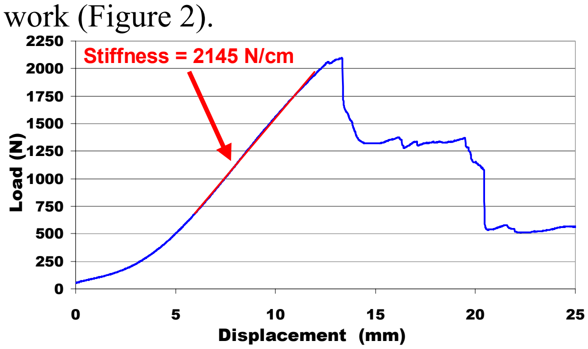

Figure 2: Quasistatic Knee Stiffness Test

Finally, the tibia was able to sustain significant posterior subluxation in several tests with little or no apparent injury to the PCL and knee complex (Figure 3).

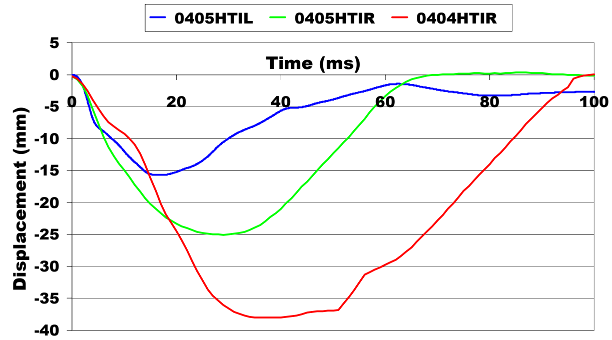

Figure 3: Posterior tibia displacement from three subject legs which did not result in visible PCL injury

Clinically, tibia posterior displacement of 15 mm of a flexed lower extremity would be classified as a grade III PCL injury (complete rupture.) These displacements indicated a greater elastic component in the knee complex without injury than previously thought.

REFERENCES

[a]Kuppa, S. et al. (2001). *Proc. 17th ESV*, Paper No. 457, NHTSA, Washington, DC.

[b]Viano, D.C. et al. (1978). *SAE Paper No. 780896*, Society of Automotive Engineers.

ACKNOWLEDGEMENTS

This project was funded by the Vehicle Research and Test Center in collaboration with the Transportation Research Center.

THE INFLUENCE OF SEAT HEIGHT IN SIT TO STAND IN THE ELDERLY: A SIMULATION STUDY

Zachary J. Domire [1] and John H. Challis [2]

[1] Division of Kinesiology and Health, The University of Wyoming, Laramie, WY, USA
[2] Biomechanics Laboratory, The Pennsylvania State University, University Park, PA, USA
E-mail: zdomire@uwo.edu

INTRODUCTION

Lowering seat height has been shown to increase the difficulty of rising from a chair (Arborelius et al., 1992). The impact of this increasing difficulty is particularly important for elderly individuals, because rising from a chair can be a near maximal strength task (Hughes et al., 1996). Two strategies while in contact with the seat have been proposed for dealing with decreases in seat height: moving the trunk farther forward or increasing the forward momentum of the trunk (Weiner et al., 1993; Schenkman et al., 1996).

The following study uses a computer simulation model with muscle properties adjusted to be reflective of the elderly to examine how kinematics are adjusted to deal with the increasing difficultly of standing from progressively lower seat heights.

METHODS

An optimal control direct dynamics muscle moment driven model was used to simulate rising from a chair. The objective function used was proposed by Pandy et al. (1995). The inertial parameters for the model's links were the same as those for a typical experimental subject (mean age 71.8 years) from the study of Burgess (2003).

The model was actuated by eight muscle models representing the major muscle groups of the lower extremity. Each muscle model had force-length and force-velocity properties as well as activation dynamics (Gallucci & Challis, 2002). To reduce simulation time muscles were modeled with rigid series elastic elements. The original parameters values for the muscle model were based on the data presented by van Soest et al. (1993) and Friederich and Brand (1990). Adjustments were made to these parameters to make them reflective of an older subject (approx. age 70 years).

Sit to stand was simulated from three different seat heights. The shank and the trunk were vertical at the start of each of the simulations. Changing seat height was accommodated by rotation of the thigh segment.

RESULTS AND DISCUSSION

The simulation from the 42 cm seat produced a similar kinematics and kinetics as a typical subject from Burgess (2003).

Changes in trunk movement prior to seat off as seat height decreased did not support either strategy proposed to deal with this increased difficultly (Table 1). The hip angle at seat off increased as seat height decreased. However, because of the higher initial hip angle, the resulting anterior trunk rotation decreased as seat height decreased. Maximum hip flexion velocity also decreased as seat height decreased.

Table 1: Trunk motion prior to seat off for each seat height.

	Seat Height		
	38 cm	42 cm	50 cm
Hip Angle	102°	101°	95°
Trunk Angle	7°	10°	15°
Maximum Hip Flexion Velocity	37 °/s	54 °/s	85 °/s

Moments expressed as a percentage of maximum available moment available at a given joint angle increased as seat height decreased (Table 2). As seen in other studies the maximum knee moment for the lowest seat height was close to maximal.

To accommodate the lower seat heights initial hip flexion had to increase; this additional hip flexion moved the hip extensors to a less favorable region of the force-length curve. This is complicated by the knee extensors being near maximally stressed at this time, therefore activation of the hamstrings is undesirable. In the simulation from the lowest seat height the gluteal muscles are 90 percent activated to reverse the direction of the hip movement, thus not allowing increased forward trunk rotation.

SUMMARY

Two strategies for motion prior to losing contact with seat have been proposed for dealing with decreases in seat height: rotating the trunk farther forward or increasing the forward momentum of the trunk. Evidence from this study does not support adoption of either of these two strategies. Here as seat height decreased both the forward rotation and angular velocity of the trunk decreased. This is a consequence of the higher initial hip angles placing the hip extensors on a less favorable region of the force-length curve.

REFERENCES

Arborelius, U. P. et al. (1992). *Ergonomics*, **35,** 1377-91.

Burgess, R.M. (2003). Unpublished M.S. thesis, Penn State.

Friederich, J.A., & Brand, R.A. (1990). *J. Biomech*., **23**, 91-95.

Gallucci, J.G., & Challis, J.H. (2002*). J. App. Biomech*., **18**, 15-27.

Hughes, M.A. et al. (1996). *J. Biomech*., **29,** 1509-13.

Pandy, M.G. et al. (1995). *J. Biomech. Eng*., **117,** 15-26.

Schenkman, M. et al. (1996). *J Am Geriatr Soc*, **44,** 1441-6.

Van Soest, A.J. et al. (1993). *J. Biomech*., **26**, 1-8.

Weiner, D. K. et al. (1993). *J Am Geriatr Soc*, **41,** 6-10.

ACKNOWLEDGEMENTS

This research was in part support by a grant from The Whitaker Foundation.

Table 2. The maximum joint moments for the simulations from the three seat heights, and presented as a percentage of maximum moment available at given joint angles and velocities.

	38 cm	**42 cm**	**50 cm**
Maximum Hip Extension Moment	70 Nm (67%)	82 Nm (36%)	87 Nm (41%)
Maximum Knee Extension Moment	266 Nm (98%)	271 Nm (96%)	229 Nm (74%)
Knee Extension Moment at Seat Off	245 Nm (93%)	239 Nm (84%)	200 Nm (66%)
Maximum Dorsiflexion Moment	266 Nm (99%)	278 Nm (89%)	238 Nm (80%)

Note - Moments presented are for both legs.

CHARACTERIZATION OF PLANTAR TISSUES UNDER THE METATARSAL HEADS

Andrew R. Fauth[1,2] and Neil A. Sharkey[1,2,3]

[1]Center for Locomotion Studies, The Pennsylvania State University, University Park, PA
[2]Dept. of Kinesiology, The Pennsylvania State University, University Park, PA
[3]Dept. of Orthopaedics and Rehabilitation, The Pennsylvania State University, Hershey, PA
email: nas9@psu.edu url: www.celos.psu.edu

INTRODUCTION

Reports in the literature of the material properties of human plantar tissues have mainly been limited to the heel, many of which are *in vivo* impact tests of the plantar surface (Valiant, 1884; Aerts et al., 1995). Others have used ultrasonic methods to characterize the hyperelasticity of heel tissue for inverse finite element analysis (FEA) (Erdemir et al., 2003). *In vitro* methods have also been used to determine the material properties of heel pad soft tissues under compression for input into FEA (Miller-Young et al., 2002; Ledoux et al., 2002). Despite the extensive examinations of the heel soft tissues, reports of the plantar tissue properties under the metatarsal heads are limited. Ledoux et al. (2003) reported on the rate and location sensitivity of the plantar fat pad, noting significant differences in stress and modulus between the heel and submetatarsal regions. The purpose of this study was to describe the stress-strain behavior of the plantar tissue under the first and second metatarsal heads as well as to quantify the hyperelastic material parameters in both constrained and unconstrained tissues. These data are useful in constructing more realistic numerical models of the foot. Furthermore, differences in these material parameters across test conditions may indicate the influence of boundary effects that can occur with structural indentation testing.

METHODS

The plantar tissues from 8 fresh-frozen, non-diabetic, cadaveric feet (average age 68.6) were used for this study. Each specimen was thoroughly thawed and allowed to fully acclimate to a 37° C water bath prior to testing. A dorsal approach was used to dissect out the first and second metatarsal heads and the sesamoids, leaving only the plantar fat pad and skin. A 4 cm x 1 cm platen was used to compress the plantar tissues under the first and second metatarsals. Following the initial compression test, relief cuts were made completely through the fat pad and skin at both ends of the platen along its short axis, and the testing regime was repeated. Testing was done on a servo-hydraulic testing machine (MTS Corp., MN, USA) at a test rate of 1Hz. Each specimen was sinusoidally cycled 100 times under load control to 300 N of compression while force and displacement data were collected every 10th cycle. The force-displacement data for both the non-relieved and relieved conditions were normalized by tissue thickness and platen area to obtain mean stress-strain curves across all specimens. A root mean squared routine was employed to characterize the loading portion of the mean stress-strain curves. Stress-strain data was imported into Abaqus (Abaqus, Inc., Pawtucket, RI, USA) where the Ogden strain energy function was used to calculate the incompressible hyperelastic material parameters μ (initial shear modulus) and α (measure of the increase in material stiffness as a result of loading).

Table 1: Polynomial fits and RMS values for the loading curves

Condition	*Polynomial Fit Equations for the Loading Curves*	*RMS (MPa)*
No Relief	$Y = 7.382*X^4 - 1.038*X^3 + 0.061*X^2 + 0.0014*X + 0*C$	.0078
With Relief	$Y = 1.622*X^4 - 0.230*X^3 + 0.012*X^2 + 0.0001*X + 0*C$	.0092

RESULTS AND DISCUSSION

The stress-strain curves for both test conditions exhibited nonlinear, viscoelastic behavior with significant hysteresis (Figure 1). Each loading curve was characterized by a fourth-order polynomial with rms values less than 2 percent max stress (Table 1). It is difficult to compare these data to previous soft tissue examinations due to differences in test frequency, methodology, and location on the foot. Ledoux et al. (2003) tested unconstrained tissue beneath the 1st, 3rd, and 5th metatarsal head at 1 Hz, but their samples comprised only the fat pad without the skin. While the inclusion of the skin in this study differs from other *in vitro* tests in the literature, many FEA models of the plantar surfaces lump both the skin and fat pad together. Therefore, data regarding the material behavior of the skin-fat pad construct is useful. Differences in the stress-strain curves between the non-relieved and relieved tests may be a result of boundary effects from adjacent tissue at the platen edges, which is relevant to impact-type material testing. However, the hyperelastic material parameters, μ and α (Table 2) were not found to be statistically different across test conditions, indicating that boundary effects did not dictate the stress-strain relationship. Future development of an inverse FEA hyperelastic model would help to elucidate any boundary effects that may actually be occurring.

Table 2: Hyperelastic material properties

	μ *(MPa)*	α
No Relief	0.985 (±0.105)	12.77 (±1.456)
With Relief	1.065 (±0.209)	14.52 (±2.131)

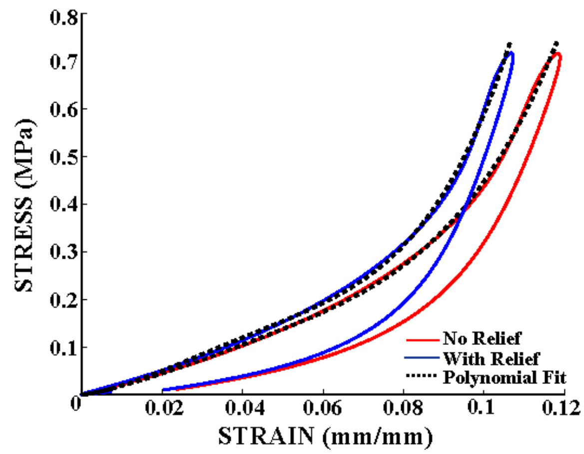

Figure 1: Stress-strain curves and polynomial fits

SUMMARY

These data describe the *in vitro* material properties of the plantar soft tissues beneath the first and second metatarsal heads and can be used in detailed hyperelastic numerical models of the soft tissues on the plantar surface of the foot.

REFERENCES

Aerts, P. et al. (1995) Journal of Biomechanics **28** (11): 1299-1208.

Erdemir, A. et al. (2003) *ASME Summer Bio-engineering Conference*, FL.

Ledoux, W. R. et al. (2002) Proceedings of the 4th World Cong. of Biomechanics.

Ledoux, W. R. et al. (2003) Proceedings of the 27th Annual ASB Meeting.

Miller-Young, J.E. et al., (2002) *Journal of Biomechanics* **35**(12): 1523-31.

Valiant, G. A. (1984) Ph.D. Thesis, Penn State University, University Park, Pa.

ACKNOWLEDGEMENTS

We would like to acknowledge the help of Ahmet Erdemir, Ph.D. and Todd Pataky, M.S. This work was supported by NIH Grant # 5R01HD3744302, P.I. Peter Cavanagh, Ph.D.

BONE STRENGTH IS NOT COMPROMISED WITH AGING IN BLACK BEARS (URSUS AMERICANUS) DESPITE ANNUAL PERIODS OF DISUSE (HIBERNATION)

Seth W. Donahue[1, 2] and Kristin B. Harvey [1]

Departments of [1]Mechanical Engineering - Engineering Mechanics and [2]Biomedical Engineering, Michigan Technological University, Houghton, MI 49931, USA
E-mail: swdonahu@mtu.edu Web: http://www.biomed.mtu.edu/swdonahu/

INTRODUCTION

Disuse osteoporosis is well documented in humans and animals including hibernating bats and ground squirrels (Kwiecinski, 1987). A reduction in bone's mechanical stress environment stimulates increased osteoclastic bone resorption coupled with decreased osteoblastic bone formation (Weinreb, 1989). This leads to bone loss and decreased material properties (Kaneps, 1997). Upon remobilization after a prolonged period of disuse, bone loss may not cease immediately and may take 2-3 times the length of the disuse period to be completely recovered (Weinreb, 1997). Since black bears hibernate for 5-7 months annually, these previous findings raise an important question regarding the maintenance of bone in hibernating black bears: how can black bears maintain bone mass and strength when annual hibernation (i. e., disuse) and active periods are approximately equal (6 months)?

The answer may be explained by their regulation of bone formation. We previously found that even though bone resorption increases in bears during hibernation, bone formation does not decrease (Donahue, 2003). Furthermore, bone formation increases 2-5 fold immediately upon remobilization. The goal of the work presented here was to assess how annual periods of disuse affect the material behavior of black bear bone.

METHODS

Tibias were obtained from 26 black bears that were killed late in their active period (i.e., October) by licensed hunters in the Upper Peninsula of Michigan; 15 were from male bears (ages 2 to 8 years) and 11 were from female bears (ages 2 to 14 years). Bending coupons were milled from the medial quadrant of the mid-diaphysis into 2mm x 3.5mm x 30mm rectangular bars. The specimens were loaded to failure in three-point bending at a displacement rate of 1 mm/sec. Tensile specimens were milled from the anterior quadrant into dumbbells with square cross-sections: 2mm x 2mm x 10mm in the gage region. They were loaded monotonically to fracture in uniaxial tension at a strain rate of $0.03s^{-1}$. One half of each fractured specimen was used to calculate the ash fraction and the other half was used to calculate porosity.

For ashing, the bone samples were placed in a furnace at 100°C for 24 hours to remove the water, and then at 600°C for 48 hours to remove the organic material, leaving only the bone mineral. The ash fraction was calculated as the ash mass over the dry mass. The histological specimens were dehydrated in ethanol and then embedded in methyl methacrylate. Cross-sectional wafers with a thickness of 100 microns were extracted adjacent to the fracture surface and examined by light microscopy. Porosity was calculated by point counting. All parameters were linearly regressed against age. The bending, ash, and porosity data were compared to human data for the same relative ages (growth through maturity) since humans do not routinely experience disuse.

RESULTS AND DISCUSSION

The tensile strength did not significantly (p=0.16) change with age (Figure 1).

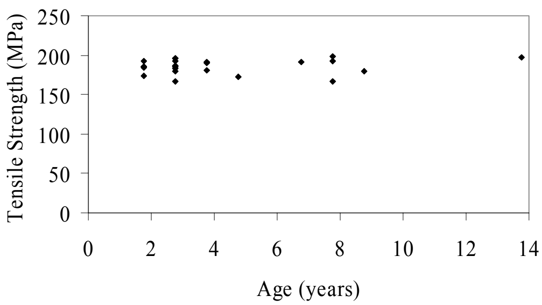

Figure 1: Tensile strength vs age.

However, the bending strength significantly (p=0.01) increased with age (Figure 2). This age-related increase in bending strength is similar to that seen in human (ages 2-48 years) cortical bone (Currey, 1975). Bending modulus (p=0.04) and ash

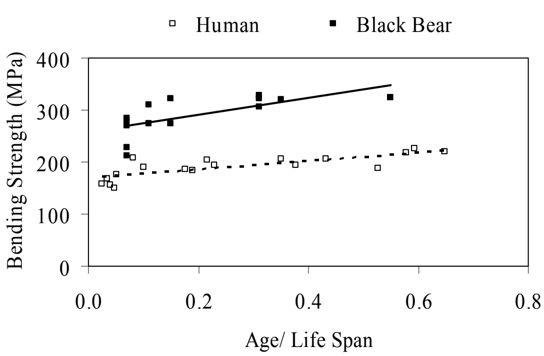

Figure 2: Black bear and human bending strengths show similar significant increases with age. However, black bear bone is stronger. And humans do not routinely experience disuse annually. Human data from Currey (1975).

fraction (p=0.03) also increased with age, as it does in human bone. Fracture energy in bending did not change (p = 0.91) with age in bears, unlike the age-related decrease seen in human bone. Furthermore, black bear cortical bone porosity did not significantly (p = 0.12) change with age, unlike the age-related increase in porosity in human cortical bone. These findings provide further support for the hypothesis that black bears are resistant to disuse osteoporosis.

SUMMARY

We found that black bear bone material properties are not compromised with aging despite the fact that bears are inactive for 6 months annually. The biological mechanisms for the black bear's ability to resist disuse osteoporosis are currently under investigation. These mechanisms may have important implications for understanding human osteoporoses and developing pharmaceutical therapies.

REFERENCES

Currey, J. D., Butler, G. (1975). J Bone Joint Surg Am 57, 810-4.

Donahue, S. W., et al. (2003). J Exp Biol 206, 4233-9.

Kaneps, A. J., et al. (1997). Bone 21, 419-23.

Kwiecinski, G. G., et al. (1987). Am J Anat 178, 410-20.

Weinreb, M., et al. (1989). Bone 10,187-94.

Weinreb, M., et al. (1997). Virchows Archiv 431, 449-52.

ACKNOWLEDGEMENTS

This research was supported by NIH and NASA. The authors thank Doug Wagner from the Michigan Department of Natural Resources for providing the bone specimens.

REALISTIC TESTING OF RIOT HELMET PROTECTION AGAINST PROJECTILES

Cathie L. Kessler, Jean-Philippe Dionne, Doug Bueley, Aris Makris

Med-Eng Systems Inc., Ottawa, Ontario, Canada
E-mail: ckessler@med-eng.com Web: www.med-eng.com

INTRODUCTION

The NIJ and CSA standards for testing of riot helmets [NIJ, 1984; CSA, 2002] require drop tower testing, in which helmeted headforms are dropped on anvils and stationary helmets are impacted by falling objects. The CSA standard also provides information regarding weights and impact energies of typical projectiles used in crowd management situations. In the current testing, inertia effects introduced by artificial supports are removed by impacting a free-falling mannequin with objects representative of these projectiles.

METHODS

All testing was performed on a Hybrid II mannequin representing the 50th percentile. Spherical objects representing a billiard ball (210 g, 98 km/h), full beverage can (360 g, 87 km/h), and half-brick (954 g, 67 km/h) were propelled at the mannequin using a standard baseball pitching machine. A tri-axial cluster of accelerometers (PCB Piezotronic 350A03) was located in the head of the mannequin, with the origin of the coordinate at the nasal root. High-speed digital video was taken at 500 fps, and data was collected through a computerized data acquisition system at a rate of 10 kHz and filtered at 1650 Hz with a 4-pole, low-pass, Butterworth filter [SAE, 1995].

The mannequin was hung from a quick-release mechanism (Fig. 1(a)), allowing it to be in a state of free-fall (i.e. unsupported) at the time of impact. As the ‘ball’ exited the pitching machine, it passed through an optical sensor, triggering the release mechanism, the camera, and the data acquisition. Impacts were aimed at the forehead (unprotected), or the centre/top of the visor (protected). Because of the difficulty in accurately aiming the impacts, a minimum of ten data points was taken in each case. A single helmet was used throughout the testing. In order to reduce the number of ‘misfire’ impacts (in which the projectile hits too low on the visor or glances off the side), a plastic and foam ‘filter’ with a 20 cm diameter hole in the centre was placed immediately in front of the mannequin (Fig. 1(b)).

Figure 1: (a) Shoulder-blade connection of mannequin to quick-release mechanism; (b) Test setup for protected impacts.

RESULTS AND DISCUSSION

The Head Injury Criterion (HIC) was used to assess the probable level of injury due to head acceleration [Versace, 1971]. The HIC is calculated as follows:

$$HIC = \left\{ \left(t_2 - t_1\right)^{-1.5} \left[\int_{t_1}^{t_2} a(t)\,dt \right]^{2.5} \right\}_{\max}$$

where t_1 and t_2 are chosen to maximize the HIC parameter. This value was then used to calculate the scores for the Abbreviated Injury Scale (AIS), which gives the probability of the injury falling into various levels of severity [Prasad et. al, 1985]. A weighted average of the AIS values obtained for the given HIC was also calculated.

Values of the peak acceleration, HIC, and average AIS are shown in Table 1. As can be seen, the impacts on an unprotected head consistently produce a very high probability of a lethal injury (AIS 6 represents a fatal injury; AIS 5 represents an injury causing unconsciousness for more than 24 hours), while the impacts against a helmeted head produce a 100% probability of no injury at all.

SUMMARY

An unconstrained mannequin was subjected to projectile impacts in the head, both with and without a helmet. Estimates of the severity of the head injury were made using the Head Injury Criterion (HIC) and the Abbreviated Injury Scale (AIS), allowing for comparison between the protected and unprotected cases. For all three objects tested, the results show that wearing a helmet makes the difference between sustaining a lethal injury and remaining virtually unharmed. These tests differ from those required by most helmet standards, in that an unconstrained mannequin was used, thereby accounting for imparted inertia. Further, a realistic impact was generated. These, together, make the testing much more representative of actual use, and also make comparisons with the unprotected case possible. These results are similar to those of previous 'realistic' riot helmet testing performed with baseball bat impacts [Kessler et al., 2003].

REFERENCES

1. Canadian Standards Association (2002), Standard Z611-02
2. Society of Automotive Engineers (1995). *SAE-J211/1*.
3. Versace, J. (1971). *Proceedings of 15th Stapp Car Crash Conference*, 771-796
4. Prasad P, Mertz HJ (1985), *Society of Automobile Engineers*, SAE Paper Number 85-1246
5. Kessler, C. et al. (2003). *Proceedings of the 27th Annual Meeting of the American Society of Biomechanics*

Table 1: Results for Impacts of Protected and Unprotected Mannequin Heads

	Unprotected Impacts – Average of 10 (± SD)			
Mass (kg)	Impact Energy (J)	Peak Acc. (g's)	HIC	AIS
0.210	80.2 (1.6)	440 (113)	3121 (619)	5.85 (0.36)
0.360	94.6 (27.2)	660 (81)	7226 (1882)	6 (0)
0.954	144.6 (12.2)	635 (197)	9630 (5612)	5.80 (0.62)
	Protected Impacts – Average of 10 (± SD)			
Mass (kg)	Impact Energy (J)	Peak Acc. (g's)	HIC	AIS
0.210	77.4 (2.6)	23 (3)	6.2 (1.7)	0 (0)
0.360	103.4 (2.0)	41 (7)	22.6 (5.4)	0 (0)
0.954	146.4 (11.8)	64 (10)	69.9 (26.5)	0.04 (0.04)

The Role of Select Biarticular Muscles During Slope Walking

Andrea N. Lay[1], Chris J. Hass[2], Robert J. Gregor[3]

[1] School of Mechanical Engineering, Bioengineering Program, Georgia Tech, Atlanta, GA, USA
[2] Dept of Biobehavioral Sciences, Teachers College, Columbia University, New York, NY, USA
[1] School of Applied Physiology, Georgia Tech, Atlanta, GA, USA
E-mail: gtg449j@mail.gatech.edu

INTRODUCTION

Negotiating sloped surfaces is a challenge in our daily environment that places unique demands on the neuromuscular system. This task has been studied in detail using quadruped models in order to gain insight into neural control of locomotion (Carlson-Kuhta, 1998; Smith, 1998). Similar studies in humans would enhance our understanding of possible strategies employed by the neuromuscular system to successfully navigate challenging environments. An initial step towards this goal would be to characterize the changes in mechanical demand and muscular activity that occur in the lower extremity during slope walking. The purpose of this study was to focus on such changes at the knee and hip, and in particular, on biarticular muscles acting at these adjacent joints.

METHODS

Ten healthy adults were recruited from the student population at Georgia Tech (5 M, 5 F, mean age = 24.3 yrs). Participants were fitted with fifteen retroreflective markers according to the Helen Hayes marker system and with four pairs of self-adhesive Ag – AgCl electrodes (over the RF, VM, BF, SM) on their self-selected limb (6 R, 4 L). Subjects performed five walking trials on a custom ramped walkway at each of five different grades (level, ± 15, ±39%). Starting positions were adjusted so each subject struck the force plate with their EMG-instrumented limb on every trial.

Ground reaction forces (GRF) were sampled at 1200 Hz from a force plate (Bertec Corp., Columbus, OH) secured in the ramp structure and reinforced from below with vertical struts. Kinematic data were captured at 60 Hz using a six camera 3D Optical Capture system (Peak Performance, Englewood, CO). Electromyographic data were colleted at 1200 Hz using a telemetred EMG system (Konisburg Instruments, Pasadena, CA). All data were time synchronized in the Peak Motus analysis system. GRF and kinematic data were exported to in-house software for inverse dynamics calculations. Trials where the average ASIS marker speed was in the range of 0.8 - 1.6 m/s were used for analysis. Joint moment and power data were time normalized to 300 points over the stride (200 stance, 100 swing) and then ensemble averaged across all subjects for each grade.

RESULTS AND DISCUSSION

Average joint moment data for the knee and hip joints are shown in Figure 1. The magnitudes of the joint moments increase during upslope walking, but the joint moment patterns remain relatively similar to those for level walking. For downslope walking, the joint moment magnitudes also increase, but the moment patterns are different from level walking. For example, the absence of a knee flexor in mid-stance, and an earlier onset of the stance phase hip flexor moment were observed during downslope walking.

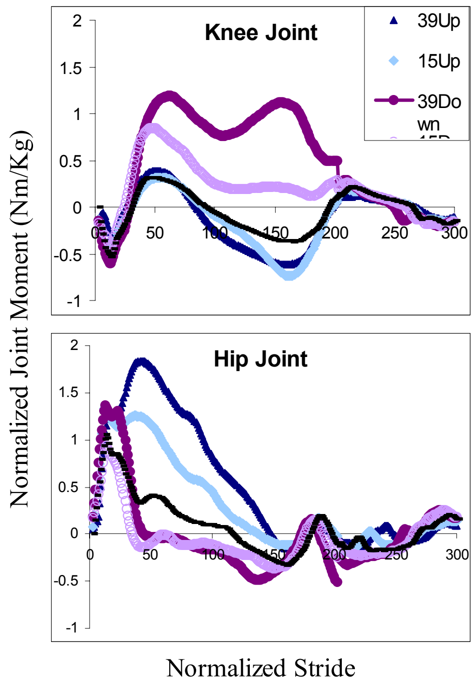

Figure 1. Knee and hip joint moments, normalized to body mass, positive is extension. Vertical line marks toe off.

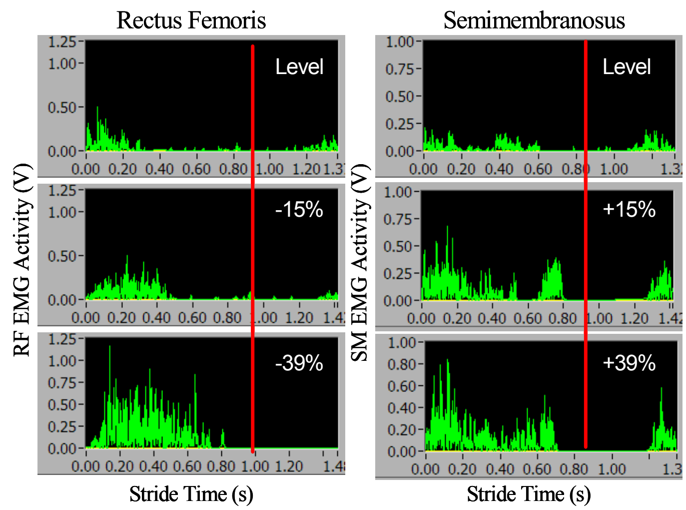

Figure 2. RF and SM EMG activity for six representative trials from one subject. Data were bandpass filtered (20-500Hz), rectified, and wavelet filtered. Red line marks toe off.

These changes during downslope stance result in a combination of joint moments that is different than that observed during level walking (i.e., there is a knee extensor and hip flexor moment during midstance), and that may be produced most efficiently by activation of the biarticular rectus femoris (RF) rather than other uniarticular knee extensors and hip flexors (Prilutsky, 2000). Since this combination of joint moments does not exist during level walking, we might expect the RF to be less active during level walking. Indeed, RF activity was observed during midstance for the two downslope conditions but not for level walking (Figure 2). RF activity also increases in magnitude as the slope decreases, which relates to the increasing knee extensor moment. In addition, although VM activity (not shown) increases in magnitude during downslope stance, its firing duration remains very similar to that of level walking, which further supports the idea of preferential RF activation.

Finally, because joint moment patterns are similar for level and upslope walking, the biarticular hamstrings should not show the same preferential activation as seen with the RF. Figure 2 shows semimembranosus (SM) firing patterns that are similar for level and upslope walking. The increasing SM activity levels correspond to the increasing hip extensor moment.

SUMMARY

These data allow us to begin analyzing the control strategies used by the nervous system and the role of biarticular muscles in such strategies. The data also suggest that a change in strategy may be necessary to successfully achieve downslope walking.

REFERENCES

Carlson-Kuhta, P et al. (1998). *J Neurophysiol,* 79, 1687-701.
Prilutsky, BI (2000). *Motor Control,* 4, 1-44.
Smith, JL et al. (1998). *J Neurophysiol,* 79, 1702-16.

ACKNOWLEDGEMENTS

This work is supported by an NSF GRF.

ASYMMETRIES DURING WEIGHTED LOADS: A COMPARISON BETWEEN 1-STRAP AND 2-STRAP CONDITIONS

W. Brent Edwards, Josh P. Vavao, Melissa Jensen, Toran D. Furch, Maharisha C. Belton, Shabnam R. Dezfouli and Alan Hreljac

Biomechanics Lab, California State University, Sacramento, CA, USA
E-mail: edwardswb@earthlink.net

INTRODUCTION

School children, adolescents, and adults often carry heavily loaded backpacks. Studies have shown that as loads increase, stride frequency and double support time increases and stride length and single support time decreases (Martin & Nelson, 1986). Recently, it has become increasingly popular to carry a backpack over one shoulder (one strap). Pascoe et al. (1997) concluded that utilizing only one strap on a backpack produced asymmetries during gait. If carrying a backpack on one shoulder yields gait asymmetries, could these asymmetries possibly lead to injury? Pascoe et al. (1997) stated that potential for acute or long-term injury resulting from weight bearing carriage using only one strap may be considerable.

The purpose of this study was to analyze walking patterns and asymmetries between left and right step parameters under three different loading conditions (0, 10, 20% BW), and two strap conditions (2-strap & 1-strap). Symmetry was defined as the perfect agreement of the kinematics of the left and right legs (Herzog et al., 1989).

METHODS

Six subjects (three male, three female, right limb dominant; mean age 26.7 yrs; mean weight 78.7 kg; mean height 1.72 m) walked on a treadmill under six different conditions, completing trials with 0% BW, 1 and 2-strap (0-1, 0-2), 10% BW, 1 and 2-strap (10-1, 10-2), and 20% BW, 1 and 2-strap (20-1, 20-2). In all 1-strap conditions, backpacks were carried on the right shoulder. Subjects were free from anthropometric, neurological and orthopedic disorders. Prior to testing reflective markers were placed on the following bilateral anatomical landmarks: the greater trochanter, lateral femoral epicondyle, lateral maleolus, and head of the fifth metatarsal.

Experiments were performed on a Precor C964i treadmill. The backpack was loaded with York plate weights secured with 1/4″ nylon rope. Subjects walked at 1.29 m/s (average preferred speed of sample), while data were collected using a 6 camera Peak Motus 3-D motion analysis system, at a collection rate of 60 Hz for 8 seconds. Heel strike and toeoff times were determined using the algorithm of Hreljac & Marshall (2000).

The three 2-strap conditions were compared to determine effects of added weight on stride length. The absolute step difference between the three 1-strap conditions and left and right step lengths within each condition were compared to assess asymmetry. Paired t-tests were used to identify significant differences ($p<0.05$).

RESULTS & DISCUSSION

No significant differences were found between the 0-2/10-2, 0-2/20-2, & 10-2/20-2 conditions in stride length (Fig. 1). As no decrease in stride length was found with increases in weight, this study is in disagreement with Pascoe et al. (1997). This may be due to differences in the sample populations. The Pascoe et al. (1997) study utilized children ages 11-13 yrs, while this study's sample consisted of young, healthy adults ages 23-33 yrs.

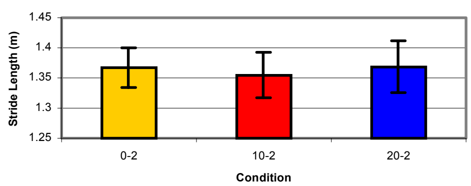

Figure 1: Stride length of the 2 strapped (equal weight distribution) condition.

No significant differences were found in bilateral step difference between the 0-1/10-1, 0-1/20-1, & 10-1/20-1 condition (Fig. 2). However, a trend toward becoming more asymmetrical as weight increased was identified, as depicted by an increase in step difference.

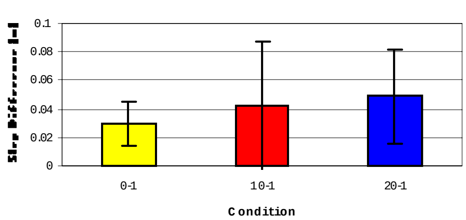

Figure 2: Absolute step difference of the 1 strapped (unequal weight distribution) condition.

A significant difference was found between the left and right step length at the 20-1 condition only. The left step length was greater than the right step length by an average of 4 cm for this condition.

SUMMARY

Findings suggest that 20% BW is not enough weight to elicit a decrease in stride length in young, healthy adults. Though not significant, increases in step difference while using 1-strap were found with as little as 10% BW and a significant difference between left and right step length was calculated at the 20-1 condition. Noted differences may be a result of deviation of the center of mass due to unequal weight distribution. This asymmetrical mechanical loading of the musculoskeletal system could potentially lead to injury. Pascoe et al. (1997) also states that the ramifications of this weight bearing induced stress can be a serious issue when considering children still experiencing physical growth and motor development.

To further assess gait asymmetries during 1-strap weighted backpack conditions, multiplanar analyses may be necessary. Gait parameters should also be considered after a substantial amount of walking time (i.e. 5, 10, 15 min) to mimic the normal everyday practice of 1-strap backpack walking.

REFERENCES

Herzog, W. et al. (1989). *Med Sci Sports Exerc*, **21**, 110-114.

Hreljac, A., Marshall, R.N. (2000). *J. Biomech*, **33**, 783-786.

Martin, P.E, Nelson, R.C. (1986). *Ergonomics*, 29, 1191-1202.

Pascoe, D.D. et al. (1997). *Ergonomics*, **40**, 631-641.

WHAT CAUSES A CROSS-OVER STEP WHEN WALKING ON UNEVEN GROUND? A STUDY IN HEALTHY YOUNG WOMEN

Sibylle B. Thies and James A. Ashton-Miller

[1] Biomechanics Research Laboratory, Dept. of Biomedical Engineering, University of Michigan, Ann Arbor, MI, USA

E-mail: sthies@umich.edu Web: http://me.engin.umich.edu/brl/

INTRODUCTION

Some 24% of falls in the elderly occur while walking on uneven ground (Berg et al. 1997). Although both step width (SW) and step time (ST) variability have been quantified in healthy and impaired adults walking on irregular surfaces (Menz et al. 2003, Richardson et al., in press), the underlying mechanisms by which surface irregularities affect SW and ST or cause cross-over steps during level gait are presently unknown. SW is important because it is used to maintain frontal plane stability (Bauby & Kuo 2000), while increased ST variability is elevated in fallers (Haussdorff et al. 2001).

We hypothesized that sudden ankle inversion, caused by stepping on an object with the medial forefoot of the stance limb, as compared to no object, will:

- decrease ankle eversion moment (M_a)
- increase maximum lateral velocity ($\dot{x}_a$) of the ankle joint center (AJC) and foot angular acceleration ($\ddot{\theta}_f$) in the frontal plane, and
- decrease the next-step SW and ST.

METHODS

Twelve healthy young women (mean ± SD: 22 ± 2.4 years) participated in the study. Subjects were instructed to walk at a comfortable speed to the end of a 6-m level walkway wearing flat-soled sandals. They carried a tray to prevent any visual monitoring of foot placement. Their starting position was such that their 2nd, 3rd, and 4th step would each fall on consecutive AMTI force plates. The second force plate was marked with a rectangular grid of thirty 10x6 cm cells. Normal walking trials were recorded until the subject's left forefoot landed three consecutive times in the same cell. Next, a solid triangular prism (H*W*L:1.2*3.5*10 cm) was placed inside that cell's boundaries and enough trials were recorded until three trials were obtained in which the medial forefoot landed on the prism while subjects walked to the end of the walkway.

A custom MATLAB® algorithm was used to process kinematic data collected at 50 Hz from 28 Optotrak markers, and force plate and plantar pressure (F-scan) data collected at 100 Hz. The lateral locations (x) of the center of pressure (x_{cop}) and ankle joint center (x_a) were calculated during left leg single support (3rd step), as were M_a, $\dot{x}_a$, and $\ddot{\theta}_f$. SW, measured in the frontal plane from the left to the right ankle joint center, and ST were obtained for the 4th step. The hypotheses were tested using paired two-tailed t tests ($p<0.05$ considered significant), and Pearson correlations (R) were performed between the salient gait parameters.

RESULTS AND DISCUSSION

The hypotheses were supported in that a medial forefoot perturbation during single support decreased M_a ($p<0.001$) [see Fig. 1 sample results from one individual: the horizontal locations of the COP and AJC approach and cross one another in the perturbation trial, while M_a switches sign from eversion (+) to inversion (-).]

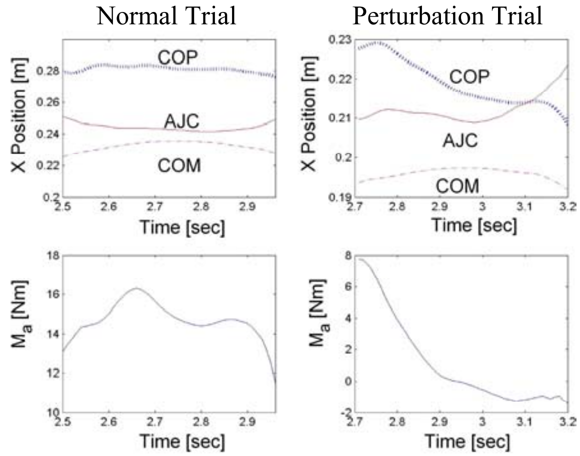

Fig. 1: *Horizontal kinematic trajectories in single support (top) and M_a for a normal (left) and a medial perturbation trial (right).*

Stance limb $\dot{x}_a$ and $\ddot{\theta}_f$ were significantly increased stepping on the object ($p=0.004$ and $p=0.017$, respectively). SW and ST of the 4th step were significantly reduced following a medial perturbation on the 3rd step ($p<0.001$ and $p=0.049$, respectively). Minimum M_a was inversely correlated with maximum $\dot{x}_a$ ($p<0.001$, $R= -0.48$) which, in turn, was correlated with $\ddot{\theta}_f$ ($p=0.027$, $R=0.26$). $\ddot{\theta}_f$ correlated negatively with SW ($p<0.001$, $R=-0.48$, Fig. 2) and ST ($p=0.003$, $R=-0.34$). Following a perturbation, 70% and 76% of next-step SW and ST, respectively, were shorter than the subject's mean unperturbed SW and ST, and 15% of the post-perturbation steps were cross-overs (Figs. 2&3). The cross-over step is apparently a strategy to rapidly unload the perturbed ankle.

SUMMARY

A cross-over step is caused by an unexpected ankle inversion on irregular ground. The larger the inversional foot acceleration, the shorter the next-step ST and smaller the next-step SW will be.

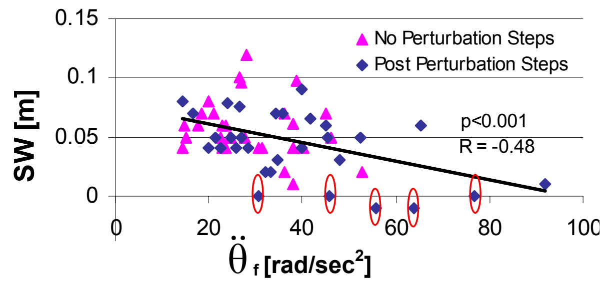

Fig. 2: *Correlation between $\ddot{\theta}_f$ and next-step SW. Cross-over steps (defined as SW≤ 0) are circled in red.*

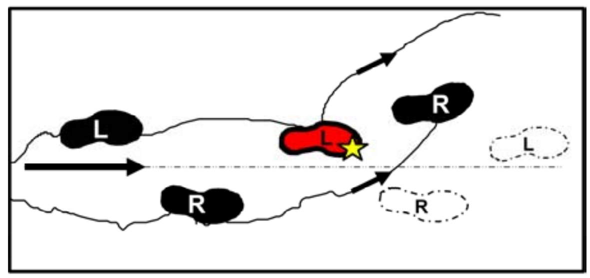

***Fig. 3**: Sample AJC trajectories in single (solid line) and dual support (foot prints). The arrows denote progression direction. A medial perturbation (under the left foot, L, in red) caused the next step (R) to "cross over" the midline rather than continue the average unperturbed stepping pattern (dashed open foot prints).*

REFERENCES

Berg, W.P., et al. (1997) *Age Aging,* **26**,261-268.

Bauby, C.E. & Kuo, A. (2000) *J Biomech,* **33**, 1433-1440.

Hausdorff, J.M., et al. (2001) *Arch Phys Med Rehabil,* **82**, 1050-1056.

Menz, H.B., et al. (2003) *Gait Posture* **18**, 35-46.

Richardson, J.K., et al. *J Am Geriatr Soc,* in press.

ACKNOWLEDGEMENTS

Support of PHS grant AG P60 08808.

DROP LANDING EXERCISE DOES NOT INCREASE MAXIMUM JUMP HEIGHT IN CHILDREN

Allison T. Lulay, Jeremy J. Bauer, Christine M. Snow, and Michael J. Pavol

Department of Exercise and Sport Science, Oregon State University, Corvallis, OR, USA
E-mail: mike.pavol@oregonstate.edu

INTRODUCTION

A 7-month program of repeated drop landing has been shown to increase bone mass in prepubescent children (Fuchs et al., 2001), raising the question of whether these exercises might also have beneficial effects on the neuromuscular system. During landing after a drop from a height, the body's energy is partially absorbed through eccentric contraction of the same muscles that are used in vertical jumping. The eccentric contractions from repeated landings could thus produce an increase in coordinated muscle strength that would allow a child to jump higher. Maximum vertical jump height is known to increase with increased knee extensor strength in young adults (Colliander and Tesch, 1991). This study investigated whether a 7-month program of repeated drop landing would act to increase the maximum vertical jump heights of prepubescent boys and girls.

METHODS

Subjects were 49 prepubescent children aged 7-11 years. An intervention group of 9 boys and 6 girls (mean ± SD age: 9.3 ± 0.9 yrs.; height: 1.35 ± 0.09 m; body mass index [BMI]: 17.6 ± 2.5 kg/m^2) had performed 100 drop landings from a 61 cm height on each of 5 days per 2-week period over the preceding 7 months as part of their physical education class. A control group of 20 boys and 14 girls (age: 8.7 ± 1.0 yrs.; height: 1.39 ± 0.09 m; BMI: 18.4 ± 3.4 kg/m^2) participated in a physical education class that did not include the drop landing exercises. Group membership was determined by the child's school. Subjects and parents provided their informed consent.

During testing, each subject performed 5 maximum-height vertical countermovement jumps. Before each jump, the subject stood as still as possible on a pair of force plates (Bertec, Columbus, OH). Upon an oral signal, the subject jumped upward and attempted to touch as high as they could on a string dangling above them. Vertical ground reaction forces were measured at 1080 Hz from each force plate. Verbal encouragement and feedback was provided between jumps. Five warm-up jumps preceded the testing.

For each jump, the maximum height of the body center of mass (COM), relative to its height during standing, was computed. First, the vertical velocity and height of the COM at take-off were found by single and double integration, respectively, of the vertical acceleration of the COM from the start of the countermovement until take-off. COM vertical acceleration was computed from the bilateral ground reaction forces, the measured body mass, and gravity. Integration endpoints were identified from the force traces. From the COM height and velocity at take-off, projectile motion equations were used to compute the maximum COM height during the jump. Maximum jump height was defined as the average of a subject's two highest jumps. Jump height was normalized to body height.

A 2-factor analysis of variance determined whether maximum jump height differed between jumpers and controls, or between boys and girls. Body Mass Index (BMI = [body mass]/[body height]^2) and subject age were included as covariates in the analysis. A significance level of 0.05 was used.

RESULTS AND DISCUSSION

Maximum jump height in these children was highly correlated to BMI (r = -0.56; p < .001); children with lower BMI jumped higher (Figure 1). After accounting for the effects of BMI, there was no difference in maximum jump height between the children who had performed 7 months of drop landing exercises and the children who had not (p = .59; Table 1), independent of sex (p = .98). Maximum jump height also did not differ between boys and girls (p = .42). Finally, maximum jump height was unrelated to age in these children (p = .45).

The present results are consistent with a previous study of young men in which two different drop-jump training methods failed to increase vertical jump performance after 6 weeks (Young et al., 1999). It is likely that the drop landings from a 61 cm height did not provide a stimulus of the intensity or specificity needed to produce an increase in the coordinated muscle strength that would lead to higher vertical jumping ability.

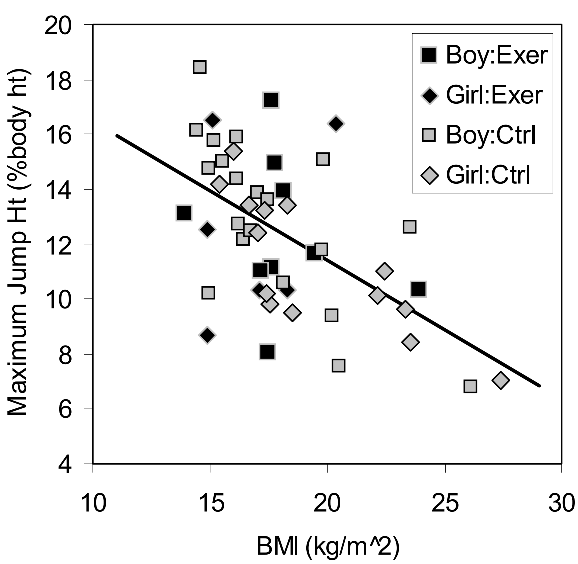

Figure 1: Relationship between BMI and maximum jump height in boys and girls in the exercisers (Exer) and controls (Ctrl)

Table 1: Mean ± SD maximum jump heights (% of body height)

	Exercisers	Controls
Boys	12.4 ± 2.7	12.9 ± 3.0
Girls	12.5 ± 3.3	11.3 ± 2.4

The lack of a differential effect of sex on maximum jump height and on the influence of the drop landing exercises is consistent with previous findings of similar motor skills in prepubertal boys and girls (Branta et al., 1984). Only after adolescence do males typically exhibit a relative advantage in skills requiring strength and power.

While drop landing exercises have beneficial effects on the bone mass of prepubescent children, it appears that the benefits of these exercises do not extend to increases in maximum vertical jump height.

REFERENCES

Branta, C. et al. (1984). *Exerc Sport Sci Rev*, **12**, 467-520.

Colliander, E.B., Tesch, P.A. (1991). *Acta Physiol Scand*, **141**, 149-156.

Fuchs, R.K. et al. (2001). *J Bone Miner Res*, **16**, 148-156.

Young, W.B. et al. (1999). *Int J Sports Med*, **20**, 295-303.

ACKNOWLEDGEMENTS

Funded by an URISC award from Oregon State University (to A.T.L.) and NIH R01 AR-45655-01 (to C.M.S.).

EFFECT OF VERTEBRAL BONE ENDPLATE CURVATURE ON LOAD TRANSMISSION

Shreedhar P Kale[1], Noshir A Langrana[1], Thomas Edwards[2] and Casey K Lee[3]

[1]Department of Mechanical and Aerospace Engineering, Rutgers University, Piscataway, NJ.
[2]Kessler Medical Rehabilitation Research & Education Corp., West Orange, NJ, [3]Roseland, New Jersey.
Email: spkale@eden.rutgers.edu
Mechanical and Aerospace Engineering Department, Rutgers: http://mechanical.rutgers.edu/

INTRODUCTION

The vertebral endplates of the lumbosacral spine have various degrees of concavity and/or convexity. Differences in these curvatures will increase stress in some regions and decrease stress elsewhere as the spine is compressed. This has important implications for the design of disc implants and for rehabilitation following injury.

In our previous study [Kale et al, 2003], lumbar vertebral endplate curvatures in the anterior-posterior and medial-lateral directions on human cadaver lumbar vertebrae were measured. Six sets of measurements (on human male-female L4 lower to S1 upper endplates) were performed. The data was later used in a linear elastic cylindrical model containing cortical shell and trabecular core. Finite element analysis on the cylindrical model was performed to study the effects of the location of maximum curvature on the stress distribution. In the current study, a vertebral bone model is created, with a more realistic, characteristic kidney shaped cross section and linearly varying height. The endplates were assigned curvatures extracted from our human cadaver data.

METHOD

Vertebral bone model. The techniques used in the past to study the lumbar vertebral bones, either used patient specific CT scans [Homminga, at al, 2001] or flat endplate models [Smit et al, 1997, Liebschner et al, 2003, Cao et al, 2001]. In this study, we use parametric equations [Mizrahi et al., 1993] to develop a solid model of the vertebral bone in Pro-Engineer [Higgins, et al, 2002]. This model has side curvatures varying linearly with height and a thin outer cortical shell. The top endplate has a curvature of depth 2.5mm, which directly matches one of the bone samples. Two models were used to examine the placement of the center of curvature. The first model has the maximum curvature at the center of the endplate. In the second model, the curvature is shifted by 20% posteriorly from the center. The cortical and trabecular bone materials have a ratio of four in their modulus of elasticity values. The commercial FE analysis code, ANSYS, was used for the analyses.

Boundary conditions. The bottom endplate was constrained from any motion. A pressure of 25MPa was applied to the top endplate. Displacement as well as stress contours were computed and compared.

RESULTS AND DISCUSSION

The normal compressive stress distribution for the two cases, normalized to the same scale, is shown in figures 1 and 2. The FE Analysis demonstrates that the shell takes higher load compared to the core, which is in accordance with theory considering that it has a higher modulus of elasticity compared to the core. However, the stress distribution is affected as the location of the maximum curvature is shifted from center to a location more posterior.

MODEL 1 **MODEL 2**

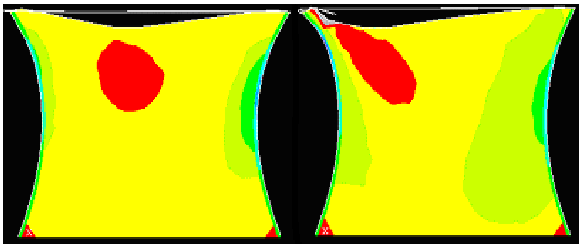

Figure 1 Axial normal stress (MPa), sagital plane

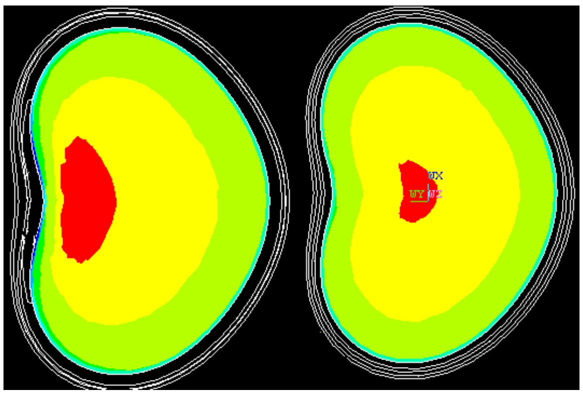

=5MPa = 25MPa =50MPa =200MPa

Figure 2 Axial normal stress (MPa), horizonal plane

The minimum compressive stress of 5 MPa occurs just below the maximum curvature in both the cases. As shown, this location is shifted in the second case (fig. 2). The stress in most of the central region, in both of the cases, corresponds to 25 MPa, which is the applied pressure loading. The stresses in the core decrease up to 25% posteriorly when the curvature is shifted posteriorly (fig 1). The posterior shell then absorbs approximately 20% more of the stress compared to the first case. The stresses at the anterior shell also decrease in the second case, with the core taking more of the stress in the anterior portion of the vertebra.

CONCLUSIONS

The Mizrahi's equations, used to model the bone geometry, are governed by curvature parameters that define the characteristic kidney shape of the bone. Therefore, selecting these parameters can create the shape of vertebral bone of any individual at any level. Here the curvatures of the adjacent endplates for each level was based on our previous study.

In this study, the stress distribution changes due to curvatures in a vertebral bone were quantified. This correlation of higher stress to the amount of curvature and location of the maximum curvature provides vital information for rehabilitation as well as surgical techniques. The information gathered in this study will also contribute in the designs of interbody devices like fusion cages, bone grafts and disk prosthesis.

REFERENCES

Cao, K. D., Grimm, M. J., et al (2001), *SPINE* **26**: E253-E260.

Higgins, K.B., Langrana, N.A. (2002), *PhD thesis*, Rutgers The state university of NJ.

Homminga, J., at al, (2001) *SPINE*: **26(14):** 1555-1560.

Kale, S. P., Langrana, et al, (2003), *Proceedings on IMECE'03.*

Liebschner, M. A. K., Kopperdahl, D. L., et al, (2003) *SPINE* **28** **(6)**: 559-565.

Mizhari et al, (1993) *SPINE* **18(14)**: 2088-2096.

Seenivasan G., Goel, V. K., (1994), *IEEE Eng. In Med. & Biol.,* Vol. 13, 508-516.

Smit, T. H., Odgaard, A., et al, (1997), *SPINE* **22**: 2823-2833.

ACKNOWLEDGEMENTS

This study was supported, in part, by funds from the Henry H. Kessler Foundation. The authors would like to thank the Department of Mechanical and Aerospace Engineering, Rutgers, The state university of New Jersey for their computer laboratory support.

QUANTITATIVE PREDICTION OF ARTICULAR CARTILAGE DEGENERATION FOLLOWING INCONGRUOUS INTRA-ARTICULAR FRACTURE REDUCTION

Yang Dai[2], Thomas D. Brown[1, 2], J. Lawrence Marsh[1]

[1]Department of Orthopaedics and Rehabilitation, University of Iowa, Iowa City, IA, USA
[2] Department of Biomedical Engineering, University of Iowa, Iowa City, IA, USA
E-mail: tom-brown@uiowa.edu

INTRODUCTION

Treatment of a displaced intra-articular fracture poses great orthopaedic challenges. It is believed that the residual incongruities after treatment induce stress aberration in the articular cartilage, and provoke an adverse mechano-response leading to degeneration of the cartilage (secondary osteoarthritis). Therefore, reduction of the fracture, to restore as smoothly congruent an articular surface as possible, is often viewed as critical to patient management [3].

Conventionally, geometric descriptors (e.g. gaps, step-offs) obtained from xrays or intra-operative fluoroscopic images are utilized to evaluate the accuracy of the reduction. Such geometric estimations are not only surgeon- and image- dependent, but they have limited relationship with quantity of primary physical interest: the cartilage stress magnitude accompanying residual incongruity.

A new formulation using Discrete Element Analysis (DEA) [2] was developed to expeditiously compute the stress distribution throughout the gait cycle for an incongruous fracture situation. Combining such stress data with activity level, cumulative pressure exposure can be calculated, to assess the functional adequacy of provisional reductions and to find optimum fragment realignment.

METHODS

Acetabular fractures are useful as an example to present the method. A 3D voxel hip joint model was reconstructed from segmented serial CT slices. A custom-written Matlab program was developed to pave the potential contact surfaces of the femoral head and acetabulum with smoothed triangular facets (Fig. 1).

Figure 1
A: Proximal fragment cartilage
B: Distal fragment cartilage
C: Femoral head cartilage

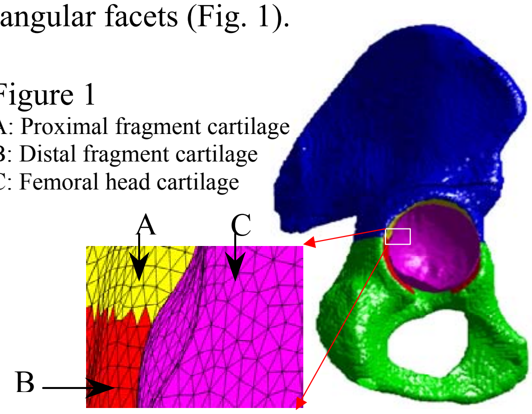

Treating the femoral head and acetabulum as rigid bodies, the region between them, i.e. the cartilage, is represented as an array of linear elastic compressive springs. The springs pass from the centroids of the acetabular facets to the nearest counterparts on the femoral head surface. The springs' stiffnesses in the normal direction (Equation 1) depend on the cartilage modulus (E), Poisson ratio (ν) and thickness (h). Due to the lubrication of the joint, the stiffness in the shear direction can be neglected.

$$k_n = \frac{E(1-\nu)}{(1+\nu)(1-2\nu)h} \qquad [1]$$

A trans-tectal displaced fracture model was created by transversely sectioning the acetabulum, and displacing the proximal fragment in the supero-medial direction. Serial input (n=16) loads and positions of the femoral head, corresponding to discrete instants in the gait cycle, were used to calculate the stress distribution. For each facet, the difference between the deformed spring length and the intact spring length in the normal direction was used to compute the local pressure on the acetabular surface. From the stress distribution (P) thus obtained, a pressure damage threshold (P_d, 2MPa [1]), the time elapsed for each gait cycle increment (t_i), and number of steps (N, 2 million) and seconds (SY) in a year, cumulative pressure exposure (P_c) for the cartilage was calculated (Equation 2). The results were scaled to compare with literature on chronic cartilage pressure tolerance. [1]

$$P_c = \frac{\left(\sum_{i=1}^{16}(P-P_d)t_i\right)*N}{SY}*Years \qquad [2]$$

RESULTS AND DISCUSSION

For different residual step-offs (2.5, 2.0, 1.5, 1.0, 0.5 and 0mm), the cumulative pressure exposures were calculated for a 2-year time span. Taking 10MPa-years as a threshold for OA onset [1], any region experiencing a supra-threshold cumulative pressure dosage is considered as at risk for degeneration. (Figure 2)

MPa-Years [1]

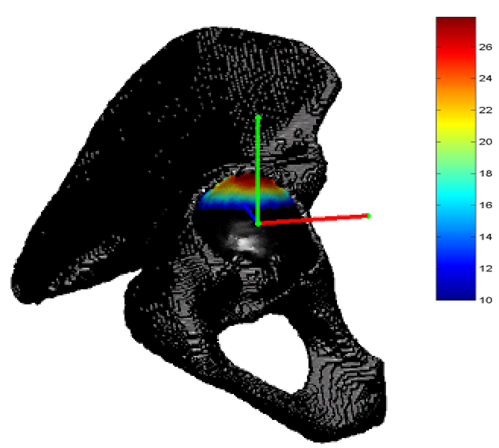

Fig. 2 Distribution of cumulative pressure exposure at 2 years, for a 2mm step-off

Table 1: Cartilage area experiencing over 10MPa-years of cumulative over-pressure (Total potential contact area = 3402.9mm^2)

Step-off (mm)	2-year Overpressure Area (mm^2)	Years needed for 5% area to reach 10MPa-years
0	0	N/A
0.5	6.68	2.3
1.0	486.89	1.5
1.5	576.34	1.2
2.0	700.60	0.9
2.5	988.94	0.6

From the results, the area with P_c over 10MPa-years, and the rate at which that threshold is approached increase with the enlargement of the step-offs. For the displaced intra-articular fractures with over 1mm of residual step-off, more than 15% of the acetabular cartilage becomes at risk for degeneration in 2 or less years. OA onset times in the range of 0.5-2 years are commonly observed clinically for similar injuries. [3]

For this particular fracture model, most of the degeneration-prone regions are at the superior rim of the acetabulum. The reason is that, with "widening" of the acetabulum due to the incongruity, the femoral head can be displaced (subluxated) under loading. With such displacement, the femoral head comes into preferential contact with the rim of the acetabulum.

With refinement this technique lends itself to use computerized datasets to predict clinically relevant joint contact loading for articular fractures. This information could help determine the need for operative intervention, assess the predicted loading and prognosis after operative intervention and in the future be used real-time during surgery to guide operative decision making.

REFERENCES

[1] Hadley *et al*: *J. Ortho. Res. 8: 504-513, 1990* [2] Kawai *et al*: *Conf. Comp. in Civ. Engn.: 1-16, NY ,1981* [3] Matta *et al*: *JBJS 1996 78A 1632-45*

OCCUPATIONAL VIBRATION AND POSITION SENSE

Sara E. Wilson and Feng Zhang [1]

[1] Human Motion Control Laboratory, Mechanical Engineering,
University of Kansas, Lawrence, KS, USA
E-mail: sewilson@ku.edu Web: http://www.engr.ku.edu/me/

INTRODUCTION

Occupational vibration exposure has long been known to be associated with low back injuries in industrial workers[1]. While research on the transmissibility of vibration is extensive, there is little research into the mechanism by which the vibration may lead to injury.[2] Current research in low back injuries suggests that loss of low back stabilization may play a role in the etiology of these injuries[3, 4]. Indeed, Wilder et al. found in experiments on sudden loading dynamics that muscular response time after vibration exposure was increased[5]. One potential mechanism for these changes is changes in proprioception and position sense with vibration. In this research, the effect of vibration on position sense was measured experimentally. In addition, the possible effects of changes in position sense on response time and dynamic stabilization were examined using a computation model.

METHODS

Nineteen subjects (10 men, 9 women) aged 19 to 32 years, participated in this study with human subjects approval. Electromagnetic markers were attached to the skin using double sided tape over the manubrium and the T10 and S1 spinous processes. Lumbar curvature was defined as the difference in angle of the T10 and S1 markers. Reposition sense was measured using a previously developed protocol[6]. This protocol is an active-active procedure consisting of training trials where the subjects learn a lumbar curvature followed by assessment trials where the subjects attempt to reproduce the lumbar curvature. During the training trials, lumbar curvature was displayed and subjects were asked to match their curvature to the target. After two training trials, the display was removed and subjects were asked to repeat lumbar curvature from memory. Training trials were then alternated with assessment trials for a total of 3 assessment trials. Between the trials subjects were asked to perform a flexion task. Both the directional reposition error (the difference between lumbar curvature and target) and the absolute reposition error (the absolute value of the difference between lumbar curvature and target) were measured.

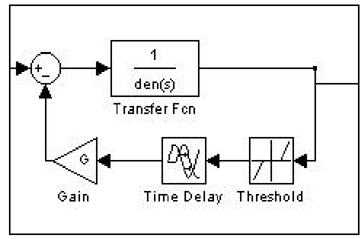

Figure 1. *A simulink model was created to assess the possible effects of changes in threshold (position sense) on changes in muscular response to sudden loading and dynamic stabilization.*

The reposition sense protocol was performed before vibration exposure, during the exposure and after the exposure. Three vibration exposures were assessed at 5, 20 and 50 Hz in a random order. The vibration exposures lasted 7 minutes and was followed by a 15 minutes recovery period. A vibratatory stimulus of 2 mm amplitude was applied over the left and right multifidus muscle at the L2/L3 level.

Frequency	Pre Vibration	During Vibration	After Vibration
5 Hz	2.1 ± 1.3	2.2 ± 1.4	2.3 ± 1.2
20 Hz	2.3 ± 1.2	3.0 ± 1.8	2.9 ± 1.6
50 Hz	2.1 ± 1.4	3.0 ± 1.1	2.4 ± 1.5

a. Absolute Reposition Error

Frequency	Pre Vibration	During Vibration	After Vibration
5 Hz	0.7 ± 2.2	0.2 ± 2.1	0.1 ± 2.1
20 Hz	-0.2± 1.8	-1.4± 3.0	-0.3± 3.2
50 Hz	-0.3± 1.1	-1.8± 3.1	-0.8± 2.3

b. Direction Reposition Error

Table 1. *Absolute reposition error increased both during and after vibration. Direction reposition error increase only during vibration.*

A control feedback model of the sudden loading response was created using Simulink in Matlab (Natick, MA). In this model the sudden loading response was modeled as a second order system with a proportional negative feedback response. Within the negative feedback response, a gain, a reflex delay, and a response threshold were incorporated. The response threshold, which represents the position sense, was set to the position sense error measured experimentally.

RESULTS AND DISCUSSION

Both absolute reposition error and direction reposition error were significantly increased during exposure to vibrations of 20 and 50 Hz ($p<0.05$). Subjects assumed more lordotic postures during vibration, consistent with previous evidence of muscle lengthening kinesthetic illusions with vibration[7-9]. Vibration exposures of 5 Hz did not produce kinesthetic illusions or changes in reposition error (either absolute or directional) during the vibration.

After removal of the vibration absolute reposition error was found to be higher than before the vibration at all frequencies (ANOVA, $p<.05$). No directional error increase was observed after vibration exposure. The increase absolute error observed after vibration was found to be highest at 20 Hz.

The control feedback model was used to examine the effect of the changes in position sense observed experimentally on the dynamics of trunk in response to a sudden perturbation. It was found that increasing the response threshold increased the response time for muscular activity. The effective stiffness of the torso was also reduced with the increases in response threshold.

SUMMARY

In this study, vibration exposure was found to have two effects on position sense. During the vibration, higher frequency vibrations were found to cause kinesthetic illusions in the low back leading the subjects to assume more lordotic postures. After the removal of the vibration, habituation to the vibration led to increased reposition error but no kinesthetic illusion. This increased error is important because, as the modeling shows, it increases the time it takes the muscle activity to respond to sudden loading, decreasing the stabilization of the lumbar spine.

REFERENCES

1.J. W. Frymoyer *et al.*, *J Bone Joint Surg Am* **65**, 213-8. (1983).
2. M. H. Pope *et al.*, *Clin Orthop*, 241-8. (1998).
3. J. J. Crisco *et al.*, *Clinical Biomechanics* **7**, 19-26 (1992).
4. J. Cholewicki, *et al.*, *Spine* **22**, 2207-12 (1997).
5. D. G. Wilder, *Am J Ind Med* **23**, 577-88. (1993).
6. S. E. Wilson *et al.*, *Spine* **28**, 513-8. (2003).
7. S. Brumagne *et al.*, *Spine* **25**, 989-94. (2000).
8. J. P. Roll *et al.*, *J Vestib Res* **3**, 259-73. (1993).
9. P. J. Cordo *et al.*, in *Progress in motor control* pp. 151-72.

ACKNOWLEDGEMENT

This publication was made possible by NIH grant number P20 RR016475.

SPATIO-TEMPORAL ORDER IN EMG FROM A LOW BACK SURFACE ELECTRODE ARRAY

Zhi He [1], Martin H. Krag [2], James R. Fox [2], Dryver R. Huston [1] and Alan B. Howard [3]

[1] Department of Mechanical Engineering, University of Vermont, Burlington, VT, USA
[2] Vermont Back Research Center, Department of Orthopedics and Rehabilitation, University of Vermont, Burlington, VT, USA
[3] Academic Computing Services, University of Vermont, Burlington, VT, USA
E-mail: zhe@emba.uvm.edu Web: http://www.emba.uvm.edu/me

INTRODUCTION

Surface electromyography (EMG) has been used to study muscle disease and muscle biomechanics. The relationship between muscle activation and EMG signals is complex. This study was undertaken as part of a larger project that aims to identify abnormalities in the three-dimensional motion of individual lumbar vertebrae (motion segment dyskinesias), hypothesized to be involved in some cases of low back pain. It seems plausible that such motion abnormalities would have associated, simultaneous lumbar muscle activation abnormalities (as either cause or effect) and that these, in turn, would have associated EMG abnormalities.

Such EMG abnormalities may involve only one or a few of the muscle slips that attach to a single vertebra and would thus be spatially limited. The abnormality may be only transient and would thus be temporally limited. Currently available EMG techniques do not seem capable of detecting such abnormalities.

The objective of this study was to develop EMG techniques likely to be capable of detecting these abnormalities. Rather than trying to understand the surface activity in terms of motor unit behavior, our current approach is to look for patterns in the array data that plausibly would be altered if one or more individual vertebral muscle slips were activated abnormally. Because the vertebral dyskinesias of interest may be of only brief duration, the EMG analysis method must involve little or no temporal smoothing.

This report describes the data collection, display, and analysis methods developed, and gives representative results and some initial observations. Subsequent reports will describe results from applying these methods to normal and low back pain subjects performing static and dynamic tasks.

METHODS

Thirty monopolar electrodes were arranged in a rectangular array in the right lumbar region. Each of 5 rows was aligned with the midpoint of the spinous process of each of the lumbar vertebrae (L1-L5). There were 6 columns, the first of which was 15mm from the midline. The other 5 were spaced 15mm center-to-center. The technical details of the EMG array itself are described more fully in Coates (2000). Initial data processing includes 60Hz notch filtering and the removal of cardiac depolarization.

Figure 1 shows a “B-mode display.” The voltage from each of the 30 electrodes for each millisecond over 1000 msec is linearly mapped to a gray scale. The x axis is the electrode number. The y axis is time. The resulting band-like structure indicates the presence of spatio-temporal order. This was not found in a B-mode display of random data (not shown).

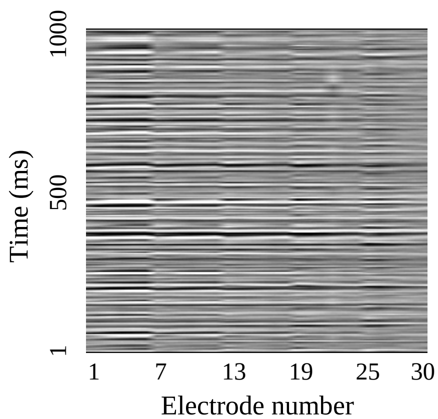

Figure 1: B-mode display.

RESULTS AND DISCUSSION

To quantify this spatio-temporal order, correlation coefficients between various pairs of electrodes were calculated over a specified time interval. Figure 2 shows the results for the inner column of electrodes over a 50 msec time interval. The L5 electrode was compared to each of L5, L4, L3, L2 and L1.

Note the gradual decrease with increasing inter-electrode distances. This contrasts to Figure 3 that shows results from random data.

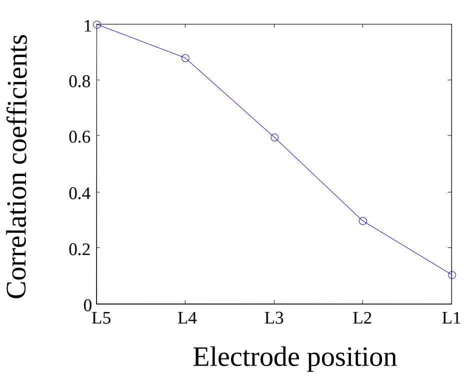

Figure 2: EMG data correlation results.

To check whether specific frequency bands were disproportionately contributing to the spatio-temporal order, coherence values were calculated. This showed that coherence was approximately equal across frequency and decreased with inter-electrode distances.

SUMMARY

This novel approach shows quantitatively the presence of spatio-temporal order between multiple surface EMG electrodes. Additional inter-electrode-based analyses are being developed. These will be applied to EMG data obtained from healthy and from low back pain subjects performing static and dynamic tasks. Simultaneous intervertebral kinematic measurements will be obtained. Correlation between EMG and kinematic parameters will be investigated.

REFERENCES

Coates A.D. (2000). *The Design, Development, and Validation of the EMG Grid*. Master Thesis, University of Vermont.

ACKNOWLEDGEMENTS

This work was supported by a grant from NIH-NIAMDD (1-R01-AR-45935).

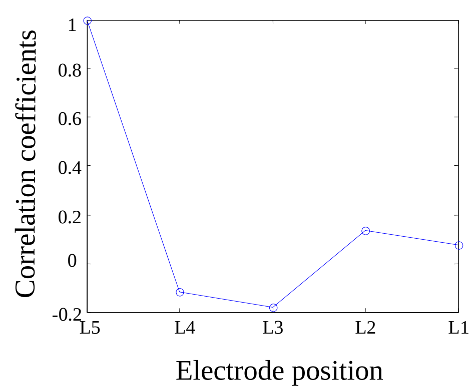

Figure 3: Random data correlation results.

DETECTING A LOSS OF BALANCE IN YOUNG ADULTS PERFORMING A MAXIMAL FORWARD REACH

Alaa A. Ahmed[1], M.S. and James A. Ashton-Miller[1,2], PhD.

Biomechanics Research Laboratory
Departments of [1]Biomedical and [2]Mechanical Engineering
University of Michigan, Ann Arbor, MI, U.S.A.[aaahmed@umich.edu]

INTRODUCTION

The hypothesis was tested that a loss of balance (LOB) is actually a loss of effective control, as evidenced by a control error signal anomaly (CEA: see Methods). Previous work (Ahmed & Ashton-Miller, 2004) has shown that CEA is detectable and can reliably predict a compensatory reaction in young adults performing a one degree-of-freedom (dof), whole body, planar balancing task. A model-reference adaptive controller and failure-detection algorithm were used to represent central nervous system decision-making based on input and output signals obtained during the task. Our goal is to extend this method to a more complex , challenging three dof task: a maximal forward reach. We therefore tested the hypothesis that a CEA is indeed detectable in 10 healthy young female adults performing a maximal forward reach. Evidence of successful detection was the initiation of an observable compensatory response (forward step), no earlier than 100 ms after CEA detection and no later than 2s.

METHODS

Ten healthy young women (18-30 yrs) volunteered as subjects. Subjects were asked to reach forward as far as they could with both hands towards a circular target (Fig.1). They were allowed to lift both heels but not to bend their knees as they performed the task.

The target was randomly positioned at varying percentages of their maximum reach distance (100, 105, 110, 115,120, and 125%). They were instructed to attempt to reach the target and hold the position for 10s. Sufficient reach trials were recorded to accumulate 10 trials, each with an involuntary step.

Body segment orientation and location in three-dimensional space was measured at 100 Hz using infrared light-emitting diodes (LED) markers and an Optotrak 3020 system. Nine markers were placed on bony landmarks up the right-side of the body, obtaining the kinematics of the foot, shank, thigh, torso and head (Fig. 1). Subjects stood with each foot on a separate AMTI six-channel force-plate. Three dimensional ground reaction forces and moments were recorded at a sampling frequency of 100 Hz. The task was modeled as a triple inverted pendulum, consisting of the FOOT, shank-thigh (LEG), and head-arms-torso (HAT) segments. Joint torques (T_{hip}, T_{ankle}, T_{toe}) were obtained through inverse dynamics. Height, weight, and body segment lengths were measured for each subject.

The joint torques represented the system inputs. Angular acceleration of the FOOT

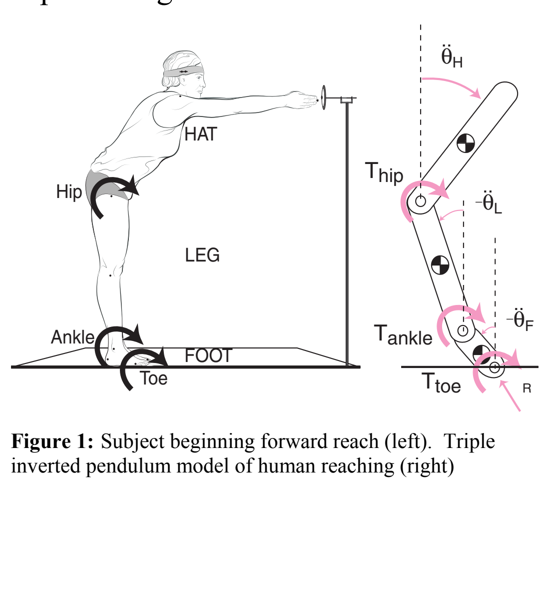

Figure 1: Subject beginning forward reach (left). Triple inverted pendulum model of human reaching (right)

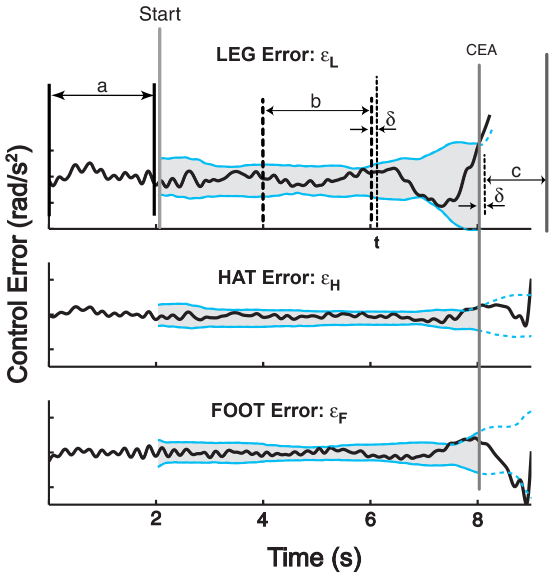

Figure 2: Schematic of three control error signals: ε_L, ε_H, ε_F (black) and ± 3Σ thresholds (shaded). 3Σ algorithm is described on ε_L (top).

($\ddot{\theta}_F$), LEG ($\ddot{\theta}_L$), and HAT ($\ddot{\theta}_H$) constituted the three dof freedom system outputs. Three control error signals were formed, ε_F, ε_L, and ε_H, defined as the residuals generated when each of the actual system outputs is compared to the corresponding predicted output of a nominal forward internal model using the given torque inputs. CEA was detected once an error signal first crossed a threshold level set at three standard deviations (3Σ) beyond the mean value in a 2-second-wide moving window, **b**, which trailed the current time instant, t, by 100 ms (**δ**). (Fig 2: The threshold calculation begins at '**Start**', initially using baseline data in window **a**.) LOB was confirmed by the occurrence of a step within 2 s of and no earlier than 100 ms from CEA detection (window **c**). The occurrence of a step was defined as a compensatory response, and evidence of CEA perception.

RESULTS AND DISCUSSION

In 83.6% of 98 trials a CEA was detected when ε_L crossed either the upper or lower 3Σ threshold. Monitoring ε_H or ε_F provided similar reliability (χ^2: $p > 0.1$). The optimal threshold level was 2.6Σ, with 85.4%

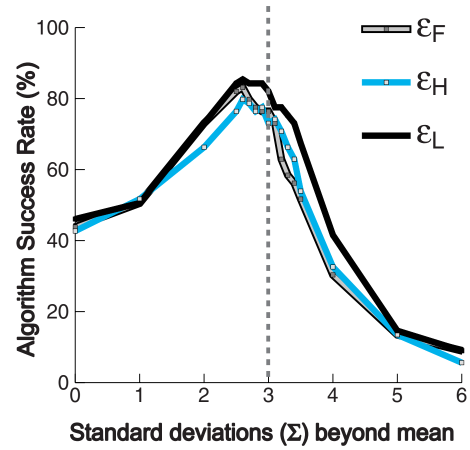

Figure 3: Threshold sensitivity analysis for each of the three control error signals

reliability, slightly greater than the 83.6% obtained with 3Σ (Fig 3). Monitoring both thresholds on ε_L provided a 72.4% success rate ($p > 0.05$). Detection algorithms based on absolute velocity or position thresholds (maintaining the center of mass, COM, within the base of support, BOS) were significantly less reliable in detecting LOB: 56% and 29%, respectively ($p < 0.005$). It is noteworthy that CEA detection does not require calculation of the COM kinematics or the BOS. There is also no need for an absolute position reference, or maximum strength estimates.

SUMMARY

The results support the hypothesis that a LOB is a loss of effective control. The 3Σ algorithm detected a CEA and predicted the need for a compensatory response using this multi-input, multi-output model of an activity of daily living-type task.

REFERENCES

Ahmed, A.A., Ashton-Miller, J.A. (2004) *Gait & Posture, epub/in press*.

ACKNOWLEDGEMENTS

NIH grants P01 AG 10542, T32 AG 00116 and P60 AG 08808

DETERMINING THE MOST APPROPRIATE MEASURE OF MECHANICAL DEMAND

Sean P. Flanagan[1] and George J. Salem[2]

[1]Department of Kinesiology, California State University, Northridge, Northridge, CA, USA
[2]Musculoskeletal Biomechanics Research Laboratory, Department of Biokinesiology and Physical Therapy, University of Southern California, Los Angeles, CA, USA
Email: sflanaga@usc.edu

INTRODUCTION

Mechanical demand at the joint level may be characterized by numerous mechanical measures , including the peak (PM), average (AM), and integrated (IM) net joint moment, and the peak (PP), average (PA), and integrated (IP; work) joint power. Some, or all, of these measures have been reported without attempts to provide insight into which is most appropriate for a given activity. This practice may be acceptable if all of the variables lead to the same conclusion; however, many times, when comparing individuals or tasks, different conclusions can be reached depending upon which variables are examined. It would seem logical to assume that the most appropriate measure is the one that is the most highly correlated to the task objective. The purpose of this investigation was to relate each of the above measures to the performance of a task in which the objective was both easily quantifiable and manipulated.

METHODS

The propulsive phase of a barbell squat exercise was chosen for this investigation because it met both of the above criteria. Experienced subjects (N = 18) performed 3 sets of 3 repetitions using a resistance load of 25% and 50% of a pre-determined 3 repetition maximum both at a self-selected speed and "as quickly as possible." A lower extremity marker set was attached to each subject, and the repetitions were performed with a force platform (AMTI, Watertown, MA) under each foot. Kinematic data was captured with a motion analysis system (Vicon 370, Oxford, UK) at 120 Hz and kinetic data was captured at 2400 Hz. The net joint moment was calculated as the moment required to satisfy the Newton-Euler equations of motion. The net joint moment power was calculated as the dot product of the net joint moment and angular velocity. Both of these calculations were performed using standard software (Vicon Workstation, Oxford Metrics, Oxford, UK). Peak, average and integrated values were obtained using signal processing software (Datapac, Run Technologies, Laguna Hills, CA). Each of these values was summed bilaterally to create measures for the hip, knee, and ankle. The 9 repetitions were then averaged for each loading condition.

The objective of the task was to perform a certain amount of work (e.g. lift a given weight a specified distance (45% of the subject's leg length) – in as short a time as possible. Thus, the goal was to maximize the average power of the center of mass (COM). Six multiple regression analyses were performed. For each analysis, the average power (the task objective) was the dependent variable. A separate analysis was performed using each measure of interest (PM, AM, IM, PP, AP, IP) with three inputs (hip, knee, and ankle) as the independent variable.

RESULTS AND DISCUSSION

All of the measures were significantly correlated with the task objective, except IM. Depending on the significant measure chosen, anywhere from 50-93% of the variance in the work performed by the subject was explained by one of the kinetic measures. Results are presented in Table 1, and are listed in descending order with the highest coefficient listed at the top. AP was the most highly correlated measure, followed by PP and PM. There was little appreciable difference between PP and PM. We suggest that AP be measured when the goal of the task is to maximize average power output at the center of mass. Average values may be more appropriate than peak measures when trying to determine the demand during the entire task. AM and IP were not as highly correlated. The results of the integrated measures (IM and IP) were anticipated. The moderate correlation between AM and power at the COM was somewhat surprising. These findings suggest that average power, and not peak power, should be maximized when attempting to improve performance. Further investigation will be necessary to determine how exercise prescriptions featuring activities that generate high joint APs, PPs, and AMs influence tissue (bone, muscle) and performance adaptations.

SUMMARY

The average NJM power, peak NJM power, or peak NJM should be used when analyzing the mechanical demand at the joint level during the propulsive phase of squatting activities performed rapidly.

Table 1. Results of Multiple Regression Analyses.

Model Inputs	R	R^2	SEE	CV
AP	.963	.927	70.59	.102
PP	.908	.825	109.27	.158
PM	.893	.797	117.6	.170
AM	.836	.700	143.14	.207
IP	.707	.500	184.14	.267
IM	.183	.033	256.79	.371

* R, Correlation Coefficient. R^2, Coefficient of Determination. SEE, Standard Error of the Estimate. CV, Coefficient of Variation. AP, Average Power. PP, Peak Power. PM, Peak Moment. AM, Average Moment. IP, Integrated Power or Work. IM, Integrated Moment.

LIGAMENTOUS INJURY DURING SIMULATED FRONTAL IMPACT

Manohar M. Panjabi, Adam M. Pearson, Shigeki Ito,
Paul C. Ivancic, S. Elena Gimenez, Yasuhiro Tominaga

Biomechanics Research Laboratory, Yale University School of Medicine, New Haven, CT, USA
E-mail: paul.ivancic@yale.edu

INTRODUCTION

Clinical and biomechanical studies have documented injuries to cervical spine ligaments during frontal impact. There are no biomechanical studies investigating subfailure injury mechanisms to the cervical spine soft tissues during simulated frontal impact. Accordingly, the goals of this study were to quantify the strains in the cervical spine ligaments during simulated frontal impact, and investigate the injury mechanisms.

METHODS

A lateral radiograph of the intact human osteoligamentous cervical spine (occiput to T1; n=6) with vertebral motion tracking flags was taken to define rigid body relationships between the flag markers and the ligament attachment points. The flags, each with two white, spherical, radio-opaque markers, were attached to each vertebra. Sagittal flexibility testing up to 1.5 Nm was performed to determine the physiological ligament strains.

The whole cervical spine with muscle force replication and surrogate head were used to simulate frontal impacts at 4, 6, 8, and 10 g horizontal accelerations of the T1 vertebra using a bench-top sled (Panjabi et al., 2004). A high-speed camera recorded the spinal motions at 500 frames/sec. The peak strains in the supraspinous (SSL) and interspinous (ISL) ligaments, ligamentum flavum (LF), capsular (CL) and posterior longitudinal (PLL) ligaments at C2-C3 to C6-C7 during frontal impact were statistically compared to the physiological strain limits (**Figure 1**).

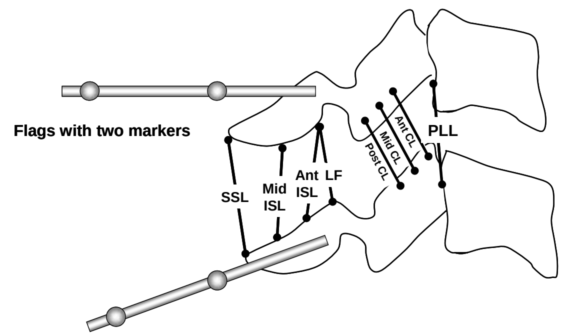

Figure 1: Schematic showing a functional spinal unit and points used to calculate ligament strains.

RESULTS

The SSL and ISL strain increases ($p<0.05$) began at 4 g at C2-C3, C3-C4 and C6-C7 and subsequently spread to all intervertebral levels at 6 g (**Figure 2A**). The highest SSL strains of 83.5 % and 71.2 % occurred during the 10 g impact at C3-C4 and C5-C6, respectively. The greatest ISL strains tended to occur in the middle fiber, with the largest strain of 83.2 % observed at C3-C4.

The LF strains exceeded physiological limits at C6-C7 during the 4 g impact and at C2-C3, C3-C4 and C5-C6 at the 6 g impact (**Figure 2B**). The greatest LF strain of 94.5 % was observed at C3-C4 followed by 78.7 % at C5-C6, both during the 10 g impact.

The CL strain, generally less than 30 %, exceeded physiological limits only during the 10 g impact (**Figure 2B**). The PLL strain typically remained under 20 %, and never exceeded the physiological limits.

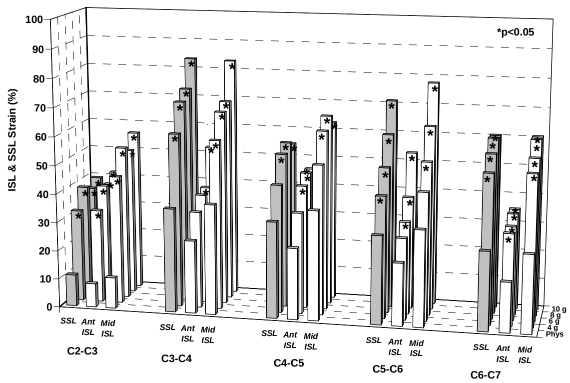

A

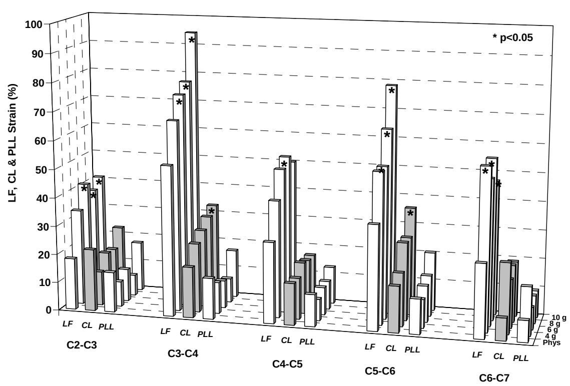

B

Figure 2. Average peak (**A**) SSL and anterior and middle ISL strains and (**B**) LF, CL, and PLL strains during simulated frontal impact. The physiological strain limits are also shown. Significant differences (p<0.05) between the peak frontal impact and corresponding physiological strains are indicated by *.

DISCUSSION AND SUMMARY

Frontal impacts may cause soft tissue cervical spine injuries, resulting in both acute and chronic pain. An improved understanding of the injury mechanisms could aid in the improvement of prevention strategies and diagnostic techniques. The present study determined cervical ligament strains during simulated frontal impact using a biofidelic fresh-frozen cadaveric whole cervical spine model with muscle force replication. Significant increases (p<0.05) over physiological strains were observed in the SSL, ISL and LF beginning at the 4 g horizontal acceleration of the T1 vertebra. These ligaments had the highest peak strains occurring at C3-C4, suggesting that this intervertebral level may be at the greatest risk for injury during frontal collision. By contrast, few significant increases were observed in the CL strains, and none in the PLL strains.

Few previous studies have documented injury mechanisms of frontal impacts. The present study demonstrated that strains in excess of the physiological limits occurred in the SSL, ISL and LF during simulated frontal impact. Ligament injury during frontal collisions may contribute to chronic pain. Future clinical and biomechanical studies are needed to delineate the relationship between excessive SSL and ISL strains and neck pain generation.

REFERENCES

Panjabi, M.M.et al. (2004). *Clin Biomech*, **19**, 1-9.

ACKNOWLEDGEMENTS

This research was supported by NIH Grant 1 R01 AR45452 1A2 and the Doris Duke Charitable Foundation.

CARPAL TUNNEL SYNDROME AFFECTS FINGER FORCE PRODUCTION

Shouchen Dun, Robert J. Goitz, Zong-Ming Li

Hand Research Laboratory, Departments of Orthopaedic Surgery and Bioengineering
University of Pittsburgh, Pittsburgh, PA, USA Email: zmli@pitt.edu

INTRODUCTION

Within the hand, the median nerve provides sensation in the palmar areas of the thumb, index, middle, and radial half of the ring fingers. It also innervates the thenar muscles and the radial two lumbricals. Carpal tunnel syndrome (CTS) is the most common peripheral neuropathy and is caused by the compression of the median nerve in the carpal tunnel. CTS impairs grip force coordination during precision grip (Lowe and Freivalds 1999). A lower median nerve lesion simulated by a nerve block at the wrist degrades motor function of the thumb (Li, et al. 2004) and fingers (Kozin, et al. 1999). However, little is known about how CTS affects the motor function of individual fingers and their force coordination. The purpose of this study was to investigate the effects of CTS on finger force production and coordination.

METHODS

Fourteen right-handed females afflicted with CTS volunteered to participate in this study. The subjects' age, height, and weight were 41.1 ± 10.4 years, 1.63 ± 0.08 m, and 75.3 ± 18.5 kg, respectively. A control group of 13 right-handed, healthy females (age 43.4 ± 12.8 years, height 1.66 ± 0.07 m, weight 66.4 ± 12.6 kg) were recruited.

A suspension device (Figure 1) with 4 unidirectional piezoelectric force sensors measured the maximal voluntary contraction (MVC) forces of individual fingers.

The participant's forearm was strapped on an arm holder with the wrist restrained at 20° extension. The interphalangeal joints were immobilized using wooden splints on the palmar side of the finger. All the fingers were positioned inside the corresponding loops at the bottom end of each wire. Each loop was secured around the proximal interphalangeal (PIP) joint of the finger with sports tape, ensuring that the forces were always applied at the PIP joints. The experimental tasks were to voluntarily press down as hard as possible with a single finger (the index, middle, ring, or little) or all 4 fingers. Each participant performed three trials of each task. Analog data was digitized by a 16-bit analog-digital converter at a sampling rate of 100 Hz.

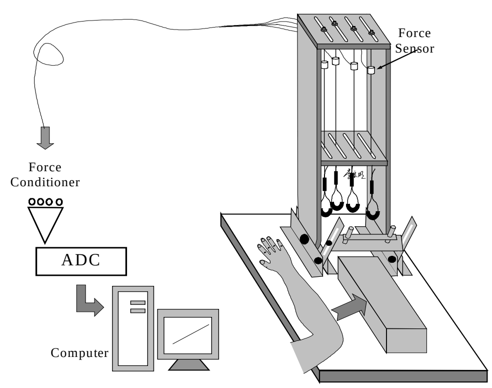

Figure 1. Schematic of suspension device

For the 4-finger tasks, the force data of each finger was extracted at the moment when the total MVC value was reached. Force sharing in a 4-finger task was defined as the percentage contribution of each individual finger to the total force. The force deficit was defined as the difference between 100% and the percentage of the total MVC force in the 4-finger task to the sum of the MVC forces of each individual finger in single-finger tasks. If the MVC force of any finger of a participant was less than 1 N in the 4-finger task, the participant was excluded from the analysis of force sharing. MANOVA and *t*-test were used for statistical analyses. A p-value less than 0.05 was considered to be statistically significant.

RESULTS

Compared with the control group, the MVC forces of the CTS group were significantly decreased in all single-finger tasks ($p < 0.05$). The average percentage decreases in force were 40.7%, 32.0%, 27.6%, and 27.1% for the index, middle, ring, and little fingers, respectively (Figure 2). In the 4-finger task, CTS subjects produced 41.7% smaller total MVC force than the control subjects ($p < 0.01$).

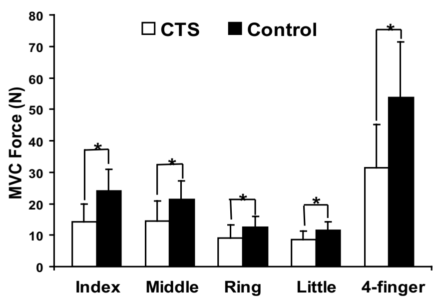

Figure 2. MVC forces in single- and 4-finger tasks. * denotes $p < 0.05$.

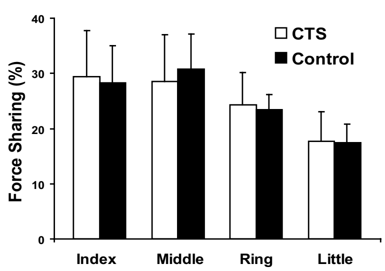

Figure 3. Force sharing (%) of individual fingers in 4-finger tasks.

One participant was excluded for the analyses of force sharing based on the exclusion criteria. During 4-finger tasks, the force sharing pattern (Figure 3) did not significantly differ between the CTS and control groups ($p > 0.80$). The force deficit of the CTS and control groups were 32.8% (± 19.6%) and 22.3% (± 19.5%), respectively. However, the difference was insignificant ($p > 0.17$).

DISCUSSION

CTS tends to preferentially impair the force production capabilities of the index and middle finger during single-finger tasks, which is in agreement with the neuroanatomical association of the median nerve with the radial side of the hand. However, the large force decreases of the ring and little fingers suggest that CTS globally impairs the motor function of all fingers. We hypothesize that neural adaptation might have occurred in the central nervous system secondary to peripheral neuropathy, leading to a decrease of central neural drive to individual fingers and therefore an overall change of the hand motor function. Interestingly, similar force sharing patterns were observed for CTS and control subjects during the 4-finger tasks. We hypothesize that additional motor control strategies (e.g. minimization of secondary moment of the hand) may have dictated or modulated individual finger forces.

REFERENCES

Kozin SH, et al. (1999). *J Hand Surg [Am]*; 24(1): 64-72.

Li ZM, et al. (2004). *J Neuroengin Rehab 2004 (submitted).*

Lowe BD, Freivalds A (1999). *Ergonomics*; 42(4): 550-64.

ACKNOWLEDGEMENTS

This project was supported by the Whitaker Foundation.

Clinical quantification of frontal plane knee angle: correlation of 2D and 3D motion analysis

John D. Willson[1] and Irene Davis[1,2]

[1] Department of Physical Therapy, University of Delaware, Newark, DE, USA
[2] Joyner Sportsmedicine Institute, Mechanicsburg, PA, USA
Email: willson@udel.edu Web: www.udel.edu/PT/davis/index.htm

Introduction

Excessive movement of the knee joint in the frontal plane during closed kinetic chain activities is suggested to contribute to the etiology of injuries such as patellofemoral pain (Ireland, 2003) and anterior cruciate ligament rupture (Hewett, 1999). Recently, several authors have utilized high speed, three-dimensional motion analysis to test for this potential injury risk factor during activities such as drop jumps and single leg squats (Ford, 2003, Zeller et al. 2003). While it is important to identify these individuals as they may most significantly benefit from intervention efforts, these methods are not practical for most practicing clinicians.

Recently, authors have expressed the need to simplify these methods to make them appropriate for more clinical environments (Ford, 2003). However, at this time, no uniform or reliable procedures for screening of this potential risk factor have been described in peer-reviewed literature. Therefore, the purpose of this pilot study was to describe a two-dimensional (2D) procedure suitable for measurement of frontal plane movement of the knee during a closed kinetic chain activity in a clinical environment. Additionally, we intended to determine whether this clinical method yields reliable measures that can be validated with 2D projected plane angles calculated from the coordinate data from standard motion analysis. Finally, we intended to correlate the frontal plane angle of this clinical method with the frontal plane angle determined from three-dimensional (3D) rigid body analysis. We hypothesized that the 2d methods would be similar and correlated. We also hypothesized that the 2D angles would be highly correlated with the 3D angles, but significantly smaller.

Methods

Retro reflective anatomical and tracking markers were placed on the lower extremity. The anatomical markers were removed after the standing trial. A six camera Vicon motion analysis system collecting at 120 Hz and V3D software were used to determine the 2D and 3D joint angles. Data were collected from five healthy subjects during one trial of single leg stance and three trials of single leg squats to 45º. During each trial, a digital image was recorded by a digital camera. This camera was mounted on a tripod 2 m anterior to the subject perpendicular to the frontal plane, and at the height of the knee joint in single leg stance. To synchronize this 2D camera image with the 3D motion analysis data, a signal was delivered to the motion analysis workstation as the digital image was recorded. Subjects performed a single leg squat to 45º as determined by hand-held goniometry. A tripod was adjusted behind the subject such that when they lowered themselves to the tripod, their knee angle was at 45º. In addition to the marker set used for motion analysis, three reflective markers were placed on the leg of each subject bisecting the proximal thigh, patella, and malleoli at the ankle to determine the frontal plane angle of the knee from the digital image. The frontal plane angle of the knee during these tests was determined using the angle measurement tool provided in commercially available graphics software (CorelDraw). For comparison, the x (frontal) and z (vertical) coordinates of these same markers were used to determine a 2D angle using a dot product calculation.

Two-tailed paired t tests were used to test for differences in knee angles between the three methods. In cases where differences were not found, one-way random ICC values were determined.

Results and Discussion

No significant difference was revealed between the 2D methods (p = .62). Further, the 2D methods were found to be highly correlated (r= 0.89) (Figure 1). The intraclass correlations between these two methods were high for both single leg squat trials (ICC (2,k) = 0.88) and the single leg stance condition (ICC (2,1) = 0.96). This suggests that the 2D projected frontal plane knee angles obtained using a digital camera is an accurate representation of the true 2D projected plane knee angle.

Three-dimensional motion analysis revealed significantly greater frontal plane knee angles than both 2D methods ($p < 0.01$). This was expected as the projected plane magnitude of a 3D angle will be smaller than the true angle. However, there was surprisingly little correlation between this measure and the angles determined using the digital image (r = -0.18) or frontal plane coordinates (r = 0.01). This may be due to variable lower extremity rotation between and within subject trials.

Subjects demonstrated considerable variability across single leg squat trials. As a group, subjects demonstrated an average of 41.9º knee flexion during the single leg squat trials. However, the confidence interval for these trials was large (95% CI = 32.8º,50.1º). Subjects also demonstrated increased variability in 2D frontal plane knee angles during single leg squats. Within subjects, the average standard deviation of the 2D frontal plane knee angle was 3.5º. Therefore, we recommend taking the average of three trials of single leg squats to more accurately represent the frontal plane angle the individual tends to display.

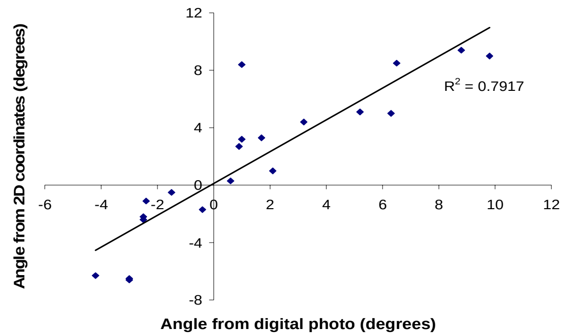

Figure 1: Correlation of frontal plane knee angles using different 2D methods.

Summary

Based on the results of this preliminary study, we feel that the frontal plane knee angle determined from a digital image provides an accurate representation of the projected plane angle of the knee. However, this angle does not appear to represent the true 3D frontal plane angle of the knee obtained using more sophisticated techniques. Factors such as inconsistent knee flexion angles and lower extremity rotation during single leg squats may adversely affect the relationship between the 2D and 3D techniques.

References

Ford, K.R., Myer, G.D., Hewett, T.E. (2003). Am J Sports Med, **35**, 1745-1750.

Ireland, M.L., Willson, J.D., Ballantyne B.T., et al. (2003). J Orthop Sports Phys Ther, **33**, 671-676.

Hewett, T., Lindenfeld, T., Riccobene, J., et al. (1999). Am J Sports Med, **27**, 699-706.

Zeller, B.L., McCrory, J.L., Kibler, W.B., et al. (2003). Am J Sports Med, **31**,449-456.

RELATIONSHIP OF KNEE EXTENSION STRENGTH AND ANTHROPOMETRIC VARIABLES TO ALPINE SKI RACING SUCCESS

Benjamin A. Crockett and Randall L. Jensen

Dept of HPER, Northern Michigan University, Marquette, MI, USA
E-mail: rajensen@nmu.edu Web: http://www.nmu.edu/hper/faculty/jensen.htm

INTRODUCTION

A large amount of knee extensor strength is often sited as a requirement for alpine ski racing success.

Several studies have attempted to show a relationship between isometric, isotonic or isokinetic quadriceps strength and ski racing ability. Takashi et al (1992) found that eccentric knee extension and flexion strength may be related to racing success in national caliber athletes. In contrast, Neumayr et al (2003) found no correlation between muscle strength and racing performance in world class athletes. Few studies have examined these types of relationships in recreational athletes.

Tesch (1995) showed ski racing depends heavily on slow forceful eccentric muscle actions. Kues et al (1994) found a strong correlation between slow eccentric contraction strength and isometric contraction strength in muscle testing. The current study examined the relationship between isometric strength of the knee extensors and success in recreational alpine ski racing. In addition, the relationship of several anthropometric measurements to racing ability was also examined.

METHODS

Twenty-two subjects (9 male, 13 female) were selected from an open-entry citizen-type alpine ski race. All subjects were greater then 15 years of age. (Mean 25.6). Heights and weights were obtained for all of the subjects (Means 168.8 cm, 72.4 kg). Segment length measurements were gathered for the dominant leg using a flexible steel tape. The shank of the leg was measured from the lateral malleolus to the head of the fibula. The upper leg was measured from the lateral epicondyle to the greater trochanter. These anatomical structures were found through palpation. Knee joint flexibility was determined with a manual goniometer. The subject stood upright with the anterior surfaces of both legs against a vertical surface. They then independently flexed each knee as far as possible and the knee angle was measured using the greater trochanter and lateral malleolus as aligning landmarks.

Peak isometric knee extension torque was measured at 90 degrees of flexion. The subjects were seated on a bench with an adjustable cuff secured 10 cm below the tibial tuberosity on their dominant leg. This cuff was securely fastened by cable to an OR6-7-2000 (AMTI, Watertown, MA) force platform located behind the subject(Figure 1). The subject's non-restrained leg was also at 90 degrees with the foot resting on the floor. The subjects pushed against the cuff by extending their knee with maximum effort for a period of 5 sec. Data was collected from the force platform and analyzed with an IBM compatible computer using Biosoft 1.0. (AMTI, Watertown, MA)

Ski racing ability was determined using the race times from a 25 gate citizen slalom race.

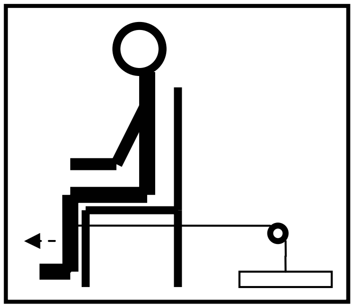

Figure 1. Set-up for measuring isometric knee extension strength

RESULTS AND DISCUSSION

A correlational analysis (SPSS v 11.5) indicated that, for the variables tested, only subject height was significantly correlated to ski racing time ($r = -.561$, $p < 0.01$). Isometric knee extensor strength, knee flexibility, and other anthropometric variables were not significant ($p > 0.05$)

Table 1. Correlation of ski racing time to independent variables (N=22)

Independent Variable	Race Time (sec)	
Age	0.299	
Gender	-0.366	
Height (cm)	-0.561	*
Weight (kg)	-0.120	
Right knee flex (degrees)	-0.297	
Left knee flex (degrees)	-0.279	
Shank length (cm)	-0.332	
Leg length (cm)	-0.318	
Avg. isometric knee strength (N)	-0.221	

* Significant correlation (P < 0.01, 2-tailed)

The data from 16 subjects were randomly chosen from the pool of 22 to form a regression equation. The six remaining subjects were used to cross-validate this equation. Regression analysis was performed (SPSS v 11.5) 20 times using the re-sampling cross-validation technique (Jensen and Kline, 1994). Height was the first variable entering the equation in 17 out of 20 samples with mean multiple r of 0.65. Left knee flexibility, sex, and knee strength entered the equation first one time each.

In recreational alpine ski racing height seems to be an advantage, in contrast to the findings of Piper et al (1987). Taller athletes may be able to put more leverage on the ski, causing them to turn faster. However, isometric knee extension strength was not a factor. Moreover gender, which was also related to height, was not a factor in racing performance.

Table 2. Summary of statistics for predicting ski racing time from 20 regression equations and cross-validations.

	Mean	SD
Development		
Multiple R	0.65	0.121
SEM	4.14	0.947
Beta Coefficients		
Height	-0.428	0.082
Constant	100.9	27.19
Validation		
Correlation	0.49	0.358
Mean Difference	-1.88	5.857
t-value	0.378	0.349

SUMMARY

The major finding of this study was the inability to correlate isometric knee extension strength to racing time in recreational alpine skiers. However, subject height was correlated to racing time.

REFERENCES

Jensen, R., Kline, G. (1994). *Med Sci Sport Exerc*, **26**, 929-933.

Kues, J. et al. (1994). *Phys Ther,* **74**, 647-683.

Neumayr, G. et al. (2003). *Int J Sports Med,* 571-575.

Piper, F.C. et al. (1987) *J Sports Med,* **27**: 478-482.

Takashi, A. et al. (1992). *J Sports Med Phys Fitness*, **32**, 353-357.

Tesch, P. A. (1995). *Med Sci Sport Exerc,* **27**, 305-309.

COMPARING MOMENTUM AND STABILITY TRADEOFFS DURING BI-DIRECTIONAL GAIT INITIATION IN OLDER ADULTS AND PARKINSONISM

Chris J. Hass[1,2], Dwight E. Waddell[1], Steve L. Wolf[3], Jorge L. Juncos[2], Robert J.Gregor[1]

[1] Center for Human Movement Studies, Georgia Institute of Technology, Atlanta, GA, USA
[2] Department of Neurology, Emory University, Atlanta, GA, USA
[3] Department of Rehabilitation Medicine, Emory University, Atlanta, GA, USA
E-mail: chass@emory.edu Web: http://www.emory.edu/WHSC/MED/NEUROLOGY/CAM

INTRODUCTION

Gait initiation (GI) is a functional task requiring voluntary destabilization of the whole body center of mass (COM) and a transition from a large to small base of support. The two requirements for successful GI are the generation of momentum and the maintenance of stability. Polcyn (1998) indicated that the most important consideration during GI is the generation of momentum via displacement of the center of pressure (COP) while maintaining the COM within the base of support to ensure stability. Initially, the COP moves towards the swing limb and backward before moving towards the stance limb and forward as the swing phase begins. This initial posterolateral movement towards the swing limb generates momentum in the forward and stance side direction.

Changing direction during GI is a common task performed daily such as when moving away from a kitchen counter. Since many older adults report falling when turning or directing motion laterally (Rogers, 2003), it is surprising that the effects of changing direction during GI have received little attention

The purpose of this study was to examine changes in the translation of the COP during forward and lateral-oriented GI in two populations of older adults who are particularly susceptible to postural instability.

METHODS

Twenty-eight older adults (mean age 80.2± 6.1yrs, mass 65.7± 12.1 kg; height 162.3± 10.2cm) were recruited for this investigation from 20 congregate living facilities. All participants were transitioning to frailty (TF), based on criteria proposed by Speechley (1991). In addition, 16 patients with idiopathic Parkinson's disease (PD) (mean age 66.6± 6.4 yrs; mass 79.1±15.4 kg; height 174.7± 8.1 cm; Hohen & Yahr 2.4± 0.4) were recruited from the Movement Disorders Clinic at Emory University School of Medicine.

GI trials began with the participant standing quietly on the force platform. Initial positioning of the feet was self selected. In response to a cue, the participants initiated walking in the instructed direction and they continued to walk for several steps. Participants performed both forward and lateral GI in a random order. In the lateral conditions, the participant began walking by stepping 90 degrees to the side of the instructed leg. For each participant, three data collection trials were collected for each leg performed at a self selected pace in both GI directions. Thus, 12 GI trials (6 forward and 6 lateral) were analyzed per participant.

Ground reaction forces were collected using a multi-component force platform (Kistler Instruments). The platform was mounted flush with the surface of a level walkway. Forces and moments along the 3 principal axes were sampled at 300 Hz. Force platform data were subsequently used to calculate the instantaneous COP and the dependent variables of interest using software (LabView) developed at the Center for Human Movement Studies.

The COP during GI was divided into three periods (S1, S2, S3) by identifying two landmark events as described previously (Hass, 2004). Data from the right and left legs were averaged for statistical analysis. Five dependent COP variables were computed to include: a) displacement in the X direction; b) displacement in the Y direction; c) average velocity in the X direction; d) average velocity in the Y direction; and e) smoothness. Separate 2 x 2 (Group x Direction) MANOVA's were used to test for overall group differences during each GI period. Separate ANOVA's were performed for follow-up testing when the MANOVA test identified significant differences.

RESULTS AND DISCUSSION

An exemplar record of an overhead view of the path of the COP during forward (left panel) and lateral (right panel) oriented gait initiation when stepping with the left foot is presented in Figure 1.

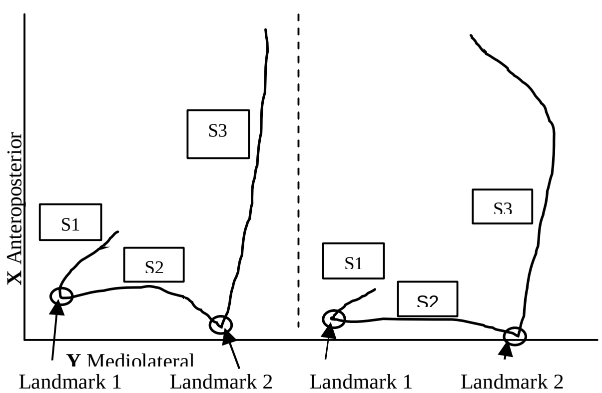

Figure 1. Exemplar COP trajectory during forward and lateral oriented gait initiation.

In general, the TF group produced larger, faster, and more coordinated movement of the COP during lateral and forward directed GI. The TF adults were able to scale the output of the GI motor program so that forces were maximized to propel the COM in the intended direction of movement. For example, the TF group produced a significantly greater posterior displacement of the COP during S1 of the forward directed GI, which functions to generate forward momentum of the COM. Similarly, the TF group produced a greater swing-side COP displacement during S1 of the lateral GI, producing greater momentum along the direction of the intended step. Conversely, the PD patients appear to use a strategy that optimizes stability rather than momentum generation. During the S1 portion of forward directed GI, PD patients produced a reduced posterior COP displacement thereby reducing forward COM momentum. In addition, these patients produced greater swing side COP displacement so that the body's COM is propelled as close to the stance limb as possible prior to taking a step thereby enhancing stability. During lateral directed GI, PD patients produced swing-side COP displacements that were 12.5% less than in the TF. Limiting this displacement reduces the forces acting to propel the body in the lateral direction enhancing stability.

SUMMARY

These findings suggest that PD patients are placing greater emphasis on postural stability than on generating momentum during GI.

REFERENCES

Hass et al. (2004). *Arch Phys Med Rehabil* In press.

Polcyn et al. (1998). *Arch Phys Med Rehabil* **79**,1582-9.

Rogers et al. (2003) *Exerc Sport Sci Rev* **31**, 182-187.

Speechley & Tinetti M.(1999). *J Am Geriatr Soc* ;**39**, 46-52

ACKNOWLEDGEMENTS

Supported by NIH grant #RO-1AT00612-01;NIA grant AG 14767

SIMULATION MODEL OF THE LOWER LIMB

Alexandra Schonning[1], Binu Oommen[2], Irina Ionescu[3], and Ted Conway[4]

[1] Mechanical Engineering; University of North Florida; Jacksonville, FL
[2] Materials Science and Engineering; Massachusetts Institute of Technology; Boston, MA
[3] Scientific Computing and Imaging Institute; University of Utah; Salt Lake City, UT
[4] Mechanical, Materials, and Aerospace Engineering; University of Central Florida; Orlando, FL

E-mail: aschonni@unf.edu Web: http://www.unf.edu/~aschonni/

INTRODUCTION

The motivation for performing this research is to ultimately develop a customized simulation model of the human lower limb. This model is to be used as a design and analysis tool for medical practitioners. The model is under development but initial results on a generic model have been obtained. The model is based on Computed Tomography (CT) data from the National Institute of Health. This data has been used to develop three-dimensional models which form the basis for the finite element model.

METHODS

CT data was obtained from the National Institute of Health. It consisted of two-dimensional gray scaled images of a normal human male. The images were converted into three-dimensional models using an interpolation algorithm embedded in a medical imaging software called Mimics, by Materialize [Mimics]. The gray-scaled values of the images represent the density of the material scanned. By setting threshold values it was possible to separate the cortical, cancellous bone and the bone marrow. Since the material properties vary for the cortical bone, cancellous bone and the marrow cavity, different geometrical volumes were generated for these.

The three-dimensional volumes were then imported into a data editing software called Geomagics by Raindrop Geomagic [Geomagics]. This software includes functions that allow the surfaces to be smoothed. This is necessary to reduce the mesh size and to increase the quality of the computational mesh generated. Geomagics is also used to convert the geometry into Non-Uniform Rational B-Splines (NURBS) format. The NURBS curves are created by the use of a regression analysis technique. Points are connected in a format that can better be understood by the finite element modeling software. This gives the user higher control over the geometry to be exported for finite element meshing. It is important to develop a good NURBS geometry so that a high quality meshes can be generated.

Once the geometry is completed, the next step is to import it into a finite element modeling software. It has been found that hexahedral meshes perform well for polygonal models such as the lower limb [Cattaneo]. For this reason, it was decided to use a meshing software that is specialized at generating hexahedral meshes for complicated geometry. The meshing software utilized is called True Grid by XYZ Scientific Applications Inc. [Truegrid]. This software requires a significant amount of user interaction to generate the mesh. While this is a challenging task, it also gives the user total control. In the case of the femur, a bone marrow cavity mesh was first generated and then projected in an outward fashion to develop the cancellous and cortical mesh. True Grid is organized in a fashion where the user defines a computational block structure and then projects these blocks onto the geometry, resulting in the mesh. The generated mesh file can easily be modified by the user.

RESULTS AND DISCUSSION

The model has been analyzed in the upright position with the weight of a 50th percentile male applied. Both forces and appropriate moments were applied to the femoral head. In order to generate the moments, elements were used that could transfer all six degrees of freedom. To distribute the load over the femoral head a constraint element was utilized. The connection between different bones was modeled using spring elements. Future versions of the model will utilize different techniques to transfer the load between the bones. The distal end of the tibia was constrained from motion in all six degrees of freedom. While the elements only have translational stiffness a combination of constraints resulted in the indirect removal of both translational and rotational degrees of freedom.

The femur included stresses as a result from both bending moments and normal loads while the tibia mostly showed stresses as a result from the normal load. The stress distribution on the femur is shown in Figure 1. It is expected that a similar stress distribution will result from a model that utilizes contact elements to model the connections between the bones.

Modifications will be needed to the model before it can be used by the medical community in developing new and improved implant designs and treatment techniques. Some of these include modifications to the material properties, contact modeling, application of the muscle forces and analysis of numerous stances.

Figure 1: Stress Distribution

The current model represents the initial step towards creating a model that can be used by engineers and medical practitioners to develop improved treatment techniques for patients suffering from orthopedic disease or deformity.

REFERENCES

Materialise's Interactive Medical Image Control System (MIMICS) 7.0: User Manual, 2003, Materialise, http://www.materialise.com/mimics/.

GEOMAGIC Studio 4.1, User Manual, Raindrop Geomagic Inc., 2002 http://www.geomagic.com.

Cattaneo, P., Dalstra, M., Frich, L., "A Three Dimensional Finite Element Model from Computed Tomography data: a semi-automated method", *Proceedings Institute of Mechanical Engineers [H],* 2001, **vol. 215(2)**, pp. 203-13.

TRUEGRID, User Manual, XYZ Scientific Applications, Inc., 2003, http://truegrid.com.

MEASURING REAL TIME HEAD ACCELERATIONS IN COLLEGIATE FOOTBALL PLAYERS

Stefan Duma[1], Sarah Manoogian[1], Gunnar Brolinson[2,3], Mike Goforth[3], Jesse Donnenwerth[3], Richard Greenwald[4], Jeffrey Chu[4], Bill Bussone[1], Joel Stitzel[1], Joseph Crisco[5]

[1] Virginia Tech – Wake Forest Center for Injury Biomechanics; [2] Edward Via Virginia College of Osteopathic Medicine; [3] Virginia Tech Sports Medicine; [4] Simbex; [5] Brown Medical School
E-mail: duma@vt.edu Web : CIB.vt.edu or Simbex.com

INTRODUCTION

Traumatic brain injuries occur in 1.5 million people in the United States each year, of which 75 percent are mild traumatic brain injuries (MTBIs) like concussions (McCrea, 2003). Sports related concussions constitute 300,000 of these injuries. Football has the most total concussions of any sport and has had an increasing rate of injury in the last seven years.

Using video analysis of concussive events in the National Football League, previous research has reconstructed head acceleration injury limits using instrumented Hybrid-III crash test dummies (Pellman, 2003). The dependence on video reconstruction and dummy reenactments is expensive, time intensive, and does not allow for the data to be used clinically on the field. The purpose of this paper is to introduce a new method for accurately collecting and analyzing real-time on-field head impact data in collegiate football and to present data collected from one season.

METHODOLOGY

A total of 8 players were instrumented for each practice or game with a new set of players randomly chosen on a weekly basis. Institutional Review Board approval was obtained from Virginia Tech and the Edward Via Virginia College of Osteopathic Medicine. Over the course of the 2003 season, data were collected from 38 different players from all primary offensive and defensive positions.

This study utilized the Head Impact Telemetry System (HIT System) (Simbex, Lebanon, NH), a wireless system that provides real time measurements of a player's head acceleration and impact location on up to 64 simultaneous players. Each monitored player wears a player unit designed to fit a large or extra-large Riddell VSR-4 football helmet (Figure 1). The player unit consists of sensors (6 linear accelerometers and 1 temperature), a wireless transceiver (903-927 MHz), on-board memory (up to 33 impacts), and data acquisition capabilities (8 bit; 1000 Hz / Ch). Data are collected for 40 ms when any accelerometer detects accelerations that exceed a user-selected threshold (10g). The acceleration data are time-stamped (+/- 5 ms resolution) and wirelessly transmitted to a sideline receiver interfaced to a laptop. These data are processed using a novel algorithm (Crisco, 2002) that calculates linear head acceleration and impact location. If wireless communication is not present, data are stored on non-volatile memory and downloaded once communication has been re-established.

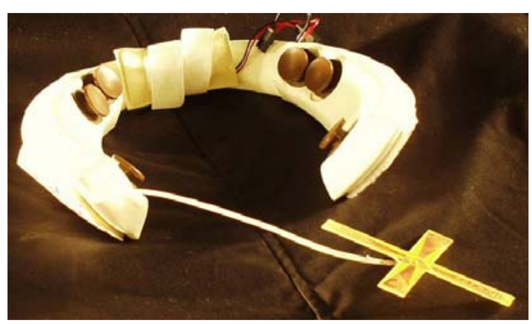

Figure 1: Six accelerometers, FM-antenna, and rechargeable battery pack of the HIT system prior to instillation in a helmet.

The HIT system was validated using a series of impact tests with a helmet-equipped Hybrid-III dummy that featured a 3-2-2-2 head accelerometer array. The data correlated well with the 3-2-2-2 data (R^2=0.97) and had a ±4% error for linear and rotational accelerations as well as HIC. In addition to the acceleration data, the sports medicine staff maintains detailed player histories, including pre-season neuropsychological records.

RESULTS AND DISCUSSION

For the entire season a total of 3,312 valid head impacts were recorded with 1,198 occurring in 10 games and 2,114 in 35 practices. For all players over the entire season, the average peak head acceleration was 25.8 g ± 21.3 g (range 0 g to 185.7 g). The majority of the impacts were less than 50 g in a non-normal distribution (Figure 2). The average GSI was 22.2 ± 58.7 (range 0 to 1327) and the average HIC was 15.7 ± 40.5

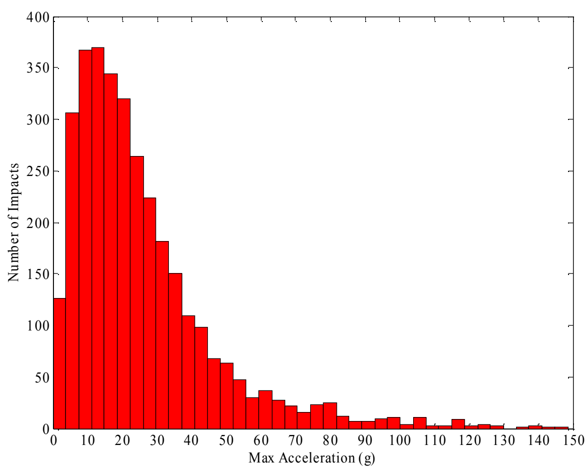

(range 0 to 794.5).

Figure 2: Histogram of peak head acceleration for all players all season.

Impact exposure and location differences by player position were measured. Linebackers (LB) and linemen observed more head impacts compared to running backs (RB), defensive backs (DB), wide receivers (WR), tight ends (TE), and quarterbacks (QB) (Figure 3). Furthermore, location data demonstrated differences by player positions and style of play.

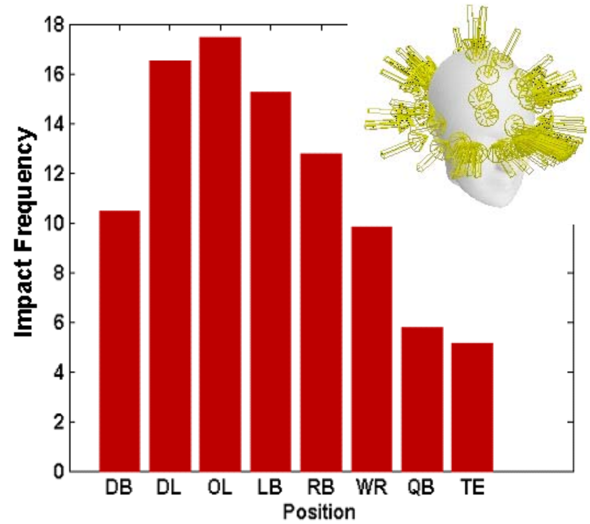

Figure 3: Histogram of athlete impact exposure by position and impact direction from a RB for one game (insert).

The primary finding of this study is that the HIT system proved effective at collecting thousands of head impact events and providing real-time on-field data analysis. A few players exhibited impact magnitudes greater than the reported 98g concussed average (Pellman, 2003) without sustaining an injury. Through continued use of this system, it is anticipated that on-field impact measurements will help improve head injury criteria and clinical evaluation techniques.

REFERENCES

McCrea, M., (2003) *J. American Medical Association*, 290(19), 2556-2563.

Pellman, E. (2003) *J. Neurosurgery*, 53(4), 799-814.

Crisco, J.J. (2002) World Congress of Biomechanics.

ACKNOWLEDGEMENTS

The authors gratefully thank our funding groups: Edward Via Virginia College of Osteopathic Medicine, the Virginia Tech College of Engineering and Department of Sports Medicine, and Simbex. This work was supported in part by NIH 2R44HD40473.

JOINT MECHANICAL CONTRIBUTIONS VARY WITH SQUATTING DEPTHS

Joo-Eun Song[1], and George J. Salem[1]

[1] Musculoskeletal Biomechanics Research Laboratory, Dept. of Physical Therapy and Biokinesiology, University of Southern California, Los Angeles, CA, USA

E-mail: jooeunso@usc.edu Web: www.usc.edu/go/mbrl

INTRODUCTION

Squatting exercises are common activities used to prevent injury, improve sport performance and rehabilitate patients following trauma/surgery. Squatting is a popular training exercise because it requires balance and stability, mimics important functional activities, and targets multiple lower extremity muscle groups bilaterally. Although muscles about the ankle, knee, and hip are required to perform squatting activities, the *relative* mechanical contributions of these joints, across varying movement depths, have not been adequately characterized. Thus, the purpose of this investigation was to quantify the mechanical contributions of ankle, knee and hip across squatting activities performed at three different depths.

METHODS

Ten participants (mean age = 29.3yr± 3.77) performed two trials of the squat activity at three different depths, which were standardized based upon previously measured knee-flexion angles (70,90, & 110º). Limit bars were used to provide a consistent squatting depth.
The ground reaction forces were measured using 2 force plates (AMTI, Watertown, MA) at 1200 Hz. A motion analysis system (Vicon 370, Oxford, UK) captured the kinematics (60 Hz), and standard inverse dynamics techniques were used to calculate the sagittal plane net joint extensor impulse (IMP; integrated area beneath the net joint moment/time curve). ANOVA with repeated measures were used to assess differences in kinematics and the % contribution of the hip, knee, and ankle extensor impulse, among the three squatting depths. (α=0.05).

RESULTS AND DISCUSSION

Maximum ankle angle remained constant throughout the varying squat depths; whereas, the maximum hip joint angle varied from 45º-93º with increasing knee flexion angle ($p<0.05$) (Figure 1).

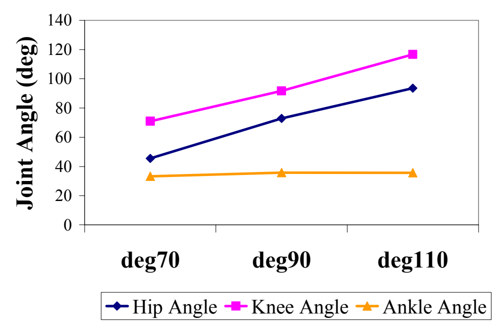

Figure 1: Joint displacement of hip, knee, and ankle across depths

Knee and hip average extensor IMP increased with increasing depth; whereas, ankle plantar flexor IMP remained fairly constant across depths (Figure 2). The percent contribution of the ankle decreased from 26-19% as depth increased ($p<0.05$). The percent contribution of the hip increased from 28-44% as depth increased ($p<0.05$). The percent contribution of knee, however, remained constant across depths.

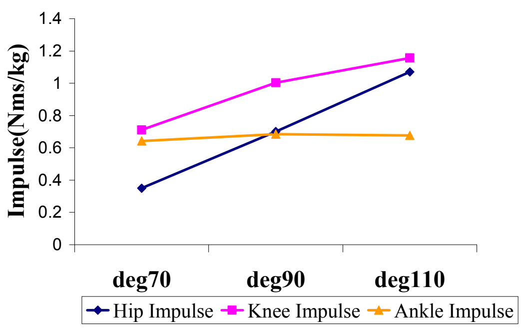

Figure 2: Joint impulse of hip, knee, and ankle across depths

Findings suggest that squatting depth influences the relative mechanical contributions of the ankle, knee, and hip extensors. The percent contribution of hip impulse increased as knee flexion angle increased, whereas the percent load demand on the ankle joint decreased. The percent contribution of the knee extensors remains fairly stable throughout increasing flexion angles. Joint extensor impulse patterns varied in conjunction with the sagittal joint displacement.

SUMMARY

In general, it appears as though a consistent percent contribution of knee extensor impulse (45%) is required during squatting, despite differences in knee joint angle and squatting depth. These findings may be used by physicians and physical therapists to more appropriately prescribe squatting exercises during rehabilitation. For example, therapists should not assume that increased squatting depth will increase the mechanical demand at all joints, including the ankle. Additionally, therapists should consider the relatively large increased demand at the hip when squatting depth increases.

REFERENCES

Escamilla, R.F. et al. (1998). *Med Sci. Sports Exerc*, **30**:556-569.

Isear, J.A. et al. (1997). *Med Sci. Sports Exerc*, **29**:532-539.

Salem, G.J., Salinas, R., and Harding, F.V. (2003). *Arch Phys Med Rehabil*, **84**(8):1211-1216.

ACKNOWLEDGEMENT

Supported by James H. Zumberge Research Fund.

The Effects of Varying Nucleus Implant Parameters on the Compressive Behavior of the Human Lumbar Intervertebral Disc

Abhijeet Joshi[1], Samir Mehta[2], Edward Vresilovic[3], Andrew Karduna[4] and Michele Marcolongo[1,3]

[1]Dept. of Materials Science and [3]Biomedical Engineering, Drexel University, Philadelphia, PA, USA
[2]Dept. of Orthopaedic Surgery, University of Pennsylvania, Philadelphia, PA, USA
[4]Dept. of Exercise and Movement Sciences, University of Oregon, Eugene, OR, USA
E-mail: marcolms@drexel.edu

INTRODUCTION

The origin of low back pain is often a degenerated lumbar intervertebral disc (IVD). We are investigating replacing the nucleus pulposus (NP) of the IVD with a polymeric hydrogel implant, with the goal of restoring the normal mechanical behavior to the natural IVD. In this study, we examined the effect of variation of the nucleus implant material and geometric parameters on the compressive stiffness of the IVD. We hypothesize that the nucleus implant parameters will have a significant effect on the IVD compressive mechanical behavior.

METHODS

A 10% polymer mixture was prepared from a 95/5 blend of poly (vinyl alcohol) (PVA) and poly (vinyl pyrrolidone) (PVP) to make hydrogel implants. The solution was cast into the molds of three different diameters (D_1=15mm, D_2=16mm, D_3=17mm). Implants were prepared in three heights (H_1=H_2-1mm, H_2, H_3=H_2+1 mm), where H_2 is the average height of the tested IVD. Three implant moduli were studied. Moduli (E_1=50 kPa and E_2=150 kPa, @ 15% strain) were obtained by varying the number of freeze-thaw cycles during the preparation [1]. A third higher modulus implant (E_3=1.5 MPa @ 15% strain) was made from Silastic T2, a commercially available polymer mixture (Dow Corning®).

Lumbar spines were harvested from 4 cadavers (1 male, 3 females) with an average age of 63 years. Motion segments (n=9) from L1-L5 levels were prepared by removing the facet joints and ligaments.

A series of compressive tests were run on each of the nine specimens. First the intact specimen was tested. The upper vertebra was then core drilled (16 mm diameter) from the proximal surface through the upper end plate. This created a cylindrical bone plug (BP), which remained in its original position and the specimen was tested again (BI condition). The BP was then removed, the NP was excised in-line with the core drilling of the upper vertebrae and the specimen was tested again (DN condition). A parametric study of the effect of NP implant moduli, heights and diameters was then conducted by inserting the appropriate implants into the disc, replacing the BP and repeating the test protocol. The order of the implant testing was randomized.

For each specimen, the implant modulus was varied (E_1/E_2/E_3) with a constant height (H_2) and diameter (D_2). Similarly, the implant height was varied (H_1/H_2/H_3) with a constant modulus (E_2) and diameter (D_2). Finally, the implant diameter was varied (D_1/D_2/D_3) with a constant modulus (E_2) and height (H_2). In the end, the specimen was re-tested in the denucleated condition (DN-1).

A combination of ANOVA and Fisher's LSD was used for statistical analysis.

RESULTS

Denucleation (DN condition) significantly reduced the compressive stiffness of the specimen in comparison to the BI condition (p<0.001) (Figure 1). Insertion of implants restored the compressive stiffness of the DN specimen to that of the BI except for H_1 and D_1 implants (p=0.01). The DN and DN-1 conditions were not different (p>0.05).

DISCUSSION

The methodology used here has been previously validated to the literature for the intact condition [2]. The major finding from our previous work was that the hydrogel nucleus implant was able to reproduce the compressive stiffness of the BI condition. In addition, the independent stiffness of the implant alone (2 N/mm) and the DN condition (672 N/mm) did not algebraically sum to the stiffness of the implanted condition (1351 N/mm), indicating a non-linear increase in stiffness. We hypothesized that this behavior was the result of a synergistic interaction between the implant and an intact annulus (AF), where Poisson's ratio of the implant played a major role.

The effect of implant parameters on the compressive stiffness of the IVD at 15% strain is shown (Figure 1). E_1 and E_2 were different (p<0.05), but E_2 and E_3 were not different. There is likely a threshold where the modulus will affect tensioning of the AF, after which, it does nothing to further the stiffness of the system. In the cases of undersize implants (H_1 and D_1), lack of initial interaction between the implant and AF resulted in limited stiffness restoration. In the cases of line-to-line fit and oversize implants, complete restoration (99% of BI) of the stiffness was observed (p>0.6). The oversized implant may be exerting a pre-stress on the AF, pushing it radially outwards. This may mimic the natural load transfer phenomenon, where the intradiscal pressure creates tension in the AF.

SUMMARY

The effect of nucleus implant modulus and 'fit and fill' effect of the nuclear cavity is shown. Implant geometric parameters variations were observed to be more effective than that of implant moduli examined for IVD stiffness restoration.

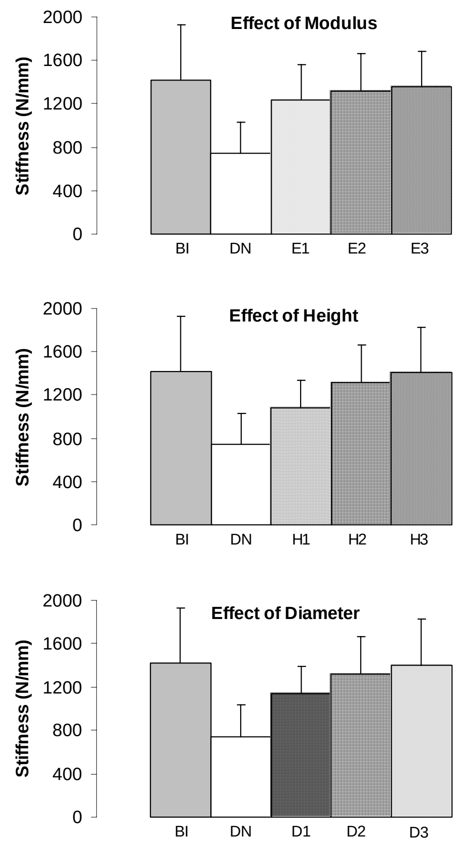

Fig.1: Effect of Nucleus Implant Parameters at 15% compressive strain

REFERENCES

[1] Hickey et al., *Journal of Membrane Science*, 107 (3), 1995 [2] Joshi et al., *Society for Biomaterials*, Annual Meeting 2003, Reno.

ACKNOWLEDGEMENT

NSF Grant # BES 0085383

DYNAMIC CADAVERIC GAIT SIMULATION: STEPS INTO THE FUTURE

Andrew H. Hoskins[1, 2], Andrew R. Fauth[1, 3], and Neil A. Sharkey[1, 3, 4]

[1] Center for Locomotion Studies, [2] Dept. of Mechanical and Nuclear Engineering, and
[3] Dept. of Kinesiology, Pennsylvania State University, University Park, PA, USA
[4] Dept. of Orthopaedics and Rehabilitation, Pennsylvania State University, Hershey, PA, USA
E-mail: nas9@psu.edu www.celos.psu.edu

INTRODUCTION

Experiments utilizing cadaveric models can be designed to investigate a variety of issues related to functional anatomy and orthopedic pathology. Examining isolated components of the foot or ankle is useful but may not provide meaningful insight into the structure's overall *in vivo* function during activities of daily living. Recently cadaver models, consisting of the entire foot and ankle complex, have been developed in order to gain a better understanding of lower extremity biomechanics in health and disease.

This presentation focuses on describing advances incorporated into the latest iteration of a device first described by Sharkey and Hamel in 1998, the Dynamic Gait Simulator (DGS). This unique research tool was integral in completing several investigations into foot and ankle mechanics, including examinations of internal kinematics (Hamel et al., 2003), metatarsal and tibial strain in relation to cyclic overload and stress fractures (Donahue et al., 1999; Donahue et al., 2000) and bone maintenance (Peterman et al., 2001), plantar fascia function (Hamel et al, 2001; Erdemir et al., 2002), ankle trauma and reconstruction (Michelson et al., 2002), as well as issues related to the surgical management of diabetes (Sharkey and Hamel, 2000).

MOTIVATION

The DGS was designed to reproduce lower leg motion as well as the actions of the extrinsic muscles of the foot in simulations of the stance phase of walking. Despite the success of the DGS in providing researchers with a means of conducting invasive procedures on the human foot and ankle under physiologic loading conditions, model shortcomings were of concern and prompted complete redesign of the apparatus.

The motion of the knee joint in the original DGS was recreated with a cam profile that was machined into plates making modifications to the prescribed knee motion arduous and expensive. Furthermore, this lack of flexibility affected simulation fidelity and made it difficult to study specimens of varying dimensions.

In a living person, muscles that cross the knee impart a resistive moment to counteract the moments induced by ground contact, so that the joint does not freely rotate. Rotation of the simulated knee joint in the DGS had no such constraint, therefore reducing the overall fidelity of the model. In particular we noted that the minima in vertical ground reaction force that occurs in midstance was consistently lower than that measured in live subjects.

EXPERIMENTAL DESIGN

The motion of the proximal shank is recreated in the current version of the DGS with a system of three linear actuators as opposed to the cam-carriage mechanism used previously. The three actuators are programmed to recreate the 2-dimensional sagittal kinematics of the proximal fibular head and lateral maleolus during any activity that can be captured using standard gait analysis hardware and techniques. Two of these actuators are used to recreate vertical movement of the proximal shank and constrain its angle as prescribed by data gathered in the gait lab. The third actuator reproduces the motion of the knee in the direction of travel (anterior progression in the sagittal plane)

This architecture offers the distinct advantage over the previous version by allowing researchers to investigate the effects of variations in lower leg kinematics quickly and easily. Kinematic profiles from different sized individuals under different conditions can be quickly loaded into the control algorithm to better match kinematics to specimen dimensions. This is an important improvement because of the sensitivity of internal loading to mismatches between kinematics and specimen dimensions. In addition, this feature increases the versatility of the machine as it is no longer constrained to simulate just walking. Future research is likely to investigate internal biomechanics as a function of running and jumping.

As in the original DGS, the latest version incorporates the actions of six different extrinsic muscles or muscle groups. The muscles have been grouped based on EMG measures of activation throughout the stance phase of walking. The protocol used to recreate the muscle forces incorporates independent force feedback control of the six muscle groups, as described in detail by Sharkey and Hamel in 1998. Our new iteration uses the same control strategy but the actuators used to simulate muscle contraction have been removed from the carriage assembly to reduce inertial effects and are now linked to the extrinsic tendons through cables. Control hardware has also been upgraded and improved.

RESULTS

Figure 1 compares GRFs produced by the new simulator with those generated *in vivo* by a subject whose lower leg kinematics were used to control the simulation.

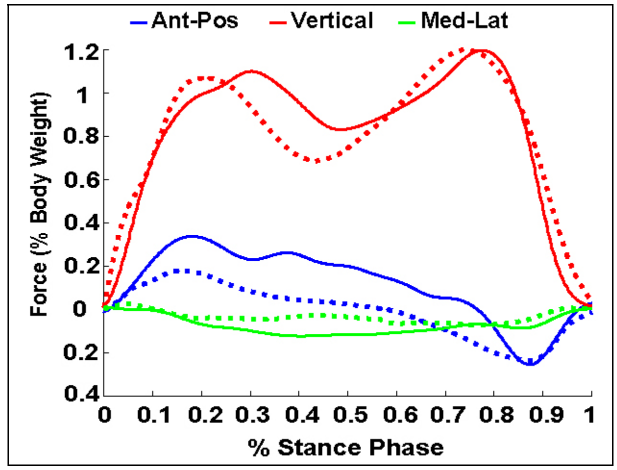

Figure 1: GRFs from a walking simulation (solid) and an *in vivo* walking trial (dashed).

SUMMARY

Computer controlled actuators incorporated into the latest version of the DGS have increased the versatility and fidelity of dynamic *in vitro* simulations of the human lower extremity.

REFERENCES

Donahue, SW, et al. (2000) *Bone*, **27**, 827.

Donahue, SW, et al. (1999) *JBJS*, **81A**, 1236.

Erdemir, A, et al. (2002) *J. Biomech*, **35**, 857.

Hamel, AJ, et al. (2003) *Gait and Posture*, (In Press)

Hamel, AJ, et al. (2001) *Clin Orth,* 393, 326.

Michelson, JD, et al. (2002) *JBJS,* **84A**, 2029.

Peterman, MM, et al. (2001) *J. Biomech*, **34**, 693.

Sharkey, NA and Hamel, AJ. (1998) *Clin Biomech*, **13**, 420.

Sharkey, NA and Hamel, AJ. (2000) *46th Orth. Res Soc. Meet.*, 0192.

ACKNOWLEDGEMENTS

This work was partially supported by grants from NIH (R01HD3744302) and NASA (NAG9-1264)

THE EFFECTS OF AN OVER-THE-COUNTER ORTHOTIC ON LOWER EXTREMITY KINEMATICS IN MALE AND FEMALE RECREATIONAL RUNNERS

Ahmed M. Alzahrani, Aric J. Warren, and Robert W. Gregory

Biomechanics Laboratory, Dept. of Health, Sport and Exercise Sciences, University of Kansas, Lawrence, KS, USA
E-mail: amz5582@ku.edu Web: www.soe.ku.edu/hses/

INTRODUCTION

Abnormal foot mechanics during the stance phase of running may affect the kinematics of the lower extremities and predispose an individual to injuries of the foot, ankle, and knee. Custom made foot orthotics are often prescribed to correct abnormal mechanics during running by restoring dynamic stability to the closed chain of the lower extremity. However, custom made orthotics are expensive and must be made by a specially trained professional. An alternative to custom made orthotics are several brands of over-the-counter orthotics. However, there has been no research to examine the efficacy of using an over-the-counter orthotic to correct abnormal gait mechanics. One of the purposes of this study was to examine the effects of an over-the-counter orthotic on ankle and knee joint kinematics during running in individuals identified as excessive pronators.

In addition, females are reported to demonstrate different lower extremity mechanics during running as compared to males. As a result, females are more likely to sustain injuries due to running than their male counterparts. The second purpose of this study was to determine if there are gender specific effects of orthotics on ankle and knee joint kinematics during running, as well as to determine if orthotics are more effective in reducing abnormal gait mechanics in female versus male runners.

METHODS

Twenty college-age recreational runners (10 males, 10 females) identified as being excessive pronators participated in this study. Excessive pronation was defined as those individual with a navicular drop of greater than or equal to 9 mm.

Subjects were required to perform two testing sessions in which they ran with and without orthotics. The orthotic used in this study is a commercially available over-the-counter orthotic (Flat Foot Products, Marathon Shoe Co.). In addition, all subjects used an identical pair of running shoes for both testing sessions (Air Max Moto II, Nike Inc.)

During both testing sessions, the subjects ran on a treadmill at a velocity of 3.35 m/s for 15 min. A three-dimensional motion capture system (Visualeyez VZ 3000, PhoeniX Technologies Inc.) was used to record the position of light emitting diodes placed on the foot, shank, and thigh segments at 100 Hz for 50 complete gait cycles during the last 5 min of each session.

Range of motion, peak angular velocity, and peak angular acceleration at the ankle and knee joints were calculated for the frontal, sagittal, and transverse planes of motion. A two-way ANOVA was used to assess the effects of the orthotic and gender on all kinematic variables.

RESULTS AND DISCUSSION

No differences between the orthotic and non-orthotic conditions across gender were found for ankle joint kinematics (range of motion, peak angular velocity, and peak angular acceleration) in the frontal, sagittal, and transverse planes of motion. One finding of note is that there was no difference in the amount of pronation between the orthotic condition (4.1±2.7°) and the non-orthotic condition (3.5±2.8°). This contradicts the common finding that soft orthotics reduce pronation (Eng and Pierrynowski, 1994; Smith et al., 1986).

In addition, no differences between the orthotic and non-orthotic conditions across gender were found for knee joint kinematics (range of motion, peak angular velocity, and peak angular acceleration) in the frontal and sagittal planes of motion. However, there was significantly greater (p<0.05) transverse plane motion in the orthotic condition (4.6±2.9°) as compared to the non-orthotic condition (1.7±1.2°). Increased knee joint range of motion during running when using soft orthotics has also been documented by Eng and Pierrynowski (1994).

No significant differences in lower extremity kinematics between males and females were found; this contradicts the findings of Ferber et al. (2003). However, there was a strong trend for greater pronation in females than males (7.2±1.5° vs. 4.0±1.4°). Anatomical differences at the hip and knee between genders may predispose females to increased pronation.

Finally, it should be noted that there were no significant interaction effects between gender and orthotics on ankle and knee joint kinematics. Therefore, orthotics do not have a gender specific effect on lower extremity mechanics during running.

SUMMARY

The results show that the over-the-counter orthotic used in this study was not effective in altering the lower extremity kinematics in male and female recreational runners identified as excessive pronators. It can be concluded that over-the-counter orthotics provide mostly cushioning and little, if any, functional control. For individuals with gait pathomechanics, the use of a custom made rigid or semi-rigid orthotic may be necessary.

Also, while there are differences in lower extremity mechanics between male and female runners, there are no gender specific effects of orthotics on ankle and knee joint kinematics during running. Therefore, orthotics are no more effective in reducing abnormal gait mechanics in females versus males during running.

REFERENCES

Eng, J.J., Pierrynowski, M.R. (1994). *Physical Therapy*, **74**, 836-843.

Ferber, R. (2003). *Clinical Biomechanics*, **18**, 350-357.

Smith, L.S., et al. (1986). *Journal of the American Podiatric Medical Association*, **76**, 227-233.

ACKNOWLEDGEMENTS

This study was funded by a grant from the Mid-America Athletic Trainers Association. The orthotics used in this study were provided by Marathon Shoe Co. The authors would like to thank Dorian Amend and Matt Stensrud for assistance with data acquisition and analysis.

SPINAL INSTABILITY DUE TO SIMULATED FRONTAL IMPACTS

Adam M. Pearson, Manohar M. Panjabi, Paul C. Ivancic, Shigeki Ito,
Bryan W. Cunningham, Wolfgang Rubin, S. Elena Gimenez

Biomechanics Research Laboratory, Yale University School of Medicine, New Haven, CT, USA
E-mail: paul.ivancic@yale.edu

INTRODUCTION

Current imaging modalities are unable to detect subfailure soft tissue injuries that occur during automotive collisions. The purpose of this study was to identify, quantify and determine the mode of soft tissue subfailure injuries sustained during simulated frontal impacts.

METHODS

Six fresh-frozen human cervical spines (occiput to T1) were dissected of all non-osteoligamentous soft tissues. Motion tracking flags were attached to each vertebra. The whole cervical spine specimen with muscle force replication and surrogate head was used to simulate frontal impacts at 4, 6, 8, and 10 g T1 accelerations (**Figure 1**).

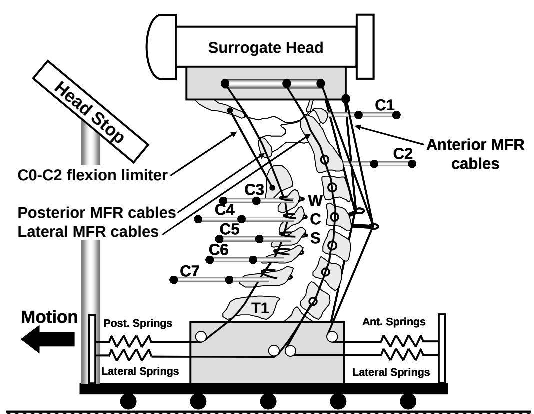

Figure 1. The whole cervical spine (WCS) model with muscle force replication (MFR) subjected to frontal impact simulation.

Sagittal flexibility testing with physiological 1.5 Nm pure moments was performed before and after each frontal impact. Flexibility parameters of neutral zone (NZ) and range of motion (ROM) were determined for all intervertebral levels. ANOVA and Bonferonni post-hoc tests were used to determine significant increases in the flexibility parameters.

The Injury Potential was defined as the relative percentage increase in a flexibility parameter following the frontal impact ($Flex_{Frontal\ Impact}$) as compared to the corresponding value after the 2 g dynamic preconditioning ($Flex_{2g}$) (Panjabi et al., 1998). Expressed mathematically, it was:
Injury Potential (%) =
$(Flex_{Frontal\ Impact} - Flex_{2g})*100/Flex_{2g}$.

Spinal injury was defined as a significant increase ($p<0.05$) in the intervertebral flexibility of the cervical spine due to simulated frontal impact. The spinal injury threshold acceleration was the lowest T1 horizontal peak acceleration that caused an intervertebral flexibility increase ($p<0.05$).

RESULTS

At the 8 g frontal impact simulation, the injury threshold was noted in the C6-C7 flexion NZ and ROM. Following the 10 g impact, significant increases in flexion flexibility parameters were observed at C2-C3, C3-C4, C4-C5, and C6-C7.

The Injury Potential parameters illustrate the relative sensitivity of the NZ as compared to the ROM (**Figure 2**).

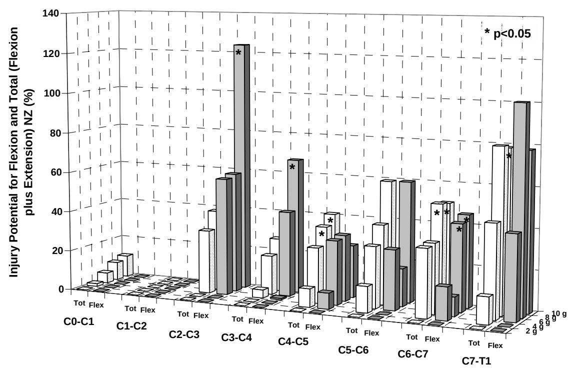

A

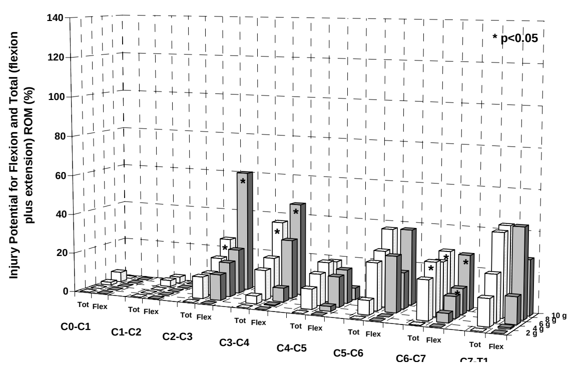

B

Figure 2. Average Injury Potentials for flexion (Flex) and total (Tot) (**A**) neutral zones and (**B**) ranges of motion for each intervertebral level (C0-C1 to C7-T1) due to frontal impact simulations. Statistically significant increases ($p< 0.05$) are indicated by *.

Although both NZ and ROM showed significant increases over physiological limits beginning at 8 g, NZ detected injury at more intervertebral levels than ROM. Total (flexion plus extension) NZ detected injury at 10 g in all levels except for C0-C1, C1-C2 and C5-C6 (**Figure 2A**). In contrast, at 10 g, total ROM detected injury at only three intervertebral levels (C2-C3, C3-C4 and C6-C7) (**Figure 2B**). Overall, the injuries involved the middle and lower cervical spine, and excluded C5-C6 as well as the upper cervical spine levels of C0-C1 and C1-C2. The Injury Potential parameters also demonstrated that increases in total (flexion plus extension) NZ and ROM were mirrored closely by increases in flexion NZ and ROM. This indicated that the predominant mode of injury during simulated frontal impact was flexion.

DISCUSSION AND SUMMARY

Subfailure injuries may lead to chronic pain due to accelerated degeneration or altered loading via clinical instability. The current study identified the soft tissue injury threshold using flexibility testing of the whole cervical spine model with muscle force replication before and after simulated incremental frontal impact at peak accelerations of 4, 6, 8, and 10 g.

The T1 horizontal acceleration of 8 g was the injury threshold acceleration, as indicated by increases over physiological limits of flexion NZ and ROM. The results presented here may aid in developing improved methods of detecting and treating clinically occult injuries of the cervical spine. Future clinical and biomechanical studies are necessary for an improved understanding of the relation of subfailure injury to chronic pain.

REFERENCES

Panjabi, M.M.et al. (1998). *Eur Spine J,* **7**, 484-492.

ACKNOWLEDGEMENTS

This research was supported by NIH Grant 1 R01 AR45452 1A2 and the Doris Duke Charitable Foundation.

A ROBOT-ASSISTED MEASURE OF FINGER JOINT STIFFNESS

Gregg Davis, Shouchen Dun, and Zong-Ming Li

Hand Research Laboratory, Departments of Orthopaedic Surgery and Bioengineering
University of Pittsburgh, PA, USA
E-mail: zmli@pitt.edu

INTRODUCTION

Excessive finger joint stiffness commonly occurs in individuals suffering tightness of the intrinsic muscles (e.g. the lumbrical). Clinicians routinely evaluate intrinsic tightness by estimating finger joint stiffness with the Bunnell-Littler test (Bunnell, 1953). This test involves an evaluation of proximal interphalangeal (PIP) joint resistance against a manually applied force at both full extension and full flexion of the metacarphalangeal (MCP) joint. However, the Bunnell-Littler test is subjective and largely depends on the experience and skill of the tester. The objective of this study was to develop a quantitative approximation of the Bunnell-Littler test.

METHODS

A robot-assisted testing apparatus (Figure 1) was constructed to collect passive PIP joint torque-angle data of the index finger for extended (0°) and flexed (60°) MCP joint positions. A low payload (3 kg) industrial robotic arm (KR 3, KUKA Robotics Corporation, Augsburg, Germany) induced cyclic motion of the PIP joint, and a miniature 6-DOF force/torque transducer (Nano17, ATI Industrial Automation, NC, USA) attached to the end-effecter of the robot arm measured the passive PIP joint torque. A thermoplastic splint maintained a functionally neutral wrist angle of 15° extension. A lockable linkage with a finger clamp was mounted on the splint to prescribe the desired MCP joint angles.

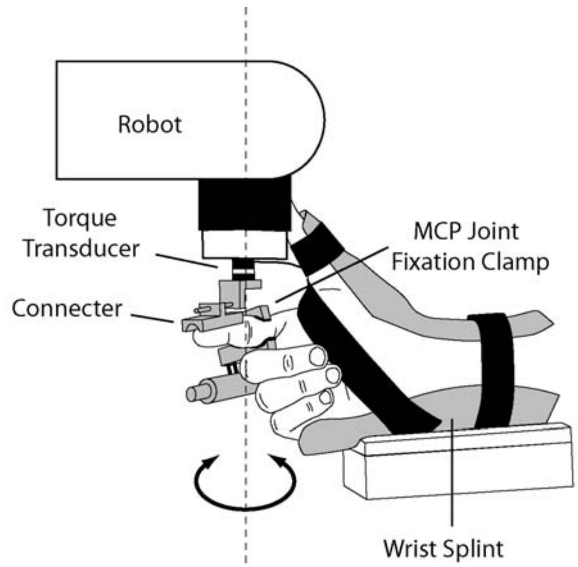

Figure 1. Schematic of experimental setup. Aluminum safety cage not shown.

Six male subjects aged 28 ± 4 years (mean ± SD) without diagnosed intrinsic muscle tightness participated in this study with IRB approval. Each subject was tested once at MCP extension and flexion in a random order. The angular motion was applied to the PIP joint in a cyclic manner between full extension (0°) and 90° of flexion at 7° per second. Each trial consisted of twenty flexion/extension cycles. Throughout testing, the subject was instructed to remain relaxed and offer no voluntary resistance to the induced motion.

For each trial, the first ten cycles of torque-angle data were considered preconditioning, and the last ten cycles were averaged. The equilibrium angle of the PIP joint was determined by the zero torque intercept of the flexion curve. PIP joint stiffness was calculated as the slope of the induced flexion curve in a 20° window starting from the equilibrium angle (Figure 2). Paired t-tests were performed for the statistical analyses with a significance level of α = 0.05.

RESULTS AND DISCUSSION

The averaged torque-angle relationship of the six subjects is shown in Figure 2. The results include induced flexion and extension curves at each MCP joint position. The curves at both MCP positions show distinct hysteresis. The equilibrium angle changed significantly from 52.6° ± 6.9° with the MCP joint extended at 0° to 29.4° ± 4.0° with the MCP joint flexed at 60° ($p < 0.001$). This may be due to passive tightening of the PIP joint extensors as the MCP joint assumes a flexed position.

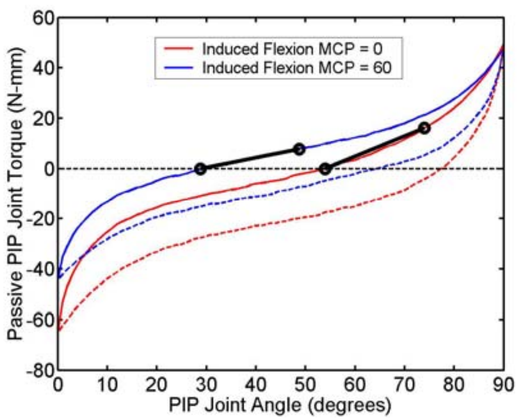

Figure 2: Averaged (n = 6) PIP torque-angle data for induced flexion-extension at MCP angles of 0° and 60°.

The PIP joint showed a significant increase in stiffness from 0.40 ± 0.11 N-mm/degree with the MCP joint flexed at 60° to 0.74 ± 0.23 N-mm/degree with the MCP joint extended at 0° ($p < 0.01$). This increase (85%) is most likely due to a passive tightening of the intrinsic muscles as the MCP assumes an extended position, because passive tightening of the intrinsic muscles provides an additional PIP extension torque due to their attachment to the extensor hood via the lateral bands (Figure 3).

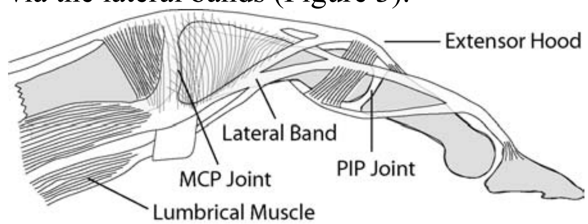

Figure 3. Illustration of relevant finger anatomy.

Our results support the underlying theory behind the Bunnell-Littler test. In future studies, we will compare PIP joint stiffness between asymptomatic hands and hands with intrinsic muscle tightness. We expect to quantify a much higher elevation in PIP joint stiffness when the MCP joint changes from flexion to extension for hands with intrinsic tightness. Additional studies will examine the effectiveness of surgical procedures of intrinsic muscle release.

SUMMARY

We have successfully developed a quantitative measure of PIP joint stiffness and framed it within a clinical context. PIP joint stiffness is dependant on the MCP joint angle, supporting the regulation role of the intrinsic muscles on PIP joint stiffness. Our method of quantifying finger joint stiffness has the potential to accurately evaluate the level of intrinsic muscle tightness.

REFERENCES

Bunnell S, (1953). *J Bone & Joint Surg*; 35-A(1): 88-101.

ACKNOWLEDGEMENTS

This study was supported by the Pittsburgh Foundation, Albert B. Ferguson, M.D., Orthopaedic Fund.

EFFECTS OF CHANGING PROTOCOL, GRADE, AND DIRECTION ON THE PREFERRED GAIT TRANSITION SPEED DURING HUMAN LOCOMOTION

Alan Hreljac, Rodney Imamura, W. Brent Edwards, and Escamilla, R. F.

Kinesiology and Health Science Department, California State University, Sacramento
E-Mail: ahreljac@hhs4.hhs.csus.edu

INTRODUCTION

A gait transition during human terrestrial locomotion naturally occurs as the speed of walking increases or the speed of running decreases. Although transition speeds reported by various researchers are relatively consistent, the difference between the walk-run (WR) and the run-walk (RW) transition speed varies considerably, ranging from -0.08 $m \cdot s^{-1}$ (Turvey et al., 1999) to 0.24 $m \cdot s^{-1}$ (Beuter & Lefebvre, 1988). The negative sign indicates that RW was greater than WR. The discrepancy in the amount of hysteresis reported may be partly due to methodological differences between the various studies. In six studies (e.g. Diedrich & Warren, 1998; Thorstensson & Roberthson, 1987) in which a constantly accelerating treadmill was utilized, an average hysteresis of 0.10 $m \cdot s^{-1}$ was reported. In six studies in which the treadmill speed was increased incrementally (e.g. Hreljac, 1995; Raynor et al., 2002), an average hysteresis of 0.04 $m \cdot s^{-1}$ was reported. No studies used both protocols, while several other studies did not report both WR and RW. Another factor which has an effect on WR and RW is the treadmill inclination. Increasing grade appears to decrease hysteresis (e.g. Diedrich & Warren, 1998). The purpose of this study was to determine whether hysteresis is affected by the protocol (continuous or incremental) or by the treadmill inclination.

METHODS

The preferred WR and RW of nine young, healthy subjects (6 males, 3 females) who were familiar with treadmill locomotion was found using two different protocols (continuous and incremental) and three inclination conditions (0%, 10%, and 15% grades). Conditions were randomly ordered, and repeated at least twice. To find WR using the continuous protocol, the treadmill was set to a slow walking speed, and continually accelerated until the subject was running. The instant of WR was determined from observation of a sagittal plane video recording (240 Hz), and defined to occur at toeoff of the step during which the subject switched from an inverted pendulum to a bouncing ball model. Treadmill speed at WR was found by digitizing a marker on the treadmill. To find RW, the process was repeated in reverse, with the RW defined to occur at heelstrike of the first walking step.

To determine WR using the incremental protocol, the treadmill was initially set to a comfortable walking speed. Subjects were given a 30 s decision period to determine whether walking or running was the preferred gait at this speed. After stopping the treadmill, subjects dismounted before the treadmill speed was increased by 0.2 mph ($\approx$0.1 $m \cdot s^{-1}$), and the subject remounted. This procedure was repeated until a speed was reached at which the subject asserted that running was the preferred gait at that speed. The procedure was repeated in reverse for determination of RW. A repeated measures ANOVA tested for differences in speed between protocols, transition direction, and treadmill inclination ($p < 0.05$).

RESULTS AND DISCUSSION

Regardless of protocol, both WR and RW decreased significantly as inclination increased. At the 10% and 15% conditions, WR and RW were greater with the continuous than the incremental protocol (Figure 1), but there was no difference between WR and RW at the 0% condition.

With the incremental protocol, there was a significant difference between WR and RW at all inclination conditions. The differences between WR and RW (0.08, 0.08, and 0.09 $m \cdot s^{-1}$) was consistent with previous studies which used this protocol (e.g. Hreljac, 1995), and within the range of what was expected. Because of the stepping nature of this protocol, the expected amount of hysteresis would be equal to the speed increments employed. For all inclination conditions, speed increments were the same (≈ 0.09 $m \cdot s^{-1}$), so it is not surprising that hysteresis was unaffected by inclination with the step protocol.

With the continuous protocol, there was a significant difference between WR and RW at the 0% and 10% conditions, but no significant hysteresis at the 15% condition. This is consistent with the results of Diedrich and Warren (1998) who reported that the hysteresis effect decreased with increasing inclination when using a continuous protocol.

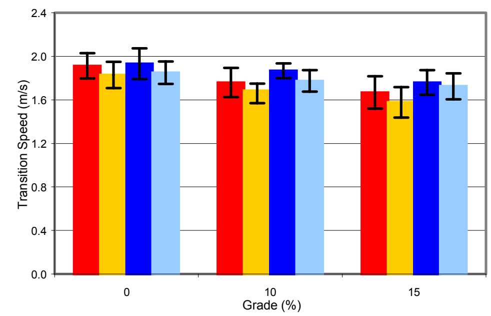

Figure 1: Preferred transition speed for Step-WR, Step-RW, Cont-WR, and Cont-RW (left to right bars) at each of the three inclination conditions.

SUMMARY

The results of this study suggest that the choice of protocol makes little difference in the determination of the preferred transition speed or in the amount of hysteresis found when using a level treadmill condition. When using inclined conditions, however, researchers should be aware that the choice of protocol may affect both the preferred transition speeds and the amount of hysteresis. Although it was not tested in this study, the amount of hysteresis found when using the incremental protocol appears to be related to the speed increments used.

REFERENCES

Beuter, A., Lefevbre, R. (1988). *Can. J. Appl. Sports Sci.,* **13**, 247-253.

Diedrich, F.J., Warren, W.H. (1998). *J. Mot. Behav.*, **30**, 60-78.

Hreljac, A. (1995). *J. Biomech.*, **28**, 669-677.

Raynor, A.J. et al. (2002). *Hum. Mov. Sci.*, **21**, 785-805.

Thorstensson, A., Roberthson,H. (1987). *Acta Physiol. Scand*., **131**, 211-213.

Turvey, M.T. et al. (1999). *J. Mot. Behav.*, **31**, 265-78.

THE ROLE OF THE VASTUS MEDIALIS AND VASTUS LATERALIS IN MEDIAL-LATERAL KNEE JOINT STABILITY

Alex E. Albertini [1] and Yasin Y. Dhaher [2]
[1] Biomedical Engineering, Northwestern University, Evanston, IL, USA
[2] Sensory Motor Performance Program, Rehabilitation Institute of Chicago, Chicago, IL, USA
Email: y-dhaher@northwestern.edu Web: www.smpp.northwestern.edu

INTRODUCTION

It has been shown that activation of some or all of the quadriceps with the proper distribution would alter the patellar kinematics [1]. Change of patellar kinematics may influence the individual quadriceps moment output at the knee joint [2]. The goal of our study is to examine the effect of patellar kinematics on the role of individual quadriceps muscles in medial-lateral control of the knee. To achieve this, patellar kinematics are changed by providing different background activation of all quadriceps prior to the selective electrical stimulation of an individual knee muscle. The quadriceps muscles examined were the vastus lateralis (VL) and the vastus medialis (VM). The resulting abduction/adduction to extension moment ratio, obtained under the superimposed selective stimulation, is then compared across the different background activation levels.

METHODS

Six healthy young males with no history of knee degeneration or neurological diseases participated in the study (25.5 +/- 3.9 yrs; 70.9 +/- 4.5 in; 174.7 +/- 34.2 lbs). The subject was seated upright with the knee flexed at an angle of 20° from a fully extended position. Twenty degrees was selected because the vasti muscles are most active between 10 and 20° of flexion. Prior to each experiment, the subject's Maximum Voluntary Contraction (MVC) extension moment (M_{ext}^{MVC}) was recorded using a six degree-of-freedom (6-DOF) load cell. Prior to the electrical stimulation experiments, subjects were asked to generate an extension moment (M_{ext}) as a percentage of their MVC extension moment using a visual display of the desired level $(M_{ext}^{back} = 100 \cdot M_{ext} / M_{ext}^{MVC})$. Eight pre-activation levels (0 to 30-35% of M_{ext}^{MVC}) were used. Selective electrical stimulation was applied to the VM and VL in alternating trials, with the resulting forces and moments measured using the 6-DOF load cell. The load cell was centered at the lateral femoral condyle of the knee with its long axis aligned with the transcondylar line of the femur. Two sterilized bipolar intramuscular electrodes (50µm) were inserted using 27 gauge hypodermic needles. The interelectrode distances and the electrode locations were confirmed by stimulating the muscle and verifying that the appropriate muscle contraction had occurred. The stimulus intensity was chosen to maintain sufficient muscle force with minimal discomfort. To insure selectivity of the electrical stimulus, EMG activity of the neighboring muscles was recorded with intramuscular electrodes to detect the maximum level of current that could be used with minimal electrical spread. The stimulus profile was a rectangular mono-phasic constant current with 0.3 ms pulse duration. Train duration was 500 ms with a 20 ms interval, repeated every 2 s. For each subject, at least fifteen contraction cycles were obtained. The three-dimensional moments measured at the load cell center were transformed to the center of the knee joint, defined as the midpoint of the transcondylar line of the femur, and the adduction/abduction moment to the extension moment ratio was then computed.

RESULTS AND DISCUSSION

To assess the effect of changing patellar kinematics on the medial-lateral stabilizing role of the quadriceps, moment ratio was computed from knee moments measured as a result of the selective electrical stimulation of lateral (VL) and medial (VM) muscles. In figures 1 and 2, a positive ratio indicates an abduction torque production. The data shown in Figures 1 and 2 indicate that both VM and VL are capable of generating sufficient off-axis moments. The VL moment ratio was consistent in its trend and sign across all six subjects (data not shown). The magnitude of the moment ratio increased systematically with increasing of M_{ext}^{back} (see Figure 1). Across all subjects, change of the patellar kinematics induced by the different M_{ext}^{back} had no impact on the fundamental role of VL. On the other hand, the medial-lateral role of the VM muscle varied significantly across subjects. For example, while the moment ratios obtained on S1 and S2 were similar in sign and magnitude at low M_{ext}^{back}, they were significantly different at higher levels of M_{ext}^{back} (see Figure 2). At higher background activations, only modest variation of the S2 moment ratio occurred while a significant decrease of the same ratio was evident for S1. In fact, moment ratio data of S1 reversed sign, indicating that at higher pre-activation levels, the VM muscle reversed role from an abductor to an adductor of the knee joint. Contrary to the S1 and S2 data shown in Figure 2, in other subjects, activation of VM at rest generated adduction moment and moved towards abduction as the M_{ext}^{back} levels were increased (data not shown).

SUMMARY

Across all subjects, the VL was found to be predominantly an abductor of the knee joint. These results were not as clear for the traditionally known adductor of the knee, the VM muscle. Our preliminary data indicates a potential role reversal of the VM as a function of the patellar kinematics or background extension moment. The cause of across subject variability in the role of the VM is not yet clear from the current data. This matter could potentially be addressed with a larger number of subjects.

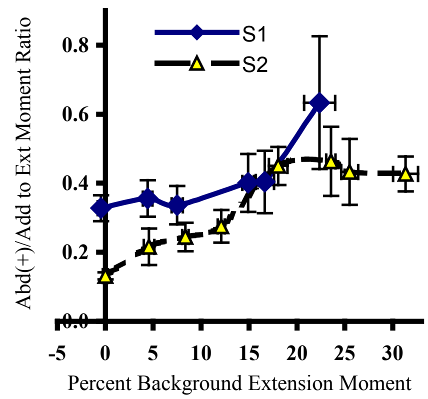

Figure 1: VL moment ratio obtained on two representative subjects, S1 & S2.

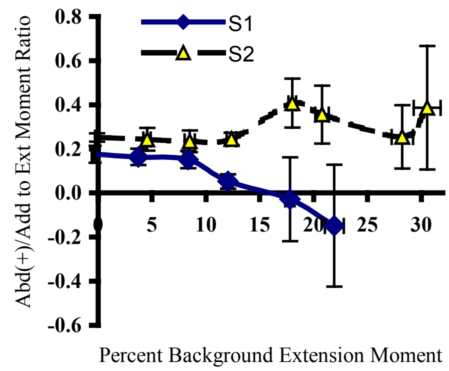

Figure 2: VM moment ratio obtained on two representative subjects, S1 & S2.

ACKNOWLEDGEMENTS

This study was funded by the Whitaker Foundation

REFERENCES

1.Goh, J.C., et al. Journal of Bone & Joint Surgery - British Volume, 1995. **77**(2): p. 225-31.
2.Lafortune, M. and P. Cavanagh, eds. International Series on Biomechanics, ed. B. Jonsson. Vol. Biomechanics X-A. 1987, Human Kinetics Publishers, Champaign, Illinois. 337-341.

COMPUTATIONAL ASSESSMENT OF CONSTRAINT IN POSTERIOR-STABILIZED TOTAL KNEE REPLACEMENTS

Matthew F. Moran[1,2], Safia Bhimji[5], Joseph Racanelli[5] and Stephen J. Piazza[1,2,3,4]

[1]Center for Locomotion Studies and Departments of [2]Kinesiology, [3]Mechanical Engineering, and [4]Orthopaedics and Rehabilitation, The Pennsylvania State University, University Park, PA
[5]Stryker Orthopedics, Mahwah, NJ
E-mail: *steve-piazza@psu.edu* Web: *www.celos.psu.edu*

INTRODUCTION

The American Society of Testing Materials (ASTM) provides a standard mechanical testing protocol of total knee implants to determine constraint criteria. Posterior-stabilized (PS) implants are constrained in the anterior-posterior (AP) direction by a cam and post mechanism and rotationally by curved bearing surfaces.

Computational prediction of constraint within total knee implants has two potential advantages over standard bench-top testing. First, inherent experimental inaccuracies and variation in testing devices between facilities may invalidate implant comparisons. Second, a computational model that accurately predicts constraint could be used as a design tool before resources are spent in prototyping and physical testing of implants. Similar computational approaches have been used to predict wear and constraint within knee implants in a mechanical tester (1,2). The purpose of this study was to develop a computer model that could predict the constraint demonstrated by a PS knee implant in a mechanical knee tester undergoing standard ASTM protocol (3).

METHODS

A Duracon PS knee implant (Stryker Orthopedics) was mechanically tested for AP and rotational constraint at 0º, 30º, 60º, 90º, and 120º flexion in an MTS 858 Bionix Test Frame. For the AP trials the tibial insert was cycled at a frequency of 0.125 Hz from neutral position to peak posterior/anterior displacement and the required force to produce this motion was collected. For the rotational trials, the tibial insert was locked in place and the femoral component was rotated at the same frequency through ±20º internal/external rotation. Similarly, the required torque to produce this motion was collected. In all trials the femoral component was free to move in varus/valgus and to translate vertically.

The experimental setup was modeled as 7 segments, two of which were the femoral and tibial implants. Segmental masses, geometry, damping and compliance parameters were measured and prescribed within the model. Manufacturer supplied CAD files defined the implant surfaces, and joint contact was implemented using a rigid body spring model (4). Polynomial and Fourier fitted curves were used to model the compressive load that varied from 0 – 300N throughout the trials. Prescribed motion for each simulation matched the corresponding experimental trial.

Equations of motion were formulated and integrated forward in time via the SIMM/Dynamic Pipeline (Musculographics, Inc.) and SD/FAST (Parametric Tech Corp.) software packages. Custom MATLAB (Mathworks Inc.) software was used to compute root mean square (RMS) differences between model and experimental forces and torques.

RESULTS AND DISCUSSION

Computer model constraint forces and torques for both AP and rotational simulations, respectively, compared favorably to experimental outputs (Figure 1). The curves had qualitatively similar shapes, but since contact friction was not included the computer model forces and torques were slightly less than the experimental values. The RMS differences between model and experimental averaged 31.8 N for AP tests and 1080.3 N·mm for rotational tests.

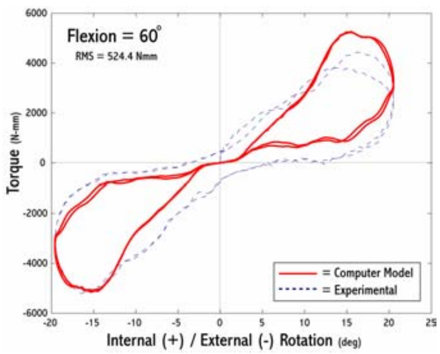

Figure 1. Rotational constraint comparison for a given flexion angle. Qualitatively the curves matched well for all flexion angles.

The purpose of the ASTM standard is to build a database of constraint criteria for the unbiased comparison of total knee implants (3). Such a database could serve as a clinical tool in the selection of implants for specific patients based upon constraint criteria. However, inherent inaccuracies and artifacts present in bench-top experiments could bias this database. In the present setup, there was found to be fixture compliance within the vertical testing arm. Computer simulations of AP constraint trials without this measured fixture compliance resulted in significantly larger forces when the cam contacted the posterior aspect of the post (Figure 2A). Similarly all simulations were sensitive to the initial starting or "neutral" point (Figure 2B). Computer models such as this are promising as a means for meaningfully comparing constraint differences between implants because they are free from experimental artifacts.

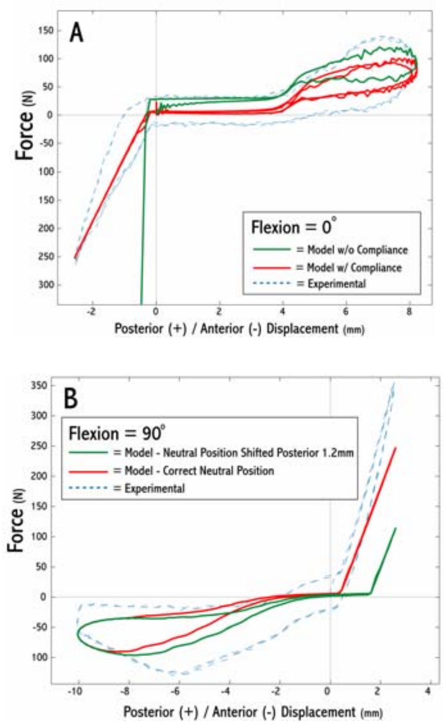

Figure 2. Sensitivity to AP fixture compliance (**A**) and to starting "neutral" position (**B**) on model constraint force during an AP simulation.

REFERENCES

1. Fregly et al. (2003). *J Biomech*, 36: 1659-1668.
2. Sathasivam et al. (1997). *J Biomech*, 30: 177-184.
3. "F1223-03 Standard Test Method for Determination of Total Knee Replacement Constraint," ASTM International.
4. Li et al. (1997). *J Biomech*, 30: 635-638

ACKNOWLEDGMENTS

This work was supported by:

- ISB (*Matching Dissertation Grant*)
- PSU (*Academic Computing Fellowship*)
- Stryker Orthopedics

FINITE ELEMENT ANALYSIS OF HUMAN FACET JOINT CAPSULE DURING PHYSIOLOGICAL MOTIONS FOR TWO LUMBAR MOTION SEGMENTS

Anita C. Saldanha[1], Yi-Xian Qin[1], Vijay K. Goel[2], Partap S. Khalsa[1]

[1]Biomedical Engineering Department, Stony Brook University, Stony Brook, NY, 11794 USA
Email: Partap.Khalsa@stonybrook.edu

[2]Bioengineering Department, University of Toledo, Toledo, OH, 43606 USA

INTRODUCTION

Eighty percent of Americans will experience low back pain (LBP) in their lifetime [Cassidy, 1998]; for the majority of LBP patients, the etiology continues to be poorly understood. A known cause of LBP is the activation of mechano-nociceptors innervating lumbar facet joint capsules. In isolated, but intact, nerve – capsule (as well as nerve – skin & nerve – muscle) mechanoreceptors and nociceptors appear to encode the local stress rather than the local strain during loading [Khalsa 1997].

In-vivo, it is virtually impossible to directly measure capsule stress; however, robust estimates of capsule stress are possible using the finite element method (FEM). Previous FEM models of the lumbar spine have not included accurate representations (geometry or material properties) of the facet joint (FJ) and its posterior capsule. The purpose of this study was to create a geometrically correct FEM model of the lumbar FJ, incorporate it into an existing lumbar spine model [Goel, 1995], and subject it to normal physiological loading conditions.

METHODS

Model Geometry: 13 1-mm high-resolution computed tomography (CT) images of the left L_{3-4} FJ from a lumbar spine were used to define the non-linear geometry of the FJ in the model. Custom software was written in PVWAVE (Visual Numerics Inc.) to perform pre-processing for FEM mesh development. The perimeter nodal points for both the superior and inferior facet processes served as a framework to build a surface mesh in ABAQUS (v. 6.3, HKS, Inc.). ABAQUS's automatic mesh generating algorithm was used to build slices consisting of linear elastic elements (continuum 3D, 8-noded, brick elements).

In MATLAB (ver. 6.5; The MathWorks Inc.), the articular cartilage and capsular ligament perimeter geometry was developed based on the superior and inferior process geometry, and subsequently modeled as linear elastic and 3-D hybrid elastic elements in ABAQUS. The 3D mesh of the facet joint was then incorporated into the L_{3-4} and the L_{4-5} joint levels of a previously validated L_{3-5} spine model [Goel, 1995].

Material Properties: Linear isotropic material properties were assigned to the vertebrae, intervertebral disks, FJ (3.5GPa, ν=0.25), including articular cartilage and FJ capsule (6MPa, ν=0.3). All other ligaments were modeled as hypoelastic materials.

Boundary and loading conditions: The nodes along the symmetry line on the L_5 inferior surface (X-axis for flexion/extension and Y-axis for bending) were fixed in all directions. Displacements of 7, 14, 20 and 28 mm, which correspond to 10, 20, 30 and 40 mm at the T_{12} vertebra, were applied along the line of symmetry nodes on the top surface of the L_3 vertebra to simulate flexion, extension, left and right lateral bending.

RESULTS AND DISCUSSION

A 3D FEM mesh of the superior and inferior processes, articular cartilage, and capsule ligament, consisting of 2988 elements and 3882 nodes was constructed (Fig. 1). This geometry was then incorporated into an existing lumbar spine model (Fig. 2).

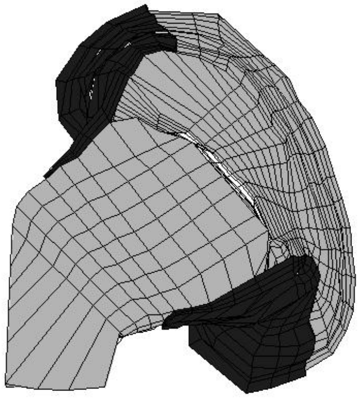

Fig. 1: FEM of facet joint capsule consisting of bony facets (gray), capsule ligament (black) and cartilage (white).

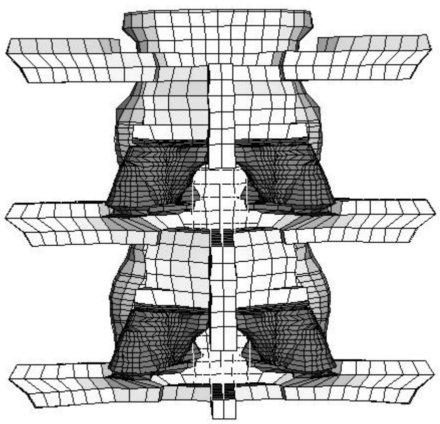

Fig. 2: Lumbar spine model (white) with new facet geometry (gray) at the L_{3-4}, and L_{4-5} joint levels.

The FE model representing the intact lumbar spinal unit was validated using FJ capsule strain data from a prior study in cadaveric lumbar spines (Ianuzzi, 2004). During all motion types, the facet joint capsule strains computed by the model were within the 95% confidence intervals of the capsule strains that occurred experimentally (Fig. 3, extension/flexion shown).

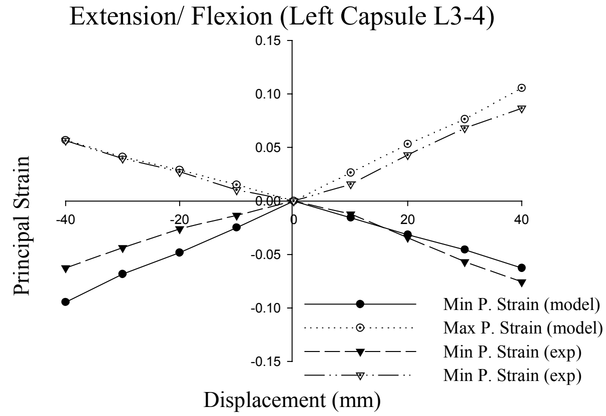

Fig. 3: During extension/flexion, left L_{3-4} facet joint capsule strain magnitudes computed by the model were similar to those that occurred experimentally.

The 3D FEM model of the facet joint capsule within the lumbar spine provides a foundation to simulate and determine the mechanical states of this joint. Future work includes incorporating the relation between mechanically sensitive neurons and stress states during physiological motions.

SUMMARY

A 3D FEM of the human FJ capsule was created and incorporated into an existing lumbar spine model. It was then used to simulate normal physiological loading conditions on the FJ capsule. Simulated strain results in the FJ was validated and highly correlated with previously published in-situ capsule strains.

REFERENCES

Cassidy, J.D., et al. (1998) *Spine*, **23**,1860-6.
Khalsa, P.S., et al. (1997) *J Neurophysiology* vol. **77**(7) 492-505.
Goel, V.K., et al. (1995) *Trans.of ASME* **117**:266-271.
Ianuzzi, A., et al. (2004). *Spine J*, **4**(2), 141-152.

ACKNOWLEDGEMENTS

Funded by NIH/CCCR and the Whitaker Foundation (RG-99-24).

HYPERELASTIC PROPERTIES OF NORMAL AND DIABETIC HEEL PADS FROM AN INVERSE FINITE ELEMENT MODEL OF INDENTATION

Ahmet Erdemir[1], Meredith L. Viverios[2], Jan S. Ulbrecht[3], and Peter R. Cavanagh[1]

[1] Department of Biomedical Engineering, Cleveland Clinic Foundation, Cleveland, OH, USA
[2] Instron Corporation Headquarters, Canton, MA, USA
[3] Depts of Biobehavioral Health and Medicine, Penn State University, University Park, PA, USA
E-mail: cavanagh@bme.ri.ccf.org Web: http://www.lerner.ccf.org/bme/cavanagh/lab/

INTRODUCTION

In vivo characterization of heel pad material properties can provide insight into connective tissue changes that may occur in diseases such as diabetes. The process is also essential for patient-specific models of the foot that can be applied to the study of therapeutic footwear. This study aims i) to provide hyperelastic models of normal and diabetic heel pad behavior under compressive loading and ii) to compare normal and soft tissue response at the material level. This investigation is an extension of the studies of Hsu et al. (2000) and Klaesner et al. (2002) which assessed diabetic plantar tissue at a structural level, but without a true stress-strain response.

METHODS

The left and right heels of 40 subjects (20 age, gender and body mass index matched pairs of normal controls and diabetic patients) were indented. Displacement of the indenter tip relative to the underlying bone was measured with ultrasound (SSD-500, ALOKA Co., Ltd.). Indentation forces were simultaneously recorded with a load cell (Kistler Instrument, Corp.). A finite element model of a generic heel was adjusted to represent the subject-specific tissue thickness measured during the experiment (Figure 1). All plantar soft tissue was modeled as a single incompressible hyperelastic material layer with strain energy, U, given by Eq. 1.

$$U = \frac{2\mu}{\alpha^2}\left(\lambda_1^\alpha + \lambda_2^\alpha + \lambda_3^\alpha - 3\right) \tag{1}$$

where λ_i (i: 1-3) are the deviatoric principal stretches. Heel-specific material parameters (μ, α) were obtained by inverse finite element analysis of the indentation procedure, which minimized the error between model predicted and experimental force-displacement curves (Erdemir et al. 2003).

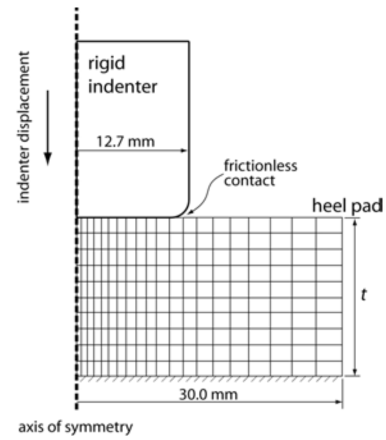

Figure 1: Axisymmetric model of the heel.

The influence of diabetes on material properties was assessed for each pair of subjects by defining two indices:

$$MI_{LS} = \sqrt{\frac{\mu_{LD}\cdot\mu_{RD}}{\mu_{LC}\cdot\mu_{RC}}};\quad MI_{HS} = \sqrt{\frac{\alpha_{LD}\cdot\alpha_{RD}}{\alpha_{LC}\cdot\alpha_{RC}}} \tag{2}$$

Where L and R stand for left and right; C and D represent control and diabetic. MI_{LS} represents a change in low strain behavior since μ is the initial shear modulus and therefore linearly related to initial elastic modulus (ABAQUS, 2002). MI_{HS} describes a change in high strain behavior, as α is a measure of increase in material stiffness with increased deformation. Side (L or R) dependency was eliminated by these indices, therefore providing a global measure of change in tissue property. A Student's *t*-test, with a level of significance 0.05, tested the hypothesis that each index was greater than 1. This would indicate stiffer heels in patients with diabetes.

RESULTS AND DISCUSSION

Experiment data (indentation depth and rate) and root-mean-square errors (RMS) of inverse modeling were not statistically different between control and diabetic groups (Table 1). These findings allowed appropriate comparisons of material properties. Tissue thicknesses were not different either, further supporting the findings of Hsu et al. (2000). Data for left and right sides were pooled for the summary of results (Table 1) since side did not have a significant effect on material properties.

Table 1: Material coefficients, tissue thickness, experiment conditions (depth and rate) and fit errors (RMS).

	Control	Diabetic
μ (kPa)	16.45 (8.27)	16.88 (6.70)
α	6.82 (1.57)	7.02 (1.43)
thickness (mm)	18.63 (2.00)	18.38 (2.25)
indentation depth (% thickness)	50.3 (5.8)	48.9 (5.7)
indentation rate (% strain/sec)	139 (20)	144 (16)
RMS error (N)	1.46 (0.72)	1.63 (0.72)
RMS error (% Max Force)	2.23 (0.99)	2.45 (0.90)

MI_{LS} and MI_{HS} were not significantly greater than 1. MI_{LS} was 1.171 ± 0.505 ($p = 0.073$), MI_{HS} was 1.061 ± 0.258 ($p = 0.151$). Subject variability was high in each group, as also shown by the mean and standard deviation of derived uniaxial stress-strain curves (Figure 2). Our results agree with those of Hsu et al. (2000) and Klaesner (2002) who did not find increased stiffness at the heel of diabetic patients. Our analysis provides a material behavior representation to supplement their derivations of structural properties of the heel.

Statistical analysis of MI_{LS} and MI_{HS} shows a trend for diabetic tissue to be stiffer (*p*-values of 0.073 and 0.151, respectively). Yet, this trend was concealed by high intersubject variability. The numerical-experimental approach presented here may induce errors in the determination of material properties particularly due to simplified heel geometry (Erdemir et al., 2003). Nevertheless, these errors are likely to be systematic rather than a cause of high subject variability. Our findings highlight the importance of subject-specific assessment of material properties for prospective use in finite element analysis of therapeutic interventions.

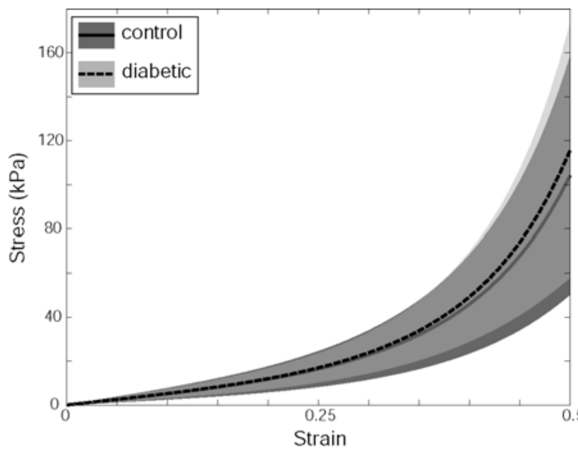

Figure 2: Normal and diabetic soft tissue under uniaxial compression.

REFERENCES

ABAQUS Theory Manual (2002). *Hibbitt, Karlsson & Sorensen, Inc*. Pawtucket, RI.

Erdemir. A. et al. (2003). *ASME Summer Bioengineering Conference*.

Hsu, T.-C., et al. (2000). *Diabetic Medicine*, **17**, 854-859.

Klaesner, J.W. et al. (2002). *Arch, Phys. Med. Rehabil.,* **83**, 1796-1801.

ACKNOWLEDGEMENTS

This study was supported by NIH Grant #5R01 HD037433. The assistance of Mary Becker, R.N., is gratefully acknowledged.

DIRECTIONAL FORCE CONTROL OF THE THUMB

Laurel Kuxhaus, Daniel A. Harkness, and Zong-Ming Li

Hand Research Laboratory, Departments of Orthopaedic Surgery and Bioengineering
University of Pittsburgh, Pittsburgh, PA, USA
E-mail: zmli@pitt.edu

INTRODUCTION

A well-controlled thumb requires successful modulation of force magnitude and application direction via muscle synergy, (Kaufman *et al.*, 1999, Valero-Cuevas, 2000) joint-torque balance, and cortical regulation (Georgopoulos *et al.*, 1992). We investigated the control of submaximal thumb forces in eight directions and predicted that this control is influenced by and aligned with the target direction.

METHODS

Eleven self-reported right-handed male volunteers indicated their informed consent via a form approved by the University of Pittsburgh's Institutional Review Board. The subjects were 26±3.5 (mean±SD) years and free of upper extremity trauma or disorders. We splinted the right thumb's interphalangeal joint and standardized the arm position. An aluminum ring around the thumb's proximal phalanx coupled it to a six-degree-of-freedom force/torque sensor (Mini40, ATI, Apex, NC). Subjects produced maximal forces in eight different randomly-presented directions spanning the dorsal-ulnar plane of the thumb. We provided visual feedback about force production in the dorsal-ulnar plane via custom LABVIEW (National Instruments, Austin, TX) software and collected force data at 100 samples-per-second. We then asked subjects to produce and hold 25% of their maximal force in each direction for sixty seconds. The target force was displayed with the subject's current force production. Two minutes' rest was required between trials.

To eliminate ramp-up and down effects, only the center fifty seconds of data were analyzed. Custom MATLAB (The Math Works, Natick, MA) routines expressed the force data relative to the target force in the radial and tangential directions (Figure 1), fit an ellipse to each force cluster, computed its major and minor axes relative to the target radial direction, and computed the force variations in the radial (force magnitude) and tangential (directional control) directions and their ratio. Repeated-measures ANOVAs using SPSS (SPSS Inc., Chicago, IL) assessed the significance of target direction on the radial and tangential force variations and on the major axis orientation ($\alpha=0.05$).

RESULTS AND DISCUSSION

Thumb forces closely matched the target forces (Figure 1). Mean radial and tangential variations ranged from 0.49N to 1.1N (Table 1). Direction influenced the relative radial and tangential variations ($p<0.02$). For example, the variation in the tangential direction was half the radial in extension and flexion (#2, #6, Table 1, tan/rad), and less extreme for other directions. The orientation of each cluster's major axis relative to its target is influenced by target direction ($p<0.004$) (e.g. #6 only deviates -0.34±4.3° from its target direction). In addition, the major and minor axis lengths were significantly different (p<0.001). A longer major axis (#2, #6, Figure 2) indicates different directional control than magnitude control, while comparable lengths of major and minor axes (#0, #4) indicate similar variations in all directions and more homogeneous control around the target. Radial variation

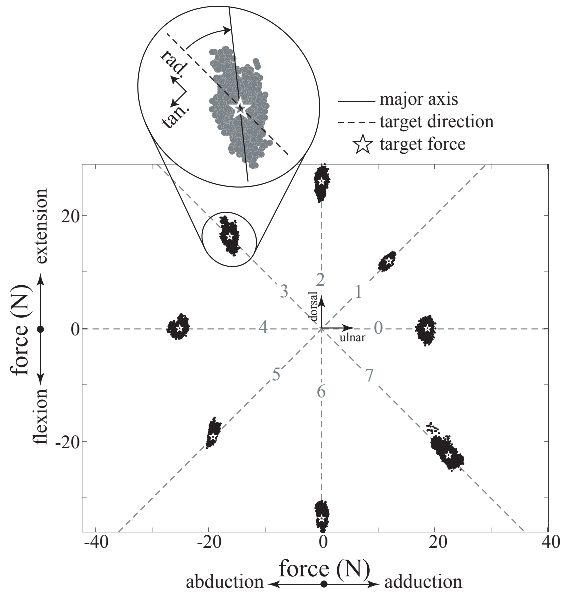

Figure 1: Force clusters from one representative subject. Numerals indicate the eight directions. Inset shows the radial and tangential directions, the major axis and its angle relative to the target direction.

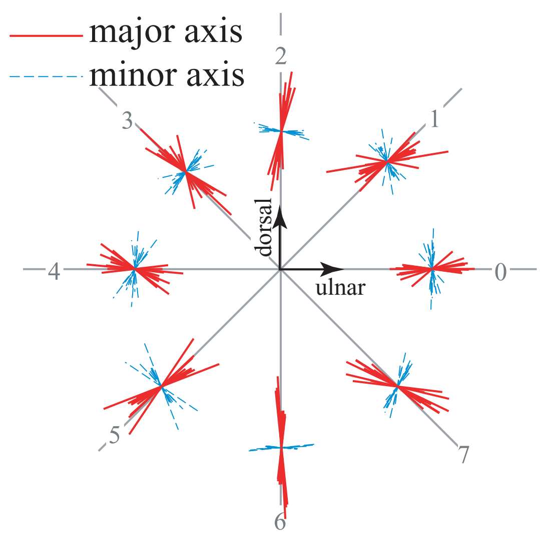

Figure 2: Major and minor axes for each force cluster.

Table 1: Force variations. Mean (SD).

direction	radial variation (N)	tangential variation (N)	tan/rad
0	0.65 (0.16)	0.92 (0.27)	1.4 (0.19)
1	0.83 (0.27)	0.61 (0.18)	0.75 (0.16)
2	1.0 (0.25)	0.49 (0.16)	0.49 (0.10)
3	0.75 (0.26)	0.74 (0.22)	1.0 (0.20)
4	0.65 (0.19)	0.80 (0.21)	1.2 (0.15)
5	0.91 (0.27)	0.77 (0.32)	0.83 (0.15)
6	1.1 (0.36)	0.50 (0.19)	0.45 (0.069)
7	0.99 (0.26)	0.73 (0.16)	0.76 (0.12)

dominance agrees with the idea that muscle activation patterns for submaximal forces are scaled versions of those for maximal forces (Valero-Cuevas 2000). However, the similar radial and tangential variations (#0, #4) suggest modulation of both the activation level of and the synergy among the muscles. The general alignment of the major axes with the target direction suggests that there may be distinct control signals at the cortical level to regulate forces (Georgopoulos *et al.*, 1992).

In conclusion, we have shown that the controllability of submaximal thumb forces changes with the target direction. Our future work will examine the temporal force variation, correlate muscle coordination patterns with our results, explore the role of feedback on force control, and study the effects of peripheral neuropathies on the ability to control thumb forces.

REFERENCES

Georgopoulos, A.P., *et al.* (1992). *Science*, **19**(256),1692-1695.

Kaufman K.R., *et al.* (1999). *Clin. Biomech.,* **14**(2),141-50.

Valero-Cuevas, F.J. (2000). *J Neurophysiol.,* **83**, 1469-1479.

ACKNOWLEDGEMENTS

This material is based upon work supported under a National Science Foundation Graduate Research Fellowship (LK) and the Whitaker Foundation (ZML).

DIRECTION-DEPENDENCE OF POLYETHYLENE WEAR FOR METAL COUNTERFACE SCRATCH TRAVERSE

Matthew C. Paul[2,1], Liam Glennon[2,1], Thomas E. Baer[1], Thomas D. Brown[1,2]
[1]Dept. of Orthopaedics and Rehabilitation, [2]Dept. of Biomedical Engineering, Univ. of Iowa
*email:*matthew-paul@uiowa.edu *web:*poppy.obrl.uiowa.edu/OBL_Lab_Website/index.html

INTRODUCTION

Scratches produced by third-body debris in total joint replacements substantially accelerate wear. In metal-on-polyethylene designs, scratches on retrieved metal components often show a locally prevailing direction of scratching. Because wear of polyethylene is an adhesive-abrasive process, the direction of scratching relative to counterface motion would seemingly influence wear.

In this investigation, a reciprocating motion physical wear test protocol was employed to identify the direction-dependence of wear of polyethylene as a function of relative scratch orientation. Concurrently, a local finite element (FE) model of scratch traverse was developed to identify surrogate stress/strain measures showing similar direction-dependence.

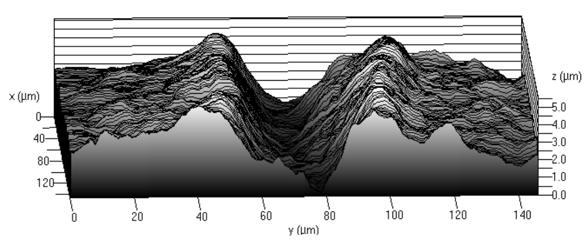

Figure 1. Laser scanning micrography image of custom scratch profile created on 316L stainless steel. Surface roughness R_a=1-1.5 µm.

METHODS

Wear test protocol

Arrays of parallel scratches were produced at 150 µm intervals on polished plates (316L stainless steel, R_a 250-500 nm) using diamond styli under an applied (spring) load of 3N. To form the scratches, a row of eleven diamond styli of tip radii 50.8 µm was dragged across the plate and then incrementally offset, until the plate was uniformly scratched. Scratching speed was 3 mm/s. This method created scratches with typical lip heights, lip widths and furrow widths of 1.3, 22 and 23 µm, respectively (Figure 1).

The scratched plates were mounted in a custom-built pin-on-plate fixture, installed for loading on a biaxial MTS 858 Bionix materials testing machine. The scratched plates were driven reciprocally against a 25.4 mm diameter polyethylene pin, loaded by 1269 N (nominal stress 2.5 MPa). Total linear excursion per cycle was 48 mm. The counterface scratch plate was moved across the polyethylene pin, at angles of 0, 2.5, 5, 15, 30, 45, 60, and 90º relative to the scratch orientation. Parametric tests were conducted for both conventional and highly-crosslinked UHMWPE (HXPE). The contact surface was immersed in bovine serum, and the plate was cooled by water circulating through the aluminum mounting block.

Wear tests were run for increments varying between 3 and 11 hours (8,000 and 30,000 cycles). After each such increment, the pin was removed and a gravimetric measurement (precision 100 µg) recorded to document the material lost. The pin was then remounted in the same orientation, and the test continued. Typically after 60,000 cycles the wear rates approximated steady state.

Finite element model

A 3-d FE model was utilized to study localized scratch/polyethylene interaction. A representative scratch profile was developed from interferometry readings of the

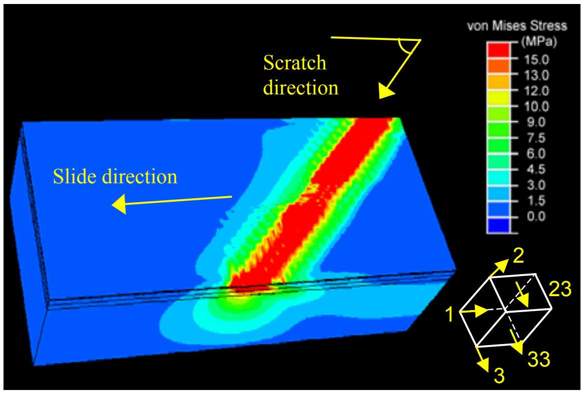

Figure 2. Instantaneous stress induced in polyethylene by a counterface scratch lip sliding at an angle of 45º.

scratched metal platen. The physical system's geometric periodicity lent itself to analysis by nonlinear computational models of tractable size, typically 45,000 elements. The model included both geometric (contact) and constitutive [Cripton, 1993] nonlinearities.

To impart the same local effect as for the load used experimentally, the computational load per unit scratch length was calculated by assuming the applied physical load to be uniformly distributed over the entire length of scratches experimentally in contact with the polyethylene plug at a given instant. The loaded scratch was then displaced across the polyethylene surface at constant velocity (Figure 2), replicating the traverse directions of the physical experiment.

Stress/strain data were output at serial instants during the event of scratch approach, overpass, and recession. A post-processing algorithm was developed to "integrate" the mechanical disturbance history experienced at a given site on the polyethylene surface, due to scratch passage.

RESULTS AND DISCUSSION

Experimentally, a scratch oriented at 15º with respect to the sliding direction was found to produce the greatest wear for conventional UHMWPE. The direction of greatest sensitivity for HXPE was 5º (Figures 3,4). The angle-specific wear rates were normalized for comparison with the results of the finite element analysis.

Three full-field stress/strain tensorial components in the FE model were found to behave consistently with observed direction-dependent wear of HXPE. These were primary strains ε_{33}, shear strains ε_{23}, and shear stresses σ_{23}, for a scratch loaded normal to the 2-plane and sliding normal to the 1-plane. For conventional UHMWPE, primary strains ε_{33} showed dependence similar to observed wear (Figures 3,4). For purposes of wear modeling at the macroscopic level, these parameters arguably could be used as surrogates for orientation-dependent wear in UHMWPE.

REFERENCE

Cripton, P.A. [MSc Thesis] Queen's University at Kingston. 1993.

ACKNOWLEDGEMENTS

Supported by NIH grants AR46601 and AR47653, with technical help from D.R. Pedersen, K.J. Stewart and R.M. Hall.

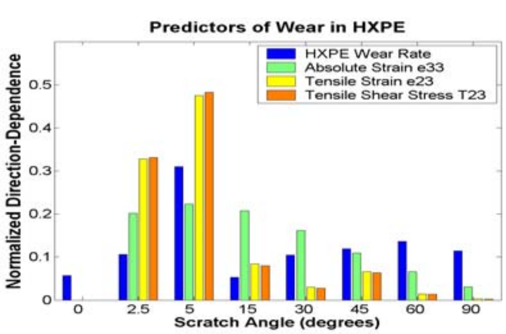

Figure 3. Surrogate predictors of wear as a function of scratch orientation in highly-crosslinked UHMWPE.

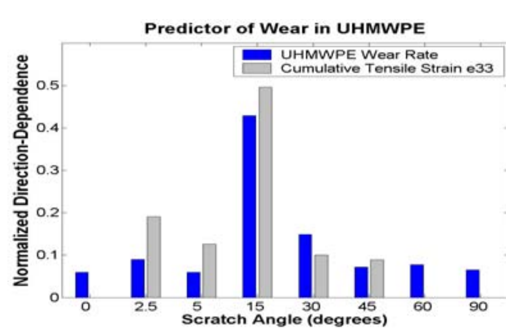

Figure 4. Tensile strain ε_{33} as a predictor of wear dependence in conventional UHMWPE (p=.0015).

TRUNK MOVEMENT PATTERNS AND PROPULSION EFFICIENCY IN WHEELCHAIR USERS WITH AND WITHOUT SCI

Alicia M. Koontz, Michael L. Boninger, Ian Rice, Yusheng Yang, Rory A. Cooper
Human Engineering Research Laboratories, VA Medical Center, Pittsburgh, PA, USA
University of Pittsburgh, Dept. of Rehabilitation Science and Technology, Pittsburgh, PA
E-mail: akoontz@pitt.edu Web: www.herlpitt.org

INTRODUCTION

Handrim wheelchair propulsion is a mechanically inefficient mode of locomotion in comparison to arm cranking and cycling (de Groot et al., 2002). In addition, wheelchair propulsion has been associated with high physical strain and repetitive strain injuries (Janssen et al., 1994). The inefficiency of wheelchair propulsion has been attributed to factors such as, improper fit of the user to the wheelchair, decreased strength and poor technique. A recent study found that during propulsion, individuals with paraplegia exhibited paradoxical trunk movements; that is, the trunk moved in the opposite direction of the arms during force production (Rice et al., 2004). The authors suggested that this might be a result of impaired trunk stability due to paralysis of the back and abdominal core muscles. Thus, lack of trunk control may also be associated with lower mechanical efficiency (ME). The purpose of this study was to examine paradoxical trunk movements and ME during two speeds of wheelchair propulsion in two groups of individuals; a group with paraplegia and a group of unimpaired individuals. We hypothesized that the group without paraplegia would be more efficient at propelling a wheelchair despite their lack of experience and training.

METHODS

Subjects: Eighteen individuals (12 men and 6 women) with spinal cord injuries (SCI) ranging from T4 to L4 and seventeen unimpaired individuals (7 men and 10 women) provided informed consent prior to participation in the study. The mean age and years post injury for the SCI group were 37 and 15 years, respectively. The age range for the unimpaired group was 23 – 62 years (mean 36 years) and they had limited to no knowledge about wheelchair propulsion technique.

Experiment protocol: Subjects' with SCI used their own personal wheelchairs while the unimpaired individuals were provided with a test wheelchair that matched their body dimensions. The wheelchairs were fitted on the right side with a SMART$^{\text{Wheel}}$ (Three Rivers Holdings, Inc., Mesa, AZ), force and torque sensing pushrim, which measures three-dimensional 3-D forces and moments in a global reference frame. A carbon fiber rigid body chest piece was fitted around the torso via cloth and Velcro$^{\text{TM}}$ straps. An infrared emitting diode marker was placed on the chest piece and a three-dimensional camera system recorded the 3-D coordinates (OPTOTRAK, Northern Digital Inc., Waterloo, CA). Subjects were instructed to propel at two steady-state speeds 0.9 m/s (2 mph), and 1.8 m/s (4mph). Propulsion speed was displayed on a 17-inch computer screen placed in front of the subjects. Upon reaching the target speed for one minute, data collection was initiated and continued for 20 seconds.

Data analysis: Kinetic data (sample rate 240 Hz) were filtered and linearly interpolated for synchronization with the filtered kinematic data (sample rate 60 Hz). The propulsion cycle was divided into two phases, push or recovery phase based on the presence or absence of pushrim forces. Number of strokes per second (cadence), percentage of the cycle that comprised the push phase, trunk anterior/posterior range of motion (ROM), and ME for the first ten consecutive cycles were determined and a mean was computed (Table 1). Mechanical efficiency was defined at $Ft^2/Ftotal^2$, where tangential force (*Ft*) was calculated by dividing wheel torque by the radius of the wheel. We also determined the proportion of the phase (%) that the trunk was moving backward and rearward excursion (mm) of the trunk for the same ten strokes, and for both push and recovery phases (Table 2). A mixed-model ANOVA was applied with within subject factor: speed (slow and fast) and between subject factor: group (unimpaired and SCI) The α value was set at 0.05.

RESULTS AND DISCUSSION

As speed increased, the unimpaired group pushed with fewer strokes per second and spent more time in contact with the rim delivering forces in comparison to the SCI group. ME was higher for the unimpaired group and increased with increasing speed whereas in the SCI group, ME was smaller and decreased with increasing speed. The SCI group exhibited paradoxical motion of the trunk during force production to a greater extent than their unimpaired counterparts during the faster speed condition. In addition, the SCI group had more rearward excursion of their trunk than their unimpaired counterparts at both speed conditions during the push phase.

The unimpaired subjects had no training in propulsion technique and were inexperienced but yet pushed with greater ME than the SCI group which consisted of seasoned wheelchair users. Persons with volitional trunk control can use abdominal and back muscles to some extent to minimize the degree to which reactive forces from pushing forward sends the trunk backwards. In SCI, the body achieves trunk stability in the wheelchair through postural adaptations (e.g, kyphotic posture) that may not be optimal for propulsion. As a result adequately directing the forces tangentially to the wheel may be more difficult or require greater energy expenditure. It's possible that a rigid back support combined with training, may improve ME in persons with SCI.

REFERENCES

De Groot, S. et al. (2002). *Clin. Biomech.,* **17**(3): 219-226.

Janseen, T. W. et al. (1994). *Med. Sci. Sports Exerc.* **26**(6): 661-670.

Rice, I. et al. (2004). *Proceedings of RESNA'04.*

ACKNOWLEDGEMENTS

VA Rehab R&D Service and NIDRR H133A011107.

Table 1: Propulsion measures at both speeds (mean± SD).

	Cadance (1/sec)[b,c]		Push Phase (% cycle)[a,c]		Trunk ROM (mm)[a,b]		Mechanical Efficiency[b,c]	
Speed (m/sec)	**0.9**	**1.8**	**0.9**	**1.8**	**0.9**	**1.8**	**0.9**	**1.8**
UI	1.18 (0.25)	0.83 (0.14)	54.8 (6.8)	52.4 (7.4)	25.5 (10.9)	27.0 (16.2)	0.64 (0.14)	0.74 (0.19)
SCI	1.01 (0.15)	1.33 (0.16)	49.6 (4.9)	45.7 (6.4)	15.7 (5.3)	30.4 (13.0)	0.54 (0.20)	0.46 (0.16)

Table 2: Percent of the phase that trunk was moving backward and excursion during push and recovery (mean± SD).

	Push Phase (%)[b,c]		Push Excursion (mm)[b,c]		Recovery Phase (%)[a,b,c]		Recovery Excursion (mm)[a,b]	
Speed (m/sec)	**0.9**	**1.8**	**0.9**	**1.8**	**0.9**	**1.8**	**0.9**	**1.8**
UI	43.9 (13.7)	30.2 (12.3)	6.54 (3.2)	5.14 (2.4)	62.5 (23.6)	80.3 (13.6)	9.1 (6.2)	22.4 (15.6)
SCI	42.6 (18.0)	52.7 (22.0)	10.0 (5.8)	15.4 (10.4)	59.4 (20.9)	54.2 (19.3)	15.8 (11.8)	16.1 (10.5)

a = significant difference between within-subject factor speed ($p < 0.05$), b = significant difference for interaction between speed and group ($p < 0.05$), c = significant difference for between-subject factor group ($p < 0.05$)

OPTIMIZATION OF BONE ALIGNMENT TO REPRODUCE PLANTAR PRESSURES IN A SUBJECT-SPECIFIC FINITE ELEMENT FOOT MODEL

Ahmet Erdemir[1], Marc Petre[1,2], Sachin Budhabhatti[1,3] and Peter R. Cavanagh[1]

[1]Dept. of Biomedical Engineering, Cleveland Clinic Foundation, Cleveland, OH, USA
[2]Dept. of Biomedical Engineering, Case Western Reserve University, Cleveland, OH, USA
[3]Dept. of Chemical & Biomedical Engineering, Cleveland State University, Cleveland, OH, USA
E-mail: cavanagh@bme.ri.ccf.org Web: http://www.lerner.ccf.org/bme/cavanagh/lab/

INTRODUCTION

Finite element analysis of the foot has the potential to identify mechanisms of foot disorders and to provide a-priori information on therapeutic interventions (Gefen et al., 2000; Chen et al., 2001; Camacho et al., 2002). Prediction of plantar foot pressures is particularly attractive due to the relationship with diabetic foot ulceration. Various models have shown the capacity to provide this information (Chen et al., 2001; Gefen, 2003), but previous models have not been subject-specific. Calculations of plantar pressures are sensitive to inaccuracies due to loading, tissue properties, and relative bone configuration. The objectives of this study are i) to develop a strategy for optimal alignment of bones, and ii) to illustrate its usefulness in a model of the first ray of the foot.

METHODS

A finite element model of the first ray of the right foot of a male subject (95 kg, 1.88 m) was developed (Figure 1) based on MRI data. Bones (proximal and distal phalanges, metatarsal including sesamoids) were assumed to be rigid, soft tissue was modeled as hyperelastic, and a frictional contact between the soft tissue and the floor was incorporated. The model had 18 degrees of freedom (DoFs) to describe bone alignment. Six DoFs described the metatarsal pose and orientation relative to the floor. Relative movements between the three bones of the first ray were represented by additional DoFs (six for each bone pair). In an analysis

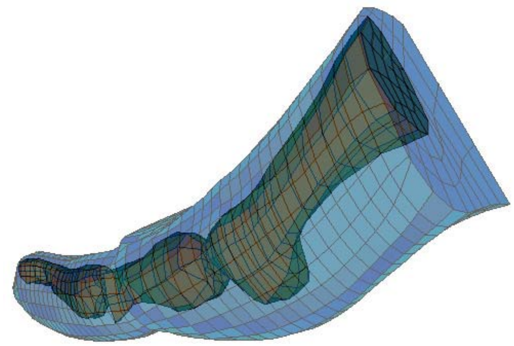

Figure 1: The first ray model.

the operator could either prescribe the DoFs or apply a load case.

Barefoot plantar pressures were recorded from the subject during five trials of walking at a self-selected speed (EMED, Novel, Inc). Pressure distributions underneath the first ray were extracted for the initiation of late stance phase, at a time when forefoot loading was maximal.

Finite element simulations were completed for each experimental trial. The vertical force applied to the metatarsal was calculated by integrating the pressure data over total contact area. Horizontal force was estimated to be 20 % of the vertical force (Chao et al., 1983). The whole model was initially configured to approximate the orientation of the metatarsal head at the initiation of late stance. Fine tuning in bone alignment was performed by minimizing the difference between the model predicted and experimentally measured pressures by iteratively changing the DoFs. Relative bone movements were constrained in order to prevent unrealistic joint configurations. Matlab (Mathworks, Inc) code interacting with ABAQUS (Abaqus, Inc) solved the minimization problem using Sequential Quadratic Programming (Schittkowski, 1986) as the optimization algorithm.

RESULTS AND DISCUSSION

Changing bone alignment allowed realistic load distribution between the metatarsal head and the distal hallux (Figure 2). Peak pressures along the longitudinal axis of the first ray were in good agreement with experimentally derived values, particularly for the aforementioned sites (Figure 3).

Root mean square errors of model predicted pressures were 61.8 ± 21.4 kPa (11.1 ± 2.3 % max. pressure). The RMS errors were 85.8 ± 17.3 kPa (16.6 ± 6.1 % max. pressure) before alignment. A finer mesh may further decrease these errors and may also account for discrepancies underneath the base of the proximal phalange. However, the computational cost of the optimization would be elevated.

Our methodology offers a solution to the uncertainty of model configuration or joint loading in a finite element model. Variables that are difficult to measure during gait can reliably be estimated, e.g. plantarflexion of the first metatarsophalangeal (MTPJ1) and interphalangeal (IPJ1) joints (1.4° ± 2.0° and 6.2° ± 3.0°). These joints were at their neutral angles (0°) before alignment. The solution also generates loading information such as MTPJ1 and IPJ1 plantarflexion moments (5.86 ± 1.0 and 0.57 ± 1.97 Nm). Pressure relief by preventive and therapeutic interventions can now be investigated under the same geometric configuration (joint angles specified) or the same loading conditions (joint torques provided). The technique can also be extended to the whole forefoot once a model becomes available. Realistic estimations of peak pressures are critical, especially for simulation-based interventions to prevent pressure related ulceration underneath the diabetic foot.

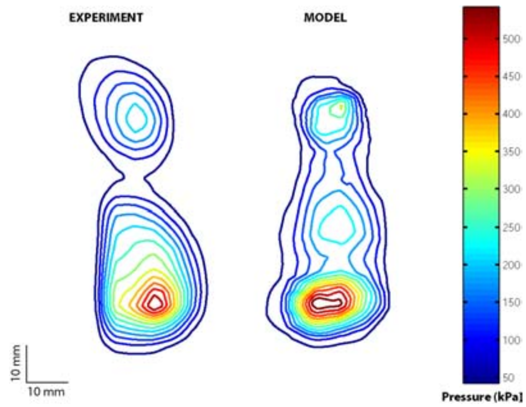

Figure 2: Average pressure distribution.

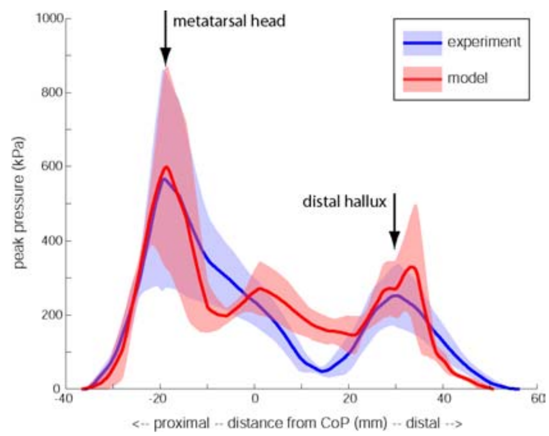

Figure 3: Peak pressures (mean ± SD) along the longitudinal axis of the first ray.

REFERENCES

Camacho, D.L.A. et al. (2002). *J Rehab Res Dev*, **39**, 401-410.

Chao, E.Y. et al. (1983). *J Biomech*, **16**, 219-233.

Chen, W.-P. et al. (2001). *Clin Biomech*, **16**, 614-620.

Chen, W.-P. et al. (2003). *Clin Biomech*, **18**, S17-S24.

Gefen, A. (2003). *Med Eng & Phys*, **25**, 491-499.

Gefen, A. et al. (2000). *J Biomech Eng*, **122**, 630-639.

Schittkowski, K. (1986). *Annals of Operations Research*, **5**, 485-500.

ACKNOWLEDGEMENTS

This study was supported by NIH Grant #5R01 HD037433.

INTERVERTEBRAL NECK INJURY CRITERION FOR SIMULATED FRONTAL IMPACTS

Paul C. Ivancic, Shigeki Ito, Manohar M. Panjabi, Adam M. Pearson, Yasuhiro Tominaga, Jaw-Lin Wang, S. Elena Gimenez

Biomechanics Research Laboratory, Yale University School of Medicine, New Haven, CT, USA
E-mail: paul.ivancic@yale.edu

INTRODUCTION

Automobile collisions may result in soft-tissue injuries to the cervical spine leading to chronic symptoms. In order to predict these injuries, a validated cervical spine injury criterion is needed. The Neck Injury Criterion (NIC) is based on the hypothesis that sudden changes in spinal fluid pressure may cause neural injuries, and was formulated using a rear impact porcine model (Bostrom et al., 1996). The Intervertebral Neck Injury Criterion (IV-NIC) is based on the hypothesis that intervertebral motion beyond the physiological limit may injure cervical soft tissues (Panjabi et al., 1999). The goals of this study were to use a biofidelic whole human cervical spine model with muscle force replication in frontal impact simulations to determine the IV-NIC injury threshold at each intervertebral level, and to compare IV-NIC with NIC.

METHODS

The IV-NIC was defined as the dynamic intervertebral rotation during simulated frontal impact, $\theta_{dynamic,\,i}(t)$, divided by the corresponding physiological range of motion (ROM) limit, $\theta_{physiological,\,i}$, where i is the intervertebral level. Thus,

$$IV-NIC_i\,(t) = \frac{\theta_{dynamic,\,i}(t)}{\theta_{physiological,\,i}}, \qquad (1)$$

where t represents time.

The NIC is given by the following equation:

$$\mathrm{NIC}(t) = 0.2 \cdot a_{rel}(t) + v^2{}_{rel}(t), \qquad (2)$$

where $a_{rel}(t)$ and $v_{rel}(t)$ are the relative horizontal acceleration and velocity, respectively, between the head center of mass and T1 vertebra.

Six intact human osteoligamentous cervical spine specimens (occiput to T1) were prepared with vertebral motion tracking flags. The flags, each with two white, spherical, radio-opaque markers, were attached to each vertebra. Sagittal flexibility testing up to 1.5 Nm was performed to determine the intervertebral flexibility parameters of neutral zone (NZ) and ROM of the intact specimens and following each frontal impact. The whole cervical spine with muscle force replication and surrogate head were used to simulate frontal impacts at 4, 6, 8, and 10 g horizontal accelerations of the T1 vertebra using a bench-top sled (Panjabi et al., 1998). A high-speed camera recorded the spinal motions at 500 frames/sec. Accelerometers were mounted to the sled and head center of mass to determine the T1 and head horizontal accelerations, respectively. The IV-NIC and NIC were computed as functions of time using equations (1) and (2), respectively.

The soft tissue injury was defined as a statistically significant increase ($p<0.05$) in NZ or ROM, due to frontal impact simulation above the corresponding baseline values. The soft tissue injury threshold was the lowest T1 horizontal peak acceleration that caused the soft tissue injury. The IV-NIC injury threshold was the average peak IV-NIC at the soft tissue injury threshold.

RESULTS

The IV-NIC flexion peaks were greater than the extension peaks at all intervertebral levels, excluding C0-C1 and C1-C2 (**Figure 1**). The soft tissue injury threshold acceleration was found to be 8 g, as determined by significant increases above the corresponding baseline values in total NZ or ROM at C4-C5 and C6-C7 following the 8 g impact acceleration. The average IV-NIC (95% confidence interval) at the injury threshold varied among intervertebral levels, and ranged between 2.0 (1.2-2.8) at C4-C5 and 3.5 (2.4-4.6) at C7-T1, during the 8 g and 10 g impacts, respectively (**Table 1**). At the soft tissue injury threshold, the average peak NIC was 18.4 (17.8-19.0) m^2/s^2.

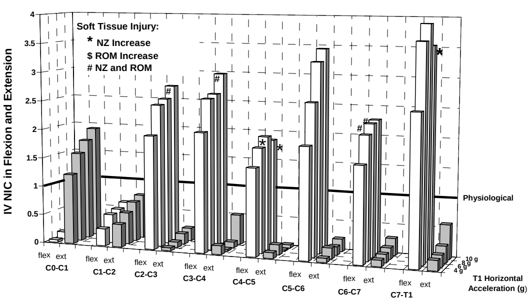

Figure 1. The average IV-NIC peaks in flexion and extension for each intervertebral level (C0-C1 to C7-T1).

DISCUSSION AND SUMMARY

The IV-NIC injury threshold was determined at each intervertebral level that was injured due to simulated frontal impact, using the whole human cervical spine whiplash model with muscle force replication. The many advantages of the IV-NIC over NIC in predicting soft tissue injuries include the ability to predict the intervertebral level, mode of loading, and time of injury during frontal impact. The development and validation of an injury criterion which helps predict these clinically relevant parameters is valuable in efforts to advance injury prevention measures as well as to develop better means of diagnosis and more efficient treatment.

REFERENCES

Bostrom, O.et al. (1996). *IRCOBI*, 123-136.

Panjabi, M.M.et al. (1998). *Spine,* **23**, 17-24.

Panjabi, M.M.et al. (1999). *IRCOBI*, 179-190.

ACKNOWLEDGEMENTS

This research was supported by NIH Grant 1 R01 AR45452 1A2 and the Doris Duke Charitable Foundation.

	IV-NIC (dimensionless)								NIC (m^2/s^2)
	C0-C1	**C1-C2**	**C2-C3**	**C3-C4**	**C4-C5**	**C5-C6**	**C6-C7**	**C7-T1**	**C0-T1**
4 g	no injury	no injury	no injury	no injury	no injury	no injury	no injury	no injury	7.4 (6.4-8.4)
6 g	no injury	no injury	no injury	no injury	no injury	no injury	no injury	no injury	11.9 (10.9-12.9)
8g	no injury	no injury	no injury	no injury	2.0 (1.2-2.8)	no injury	2.3 (1.2-2.8)	no injury	18.4 (17.8-19.0)
10 g	no injury	no injury	2.7 (1.6-3.8)	3.0 (2.4-3.6)	1.9 (1.1-2.7)	no injury	2.3 (1.6-3.0)	3.5 (2.4-4.6)	22.3 (20.9-23.7)

Table 1. Average IV-NIC, with 95% confidence intervals, for each intervertebral level that was injured due to simulated frontal impact. The average NIC, with 95% confidence intervals, is shown in the last column for each impact.

PLANTAR PRESSURE REDUCTION BY FOOTWEAR: A FINITE ELEMENT MODEL

Sachin Budhabhatti[1,2], Ahmet Erdemir[1], Marc Petre[1,3], and Peter R. Cavanagh[1]

[1]Dept. of Biomedical Engineering, Cleveland Clinic Foundation, Cleveland, OH, USA
[2]Dept. of Chemical & Biomedical Engineering, Cleveland State University, Cleveland, OH, USA
[3]Dept. of Biomedical Engineering, Case Western Reserve University, Cleveland, OH, USA
E-mail: cavanagh@bme.ri.ccf.org Web: http://www.lerner.ccf.org/bme/cavanagh/lab/

Therapeutic footwear is routinely prescribed to provide plantar pressure relief at highly loaded areas underneath the feet of people with diabetes (Foto and Birke, 1998). A number of researchers have investigated the effect of flat and total contact orthoses and their thickness on plantar pressure re-distribution using two or three dimensional finite element (FE) models (Lemmon *et al.*, 1997; Chen *et al.,* 2003). These analyses have been performed at only one instant during the support phase of walking. Peak pressures are likely to occur at different stages of gait depending on the anatomical location of interest (e.g. hallux vs. metatarsal heads).

The objectives of this study were i) to simulate plantar pressure under the first ray for the entire duration of the late support phase and ii) to investigate the influence of five different insole materials on plantar pressure redistribution under the areas that have a high risk of ulcer formation in the setting of diabetic peripheral neuropathy (first metatarsal head and hallux). A FE model of the foot and the insole was chosen as a tool to simulate these conditions.

METHODS

A FE model of the first ray of the right foot of a male subject (95 kg, 1.88 m) with a flat insole was developed (Figure 1). The details of the model have been explained elsewhere (Budhabhatti *et al.*, 2004). Bone orientation and the loads applied to the model were calculated by an optimization procedure that

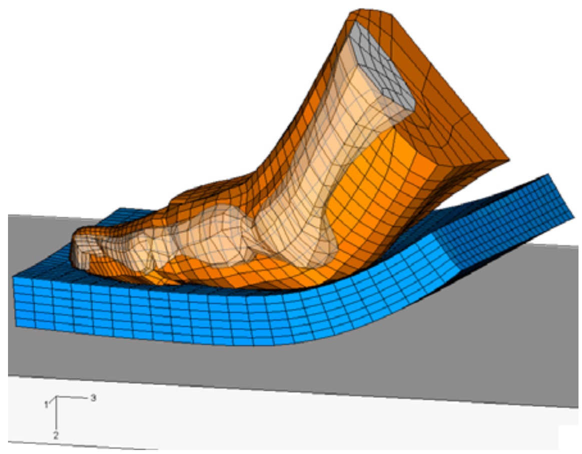

Figure 1: FE model of foot & insole during push-off.

minimized the difference in barefoot pressures predicted by the model and measured experimentally at the initiation of late stance (Erdemir *et al.,* 2004). The model was first configured and loaded to simulate the initiation of late stance. To model the push-off phase, the forces applied to the base of the metatarsal head and the metatarsophalangeal joint moment were incrementally decreased to zero. Simultaneously, the first metatarsal was subjected to an incremental rotation in its orientation with respect to the ground up to 45 degrees (Fauth, 2002). Five different footwear materials (Firm and Medium Plastazote, Puff, Puff-lite, and Poron) were simulated. Material thickness was set at 15 mm and material properties were obtained from data fits to compression tests (Figure 2). Hyperform material properties were used in the model (ABAQUS Theory Manual) and frictional contacts between the foot and insole and the insole and ground plane were modeled.

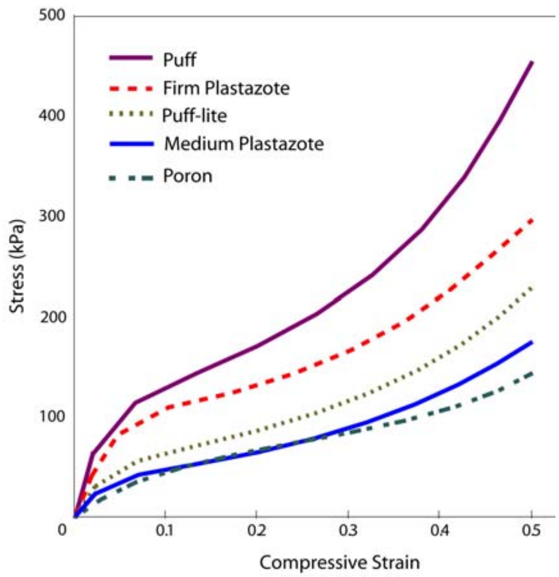

Figure 2: Stress-strain behavior of insole materials.

RESULTS AND DISCUSSION

The peak plantar pressures for the barefoot condition (experimental and model) along with five footwear materials are shown in Figure 3. Barefoot model predictions of peak hallux and metatarsal head pressures were in good agreement with experimental measurements. The simulation protocol was capable of identifying both peak metatarsal head and hallux pressures that occurred at different instants of push-off. The time of occurrence of peak hallux pressures (approximately 55% of push-off phase) was later than peak metatarsal loading (approximately 15% of push-off phase), an observation made possible by simulation of the entire late-support phase.

All materials resulted in a reduction of peak pressures compared to the barefoot walking simulation underneath the regions of interest (Figure 3). Poron resulted in a 70% decrease in hallux pressures and 50% reduction in metatarsal head peak pressure. Puff reduced pressures by 12% and 22% although it is rarely used in a single layered insole.

The methodology presented here can be used to predict plantar pressure relief under various conditions. This study can also be extended to test therapeutic footwear interventions that combine different insole materials and geometries and to the study of subject-specific models.

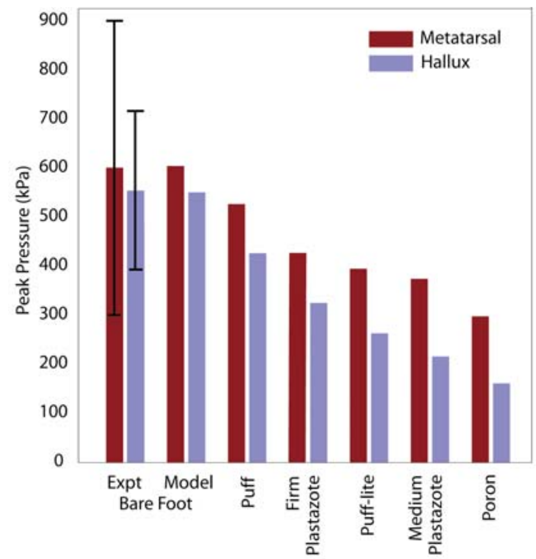

Figure 3: Peak plantar pressures for different footwear materials. Mean ± SD of five barefoot walking trials of the subject from whom model geometry was obtained is also shown (Expt).

REFERENCES

Abaqus Theory Manual, 2002, Hibbitt, Karlsson & Sorensen, Inc., Pawtucket, RI.

Foto, J.G. and Birke, J.A. (1998) *Foot & Ankle International* **19,** 836-841.

Budhabhatti, S., et al. (2004) *Research ShowCASE abstract*, 2004

Chen et al. (2003) *Clinical Biomech.*, **18,** S17-S24.

Erdemir A., et al. (2004) *ASB Abstract.*

Fauth A. (2002) *MS. Thesis, PSU, PA.*

Lemmon, D., et al. (1997) *J Biomech.* **30,** 615-620.

ACKNOWLEDGEMENTS

This study was supported by NIH Grant #5R01 HD037433.

MODELING THE EFFECT OF HALLUX LIMITUS ON FIRST RAY PLANTAR PRESSURE DISTRIBUTIONS

Marc Petre[1,2], Ahmet Erdemir[1], Sachin Budhabhatti[1,3] and Peter R. Cavanagh[1]

[1]Dept. of Biomedical Engineering, Cleveland Clinic Foundation, Cleveland, OH, USA
[2]Dept. of Biomedical Engineering, Case Western Reserve University, Cleveland, OH, USA
[3]Dept. of Chemical & Biomedical Engineering, Cleveland State University, Cleveland, OH, USA
E-mail: cavanagh@bme.ri.ccf.org Web: http://www.lerner.ccf.org/bme/cavanagh/lab/

INTRODUCTION

Hallux limitus (HL) refers to a stiffening and consequent limited mobility of the first metatarsophalangeal joint (MTPJ1). In the extreme case of hallux rigidus, the normal 55-65° joint range of motion is effectively reduced to zero. During mid-support in normal gait, the phalanges remain parallel to the ground providing a large base of support as the metatarsals rotate. In HL, the force is believed to be localized at the distal plantar surface of the hallux leading to high plantar pressures.

Rigidity in MTPJ1 can be biomechanically accommodated in a number of ways including foot inversion, premature liftoff of the toes, and a more vertical toe-off (Dananberg, 1986). These changes in gait shift load to other regions of the foot and help protect the stiffened hallux. However, in patients with diabetic neuropathy, increased pressure may go unnoticed and eventually lead to sub-hallux ulceration (Dannals, 1989).

Patients with insensate feet can be provided with artificial accommodation in the form of therapeutic footwear. Custom insoles and rocker or roller bottom shoes have shown promise in patients with HL, but parameters associated with these treatments are still a matter of debate (van Shie et al., 2000). A finite element (FE) model of HL would allow an extensive analysis of footwear that may not be feasible with human subjects. The objective of this study is to produce a model capable of representing HL for prospective therapeutic footwear designs.

METHODS

A three dimensional FE model of the right foot first ray of a male subject (95 kg, 1.88 m) was used to model HL (Figure 1). The first ray model is described elsewhere in greater detail (Budhabhatti, 2004). Model forces and bone orientations were determined by minimizing differences between model generated plantar pressures and experimental pressures collected from the subject whose foot was modeled (Erdemir, 2004).

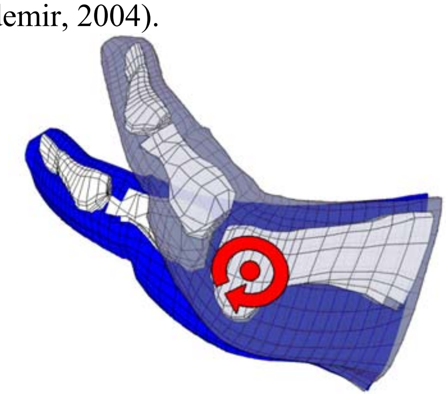

Figure 1: First ray model showing dorsiflexion about the MTPJ1. The range of motion is restricted in hallux limitus.

The model MTPJ1 degrees of freedom were progressively restricted to reflect the pathology of HL. Stiffness of MTPJ1 was modeled as a combination of inherent passive joint stiffness and a 'locking angle' at which the joint will no longer extend. The passive properties of joints were taken from measurements in the literature on normal subjects and subjects with HL (Birke et al., 1988). Values for the locking angle ranged from 58° dorsiflexion (unrestricted normal joint) to 0° dorsiflexion (severe HL).

The FE simulations started at the initiation of late stance (as defined by the second peak in vertical ground reaction force) and ended with toe-off. The peak metatarsal and hallux pressures during this movement were extracted from the model output along with their times of occurrence.

RESULTS AND DISCUSSION

A peak pressure of 600 kPa under the first metatarsal head occurred at the same time point in late stance for all locking angles (Figure 2). Hallux peak pressure was more dependent on available dorsiflexion and increased significantly as the joint range of motion was restricted. In this model, approximately 25° of dorsiflexion appears to be sufficient to keep peak pressures closer to normal. Peak hallux pressures occurred earlier in models with limited MTPJ1 movement (Figure 3).

Peak pressures collected during gait from the subject with unrestricted MTPJ1 motion from whom the model was derived were 570 and 485 kPa for the metatarsal and hallux respectively. Overestimation by the model could be due to the assumption of fixed interphalangeal joints. Free joints would provide some additional compensation and load sharing. Peak hallux pressures above 1200 kPa are rarely seen in practice, yet predicted by this model because biomechanical compensation methods were not considered. The model is, in effect, a worst-case scenario showing what the peak pressures could be with no active compensation mechanism. The effect of element size in the experimental pressure measurement device must also be considered.

This modeling approach provides a useful representation of the pathology of HL. The techniques described can now be used to investigate the efficacy of therapeutic footwear in the reduction of peak pressures (i.e. design of a rigid rocker or insole material selection). Previous studies have shown that optimal designs are highly subject dependent (van Shie et al., 2000). As subject specific models become available, this modeling approach can be used in the design of patient-specific footwear.

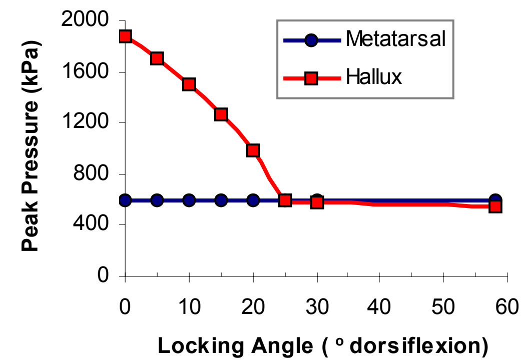

Figure 2: Peak pressures at the metatarsal and hallux for different levels of MTPJ1 rigidity. Hallux pressures increase as the joint is further restricted.

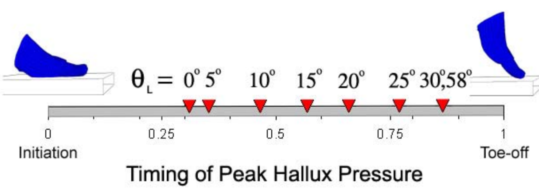

Figure 3: As the locking angle, θ_L, decreases, the hallux peak pressure occurs earlier in late stance.

REFERENCES

Birke, J.A. et al. (1988). *J Ortho Sports Physical Therapy*, **10**, 172-176.

Budhabhatti, S. et al. (2004). *Research ShowCase Abstract.*

Dananberg, H.J. (1986). *J American Podiatric Medical Assoc*, **76**, 648-652.

Dannals, E. (1989). *J American Podiatric Medical Assoc*, **79**, 447-450.

Erdemir, A. et al. (2004). *ASB Abstract.*

van Shie, C. et al.(2000). *Foot & Ankle International,* **21**, 833-844.

ACKNOWLEDGEMENTS

This study was supported by NIH Grant #5R01 HD037433.

DOES PLYOMETRIC TRAINING IMPROVE SWIM START PERFORMANCE?

Gregory M. Gutierrez, Elizabeth V. Macbeth, Mark D. Tillman and John W. Chow

Center for Exercise Science, University of Florida, Gainesville, Florida
Email: mtillman@hhp.ufl.edu

INTRODUCTION

The swim start is only a small portion of the overall race time; however, improvements in the start could result in a winning race time. A typical swim start consists of three phases: the loading phase, the push phase, and the flight phase. The first two phases of the start may be considered plyometric in nature. Plyometric activities are frequently recommended as a training method for increasing muscular output and improved performance in explosive activities (Ebben, 2001). A more explosive, stronger takeoff during a swim start will lead to a greater horizontal linear impulse and an improved start time. It is also important to optimize the takeoff angle at the start so as to maximize the flight time while achieving a shallow entry (Miller et al., 1984). Flight time should be maximized because air resistance is much smaller than water resistance. Swimmers must also not enter the water at a large angle, relative to the horizontal, since this will bring them down toward the bottom of the pool and they will have to use extra effort to rise back to the top. The purpose of this study was to determine whether plyometric training is a viable form of training to improve swim start performance by testing how it affects grab and track style swim starts.

METHODS

Thirty-six members (21 female, 15 male) of a Division I collegiate swim team participated in the study. The subjects were randomly assigned to one of four plyometric training groups: vertical, horizontal, combination, or control. In addition to the normal team training regimen, subjects in the vertical plyometric group performed vertical plyometric drills, the horizontal plyometric group performed bounding plyometric drills, and the combination plyometric group performed both vertical and bounding plyometric drills. The control group did not perform any additional plyometric activities.

All swim start trials were performed on a custom made starting block that was constructed to keep the size and angle (10˚) measurements typical of a USAA starting block. This starting block was fitted with a force plate operating at 1000 Hz. Two twin-sized air mattresses were stacked and secured on a rolling platform to allow for safe landing 30cm below the level of the starting block. A high-speed camera sampling at 250 Hz was positioned 8.5 m from the starting block and provided a sagittal view. A signal generating unit with a light and a buzzer was used to trigger the swimmers for their swim starts using the normal USAA competitive method. A Peak Motus® 2000 system was used to digitize kinematic data and record ground reaction forces.

All subjects performed a pretest session consisting of three trials of a grab start, with the hands grabbing outside the feet, and a track start, with the left leg back. Eight weeks of training were completed and a second testing session was performed. To assess the relationship between plyometric training group and test session in relation to the grab start and the track start in the laboratory, the following nine dependent variables were examined: block time, maximum and average block reaction forces, horizontal and vertical impulse, resultant takeoff velocity, takeoff angle, horizontal distance, and estimated flight time. Two separate 4 X 2 MANOVA (Training Group x Test Session) were used for each start type (grab and track). When significant main effects were observed univariate analyses were performed with the Tukey HSD (Honestly Significant Difference) post hoc test. The level of significance was set at a traditional level (α=0.05).

RESULTS AND DISCUSSION

Multivariate testing revealed a main effect for the test session condition for the grab start (Wilks' lambda = .315, $F(9,24) = 9.833$, $p < .001$) and for the track start (Wilks' lambda = .139, $F(9,24) = 16.542$, $p < .001$). Although no main effect for start type was detected, univariate follow-up testing revealed several pre-post differences (Table 1). Contrary to the original hypotheses, no main effects were detected for the training group condition. This lack of significance could be due to the high level of normal training already being completed. The swimmers were performing their standard team training, including running stadium stairs, which are plyometric in nature. The amount of standard training performed may have outweighed the potential benefits of the added plyometric drills.

SUMMARY

For both swim starts, six out of nine variables were significantly different as a result of training. Overall improvements were seen, but were quite variable. Based on the findings of this study, it is evident that plyometric training is not a detriment to a swim training program. It cannot be conclusively determined whether plyometrics actually improve swim start performance. Further testing in a more controlled environment may elicit more significant results.

REFERENCES

Ebben, W. P. (2001). *Strength Cond. J.* **23**(5), 47-50.

Miller, J.A. et. al. (1984). *J. Sports Sci.* **2**, 213-223.

Table 1. Pre- and Post-test Swim Start Results (mean ± standard deviation)

	Pre-test (Grab)	**Post-test (Grab)**	**Pre-test (Track)**	**Post-test (Track)**
BT (s)	.96 ± .07 *	.93 ± .07 *	.94 ± .09	.92 ± .13
RGRFM (BW)	1.9 ± .17*	1.8±.19 *	2.0 ± 1.0	1.7 ± .13
RGRFA (BW)	1.2 ± .08 *	1.1 ± .04 *	1.2 ± .06 *	1.1 ± .06 *
Ih (Ns)	269.0 ± 81.2	287.1 ± 42.8	265.5 ± 40.3 *	290.2 ± 43.5 *
Iv (Ns)	69.1 ± 26.4 *	41.2 ± 25.3 *	55.3 ± 27.3 *	26.0 ± 28.3 *
Vr (m/s)	3.8 ± 0.7	3.9 ± .26	3.7 ± .22 *	4.0 ± .22 *
TA (degrees)	15 ± 5.7 *	8.1 ± 4.6 *	11.8 ± 5.4 *	5.1 ± 5.6 *
Dh (m)	2.3 ± .49	2.3 ± .22	2.2 ± .18	2.2 ± .23
FT (s)	.64 ± .04 *	.59 ± .04 *	.62 ± .05 *	.56 ± .05 *

*denotes significant main effect between pre-test and post-test

BT – Block Time
RGRFM – Maximum Resultant Ground Reaction Force
RGRFA – Average Resultant Ground Reaction Force
Ih – Horizontal Impulse
Iv – Vertical Impulse
Vr – Resultant Velocity
TA – Take-off Angle
Dh – Horizontal Distance
FT – Flight Time

Characterizing How the Assumed Quadriceps Force Distribution Influences the Patellofemoral Pressure Distribution

John J. Elias

Medical Education and Research Institute of Colorado, Colorado Springs, CO
e-mail: elias@meric.info web: www.meric.info

INTRODUCTION

For in vitro experimental models and computational models representing the patellofemoral joint, the quadriceps force is typically distributed among the four muscles of the quadriceps group based on the physiological cross-sectional area (PCSA) of each muscle (Farahmand et al., 1998). Recently, EMG has been utilized to estimate the contribution of each quadriceps muscle to the extension moment during knee extension (Zhang et al., 2003). The hypothesis of the current study is that altering the assumed quadriceps force distribution will alter computational predictions of the patellofemoral pressure distribution.

METHODS

Both the PCSA-based and the EMG-based quadriceps force distributions were simulated while computationally determining the influence of the Q-angle on the patellofemoral pressure distribution. As described previously (Elias et al., in press), four knee models were flexed from 40° to 90° with the Q-angle set at 15° and with the tibial tuberosity lateralized to increase the Q-angle to 25°. Force vectors representing the four muscles of the quadriceps group and the patella tendon were applied to the patella, and a quadriceps moment was applied at each flexion angle to simulate a knee extension exercise against 25 N of resistance at the ankle. Both the PCSA-based and EMG-based estimates of the quadriceps force distribution were used to determine the force applied by each muscle (Table 1). For each loading case, the patellofemoral pressure distribution was quantified by minimizing the potential energy stored within springs representing the cartilage and the joint capsule. At each flexion angle, a repeated measures ANOVA and Student-Neuman-Keuls post-hoc test were used to examine for statistically significant ($p < 0.05$) variations in the components of the resultant force and moment applied to the patella by the quadriceps muscles and the patella tendon, the maximum patellofemoral pressure and the mean patellofemoral pressure between the four tests cases (2 Q-angles and 2 quadriceps force distributions).

Table 1: Distribution of Total Quadriceps Force among Quadriceps Muscles

	RF	VI	VL	VM
PCSA	15%	22%	38%	25%
EMG	21%	49%	20%	10%

RF: rectus femoris, VI: vastus intermedius, VL: vastus lateralis, VM: vastus medialis

RESULTS AND DISCUSSION

The quadriceps force distribution had little influence on the lateral force acting on the patella. Increasing the Q-angle increased the lateral component of the resultant force applied to the patella by the quadriceps and the patella tendon from 40° to 90° of flexion for both estimates of the quadriceps force distribution. No significant differences were found between the two quadriceps force distributions (Fig. 1). For both Q-angles, changing the quadriceps force distribution from a PCSA-based estimate to an EMG-based estimate significantly decreased the moment acting to tilt the patella laterally from 40° to 90° of flexion, and significantly decreased the moment acting to rotate the distal patella laterally at 50° and 60° of flexion. Changes in the resultant tilt and rotation moments have less influence on the pressure distribution than changes in the resultant lateral force (Elias et al., in press), however.

Changes in the maximum and mean cartilage pressure were similar to changes in the resultant lateral force. For both estimates of the quadriceps force distribution, increasing the Q-angle significantly increased the maximum pressure from 40° to 70° of flexion (Fig. 2) and significantly increased the mean pressure from 40° to 90° of flexion (Fig. 3). For both Q-angles, no significant differences in the maximum or mean pressure were found between the two estimates of the quadriceps force distribution.

SUMMARY

Changing from a PCSA-based to an EMG-based distribution of forces among the muscles of the quadriceps group had little influence on the pressure distribution, primarily due to the fact that increasing the forces applied by the vastus intermedius and rectus femoris while decreasing the forces applied by the vastus lateralis and vastus medialis produced little change in the lateral force acting on the patella.

REFERENCES

Farahmand, F., et al. (1998). *J Orthop Res*, **16**, 136-143.

Zhang, L.-Q., et al. (2003). *J Orthop Res*, **21**, 565-571.

Elias, J.J., et al. (in press). *Am J Sports Med.*

ACKNOWLEDGEMENTS

Funding was provided by a research grant from the Whitaker Foundation

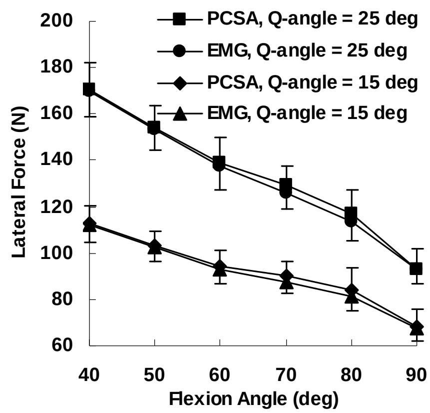

Figure 1: The lateral resultant force.

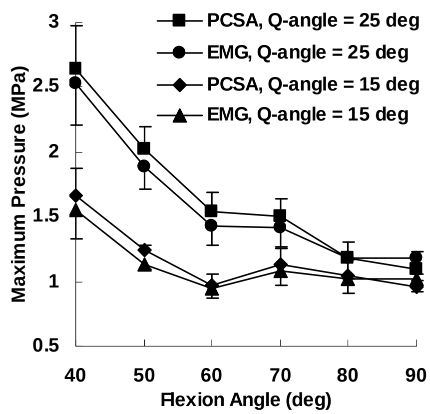

Figure 2: The maximum cartilage pressure.

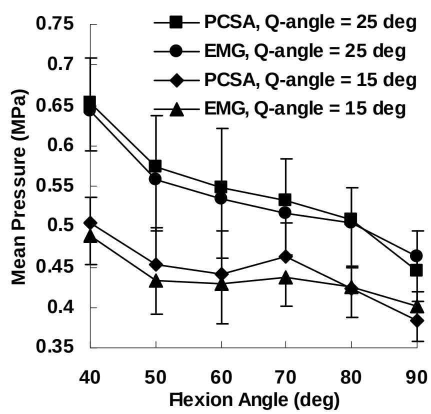

Figure 3: The mean cartilage pressure.

THE EFFECT OF FOOT TYPE ON PLANTAR PRESSURE

William R. Ledoux[1,2,3], Eric S. Rohr[1], Charles Harp[1,3], Randal P. Ching[1,3], and Bruce J. Sangeorzan[1,2]

[1]RR&D Center of Excellence for Limb Loss Prevention and Prosthetic Engineering,
VA Puget Sound Health Care System, Seattle, WA
Departments of [2]Orthopaedics and Sports Medicine and [3]Mechanical Engineering,
University of Washington, Seattle, WA
E-mail: wrledoux@u.washington.edu Web: www.seattlerehabresearch.org

INTRODUCTION

It has long been held that foot structure can affect foot function. Foot type is a means of structurally describing the foot. Feet can be classified as pes cavus (PC, high arch), neutrally aligned (NA, normal arch), and pes planus (PP, low arch). Pes planus feet may be further subdivided into asymptomatic (PPA) and symptomatic (PPS) groups. Plantar pressure is considered a measure of foot function. It has been retrospectively and prospectively associated with ulceration (Boulton *et al.* 1983; Veves *et al.* 1992) and it has been correlated to measures of foot shape (Morag and Cavanagh 1999). The purpose of this study was to explore how foot type (structure) affects plantar pressure (function).

METHODS

A total of 40 subjects were enrolled with ten in each of four foot type groups: PC, NA, PPA, and PPS. Each subject contributed one foot to this analysis. Foot type was determined via clinical examination by an orthopaedic surgeon. Each foot was X-rayed (AP and lateral) and a weight-bearing CT scan was performed. The X-ray and the CT measurements of foot shape were both used to support the determination of foot type (i.e., there were significant differences between foot types, data not shown). Age, weight, height and gender were recorded.

Ten trials of barefoot plantar pressure data were collected with an EMED-SF system. Velocity was recorded with two infrared emitter-reflector-detector systems placed a fixed distance apart on either side of the pressure plate. Stance phase was divided into contact phase (heel strike to foot-flat), mid-stance phase (foot-flat to heel-off) and propulsion phase (heel-off to toe-off). Peak pressure and the pressure-time integral (PTI, i.e., a measure of high pressure dosage) was determined over the entire foot as well as 10 subdivisions: the hallux, lesser toes, first through fifth metatarsal heads, medial midfoot, lateral midfoot and heel. These subdivisions were obtained by overlaying the AP X-ray on top of an actual-size composite peak plantar pressure print out. The Center of Pressure Excursion Index (CPEI), a measure of dynamic foot function, was also determined, as was foot angle (the angle of the foot bisection with the sagittal plane). Adjusting for age, body mass index, and velocity, a linear mixed effects model was used to explore differences between foot types.

RESULTS

There were no significant differences in age, BMI or gender between the four groups, but PC subjects walked significantly slower than all other foot types (Table 1, $p<0.0001$). PC subjects spent significantly more time in midstance ($p<0.0001$) and less time in propulsion (p=0.002) than all other foot types. They also spent less time in contact phase than NA feet (p=0.003). There were no significant differences in CPEI or foot angle. Over the entire foot, PC feet had higher peak pressures than NA or PPA feet, while the PPS had higher peak pressures than NA feet (p=0.001). The PC feet had less pressure beneath the hallux (p=0.0004) and second metatarsal (p=0.002) than all other foot types, and less pressure under the toes (p=0.002) than the PP feet, but higher peak pressure at the fifth metatarsal than either pes planus group (p=0.008). PPS feet had higher peak pressures beneath the first metatarsal compared to the PPA and NA feet (p=0.012). The PC feet also had a higher PTI over the entire foot compared to the PPA and NA feet (p=0.001). PC feet have a smaller PTI under the hallux (p=0.004) and toes (p=0.008) than either PP group, and a smaller PTI than NA and PPA feet under the 3rd metatarsal (p=0.013), and a larger PTI than the PPA feet for the heel (p=0.045). Finally, the PC feet have a larger PTI than PPS feet (p=0.054) for the 5th metatarsal.

DISCUSSION

Subjects with PC feet walked slower and with more time in midstance than the other foot types. PC and PPS foot types are considered pathologic, and thus several differences in peak pressure and PTI from the more benign NA and PPA foot types were seen, indicating aberrant foot function.

REFERENCES

Boulton, A. J., *et al.* (1983). *Diabetes Care* **6**, 26-33.

Morag, E., Cavanagh P. R. (1999). Journal of Biomechanics **32**, 359-70.

Veves, A. *et al.* (1992). *Diabet.* **35,** 660-3.

ACKNOWLEDGEMENTS

This work was supported by the Department of Veteran Affairs project #A2180R. Jane Shofer performed the statistical analysis.

Table 1: Significantly different gait measures (mean ± SE adjusted for age, BMI, and velocity).

	PC (n=10)	NA (n=10)	PPA (n=10)	PPS (n=10)	p*
Velocity (m/s)	0.93 ± 0.05	1.26 ± 0.04	1.20 ± 0.04	1.17 ± 0.05	.0001[abc]
Contact (%)	6.9 ± 0.7	11.0 ± 0.6	9.3 ± 0.6	9.3 ± 0.6	.003[a]
Midstance (%)	69.4 ± 2.7	51.4 ± 2.4	54.1 ± 2.4	52.6 ± 2.6	.0001[abc]
Propulsion (%)	24.0 ± 2.6	37.6 ± 2.4	36.6 ± 2.3	38.1 ± 2.5	.002[abc]
PeP - total (	89.2 ± 6.2	53.6 ± 5.4	63.5 ± 5.7	77.7 ± 5.9	.001[abe]
PeP - hallux	13.3 ± 6.9	41.2 ± 6.4	55.6 ± 6.8	55.0 ± 7.0	.0004[abc]
PeP - 1st metatarsal	31.5 ± 7.4	24.4 ± 7.0	20.2 ± 7.3	53.9 ± 7.4	.012[de]
PeP - 2nd metatarsal	22.1 ± 3.9	39.7± 3.7	43.8 ± 3.9	42.2 ± 3.9	.002[abc]
PeP - 5th metatarsal	47.6 ± 6.5	25.2 ± 5.8	22.6 ± 6.1	14.5 ± 6.1	.008[bc]
PeP - toes	7.7 ± 2.3	13.1 ± 2.1	19.9 ± 2.2	19.0 ± 2.3	.002[bc]
PTI - total	32.7 ± 2.3	20.2 ± 2.1	20.4 ± 2.1	25.4 ± 2.2	.001[ab]
PTI - hallux	2.7 ± 1.6	8.3 ± 1.5	11.0 ± 1.6	10.6 ± 1.6	.004[bc]
PTI - 3rd metatarsal	6.4 ± 0.8	9.8 ± 0.7	9.5 ± 0.8	8.0 ± 0.8	.013[ab]
PTI - 5th metatarsal	10.4 ± 1.6	7.1 ± 1.5	6.2 ± 1.6	3.8 ± 1.6	.054[c]
PTI - toes	1.5 ± 0.6	3.0 ± 0.5	4.0 ± 0.6	4.4 ± 0.6	.008[bc]
PTI - heel	13.1± 1.7	8.2 ± 1.6	6.4 ± 1.7	7.5 ± 1.7	.045[b]

PeP = peak pressure, PTI = pressure time integral, [a]PC v. NA, [b]PC v. PPA, [c]PC v. PPS, [d]PPS v. PPA, [e]PPS v. NA

COMPARISON OF KNEE JOINT MOMENTS REPORTED IN DIFFERENT SEGMENTAL REFERENCE FRAMES

Kristian M. O'Connor, Sarika K. Monteiro, and Jennifer E. Earl

Department of Human Movement Sciences, University of Wisconsin - Milwaukee, WI, USA
E-mail: krisocon@uwm.edu Web: www.uwm.edu

INTRODUCTION

Three-dimensional joint moments have recently been used to investigate movement coordination and joint loading during dynamic tasks such as a cutting maneuver (Besier et al., 2001a) in order to assess joint injury risk. One confounding factor is that three-dimensional net joint moments can be reported in a number of reference frames. There is currently no accepted standard for reporting these moments. Many studies have reported net joint moments in the global reference frame (Eng & Winter, 1995). These moments, however, may not relate to the moments acting about the anatomical axes of the body. Also, for activities such as cutting where the movements do not occur orthogonally to the global coordinate system, a body segment-based coordinate system is more anatomically relevant (Davis et al., 1991). Some studies have reported knee moments in the segment proximal to the joint (Besier et al., 2001a; Davis et al, 1991). Knee joint moments, to our knowledge, have not been reported in the distal reference frame. If the intent is to make clinically relevant inferences of loading of the leg, then reporting knee joint moments in the reference frame of the leg may be more appropriate.

The purpose of this study was to compare three-dimensional knee joint moments reported in the proximal (thigh) and distal (leg) reference frames for a cutting maneuver.

METHODS

Ten active college-age male subjects with no current lower extremity impairment volunteered to participate. All subjects wore a standard running shoe.

Three-dimensional kinematic data were collected at 200 Hz and ground reaction force data were collected at 1000 Hz. Subjects ran 4.5-5.0 m/s and watched for a visual cue to run straight ahead, stop, or cut at 45° to the left. This design was intended to elicit an unanticipated cutting response, which has been shown to differ from anticipated cutting maneuvers (Besier et al., 2001b). The right lower extremity was recorded for all subjects. Five trials were collected for each condition, which were randomly presented. Only the cutting trials were analyzed.

Three-dimensional knee joint kinetics were calculated using an inverse dynamics approach. Knee joint moments were reported in both the thigh and leg reference frames.

RESULTS AND DISCUSSION

The net joint moments in the sagittal plane were nearly identical (Figure 1). In the frontal plane, the profiles were similar, although there was a slight difference in magnitude. The transverse plane moment, however, was quite different. The thigh reference frame yielded an internal rotation moment during mid-stance, while the leg-based reference frame yielded an external rotation moment at mid-stance.

While relatively small when compared to the sagittal plane moment, Besier et al. (2001a) argued that the transverse plane moment may be an important contributor to the risk of knee injury. The choice of reference frame, however, has the potential to alter conclusions about the role of the transverse plane moments. At the ankle, the choice of reference frame has been shown to greatly alter the interpretation of the non-sagittal plane moments (O'Connor, 2002).

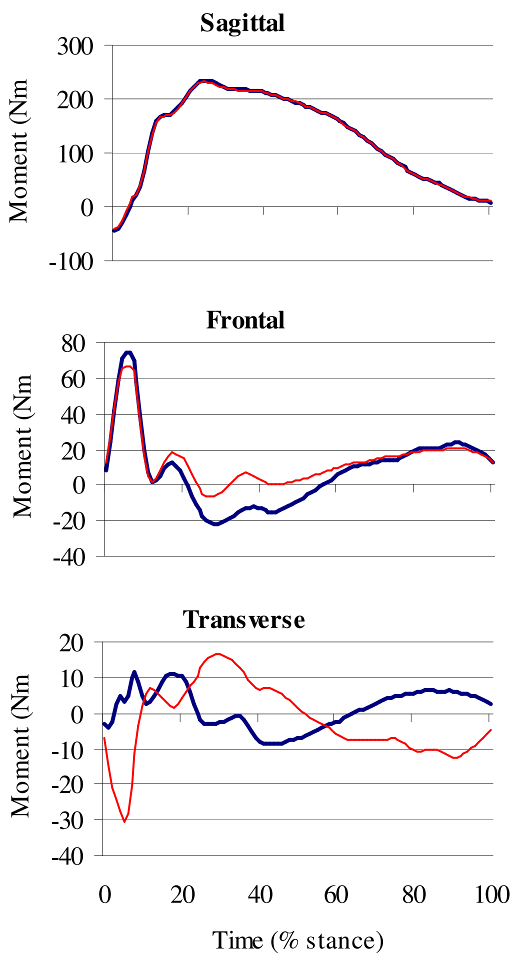

Figure 1: Ensemble average sagittal, frontal, and transverse plane moments at the knee reported in the thigh (thin red) and leg (thick blue) reference frames during a cutting maneuver.

SUMMARY

There were relatively minor differences in the sagittal and frontal plane moments between the two reference frames. The transverse plane moments, however, were characteristically different. It was concluded that the distal reference frame was more appropriate, because the transverse plane moment reported in the distal segment will more accurately reflect the internal/external rotation moment acting on the leg at the knee. When the knee flexes, the transverse plane of the thigh does not coincide with that of the leg.

Given that the choice of reference frame can influence interpretation of non-sagittal joint loading, care should be taken in choosing the appropriate convention.

REFERENCES

Besier, T.F. et al. (2001). *MSSE,* **33,** 1168-1175.
Besier, T.F. et al. (2001). *MSSE,* **33,** 1176-1181.
Davis, R.B. et al. (1991). *Human Movement Science,* **10**, 575-587.
Eng, J.J., Winter, D.A. (1995). *J. Biomechanics,* 28, 753-758.
O'Connor, K.M. (2002). University of Massachusetts.

ACKNOWLEDGEMENTS

UWM College of Health Sciences (SEED Grant)

FACTORS AFFECTING THE ACCURACY OF 2D-DLT CALIBRATION

Scott P. McLean[1], Peter F. Vint[2], Richard N. Hinrichs[3], John K. DeWitt[4], Bryan Morrison[3], and Jason Mitchell[1]

[1]Biomechanics Laboratory, Kinesiology Dept., Southwestern University, Georgetown, TX, USA
[2]Research Integrations, Inc., Tempe, AZ, USA
[3]Biomechanics Laboratory, Kinesiology Dept., Arizona State University, Tempe, AZ, USA
[4]Exercise Physiology Laboratory, NASA-Johnson Space Center, Houston, TX, USA
e-mail: mcleans@southwestern.edu

INTRODUCTION

A simplified version of the direct linear transformation (DLT) (Abdel-Aziz and Karara, 1971) known as the two-dimensional (2D) DLT (Walton, 1981), offers an alternative to the use of the simple scaling technique for calibrating an image plane. Brewin and Kerwin (2003) found camera pitch angles ranging from 2° below horizontal to 6° above horizontal had little effect on 2D-DLT calibration accuracy. However, little additional research has systematically investigated factors that would affect the accuracy of the 2D-DLT. The purposes of this project were to evaluate the effect of the number of control points used for calibration, the distance from the camera to the calibration plane (camera distance), and the camera yaw angle relative to the calibration plane (camera angle) on 2D-DLT calibration accuracy.

METHODS

A planar calibration object (120 cm × 120 cm) with a 12 × 12 grid of 2.5 cm diameter markers spaced 10 cm apart was constructed of MDF board (Figure 1). The location of the center of each grid marker was surveyed to the nearest 0.1 cm using triangulation. The calibration object was oriented vertically.

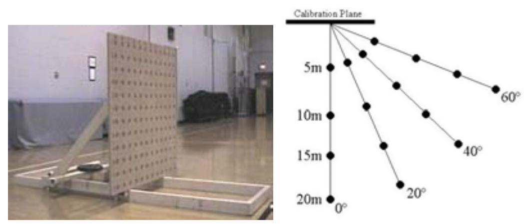

Figure 1. 2D-DLT calibration object and camera positions for filming.

A digital camcorder was mounted and leveled on a tripod. The camera was zoomed to maximize image size. The control object was filmed with the camera positioned at four distances (5m, 10m, 15m, and 20m) from the control object and at each of four yaw angles (0°, 20°, 40°, and 60°) (Figure 1).

All 144 grid points were digitized in a single video frame using the Motus system (Peak Performance Technologies, Inc., Englewood, CO). DLT camera parameters based on specified grid points (control points, CP) were computed using custom 2D-DLT software for each camera position. The remaining grid points were defined as non-control points (NCP).

Average resultant prediction error of non-control points was evaluated for combinations of control points ranging from 4 to 56 points to determine the minimum number of control points needed to produce the most accurate calibration. Additional analyses were conducted to assess the prediction error of non-control points as a function of camera position, and camera angle.

RESULTS AND DISCUSSION

Although resultant prediction error was small for all combinations of control points, this error approached a constant value of approximately 0.12 cm with a minimum of 24 control points (Figure 2). Subsequent analyses were based on calibrations that used 24 control points. Prediction errors represented the average resultant error for the remaining 120 non-control points.

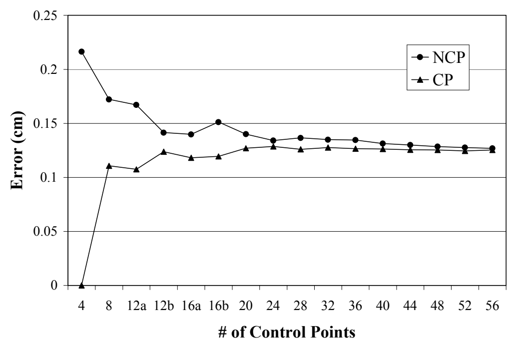

Figure 2. Prediction error as a function of number of control points.

The 2D-DLT was not affected by camera distance. The range in average resultant prediction error for the image plane was generally less than 0.1 cm between different camera distances when camera angle was held constant (Figure 3). A common recommendation for using the scaling technique for 2D calibration is to move the camera as far from the image plane to minimize perspective error. This suggests that a major advantage of 2D-DLT over the scaling technique is the ability to calibrate with the camera close to the object plane.

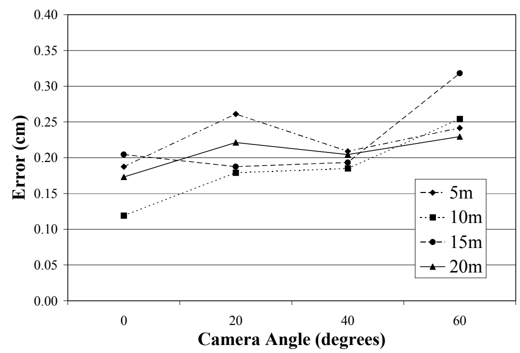

Figure 3. Prediction error as a function camera yaw angle and camera distance.

Although there was a trend for average resultant prediction error to increase as camera angle increased, these errors remained small (< 3 mm or 0.2% of the calibration object diagonal) through a camera angle of 60° (Figure 3). This suggests that a second advantage of the 2D-DLT is the ability to calibrate an object plane when the camera is positioned oblique to the plane.

SUMMARY

Use of a minimum of 24 control points is recommended for best 2D-DLT calibration accuracy. The 2D-DLT provides a robust alternative to the simple scaling technique for calibrating a 2D object space because camera distance has little effect on calibration accuracy and camera positions oblique to the calibration plane only slightly decrease calibration accuracy.

REFERENCES

Abdel-Aziz, Y.I. and Karara, H.M. (1971). *Proc. Am. Society of Photogrammetry.*

Brewin, M.A. and Kerwin, D.G. (2003). *J. Appl. Biomech.*, **19**, 79-88.

Walton, J. (1981). *Unpublished dissertation*, Pennsylvania State University.

Patellofemoral Lesions Increase Pressure Applied to Surrounding Cartilage

John J. Elias[1], Derek R. Bratton[1], David M. Weinstein[1], Andrew J. Cosgarea[2]

[1]Medical Education and Research Institute of Colorado, Colorado Springs, CO
[2]Department of Orthopaedic Surgery, Johns Hopkins University, Baltimore, MD
e-mail: elias@meric.info web: www.meric.info

INTRODUCTION

Isolated cartilage lesions are common in patients with patellofemoral pain and/or instability. The lesions do not preferentially develop at any one position on the patella. Although a primary goal of treatment is unloading existing lesions, how lesions influence the patellofemoral pressure distribution is not well understood. The current study was performed to determine how the position and severity of patellofemoral lesions influence the pressure applied to the surrounding cartilage.

METHODS

Four computational models of the knee were created using a technique which has been shown to accurately characterize how variations in patellofemoral loading influence the pressure applied to the cartilage (Elias et al., 2004). As described previously (Elias et al., in press), a knee squatting activity was simulated while force vectors representing the four muscles of the quadriceps group and the patella tendon were applied to the patella. At flexion angles ranging from 40° to 90°, the patellofemoral pressure distribution was quantified by minimizing the potential energy stored within springs representing the cartilage and the joint capsule.

The pressure distribution was quantified for normal cartilage and for simulated cartilage lesions. Each lesion was circular with a radius of 8 mm (Huberti and Hayes, 1988). A proximal lesion was positioned with the proximal edge of the lesion aligned with the proximal edge of the patellofemoral contact surface (Fig. 1). The same technique was used to position lateral, medial, and distal lesions. A central lesion was placed midway between the lateral and medial lesions. The stiffness of the cartilage at each lesion site was decreased by 50% and 75% to represent varying degrees of softening. Changes in the pressure distribution were characterized in terms of the maximum pressure and the mean pressure ratio. The mean pressure ratio is the mean pressure in the cartilage outside the borders of the lesion when the cartilage stiffness is decreased, divided by the same measurement when the cartilage stiffness is not decreased. A repeated measures ANOVA and Student-Neuman-Keuls post-hoc test were used to examine for statistically significant ($p < 0.05$) variations in the measured parameters.

RESULTS AND DISCUSSION

The distal and central lesions caused the greatest pressure increase near 40° of flexion, while the proximal lesion caused the greatest pressure increase near 90°. For a 50% cartilage stiffness decrease, the distal lesion significantly increased the maximum pressure, compared to the case of no lesion, at 40° and 50°of flexion (Fig. 2), while the proximal lesion significantly increased the maximum pressure at 90°. The proximal lesion also created a significantly larger mean pressure ratio than all other lesions at 80° and 90° (Fig. 3). The central lesion created the second largest average mean pressure ratio from 70° to 90° of flexion, and created the largest average mean pressure ratio from 40° to 60° of flexion. The lateral lesion had less influence on the mean pressure ratio than the central lesion, but had a similar influence on the maximum pressure. The medial lesion typically had the least influence on the maximum pressure and the mean pressure ratio during flexion.

Changing the decrease in the stiffness of the cartilage at the site of a lesion from 50% to 75% increased the maximum pressure and mean pressure ratio for all lesions. For a proximal lesion, this change increased the average maximum pressure and the mean pressure ratio at 90° of flexion by 26% and 17%, respectively. For a distal lesion, this change increased the average maximum pressure and the mean pressure ratio at 40° of flexion by 12% and 11%, respectively.

SUMMARY

When a cartilage lesion develops on the patella, the pressure applied to the normal cartilage surrounding the lesion increases. Proximal lesions cause a particularly large pressure increase near 90° of flexion, which worsens as the properties of the cartilage at the lesion site deteriorate.

REFERENCES

Elias, J.J., et al. (2004). *J Biomech*, **37**, 295-302.

Elias, J.J., et al. (in press). *Am J Sports Med.*

Huberti, H.H., Hayes, W.C. (1988). *J Orthop Res*, **6**, 499-508.

ACKNOWLEDGEMENTS

Funding was provided by a research grant from the Whitaker Foundation

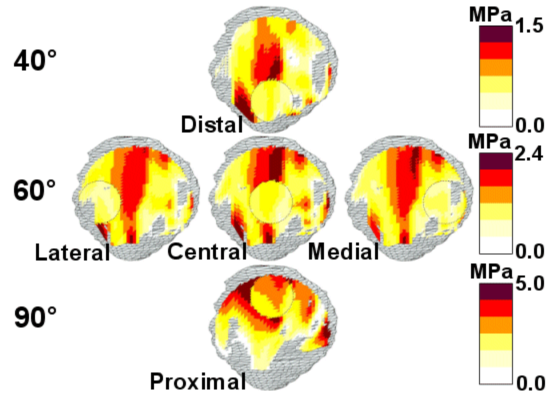

Figure 1: The patellofemoral pressure distribution for all lesion positions on one model at various flexion angles for a 50% cartilage stiffness decrease.

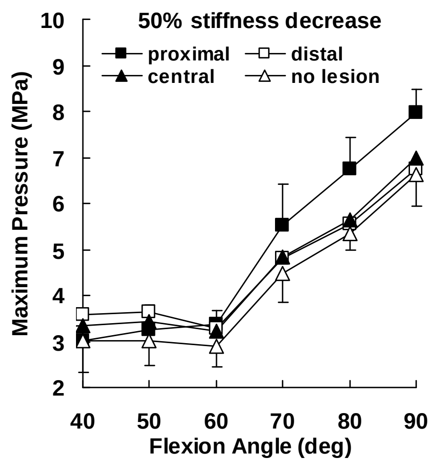

Figure 2: The maximum cartilage pressure for select lesions for a 50% cartilage stiffness decrease.

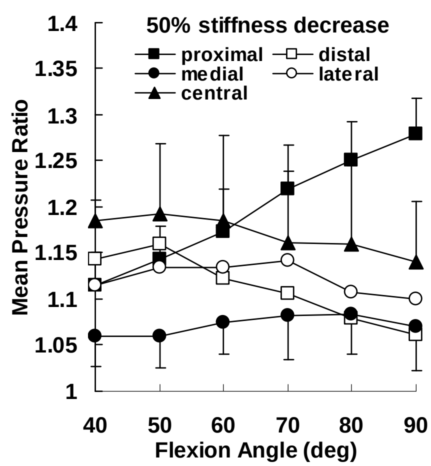

Figure 3: The mean pressure ratio for all lesions for a 50% stiffness decrease.

EFFECTS OF EXAGGERATED PRONATION AND SUPINATION ON KNEE MECHANICS DURING A CUTTING MANEUVER

Jennifer E. Earl, Sarika K. Monterio, and Kristian M. O'Connor

Department of Human Movement Sciences, University of Wisconsin - Milwaukee, WI, USA
E-mail: jearl@uwm.edu Web: www.uwm.edu

INTRODUCTION

Non-contact injuries to the anterior cruciate ligament typically occur as a result of sudden twisting, cutting or change of direction without direct contact with an external object. The mechanism of non-contact ACL injury is commonly associated with a position of knee valgus and tibial external rotation. There is contradiction in the literature about how foot pronation relates to knee motion and ACL injury. Excessive pronation has consistently been identified as a risk factor for non-contact ACL injury. However, pronation contributes to tibial internal rotation, which is contradictory to the reports of external rotation occurring at the time of injury.

The purpose of this study was to determine how exaggerated pronation or supination influenced knee kinetics and kinematics during a side cutting maneuver.

METHODS

Ten active college-age males, with no current lower extremity impairment, volunteered to participate.

Three-dimensional kinematic data were collected at 200 Hz and ground reaction force data were collected at 1000 Hz. Subjects ran 4.5-5.0 m/s, and watched for a visual cue to run straight ahead, cut 45° to the left, or stop quickly. This design was intended to elicit an unanticipated cutting response, which has been shown to differ from anticipated cutting maneuvers (Besier et. al., 2001b) The right leg of all subjects was tested. Only the cutting trials were analyzed.

Subjects wore custom made running shoes: a pair with a neutral-posted midsole, a pronated pair with an 8° lateral rearfoot wedge, and a supinated pair with an 8° medial rearfoot wedge. Five trials of each activity were collected in each of the three shoes, for a total of 45 trials.

Three-dimensional knee joint kinematics and kinetics were calculated using an inverse dynamics approach. Knee joint moments were reported in the leg reference frame. Peak joint angle and moment data were extracted from the stance phase, and analyzed using repeated measures ANOVA. ($p<0.05$).

RESULTS AND DISCUSSION

ANOVA revealed a significant difference in knee external rotation moment ($f_{2,18}=4.407$, $p=0.03$), with the pronated shoe causing significantly less external rotation moment than the neutral or supinated shoe (Figure 1). There were no significant differences in the sagittal or frontal plane moments, or in any of the kinematic variables. There was, however, a trend toward a decrease in the knee abduction moment in the pronated shoe compared to the neutral and varus shoes, although this difference did not reach statistical significance ($p=0.12$) (Figure 2).

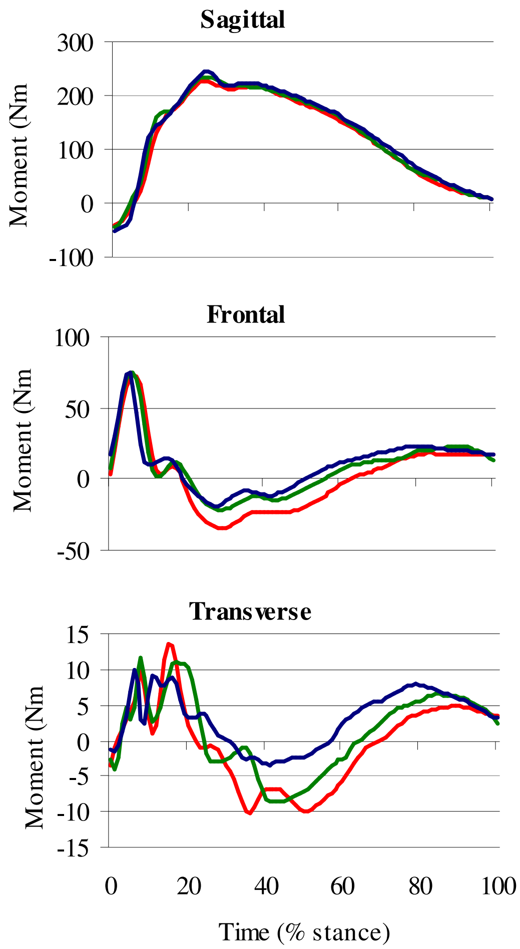

Figure 1: Sagittal, frontal, and transverse plane moments at the knee during a cutting maneuver. Red = varus shoe, Green = neutral shoe, Blue = valgus shoe.

Joint angle patterns observed in this study are similar to those previously reported. (McLean et. al. 1998, Neptune et. al., 1999) Besier et al (2001a) reported similar patterns of knee joint moments in the sagittal and frontal planes during a cutting maneuver, but the pattern in the transverse plane is different from what was seen in this study. Besier et. al. (2001a) reported a small external rotation moment during the weight acceptance phase, which increased during midstance, and decreased at push off. Results from the current study show a pattern that reversed from an internal rotation moment at weight acceptance, to an external rotation moment during midstance, to an internal rotation moment during push off. This difference may be a result of a slower running speed, or other variations in the protocol or footwear.

SUMMARY

Wearing a pronated shoe during cutting decreased the knee external rotation moment during stance. Because there were no differences in knee joint angles, other forces must be acting on the lower leg and thigh to slow internal rotation motion during stance. Based on these data, increased pronation of the foot does not appear to increase the stresses on the knee joint during a cutting maneuver. The hypothesis of increased pronation contributing to excessive loading at the knee and greater injury risk does not appear to be supported by these data. The relationship between knee joint moments and those at the ankle and hip will be explored in future reports.

REFERENCES

Besier, T.F. et al. (2001a). *Medicine and Science in Sports and Exercise*, **33**, 1168-1175.

Besier, T.F. et al. (2001b). *Medicine and Science in Sports and Exercise*, **33**, 1176-1181.

McLean, S.G. et al. (1998). *Bulletin Hospital for Joint Diseases*, **57**, 30-38.

Neptune, R.R. et al (1999). *Medicine and Science in Sports and Exercise.* **31**, 294-302.

ACKNOWLEDGEMENTS

UWM College of Health Sciences SEED grant.

PREDICTING OUT-OF-PLANE POINT LOCATIONS USING THE 2D-DLT

Richard N. Hinrichs[1], Bryan Morrison[1], Peter F. Vint[2], John K. DeWitt[3], Jason Mitchell[4] and Scott P. McLean[4]

[1]Biomechanics Laboratory, Kinesiology Dept., Arizona State University, Tempe, AZ, USA
[2]Research Integrations, Inc., Tempe, AZ, USA
[3]Exercise Physiology Laboratory, NASA-Johnson Space Center, Houston, TX, USA
[4]Biomechanics Laboratory, Kinesiology Dept., Southwestern University, Georgetown, TX, USA
e-mail: hinrichs@asu.edu

INTRODUCTION

McLean et al. (2004) demonstrated that the two-dimensional (2D) direct linear transformation (DLT) (Walton, 1981) is a robust alternative to the simple scaling technique often used to calibrate an object plane. However, often joint markers or body landmarks move out of the calibrated plane. The use of the 2D-DLT in such situations requires an extrapolation of the calibration. The purposes of this project were (1) to examine prediction of points out of the calibration plane, and (2) to assess the effects of altering the distance from the camera to the calibration plane (camera distance), and the camera yaw angle relative to the calibration plane (camera angle) on the accuracy of extrapolated point prediction using the 2D-DLT.

METHODS

A planar calibration object (120 cm × 120 cm) with a 12 × 12 grid of 2.5 cm diameter markers spaced 10 cm apart was constructed of MDF board (Figure 1). The location of the center of each grid marker was surveyed to the nearest 0.1 cm using triangulation. The calibration object was oriented vertically and could be translated horizontally through a distance of 1 m at 0.1 m increments. The middle plane of this translation space was defined as the calibration plane (0 cm of extrapolation). The extrapolated planes extended from 50 cm behind the calibration plane (–50 cm) to 50 cm in front of the calibration plane (+50 cm).

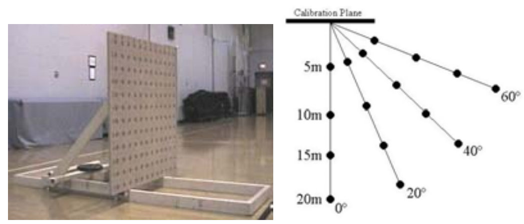

Figure 1. 2D-DLT calibration object and camera positions for filming.

A digital camcorder was mounted and leveled on a tripod. The calibration object was filmed in each extrapolation position at 16 camera positions (Figure 1). For each camera position the camera was zoomed to maximize image size in the +50 cm plane but focused in the 0 cm plane.

All 144 grid points were digitized in a single video frame using the Motus system (Peak Performance Technologies, Inc., Englewood, CO). DLT camera parameters based on 24 control points (CP) were computed for each camera position using custom 2D-DLT software. These were used to predict coordinate locations of the remaining 120 non-control points (NCP). Average absolute prediction error in the horizontal (X) and vertical (Y) directions and the resultant prediction error were used for comparison.

RESULTS AND DISCUSSION

Extrapolation outside of the calibrated plane increased prediction error (Figure 2). Furthermore, the magnitude of this error was mediated by camera distance such that prediction error was reduced when the camera was placed further from the image plane.

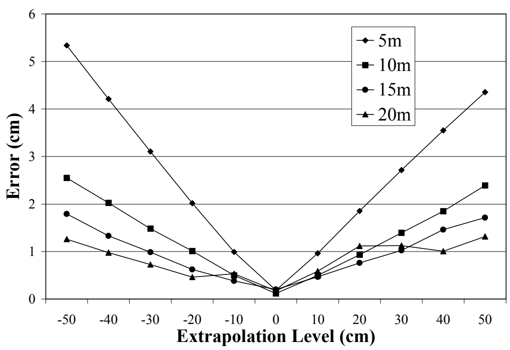

Figure 2. Prediction error as a function of extrapolation with a 0° camera angle.

The 2D-DLT allowed calibration of an image plane using non-zero camera angles with only small increases in prediction error. However, use of oblique camera angles had a substantial effect on prediction error of points outside of the calibrated plane (Figure 3).

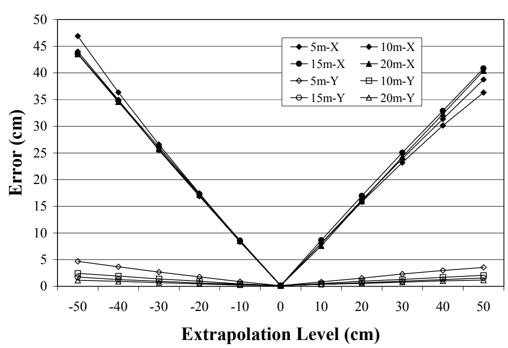

Figure 3. X and Y prediction error as a function of extrapolation with a 40° camera angle.

The magnitude of this error increased with camera angle. This increase was due primarily to increased error in the prediction of horizontal coordinates (Figure 4). Increasing camera distance reduced extrapolation error of the vertical coordinates but had little effect on the extrapolation errors of the horizontal coordinates.

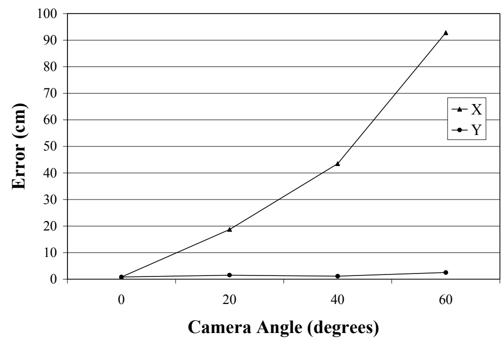

Figure 4. X and Y prediction error as a function of camera angle (-50cm extrapolation plane, 20m camera distance).

SUMMARY

Care must be taken when using the 2D-DLT if extrapolation is necessary. Increasing camera distance reduces prediction error in horizontal and vertical coordinates for a 0° camera angle but only the vertical coordinates of non-zero camera angles. Furthermore, the substantial increases in prediction error of the horizontal coordinates with non-zero camera angles suggest that extrapolation should be avoided in these situations.

REFERENCES

McLean, S.P. *et al.* (2004). *Proc. of ASB '04*.

Walton, J. (1981). *Unpublished dissertation*, Pennsylvania State University.

COMPUTATION OF MOTION PATTERNS OF THE COCHLEAR PARTITION

Hongxue Cai, Brett Shoelson, and Richard S. Chadwick

Section on Auditory Mechanics, NIDCD/NIH, Bethesda, MD 20892
E-mail: hongxuec@helix.nih.gov

INTRODUCTION

The relative motions of the different parts of the cochlear partition (CP) in the inner ear, which are directly related to the bending of the hair bundles of the mechano-sensory cells, remain unclear. Experiments to determine the motion of the CP and surrounding fluid are extremely challenging. As a result, the motion data are incomplete and often contradictory. One potential bending mechanism of the stereocilia is thought to be the tectorial membrane (TM) radial resonance. Gummer et al. and Hemmert et al. showed a radial resonance of the TM motion. However, these findings contrast those of Ulfendahl et al., who reported almost no radial TM motion. Another controversy involves the transverse mode shape of the basilar membrane (BM), i.e. the variation in phase across the width of the BM. Both monophasic and multiphasic responses have been reported in the basal turn of the guinea pig cochlea. While the BM is accessible at the base, the TM and organ of Corti (OC) are not. In contrast, the TM and OC are accessible at the apex, but the BM is difficult to probe.

In this study, we: (a) develop and apply a new 2-D incompressible optical flow technique in the hemicochlea preparation, and (b) use a hybrid analytical/finite-element approach to model both the basal and apical regions of the guinea pig cochlea. In (a), we formulate a mathematically well-posed problem by introducing an in-plane incompressibility constraint, and solve the resulting system using a Lagrangian description of the conservation equations. In (b), we solve a fluid-solid interaction eigenvalue problem for the axial wavenumber, fluid pressure, and vibratory relative motions of the CP as functions of frequency. We find, for the first time in a complex continuum model, evidence of TM radial motion at both the base and apex of the hearing organ.

METHODS

2-D incompressible optical flow The optical flow method is usually mathematically ill-posed, because the single scalar equation representing the conservation of local intensity (I), $\partial I/\partial t + \mathbf{v} \cdot \nabla I = 0$, contains more than one unknown velocity component ($\mathbf{v} = v_x\mathbf{i} + v_y\mathbf{j}$). Instead of regularizing the problem using optimization techniques, we introduce an in-plane incompressibility constraint ($\nabla \cdot \mathbf{v} = 0$), which implies that infinitesimal elements conserve area as they move. We follow the same material points in a region of image area as the region moves or deforms. With this Lagrangian approach, the displacement of isointensity contours on sequential images determines the normal component of velocity of an area element, while the tangential component is computed from the local constant area constraint.

Hybrid WKB/finite-element approach We use the WKB perturbation method to treat the axial propagation of the traveling waves, and use finite-element analysis in the cross-sections of the cochlea, which are divided into fluid and solid domains. The elastic domain representing the OC is further divided into sub-domains to include discrete cellular structures. The elastic sub-domains are assigned different values for Young's modulus. The cochlear fluid is viscous and incompressible with dynamics following the linearized Navier-Stokes equations. The BM is treated as an orthotropic plate, and the TM and reticular lamina (RL) are elastically coupled through the stereocilia bundle stiffness. The outer hair cells (OHCs) are treated as passive structural elements; we do however inves-

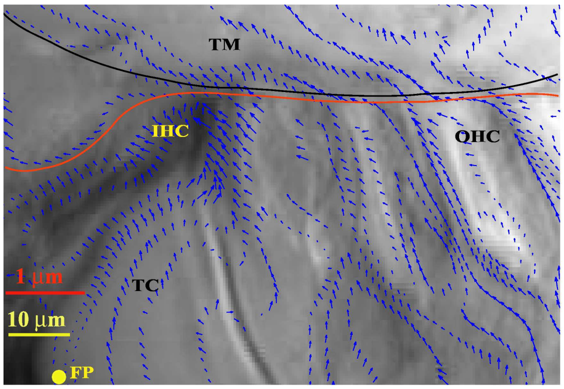

Figure 1: Optical flow field computed from two video images of the hemicochlea preparation excited at 1.8 kHz. results are shown for the sub TM-RL-OHC-IHC region.

tigate the effect of introducing a negative bundle stiffness parameter. It is important to emphasize that although the computations are performed in planes, we still retain coupling in the axial direction through the wavenumber k, both in the fluid and solid domains. Details of our model, including the governing equations, boundary conditions, and iterative computational algorithm, can be found in Cai and Chadwick (2003).

RESULTS AND DISCUSSION

Figure 1 shows the computed optical flow field for a hemicochlea stimulated at 1.8 kHz. A shear motion exist between the TM and RL, essentially induced by a rotation of the RL about the foot plate (FP) of the inner pillar cell. Our modified optical flow method is a new, fast and efficient geometry-based approach, which has a better performance than the Lucas and Kanade algorithm when it is applied to to the image sequences from the the hemicochlea preparation, where motions are complex and extremely small (Cai et al., 2003).

Figure 2 shows the comparison of the detailed relative motions within the CP at the apex of cochlea, stimulated at 300 Hz and 1 kHz, respectively. The vibratory mode of the BM is monophasic at both the

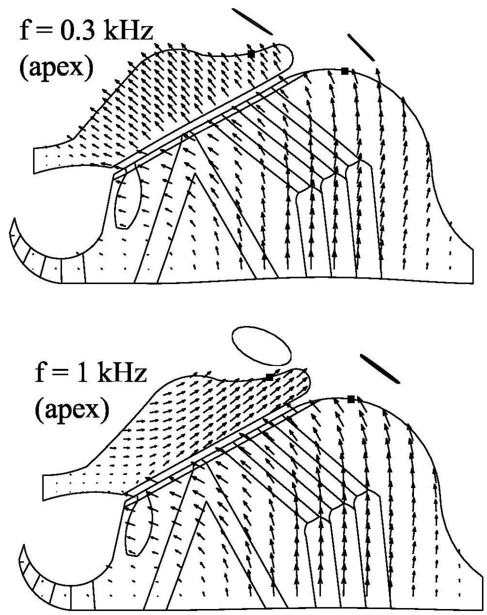

Figure 2: Detailed movements within the OC and TM at cochlear apex. Orbits are shown for two simulated microspheres.

apical and basal portions of the cochlea. Nevertheless we find a transition to an evident TM radial motion around 850 Hz. At 300 Hz the vector patterns resemble those obtained by the optical flow technique in Fig.1. At 1 kHz, however, the direction of the vectors on the TM changes dramatically to show an evident radial motion. The trajectories of "simulated microspheres" affixed to the top of the TM and Hensen cells are in excellent quantitative agreement with measurements (Gummer et al. 1996, Hemmert et al., 2000). Note that we also find a transition to an evident TM radial motion in the frequency range from 11 to 14 kHz at the cochlear base (Cai et al., 2004).

Cai, H. et al. (2004). *Proc. Natl. Acad. Sci. USA*, (in press).

Cai, H., Chadwick, R.S. (2003). *SIAM J. Appl. Math.*, **63.4**, 1105-1120.

Cai, H. et al. (2003). *Biophys. J.*, **85**, 1929-1937.

Gummer, A.W. et al. (1996). *Proc. Natl. Acad. Sci. USA*, **93**, 8727-8732.

Hemmert, W. et al. (2000). *Biophys J.*, **78**, 2285-2297.

Ulfendahl, M. et al. (1995). *Neuroreport*, **6**, 1157-1160.

INFLUENCE OF SEX AND GENOTYPE ON SKELETAL FRAGILITY

Marie Shea[1], Brenden L. Hansen[1], Dawn A. Olson[2], Denise Dinulescu[2], Ben Orwoll[2], John K. Belknap[2], Eric S. Orwoll[2], and Robert F. Klein[2]

[1]Orthopaedic Biomechanics Laboratory, Oregon Health & Science University, Portland, OR, USA
[2]Bone and Mineral Unit, Oregon Health & Science University, Portland, OR, USA
sheam@ohsu.edu

INTRODUCTION

Genetic factors play an important role in determining bone mineral density (BMD), size, and shape, all key contributors to bone strength. Although the chromosomal loci of genes responsible for the heritable differences in BMD are being explored, the specific biomechanical characteristics that describe the integrity of skeletal tissue in commonly used laboratory mice are unknown. To explore these characteristics, we examined both sex-dependent and strain-dependent differences in femoral BMD, geometry and failure properties in 8 genetically distinct inbred mouse strains.

METHODS

Adult (20 week-old) male and female mice (10-16/sex/strain) were bred at the Portland VA Veterinary Medical Unit from stock originally obtained from the Jackson Laboratories. Strains were: C3H/HeJ (C3H), AKR, A/J, BALB/cByJ (BALBc), Castaneus (CAST), 129S1, C57Bl/6J (B6), and DBA/2J (DBA).

Excised femora were scanned with a Piximus scanner to determine BMD and with a Skyscan micro computed-tomograph to determine midpoint geometric properties (moment of inertia, cortical thickness; and all cross-sectional areal measurements). Femora were tested to failure in 3-point bending on a material testing machine to determine failure or ultimate load, stiffness, strength, modulus, work to failure, and ductility.

RESULTS

Figure 1 Femoral midshaft slices show that cortical thickness (B6, C3H) and specimen shape (AKR, DBA) vary significantly among strains.

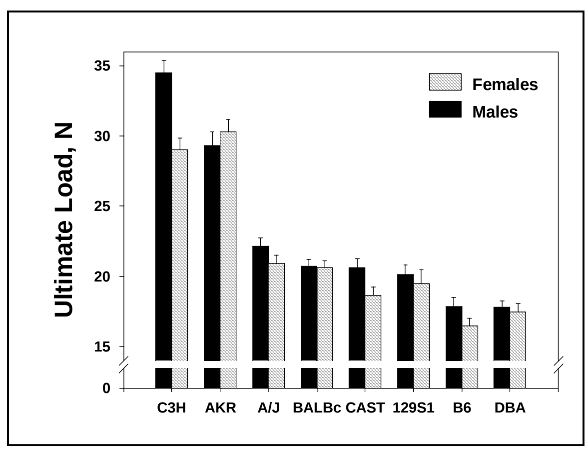

Figure 2: Ultimate load varied widely among strains, and there was a striking difference between sexes with values of males exceeding those of females in all strains but AKR.

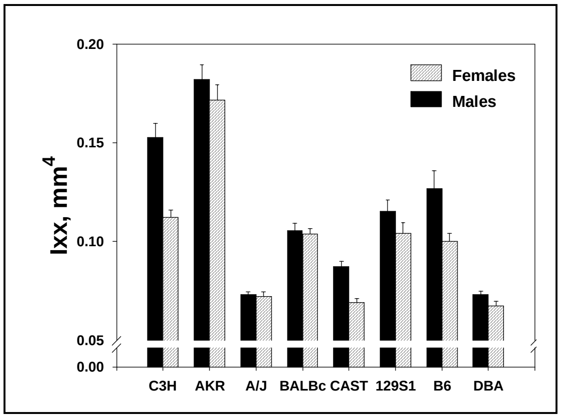

Figure 3: Moment of inertia, Ixx, varied 2.5-fold across strains, and was consistently higher in males (8/8 strains).

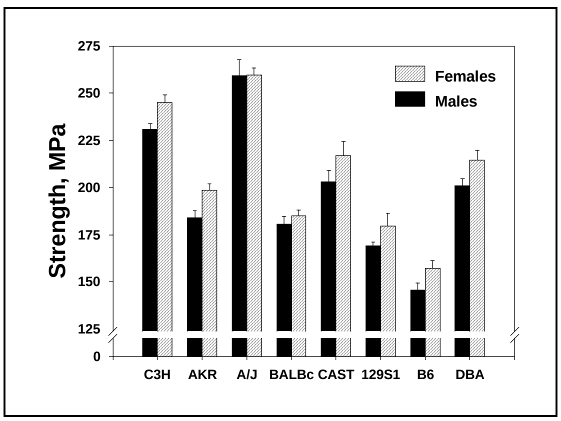

Figure 4: Tissue strength (and modulus) varied nearly 2-fold across strains and interestingly were both higher in females (8/8 strains strength, 7/8 strains modulus).

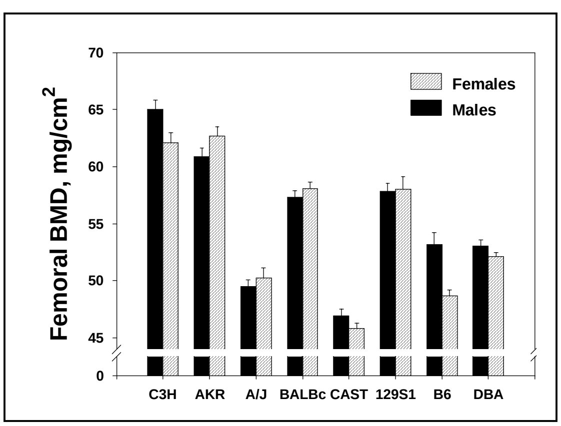

Figure 5: Femoral BMD also varied 2.5 -fold across strains.

Across strains, there was a strong correlation between femoral ultimate load and femoral BMD (R=0.725)

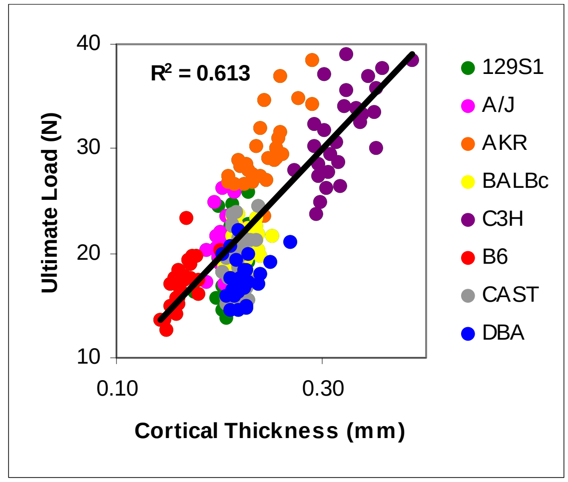

Figure 6: Across strains, there was a strong correlation between femoral ultimate load and all femoral geometric measures (R=0.457-0.861) except marrow area.

DISCUSSION

These data indicate that the key determinants of bone strength are under significant genetic control in these common mouse strains. Geometry varied widely among strains and played a large role in femoral ultimate loads. These data also highlight the important role of gender in the inheritance of skeletal strength. Since the male phenotype is associated with considerable fracture risk reduction in humans, an improved understanding of the nature of the gender divergence in murine skeletal traits could provide for novel diagnostic, preventative or therapeutic approaches.

ACKNOWLEDGEMENT

This work was supported by Roche Pharmaceuticals, Veterans Affairs Medical Research Service and the National Institutes of Health (AE44659).

Effects of Gait Velocity on COP Symmetry Measures in Individuals with Stroke

Mary M. Rodgers, Larry Forrester, Christopher Mizelle, Michelle Harris-Love

Department of Physical Therapy and Rehabilitation Science,
University of Maryland School of Medicine, Baltimore, MD, USA
E-mail: mrodgers@umaryland.edu Web: http://pt.umaryland.edu

INTRODUCTION

Asymmetry is a prominent characteristic of hemiparetic gait of stroke survivors and gait velocity is viewed as an indicator of functional ability. Several biomechanical indicators of improvement in the quality of walking gait for individuals with stroke have been identified including stance-time symmetry (Harris-Love et al., 2001), stride length symmetry and walking velocity (Gaviria et al., 1996). However, the relationship of hemiparetic gait asymmetry to walking speed is not well understood. The purpose of this study was to compare the sensitivity of insole center of pressure (COP) symmetry measures to gait velocity among individuals with stroke.

METHODS

Subjects included 36 individuals (24 male, 12 female; 24 with left side hemiparesis, mean age 67 ± 10 yrs;) more than 6 months post-stroke. Mean Berg Balance scores were 36±10 (6 to 54 range) and no assistive devices were used during testing. After informed consent, three walking trials at the individual's self-selected velocity were collected with five complete cycles. Walking speed was measured on a 24-foot GaitRite (CIR Systems, Clifton, NJ, USA) gait mat. Pressures were measured using a Pedar insole pressure distribution system (Novel, Munich, Germany). Pressure variables included anteroposterior (A-P) and mediolateral (M-L) mean displacement ranges of the COP for each side (paretic and non-paretic) and the composite total COP path lengths. Symmetry indices were derived as: 1) the ratio of bilateral COP paths (paretic/non-paretic) and 2) ratios of the COP path ranges (paretic/non-paretic) for A-P and M-L displacements. Linear regression analyses were performed to determine the relationship of these variables to walking velocity using SAS (Cary, NC) statistical package with significance at the $p<0.05$ level.

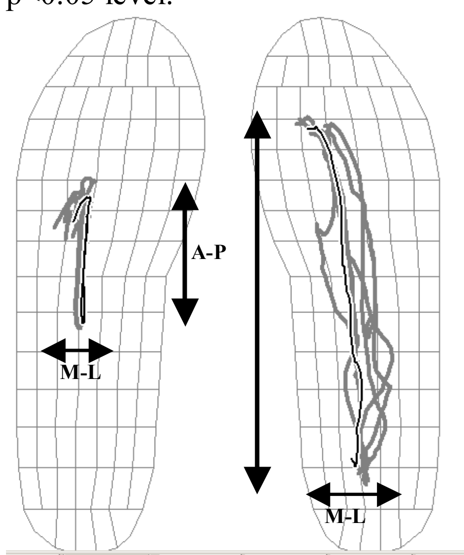

Figure 1: COP path from one subject with left hemiparesis.

RESULTS AND DISCUSSION

Mean walking velocity for all subjects was 38.2 ± 22.4 cm/s, indicating considerable gait impairment. Regression analysis results are summarized in Table 1. Total COP path length and A-P COP ratios demonstrated a trend toward greater symmetry with increasing velocity (Figure 1A). Further analysis of the COP variables for each foot demonstrated a differential response to velocity from the paretic foot (Figure 1B).

SUMMARY

COP measures and symmetry indices show a positive relationship to walking velocity in individuals with chronic stroke. The symmetry indices may provide documentation of the restitution of gait ability in more impaired subjects.

REFERENCES

Harris-Love, M.L. et al. (2001). *Neurorehabil Neural Repair,* 105-112.

Gaviria M. et al. (1996). *Gait Posture,* 297-305.

ACKNOWLEDGEMENTS

This work was supported by NIH P50 AG12583 and Department of Veterans Affairs: Rehabilitation Research and Development Service Career Development Award.

Table 1: Regression analysis results for insole center of pressure (COP) variables (*significant at the $p<0.05$ level)

COP Variable	Mean	Standard Deviation	Intercept	Slope	R^2	Slope p-value
Path Length Ratio	0.77	0.19	0.646	0.0032	0.14	**0.027***
Anteroposterior (A-P) Ratio	0.81	0.22	0.676	0.0035	0.13	**0.031***
Mediolateral (M-L)Ratio	0.91	0.32	0.828	0.0022	0.02	0.363
Nonparetic Foot Path Length (mm)	319.5	61.9	312.7	0.1758	<0.01	0.708
Nonparetic Foot A-P Range (mm)	173.1	24.1	162.1	0.290	0.07	0.108
Nonparetic Foot M-L Range (mm)	35.9	9.5	30.5	0.142	0.12	**0.042***
Paretic Foot Path Length (mm)	242.6	67.2	203.1	1.033	0.12	**0.037***
Paretic Foot A-P Range (mm)	141.1	44.3	110.3	0.807	0.17	**0.012***
Paretic foot M-L Range (mm)	31.4	9.7	23.4	0.208	0.24	**0.002***

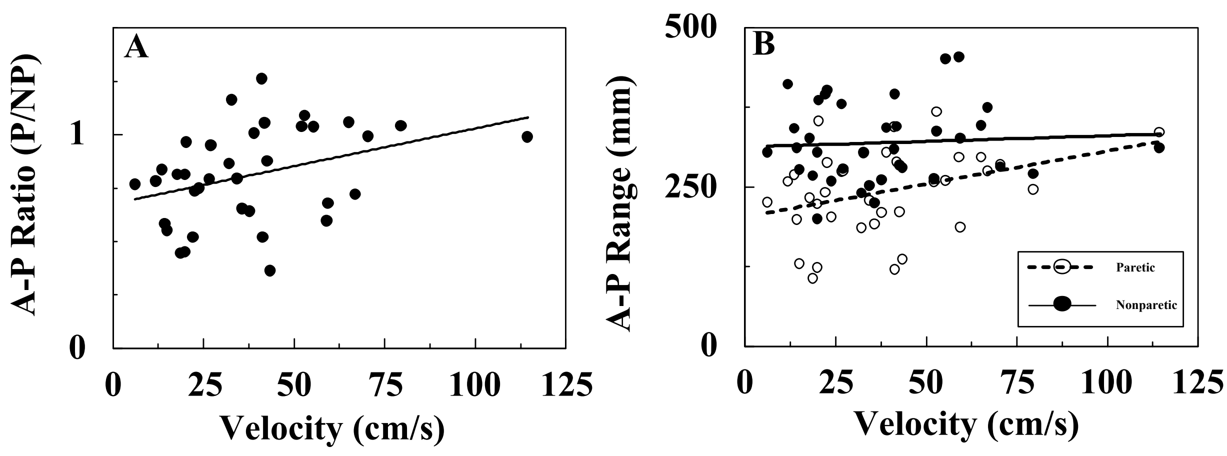

Figure 1: Regression analysis results for two COP measures. 1-A shows the relationship of the paretic/nonparetic ratio of the anteroposterior (A-P) COP to walking velocity. 1-B shows that the primary contribution to this relationship is from the A-P COP range for the paretic foot.

INVESTIGATING CHRONIC STRESS EXPOSURE FOLLOWING INTRA-ARTICULAR FRACTURE USING A FINITE ELEMENT MODEL OF THE ANKLE

Donald D. Anderson, Nicole M. Grosland, and Thomas D. Brown

Department of Orthopaedics and Rehabilitation, The University of Iowa, Iowa City, IA, USA
e-mail: don-anderson@uiowa.edu web: poppy.obrl.uiowa.edu/OBL_Lab_Website

INTRODUCTION

Post-traumatic osteoarthritis (OA) is a disturbingly frequent outcome following intra-articular fracture. It has long been felt that altered articular surface anatomy is the primary culprit, subjecting cartilage to chronically aberrant contact stress distributions which eventually lead to OA. But current knowledge concerning the relationships between altered surface anatomy and contact stress is sorely inadequate. With the advent of patient-specific finite element (FE) modeling techniques comes the ability to address this issue more definitively.

The ankle is an ideal joint in which to study the pathogenesis of post-traumatic OA, since OA often develops in it following fractures, but rarely develops in the absence of traumatic injury. In this study, we present preliminary work towards characterizing chronic stress exposure following intra-articular fracture using FE models of intact and fractured ankles from patients.

METHODS

Two different ankles were studied, one from an intact cadaver, the other from a 4-month post-operative intra-articular fracture patient. The fracture involved an antero-medial fragment, reduced with a single screw, but healed in a somewhat depressed position. In both cases, CT studies were obtained following a standard clinical protocol, and 3-d finite element models were created (Figure 1) using voxel-based

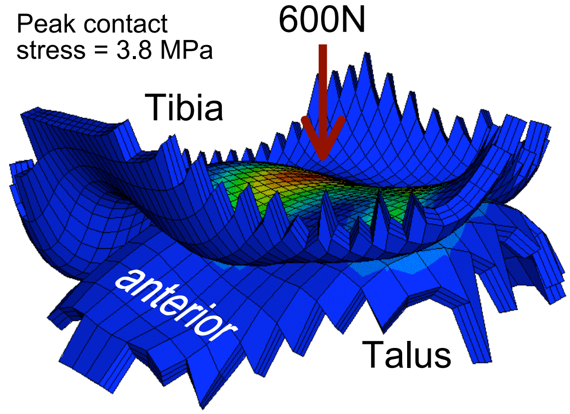

Figure 1: Schematic of ankle FE model with provisional 600N compressive seating load. The tibia is rotated about a flex/ext axis in the talus.

techniques previously described (Grosland and Brown, 2002). In brief, the subchondral surfaces of the distal tibia and the proximal talus are segmented, rigid surfaces connoting the bones are defined, and 1.5 mm layers of articular cartilage (E=12MPa, ν=0.42) are meshed to cover these surfaces. The apposing surfaces of these cartilage regions are defined as deformable contact pairs with a frictionless interface. The simulations were carried out using ABAQUS (v6.4) FE code.

To accommodate minor misalignments in the bones associated with a relaxed posture during CT scan acquisition, weak linear and torsional springs are defined to resist talar motion during provisional loading (straight compressive force to 600N – Figure 1). The tibia is then rotated about a flex/extension axis located within the talus so as to produce a neutral ankle posture, while still subject to the 600N load. The torsional springs are removed, and a sequence of thirteen loading conditions (10 to 2800N loads, rotations from 5° plantar- to 9° dorsi-flexion) taken from Stauffer et al. (1977) are applied to the tibia to simulate the stance phase of gait.

In order to characterize the contact stress exposure to which the cartilage is subjected, computed contact stress values were summed at each surface node across the stance phase of the gait cycle.

RESULTS AND DISCUSSION

Intuitively credible solutions were obtained with both models (Figure 2). Contact stress distributions in the post-op fracture case tended to line up along the residual fracture step-off. At sites away from the fracture, contact stresses were decreased compared to those in the intact ankle. The peak cumulative local stress for the fracture case was 25% higher than in the intact ankle, and located several mm from the incongruity lip.

The contact stress exposures, appropriately scaled across a period of service, might logically be compared to previously published values for chronic stress tolerance in articular cartilage (Hadley et al. (1990)).

SUMMARY

These patient-specific FE models of ankle loading during the stance phase of gait provide insight into the contact stress histories which articular cartilage experience over many cycles each day. The long-theorized chronic stress exposure following intra-articular fractures healed with residual incongruity may now be studied in the living ankle. This opens new avenues to study the link between chronic stress exposure and the onset of post-traumatic OA.

REFERENCES

Grosland, N.M. and Brown, T.D. (2002). *Comp Meth Biomechanics & Biomed Engineering*, **5**, 21-32.

Hadley, N.A. et al. (1990). *J Orthop Res*, **8**, 504-513.

Stauffer R.N. et al. (1977). *Clin Orthop & Rel Res*, **127**, 189-196.

ACKNOWLEDGMENTS

Funded by the Arthritis Foundation and the NIH (AR46601 & AR048939). The efforts of John Hill and Kiran Shivanna are gratefully acknowledged.

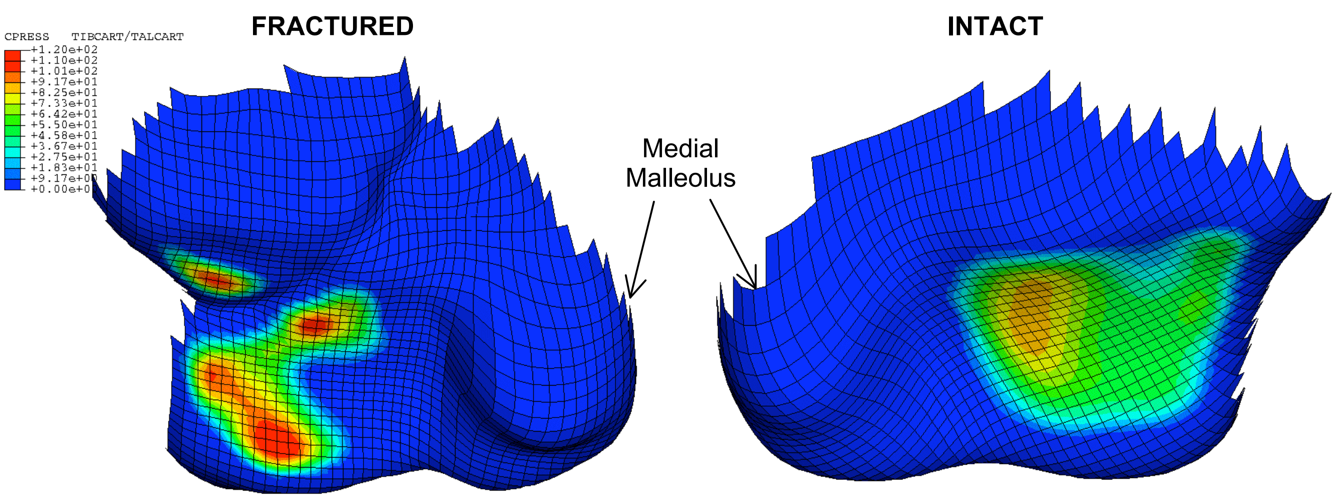

Figure 2: In these anterior views of the inferior aspect of the tibial articular surface, plots of contact stress exposure (effectively time integrals of instantaneous contact stress summed over the stance phase of gait) demonstrate contact stress aberration following a healed intra-articular fracture.

STRUCTURAL BEHAVIOUR OF THORACIC SPINAL UNIT; THE ROLE OF THE POSTERIOR ARTICULAR FACETS IN SPINAL DEFORMITY

Behnam Heidari[1], David FitzPatrick[1], Keith Synnott[2] and Damien McCormack[2]

[1] Department of Mechanical Engineering, University College Dublin, Dublin, Ireland
[2] Spinal Unit Research Group (SURG), National Spinal Centre, Mater Misericordiae Hospital, Dublin, Ireland
E-mail: behnam.heidari@ucd.ie

INTRODUCTION

Spinal deformities, such as Adolescent Idiopathic Scoliosis (AIS), frequently involve rotational deformity of the vertebrae. In AIS it is common to define the scoliotic deformity in terms of spinal curvature in the frontal plane. However, it is actually a three-dimensional problem of torsion, angulation and translation simultaneously occurring in the transverse, coronal and sagittal planes.

The vertebral axial rotation is usually rotates the spinous processes towards the concavity of the scoliosis (Stokes et al., 1991). The initiation of spinal deformities such as AIS is not clearly understood, either in the fundamental nature or the sequence of expression of its structural deformities (Burwell et al., 2000).

The geometry of the facet joints has been mentioned as an important factor in the mechanical behaviour of the thoracolumbar spinal units (Oxland et al., 1992). Also, pathological spinal deformation is usually a result of at least one unstable motion segment. Therefore, detail study on the structural behaviour and significance of the posterior elements of the thoracic spine is important and will provide better insight to the aetiology and leads to efficient treatment of spinal deformities.

OBJECTIVES:

The objectives of this study are: 1) to develop a three-dimensional accurate finite element model of T7-T8 motion segment and 2) to identify the significance of the posterior articular facet joint geometry and coupling phenomena on the mechanical behaviour of thoracic functional unit.

METHODS

A three-dimensional finite element model of thoracic spinal unit was developed using CT scan data of T7-T8 motion segment. The T7-T8 motion segment was chosen because it is located at the apex of the thoracic curve and because the apex of most spinal deformity occurs in this region.

The model of the vertebral body included the cortical shell, cancelous core, pedicles, laminae, transverse processes, spinous processes, and endplates. The intervertebral disc was modeled with annulus fibrosus having four layers containing bi-directional fibers, surrounding the nucleus pulposus. All seven ligaments were modelled as tension only fibers, oriented with the use of anatomical data.

The boundary conditions were chosen to match as close as possible those of the experimental studies (Panjabi et al., 1976), in order to validate the results. The lower part of the inferior vertebra was fixed and all loads applied to the upper part of the superior vertebra. The model was subjected to axial compression [250 to 1000 N], flexion/extension [1.5 to 9 Nm], lateral bending [1 to 6 Nm], and axial rotation [1 to 6 Nm].

RESULTS AND DISCUSSION

The finite element model (Figure 1) was validated in compression, flexion/extension, lateral bending, and axial rotation by comparing to experimental results of Panjabi et al., 1976 (Figure 2).

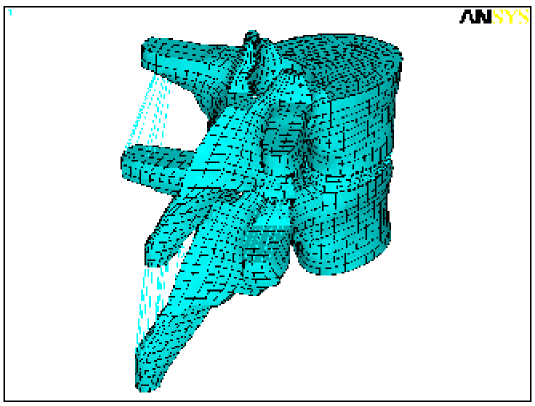

Figure 1: 3D finite element model of T7-T8

The results demonstrate that in the presence of axial rotation, the coupling effect of the posterior elements will cause lateral deviation of spine (Figure 3). This coupling effect results in asymmetrical loading of the spine, which in long term can cause morphological changes of vertebrae.

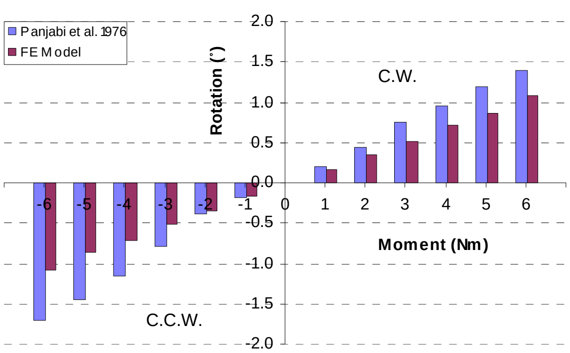

Figure 2: Validation of T7-T8 motion segment of spine under axial rotation.

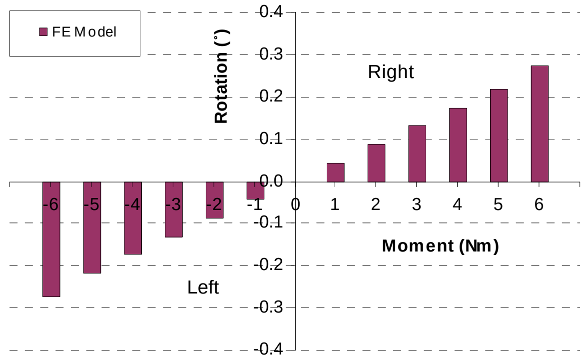

Figure 3: Induced lateral bending due to coupling effect in axial rotation.

Induced axial rotation has been shown (Heidari et al., 2004) to be sufficient to generate scoliotic deformity. Combined axial rotation and coupled lateral bending, demonstrated in this study, will serve to further increase the level of deformity.

Accurate description of the spinal deformity will provide better understanding of deformation mechanisms that may allow the development of more appropriate treatment for scoliosis correction.

REFERENCES

Burwell, R.G., Dangerfield, P.H. (2000). *Spin: State of the Art Reviews.* 319-33 Hanley & Belfus, eds.

Heidari, B. et al. (2004). *Clin Biomech,* **19**: 217-224.

Oxland, T.R. (1992). *J Orthop Res,* **10**: 573-80.

Panjabi, M.M. et al. (1976). *J Bone Joint Surg,* **58-A**: 642-652.

Stokes, I.A.F., Gardner-Morse M.G. (1991). *J Biomech*, **24**: 753-759.

ACKNOWLEDGEMENTS

This research project (PRP/00/MI/14) is supported by a grant from Enterprise Ireland.

KNEE KINEMATICS DURING ACTIVITY IN ACL DEFICIENT PATIENTS ARE LESS AFFECTED IN THOSE WHO COPE WELL WITH THE INJURY

Peter J. Barrance [1], Glenn N. Williams [2], Thomas S. Buchanan [1]

[1] Center for Biomedical Engineering Research, University of Delaware, Newark, DE
[2] Graduate Program in P.T. & Rehabilitation Science, The University of Iowa, Iowa City, IA

E-mail: peteb@udel.edu

INTRODUCTION

Pathological knee kinematics, such as increased anterior translation of the tibia, have been observed during activity in people with ACL deficiency. ACL injury has been associated with the development of osteoarthritis. Changes in functional kinematics due to the loss of joint stabilization have been proposed to contribute to the cartilage degeneration process in people with this injury. While reconstructive surgery is recommended for most young, athletic ACL deficient patients, non-operative management has been successful in a select group of these people. These ACL deficient 'copers' have been able to return to their pre-injury levels of activity in sports that challenge knee stability without experiencing giving-way episodes. The purpose of this study was to compare the knee kinematics of ACL deficient copers, ACL deficient non-copers, and people without a history of knee injury during a common dynamic task. We hypothesized that copers would exhibit knee kinematics similar to those of uninjured controls.

METHODS

Cine phase contrast magnetic resonance imaging (cine-PC MRI) and a previously reported cine-PC rigid body tracking technique (Barrance et al. 2002) were used to measure the six degree-of-freedom knee kinematics of subjects who performed cyclic knee flexion/extension while lying supine within the bore of an MRI scanner (GE Signa LX). The motions of 3-D geometric models of each bone are registered with the cine phase contrast data. Knee kinematics are calculated from anatomical coordinate systems embedded in each 3-D model. For data collection, the thigh was placed on a ramp to put the hip in a flexed position, and knee extensions were performed against the weight of the shank. The ramp was adjusted to achieve full knee extension when the toe touched the highest point of the imager's bore; this allowed flexion of the knee to approximately 30 degrees, depending on subject size. Subjects voluntarily synchronized their flexion/extension motions to the beat of a metronome set to produce a repetition frequency of 35 cycles per minute. The scan duration was about six minutes.

Twenty-seven subjects volunteered to participate in this study. Nine of these were non-copers (mean age: 21.4±9.2 yrs) who had sustained a complete isolated unilateral ACL ruptures within six months of testing and were scheduled to undergo reconstructive surgery. Nine other subjects were ACL deficient copers (mean age: 35.9+/-9.0 yrs) who had sustained complete, isolated ACL ruptures and had returned to participation in high-risk sports for at least one year without reporting knee instability or noteworthy functional deficits. The remaining nine subjects were people (mean age: 21.0+/-7.1 yrs) with no history of knee injury that were age, sex, and activity-level matched to the non-copers. The copers and uninjured subjects were regular participants in sports requiring cutting, pivoting, and-or jumping at the time of testing, whereas the non-copers had been immediately prior to their acute ACL injuries. There were seven males and two females in each group. All subjects gave written informed consent to participation in this University of Delaware Human Subjects Review Committee approved study.

Paired t-tests (significance level p=0.05) were used to test for differences in kinematic parameters at each flexion angle between pairs of knees in each group. For the non-coper and coper groups, side-to-side differences were evaluated by comparing injured knees to their uninvolved knees. The knees chosen to serve as the test knee of the control subjects in the side-to-side comparisons were assigned by selecting the side that corresponded with the injured knee of the non-coper subjects to which they were matched; the opposite knee served as the reference.

RESULTS AND DISCUSSION

The tibial position of the non-copers' involved knees was significantly anterior to that of their uninjured knees at angles between 5 and 20 degrees (Fig. 1). The average value of the mean difference over the flexion range of motion was 2.8±0.2 mm. The mean differences in side-to-side A/P tibial position in the copers and control subjects were similar (1.0±0.7 mm, -1.3±0.7 mm). The peak side-to-side tibial position differences were greatest in the non-copers (3.1±2.7 mm at 20º). The copers' side-to-side differences in six degree-of-freedom knee kinematics usually fell between those of the non-copers and the uninjured controls. However, the between-subject variability in side-to-side kinematic differences was

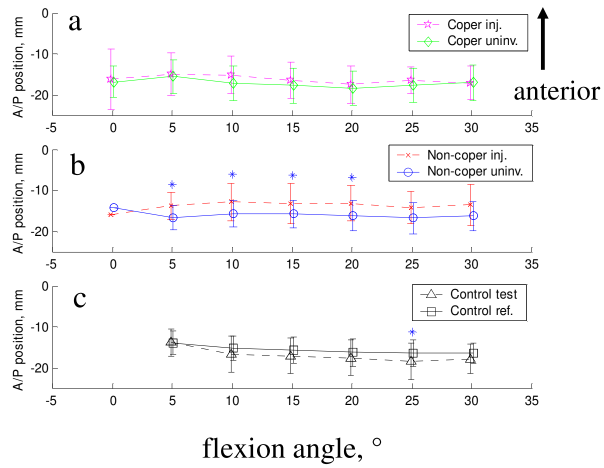

Figure 1: Anterior/posterior position parameter at 5º increments of flexion angle. (a) Copers, (b) Non-copers, (c) Control group. *: Significant difference between means within group.

greatest within the coper group, suggesting that copers have idiosyncratic responses to ACL injury. This is consistent with previous reports.

SUMMARY

The tibias of the non-copers' ACL deficient knees were positioned significantly anterior to the tibias of their opposite knee when the kinematic patterns of their knees was compared. The copers' knee kinematics did not differ significantly from that of people with no history of knee injury. Greater within group variability was observed in the copers' knee kinematics, suggesting that their response to ACL injury is idiosyncratic. Future studies, using in vivo measurements of kinematics during dynamic tasks promise to further elucidate these differences.

REFERENCES

Barrance, PJ. et al, *Fourth World Congress of Biomechanics*, August 2002.

ACKNOWLEDGMENT

Supported by NIH Grant R01AR46386.

RELATIONSHIP OF MUSCLE FIBER PENNATION ANGLE TO EMG AND JOINT MOMENT DURING GRADED ISOMETRIC CONTRACTIONS USING ULTRASOUND IMAGING

Dustyn P. Roberts and Thomas S. Buchanan

Center for Biomedical Engineering Research, University of Delaware, Newark, DE
E-mail: robertdp@me.udel.edu

INTRODUCTION

The angle that muscle fibers insert into tendon in pennate skeletal muscles is an important determinate of the muscle's functional characteristics. Pennate muscles allow more fibers to align in parallel, increasing the contractile force potential compared to a muscle of identical composition and volume with longitudinal fibers. Consequently, the pennation angle is an important parameter in musculoskeletal modeling when predicting musculotendon length, force generation, and contribution to joint moment. Historically, pennation angles were measured *post mortem* using cadaver muscles (e.g., Frendrich & Brand, 1990) and any changes in the angle during contraction were considered negligible (e.g., Zajac, 1989). However, ultrasonography has recently been used as a tool to measure pennation angle *in vivo* and significant changes in pennation angle between rest and isometric maximum voluntary contraction as measured through electromyography (EMG) and dynamometry have been documented for several muscles (Hodges *et al.*, 2003; Maganaris *et al*., 1998). Other studies have shown pennation angle of specific muscles to vary significantly with age, gender, repeated muscle contractions, muscle hypertrophy, and atrophy/disuse. Clearly, incorporating changes in pennation angle into any musculoskeletal model will therefore increase anatomical and physiological accuracy. However, a relationship between pennation angle and muscle contraction must first be determined *in vivo* to be practical and applicable to modeling. This study will use electromyography and dynamometry to measure muscle activity and external joint moment while simultaneously imaging the muscle using ultrasonography during graded isometric contractions to measure pennation angle. The goal is to establish predictive relationships between pennation angle, moment, and EMG in healthy subjects as well as subjects with unilateral lower limb injuries.

METHODS

Subjects are recruited into two patient populations: group A includes 20 healthy subjects with no history of musculoskeletal injuries to either leg, and group B includes subjects with acute or chronic unilateral injuries to the lower limb. The muscles studied are the prime movers of the ankle joint in the sagittal plane. The main dorsiflexor is the tibialis anterior (TA), and the muscles of the triceps surae complex form the plantarflexion muscle group: medial gastrocnemius (MG), lateral gastrocnemius (LG), and soleus (SOL).

Muscle activity in the TA, MG, LG, and SOL are measured simultaneously using a custom EMG processor, a Biodex dynamometer, and an Aloka 5000 ultrasound unit. Each subject is first prepared for EMG collection on the indicated muscles of each leg. Surface electrodes are fixed over the TA, MG, and LG, and fine wire electrodes are used for the SOL to minimize cross-talk from adjacent muscles. The subject is then seated in a Biodex dynamometer and performs a series of isometric dorsiflexion and plantarflexion contractions with the leg extended parallel to the floor and the ankle fixed in neutral (the foot at 90 degrees to the shank). The root mean square amplitudes of the EMG and moment signals for 2 seconds of each contraction are taken as the representative signal. Ultrasound images are collected through a linear 10 MHz transducer for each muscle at rest and during each contraction. Measurements of pennation angle are performed online.

RESULTS

Statistical analysis of preliminary data collected from the TA in a healthy male subject showed that the relationships between pennation angle and EMG as well as between pennation angle and moment are best represented by a squared polynomial regression. The R^2 values of .90 and .91, respectively, confirm the strength of the relationship between the indicated variables.

Data were also analyzed from the TA of one female subject two days following cast removal from an injury resulting in fractured talus and calcaneus bones in the left ankle complex. Because of extreme atrophy and residual pain it was not possible to test graded isometric contractions, so measurements at maximum dorsiflexion and rest were taken from each leg and compared using paired t-tests instead of regression analysis. Borderline significant results were indicated by P values of 0.05 and 0.06 when moment and EMG were compared between injured and uninjured legs. No significant differences in pennation angle were noted between legs or between rest and contraction of either leg at this time.

DISCUSSION

The results in healthy subjects comparing pennation angle and moment support findings by Maganaris *et al.* (1998), who also found a squared polynomial relationship between these variables. When comparing pennation angle to EMG, the current study found a squared polynomial relationship while a similar study showed a logarithmic regression to have a better fit (Hodges *et al*., 2003). A larger sample size will be recruited to increase statistical power to show significance of regression.

The limited data available from the group B subject showed promising results (as indicated by the p values from the paired t-tests) when comparing differences in maximum moment and EMG production capabilities in the injured and uninjured muscle. Statistical power will be increased by recruitment of more subjects, at which time regression analyses will also be possible and paired t-tests may confirm the suggested significance indicated in these preliminary findings. The lack of significant changes in pennation angle between legs is most likely due to the small subject population and is not likely representative of the general differences observed in disuse/atrophy.

REFERENCES

Friederich J.A. and Brand R.A. (1990) *J. Biomech*. 23: 91-95.
Hodges P.W., et al. (2003) *Muscle & Nerve*. 27: 682-692.
Maganaris, C.N., et al. (1998) *J. Physiol*. 512.2: 603-614.
Zajac F.E. (1989) *Crit. Rev. Biomed. Eng.* 17: 359-411.

ACKNOWLEDGEMENTS

This work supported, in part, by NIH R01 HD38582.

Are fast-moving elephants really running?

Despite their unseemly bulk, elephants can hit high speeds — but use an unusual style.

It is generally thought that elephants do not run[1–5], but there is confusion about how fast they can move across open terrain and what gait they use at top speed. Here we use video analysis to show that Asian elephants (*Elephas maximus* L.) can move at surprisingly high speeds of up to 6.8 m s^{-1} (25 km h^{-1}) and that, although their gait might seem to be a walk even at this speed, some features of their locomotion conform to definitions of running.

Elephants moving rapidly have been estimated[2–4] to reach speeds of about 4 m s^{-1} (15 km h^{-1}), although anecdotal evidence[1] claims that they can reach 11 m s^{-1} (40 km h^{-1}). To investigate the gait used by elephants at top speeds, we used video analysis to study 42 healthy, active Asian elephants throughout Thailand (for details, see supplementary information). The skin was marked with non-toxic tempera paint dots over the limb-joint centres of the elephants (right fore- and hindlimbs; Fig. 1), estimated by palpation and manipulation of the joints; these dots were used for later video digitizing. Mahouts guided the elephants along a 30-metre course, parallel to the field of view of the video camera (60 Hz). Elephants had at least 10 m to accelerate or decelerate before and after this 30-m course. A total of 188 trials were carried out; trials with sudden accelerations or decelerations in the 10-m videotaped stretch of the course were omitted.

Our digitization of the hip-joint markers (using Peak Motus, Peak Performance, Colorado) measured the average velocity along the central 10 m of the track. We used the length of the thigh segment (between the centres of hip- and knee-joint markers) to scale the digitized video coordinates to real dimensions. Photocell timers at either end of the track gave an average velocity across the entire 30 m, which was used as a preliminary gauge of which elephants were the fastest, as well as for comparison with the 10-m velocity to monitor speed changes. Speeds over the 10-m and 30-m courses were generally similar, indicating that the elephants did not suddenly speed up or slow down.

Of the elephants, 32 reached top speeds of over 4.0 m s^{-1}, 20 exceeded 5.0 m s^{-1}, and three attained speeds greater than 6.0 m s^{-1}. The fastest gait used by elephants has been variously described as a walk, amble, trot, pace, rack or a running walk[1–5], but — given that these speeds are relatively fast — how well does this gait of the fastest elephants fit the definitions of running?

Several kinematic factors distinguish quadrupedal walking from running. First, trotting and galloping are running gaits with footfall patterns that are distinct from walking[5]. Second, an aerial phase (a period during which no foot touches the ground) often marks the transition from walking to running[5]. Third, a run has been defined as any gait with a duty factor (the fraction of a complete sequence of footfalls for which a given foot is in contact with the ground) of less than 0.50 (ref. 5). Our elephants maintained the same walking footfall pattern (Fig. 2a) and always kept at least one foot in contact with the ground, although they used duty factors as low as 0.37.

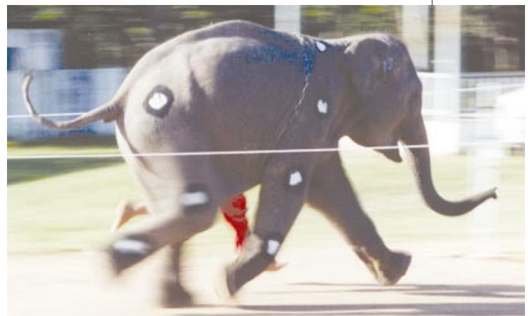

Figure 1 An Asian elephant marked with dots for gait analysis.

R. LAIR

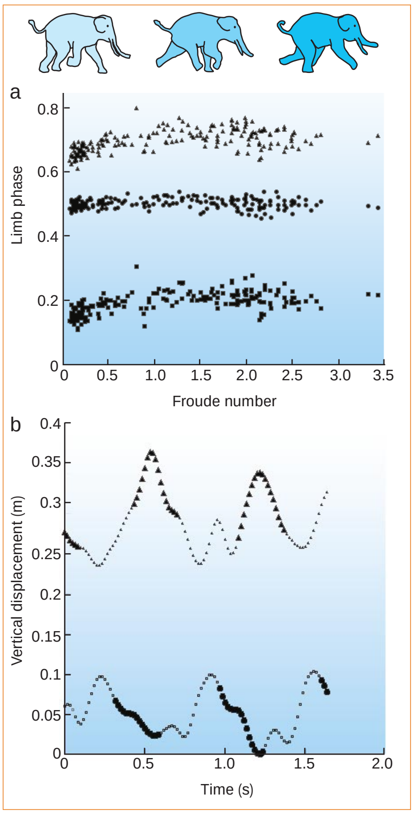

Figure 2 Biomechanics of rapid movement by Asian elephants (*Elephas maximus* L.). **a,** Relative limb phase (fraction of stride time for which each foot comes into contact with the ground after the left hind foot) plotted against dimensionless speed (Froude number). At all speeds, the left hind foot, then the left front (squares), then the right hind (circles), then the right front foot (triangles) contact the ground in the same sequence. Images of elephants moving at 6.6 m s^{-1} (Froude number, 3.1; see movie in supplementary information) illustrate these footfall patterns, which are typical of quadrupedal walking[5]. **b,** Vertical displacements of the hip (circles) and shoulder (triangles) joints plotted against time for one individual moving at 6.8 m s^{-1} (Froude number, 2.8). Large symbols indicate stance phase; small symbols indicate swing phase. This downward hip movement was typical of all fast-moving elephants; many showed a downward-then-upward pattern during stance. Roughly 2.5 strides are shown, beginning just before and ending just after the 10-m section of the observation course.

Walking and running can also be distinguished by the forces involved. The Froude number (Fr) is a dimensionless speed[6] calculated as velocity^2/(acceleration of gravity $\times$ hip height). At speeds beyond Fr 1.0, the force needed to keep the body mass on a circular arc during stance exceeds the force of gravity. Theoretically, this requires a walking animal to leave the ground and run. Most animals usually switch from a walk to a run at Fr $\approx$ 0.50, presumably because of an energetic or mechanical trigger[7], and quadrupeds switch from a trot to a gallop at Fr $\approx$ 2.5 (ref. 6). The elephants routinely exceeded Fr 1.0, reaching Fr values as high as 3.4 — speeds that are inconsistent with a quadrupedal walking gait. Other animals, such as running birds[8], also have non-aerial gaits at high Froude numbers.

It is the exchange of gravitational potential and kinetic energy that fundamentally distinguishes walking and running[9–11]. The centre of mass is highest at mid-stance in walking, but lowest at mid-stance in running[12]. Our analysis shows that at low speeds, as expected for walking, elephants' shoulder and hip joints rise and then fall (indicating vertical motion of the centre of mass) during the stance phase. At the highest speeds, the vertical movements of the shoulder indicate walking, but hip motion indicates running (Fig. 2b). During the stance phase of the forelimb, shoulder motion resembles walking, moving upwards and then downwards while the front foot is on the ground, whereas the hip's motion during the stance phase of the hindlimb is characteristic of running, moving downwards and then upwards.

Usually, the various criteria for walking and running are consistent, making it relatively easy to distinguish walking from running, but this is not true in the case of elephants. Our observations suggest that, at greater speeds, elephants do more than merely walk. Ground-reaction-force data are needed to demonstrate conclusively whether the elephants' gait involves spring-like running kinetics[9–12] and to understand why elephants avoid using an aerial phase.

John R. Hutchinson*, Dan Famini†, Richard Lair‡, Rodger Kram§

**Biomechanical Engineering Division, Stanford University, Stanford, California 94305-4038, USA*
e-mail: jrhutch@stanford.edu
†School of Veterinary Medicine, University of California, Davis, California 95616, USA
‡Thai Elephant Conservation Center, Lampang 52000, Thailand
§Department of Kinesiology and Applied Physiology, University of Colorado, Boulder, Colorado 80309-0354, USA

1. Howell, A. B. *Speed in Animals* (Chicago Univ. Press, 1944).
2. Muybridge, E. *Animals in Motion* (Dover, New York, 1957).
3. Gambaryan, P. P. *How Mammals Run* (Wiley, New York, 1974).
4. Alexander, R. McN. *et al. J. Zool. Lond.* **189,** 135–144 (1979).
5. Hildebrand, M. *Am. Zool.* **20,** 255–267 (1980).
6. Alexander, R. McN. & Jayes, A. S. *J. Zool. Lond.* **201,** 135–152 (1983).
7. Farley, C. T. & Taylor, C. R. *Science* **253,** 306–308 (1991).
8. Gatesy, S. M. *J. Morphol.* **240,** 115–125 (1999).
9. Dickinson, M. H. *et al. Science* **288,** 100–106 (2000).
10. Cavagna, G. A. *et al.* in *Scale Effects in Animal Locomotion* (ed. Pedley, T. J.) 111–125 (Academic, New York, 1977).
11. Heglund, N. C., Cavagna, G. A. & Taylor, C. R. *J. Exp. Biol.* **97,** 41–56 (1982).
12. McMahon, T. A. *et al. J. Appl. Physiol.* **62,** 2326–2337 (1987).

Supplementary information accompanies this communication on *Nature*'s website.

Competing financial interests: declared none.

Cell biology

Developmental predisposition to cancer

Many human cancers occur in renewing epithelial tissues, in which cellular lineages typically go through two distinct phases: early in life, cell populations expand exponentially to form the tissue, and for the remainder of life, the tissue is renewed by stem cells dividing to create an almost linear cellular history[1]. Here we use a simple mathematical model to show that mutations that arise during the exponential phase probably seed tissues with stem cells carrying mutations that may predispose to cancer. Susceptibility to late-life cancers, such as those of the skin and colon, may therefore be influenced by somatic mutations that occur during early development.

Mutations accumulate during exponential cellular growth according to the Luria–Delbrück distribution[2]. Let u_e be the mutation probability per cell division during exponential growth, and N the number of stem cells produced during development to seed the tissue. Starting with one cell, the number of cell divisions required to produce N cells is $N-1$, and the total number of mutation events during the cellular history is $M=u_e(N-1)\approx u_eN$. (The phases of cellular growth are shown in Fig. 1a.)

Figure 1b shows the probability distribution for the number of stem cells that carry mutations. These are the mutations that arise during exponential growth, before further division of the stem lineages to renew the local tissue. The average frequency of stem cells with mutations is $\bar{x}\approx u_e\ln(N)$ (ref. 2).

Although the frequency of stem cells that initially contain a mutation may be small, those mutations can contribute substantially to the total risk, R_T, of cancer. Suppose that k rate-limiting mutations are needed for cancer to develop[3,4], then the total risk is $R_T=N(1-x)R_k+NxR_{k-1}$, where x is the frequency of stem cells that start with one mutation, and R_k is the risk that a particular stem-cell lineage acquires k mutations during the phase of linear division and tissue renewal. The risk, R_k, is given roughly by the gamma distribution, which describes the probability of the occurrence of the kth event over a particular time interval. From the gamma distribution, $R_k\approx(u_s\tau)^k/k!$, where u_s is the mutation rate per stem-cell division, and τ is the total number of stem-cell divisions.

The expected fractional increase in cancer risk arising from stem cells that begin with one mutation can be calculated as $F=\bar{x}\,R_{k-1}/R_k\approx u_e\ln(N)k/u_s\tau$. The next step is to assign approximate magnitudes to these quantities. We can take $k\approx5$ for the number of rate-limiting mutations required to cause epithelial cancer in humans[3,4], $\ln(N)\approx20$, and τ to range from 100–1,000. This gives the fractional increase in cancer risk, F, ranging from $u_e/10u_s$ to u_e/u_s.

If mutations accumulate with the same probability per cell division during exponential growth and linear stem-cell division ($u_e=u_s$), then the increase in risk from mutations arising in development ranges from 10–100%. If, as has been claimed[5], mutation rates in stem cells are much lower than those during exponential growth, ($u_s \ll u_e$), then almost all cancer arises from predisposed stem-cell lineages that were mutated during development.

The risk of cancer from somatic mutations during development could be quantified by studying inbred rodents. The number of predisposing mutations per individual will vary according to the Luria–Delbrück distribution (Fig. 1b). Individuals with many predisposing mutations are likely to develop multiple independent tumours relatively early in life, whereas those with few predisposing mutations should develop few tumours relatively late in life. Controlled experiments have shown variability in cancer susceptibility among inbred rodents[6], but the causes of this variability have not been determined.

Mutations during development seed a young individual with a small fraction of mutated stem cells. Those relatively few mutated lineages may therefore be responsible for a substantial proportion of the cancers that develop later in life.

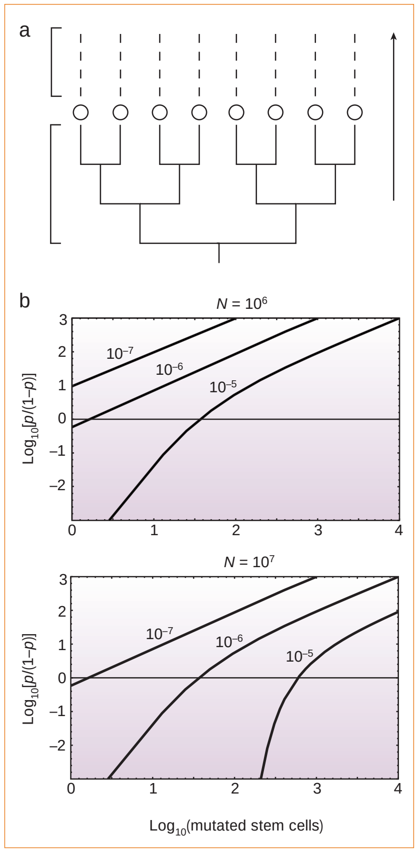

Figure 1 The role of tissue architecture in the accumulation of mutations during development. **a,** The phases of cellular growth in epithelial tissues. Cell populations increase exponentially during development, shown by a branching phase of division; at the end of development, stem cells differentiate in each tissue compartment (circles); stem cells renew each compartment by dividing to form a nearly linear cellular history (dashed lines) — each stem-cell division gives rise to one daughter stem cell that continues to renew the tissue and to one daughter transit cell that divides rapidly to produce a short-lived lineage that fills the tissue. **b,** The cumulative probability, p, for the number of stem cells mutated during development. By plotting $\log_{10}[p/(1-p)]$, the zero line gives the median of the distribution. N, number of stem cells produced during exponential growth. The number above each line is u_e, the mutation probability per cell added to the population during exponential growth. For a single gene, u_e is probably of the order of 10^{-7}; thus, if there are 100 genes for which initial mutations can influence the progression to cancer, then u_e is roughly of the order of 10^{-5}. The Luria–Delbrück distribution plotted here was calculated using equation (8) of ref. 7.

Steven A. Frank*, Martin A. Nowak†

**Department of Ecology and Evolutionary Biology, University of California, Irvine, California 92697-2525, USA*
e-mail: safrank@uci.edu
†Institute for Advanced Study, Einstein Drive, Princeton, New Jersey 08540, USA

1. Cairns, J. *Nature* **255,** 197–200 (1975).
2. Zheng, Q. *Math. Biosci.* **162,** 1–32 (1999).
3. Knudson, A. G. *Proc. Natl Acad. Sci. USA* **90,** 10914–10921 (1993).
4. Hanahan, D. & Weinberg, R. A. *Cell* **100,** 57–70 (2000).
5. Cairns, J. *Proc. Natl Acad. Sci. USA* **99,** 10567–10570 (2002).
6. Prehn, R. T. *Science* **190,** 1095–1096 (1975).
7. Zheng, Q. *Math. Biosci.* **176,** 237–252 (2002).

Competing financial interests: declared none.

EFFECTS OF PREPARATION ON POSTURAL STABILITY WHILE ACCEPTING A WEIGHT IN THE OUTSTRETCHED HANDS

[1]Jennifer Rattenbury, [2]Ted Milner [1]Stephen N. Robinovitch,

[1]Injury Prevention and Mobility Laboratory, [2]Biomechanics Laboratory; School of Kinesiology, Simon Fraser University, Burnaby, British Columbia, Canada
Email: jrattenb@sfu.ca

or: are a common cause of falls?

INTRODUCTION

Destabilizing movements that bring the body's COG close to the edge of its base of support are associated with increased risk of falling in elderly (Cumming and Klineberg, 1994). Many activities of daily life require elderly individuals to complete reaches and/or movements to accept weight with the outstretched hand. ~~Reaching and accepting a weight in the outstretched hand are considered destabilizing movements~~ and therefore put elderly ~~at an increased~~ risk for falling.

how do you define perturbation here?

Studies have shown ~~that individuals~~ decrease the amount of perturbation due to these destabilizing activities by anticipating and countering the upcoming joint torques and COG movements (Toussaints et al., 1997, Kaminski and Simpkins, 2001). These anticipations can be seen in the form of early muscular activation and early movement of the COP to minimize the upcoming COG movement and decrease the chances of it moving outside the base of support.

how exactly do they "counter" the perturbation? e.g.

The aim of the present research was to understand the effects of varying degrees of preparation on the movement of the COG and COP when a weight is accepted in the outstretched hands. It was hypothesized that the COP and the COG displacement would be greater in involuntary compared to voluntary weight acceptance. As well, we hypothesize that there will be early COP movement prior to COG displacement in voluntary trials but delayed COP movement in involuntary trials.

Vague "to determine" is better

METHODS

Eight young women (18-26 years, mean=)were instructed to reach forward and accept the weight of an object suspended in front of them ~~by~~ on an ~~adjusta~~ble rope (Figure 1). Instructions were given to begin the trial in a reaching position pending weight acceptance. The weight was then accepted in the outstretched hands in one of three ways; 1) through voluntary lifting 2) by voluntarily releasing the tension in the suspending rope ~~by turning off the magnet and releasing the object into the hands or~~ 3) by accepting the weight ~~at an unknown time~~ after the investigator released the tension in the suspending rope ~~by turning off the magnet~~. The object position varied in height and distance from the subject.

confusing

colon

awkward

include?

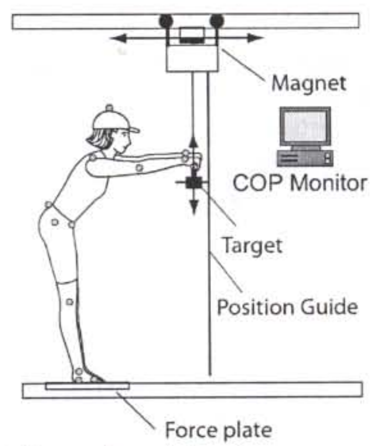

Figure 1. Experimental set up

voluntary lifting vs

We used an 8-camera 120Hz motion capture system (Eagle, Motion Analysis) with 61 markers, a force plate (6090-15, Bertec),and two load cells to capture data. — what data? (kinematic motion; foot contact forces)

RESULTS AND DISCUSSION

As we hypothesized, a significant main effect ($t_{0.5,7}$ = , p<) was seen for the preparation time using a 3 way repeated measures ANOVA. Post hoc analysis revealed significantly more COP and COG displacement for involuntary (+/-) compared to voluntary (+/-) released trials and greater displacement for voluntary released than voluntary lifting (+/-).

match btwn COP and COG is very close in VL, with COP always ahead of COG. This is nearly the case in VR, but not in IVR

at what instant do you match COP & COG?

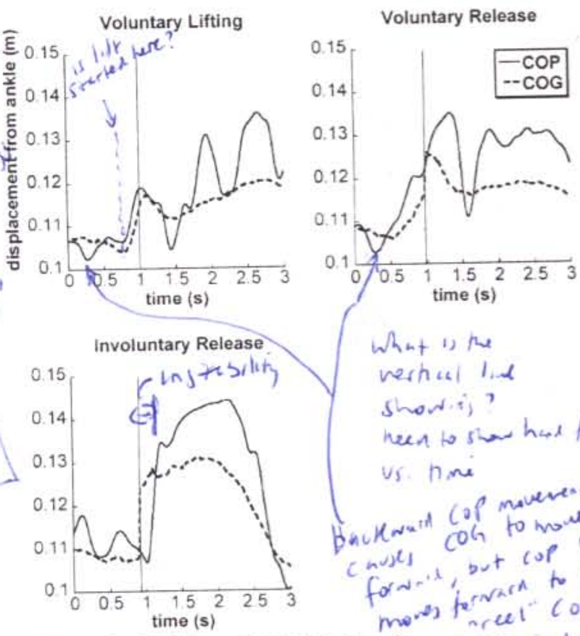

is this started here?

instability

What is the vertical line showing? need to show hand force vs. time

Backward COP movement causes COG to move forward, but COP then moves forward to try and "arrest" COG in and prepare for weight acceptance

Figure 2. COP and COG displacement against time across weight acceptance conditions

These results suggest that with less time for preparation there is a greater perturbation to the subject. The larger perturbation therefore requires a greater displacement of the COP and the COG to generate ankle torques to minimize instability and maintain posture.

we don't really vary the time, just the nature of preparation

how was size of the perturb. measured? weight remains constant

(i.e., doesn't affect TA)

Furthermore, a significant main condition effect ($t_{0.5,7}$=,p=) was seen for time between COP and COG movement. The COP moved prior to the COG in voluntary trials and was delayed in involuntary trials. Additionally, anticipatory COP movements were earlier in lifting versus voluntary released trials (Figure 2).

Similar to other studies (Heiss, Shields and Yack, 2002, Shiratori and Latash, 2001) the results suggest that subjects were able to minimize the instability of the weight acceptance through anticipation in voluntary lifting and release trials but not in involuntary trials. what type?

This research provides an understanding of the type and amount of biomechanical preparation required to counter the weight acceptance perturbation. Future studies will examine the preparation requirements associated with such a task in elderly individuals.

vague → need more specific take home

SUMMARY

Effects of preparation on postural stability during weight acceptance in the outstretched hands were tested using voluntary and involuntary weight acceptance conditions. Involuntary weight acceptance was a greater perturbation to postural ~~stability and~~ prevented normal anticipatory movements of the COP.

REFERENCES

1) Cummings, S.R. and Klineberg, R.J.(1994). *JAGS*, **42**, 774-8.,2) Heiss et al. (2002). *Arch Phys Med Rehabil*, **83**, 48-59.,3) Kaminiski and Simpkins (2001). *Exp Brain Res*, **136**(4), 439-46. ,4) Shiratori and Latash (2001). *Clin Neurophysiol*, **112**(7), 1250-65.,5) Toussaint et al.(1997). *Med Sci Sports Exerc*, **29**(9), 1216-24.

ACKNOWLEDGEMENTS

Grant??

why do you want the COG to move forward prior to weight acceptance? Is it to allow the COP to also move forward (in preparation for weight acceptance) while maintaining dynamic equilibrium?

INTERSEGMENTAL DYNAMICS OF THE SWING PHASE OF WALKING IN TRANS-TIBIAL AMPUTEES

Philip E. Martin and Jeremy D. Smith

Department of Kinesiology, Penn State University, University Park, PA 16802
Email: pmartin@psu.edu Web: http://www.hhdev.psu.edu/kines/

INTRODUCTION

Unilateral, trans-tibial amputees reflect significant inertial asymmetries between the intact and prosthetic limbs (Mattes et al., 2000) and also exhibit temporal, kinematic, and kinetic gait asymmetries during walking (e.g., Sanderson & Martin, 1997). Early modeling research (Tsai & Mansour, 1986) suggested lower extremity inertial symmetry may lead to more symmetrical gait patterns in unilateral amputees. Mattes et al. (2000), however, found that matching inertial properties exacerbated existing temporal asymmetries. In an effort to better understand the influence of inertial manipulation on swing phase dynamics for unilateral, trans-tibial amputees, we examined the effect of matching the inertial properties of prosthetic and intact legs on intersegmental dynamics at the knee and hip during walking.

METHODS

Six males with unilateral, trans-tibial amputations (age: 32±12 yrs, body mass: 85±6 kg, body height: 179±6 cm) served as subjects. Time since amputation ranged from 3 to 15 years. Participants were fully ambulatory and used energy storing prosthetic limbs in their daily activities.

Participants completed an orientation session during which they were acclimated to treadmill walking and load conditions. Inertial properties of the intact and prosthetic limbs were also measured or estimated (de Leva, 1996a, 1996b).

Subjects completed overground walking trials at 1.34 m/s as sagittal plane motion and ground reaction force data were sampled (60 Hz and 480 Hz, respectively). Three inertial conditions were examined: 1) a baseline condition in which no load was added to the prosthetic limb, 2) a 100% mass condition in which prosthetic limb mass and moment of inertia about a transverse axis through the knee were matched to those of the intact limb, and 3) a 50% mass condition in which the added load was half that added to the limb for the 100% condition. An intersegmental dynamics approach was used to partition the net moments about the knee and hip into interaction, gravitational, and muscle components (e.g., Schneider et al., 1989).

RESULTS AND DISCUSSION

Increasing the mass and moment of inertia of the prosthetic limb had no effect on intersegmental dynamics at the knee and hip of the intact limb, but significantly altered the knee and hip moments of the prosthetic limb. At the knee of the prosthetic limb, the interaction moment showed little change, whereas the gravitational moment increased modestly (Figure 1) and the muscle moment increased substantially at both the initiation and cessation of the swing phase (Figure 2). Although the asymmetry in swing time was increased as the limbs became more closely matched with respect to their inertial properties (Mattes et al., 2000), interlimb symmetry improved for both the gravitational and muscle moments.

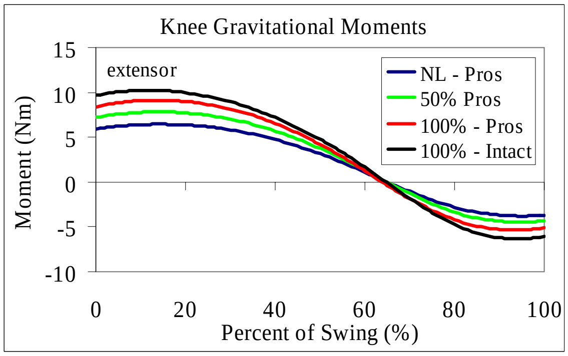

Figure 1. Gravitational moment about the knee increased modestly as load on the prosthetic limb increased.

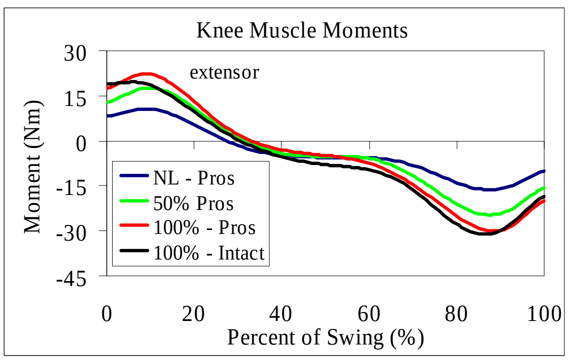

Figure 2. Muscle moment about the knee increased systematically with increases in prosthetic limb mass and moment of inertia.

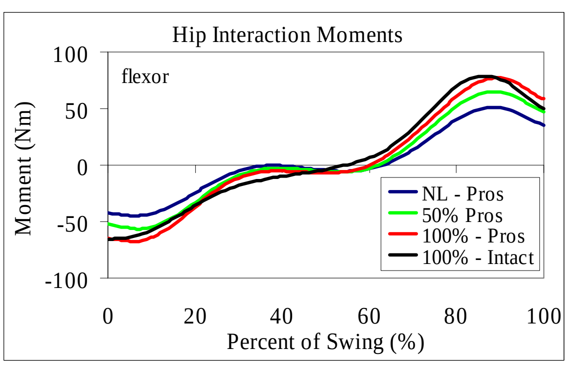

Figure 3. The interaction moment at the hip increased as prosthetic limb inertia was increased.

At the hip, both interaction and muscle moments increased with prosthetic limb load (Figures 3 and 4, respectively). The gravitational moment, which made small contribution to the net moment, showed little change as limb inertia was increased.

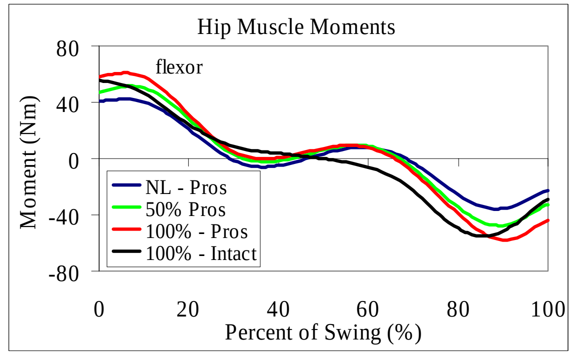

Figure 4. Muscle moment about the hip increased due to prosthetic limb loading.

SUMMARY

The increased muscle moments at the hip and knee as limb inertia was increased were consistent with an increase in metabolic cost of walking (Mattes et al., 2000). Higher hip and knee muscle contributions at swing initiation may be related to the reduced push-off attributed to the loss of plantar flexor function in the prosthetic limb and the need to rely on an alternative mechanism to drive the swing phase.

REFERENCES

de Leva, P. (1996a). *J Biom*, **29**, 1223-30.

de Leva, P. (1996b). *J Biom*, **29**, 1231-33.

Mattes, S.J. et al. (2000). *Arch Phys Med Rehab*, **81**, 561-68.

Sanderson, D.J., Martin, P.E. (1997). *Gait and Posture*, **6**, 126-36.

Schneider, K. et al. (1989). *J Biom*, **22**, 805-17.

Tsai, C.S., Mansour, J.M. (1986). *J Biomed Eng*, **108**, 65-72.

DYNAMICS AND MULTIJOINT CONTROL DURING SINGLE LEG SQUAT WITH AND WITHOUT ACTIVATION OF ABDOMINAL OBLIQUE MUSCLES

Roongtiwa Vachalathiti[1], Jill L. McNitt-Gray[2,3,4], Witaya Mathiyakom[2,5], Heather Boni[2]
[1]Faculty of Physical Therapy and Applied Movement Science, Mahidol University, Bangkok, Thailand
[2]Departments of Kinesiology, [3]Biomedical Engineering, [4] Biological Sciences, [5]Gerontology, University of Southern California, Los Angeles, CA, USA
E-mail: mcnitt@usc.edu

INTRODUCTION

Control of the pelvis and lumbar spine is an important component of goal-directed whole-body movements. Previous research has shown that activation of deep abdominal muscles provides dynamic stability of the pelvis and lumbar spine in functional tasks (Cholewicki and McGill, 1996). Motion of the trunk is known to influence control of lower extremity during dynamic weightbearing movements (McNitt-Gray et al., 2001). This led us to hypothesize that trunk stabilization, by means of engaging the abdominal oblique muscles, facilitates control of the pelvis and lower extremity during weightbearing tasks.

Squating during single-leg support is a common component of functional tasks and sport activities and has been used as part of clinical screening tests for assessing hip strength and trunk control (Kendall et al., 1993). To successfully perform the task, subjects need to coordinate the trunk and lower extremity so that the position of center of mass (CM) is over the base of support.

The aim of this study was to investigate the role of trunk stabilization in controlling the center of mass trajectory and the relative angle between the lower extremity segments and the reaction force during the single leg squat with (SLSO) and without (SLS) engaging of abdominal oblique muscles.

METHODS

Skilled female volleyball players (n=6) volunteered to participate in accordance with the Institutional Review Board. Single leg squats were performed with and without activating the abdominal oblique muscles. Frontal plane kinematics (200 fps), EMG (1,200 Hz) and reaction forces (1,200 Hz) were simultaneously recorded. Digitized x and y coordinates of body landmarks (de Leva, 1996) were individually filtered using a fourth order Butterworth filter (Saito and Yokio, 1982) with cut-off frequency based on a method described by Jackson (1979). The CM and leg position vectors, relative to the center of pressure (CP) were used to differentiate the role of the legs and trunk in controlling the CM relative to the reaction force. Frontal plane joint kinetics were determined using Newtonian mechanics, reaction forces, and frontal plane segment kinematics.

RESULTS AND DISCUSSION

Trunk stabilization by means of engaging the abdominal oblique muscles induced between task differences in CM trajectory and the relative orientation between the lower extremity segments and the reaction force. As a result, between task differences in lower extremity net joint moments were observed.

The mechanical demand imposed on the ankle, knee and hip was dependent on the orientation of the reaction force relative to foot, shank and thigh segments. The more horizontal the segment, the larger the moment created by the net joint forces acting on the segment, thereby creating the need to generate greater NJMs to control segment rotation. The EMG activity was consistent with the magnitude and direction of the lower extremity NJMs.

SLSO tasks exhibited more vertical segment positions at the time of single leg stance and throughout the squatting motion as compared to the SLS task (Fig. 1a). These between task differences in segment angles during the SLSO tasks, reduced the relative angle between the lower extremity segments and the reaction force, and as a result, less knee and hip abductor NJMs were needed during the SLSO task as compared to the SLS task (Fig. 1b).

With SLSO, subjects demonstrated a significant decrease in vertical displacement of CM as compared to the SLS task. Therefore, the between task differences in segment orientation relative to reaction force were compared at the minimum CM position of SLSO task. At this CM position, the orientation of the CM position vector and the resultant reaction force were vertical and aligned. However, between subject differences in lower extremity segment orientations relative to the leg orientation were observed. In SLSO task, four out of six subjects demonstrated closer alignment between segment angle and leg angle as compared to SLS.

SUMMARY

Activation of the oblique muscles altered control of the lower extremity during single leg squat. Closer alignment of the shank and thigh segments, as observed in the SLSO task, reduced the relative angle between the segments and the reaction force, thereby reducing NJM magnitude and muscle activation needed to control the lower motion.

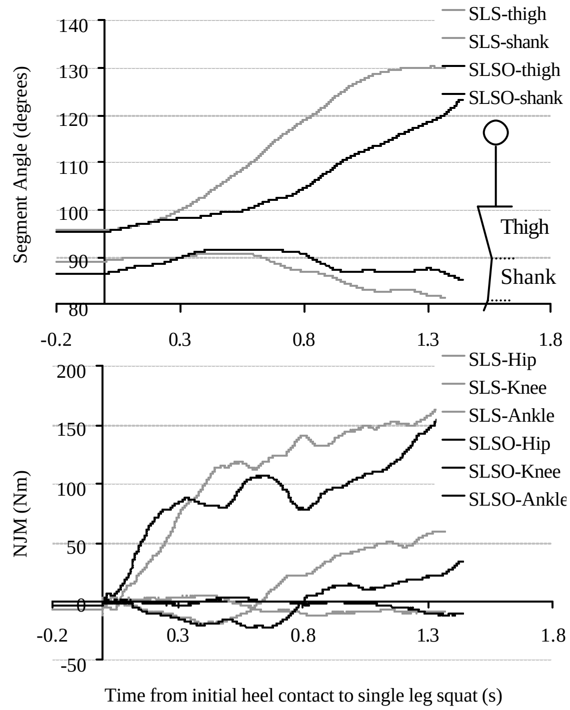

Figure 1: Between task differences in a) orientation of the lower extremity segments, and b) net joint moments of an exemplar subject.

REFERENCES

Cholewicki, J., McGill, S.M. (1996). *Clinical Biomechanics*, **11**, 1-15.

McNitt-Gray, J.L. et al. (2001). *J. Biomech*, **34**, 1471-1482.

Kendall, F.P. et al. (1993). *Muscles testing and function*. Williams & Wilkins.

de Leva, P. (1996). *J. Biomech*, **29**, 1223-1230.

Saito, S., Yokio, T. (1982). *T. Bull of Health and Sport Science.* University of Tsukuba. 201-206.

Jackson, K.M. (1979). *IEEE Trans Biomed Eng*, **26**, 122-124.

ACKNOWLEDGEMENTS

Ministry of Education, Thailand. Intel, Women in Science and Engineering, USC.

THE INFLUENCE OF DIFFERENT MIDSOLE HARDNESS ON KNEE JOINT LOADS DURING RUNNING

Katja J. Michel [1,2] Frank I. Kleindienst [1] Alex Stacoff [2] Berthold Krabbe [1] Edgar Stüssi [2]

[1]Biomechanical Lab, adidas Innovation Team, adidas-Salomon AG, Scheinfeld, Germany
[2]Biomechanical Laboratory, Department of Materials, Swiss Federal Institute of Technology, Zürich, Switzerland
E-mail: katja.michel@adidas.de

INTRODUCTION

Millions of people are involved in running and jogging activities. The reported yearly incidence of injuries ranges between 37 and 56% (Van Mechelen, 1992). The knee has been shown to be a common site of injury for runners and Patellofemoral Pain Syndrome (PFPS) is the most common complaint within the injuries to the knee. High abduction and external rotation moments in the knee joint are related to overuse injuries like PFPS (Stefanyshyn et al., 2001).

It has been shown that shoe constructions influence kinetics (Frederick et al., 1986) and kinematics (Stacoff et al., 2000) of runners. However, the influence of different midsole hardness on knee joint moments has not been studied yet. Therefore the purpose of this study was to investigate the influence of different midsole hardness on 3-dimensional knee joint moments during running.

METHODS

Subjects were 10 male runners (age: 32 ±4yr; ht: 175 ±5cm; mass 68 ±7kg; shoe size: 8.5 UK) with an average weekly running distance of 58km. According to a medical examination by an orthopedic surgeon, all subjects were injury free during the study. Two shoe types (adidas® Unity), differing exclusively in midsole hardness (40 Shore C, 70 Shore C respectively) were used for the running trials.

Kinematic data were collected using a 4-camera 3-dimensional Vicon System (200Hz). Reflective markers were placed on the pelvis, upper leg, lower leg and foot (3 per segment). Kinetic data were collected using a Kistler force plate (1000Hz). Subjects ran across the force plate in the middle of a 25m runway at a velocity of 3.6 ±0.2ms^{-1}. Kinematic and kinetic data were collected for 5 valid trials for each subject and shoe condition (10 trials per subject; total: 100 trials). 3-dimensional knee joint moments were calculated during the stance phase using an inverse dynamics approach. Force and moment curves were normalized to bodyweight. Selected values were determined from each curve and averaged for each condition and subject. Significant differences between the two shoe conditions were detected using non-parametrical tests (Friedmann and Wilcoxon).The significance level was set to $p \leq 0.05$.

RESULTS AND DISCUSSION

Different midsole hardness influence mean abduction moments (Figure 1) as well as mean external rotation moments (Figure 2) in the knee joint. However, knee extension moments are not effected.

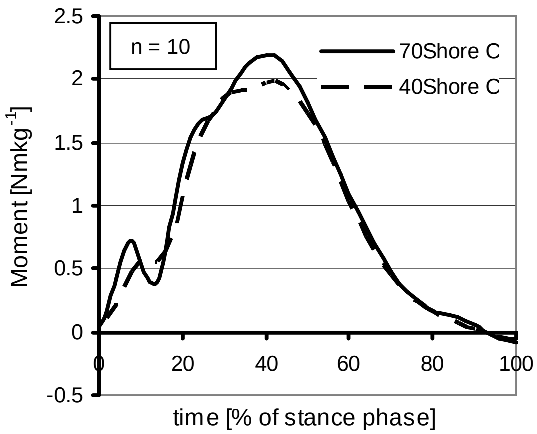

Figure 1: Knee abduction moments

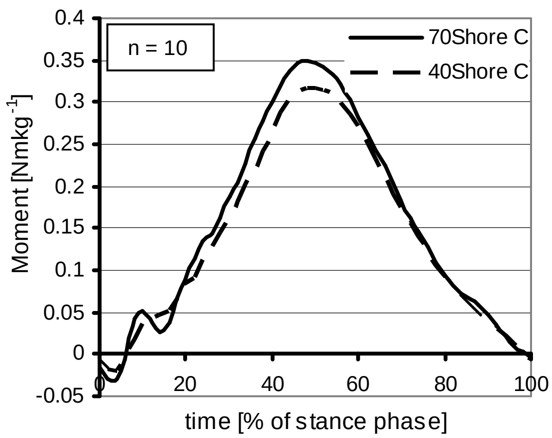

Figure 2: Knee external rotation moments

The hard shoe condition provokes significantly higher maximum abduction moments (Figure 3) and higher maximum external rotation moments (Figure 4) than the soft shoe condition.

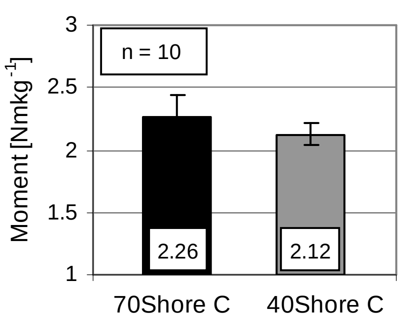

Figure 3: Max. knee abduction moments

These results are in accordance with the significantly higher amplitudes of the medio-lateral ground reaction forces and the significantly higher tibia rotation angles for the hard shoe condition.

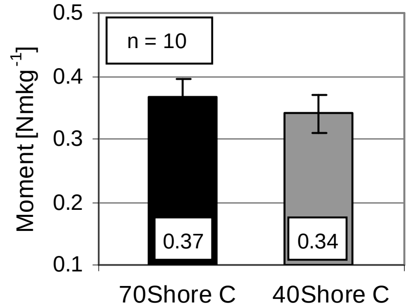

Figure 4: Max. knee ext. rotation moments

Due to the influence of varying midsole hardness on knee joint moments, further investigations with heterogeneous subject groups would be useful in order to develop appropriate running shoes for groups of runners differing in gender, bodyweight, age or performance (product differentiation and mass customization).

SUMMARY

Midsole hardness influences abduction as well as external rotation moments in the knee joint. The hard shoe condition provokes significantly higher maximum abduction moments and higher maximum external rotation moments than the soft shoe condition. The results indicate that appropriate midsole hardness could have a positive effect on knee joint moments and subsequently on the reduction of overuse injuries.

REFERENCES

Frederick, E.C., Hagy, J.L. (1986). *Int. J. Sport Biomech.*, **14**, 498.

Stacoff, A. et al. (2000). *Foot Ankle Int.*, **21**, 232-239.

Stefanyshyn, D.J. et al. (2001). *Proc. of the 5th Symp. on Footwear Biomechanics*, Zürich, 74-75.

Van Mechelen, W. (1992). *Sports Med.*, **14**, 320-335.

SAFETY AND EFFICACY OF THE SYNTHES THORACIC HOOK LOCKING SCREW

Ronald Turker[1], Joel Gillard[1,2], Michael Binette[1], Marie Shea[1]
[1]Department of Orthopaedics, Oregon Health & Science University, Portland, OR,
[2]Acumed Inc., Hillsboro, OR
E-mail:turkerr@ohsu.edu

INTRODUCTION

Posterior spinal fusion and instrumentation using rods attached to hooks, wires, or screws is commonly used to correct severe thoracic scoliosis deformities. Posterior and lateral forces are applied to the spine through an interface between the rod and the posterior vertebral elements. The advantage of pedicle hooks is the footplate's broad surface area through which forces are applied. Hooks are relatively easy to insert compared to wires and pedicle screws, decreasing the potential for neurologic or dural injury. However, the hooks can easily dislodge during corrective maneuvers. Pedicle screws in the thoracic spine have been gaining popularity but are clearly more technically challenging to place safely.

The Universal Spine System (USS, Synthes Spine Corp., Paoli, PA) contains a locking screw that passes through the body of the hook, traversing the pedicle and into the cranial endplate of the vertebral body, creating fixation between the hook and pedicle. During placement it is possible that either the drill bit or the screw may come into contact with neural elements. We compared the safety and ease of placement of this construct with 2 separate screw lengths against thoracic pedicle screws.

Our specific aims were: 1) to determine if the pedicle screw, the longer hook locking screw or the shorter hook locking screw could be consistently placed such that the screw does not impinge on the neural elements; and 2) to assess the lateral and posterior pullout strength of these three constructs.

METHODS

Three groups of implants were placed in 7 intact fresh frozen cadaveric thoracic vertebrae (T1-T12, average age 59 yrs). T12 bone mineral density (BMD) was determined for each specimen using dual energy x-ray absorptiometry (DXA) in order to normalize the pullout data for varying specimen density. The groups consisted of: 1) thoracic pedicle hooks with a 40 mm locking screw, 2) thoracic pedicle hooks with a 20 mm locking screw, or; 3) 4.2 mm standard thoracic pedicle screws. The implants were alternated by vertebral level. No real time radiographic imaging was used for placement of either implant.

Each level was then inspected to determine the anatomic proximity of the implants to the neural elements, based on the known typical location and course of nerve roots and the thecal sac. The vertebral bodies were then disarticulated and embedded in aluminum fixtures; the transverse and spinous processes and the hardware were left unembedded. The constructs were tested to failure in either a lateral or posterior direction. Only a single hook or screw at each level was tested and the side was alternated.

Maximum pullout force and stiffness data were analyzed using a multifactorial analysis of variance with specimen, screw type, and pullout direction as separate factors. If screw type and loading direction had an effect on pullout force or stiffness, we performed a Tukey Post Hoc analysis to detect group differences at $p<0.05$.

RESULTS

Safety: Of 37 hooks with short locking screws, 4 screws (11%) had potential neural contact medially without significant canal compromise or likely neurologic sequelae in-vivo. Three (8%) screws were misplaced laterally, which would not likely have any neural contact.

Of 38 hooks with long locking screws, 1 screw (3%) intersected the path of the nerve root as it exited the foramen, having a high possibility of encroachment or nerve root injury in-vivo. Ten (26%) of the long locking screws were misplaced laterally, which would not likely have any neural contact.

Of 42 pedicle screws inserted, 2 (4%) screws had potential neural contact. One was angled too caudally by 38^o, placing the screw directly across the path of the nerve root as it exited the foramen. The second screw broke through the medial pedicle wall, mildly reduced the volume of the lateral recess and had a low probability of clinically significant neural contact.

Strength: During pullout testing, all constructs had equivalent failure load (Table 1). During posterior pullout testing, the pedicle screw was stiffer than both locking screws ($p<0.0005$, 95% power).

Table 1: Data (mean $\pm$ standard deviation, sample size) for the 3 screw types. [a]Pedicle screw stiffness in the posterior direction was significantly greater than the long or short screws.

Corrected for BMD (Mean $\pm$ SD)					
Screw	**Direction**	**Stiffness (N/mm)**	**n**	**Failure Load (N)**	**n**
Long	Lateral	168 $\pm$ 65	8	668 $\pm$ 247	9
Short	Lateral	181 $\pm$ 81	11	449 $\pm$ 241	11
Pedicle	Lateral	229 $\pm$ 112	10	499 $\pm$ 182	11
Long	Posterior	423 $\pm$ 143	11	861 $\pm$ 231	11
Short	Posterior	593 $\pm$ 246	11	1098 $\pm$ 315	11
Pedicle	Posterior	[a]1245 $\pm$ 302	8	840 $\pm$ 203	9

DISCUSSION

Of 119 implants placed, 4% of the pedicle screws and 37% of the hook locking screws missed their intended path. One long locking screw and one pedicle screw directly crossed the anatomic path of a thoracic nerve.

Four of the short locking screws and 1 long locking screw were placed against the medial wall of the pedicle in the lateral recess of the neural canal. One pedicle screw was placed slightly medial and broke the medial cortex of the pedicle decreasing the space available for the nerve root within the lateral recess. Six additional locking screws were near the nerve root but not as likely to have clinical impact as the locking screw and pedicle screw that traversed the course of the nerve roots.

Theoretically, the placement of the locked hook should be technically easier than placement of the standard pedicle screw. However, we found more variation in the anatomic placement of the hook locking screws, though this did not result in increased risk of nerve root injury. Despite an increased risk of malposition, the locked hooks had equivalent failure loads to the pedicle screws, and equivalent stiffness in the lateral direction.

While pedicle screws have gained popularity for their significant contribution to stability in spinal instrumentation, there are ongoing concerns about the safety of pedicle screw implantation. The goal of this ongoing design effort is to equal the stiffness and failure load of pedicle screw instrumentation with an implant that can be safely placed by a wide population of surgeons.

ACKNOWLEDGEMENT

Funded by Synthes Spine Corp., Paoli, PA.

JOINT LOADING AND BONE MINERAL DENSITY IN PERSONS WITH UNILATERAL, TRANS-TIBIAL AMPUTATION

Todd D. Royer and Michael Koenig

Dept of Health, Nutrition and Exercise Sciences, Univ of Delaware, Newark, Delaware, USA
Email: royer@udel.edu

INTRODUCTION

Persons with unilateral, trans-tibial amputation have an asymmetrical gait pattern, most likely the result of pain, weakness, and/or instability on the prosthetic side. As a result, the intact limb experiences excessive joint loading (Sanderson & Martin, 1997), predisposing it to greater risk of developing degenerative joint disease, e.g., osteoarthritis (OA).

Previous research on osteoarthritic gait has demonstrated an important link between abnormal joint loading and bone mineral density (BMD). Patients with medial compartment knee OA have large knee abduction moments and elevated proximal tibia BMD (Wada et al., 2001); likewise, larger hip joint moments corresponded to greater proximal femoral BMD in subjects with end-stage hip OA (Hurwitz et al., 1998a). There is an associated link between increased BMD and osteoarthritis, however the causative relationship is not clear (Hurwitz et al., 2001). Osteoarthritis is a degradation of articular cartilage, nonetheless, Radin and Rose (1986) have suggested that OA is initiated by or prompted to progress by increased density of subchondral bone.

The purpose of this study was to examine gait mechanics and BMD in persons with unilateral, trans-tibial amputation. We hypothesized that peak net internal abduction moments and BMD of the intact knee and hip would be significantly greater than that of the prosthetic side.

METHODS

Six males and one female ($M_{age} = 45.7 \pm 7.9$ yrs; $M_{height} = 169.2 \pm 18.9$ cm; $M_{mass} = 98.4 \pm 19.9$ kg) with a unilateral, trans-tibial amputation served as subjects. All were recreationally active and utilized an energy storing prosthetic limb.

To obtain data used in calculating gait mechanics, lightweight reflective markers were placed bilaterally on the legs and feet of the subject using the Helen Hayes marker set. Motion analysis cameras captured three-dimensional position data (60Hz) of these markers and a force platform captured ground reaction force data (480Hz) as the subject walked at their freely chosen speed ($M_{speed} = 1.3 \pm 0.2$ m/s) overground along a 20-meter walkway. Peak net internal abduction moments for the knee (MK_{abd}) and hip (MH_{abd}) of both legs were determined using an inverse dynamics approach and normalized to body mass (Orthotrak software, Motion Analysis Corporation). BMD of the hip (femoral neck) and knee (medial compartment of the proximal tibia) was measured bilaterally via dual energy x-ray absorptiometry (Hologic Delphi W).

Dependent t-tests were used to test for significant differences in knee and hip frontal plane joint moments and bone mineral density between limbs ($p<.05$).

RESULTS AND DISCUSSION

MK_{abd} for the intact limb was 71.8% greater than the prosthetic side (Figure 1). The between limb difference in mechanical loading is reflected in the intact proximal tibia BMD which was 54.1% larger than the prosthetic side (Figure 2). MK_{abd} for the intact limb was 0.53 Nm/kg, which is 12.7% greater than normal (approximately 0.47 Nm/kg) reported by Hurwitz and colleagues (1998b). This suggests that the intact limb of unilateral, trans-tibial amputees is concomitantly made more susceptible to degenerative joint disease, specifically OA. Indeed, Melzer et al (2001) reported 65% of unilateral, lower-extremity amputees had some degree of knee OA in the intact limb.

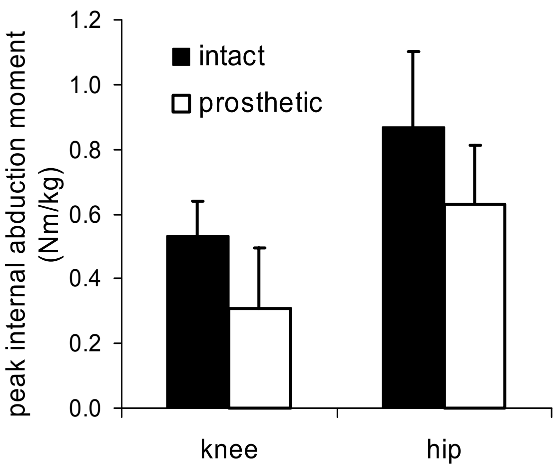

Figure 1. Peak internal abduction moments for the intact limb were larger ($p<.05$) than the prosthetic side.

MH_{abd} for the intact limb was 37.5% greater than the prosthetic limb (Figure 1). The between limb difference in mechanical loading was also evident in the intact femoral neck BMD which was 10.9% greater than the prosthetic side (Figure 2). Hurwitz and colleagues (1998a) reported a significant positive correlation between hip joint loads and femoral neck bone mineral density, which may be associated with increased risk of OA. In our study, MH_{abd} for the intact limb was 0.86 Nm/kg, which is 2.4% greater than normal (approx 0.84 Nm/kg) reported by Hurwitz et al (1998a).

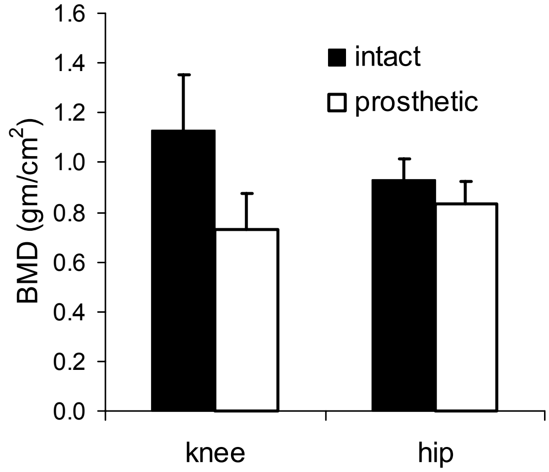

Figure 2. Bone mineral densities of the knee and hip were greater for the intact limb than for the prosthetic side ($p<.05$).

SUMMARY

Individuals with unilateral, trans-tibial amputation have greater mechanical loads on the intact knee and hip, which is reflected in the BMD at the knee and hip. Increased BMD may indicate risk of osteoarthritis.

REFERENCES

Hurwitz, D.E., et al (1998a) *J Biomech*, **31**, 423-30.

Hurwitz, D.E. et al (1998b). *J Biomech*, **31**, 919-25.

Melzer, I., et al. (2001). *J Rheumatol*, **28**, 169-72.

Radin, E.L. & Rose, R.M. (1986). *J Orthop Res,* **2**, 221-234

Sanderson, D.J., & Martin, P.E. (1997). *Gait and Posture*, **6**, 126-36.

Wada, M. et al. (2001). *Rheumatology*, **40**, 499-505.

ACKNOWLEDGEMENTS

Support from NIH-RR16548 (Tom Buchanan, PI) is acknowledged.

Characterizing Kinematics of 3-D Human Movements Using Quaternions

Laurie Held[1], Jill L. McNitt-Gray[1,2,3], Henryk Flashner[3,4]
Biomechanics Research Lab, Departments of Biomedical Engineering[1], Kinesiology[2], Biological Sciences[3], and Aerospace and Mechanical Engineering[4]
University of Southern California, Los Angeles, CA
held@usc.edu

INTRODUCTION

Dynamic models of the human body allow us to study control strategies implemented by the nervous system during goal directed multijoint tasks. Before a dynamic model is used to test hypotheses regarding control, it is experimentally validated using kinematic and reaction force data.

Human motion is characterized using observed segment kinematics. To determine segment orientation in three dimensions, accurate position data of three non-collinear points (tracking markers) located on the segment must be detected. Accuracy of the kinematic characterization depends on the interaction between marker measurement error, modeling assumptions, and the method of attitude parameterization.

The quaternion parameterization provides computational and conceptual advantages for characterizing segment orientations in space. Quaternions are an extension of complex numbers that parameterize rigid body 3-D orientations as one rotation about a single axis. The axis/angle information embedded in the quaternion can help validate model assumptions by quantifying out of plane motion and providing instantaneous axes of rotation about a joint.

In this study, we 1) developed a quaternion-based approach for characterizing human motion and 2) determined the effect of data acquisition error on joint kinematics calculated using the quaternion approach.

METHODS

Approach: A model was used to generate marker coordinate data representative of what we would acquire experimentally. 3D coordinates of anatomical and tracking markers were obtained at the end of the simulation and exported into Matlab. Quaternions were computed from the tracking marker position data for each segment at each moment in time. These quaternions were used to calculate segment orientations and joint angles over time.

To simulate digitizing error, noise (zero-mean, ±5mm error) was added to each marker coordinate and the quaternion calculations performed again. Joint angles computed from both the clean and noisy tracking marker coordinate data were compared to the actual joint angles calculated using the anatomical coordinates. Comparison of these results quantifies the computational and noise generated error associated with the quaternion method.

Model: A four-segment model was created using ADAMS software (Mechanical Software, Ann Arbor, MI) with spherical joints at the ankle (fixed to the ground) and hip, and hinge joints at the knee and shoulder. Link dimensions were chosen to best approximate body segments (de Leva, 1996). Four tracking markers were placed on each segment. To induce out of plane motion, angular displacement about the y axis was imposed at the hip joint. The simulation ran for 0.25 seconds (500 steps), which corresponds to typical landing phase durations (McNitt-Gray et al., 1999).

RESULTS AND DISCUSSION

A representative plot of calculated joint angles over time computed using clean data is shown in Figure 4 along with the actual joint angles. Root mean square error of the calculated angles was 0.44°, 0.45°, and 0.19° for the ankle, knee, and hip, respectively.

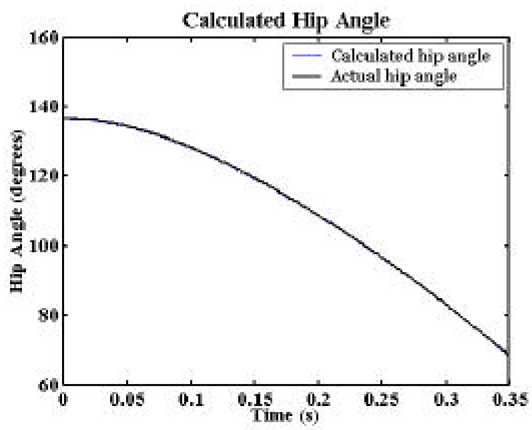

Figure 4. Actual and calculated hip angles using data with no noise.

A representative plot of calculated joint angles over time computed using noisy data is shown in Figure 5 along with the actual joint angles. Root mean square error in all calculated joint angles was between 2° and 3° for all sets of noisy data.

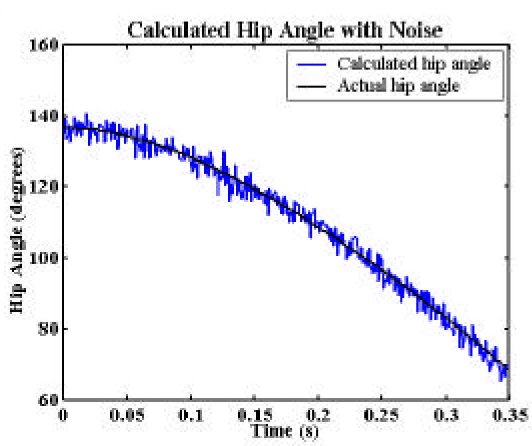

Figure 5. Actual and calculated hip angles using data with noise.

These results show that the quaternion parameterization, which provides computational and interpretational benefits, does not compromise joint angle calculations when using data with noise.

SUMMARY

In this study, we developed and evaluated a quaternion-based approach to characterize segment orientation. This method will allow us to quantitatively validate models and to answer questions about joint axes of rotation. The method was shown to be accurate for calculating segment kinematics from position data with measurement error. Knowledge of the magnitude of the error associated with the method of parameterization allows us to better assess the accuracy of dynamic models.

In the future, filtering algorithms will be integrated at the coordinate data and/or the quaternion levels to reduce the error in the segment and joint velocities and accelerations. The quaternions themselves can be used directly to answer biomechanical questions about joint centers and out-of-plane motion.

REFERENCES

Zatsiorsky (1998). *Kinematics of Human Motion*.
Kim, Injung et al.(2001) *Advances in the Astronautical Sciences, Spaceflight Mechanics 2001*, **108**, 571-586
De Leva, P. (1996). *J Biomech*, **29**, 1223-30.
McNitt-Gray et al. (2001). *J Biomech*, **34**(11)
Kuipers (1999). *Quaternions and Rotation Sequences*. Princeton University Press.

ACKNOWLEDGEMENTS

Intel, Women in Science and Engineering Fellowship, Oakley Fellowship, Witaya Mathiyakom

3D COMPUTER SIMULATION OF ROUNDHOUSE KICK IN TAEKWONDO

Young-Kwan Kim [1], Gary T. Yamaguchi [2], and Richard N. Hinrichs [1]

[1] Department of Kinesiology, Arizona State University, Tempe, AZ, USA
[2] Exponent®, Inc., Phoenix, AZ, USA
E-mail: Young-Kwan.Kim@asu.edu

INTRODUCTION

Taekwondo, a form of Korean martial arts, has gained popularity throughout the world as an excellent physical conditioning activity as well as a method of self-defense. Its popularity is largely due to the use of various kicks in competitive sparring. Considering all the alternatives, the roundhouse kick is the most popular kick during sparring because of its fast speed and excellent accuracy. The roundhouse kick consists of flexion and extension of the knee along with flexion of the hip joint while simultaneously rotating the trunk and abducting the hip joint.

Kicking, a fundamental motor skill, uses a proximal-to-distal sequence of segmental interaction in an attempt to maximize the linear velocity of the foot. Since the roundhouse kick begins in the sagittal plane and ends in the transverse plane, three-dimensional (3D) analysis is required to understand the characteristics of the kick. However, no studies on 3D computer simulation or joint torque contribution to the performance of the roundhouse kick have been found in the literature.

The purpose of this study was to develop a 3D model of the roundhouse kick and to use it to perform a sensitivity analysis of each joint torque on kicking performance. Implementing computational modeling of lower extremity might shed light on the understanding the kinematic characteristics of the roundhouse kick and the musculoskeletal system functioning of the lower limb.

MODEL

The kicking model consisted of four bodies (HATP [head, arms, trunk, and pelvis], thigh, shank, and foot) and included six degrees of freedom (θ_1 to θ_6) (Figure 1).

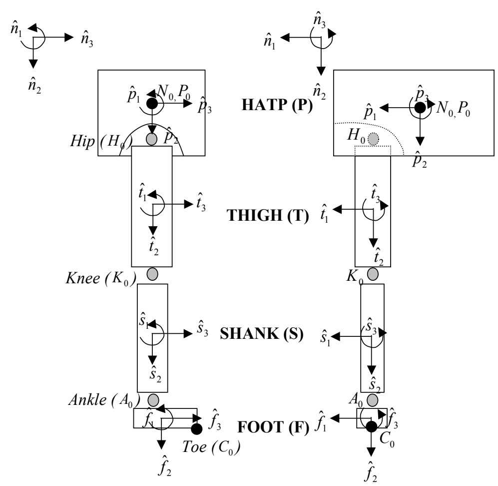

Figure 1. The sagittal and frontal plane model and coordinate system of the kicking leg.

θ_1 was defined as the rotation about $\hat{p}_3$ (trunk lateral deviation), θ_2 the rotation about $\hat{p}_2$ (trunk rotation to L/R), θ_3 the rotation about $\hat{t}_3$ (hip ab-/adduction), θ_4 the rotation about $\hat{t}_1$ (hip flexion/extension), θ_5 the rotation about $\hat{s}_1$ (knee flexion/extension), and θ_6 the rotation about $\hat{f}_1$ (ankle plantar /dorsi flexion). The model followed the forward dynamics approach using Kane's dynamic method (Kane & Levinson, 1985). The reference coordinates were transformed by the multiplication of each direction cosines, where the abbreviations were $c_i \equiv \cos(\theta_i)$ and $s_i \equiv \sin(\theta_i)$.

$$\begin{bmatrix}\hat{n}_1\\\hat{n}_2\\\hat{n}_3\end{bmatrix}=\begin{bmatrix}c1 & -s1 & 0\\ s1 & c1 & 0\\ 0 & 0 & 1\end{bmatrix}\cdot\begin{bmatrix}c2 & 0 & s2\\ 0 & 1 & 0\\ -s2 & 0 & c2\end{bmatrix}\cdot\begin{bmatrix}c3 & -s3 & 0\\ s3 & c3 & 0\\ 0 & 0 & 1\end{bmatrix}\times$$
$$\begin{bmatrix}1 & 0 & 0\\ 0 & c4 & -s4\\ 0 & s4 & c4\end{bmatrix}\cdot\begin{bmatrix}1 & 0 & 0\\ 0 & c5 & -s5\\ 0 & s5 & c5\end{bmatrix}\cdot\begin{bmatrix}1 & 0 & 0\\ 0 & c6 & -s6\\ 0 & s6 & c6\end{bmatrix}\cdot\begin{bmatrix}\hat{f}_1\\\hat{f}_2\\\hat{f}_3\end{bmatrix}$$

The angular and linear velocities at the end of foot were defined as followings.

$${}^{N}\vec{\omega}^{F}={}^{N}\vec{\omega}^{P}+{}^{P}\vec{\omega}^{T}+{}^{T}\vec{\omega}^{S}+{}^{S}\vec{\omega}^{F}$$
$${}^{N_0}\vec{v}^{C_0}={}^{N_0}\vec{v}^{P_0}+{}^{P_0}\vec{v}^{H_0}+{}^{H_0}\vec{v}^{K_0}+{}^{K_0}\vec{v}^{A_0}+{}^{A_0}\vec{v}^{C_0}$$

The joint torques, consisting of the summation of active torque and passive torque, were applied at each degree of freedom. Passive torques were obtained from Yamaguchi (2001). Active torques were systematically assigned in order to produce a kick that was similar to that described in an experimental study by Kim and Kim (1997).

The sensitivity analysis was performed by applying ±10% variations of baseline active joint torque at each degree of freedom except hip ab-/adduction to determine the effect on kicking performance.

RESULTS AND DISCUSSION

The baseline kick demonstrated proximal to distal coordination of segments (Figure 2). A 10% increase in trunk rotational torque produced a large increase in kicking speed (+73%). It lowered kicking height by 30% from the baseline kick height because the increased trunk rotation torque tended to extend the hip and this conflicted with hip flexion during lifting of the lower extremity. A 10% increase in hip flexion torque increased kicking height (+16%) and foot speed (+27%), whereas a 10% decrease in hip flexion torque reduced kicking height (–44%) and foot speed (–9%) from the baseline. A 10% increase in knee extension torque increase foot speed (+26%), while a 10% decrease in knee extension torque reduced foot speed (–17%). Both 10% increase in trunk rotation torque and hip flexion torque increased foot speed (+57%) without losing kicking height (+2%).

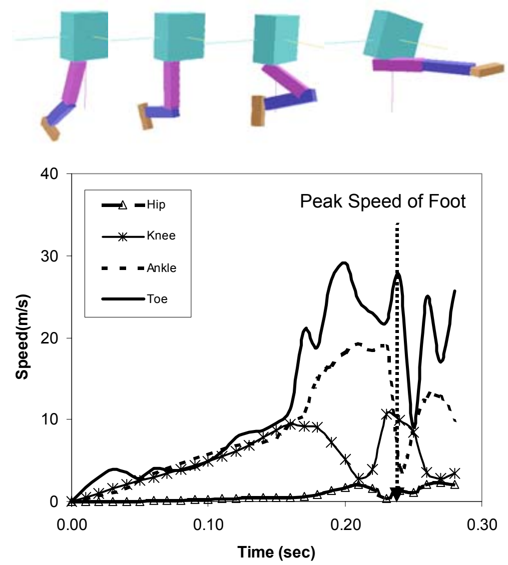

Figure 2. Linear speed of baseline roundhouse kick at each joint.

SUMMARY

Trunk rotation was found to be the most important factor for producing foot speed in roundhouse kick. However, without also increasing hip flexor torque the increased trunk rotation torque produces a kick at the wrong height.

REFERENCES

Kane, T.R., Levinson, D.A. (1985). *Dyanmics: Theory and Applications*. McGraw-Hill, New York, NY.

Kim, S.,-B., Kim, J.,-S. (1997). *Korean J. of Phy. Edu.*, **36**, 348-360.

Yamaguchi, G.T. (2001). *Dynamic Modeling of Musculoskeletal Motion.* KAP, Norwell, MA.

QUANTIFICATION OF MUSCULAR CHALLENGE DURING OBSTACLE CROSSING IN THE ELDERLY: EMG vs. JOINT MOMENT

Li-Shan Chou, Heng-Ju Lee, and Michael E. Hahn

Motion Analysis Laboratory, Department of Exercise and Movement Science
University of Oregon, Eugene, Oregon, U.S.A
E-mail: chou@uoregon.edu

INTRODUCTION

Skeletal muscle strength involved in postural control and locomotion is known to decline with age and disease (Fiatarone and Evans, 1993). It is important to be able to quantify the relationship between muscular demands and gait/balance deviations in the elderly. To better examine the level of challenge imposed on a muscle group, a quantitative index is needed to take into account both strength capacity and strength requirement during performance.

Studies used the ratio of peak calculated joint moments required during activities of daily living (ADL) to peak measured dynamometric torques during maximum voluntary contractions (MVC) and found that older adults required a significantly higher fraction of measured MVC torque in the lower extremity than young adults to perform a majority of the ADLs (Hortobagyi et al., 2003). It should be noted that joint moments computed through inverse dynamics only indicate the net moment from all muscular effort, which provides little information on the level of mechanical demand imposed on an individual muscle group.

Dynamic EMG data allows us to examine the timing and relative intensity of the muscle effort (Perry, 1993). The ratio between the EMG amplitudes collected during functional tasks and the peak EMG amplitude collected during the maximum effort manual muscle testing (MMT) can be used to quantitatively identify the utility of available strength of a muscle group. The purpose of this study was to evaluate and compare two muscular activating ratios, defined by EMG and net joint moment, of selective lower extremity muscles between young and elderly adults during level walking and while crossing an obstacle.

METHODS

Eleven young adults (6 males/5 females; mean age 24.8yrs) and sixteen elderly adults (8 males/8 females; mean age 71.3yrs) were recruited for this study. All participants were determined to be free of neuromuscular or orthopedic pathologies.

Pre-amplified surface electrodes were attached bilaterally to bellies of the gluteus medius (GM), vastus lateralis (VL) and gastrocnemius (medial head, GA). Maximum effort MMT was performed for isometric hip abduction, knee extension, and ankle plantar flexion. EMG signals were collected at 960Hz using the MA-300™ system (Motion Lab Systems, Baton Rouge, LA). MVC tests were performed with a KinCom dynamometer (Chattecx, Hixson, TN) on hip abductors, knee extensors, and ankle plantar flexors. Subjects were then asked to walk at a self-selected pace with barefoot during unobstructed level walking and when stepping over an obstacle of height corresponding to 2.5%, 5%, 10%, or 15% of the subject's height. The order of obstacle height was randomly selected. Motion analysis was performed with a 6-camera ExpertVision™ system (Motion Analysis Corp., Santa Rosa, CA). Two force plates (AMTI, Watertown, MA) were used to collect ground reaction forces with a sampling rate at 960 Hz.

Filtered EMG signals from gait trials were normalized to the MMT signal maximum for each muscle to indicate relative activation levels. OrthoTrak software (Motion Analysis Corp., Santa Rosa, CA) was used to calculate joint moments of both limbs during the crossing stride. Similarly, peak joint moments were normalized to the maximum joint moment collected from MVC to derive relative activation levels. Normalized EMG (N-EMG) and joint moment (N-moment) ratios were analyzed for the effects of age group and obstacle height with a two-factor ANOVA with repeated measures.

RESULTS AND DISCUSSION

Compared to young adults, elderly adults demonstrated significantly higher N-EMG ratios in the VL and GM of both limbs ($p<0.05$). Similarly, elderly adults also showed significantly greater N-joint moment ratios in hip abductors and ankle plantar flexors of both limbs ($p<0.05$) than young adults. However, young adults demonstrated significantly greater N-moment ratios in knee extensors of both limbs than elderly adults ($p<0.05$; Fig. 1).

Increasing obstacle height resulted in significantly greater N-EMG ratios for all muscles of both limbs in all subjects ($p<0.05$), except for the trailing limb VL of elderly adults. Significant obstacle height effects on N-moment ratios were only detected for the trailing hip abductor and leading knee extensor ($p<0.05$).

The opposite trend found between the VL N-EMG and knee extensor N-moment of the leading limb could be interpreted as although the net knee joint moment decreases with higher obstacles, greater co-activations of both agonist and antagonist muscles are required. This indicates that N-EMG ratios may be better to truly quantifying the level of challenge imposed on a muscle group.

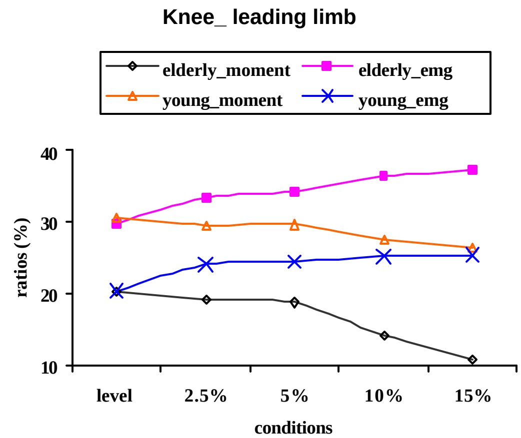

Figure 1. N-EMG ratios of the VL and N-moment ratios of the knee extensor of the leading limb.

SUMMARY

Elderly adults required significantly greater relative activation levels, compared to young adults, to successfully negotiate an obstacle during gait. N-EMG ratios might allow us to better quantify muscular challenge and to assess the relationship between muscular demands and gait/balance deviations in the elderly.

REFERENCES

Fiatarone and Evans (1993), *J Gerontol* **48S**, 77-83.

Hortobagyi et al. (2003), *J Gerontol* 5**8A**, 453-460.

Perry, J. (1993) *Gait Analysis*. Thorofare, NJ, Slack Inc.

ACKNOWLEDGEMENTS

This study was supported by the NIH (AG 022204-01; HD 042039-01A1). Assistance from Jung-Hung Chien in data reduction is greatly appreciated.

In Vivo Shoulder Kinematics: A Comparison of Measurement Methods

Duane A. Morrow, Diana K. Hansen, Denny J. Padgett, Kai-Nan An, Kenton R. Kaufman
Motion Analysis Laboratory, Division of Orthopedic Research, Mayo College of Medicine, Rochester, MN, USA
Email: kaufman.kenton@mayo.edu

INTRODUCTION

Clinical examination of the upper extremity (UE) remains a difficult challenge. With all of the degrees of freedom in the shoulder and the indeterminate system that provides its range of motion and stability, it is perhaps our most complex joint. Additionally, there is a large degree of accompanying skin movement that allows for this high range of motion. These compounding factors do not make in vivo measurement of shoulder kinematics any easier. Most marker-based motion analysis systems, including the Helen Hayes and Cleveland Clinic marker sets (Motion Analysis Corp., 2001), in fact, identify 'shoulder' motion using markers on the 'thorax' (the spinous process of C7 (C7), the xiphoid process (XP), and the sternal notch (SN)) and upper arm (acromion process (AP), medial (ME) and lateral epicondyles (LE)). This use of the thoraco-humeral pseudo-joint completely neglects the role of the scapula as a prime mover of the upper extremity. A thorough understanding of UE kinematics requires that the involvement of the scapula be accounted for.

Recently, a new method has been validated to track the movement of the scapula (Karduna, 2001). Using the tracker described in the paper, motion of the scapula can be accurately recorded. While the referenced paper used an electromagnetic tracker to characterize scapular motion, we have modified the technique to use retroreflective marker based measurement. This method was used in conjunction with a standard UE marker set to compare the results of UE cardinal-plane motions.

METHODS

Right UE motion was collected using nine retroreflective markers to define three segments: thorax using C7, XP, SN; humerus using AP, ME, LE; and scapula using three markers on the scapular tracker). Data was collected using a 10-camera RealTime Motion Analysis System (Motion Analysis Corp., Santa Rosa, CA) at 60 Hz. A single subject was asked to perform a UE evaluation consisting of moving the upper arm in the cardinal planes (Flexion/ Extension (FE), Ab/Adduction (AB), and Internal/External Rotation). A neutral position capture was first collected with the subject's arm resting at his side, thumb forward. For FE trials, the shoulder was flexed with the elbow fully extended, through a comfortable range of motion. Likewise, in the AB trials, the elbow was extended as the shoulder was raised into abduction, and lowered again, with the hand rotating from thumb forward at the beginning of the motion, to thumb facing rearward when the hand is above the head. For the IE trials, the elbow was held, locked at 90º of flexion while the shoulder rotated, bringing the forearm from across the midsection to the comfort limit of external rotation. Three trials of each motion were collected.

Relative rotation matrices were calculated using the method of Soderkvist (Soderkvist, 1993). Glenohumeral (GH) motion was defined as the relative rotations between the Humerus and Scapula, and thoraco-humeral (TH) was defined as rotations between that humerus and thorax. These rotation matrices were then decomposed using the method of Euler Angles into flexion, abduction, and internal rotation.

RESULTS

Results for the ab/adduction rotations are shown (for the motion of the same name) in Figure 1. It can be seen that the GH motion was consistently 31.6% less than the TH motion. A similar discrepancy was found for ab/adduction during the flexion/extension trial. As one might expect, given the little scapular motion anticipated during shoulder IE, there was little to no discrepancy between GH and TH motions in any of the planes (AB shown in Figure 2).

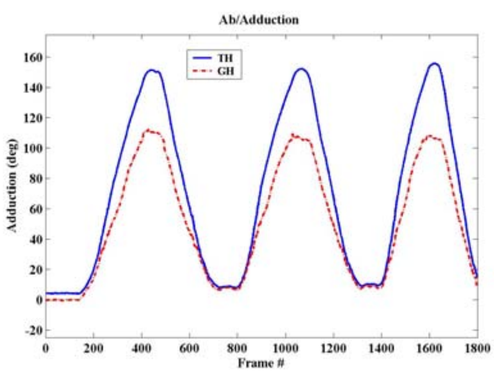

Figure 1. Adduction angle shown for glenohumeral (GH) and thoraco-humeral (TH) motion as a subject abducts his arm over his head.

DISCUSSION

Previous studies have lead to the general consensus that there is a 2:1 ratio of humeral motion to scapular motion during shoulder abduction (Hoppenfield, 1976). This study roughly validates that belief in general. It also calls to mind the potential importance of collecting scapular motion as available in determining a complete analysis of UE kinematics.

SUMMARY

While most currently used motion analysis full-body marker sets do not use markers on the scapula to allow for measurement of glenohumeral kinematics in vivo, it is clear that such measurements are important in assessing total shoulder motion.

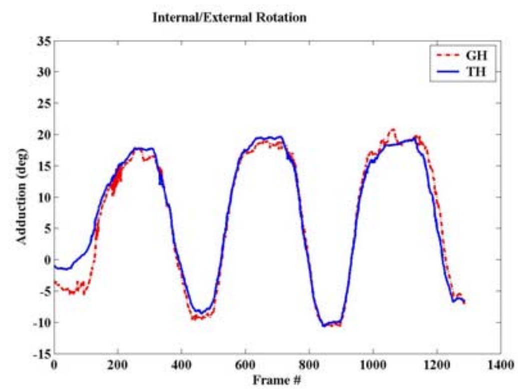

Figure 2. Adduction angle shown for glenohumeral (GH) and thoracohumeral (TH) motion as a subject internally and externally rotates his shoulder.

REFERENCES

Hoppenfield, S. (1976) *Physical Examination of the Spine and Extremities*. Appleton-Century-Crofts.

Karduna, A.R. et al. (2001). *J. Biomech. Eng.*, **123**, (184-190).

OrthoTrak 5.0 Reference Manual, Motion Analysis Corporation, 2001.

Soderkvist, I., Wedin, P.-A. (1993). *J. Biomech.*, **26**, 1473-1477.

ACKNOWLEDGEMENT

The authors would like to gratefully acknowledge the Mayo Foundation for their support of this project.

SAGITTAL PLANE BIOMECHANICS DURING SPORT MOVEMENTS DOES NOT EXPLAIN HIGHER INCIDENCE OF ACL INJURY IN FEMALES

Scott G. McLean[1,2], Anne Su[1] and Antonie J. van den Bogert[1,2]

[1] Department of Biomedical Engineering, The Cleveland Clinic Foundation, Cleveland OH
[2] The Orthopaedic Research Center, The Cleveland Clinic Foundation, Cleveland OH
email: mcleans@bme.ri.ccf.org web: www.lerner.ccf.org/bme

INTRODUCTION

Anterior cruciate ligament (ACL) injury is a common and traumatic sports injury, particularly for females. Female neuromuscular control patterns can contribute to their increased risk of ACL injury. For example, women tend to land in a more extended (hip and knee) position than men (e.g. Malinzak et al., 2001). This places the patellar tendon in a more anterior orientation (Herzog and Read, 1993), which is theorized to increase the amount of quadriceps-induced ACL force, and thus contribute to ACL injury (DeMorat et al., 2004). During athletic movements, however, the quadriceps force and ground reaction force are not independent of flexion angle, or of each other, and this is not incorporated within this theory. The purpose of this study is, therefore, to collect data from human subjects of both genders, and quantify the contributions of sagittal plane knee biomechanics to the force in the ACL during an athletic movement that has been associated with ACL injury.

METHODS

Ten male and ten female NCAA basketball players had lower limb 3D kinematics and kinetics quantified during the stance phase of ten sidestep cutting maneuvers. A dynamic model of the pelvis and lower extremity was generated for each subject as described previously (McLean et al. 2003). Joint angles were obtained from Mocap Solver (Motion Analysis Corporation, Santa Rosa, CA) and intersegmental 3-D forces and moments at the knee were solved using standard inverse dynamics. Intersegmental loads were defined as components of external load on the joint, expressed in a joint coordinate system. Anterior tibial shear force (F_{ant}), external flexion (M_{flex}), valgus (M_{val}), and internal rotation moments (M_{int}) were used for further analysis.

ACL force (F_{ACLsag}) due to the sagittal plane joint loading mechanism was estimated as:

$$F_{\text{ACLsag}} = F_{\text{ant}} + \left(\frac{M_{\text{flex}}}{d(\theta)}\right) \times \sin\alpha(\theta)\,,$$

where d is the moment arm of the patellar tendon as a function of knee flexion angle θ, and α represents the angle between the patellar tendon and the long axis of the tibia in degrees, also a function of knee flexion (Herzog and Read, 1993). This equation does not incorporate the force contributions of the hamstring muscles, and thus represents a worst-case scenario in terms of ACL injury potential during sidestepping.

Peak loads and initial contact knee flexion data were obtained from each trial, averaged for each subject, and compared between genders using a Student t-test ($p<0.01$ after Bonferroni correction).

RESULTS AND DISCUSSION

Women landed with less initial knee flexion (Table 1), similar to previous observations (Malinzak et al., 2001). No significant gender differences were found in the kinetic variables (Table 1). The sagittal plane loading mechanism failed to significantly load the ACL for either gender (Figure 1). In fact, the joint forces were mainly posterior, loading the PCL rather than the ACL. Females loaded the ACL during early stance, but the magnitude was small compared to known failure loads. The closed-chain relationship between flexion angle, external ground reaction force, and quadriceps force appears to protect the ACL from excessive sagittal plane loading. During early stance, the ground reaction force acts posteriorly on the tibia, protecting the ACL. Quadriceps force does not become large until later in stance, when the flexion angle is such that the patellar tendon orientation is no longer harmful.

Females had larger valgus loads at the knee, though not significantly so (Figure 2). However, these differences in load during normal movement may indicate a much larger difference in injury risk, which occurs at the tail of the probability distribution. These observations support the evolving hypothesis that knee valgus is the primary extrinsic contributor to the female injury mechanism. We have made comparable observations using forward dynamic simulations of ACL injury mechanisms (McLean et al., 2003).

Table 1: Gender comparisons *(p<0.01).

Variable	Male	Female
θ_{init} (deg)*	30.4 ± 3.6	24.0 ± 1.3
F_{ant} (N)	294 ± 126	194 ± 85
M_{flex} (Nm)	311 ± 84	282 ± 60
M_{val} (Nm)	58 ± 25	68 ± 27
M_{int} (Nm)	39 ± 14	27 ± 21
F_{ACLsag} (N)	378 ± 173	287 ± 110

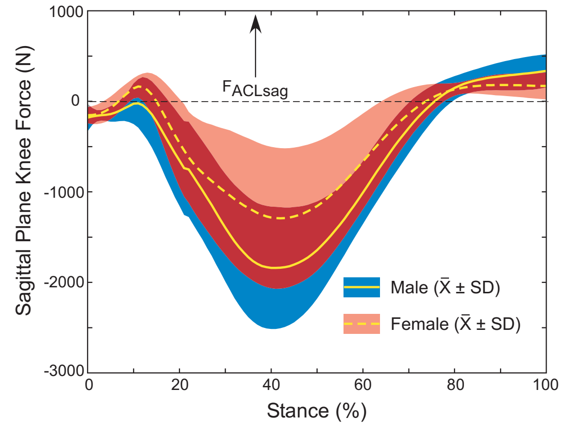

Figure 1: Sagittal plane ACL loading.

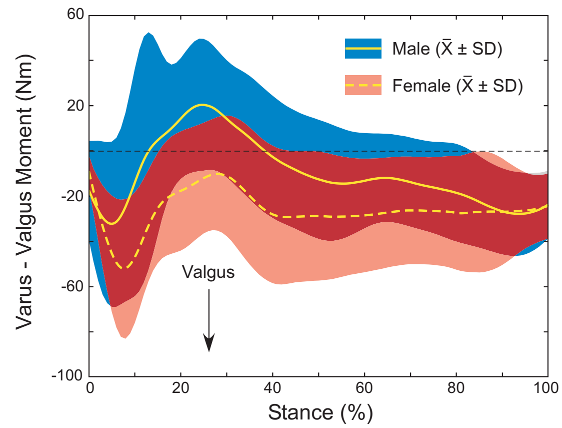

Figure 2: Knee valgus loading.

SUMMARY

Gender differences in sagittal plane knee biomechanics do not appear related to the higher incidence of ACL injury in women.

REFERENCES

DeMorat, G. et al. (2004). *Am. J. Sports Med.*, **32**, 477-483.

Herzog, W., Read, L.J. (1993). *J. Anat.*, **182**, 213-230.

Malinzak, R.A. et al. (2001). *Clin. Biomech.*, **16**, 438-445.

McLean, S.G. et al. (2003). *J. Biomech. Eng.*, **125**, 864-874.

ACKNOWLEDGMENT

This research is supported by the National Institutes of Health (R01AR47039).

FOOTWEAR THAT ALLOWS RELATIVE HORIZONTAL MOVEMENT BETWEEN THE FOOT AND OUTSOLE REDUCES KNEE JOINT MOMENTS DURING RUNNING

Darren J. Stefanyshyn, Jay T. Worobets and Brady Anderson

Human Performance Laboratory, University of Calgary, Calgary AB, Canada
E-mail: darren@kin.ucalgary.ca Web: www.kin.ucalgary.ca/hpl/

INTRODUCTION

Patellofemoral pain syndrome (PFPS) accounts for about 25% of all running injuries (Taunton et al, 2002). It has been shown that subjects who developed PFPS during running had higher internal knee abduction and external rotation moments than asymptomatic subjects in both a retrospective (Stergiou et al., submitted) and prospective study (Stefanyshyn et al., submitted). In addition, high knee joint moments appear to be a potential cause of other running related injuries (Stefanyshyn, et al., 2001).

Footwear can significantly influence joint moments at the knee and ankle (Webster et al., 2001; Mündermann et al., 2003). Therefore, it was speculated that footwear could be developed specifically to reduce knee joint moments, primarily in the transverse and frontal planes. A new prototype was developed to allow the foot to displace both in a medial-lateral and anterior-posterior direction relative to the outsole. The prototype employed a ball and socket design where the rear foot portion of the midsole could move independently of the rest of the shoe (termed Ball and Socket). The shear forces developed due to the horizontal ground reaction forces result in additional horizontal movement within the shoe.

The purpose of this study was to determine if the prototype footwear allowing relative movement between the foot and outsole would reduce three-dimensional knee joint moments during running.

METHODS

Eleven male subjects provided informed written consent and participated in this study. Data were collected while they ran with the different shoe conditions at speeds of 3 and 5m/s. The shoe conditions consisted of a fixed and functional version of the Ball and Socket prototypes. The fixed versions served as the control condition and did not allow any horizontal movement, the technology was incorporated in the footwear but it was secured and not allowed to move.

Kinetic data were collected with a Kistler force platform sampling at 2400 Hz. Kinematic data were collected simultaneously with the kinetic data using a Motion Analysis six video camera system at 120 Hz. Spherical reflective markers were placed on the thigh, shank and shoe. Five trials were collected for each condition and prior to calculation of any variables, the kinematic (cutoff frequency of 12 Hz) and the kinetic data (cutoff frequency of 50 Hz) were filtered with a fourth-order low-pass Butterworth filter. Internal knee joint moments were calculated using an inverse dynamics analysis. Traditional variables such as eversion, eversion velocity, tibial rotation, peak impact forces and peak impact force loading rates were also calculated.

Paired student T-tests were performed to compare between the shoes with functional and fixed systems. The α-level chosen was 0.05.

RESULTS AND DISCUSSION

There was a significant reduction of about 11% in peak knee abduction moments with the Ball and Socket shoe while running at 3m/s (Fig. 1). All 11 subjects had a reduction while running at the slow speed. Eight of the eleven subjects also had a reduction while running at 5m/s but on average, the reduction was not significant.

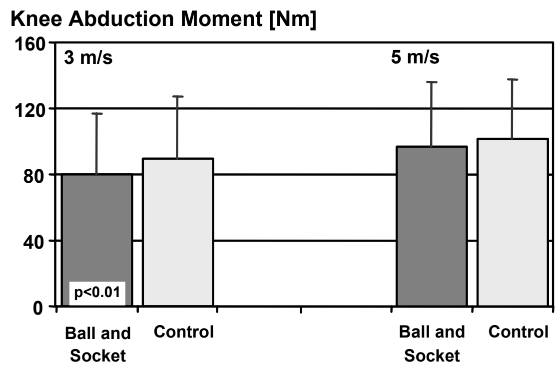

Figure 1: Average (n=11) peak abduction knee joint moments.

The peak external rotation moments at the knee were highly variable between subjects. However, the Ball and Socket shoe significantly reduced the external rotation moments at the knee during running at 3m/s (Fig. 2). The reduction was approximately 18%. There was also a trend toward reduced external rotation moments during fast running. Eight of the subjects had consistent reductions in peak moments with the prototype shoe.

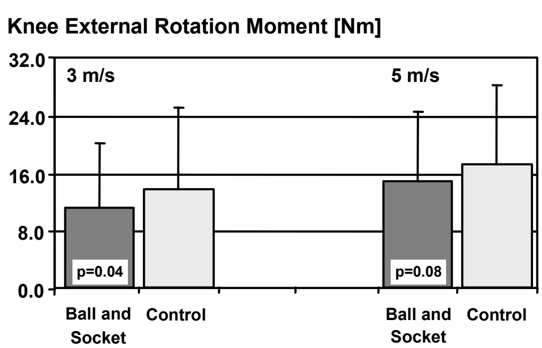

Figure 2: Average (n=11) peak external rotation knee joint moments.

There were no significant differences in eversion, eversion velocity, tibial rotation, peak impact forces and peak impact force loading rates between the two footwear conditions.

Although running shoe manufacturers have contributed substantial resources toward minimizing rear foot pronation and impact forces, there is very little retrospective and virtually no prospective evidence to suggest that these variables cause running related injuries. Recent data suggest that knee joint moments could be related to running injuries and development of footwear that can reduce these moments should be pursued further. Future intervention studies with moment reducing footwear should be used to determine if running injuries can be reduced.

SUMMARY

Since high knee abduction and external rotation moments have been proposed to be associated with knee injuries, especially PFPS, the decreased moments with the new prototype Ball and Socket shoes may help in preventing running related injuries.

REFERENCES

Mündermann et al. (2003) Clin. Biom. **18**, 254-262.
Stefanyshyn et al. (2001) Proc. 5th ISB Footwear Symp., 74-75.
Stefanyshyn et al. (sub) Clin. J. Sports Med.
Stergiou et al. (sub) Clin. J. Sports Med.
Taunton et al. (2002) Br. J. Sports Med. **36,** 95-101.
Webster et al. (2001) Proc. 6th Gait Clin. Mov. Analys.

ACKNOWLEDGEMENTS

adidas International.

HORIZONTAL IMPULSE GENERATION CHARACTERISTICS DURING THE SPRINT START ARE INFLUENCED BY SHANK SEGMENT CONTROL

Kathleen E. Costa[1] and Jill L. McNitt-Gray[2]

[1] Coaching & Sport Sciences, United States Olympic Committee, Chula Vista, CA
[2] Biomechanics Laboratory, Dept. of Kinesiology, Biomedical Engineering, Biological Sciences
University of Southern California, Los Angeles, CA, USA
E-mail: kathleen.costa@usoc.org

INTRODUCTION

The goal of the first step of a sprint start is to increase the forward horizontal momentum of the body as quickly as possible. Change in horizontal momentum of a system requires that a net horizontal impulse be applied in the desired direction. Previous investigations have found that faster horizontal running velocities are associated with shorter ground contact times, larger net horizontal ground reaction forces, and faster times to peak horizontal ground reaction force, compared to slower horizontal running velocities (Henry, 1952; Bobbert & Van Zandwijk, 1999; Weyand et al., 2000; Kuitunen et al., 2002). The purpose of this investigation was to test the hypothesis that increased rate of horizontal force development (HRFD) produces larger net horizontal impulse during the first foot contact of sprint start. Understanding impulse generation strategies during the first step of the sprint start will facilitate horizontal momentum generation early in the race, leading to an improvement in overall sprint performance (Mero, 1988).

METHODS

National level multi-event athletes (1 heptathlete, 11 decathletes) volunteered to serve as subjects in accordance with the Institutional Review Board. Each athlete performed a series of sprint starts out of starting blocks during a pre-season training camp session (United States Olympic Training Center, Chula Vista, CA). During the sprint start, two-dimensional, sagittal plane kinematics (NAC C^2S, 200Hz) and three-dimensional reaction forces (Kistler, Amhurst, MA, 0.6x0.9m, 1200Hz) were collected during the first step out of the starting blocks. Body segment landmarks (22) (Zatsiorsky and Seluyanov, 1983; de Leva, 1996) were manually digitized (Motus, Peak Performance, Inc., Inglewood, CO) during the time between touchdown (TD) and take-off (TO) of the first step of the sprint start. Digitized x and y coordinates of body landmarks were individually filtered, interpolated (1200 Hz) and synchronized with reaction force data at the time of TD. Net joint forces (NJF) and net joint moments (NJM) of the ankle, knee, and hip of the stance leg were determined using Newtonian mechanics. Changes in center of mass (CM) horizontal and vertical velocity during the contact phase were determined by integrating the net horizontal and the net vertical force-time curves normalized by body mass from TD to TO. Rate of horizontal force production was calculated as the average slope of the horizontal reaction force-time curve from minimum braking force to maximum propulsive force.

RESULTS AND DISCUSSION

Contrary to the hypothesis, an increase in HRFD did not consistently result in larger net horizontal impulse during the first foot contact of a sprint start. Athletes were found to generate similar net horizontal impulse with different horizontal force-time characteristics (e.g. high ΣF_h over short Δt, or low ΣF_h over long Δt; figure 1). Across subjects, net horizontal impulse generated during the first step ranged from 1.08-1.48m/s over a period of 0.166-0.265s.

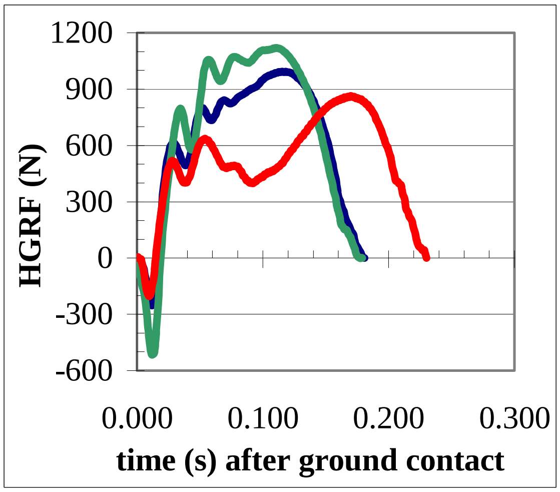

Figure 1. Horizontal ground reaction force-time curves plotted for 3 athletes who generated equal net horizontal impulse ($\Delta V_h = \Sigma F_h \Delta t$ / m = 1.29m/s) during the first step of a sprint start from starting blocks. These data demonstrate that equal net horizontal impulse magnitudes may be generated with different HRFD.

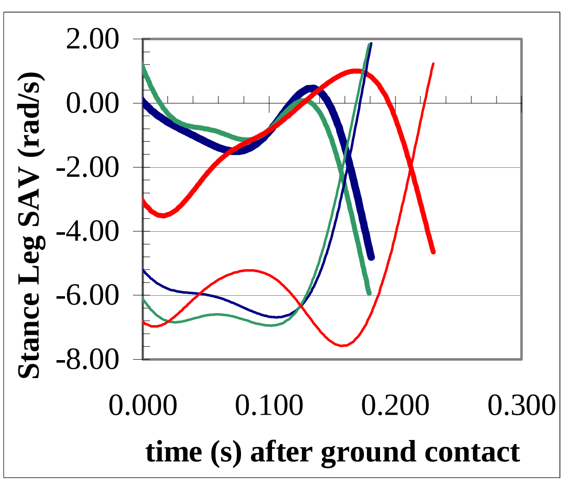

Figure 2. Support leg shank (thick lines) and thigh (thin lines) segment angular velocity (SAV)-time curves plotted for the same 3 athletes as shown in figure 1. These kinematic data suggests horizontal impulse generation characteristics may be associated with lower extremity segment control during ground contact. Specifically, trials with greater shank SAV during the impact phase, tended to have greater thigh SAV during the post-impact leading to a delay in HGRF generation. Whereas, trials with lower shank SAV during impact appeared to provide a base for quicker thigh rotation over the knee thereby contributing to a quicker generation of HGRF.

SUMMARY

Rate of horizontal force development was not found to be directly related to horizontal impulse generation during the first step of a sprint start. Individual horizontal impulse generation characteristics (e.g. large ΣF_h over short Δt, or small ΣF_h over long Δt) appears to be related to lower extremity segment control at touchdown and during ground contact phase.

REFERENCES

Bobbert & Van Zandwijk (1999) *Biol Cybern.*, 81:2, 101-8.

de Leva P (1996) *J Biom*, 29:9, 1223-30.

Henry, F.M. (1952) *Res Quart*, 23:4, 301-18.

Kuitunen et al. (2002) *MSSE*, 34:1, 166-73.

Mero A. (1988), *Res Quart*, 59:2, 94-8.

Weyand et al., (2000) *J Appl Phys*, 89, 1991-9.

Zatsiorsky & Seluyanov (1983) *Biom VIII-B*, 1152-9.

ACKNOWLEDGEMENTS

USOC C&SS, USA Heptathlon, USA Decathlon

SAGITTAL AND FRONTAL SWAY ANGLES DURING LOCOMOTION IN THE ELDERLY

Heng-Ju Lee and Li-Shan Chou

Motion Analysis Laboratory, Department of Exercise and Movement Science, University of Oregon
Eugene, Oregon, U.S.A
E-mail: chou@oregon.edu

INTRODUCTION

Falls are the leading cause of injuries in elderly adults and the leading cause of accidental death in those over age 85. Epidemiological studies of falls have shown that most falls during some forms of locomotion (Overstall et al., 1977). Therefore, an accurate assessment of balance control during dynamic activities is critical to reducing the incidence of falls.

Motion of the whole body center of mass (COM) has been used as a biomechanical measure to identify dynamic instability in the elderly (Hahn and Chou, 2003; Chou, et al., 2003). However, linear COM excursions might be affected by the individual's stature (Berger et al., 1992). In addition, the COM motion has to be precisely coordinated with the center of pressure (COP) of the stance foot to avoid imbalance. Therefore, biomechanical measures that could provide information on instantaneous coordination between the COM and COP and exclude inter-subject variability are needed to better define dynamic stability.

In this study, instantaneous sagittal and frontal sway angles of an inverted pendulum, defined by the COM and COP, during unobstructed and obstructed walking were assessed. It was hypothesized that sway angles were able to identify older adults who are at a greater risk of falling.

METHODS

Six healthy elderly adults, (3 males and 3 females; 77.2± 3.4 years; 170.7 ± 9 cm; 73± 7.4 kg) and six elderly patients with complaints of imbalance during walking (3 male and 3 female; 80 ± 4.8 years; 162.1 ± 11 cm; 75.7 ± 18 kg) were recruited for this study. The experimental protocol included unobstructed level walking and stepping over an obstacle set to a height equal to 2.5 or 10% of the subject's body height (BH). Subjects were asked to walk at a self-selected pace along a 10-m walkway while barefoot.

Whole body motion analysis was performed with a 6-camera ExpertVision™ system (Motion Analysis Corp., Santa Rosa, CA). Twenty-seven reflective markers were placed on bony landmarks of each subject. Three-dimensional marker trajectory data were collected at 60 Hz. Both external markers and estimated joint centers (of both distal and proximal ends) were used to calculate the three-dimensional locations of segmental COMs. Whole body COM position data was calculated as the weighted sum of each body segment, with 13 segments representing the whole body (head-neck, trunk, pelvis, upper and lower arms, upper and lower legs, feet). The COP position was calculated from the ground reaction forces/moments collected from two force platforms (AMTI, Watertown, MA) at 960 Hz.

Instantaneous sway angles in the sagittal and frontal planes were defined as the angle between the inverted pendulum, defined by the COP and COM, and the vertical line (Fig. 1). Effects of subject group and obstacle height on sway angles were assessed using a two-factor ANOVA with repeated measures of obstacle height.

RESULTS AND DISCUSSION

Profiles of the sway angle, started from the leading limb toe-off to the time right before trailing limb heel-strike, were similar in both subject groups (Fig. 2). Peak anterior sway angle occurred right at leading limb heel strike.

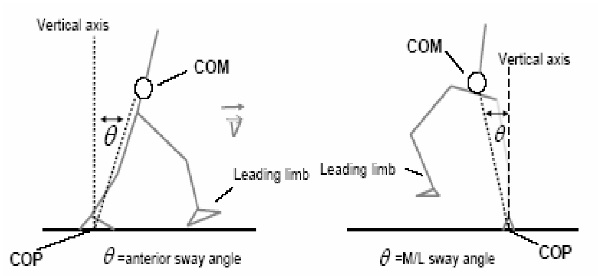

Figure 1.

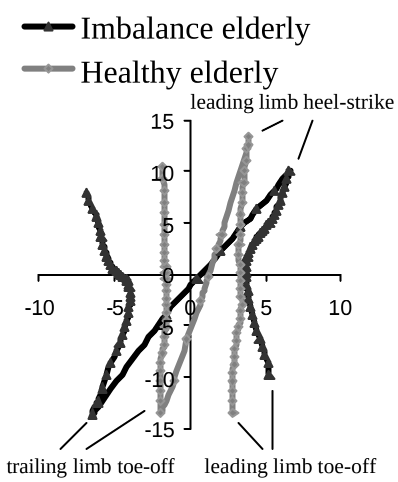

Y axis - A/P sway angle (degrees)

X axis - M/L sway angle (degrees)

Figure 2. Typical patterns of the A/P and M/L sway angles during a crossing stride when stepping over an obstacle of 2.5% BH.

Elderly adults with imbalance demonstrated significantly greater range of M/L sway angles, greater peak M/L sway angles and smaller peak A/P sway angles than healthy elderly adults. Increasing obstacle height resulted in a linear increase ($p< 0.05$) in the peak anterior sway angle (Table 1).

Our results indicated that sway angles in both sagittal and frontal planes during walking were able to distinguish elderly individuals with imbalance. Significant reduction of the A/P sway angles in elderly adults with imbalance might be due to their adoption of a conservative strategy, such as a slower walking speed with a shorter step length. On the other hand, significant greater M/L sway angles observed in the elderly with imbalance could indicate their inability to control COM motion in the frontal plane.

SUMMARY

Instantaneous sway angles in both the sagittal and frontal planes during walking provide information about an individual's ability to control COM position in relation to the corresponding COP. These measures might allow us to better detect elderly individuals at risks for imbalance or falls.

REFERENCES

Berger, W. et al. (1992). *Acta Otolaryngol*, ***112***, 22-30
Chou, L-S. et al. (2003). *Gait and Posture*, ***18***, 125-133
Hahn, M.E., and Chou, L-S. (2003). *Clin Biomech*, ***18***, 734-44.
Overstall et al. (1977) *Br. Med. J* 1, 261-264.

ACKNOWLEDGEMENTS

This study was supported by the NIH (AG 022204-01; HD 042039-01A1).

Table 1: Sway angles (degree), group means (SD)

Obstacle Height	None		2.5%		10%		Effect
	Healthy	Imbalance	Healthy	Imbalance	Healthy	Imbalance	
Max. anterior sway angle	12.4(2)	9(1)	14.2(1)	10.2(1)	14.6(2)	11.1(2)	a,b
Range of M/L sway angle	8.1(1)	11.1(1)	7.5(2)	11(1)	8.4(1)	11.2(1)	a
Max. M/L sway angle	4.3(1)	6.1(1)	4.2(1)	6(1)	4.6(1)	6.3(1)	a

a. significant group difference, $p<0.05$; **b**. significant obstacle height effect, $p<0.05$

FE ANALSIS OF THE MECHANICAL BEHAVIOR OF CHONDROCYTES

S.-K.Han[1], S. Federico[1], A. Grillo[2], F. Musumeci[2], G. Giaquinta[2], and W. Herzog[1]
[1]Human Performance Laboratory, the University of Calgary, Canada
[2]Dept of Physical and Chemical Methodologies for Engineering, University of Catania, Italy
Corresponding Author: Sang Kuy Han, e-mail: shan@ucalgary.ca

INTRODUCTION

Chondrocytes are the living cells in articular cartilage (AC). They synthesize and maintain the extracellular matrix. Their activity is regulated by the interplay of genetic and environmental factors, such as soluble mediators, extracellular matrix composition, and mechanical factors. The mechanical environment of the chondrocytes has a significant influence on the health of the joint. In past studies of the mechanical behavior of chondrocytes (Wu and Herzog, 2000; Guilak and Mow, 2000), articular cartilage was described as a biphasic material consisting of a homogeneous, isotropic, linearly elastic solid phase, and an inviscid fluid phase, although AC is known to be highly anisotropic and inhomogeneous. In this study, AC is modeled by using the microstructure-based transversely isotropic, transversely homogeneous (TITH) model proposed by Federico et al. (2003, 2004). The purpose of this study was to analyze the mechanical behavior of chondrocytes as a function of location within the tissue, and to compare the predictions of classical isotropic, homogeneous (IH) models with those obtained using the TITH model.

METHODS

In order to model chondrocyte deformation, we used a multi-scale step method (e.g., Wu and Herzog, 2000; Guilak and Mow, 2000), consisting of a macro-scale and micro-scale description for the entire tissue and the cells, respectively. At the macro-scale level, articular cartilage was assumed to be biphasic, and the elastic solid phase was modeled by use of the TITH model, i.e., as a composite made of a proteoglycan matrix, a cell inclusion phase, and a depth-dependent, statistically oriented collagen fiber phase. The fluid phase was assumed to be inviscid and incompressible, with a deformation-dependent permeability (Holmes and Mow, 1990). All material properties for the TITH model were taken from the published literature. Cells were assumed to be axi-symmetric ellipsoids and their aspect ratio $\alpha = a/b$ (a and b being the vertical and the transverse semi-axes, respectively) and volumetric concentration depended on their depth location within the cartilage. Chondrocytes are typically flattened ($\alpha < 1$) in the superficial zone, spherical ($\alpha = 1$) in the middle zone, and elongated ($\alpha > 1$) in the deep zone (Clark et al., 2003). At the micro-scale level, a single cell was embedded in a cylinder with the same aspect ratio as the cell. The cylinder was made up of extracellular matrix (proteoglycan matrix plus collagen fibers). The homogenized elastic properties of the matrix were obtained by applying the TITH model to the proteoglycan matrix and fibers alone. The volume of the cylinder was given by the ratio of the cell volume (which was assumed constant in the initial unloaded state) and the cell volumetric concentration. The displacement and fluid pressure fields calculated at the macro-scale level were used as the time-dependent boundary conditions for the micro-scale model. In order to compare the TITH model with the IH model, the elastic constants for the IH model were taken to be equal to the average properties of the TITH model. Numerical simulations were made by means of the commercially available software ABAQUS v6.3, and in accordance with experimental configurations (Guilak, 1995). The cartilage specimen was assumed cylindrical, 1.0*mm* thick, and had a diameter of 6.0*mm*. The specimen was subjected to a 15% unconfined compression load, at a constant rate during a ramp period of 30 *s*, and the deformation was then kept constant until 1200 *s*. Three chondrocyte locations were chosen for analysis. The locations of these chondrocytes were on the axis of symmetry (*z*-axis) which runs from the bone-cartilage interface to the articular surface: superficial ($z = 0.9, a = 1/3$), middle ($z = 0.5, a = 1$), and deep zone ($z = 0.1, a = 3/2$).

RESULTS AND DISCUSSION

In the superficial and middle zone, the normalized cell height predicted by the TITH model was significantly smaller than that predicted by the IH model throughout the loading and recovery phase (Fig. 1). The percentage decrease in cell height in the middle zone predicted by the TITH model was 14.5%, a value that compares well with the experimental value (14.7±6.4%) found by Guilak (1995). The TITH model predicted a smaller normalized cell volume, compared to the IH model, at all locations (Fig. 2). In particular, in the middle zone, the TITH model predicts a small volume decrease during the loading phase, and a short-term increase, followed by a decrease, in the recovery phase, whereas the IH model predicts a monotonic decrease. We speculate that this difference is caused by the different fluid flows in the two models.

SUMMARY

The results of this study indicate that anisotropy and inhomogeneity of AC dramatically influence the mechanical properties of the tissue on the macro- and microscopic level. We believe that studies at the micro- and macro-scale level will provide new insight into understanding the relationship between mechanical loading of AC and adaptive and degenerative biological responses controlled by the chondrocytes.

REFERENCES

Wu, J.Z., Herzog, W. (2000) *J. Biomech. Eng*, **28**, 318-330. Guilak, F., Mow, V.C. (2000) *J. Biomech.* **33**, 1663-1673. Federico, S. et al. (2003) Proc. XIX ISB Congress, 100. Federico, S. et al. (2004) *J. Mech. Phys. Solids*, accepted. Guilak, F. (1995) *J. Biomech.* **28,** 1529-42. Holmes, M.H., Mow, V.C. (1990) *J. Biomech* **23,** 1145-56. Shin, D., Athanasiou. K. A. (1997) *Trans. Orthop. Res. Soc*. **22**:1: 352. Clark, A.L. et al. (2003) *J. Biomech.* **36**, 553-568

ACKNOWLEDGEMENTS

NSERC, CHIR, Arthritis Society of Canada.

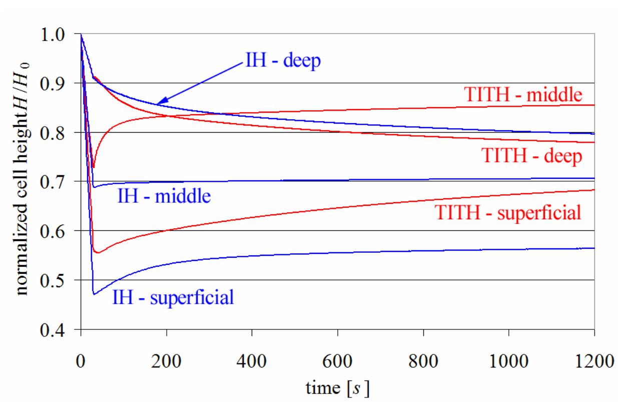

Figure 1. Normalized cell height

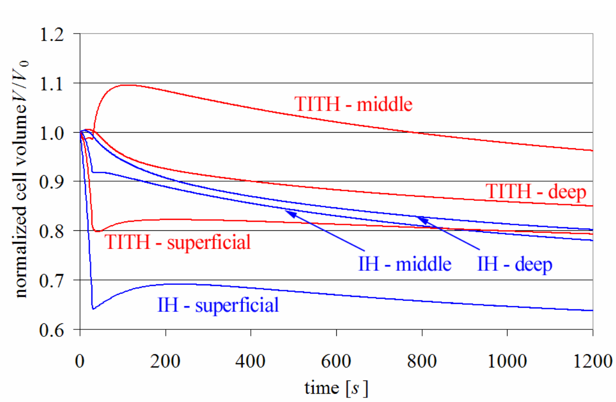

Figure 2. Normalized cell volume

KNEE VARUS/VALGUS MOMENTS DURING TAI-CHI EXERCISE AND NORMAL WALKING IN PATIENTS WITH KNEE ARTHRITIS SYMPTOMS

INTRODUCTION

Musculoskeletal disease, including osteoarthritis (OA), is the leading cause of physical activity limitation for adults in the United States. Recently, alternative approaches have been employed in the treatment of OA, attempting to decrease pain and stiffness. One approach, Tai Chi Chuan (TCC) has begun to draw more attention. For specific groups such as patients with OA, Tai Chi Chuan may provide unique benefits of improved function and decreased pain compared to regular exercise walking programs. In order to understand the mechanisms of how TCC may be beneficial to persons with arthritis, it is important to look at the loading demands TCC exercise places on the knee joint. The Varus/Valgus moments are particularly important because of their relationship to medial and lateral tibial compartment loading (Andriacchi, 2000). The purpose of this pilot study was to assess the knee Varus/Valgus moment patterns during normal walking and TCC exercise in patients with self-reported knee arthritis.

METHODS

Four subjects ages (45 to 55) who were experienced in Tai-Chi exercise volunteered for this study. Two patients complained of bilateral knee pain, and two complained of right knee pain. All subjects reported having signs or symptoms of arthritis (morning stiffness, decreased ROM, pain with stairs, crepitus, and/or chronic swelling) in one or both knees. All subjects reported being told by their physician that they had some knee arthritis. All subjects had been practicing TCC for at least 1 yr. Subjects were asked to walk across a level 5 m walkway at a self-selected pace and to perform the beginning part of their TCC exercise which required them to step out with their left leg. An Optotrack® motion analysis system (Northern Digital Inc. Ontario, Canada) recorded three-dimensional kinematics of left lower extremity at 100Hz sampling rate. A force platform (AMTI, Watertown, MA, USA) recorded ground reaction forces (GRF) during the stance phase of gait and the TCC step. Knee moments in the frontal plane were calculated during the stance phase of each task using an inverse dynamics approach.

RESULTS AND DISCUSSION

Knee varus/valgus moments for all four subjects are shown in Figure 1a (during Tai-Chi stepping) and Figure 1b (during the stance phase of normal gait). For the two patients with bilateral knee pain, valgus moments occurred during the normal stance phase of gait and were maintained during Tai Chi stepping with greater variability. The two subjects with unilateral pain could be considered control subjects because the analysis was done on their uninvolved side. During normal stepping they exhibited varus moments up to 50% of stance, which then shifted into slight valgus moment. However, during Tai Chi stepping they maintained a varus moment during the entire period.

SUMMARY

The two patients with bilateral pain could have learned to do activities with more Valgus loading to limit medial compartment forces. The increased Varus loading, even though it was on the uninvolved knee could indicate poor compensation to Tai-Chi exercise. The study is the first study to look at the knee joint kinetics pattern during the normal walking and TC exercise, but limited by the sample size and by the fact that only one leg analysis was performed. Nevertheless, it does begin to probe the biomechanical effects of Tai-Chi exercise, which is becoming a popular exercise for patients with arthritis. Further study is warranted to assess whether Tai Chi exercise creates potential deleterious joint loading for arthritis patients

REFERENCES

1. Andriacchi, T.P et al. (2000) J. Rehab. Res. and Develop, 37(2) 163-170

ACKNOWLEDGEMENTS

This study was funded by a grant from The Center for Complimentary and Alternative Medicine, University of Maryland School of Medicine

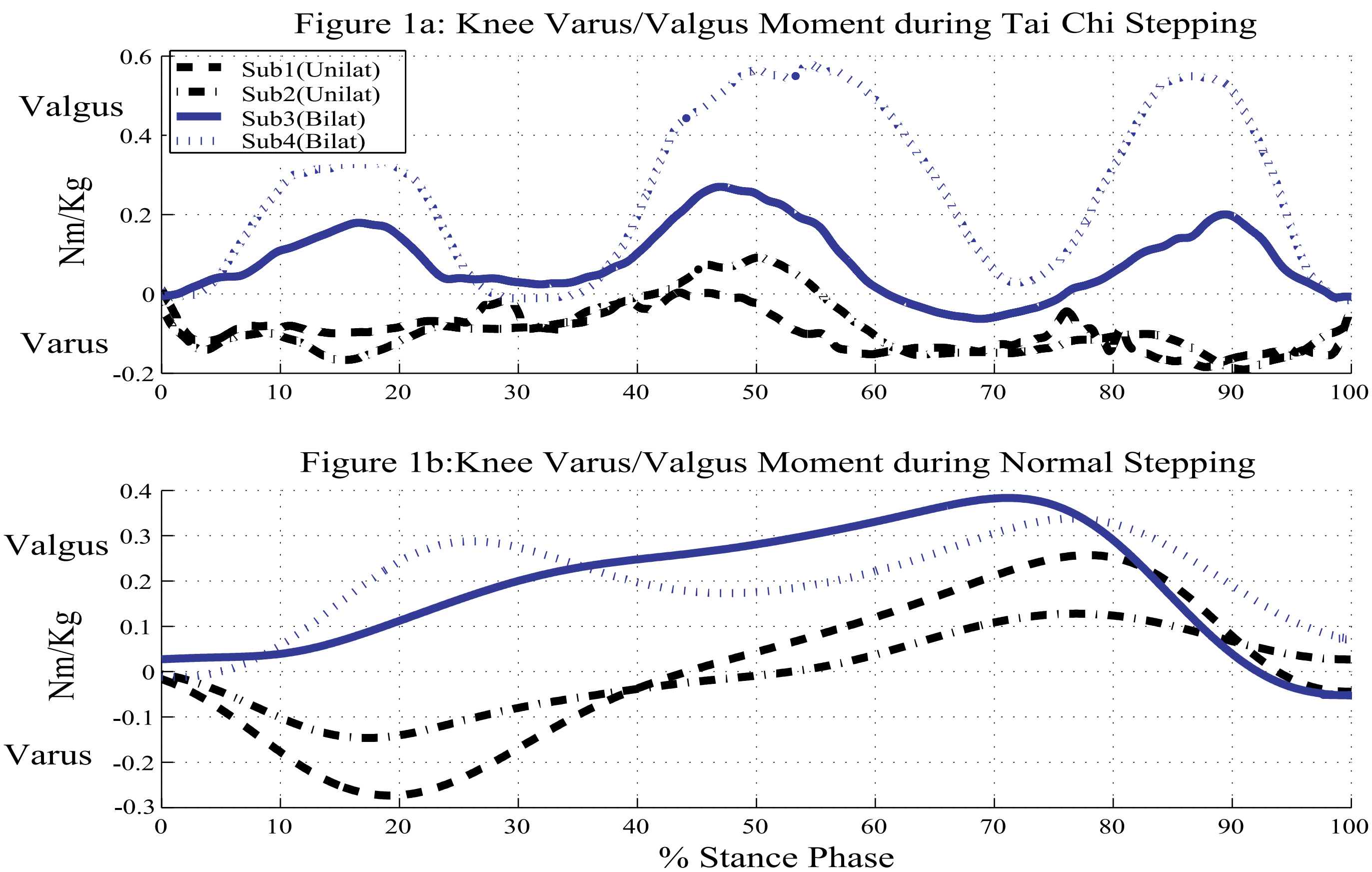

Figure 1a: This graph illustrates knee varus and valgus moment during Tai Chi Stepping

Figure 1b: This graph illustrates knee varus and valgus moment during Tai Chi Stepping

EFFECT OF LOADING RATE ON COMPRESSIVE FAILURE MECHANICS OF THE PEDIATRIC CERVICAL SPINE

Paul Z. Elias, David J. Nuckley, and Randal P. Ching

Applied Biomechanics Laboratory, Dept. of Mechanical Engineering, University of Washington, Seattle, WA, USA
E-mail: rc@u.washington.edu Web: depts.washington.edu/uwabl

INTRODUCTION

To date, the effort towards prevention of pediatric cervical spine injuries has been hindered by a lack of data on pediatric spine mechanics. Although pediatric injuries to the cervical spine are not particularly common, they are associated with significant rates of mortality and disability (Brown et al., 2001). To reduce such injuries, various crash-test dummies, computational models, and safety standards have been developed by scaling adult injury tolerance data to children. While animal models have been used to establish pediatric tensile (Ching et al., 2001) and compressive (Nuckley et al, 2002a) scaling factors, the viscoelastic behavior of biologic tissues requires that loading rate be taken into account for a thorough understanding of cervical spine mechanical properties. As such, this study aims to contribute data on the compressive failure mechanics of the cervical spine with an emphasis on the effect of loading rate, using a baboon model.

METHODS

12 fresh-frozen baboon cadavers, age 9 ± 1 human equivalent years, were inspected for spinal injury and pathology before gross dissection to remove musculature and soft tissues. The remaining full and intact cervical spines were each dissected into 3 segments, each comprised of 2 functional spinal units (Occiput – C2, C3 – C5, and C6 – T1). Segments were wired through the vertebral body and lateral masses inferiorly and superiorly before being embedded in PMMA. Segments were then attached inferiorly to a 6-axis load cell and superiorly to an MTS ram (Figure 1).

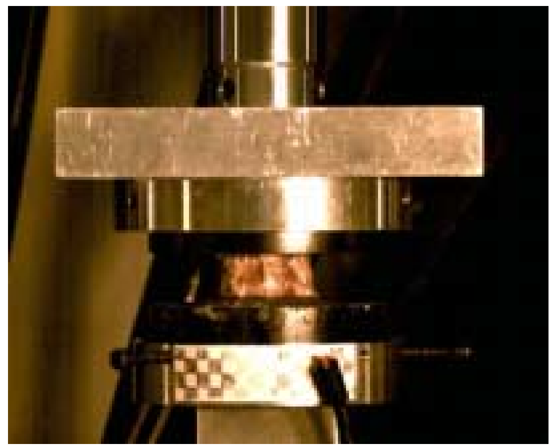

Figure 1: Segment attached inferiorly to a 6-axis load cell and superiorly to the MTS ram

Displacements were measured using both LVDT and high-speed video. Each segment was randomly assigned to a loading rate group of 5, 50, 500, or 5000 mm/sec, ensuring that each group contained 3 Oc-C2, 3 C3-C5, and 3 C6-T1 segments. All segments were preconditioned for 50 cycles at 1 Hz, up to 100 N. Following preconditioning, each segment was failed in axial compression via a haversine displacement-controlled input to a strain of 60 %. Stiffness, failure load, and displacement at failure were determined from load-displacement curves. Due to the lack of a single linear region for calculation of stiffness, an average linear stiffness was determined by dividing the failure load by the displacement at failure, with displacement measured from the point where the specimen first began taking load. Failure loads were determined by identifying the first sharp drop in load, accompanied by increasing displacement.

RESULTS AND DISCUSSION

Post-failure radiographs showed mostly general compression fractures for the 5 mm/sec tests, while the higher rates produced mostly burst fractures. Stiffness was found to increase significantly with increasing loading rate ($p = 0.0379$). Mean stiffness of the 5000 mm/sec loading rate group was found to be approximately 30 % higher than that of the 5 mm/sec group (Figure 2). Such rate dependence is consistent with the general viscoelastic behavior of biologic tissues (Danto and Woo, 1993), and also with previous tests using cervical spine motion segments (Yingling et al., 1997).

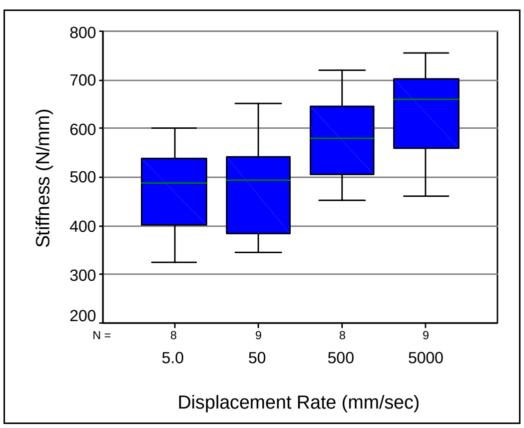

Figure 2: Stiffness vs. Loading Rate

A trend towards increasing failure load with loading rate was also observed, but no statistical difference existed between the loading rate groups. It appears, therefore, that the failure load rate dependence of cervical spine motion segments is much greater between quasi-static and dynamic rates, rather than between the various dynamic rates tested in this study (Yingling et al., 1997). Finally, the displacement at failure was found to be independent of loading rate, which is consistent with previous literature indicating that the failure mechanism in cervical spine motion segments is based on strain rather than stress (Nuckley et al., 2002b).

SUMMARY

This study aimed to determine the effect of loading rate on compressive failure mechanics of the pediatric cervical spine. It was found that stiffness increased significantly with loading rate, while displacement at failure was independent of rate. Failure load showed an increasing, but not statistically significant, trend with increasing loading rate. The results of this research may be useful for development of better pediatric automotive safety standards, improved biofidelic crash-test dummies, and more accurate computational models.

REFERENCES

Brown, R.L et al. (2001). *J. Pediatric Surg.*, **36(8)**, 1107-1114.
Ching, R.P. et al. (2001). *Stapp Car Crash J.*, **45**, 329-336.
Danto, M.I. and Woo, S.L. (1993). *J. Orthop. Res.*, **11(1)**, 58-67.
Nuckley, D.J. et al. (2002a). *Stapp Car Crash J.*, **46,** 431-440.
Nuckley, D.J. et al. (2002b). *World Congress of Biomech IV, Calgary, Alberta*
Yingling, V.R. et al. (1997). *Clin. Biomech.*, **12(15)**, 301-305.

ACKNOWLEDGEMENTS

This research was funded by The National Center for Injury Prevention and Control, Centers for Disease Control.

PARAMETERS AFFECTING AXIAL STIFFNESS OF TIBIAL FIXATION IN AN ILIZAROV ANKLE DISTRACTOR

Jonathan K. Nielsen [2], Charles L. Saltzman [1,2], Thomas D. Brown [1,2]

[1] Department of Orthopaedics and Rehabilitation, University of Iowa, Iowa City, IA, USA
[2] Department of Biomedical Engineering, University of Iowa, Iowa City, IA, USA
E-mail: jonathan-nielsen@uiowa.edu Web: mnypt.obrl.uiowa.edu/OBL_Lab_Website

INTRODUCTION

For end-stage osteoarthritis patients, ankle distraction to permit partial regeneration of the articular surface is an attractive treatment alternative to arthrodesis and arthroplasty (van Roermund 2002). Although many of the mechanisms influencing the efficacy of distraction treatment are not well understood, it is known that joints experiencing even slight articular contact are exposed to stress levels an order of magnitude greater than those seen in ankles in which distraction is maintained.

In ongoing clinical study of this intriguing new treatment, it is desirable to ensure that the distracted articular surfaces (5 mm separation intraoperatively) do not make contact during weight bearing. Therefore, a configuration-specific finite element model of an Ilizarov ankle fixator was developed to identify frame configurations adequate for that purpose.

Figure 1: Ilizarov ankle fixator.

METHODS

The finite element model was constructed primarily using beam elements, which allowed extremely fast solution times of less than 15 seconds, due to small problem size (157 elements in baseline configuration).

Baseline model geometry was based on a typical fixator construct (Figure 2A). Configuration-specific model geometry was entered using a MATLAB-based graphical user interface that allowed specification of thirteen parameters, such as half-pin position and ring spacing. The interface program created an input file for the model, submitted it for analysis in ABAQUS finite element code, monitored the progress of the analysis job, and output the corresponding tibial displacement relative to the talus (Figure 2B).

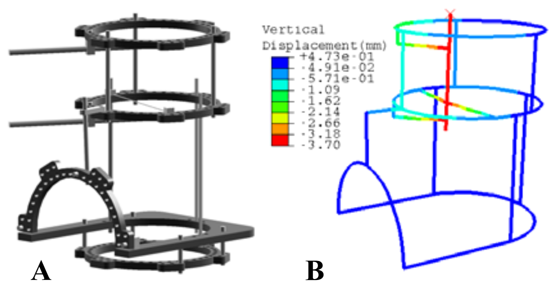

Figure 2: The baseline left ankle fixator configuration (A) and corresponding FE model vertical displacement output (B).

RESULTS AND DISCUSSION

The dominant factors influencing tibial displacement were those relating to the stiffness of the half-pins fixed to the antero-medial segment of the tibial rings. Reducing pin length by mounting the tibia 25 mm more anteriorly or medially reduced vertical displacement by 31% and 24%, respectively, compared to the baseline configuration's displacement of 3.67 mm. Increasing the half-pin diameter from 6 mm to 7 mm resulted in a 21% decrease in displacement, while reducing the diameter to 4 mm increased displacement by 84%. The tibial displacement was also increased 3% by angling the pins 10˚ downward, but was reduced 2% by angling them upward. In keeping with the goal of reducing their length, placing the pins on the tibial rings at the nearest circumferential location to the bone minimized displacement (Figure 3).

Pin	Displacement
2	4.03 mm
3	3.86 mm
4	3.71 mm
5	3.62 mm
6	3.67 mm
7	3.72 mm
8	3.77 mm
9	3.84 mm
10	3.94 mm
11	4.07 mm

A

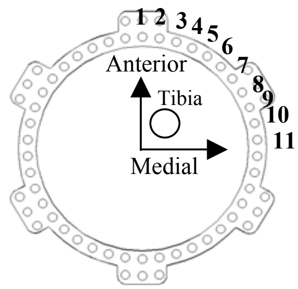

B

Figure 3: The effect of half-pin circumferential position on tibial displacement (A). Pins labeled as in (B).

Selection and placement of the tibial rings also contributed to tibial displacement. Using larger diameter tibial rings (180 mm vs. 155 mm) and the same tibial mounting position increased vertical displacement of the bone by 56%. Replacing the aluminum rings in the model with available carbon fiber or stainless steel rings decreased displacement by 25%. Placing the tibial rings farther apart also reduced displacement: increasing the ring spacing from 10 cm to 13 cm resulted in a 2% decrease in displacement.

The superposition of non-vertical loads derived from force plate data did not strongly affect vertical tibial displacement: 30N loads in anterior, posterior, medial, and lateral directions each altered baseline fixator displacement by less than 2%.

The height of the half-pin mounting clamps affected the tibial displacement, as well. For each pin-mounting hole above the hole nearest to the tibial ring, displacement increased by 20% of the baseline value.

As anticipated, adding a transfixion wire to the proximal ring, or extra half-pins on either tibial ring, decreased the displacement of the tibia according to the number and location of the additions. Additional pins were most effective when mounted in the same clamp as the existing pin. While the distal wire was most effective when nearly parallel with the half-pins, the converse was true for the (additional) proximal wire.

SUMMARY

The development of a very fast-running finite element model provided a tool for identifying factors contributing to fixation rigidity. Tibial displacement was most effectively reduced by minimizing the length of the fixator half-pins, achieved by mounting the bone as close as possible to the pin clamping sites. Displacement was also limited by the addition of transfixion wires and half-pins to the system. The versatility and speed of this FE model and interface program invite their application intraoperatively for patient-specific determination of fixation rigidity in the contexts of distraction, fracture fixation, and limb lengthening.

REFERENCES

van Roermund P.M. et al. (2002). *Foot Ankle Clin.*, **7(3)**, 515-27.

ACKNOWLEDGEMENTS

Funded by NIH grant 5 P50 AR04893

COMPARISON OF DYNAMIC ENGINES FOR MUSCULOSKELETAL MODELING SOFTWARE MSMS

Peman T. Montazemi, Rahman Davoodi and Gerald E. Loeb

A. E. Mann Institute and Biomedical Engineering Department, University of Southern California
Los Angeles, CA 90089, USA
E-mail: montazem@usc.edu Web: http://ami.usc.edu/

INTRODUCTION

The dynamics of articulated mechanical or skeletal systems can be modeled by a set of differential-algebraic equations. For simple physical systems, it is easy to manually derive the closed form governing equations. But for more elaborate systems, this task becomes very difficult, even impossible. In that case, the intervention of an equation generator, called a "dynamic engine", is necessary.

Dynamic engines use different formulation methods such as Lagrange, Newton-Euler, Hamilton, Kane, and Featherstone. The newer Order-N formulations have also been developed that are more efficient. What is meant by Order-N is that the computational effort per temporal integration step increases as a linear function of the number of generalized coordinates. This feature is very useful for faster responses, especially when the number of segments in a system is >10. We are developing a new musculoskeletal modeling software (MSMS) [Davoodi et al. – 2004] that needs a dynamic engine to automatically derive the equations of motion for the skeletal system. Here, we report on a comparison study to select the appropriate dynamic engines for inclusion in MSMS software. The main criteria for selection were accuracy and speed but other general criteria such as ease of integration with MSMS software were also considered.

METHODS

The comparison is based on accuracy/precision, speed of execution and a number of other general features such as the capability to model closed-chain systems, the dynamic formulation method and cost. Closed chain is an option that some dynamic engines offer in order to consider not only tree-structure systems but also closed chain or loop systems such as occurs when a subject is standing on two feet. In the selected dynamic engines (Table 1)[1], only Robotics Toolbox [Corke – 2000] does not offer this option. For the speed of execution parameter, two distinct groups were considered: the "C/C++ based" dynamic engines (Autolev [Reckdahl and Mitiguy – 1996], Dynamechs [McMillan et al. – 1995] and SD/Fast [Hollars et al. – 1994]), and the "Matlab based" dynamic engines (Robotics Toolbox and SimMechanics [Wood and Kennedy – 2003]). Obviously the attainable speed will depend on both the efficiency of the algorithm itself and the speed of execution of the language in which it is written. For all simulations, no external force besides gravity has been added. The following models were implemented for each dynamic engine:

1) A single pendulum is modeled because its closed-form equation of motion is known. This model will test the accuracy/precision of all engines.
2) A four-bar mechanism, for testing the capability of the dynamic engines in simulating closed chain systems. Besides "Robotic Toolbox", all other dynamic engines included.
3) A five-bar pendulum for measuring the speed

[1] This selection was based on a search among all applicable dynamic engines available on the market/internet. In some cases, only free (limited) versions were considered.

of execution of each dynamic engine. This last mechanical system has a high order of complexity and combined with a small time step can induce a measurable execution time. The speed of execution values were measured 10 times using a stopwatch. The average of these values is presented in this study.

RESULTS AND DISCUSSION

The accuracy test confirmed that all tested dynamic engines are equivalent within 0.01% of error. The results of the accuracy and speed benchmarks are summarized in Table 1 on a one-to-ten based scale. Dynamechs is a free collection of C/C++ libraries that are easier to integrate with MSMS but it is a work in progress that needs further improvements. In particular, it had some computational instability that was sensitive to mass properties of the system. Autolev was revealed to be the fastest dynamic engine in the speed benchmark. The main disadvantage is that a specific Autolev code has to be generated every time that a mechanism needs to be assembled. This feature makes Autolev very difficult to integrate with MSMS or other modeling software. If this step could be automated, it would save the user a considerable amount of time in pre- and post-processing. SD-Fast is fast, easy to integrate with MSMS, and has many additional utilities and analysis. Further, its use in other modeling software has shown that it is a robust dynamic engine. Robotics Toolbox for Matlab does not support closed-loop systems that occur very often in musculoskeletal systems.
By contrast, SimMechanics supports both forward and inverse dynamics and is a toolbox that is specifically designed to work with Simulink numerical integrators. Therefore, it is better suited for simulations in Simulink environment.

SUMMARY

In this study we compared several dynamic engines based mostly on accuracy/precision, speed of execution, closed loop capabilities and cost. Three simple physical models were implemented in each software in order to compare them. Considering all the important criteria, we conclude that the most suitable software for inclusion in MSMS are SD-Fast for simulation in C and SimMechanics for simulations in Simulink. Dynamechs on the other hand is a free dynamic engine that could be used in place of expensive SD-Fast but it requires further development.

REFERENCES

Corke P.I., "*Robotics Toolbox for Matlab Release 6*" Queensland Center for Advanced Technologies, Copyright © 2000 QCAT.
Davoodi, R. et al.(2004). "*Clinician-friendly software for biomechanical modeling and control of movement*" This proceedings.
Hollars M.G., Rosenthal D.E. and Sherman M.A., "*SD/Fast User's Manual Version B.2*" Symbolic Dynamics, Inc., 1994.
McMillan S., Orin D.E. and McGhee R.B., "*Underwater Robotic Vehicles: Design and Control*" (J. Yuh, ed.) TSI Press, pp. 73-98, 1995.
Reckdahl K.J. and Mitiguy P.C., "*Autolev 3.0 Tutorial*" Online Dynamics, Inc., 1996.
Wood G.D. and Kennedy D.C., "*Simulating Mechanical Systems in Simulink with SimMechanics*" The MathWorks, Inc., 2003.

ACKNOWLEDGEMENTS

Funded by A. E. Mann Institute for Biomedical Engineering, University of Southern California.

Table 1: Comparison of Dynamic Engines for MSMS Software (1 = poor; 10 = excellent)

Comparison	SD-Fast	Autolev	SimMechanics	Rob. Tool.	Dynamechs
Accuracy	10	10	10	10	9
Speed (seconds)	12.24 s	5.04 s	115.61 s	334.41 s	23.68 s

INFLUENCE OF TORSO ROTATION AND ARM COCKING STYLES ON ELBOW VARUS TORQUE IN BASEBALL PITCHING

Jeff T. Wight [1], Guy B. Grover [1], John W. Chow [1], James G. Richards [2], and Mark D. Tillman [1]

[1] Center for Exercise Science, University of Florida, Gainesville, FL, USA
[2] Dept. of Health, Nutrition, and Exercise Sciences, U. of Delaware, Newark, DE, USA
E-mail: jwight@ufl.edu

INTRODUCTION

Considerable variation in pelvis rotation patterns exists among baseball pitchers as pelvis orientation at stride foot contact (SFC) varies from 0-60º (Wight et al., 2004). The pitcher in Figure 1 is approaching a pelvis orientation of 90º (facing home plate). Pitchers who rotate the pelvis prior to SFC (pelvis orientation > 30º at SFC) have been previously classified as early rotators while pitchers who wait until SFC to initiate pelvis rotation (pelvis orientation < 30º at SFC) have been classified as late rotators (Wight et al., 2004). Additional kinematic factors were found to be associated with early and late rotators including arm cocking patterns and pitch delivery time. Kinetic patterns were also established as late rotators demonstrated significantly higher maximum loads on the throwing elbow and shoulder. Among the significant elbow loads was the maximum varus torque (59.0 N·m vs. 29.9 N·m). This torque was previously identified by Fleisig et al., (1995) as a critical instant associated with pitching injuries (Figure 1). However, the effect of overall pitching mechanics during the arm cocking phase on the maximum varus torque is not well understood. The purpose of this study was to identify distinguishable arm cocking and upper torso rotational characteristics that may relate to the differences in the maximum elbow varus torque experienced by early and late rotators.

Figure 1. The elbow maximum varus torque occurs while the arm is decelerating late in the cocking phase.

METHODS

This study represents a further analysis of a group of pitchers reported in Wight et al. (2004). Twenty pitchers (11 college, 9 high school) participated in the study. Subjects ranged in age from 16-22 years. Kinematic data were collected using an 11-camera Eagle Digital Motion Analysis system at 240 frames per second. Data from 3 maximum effort fastball strikes were averaged for each pitcher. The five pitchers that landed with the most closed pelvis orientation (5.6-15º) were designated as late rotators and the five pitchers that landed with the most open pelvis orientation were designated as the early rotators (37.8-56.3º). There were no significant differences in age, height, mass, or throwing velocity between the groups. Independent T-tests ($p<0.05$) were used to assess differences in arm cocking and upper torso characteristics between late and early rotators

RESULTS AND DISCUSSION

Late rotators rotated the upper torso and cocked the arm faster than the early rotators as demonstrated by the upper torso maximum axial rotational angular velocity (1001±122º/s vs. 804±89º/s [t_8=2.899, p=0.020]) and the shoulder maximum external rotation angular velocity (1428±128º/s vs. 1227±205º/s [t_8=1.844, p=0.102]), respectively.

The two groups used different upper torso rotational styles which may help to explain the differences in maximum angular velocities. Late rotators landed at SFC with a significantly (t_8=-5.169, p=0.001) more closed upper torso orientation (-23.1±9.6º) in comparison to early rotators (9.9±10.5º). Interestingly, late and early rotators achieved maximum upper torso velocities at similar upper torso orientations (42.9±11.5º vs. 40.9±10.4º [t_8=0.287, p=0.782]). This implies that late rotators rotated the upper torso over a greater range of motion (66.0º vs. 31.1º) while the stride foot was in contact with the ground during the cocking phase. This may explain the significantly greater maximum torso rotational angular velocity in late rotators.

The observed trends in arm cocking patterns may also help to explain differences in maximum varus torques between the groups. First, late rotators externally rotated the shoulder throughout a greater range of motion (123.2º vs. 48.6º) while the stride foot was in contact with the ground (defined as the time from stride foot contact to maximum varus torque). Second, late rotators had a higher maximum shoulder external rotation angular velocity as previously mentioned. Third, there was no significant difference (t_8=0.896, p=0.397) in the duration of the deceleration phase of arm cocking between late (0.066±0.014s) and early rotators (0.074±0.012s).

CONCLUSIONS

In conclusion, late rotators demonstrated higher upper torso and arm cocking angular velocities. This may be due to the fact that during the cocking phase both the torso and arm of late rotators covered a greater range of motion while the stride foot was in contact with the ground. In addition, the arm cocking deceleration phase was of similar length for the two groups. These trends associated with each pitching style may explain the significant difference in elbow maximum varus torque between early and late rotators.

REFERENCES

Fleisig, G. S. et al., (1995). *The American Journal of Sports Medicine*, **23**, 233-239.

Wight, J.T. et al., (2004). *Sports Biomechanics*, **3**(1), 67-83.

THE USE OF CENTER OF MASS ANALYSIS FOR GAIT ASSESSMENT IN CHILDREN WITH CEREBRAL PALSY

Bradford C. Bennett, Adam Wolovick, Tim Franklin, Paul E. Allaire, & Mark F. Abel
Motion Analysis and Motor Performance Laboratory, University of Virginia,
E-mail: bcb3a@virginia.edu

INTRODUCTION

There has been considerable interest in the movement of the center of mass (CoM) in walking as an important indicator or collective variable of energy costs in both normal and pathological gait. It has been suggested that healthy walkers have developed movement strategies, which limit the vertical excursion of the CoM to minimize energy consumption. This view is reinforced by the fact that in typical walking more than half of the total energy consumed is lift work on the CoM(Duff-Raffaele *et al.*, 1996). Inverted pendulum models of walking suggest another manner in which energy costs are minimized is through the passive transfer between potential (PE) and kinetic energy (KE) of the COM. The CoM mechanics of walking have not been studied in children with cerebral palsy (CP).

This study examined the work performed, energy recovery factor, and the phasic and magnitude relationships between KE and PE of the COM at preferred walking speed of children with CP and age matched controls.

METHODS

Kinematic data (3-D) were collected on 15 children with spastic diplegia CP and five able bodied children at their preferred walking speed. The average age of the children was 10.5 ± 3.6 years. COM position was determined from anthropometric measurements, estimates for segment masses(Jensen, 1986), and kinematic data. The COM vertical excursion was computed and normalized by the excursion of a compass gait model to account for both leg and step length variation. The KE per unit mass ($0.5 \bullet |v|^2$) was computed and compared to the potential energy (PE) per unit mass ($g \bullet h$). The continuous relative phase of the PE relative to the KE was computed with the cross-spectral density function(Duarte, 2002). The energy recovery factor*(R)* for the CoM was determined. *R*, the percentage of energy recovered via passive exchange between KE and PE is defined as(Winter, 1990):

$$R = 100 * \frac{(W_{ne} - W_{ext})}{W_{ne}}$$

where W_{ext} is the external work performed and W_{ne} is the work done assuming no energy exchanges.

Repeated measures ANOVA's were used to test for between group differences of the dependent measures.

RESULTS AND DISCUSSION

The children with CP performed more external work to walk than the controls (1.31 vs 0.54 J/kg/m, $p < 0.003$). The normalized vertical CoM excursion of children with CP was 70% greater ($p<0.03$) than that of the controls, while there was no difference in lateral excursion. The larger change in PE combined with the tendency of the patients to walk slower resulted in a larger ratio of PE to KE than the controls (2.15 vs. 1.3, $p < 0.003$). In addition, the relative phase of PE to KE was 165^{o} in the able bodied children (Figure 1a) vs. 144^{o}, ($p <0.04$) in the children with CP (Figure 1b). The closer the relative phase is to 180°, the better the passive energy transfer, which conserves energy. This is clearly seen in the energy recovery factor which encompasses the effects of both phasing and energy ratios. The children with CP recovered only 43% of the possible energy while the controls recovered 69% ($p < 0.001$).

CoM analysis also provided insight into walking strategies. Figure 1 shows where energy transfers can and cannot occur relative to the phases of walking. For an able-bodied child (Figure 1a) there is very little time during which energy transfer cannot occur because the relative phase of the two energies is nearly 180°. This can be contrasted with a plot of energies of a child with CP, Figure 1b. While there is much diversity in energy plots of children with CP, typically the peak in KE occurs before the minimum in PE. This results in a period of time where the CoM is "falling" and the walker is decelerating, meaning there can be no energy transfer. In this case the child flexes the knee of the front leg upon foot contact thus lowering the CoM while decelerating. Thus the poor energy use of children with CP is a combination of large vertical excursions of the CoM and poor timing of this movement.

The greater energy use by children with CP has been well documented, but its sources are much less well understood. The ratio of work on the CoM is quite similar to differences in metabolic cost found measuring O_2(Unnithan *et al.*, 1999), suggesting the importance of external work in the increase in metabolic cost. In addition, these results show that the increase in work is a result of both excessive vertical motion of the CoM and the timing of this motion.

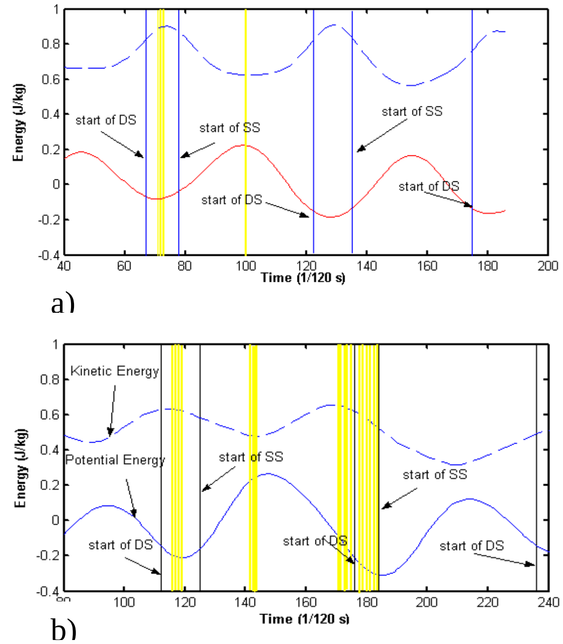

Figure 1 Plots of KE (dashed line) and PE (relative to mean CoM position) during walking. Shaded areas are times when energy transfer cannot occur. DS = Double Support, SS = Single Support a) Able-bodied child walking. b) Child with CP walking.

SUMMARY

The results of this study show that CoM analysis can provide insights into walking strategies of children with CP. This information is important as it can be used to understand the effects of interventions to improve walking in patients with CP. Current research is examining the effects of ankle foot orthoses on CoM mechanics. Future work will also quantify the relationships between CoM work and O_2 consumption.

REFERENCES

Duarte,M. (2002) *Matlab Software site* http://www.usp.br/eef/lob/md/software/.

Duff-Raffaele,M.et al. (1996) *Amer. J. of Physical Med. & Rehab.* **75,** 375-379.

Jensen,R.K. (1986) *J. of Biomechanics* **19,** 359-368.

Unnithan,V.B.et al. (1999) *Med. & Science in Sports & Exercise* **31,** 1703-1708.

Winter,D.A. (1990) *Biomechanics and motor control of human movement*. Wiley-Interscience, N.Y.

CERVICAL SPINE TOLERANCE TO DYNAMIC TENSILE LOADING

Eno M. Yliniemi [1], Joseph A. Pellettiere [2], Erica J. Doczy [3], David J. Nuckley [1], and Randal P. Ching [1]

[1] Applied Biomechanics Laboratory, Department of Mechanical Engineering, University of Washington, Seattle, WA, USA
[2] Biomechanics Branch, Air Force Research Laboratory, Wright-Patterson AFB, Dayton, OH, USA
[3] General Dynamics, Dayton, OH, USA
E-mail: enomaria@u.washington.edu Web: http://depts.washington.edu/uwabl

INTRODUCTION

Injury-causing tensile loading may occur in the cervical spine during events such as airbag deployments and pilot ejections. However, great disparity exists among neck injury tensile tolerance limits in the literature because of varied methods and specimen demographics. The objective of this study was to provide tensile neck injury tolerance values by testing a younger population using a dynamic loading rate.

METHODS

Nine un-embalmed adult (49 ± 9 yrs, 6M/3F) human cadaveric specimens (head and upper torso including skin and muscle) were exposed to axial tensile loads from a custom servohydraulic Material Testing System (MTS). The input displacement profile was a haversine curve with a linear slope of 500 mm/sec corresponding to 33,000 N/s in a Hybrid III neck (loading rate measured in manikin windblast tests).

Figure 1 shows a schematic of a specimen in the testing apparatus. A shoulder harness system assisted in securing the torso to an aluminum plate. In addition, thoracic vertebrae, T8-T11, were embedded in polymethylmethacrylate and affixed to the plate. Axial tensile loading was applied using a custom helmet system with a reinforced integrated chin-nape strap. Linear and rotational bearings in the helmet-ram bracket assured tension was the primary mode of loading. Six-axis load cells measured forces and moments. A high-speed video camera was used to capture the test at 1000 fps. Pins with video tracking markers were inserted into the skull and the spinous processes of C2-T1. Anthropometric measurements of the specimens were recorded prior to testing.

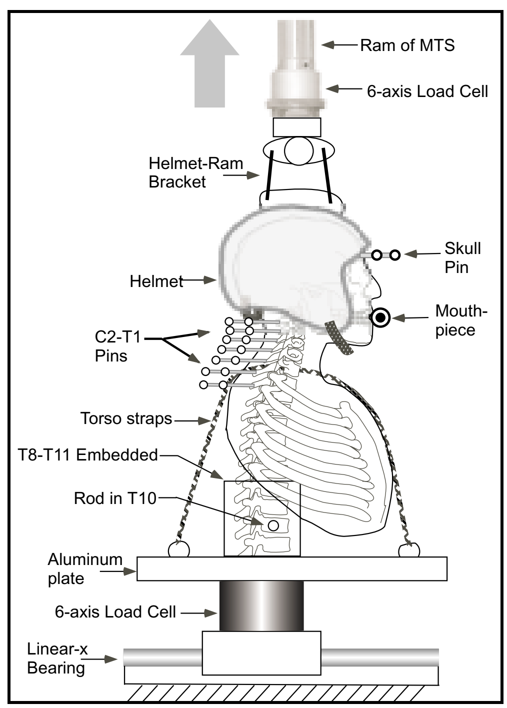

Figure 1: Schematic of dynamic tensile testing apparatus.

RESULTS AND DISCUSSION

Post-test radiographs and dissections were performed to determine location and severity of injury. All injuries occurred in either the upper (skull-C3) or lower (C5-T1) cervical spine and consisted of skull fractures, atlanto-occipital dislocations, dens fractures, atlanto-axial dislocations, and endplate fractures. The mean catastrophic tensile load for the nine specimens was approximately 3160 N ± 760 N.

A similar study by Yoganandan et al. (1996) tested three specimens in tension at 1 m/s (Schlick 2002) and reported a mean failure load of 3370 ± 839 N. Figure 2 shows cervical spine failure loads for the nine specimens in this study along with those found by Yoganandan et al. The figure also displays cervical tensile load limits proposed by the following entities: National Highway Traffic Safety Administration (NHTSA)—4500 N (Eppinger et al. 2000), Alliance of Automotive Manufacturers and Association of International Automobile Manufacturers (AAM-AIAM)—4170 N (Eppinger et al. 2000), and Naval Biodynamics Laboratory (NBDL)—2450 N (Weiss 1986). All specimens in this study failed at lower loads than two of the proposed limits.

The influence of anthropometry on neck dynamic tensile failure load was considered. Direct correlations between neck strength and height, weight, BMI, or neck circumference were not found. However, the circumference of the load-carrying neck structures (excluding skin/fat layer) appeared to correlate with failure load.

SUMMARY

Nine human cervical spines were tested in dynamic tension to determine their failure loads. The tensile failure load values were similar to those found in another experimental study, but all were below the maximum allowable values proposed by automotive safety standards.

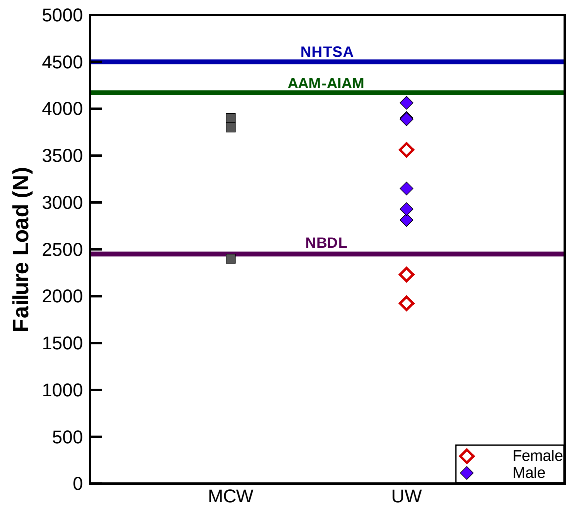

Figure 2: Dynamic tensile cervical failure loads measured in this study (UW, n=9) are shown with failure loads measured by Yoganandan et al. (MCW, n=3). The neck tensile force limits proposed by NHTSA, AAM-AIAM, and NBDL are also displayed

REFERENCES

Eppinger, R., et al. (2000). 208 Final Rule Docket: NHTSA-00-7013.

Schlick, M. (2002). Personal Communication. Medical College of Wisconsin, Milwaukee, WI.

Weiss, M.S.L., Leonard S. (1986). Guidelines for safe human experimental exposure to impact acceleration. NBDL-86R006.

Yoganandan, N., et al. (1996). Human head-neck biomechanics under axial tension. *Med Eng Phys* **18**(4): 289-94.

ACKNOWLEDGEMENTS

This research was funded by the Air Force Research Laboratories via a subcontract through General Dynamics.

EFFECTS OF FOOT ARCH IMPEDANCE ON NAVICULAR DROP AND CALCANEAL EVERSION DURING WALKING

Shing-Jye Chen and Li-Shan Chou

Motion Analysis Laboratory, Department of Exercise and Movement Science
University of Oregon, Eugene, OR, USA
E-mail: chou@uoregon.edu

INTRODUCTION

Excessive calcaneal eversion/ pronation have been linked to foot problems during walking and running. As calcaneal eversion occurs primarily through the midtarsal joints such as talonaviclar (Ouzounian, 1989), the midfoot navicular drop is found to positively correlate with calcaneal eversion during walking (Cornwall, 2002). The magnitude of navicular drop during standing has also been used as an indicator to predict excessive calcaneal eversion during walking (Muller, 1993).

A general goal for the use of foot orthoses or arch supports is to confine the foot in its neutral position and to reduce excessive rearfoot motion. However, contradictory findings have been reported. Increases in peak calcaneal eversion during mid-stance were observed while running with orthoses (Williams III, 2003). Furthermore, increases in eversion between calcaneus and talus were found in vitro while navicular height was impeded by an arch support with different loads (Kitaoka, 1997). Therefore, the purpose of this study was to examine and quantify the navicular arch height displacement and peak calcaneal eversion during level walking with and without arch height impedance.

METHODS

Three healthy male adults (mean age, 25.0 ± 3.2 years) were recruited and tested after being examined by a local podiatrist and ruled out any foot-related pathologies. Nine 8-mm superficial skin markers were placed on the left lower limb: 4 on tibia, 4 on rear foot, and one on navicular tubercle. Motion data were collected using a six-camera ExpertVision^{TM} system (Motion Analysis Corp., Santa Rosa, CA) while quiet stance and during level walking with barefoot (BF) and with arch supports. KinTrak software (Motion Analysis Corp., Santa Rosa, CA) was used to analyze the motion data.

Two pairs of customized arch supports, one deformable (AS1) and one rigid (AS2), were prescribed to each subject. Heel cups of both supports were removed to eliminate any effects on rearfoot motion. Subjects first walked with barefoot at a self-selected speed, and then followed by AS1 and AS2 conditions. Supports were directly attached to the plantar surface of the feet and secured by double sided adhesive tapes

The navicular arch height (AH) displacement was defined as a range of vertical AH change between the highest and lowest positions of the navicular marker (AH_{max} – AH_{min}) during the mid-stance period of walking trials of each testing condition (BF, AS1 & AS2). The mid-stance was defined as the period between initial ground contact of the first metatarsal head and initial heel off. The peak calcaneal eversion was defined as a maximum angle occurring on frontal plane between the tibia and calcaneus. Joint coordinate systems were applied to calculate the eversion angle between the quiet standing and dynamic walking trial (Grood & Suntay, 1983). One-way within-subjects ANOVA was conducted to detect effects of arch impedance on the range of AH displacement and peak calcaneal eversion.

RESULTS AND DISCUSSION

Neither average walking speeds nor mid-stance durations were significantly affected by the arch impedance (mean values: 1.38 ± 0.01 m/s and 42.9 ± 1.62 % of gait cycle, respectively).

Significant arch impedance effects on the range of the vertical AH displacement across subjects were found ($p < .02$, Fig 1) decreasing from the BF (2.98 ± 0.99 mm) to the AS1 (2.73 ± 0.85 mm), and to the AS2 (2.24 ± 0.71 mm) conditions. No significant arch impedance effects on the peak calcaneal eversion across subjects were detected ($p = .31$; Fig. 2). However, the peak eversion showed an increasing trend from the BF (1.93° ± 1.70°) to the AS1 (2.83° ± 1.19°), and to the AS2 (3.41° ± 1.40°) conditions.

Reductions in the range of vertical AH displacement with the use of arch supports demonstrated that the navicular drop was successfully impeded by the arch support. The tendency of increasing peak calcaneal eversion with impeded arch may imply compensation to the lack of the navicular drop in order to restore the arch height functions during barefoot walking.

SUMMARY

These preliminary findings suggested a greater calcaneal eversion might occur when the foot arch is impeded during the mid-stance of walking. As orthoses are often prescribed to correct excessive rearfoot motion, constraint on midfoot navicular drop needs to be considered.

REFERENCES

Cornwall, M.W. & McPoil, T.G. (1999). Foot & Ankle International, 20(8), 507-512.

Grood & Suntay (1983). Journal of Biomechanical Engineering, 105(2), 136-44.

Kitaoka, H. B. et al. (1997). Clinical Orthopaedics and Related Research, 341,250-6.

Kitaoka, H. B. et al. (1997). Archives of Physical Medicine Rehabilitation, 83, 876-9.

Muller, M.J. et al. (1993). Journal of the American Pediatric Medical Association, 83(4), 198-202.

Ouzounian, (1989). Foot & Ankle. 10(3), 140-6.

Williams III, D.S., et al. (2003). Medicine & Science in Sports & Exercise, 35(12): 2060- 68.

ACKNOWLEDGEMENTS

This work was supported by the University of Oregon and ISB Dissertation matching grant.

Fig 1. AH range (max- min)

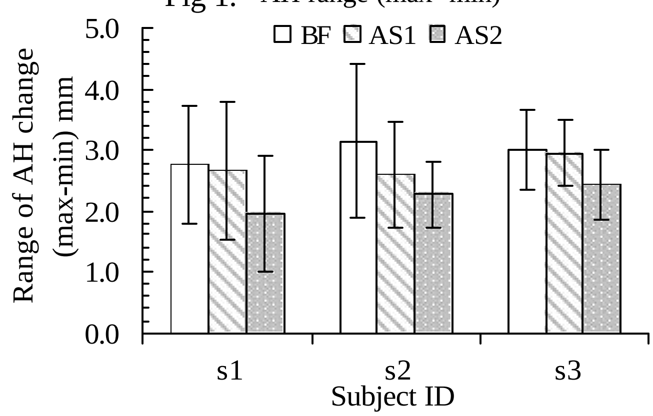

Fig 2. Peak calcaneal eversion

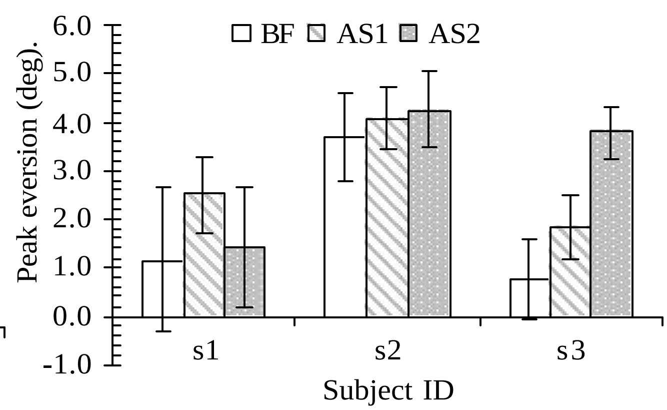

COMPUTATIONAL SIMULATION OF CORNEAL APPLANATION

T.-H. Kwon[1], D. A. Pecknold[1], J. Ghaboussi[1], S. Sayegh[2], and Y. M. Hashash[1]
[1] Dept. of Civil and Env. Engrg., Univ. of Illinois at Urbana-Champaign, IL 61801
[2] Medical Director, The EYE Center, Champaign, IL 61820
E-mail: pecknold@uiuc.edu Web: www.cee.uiuc.edu

INTRODUCTION

We have developed methods for realistic finite element modeling of the human cornea, including the effect of aqueous humor. In this paper we report on the use of this FE modeling method to simulate the measurement of intra-ocular pressure (IOP) via applanation tonometery.

Open-angle glaucoma arises from serious damage to the optic nerve and is strongly correlated with high IOP (Sommer 1989). Glaucoma usually has no early symptoms; by the time that loss of peripheral vision starts to become noticeable, irreversible damage to the optic nerve has already occurred. Since IOP measurement is used as the main screening mechanism for early detection of those at risk, it is evident that accurate measurement of IOP is of primary importance. The most widely used clinical method of measuring IOP is Goldmann applanation tonometry. However, there is a growing awareness that applanation tonometry measurements (IOPG) can differ from true intraocular pressure (IOPT) due to a number of different factors, including corneal bending resistance which is influenced by central cornea thickness (CCT) (Orssengo 1999).

MODELING METHODOLOGY

The (axisymmetric) aspheric surfaces of the cornea are described by the equation

$$x^2 + y^2 + (1+Q)z^2 - 2zR = 0, \qquad (1)$$

where the z axis points inward along the optic axis, and R is the radius of curvature of the corneal surface at the apex. The parameters used in this study are given in the following table (Liou 1997). Astigmatism was neglected.

Table 1. Conicoid parameters for cornea

Surface	Radius(R)	Asphericity(Q)
Anterior	7.77	-0.18
Posterior	6.40	-0.60

The cornea was modeled using 4 node axisymmetric solid finite elements. As shown in Figure 1, the boundary condition at the base of the finite element model of the cornea was assumed as fixed. It has been shown (Raymond 1992) that the applanating force is not significantly affected by the choice of boundary conditions. The (Goldmann) applanation tonometer was modeled by axisymmetric rigid elements with a diameter of 3.06 mm. Contact elements were used at the interface between tonometer and cornea. Representing the IOP as a constant pressure load on the interior surface of the cornea does not fully account for the behavior of the aqueous humor during applanation. Our studies have shown that the interaction of the aqueous humor and cornea, as well as outflow of the aqueous humor from the anterior chamber, may play an important role.

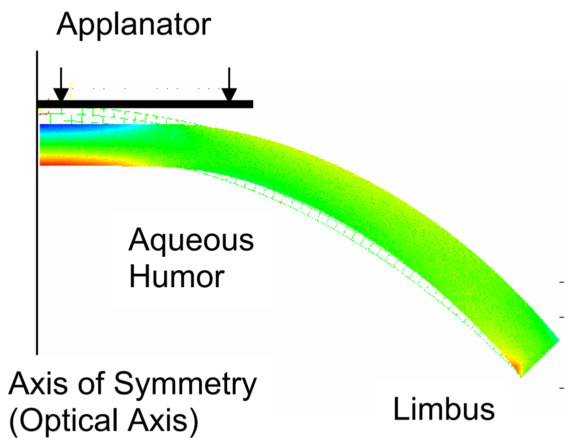

Figure 1: Axisymmetric finite element model for applanation tonometry analysis

Therefore, we have modeled the aqueous humor with a hydrostatic fluid element, allowing for time-dependent outflow during applanation. We have used a nonlinear transversely isotropic material model, based on Fung's (1979) exponential strain energy function, to define the mechanical behavior of the cornea, and implemented it via the user-defined subroutine UMAT in ABAQUS.

RESULTS AND DISCUSSION

Experimental data by Bryant (1996) was used in order to calibrate the nonlinear material model (Figure 2). They recorded the apical displacement of a cornea mounted in a testing frame during membrane inflation.

Figure 3 shows typical results of the simulation of applanation tonometry. The measured (IOPG) and true (IOPT) IOP values are plotted as a function of the central corneal thickness (CCT). It can be seen that the error in measured IOP (IOPG) increases as the corneal bending resistance increases with CCT. The IOP (initial value =15 mmHg) also increases slightly during applanation.

REFERENCES

Sommer, A (1989). *Am J Ophthalmol* **107,** 186-188.
Orssengo, GJ et al. (1999). *Bul Math Biology*, **61**, 551-572
Liou, H-L et al. (1997). *J Opt Soc Am*, **14**, 1684-1695.
Vito, RP et al. (1992). *Refractive & Corneal Surgery*, **8**, 146-151.
Fung, YC et al. (1979). *Am J Physiol*, **237**, H620-H631
Bryant, MR et al. (1996). *J Biomech Engrg*, **118**, 473- 481.

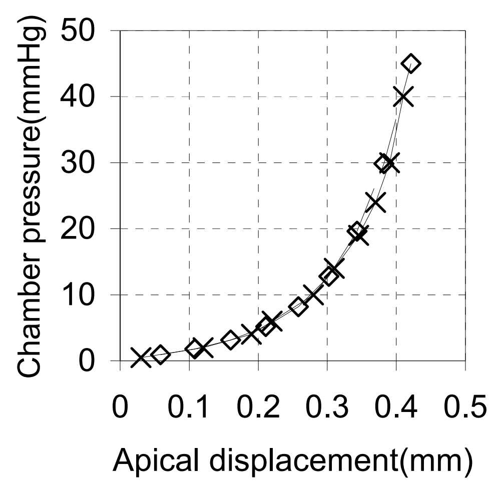

Figure 2: Material model calibration, ◊: FEA, ×: experimental data

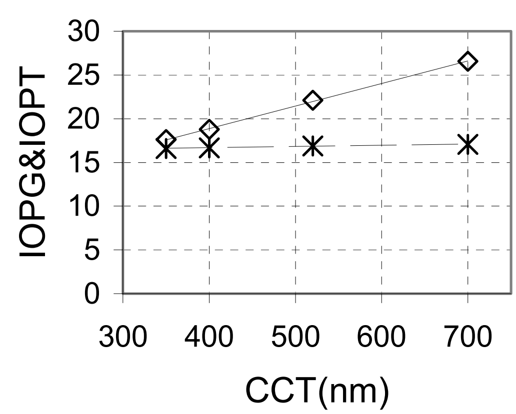

Figure 3: IOPG and IOPT versus CCT, Initial IOP = 15mmHg, ◊: IOPG, ×: IOPT

Evaluating Symmetry of the Swing Leg During Running with Velocity-Velocity Profiles

Ryan A. Jorden[1], Gary D. Heise[2], Kendall Mallory[3], and Dan Packard[3]

[1]Department of Kinesiology, Westmont College, Santa Barbara, CA 93108
[2] Sport and Exercise Science, [3] Physics, University of Northern Colorado, Greeley, CO 80639
E-mail: rjorden@westmont.edu Web: www.unco.edu/hhs

INTRODUCTION

Researchers who study running traditionally examine sagittal plane motion, and often assume that the kinematics of gait are symmetrical. Those who do study nonsagittal motion of the leg and foot often examine the stance phase of running. Studies which focus on rearfoot motion usually attempt to identify connections between frontal plane mechanics with a person's predisposition to leg and foot injuries (e.g., Williams et al., 2001). Focusing on the stance phase of running makes sense because of the high forces encountered by the single support leg; however, an analysis of lower extremity motion outside the sagittal plane during swing phase is often not addressed.

The latter part of swing has been identified as a crucial phase of locomotion with respect to injury. Radin and colleagues (1991) went so far as to say that uncoordinated motion prior to foot contact ("microklutziness") may predispose persons to knee pain and ultimately, osteoarthritis. This suggests the motion of the leg during swing may contribute to poor mechanics during stance.

In a previous study, we identified asymmetrical runners from a cursory examination of mediolateral (ML) swing leg motion (Heise et al., 2003). In the present investigation, we more closely scrutinized the ML motion of the asymmetrical runners and matched controls. Specifically, we examined the following in both groups of runners: repeatability of swing leg kinematics; and a correlation analysis of symmetry using ML velocity of the lower extremity in combination with antero-posterior (AP) velocity.

METHODS

Previously, we examined eighteen runners (10 men and 8 women) for symmetrical swing leg kinematics during treadmill running. During one testing session, participants ran on two different treadmills at 3.5 m/s (9 min/mile pace). Treadmills were located next to each other, but faced opposite directions (see Fig 1). Two 60-Hz video cameras recorded the motion of the right leg on one treadmill and then after a brief rest, the motion of the left leg on the adjacent treadmill. Direct linear transformation (DLT) was used to calibrate a 1.25 m × 0.80 m × 0.90 m volume, which included both treadmills. A 13-point calibration object was used resulting in an overall error of 0.22%.

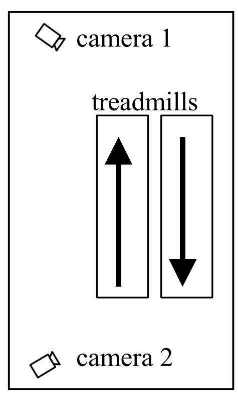

Fig 1. Experimental set-up showing two cameras and treadmills

From our original sample, five subjects (2 women and 3 men) were categorized as having bilaterally asymmetrical swing characteristics. These runners were matched (based on gender, body weight and running experience) with subjects classified as having bilaterally symmetrical swing patterns for further comparison. Consistency across five consecutive strides for each of the ten subjects was examined in the context of swing phase velocity-velocity plots. Correlations were performed to assess repeatability and symmetry.

RESULTS AND DISCUSSION

The repeatability for the motion of both legs in each group was high. The right vs. left correlation was significantly higher in the symmetrical group (see Table 1).

	symmetrical	asymmetrical
right leg	.853	.857
left leg	.808	.778
right vs. left *	.771	.404

Table 1. Correlation coefficient means.
* ($p < 0.05$) between groups

The symmetrically classified runners were shown to have reproducibly similar velocity-velocity swing patterns (see Fig 2a), whereas the asymmetrically classified runners showed bilateral differences (see Fig 2b). The velocity plots of the symmetrical subjects displayed a (typical) horseshoe-shaped pattern. This result is expected since the movement of the swing leg elicits a motion similar to that of a pendulum completing a full ML cycle (out and back) and a half pendular cycle in the AP direction (forward only).

Similar to the findings of Radin et al. (1991), no gross, qualitative, or discernible differences were noted by a trained eye, however, stark kinematic differences were noted as outlined above. Future work will include the quantitative assessment of the bilateral deviation from a mathematical model to enhance classification of mediolateral swing asymmetries in runners.

In conclusion, our analysis was successful in classifying swing leg symmetry and we found that all runners regardless of symmetry displayed high cycle repeatability.

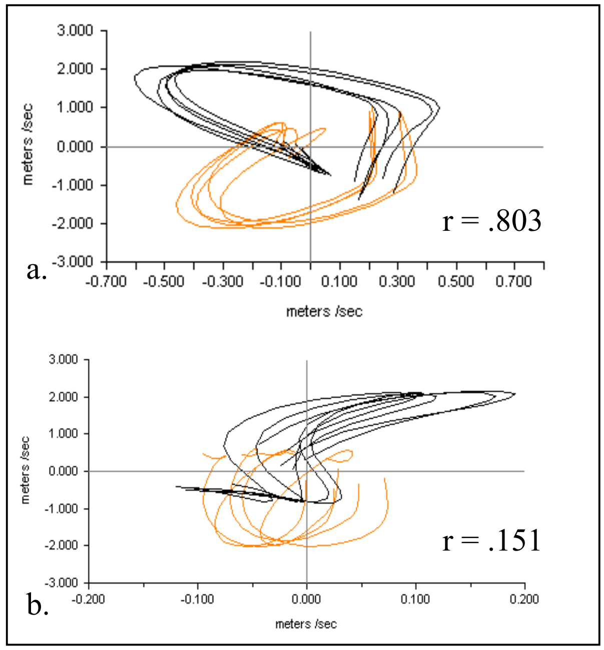

Fig 2 a, b. Knee AP velocity (vertical) vs. ML velocity (horizontal) during swing for a representative symmetrical runner (a) and asymmetrical runner (b). Five consecutive strides (for left • and right • legs) are shown.

REFERENCES

Abdel-Aziz, Y.I. & Karara, H.M. *Proc of the ASP/UI Symposium on Close-Range Photogrammetry*, Amer Soc Photogr, pp. 1-18, 1971.

Fredericson, M. et al. *Clin J Sport Med*, 10, 169-175, 2000.

Heise, G.D. et al. *Proceedings of ASB,* Abstract, 2003.

Radin, E.L. et al. *J of Ortho Res*, 9, 398-405, 1991.

Williams, D. S., et al. *J of App Biomech*, 17, 153-163, 2001.

BIOMECHANICAL PATTERNS OF THE ANKLE IN GRAND-PLIÉ MOVEMENT

Cheng-Feng Lin[1], Hong-Wen Wu[2], Fong-Chin Su[3]
[1]Center for Human Movement Science, Division of Physical Therapy, School of Medicine, University of North Carolina at Chapel Hill, Chapel Hill, USA
[2]School of Physical Therapy, China Medical University, Taichung, TAIWAN
[3]Institute of Biomedical Engineering, National Cheng Kung University, Tainan, TAIWAN
E-mail: feng1368@email.unc.edu

INTRODUCTION

The most common occurred injury in ballet dancers was as a result of abnormal force distribution at the joints for compensating insufficient flexibility and strength at the other joints (Schon and Weinfeld 1996). These deficient joint ranges of motion (ROM) and asymmetric force distribution in lower extremities will affect the normal pattern of ankles and their performance. Few biomechanical studies of the population had been conducted till now to get basic understanding of ankle contributions in ballet movements. Therefore, the major objective of this study was to investigate the ankle biomechanics of ballet dancers in one fundamental ballet movement : grand-plié, which is with knee maximal flexion, heel raising from floor, entire weight is borne on the metatarsal head regions and toes (Clouser 1994, Trepman et al. 1998). By examining the joint motion and moment of the ankle, the normal ankle biomechanics of grand-plié can be better understood.

MATERIALS AND METHODS

Thirteen ballet dancers (19.15±1.9 y/o, 159.69±5.92 cm, 49.15±6.39 kg) with 11.3±3.9 years of dance training were recruited in this study. All of them are right side dominant. Five trials with pointé shoes were collected and three trials with highly consistent patterns were selected to analyze. The HIRE Motion Analysis system (Motion Analysis Corp., CA) was used to collect the trajectories of the landmarks at 60 Hz and two force platforms (Kistler Instrument Co, Switzerland) were used for measurement of ground reaction of each foot at 1000 Hz, respectively. Based on the inverse dynamics method, the three-dimensional ankle joint moments were calculated by the custom code. This study only focused on plantarflexion-dorsiflexion plane due to the limitation of whole foot as one segment. The analytic phase, transient phase, was defined from the instant the dancer began action to the instant the sacral marker moved to the lowest point with maximum knee flexion in the movement. Figure 1 was the end gesture of the transient phase.

RESULTS AND DISCUSSIONS

Figure 2a shows the basic biomechanical excursion patterns in grand-plié. The ankle dorsiflexion angles were -47.8±7.3° and -49.0±7.0° at right and left, respectively. The peak ankle plantarflexor-dorsiflexor moments of the dominant (right) and non-dominant (left) side were 0.65±0.22 Nm/BW and 0.69±0.13 Nm/BW, respectively. There was no significant difference between right and left sides (Fig. 2b). Three moment patterns were discovered at the non-dominant ankle. Less variation of the moment pattern at the dominant ankle might indicate that the dominant side had better control during the movement than non-dominant side (Fig. 2c). The excursion of moment patterns in Figure 2c also demonstrated the difference at initial value between right and left sides. As we knew, the grand-plié was a symmetric movement but some differences were found in this study, including the moment excursion patterns and initial weight-bearing values. These meant the dominant and non-dominant sides played different roles throughout the movement (Koceja et al. 1991) and different strategies were recruited by these ballet dancers. In addition, the coordination of R/L could not be decided only by ankle ROM demanding. The moment exertion patterns should be considered. Meanwhile, the fundamental biomechanical movement excursion patterns in grand-plié were also investigated.

REFERENCES

Schon L.C. Weinfeld S.B. (1996) Lower extremity musculoskeletal problems in dancers. *Current Opinion in Rheumatology*, **(8):**130-142.

Clouser J. (1994) The grand-plié: some physiological and ethical consideration. *Impulse*, **2:**83-86.

Trepman E. et al (1998) Electromyographic analysis of grand-plié in ballet and modern dancers. *Med Sci & Sports Exerc*, **30(12):**1708-1720.

Koceja D.M. et al (1991) Organization of segmental reflexes in trained dancers. *Int J Sports Med*, **(12):**285-9.

Figure 1: End posture of transient phase in grand-plié.

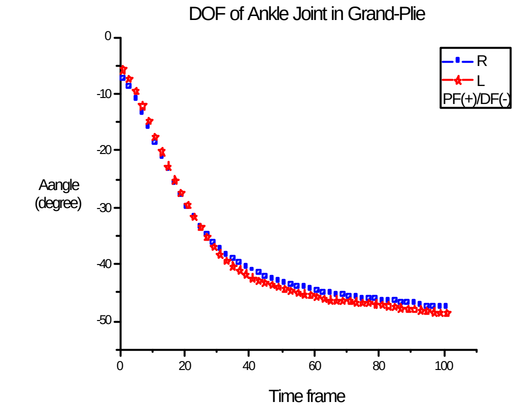

(a)

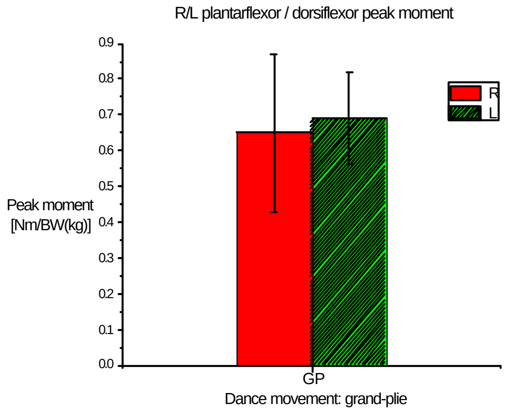

(b)

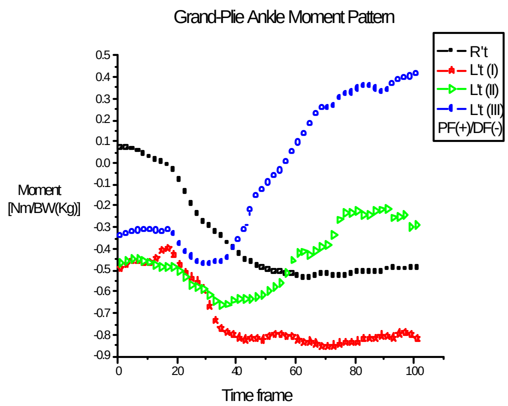

(c)

Figure 2: Ankle movement in grand-plié: (a) excursion (b) peak moment comparison at R/L side (p-value: 0.47), (c) plantarflexor/dorsiflexor moment. (Significant difference level, $p<0.05$).

AMPLITUDES OF MUSCLE ACTIVITY DURING EARLY PRACTICE TRIALS COMPARED WITH THOSE OF A WELL-LEARNED SKILL

Gary D. Heise and Cory Christiansen

School of Sport and Exercise Science, University of Northern Colorado, Greeley, CO, USA
E-mail: gary.heise@unco.edu Web: www.unco.edu/hhs

INTRODUCTION

Traditional skill acquisition research has focused on the outcome or goal of a movement as the primary dependent variable. Conclusions from these studies have implications for skill training concerns (e.g., training schedules, types of feedback), however, little is added to our understanding of how the learner acquires control for a certain skill.

From a dynamical systems perspective, a learner will acquire the most economical coordination strategy available, which may include exploiting reactive forces present in the link-segment system (Bernstein, 1967). Within this context, Vereijken et al. (1992) studied a multijoint task and found significant improvements in task outcomes and movement dynamics by the 20th practice trial. Changes in muscle activation during early stages of practice, however, are not as well known (Young & Marteniuk, 1995).

Therefore, the purpose of this study was to examine the changes in muscle activity during the first day of practice of a multi-joint, "ski-simulation" task. Specifically, we examined the ratios of EMG amplitudes between knee extension and flexion.

METHODS

Five healthy men who were unfamiliar with the ski simulator volunteered as subjects (mean body mass = 78.5 $\pm$ 13.2 kg; mean body height = 179 $\pm$ 6 cm). Each subject attended four test sessions in which 25 trials were performed during each session. A trial consisted of a 30-s attempt to go "as fast and as far as possible" on a ski simulator (see Fig 1). Subjects applied force in a lateral direction against the movable platform which sat on curved rails. Once the platform reached the most lateral position, it sprang back towards the center because of elastic bands attached to it.

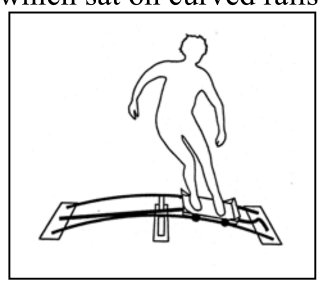

Figure 1: Ski simulator apparatus (from Vereijken et al., 1992)

Prior to testing on days 1 and 4, and after appropriate skin preparation, surface EMG electrodes were positioned over the bellies of the following muscles on the right lower extremity: rectus femoris (RF); vastus lateralis (VL); medial hamstrings (MH = semimembranosus + semitendinosus); the long head of biceps femoris (BF); and the lateral head of gastrocnemius (LG). An electrogoniometer was placed over the right knee to monitor knee joint angle and a photocell was used to produce an event signal whenever the platform crossed top dead center (TDC). Data were sampled at 780 Hz for a duration of 3 s.

Variables that assessed task performance were lateral platform displacement and cycle frequency. Platform displacement was measured with a video-based motion analysis system (Peak Performance, Inc.). Cycle frequency was determined from a photocell signal with a cycle defined as the time it took a subject to go from TDC, to the far right, and back to TDC. EMG signals were full-wave rectified and integrated (IEMG) over two durations within a cycle: knee extension (KE); knee flexion (KF). A ratio was then calculated:

$$\text{IEMG RATIO} = \frac{\text{IEMG}_{\text{KE}}}{\text{IEMG}_{\text{KF}}}$$

Four blocks of trials from the first day of practice were compared to one block taken from the end of the fourth day of practice.

RESULTS AND DISCUSSION

Task performance improved as represented by an increase in lateral platform displacement (60.2 cm early in practice to 82.0 cm late in practice) and an increase in cycle frequency (1.7 Hz to 2.1 Hz).

During the first day of practice, IEMG RATIOs remained near 1.0, with slight changes occurring in Blocks 3 and 4 (see Fig. 2). With the exception of MH, the relative differences in IEMG RATIOs between the muscles began to display a profile consistent with the well-learned skill (day 4), albeit at much lower values.

The IEMG RATIOs of the two knee extensors, RF and VL, increased dramatically from day 1 to day 4 because of the decreased activity in these muscles during knee flexion. The IEMG RATIO for BF increased for the same reason. These amplitude results underscore our earlier temporal-based findings (Heise et al., 1996). In contrast, the ratio for LG increased because of an increase in its activity during knee extension.

In conclusion, extension-flexion EMG amplitudes early in practice did not reach levels shown by subjects late in practice.

REFERENCES

Bernstein, N. (1967). *The Co-ordination and Regulation of Movements*, Pergamon: Oxford.

Heise, G.D. et al. (1996). *Proceedings of ASB,* 63-64.

Vereijken, B. et al. (1992). *J. Motor Behavior,* **24**, 133-142.

Young, R.P. & Marteniuk, R.G. (1995). *J. Biomech,* **28**, 701-713.

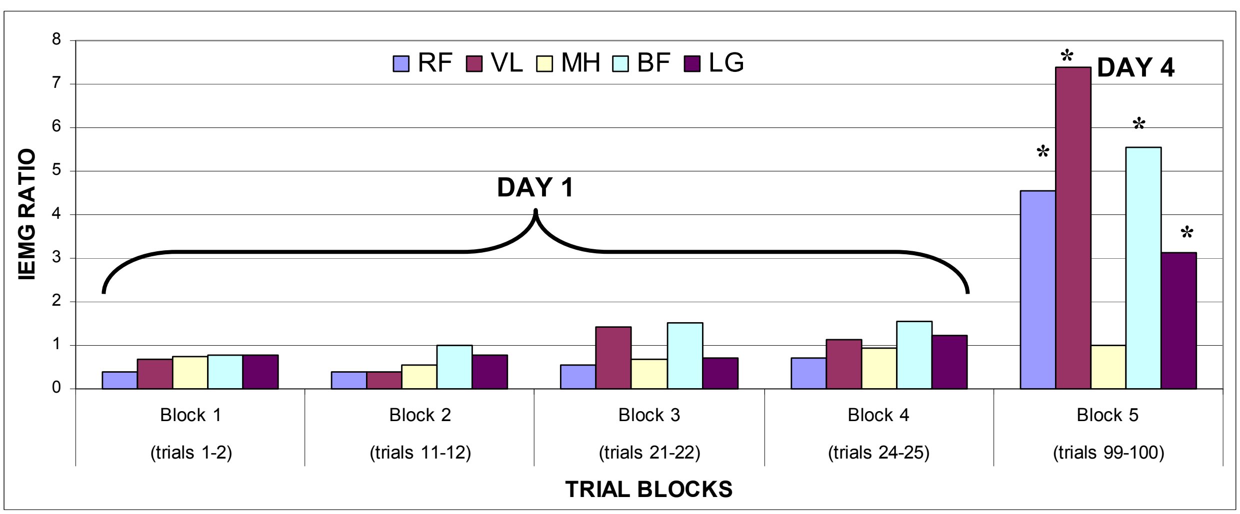

Figure 2: IEMG RATIOs averaged across subjects for five blocks of practice.
* significantly higher than Day 1, p < .05

EMOTION RECOGNITION FROM BODY MOVEMENT KINEMATICS

M. Melissa Gross[1], Geoffrey E. Gerstner[2], Daniel E. Koditschek[3], Barbara L. Fredrickson[4] and Elizabeth A. Crane[1]

[1]Department of Movement Science, [2]Department of Biologic and Materials Science, [3]Department of Electrical Engineering and Computer Science, and [4]Department of Psychology
University of Michigan, Ann Arbor, MI, USA
E-mail: mgross@umich.edu Web: www.kines.umich.edu/facstaff/gross.htm

INTRODUCTION

Emotions can be recognized from body movements presented to observers as point light displays, either from videos or from simulations derived from motion capture data (Montepare 1987; Pollick 2001; Troje 2002). The specific aspects of the movements responsible for emotion recognition are not known because either the kinematics have not been analyzed or the emotional content has not been validated in previous studies.

The purpose of this study was to quantify the emotion-specific kinematics of movements in which specific emotions were elicited in actors and were recognized by observers. The emotion-specific kinematics were determined by first reducing the complexity of the high-dimensional dataset using principal components analysis and then using discriminant analysis to determine the recognition rate of emotions based on the kinematic data.

METHODS

Six female college students (mean age = 21 yrs) with community and university acting experience participated in the study after giving consent. Motion data were captured at 120 Hz from 35 markers placed on the actors that demarcated head, neck, shoulder, arm, forearm, upper spine, pelvis, thigh and leg segments. Six target emotions (anger, anxious, content, joy, pride, sad) and neutral emotion were elicited using an autobiographical memories paradigm. Actors knocked on a vertical surface after recalling each of the emotion memories. Actors performed three trials for each emotion and their self-selected best trial was included in the analysis. Following each set of three trials the actors rated the intensity of their feelings for the target emotions and ten other emotions using a Likert scale ranging from 1 (“not at all”) to 5 (“extremely”).

Joint angle data were calculated for head tilt and rotation, neck flexion, shoulder abduction and flexion, elbow flexion, knee flexion, ankle dorsiflexion and spine lateral flexion, rotation and flexion. The knocking epoch began with the onset of shoulder flexion and ended when the arm returned to the side. Principal components analysis was used to reduce the complexity of the epoch data. Discriminant analysis was used to classify the principal components by emotion.

To validate the emotion content of the movements, videos of the actors’ knocks with each emotion were randomized and assembled into three different composite video sequences. The composite videos were shown to male (n=14) and female (n=21) college students who rated the intensity of 16 emotions in each knocking trial using the same questionnaire as the actor self-reports. A mixed model ANOVA was used to detect significant differences in intensity among actors, observers, and sequences.

RESULTS AND DISCUSSION

Emotion elicitation. The self-report data indicated that the actors experienced the target emotions. At least half of the actors reported intensities of “quite a bit” or “extremely” for all emotions. Mean intensity scores for anger, anxious, content, joy, proud and sad were 3.7, 4.2, 4.2, 4,7, 4.8 and 4.0, respectively.

Validation of emotion recognition. Observer recognition of emotion depended on actor and emotion. Two of the six actors had consistently low intensity scores; data from these actors were not included in the subsequent analyses. Recognition rates for the target emotions for the remaining actors, based on a mean intensity score of “moderately” or better, were 93.6, 77.9, 39.3, 52.9, 65.7 and 52.9% for anger, anxious, content, joy, pride and sad, respectively. Sequence and observer effects did not affect emotion recognition.

Kinematics-based emotion classification. The first 3 principal components captured more than 95% of the variability in the kinematic data for each actor and emotion. Joint angles reconstructed from the first 3 principal components were very similar to the original joint data (Fig. 1).

The emotion recognition rate was 76.5% using discriminant analysis with the principal components data. The joint angles most important for the correct classification of emotion were head rotation, head tilt and ankle angle. The recognition rate dropped considerably if the two actors with poor validation scores were included in the analysis.

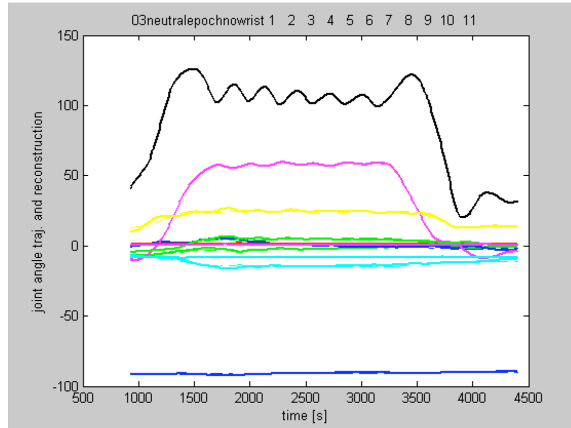

Figure. 1: Original (solid lines) and reconstructed (dashed line) joint angles during knocking with neutral emotion for one actor.

SUMMARY

Target emotions were elicited in the actors, recognized by observers, and classified with the kinematic data. The validation and discriminant analyses agreed on which actors communicated the target emotions and which actors did not. The results suggest that recognition of emotion depended on subtle postural movements rather than the relatively large movements of the arm during knocking.

REFERENCES

Montepare J. M., et al. (1987) *J. Nonverbal Behavior*, **11**, 33-42.

Pollick, F.E., et al. (2001). *Cognition*, **82**, B51-B61.

Troje, N.E. (2002). *J. Vision*, **2**, 371-387.

ACKNOWLEDGEMENTS

The authors thank Zaineb Bohra, Daniel Hoffman, Shannon Kruger, Jonathon Priebe and Brady West for their assistance with the project. Supported by a grant from Rackham Graduate School, University of Michigan.

QUIET STANDING AND STABILITY LIMITS: EFFECT OF WORK EXPERIENCE AND AGE

Steven R. Torgerud[1], Shirley Rietdyk[1], James D. McGlothlin[2] and Mark J. Knezovich[2]

[1]Biomechanics Laboratory, [2]School of Health Sciences, Purdue University, IN, USA
E-mail: srietdyk@purdue.edu

INTRODUCTION

Occupational falls threaten the health and well-being of workers and result in decreased productivity for employers (Hsiao et al. 1997). Each year, approximately 100 falls from roofs are fatal (Suruda et al. 1995).

Roofers are exposed to a unique visual environment (few visual references and a dynamic background) and must adapt to various slopes and weather conditions. A fall from a roof has much greater consequences than on ground level. Therefore, roofers may have enhanced balance control. However, as a person ages, decrements in balance control are observed (Perrin et al. 1997).

The purpose of this study was to examine quiet standing and stability limits of older and younger roofers and non-roofers to determine if roofers exhibit improved balance, and if improved balance was maintained with age.

METHODS

Forty volunteer subjects participated in this study with their informed consent (Table 1). They stood on a forceplate (AMTI) using a self-selected stance width.

Quiet standing with the eyes open and the eyes closed was documented with root mean square (RMS) and mean power frequency (MPF).

Stability limits were examined by instructing the subjects to lean as far as they could in both the anterior posterior (AP) and medial lateral (ML) directions without removing either foot from the forceplate. COP displacement was expressed in cm and as a percentage of foot length and stance width.

RESULTS AND DISCUSSION

During quiet standing, roofers' displacement was similar to non-roofers, but they moved at a higher frequency (Figure 1). Age resulted in an increase in displacement but

Table 1: Summary of participant characteristics (mean ± std).

Group	N	age (yrs)	height (cm)	mass (kg)	roofing experience (yrs)
Young Roofers	10	26.3 ±3.1	175.4 ± 17.9	74.5 ± 6.8	6.3 ± 4.6
Young non-Roofers	10	26.2 ± 3.7	179.5 ±5.5	80.7 ± 15.28	N/A
Older Roofers	10	50.6 ± 4.2	176.0 ± 8.0	83.7 ± 10.2	17.6 ± 9.1
Older non-Roofers	10	55.1 ± 4.5	179.4 ± 7.5	97.3 ± 22.7	N/A

no change in frequency (AP RMS: 3.8 ± 1.4 mm vs. 4.9 ± 1.8 mm, $p < 0.0001$ and ML RMS: 1.6 ± 0.87 mm vs. 1.9 ± 0.84 mm, $p = 0.002$); the age effect was not dependent on work experience (age x work $p > 0.0795$).

Closing the eyes increased the magnitude of COP displacement in both directions and increased the frequency of COP displacement in the AP direction ($p < 0.005$). The vision effect was not dependent on work experience or age ($p > 0.1442$).

AP stability limits were similar across age and work experience whether expressed as an absolute magnitude or as a percentage of foot length ($p > 0.1572$). In the ML direction, roofers adopted a 1.55 cm wider stance than non-roofers ($p < 0.0013$). The older roofers exhibited the largest stability limit both in absolute magnitude and as a percentage of stance width (Figure 2).

SUMMARY

The increase in frequency observed in roofers may be a strategy to obtain more visual and vestibular information for balance control. The effect was maintained in older roofers. The older roofers had an increase in sway magnitude similar to the older non-roofers relative to the younger groups. The roofers adopted a safer stance width and the older roofers were more willing to approach the edges of their base of support.

REFERENCES

Hsiao et al (1997) *Int J Ind Ergon* **20**:501-508.
Perrin et al (1997) *Gerontology,* **43**:223-231.
Suruda et al (1995) *J Safety Res*, **26**(1):1-8.

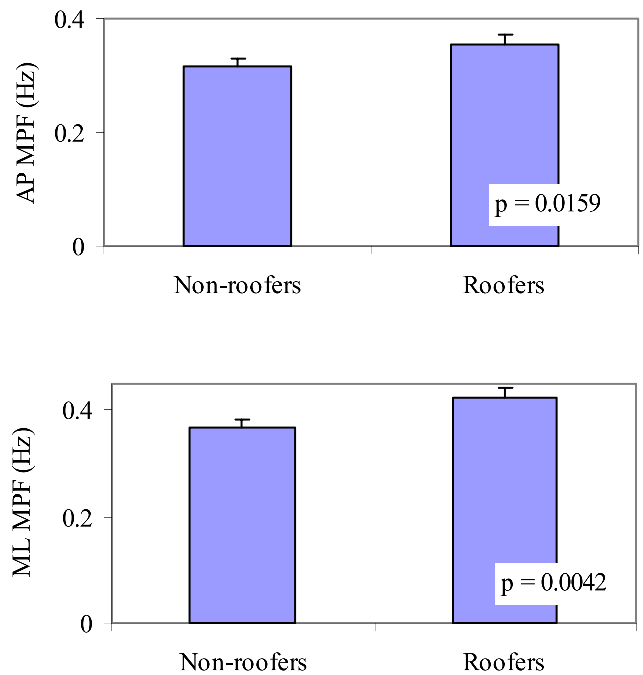

Figure 1: AP MPF (top) and ML MPF (bottom).

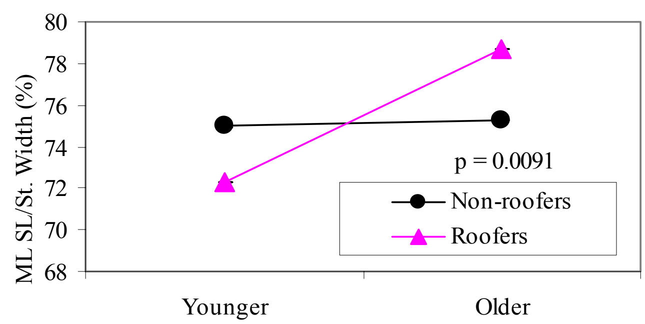

Figure 2: ML stability limit, expressed as a percentage of stance width.

ACKNOWLEDGEMENTS

Mark van Paemel, Josh Williams, Jessica Barber, Billy Block, Tiffany Featherstone, and Scott Thompson are acknowledged for their assistance with data collection. This research study was supported by the NIOSH Pilot Project Research Training Program of the University of Michigan COHSE

MAGNETIC RESONANCE ELASTOGRAPHY FOR THE ASSESSMENT OF MUSCLES IN HYPERTHYROIDISM

Stacie I. Ringleb[1], Laurel Littrell[2], Qingshan Chen[1], Sabine Bensamoun[1], Michael D. Brennan[3], Kenton R. Kaufman[4], Richard L. Ehman[2], Kai-Nan An[1]

[1]Orthopedics Biomechanics Laboratory, Mayo Clinic College of Medicine, Rochester, MN
[2]MRI Research Laboratory, Mayo Clinic College of Medicine, Rochester, MN
[3]Department of Endocrinology, Mayo Clinic, Rochester, MN
[4]Motion Analysis Laboratory, Mayo Clinic College of Medicine, Rochester, MN
E-mail: Ringleb.Stacie@mayo.edu Web:mayoresearch.mayo.edu/mayo/research/biomechanics

INTRODUCTION

Skeletal muscle is an important target of thyroid hormone action. Muscle weakness and atrophy are commonly encountered among patients with thyroid gland dysfunction. Graves disease is a common cause of hyperthyroidism that is accompanied by muscle weakness that is reversible with correction of the hyperthyroid state. The pathogenesis of muscle weakness in this condition is incompletely understood and there is little or no information on the *in vivo* mechanical properties of skeletal muscle in this condition.

Magnetic Resonance Elastography (MRE), a non-invasive phase contrast MRI technique, can visualize small displacements from applied shear waves and quantify the stiffness of soft tissues *in vivo* (Manduca, 2001). When this technique is applied to muscle, the wave travels primarily along the direction of the fiber (Dresner, 2001) and the wavelength increases as load is applied. The purpose of this study was to compare the relationship between the applied load and the measured stiffness in the vastus lateralis in patients with Graves Disease and in healthy asymptomatic volunteers.

METHODS

Three healthy, asymptomatic volunteers (mean age 30.89±0.1 years) and three patients with Graves disease (mean age 51.69±16 years) were tested. Isometric loads, with the knee fully extended and the hip flexed at approximately 45˚, were resisted in increasing 1 kg increments until the subject could not resist the load for one minute.

An electromechanical driver placed over the quadriceps applied shear waves to the vastus lateralis at 100 Hz. A 2D 5 mm thick slice (Figure 1a) of the vastus lateralis was imaged with a gradient-echo, cyclic motion sensitizing sequence (TR/TE of 100ms/min full, 256x64 acquisition matrix, 24cm FOV). Each scan took 64 seconds to complete.

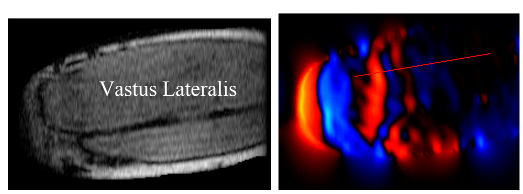

(a) **(b)**

Figure 1: 2D slice of vastus lataralis: a) MRI image b) phase difference image

The stiffness of the muscle (μ) was calculated with the following equation (Dresner, 2001), where ρ is the density (assumed to be 1), *f* is the frequency of the shear wave applied to the muscle and λ is the wavelength of the wave measured from the phase difference image (Figure 1b).

$$\mu = \rho f^2 \lambda^2 \qquad (1)$$

The stiffness values were normalized by the cross sectional area (Figure 2 and Table 1) of the vastus lateralis.

RESULTS AND DISCUSSION

The muscle in patients with Graves Disease was stiffer at a given load than in healthy volunteers. Additionally, the stiffness of the muscle increased at a higher rate in patients than in volunteers (Figure 2 and Table 1).

A previous study demonstrated that the slope of the stiffness vs. load curve increases as the cross sectional area of the muscle decreases (Dresner, 2001). We observed an increase in slope that was significantly larger than the change in cross sectional area. Studies of patients with hyperthyroidism have shown that systematic changes occur with changes in muscle enzyme activity, a decrease in glycogen stores, a decrease in the number of slow twitch muscle fibers and an increase in fast twitch muscle fibers (Canepari, 1998, Celsing, 1986). In addition to the decrease in cross sectional area, these physiological changes may also contribute to the large increase in slope and the increase in the stiffness, observed in patients with Graves Disease.

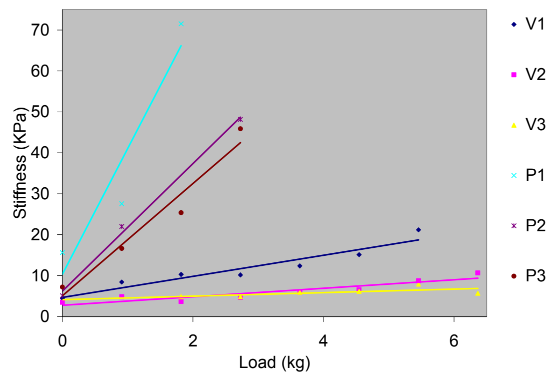

Figure 2: Stiffness vs. Load for healthy volunteers (V1-V3) and patients with Graves Disease (P1-P3).

SUMMARY

Magnetic Resonance Elastography was able to detect larger muscle stiffness in response to applied load between healthy volunteers and patients with Graves Disease.

REFERENCES

Canepari, M. et al. (1998). *Arch Physiol Biochem,* **106**, 308-315.

Celsing, F. et al. (1986). *Clin Physiol,* **6**, 181-181.

Dresner, M.A. et al. (2001). *J. Magn Reson Imaging*, **23**, 269-276.

Manduca, A. et al. (2001). *Medical Image Analysis,* **5**, 237-254.

ACKNOWLEDGEMENT

This research was funded by NIH (NIBIB) Grant # EB00812-04A1.

Table 1: Cross sectional area of the vastus lateralis and the slope (KPa/kg) and y-intercept of the stiffness vs. load curve.

	V1	V2	V3	P1	P2	P3
A (cm^2)	15.45	14.52	15.91	7.22	10.89	10.42
Slope	2.58	1.04	0.43	30.73	15.59	13.72
y-intercept	4.70	2.77	4.15	10.31	6.21	5.07

Modeling the Influence of Flight Phase Control on Center of Mass Trajectory and Reaction Forces During Landing

J. L. McNitt-Gray[1,2,3], P. S. Requejo[1], H. Flashner[3,4], and L. Held[2]

Biomechanics Research Laboratory
[1]Departments of Kinesiology, [2]Biomedical Engineering,
[3]Biological Sciences, and [4]Aerospace and Mechanical Engineering
University of Southern California, Los Angeles, CA 90089, USA

INTRODUCTION

Complex goal-directed human movements consist of a series of phases with multiple objectives. Knowledge of the relationship between control and dynamics during flight and subsequent contact phase is essential for improving landing performance without sustaining injury.

The purpose of this study was to 1) model the relationship between the flight phase control, the center of gravity (CG) trajectory and the reaction force during contact with the landing surface and 2) determine how control of the lower extremities prior to contact, as observed experimentally, influences the reaction force during impact.

METHODS

Approach: First, the dynamics of the interaction between the multi-link system model of the human musculoskeletal system and the model of the visco-elastic landing mat (McNitt-Gray et al., in press) were developed. Second, the model was experimentally validated using landing kinematics and reaction forces. Third, a simulation study was performed to determine how modification in knee joint torque prior to contact influenced CG trajectory and reaction force during contact.

System Model: The human body was modeled as rigid links (n=6) with rotational joints (Fig. 1). The dynamic model of a multi-link system was represented by a set of differential equations in matrix form as follows:

$$\mathbf{M(q)\ddot{q}} + \mathbf{V(q,\dot{q})} + \mathbf{G(q)} = \mathbf{Q} + \boldsymbol{\lambda}\left[\partial P_f / \partial \mathbf{q}\right]^T$$

$$\left(\partial P_f / \partial \mathbf{q}\right) \cdot \dot{\mathbf{q}} = 0$$

where $\mathbf{M(q)}$ is the mass matrix, $\mathbf{V(q,\dot{q})}$ is vector of centrifugal and Coriolis terms, $\mathbf{G(q)}$ is a vector of gravity terms, $\mathbf{Q}$ is a vector of generalized forces, $\boldsymbol{\lambda}$ is the reaction constraint force at the foot/mat interface, $\left[\partial P_f / \partial \mathbf{q}\right]^T$ is the Jacobian constraints expressed as a function of the generalized coordinates equations. The landing mat was modeled as a first order nonlinear spring-damper system.

$$(m + \mu_m)(\ddot{x} - g) + k|x|^\alpha + C|x|^\beta \dot{x} = 0$$

where x is the displacement of the mat.

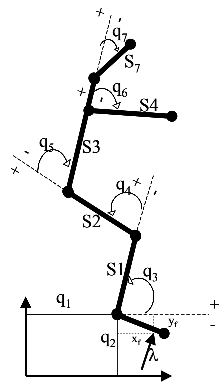

Figure 1: Multi-link model of the human body

Landing Experiment: Experimental data was collected from drop landings (0.72 m) performed by a male collegiate gymnast onto a landing mat (0.12 m thick) in accordance with the Institutional Review Board. Reaction forces at the mat/plate interface were quantified using two force platforms (0.4 x 0.6 m, 800 Hz, Kistler). Two-dimensional sagittal plane kinematics were recorded (200 Hz) and digitized (Peak) according to body landmarks specified by deLeva (1996). Kinematic data were smoothed (14Hz) and derivatives were generated using splines (Woltring, 1986).

Simulations: Landings were simulated under the following conditions: a) experimental segment configurations at touchdown with immovable joints and b) experimental kinematics at touchdown with moving joints (ADAMS, MSC). Input parameters to the multi-link ADAMS model included segment lengths, masses, center of mass, and moments of inertia and either time varying joint accelerations (motion-driven) or time varying joint torques (torque-driven) as in (Requejo, 2002).

RESULTS

Simulated landings with fixed joints resulted in greater reaction force magnitudes and longer times-to-peak force than observed experimentally (Fig. 2). Landing simulations with progressive increases in knee extensor torque prior to touchdown reduced the relative velocity between the CM and the legs ("pull-up") and resulted in a) more vertical shank positions at touchdown, b) greater rates of vertical and horizontal impulse generation c) greater peak forces during the contact phase and d) greater reductions in the CGVy and CGVx during the initial part of the contact phase (Fig. 3).

DISCUSSION

A multi-link model of a gymnast and a model of the gymnastics mat were developed and experimentally validated. Modification of the knee joint torque prior to touchdown simulated the leg "pull-up" behavior often observed prior to contact (McKinley et al., 1992; McNitt-Gray et al., 2001). These results support the hypothesis that modifications in flight phase control provides a mechanism for regulating the magnitude of the reaction forces experienced during contact.

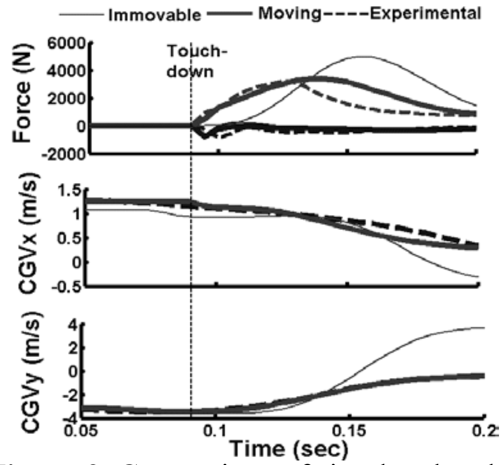

Figure 2. Comparison of simulated and experimental reaction forces and CG trajectories.

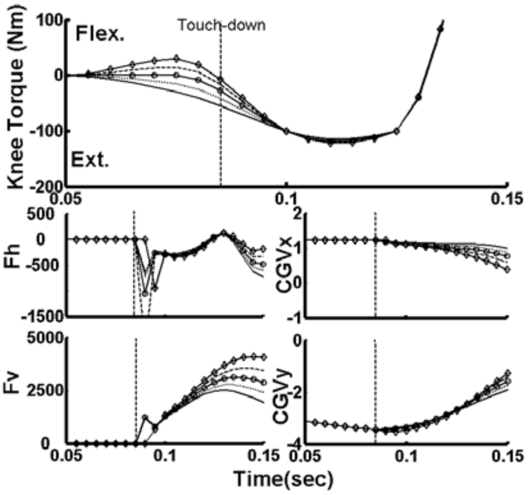

Figure 3. Simulated knee joint torque, reaction forces, and CG velocity

REFERENCES

deLeva, P. J. (1996). *J. of Biomech.,* **29**(9), 1223-1230.

McKinley, P., & Pedotti, A. (1992). *Exp. Brain Res.*, **90**(2), 427-440.

McNitt-Gray, et al. (2001). *J. of Biomech.*, **34**(11), 1471-1482.

McNitt-Gray, et al. (in press). *ISEA*

Requejo, P. S. (2002). *PhD. Dissertation.*

Woltring, H. (1986). *Ad. Eng. Software*, **8**(2), 104-113.

EFFECT OF VARIATIONS IN CORNEA CHARACTERISTICS ON MEASURED INTRAOCULAR PRESSURE

T.-H. Kwon[1], D. A. Pecknold[1], and J. Ghaboussi[1]
[1] Dept. of Civil and Env. Engrg., Univ. of Illinois at Urbana-Champaign, IL 61801

E-mail:pecknold@uiuc.edu Web: www.cee.uiuc.edu

INTRODUCTION

Measurement of intarocular pressure (IOP) in the human eye is the primary screening method for early detection of those at risk for glaucoma. The most common method for IOP measurement is applanation (Goldmann) tonometry, in which an instrument is used to flatten the central part of the cornea. A number of studies (e.g. Ehlers 1975) have been carried out on human eyes *in vivo*. These data show systematic errors in IOP tonometer readings that correlate with increased central corneal thickness (CCT). Such errors have significant implications for glaucoma screening. Doughty and Zaman (Doughty 2000), in a thorough analysis of the literature published over the period 1968-1999, find a statistically significant correlation between apparent IOP and CCT.

However, all of the results show a high degree of scatter. We demonstrate in this paper, via a series of computational simulations, that variations in other mechanical characteristics and properties of the cornea, that are not controlled in these various studies, are quite likely responsible for the observed scatter.

It is clear that central corneal thickness is only one of the factors that influences corneal bending resistance. The elastic properties, as well as the structure, of the individual cornea must be recognized in order to properly correct for corneal bending resistance and obtain reliable and accurate tonometric IOPs.

METHODS

In this paper, we used a finite element (FE) modeling approach, described in a companion paper, to study the response to Goldmann applanation of a set of 50 cornea models with varying characteristics (CCT, true IOP and elastic modulus Ep). The elastic behavior of the cornea was represented by a nonlinear transversely isotropic material model which was implemented in the user-defined routine UMAT in ABAQUS.

The (axisymmetric) aspherical FE model of the cornea was composed of 4-noded axisymmetric solid elements with anterior and posterior surface geometry defined by conicoids (Liou 1997) (Figure 1).

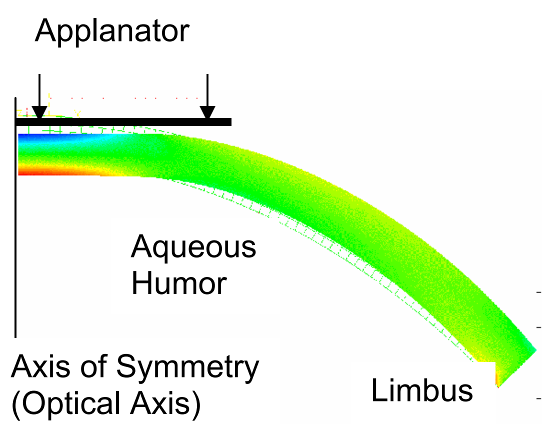

Figure 1: Axisymmetric finite element model for applanation tonometry analysis

Fifty different cornea models were generated by randomly sampling the three variables. The variables were assumed normally distributed and uncorrelated with (mean ± SD) as follows: CCT (536 ± 31nm), in-plane Young's modulus Ep (0.2 ± 0.05Mpa), and true IOP (16 ± 3mmHg).

RESULTS AND DISCUSSION

The 50 cornea FE models were analyzed using the commercial software ABAQUS 6.3.1. Plots of measured (i.e. computed) IOPs are plotted vs CCT in Figure 2, in which random variations of E_p and true IOP are present. Clinical measurements are also provided for comparison (Figure 3).

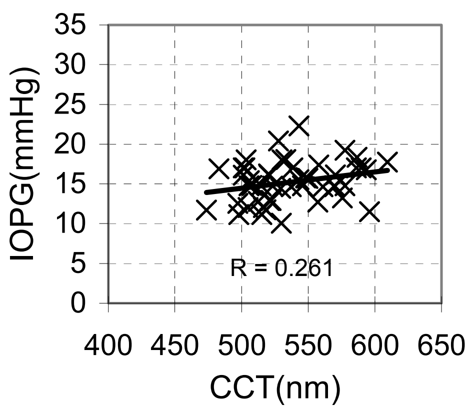

Figure 2: Measured IOP versus CCT in 50 cornea models

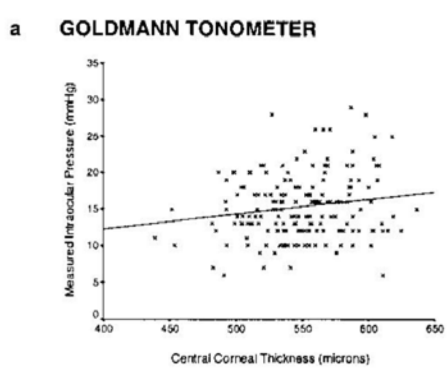

Figure 3: 2001 Bhan et al, 181 normal corneas of 94 patients

The similarity of Figures 2 and 3 is obvious. A second set of cornea models was analyzed (Figure 4), with 2 of the 3 variables (E_p and true IOP) "controlled" by reducing their standard deviations to 20 percent of their original values. The correlation of measured IOP with CCT shows much less scatter as expected.

These results demonstrate that plausible variations in corneal characteristics, other than CCT, may have as much effect on IOP measurement accuracy as variations in CCT.

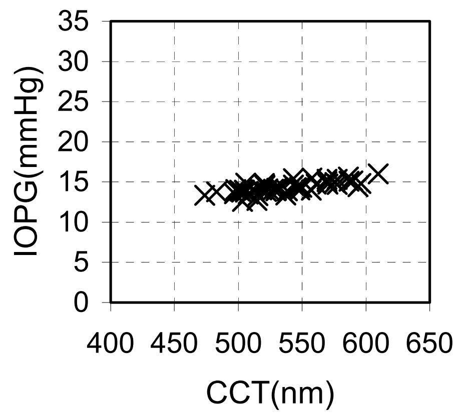

Figure 4: IOP reading versus CCT. CCT 536 ± 31nm, Ep 0.2 ± 0.01Mpa, and IOP itself 16 ± 0.6mmHg

REFERENCES

Ehlers, N (1975). *Acta. Ophthalmol.*, **53,** 34-43.

Bhan, A. et al. (2002). *Investigative* Ophthalmology & Visual Science, **43**, 1389-1392.

Doughty, MJ and Zaman, ML. (2000). *Survey of Ophthalmology*, 44, 367-408.

Liou, H-L et al. (1997). *J Opt Soc Am*, **14**, 1684-1695.

QUANTITATIVE SHEAR WAVE MAGNETIC RESONANCE ELASTOGRAPHY: COMPARISON TO A DYNAMIC SHEAR MATERIAL TEST

Stacie I. Ringleb[1], Qingshan Chen[1], Armando Manduca[2], Richard L. Ehman[2], Kai-Nan An[1]

[1]Orthopedics Biomechanics Laboratory, Mayo Clinic College of Medicine, Rochester, MN
[2] MRI Research Laboratory, Mayo Clinic College of Medicine, Rochester, MN
E-mail: Ringleb.Stacie@mayo.edu Web: mayoresearch.mayo.edu/mayo/research/biomechanics

INTRODUCTION

In clinical applications, such as tumor detection, changes in the mechanical properties of soft tissues are assessed with palpation, which is subjective and has low sensitivity. In muscle, there is no clinically routine method used to measure the mechanical properties of muscle *in vivo*. Such a tool would greatly improve understanding of changes that occur in muscle with pathologies and treatment.

Magnetic Resonance Elastography (MRE), a non-invasive phase contrast MRI technique, can visualize small displacements from applied shear waves and quantify the stiffness of soft tissues *in vivo* (Muthupillai, 1995). This method has been applied to *in vivo* soft tissues including kidney, liver, and muscle (Kruse, 2000). However, attempts to validate the technique by comparing its stiffness estimate with a mechanical test have used only compression tests (Hamhaber, 2003).

Dynamic mechanical analysis (DMA) is a non-destructive dynamic material test that can measure the shear modulus over a given frequency range. The purpose of this study was to compare the MRE stiffness estimate to the shear modulus measured with the DMA in soft tissue mimicking agarose gel.

METHODS

Prismatic agarose gel samples (7x13.4x20.5 cm) with concentrations ranging from 1.5-3.5% in 0.5% increments were prepared. The samples were placed in a head coil and an electromechanical driver was placed on top of the sample that generated shear waves at 100, 150 and 200 Hz. The MRE tests were conducted in a 1.5 T General Electric Signa scanner. A 2D slice of the sample was imaged with a gradient-echo, cyclic motion sensitizing sequence (TR/TE of 100ms/min full, 60° flip angle, 256x64 acquisition matrix, 24cm FOV). Each sample was tested three times. The stiffness (μ) was calculated manually (equation 1), where ρ is the density (assumed to be 1), *f* is the frequency of the shear wave and λ is the wavelength manually measured from the displacement image (Figure 1).

$$\mu=\rho f^2\lambda^2 \qquad (1)$$

Stiffness was also estimated with two inversion algorithms, local frequency estimation (LFE) and matched filter (Manduca, 2001). The dynamic shear moduli of the gels were tested three times with a DMA 2980 (TA Instruments, New Castle, DE) in the shear sandwich mode.

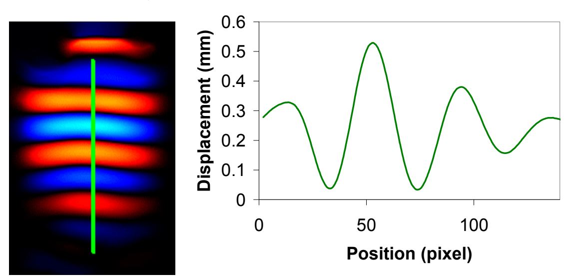

(a) **(b)**

Figure 1: a) Displacement image in 3% agar gel **b)** wave propagating through phantom along profile (green line) in (a).

RESULTS AND DISCUSSION

The shear modulus measured from the DMA was plotted against the MRE stiffness estimates determined from manual calculation and the LFE and matched filter inversion algorithms (Figure 2). The slope, y-intercept, and correlation coefficient (R^2) were recorded (Table 1).

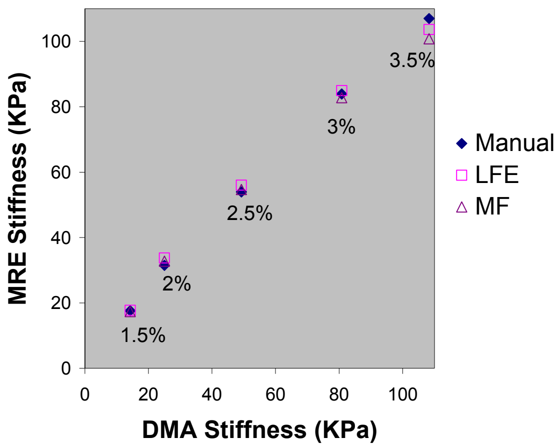

Figure 2: DMA vs. MRE stiffness estimates

In a previous study, MRE measurements were compared with a compression test with concentrations ranging from 0.5-2.5% of agar-agar gel (Hamhaber, 2003). While generally good agreement was obtained, the differences between their manually calculated shear moduli and their compression test results showed somewhat greater deviation than our comparison of the shear modulus measured with a DMA. This suggests that a shear test may be a more appropriate material test for validating the stiffness estimate of MRE.

Our results also demonstrated that the manual stiffness calculation gave the best correspondence to the shear modulus measured with DMA. The inversion algorithms, while showing fairly good agreement as well, had systematically lower slopes and larger discrepancies than the manual calculation. This may be because inversion algorithms are sensitive to noise and edge effects from the container holding the gel (Manduca, 2001).

SUMMARY

MRE was successfully validated using a shear test in a DMA. The manual calculation of stiffness yields the closest comparison to the measured shear stiffness.

REFERENCES

Hamhaber, U et al. (2003). *Magnetic Resonance in Medicine,* **49**, 71-77.

Kruse, S.A. et al. (2000). *Phys Med Biol,* **45**, 1579-90.

Manduca, A. et al. (2001). *Medical Image Analysis,* **5**, 237-54.

Muthupillai, R. et al. (1995). *Science,* **269**, 1854-57.

ACKNOWLEDGEMENT

This research was funded by NIH (NIBIB) Grant # EB00812-04A1

Table 1: Slope, y-intercept and correlation coefficient coefficient of MRE vs. DMA stiffness estimate plots.

	Manual Calculation	LFE	Matched Filter
Slope (KPa/KPa)	0.9419	0.9027	0.8777
y-intercept	6.4793	9.0933	8.9231
Correlation Coefficient (R^2)	0.9977	0.9906	0.9904

LASER SPECKLE MEASUREMENTS FOR SKIN MECHANICS AND DIAGNOSTICS

Sean J. Kirkpatrick

[1]Department of Biomedical Engineering, Oregon Health & Science University, 20000 NW Walker Rd., Beaverton, OR 97006, USA
E-mail: sean.kirkpatrick@bme.ogi.edu
Web: http://www.bme.ogi.edu/biomedicaloptics/kirkpatrick/

Introduction

Laser speckle strain or displacement measurements in soft tissue are often confounded by the very rapid decorrelation of the speckle patterns due to tissue and water movement, as well as the depolarization of the speckle fields. This decorrelation is largely a result of the tissue behaving as a volume scatterer as opposed to a surface scatterer, such as lightly abraded metals. Because of theses issues, classical speckle interferometric methods are often not suitable for mechanical measurements in fully hydrated tissues. Herein, we present a variation on a laser speckle strain gauge that does not rely upon the formation of correlation fringes for displacement measurements. The gauge is relatively insensitive to modest speckle decorrelation, has no dependence on the polarization state of the scattered light, and is highly sensitive (sub-microstrain resolution). This system has potential applications in medical diagnostics, as well as basic biomechanical studies.

The key to the strain gauge is the efficient and accurate estimation of the speckle shift between successive records as a result of an imposed load. For small shifts (<0.5 pixels/record), the maximum likelihood estimator has been shown to be superior to the other approaches (Duncan and Kirkpatrick, 2002).

Methods and Materials

The fundamental method employed in this study was to use an acoustic speaker to supply a low frequency, sinusoidally varying acoustic stress to the skin. Simultaneously, specific points on the skin were illuminated with coherent laser light and the motions of the backscattered speckle patterns as a function of the driving acoustic stress wave were recorded. The magnitude and the time-resolved pattern of the speckle shift were calculated using the maximum likelihood estimator.

All of the experiments were performed using samples of fresh porcine flesh obtained from a local abattoir. The tissue samples consisted of skin, adipose tissue and underlying muscle tissue. Typical dimensions of the tissue sample were 20 cm X 10 cm X 5 cm in the *x, y,* and *z* dimensions, respectively. Tissues were kept refrigerated until approximately ½ hour before testing at which time they were removed from refrigeration, surrounded on all sides, except for the skin surface, with damp paper towels and allowed to equilibrate to room temperature. To apply the acoustic stress wave, a small speaker (87 W, 7.0 cm diameter) was placed in direct contact with the skin at one end of the sample. The speaker was sinusoidally driven at 1 Hz by a sine wave originating from a function generator. In addition, the speaker was assumed to have remained in solid contact with the skin during excitation. Optical illumination was supplied by a 5 mW green HeNe laser ($\lambda = 543$ nm) coupled through single-mode fibers. This wavelength was chosen as it restricted the interrogation depth to depths on the order of 100 μm.

The measurement of tan δ relies upon determining the relative phase difference between the driving acoustic sinusoid and the sinusoidal shift in the speckle pattern from a single illuminated spot. In this case, the illuminated spot was located 5 cm from the edge of the speaker. The speaker was again driven with a 1 Hz sinusoid from a function generator and the backscattered speckle pattern was imaged with the linear array CCD camera. The speckle shift was plotted along with the driving waveform as a function of time (or record number). Based on the measured Rayleigh wave velocity, C_R, a correction was made for time of flight of the surface acoustic wave and the phase difference, δ, between the driving acoustic wave and the resulting speckle shift was calculated. The phase of each waveform was determined as the arctangent of the ratio between the imaginary and real parts of the waves. This procedure was conducted on 3 different locations each on 5 separate skin samples.

Results

Based on the phase differences between the driving acoustic sinusoid and the sinusoid describing the time-resolved speckle shift, the mean value of tan δ was 0.14 ± 0.07, or a phase angle of approximately 8º. Table 1 shows the actual values for each skin sample and their standard deviations.

Table 1

Skin Sample	Tan δ (mean ± s.d.)
1	0.166 ± 0.04
2	0.237 ± 0.12
3	0.154 ± 0.07
4	0.140 ± 0.04
5	0.057 ± 0.03
Overall	0.14 ± 0.07

Discussion

The variation in tan δ values between samples simply reflects the natural variation in tissues, and the fact that the mechanical properties of skin are very dependent upon location on the body and physiological parameters. However, if a large area of skin, including a suspected pathological site, were to be illuminated and a sequence of speckle images were taken as the skin is acoustically stressed, then neighborhood variations in the speckle shift across the images could be determined by extending the speckle shift algorithm to 3 dimensions (the 3rd dimension being time). In this manner, the tissue surrounding the suspect tissue would serve as an internal 'control'. Stiffer tissue areas would exhibit less speckle motion, while less stiff areas would exhibit greater motion under the same acoustic stress, indicating local variations in mechanical properties.

References

Duncan, D.D., Kirkpatrick, S.J. (2002) *Opt.Express* 10, 927-941.

Acknowledgements

This work was funded in part by NSF Grant BES-0196172.

THE EFFECTS OF A RIGID SHANK SHOE ON PLANTAR FASCIITIS IN RUNNERS

Susan E. D'Andrea[1], Kasey R. Parker[1,3], Jason Novick[2], Michael Kahelin[1], Patrick McKee[2] and Alex Kor[2]
Departments of [1]Biomedical Engineering and [2]Orthopaedic Surgery, The Cleveland Clinic Foundation, Cleveland, OH
[3]School of Human Kinetics, University of Ottawa, Ottawa, Ontario, CANADA
Contact information: dandreas@bme.ri.ccf.org, http://www.lerner.ccf.org/bme/biomechanics/

INTRODUCTION

Plantar fasciitis is a common inflammation of the broad-based ligament extending from the calcaneus to a point just proximal to the metatarsal heads (Hlavac, 2001). In high impact, repetitive sports such as running, 10% of all injuries can be attributed to this condition (Tauton et al, 2002). Although medical experts do not entirely agree on the specific cause, most practitioners and investigators include the following etiologies: shape and structure of the foot, activity level of the patient, weight of the patient, the playing surface and the quality of the shoe gear (Thomas et al, 2001; Wilke, Fischer and Gutierrez, 2001).

The current study focuses on the concept that an increase in the rigidity of the shank region of running shoes will decrease the overload on the plantar fascia and thus alleviate the symptoms of plantar fasciitis. To date, shoe stiffness and dynamic deformation have been assessed through computerized gait analyses, ground reaction forces and mechanical three-point bending tests.

METHODS

Running shoes from the stability, motion control and cushioned categories were evaluated and selected by an experienced podiatrist. Each pair was obtained unused from a local running shoe store. Selections for the study were based on the flexibility of the shank of the shoe. Two flexible shoes and two rigid shoes were assigned to the stability and motion control categories. Two flexible and one rigid shoe were assigned to the cushioned shoe group.

Three point bending tests were performed on all shoes (Figure 1, MTS, Minneapolis, MN). Load was applied through displacement control at 5 mm/s to a maximum of 30 mm. This position was maintained for 1 second and then the load was released at 5 mm/s. This cycle was repeated 5 times with a 30 second hold between cycles allowing the material to relax. Force and deformation were recorded for each cycle and stiffness values were calculated in the steepest region of the elastic portion of the each curve.

Figure 1. MTS Testing Apparatus

In order to determine the dynamic range of the shoe shank, motion analysis data was recorded while the subject was running on an instrumented treadmill at 10 km/hr. Eight retro-reflective markers were place on the tibia and shoe (Figure 2).

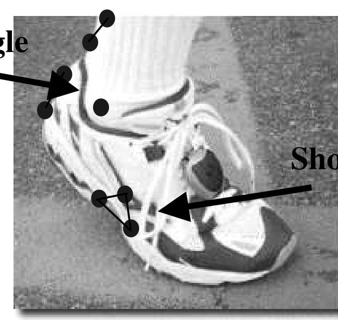

Figure 2: Marker Placement

Subjects were grouped according to foot type–cavus, pes planus or neutral. Two subjects were selected for each group and fitted with the appropriate shoes – cushioned, motion control and stability, respectively. Each subject tested three or four pairs of shoes.

Marker position and ground reaction force data were collected for ten seconds. The rear foot angle and the shoe shank angle, as defined by the apex of the triangle on the shank of the shoe, were calculated and a custom LabVIEW (National Instruments, TX) program segmented and normalized each gait cycle according to the force profile. The maximum range was determined for both the rear foot and shoe shank angles during stance. Angular data were correlated with stiffness values by shoe type.

RESULTS AND DISCUSSION

Since it is widely accepted that the flexibility in a shoe can be a major contributing factor to the onset of plantar faciitis, a shank-bending threshold was determined based upon stiffness values (Figure 3). The threshold was established based upon group wise comparisons and represents the level of shoe stiffness below which the stretch in the arch during repetitive loading of the foot would be amplified. Only shoes with stiffness values above 27 N/mm were used in subsequent investigations.

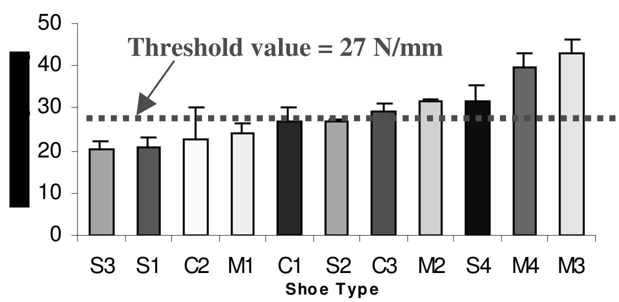

Figure 3: Average Stiffness by Shoe Type. **C**: cushion type shoe; **M**: motion control type shoe; **S**: stability type shoe

Calculated rear foot and shoe shank angles were consistent within and between subjects and corresponded with values found in the literature (Areblad et al, 1990; Figure 4).

The dynamic range of the shoe was evaluated by the change of the shoe shank angle during running. The relationship between the angle range and the shoe stiffness was strongest in the cushion-type shoes ($\mathbf{R^2}$> 0.88, Figure 5).

Correlations between these variables for other shoe types were not as straight forward and further analysis is necessary to determine peripheral factors.

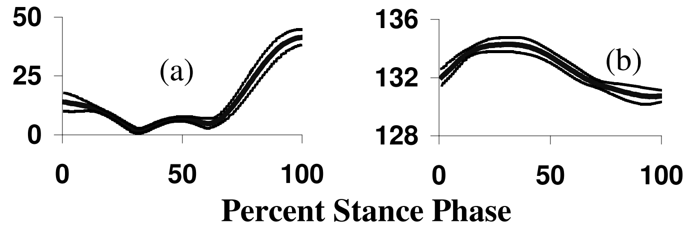

Figure 4: Representative rear foot (a) and midfoot (b) angles during the stance phase of running.

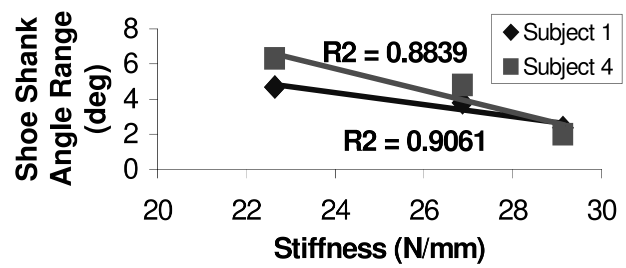

Figure 5: Relationship between three-point bending shoe stiffness and shoe shank motion.

SUMMARY

Currently, longitudinal studies are being completed to evaluate thirty runners with plantar fasciitis after being given a stiffer shoe as indicated by the present analysis. Data will help to ascertain the effectiveness of a rigid shoe shank on the outcome and recovery of this condition.

REFERENCES

Areblad et al. (1990). *Journal of Biomechanics*, **23**(9): 933-940.

Hlavac (2001). *Podiatry Today*, **14**(11): 41-44.

Tauton et al., (2002). *British Journal of Sports Medicine*, **36**: 95–101.

Thomas et al. (2001). *The Journal of Foot and Ankle Surgery*, **40**(5): 329-340.

Wilke, et al. (2001). *Journal of Orthopaedic and Sports Physical Therapy*, **30**(1): 21-31.

ACKNOWLEDGEMENTS

Thanks to the American Academy of Podiatric Sports Medicine for funding this project, Bill Dieter and the staff at Second and Cortney Popowitz for assistance with data collection.

POSTURAL SWAY RESPONSES TO PREDICTABLE AND UNPREDICTABLE MOVING VISUAL SCENES

Mark Musolino[1,2,4], Patrick Loughlin[1,2,3] and Mark Redfern[1,2,4]

[1]Human Movement and Balance Laboratory
[2]Dept. of Bioengineering, [3]Dept. of Electrical Engineering, and [4]Dept. of Otolaryngology
University of Pittsburgh, Pittsburgh, PA, USA
Email: markmuso@pitt.edu Web: www.mvrc.pitt.edu

INTRODUCTION

While much is known about the sensory processes that contribute to postural control, a clear picture of how the central nervous system combines and interprets visual, vestibular and somatosensory afferents in order to maintain stability has yet to emerge. For example, some studies have concluded that feedback (corrective) mechanisms alone can account for experimental observations of postural behavior (Peterka 2002), while others have reported that feedforward (predictive) processes must be involved as well (Jeka et al. 2000). If indeed a predictive component to postural control exists, then one would expect to observe differences in postural responses to external perturbations that vary in their degree of predictability. *The purpose of the present study was to investigate postural sway responses to predictable and unpredictable moving visual stimuli.*

METHODS

Postural sway was examined in 6 healthy young adults that viewed a bullseye-and-checkerboard pattern that oscillated in a periodic ("predictable") or non-periodic ("unpredictable") fashion. Tests were performed in the BNAVE, a custom built virtual environment that projects computer generated images onto several adjoining screens (Jacobson et al. 2001). Scene motion was driven by one of five signals: (1) ±8cm 0.1Hz sinusoid, (2) ±8cm 0.3Hz sinusoid, (3) ±8cm 0.5Hz sinusoid, (4) a ±8cm periodic sum of these sinusoids (0.1 + 0.3 + 0.5 Hz = PSUM), or (5) a ±8cm non-periodic counterpart ($0.1 + \pi/10 + 0.5$ Hz = NPSUM). Subjects stood barefoot on a force plate, 1 meter from the front screen, with arms folded across the chest (fig 1).

Figure 1: Subject viewing a scene in the BNAVE

Trial duration was 80 seconds. The five scene movements were shown only once, and presented in random order, with a 2-minute rest period between successive trials. A 30-second quiet stance (QS) trial was performed prior to the moving scene trials. Postural responses were examined through measurements of head and center-of-pressure (COP) displacements in the sagittal plane. Sway power at each of the stimulus component frequencies was used as the means of comparison between PSUM and NPSUM responses. Differences were tested for statistical significance using a full-factorial repeated measures ANOVA.

RESULTS AND DISCUSSION

All of the moving visual scenes evoked an increase in sway below 0.2Hz, relative to QS (fig 2). At each component frequency, both PSUM and NPSUM scenes elicited sway which was significantly larger than that for QS (fig 3); this difference was particularly large (≥ 10dB) at 0.5Hz. In addition, PSUM and NPSUM responses were nearly identical at 0.1Hz and 0.3Hz, but significantly different at 0.5Hz, with PSUM larger by over 6dB (fig 3). The power increase at 0.5Hz (relative to QS) in the sum-of-sinusoids responses was comparable to that evoked by the 0.5Hz pure sinusoid (fig 2). In contrast, power at 0.3Hz for the PSUM and NPSUM trials was much lower than that elicited by the 0.3Hz pure sinusoid (fig 2).

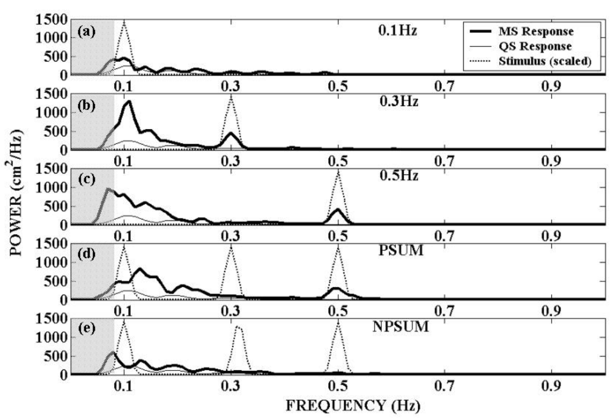

Figure 2: Ensemble power spectra (n=6) of head responses to the moving scenes (MS response). Top-to-bottom: 0.1Hz, 0.3Hz, 0.5Hz, PSUM, NPSUM. Shaded area indicates signal attenuation via high-pass filter (-3dB at 0.08Hz). COP responses were similar.

This differential response at 0.3Hz and 0.5Hz suggests that the postural system may have been sensitive to stimulus *velocity*, and therefore influenced primarily by the sinusoidal component with highest velocity (0.5Hz). Such velocity sensitivity has been reported by others (Dijkstra et al. 1994). In addition, the differences observed between PSUM and NPSUM groups, as well as the heightened response at some non-stimulus frequencies, indicates that the postural system was not operating in a linear time-invariant manner. Possible causes include saturation nonlinearities (Peterka & Benolken 1995) and sensory reweighting (Peterka & Loughlin 2004).

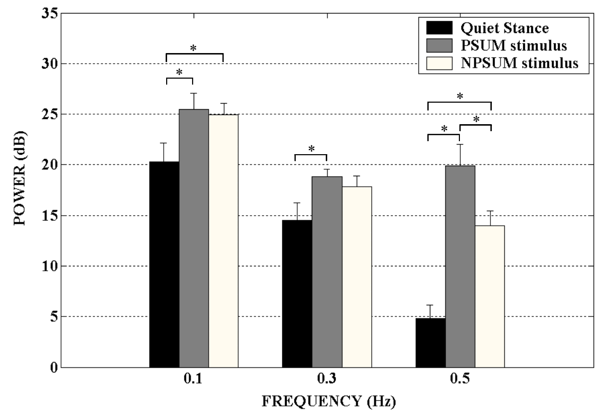

Figure 3: Head sway response power at each of the stimulus frequencies for the QS and sum-of-sinusoids trials (mean +/- std error (in dB) for n=6 subjects). Asterisks denote significant differences ($p<0.05$). COP responses were similar.

SUMMARY

These results show that predictable and unpredictable optic flow with very similar spectral content evoked significantly different sway responses. However, contrary to what one might expect in a system that utilized prediction to maintain stability, sway was largest in response to predictable stimuli. Future studies are planned to further investigate these findings and develop models of underlying mechanisms.

REFERENCES

Dijkstra, T.M. et al. (1994). *Biol Cyb* **71(6)**: 489-501.
Jacobson, J. et al. (2001). *Proceedings of the Virtual Reality Software & Technology Mtg.*
Jeka, J.J. et al. (2000). *Exp Brain Res* **134(1)**: 107-25.
Peterka, R.J., Benolken, M.S. (1995). *Exp Brain Res* **105(1)** : 101-10.
Peterka, R.J (2002). *J Neurophys* **88(3)**: 1097-118.
Peterka, R.J., Loughlin, P.J. (2004). *J Neurophysiol* **91(1)**: 410-23.

ACKNOWLEDGEMENTS
This work was supported by NIH grants R01-AG14116 and R01-DC04435.

FINGER COORDINATION DURING MOMENT PRODUCTION ON A MECHANICALLY FIXED OBJECT

Jae Kun Shim [1,2], Mark L. Latash [2], and Vladimir M. Zatsiorsky [2]

[1] Biomechanics Laboratory and [2] Motor Control Laboratory, Department of Kinesiology,
The Pennsylvania State University, State College, PA, USA
E-mail: jus149@psu.edu, Web: www.psu.edu/dept/biomechanics/

INTRODUCTION

This study deals with the fingertip forces exerted during moment production on a handle affixed to an unmovable support, which is a quite common task in everyday life. As compared to holding a free object — to date the most popular object for studying prehension (Augurelle et al. 2003; Shim et al. 2003, 2004; Zatsiorsky et al. 2003)—this task possesses one essential distinction. When a handle is affixed to an external support, the forces exerted on the handle can be of any magnitude; in this sense, the task is constraint free and it is not dictated by typical static equilibrium constraints ($\sum \boldsymbol{M}=0$, $\sum \boldsymbol{F}=0$).

The goal of this study has been to investigate effects of three task parameters—(1) the mechanical advantage of the fingers, (2) the magnitude, and (3) the direction of the produced moment—on the following outcome variables: (a) the net forces exerted on the object, (b) the internal grasp force, (c) the percentage contribution of the free moment (a force couple) and the net force to the total moment production, (d) the agonist and antagonist moments, and (e) the individual finger forces.

METHODS

Equipment: Five six-component (three forces and three moments) transducers (Nano-17, ATI Industrial Automation, Garner, NC, USA) were attached to an aluminum handle which was fixed to a small force plate (PY6, Bertec Co., Columbus, OH, USA).

Experimental Procedure: Subjects (n=13, male, right-handed) sat on a chair and flexed the right elbow joint 90° in the sagittal plane. The forearm was in a neutral position between pronation and supination. The instruction to the subjects was to grasp the handle by placing the digit tip centers over the centers of the corresponding sensors and to produce a required moment about the moment axis as accurately as possible. The moments were generated in the counterclockwise (pronation, positive) and clockwise (supination, negative) directions, in total four moments: –2.0 Nm, –1.0 Nm, 1.0 Nm, and 2.0 Nm. The position of the handle with respect to the moment axis, P (6.0 cm, 4.0 cm, 2.0 cm, 0 cm, –2.0 cm, –4.0 cm, and –6.0 cm) defined the finger force moment arms that varied systematically across trials.

RESULTS AND DISCUSSION

The performance variables changed symmetrically with P. In particular, the magnitudes of the net horizontal and vertical forces both showed an S-shape change (Fig.1). The internal grasp force varied as a function of P being maximal at P=0 (Fig.2).

The index finger produced 69% of the total normal force during positive torque tasks while the little and the middle together produced 70% during negative torque tasks (Table 1).

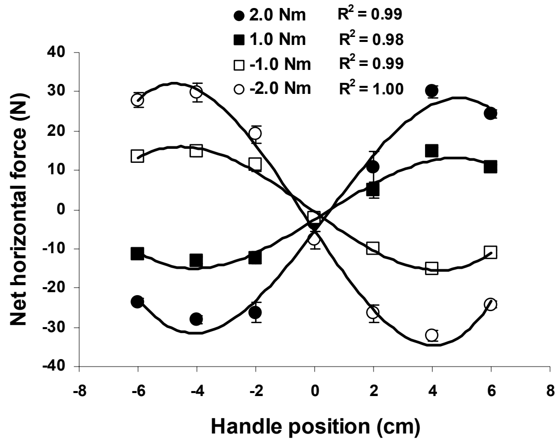

Figure 1. Net horizontal force.

The position of the point of zero free moment (PZFM) was determined. For the intermediate grasp locations (when $0<|P|<\text{PZFM}$), the contributions of M_{free} (moment produced by pronation or supination effort) and the moment of the resultant force (moment generated mainly by pushing) into the total moment production scaled linearly with P.

The magnitudes of both agonist and antagonist moments (those acting in and against the direction of the required moment, respectively) of normal forces increased with $|P|$ while the magnitude of agonist moments of tangential forces decreased.

For individual fingers, the ratio of finger force to its moment arm was not constant.

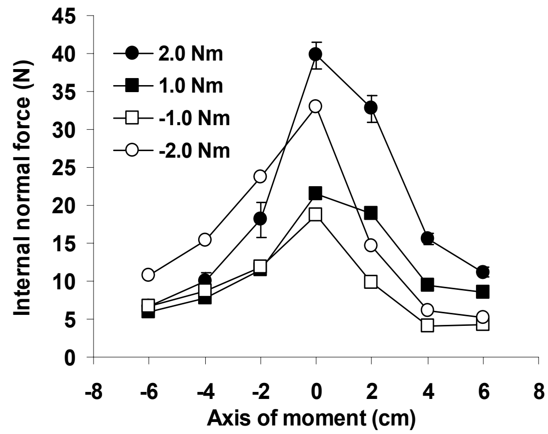

Fig.2. Internal grasping force

The mechanical advantage hypothesis was successful in explaining some of the data but could not cope with other findings. We assume, therefore, this hypothesis is limited in its applicability and may be task and effector specific.

REFERENCES

Augurelle A.S. et al. (2003). *Exp Brain Res* **148**,533-540.

Shim J.K. et al. (2003). *Exp Brain Res,* **152**, 173-184.

Shim J.K. et al. (2004). *J Appl Physiol,* 2004 Mar 5 [Epub]

Zatsiorsky et al. (2003). *Exp Brain Res*, **148**, 77-87.

ACKNOWLEDGEMENTS

AR-048563, AG-018751 and NS-35032 from NIH.

Table 1. Sharing total normal and tangential force among individual fingers, %. Mean ≤ S.D.

Task moment	Normal force (%) I	M	R	L	Tangential force (%) I	M	R	L
2.0 Nm	68.4≤4.3	14.9≤2.4	11.8≤2.1	4.9≤1.2	50.0≤16.1	***19.0±12.1**	6.5≤6.3	9.6≤3.0
1.0 Nm	69.0≤4.0	14.8≤2.4	11.4≤1.9	4.8≤1.0	48.0≤16.3	***14.2±11.8**	6.3≤4.0	8.8≤2.5
-1.0 Nm	***14.1±4.1**	***15.9±2.5**	36.1≤1.8	34.0≤1.0	18.3≤17.7	23.3≤12.0	27.0≤4.4	***28.2±2.7**
-2.0 Nm	***12.2±4.3**	***17.3±2.4**	35.4≤2.0	35.0≤1.0	15.3≤18.2	26.6≤11.7	26.5≤4.3	***31.1±2.7**

Mean and S.D. values were calculated over all handle positions for all subjects. *Significant ($p<0.05$) differences of finger force sharing between 2.0 Nm and 1.0 Nm or between –2.0 Nm and –1.0 Nm.

RELATIVE TIMING OF MUSCLE FATIGUE AND COORDINATION CHANGES DURING REPETITIVE DUMBBELL LIFTING

Kyle R. Voge, B.S. and Jonathan B. Dingwell, Ph.D.

Nonlinear Biodynamics Lab, Dept. of Kinesiology, University of Texas, Austin, TX, USA
email: jdingwell@mail.utexas.edu web: http://www.edb.utexas.edu/faculty/dingwell

INTRODUCTION

Repetitive stress injuries (RSI) affect tens of thousand Americans each year and are very costly, with some estimates of the yearly total costs nearing a billion dollars (Webster & Snook, 1994). For repetitive tasks, muscle fatigue is often associated with altered movement coordination and some of these altered movement patterns may lead to the development of RSI (Mizrahi et al., 2000). While some studies have examined coor-dination patterns pre- vs. post-fatigue, no study has yet examined the time course over which muscle fatigue and movement pattern changes manifest themselves. The goals of this study were to determine, for a repetitive upper extremity task, (1) if changes in muscle fatigue and coordination progress monotonically and (2) if changes in muscle fatigue precede changes in coordination.

METHODS

Six healthy right-handed male subjects (age 23.7±4.2) gave informed consent before participating. Subjects performed dumbbell rows with 6% of their max isodynamic lifting strength at 40 lifts/min until volitional exhaustion. The test was repeated for each arm about one week apart, in random order.

3D motions of 12 reflective markers placed on the torso, upper arm, and forearm were recorded at 60Hz (Vicon-612, Oxford Metrics, Oxford, UK). Inverse kinematic analyses were performed and Cardan angles for shoulder flexion, abduction, and rotation were calculated. Maximum angles *for each lift* were extracted from these data.

Eight bipolar surface electrodes (Delsys Inc, Boston, MA, USA) recorded EMG from the biceps brachii; pectoralis major (clavicular portion); anterior, medial, and posterior deltoids; upper and mid trapezius; and latissimus dorsi at 1080Hz. The median frequency (MdPF) for each muscle for each lift was calculated as a measure of fatigue status. Cross correlations between MdPF and maximum joint angles were computed to determine the temporal sequencing of fatigue and movement pattern changes.

RESULTS

Subjects averaged 401±83 lifts with their right arm and 382±46 lifts with their left. This was consistent with findings that the dominant arm is usually more resistant to fatigue (Tanaka et al, 1984). Shoulder flexion and rotation and elbow flexion angles remained consistent across trials. Shoulder abduction motions were much more variable (Fig. 1). Unlike isometric or single degree-of-freedom fatiguing tasks, changes in kinematics and EMG activity were *not* monotonic for this multi-joint task.

Variations of max shoulder abduction and mid-trapezius MdPF for a typical subject are shown in Fig. 2. Cross-correlation analysis yielded a negative correlation (r = -0.599) at a negative lag (-20 lifts). This indicates that for this subject, changes in muscle fatigue states occurred about 20 lifts *before* changes

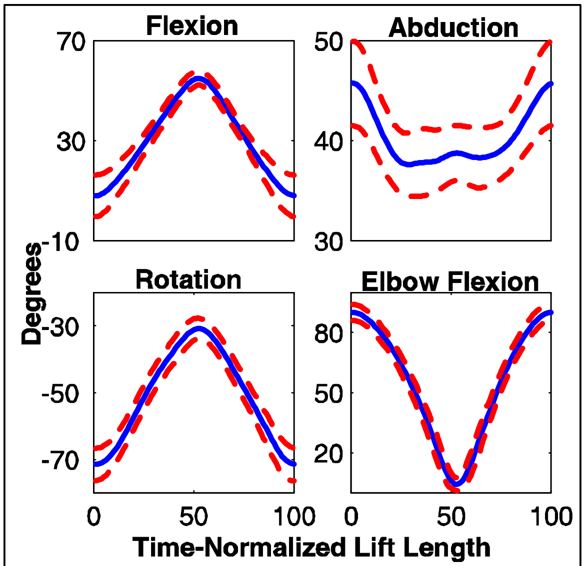

Figure 1: Normalized shoulder flexion, abduction, rotation, and elbow flexion for a typical subject. Mean (-), ±1 SD (- -).

in shoulder abduction coordination. Of 9 sets of cross correlations in mid-trap MdPF with max abduction collected so far, 2 had max correlations at negative lags, 1 at positive lags, 2 at zero lag, and 4 showed no significant correlation.

DISCUSSION

During multi-joint movement tasks, humans can and do alter their inter-segmental movement patterns while maintaining constant output to offset the effects of muscle fatigue (Côté et al., 2002). Our results indicate that changes in kinematics and fatigue states were *not* monotonic, but varied continuously during each trial. This finding was highly consistent across all subjects. Cross-correlation analyses also demonstrated that shifts in coordination often depended on specific changes in muscle fatigue state. However, these nature of these changes varied widely across subjects.

Differences in correlations may result from different subjects using different strategies to compensate for muscle fatigue. Changes

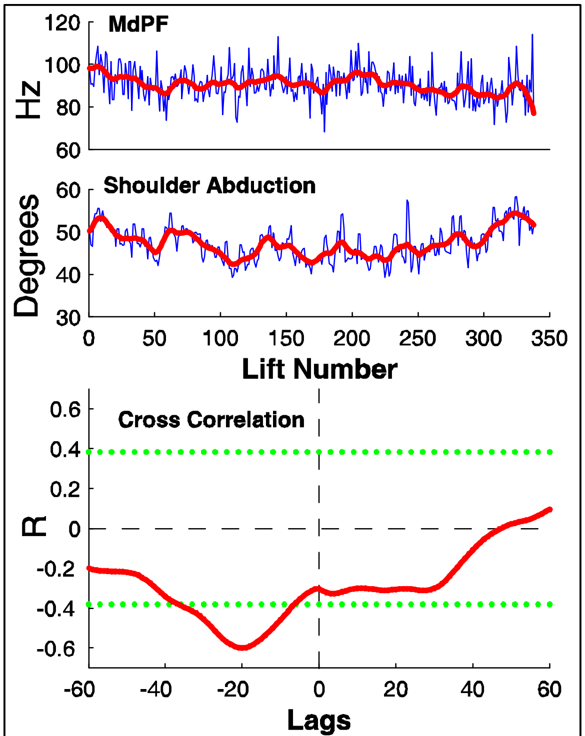

Figure 2: Cross correlation between mid-trap MdPF (top) and max shoulder angle (middle) for consecutive lifts. Actual data (-), moving average trends (-), and ±95% CI for zero correlation (•••).

in coordination at any one joint may also result from a more complex combination of changes in fatigue state across multiple muscles simultaneously. Future research will be aimed at clarifying these issues.

ACKNOWLEDGEMENTS

Partial funding was provided by a Research Grant from the University of Texas Office for the Vice President for Research.

REFERENCES

Côté J.N., et al. (2002). *Exp. Brain Research*, **146**, 394-398.
Mizrahi J., et al. (2000). *Annals of Biomedical Engineering*, **28**, 463-469.
Tanaka M., et al. (1984). *Eur. J. Appl. Physiol. Occup. Physiol.*, **53**, 17-20.
Webster B.S. and Snook, S.H. (1994). *J. Occup. Med.*, **24**, 543-555.

FACTORS INFLUENCING THE ACCURACY OF ARTICULAR CARTILAGE THICKNESS MEASUREMENT FROM MRI

Seungbum Koo[1], Peter Kornaat[2], Garry Gold[2] and Thomas P. Andriacchi[1,3]

[1] Biomotion Laboratory, Stanford University, Stanford, CA, USA
[2] Department of Radiology, Stanford University, Stanford, CA, USA
[3] Department of Orthopaedic Surgery, Stanford University, Stanford, CA, USA
E-mail: koosb@stanford.edu Web: http://biomotion.stanford.edu

INTRODUCTION

Accurate measurement of articular cartilage thickness is important in the analysis, diagnosis and treatment of degenerative changes associated with osteoarthritis. While magnetic resonance imaging (MRI) is frequently used to diagnose articular cartilage disease in-vivo (Peterfy 2004), measuring cartilage thickness in co-planar MRI has a problem of overestimation (McGibbon 1998). Three-dimensional (3D) computer models of articular cartilage using MRI (Stammberger 1999, Koo 2003) provide a viable alternative to co-planar methods. However appropriate accuracy testing of thickness measurements using 3D models has been limited (Eckstein 2000 and Graichen 2003) and not addressed the influences of factors such joint curvature, bone defects or imaging properties of adjacent tissue on the accuracy of thickness measurement.

The purpose of this study was to evaluate the several factors that potentially influence the accuracy of cartilage thickness measured from MRI.

METHODS

MR images from an intact porcine knee with a subchondral cyst (Sagittal plane, 3D-SPGR, fat-saturated, TR=60ms, TE=5ms, FA=40°, matrix 256x256, rectangular FOV 14x14cm slice thickness 1.5mm, 60 slices.) were used to construct a 3D computer model of the femoral cartilage (Koo 2003) and its thickness was calculated to generate a thickness map (Figure 1a). The distal end of the femur was removed for laser scanning (Cyberware, Monterey, CA, USA) with an accuracy of 50µm. The cartilage surface was coated with a powder spray of negligible thickness to prevent laser scan error due to optical properties of the cartilage (Sommers 2003). After the initial scan, the cartilage was removed using a 6.0% sodium hypochlorite solution for four hours to digest the cartilage and second laser scan was performed to measure the surface shape of the subchondral bone. The two laser scans were combined to create a 3D computer model of the articular cartilage, and its thickness was calculated to generate a thickness map (Figure 1b). The two cartilage thickness maps were registered to compare cartilage thickness of the same regions. Accuracy measurements were evaluated in three central regions and twelve boundary regions (Figure 2) on each condyle. Average thicknesses were compared between the MRI and laser scanned models.

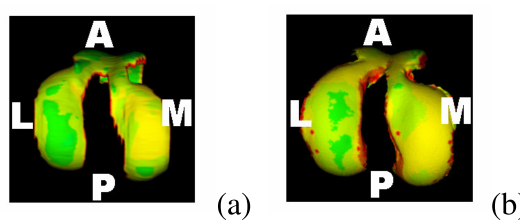

Figure 1: Thickness map of 3D cartilage model from (a)MRI (b)Laser Scan

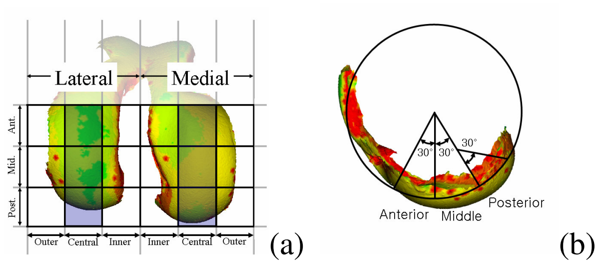

Figure 2: Criteria of selecting regions (a)front view (b) side view

RESULTS AND DISCUSSION

The differences in average thickness between the MRI and laser models were less than 0.3 mm in all central regions (Table 1) with the exception of middle Lateral-Central region (underlying bone cyst) and Medial Central region (in contact with muscle) whose MRI are shown in Figure 3. The lack of contrast between cartilage and muscle made it more difficult to delineate the cartilage. Overall, there were larger errors in the boundary regions. Cartilage in boundary regions is more difficult to segment due to other adjacent soft tissues. In addition the smaller radii along the scanning direction (sagittal plane) in these regions cause large partial volume effects in MRI.

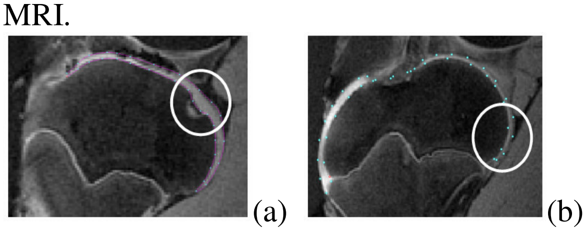

Figure 3: (a)Underlying bone cyst (b)Cartilage in contact with muscle

SUMMARY

Cartilage thickness measurements obtained from 3D models of articular cartilage derived from MRI showed high accuracy that was better than 0.3mm under ideal conditions. Error was increased to a range between 0.35 and 0.65mm in regions with adjacent bony defects, adjacent soft tissue and smaller radii in boundary regions. These results suggest that MRI derived thickness measurements using 3D models in the central load bearing areas of the joint are quite accurate and useful for studies of in vivo cartilage thickness.

REFERENCES

Eckstein, F. et al. (2000). *J. Magnetic Resonance Imaging*, 11, 161-167.
Graichen, H. et al. (2003). *OsteoArthritis and Cartilage*, 11, 475-482.
Koo, S. et al. (2003). *ASME Summer Bioengineering Conference*, 2003.
McGibbon, C.A. et al. (1998). *Medical Engineering & Physics*, 20(3), 169-176.
Peterfy, C.G. et al. (2004). *Osteoarthritis and Cartilage*, 12(3), 177-190.
Sommers, M. et al. (2003). *27th Annual meeting of ASB*.
Stammberger, T. et al. (1999). *Magnetic Resonance in Medicine*, 41, 529-536.

ACKNOWLEDGEMENTS

The laser scan data was processed using the RapidForm (INUS, Korea).
This study is funded by NIH EB002524 and NIH AR049792.

Table 1: The difference of average thickness of each region (mm). Thicknesses larger than 0.3mm are highlighted in gray.

	Lateral			Medial		
	Outer	Cenral	Innner	Innner	Central	Outer
Anterior	0.33±0.10	0.19±0.13	0.26±0.11	0.39±0.19	0.14±0.08	0.64±0.51
Middle	0.25±0.18	0.32±0.07	0.38±0.08	0.38±0.20	0.11±0.07	0.09±0.07
Posterior	0.34±0.13	0.23±0.16	0.36±0.28	0.49±0.29	0.35±0.15	0.18±0.16

INITIAL HORIZONTAL MOMENTUM ALTERS CONTROL OF THE REACTION FORCE RELATIVE TO THE CENTER OF MASS

Witaya Mathiyakom,[1,5] Jill McNitt-Gray,[1,2,3] and Rand Wilcox[4]
Departments of [1]Kinesiology, [2]Biomedical Engineering, [3]Biological Sciences, [4]Psychology, and [5]Gerontology
University of Southern California, Los Angeles, CA, USA
E-mail: mathiyak@usc.edu

INTRODUCTION

Generation of angular impulse during the contact phase of goal directed tasks requires that the performer control the center of mass (CM) relative to the reaction force so that linear and angular related task objectives at take-off are satisfied. During goal directed tasks initiated from rest, the CM position relative to the feet is controlled by coordinating the trunk, arms, and leg motion, and the reaction force is generated by rapid extension of the joints (Miller and Munro, 1984). In contrast, during tasks performed with an initial CM velocity, the position of the feet relative to the CM is controlled at touchdown so that the CM trajectory and the net linear and angular impulse generated during foot contact satisfies the linear and angular related task objectives (Hay, 1986). These observed between task differences in CM control relative to the feet led us to hypothesize that the initial total body momentum contributes to between task differences in 1) mechanisms of reaction force generation and 2) mechanisms of coordinating trunk-leg motion to satisfy CM trajectory requirements of the task.

METHODS

Highly skilled performers (n=5) executed a series of standing and running forward somersaults from a force platform onto a landing pit. Sagittal plane kinematics (200 fps) and reaction force (1,200 Hz) were simultaneously recorded and synchronized at plate departure. Each coordinate of the body landmarks was digitized, filtered using a fourth order Butterworth Filter (Saito & Yokio, 1982) with cut-off frequencies determined using a method based on Jackson (1979). Body segment parameters of an athletic population (de Leva, 1996) were used to calculate the body segment and CM. The CM and hip position vectors originated from the center of pressure (CP) were used to identify CM and leg orientation, respectively. In addition, trunk orientation relative to the right horizontal passing through the hip was also calculated. Angular impulse was calculated as the area under moment-time curve.

RESULTS AND DISCUSSION

Between task differences in initial momentum induced between task differences in the control of CM trajectory and reaction forces. During the take-off phase of the running FRONT somersault, the initial momentum afforded the use of the lower extremities to reduce the excessive horizontal CM velocity at touchdown by placing the feet in front of the CM at touchdown. The orientation of the reaction force relative to the CM was mediated by altering leg orientation at touchdown (Fig.1). Forward rotation of the trunk after contact placed the CM more vertical relative to the leg thereby, increasing the relative angle between the CM and the reaction force. Coordinated motion of the trunk and legs was established at touch down and was maintained throughout the take-off phase of the running FRONT somersault (Fig. 2).

During the standing front somersault, the initial momentum was negligible. As a result, an increase in the relative angle between the CM and the reaction force was initiated by moving the CM forward relative to the feet via forward trunk rotation. Forward trunk motion about the hip prior to joint extension reoriented the CM in front of the reaction force, thereby, increasing the magnitude of the angular impulse.

Although the mechanism for generating the reaction forces were different between tasks (e.g. impact vs joint extension), the control of the legs was associated with reaction force magnitude and direction (Hay, 1986). Control of the trunk motion served as the primary vehicle for altering CM trajectory (Miller and Munro, 1984).

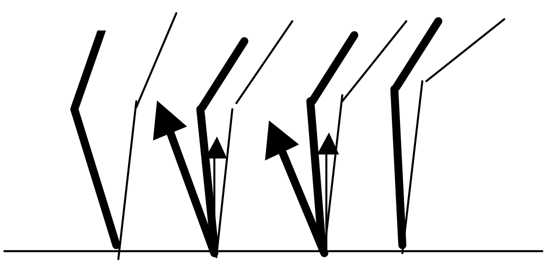

Figure 1: Orientation of the trunk, leg and reaction force during the take-off phase of the standing front somersault (thin line) and running FRONT somersault (thick line).

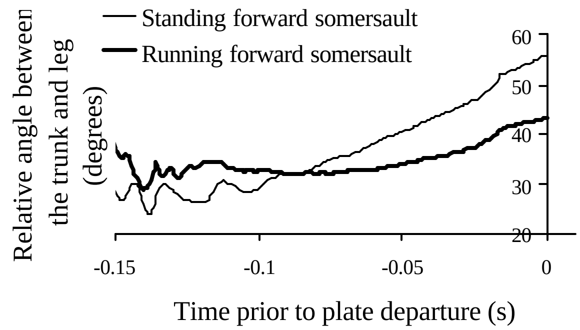

Figure 2: Relative angle between the trunk and leg angle during the take-off phase of task initiated with (running) and without (standing) initial momentum of an exemplar subject.

SUMMARY

Between task differences in initial momentum induced between task differences in mechanisms used to generate angular impulse. However, the role of legs and trunk contributing to the CM orientation and reaction force generation were consistent between tasks.

REFERENCES

de Leva, P. (1996). *J Biomech,* **29**, 1223-1230.

Hay, J. (1986). *Exer Sport Sci Rev*, **14**, 401-446.

Jackson, K. (1979). *IEEE Trans Biomed Eng*, **26**,122-124.

Miller, D., Munro, C. (1984). *Med Sci Sports Exerc*, **16**, 234-242.

Saito, S., Yokio, T. (1982). *T. Bull of Health and Sport Science*, University of Tsukuba. 201-206.

DRAG FORCE NORMALIZED WHEELCHAIR PROPULSION FORCES

W. Mark Richter, Russell Rodriguez, Kevin R. Woods, and Peter W. Axelson

BioMobility Laboratory, Beneficial Designs, Nashville, TN USA
mark@beneficialdesigns.com   www.beneficialdesigns.com

INTRODUCTION

Ground reaction forces are commonly normalized by subject body weight in gait biomechanics studies. This method of normalizing is justified since the reaction forces are directly related to body weight. Handrim forces are used instead of ground reaction forces when studying wheelchair propulsion biomechanics. Just as in gait studies, it is desirable to normalize the resulting handrim forces to allow users of varying weights to be compared. However, it is the wheelchair wheels, not the handrim forces that support the user's body weight when using a wheelchair. While an association has been found between a user's body weight and the magnitude of peak forces on the handrim for level propulsion (Boninger, 2000), it is likely that this relationship is driven by secondary factors such as the propulsion technique of the heavier population. This pilot study investigates an alternative normalizing value, the effective drag force (EDF), for use in propulsion studies. The EDF represents the minimum handrim force required to maintain forward propulsion for any particular user on any particular propulsion environment.

METHODS

A single full-time manual wheelchair user was recruited to participate in the study. The subject's rear wheels were replaced by propulsiometer instrumented test wheels, which measure the 3D forces and moments applied to the handrim during propulsion. The subject sat in his wheelchair, with his hands in his lap, and the wheelchair tethered to the front of a research treadmill (Figure 1). The tether was instrumented with a load cell to measure the drag force.

Figure 1: The experimental setup included a load cell instrumented tether to measure the drag force. Handrim forces were measured using a propulsiometer instrumented wheel.

Drag force was measured for treadmill speeds of 0.45 and 1.34 m/s on grades of 0, 3, 6, and 9 degrees. The effective weight of the subject was then increased, by adding 11.3 kg (25 lb) of mass under the seat, and the drag force was re-measured for each of the treadmill speeds and grades.

The subject was then asked to propel at a self-selected speed on each of the treadmill grades for 20 pushes while handrim forces were measured. The subject then repeated the process with the additional mass under his seat. The peak forces for the 20 pushes were averaged for each of the experimental conditions. The average peak forces were normalized by the subject's body weight (bw) and by the effective drag force (EDF). The EDF was calculated according to equation (1), using ½ the measured drag force (DF), since for straight propulsion, handrim forces from only one side of the wheelchair are required due to symmetry. D_w and D_{hr} were the diameters of the wheel and handrim respectively.

$$EDF = \frac{1}{2} DF (D_w/D_{hr}) \qquad (1)$$

RESULTS AND DISCUSSION

The resulting drag force for each of the speed, grade, and weight combinations are given in Figure 2. Drag force was not affected by treadmill speed. On the level surface, drag force was not substantially affected by the additional weight. However, as the grade was increased, the drag force increased proportionally to the sine of the treadmill grade.

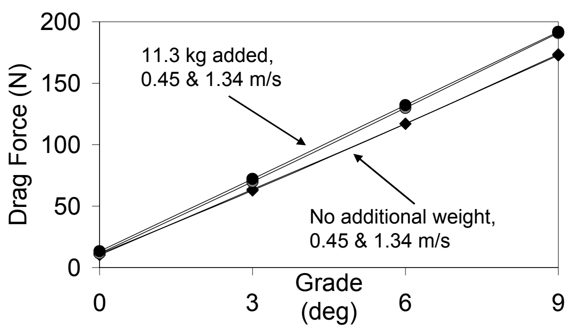

Figure 2: Drag force for varying speed, grade, and weight conditions.

The resulting peak handrim forces for the subject and the weight-added subject are shown in Figure 3 (top). The self-selected speeds for the increasing grades were: 1.48, 0.85, 0.58, and 0.49 m/s. As expected, the handrim forces increased for propulsion on increasing grades. The body weight normalized forces are simply scaled versions of the un-normalized forces. The body weight normalized scale is given on the right.

The EDF normalized forces for the subject and weight-added subject are given in Figure 3 (bottom). The EDF normalized forces exhibited a unique and insightful relationship with treadmill grade. As grade increased, the normalized forces decreased, approaching but never reaching the 1.0 physical limit. As was expected, the results were very similar between the subject and weight-added subject trials, demonstrating the effectiveness of EDF normalizing.

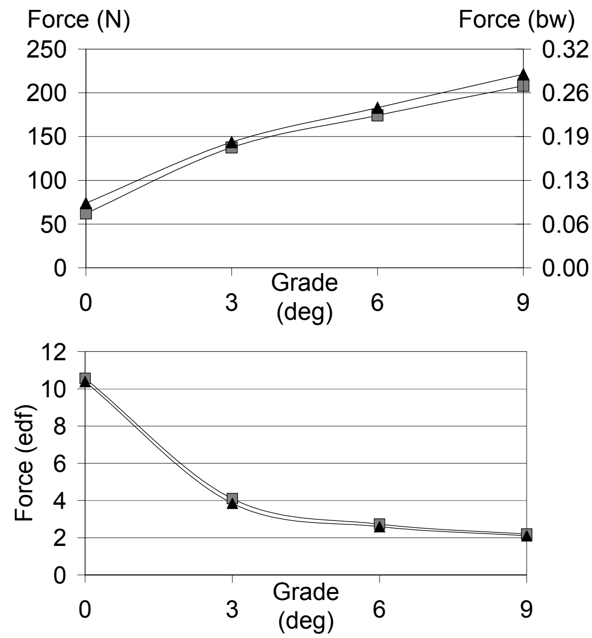

Figure 3: Peak handrim forces in both un-normalized and normalized forms. Triangular markers represent forces with 11.3 kg of mass added to the subject.

SUMMARY

The results of this pilot study suggest that normalizing wheelchair propulsion forces by the effective drag force is an effective and more analytically appropriate method for comparing biomechanics across users of varying body weights.

REFERENCES

Boninger,M.L., Cooper,R.A., *et al.* (1999) Wheelchair pushrim kinetics: body weight and median nerve function. *Arch Phys Med Rehab* **80**, 910-5.

ACKNOWLEDGEMENTS

This research was funded by NIH through SBIR Grant #2 R44 HD36533-02A2

FOOT PATH MEASUREMENT USING ACCELEROMETRY

Ken R. Fyfe and Anne H. Gildenhuys
Dynastream Innovations, Inc., Cochrane, Canada.
Email: anne.gildenhuys@dynastream.com. Web: www.dynastream.com

INTRODUCTION

The most common method for measuring the motion of body segments in space is using high-speed video camera systems. However these systems are expensive and have a limited field of view that restricts their effectiveness for studying activities outside the laboratory environment. Accelerometers can be used outside of a laboratory to detect phases of gait or to measure impact forces (Ledoux, 2001; Williamson, 2000). Others have used gyroscopes or other sensors in combination with accelerometers to get more detailed kinematics (Mayagoitia, 2002; Sabatini, 2004). Frequently these techniques are computationally demanding and thus are only applicable off-line.

In the present work, the path of the foot segment during over-ground walking and running was of particular interest since this would enable computation of instantaneous speed and total distance traveled. The goal of this project was to develop an accelerometer-based technique, applicable in real-time, that measures the path of the foot in the sagittal plane outside the lab.

METHODS

Two accelerometers (one bi-axial and one uni-axial) are mounted inside a plastic housing that attaches to the top of the foot via the shoelaces (Figure 1). The accelerometers are sampled and filtered for analysis. First the difference between the two parallel acceleration readings (*A* and *C*) is used to compute the angular acceleration of the foot. From this, the foot angle is calculated through double-integration. Knowing the angle of the foot at every instant makes it possible to resolve the signals from the bi-axial accelerometer (*A* and *B*) into horizontal and vertical components. Double integration of these components of the acceleration enables tracking of the horizontal and vertical position of the foot as it travels through space. These algorithms are implemented in real-time within the sensor pod such that summary data can be displayed on a small screen, communicated to another device (e.g. watch), or stored in memory for later uploading to a computer.

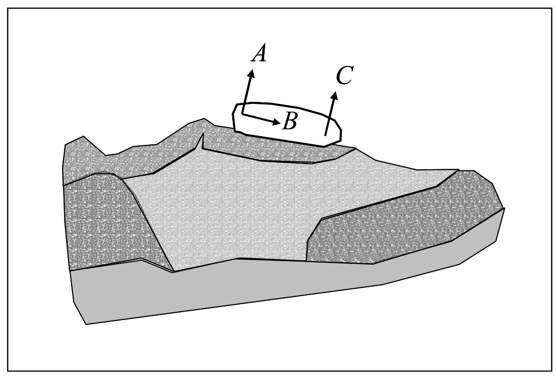

Figure 1: Sensor pod on the shoe and the orientation of the accelerometer axes within the pod.

RESULTS

The path of the foot in the sagittal plane, measured using this technique, is shown for four different speeds of locomotion (Figure 2). Also computed is the angle of the foot and the speed the foot travels. This analysis is performed in real-time on the sensor pod.

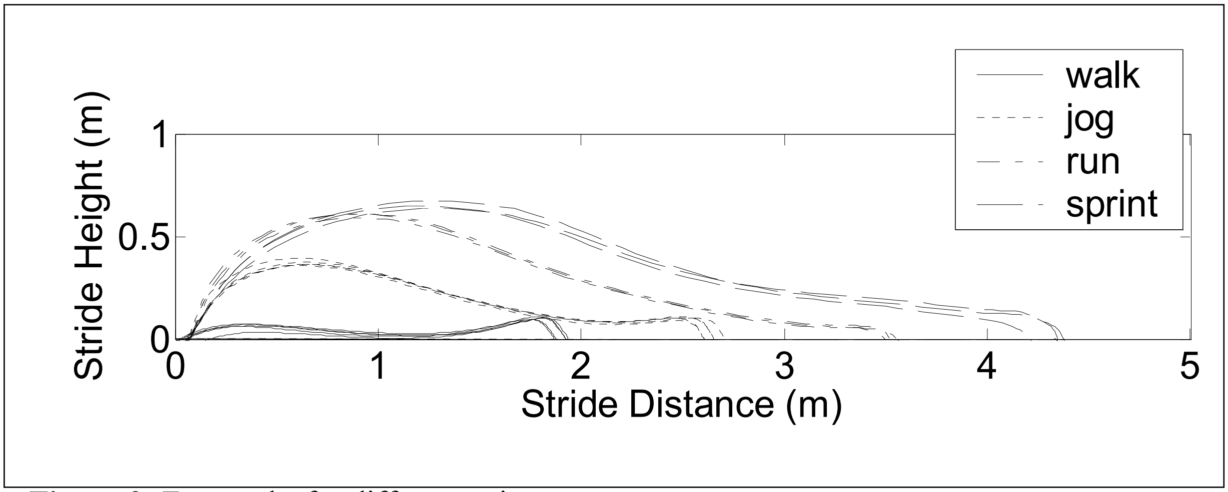

Figure 2: Foot paths for different gaits.

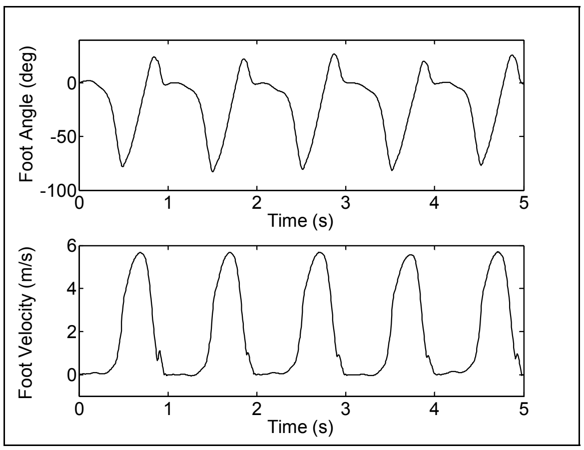

Figure 3: Foot angle and horizontal foot velocity for consecutive walking strides.

DISCUSSION

The novel technique presented here, using accelerometers to track foot paths in real-time, has many applications for gait analysis outside the laboratory environment. Research applications include analysis of gait kinematics in different populations or under different conditions (e.g. different footwear or orthotics). Other potential uses include providing real-time gait feedback during rehabilitation or for coaching purposes in a training setting.

The ability to track the path of the foot enables determination of stride lengths which, when accumulated over a run or walk, gives the total distance traveled. The technique described herein has already been applied in commercially available speed and distance monitors that have accuracies of approximately 97% (Fyfe, 1999). Another commercial application of this technique is in activity monitors that are worn on the ankle for up to one week and display the number of steps taken, the distance traveled, walking speed, cadence, step length, and more.

In summary, a technique has been described that uses accelerometry to track foot paths over multiple steps during over-ground walking or running outside of a laboratory environment.

REFERENCES

Fyfe, K.R. (1999). *US Patent 5,955,667*.
Ledoux, W.R., Hillstrom, H.R. (2001). *Clin. Biomech.*, **16**, 608-613.
Mayagoitia, R.E. et al. (2002). *J. Biomech.*, **35**, 537-542.
Sabatini, A.M. et al. (2004). *Electronic Letters*, **40**, 95-96.
Williamson, R., Andrews, B.J. (2000). *IEEE Trans. Rehab. Eng.*, **8**, 312-319.

DAILY ACTIVITY PROFILE OF TOTAL KNEE REPLACEMENT PATIENTS

William Nechtow [1,2], Thorsten Schwenke[1], Kirsten Moisio[1], and Markus Wimmer[1,2]

[1] Department of Orthopedic Surgery, RUSH University Medical Center Chicago, IL, USA
[2] Department of Bioengineering, University of Illinois at Chicago, Chicago, IL, USA
E-mail: Markus_A_Wimmer@rush.edu Web: http://www.ortho.rush.edu/tribology/

INTRODUCTION

The performance of Total Knee Replacement (TKR) components is evaluated pre-clinically using mechanical knee joint simulation devices. Contemporary simulators use input data based on gait analysis studies of normal individuals. Unfortunately, tibial component wear patterns and distributions reported from simulations do not match with wear patterns observed on retrieved tibial components [Harman, 2001]. This may be a consequence of unrealistic simulation input parameters that implement walking alone. Currently 1 million gait cycles is used to simulate a year of TKR patient activity [Seedhom, 1973]. This does not accurately reflect the actual activity range of TKR patients. The daily activity profiles, including sitting, standing, laying, walking, and stair climbing of American TKR patient life are yet undetermined.

The purpose of this study was to quantify the daily amount of time TKR patients spent sitting, standing, laying, walking, and stair stepping, and to count TKR patient daily walking steps and stair steps.

METHODS

Ten TKR patients gave informed consent to participate in this study (3 unilateral, 7 bilateral; age 78.9±7.2 yrs; height 169.3±9.9 cm; weight 77.2±17.46 kg; 5 female, 5 male). From the overall database, patients were excluded from the study if they had undergone a revision of the original MGII, a neurological diagnosis, a history of total hip arthroplasty, or were not able to walk independently without an assistive device. All tested patients had a successful TKR utilizing the MGII prosthesis (Zimmer Inc., USA). Patients were an average of 138 (range 108 to 193) months post operative and had an average RUSH modified functional knee evaluation score of 94.9±4.0.

Figure 1: Subject wearing the activity monitor.

Daily activities were monitored using a mobile data acquisition system [Wimmer, 2002]. A portable data logger sampled data from three sensors at a frequency of 30 Hz (Biomedical Monitoring Ltd., UK). Sagittal plane inclinations in the global coordinate system of the thigh and shank were measured by absolute inclination sensors (range ±70º, resolution 0.01º, SEIKA N4, Germany). The sensors were placed laterally on the operated leg and their axes were aligned with the axes of the thigh and shank. Direct knee angles were measured by an electro-goniometer placed laterally on the operated knee joint (range 270º, resolution 0.01º, Contelec, Switzerland). Sensor placement was done by the same trained physical therapist in all subject tests.

Data collection began at the subject's home in the morning. It ended in the evening immediately prior to each subject's individually specified bedtime. Patients were instructed to go about their typical daily activities. The durable and lightweight system (100g) did not inhibit movement, and normal clothing could be worn over the device (Figure 1).

A classifying algorithm was used to accurately identify standing, sitting, laying, walking, and stair stepping [Morlock, 2001]. Prior to testing, a calibration file was collected for each test subject. Based on the calibration file, the algorithm separates static and dynamic activities, then classifies activity periods as sitting, standing, laying, walking, or stair stepping. Data was normalized to a 12 hour day.

RESULTS

Measurement durations lasted an average of 719.5±51.2 minutes. Table 1 shows TKR patient daily activity percentages. The average quantity of walking steps was (3024.72±1379.23). The average quantity of stair steps was (57.56±46.91).

DISCUSSION

This study quantified the daily amount of time our patient population spent sitting, standing, laying, walking, and stair stepping, and counted TKR patient daily walking and stair steps. Contrary to the current TKR simulator testing protocol, a majority of this patient population's daily activity involved activities other than walking. A more accurate daily activity profile for a year of American TKR patient activity will provide useful input for TKR simulations, and will improve predictions of in vivo TKR component damage. Patients tested were all from the same geographical region. Different regions might experience different activity profiles. An older patient population was examined, and a more broad age group should be examined in the future.

REFERENCES

Harman, M., DesJardins, J., et al. (2001). *Proceedings of ORS'01, 1003.*

Seedhom, B., Dowson, D., et al. (1973). *Wear,* **24**, 35-51

Wimmer, M.A., Hänni, M., et al. (2002). *Proceedings of ORS'02*, 740.

Morlock, M., Schneider, E., et al. (2001). *Journal of Biomechanics*, **34**, 873-881.

ACKNOWLEDGEMENTS

This study was funded in part from Zimmer Inc., USA.

Table 1: Percent of the day spent standing, sitting, laying, walking, and stair climbing. Missing to 100% due to unclassified activities.

	% standing	% sitting	% laying	% walking	% stair climbing
Average	10.60	62.67	8.26	7.90	0.16
St. Dev.	3.80	13.12	11.66	3.71	0.16

LARGE DEFORMATION AND FLUID MODELING IN THE ANTERIOR CHAMBER IN IMPACTS TO THE HUMAN EYE

Joel Stitzel[1], Stefan Duma[1], Joseph Cormier[2]

[1] Virginia Tech – Wake Forest University Center for Injury Biomechanics
[2] Biodynamics Research Corporation

E-mail: jstitzel@wfubmc.edu Web: www.cib.vt.edu

INTRODUCTION

Recent biomechanical studies have presented dynamic computational models of fluid-filled biological tissues, such as the human aorta, uterus, and eye. These models have treated the fluid-filled volume as a control volume, with pressure-volume relationships determined by the overall change in size of the control volume. A drawback to this approach is that the mass of the fluid within the control volume does not contribute inertially to the model, a potentially important effect when the fluid density nears that of water. Four methods are detailed in the current study to model the anterior chamber of the human eye during high speed BB impacts. The first method treats fluids with linearly elastic material with low stiffness. The second uses Lagrangian elements and a modulus of compressibility, or bulk modulus. The third models the fluid with a control volume and pressure-volume relationship calculated with bulk modulus. The final approach uses a Lagrangian representation for the solids and an ALE (Arbitrary Lagrangian-Eulerian) approach for the fluids. In the case of the human eye, only the ALE approach was feasible, resulting in an accurate prediction of the stresses and strains in the globe.

METHODS

Four approaches are detailed here in order to understand the differences between several fluid/solid modeling scenarios.

1. Modeling the interior of the eye using solid elements of low young's modulus to approximate the fluid (Power, 2000, eye).

2. Modeling with a lagrangian approach with elastic fluid elements, with a bulk modulus model.

3. Modeling using a control volume, and a pressure-volume relationship as with an airbag. (Shah, 2001, aorta)

4. Modeling with an arbitrary lagrangian-eulerian (ALE) approach, with fluids as ALE and solids as lagrangian (Stitzel, 2002).

Each of these four approaches has advantages and disadvantages that will be discussed in terms of computational efficiency, accuracy, and realism. The geometry used for the finite element eye is the same as a geometry presented by Woo *et al* (1972) (Figure 1). Each model is impacted with a projectile frontally to elucidate these differences.

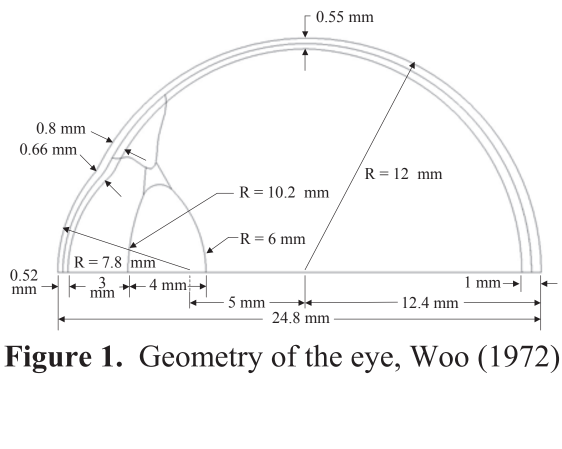

Figure 1. Geometry of the eye, Woo (1972)

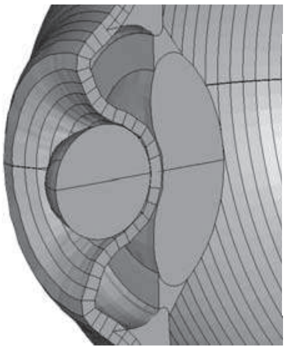

Figure 2: Front Portion of Eye with High Deformation

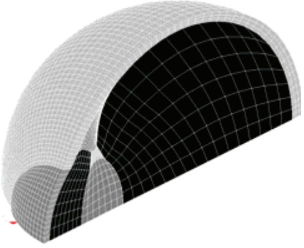

Figure 3: Model for Lagrangian Approaches

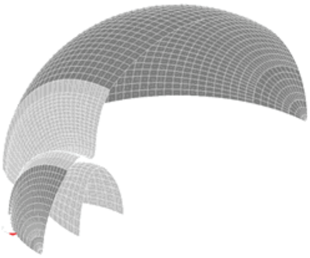

Figure 4: Control Volume Model Approach

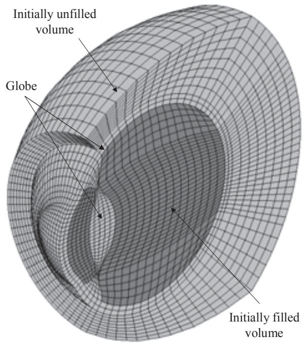

Figure 5: Eulerian Model – Eulerian Flow Field

RESULTS AND DISCUSSION

BB impacts sufficient to rupture the globe result in large deformations in the anterior chamber (Figure 1). The speeds modeled with the BB impacts were sufficient in all experiments conducted to rupture the globe, at stress of 22 MPa (Stitzel, 2002).

In both the approaches 1 and 2, the lagrangian approach for modeling interior components, and the eulerian approach, the stresses in the membrane were insufficient to cause globe rupture (Peak stress < 22 MPa). Large deformation in the anterior chamber causes a decrease in the size of elements in the anterior chamber, and a reduction in time step, so simulations could not be completed. This may seem to be the cause of lower stress, however the stresses had already peaked in simulations and thus a fundamental problem exists for stress prediction using these modeling approaches.

In the control volume model approach, large deformation was possible (Figure 4). This method is computationally the least costly of all the methods, as no elements are required for the control volume. However, in this approach, the method used by Shah (2001) is used, with a linear_fluid option. With this option, the mass of the fluid is not considered. There is unrealistic collapse of the anterior chamber, as the pressure changes uniformly throughout the eye during a dynamic event. The response of the eye visually and in terms of stress is not biofidelic, (<22 MPa in the shell).

In the ALE approach, the lagrangian mesh, embedded in an ALE control volume, shows a realistic behavior (Figure 2, Figure 5). No problems are observed with the time step and the simulation was able to run to completion. Also peak stresses were sufficient to rupture the globe, as in experiments (22+ MPa).

SUMMARY

The ALE method requires the most computational time, but is most accurate for fluid-filled tissue with large deformation.

REFERENCES

Power ED (2001) MS Thesis, Virginia Tech.
Shah CS, Yang KH, Hardy WN, Wang HK, King AI. (2001) 45^{th} Stapp. Pp. 161-182
Stitzel JD, Duma SM, Cormier JM, Herring IP (2002) 46th Stapp, Pp.
Woo SL, Kobayashi AS, Lawrence C, Schlegel WA (1972) *Ann Biomed Eng* 1:87-98.

SIMULATION OF FORWARD FALLS: EFFECT OF LOWER EXTREMITY CONTROL STRATEGY ON INJURY RISK

Jia-Hsuan Lo and James Ashton-Miller

Biomechanics Research Laboratory, Department of Mechanical Engineering, University of Michigan, Ann Arbor, MI, USA
E-mail: joshualo@umich.edu Web: http://me.engin.umich.edu/brl/

INTRODUCTION

Skilled use of the upper extremities can reduce the magnitude of the fall-related impact force on the distal forearm during a forward fall (DeGoede & Ashton-Miller, 2002). This corroborates the finding that skilled lower extremity use can reduce impact velocity during a backward fall (Sandler & Robinovitch, 2001). It is not yet known whether skilled lower extremity use can affect the impact forces resulting from forward falls. We therefore simulated the effect of different knee and hip joint control strategies during the descent phase of forward falls on the impact severity. Our main hypothesis was that modulation of hip and/or knee joint movements during the fall affect impact injury risk Φ (defined in Methods). If the hypothesis was supported, we would further identify the descent phase strategies for hip and knee control leading to the lowest (“L”) and highest (“H”) Φ, and perform an accompanying energetics analysis.

METHODS

To model forward falls from 20^{o} inclination, the linkage dynamics was modeled by a 2-D, 7-segment rigid body models using 50-percentile male anthropometric data. Segments were connected by revolute joints, and the movement of each joint was driven by a pair of agonist and antagonist joint muscle torque actuators. Each actuator employed a Hill-type model with muscle excitation-activation dynamics (Pandy et al. 1990). A feedback PID controller was used to drive each joint to a prescribed configuration (given target angle maintained with zero angular velocity) for impact.

To examine the effects of modulating knee and hip impact configuration, a factorial parametric study was conducted using target knee and hip angles as design factors. Each of the two factors was divided into five levels, and a full-factorial, 25-trial simulation was conducted. For each trial of simulation, the arm configuration was optimized via a global nonlinear programming method (“gclsolve”, Holmstroem 1999)

The outcome measure of each trial is the Hayes impact injury risk Φ, defined as the ratio of the peak impact forces at wrist, elbow, and knee to their corresponding fracture tolerances. A non-linear model predicted the vertical ground reaction force (DeGoede & Aston-Miller, 2003). Analysis of variance (ANOVA) was used to investigate the hip and knee target angle effects. $P<0.05$ was considered significant. A healthy 56 yr (81 Kg, 1.88 m) male was tested to validate the model. He performed three forward falls (from a slightly inclined stance) and landed on double-thickness gymnastic mats naturally (3 “natural” trials) and with minimum impact (3 “minimum impact” trials). Kinematic (200 Hz) and kinetic data (2 kHz) were collected using dual Optrotrak 3020s and AMTI force plates.

RESULTS AND DISCUSSION

The hypothesis was supported (ANOVA, p=0.0027, Fig.1).

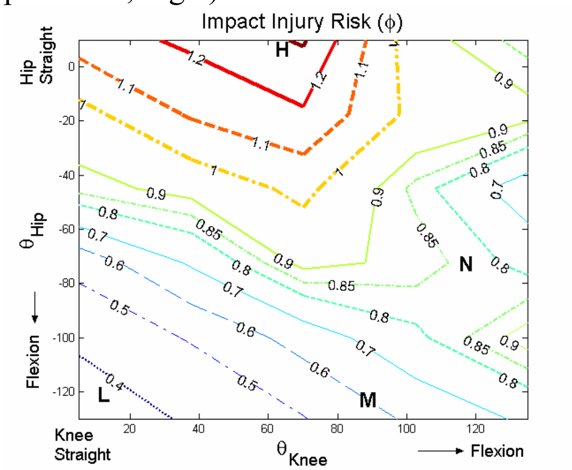

Figure 1: *Predicted Φ contours.* ***L*** *and* ***H*** *represent the low- and high-impact falls, respectively (see Fig. 2).* ***N*** *(landing on knees and hands) and* ***M*** *(landing on hands only) represent the measured natural and minimum impact trials, respectively.*

The low-impact (L) strategy involved flexed hips and extended knees, while the high-impact (H) strategy involved the opposite (Fig. 2). The pre-impact decrease in potential energy (PE) was much less in the L than the H fall (Fig. 2). Prior to impact, the hip and knee muscles performed considerable negative work in the L fall, resulting in reduced kinetic energy in the L fall. The subject volitionally modulated knee/hip angles to reduce Φ by 33%, not far from the 27% value we predicted.

SUMMARY

Lower extremity control strategy can effectively change the impact injury risk in a no initial momentum, forward fall. The sample experiment shows the potential for a middle-aged male to significantly adjust joint angles to alleviate impact severity.

REFERENCES

DeGoede, K.M. & Ashton-Miller, J.A. (2002) *J Biomech*, **35:**843-848.

Sandler, R., Robinovitch, S. N. (2001) *Trans ASME*, **123:**590-598.

Pandy, M.G., et al., (1990) *J Biomech* **23:**1185-1198.

Holmstroem, K. (1999) *Adv Model Optim*, **1:**47.

DeGoede, K.M. & Ashton-Miller, J.A. (2003) *J Biomech* **36:**413-20.

ACKNOWLEDGEMENTS

PHS grants AG 10542 and 08808.

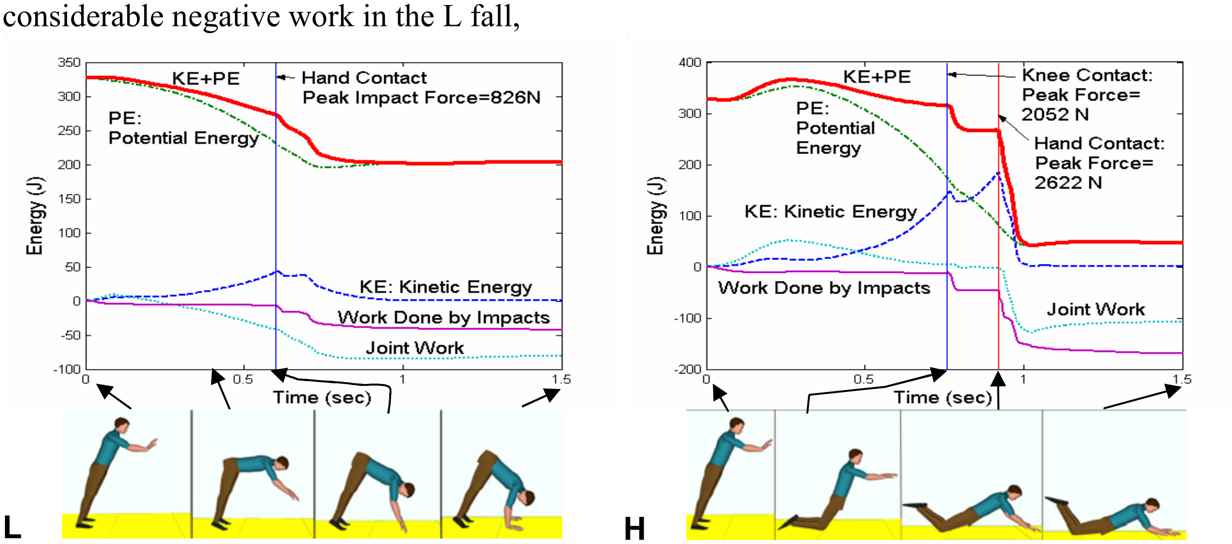

Figure 2: Energy histories of best (**L**, left) and worst (**H**, right) forward fall strategies

A BIOMECHANICAL MODEL FOR TISSUE INJURY IN PELVIC ORGAN PROLAPSE

Amanda Clark MD,[1] Qi Liu,[2] Marie Shea MS[2]

[1] Division of Urogynecology and Reconstructive Pelvic Surgery, [2] Orthopaedic Biomechanics Laboratory, Oregon Health & Science University, Portland, OR, USA
Email: clarka@ohsu.edu Web: www.ohsu.edu/obgyn/urogyn/urogyn.html

INTRODUCTION

The pelvic floor is a complex, soft tissue diaphragm that is suspended across the pelvis and supports the abdominal contents against gravity and activities that raise intraabdominal pressure. During childbirth, the pelvic soft tissues in women must distend greatly to accommodate delivery of a large fetal cranium. During birth, the vaginal connective tissues rapidly undergo a 4-5 fold elongation. After childbirth, the tissues must remodel back into a structure that can provide support for 40-60 years. Mechanical failure of pelvic floor is common in older women, and results in conditions such as pelvic organ prolapse and urinary incontinence. Women face an 11% lifetime risk for undergoing surgery for pelvic organ prolapse. (Olsen, 1997)

The anterior vagina forms the most superior layer of pelvic floor support and the most common site of vaginal prolapse. In contrast to ligamentous supports, the vagina is composite of several tissue types, smooth muscle, connective tissue, and epithelium. (Figure 1) Gynecologic surgeons posit that prolapse occurs due to attenuation or discrete breaks in the fibromuscular layer, followed by abnormal elongation of the vaginal epithelium. Surgeons believe that the fibromuscular layer lends strength to the vagina, and surgical repair aims to repair this layer. This assumption cannot be studied in human women due to the deep, inaccessible location of these tissues.

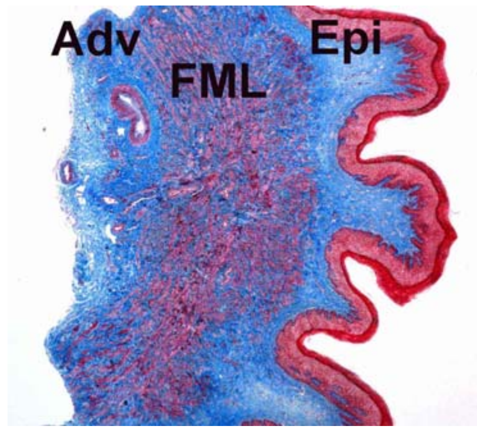

Figure 1. Full thickness histological section of anterior vaginal wall: **Adv,** adventitia; **FML,** fibromuscular layer; **Epi,** epithelium. With trichrome, smooth muscle and epithelium stain red, connective tissue, blue.

We've chosen an animal model in which to study the biomechanics of vaginal support. The Rhesus is similar to humans with respect to its semi-upright posture, its pelvic anatomy, and childbirth. Biomechanical assessment of these tissues represents a novel approach to studying the pelvic floor.

METHODS

Longitudinal strips of full thickness anterior vaginal wall were cut in a standardized "dog bone" shape. Uniaxial tensile failure load was measured on an Instron tensiometer. Deflection was measured by synchronizing optical capture of markers sutured to the specimens. A customized cryo-fixture was used to attach specimen to the tensiometer. The loading rate was 20 mm/min. The tissue dimensions were measured from digital photographs of the gross specimens and by image analysis of histological specimens.

RESULTS AND DISCUSSION

In contrast to tensile testing of ligament or skin, ultimate failure load occurred coincident with a small break in the specimen, while the majority of the tissue is visibly intact. (Figure 2a) Visible (clinical) failure of the tissue didn't occur until the load dropped almost to zero. (Figure 2b)

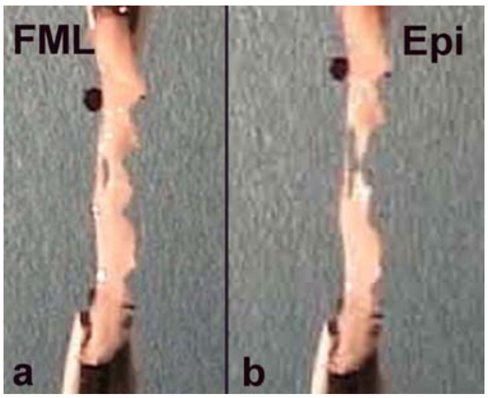

Figure 2. Lateral view of test specimens; **a.** At ultimate failure load, **b.** Just prior to clinical failure

In a majority of specimens, 80%, the 1st break occurred in the fibromuscular layer, separately or coincident with an adjoining layer. (Table 1) The remaining adventitia and epithelium undergo significant plastic elongation before complete loss of continuity of the tissue.

Table 1. Results of testing

First Layer of Break	N=83
FML	56 (67%)
FML+Adv simultaneously	8 (10%)
FML+Epi simultaneously	2 (2%)
All layers simultaneously	2 (2%)
Epi→FML→Adv	7 (8%)
Unable to visualize	8 (10%)

Ultimate elastic elongation was measured as 24% of the original length. Plastic elongation was even greater, 33% of original length before complete loss of continuity.

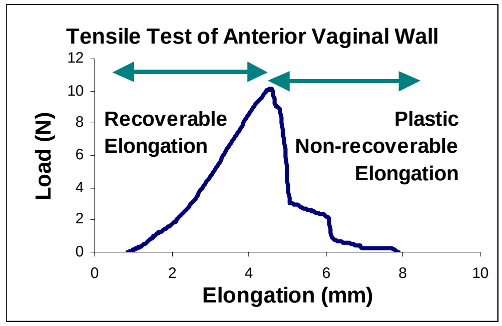

Figure 3. Example of load deflection curve demonstrating elastic and plastic elongation

SUMMARY

Our model closes represents the condition of pelvic organ prolapse, in which abnormal elongation of the vagina is associated with specific defects in the fibromuscular layer. We've shown that the injury required to weaken the vagina can occur without a visible change in the vaginal epithelium. Our work supports the clinical hypothesis that sub-clinical injury to the fibromuscular layer, as may occur during childbirth, markedly reduces the ability of the vagina to resist plastic deformation, thus leading to the development of pelvic organ prolapse.

REFERENCES

Olsen, A. L., V. J. Smith, et al. (1997). "Epidemiology of surgically managed pelvic organ prolapse and urinary incontinence." Obstet Gynecol **89**(4): 501-6.

ACKNOWLEDGEMENTS

Supported by NIH NICHD HD38673

Initial Condition Variables and Age Group as Determinates of Slip Severity

Brian E. Moyer (bmoyer@pitt.edu), April J. Chambers, Mark S. Redfern, and Rakié Cham

Human Movement and Balance Laboratory (http://www.engr.pitt.edu/hmbl),
Bioengineering Department, University of Pittsburgh, Pittsburgh, PA, USA

INTRODUCTION

Slip/fall research has primarily focused on subjects' postural reactions generated in response to slipping, based on the assumption that slip outcomes (recovery or fall) are predominantly governed by reactionary biomechanics. Although this is certainly true, subjective gait biomechanics likely contribute to the initial conditions affecting slip magnitudes as well. The relationships among initial condition variables, age group, and slip magnitude resulting from stepping onto a slippery surface are reported herein.

METHODS

A total of 27 healthy adults, 11 older individuals aged 55 to 67 years and 16 younger individuals aged 20 to 33 years old, participated in the study (Table 1). Prior to participation, each individual signed a consent form approved by the University of Pittsburgh Institutional Review Board. Exclusionary criteria included a history of neurological, orthopedic, cardiovascular and pulmonary abnormalities as well as any other difficulties hindering normal gait.

Table 1: Average subject age, height, and weight with standard deviations.

	Fem	Male	Age	Height (cm)	Weight (kg)
Young	9	7	23.5 (3.2)	171.2 (8.9)	67.6 (10.5)
Old	7	4	60.9 (4.0)	166.2 (8.1)	78.2 (10.9)

Subjects walked on a raised platform, surfaced with Armstrong commercial tile while an eight camera Vicon 612 measurement system acquired 3D motion data at 120 Hz from markers placed on their left feet. Ground reaction forces were recorded at 1080 Hz from two Bertec forceplates located near the center of the 9 m gait path. All participants wore the same brand/model of appropriately sized polyvinyl chloride hard-soled shoes. A harness protected subjects from ground contact injuries.

The gait start location was adjusted to ensure appropriate contact with the forceplates for each subject walking at their self-selected comfortable pace. After sufficient practice, subjects were informed that the first few trials would be dry and two to three trials were collected. Then, without a subject's knowledge, a diluted glycerol solution (75% glycerol, 25% water) was applied onto the left (leading) foot forceplate (0.75 x 0.4 m) and another gait trial was conducted. The coefficient of friction of the shoe-floor interface was 0.53 and 0.03 for the dry and slippery surfaces, respectively, as measured with the English XL VIT slipmeter (ASTM F1679). To mask contaminate application clues, subjects faced away from the gait path for one minute between trials while listening to loud music, all trials were conducted with lights dimmed, and subjects were instructed to focus on a target centered on the wall at the end of the gait path during ambulation. To reduce anticipatory and learning gait adjustment effects, analysis for this paper has been limited to one (unexpected) slip.

RESULTS AND DISCUSSION

Slip type was categorized as hazardous (slip distance > 10 cm) or non-hazardous (slip distance < 10 cm); note, none of the non-hazardous slips resulted in falls. Four of eleven older subjects and six of sixteen younger subjects experienced non-hazardous slips as illustrated in Figure 1.

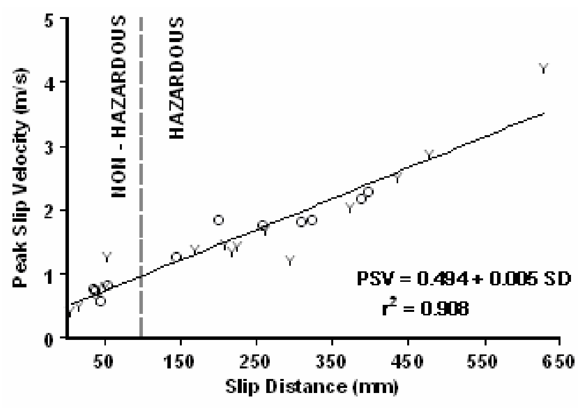

Figure 1: Peak slip velocity (PSV) versus slip distance (SD) for Young (Y) and Older (O) subjects.

To better understand why some subjects experienced non-hazardous slips while others did not, several temporal and spatial gait variables were derived: **CAD**, cadence (steps/min); **SLR**, step length ratio (step length normalized to left leg length); **GS**, gait speed (m/s); **FFA**, foot-floor angle at heel strike (deg); **FFAS**, slope of foot-floor angle at heel strike (deg/s); **LLR**, left foot normal force rate of change after heel strike (N/s). Some of these gait variables were well correlated (Table 2) including SD and PSV (Figure 1) which were both well correlated with SLR, FFA, FFAS, and LLR.

Table 2: Variable correlations

SD	0.95	-0.34	0.51	0.24	0.48	-0.47	0.49
	PSV	-0.37	0.57	0.25	0.46	-0.46	0.55
		CAD	-0.18	0.51	-0.38	0.14	0.00
			SLR	0.51	0.67	-0.70	0.67
				GS	0.17	-0.43	0.61
					FFA	-0.73	0.22
						FFAS	-0.38
							LLR

A series of two-factor (age group and slip type) ANOVAs were conducted on these variables. In general, there were significant differences (except for LLR and GS) between hazardous and non-hazardous slips. Significant age-group differences were seen in SLR, FFA and FFAS (Figure 2). No secondary interaction (age, slip type) effects were significant.

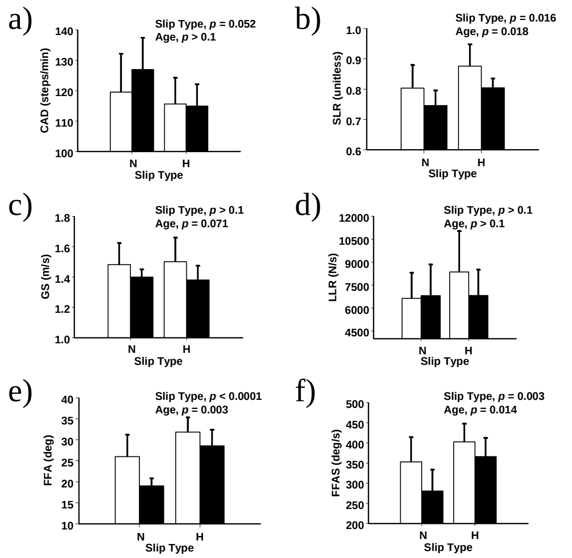

Figure 2: Associations among age-group: unfilled = young, filled = old; slip type: (N)on-Hazardous and (H)azardous; and variables of interest, a) CAD, b) SLR, c) GS, d) LLR, e) FFA, and f) FFAS. Means with standard deviations illustrated.

Because they can be determined *a priori*, initial condition variables may be useful predictors of slip severity. The outcome of a hazardous slip (fall or recovery) was not differentiable based on these variables due in large part to active recovery reactions which play a critical role in a subjects' attempts to regain balance.

ACKNOWLEDGEMENTS

Funding source: NIOSH R03 OH007533

INDUCED ACCELERATION CONTRIBUTIONS TO LOCOMOTION DYNAMICS ARE NOT PHYSICALLY WELL-DEFINED

George Chen

Honda Fundamental Research Laboratories, Mountain View, CA
Email: chen@rrdmail.stanford.edu

INTRODUCTION

Induced acceleration analysis quantifies the contributions of individual forces and moments to the accelerations, reaction forces, and powers produced during a task (Zajac *et al*., 2002). The analysis has been advocated in the assessment of muscle and joint moment function during locomotion (Anderson *et al.*, 2003; Neptune *et al.*, 2004; Siegel *et al.*, 2004; Zajac *et al.*, 2003). However, results and interpretations drawn from the analysis have differed considerably between studies. In this abstract, the induced power contributions of individual joint moments are shown not to be physically well-defined for a theoretical locomotor task.

METHODS

The theoretical locomotor task was based on a planar, rigid-body simulation created using dynamical-equations-of-motion generated by SD/FAST. The body consisted of four rigid segments – the trunk, and thigh, shank, and foot of the supporting leg. The contralateral leg was not included. Joint moments at the hip, knee, and ankle were prescribed to posturally support the configuration of the body as it rolled forward, in a pendular motion, over a pin joint connecting the tip of the foot to the ground.

Induced acceleration analyses (Zajac et al. 2002) were performed using four models in determining the contributions of joint moments and centrifugal and gravity forces to the mechanical power of the trunk and leg. Model 1 represented all body degrees of freedom, and Models 2 through 4 represented progressively fewer degrees of freedom by locking the ankle, knee, and hip joints. Since these degrees of freedom did not accelerate during the task, all four models completely described its simulated dynamics.

RESULTS

The powers contributed by each moment or force differed (both in magnitude and direction) between models, even though the total contributions were identical for all models and equal to the simulated powers (Fig. 1). Since the joint moments did not generate nor absorb energy, they redistributed power between the trunk and leg such that the contributed leg powers were equal in magnitude to the contributed trunk powers but opposite in sign. In Model 1, the knee moment redistributed much power from the trunk to the leg (i.e., power contribution to trunk was negative, contribution to leg positive), but its effect was mostly cancelled from the power redistributed from the leg to the trunk by the hip and ankle moments. As the joints were progressively locked in Models 2 and 3, the moments acting at the joints that were left unconstrained redistributed less power. In Model 4, the total redistribution of power from the trunk to the leg was attributed to gravity, without any cancellation of power flows.

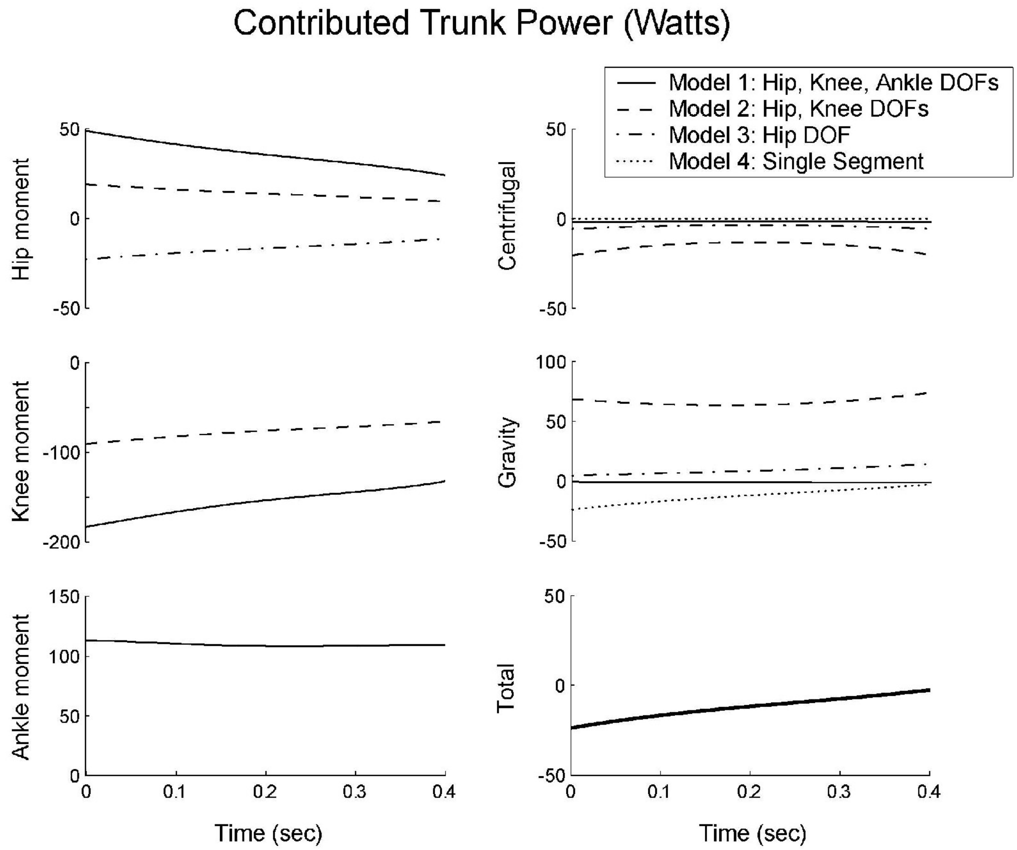

Figure 1: Trunk power contributed by each moment or force and total contribution using Models 1 through 4. Note: Total was the same for all models. The contributed leg powers were equal in magnitude but opposite in sign.

DISCUSSION

Even though all four models completely described the simulated dynamics of the task, the decomposition of mechanical powers differed between models. Clearly, these differences cannot be attributed to estimation errors. Moreover, the representation of body degrees of freedom that were posturally supported and did not accelerate during the task resulted in greater power redistribution attributed to individual joint moments. These redistributions mostly cancelled and did not contribute importantly to net changes in individual segmental energy. To conclude, induced acceleration contributions to the dynamics of a task are not physically well-defined. The application of induced acceleration analysis in the assessment of muscle and joint moment function during locomotion should be critically reevaluated.

REFERENCES

Anderson, F.C. et al. (2003) *Gait & Posture*, **17**, 159-69.

Neptune, R.R. et al. (2004) *Gait & Posture*, **19**, 194-205.

Zajac, F.E. et al. (2002) *Gait & Posture*, **16**, 215-232.

Zajac, F.E. et al. (2003) *Gait & Posture*, **17**, 1-17.

Siegel K.L. et al. (2004) *Gait & Posture*, **19**, 69-75.

STIFFNESS DURING WALKING: A COMPARISON BETWEEN CHILDREN WITH AND WITHOUT SPASTICITY

Robin D. Dorociak[1], Molly P. Nichols[1], Susan Sienko Thomas[2], and Cathleen E. Buckon[2]

[1]Motion Analysis Laboratory and [2]Clinical Research, Shriners Hospitals for Children Portland, Portland, OR, USA
E-mail: rdd@shcc.org

INTRODUCTION

During movement, the body seems to "spring" forward on muscles, tendons, and ligaments that store and return energy. This observation has led to the development of a simple spring-mass model for hopping and running (Farley, et al 1991, 1993). Similar models have been developed for walking. Holt et al (2003) proposed the calculation of vertical stiffness, k_{vert} from the excursion of the center of mass (COM); while Davis et al (1996) proposed a rotary spring model that found the stiffness, k_{rot} from the slope of the ankle moment as a function of ankle kinematics.

Muscle spasticity contributes to joint stiffness and resistance to motion. The purpose of this study was to determine whether stiffness models are able to differentiate the stiffness characteristics of children with and without spasticity.

METHODS

Twenty-one children with a diagnosis of spastic hemiplegia mean age 7.0 (± 2.3) and twenty-one age-matched peers, mean age 7.2 (± 2.2) were evaluated in the motion lab using a 6 camera VICON 370 system with two AMTI force plates. Thirteen reflective markers were placed on the lower extremities in accordance with the model described by Vicon Clinical Manager (VCM).

The vertical stiffness, k_{vert} was calculated from the pelvic origin (PO), which was assumed to be the COM, using the following equation:

$$mA_{POz} = -k_{vert}\,(POz\text{-}POz_0)$$

where m is the subject mass, A_{POz} is the vertical acceleration of the PO calculated by a three point finite difference equation (Winter 1988), POz is the current vertical position of the PO, POz_0 is the equilibrium position of the PO which was calculated to be the mean position during stance, and k is the spring constant. A linear regression model was applied to the vertical component of the acceleration and position during compression. Compression was determined to be when the PO was descending in stance.

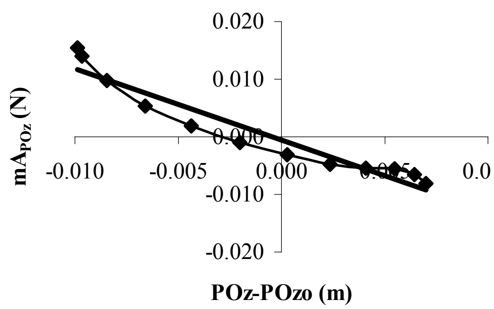

Fig. 1 mA_{POz} vs $(POz\text{-}POz_0)$ during compression in stance k_{vert} is the slope of the regression line

The rotation stiffness, k_{rot} at the ankle was calculated using a linear regression model that was applied to the ankle moment and kinematics during the period of second rocker.

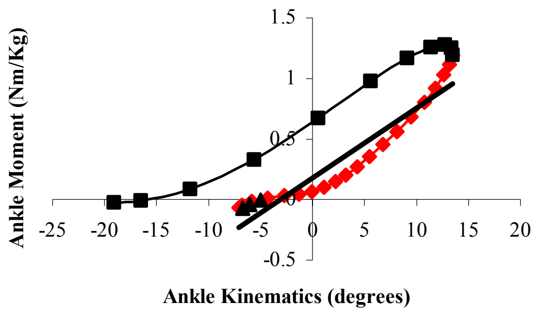

Fig. 2 Ankle Moment vs Kinematics during stance phase. k_{rot} is the slope of the regression line during second rocker (red).

For data analysis, one side was randomly chosen for the age-matched peers and the involved side was chosen for the subjects with hemiplegia. k_{vert} and k_{rot} were calculated from three trials for each subject and the mean value was used for analysis. An unpaired t-test was used to determine if a statistically significant difference for k_{vert} and k_{rot} existed between the two groups. Significance was set at $p<.05$. A step-wise regression was used to determine if any correlation existed between the k values and age, cadence, velocity, and stride length.

RESULTS AND DISCUSSION

There was no significant difference between the two groups for k_{vert} $p = .67$. The lack of difference between the groups reveals that children with mild spastic hemiplegia are able to make compensatory changes to minimize their COM excursion. A linear correlation did exist between k_{vert} and age for the two groups (control R^2 =.812 and hemi R^2 = .579), but no strong correlation existed for velocity, stride length, and cadence. The strong correlation for the age-matched peers is indicative of the normal aging process, where the children with mild hemiplegia demonstrated greater stiffness at a younger age.

There was a significant difference between the two groups for k_{rot} $p < .0001$. Four subjects in the hemiplegic group were eliminated due to the absence of second rocker. The significant difference between the groups reflects the primary involvement at the ankle in the children with mild hemiplegia. No linear correlation existed between age, cadence, stride length, and velocity.

	Control (SD)	Hemi (SD)
k_{vert}	-0.462 (0.221)	-0.491 (0.230)
R^2	0.950 (0.073)	0.940 (0.094)
k_{rot}	0.070 (0.012)	0.048 (0.017)
R^2	0.852 (0.099)	0.869 (0.104)

Table 1. k and R^2 for the two groups

SUMMARY

In summary, the stiffness models utilized in this study reveal that more than one model is needed to obtain a thorough understanding of how stiffness impacts movement.

REFERENCES

Davis, R.B. et al.(1996) *Gait & Posture*, 4:224-231

Farley, C.T. et al.
(1991) *J. of Exp Biol.*, 71:2127-2132
(1993) *J. of Exp Biol.*, 185:71-86

Holt, K.G. et al.
(2003) *J. of Biomechanics*, 36:465-471

Winter, D.A. (1988) *The Biomechanics and Motor Control of Human Gait*

ACKNOWLEDGEMENTS

Thank you to all of the subjects that volunteered and the clinical staff of the Motion Analysis Lab. This research was funded by the Shriners Hospitals for Children.

SHORTENING AND LENGTHENING FORCE-VELOCITY PROPERTIES OF HUMAN SINGLE MUSCLE FIBERS

David C. Lin[1,2] and Kasey Schertenleib[2]

[1]Programs in Bioengineering and Neuroscience and [2]Dept. of Veterinary and Comparative Anatomy, Pharmacology and Physiology, Washington State Univ., Pullman, WA, USA
Email: davidlin@wsu.edu Web: www.bioengineering.wsu.edu/alias/?davidlin

INTRODUCTION

Studies on single muscle fibers have proven extremely valuable because the contractile properties of fibers can be measured and their contractile protein isoforms identified. The force-velocity (F-V) relationship is an important property which depends upon the myosin heavy chain (MHC) isoform of a fiber. Although single fiber studies have been used extensively for some time, only a few studies have been conducted on human fibers. Specifically, only isometric and shortening data have been obtained (Bottinelli *et al.,* 1996). Lengthening F-V data are also important, especially when formulating and validating mathematical models of muscle mechanical properties.

The aim of this study is to measure F-V properties for shortening and lengthening in MHC type-identified single muscle fibers obtained from the human soleus muscle. One difficulty in obtaining lengthening F-V data is that lengthening contractions tend to damage single fibers, thus it is not possible to record a series of lengthening isotonic loads. This study circumvents this problem by application of a “force ramp” (FR) load (a linear increase in force over time), which enables recording lengthening F-V data within one perturbation (Lin and Nichols, 2003). Further, these data can and will be used in the development of single-fiber muscle models, which can be later incorporated into population models to simulate whole muscle properties.

METHODS

Excisional biopsies from the soleus muscle were taken during Achilles tendon repair surgeries. The biopsies were stored in a cold (-20ºC) skinning solution so that single fibers could be separated for mechanical experiments. Institutional Review Board approval was obtained for these procedures.

Single fibers were attached to a force transducer and motor. Sarcomere length was set to 2.5 μm by laser diffraction. Fibers were maximally activated at room temperature (21ºC) in a high calcium concentration solution (pCa=4.0). During activation, a shortening FR load was applied first, followed by an isometric period which allowed the force to return a steady-state level, a lengthening FR load, and a final isometric period. Force and length changes were recorded. MHC type of the fiber was analyzed by SDS-PAGE electrophoresis.

The mechanical data were first inspected for changes in the isometric force before and after the FR protocol. If a greater than 10% decrease in isometric force was observed, the data from that fiber was not used. Length data were lowpass filtered at 50 Hz and differentiated to calculate velocity. F-V plots were generated by plotting the force (normalized by isometric force, F_o) and velocity (normalized by initial fiber length, L_o) at each point in time. Two hyperbolic functions, one for shortening and another for lengthening (Mashima, 1972), were fitted to the F-V data for each fiber. Average F-V curves were calculated from these fits.

RESULTS AND DISCUSSION

Experimental data have been obtained from 18 single fibers. 13 of the fibers were 100% of type I MHC and the remaining fibers were "hybrid" fibers, which have more than one type of MHC isoform (types I, IIx, and IIa). The experimental data reported here will be of the type I MHC fibers.

Experimental data obtained from a type I soleus fiber in response to the FR loads are shown in figure 1 (only the FR portions of the perturbation are shown). Similar to single fibers from cat soleus muscle, the FR loads produced hyperbolic F-V curves with a velocity offset for both shortening and lengthening loads (Lin and Nichols, 2003). Average F-V data from the 13 type I fibers are shown in figure 2.

Comparison to the shortening F-V data obtained by Bottinelli *et al.* (1996) cannot be made directly because only F-V data from 12ºC were reported. Maximal shortening velocity for type I fibers at 22ºC was measured to be approximately 1 L_o/s in this study. Lengthening F-V data have not been recorded in human single fibers. Cat soleus

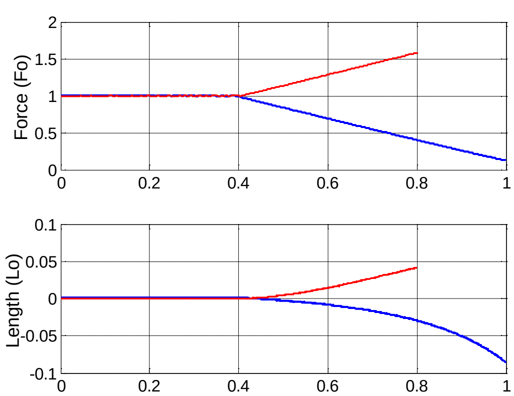

Figure 1. The shortening and lengthening FR portions of the perturbation during activation of a single muscle fiber.

(type I) fibers show a maximal force of ~1.5 F_o, while caudofemoralis fibers (type IIx) show a much greater maximal force of >1.8 F_o (Lin and Nichols, 2003; unpublished data). In this respect, human type I fibers in this study are comparable to type IIx fibers in the cat. This suggests that not all type I fibers behave similarly, rather depending on species differences, probably at the level of crossbridge kinetics.

SUMMARY

Force-velocity data were collected from type I MHC single muscle fibers obtained from human soleus biopsies. Both shortening and lengthening data were obtained. Lengthening data in this study showed significant differences from cat type I fibers.

REFERENCES

Bottinelli, R., *et al.* (1996). *J. Physiol. (Lond.)*, **495.2**, 573-586.

Lin, D.C. and Nichols, T.R. (2003). *ASME J. Biomech. Eng.*, **125**, 132-140.

Mashima *et al.* (1972). *Jpn. J. Physiol.*, **22**, 103-120.

ACKNOWLEDGEMENTS

Support provided by the Whitaker and Cadeau Foundations.

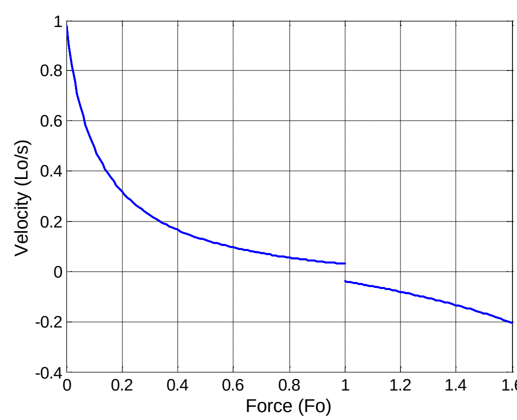

Figure 2. Average F-V data for type I single fibers.

MRI-BASED GEOMETRY OF NECK MUSCLES FOR BIOMECHANICAL MODELS

Richard Lasher[1], Travis Meyer[1], Kyle Kraemer[1], Patrick Gavin[2], Anita Vasavada[1]

[1]Program in Bioengineering, [2]Department of Veterinary Clinical Sciences (Radiology)
Washington State University, Pullman, WA USA
E-mail: vasavada@wsu.edu Web: www.bioengineering.wsu.edu\alias\?AnitaVasavada

INTRODUCTION

Accurate representation of muscle paths is important to compute muscle length, moment arm and force-generating capacity for biomechanical analyses. Neck muscles are constrained by surrounding musculature, soft tissue and bones, and differences between the actual path and straight line models may be significant, especially for the superficial neck muscles such as trapezius. Our goals are to improve an existing biomechanical model (Vasavada *et al.*, 1998) by calculating centroid paths of neck muscles from magnetic resonance images (MRI) and determining geometric constraints over a 3-D range of motion.

METHODS

MRI scans were taken of two male subjects. In the first subject, scans were taken in the neutral posture only. In the second subject, scans were taken in five positions: neutral, 30° flexion, 30° extension, 30° axial rotation and 20° lateral bending, using a jig that ensured proper head positioning. Axial proton density weighted MR images (TR = 2500 ms; TE = 18 ms; slice thickness 4.5 mm; gap 0.5 mm) were obtained from the base of the skull to T2. The boundaries of 15 major neck muscles were outlined (Figure 1), and muscle centroids from each image plane were used to define the muscle paths. In each posture, we calculated the difference between centroid and straight line path lengths, and the change in centroid path length from neutral. Centroid paths were fit to straight lines, circles and ellipses to determine the best fit geometry.

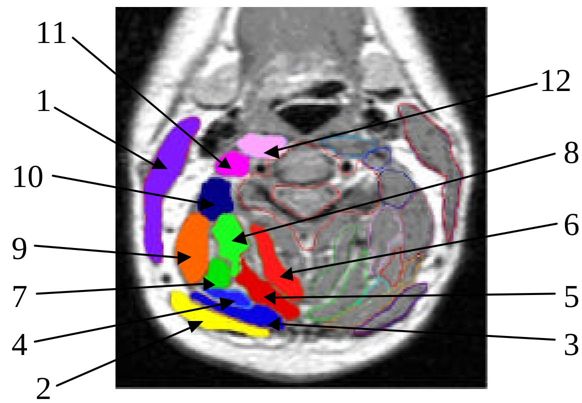

Figure 1. Axial proton density weighted MRI scan of subject 1 at the level of C4, with neck muscles outlined and identified. 1(purple)=Sternocleidomastoid, 2(yellow)=Trapezius, 3(blue)=Splenius Capitis, 4(blue)=Splenius Cervicis, 5(red)=Semispinalis Capitis, 6(red)=Semispinalis Cervicis, 7(green)=Longissimus Capitis, 8(green)=Longissimus Cervicis, 9(orange)=Levator Scapulae, 10(navy)=Scalenus, 11(dark pink)=Longus Capitis, 12(light pink) = Longus Colli.

RESULTS AND DISCUSSION

Centroid paths and the original model straight line paths are depicted (Figure 2) using Software for Interactive Musculoskeletal Modeling (SIMM; Musculographics, Santa Rosa, CA). We compared straight line and centroid path lengths in four neck muscles (trapezius, sternocleidomastoid, scalenus and levator scapula) and five postures for subject 2. For sternocleidomastoid, scalenus and levator scapula, the difference between straight line paths and centroid paths ranges from 4-8% in all postures. For trapezius, straight line paths underestimate the centroid path length by 17-21% in all postures.

The change in muscle length from neutral to a rotated posture was normalized by the angular change in radians. This is an estimate of a muscle's moment arm for that direction of motion. (The exact calculation of moment arm is the instantaneous change in length with rotation). Trapezius shortens most in extension, followed by ipsilateral bending and contralateral axial rotation. Sternocleidomastoid shortens most during flexion, followed by ipsilateral bending and contralateral rotation. In contrast, the model predicts greater shortening in lateral bending than flexion or extension for both of these muscles. Levator scapula and scalenus shorten mostly in lateral bending.

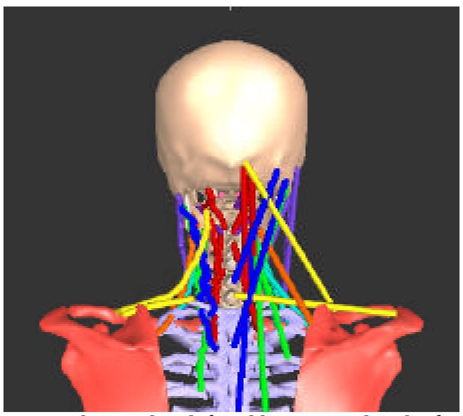

Figure 2. Neck muscles defined by centroid paths from subject 1 (left) and original model with straight line paths (right) in SIMM. Muscles are identified by color in Fig. 1.

Some muscles shorten in two opposite directions in the same plane. For example, sternocleidomastoid is shorter in both flexion and extension compared to neutral. This suggests that sternocleidomastoid is longest near the neutral posture and has flexion moment arms in flexed postures and extension moment arms in extended postures. This result is predicted in the model of the cleiod-occipital segment of sternocleidomastoid. In addition, levator scapula shortens slightly in both extension and flexion, and scalenus shortens in both ipsilateral and contralateral bending. These results were not predicted from the model.

For all muscles and all positions, centroid paths have better fits with curved lines (circles or ellipses) than straight lines. Sternocleidomastoid and scalenus are closest to straight lines: R^2 values for linear fits range from 0.91-0.95, whereas R^2 for ellipses range from 0.94-0.97 for all postures. R^2 values for linear fits to levator scapula range from 0.89-0.91, whereas R^2 values for ellipses range from 0.93-0.94. Trapezius had the worst fits to straight lines (R^2 0.74-0.81); fits to ellipses yielded R^2 values of 0.95-0.96. These fits could be improved by examining the curvature changes in specific regions of the muscle.

A limitation of this study is that centroid path data are spaced at 5 mm axial intervals, and exact locations of origins and insertions are difficult to identify. Further, more positions may be needed to compare to model predictions of muscle length and moment arms.

SUMMARY

We have characterized the geometry of neck muscle paths based on MR images. These data can be used to improve the model representations of neck muscles. The centroid paths will be incorporated into the existing neck model in SIMM, and wrapping surfaces will be used to mimic anatomical constraints. Having centroid data from different postures ensures that the wrapping surfaces constrain the muscles accurately through the range of motion. These improved models will be used to analyze neck muscle mechanics, control and injury.

REFERENCES

Vasavada *et al.* (1998). *Spine*, **23**: 412-421.

ACKNOWLEDGEMENTS

We thank Rob Houston, Christopher Robinson and Kasey Schertenleib for technical assistance. Funding has been provided through the Whitaker Foundation.

ANGULAR ACCELERATION OF THE HEAD/NECK SYSTEM INDUCED BY STERNOCLEIDOMASTOID

Prasanna Krithivasan[1] and Anita Vasavada[1,2]
[1]Department of Mechanical and Materials Engineering, [2]Program in Bioengineering
Washington State University, Pullman, WA USA
E-mail: vasavada@wsu.edu Web: www.bioengineering.wsu.edu\alias\?AnitaVasavada

INTRODUCTION

Sternocleidomastoid (SCM) is a major muscle connecting the head to the shoulder girdle. The muscle originates on the sternum and clavicle and inserts on the mastoid process and occipital region of the skull. SCM has an extension moment arm in the upper cervical region (skull to C2) and a flexion moment arm in the lower cervical region (C2 to T1) (Vasavada *et al*. 1998). The posterior translation and extension of the head relative to the torso that occur during whiplash potentially damage SCM and other structures of the neck. SCM appears to have the capability to resist these motions; however, there have been no studies documenting the accelerations induced by SCM. The goal of this study was to calculate the angular acceleration generated by SCM with changes in head and neck posture.

METHODS

We used a biomechanical model of the neck (Vasavada *et al*. 1998) developed in Software for Interactive Musculoskeletal Modeling (Musculographics, Santa Rosa, CA). Sternocleidomastoid is defined as three subvolumes: sternomastoid, cleidomastoid and cleido-occipital (Figure 1). Head and neck kinematics were simplified to two degrees of freedom in the sagittal plane. The lower cervical joint includes flexion/extension motion between C2 and T1, and the upper cervical joint includes flexion/extension between the skull and C2. SCM moment was calculated at each joint by multiplying peak muscle force by the moment arm.

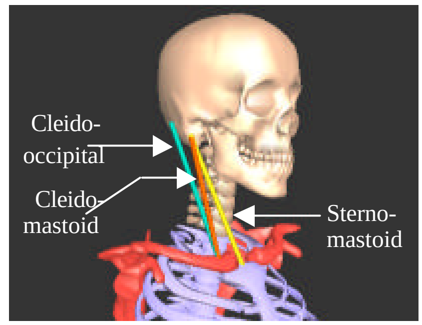

Figure 1: Model of sternocleidomastoid illustrating the three subvolumes.

The lower cervical segment length is the distance from the center of rotation (CR) of C7-T1 to the CR of C2-C3, and the upper cervical segment length is the distance from the CR of C2-C3 to the head center of mass (Table 1). To estimate the moment of inertia of the lower cervical segment, it was assumed to be a cylinder with a circumference equal to the 50th percentile male neck (Gordon *et al*., 1989).

Table 1: Mass, length, moment of inertia of segments. *Data from Garcia and Ravani (2003).

	Upper Cervical	Lower Cervical
Mass (kg)	5.5*	1.476*
Length (m)	0.081	0.102
Moment of Inertia ($kg\text{-}m^2$)	0.035*	0.0045

The equations of motion of a double inverted pendulum were used to calculate the angular accelerations. The torques exerted on one segment due to the motion of the other segment depend on angular acceleration and velocity of both segments, as well as their relative orientations. Initial angular velocities were equal to zero.

RESULTS AND DISCUSSION

The moment generated by SCM at either joint depends on the orientation of both joints (Figure 2). The upper cervical extension moment increases with both upper and lower cervical extension. The lower cervical flexion moment increases with both upper and lower cervical flexion.

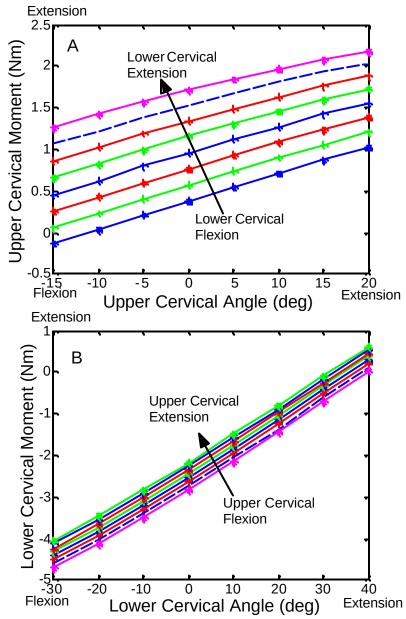

Figure 2: SCM moments. (A) Upper cervical moments with lower cervical angle from –30º flexion to 40º extension. (B) Lower cervical moments with upper cervical angle from -15º flexion to 20º extension.

In the neutral posture, SCM accelerates the lower cervical segment into flexion and the upper cervical segment into extension (Figure 3). Both the extension acceleration of the upper segment and the flexion acceleration of the lower segment decrease with upper cervical flexion. Conversely, these accelerations increase with upper cervical extension. With flexion of the lower cervical segment, both extension acceleration of the upper segment and flexion acceleration of the lower segment increase. When the lower segment is extended, both the upper cervical extension acceleration and lower cervical flexion acceleration decrease. In fact, when the lower cervical segment is extended more than 25º, SCM induces an *extension* rather than flexion acceleration in the lower cervical segment. This an example of a multiarticular muscle accelerating a joint in the direction opposite to its applied torque (Zajac and Gordon, 1989).

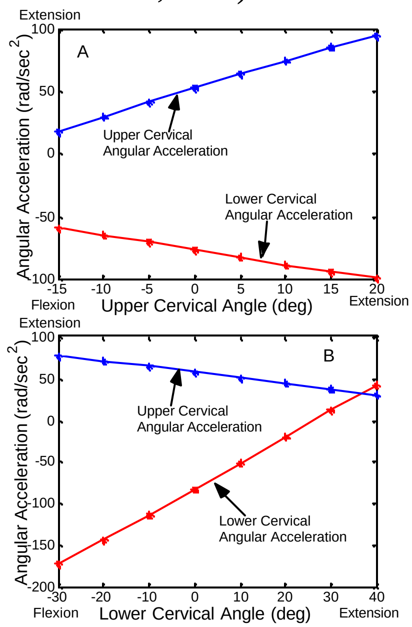

Figure 3: Angular acceleration induced by SCM. (A) Varying upper cervical angle with lower cervical angle at neutral (0º). (B) Varying lower cervical angle with upper cervical angle at neutral (0º).

SUMMARY

We calculated the induced accelerations of sternocleidomastoid with variations in head and neck posture. Although SCM generally accelerates segments in the same direction as its moment arm, in some extended postures the induced accelerations are opposite to its moment arm in the lower cervical region. If non-zero initial velocities were simulated, there may be other postures where induced accelerations are opposite to moment arm. In the future we plan to calculate the induced accelerations of SCM during the head and neck kinematics that occur during whiplash.

REFERENCES

Garcia and Ravani (2003). *J Biomech Eng*, **125**:254-265.

Gordon *et al.* (1989). US Army, Natick, MA.

Vasavada *et al.* (1998). *Spine*, **23**: 412-421.

Zajac and Gordon (1989). *Ex Sport Sci Rev*, **17:**187-230.

ACKNOWLEDGEMENTS

Funding from the Whitaker Foundation.

INSTRUMENTATION SYSTEM FOR BIOMECHANICAL ANALYSIS OF FACTORS AFFECTING BACKPACK USER COMFORT

Jennifer L. Springer, B.S. and David A. Hawkins, Ph.D.

Human Performance Laboratory, Biomedical Engineering Graduate Group,
University of California, Davis, CA

INTRODUCTION

Backpacks provide a convenient means of hands-free load carriage and are used by many people in a variety of settings. The primary purpose of backpacks is to maximize load carriage capacity while minimizing user discomfort. Discomfort is difficult to quantify because it may result from many factors and user sensitivity to these factors varies. However, feedback from backpack users suggest that localized pressure (perhaps blocking circulation and/or causing nerve impingement), localized temperature, motion of the pack relative to the user (causing chaffing), and muscle fatigue are important factors affecting comfort. These factors are directly related to backpack design variables such as load capacity and distribution, materials and venting, shoulder and hip belt area and contour. Studies have been conducted to understand how backpack design affects these factors (LaFiandra et al. 2002, Stevenson et al. 2003), but to date there is no instrumentation system available to record, in-the-field, those quantities indicated above. The purpose of this study was to develop an instrumentation system that could assist backpack designers by recording shoulder and hip pressure profiles, localized skin temperature, relative motion of the pack relative to the user, and muscle activation during in-the-field backpack usage.

METHODS

We established the following design criteria for the backpack instrumentation system.

1. Measure dynamic pressures acting between the pack and body in real-time (pressure levels between 0 and 48 kPa).
2. Measure skin temperature along back and under the hipbelt (temperature range of 25 to 40°C and a resolution of 0.2°C).
3. Measure relative motion of the pack and torso to within 2 cm accuracy.
4. Measure muscle activity of four to six muscle groups.
5. Measure forward lean of the backpacker (50° range and 0.05° resolution).
6. Instrumentation system should have minimal affect on backpack user movement and should be portable.

A single subject was tested to determine the utility of the instrumentation system. A 23 year old female subject walked on a level treadmill at a rate of 1.1 m/s with an internal frame backpack with hipbelt. Trials were done with a 19 kg load (about 33 % body mass) placed in high and low positions within the backpack, and with and without a hipbelt (load in high position). Sample results of muscle usage and localized pressure levels are presented to illustrate the utility of the system.

RESULTS AND DISCUSSION

The instrumentation system designed to satisfy the stated design criteria consisted of:

1. Tekscan FlexiForce® 0-4.45 N sensors which have acceptable drift, repeatability, linearity and hysteresis under static loading on either a flat or curved surface with a radius of curvature greater than 32 mm (Ferguson-Pell et al. 2000). With a sensing area of 0.79 cm^2, approximately 48 of these sensors will be needed to measure the force and pressure applied under a shoulder strap.
2. Two YSI thermisters with a range of 0 to 100°C accurate to within ±0.2°C and thin enough to fit comfortably between the backpack and body will be used.
3. Memsic ±10g dual axis accelerometers will be placed as close to one another as possible on the backpack and body. Acceleration signals will be double integrated to quantify relative motion.
4. A custom EMG system with surface electrodes allows up to six different muscle groups to be monitored.
5. The Applied Geomechanics 902 biaxial tilt sensor with a 50° range and 0.01° resolution meets the desired criteria.
6. Amplification/conditioning circuits were designed for the above transducers. Conditioned transducer outputs were wired to a 68-pin connector that was connected to a data acquisition PC-Card manufactured by National Instruments (DAQCARD-Al-16E-4) housed in a laptop computer (Hewlett Packard Pavillion notebook n5425). The entire system weighs less than 45 N and can fit into standard backpacks.

Sample muscle activity and localized shoulder force data are shown in Figure 1 and Figure 2 respectively. Abdominal muscle activity increases as the load is moved to lower positions. Force levels between the body and shoulder straps in positions on top of the shoulder just above the clavical bone (1), on the clavical bone(2), under the clavical bone (3), and two inches down on the anterior shoulder (4) show that the force and pressure levels are highest on the top of the shoulder, specifically on the clavical bone.

SUMMARY

The backpack instrumentation system satisfies all the stated design criteria and provides a useful tool for analyzing biomechanical factors that affect backpack user comfort. Force sensors measure force distribution to the shoulders and can provide a pressure mapping of contact areas. Temperature sensors locate high temperature areas. Accelerometers measure relative motion of the backpack. Electromyography monitors muscle activity. And a tilt sensor measures forward lean of the backpacker.

REFERENCES

Ferguson-Pell, M. et al. (2000). *Medical Engineeing & Physics*, **22**, 657-663.

LaFiandra, M. et al. (2004). *Medicine and Science in Sports and Exercise*, **36**, 460-467.

Stevenson, J. et al.(2003). *ASB 2003*.

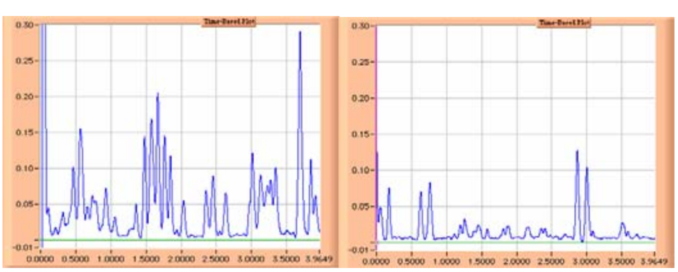

Figure 1: Abdominal activity with low and high load position

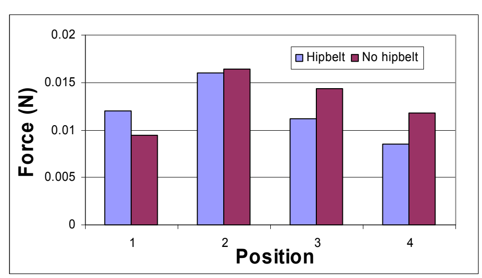

Figure 2: Force under shoulder strap

MUSCLE-TENDON ULTRASOUND: QUANTITATIVE CONSIDERATIONS

Lisa Coughlin, B.S. and David Hawkins, PhD.

Human Performance Laboratory, Biomedical Engineering Graduate Group
University of California, Davis, CA USA
E-mail: dahawkins@ucdavis.edu Web: http://www.exb.ucdavis.edu/faculty/hawkins/index.htm

INTRODUCTION

In the last ten years ultrasound has been used as a non-invasive tool for characterizing muscle-tendon structure and behavior in vivo. Ultrasonography is an exciting tool, but it has limitations that have not been adequately considered by many using it to quantify muscle-tendon structure and deformation. Ultrasound images of biological structures are based on an assumed speed of sound (SOS) through these structures and the signal attenuation. However, biological tissues transmit and attenuate sound waves differently. Therefore ultrasound images may be distorted in the direction perpendicular to the ultrasound probe surface if the SOS in the biological structures varies from the value used in the ultrasound algorithms. This distortion would directly affect structure thickness and cross-sectional area measurements, important biomechanical quantities that appear to have been reported in the past without consideration for this distortion (Gillis et al 1993, 1995; Kawakami et al 1995; Kubo 2003[1], 2003[2]; Ito et al 1998; Sipila et al 1996). The purpose of this study was to investigate the error associated with tendon, fat and muscle thickness measurements obtained using a commercial ultrasound system.

METHODS

Experiments were conducted to quantify the speed of sound in tendon, fat and muscle for the purpose of determining thickness errors that could result when using a commercial ultrasound system. Sutures were tied to the ends of bovine tendon and fat, and chicken muscle samples. Samples were tested sequentially. The free ends of the suture were secured to a suspension device located in a tank and the sample was slightly loaded in tension (Figure 1). The sample's thickness was measured six times with calipers. The tank was filled with water and a Hitachi EUP L53 ultrasound probe was positioned over the sample. Ultrasound images were collected and the thickness of the sample was measured six times from digital images created from the Hitachi EUB 6500 Ultrasound System (this system assumes an average speed of sound in body tissues of 1540 m/s). Thickness measurements were repeated with the calipers to check for any hydration changes. Average caliper and ultrasound image thickness measurements were compared.

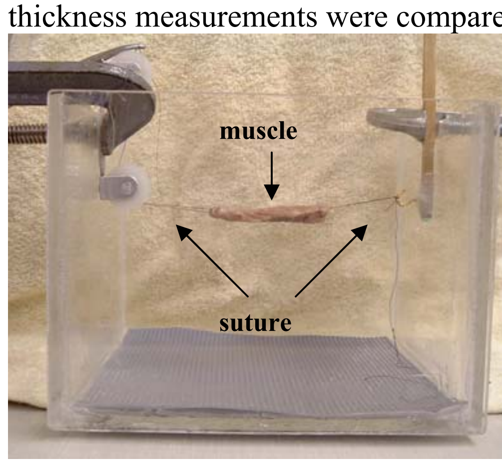

Figure 1: Suspended muscle in test chamber.

The SOS within each sample was determined from

$$SOS = \frac{Tc \bullet 1540}{Tu}$$

where Tc and Tu are the sample thickness measured using calipers and from the ultrasound images, respectively, and 1540 m/s is the SOS used to create the ultrasound image.

Speed of sound measurements were compared to literature values. The percent errors between the thickness measured using calipers and from the ultrasound images were determined.

RESULTS AND DISCUSSION

The calculated SOS values, percent difference from the thickness calculated for the ultrasound system (1540 m/s), and the percent difference from the thickness estimated with literature SOS values appear in Table 1 for tendon, fat, and muscle. The SOS values calculated using the caliper measured thickness matched well with literature values. Small SOS variations can be attributed to species, temperature and tissue density variations.

SUMMARY

In order to determine tendon material properties such as stress, it is necessary to measure both force and cross-sectional area. As stated previously studies have used tendon cross-sectional area values from ultrasound measurements without considering the differences between the SOS in body structures and the SOS used by the ultrasound system to create the images. These experiments show that ultrasound underestimates the thickness, and therefore area of a tendon by about 5 %, overestimates these dimensions for fat by about 7 %, and underestimates the thickness for muscle by about 1 %.

REFERENCES

Canals, R. et al. (1999) *IEEE*, **46**, 1527-1538.

Garcia, T. et al. (2003) *Ultrasound Med Biol.,* **29**, 1787-1797.

Kawakami, Y. et al. (1995) *Eur J Appl Physiol.,***72**, 37-43.

Kubo K, et al. (2003[1]) *Med Sci Sports Exerc.,* **35**, 39-44.

Kubo K, et al. (2003[2]) *Acta Physiol Scand.*, **178**, 25-32.

Gillis, CL. et al. (1993) *Am J Vet Res.,* **54**, 1797-1802.

Gillis, CL. et al. (1995) *Am J Vet Res.*, **56,** 1270-1274.

Ito, M. et al. (1998) *J Appl Physiol.,* **85**, 1230-1235.

Sipila, S. et al (1996) *Arch Phys Med Rehabil.*, **77,** 1173-1178.

ACKNOWLEDGEMENTS

This work was supported by the National Science Foundation BES 02-01829

Table 1: Tendon, Fat, and Muscle SOS Results and % Difference in Thickness.

Tissue	Reference	SOS m/s	% Diff. to 1540 m/s	% Diff to Literature
Tendon	Coughlin	1618	-5.09 %	1.92 % (1)
Tendon	Garcia (1)	1650	-7.14 %	N/A
Fat	Coughlin	1432	7.00 %	1.23 % (2)
Fat	Canals (2)	1450	5.84 %	N/A
Muscle	Coughlin	1572	-1.21 %	0.454 % (3)
Muscle	Canals (3)	1580	-2.6 %	N/A

IN VIVO QUANTIFICATION OF ACHILLES TENDON DYNAMIC CREEP

Russell Dunning, B.S. and David A. Hawkins, Ph.D.

Human Performance Laboratory, Biomedical Engineering Graduate Group
University of California, Davis
Email:dahawkins@ucdavis.edu Web: http://www.exb.ucdavis.edu/faculty/Hawkins/index.htm

INTRODUCTION

Tendons are important viscoelastic structures, transmitting forces between muscle and bones. A muscle's ability to actively develop force depends in part on its length and velocity, which are directly affected by the stiffness of the muscle's associated tendons. The stiffer the tendon, the smaller the length change and velocity during shortening and the greater the length change and velocity during lengthening. Understanding the viscoelastic behavior of tendon is fundamental for understanding muscle-tendon mechanics and for advancing preventative, therapeutic, and sports medicine.

Ex-vivo studies show tendons elicit viscoelastic behavior (stress relaxation, creep, hysteresis, etc.) (De Zee, et. al., 2000) and often experience permanent deformation and stiffness changes in response to repetitive loading. This raises some perplexing questions about how these tendons respond to repetitive loading in-vivo (tendons obviously restore rest-length over some finite time in-vivo) and whether ex-vivo studies accurately reflect in-vivo tendon behavior.

This study quantified the magnitude of Achilles tendon dynamic creep in-vivo and compared these results to ex-vivo results. This is the first study to the authors' knowledge that has quantified dynamic creep during submaximal loading of the Achilles tendon without preconditioning.

METHODS

Dynamic creep of the Achilles tendon was quantified in-vivo for a healthy male subject (42 years of age, 734 N). The testing setup included an ultrasound system (Hitachi EUB 6500) with two EUP L53 linear probes, a 4000 N force sensor (Omega Engineering), and a water tank to house the lower limb (Figure 1). The knee and ankle joints were maintained at 90° angles. One ultrasound probe was located directly over the Achilles tendon-calcaneus osteotendinous junction (OTJ). The second probe was located directly over the Achilles tendon-Gastrocnemius muscle-tendon junction (MTJ) a known distance from the first probe. Labview software was developed to capture force and ultrasound images simultaneously. Data were collected at 30 Hz.

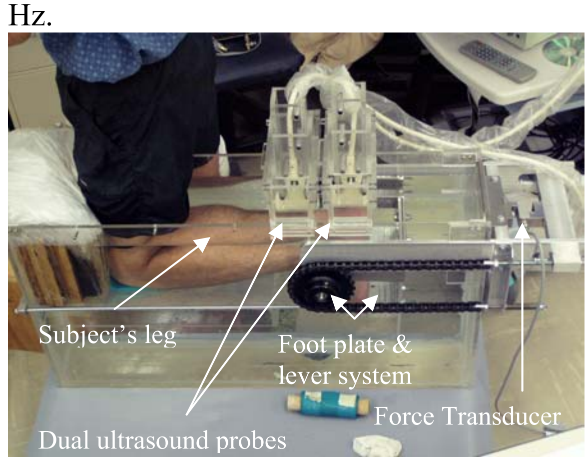

Figure 1: Testing setup used to quantify the dynamic creep of the Achilles tendon.

The subject avoided placing load on the Achilles tendon of the right leg for approximately one hour prior to testing. The subject then performed over 300 cyclic contractions attempting to produce 25 % of maximum voluntary force in 1 second intervals. Data were collected for the initial 3 cycles and then for 5 cycles after every 50 cycles.

Force data were reviewed to identify contractions of similar force magnitude and ultrasound images were digitized to determine Achilles tendon length. The images were analyzed via National Instruments software, IMAQ Vision Builder 6.1. Achilles tendon length was calculated as the length between OTJ and MTJ. Tendon strain was defined as the difference between tendon length at peak force during a contraction and in its rest state prior to the start of testing, divided by the initial rest length. Tendon strain was plotted as a function of cycle number.

RESULTS & DISCUSSION

The Achilles tendon experienced dynamic creep. Tendon strain increased from 1 % to 2.4 % over the first three cycles and increased to 3 % over 50 cycles, appearing to plateau to 3.2 % thereafter (Figure 2). The asymptotic response equates to an elongation of 7 mm for this particular subject with a relaxed Achilles tendon length of 216 mm. The first 3 cycles deform much less than later cycles displaying high stiffness relative to later cycles. This initial response of relatively high stiffness is not accounted for in two other studies reporting dynamic creep (De Zee, 2000 and Maganaris, 2002). This difference is likely due to pre-conditioning that is commonly performed prior to ex-vivo testing and that occurs naturally prior to most human testing.

Although this experiment shows an asymptotic response, it is unclear if and when dynamic creep ceases to take place beyond 300 cycles. How the body adapts to dynamic creep and the overall effect it has on functional performance is uncertain.

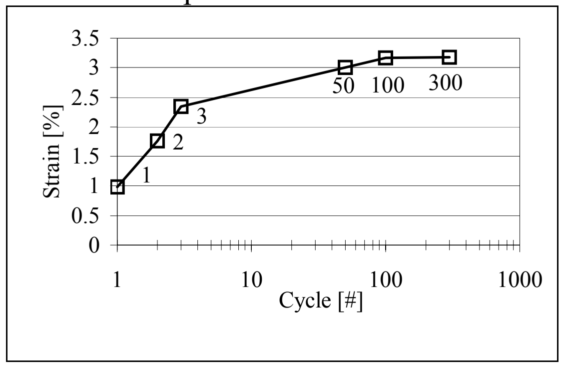

Figure 2: Tendon strain (%) for cyclic loading of the Achilles tendon. Note the logarithmic scale.

SUMMARY

Ultrasound and a force transducer were used to quantify Achilles tendon dynamic creep during submaximal loading of over 300 cycles in-vivo. Dynamic creep occurred over approximately the first 100 cycles increasing from 1% strain to over 3% strain. The asymptotic strain response is similar in magnitude to results observed in pig tendon ex-vivo cyclic testing (~3.2%, De Zee, 2000) and in-vivo human Achilles tendon during maximum muscle stimulation testing (~5-6 %, Maganaris, 2002). Novel in this study is the observed ~1.5% dynamic creep observed during the initial loading cycles for a non-preconditioned state. The next phase of testing will be to determine the time required for the tendon to recover from dynamic creep, to determine whether dynamic creep can be cumulative over multiple bouts of exercise, and to quantify creep variability between different people.

REFERENCES

De Zee, M. et al. (2000). *J Appl Physiol*, **89**, 1352-1359.
Maganaris, C.N. (2002). *J Biomech,* **35**, 1019-1027.

RELATIONSHIPS BETWEEN EMG FREQUENCY SPECTRUM AND RATE OF FORCE DEVELOPMENT CHANGES

Loren Z.F. Chiu [1], Andrew C. Fry [2], Brian K. Schilling [2], and Lawrence W. Weiss [2]

[1] Musculoskeletal Biomechanics Research Laboratory, Biokinesiology & Physical Therapy, University of Southern California, Los Angeles, CA, USA
[2] Musculoskeletal Dynamics Laboratory, Human Movement Sciences & Education, The University of Memphis, Memphis, TN, USA
E-Mail: CDNAthlete@comcast.net Web: www.usc.edu/go/mbrl

INTRODUCTION

Controversy exists as to whether or not the EMG frequency spectrum is related to isometric rate of force development (RFD). In the elbow flexor muscles, significant correlations exist between mean power frequency and maximal RFD (Bilodeau et al. 2002; Gabriel et al. 2001). To the authors' knowledge, these results have not been reproduced in knee extensor muscles.

While maximal RFD is commonly used to assess explosive strength, our previous work suggests this may not be the most robust variable for the rise of the force-time curve (Chiu et al. in press). As such, the different parameters describing this portion of the force-time curve may illustrate distinct aspects of explosive strength performance.

Additionally, we have found relationships between change scores for RFD and myosin heavy chain parameters following fatiguing exercise (Chiu et al. in press). These data indicate that factors contributing to explosive strength performance may be best elucidated following an exercise protocol.

The research purpose was to determine the relationship between RFD parameters and the EMG frequency spectrum before and after an overreaching training protocol.

METHODS

Recreationally trained male subjects performed a one-week phase of high volume, high power resistance exercise designed to induce overreaching. The details of the training protocol have been reported elsewhere (Chiu et al. 2003).

Subjects performed isometric knee extensor tests before (PRE) and after the week of training (HPT). Force was obtained via a load cell. Isometric force-time curves were analyzed for peak force, peak RFD and average RFD. EMG was obtained using a Ag-AgCl bipolar electrode on the vastus lateralis muscle. Mean (MPF) and median frequency of the power spectrum were determined for the time from the onset of the EMG signal to peak force.

Significance of differences was calculated using paired t-tests. Correlations were determined between RFD and EMG parameters. RFD parameters were normalized to body mass. Additionally, correlations were determined between the change scores for RFD and EMG parameters from PRE to HPT.

RESULTS

PRE and HPT RFD and EMG parameters are presented in Table 1. Peak force was significantly impaired following training ($p=0.02$). No significant differences existed for the group from PRE to HPT. No significant correlations were found between RFD and EMG parameters. A significant correlation existed between the change in average RFD and change in MPF from PRE to HPT (Figure 1; r=0.70; p=0.02).

Table 1: RFD and EMG parameters before and after training. Mean ± S.D. * denotes significantly different from PRE.

Measure	PRE	HPT
MPF (Hz)	59 ± 16	54 ± 16
MDPF (Hz)	45 ± 21	40 ± 19
Peak Force (N)	668 ± 122	*577 ± 150
Average RFD ($N \cdot s^{-1}$)	1717 ± 608	1800 ± 681

DISCUSSION

Contrary to earlier reports for the elbow flexor muscles, no relationship existed between knee extensor RFD and the EMG frequency spectrum. A limitation of this investigation is measuring only the vastus lateralis EMG. However, Gabriel et al. (2001) measured only biceps brachii and Bilodeau et al. (2002) measured biceps brachii and brachioradialis – neither collected from brachialis muscle. Further investigation is required to determine the variability of the frequency spectrums of the different knee extensor muscles.

Similar to our previous findings (Chiu et al. in press), the current investigation found a significant correlation between two change scores. The positive relationship between the change scores for RFD and MPF indicates that a decrease in EMG frequency is associated with a decrease in RFD and an increase in EMG frequency is associated with an increase in RFD.

Decreased MPF may result in decreased activation of high threshold motor units. High threshold motor units contain muscle fibers with MHC IIa which is positively correlated to RFD (Chiu et al. in press). Thus, decreased recruitment of high threshold motor units would result in decreased RFD. Similarly, increased recruitment of high threshold motor units would result in increased RFD. Gabriel et al. (2001) also proposed increased MPF enhanced motor unit rate coding, also consistent with increased RFD.

In summary, prior to exercise, no relationships exist between RFD and EMG frequency spectrum parameters. However, the change in average RFD and MPF following a period of training are related. This relationship may be a result of altered motor unit recruitment patterns.

REFERENCES

Bilodeau, M. et al. (2002). *J. EMG Kines.*, **12**, 137-145.
Chiu, L.Z.F. et al. (2003). *Presented at SWACSM ’03.*
Chiu, L.Z.F. et al. (in press). *Eur. J. Appl. Physiol.*
Gabriel, D.A. (2001). *J. EMG Kines.*, **11**, 123-129.

Figure 1: Correlation between change in RFD and mean power frequency.

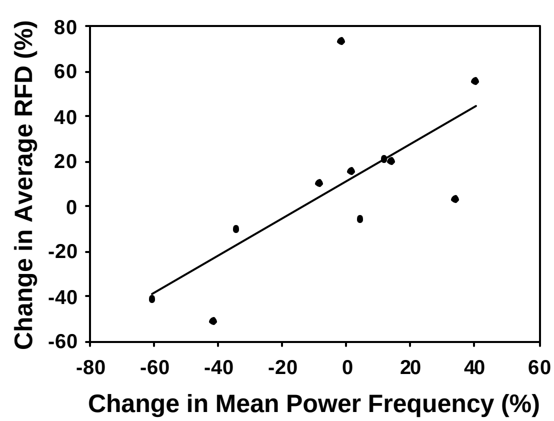

FACTORS PRODUCING A "SOFT" LANDING IN TERMS OF BOTH FORCE AND SOUND

Sara C. Novotny and Richard N. Hinrichs

Department of Kinesiology, Arizona State University, Tempe, AZ, USA
E-mail: hinrichs@asu.edu Web: www.asu.edu/clas/kines

INTRODUCTION

Many activities regularly involve landing from a jump. While studies have shown that telling subjects to decrease the volume of the sound of their landings has significant effects on reducing the landing ground reaction force (GRF) (McNair et al., 2000; Onate et al., 2001), no one appears to have systematically studied the relationship between landing sound and GRF.

Lower force landings have also been associated with more flexed joints at landing (Stacoff et al., 1988; Mizrahi & Susak, 1982). Studies have varied on which instant during landing the joint angle-force relationship has been analyzed. The purposes of this study were twofold: to investigate the relationship between maximum vertical GRF and maximum sound level for landing from a height and to analyze the relationship between maximum vertical GRF and maximum joint flexion angle for the hip, knee, and ankle.

METHODS

Forty recreationally active college-age subjects (20 men, 20 women) performed a series of eleven drop landings over the course of two data collection sessions, as part of a larger study exploring ways to assist a subject in minimizing landing force. All landings were initiated by stepping off a 30 cm platform and landing on a force platform. All subjects were outfitted with a pair of tennis shoes in order to standardize the effects of footwear across all subjects. Reflective markers were placed over anatomical landmarks on the subject's right leg and pelvis. Sagittal plane video data were recorded at 120 Hz and synchronized with the force platform data using a data pulse and corresponding LED flash. All sound data were collected via a sound meter that was mounted approximately 10 cm above the front edge of the force platform.

The video data were digitized and filtered using a Butterworth digital filter with automatically determined cutoff frequencies (Challis, 1999). The vertical force component of the GRF was filtered similarly. All sound data were filtered at 20 Hz. The maximum ankle dorsiflexion (DF) and knee joint flexion angles were calculated according Winter (1990). The maximum hip flexion angles were computed using Umberger and Martin (2001). For each trial, maximum vertical GRF and maximum sound level were also determined. Vertical GRF was normalized to multiples of body weight (BW).

Regression analyses were employed to determine the significance of the relationship between maximum vertical GRF and maximum sound level. Also examined were the relationships between maximum force and maximum joint flexion angle for the hip, knee, and ankle.

RESULTS AND DISCUSSION

Maximum sound level was determined to be a significant predictor of maximum vertical force, p<.001 (Figure 1). Controlling for individual subjects increased the explained variance to 0.294.

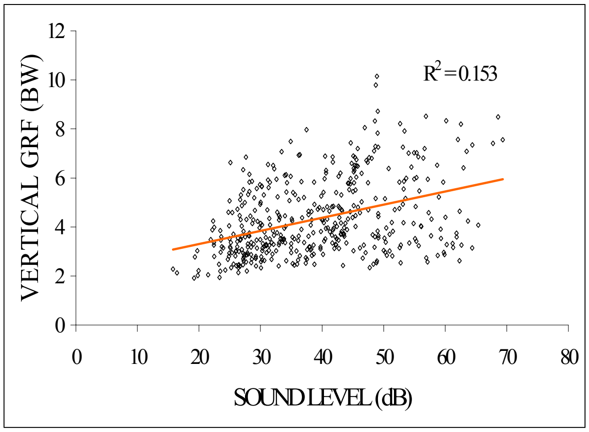

Figure 1: The relationship between maximum vertical force and maximum sound level.

Maximum joint flexion angle was a significant predictor of maximum vertical force for all three joints, the hip, the knee (Figure 2), and the ankle, p<.001. Similar but more linear relationships were present for the other two joints (hip R^2 = 0.324, ankle DF R^2=0.202).

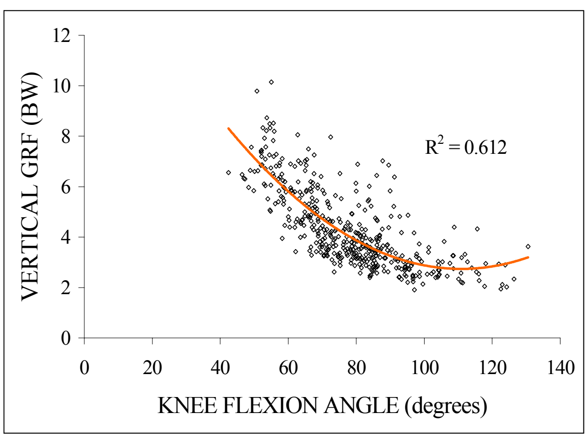

Figure 2: The relationship between maximum vertical force and maximum knee flexion angle.

The relationship between maximum vertical GRF and maximum sound level appears to be a subject-dependent relationship. When the data were examined by subject, seven out of the forty subjects demonstrated neutral or negative relationships between maximum force and maximum sound level. Although overall maximum sound level only explained 15% of the variance of maximum vertical GRF, for a particular subject sound could be used as a predictor of force. This relationship could allow for force to be inferred from sound, which in beneficial in situation where a force plate is not available.

The relationships between maximum joint flexion angle and maximum vertical force show that lower forces are associated with more flexed positions after landing.

SUMMARY

In landing, maximum vertical force is related to maximum sound level, but this relationship is highly individual. Lower vertical forces are consistently associated with greater maximum joint flexion angles, particularly at the knee.

REFERENCES

Challis, J.H. (1999). *J. Appl. Biomech.*, **15**, 303-317.

McNair, P. J. et al. (2000). *Br. J. Sports Med.*, **34**, 293-296.

Mizrahi, J. & Susak, Z. (1982). *Eng. Med.,* **11**(3), 141-147.

Onate, J. A. et al. (2001). *J. Orthop. Sports Phys. Ther.,* **31**, 511-517.

Stacoff, A. et al. (1988). *Biomechanics XI-B* (pp. 694-700). Amsterdam: Free University Press.

Umberger, B.R. & Martin, P.E. (2001). *J. Appl. Biomech.*, **17**, 55-62.

Winter, D.A. (1990). *Biomechanics and motor control of human movement*. New York: John Wiley & Sons, Inc.

AMPLIFICATION OF MUSCLE FIBER LENGTH CHANGES IN THE HUMAN SOLEUS MUSCLE-TENDON COMPLEX

John A. Hodgson[2], Ron Roiz[1], Taija Finni[4], Hae-Dong Lee[3], V. Reggie Edgerton[2] and Shantanu Sinha[3]

Departments of [1]Cybernetics, [2]Physiological & [3]Radiological Sciences, UCLA, Los Angeles, CA 90095 and [4]Department of Health Sciences, University of Jyväskylä, 40014 Jyväskylän, Finland.

Email: jhodgson@ucla.edu

INTRODUCTION

Several features in the design of the neuro-musculo-skeletal system simplify the execution of movements and improve their efficiency, leading to the notion that mechanical properties, structure and control provide an exquisitely integrated and optimized motor system. One puzzling feature of this system is the relationship between the calcaneus excursion (~30mm) in the human ankle and the length of human soleus muscle fibers (~35 – 45 mm). This presentation explores possible mechanisms that may explain how the human soleus muscle-tendon complex generates movements at the calcaneus that are almost equal to the length of its muscle fibers. Predictions based on the models presented will be tested with MRI methods designed to track the movement of tissues in_vivo.

RESULTS

Gain in the transmission of length changes from shortening muscle fibers to the aponeuroses occurs if the inward movement of aponeuroses is prevented (Gans,1982; van der Linden et al., 1998). The instantaneous gain is 1/cos(pinnation angle), giving possible length change gains of 1 – 1.3 for pinnation angles of 0 – 40° (Fig. 1). Small changes in aponeurosis separation with muscle length changes significantly decrease (aponeuroses moving closer) or increase (aponeuroses moving apart) these gains. Since muscle girth increases during shortening, we hypothesize that aponeuroses move apart, increasing the gain due to pinnation angle.

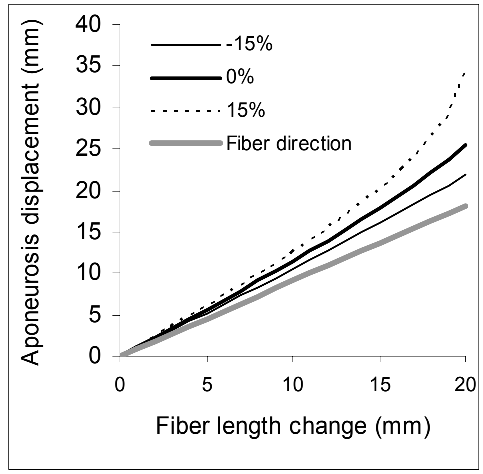

Figure 1: The relationship between muscle fiber length change and predicted movement of the aponeurosis along the long axis of the muscle. The grey line shows the result of the aponeurosis moving along the long axis of the muscle fiber. The thick solid black line shows the relationship between fiber length and aponeurosis movement if the distance between aponeuroses remain constant. The other lines indicate the relationships if the distance between aponeuroses decreases (solid line) or increases (dotted line) during a contraction.

Intramuscular pressure may provide forces normal to the muscle surface and prevent the inward movement of the aponeuroses due to muscle fiber shortening. Curvature of the muscle fibers may be one mechanism which generates intramuscular pressure with increased tension in muscle fibers (Van Leeuwen & Spoor, 1992). Others have implicated hydrostatic pressure (van der Linden et al., 1998). A finite element model of muscle was developed in ABAQUS to investigate the dimensional changes of a simple muscle composed of two elastic tendons with aponeuroses connected by muscle fibers represented as an elastic sheet in the form of a parallelogram (Fig. 2). The stiffness of the muscle fiber material was altered to simulate different levels of contraction. An identical stretch was applied to the tendons at all stiffness levels to simulate loading under isometric conditions.

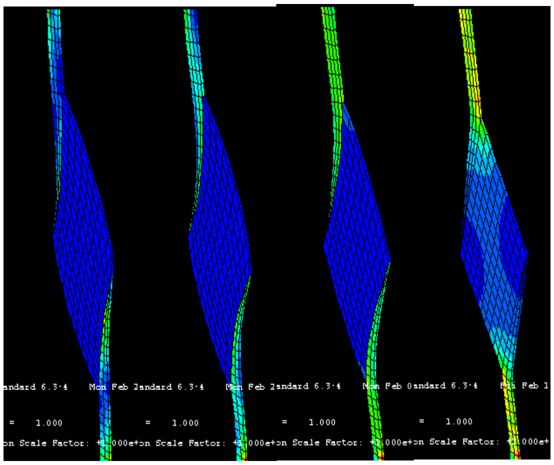

Figure 2: Simulation of a simple muscle to show the effect of increased muscle stiffness (left to right) on the shape and distribution of strain across the tendon and muscle.

Stretch resulted in rotation of the model to align it along an axis between the ends of the tendons. It also resulted in a proximo-distal bulging of the model to produce a curvature in the elements that was similar to the curvature observed in muscle fibers. Increasing stiffness of the muscle material resulted in greater shortening of the muscle element and increased stretch of the tendon. Coordinates of pairs of points corresponding to the proximal and distal ends of muscle fibers moved predominantly parallel to the axis between tendons rather than along the axis of the elements representing muscle fibers. The higher levels of stiffness in the muscle material resulted in a stress concentration at each extreme of the muscle which corresponds to the location usually affected by tendon injuries. Despite its extreme simplicity, this model exhibits behaviors that are remarkably similar to skeletal muscle, suggesting that some apparently complex behaviors of muscle tissue may be explained by relatively simple mechanisms operating in a 3-dimensional structure.

Additional mechanical gain may arise at the ankle where the Achilles tendon is pulled towards the ankle center of rotation, creating an easily observed curvature in the human Achilles tendon. Constraining the outward movement of the tendon as the calcaneus moves around the arc of a circle results in displacements of the calcaneus that exceed the length change of the musculo-tendinous unit (Fig 3).

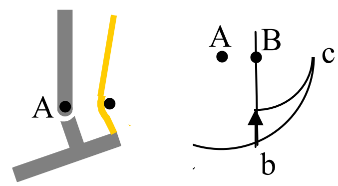

Figure 3: A diagram illustrating a possible gain mechanism at the ankle. The arc abc represents movement of the calcaneus around its center of rotation, A. Rotation along the arc would be accomplished with a muscle-tendon shortening equal to the radius of the circle. The introduction of a constraint at B, preventing outward movement of the Achilles tendon accomplishes the same movement with a tendon–muscle length change equal to the distance between the constraint and the ankle center of rotation.

REFERENCES

Gans, C. (1982) *Exerc Sport Sci Rev* **10**, 160-207.

Van Leeuwen, J.L., Spoor, C.W. (1992) *Phil Trans R Soc Lond B Biol Sci*. **336**, 275-292.

Van der Linden, B.J.J.J., Koopman, H.F.J.M., Huijing, P.A., Grootenboer, H.J. (1998) *Clin Biomech* **13,** 256-260.

ACKNOWLEDGEMENTS

This work was supported by NASA NSBRI grant NCC9-58

LIGAMENTOUS VERSUS PHYSEAL FAILURE IN MURINE MEDIAL COLLATERAL LIGAMENT BIOMECHANICAL TESTING

Hossam B. El-Zawawy; Matt J. Silva; Linda J. Sandell; Rick W. Wright
Department of Orthopaedic Surgery, Washington University School of Medicine at Barnes Jewish Hospital, St. Louis, MO.
E-mail; wrightr@msnotes.wustl.edu

INTRODUCTION

At the end of a growing long bone, the epiphysis adjacent to the articular cartilage is separated from the metaphysis and diaphysis by a cartilaginous disk known as the growth plate (physis). Growth plate physiology and timing of closure are complex events and vary between bones and among species. The choice of a research model for biomechanical experiments should account for the time of growth plate closure, particularly when dealing with joint structures such as ligaments and tendons. Kilborn et al (2002) complied from a number of sources the age of sexual maturation and its correlation to the time of growth plate closure in different animal species. In mice, sexual maturity occurs at one month for females and one and a half-months for males. Based on histological criteria, Silbermann and Kadar (1977) reported that the closure of the proximal humeral physis occurs at five months, indicating that sexual maturity precedes cessation of longitudinal bone growth by a considerable time period.

In a previous study we assessed the tensile properties of the medial collateral ligament (MCL) in mice (Wright et al, 2003). We observed that failure in some intact specimens occurred at the femoral physis rather than at the MCL although the mice were sexually mature at the time of testing. The aim of our current study is to determine the age at which the femoral physis will cease to separate in our MCL load to failure model.

METHODS

Fifteen 129X1-SVJ male mice were used in this study. The mice were purchased from the Jackson Laboratory (Bar Harbor, ME, USA) at three months of age. The animals were sacrificed in a carbon dioxide chamber at four, five and six months. Five animals were used at each time point. Following euthanasia, the mice were frozen at minus seventy degrees until the day of testing. The Animal Studies committee of Washington University approved all procedures.

We used the method described by Wright et al (2003). Prior to testing, both hind limbs from each mouse were disarticulated at the hip. Skin and muscles were then stripped from proximal and distal points of the limb to the knee. The femur and tibia were then potted in 6.4 mm diameter plastic tubes using polymethylmethacrylate (PMMA) to allow gripping of the knee during testing. The specimens were kept moist with saline solution until the time of testing. The specimens were clamped in a custom tensile testing machine with the tibia and femur at 22.5 degrees from horizontal resulting in a knee flexion angle of 45 degrees. The machine consists of a stepper-motor driven lead screw that distracts the proximal end of the specimen horizontally. A 22 N load cell (Transducer Techniques MDB-5, Temecula, CA) monitors the applied force. Force and displacement were recorded using a computerized data acquisition system (Labview 5.0 Austin, TX). Under a dissecting microscope all soft tissues structures of the knee except the medial collateral ligament were cut (LCL, ACL, PCL, and joint capsule). Specimens were then tested to failure in tension by displacing the tibia at 0.25 mm per second. The knee was observed under the microscope to determine whether the failure occurred at the physis or the ligament.

RESULTS

At four months, six (60%) of the ten specimens failed at the femoral physis with five/six (83%) occurring on the right side. At both five and six months, one (10%) of the ten specimens failed at the physis, also on the right side. Of note the 4 mice which failed at the MCL rather than the physis at five and six month of age demonstrated a trend that the right MCL failed at a higher load than the left MCL (table 1).

Table 1: Mean (± SD) ultimate force for the specimens that failed at the MCL.

Age	Mean ultimate force		P value
	Right	Left	
5 months	8.93(±1.3)	7.17(±1.5)	0.21
6 months	11.64(±2.6)	7.57(±2.8)	0.13

DISCUSSION

Previously we had carried out MCL tension to failure experiments with the assumption that mice reach skeletal maturity and sexual maturity at the same time. Our observation that a high physeal failure rate occurred in 4 month old mice specimens led us examine at what age this ceases to occur as a mean of optimizing our MCL load to failure model. We noted a strong trend that the right MCL was stronger than the left MCL. This was not the focus of our study and future studies using larger numbers of mice would be necessary to demonstrate a greater significant difference. However, previous studies have suggested that limb dominance may contribute to increased ligament strength (Denti et al, 2000). Paw preference was investigated in 114 Sprague-Dawley rats. It was reported that 70.2 percent of rats were right-pawed, 19.3 percent were left-pawed and 11.9 percent were ambidextrous (Pence 2002). The results indicated that the distribution of paw preference in rats is similar to that of other animals and to human handedness. This may explain our results of the mouse MCL being stronger in the right knee than in the left knee.

SUMMARY

Biomechanical testing of the medial collateral ligament with load to failure can result in physeal failure rather than MCL failure in skeletally immature animals. This study examined the age at which a femoral physeal failure ceased to occur in a mouse model of MCL testing. Sixty percent of the knees tested at 4 months failed at the physis rather than at the ligament. However, only ten percent of the knees tested at 5 and 6 months failed at the physis. We now consider that 5 month old mice are functionally skeletally mature and old enough to be tested biomechanically with few failures at the physis.

REFERENCES

Denti M. et al, 2000. Motor control performance in the lower extremity: normal vs. anterior cruciate ligament reconstructed knees 5-8 years from the index surgery. *Knee Surgery, Sports Traumatology, Arthroscopy* **8(5)**: 296-300.

Kilborn SH. et al, Sep 2002. Review of growth plate closure compared with age at sexual maturity and lifespan in laboratory animals. *Contemporary Topics in Laboratory Animal Science* **41(5)**: 21-26.

Pence S, 2002. Paw preference in rats. *Journal of Basic Clinical Physiology and Pharmacology* . **13(1)**: 41-49.

Silbermann M. and Kadar T., 1977. Age-related changes in the cellular population of the growth plate of normal mouse. *Acta Anatomica.* **97**: 459-468.

Wright R. et al, Sep 2003. Effect of Hemorrhage on Medial Collateral Ligament Healing in a Mouse Model. *American Journal of Sports Medicine*, **31**: 660-666

ACKNOWLEDGEMENTS

This study was funded by a grant from The National Football League (NFL) Charities, (RWW).

VARIABLE STIFFNESS PROSTHESIS FOR TRANSTIBIAL AMPUTEES

Glenn K. Klute [1,2], Joel C. Perry [1,2], Joseph M. Czernicki [1,3]

[1] Dept. of Veteran Affairs, Seattle, WA USA
[2] Dept. of Mechanical Engineering, University of Washington, Seattle, WA USA
[3] Dept. of Rehabilitation Medicine, University of Washington, Seattle, WA USA
gklute@u.washington.edu www.seattlerehabresearch.org

INTRODUCTION

Many ambulatory lower limb amputees exhibit fatigue, asymmetrical gait, and the inability to walk at varying speeds. The stiffness of their ankle/foot components are prosthetist selected and based on activity level and weight. The development of a variable stiffness prosthesis is hypothesized to reduce metabolic costs, improve gait symmetry, and facilitate changing gait speeds. This paper reports human subject data used for design requirements and results from a bench-top test of a prototype variable stiffness prosthesis where one phase of the gait cycle (loading response) was mechanically simulated.

METHODS

Twelve intact subjects free from any known gait pathology gave informed consent to participate in this Institutional Review Board approved study. Each subject performed six trials at three walking speeds: 1.0, 1.3, and 1.6 m/s (slow, medium, and fast, respectively). Kinematic and kinetic data were collected for analysis (Peak Motus with Kistler force plate). The mean ankle moment (normalized by subject weight) versus ankle plantarflexion at each walking speed was used to predict the force versus ankle plantarflexion characteristics of a prototype prosthesis during the loading response phase of gait (*i.e.*, the design requirements). These calculations assume a moment arm of 46 mm.

The prototype variable stiffness prosthesis (Figure 1) was fabricated using a Single Axis prosthetic foot (Ohio Willow Wood). Three flexible pneumatic actuators acting in parallel with two serial compression springs were used to simulate the musculo-tendon structures of the lower limb (Klute *et al.*, 2002 and Perry, 2003). Haversine input waveforms (position control) were used to mechanically simulate ankle movement from initial heel contact to midstance (MTS Model 858). Actuator pressures were calculated *a priori* using the stiffness results (design requirements) from the human subject tests (Perry, 2003).

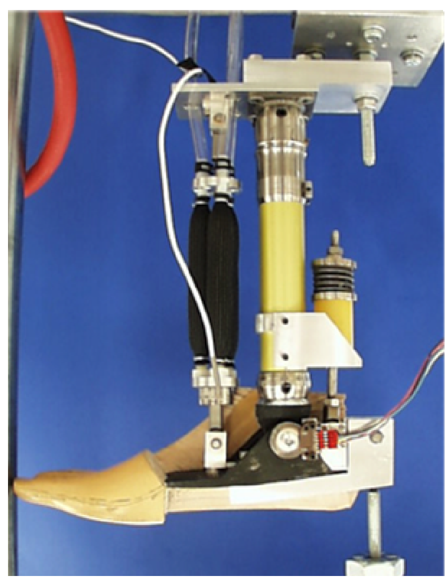

Figure 1: Prototype prosthesis.

RESULTS AND DISCUSSION

The human subject experiments revealed ankle stiffness during loading response varied with walking speed (Figure 2, dotted lines). The equivalent ankle stiffness during early stance was 32, 39, and 49 N per degree ankle plantarflexion for walking at 1.0, 1.3, and 1.6 m/s, respectively. The constant value of these stiffnesses during early stance suggests stiffness is set by muscle activation prior to initial heel contact (HS). The clockwise shape of the force versus angular displacement plot (i.e., work loop) indicates net energy absorption.

Using the properties of the flexible pneumatic actuators and series springs, the required actuator pressure for the bench-top mechanical tests were calculated to be 2.7, 2.9, and 3.4 bar. *A priori* actuator pressurization is analogous to muscle activation prior to heel initial contact.

The bench-top mechanical simulations of loading response at walking speeds equivalent to 1.0, 1.3, and 1.6 m/s revealed the capacity of the prototype to generate the desired stiffnesses during early stance (Figure 2, solid lines). Mechanical hysteresis produced a net energy absorption (clockwise work loop), however, constant activation pressure resulted in a pronounced difference between the human subject data and the prototype prosthesis as stance progressed.

SUMMARY

Intact individuals vary their ankle stiffness when walking at different speeds. A variable stiffness prosthesis capable of achieving similar results during early stance was demonstrated. Variable activation pressure (feedback control) will be necessary to achieve bio-mimetic performance.

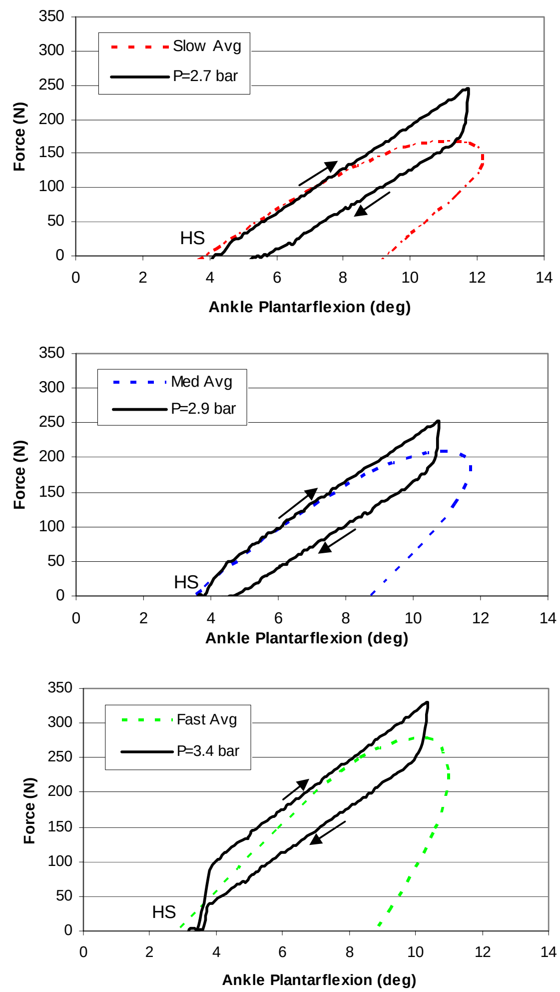

Figure 2: Force v. ankle plantarflexion during slow, medium, and fast walking from initial heel contact (HS) to midstance. Human subject data (N=12) is shown with a dotted line and prototype prosthesis results are shown with a solid line.

REFERENCES

Klute GK et al. (2002). *Int. J. Robotics Research*, **21**(4), 295-309.

Perry JC (2003). *Thesis.* University of Washington, Seattle.

ACKNOWLEDGEMENTS

This research was funded by the Department of Veterans Affairs (No.A2661C).

DYNAMIC BENDING MECHANICS OF THE DEVELOPING SPINE

David J. Nuckley, Richard M. Harrington, and Randal P. Ching

Applied Biomechanics Laboratory, Mechanical Engineering Department, University of Washington, Seattle, WA, USA
E-mail: dnuckley@u.washington.edu Web: http://depts.washington.edu/uwabl/

INTRODUCTION

Despite sophisticated new safety equipment on playgrounds and in automobiles, traumatic injuries remain the leading cause of death for children (1-24 years). Each year in the U.S. more than 8,000 children die as a result of falls or automobile crashes while a significant number survive but with debilitating life-long affects. These deaths and injuries are often the consequence of excessive dynamic bending motions of the neck. Unfortunately, the mechanical response of the pediatric cervical spine to dynamic bending inputs is not well understood, making prevention of these injuries less feasible.

Previous research has quantified the bending response of the adult cervical spine (Nightingale, 2002); however, only one study using a caprine model has examined immature spine bending mechanics (Pintar, 2000). This study reported increased stiffness with maturation in flexion and extension, but did not test dynamically or to failure. Therefore, the objective of this research was to quantify the dynamic bending mechanics (functional and failure) for the pediatric cervical spine.

METHODS

To accomplish our objective we developed an apparatus to apply "pure" dynamic bending moments about the spine. This device converts the axial motion of a servo-hydraulic MTS into a bending moment and allows linear translation of the specimen to minimize the shear forces (Figure 1).

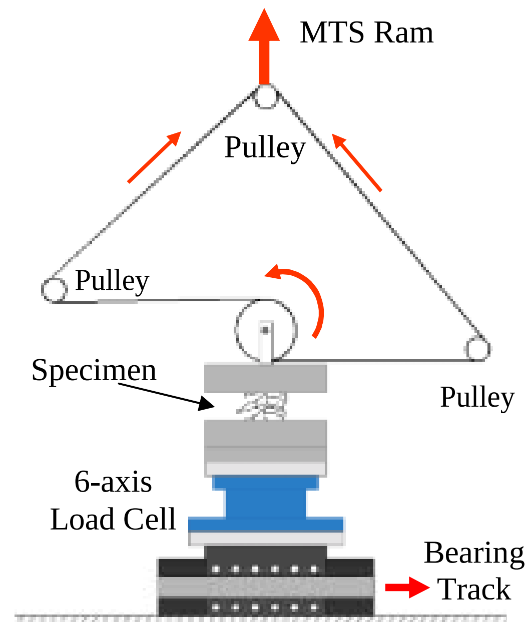

Figure 1. Apparatus to apply dynamic "pure" bending moments about the spine.

Due to the limited availability of human pediatric tissues, we employed a cadaveric baboon model for this investigation. Twenty-four male baboon specimens across the developmental spectrum (2 to 23-H.E. years)(Kuhns, 1998) were acquired from the University of Washington Regional Primate Research Center. These specimens were dissected down to osteoligamentous tissues and disarticulated giving test specimens of C3-C4 (n=13), C5-C6 (n=25), and C7-T1 (n=11). They were subsequently wired through their superior and inferior vertebrae and embedded in PMMA to ensure rigid purchase to the test apparatus.

Each specimen was mounted in the test apparatus, and a dynamic flexion, extension, or lateral bending moment was applied to the specimen. The C5-C6 specimens were randomized to flexion (n=13) and extension (n=12). The C3-C4 specimens all received right lateral bending and the C7-T1 specimens were all failed in left lateral bending. All tests were performed dynamically at a loading rate of 25-rad/sec. Each test was performed to failure and moment—angular displacement profiles were recorded. These data were then compared as a function of skeletal maturation (age) and a statistical F-test was performed to determine if the relationship was significant (alpha = 0.05).

RESULTS AND DISCUSSION

The results of this investigation demonstrate relationships between spinal maturation and dynamic failure moment (Figures 2&3). The C5-C6 failure moments were statistically correlated with maturation ($p<0.0001$) for both flexion and extension. Likewise, the C3-C4 and C7-T1 failure moments were significantly correlated with spinal development ($p<0.0001$).

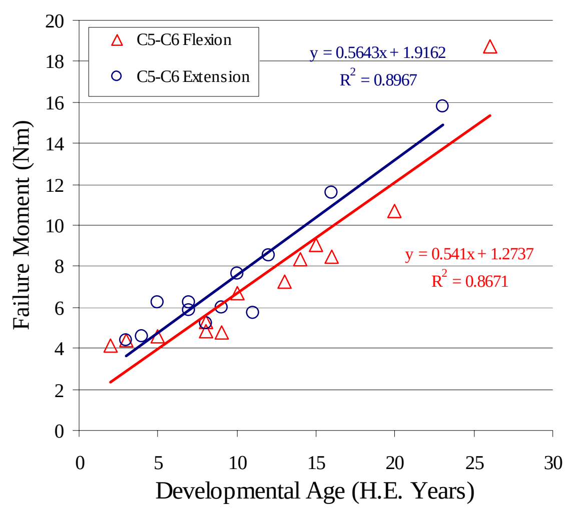

Figure 2. Failure moment of the C5-C6 spinal level in flexion and extension across the developmental spectrum.

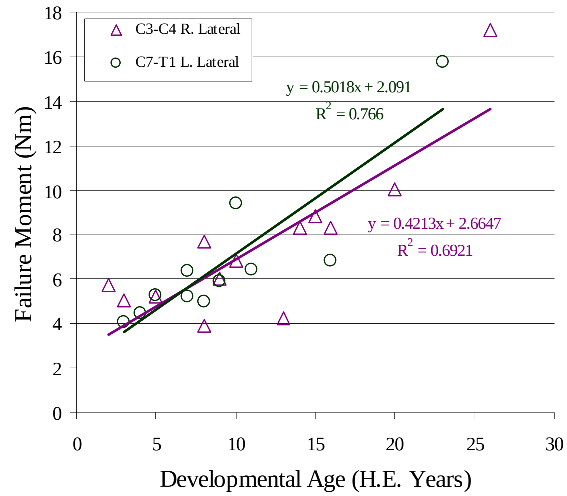

Figure 3. Lateral bending failure moments for C3-C4 and C7-T1 in the maturing spine.

SUMMARY

Clear bending failure relationships were discovered with spinal maturation. These associations are dynamically based and the resulting injuries are consistent with epidemiological data. This data set provides insight into the developmental mechanics of the cervical spine and, through age-based scaling, may be applied to modeling efforts. Armed with appropriate dynamic bending mechanics, these modeling efforts can foster improved biofidelity in anthropomorphic test devices and injury prevention strategies.

REFERENCES

Kuhns, LR (1998) *Imaging of Spinal Trauma in Children. B.C. Decker Inc.*

Nightingale, R et al.(2002) *J Biomech 35: 725-32.*

Pintar, F.A., et al. (2000) *Stapp Car Crash Journal 44: 77-84* .

ACKNOWLEDGEMENTS

Support for this research was provided by the National Transportation Biomechanics Research Center at the National Highway Traffic Safety Administration (DOT).

Characterization of a human vertebral body collapse using a 6-DOF robotic system

Wafa Tawackoli, Kay Sun, Michael A.K. Liebschner

Department of Bioengineering, Rice University, Houston, TX, USA
E-mail: wtawacko@rice.edu Web: www.ruf.rice.edu/~cebl/

INTRODUCTION

Vertebral compression fractures developed in the lumbar spine have been seen in osteoporotic patients, industrial workers, and athletes (Leigh, 1997). About half of the compressive load in the upright position results from the tension in muscles and ligaments required to maintain an erect posture, while the other half is due to body weight. In addition, many everyday activities and even such physiological functions as walking and jumping are associated with significant increase in compression loading (Cappozzo, 1984).
It seems likely that vertebrae are not loaded in one specific way, but are subjected to a large variety of forces and moments during the activities of daily life (Panjabi et al, 1989).

A study of the path of minimum resistance, therefore, may reveal how axial loads generally transfer through a human vertebra and how fracture occurs. A new testing method is proposed to investigate the strength of a single vertebral body during a full collapse by observing the path of least resistance through its weakest axis. The specimen was tested in a load feedback control to determine its response to pure axial loading up and beyond the fracture point.

METHOD

In this study, a fresh-frozen cadaveric lumbar vertebra (L4) was harvested (male, 72 years, $\rho_{QCT} = 0.167$ g/cm^3). The specimen was visually and radiographically inspected to ensure it was free of pre-existing pathologies or fractures. Specimen

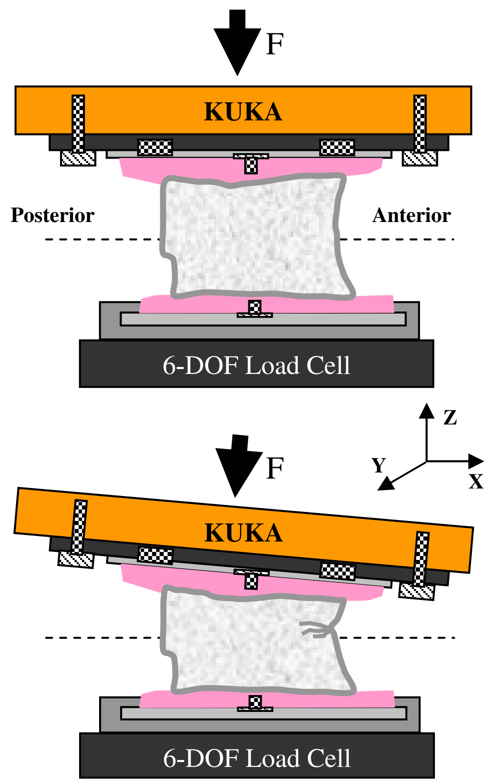

Figure 1. The top and bottom endplates were embedded in PMMA.
Top: Intact, prior to mechanical testing
Bottom: Fractured, after mechanical testing

cross-sectional area (top endplate) was measured to be 1364 mm^2.
In preparation for biomechanical testing, the specimen was thawed to room temperature and cleaned of all residual musculature and all ligamentous structures. The intervertebral discs were removed to examine the loading pattern only on the vertebral body. The PMMA was molded to the concave endplates of the vertebral body using a fixture that ensured plano-parallel ends. Additional screws were inserted into the PMMA through the square plates to ensure rigid connection. A master precision level was used to ensure that the top and the bottom surface of the aluminum plates were

parallel. After the PMMA was cured, the entire assembly was fixed between a 6-DOF robotic arm (KR150, Kuka Robotics) and a 6-DOF force/torque transducer (Omega160, ATI) (figure 1).

The specimen was loaded stepwise with a compressive axial load of ~50 N per step. After each step, both shear forces (F_x and F_y) and moments (T_x, T_y, T_z) were minimized (~zero). The transducer provided force-moment feedback to the robotic arm, thus enabling the robotic arm to operate in a force control mode. Linear and rotational displacements, based on the assigned virtual coordinate system of the robotic arm, were recorded throughout the experiment until full collapse was reached. Total failure was confirmed using plain x-rays.

RESULTS

The specimen was tested until vertebral failure (collapse) as indicated in the load-deformation curve. The compression force at collapse was measured to be ~3800 N. In addition, the specimen experienced two minor fractures at ~600 and ~1500 N (figure 2). The failure stresses at vertebral collapse was calculated to be 2.91 N/mm^2 (1st = 0.48 and 2nd = 1.21) and the initial stiffness was measured to be around 1800 N/mm.

The axial displacement (z-direction) was compared to the total displacement with tilting (z-, x-, and y-direction and rotations in flexion and abduction). The result showed that the total displacement, where the wedge fracture had occurred, is much higher compare to the linear displacement of middle portion of the vertebral body (figure 2).

DISCUSSION

Comprehensive data on the three-dimensional load displacement properties are important for studying different types of

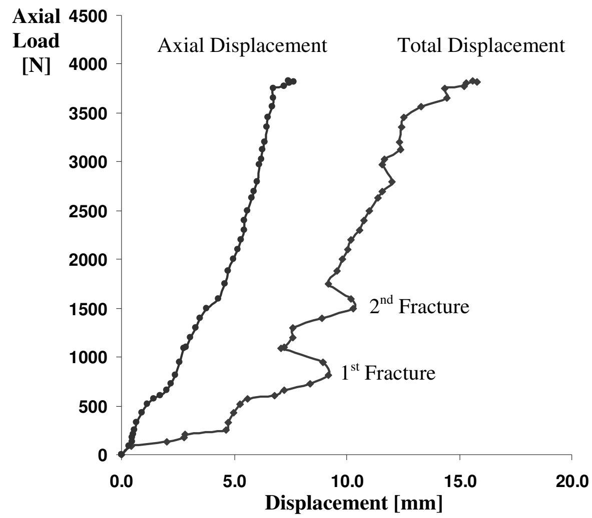

Figure 2. A comparison between compression displacements. Both the 1st and 2nd fractures are more visible in total displacement compare to axial displacement. (Ultimate strength ~ 3800N)

fracture developments in a single vertebral body. In this study, the path of least resistance was successfully pursued through our 6-DOF robotic testing system.

Standard uniaxial compression testing evaluates the strength of the strongest component within the vertebral body. However, *in vivo*, the vertebral body fractures through its weakest region. The compressive load applied in this study (minimizing shear and bending) was much less compared to the average expected ultimate load reported in previous studies.

The technique proposed in this study will allow us to further investigate and understand the complexity of the failure path in the single vertebral body for different types of spinal injury after overload.

REFERENCES

Leigh, J.P., et al., *Arch Intern Med*, 1997. **157**(14): p. 1557-68.
Cappozzo, A., *J Orthop Res*, 1984. **1**(3): p. 292-301.
Panjabi, M., et al., *Spine*, 1989. **14**(9): p. 1002-11.

Analysis of the 360 Degree Motion Envelope of Human Lumbosacral Joints

Wafa Tawackoli and Michael A.K. Liebschner

Department of Bioengineering, Rice University, Houston, TX, USA
E-mail: wtawacko@rice.edu Web: www.ruf.rice.edu/~cebl/

INTRODUCTION

Knowledge of lumbosacral joint (L5/S1) kinematics is important in understanding the cause of low back pain and in aiding in the diagnosis and subsequent treatment (Bartleson, 2001). In previous studies, the flexibility of the lumbosacral joint under a constant bending moment has been investigated only in three planes; sagittal (flexion/extension), transverse (torsion) and frontal (bilateral bending) (Panjabi et al, 1994), limiting the interpretation of spinal joint kinematics in other planes.

The purpose of the present study was to determine the load response of the lumbosacral joint to pure bending moments in a 360 degree circumference. In particular, we sought to apply such moments in a full motion path envelope to the specimen, and measure the changes in flexibility using a robotic arm and a 6-degrees of freedom (DOF) force/torque transducer.

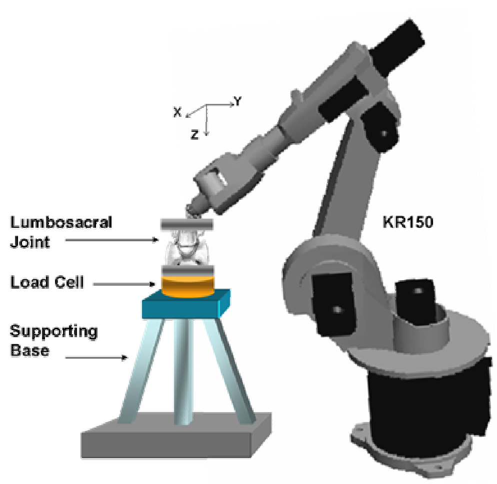

Figure 1. Experimental setup. An overall view of the robotic arm for applying pure moment in combination with compressive preloads to the multi-segment spine specimen.

The goal of this investigation was to analyze the complex motion envelope of a spinal segment in a three dimensional space for better understanding the joint kinematics, pathology of joint disease, and aid in the development of fracture prevention techniques.

METHODS

An intact lumbosacral joint from a 76 year old male donor was prepared for biomechanical testing by detaching the muscular and fatty tissues from the vertebral bodies. The ligamentous structures, facet joints, transverse processes and posterior elements were left intact. To minimize dehydration, saline-soaked gauzes were wrapped around the spinal segment and sprayed with saline solution periodically during sectioning, specimen preparation, and testing. The top and bottom of the spinal segment was permanently potted in PMMA cement. The L5 was mounted to the end of the robotic arm using a custom made connector and the S1 was rigidly fixed to the top of the transducer (Figure 1).

The robotic arm testing system consists of a 6-DOF industrial robotic arm (KR 150, KUKA Robotics Corporation) and a 6-DOF Force/Torque transducer (Omega160, ATI Industrial Automation). The neutral position of the spinal segment was determined by minimizing the forces and moments as measured by the transducer, and the top center of the L5 endplate was assigned as the origin. The specimen was tested in a load feedback control to determine the peripheral path in response to pure moments of 5, 10, and 15 N.m. with and without pure axial preload of 600-N (total of six loading cases). For each case, the motion path envelope was determined by flexing the specimen in a counterclockwise direction while maintaining the overall bending moment at a fixed value. The full motion path envelope was completed when data was collected for a full path (360 degrees in transverse plane) with approximately one set of data point for each 10 degrees increment. This protocol was repeated for the remaining five loading cases.

RESULTS

Under the application of the mobilization loads, the 360 degree motion path envelopes of lumbosacral joint under each loading regimes were mapped (Figure 2, top). A comparison between preload versus no preload showed a reduction in the projected motion fields area (mm^2) up to 35% mostly seen in the anterior portion of the motion field (Figure 2, bottom). No statistically significant decreases in moments were detected after the first loading cycle through the same path.

DISCUSSION

Through the precision and accuracy of the robotic arm, we were able to obtain the full circumferential joint motion envelope in 3-D while applying a rotating pure bending moment. In contrast to previous studies in which range of motions are generally obtained for only four points, two in the sagittal and two in the frontal planes, we were able to determine spinal flexibility in any direction within the transverse plane. In addition, the robotic arm, allowing for simultaneous movement in several axes, determined the path of minimum resistance and the helical axis of motion. Since the posterior elements were intact, restriction in motion caused by zygapophyseal joints resulted a smaller displacement in Z direction for extension than in flexion.

Characterization of such a motion envelope can provide a better understanding of the complex joint kinematics, pathology of joint disease, aid in the development of fracture prevention techniques, and improve the design of new implants with the goal of restoring joint function. A correlation between ergonomic tasks and work related injury can be drawn.

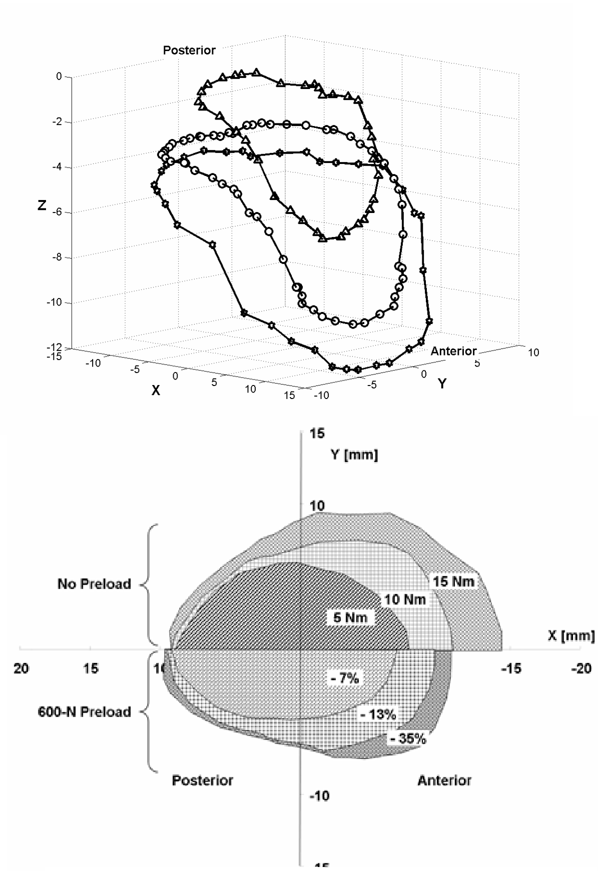

FIGURE 2. Motion path envelope of a lumbosacral joint. (top) A three-dimensional representation of motion path envelopes for a lumbosacral joint with no preload. (displacement in mm). [5 Nm = triangle, 10 Nm = circle, 15 Nm = stars].
The effect of compressive axial preload on the motion fields is shown below.

REFERENCES

Bartleson JD. *Curr Treat Options Neurol.* 2001 3(**2**):159-168.

Panjabi MM, Oxland TR, Yamamoto I, et al.. *J Bone Joint Surg Am* 1994; **76:413**-24.

Prospective Study of Structural and Biomechanical Factors associated with the Development of Plantar Fasciitis in Female Runners

Irene S. Davis[1,2], Clare E. Milner[1], and Joseph Hamill[3]

[1] Department of Physical Therapy, University of Delaware, Newark, DE, USA
[2] Joyner Sportsmedicine Institute, Lexington, KY, USA
[3] Department of Exercise Science, University of Massachusetts, Amherst, MA, USA
E-mail: mcclay@udel.edu Web: http://www.udel.edu/PT/davis/Lab.htm

INTRODUCTION

Plantar fasciitis is one of the 5 most common injuries that runners sustain (vanMechelen, 1992). It is believed that this injury is a result of repetitive strain to the plantar fascia. Warren at al. (1987) reported that runners, either currently or formerly experiencing PF, exhibited greater pronation of the foot while in a loaded stance position than runners with no history of this injury.

In a retrospective study of runners with a history of plantar fasciitis, we reported that these runners exhibited significantly greater peak eversion compared to the controls (Davis et al, 2003). A trend towards greater eversion velocity was also noted. Plantar fasciitis is also often associated with limitations in ankle dorsiflexion range of motion. It is believed that this limitation may lead to a compensatory excessive pronation. This excessive pronation, noted at both the rearfoot and midfoot, leads to increased strain of the plantar fascia.

Finally, it is possible that excessive loading, in terms of peak forces and rates of loading, may be associated with the development of plantar fasciitis. However, these loading variables have yet to be examined in runners who develop this injury.

Therefore, the purpose of this prospective study was to compare foot structure and mechanics in a group of female runners who develop plantar fasciitis (PF) to a group of healthy controls (CON). It was hypothesized the PF group would exhibit decreased peak ankle dorsiflexion, increased rearfoot eversion, and increased vertical ground reaction forces and load rates. Structurally, it was expected that the PF group would have lower arches, greater calcaneal eversion in stance and limited ankle dorsiflexion range.

METHODS

These data are part of an ongoing, prospective study of female distance runners. Female runners, aged 18 to 40 yrs., and running at least 20 miles per week are recruited into a 2-year longitudinal study. A gait analysis is performed on entry into the study. Subjects run overground at 3.7m/s in standard laboratory running shoes. Five trials are recorded using a 6-camera motion capture system at 120 Hz (Vicon, Oxford Metrics, UK) and a force platform (Bertec, OH, USA). 3D kinematics and kinetics were calculated for both lower extremities (Visual 3D, C-Motion, MD, USA). In addition to the motion analysis, a structural assessment of the runner's lower extremities is performed by an experienced physical therapist. Included in these measures are arch index (Williams et al, 2000), dorsiflexion range of motion with the knee extended, and calcaneal valgus during stance.

The subjects are then followed monthly for two years. Running mileage and injuries are tracked. To date, 10 runners, aged 32 ± 8 years, and running an average of 28 ± 12 miles per week have developed plantar fasciitis (PF). These were compared to a control (CON) group of 10 uninjured runners matched for age (31± 11 yrs) and mileage (28 ± 6 miles per week).

Variables of interest were compared between groups statistically using an independent, one-tailed t-test. Due to the preliminary nature of these data, a p value of 0.10 was used for statistical significance.

RESULTS AND DISCUSSION

Comparison of the variables of interest between groups is presented in Table 1.

Table 1: Structural and Dynamic Measures

	PF	CON	p
Peak EV (deg)	7.1	8.6	0.22
DF exc (deg)	17.8	20.8	0.12
Peak DF (deg)	25.7	27.7	0.15
Imp. Peak (BW)	1.81	1.65	0.15
Inst. Load Rate (BW/s)	124.5	109.3	0.19
Avg. Load Rate (BW/s)	86.7	77.9	0.22
Stance Calc. VAL (deg)	5	2	0.03
Arch Index (unitless)	0.339	0.353	0.19
DF rom (deg)	1	3	0.18

Surprisingly, no difference was noted in peak rearfoot eversion (EV). This is in contrast to our previous retrospective study of plantar fasciitis (Davis et al, 2003), where the injured subjects exhibited significantly greater EV than the controls. While not statistically significant, there was a trend towards a decrease in peak dorsiflexion (DF) and DF excursion. This was not associated with increased rearfoot EV in this group. However, the reduction in DF may have resulted in a compensation in the midfoot (not readily measured with standard motion analysis techniques). It is this midfoot pronation that is believed to most directly increase the strain of the plantar fascia.

All loading variables were higher in the PF group, with impact peak showing the strongest trend. Instantaneous vertical load rate was 15% higher in the PF group. Higher load rates may mean greater strain rates on soft tissues, such as the plantar fascia. These loading variables have not been previously examined in this group and may be important in the development of plantar fasciitis.

Structurally, the PF group had slightly lower arches. In addition, they presented with less ankle dorsiflexion range of motion. This may have resulted in the decreased peak dorsiflexion and dorsiflexion excursion seen during running. Finally, the PF group exhibited significantly greater calcaneal EV in stance, consistent with Warren et al. (1987). It was expected that this would be associated with greater rearfoot EV during running. While the structural measure was taken from markers placed directly on the skin, the dynamic measures were from markers placed on the shoe. This factor may have added unexplained variance to the dynamic rearfoot EV angle.

SUMMARY

Results of these preliminary, prospective data suggest that there may be predisposing structural and mechanical factors to the development of plantar fasciitis. These results may be strengthened as additional subjects are added. With additional subjects, regression analyses, utilizing both structural and mechanical variables will be performed. It is hoped that, as this research progresses, we will gain further insight into the cause of plantar fasciitis in runners. This will help us to develop optimal treatment interventions for this common injury.

REFERENCES

Davis, I et al, (2003) ISB Mtg, Dunedin, NZ
van Mechelen,W (1992). *Sport Med*, **14**, 320-35
Warren, BL et al. (1987) *MSSE*, **19**, 71-73
Williams, D et al (2000) *PhysTher* 80(9):864-71.

ACKNOWLEDGEMENTS

Supported by Dept of Defense grant DAMD17-00-1-0515. We would also like to acknowledge Kevin McCoy and Emily Mika for their assistance with data reduction.

QUANTIFICATION OF BIOMECHANICAL INTERACTIONS BETWEEN DRESSAGE HORSES AND RIDERS

Laurelyn E. Keener[1] and Morris Levy[2]

[1]Dept. of Biology
[2]Biomechanics Laboratory, Dept. of Health Physical Education and Recreation
University of Minnesota Duluth
E-mail: keen0070@d.umn.edu

INTRODUCTION

The equine sport of Dressage subjectively judges how well a horse and rider move together. Good movement has been qualitatively defined over the past four centuries. Dressage experts believe that a horse cannot move at its potential without the optimal level of balance and communication with the rider.

Cano et al. (1999) kinematically defined desirable movement of a rider-less Dressage horse as a large stride length and minimal angles of the power producing joints of the hind limb. Few studies have quantitatively measured horse-rider interactions. Peham et al. (2001) showed that measurable differences could be observed in the kinematics of multiple horses when ridden by a professional vs. amateur rider.

The availability of measurable horse-rider interactions would further benefit Dressage training, instruction and judging. Therefore, the purpose of this study was to correlate stifle- and hock- angle ranges of the horse with those of the rider hip and knee.

METHODS AND MATERIALS

Data Collection
Data collection occurred along a 12-meter track in an indoor riding arena. The footing was a mixture of shredded rubber and sand. Two pan and tilt cameras were positioned 15 meters apart, forming an equilateral triangle with the center of the track. Six eight-foot survey poles, placed at 2-meter intervals along the track, were used to calibrate the cameras.

One well-conditioned Dressage horse, accustomed to the arena in which data collection occurred, was fitted with its usual exercise tack (17.5-inch Dressage saddle and snaffle bridle). Six reflective markers were placed over palpable skeletal regions along the horse's right hind limb to aid in later identification of joint angles.

Ten adult amateur Dressage riders rode the horse. All riders had at least 4 years of riding experience and 50 hours of formal Dressage education. Reflective markers were placed on the following landmarks of each rider: top of the head, jaw, shoulder, hip, knee and ankle.

Following a five-minute warm-up period, each rider trotted (sitting) along the calibrated track. Five consecutive trials of each rider were filmed. All riders were filmed within a five-hour period, and their order was randomized.

Data Analysis
Using Peak Motus® Pan and Tilt Software, one stride cycle from each trial was captured and digitized. A stride cycle started with the right hind limb in perpendicular stance phase. The average stifle-, hock-, hip- and

knee- angle ranges of each horse-rider combination were calculated. Figure 1 illustrates the angles of interest from which correlations were derived.

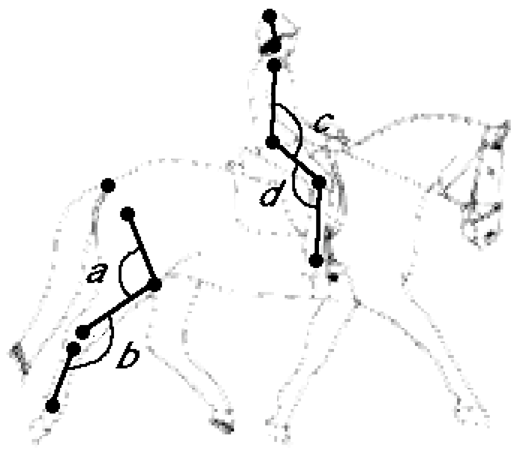

Figure 1: Outline of horse and rider shown for orientation purposes. Horse and rider marker placement and joint angles (*a* = stifle, *b* = hock, *c* = hip and *d* = knee).

RESULTS and DISCUSSION

Correlations were found between horse and rider angular kinematics. A moderately high correlation (r = -0.77) was found between the rider's hip and the horse's stifle (Table 1). Thus, a smaller change in a rider's hip angle coincided with a greater range of the horse's stifle, one of the power-producing joints identified by Cano et al. (1999). Similarly, a negative relationship between the knee angle and the stifle (r = -0.70) was observed. Therefore, rider position is strongly correlated with stifle action. However, the rider's hip- and knee- angles had low correlations (r = -0.38 and -0.31, respectively) with the horse's hock.

From the results, it appears that stifle movement is associated with rider kinematics. Traditionally, Dressage instructors and judges were mainly concerned with hock movement. These results would suggest that additional emphasis be placed on the stifle movement when considering horse-rider interactions.

Table 1: Correlation (r) and coefficient of determination (r^2) values of joint angle range during sitting trot of the riders' leg and the horse's hind limb.

Rider / Horse Angle	r	r^2
Hip / Stifle	-0.77*	0.60
Knee / Stifle	-0.70*	0.49
Hip / Hock	-0.38	0.15
Knee / Hock	-0.31	0.10

(*) $p < 0.05$

SUMMARY

Dressage, a sport based on qualitative observations, would benefit from quantitatively defining desirable interaction characteristics. In analyzing joint angles of ten riders on one horse, we found a moderately high negative correlation between rider’s hip- and knee- angles, and the horse's stifle angle. In contrast, there was little relationship between rider angular kinematics and the horse's hock angle. Further research will need to be conducted to determine how these results differ between horses.

REFERENCES

Cano, M. R. et al. (1999). *J. VET. MED,* **46**, 91-101.

Peham, C. et al. (2001). *Sports Eng.,* **4**, 95-101.

ACKNOWLEDGEMENTS

This project was funded in part by the University of Minnesota's Undergraduate Research Opportunity Program. Expressed appreciation to Nic Matack, Josh Turbes, Krissy Falk and Charles Luoma for help in data collection and processing.

COMPARING MUSCLE ACTIVITY DURING FORWARD AND BACKWARD STRIDING ON AN ELLIPTICAL TRAINER

Heather L. Clifton and Julianne Abendroth-Smith, Ed.D,

Dept. of Exercise Science, Willamette University, Salem, OR, USA
E-mail: hclifton@willamette.edu

INTRODUCTION

The elliptical trainer is a fairly new piece of exercise equipment, and despite its growing popularity, there is limited research on this training modality. Studies have examined cardiovascular responses and impact forces (Mercer, et al. 2001; Porcari, et al. 2000); however, to date there is no literature available on relative muscle activity at different grades and direction while using the elliptical trainer. Similar research on forward and backward running has shown muscle activity differences (Flynn, 1993). The purpose of this study was to determine the differences in muscle activity, as measured through electromyography (EMG), between forward and backward striding at three grades on an elliptical trainer.

Knowledge of relative muscle activity at different grades and direction would be beneficial in designing training and rehabilitation programs that incorporate the elliptical trainer. This would enable targeting specific muscle groups or avoiding re-injury, especially for athletes with muscle strains.

METHODS

Moderately active females (N = 10; age: 20.2 ± 1.0 years; mass: 66.8 ± 9.1 kg; height: 169.5 ± 7.1 cm) with previous experience using the elliptical trainer (Precor EFX546) were asked to stride both forward and backward at low, intermediate, and high grades, with the resistance and stride rate held constant. University IRB approval was obtained and all subjects signed informed consents.

Participants were asked to perform all conditions in a random order, striding for five minutes in each grade and direction setting. Surface EMG was used to determine the total integrated muscle activity averaged over two 5-second trials for four major muscle groups (gluteus maximus, rectus femoris, biceps femoris, and gastrocnemius). Recordings were taken at times during each condition without the subjects' knowledge of when the data collection actually occurred.

EMG activity was recorded using a Bortec AMT-8 Octopus cabled system, collected by Run Technologies DataPac software. EMG signals were rectified, low passed filtered (Butterworth 15 Hz, cutoff 7) and integrated. The resulting signals were normalized to the percent of signal time, and averaged per condition.

Maximum IEMG values were compared within each muscle group, between each grade x direction condition, using a repeated measures 2 x 3 ANOVA. Alpha was set at .05 level of significance.

RESULTS AND DISCUSSION

Each subject demonstrated unique patterns in muscle activity between conditions, but several trends were noted across subjects (see Figure 1). Within each muscle group, EMG activity was statistically significantly higher for the rectus femoris in backward striding when compared to forward striding ($\underline{F}$= 5.65, $\underline{df}$ = 1, $\underline{p}$= .04).

No other statistically significant differences for the main effects of grade or direction, nor for any interactions, were noted within the muscle groups. However, somewhat greater bicep femoris activity was observed in forward striding when compared to backward striding. The gluteus maximus was the only muscle that appeared to have increased EMG activity with increasing grade. The lateral gastrocnemius showed little variation with respect to either direction or grade.

SUMMARY

There is limited research on the elliptical trainer, particularly with regards to muscle activity. This information would help to design training and rehabilitation programs that either target or avoid specific muscle groups. This study found that the biceps femoris and rectus femoris were most active during forward and backward striding, respectively, while muscle activity for the gluteus maximus increased with grade, and the gastrocnemius did not demonstrate any trends. Overall, direction appears to have a greater influence on muscle activity than the grade, at least for this elliptical machine.

REFERENCES

Flynn, T.W., & Soutas-Little, R.W. (1993). *Journal of Orthopaedic and Sports Physical Therapy,* **17**(2), 108-112.

Mercer, J. et al. (2001). *Journal of Sport Rehabilitation,* **10**, 48-56.

Porcari, J. et al. (2000). *Fitness Management,* 50-53.

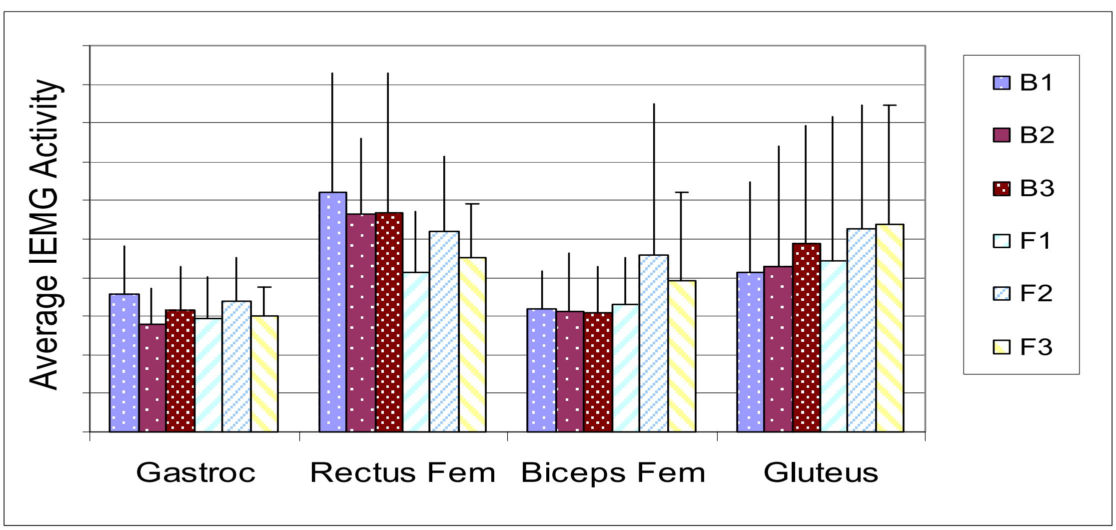

Figure 1: Average IEMG activity for each muscle group during forward (stripes) and backward (dots) striding at low (1), intermediate (2), and high (3) grades.

PREDICTED HIP JOINT REACTION FORCES DURING PRONE HIP EXTENSION WITH VARYING CONTRIBUTION FROM THE GLUTEAL MUSCLES

Cara L. Lewis[1], Shirley A. Sahrmann[2], and Daniel W. Moran[3]
[1] Movement Science Program, [2] Program in Physical Therapy, School of Medicine
[3] Department of Biomedical Engineering
Washington University in St. Louis, St. Louis, MO, USA
E-mail: lewis@wustl.edu

INTRODUCTION

Acetabular labral tears are a recently recognized source of anterior hip pain (AHP). Excessive forces have been implicated as one cause of these tears. A clinical sign of a tear is AHP with prone hip extension. We propose that the pain is due, in part, to excessive force on the anterior structures of the hip resulting from altered movement and muscle recruitment patterns. In support of this theory, if manual pressure is applied to the proximal femur and maintained in a posterior direction during active hip extension, thus countering the excessive force, the pain is reduced.

The purpose of this study is to use a 3D static musculoskeletal model to estimate the hip joint reaction forces when muscle recruitment is altered while maintaining the leg in the prone hip extended position. We hypothesize that recruitment of muscles which originate close to the axis of rotation yet insert farther from the axis will result in higher joint reaction forces when compared to recruitment of muscles which both originate and insert close to the axis of rotation.

METHODS

A six degree of freedom, 3D musculo-skeletal model of a lower leg was developed to calculate joint reaction forces in the hip, knee, and ankle. Musculoskeletal parameters were adapted from Delp 1990. Kane's Method (Kane and Levinson, 1985) and AUTOLEV 3.1 (OnLine Dynamics, Inc., Sunnyvale, CA) were used to generate the dynamic equations of motion. The general form of the dynamic equations of motion is:

$$\mathbf{M}(\vec{\mathbf{Q}})\ddot{\vec{\mathbf{Q}}} = \vec{\mathbf{T}} + \vec{\mathbf{P}}(\vec{\mathbf{Q}},\dot{\vec{\mathbf{Q}}}) + \vec{\mathbf{V}}(\vec{\mathbf{Q}},\dot{\vec{\mathbf{Q}}}) + \vec{\mathbf{G}}(\vec{\mathbf{Q}}) + \vec{\mathbf{E}}(\vec{\mathbf{Q}},\dot{\vec{\mathbf{Q}}})$$

where M is the mass matrix, T is the net joint torques contributed by the force in the muscles spanning all joints, P is the torques developed passively in the joints due to viscoelastic damping and passive joint structures, and V, G, and E are the instantaneous segmental torques caused by the inertial, gravitational, and external forces, respectively. As we were most interested in reaction forces when holding in prone the hip in a static extended, position, the only non-zero torques in the model were those due to muscles (T) and gravity (G).

Hip position was varied from 0 to 15 degrees of hip extension in one degree increments with the knee extended for all iterations. For each iteration, a pseudoinverse optimization routine was used to solve for the optimal set of muscle forces (Yamaguchi et. al. 1995) needed to hold the leg the desired position. Once the optimized muscle stresses were solved simultaneously across all joints, the model calculated the resulting 3D reaction forces in the hip.

In order to estimate the reaction forces in the hip with different contributions from the gluteal muscles, we simulated four different conditions. In the first condition, the reaction forces were estimated without any restrictions on the system. In the second, third and fourth conditions, the strength of the gluteal muscles (gluteus maximus, medius, and minimus) was reduced to 50%, 25%, and 5% of normal respectively to replicate weakness or decreased recruitment, and the reaction forces were recalculated.

RESULTS AND DISCUSSION

Failure to appropriately recruit the gluteal muscles which both originate and insert close to the hip axis of rotation, resulted in higher joint reaction forces in both the anterior and superior directions while in prone maintaining the hip in 0 to 15 degrees of extension. When the gluteals muscles were not fully recruited, the semimebranosis was recruited more to develop the appropriate hip extension moment. The utilization of the hamstring muscles, which originate close to the hip joint on the ischium and inserts distally on the tibia and fibula, results in increased muscle contraction to make up for the lost hip moment output of the gluteal muscles. These increased muscle contractions, in turn, result in increased joint reaction forces. Furthermore, as the hip extends, the line of action of the hamstrings changes more quickly due to its distant attachment.

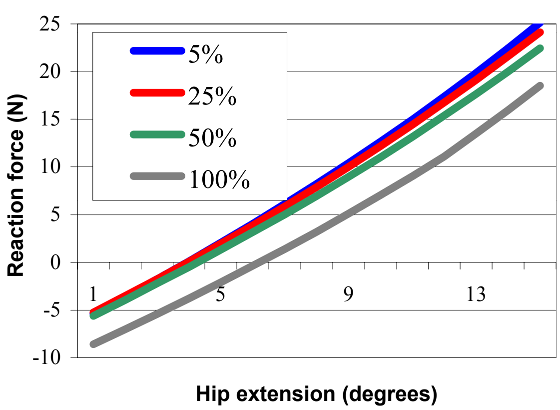

Figure 1: Anterior hip joint reaction forces with varied percentages of gluteal strength.

The anteriorly directed joint reaction forces are of particular importance. These forces are thought to result in anteriorly located tears, which are most frequent. Because the acetabulum is rotated 30° anteriorly in the frontal plane, these anteriorly directed forces must be absorbed primarily by the labrum itself, and not the boney acetabulum.

SUMMARY

A 3D musculoskeletal model was modified to estimate joint reaction forces in the hip when performing hip extension in prone with varying contributions from the gluteal muscles. When the gluteal muscles were at full strength (100%), the anterior and superior joint reaction forces were lower than in any simulation with reduced gluteal strength or recruitment. Failure to appropriately maintain strength and recruit the gluteal muscles while performing prone hip extension may result in AHP due to increased joint reaction forces.

REFERENCES

Cheng. J.Y., Buchanan, T.S. (1998). *Proceedings of NACOB'98,* 525-526.

Delp, S. L. (1990). Surgery simulation: a computer graphics system to analyze and design musculoskeletal reconstructions of the lower limb. Department Mechanical Engineering. Palo Alto, California, The Stanford University.

Jensen, J.L., Phillips, S.J. (1991). *J. Motor Behavior,* **23**, 63-74.

Jones, A.C. et al. (1988). *Simulation Techniques for Biological Systems*. Cambridge University Press.

Kane, T. R. and D. A. Levinson (1985). Dynamics: theory and applications. New York, NY, McGraw-Hill.

G.T. Yamaguchi, D.W. Moran and J. Si (1995) Computationally efficient method for solving the redundant problem in biomechanics. *Journal of Biomechanics*. Vol. 28, No.8 pp. 999-1005.

ESTIMATION OF THE ACCURACY OF A SHAPE-FROM-SILHOUETTE MARKERLESS MOTION CAPTURE SYSTEM

Lars Mündermann[1], Ajit Chaudhari[1], Gene Alexander[1], Thomas P. Andriacchi[1,2,3]

[1]Division of Biomechanical Engineering, Stanford University, Stanford, CA
[2]Bone and Joint Center, Palo Alto VA, Palo Alto, CA
[3]Department of Orthopedic Surgery, Stanford University Medical Center, Stanford, CA
lmuender@stanford.edu

INTRODUCTION

The most common methods for accurate capture of three-dimensional human motion require a laboratory environment and the attachment of markers or fixtures to the body segments. These laboratory conditions can cause adaptive changes to normal patterns of locomotion that introduce experimental artifact. For example, it has been shown that attaching straps to the thigh or shank alters joint kinematics and kinetics (Fisher 2003). Thus our understanding of normal and pathological human movement would be enhanced by a method that allows capture of human movement without the constraint of fixtures or markers placed on the body. Markerless methods are not widely available because the accurate capture of human motion without markers is technically challenging. A recently reported method in the computer vision literature using shape-from-silhouette (SFS) reconstruction offers an attractive approach (Cheung 2003). However, the factors influencing the accuracy of this method have not been addressed. The purpose of this study was to evaluate the accuracy of SFS reconstruction of a body for different camera placements, number of cameras, camera resolution and object contours.

METHODS

The analysis was conducted in a virtual environment using a realistic human form generated with a 3D laser scanner (CyberScanner, Monterey, CA) (92461 vertices; average 3D inter-point distance 4±1mm). Camera placement for SFS was evaluated using 16 virtual snapshots simulating 640×480 cameras, each with a field of view of 80°. The uniform arrangement of the 16 cameras approximated a hemisphere with each camera fully capturing a 3×2×1.5m viewing volume and directed towards the center of this volume.

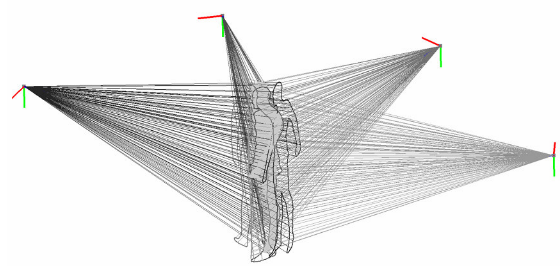

Figure 1: SFS reconstruction using four cameras.

SFS 3D point clouds were constructed from points along rays that extend from the camera positions through points along the corresponding silhouettes (Figure 1) choosing 8 out of the 16 total cameras, resulting in 12870 combinations. Accuracy was evaluated by calculating the percentage of vertices of the original mesh with a shortest distance to the point cloud smaller than a threshold value. Subsequently, the accuracy of SFS based on the number of cameras (4, 8, 16) and resolution of the camera (320×240, 640×480, 1280×960) was evaluated using the optimal camera placement. In each case, one camera was placed above the object while the remaining cameras were placed uniformly around the object in a circular plane at height 1m with one camera directly in front of the object. All cameras were directed towards the center of the rectangular viewing volume. The SFS point cloud density was determined by the distance between points along silhouettes and the spacing along the rays. The distance between neighboring points along silhouettes corresponded to pixel distance, and the distance of neighboring points along rays was set to 4mm (approximately the inter-point distance of the original mesh). SFS 3D point clouds were evaluated by calculating the shortest distances to the original mesh using Geomagic Studio (Raindrop Geomagic, NC).

RESULTS AND DISCUSSION

SFS reconstruction was sensitive to camera placement. The most accurate reconstruction based on shortest distance between the original mesh and SFS point clouds was obtained by placing one camera directly above and all others at a height of 1m, uniformly distributed in a circle around the object. Cameras with higher resolutions decreased the standard deviation (Figure 2a,b,c; Table 1). The number of points in the point clouds varied approximately proportional to the resolution. Similar results were obtained when all silhouettes were resampled with a fixed point distance of 4mm, resulting in similar numbers of points in the point clouds. While significant improvements ($P < .001$) were obtained, the relative changes were minor, suggesting that a 320×240 resolution may be sufficient to capture the body surface. Greater reduction in error occurred by increasing the number of cameras (Figure 2d,e,f; Table 1; $P < .001$). These results suggest that increasing the number of cameras is more effective than improving camera resolution. In general, SFS reconstructions were not able to capture surface depressions such as eye sockets and lack accuracy in narrow spaces (Figure 2f). For instance, the arm pits and groin region yield greater deviations than other regions of the body. Nevertheless, most of lower and upper limb surfaces were reconstructed very accurately with 8 or more cameras. This study demonstrates the feasibility of developing an accurate markerless motion capture system on the basis of SFS.

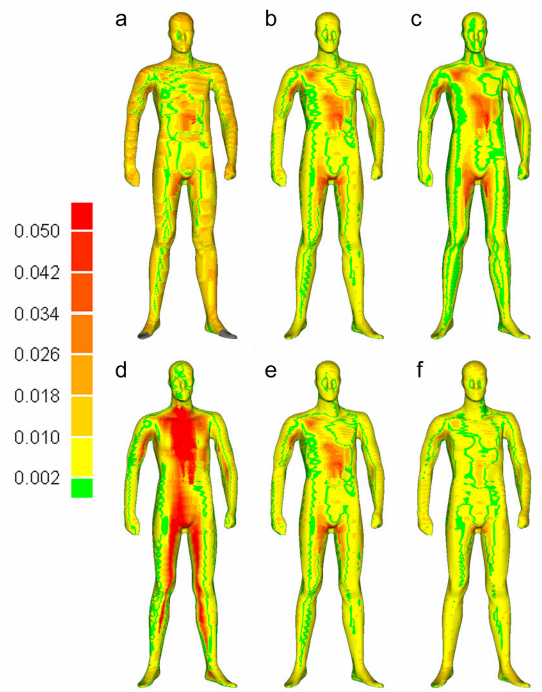

Figure 2: Absolute shortest distance between original mesh and SFS point clouds dependent on camera resolution (a) 320×240, (b) 640×480, (c) 1280×960 for 8 cameras and number of cameras (d) 4, (e) 8, (f) 16 for 640×480 cameras.

Table 1: Standard deviation and maximum distance between the original mesh and SFS point clouds and number of points in SFS point clouds dependent on camera resolution (320×240, 640×480, 1280×960) for 8 cameras and number of cameras (4, 8, 16) for 640×480 cameras.

	SD [mm]	max [mm]	points
320×240	11.4	54.6	33531
640×480	9.3	58.6	76381
1280×960	8.8	56.9	161276
4	19.8	91.0	92735
8	9.3	58.6	76381
16	6.3	40.1	71706

REFERENCES

Fisher D., et al. (2003) *ASME Bioeng. Conf.*, 849.
Cheung G. K. M., et al. (2003) *CVPR 2003*, I-77-84.

ACKNOWLEDGEMENTS

Funding provided by NSF #03225715 and VA #ADR0001129. The authors gratefully acknowledge valuable inputs by Stefano Corraza.

A VIRTUAL MODELING APPROACH FOR GENERATION, DESIGN ANALYSIS, AND FABRICATION OF 3D HUMAN SKELETAL MODELS

Charles S. Sullivan III and Denis J. DiAngelo

Department of Biomedical Engineering, The University of Tennessee Health Science Center, Memphis, TN, USA
E-mail: ddiangelo@utmem.edu Web: http://memphis.mecca.org/bme/bttlweb/

INTRODUCTION

Computer modeling of human anatomy forms the basis of several research approaches in biomedical engineering, including generic model manufacture, manufacture of implant devices, real-time animation, finite element modeling (FEM), and image guided surgery. The expense of and incompatibility between different computer aided design (CAD) and manufacturing (CAM) programs, added with the complex shape and morphology of human anatomy, have limited the creation of accurate virtual models of the human skeletal anatomy and related implant devices (Duerstock, 2003).

The Virtual Models can be used in various biomedical engineering applications: manufacture of human skeletal models and joint implants, FEM analysis of human skeletal models and joint implants, simulation and animation of biomechanical test results, and the mechanical design and FEM analysis of implant devices. The practice of combining computer tomography (CT) scans to form a 3D image of human anatomy is not new (Yoo, 2001). Using these images to produce dimensionally accurate models of complex human anatomies such as the spine, skull, jaw, teeth, hands, and feet is currently the subject of several research projects (Enciso, 2003). In this project, we generated a software \ hardware pipeline for the creation of accurate models of human skeletal anatomy.

METHODS

A method to generate a model of human skeletal anatomy suitable for use on a desktop PC was developed using the following process:

- Identify and evaluate sources for generating input data for the models.
- Identify and evaluate software and hardware for creating virtual models from input data.
- Generate the virtual 3D solid models.
- Demonstrate potential applications.

RESULTS AND DISCUSSION

Several software packages were evaluated for the model generation process. CT slices in the DICOM (.dcm) format were most commonly used for model generation, although laser surface scanning was also used. Laser scans provide an accurate point cloud of an object, but can only be used to model surface information. Laser scanning of skeletal anatomy cannot be performed on a living patient, which limits some uses for immediate patient benefit. An advantage of CT scans is that they describe both the internal and external surfaces of an object in question and they can be taken from a living patient. Medical image-processing software (SliceOmatic 4.2, Tomovision) was used to segment regions of interest (ROI) from CT scanner data. The process was performed using manual and automated tools that manipulated gray scale image thresholds for tissue separation (Figure 1).

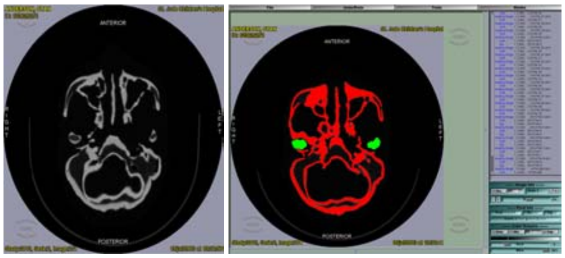

Figure 1: Example of ROI segmentation.

Output from the CT segmentation was converted into stereo lithography file formats (.stl) as point clouds. The point cloud data were imported into a volumetric surface modeling program (Geomagic Studio 5, Raindrop). Digital smoothing algorithms, in combination with manual editing techniques within this software, allowed for excellent surface reproduction from point cloud data, as shown in Figure 2.

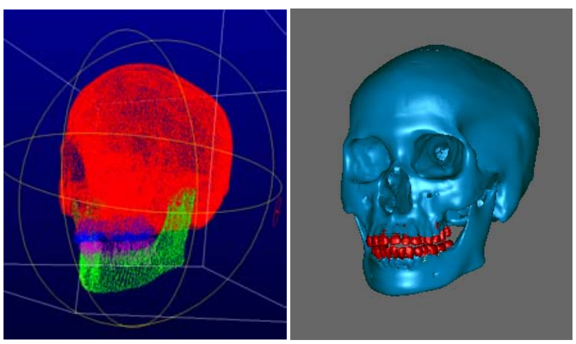

Figure 2: 3D model from point cloud data.

Geomagic Studio also provided for the conversion of the surface models into several file formats (.stl, iges, .stp, .dwg, .3do, etc.) that are compatible with many standard parametric modeling programs as well as popular FEA\FEM and CAD\CAM software. In addition, Geomagic has the ability to add datum points and axes to the models that can be used in "down stream" editing applications. Parametric modeling programs (Pro-Engineer, PTC Corp. and Unigraphics NX, EDS Inc.) were used to edit, assign material properties, and generate tool paths for CNC machining to the models, as shown in Figures 3 and 4 respectively.

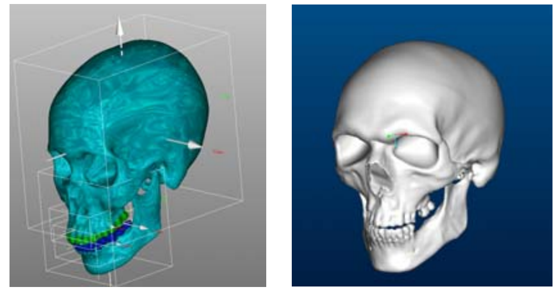

Figure 3: Left, Example of the addition of bounding boxes, axes, and textures. Right, 3D solid model of human skeletal anatomy.

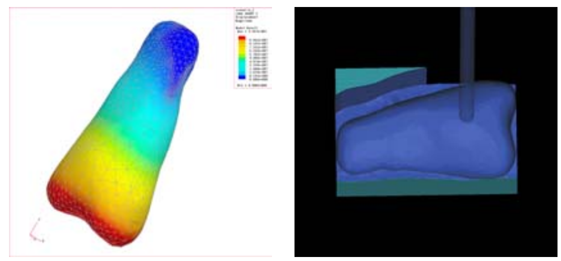

Figure 4: Examples of FEA and CNC tool path generation of a tooth modeled from CT data using appropriate software.

SUMMARY

A cost effective method for generating 3D models of human skeletal anatomy using commercially available software suitable for use on a desktop PC was developed. Optimal input data file formats (.dcm) were identified, as well as optimal output formats for surface generation (.stl) and 3D surface modeling (.iges). Software packages were identified that accomplished ROI segmentation, point cloud generation, surface smoothing\editing, and incorporation into parametric modeling programs.

REFERENCES

Enciso R. et al. (2003) *Orthod Craniofacial Res,* **6 (Suppl. 1):** 66-71.

Duerstock B. et al., (2003). *Journal of Microscopy*, **210:** 138-148.

Seung-Schik Yoo et al. (2001). *Journal of Neuroscience Methods,* **112:** 75-82.

EFFECT OF POSITIVE POSTERIOR HEEL FLARE ON KINETICS AND TIBIALIS ANTERIOR MUSCLE ACTIVATION DURING RUNNING GAIT

Robin M. Queen,[1,4] Michael T. Gross,[2,4] and Bing Yu[1,2,3,4]
[1] Department of Biomedical Engineering, [2] Division of Physical Therapy, [3] Department of Orthopedics, [4] Center for Human Movement Science,
The University of North Carolina at Chapel Hill, Chapel Hill, NC, USA
E-mail: rqueen@med.unc.edu

INTRODUCTION

Runners can develop exercise induced (EI) anterior compartment syndrome by training in running shoes that are not correct for their foot type, changing from running with a midsole strike pattern to running with a rearfoot strike pattern, running intervals, or running on banked surfaces (Blackman, 2000; Detmer, et al, 1985). The focus of this study was to determine the effect of a positive posterior heel flare (PPHF) on tibialis anterior (TA) activation, sagittal plane dorsiflexion (DF) moment requirement, and ground reaction forces (GRF) during running gait. This study was designed to identify one possible cause for the development of EI anterior compartment syndrome. A PPHF is defined as the presence of the midsole material being inclined posteriorly away from the posterior aspect of the shoe.

METHODS

Each subject was tested in two different running shoes: the Asics Gel Cumulus and the Saucony Grid Trigon. These two shoes were chosen because they had similar properties except for the degree of PPHF. The Saucony Grid Trigon had a positive posterior heel flare of $11^{\circ} \pm 1^{\circ}$ with a midsole density of 60 ± 3 durometer, while the Asics Gel Cumulus had a positive posterior heel flare of $2^{\circ} \pm 1^{\circ}$ and a midsole density of 53 ± 4 durometer. Recreational athletes were enrolled as subjects if they demonstrated a rearfoot strike pattern based on an observational video gait analysis. Subjects reported no history of lower extremity injuries in the past six months, no history of a fasciotomy, and were not using foot orthotics.

Muscle activation (telemetry EMG) and GRF (Bertec force plate) were recorded at a sampling rate of 1200Hz, while video data were collected at 120Hz. Seven trials were recorded for each shoe with the subjects running at ± 5% of their self-selected speed as determined from the average of five practice trials. Three randomly selected trials were used for analysis. These trials were averaged for the following dependent variables: slope of the vertical GRF (vGRF), peak and mean DF moment requirement, DF angular impulse, peak and mean vGRF, peak posterior GRF (pGRF), mean anterior-posterior GRF (apGRF), and mean amplitude TA activation when a DF moment requirement was present. Each dependent variable was tested using a 2x2 mixed model [one between factor (gender) and one within factor (shoe)] repeated measures ANOVA ($\alpha = 0.05$). The between trial Intraclass Correlation Coefficient [ICC (3,3)] was calculated for all subjects for each dependent variable under each shoe condition. Acceptable between trial reliability was identified as an ICC value greater than 0.70.

RESULTS AND DISCUSSION

Forty-three subjects (19 female, 24 male) ranging in age from 18 to 37 participated in the study. Female subjects had an average age of 23.4 ± 4 years, an average mass of 60.4 ± 7.7 kg, and an average height of 1.66 ± 0.05 m. Male subjects had an average age of 23.5 ± 4 years, an average weight of 74.3 ± 8.9 kg, and an average height of 1.78 ± 0.02 m. All ICC (3,3) values were greater than 0.70 for all dependent variables for both shoes, indicating acceptable reliability.

No gender by shoe interaction existed for any dependent variable. Women had significantly greater TA activation than men (p=0.029). No significant difference in TA activation existed between the two shoes, however, an increasing trend in activation was present for the Saucony (p=0.064). No statistically significant differences existed for gender or shoe for mean vGRF, peak and mean DF moment requirement, and DF angular impulse. The slope of the vGRF was significantly greater for the Asics (p=0.001), with no significant difference between genders. The peak pGRF was significantly greater for men than women (p=0.004), and significantly greater in the Asics shoe (p=0.043). Finally, the mean apGRF was significantly greater in the posterior direction for the men (p=0.002), with no difference between the shoes.

The increase in running speed for the men could explain the increase in the peak pGRF as well as the increase in the mean posterior apGRF. An increase in the PPHF for the Saucony caused a significant decrease in the slope of the vGRF, in spite of the greater midsole stiffness for this shoe. Previous research has indicated that shoes with stiffer midsoles may have higher impact loading rates than shoes with less stiff midsoles (McNair, et al, 1994; Nigg, et al, 1987). The decrease in the slope of the vGRF may have resulted from subjects landing in more DF, with greater DF excursion resulting in the vGRF being applied over a longer time, thereby decreasing the slope of the vGRF.

SUMMARY

While no significant difference existed between the shoes for the mean amplitude activation of the TA, the results indicated a trend towards an increase in TA muscle activation for the Saucony. This increase in muscle activation could possibly lead to an increase in pressure within the anterior compartment, potentially leading to the development of EI anterior compartment syndrome. An increase in the amount of ankle motion could possibly explain the attenuation of the GRF and the slope of the vGRF from heel strike to impact peak. Use of this strategy to accommodate to shoes with increased PPHF and increased midsole stiffness may also be linked to increased TA muscle activation.

REFERENCES

Blackman, P. G. A review of chronic exertional compartment syndrome in the lower leg. *MSSE*. 32:S4-S10, 2000.

Detmer, D. E., et al. Chronic Compartment Syndrome: diagnosis, management, and outcomes. *Am. J. Sports Med*. 13:163-170, 1985.

McNair, P. J. & R. N. Marshall. Kinematic and Kinetic parameters associated with running in different shoes. *British J. of Sports Med*. 28, 1994.

Nigg, B. M., et al. The Influence of Running Velocity and Midsole Hardness on External Impact Forces in Heel-Toe Running. *J. of Biomech*. 20:951-959, 1987.

ACKNOWLEDGEMENTS

Fleet Feet, Inc. & UNC Injury Prevention Research Center

A VIRTUAL MODEL OF THE HUMAN CERVICAL SPINE FOR PHYSICS-BASED SIMULATION

Hyung S. Ahn and Denis J. DiAngelo

Department of Biomedical Engineering, The University of Tennessee Health Science Center, Memphis, Tennessee, USA
E-mail: ddiangelo@utmem.edu Web: http://memphis.mecca.org/bme/bttlweb/

INTRODUCTION

With emerging computer technology, there is an effort to integrate computer graphics, diagnostic imaging tools, and computer aided design and engineering analysis programs into biomedical research. The use of computer graphics to model the cervical spine provides the opportunity to create a virtual simulator for kinematics and kinetic testing of the cervical spine. The objective was to develop a graphics - oriented interactive cervical spine model for physics-based dynamic simulation.

METHOD

Modeling of the virtual cervical spine consisted of two main phases: 1) accurately creating the 3-D bony anatomy and 2) defining the interconnecting joints and soft tissue components. In the first phase, the geometry of the skull, cervical vertebrae, and upper torso (clavicles, scapulae, ribs and sternum) were created from female computer tomography (CT) images available through the Visible Human Project® using a medical image processing software (SliceOmatic 4.2, Tomovision) and volumetric surface modeling software (Geomagic Studio 5, Raindrop). To maintain accurate reconstruction of the vertebral geometry, especially at the facet joint regions, a manual-tracing method was used to create each body (C1 to T1). The reconstructed anatomical model is shown in Figure 1. In phase two, the reconstructed Skull-Cervical vertebrae-Upper torso geometry was imported into a physics-based multibody simulation software program (VisualNastran 4D, MSC) that was used to define the interconnecting joints and soft tissue elements. The facet joints were modeled as colliding biconvex surfaces at C1-C2 and a ball on a plane joint between vertebrae C2 through T1 (Figure 2).

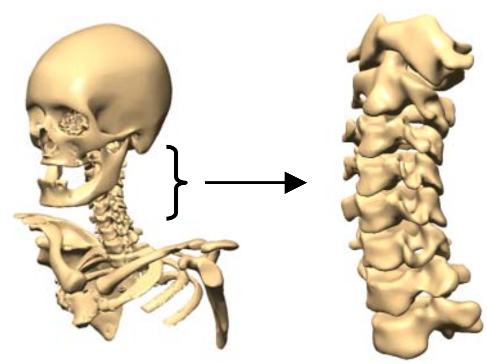

Figure 1: Reconstructed anatomical model without interconnecting structures.

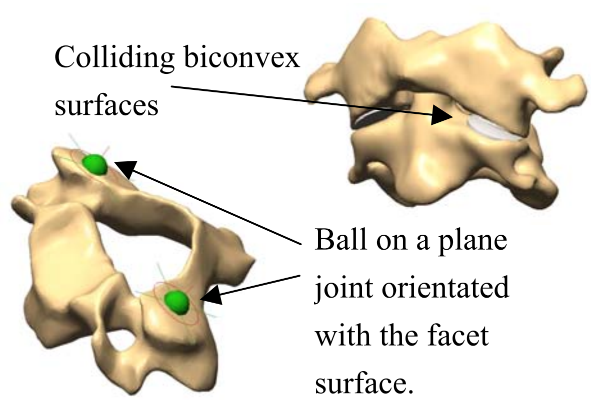

Figure 2: Modeling the Facet Joints.

Muscles were modeled by curving a series of linear actuator (Figure 3a). The actuator elements were controlled by an external application referred to as The Virtual Muscle (Cheng et al, 2000). Intervertebral discs were modeled as nonlinear, viscoelastic elements, with six-degrees of freedom (Figure 3b). Ligaments were modeled as a nonlinear spring-damper element. The material properties of intervertebral discs and ligaments were adopted from the in-vitro experimental data and the literature (Panjabi et al., 2001, Yoganandan et al., 2001).

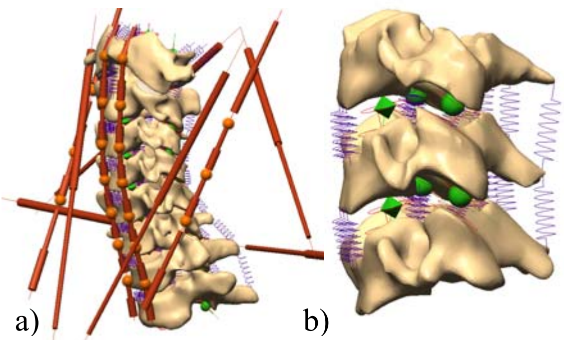

a) b)

Figure 3: (a) The reconstructed cervical spine with interconnecting structures and (b) exploded view of C3-C4-C5 segments.

RESULTS

A testing protocol replicating the physiologic motion response of the cervical spine (DiAngelo and Foley, 2003) was simulated in the virtual environment using Visual Nastran 4D (Figure 4). The motion response of the virtual spine simulator was comparable to the in vitro test results.

CONCLUDING DISCUSSION

A process for creating an accurate virtual model of human cervical spine was developed and used to simulate the dynamic flexion and extension kinetics.

The model can be used to simulate other biomechanical tests, such as the dynamic motion behavior of spinal arthroplasty or fusion hardware. With muscle control strategies, the model can also enable simulation of in vivo dynamics.

REFERENCES

Cheng, E.J. et al. (2000). *J. Neurosci. Methods* **101,** 117-130.

DiAngelo D.J., Foley K.T. (2003). *Spinal Implants: Are We Evaluating Them Appropriately?,* ASTM STP1431, 155-172.

Panjabi, M.M. et al. (2001). *Spine* **26,** 2692-2700.

Yoganandan, N. et al. (2001). *Clin. Biomech.* **16,** 1-27.

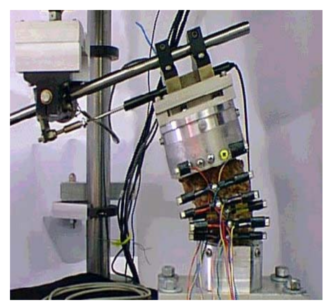

a) In Vitro Testing Arrangement

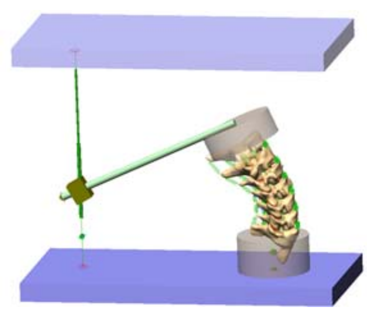

b) Virtual Simulation Model

Figure 4: Comparison of In Vitro Cervical Spine Model and Virtual Model. a) Extension testing of cervical spine mounted in biomechanical testing system. b) Simulation of the extension dynamics of the virtual cervical spine model.

CLASSIFICATION TREE ANALYSIS OF FOOT TYPES USING 3-D MEASURES

Eric S. Rohr[1], William R. Ledoux[1,2,3], Jane B. Shofer[1], Randal P. Ching[1,2,3], and Bruce J. Sangeorzan[1,2]

[1]RR&D Center of Excellence for Limb Loss Prevention and Prosthetic Engineering, VA Puget Sound Health Care System, Seattle, WA
Departments of [2]Orthopaedics and Sports Medicine and [3]Mechanical Engineering, University of Washington, Seattle, WA
E-mail: eric.rohr@med.va.gov Web: www.seattlerehabresearch.org

INTRODUCTION

From an architectural perspective, feet are shaped differently and can be generally categorized as pes cavus (PC, high arch), neutrally aligned (NA, neutral arch), or pes planus (PP, low arch). Current classification schemes are typically 2-D and may contain subjective components (Razeghi and Batt 2002). The purpose of this study was to develop and validate a 3-D, objective method for determining foot type.

METHODS

Forty subjects were recruited and examined by an orthopedic surgeon to identify their foot type. If the foot type was bilateral both feet were analyzed otherwise only the foot of interest was studied. This recruitment resulted in a total of 64 feet (31 PP, 20 NA, and 13 PC). The PP foot type was further divided into asymptomatic and symptomatic groups for other studies, thus more PP feet were analyzed in this analysis.

Simulated weight bearing CT scans of the subject's foot and ankle were studied. From the CT scans 3-D models of each bone were created using NIH Image v.1.6.2 and custom developed software. Based on each bone's surface geometry, inertial matrices were computed (assuming homogeneous bone density) to establish local Cartesian coordinate systems. These axes were then used to describe bone to bone orientation using the Z, Y', X" Euler angles (Camacho et al. 2002).

Euler angles were calculated between the 1st Metatarsal-Talus (M1Tal), 5th Metatarsal-Talus (M5Tal), Calcaneus-Talus (CalTal), 2nd Metatarsal-1st Metatarsal (M2M1), Calcaneus-Fibula (CalFib), Cuneiforms-Talus (CunTal), Cuneiforms-Navicular (CunNav), and Navicular-Talus (NavTal). The resulting twenty-four angles were used in a classification tree analysis (CTA) to determine if Euler angles can be used to classify feet into the 3 clinical foot type groups. The CTA recursively partitions the 64 feet into subgroups, which most closely approximate the three clinical foot type groups using the Euler angles. A misclassification rate was computed using a cross-validation algorithm.

RESULTS

The CTA classified the feet into subgroups using 3 partitions of data using 3 different Euler angles (Figure 1). The first measure CunTal X" represents a combination of dorsi/plantar flexion and ab/adduction of the cuneiforms relative to the talus. Thus feet with CunTal X" < 23.55° have cuneiforms that are less dorsiflexed, and more adducted and represent the PC population. The first measure that separates PP from NA is the dorsi/plantar flexion of the 1st metatarsal

(M1Tal X”). Feet that have 1st metatarsals that are plantar flexed less than 4.92° relative to the talus were classified as PP. The final determinate used to separate NA from PP was the CunNav X” angle. Feet that had cuneiforms that were adducted less than 32.14° relative to the navicular were identified as NA, whereas cuneiforms with more than 32.14° were classified as PP.

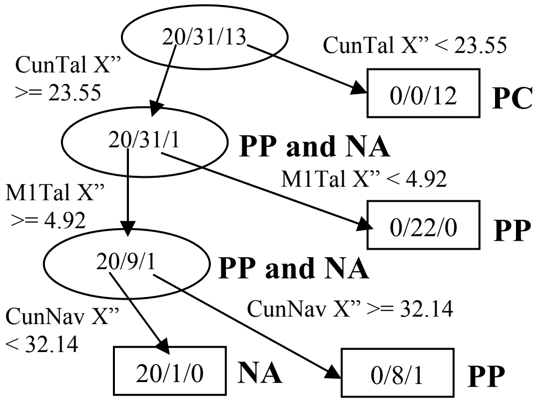

Figure 1: The Classification tree. The numbers in each branch represent the number of feet according to foot type NA/PP/PC, whereas the label indicates the category the feet should be classified as.

This classification tree demonstrates that our methods were capable of classifying 62 of the 64 feet correctly. However, the cross validated misclassification error was 20%, reflecting some degree of instability in our classification tree. Figure 2 illustrates how if partitions lines are moved by a small distance, subjects are classifed into different groups.

DISCUSSION

This methodology was able to successfully classify 97% of the feet. Figure 1 shows that one PP foot was incorrectly classified as a NA foot, and a PC foot was misidentified as a PP foot. Since the cross validation analyses showed some instability, we believe this method as a classification tool would be able to successfully classify foot types from another data set with an 80% success rate. As this method is objective and based on 3-D morphology it may be a better mechanism for classification in the future than the current means. Accurate classification of foot types can assist and improve in orthotic prescription and surgical correction.

REFERENCES

Razeghi, M. and Batt, M. (2002). *Gait Posture*, **15(3)**, 282-291.

Camacho, D. et al. (2002). *J. Rehabil Res Dev*, **39(3)**, 401-410.

ACKNOWLEDGEMENTS

This work was supported by the Department of Veteran Affairs project #A2180R

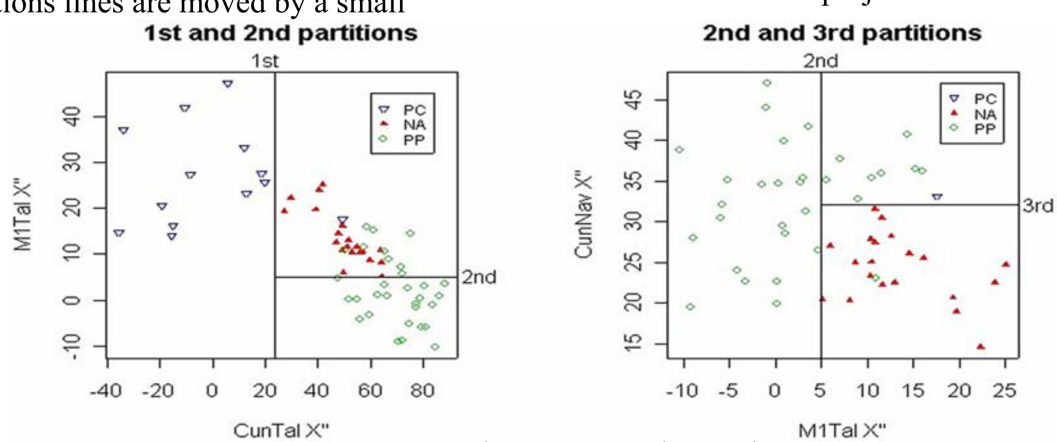

Figure 2: Euler angles used in the CTA: 2nd vs. 1st and 3rd vs. 2nd partitioning variables, with partition lines to illustrate each subgroup.

MUSCLE FUNCTION IN THE GENERATION OF PROPULSIVE AND BRAKING FORCES DURING RUNNING

Adam R. Gaines[1], Richard N. Hinrichs[1], and Philip E. Martin[2]

[1] Department of Kinesiology, Arizona State University, Tempe, AZ 85287-0404 USA
[2] Department of Kinesiology, The Pennsylvania State University, College Park, PA 16802 USA
email: adamgaines@fastem.com

INTRODUCTION

The most salient feature of the running gait has often been considered to be the generation of vertical forces in opposition to gravity. In comparison, horizontal ground reaction forces (GRFs) have traditionally been thought to play a much smaller role in running economy and muscle function. However, Chang and Kram (1999) found that by varying horizontal GRF demands, the energy cost of running could be reduced by one-third.

The purposes of this study were to find out which lower extremity muscles actively contribute to horizontal ground reaction force (GRF) production during running and to what degree muscle-tendon units use concentric or eccentric function.

METHODS

Fourteen subjects participated in this study, seven men and seven women between 20 and 39 years old. The group included sprint and endurance athletes of recreational to sub-elite ability. All were accustomed to running at least an hour per week for the past 3 months.

Each subject ran on a treadmill at 3.35 m/s while horizontal loads were applied via a waist belt attached to elastic tubing; Horizontal loads ranged from -8% body weight (BW) resistance to +12% BW assistance. Practice was given with this at least six days prior to the experimental session. A forward-directed or assistive pull increases braking impulses and reduces propulsive impulses. A rearward or resistive pull decreases braking impulses and increases propulsive impulses (Chang & Kram, 1999).

Muscle activities were measured in the soleus, gastrocnemius, tibialis anterior, vastus lateralis, rectus femoris, biceps femoris, and gluteus maximus. A sagittal plane video was recorded and combined with the regression equations of Hawkins and Hull (1990) to estimate muscle velocities.

The dependent variables for each of seven muscles were average stance activation and percent of total stance activation in concentric function. A one-factor repeated measures ANOVA was used to assess the significance of horizontal load effects (α=.05)

RESULTS

The gastrocnemius and soleus exhibited significantly lower mean stance activations with horizontal assistive loads (figure 1). Therefore, these two muscles contribute to propulsive impulses. The tibialis anterior had a significantly larger mean stance activation with horizontal assistance. All the muscles except the biceps femoris significantly increased their mean stance activation with increased horizontal resistance. Therefore all muscles except the biceps femoris may contribute to horizontal force production during faster running.

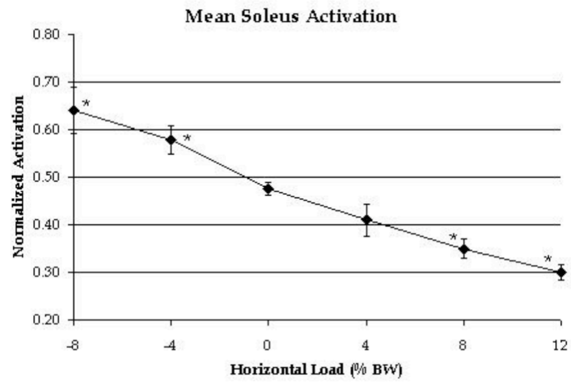

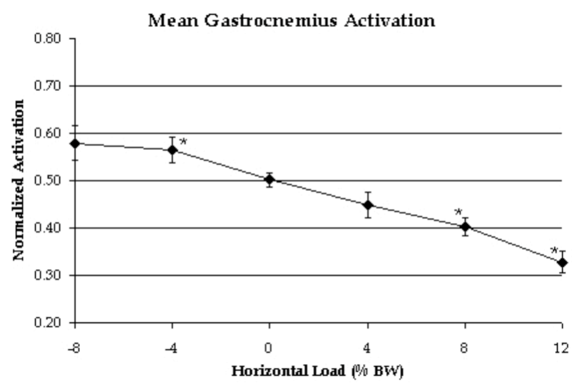

Figure 1: Mean stance activations of the soleus and gastrocnemius muscles

To address the question of whether muscles tended to function eccentrically or concentrically in producing braking and propulsive forces, integrated concentric stance activations were expressed as a percentage of the integrated stance activations. Few significant changes were observed across different horizontal loads. The idea that propulsive forces are generated concentrically and braking forces eccentrically is not supported by this study.

DISCUSSION

The gastrocnemius and soleus could potentially account for most of the energy cost of generating propulsive forces during moderate speed running, and by extension up to a third of the total cost.

Regarding eccentric/concentric function, muscles seem to rely more on adjusting activation levels generally in response to different horizontal GRF requirements than on changing shortening and lengthening activation levels independently. A potential consequence of this is that more economical runners may rely more on eccentric activations to generate propulsive forces.

A limitation was the inability to manipulate braking and propulsive forces independently. Also, only the stance leg was examined.

SUMMARY

The gastrocnemius and soleus muscles contribute to propulsive impulse generation during running. For all the other muscles measured, no results conclusively demonstrated involvement in propulsive or braking force production. Also, contrary to common assumption, braking forces do not necessarily have to be created through eccentric actions, and propulsive forces do not necessarily require concentric activation.

REFERENCES

Chang, Y., Kram, R. (1999). *J. Appl. Phys.*, **86**, 1657-1662.
Hawkins, D., Hull, M.L. (1990). *J. Biomech.*, **23**, 1163-1173.y

ACKNOWLEDGEMENTS

This study was supported by the Doug Conley Memorial Scholarship Fund.

THE EFFECTS OF MUSCLE TRAINING ON GAIT CHARACTERISTICS IN CHILDREN WITH DOWN SYNDROME

Bee-Oh Lim [1], Dong-Ki Han [2] and Young-Hoo Kwon [1]

[1] Biomechanics Laboratory, Texas Woman's University, Denton, TX 76204-5647
[2] Adapted Physical Activity Laboratory, Dept. of Physical Education, Seoul National University, Seoul, Korea
Email: imbo@biomechanics.snu.ac.kr Web: http://www.twu.edu/biom

INTRODUCTION

Patients with Down syndrome are characterized by a unique facial profile and medical complications such as heart problems, leukemia, obesity, and impaired kinesthesia. Specifically, excessive joint flexibility and weak muscles require special attention. Weak muscles cause flat-footed contact with no heel-strike, excessive abduction of the leg in the swing phase of the gait, and abnormal knee and hip flexion throughout the gait cycle (Parker, et al., 1986). Previous studies have reported increased muscle strength as a result of strength training in Down syndrome patients (Sayers, et al., 1996; Weber & French, 1988). It was suggested that training programs with exercises designed to strengthen the muscles in relatively short period time should improve the efficiency of the locomotion system (Neuman, et al., 1989). The purpose of this study was to investigate the effects of an 8-week muscle training program on the muscular fitness and gait characteristics in children with Down syndrome.

METHODS

Eight Korean male Down syndrome children (age: 12.0 ± 0.9 yrs; height: 134.9 ± 9.7 cm; mass: 34.4 ± 8.4 kg) with no history of heart problems participated in this study. Informed consents were obtained prior to the pre-test with the approvals of the primary care physicians. In both pre- and post-tests, the peak torque, work, and the average power of the knee flexors and extensors were measured using a Cybex 770 Isokinetic System at two different angular velocities: 60 deg/s and 180 deg/s. All isokinetic data were normalized to the body mass. Three-dimensional motion analyses were performed to obtain the maximum medio-lateral and vertical sway of the body center of mass (CM), toe-out, and the ankle, knee, and hip joint angles before and after the training. An AMTI force plate was used to measure the vertical and antero-posterior ground reaction forces simultaneously.

The muscle training program was composed of four leg exercises (squat, leg curl, leg extension, and toe raise) and two abdominal and back muscle exercises (sit-up and toe-raise), 3 sessions a week, 3 sets of 10-15 RM per session, for 8 weeks. The load was gradually increased, by 5 % at a time, to keep it within the 10-15 RM range. Sit-up and the hyperextension exercise were repeated until the onset of the fatigue (3 sets). The order of the exercises was randomly arranged to prevent excessive build-up of fatigue in a particular muscle group.

Repeated-measure ANOVAs were performed to see the changes in the dependent variables ($\alpha = .05$).

RESULTS AND DISCUSSION

All isokinetic variables (the peak torque, work, and the mean power) showed significant increases ($p < .05$) in response to the training (Table 1). The medio-lateral CM oscillation decreased significantly showing more stable gait. The post-test ML CM sway values were similar to that of the normal gait (5 cm). Toe-out revealed a significant decrease with the feet placed closer to the gait progression line with decreased external rotation (Table 2). The knee joint angle decreased significantly throughout the gait cycle, showing more flexed positions after the training (Table 2). The hip joint angle showed a significant decrease at foot-strike, meaning a more extended position.

The ground reaction force pattern was characterized by a wide spectrum of individual differences. In some participants, however, post-training vertical force patterns similar to the normal pattern were observed.

SUMMARY

The outcome of the 8-week muscle training program were:

1) increased muscle torque, work, and power,
2) increased postural stability with smaller medio-lateral sway of the body CM and less toe-out during the gait cycle, and
3) more upright body posture with increased hip joint angle and decreased knee joint angle.

REFERENCES

Neuman, G., et al. (1989). Development of functional stability of the musculoskeletal system in athletes in childhood and adolescence. *Arztl-Jugendkd*, **80**, 73-79.

Parker, A.W., et al. (1986). Walking patterns in Down syndrome. *Journal of Mental Deficiency Research*, **30**, 317-330.

Sayers, L.K., et al. (1996). Qualitative analysis of a pediatric strength intervention on the developmental stepping movements of infants with Down syndrome. *Adapted Physical Activity Quarterly*, **13**, 247-268.

Weber, R.C., & French, R. (1988). Down's syndrome adolescents and strength training. *Clinical Kinesiology*, **42**, 13-21.

TABLE 1: Summary of the changes in the isokinetic data (Mean ± SD; $p < .05$).

	Peak Torque (N·m)		Work (J)		Mean Power (W/kg)	
	Flexor	Extensor	Flexor	Extensor	Flexor	Extensor
Pre-Test	9.1±11.5	30.9±13.1	4.8±2.8	26.6±17.9	4.6±4.8	16.8±9.5
Post-Test	18.0±7.9	38.6±9.9	14.0±10.7	30.8±16.7	9.3±4.5	23.5±9.1

TABLE 2: Summary of the changes in the kinematic data (Mean ± SD; $p < .05$).

	M-L CM Sway (cm)	Toe-out at Foot-strike (deg)	Knee Angle at Foot-strike (deg)	Knee Angle at Toe-off (deg)	Hip Angle at Foot-Strike (deg)
Pre-Test	12.8±4.3	8.0±8.2	159.0±4.6	137.7±6.4	153.2±4.0
Post-Test	3.6±1.4	1.4±6.3	155.8±4.4	129.4±7.0	146.7±7.1

INFLUENCE OF PASSIVE ELASTIC JOINT MOMENTS ON THE METABOLIC ENERGY CONSUMPTION OF MUSCLES DURING GAIT

Darryl G. Thelen

Dept. of Mechanical Engineering, University of Wisconsin-Madison, Madison, WI, USA
E-mail: thelen@engr.wisc.edu Web: www.cae.wisc.edu/~thelen

INTRODUCTION

The passive stretch of soft tissues can produce substantial moments about the hip, knee and ankle joints (Reiner and Edrich 1999). This elastic behavior may serve as an energy storage and release mechanism during gait (Yoon and Mansour 1982). However, the extent to which passive elastic mechanisms actually reduce the metabolic cost of walking is not well understood. Furthermore, excessive passive joint stiffness may contribute to abnormal gait patterns. For example, it has been suggested that elderly adults with lower extremity impairments (e.g. knee osteoarthritis) may compensate by using tight hip flexors to passively assist swing leg movement (McGibbon 2003). The objective of this study was to estimate the effect of passive elastic joint moments on the metabolic energy consumption of lower extremity muscles during normal walking. The techniques and data provided could potentially be used to investigate the use of passive joint moments during movement in individuals with impairments.

METHODS

The body was modeled as an 8-segment, 21-degree-of-freedom articulated linkage. The model contained 64 Hill-type muscle-tendon units to represent the relationship between muscle excitation and active force development (Zajac 1989; Delp et al., 1990). Empirically derived double exponential functions were used to determine passive sagittal hip, knee and ankle moments from joint angles (Reiner and Edrich 1999). These functions included the contribution of passive muscle forces and accounted for the effect of adjacent joint angles (Figure 1).

Computed muscle control (Thelen et al., 2003) was used to determine muscle excitations that drive the model to track ensemble average kinematics and ground reactions of comfortable speed gait (1.3 m/s). A nominal simulation was first derived with passive joint moments included. A phenomological model was used to estimate the metabolic energy consumed by each muscle (Bhargave et al., 2004) over a gait cycle. Passive joint moments were then removed from the model and the gait data re-tracked to estimate the effect of elastic structures on metabolic energy consumption.

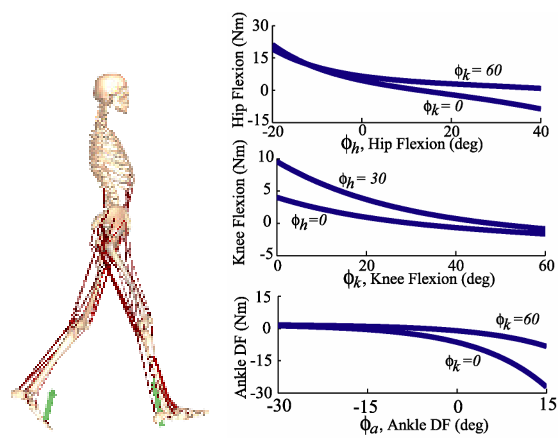

(a) (b)

Figure 1: (a) Forward dynamic musculoskeletal model used to simulate gait, (b) Passive sagittal joint moments at the hip, knee and ankle were estimated from hip, knee and ankle angles (Riener and Edrich, 1999).

RESULTS

The predicted rate of metabolic energy consumption during gait was 5.3 W/kg when passive joint moments were included about the hip, knee and ankle. Without passive moments, the energy consumption rate increased to 5.9 W/kg. Thus, a metabolic energy savings of approximately 10% was obtained via the storage and return of energy from passive elastic structures.

Passive hip moments reduced the activation required of iliopsoas and other hip flexors during late stance, thereby lowering the net energy consumed over the gait cycle by 20 J (Figure 2). The primary benefit of passive knee moments was to reduce the metabolic energy required of the hamstrings and gastrocnemius muscles during late swing. Passive ankle moments substantially reduced the metabolic energy required to the soleus during mid and late stance. However, slightly increased activation of the tibialis anterior diminished the net energetic savings attributable to passive ankle moments.

DISCUSSION

The passive force-length relationship of muscle is often included in Hill-type models that are used to simulate movement (Zajac 1989). However it is difficult to determine appropriate parameters for all the lower extremity muscles (notably optimal fiber and tendon slack lengths) that combine to represent the passive joint moment-angle behavior of individuals. It is more feasible to directly incorporate experimentally derived passive moment-angle relations within a forward simulation driven by active muscle-tendon units. This approach could be used in the generation of subject-specific simulations of gait, providing a quantitative framework within which to characterize the contributions of passive moments to both energetics and movement. Using a generic model of normal gait, we found the primary benefit of passive elastic joint moments was to reduce the metabolic energy required of the hip flexors, hamstrings, gastrocnemius and soleus muscles. A comparison of these results with gait simulations of impaired individuals may provide insights into the role that passive joint moments play in abnormal gait.

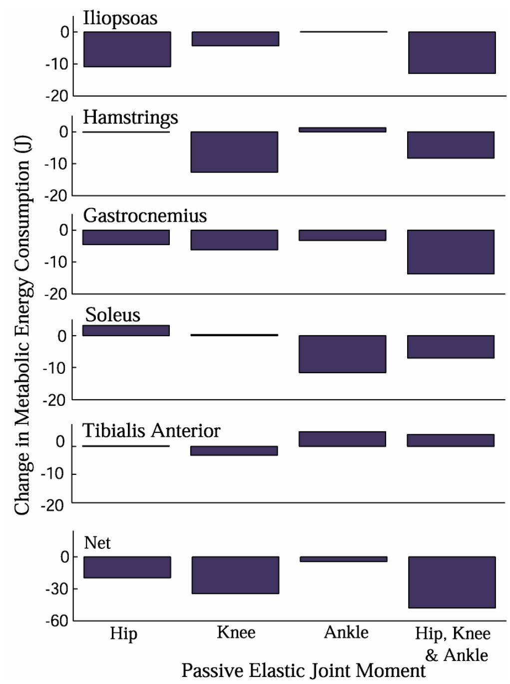

Figure 2: Reductions in metabolic energy consumption over a gait cycle due to passive elastic moments about the hip, knee and ankle.

REFERENCES

Bhargave, L.J. et al. (2004). *J Biomech*, **37**, 81-88.

Delp, S.L. et al. (1990). *IEEE Trans Biomed Eng*, **37**, 757-767.

McGibbon, C.A. (2003). *Exerc Sport Sci Rev*, **31**, 102-108.

Riener, R., Edrich, T. (1999). *J Biomech*, **32**, 539-544.

Thelen, D. G., et al. (2003). *J. Biomech.* **36**, 321-328.

Yoon, Y.S., Mansour, J.M. (1982). *J Biomech*, **15**, 905-910.

Zajac, F.E. (1989). *Crit Rev Biomed Eng* **17**, 359-411.

EFFECTS OF VIBRATION ON APPROACH TRAJECTORY OF IN-VEHICLE REACHING TASKS

Kevin A. Rider [1], Jing Wang [2] and Don B. Chaffin [1]

[1] Industrial and Operations Engineering Department, Univ. of Michigan, Ann Arbor, MI
[2] Statistics Department, Univ. of Michigan, Ann Arbor, MI
E-mail: riderk@umich.edu Web: www.humosim.org

INTRODUCTION

Target-directed reaching tasks have been analyzed using numerous qualitative and quantitative methods, ranging from simple observations to extensive laboratory experiments and analysis. The former suggests that human movements are stochastic at best, random at worst, but it is the latter that has provided the significant contributions to our current understanding of human movement.

Plamondon (1998) presents an example of the derivation of human movement by his delta-lognormal law that describes the movement as the result of a planned and executed synergy of an agonist-antagonist system. This work also provides strong support for the argument that movements are planned through the kinematics and kinetics of the end effector trajectory, rather than joint-based theories or more abstract spatial representations.

While general point-to-point trajectories can often be nicely described by Plamondon's theory, it does not take into consideration additional constraints of the task, such as movement time, accuracy, target characteristics, or even the volatility of the environment. It is this last consideration that our study is particularly concerned; how does a moving environment (i.e. vehicle motion) affect the occupant's ability to perform an in-vehicle reaching task?

Breteler et al. (2001) identified ways that end-point constraints can affect the movement trajectory with respect to the approach angle into the target and the speed of the end effector. These metrics provide a solid foundation from which to proceed towards better characterization of the kinematic changes that result from various task demands.

Another concern regarding the simplicity of Plamondon's theory is the reliance on open-loop control theory. It does not incorporate the ever-present online modification of our movements to improve the performance of the output. Particularly in the dynamic environment of vehicles, substantial perturbations are introduced to everything in the system. This ride motion effect is the focus of this study, and we specifically analyzed the trajectory as the participant's fingertip approached the target and completed the reach.

METHODS

This empirical study was conducted using the Ride Motion Simulator (RMS), a human-rated motion platform, at the US Army – Tank Automotive and Armaments Command. To investigate the basics of human dynamic response to vehicle motion, four single-frequency sinusoids were input into RMS into each of three principal axes: fore-aft, lateral, and vertical. Based on existing literature and similar results from a pilot study regarding body resonance, motion conditions were centered about an approximate resonance: stationary, 2 Hz, 4 Hz, 6 Hz, and 8 Hz.

Twelve participants were asked to perform two types of reaches, self-paced and ballistic. These reaches were performed with and without sinusoidal cab motion, under three different amplitudes. A VICON motion camera system recorded the kinematics of a seated vehicle occupant reaching towards eight cab-mounted push button targets. The fingertip trajectory was the component of principal interest for this study and results significantly support the theory end-effector-based movement planning.

RESULTS AND DISCUSSION

Figure 1 shows an example of one participant's reaches to the eight target locations. Counterclockwise from the top-left are the following views (cab-relative direction): from top (forward up), from back (top up), from right side (top up), and oblique from back-left.

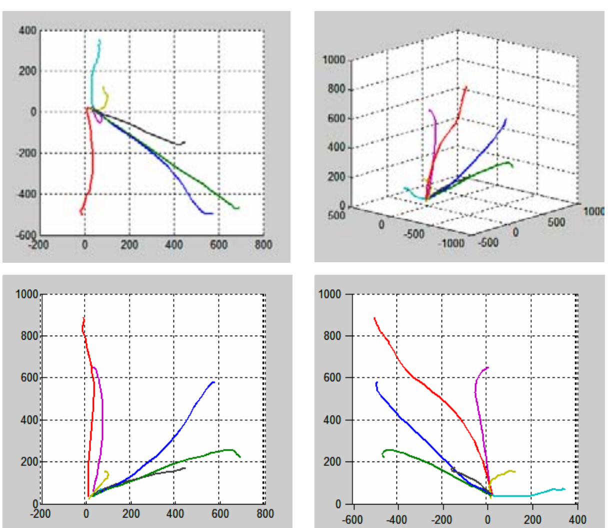

Figure 1: Reach trajectories of right index fingertip from the steering wheel to each of eight targets.

SUMMARY

For space consideration, Results and Discussion were brief or omitted to provide room for additional background. Please send questions or concerns to Mr. Rider. We will be more than happy to provide additional details if desired.

Kevin Rider: riderk@umich.edu

REFERENCES

Breteler, M., Gielen, S., Meulenbrock, R. (2001). "End-Point constraints in aiming movements: effects of approach angle and speed," *Biological Cybernetics,* **85**, 65-75.

Messier, J., Kalaska, J. (1997). "Differential effect of task conditions on errors of direction and extent of reaching movements," *Experimental Brain Research* **115**, 469-478

Plamondon, R. (1998). "A kinematic theory of rapid human movements: Part I. Movement representation and generation," *Biological Cybernetics,* **72**, 295-307.

Soechting, J., Lacquaniti, F. (1983). "Modification of trajectory of a pointing movement in response to a change in target location," *Journal of Neurophysiology,* **49(2)**, 548-564.

ACKNOWLEDGEMENTS

This research was made possible through the Automotive Research Center (ARC); a collaboration between the University of Michigan and the US Army – Tank Automotive and armaments Command (TACOM). Special thanks to Harry Zywiol, Kyle Nebel, Nancy Truong, and Kathy Mikol

Neuro-Sensory Role Of Joint Periarticular Tissue Afferents: A Human Knee Model

Yasin Dhaher
Sensory Motor Performance Program, The Rehabilitation Institute of Chicago and Department of Physical Medicine and Rehabilitation, Northwestern University, Chicago, IL 60611 USA E-mail: y-dhaher@northwestern.edu

The knee joint is surrounded by connective tissues that contain multiple nerve endings [1]. In feline preparations, several studies have reported significant increases in articular nerve discharge in response to mechanical stimuli applied to the joint capsule or ligaments [2]. Further, Baxendale et al. [3] showed that the excitability of the flexion and crossed extensor reflex pathways are influenced by the initial angle of the cat limb (i.e., initial stress in the capsule) which were abolished following joint anesthesia. These findings provide evidence that sensory inflow; mediated in part by periarticular afferents, are integrated with other reflex pathways, and can modulate muscle activation patterns at the ipsi- and contralateral limbs. It has subsequently been suggested that knee joint mechanoreceptors play a role in promoting stability by providing sensory feedback, which allows selective modulation of the activation of muscles around the knee [4, 5]. In light of the aforementioned findings, we sought to describe local (activation of muscles spanning the joint) and global (activation of muscles at distant joints) muscle activation patterns elicited by mechanical stimuli of periarticular afferents in the human knee joint. Our experimental paradigms involve frontal plane (i.e., abduction-adduction) perturbation of the knee joint. The choice of knee abduction as a model is advantageous because there is less likelihood that muscle proprioceptors will contribute to reflex activation in these directions, allowing more straight-forward examination of periarticular afferents effects. A first fundamental question, however, is, would mechanical stretching of knee joint periarticular tissue result in local activation of muscles spanning the knee**?** Previous work from our laboratory has shown that reflex activity was systematically evoked in a number of major knee muscles by angular perturbations (stretch-hold-controlled release paradigm) at the joint in the abduction direction in a seated posture [6]. The perturbation-induced reflex was characterized by a long latency response (> 70 ms, compare to 30ms latency of the tendon tap response), which consisted of an initial EMG peak, followed by a sustained reflex response that lasted throughout the holding phase of the mechanical perturbation. Furthermore, our preliminary data indicate that the sustained reflex activity exhibited a typical threshold/gain behavior as a function of the amplitude of the abduction perturbation. This overall threshold/gain pattern of activity was routinely observed for other speeds of perturbation (40°/s, 60°/s, and 80°/s) with no statistical dependence on speed. The angular threshold can be a reflection of a local state of stress or strain threshold in the receptive field of the periarticular tissues afferents. Given the documented physiological properties of the different types of mechanoreceptors, it is plausible that this threshold/gain behavior of the sustained reflex is due to slow adapting mechanoreceptors in the periarticular tissues. We further observed that the reflex activity occurred in many thigh muscles, but it was focused preferentially in medial muscles, that are potentially able to reduce the load on the medial aspect of the knee joint as a result of the abduction perturbation, which could be thought of as a local control scheme. The second key question is, how would the local muscle activation patterns observed under the seated posture paradigm change during a more functional task, like standing**?** To achieve this, similar abduction perturbations were delivered to the subject right knee via a servomotor actuator during standing posture. To eliminate potential movements of all other segments, subjects were fitted with a full-body orthosis. Prior to the perturbations, subjects were asked to maintain five different levels of load bearing on the right side (0, 0-5, 5-10, 10-15 and 15-20% of body weight) using a visual display of the vertical reaction force measured under the left foot. A total of 20 muscle activations (ipsi- and contralateral to the perturbation side) were recorded during these experiments. Across all load-bearing conditions, right knee muscle activation patterns showed preferential activation of medial muscles similar to the muscle activations observed under the seated posture experimental paradigm. In addition, our preliminary data showed significant activation of distant muscles (extensors as well as the flexors) ipsi- and contralateral to the perturbation site. Early examination of reflex latency showed that contralateral muscle activations onsets lagged the right knee muscle activity onsets by 2 to 15ms. The latencies of increased vertical ground reaction force in the contralateral limb (i.e., measured at the subject's left foot) were approximately 100 ms greater than the ipsilateral EMG onsets. It is plausible that, at least during the early stages of the perturbations, that the ipsi- and contralateral generalized activations were a result of sensorimotor interaction mediated by the periarticular tissue afferents at the right knee. The observed muscle activation and limb loading patterns could be thought of as compensatory actions or a global control scheme in response to the perturbations.

SUMMARY

We observed that reflex activity occurred in many thigh muscles in response to the mechanical perturbation, but it was focused preferentially in medial muscles, that are potentially able to reduce the load on the medial collateral ligament. These local preferential activation patterns reemerge when similar perturbations were applied at the knee during standing posture. In addition, preliminary data from the standing posture experiments showed significant activations in distant muscles ipsi- and contralateral to the perturbation site. We conclude that there is a major neurosensory role for knee periarticular tissues. Specifically, the afferents from these tissues may influence the maintenance of joint integrity by modulation of local muscle activations or by contributing to more global control schemes affecting whole-body mechanics. We believe that these findings would have a major impact on how training (physiotherapy) may influence the contribution of the different components (local & global) on the overall joint stability.

ACKNOWLEDGEMENTS

This work was supported by the Whitaker Foundation and NIH (AR46422-03).

REFERENCES

1. Kennedy, J.C., et al. American Journal of Sports Medicine, 1982. **10**(6): p. 329-35.
2. Grigg, P., A.H. Hoffman, and K.E. Fogarty. Journal of Neurophysiology, 1982. **47**(1): p. 31-40.
3. Baxendale, R.H., et al. Brain Research, 1988. **453**(1-2): p. 150-6.
4. Solomonow, M. and M. Krogsgaard. Scandinavian Journal of Medicine & Science in Sports, 2001. **11**(2): p. 64-80.
5. Johansson, H., et al. Clinical Orthopaedics & Related Research, 1991(268): p. 161-78.
6. Dhaher, Y.Y., et al. Journal of Biomechanics, 2003. **36**: p. 199-209.

A COMPLEXITY REDUCTION PRINCIPLE APPLIED TO DYNAMIC MODELING OF FINGER MOVEMENT

Sang-Wook Lee and Xudong Zhang

Biomechanics and Ergonomics Laboratory, Department of Mechanical and Industrial Engineering, University of Illinois at Urbana-Champaign, Urbana, IL, USA
E-mail: xudong@uiuc.edu

INTRODUCTION

For over decades, it has been postulated that the human behavior follows the 'optimality' principle, and many studies involve highly coordinated motions generated by the human system of kinematic redundancy, resulting in quite high degree of complexity. Two levels of complexity can be considered in this context, which characterize two aspects of the motion generation procedure respectively. Physical complexity mainly depends on the physiological properties of the human system of interest, which includes the number of body segments and corresponding actuators (muscles) involved in motion generation, and distribution of muscle forces. In contrast, control complexity of the motion is rather related to the planning or execution of the movement, and it comprises the determination of angular displacement of each segment and the temporal coordination of multi-segmental movements.

With regard to both complexities described above, human hand is one of the most complicated systems in human body, considering its multi-muscle/tendon structure and diverse motions and functions (Landsmeer and Long, 1965, Schieber, 1995). Despite the complexities, most of the hand movements are executed in a highly coordinated manner (Braido and Zhang, 2004). The reduced complexity principle is based on the premise that limited capacity of brain restoring numerous motion patterns will require those patterns to take as simple form as possible to maximize its capacity. An example of this simplification would be synchronized movements of body segments for a task, which results in reduced dimensionality in joint coordinate space. In this study, this principle was embodied in the hand movement modeling by using a simplified plant model (body) and a reduced-order controller (brain) structure. We aimed to provide a general framework that facilitates the effective coordination of the movement, and a reduced complexity principle was proposed and implemented to simulate a finger movement as an attempt to illustrate the logic.

METHODS

A digit of hand was modeled by three serially connected rigid segments. Three joint angles (DIP, PIP and MCP) were used to represent the finger movement, or the outputs of the finger system, and the torques applied on joints were defined as the inputs of the system. The equations of motion are formulated in a matrix form (Eq. (1)). The effect of gravitational force is disregarded for the sake of simplicity, assuming the gravitational force does not have a significant effect on finger motions.

$$\boldsymbol{A}(\boldsymbol{\theta}) \cdot \ddot{\boldsymbol{\theta}} = \boldsymbol{b}(\boldsymbol{T}, \boldsymbol{\theta}, \dot{\boldsymbol{\theta}}) \tag{1}$$

where ***A*** matrix incorporates the inertia terms related to the angular acceleration vector and ***b*** the other elements including velocity and torque (***T***) vector terms.

To generate a coordinated grasping movement of the hand, control schemes that reflect three different levels of complexity were applied to the hand system. First controller (C1) based on the multi-input multi-output (MIMO) linear quadratic regulator (LQR) scheme was designed at each time step, based on the identified linearized time-invariant (LTI) model at the moment, and applied to the system (Figure 1). The second controller (C2) was designed based on the approximated linear time-invariant (LTI) model. Thus, its structure remained unchanged throughout the movement, which simplified the system complexity. While previous two controllers employed three distinct controllers for three finger joints, the third controller (C3) applied the same control structure to all three joints by normalizing the angle magnitudes, which has a single-input single-output (SISO) control structure in it, and it represents the simplest control scheme.

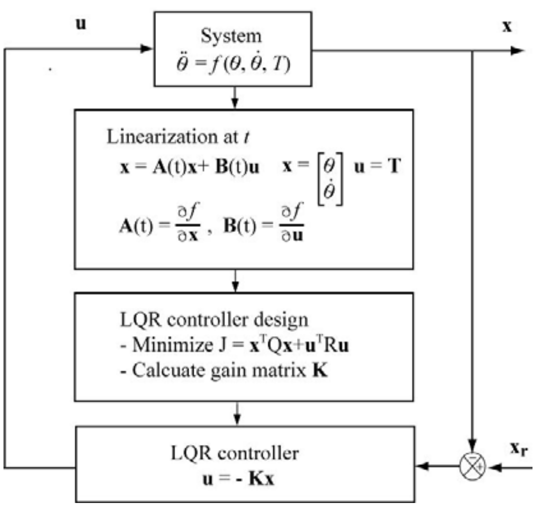

Figure 1: The logic diagram of C1

RESULTS AND DISCUSSION

Angular profiles of three joints (DIP, PIP, and MCP) generated by applying three types of controller described above were compared (Figure 2). Initial values for three joints were selected by a random number generator with zero mean. The terminal angle values were assigned to 30, 50, and 40 degrees, which are typical finger segment angles for a power grip posture.

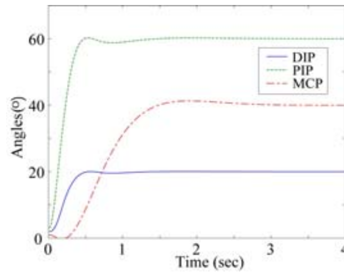

(a)

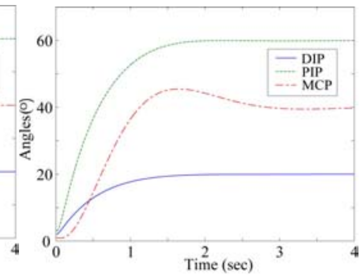

(b)

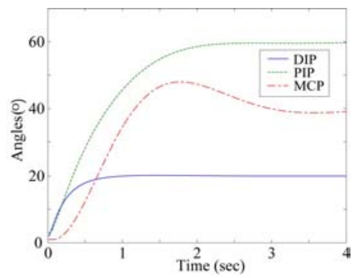

(c)

Figure 2: Angular profiles of three joints generated by three types of controller (a) C1 (b) C2 (c) C3

Angular profiles generated by controller 2 and 3 are more synchronized than ones produced by C1, and this synchronization of segment motions is similar to ones observed in human grasping movements. This can be interpreted as that some of human motions such as grasping are generated by a simplified scheme. Also the simplified scheme for the motion simulation has an advantage over full-complexity models in a sense that it requires less computation time.

Further improvement of the modeling should be followed. Passive torques applied on finger joints should be incorporated in the model, which will reduce the discrepancy between simulated and real motions, specifically in DIP joint movement. Proper tuning of control design parameters should lead to more realistic simulation.

REFERENCES

Braido.P., Zhang, X. (2004). *Human Movement Science,* **22**, 661-678.

Landsmeer, J.M.F., Long, C. (1965). *Acta Anat*. **60**, 330-347.

Schieber, M.H. (1995). *J. Neurosci.* **15**, 284-297

PREDICTION OF MUSCLE ACTIVATION PATTERNS FOR POSTURAL CONTROL USING A LINEAR FEEDBACK MODEL

Daniel B. Lockhart[1] and Lena H. Ting[2]

[1]Woodruff School of Mechanical Engineering, Georgia Institute of Technology, Atlanta, GA
[2]Coulter Department of Biomedical Engineering, Georgia Tech/Emory University, Atlanta, GA
E-mail: dlock@neuro.gatech.edu Web: http://neuro.gatech.edu

INTRODUCTION

Simple feedback control models can be used to characterize postural dynamics in response to support surface perturbations (Kuo, 1998). However, a model that can predict not only kinematics but also muscle activation patterns would allow the properties of the neural control system to be more accurately studied. Neural and muscle actuator delays were added to a simple feedback control model of posture. We used this model to predict both muscle activation and kinematics during postural perturbations in standing cats. The inclusion of delays in the feedback influences the structure of the neural control model required to accurately predict experimental results. Our model suggests that higher order derivative control is required.

METHODS

Postural dynamics of the cat were modeled as a linearized inverted pendulum on a cart. The pendulum was controlled by linear state feedback control on ankle torque using angular position, velocity and acceleration gains. This state feedback loop included a neural time delay (30 ms) and a time constant for muscle activation (20 ms). The acceleration of the cart was prescribed to be the same as that measured at the platform during each trial. Optimal feedback gains for each trial were found by minimizing a performance index relating the error between predicted and measured muscle activation and center of mass kinematics over time.

The feedback control model was driven by data from quietly standing intact cats that were subjected to perturbations of the support surface (Macpherson, 1988). Perturbations were applied along a diagonal axis that maximally elicited extensor muscle activity in the left hindlimb in one direction, and maximally elicited the flexor muscles in the opposite direction. In order to vary displacement and acceleration across trials, perturbations consisted of a short ramp (0-90 ms) in one direction followed by a longer ramp (370 ms) in the opposite direction to activate the extensor and flexor muscles in quick succession. The perturbation shown in Figure 1 consisted of a single 370 ms ramp with average velocity of 15 cm/s. Hindlimb EMGs, ground reaction forces at each paw, platform acceleration and displacement were collected. Center of mass kinematics were computed by integrating the summed ground reaction forces (Macpherson 1999).

RESULTS AND DISCUSSION

The model predicted an initial burst of EMG activity followed by a plateau, which is consistent with experimentally obtained EMG patterns (Figure 1). Moreover, optimal feedback gains were consistent over all the perturbation trials.

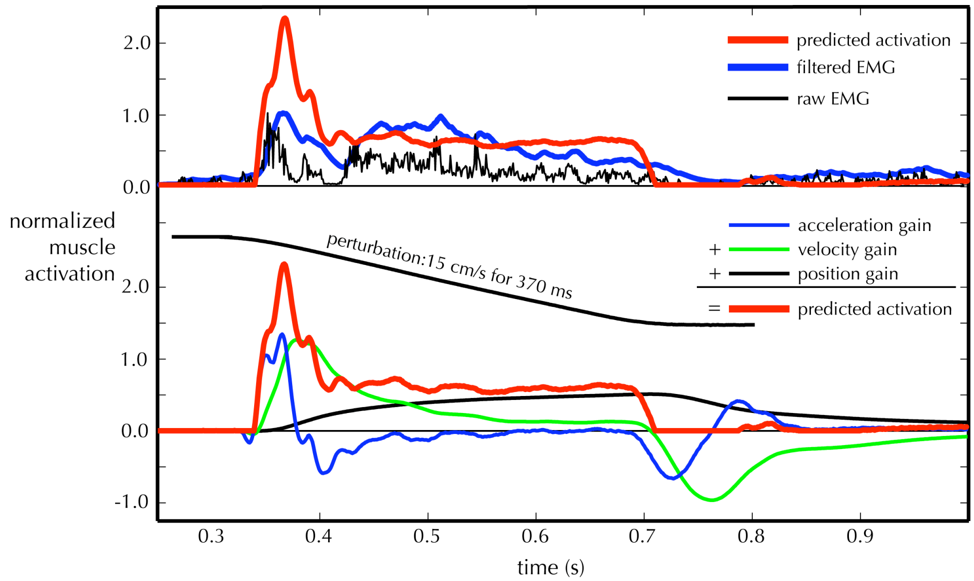

Figure 1: *Upper – Predicted muscle activation and recorded gluteus medius EMG activity. Lower – Predicted muscle activation and individual feedback components over time*

When acceleration feedback gain was removed, even after re-optimization of the remaining feedback gains, the accuracy of predicted muscle activation patterns decreased (Fig. 2). Although these gain values stabilized the inverted pendulum, the estimated muscle activation pattern did not resemble the recorded muscle activation patterns of intact cats, particularly the initial burst of EMG activity. Acceleration feedback gain was required to adequately account for the initial EMG burst. Typically, this initial burst of EMG activity has been attributed to a feedforward mechanism. Our results demonstrate that the inclusion of acceleration feedback gain can predict this initial burst.

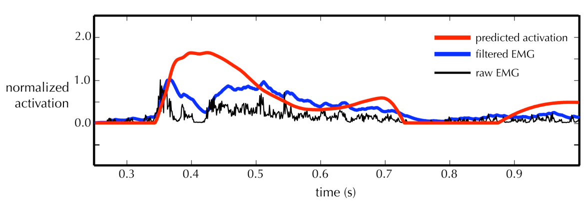

Figure 2*: Predicted muscle activation and recorded EMG activity when acceleration feedback gain is removed.*

SUMMARY

It is possible to predict muscle activation patterns of the cat hindlimb using only state feedback control. The addition of acceleration feedback control allowed the system to closely model the entire evolution of muscle activation patterns and center of mass kinematics over time during postural perturbations in an intact cat.

REFERENCES

Kuo, A. D. (1998). *Exp Brain Res*, **122**, 185-195.

Macpherson, J. M. (1988). *J Neurophysiol*, **60**, 204-217.

Macpherson, J. M. (1999). *J Neurophysiol*, **82**, 3066-3081.

ACKNOWLEDGEMENTS

Thanks to J. Macpherson for the use of the platform and the Whitaker Foundation Grant RG-02-0747

TRUNK MUSCLE ACTIVATION PATTERNS IN INDIVIDUALS WITH DEGENERATIVE DISC DISEASE: A COMPARISON OF SUBJECTS WITH AND WITHOUT LOW BACK PAIN

Sheri P. Silfies[1] and Andrew Karduna[2]
[1]Rehabilitation Sciences Biomechanics Laboratory, Drexel University, Philadelphia, PA, USA
[2]Department of Exercise and Movement Science, University of Oregon, Eugene, OR, USA
E-mail: silfies@drexel.edu

INTRODUCTION

Degenerative disc disease (DDD) is a common finding on medical imaging for individuals seeking consultation for low back pain (LBP). However, many asymptomatic individuals also demonstrate DDD on imaging (Boden et al, 1990). Why do some individuals develop symptoms while others remain pain free? One explanation is that in addition to passive spine structures, the neuromuscular system plays an essential role in promoting pain free function of the spine. Researchers have indicated that muscle co-activation is necessary to stabilize the healthy spine around a neutral spine position (Cholewicki and McGill, 1996). One hypothesis regarding injury or degeneration of the spine's passive support system, suggests that appropriate compensation by the trunk neuromuscular system is required for maintenance of stability and symptom free function (Panjabi, 1992). The purpose of this pilot study was to determine if trunk muscle activity patterns in asymptomatic individuals with evidence of DDD were different from those reporting recurrent or chronic LBP symptoms.

MATERIALS AND METHODS

Subjects-Twelve subjects (8 female, 4 male, age 31-54) were studied with IRB approval. Six patients with chronic or recurrent LBP, (current episode lasting greater than 12 months, moderate disability level) were age, gender and BMI matched to individuals with no LBP. The patients demonstrated x-ray and/or MRI evidence of DDD and had positive discography at one or more corresponding levels indicating the disc as the painful structure. The matched controls also demonstrated x-ray evidence of similar disc degeneration at the same lumbar level(s). However, these individuals had never experienced LBP that required medical imaging or examination.

EMG and Kinematics- Pre-amplified surface electrodes were applied bilaterally over the internal oblique/transverse abdominus (IOTrA), external oblique (EO), rectus abdominus (RA), lumbar multifidus (LM) and lumbar erector spinae (ES) muscle groups. Data were collected at 1248 Hz, amplified and bandpass filtered (10-750 Hz). MVICs were collected for normalization of EMG amplitude values. Three dimensional kinematic data were collected simultaneously using an electromagnetic tracking device. Anatomical axes were derived from calibration of the subject in a relaxed standing posture. Trunk angle was referenced to the global reference frame.

Protocol- Subjects performed three repetitions of active forward reaching with their arms maintained at 90°of flexion (Figure 1).

Data Analysis- EMG data corresponding to the neutral position (0° flexion) were processed using an RMS filter and normalized. The data were averaged between sides and over all three trials of forward trunk motion. Descriptive statistics were used to identify trends and statistical significance was assessed with t-tests.

Figure 1: Reaching activity mid-range.

RESULTS

Subjects with LBP exhibited higher levels of muscle activation and lower co-activation ratios at the neutral spine position (Figure 2, A). RA activity ($p = 0.04$) and the IOTrA/RA ratio ($p = 0.02$) demonstrated significant differences, while the ES muscle ($p = 0.18$), EO/RA ($p = 0.13$) and flexor/extensor ($p = 0.18$) co-activation ratios exhibited trends toward differences (Figure 2, B).

DISCUSSION

Results of this pilot study indicated that while those individuals with recurrent or chronic LBP had higher activation levels in the RA and ES muscle groups, it did not appear to adequately compensate for any biomechanical changes linked to the DDD. One explanation may be that they are unable to compensate for abnormal spine forces secondary to excessive activation of multisegmental muscles, particularly, in a situation of decreased passive stiffness and/or inadequate local muscle (IOTrA, LM) activation. Thus, there may be some maximum level of activation of multisegmental muscles above which the spine will experience reduced static and dynamic stability and pain when placed under situations requiring enhanced neuromuscular control (Hodges, 2000). The trends found in these data regarding ratio of activation between local and multisegmental muscles and the flexor/extensor ratio provides some support for this explanation. The appropriate compensation may be more related to coordination of musculature than to overall higher activation levels. Our pain free group might represent individuals able to self-adjust and adequately compensate ("copers") for lumbar spine degenerative changes. Our LBP group may represent patients who were unable to develop appropriate compensating mechanisms ("non-copers") via the neuromuscular subsystems to allow for pain free function. Collection of additional data may provide evidence to support muscle recruitment strategies that would assist rehabilitation of non-copers.

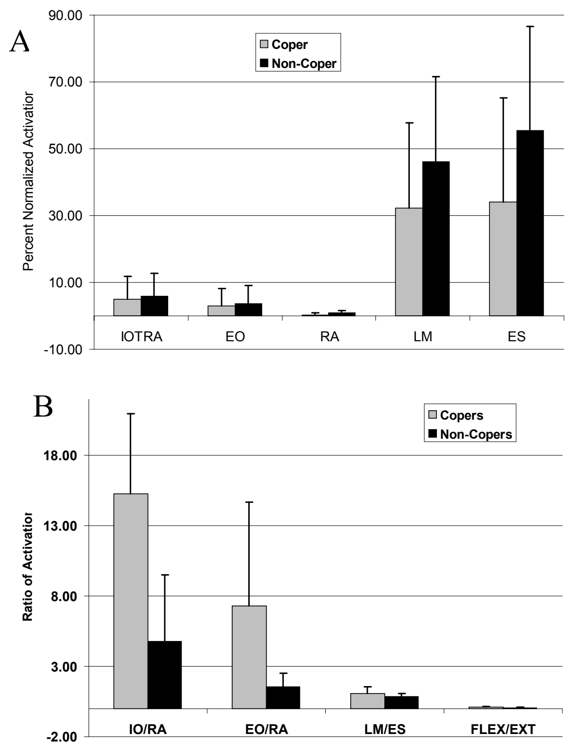

Figure 2: Normalized group mean (SD) for each (A) muscle group and (B) ratio of co-activation at the neutral spine position.

REFERENCES

Boden, et al. (1990). *JBJS,* **72-A**, 403-8.
Cholewicki J., McGill, SM. (1996). *Clin Biomech,* **11**, 1-15.
Hodges, P. (2000). *J Sci & Med Sports*, **3**, 243-53.
Panjabi, M. (1992). *J Spinal Disord,* **4**, 383-397.

EFFECT OF POSITIVE POSTERIOR HEEL FLARE ON LOWER EXTREMITY KINEMATICS DURING RUNNING GAIT

Robin M. Queen,[1,4] Michael T. Gross,[2,4] and Bing Yu[1,2,3,4]

[1] Department of Biomedical Engineering, [2] Division of Physical Therapy, [3] Department of Orthopedics, [4] Center for Human Movement Science,
The University of North Carolina at Chapel Hill, Chapel Hill, NC, USA
E-mail: rqueen@med.unc.edu

INTRODUCTION

The presence of exercise induced (EI) anterior compartment syndrome has been established within the running population. Runners can develop EI anterior compartment syndrome by running with shoes that are not correct for their foot type, changing from running with a midsole strike pattern to running with a rearfoot strike pattern, running intervals, or running on banked surfaces (Blackman, 2000; Detmer, et al, 1985). The focus of this study was to determine the effect of a positive posterior heel flare (PPHF) on lower extremity (LE) kinematics during running gait. The impetus for this study was to identify a possible factor associated with the development of EI anterior compartment syndrome. A PPHF is defined as the presence of the midsole material being inclined posteriorly away from the posterior aspect of the running shoe.

METHODS

Each subject was tested in two different running shoes: the Asics Gel Cumulus and the Saucony Grid Trigon. These two shoes were chosen because they had similar properties except for the degree of PPHF. The Asics Gel Cumulus has a PPHF of $2^o \pm 1^o$, while the Saucony Grid Trigon has a PPHF of $11^o \pm 1^o$. Recreational athletes were enrolled as subjects if they demonstrated a rearfoot strike pattern based on an observational video gait analysis. Subjects reported no history of LE injuries in the past six months, no history of a fasciotomy, and were not using foot orthotics.

A six camera, real time motion analysis system was used to record the trajectories of LE reflective markers at a sampling rate of 120Hz. Seven trials were recorded for each shoe with the subjects running at ± 5% of their self-selected speed as determined from the average of five practice trials. Three randomly selected trials were used for analysis. These trials were averaged for the following dependent variables: sagittal plane joint position of the ankle and the knee at heel strike, knee excursion from heel strike to maximum knee flexion, and peak and mean ankle angular velocities from heel strike to foot flat. Each dependent variable was tested using a 2x2 mixed model [one between factor (gender) and one within factor (shoe)] repeated measures ANOVA ($\alpha = 0.05$). The between trial Intraclass Correlation Coefficient [ICC (3,3)] was calculated for all subjects for each dependent variable under each shoe condition. Acceptable between trial reliability was identified as an ICC value greater than 0.70.

RESULTS AND DISCUSSION

Forty-three subjects (19 female, 24 male) ranging in age from 18 to 37 participated in the study. Female subjects had an average age of 23.4 ± 4 years, an average mass of 60.4 ± 7.7 kg, and an average height of 1.66 ± 0.05 m. Male subjects had an average age of 23.5 ± 4 years, an average weight of 74.3 ± 8.9 kg, and an average height of 1.78 ± 0.02 m.

The ICC analyses indicated acceptable reliability for all variables. No gender by shoe interaction existed for any dependent variable. Men ran significantly faster than the women ($p=0.026$), however, no differences in running speed existed between the two shoe conditions. Dorsiflexion angle at heel strike was not significantly different between genders, but was significantly greater for the Saucony (increased PPHF) than the Asics ($p<0.001$). Knee flexion angle at heel strike was significantly greater for the women ($p=0.003$), but not significantly different between the shoe conditions. No statistically significant differences existed for gender or shoe for either peak or mean sagittal plane ankle angular velocity. In addition, no significant difference existed for shoe or gender for knee excursion from heel strike to maximum knee flexion.

The increase in running speed for the men does not explain the decrease in knee flexion angle for the men at heel strike compared to the women. Previous studies have shown that with increased running speed, the joint range of motion decreases during terminal swing resulting in an increase in knee flexion angle at heel strike (Mann & Hagy, 1980; Vaughn, 1980). The significant difference in knee flexion angle at heel strike in our study may have resulted from differences in motion patterns between genders during running. The increase in the dorsiflexion angle at heel strike was most likely the result of the subjects contacting a more posterior portion of the shoe sooner during swing phase. Subjects could have also chosen to contact the ground earlier to attenuate the GRF by increasing the contact time between the foot and the ground.

SUMMARY

The increase in dorsiflexion angle at heel strike in the shoe with the greater PPHF could lead to an increase in muscle activation within the anterior compartment, which could lead to the development of EI anterior compartment syndrome. Further investigation is needed to determine if these kinematic changes cause changes in the dorsiflexion moment requirement, muscle activation in the anterior compartment, and changes in the ground reaction forces.

REFERENCES

Blackman, PG. A review of chronic exertional compartment syndrome in the lower leg. *MSSE*. 32:S4-S10, 2000.
Detmer, DE, et al. Chronic Compartment Syndrome: diagnosis, management, and outcomes. *Am. J. Sports Med*. 13:163-170, 1985.
Diss, C. The reliability of kinetic and kinematic variables used to analyze normal running gait. *Gait & Posture*. 14:98-103, 2001.
Mann, RA, et al. Biomechanics of walking, running, and sprinting. *Am. J. Sports Med*. 8:345-350, 1980.
Nigg, BM, et al. Influence of Heel Flare and Midsole Construction on Pronation, Supination, and Impact Forces for Hell-Toe Running. *Int. J. of Sport Biomech.* 4:205-219, 1988.
Vaughn, CL Biomechanics of Running Gait. *Crit. Rev. in Biomed Eng*. 12:1-47, 1980.

ACKNOWLEDGEMENTS

Fleet Feet, Inc. & UNC Injury Prevention Research Center

Passive and Active Sarcomere Length Non-uniformity in Skeletal Muscle

Jolene L. Lepp[1,] Dilson E. Rassier[1], Gerald H. Pollack[2], Walter Herzog[1]

[1] Human Performance Laboratory, University of Calgary, Calgary, AB, Canada
[2] Dept. of Bioengineering, University of Washington, Seattle, WA, USA
E-mail: Walter@kin.ucalgary.ca

INTRODUCTION

Sarcomeres on the descending limb of the force-length relationship in an activated myofibril are non-uniform in length, but maintain a perfect steady-state during isometric contractions (Rassier et al., 2003). Since sarcomeres in a single myofibril are all arranged in series, the force supported by each sarcomere must be identical to the force in all the other sarcomeres. With non-uniform sarcomere lengths, one would expect differences in active force production, given the differences in the degree of filament overlap in the sarcomeres (Gordon et al., 1966). In order to maintain force equilibrium in the active state, differences in passive sarcomere forces at a given sarcomere length may compensate for the differences in the active forces. However, sarcomere lengths in the passive state have been assumed uniform, with non-uniformity only developing when the sarcomeres are activated (Julian & Morgan, 1979).

The purpose of this study was to characterize passive sarcomere lengths on the descending limb of the force-length relationship in single myofibrils, and compare the results with a previous study performed with activated myofibrils. We hypothesized that sarcomere lengths in the passive myofibril are uniform throughout the test length range.

METHODS

Individual sarcomere lengths of single rabbit psoas myofibrils were imaged and recorded as described elsewhere (Rassier et al., 2003). Myofibrils (n=6) were stretched passively at ~0.1 µm increments per sarcomere, from 2.0-2.2 µm to 3.4-3.6 µm. Individual sarcomere lengths were measured after each stretch.

RESULTS AND DISCUSSION

Sarcomere lengths in the passive state demonstrated a large range at each myofibril length. The average range (±SD) was 0.29 µm (± 0.12) and 0.38 µm (±0.13) when myofibrils were stretched and shortened along the descending limb of the force-length relationship, respectively (Table1). These results suggest that the structural proteins responsible for passive force in myofibrils may have different force-elongation properties that are history dependent.

The passive sarcomere lengths ranges were compared to those measured by Rassier, et al. (2003) in the activated state on the descending limb. In that study, in which the mean sarcomere length from activated myofibrils (n=6) varied from 2.70 µm to 3.07 µm, the range of sarcomere lengths (±SD) varied from 0.31 µm (±0.09) to 0.65 µm (±0.15). In this study, passive sarcomere lengths at comparable lengths on the descending limb of the force-length relationship (2.70 µm - 3.07 µm) demonstrated a smaller mean length range of 0.29 µm (±0.14).

In order to compensate for the force differences observed in the activated myofibrils based on sarcomere length differences, sarcomeres with the largest passive forces (the shortest ones in the passive testing) would need to become the longest ones in the active state. This requires that sarcomeres change length from the passive to active state in a precisely defined manner. However, even in the passive state, there was not a unique configuration of sarcomere lengths for a given myofibril length. Therefore, sarcomeres do not seem to have a characteristic pattern of shortening when myofibrils are activated. Also, preliminary data in which we followed the length changes of myofibrils during the activation process suggest that sarcomere length changes in this phase occur in a random way.

SUMMARY

Sarcomeres in the passive state demonstrated substantial length non-uniformity. Due to the absence of a unique passive sarcomere length configuration, and in comparison to passive and active length ranges obtained in independent myofibril studies performed in our laboratory (Rassier, et al. 2003), our results suggest that active force equilibrium among sarcomeres is based on mechanisms other than compensation through passive forces. Further studies are required in order to understand the behaviour of individual sarcomeres when they change their state upon activation. Also, the force discrepancies of sarcomeres in an activated myofibril based on sarcomere lengths need reconciliation.

REFERENCES

Rassier, DE, Herzog, W, Pollack, GH. (2003). *Proc R Soc Lond B Biol Sci.,* 270(1525):1735-40.

Gordon, AM, Huxley, AF, Julian, FJ. (1966). *J Physiol.,* 184: 170-92.

Julian, FJ, Morgan, DL. (1979). *J. Physiol.*, 293: 379-92.

ACKNOWLEDGEMENTS

Natural Sciences and Engineering Research Council of Canada

Alberta Ingenuity Fund

Table 1: Summary of the sarcomere length standard deviations, and range of lengths for myofibrils (n = 6) after passive stretch and release.

Passive -Stretch	**M1**	**M2**	**M3**	**M4**	**M5**	**M6**	**Average**
SD (µm)	± 0.07	± 0.08	± 0.06	± 0.13	± 0.09	± 0.09	**± 0.09**
Length Range (µm)	0.24	0.25	0.2	0.41	0.27	0.33	**0.29**
Passive - Release							
SD (µm)	±0.12	± 0.11	± 0.06	± 0.12	± 0.2	± 0.12	**± 0.12**
Length Range (µm)	0.38	0.34	0.2	0.38	0.57	0.38	**0.38**

LOWER TRUNK KINEMATICS AND MUSCLE ACTIVITY DURING DIFFERENT TYPES OF TENNIS SERVES

John W. Chow, Soo-An Park, Mark D. Tillman and Guy B. Grover

Center for Exercise Science, University of Florida, Gainesville, FL, USA
E-mail: jchow@hhp.ufl.edu

INTRODUCTION

Lower back injuries are common among competitive tennis players. Players may be at a greater risk of lumbar disc pathology from rotational and hyperextension shearing effects (Hainline, 1995). Previous studies of the tennis serve have focused on the muscular activity and kinematics of the hitting arm and shoulder region. Limited data regarding lower trunk muscular activity and kinematics during the tennis serve are available (Chow et al., 2003).

The purpose of this study was to examine the relative motion of the middle and lower trunk and muscular activity of the lower trunk during 3 different types of tennis serves – flat, topspin, and slice – performed by skilled players.

METHODS

Twenty male tennis players were recruited as subjects (mean age 24 years, height 180 cm, weight 766 N) in two skill groups [Advanced Intermediate (AI) group: $N = 9$, NTRP rating 4.5-5.0; Advanced (AV) group: $N = 11$, NTRP rating $\geq$ 5.5]. Electromyographic (EMG) and kinematic data were collected separately in 2 sets of trials . Each set consisted of 7 trials for each of the 3 serve types. The order of the serve type was randomized for each set.

Surface EMG techniques were used to monitor the activity of 8 muscles on the left and right sides of the body: rectus abdominus (LRA, RRA), external and internal oblique (LEO, REO, LIO, RIO), and erector spinae (LES, RES). Maximum effort isometric trials were conducted for maximum EMG levels.

To obtain kinematic data, two reflective marker sets, each consisting of four markers in an inverted "T" pattern, were placed on the middle and lower back of the subject. Four gen-locked cameras (60 Hz) were used to record the serving motions. Marker locations were used for estimating the anatomical joint (AJ) angles (Vaughan et al., 1999) between the middle and lower trunk. Kinematic data were not available in 5 AV subjects.

For each subject, the 2 highest self-rated EMG and kinematic serves for each serve type were analyzed. The maximum AJ angles (expressed as the angular deviation from the AJ angle at the standing posture) for 4 trunk motions (extension, left lateral flexion, and left and right twisting) and the average EMG levels for each muscle during the four phases of a tennis serve (ascending and descending windup, acceleration, and follow-through phases) were determined.

For each muscle, the EMG parameters were compared using a 2 x 3 x 4 (Skill x Serve type x Phase) MANOVA with repeated measures on the last two factors. A 2 x 3 x 4 (Skill x Serve type x Trunk motion) ANOVA with repeated measures on the last two factors was performed on maximal AJ angles (alpha = .05).

RESULTS AND DISCUSSION

For most muscles tested, the largest average EMG levels were observed in either the descending windup or acceleration phases. When comparing overall muscle activation during a tennis serve between the two skill groups, the subjects in the AV group generally exhibited greater muscle activation than the subjects in the AI group.

The MANOVA revealed significant main effects for skill level in LRA ($p = .008$) and phases in all muscles ($p < .001$). The average EMG level of the AV group for LRA was significantly higher than that of the AI group. Two trends were observed – the AV group exhibited higher EMG levels than the AI group in the LEO ($p = .055$) and RES ($p = .069$).

The activation patterns clearly demonstrate a high degree of co-contraction during a tennis serve, especially in the descending windup and acceleration phases. In addition to the compressive load, the hyperextension and lateral flexion of the trunk during various phases of a tennis serve may cause shear loads on the lumbar spine.

The ANOVA revealed no significant main effects for serve type and skill level. However, significant differences between the two skill levels were found for the maximal AJ angles for extension ($p = 0.018$) and left lateral flexion ($p = 0.038$). The AV group had significantly smaller extension and greater left lateral flexion angles than the AI group (Table 1). It is possible that, instead of relying on lumbar hyperextension like the AI subjects did, the subjects in the AV group relied more on the hyperextension of the upper trunk (i.e., thoracic spine) to achieve the overall trunk hyperextension needed for an execution of a tennis serve.

The significantly greater maximal left lateral flexion AJ angle exhibited by the AV group indicates that highly-skilled right-handed players can reach for a greater height during a tennis serve because of the greater left lateral flexion. This result corresponds to the significantly greater LRA activity found in the AV group and implies that highly-skilled players are subjected to greater asymmetric loads on their lumbar spines due to the greater lateral flexion.

In conclusion, there was no significant variation in lower trunk motion and muscle activation among the three serve types and relatively large lumbar spinal loads are expected during the acceleration phase because of the hyperextension posture and profound front-back and bilateral co-activations in lower trunk muscles.

REFERENCES

Chow, J.W. et al. (2003). *J. Sci. Med. Sport*, **6**, 512-518.

Hainline, B. (1995). *Clin Sports Med*, **14**(1), 241-265.

Vaughan, C. et al. (1999). *Dynamics of Gait*.

ACKNOWLEDGEMENTS

United States Tennis Association (USTA).

Table 1. Means and (standard deviations) for different maximal AJ angles.

Serve Type	**Flat**		**Topspin**		**Slice**	
Motion \ Skill	**AV**	**AI**	**AV**	**AI**	**AV**	**AI**
Extension	19.3 (11.9)	27.5 (10.9)	19.3 (10.6)	31.9 (17.2)	20.0 (10.1)	26.9 (7.6)
Left Lat Flexion	16.0 (4.1)	12.3 (5.2)	15.5 (5.4)	10.9 (4.8)	15.4 (5.3)	12.4 (8.4)
Left Twisting	7.9 (4.3)	6.8 (3.8)	6.8 (4.1)	5.4 (0.9)	5.5 (3.8)	4.3 (3.1)
Right Twisting	5.6((4.5)	4.2 (1.8)	6.1 (6.9)	4.13 (0.6)	11.2 (12.7)	4.1 (3.1)

RELIABILITY OF A TECHNIQUE FOR DETERMINING SAGITTAL KNEE GEOMETRY FROM LATERAL KNEE RADIOGRAPHS

John W. Chow, Soo-An Park, Jeff T. Wight and Mark D. Tillman

Center for Exercise Science, University of Florida, Gainesville, FL, USA
E-mail: jchow@hhp.ufl.edu

INTRODUCTION

Over the years, several techniques have been proposed to quantify the knee extension mechanism using radiographs. Among these techniques, the one proposed by Grood et al. (1984) is very appealing because it considers the lines of action of the patellar and quadriceps tendons relative to the tibiofemoral and patellofemoral contacts, respectively, in determining the effective moment arm of the quadriceps force (d_e). Although the application of this technique using radiographs has been reported, the detailed analysis procedures have not been described. The purpose of this study was to examine the reliability of an analytical procedure performed on knee radiographs that is based on the Grood technique.

METHODS

Five sagittal view knee radiographs were obtained from the left knees of 2 males and 2 females (age 18-22 yrs). The 5 X-rays were taken at different knee flexion angles (20º to 85º at intervals of 15º). To load the knee joint, the subject sat on a stool located next to an x-ray film and performed isometric knee extensions with maximal effort when the radiographs were taken. A metal pin with a length of 10.15 cm was placed on the anterior surface of the patella tendon for spatial reference.

Each radiographic image was analyzed by 7 analyzers (age 20-35 yrs) using the same procedures/instructions (Figure 1):

a. Mark the ends of the linear scale (Points 1 and 2).
b. Use Points 3 and 4 to define the line of action of the patellar tendon (Line 1).
c. Points 5 and 6 define the posterior surface of the patella. The patellafemoral contact (Point 7) is a point located midway between Parallel Lines 1 and 2 on Line 2.
d. Mark the distal attachment of the quadriceps tendon (Point 8) and establish the line of action of the quadriceps tendon (Line 3). Lines 1-3 should intersect at the same point (concurrent forces).
e. Draw a line along the superior surface of the tibia (Parallel Line 3) and create 2 parallel lines that are tangent to the medial and lateral condyles of the femur (Parallel Lines 4 and 5) (Figure 2). Construct a line that is perpendicular to Parallel Line 3 and pass through the midpoint between Points A and C (Point B). The tibiofemoral contact is the midpoint between Points B and D.

The coordinates of the 12 points were used to determine d_e and other parameters (Table 1). For each radiograph, intraclass correlation coefficients (ICCs) were computed for combinations of 2-7 analysts.

RESULTS AND DISCUSSION

Overall, the high ICC values indicate an excellent inter-analyst reliability (Table 1). The results indicate that the new technique is reliable and can be used for both clinical and research purposes. Because employing multiple analysts may not be feasible in some clinics and laboratories, we performed similar tests using fewer analysts. The average ICC values for 2-6 analysts combinations are comparable to those ICCs in Table 1 but the standard deviation slightly increased when fewer analysts were used. For example, the average ICCs for the 6- and 2-analyst combinations were 0.9985±0.0003 and 0.9985±0.0015, respectively, for the 25° radiograph. It is our opinion that a single experienced analyst is sufficient for most applications. However, 2-3 analysts are recommended for research purposes.

REFERENCE

Grood, E.S. et al. (1984). *J. Bone Jt. Surg.*, **66-A**, 725-734.

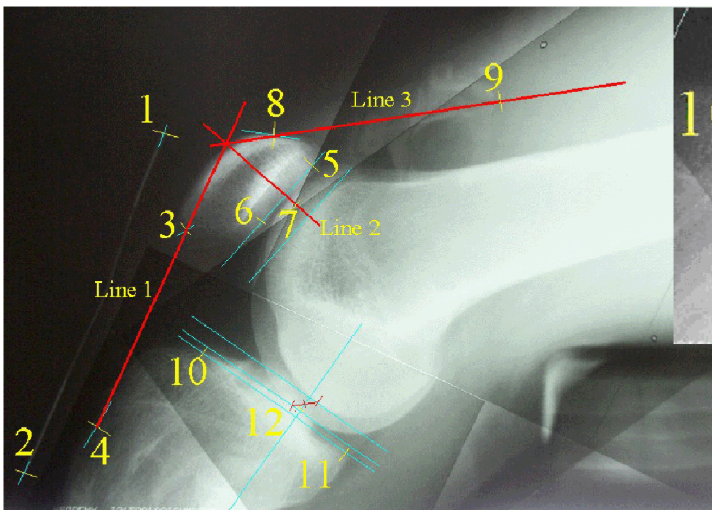

Figure 1. Points and lines identified on an X-ray.

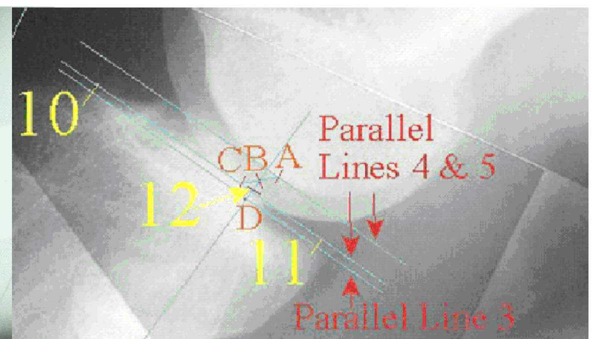

Figure 2. Tibiofemoral contact.

Table 1. Means (standard deviations) and ICC values for 7 analysts.

Knee Flexion Angle (°)	Effective moment Arm (cm)	Patella Height Ratio	Patellar Tendon Length (cm)	Tibio-femoral Joint Space (cm)	Patello-femoral Joint Space (cm)	Patellar Mechanism Angle (°)	Patellar Tendon Angle (°)	ICC
25	4.43 (0.37)	0.48 (0.07)	4.46 (0.22)	0.46 (0.07)	0.50 (0.06)	150.8 (2.6)	17.6 (5.1)	0.9985
40	4.23 (0.22)	0.51 (0.06)	4.88 (0.22)	0.40 (0.10)	0.62 (0.16)	148.3 (6.3)	12.3 (1.8)	0.9980
55	4.16 (0.30)	0.55 (0.07)	5.52 (0.28)	0.49 (0.16)	0.66 (0.32)	124.6 (6.0)	16.7 (3.4)	0.9967
70	3.22 (0.31)	0.60 (0.05)	6.17 (0.23)	0.46 (0.14)	0.58 (0.14)	116.2 (4.4)	12.7 (3.8)	0.9974
85	3.24 (0.16)	0.55 (0.09)	5.26 (0.26)	0.54 (0.23)	0.68 (0.12)	111.2 (5.3)	12.0 (3.3)	0.9967

MUSCLE ACTIVATION PATTERNS IN MALES AND FEMALES DURING DROP LANDINGS ONTO THE HEELS

Rhonda L. Boros [1] and John H. Challis [2]

[1] Applied Biodynamics Laboratory, Boston University, Boston, MA, USA
[2] The Biomechanics Laboratory, The Pennsylvania State University, University Park, PA, USA
E-mail: rboros@bu.edu

INTRODUCTION

Landing from a drop has been identified as a movement stressful to the anterior cruciate ligament (ACL) (Lephart et al., 2002). Female athletes are six times more likely to suffer a "non-contact" ACL injury compared with males (Arendt and Dick, 1995). Muscle activation patterns of males and females during the performance of various landing activities have been studied in hopes of providing insight into this phenomenon. Delayed hamstring activation coincident with peak impact force during single-leg ballistic maneuvers have been observed in males (Cowling & Steele, 2001), however few consistent or significant differences supporting a predisposition of women to ACL injury have been found relative to muscle activation patterns.

"Stiff" landings (e.g. drops onto the heels) result in large vertical ground reaction forces that must be dissipated by the individual's musculoskeletal system. Examination of muscle activity during such heel landings would determine if males and females prepared similarly for expected high impact loads. The purpose of this study was to determine if females demonstrate ACL-compromising muscle activation patterns during drop landings onto the heels.

METHODS

Vertical ground reaction force (VGRF) and EMG data on seven lower extremity muscles (tibialis anterior - TA, lateral soleus - SOL, medial gastrocnemius - GAS, vastus medialis - VAS, rectus femoris - RF, hamstrings - HAM, and gluteus maximus - GLUT) were measured as four female and four male subjects performed five trials of 2-footed heel landings onto a force plate from a 0.20 meter nominal drop height. These data were synchronized and sampled at 1920 Hz. EMG signals were differentially amplified (gain x 1000), and band pass filtered (10 to 500 Hz) with BIOPAC software.

The collected EMG signals were later high pass filtered (cutoff = 15 Hz) to remove low frequency movement artefact, full-wave rectified, and low pass filtered using a 2nd order Butterworth filter in forward and reverse directions (cutoff = 20 Hz). The EMG data from the landings were normalized and expressed as a percentage with respect to the maximum EMG signals recorded during maximum voluntary isometric contraction for each muscle. All comparisons were tested utilizing a repeated measures ANOVA ($P<0.05$).

RESULTS AND DISCUSSION

Males exhibited only slightly greater body weight normalized VGRF peaks (6.4 ± 1.4 BW) compared with females (5.9 ± 1.2 BW), while females demonstrated slightly more rapid rates of loading ($P=0.08$).

Kinetically-derived landing phase times (i.e. preparatory, descent and recovery) were not statistically significantly different between the genders. Activation times of all muscles tended to occur earlier in males compared with females (Figure 1). Mean peak EMG amplitudes were similar between males and females, with females demonstrating greater peak amplitude only in the GLUT compared with males (P=0.02).

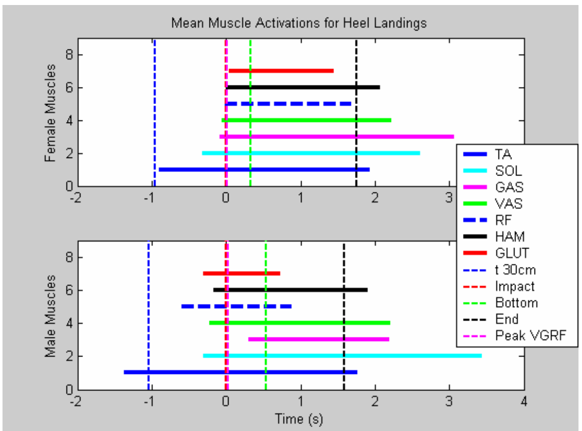

Figure 1: Mean EMG muscle activations for females and males during heel landings.

Females as a group exhibited a "bottom-up" order of muscle activation with onset coincident around initial contact. This sequence suggests the ankle is being stabilized first in preparation for impact, potentially leaving the knee unprotected at the instant of impact when peak shear forces are generally regarded to occur. Conversely, males tended to stabilize the more proximal joints first, demonstrated by an earlier and greater co-contraction across the knee and ankle prior to contact.

The coincident activation across the knee and ankle suggests males were attempting to maintain an upright torso in an effort to reduce resultant joint moments at the hip. A greater resultant joint moment at the hip could lead to an increased risk of knee injury if the heel remains firmly planted, especially if a horizontal acceleration is introduced as occurs during an off-balanced landing.

The relatively low drop height (0.2m) utilized in the present study may not have been sufficient to elicit gender differences in preparatory muscle activation. Performance of "stiff" or high impact landings from slightly greater heights (e.g. 0.4m) may reveal gender differences similar to those reported previously (Boros & Challis, 2003).

SUMMARY

Males and females demonstrated similar body weight normalized VGRF and muscle activation patterns during landings onto the heels from 0.2m, contrary to previous studies (Cowling & Steele, 2001). The more proximally located muscle activation sequence observed in males suggests they may be maintaining a more upright posture during high-impact landings, and therefore minimizing anterior shear at the knee.

REFERENCES

Arendt, E., Dick, R. (1995). *Am. J. Sports Med.*, **23**, 694-701.

Boros, R.L. and Challis, J.H. (2003). *Proceedings of the ASB 2003*.

Cowling, E.J., Steele, J.R. (2001). *J. Electromyogr. Kinesiol.*, **11**, 263-268.

Lephart, S. A., Abt, J.P., Ferris, C.M. (2002). *Curr. Opin. Orthopedics*, **14**, 168-173.

ACKNOWLEDGEMENTS

This study was funded by a financial endowment from Albert and Lorraine Kligman through the College of Health and Human Development at The Pennsylvania State University.

WHAT EFFECT DOES THE FLEXOR CARPI RADIALIS HAVE ON SCAPHOID MOTION?

Kristin D. Zhao; Jinrok Oh, MD; Steven L. Moran, MD; Maile Ceridon; Ronald L. Linscheid, MD; Kai-Nan An, PhD

Biomechanics Laboratory, Department of Orthopedic Research, Mayo Clinic, Rochester, Minnesota, USA
E-mail: zhao.kristin@mayo.edu

INTRODUCTION

Scapholunate instability is the most common cause of wrist instability. Its clinical progression eventually leads to a predictive pattern of wrist arthritis. The flexor carpi radialis (FCR) is a tendon that crosses the volar surface of the scaphoid. The FCR sits in a unique position and most likely provides a significant volar support to the scaphoid. This tendon is used frequently for tendon transfers and as a source of tendon graft in soft tissue arthroplasties of the thumb. Isolated reports have indicated that sacrifice of this tendon in patients with underlying scapholunate instability lead to a rapid progression of degenerative arthritis and exacerbation of scapholunate instability. There are no mechanical studies that examine the importance of this tendon on wrist biomechanics and its possible important role as a palmar stabilizer of wrist motion. This study investigates the role of the FCR in a cadaveric wrist model.

METHODS

Four fresh frozen cadaver wrist forearms were selected after exclusion of significant degenerative changes as determined by x-ray examination. The skin of the forearm was excised circumferentially 5 to 6 cm proximal to the wrist and a heavy suture was secured to each of the following tendons for application of tensile load: extensor carpi radialis longus (ECRL) and brevis (ECRB), extensor carpi ulnaris (ECU), flexor carpi radialis (FCR), flexor carpi ulnaris (FCU), and abductor pollicis longus (APL). The radius and ulna were transfixed with a Steinmann pin in neutral forearm rotation and the fingers were disarticulated at the metacarpophalangeal joint. Specimens were securely mounted in a custom Plexiglas holding device with polymethyl methacrylate. A 250g load was applied to each prepared tendon to simulate normal compression across the wrist due to muscle tone. A magnetic tracking system (3Space Fastrak System, Polhemus Inc.;Motion Monitor software, Innovative Sports Training Inc.) was used to record the kinematics of the scaphoid, lunate, and the 3rd metacarpal shaft. The 3Space sensors were attached to the three bones via rigid Plexiglas rods and the magnetic source was fixed to the Plexiglas experimental table.

The global coordinate system was constructed on the radius prior to data collection and flexion/extension of the bones determined using 3-D attitude representation. Passive flexion of the wrist was simulated by moving the rod in the 3rd metacarpal within a flexion/extension guide. Kinematic data was collected during flexion from the neutral position in the following conditions: intact with all muscles loaded (IN); with the FCR loading removed (FCR-NO LOAD); with the FCR soft tissue attachments around the scaphoid and trapezium removed, with loading (FRC DET-LOAD); with the FCR soft tissue attachments around the scaphoid and trapezium removed, without loading (FCR DET- NO LOAD); with the FCR cut from its insertion on the 2nd MCP (FCR CUT); and with the scaphotrapeziotrapezoidal ligament cut (STIL CUT). Two specimens were tested with the order described above (sequence A) and two specimens were tested with the STIL CUT condition followed by the FCR testing series (sequence B).

RESULTS AND DISCUSSION

The flexion/extension angle of the scaphoid relative to the radius was determined throughout the wrist flexion movement. Values of the angle in neutral, 30, and 60 degrees of wrist flexion were selected from the continuous data for all conditions. Values are presented as the difference from the intact values. Similar trends were seen for all wrist positions; a representative graph at 30 degrees of wrist flexion depicts the trends (Fig. 1).

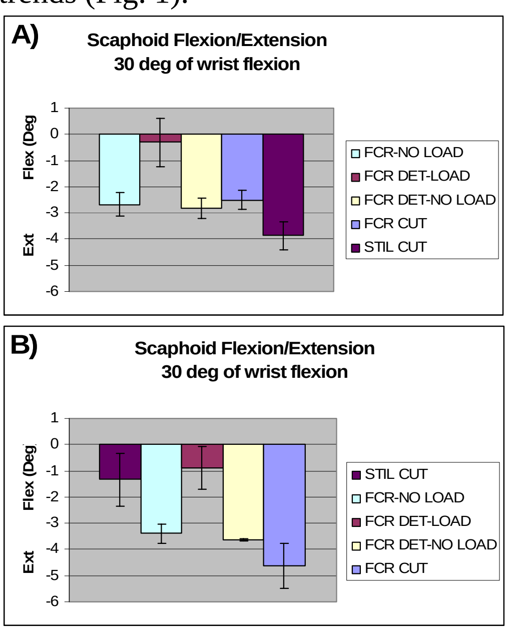

Figure 1: Mean and standard deviation of scaphoid flexion/extension angle in the radial coordinate system with the wrist in 30 degrees of flexion for A) testing sequence A, and B) testing sequence B.

Nearly all conditions depict an extension of the scaphoid relative to the intact condition. In both testing sequences, with the FCR soft tissue attachments around the scaphoid and trapezium removed and/or unloaded (FCR-NO LOAD, FCR-DET NO LOAD), or cut from its insertion on the 2nd MCP (FCR CUT), the scaphoid moves into as much as 5 degrees of extension. In addition, in the FCR DET-LOAD condition, the scaphoid is returned to within a degree of the intact condition in the first sequence and to within a degree of the STIL CUT condition in the second sequence.

SUMMARY

The results of this study show that compromising the FCR by unloading, or removing the tendon from its insertion or soft tissue attachments around the scaphoid and trapezium, moves the scaphoid into an extension position. Only in the condition with the FCR soft tissue attachments around the scaphoid and trapezium removed, and loaded, does the scaphoid return toward the intact state. This suggests that the flexion moment exerted by the FCR, both through its soft tissue attachments to the scaphoid and through its wrapping around the scaphoid, is important for maintaining scaphoid positioning. Compromise of the FCR for reconstruction operations or due to pathology may lead to further joint instability and degeneration.

ACKNOWLEDGEMENTS

Funding for this project was provided by the Mayo Foundation.

ANTERIOR CRUCIATE LIGAMENT INJURY AND PATELLAR LIGAMENT INSERTION ANGLE

Choongsoo S. Shin[1], Chris O. Dyrby[1], Brenna K. Hearn[1], Ajit M. Chaudhari[1], and Thomas P. Andriacchi [1,2]

[1] Department of Mechanical Engineering, Stanford University, Stanford, CA, USA
[2] Veterans Administration Palo Alto RR&D Center, Palo Alto, CA, USA
E-mail: scslove@stanford.edu Web: biomotion.stanford.edu

INTRODUCTION

The patellar ligament transfers the force of quadriceps contraction from the thigh to the tibia, providing the knee extensor mechanism. The patellar ligament insertion angle (PLIA), defined as the angle between the patellar ligament and the tibial shaft, determines how quadriceps force is decomposed into the anterior and superior directions. A knee with a larger PLIA would have a higher quadriceps generated anterior component of force on the tibia than a knee with a smaller PLIA. This may lead to a higher risk of ACL injury, since anterior tibial translation associated with quadriceps contraction has been suggested as a potential cause for ACL rupture (DeMorat 2004) and gait adaptations after ACL rupture (Berchuck 1990). Similarly, it has been suggested (Andriacchi 2004) that loss of the ACL would cause a shift in the nominal position of the tibia which would cause a change in the PLIA after ACL injury. The purpose of this study was to test the following hypotheses: (1) The PLIA of the uninjured, contralateral knee is larger than the control knees, and (2) the PLIA following ACL injury would decrease relative to the contralateral knee.

METHODS

Eighteen subjects were studied under IRB informed consent – nine ACL deficients (age=35.1±11.7 years, 7 male, 2 female, average 159 months past injury) and nine controls with no history of musculoskeletal injury (age=34.7±8.8 years, 7 male, 2 female). Magnetic resonance images (3DSPGR) were taken of each subject's knees in a fully extended, non-weight-bearing position. The right or left knee images of gender-matched controls were chosen to match the ACL deficient side.

To determine the PLIA of each subject, the long axis of tibial shaft was determined by bisecting the angle between the anterior and posterior sides of tibia in a midline sagittal MRI slice of the knee showing the tibial edges clearly (Figure 1a)

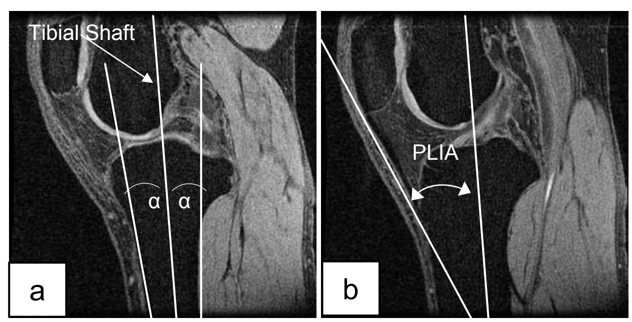

Figure 1: a) The midline of the tibial shaft was determined as the bisecting angle.
b) PLIA was measured between the patellar ligament and the tibial shaft midline.

A second slice, showing high contrast of the patellar ligament and tibial tuberosity, was used to find the patellar ligament, running from the inferior edge of the patella to the tibial tuberosity. The PLIA was then defined as the angle between the tibial shaft and patellar ligament (Figure 1b). All angles were determined using AMIRA 3.1 (TGS, Inc., San Diego, CA). A one-sided Wilcoxon test was used to test the first hypothesis and a one-sided paired Wilcoxon test was performed for the second hypothesis. Significance level of $\alpha < 0.05$ was used for all analyses.

RESULTS AND DISCUSSION

The data provide no evidence that the PLIA of the contralateral knee is larger than that of control knee ($p=0.865$). The mean (±S.D.) PLIA of the ACL deficient knee, contralateral knee, and control knee are 21.6±3.5º, 24.8±2.3º, and 27.2±4.5º, respectively (Figure 2).

After ACL injury, the PLIA of the ACL deficient knee is significantly smaller than that of the contralateral knee ($p=0.037$).

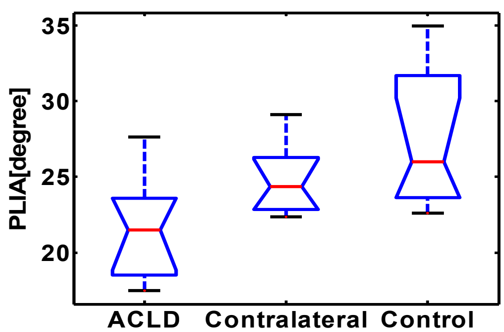

Figure 2: The PLIA for ACLD knees were reduced in comparison to contralateral and matched control knees.

These results suggest that an anatomical difference in PLIA is not likely to be a major factor causing ACL injury, since the PLIA of the contralateral knee is not larger than that of the control. Loss of the ACL, however, causes a significant reduction in the PLIA. This reduction is likely related to changes in the equilibrium condition of the soft tissues in the knee joint which decrease the PLIA. The mean difference of PLIA in the ACL injured knee compared to the contralateral knee was 3.2º. This reduced angle approximately corresponds to 3mm of anterior tibial translation given the average patellar ligament length of 51mm for these subjects.

The altered equilibrium condition of the tibia and/or patella causes both the tibio-femoral and/or patellofemoral contact points to change. This altered reference position will change joint contact mechanics and loading patterns. It has been suggested (Andriacchi 2004) that these sudden alterations in contact mechanics may lead to degenerative changes in the knee joint. ACL loss causes both tibiofemoral and patellofemoral knee osteoarthritis (Gillquist 1999; Jarvela 2001). Patellofemoral osteoarthritis is an important cause of knee pain and disability, even without concomitant tibiofemoral arthritis (McAlindon, 1992). Further study of the ACL's effect on the PLIA and loading patterns may help determine ways to prevent patellofemoral pain and osteoarthritis.

REFERENCES

Andriacchi, T.P., Dyrby, C.O. (2004). *J. Biomechanics,* accepted for publication.
Berchuck, M. et al. (1990). *J. Bone Joint Surg.,* **72A**, 871-877.
DeMorat, G. et al. (2004). *Am. J. Sports Med.,* **32,** 477-483.
Gillquist, J., Messner, K.(1999). *Sports Medicine*, **27,** 143-156.
Jarvela, T. et al. (2001). *Arthroscopy*, **17,** 818-825.
McAlindon, T.E. et al. (1992). *Ann Rheum Dis.* **51**, 844-849.

ACKNOWLEDGEMENTS

Funding source: NIH R01-AR39212

DYNAMIC FIXATION SYSTEMS COMPARED TO THE RIGID SPINAL INSTRUMENTATION-A FINITE ELEMENT INVESTIGATION

Sri Lakshmi Vishnubhotla[1], Vijay K. Goel[1], Sasidhar Vadapalli[1], Akiyoshi Masuda[1], Ashutosh Khandha[1], Miranda N. Shaw[1], Jared Walkenhorst[2], Larry Boyd[3]

[1]Spine Research Center, University of Toledo, and Medical College of Ohio, Toledo, OH
[2]Spine Wave Inc., CT
[3]Department of Biomedical Engineering, Duke University, Durham, NC
Email: svishnub@eng.utoledo.edu

Introduction:

Intervertebral disc degeneration, a contributing factor to chronic low back pain, may be partially ascribed to abnormal loading patterns on the disc. The optimum approach to treatment of degenerative disc disease is to restrict the motion of the spine to a zone or range where near normal disc loading might occur. Rigid spinal instrumentation restricts the motion but significantly alters the loading environment of the disc away from the ideal physiologic state. Hence, flexible fixation devices have been designed to provide spinal stabilization while allowing a physiologically advantageous load through the disc.

The aim of this study was to compare the motion and stresses in the disc for a rigid screw-rod system, a dynamic stabilization system (Dynesys system, Centerpulse Spinetech) and an interspinous spacer (Wallis, SpineNext) using the finite element technique.

Methods:

A 3-dimensional, non-linear, ligamentous, experimentally validated, finite element model of the intact L3-S1 segment was used, Figure 1. All of the systems were simulated across the L4-L5 level with an intact disc. The pedicle screws were 'tied' to the adjoining bone surface. The 'polymeric cylinder' and the 'ligament' of the Dynesys system were modeled as 3D elastic truss elements with the cylinder assigned "no tension" and the ligament assigned "no compression" properties.

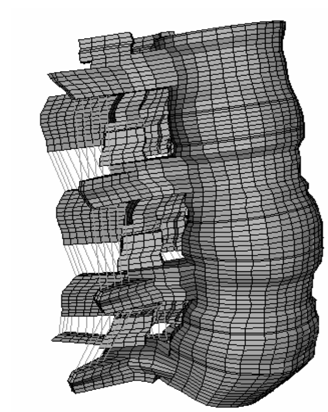

Figure 1: Finite element model of the intact ligamentous L3-S1 segment

The Wallis spacer, placed between the L4-L5 interspinous processes, was modeled using solid 3D hexahedral elements. A "tied" contact was defined for the bottom and the L5 spinous process, and hard contact, finite sliding for the top of the Wallis system and the L4 spinous process. The ligament-cables in Wallis system that tie the spacer to the spinous processes were modeled using 3D truss elements with the "no compression" option.

The models were constrained at the S1 and motion and stresses in various components were predicted for 400 N axial compression and a flexion/extension moment of 10.6 N-m applied at the top of L3 vertebra.

Results and Discussion:

In flexion, the increase in motion across L3-4 segment for the stabilized models were 11%, 10% and 4% respectively for the rigid, Dynesys and Wallis systems, as compared to the intact case. In extension, the L3-4 motion in all the three instrumented cases was closer to intact (~2% variation). At the

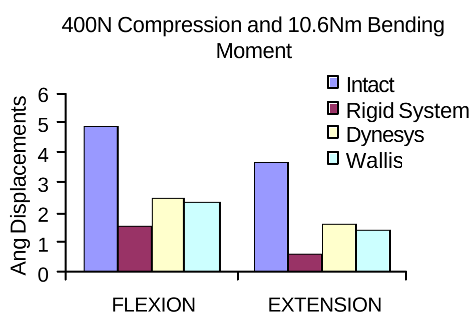

Figure 2: Comparison of relative motion at the instrumented level (L4-5) in flexion and extension for various devices.

instrumented level (L4-5) in flexion, the motion (Figure 2) decreased by 68% in rigid screw-rod system, 50% in Dynesys system and 52% in Wallis system, as compared to the intact case. In extension the corresponding reductions in motion were 84% for the rigid screw-rod system, 56% for the Dynesys and 60% for Wallis. In flexion, the peak disc stresses at the adjacent levels were comparable to the intact stresses (±5% change). The peak disc stresses at the instrumented segment reduced by 41% for the rigid system, 27% for the Dynesys system, and 31% for the Wallis system. In extension, the peak disc stresses at the adjacent levels in all the three instrumented models were almost similar to that of intact. At the instrumented level, the peak stresses of the rigid screw-rod system reduced by 80% when compared to the intact. In the Dynesys and Wallis systems, the peak stresses reduced by 45% and 56% respectively when compared to the intact.

Summary:

The trend in motion in flexion of the segment stabilized using Dynesys system is in agreement with the findings of Schmoelz et.al. (2003), supporting the validity of our model. The rigid screw-rod system gives the most restricted range of motion of spine and the most unloading of the disc at the instrumented segment. The Dynesys system allows more motion than the rigid screw-rod system, and hence allows for partial disc loading. The effect of Wallis system is between the rigid and Dynesys systems.

When compared to the rigid screw-rod system dynamic stabilization systems may allow for partial disc regeneration by allowing more physiologic levels of disc loading and a restricted range of motion at the same time. Although, we do not know at this stage the optimal value for disc loading, more physiological values could contribute to disc regeneration.

References:

Schmoelz, W. et al. (2003).*J.Spinal Disorders & Techniques*, **16**, #**4**, 418-423

Mulholland, R.C., Sengupta, D. K. (2002). *Eur Spine J*, ***11****(suppl.***2***)*, S198-S205

Acknowledgements:

Work supported in part by a grant from Spine Wave Inc., CT.

DYNAMIC FIXATION SYSTEMS COMPARED TO THE RIGID SPINAL INSTRUMENTATION-A FINITE ELEMENT INVESTIGATION

Sri Lakshmi Vishnubhotla[1], Vijay K. Goel[1], Sasidhar Vadapalli[1], Akiyoshi Masuda[1], Ashutosh Khandha[1], Miranda N. Shaw[1], Jared Walkenhorst[2], Larry Boyd[3]

[1]Spine Research Center, University of Toledo, and Medical College of Ohio, Toledo, OH
[2]Spine Wave Inc., CT
[3]Department of Biomedical Engineering, Duke University, Durham, NC
Email: svishnub@eng.utoledo.edu

Introduction:

Intervertebral disc degeneration, a contributing factor to chronic low back pain, may be partially ascribed to abnormal loading patterns on the disc. The optimum approach to treatment of degenerative disc disease is to restrict the motion of the spine to a zone or range where near normal disc loading might occur. Rigid spinal instrumentation restricts the motion but significantly alters the loading environment of the disc away from the ideal physiologic state. Hence, flexible fixation devices have been designed to provide spinal stabilization while allowing a physiologically advantageous load through the disc.

The aim of this study was to compare the motion and stresses in the disc for a rigid screw-rod system, a dynamic stabilization system (Dynesys system, Centerpulse Spinetech) and an interspinous spacer (Wallis, SpineNext) using the finite element technique.

Methods:

A 3-dimensional, non-linear, ligamentous, experimentally validated, finite element model of the intact L3-S1 segment was used, Figure 1. All of the systems were simulated across the L4-L5 level with an intact disc. The pedicle screws were 'tied' to the adjoining bone surface. The 'polymeric cylinder' and the 'ligament' of the Dynesys system were modeled as 3D elastic truss elements with the cylinder assigned "no tension" and the ligament assigned "no compression" properties.

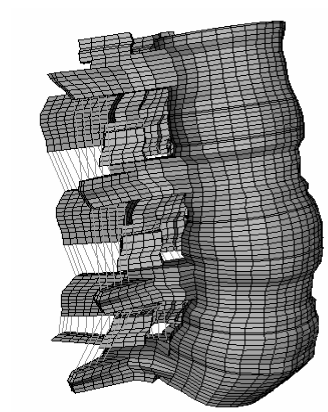

Figure 1: Finite element model of the intact ligamentous L3-S1 segment

The Wallis spacer, placed between the L4-L5 interspinous processes, was modeled using solid 3D hexahedral elements. A "tied" contact was defined for the bottom and the L5 spinous process, and hard contact, finite sliding for the top of the Wallis system and the L4 spinous process. The ligament-cables in Wallis system that tie the spacer to the spinous processes were modeled using 3D truss elements with the "no compression" option.

The models were constrained at the S1 and motion and stresses in various components were predicted for 400 N axial compression and a flexion/extension moment of 10.6 N-m applied at the top of L3 vertebra.

Results and Discussion:

In flexion, the increase in motion across L3-4 segment for the stabilized models were 11%, 10% and 4% respectively for the rigid, Dynesys and Wallis systems, as compared to the intact case. In extension, the L3-4 motion in all the three instrumented cases was closer to intact (~2% variation). At the

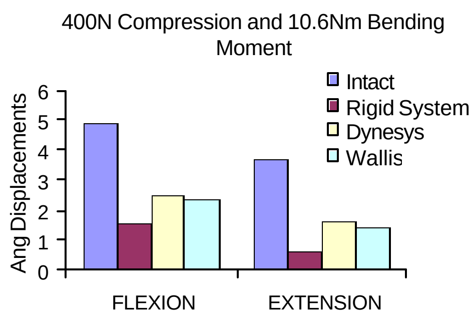

Figure 2: Comparison of relative motion at the instrumented level (L4-5) in flexion and extension for various devices.

instrumented level (L4-5) in flexion, the motion (Figure 2) decreased by 68% in rigid screw-rod system, 50% in Dynesys system and 52% in Wallis system, as compared to the intact case. In extension the corresponding reductions in motion were 84% for the rigid screw-rod system, 56% for the Dynesys and 60% for Wallis. In flexion, the peak disc stresses at the adjacent levels were comparable to the intact stresses (±5% change). The peak disc stresses at the instrumented segment reduced by 41% for the rigid system, 27% for the Dynesys system, and 31% for the Wallis system. In extension, the peak disc stresses at the adjacent levels in all the three instrumented models were almost similar to that of intact. At the instrumented level, the peak stresses of the rigid screw-rod system reduced by 80% when compared to the intact. In the Dynesys and Wallis systems, the peak stresses reduced by 45% and 56% respectively when compared to the intact.

Summary:

The trend in motion in flexion of the segment stabilized using Dynesys system is in agreement with the findings of Schmoelz et.al. (2003), supporting the validity of our model. The rigid screw-rod system gives the most restricted range of motion of spine and the most unloading of the disc at the instrumented segment. The Dynesys system allows more motion than the rigid screw-rod system, and hence allows for partial disc loading. The effect of Wallis system is between the rigid and Dynesys systems.

When compared to the rigid screw-rod system dynamic stabilization systems may allow for partial disc regeneration by allowing more physiologic levels of disc loading and a restricted range of motion at the same time. Although, we do not know at this stage the optimal value for disc loading, more physiological values could contribute to disc regeneration.

References:

Schmoelz, W. et al. (2003).*J.Spinal Disorders & Techniques*, **16**, #**4**, 418-423

Mulholland, R.C., Sengupta, D. K. (2002). *Eur Spine J*, ***11****(suppl.****2****)*, S198-S205

Acknowledgements:

Work supported in part by a grant from Spine Wave Inc., CT.

STATIC FORCE PRODUCTION IN A THREE-DIMENSIONAL MUSCULOSKELETAL MODEL OF THE CAT HINDLIMB

Lale Korkmaz [1], Thomas J. Burkholder [2] and Lena H. Ting [3]

[1] Woodruff School of Mechanical Engineering, Georgia Institute of Technology, Atlanta, GA
[2] School of Applied Physiology, Georgia Institute of Technology, Atlanta, GA
[3] Coulter Department of Biomedical Engineering, Georgia Tech/Emory University, Atlanta, GA
E-mail: lting@emory.edu Web: http://neuro.gatech.edu

INTRODUCTION

The goal of this study is to identify the extent to which the biomechanical constraints on the force generating capacity of the musculoskeletal system govern postural responses in cats. Ground reaction forces produced by a freely standing cat during postural perturbations tend to act along a diagonal axis regardless of perturbation direction – this has been dubbed the force constraint strategy (Macpherson 1988). The forces produced by individual muscles in the cat hindlimb have also been shown to have significant non-sagittal, diagonal directions when transmitted to the foot (Nichols et al 1993).

To examine how muscle forces are transformed to ground reaction forces, we developed a six degree of freedom muscolskeletal model based on the Burkholder and Nichols model (2000). We then used a static Jacobian analysis to model the directions of ground reaction force produced by each of 31 hindlimb muscles. Finally, we found the direction and magnitude of maximum force production in the limb when a combination of muscles is activated.

METHODS

A six-degree-of-freedom model of the cat hindlimb was implemented in SIMM software (Musculographics, Inc.) and consisted of three anatomical joints: the hip, knee, and ankle. The model consisted of five mechanical joints: two pin joints representing flexion and adduction rotation axes at the hip, knee and ankle. The axes of rotation were non-orthogonal at the knee and ankle. 31 hind limb muscles were modeled. Muscles were assumed to be straight lines between origin, insertion and via points.

The Jacobian matrix relating muscle force to endpoint force was derived from the model. The endpoint force and moment vector is represented by the equation:

$$\mathbf{F}=\mathbf{J}^{-\mathbf{T}}\mathbf{R}\mathbf{F}_{\mathbf{max}}\mathbf{e}$$

Where **F** is a 6x1 endpoint force and moment vector, **J** is the Jacobian matrix, **R** is a 6x31 matrix of muscle moment arms, $\mathbf{F}_{\mathbf{max}}$ is a 31x31 diagonal matrix of maximum muscle force, and **e** is a 31x1 vector of muscle activations between 0 and 1(Valero-Cuevas et al 1997). An optimization was used to find the set of muscle activation that produced the maximum endpoint force. The endpoint moment was constrained to be zero because the paw of the cat cannot support a large moment at the ground.

RESULTS AND DISCUSSION

Each muscle was found to produce a unique direction of force at the ground when activated individually (Figure 1b). Although many of the muscles have considerable medial and lateral components of force, in general the muscles forces were clustered along the diagonal axis, similar to that in the force constraint strategy (Figure 1a). It is important to note, however, that the activation of each muscle also generated an endpoint moment at the toe. At maximum activations, these moments could be unrealistically large, and would not be supported by the toe of the cat.

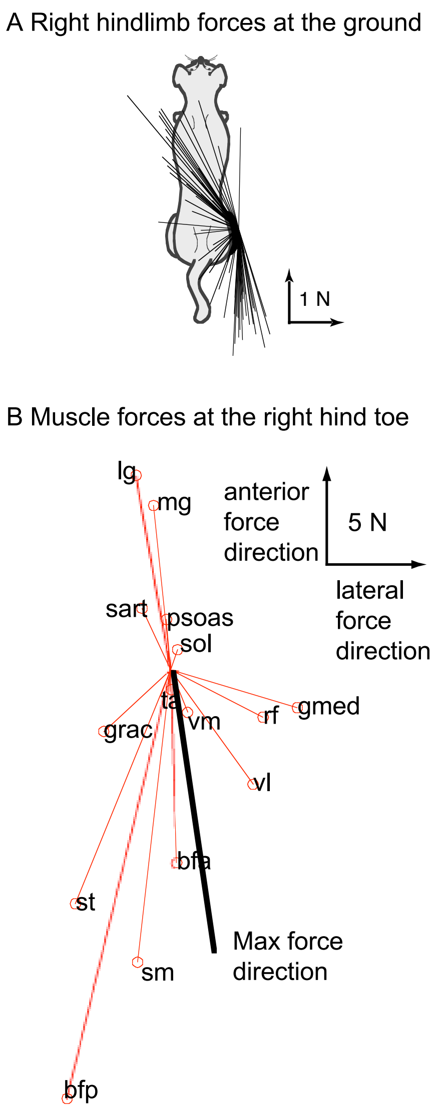

Figure 1 Forces at the ground in the right hindlimb. A) Forces during postural responses to support surface translations in 16 evenly-spaced directions in the horizontal plane B) Force generated the model due to maximal activation of individual muscles. Dark line indicates direction of maximum force production when multiple muscles are activated.

The direction of maximum force generation when the endpoint moment was constrained to be zero was directed in the downward, lateral, and posterior direction (Figure 1b, dark line), and was generated primarily by extensor muscles. This is consistent with the force direction measured during postural responses when the limb is loaded, eliciting an extensor muscle response.

The muscle activation pattern generating the maximum force had submaximal muscle activations. This is due to the fact that the foot can only support a moment equal to the ground reaction force multiplied by the length of the foot. Thus, a bang-bang solution whereby each muscle would be either off or maximally activated would render a solution that maximized both endpoint force and endpoint moment, which would be unphysiological.

SUMMARY

The nervous system may choose to stabilize the body by activating muscles such that the forces act along the direction of maximum force production of the leg. This would allow the nervous system to simply scale the amplitude of a muscle activation pattern in order to increase the ground reaction force if the necessary.

REFERNCES

Burkholder T.J. and Nichols T.R. (2000). *Motor Control* 4: 201-220.
Nichols T.R. et al. (1993) *Exp Brain Res* 97:366-371
Macpherson J.M. (1988).*J. Neurophysiol* 60: 204-231.
Valero-Cuevas et al. (1998) *J. Biomech* 31:693-703

ACKNOWLEDGEMENTS

We thank Jane Macpherson. NIH HD46922

AN IN VITRO MODEL OF SCOLIOSIS BRACING USING LOAD APPLIED TO THE HUMAN CADAVERIC TRUNK

Kristin D. Zhao[1]; Chao Yang, MD[1]; Maxime Chauvet[2]; Chunfeng Zhao, MD[1]; David Mitton, PhD[2]; Jane Matsumoto, MD[1] Anthony A. Stans, MD[1] Wafa Skalli, PhD[2]; Kai-Nan An, PhD[1]

[1] Biomechanics Laboratory, Division of Orthopedic Research, Mayo Clinic, Rochester, Minnesota, USA
[2] Laboratory of Biomechanics, Ecole National Superieure d'Arts et Metier (ENSAM), Paris, France
E-mail: zhao.kristin@mayo.edu

INTRODUCTION

Scoliosis is the most common pediatric spinal deformity and is characterized by deviation of the spine from normal alignment. Early diagnosis and treatment is essential to avoid serious spinal deformity. Spinal orthotic treatment has been widely accepted for patients with moderate curvature of the spine. Several different brace designs appear to prevent scoliosis progression, but little information is available to determine the optimal brace design. Design of a method which is able to predict maximum deformity correction, and which can be used to measure brace effectiveness, would represent a significant advancement in non-operative spine deformity treatment.

Recently, the ENSAM Biomechanics Laboratory developed a spine and trunk finite element model (FEM) using stereoradiographical techniques which will eventually be used for patient-specific brace design for scoliosis patients. The purpose of this study was to assess the effectiveness of a cadaveric spine model developed for the purpose of validating the FEM spine model.

METHODS

An in vitro model of scoliosis bracing was simulated using load applied to the human cadaveric trunk while positioned in a custom-designed apparatus which enabled biplanar radiographs to be obtained and calibrated (Fig. 1).

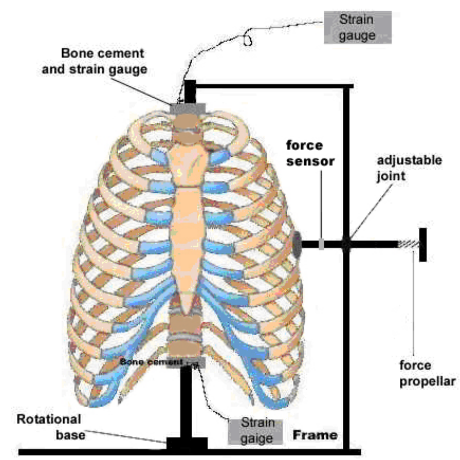

Figure 1: Spine specimen mounted in custom loading apparatus.

A fresh cadaveric spine, from vertebrae T1 to L4, was removed of soft tissue and organs. The rib cage, with ligaments and muscles intact, was harvested. T1/T2 and L4 were mounted and fixed to the custom designed apparatus via bone cement. A force transducer was positioned between the force pad (77mm diam.) and force applicator in order to measure the force applied to the rib cage.

Biplanar radiographs were obtained while applying static horizontal loads at different levels of the ribcage and at varying angles of incidence (Table 1).

Table 1: Experimental testing conditions with displayed results shown in bold.

Condition	Head Load (63N)	Lateral Load (N)	Position Lateral Load (Rib)	Angle of incidence (°)
A	**No**	**0**	**-**	**-**
B	Yes	0	-	-
C	Yes	130	5,6,7	0
D	**Yes**	**120**	**5,6,7**	**45**
E	**Yes**	**160**	**7,8,9**	**45**
F	Yes	130	7,8,9	0
G	Yes	140	7,8,9	-45

Each set of radiographs were then reconstructed using stereoradiography. Measures of relative disk rotations and 3D reconstructions were performed with a custom software package developed in collaboration between the *Laboratoire de recherche en imagerie et orthopédie,* (ETS - CRCHUM, Montréal, Canada) and the *Laboratoire de biomécanique* (CNRS-ENSAM, Paris, France). The geometry of spine and thoracic cage reconstruction using semi automatic method and NSCC (Non Stereo Corresponding Contours) have been validated (Pomero et al. 2004, Laporte et al. 2004).

RESULTS AND DISCUSSION

Results of the comparison between three experimental conditions (A, D, and E) are presented here. Figure 2 depicts the 3D reconstructions of conditions A and D respectively. Figure 3 depicts the lateral rotations of the vertebrae in conditions A, D, and E.

Realistic 3D reconstructions and resulting kinematic measures have been obtained from the cadaveric model of scoliosis bracing for assessment of the FEM spine model.

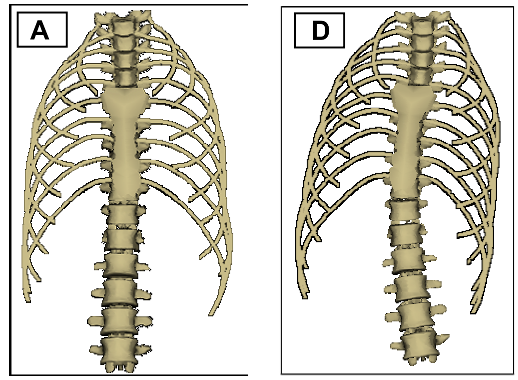

Figure 2: 3D reconstructions of the specimen in conditions A and D.

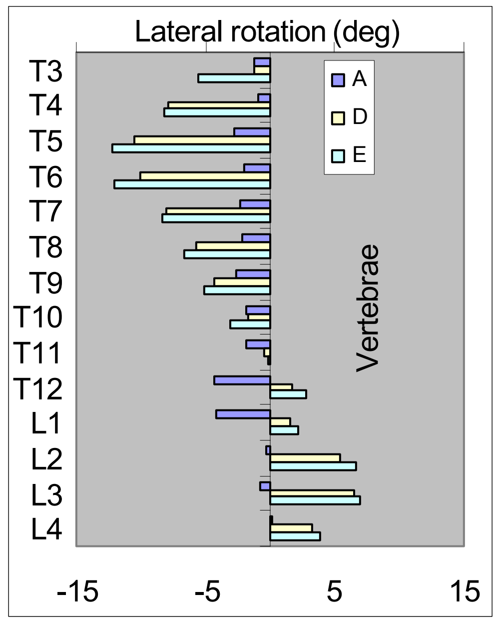

Figure 3: Lateral rotation of the vertebrae in testing conditions A, D, and E.

REFERENCES

Pomero V., Skalli W. et al. (2004) *Clin Biomech*, **19**, 240-247

Laporte S.,Mitton D. et al (2004) *Proceedings of the CARS*

Mitton D., de Guise J.A. et al. (2000) *Med Biol Eng Comput*, **38**, 133-139

ACKNOWLEDGEMENTS

The authors wish to acknowledge Joseph Kuntz and Mathieu Martinet for their contributions to this project.

A COMPARISON OF FOUR METHODS OF CALCULATING VERTICAL STIFFNESS IN DISTANCE RUNNING

Iain Hunter, Ty Hopkins, and Cindy A. Trowbridge

Department of Physical Education, Brigham Young University, Provo, UT, USA
E-mail: iain_hunter@byu.edu Web: www.byu.edu

INTRODUCTION

Vertical stiffness is a useful method for characterizing distance running. It has been correlated with stride frequency, surface, speed, and aerobic demand (Arampatzis, 1999, Heise, 1998, Farley, 1996, Kerdok, 2002, McMahon, 1990, Dalleau, 1998). However, there are limitations to the traditional method of calculating stiffness. The heel strike and initial slope compared with the final slope are poorly matched when reproducing force based upon the calculated stiffness and initial conditions (Figure 1).

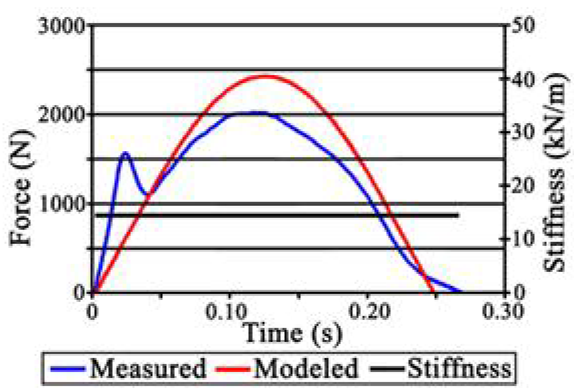

Figure 1: The traditional method of calculating vertical stiffness using a constant stiffness with modeled force.

Another approach was recently introduced measuring a stiffness that begins relatively high, and then drops to a lower stiffness around the heel strike (Hunter, 2002). This method matches reproduced force very well (Figure 2).

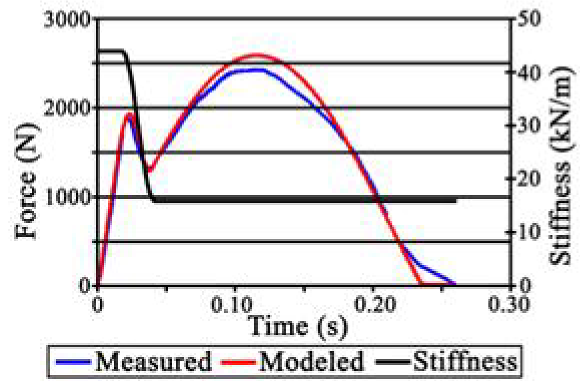

Figure 2: The variable stiffness method of calculating vertical stiffness demonstrating how well measured force matches modeled force.

This study compares the benefits and drawbacks to three different constant stiffness methods and the variable stiffness method.

METHODS

Four methods of calculating vertical stiffness were compared by their correlations with measured versus modeled vertical ground reaction forces
Traditional: The traditional method of calculating stiffness divides the maximum vertical ground reaction force by the change in vertical position of the center of mass from foot contact to the maximum displacement.
Constant low: This method differs from the traditional method by dividing by the maximum vertical displacement of the

center of mass from the lowest point to takeoff.

Constant best fit: This is a constant stiffness method using a stiffness that provides the best fit between measured and modeled vertical ground reaction forces.

Variable: This method uses a best fit model with an initial high stiffness that drops to a lower value around the heel strike. The drop begins at the peak force of heel strike and ends at the valley between heel strike and the active peak.

RESULTS AND DISCUSSION

All methods were significantly different from each other using an adjusted significance level of 0.0083 for multiple comparisons (Table 1). While the differences between most methods were practically non-significant, the variable stiffness method appeared functionally significant. It is clear visually and statistically that the variable stiffness method provides a much better fit than any other method.

The variable stiffness method may be the best fit for the following reasoning. The body reacts very stiff to the ground at initial contact. As the foot becomes flat to the ground, the center of pressure progresses forward, resulting in a lengthening of the leg spring. Since the leg spring is slightly increasing, the stiffness will decrease during this time. Once the foot is flat with the ground, the ankle becomes more involved in the stance. With an additional joint becoming a major part of the spring, the overall stiffness may decrease.

While two variables are required to use the vertical stiffness model (initial and final stiffnesses), there may be cases where only the initial or final stiffness may be of importance in the model being considered.

SUMMARY

The variable stiffness method for calculating vertical stiffness provides the best fit for modeling vertical ground reaction forces. However, there are two variables required to use this method.

REFERENCES

Arampatzis, A., Bruggemann, G. P. and Metzler, V. (1999) The effect of speed on leg stiffness and joint kinetics in human running. *J Biomech,* **32,** 1349-1353.

Farley, C. T. and Gonzalez, O. (1996) Leg stiffness and stride frequency in human running. *J Biomech,* **29,** 181-186.

Heise, G. D. and Martin, P. E. (1998) "Leg spring" characteristics and the aerobic demand of running. *Med Sci Sports Exerc,* **30,** 750-754.

Hunter, I. (2003). A new approach to modeling vertical stiffness in heel-toe distance runners. *Journal of Sci and Sports Med*, **2**, 139-143.

Kerdok, A. E., Biewener, A. A., McMahon, T. A., Weyand, P. G. and Herr, H. M. (2002) Energetics and mechanics of human running on surfaces of different stiffnesses. *J Appl Physiol,* **92,** 469-478

Table 1: Correlations between measured and modeled vertical ground reaction forces using four approaches to calculating stiffness (mean± SD) (all methods were significantly different from all others, $p<0.0083$).

Stiffness method	Method 1	Method 2	Method 3	Method 4
Correlation	0.948±0.026	0.940±0.028	0.960±0.020	0.994±0.004

CARPAL BONE SCALING IS ISOMETRIC AND NOT GENDER SPECIFIC

James C. Coburn[1], Joseph J. Crisco[1,2], Douglas C. Moore[1], M. Anwar Upal[2]

[1]Department of Orthopaedics, Brown Medical School and Rhode Island Hospital, Providence, RI
[2]Division of Engineering, Brown University, Providence, RI
E-mail: Joseph_Crisco@brown.edu Web: www.BrownBiomechanics.org

INTRODUCTION

The contribution of the individual carpal bones to overall wrist motion is similar in males and females. For example, an early study of wrist flexion and extension revealed no gender-related differences in rotations at the midcarpal joint (Brumfield, '66). Similarly, more recent 3-D studies have found no differences in the magnitude of carpal bone rotation in men and women during flexion and extension (Wolfe, '00).

Although the magnitude of carpal bone motion appears to be similar in males and females, there *are* differences in the location of the rotation axes. In particular, the rotation axes of the carpal bones in females are located more proximally than in males (e.g. Neu, '01). This suggests that the differences in rotation axis location are primarily due to differences in bone size, as opposed to shape. However, this has never been studied systematically.

This study was performed to determine whether the gender-related differences in carpal bone size are simply due to scaling. To do so we tested the hypotheses that: 1) the volume of each carpal bone relative to wrist volume did not differ with gender, 2) the dimensions of the carpal bones in men and women scale on the same continuum, and 3) carpal bone dimensions scale isometrically (by an identical factor in all coordinate directions).

METHODS

After IRB approval and informed consent, both wrists of fourteen male and fourteen female volunteers with no wrist pathology were CT scanned (mean age 24.6 years, range 21-28). The individual carpal bones were segmented from the CT volume images, and the centroid locations, principal inertial axes, and volumes of each carpal bone were calculated (Crisco '98).

Carpal bone dimensions were defined by the dimensions of a rectangular parallelepiped bounding box whose sides were parallel to the principal inertia axes, with X, Y and Z dimensions corresponding to the smallest, middle and largest inertia values, respectively (Fig. 1). The X, Y and Z dimensions of each bone were plotted as a function of carpal bone volume. To determine whether the bones scaled isometrically an average-sized set of bones was selected and the X, Y and Z dimensions multiplied by a series of isometric scaling factors (the same for all three dimensions) to generate theoretical scaling curves, which included the smallest and largest carpal bone volumes. Comparisons of carpal bone dimensions, volume, and volume as a percentage of total wrist volume were made with unpaired Students' t-tests.

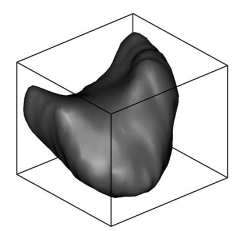

Fig. 1 Bounding box

RESULTS

As expected, the mean volume of each of the carpal bones was significantly smaller in females than in males (by an average of 30%). However, when the size of each carpal bone was calculated as a percentage of the total volume of the carpus, there were no significant differences between genders (Fig. 2).

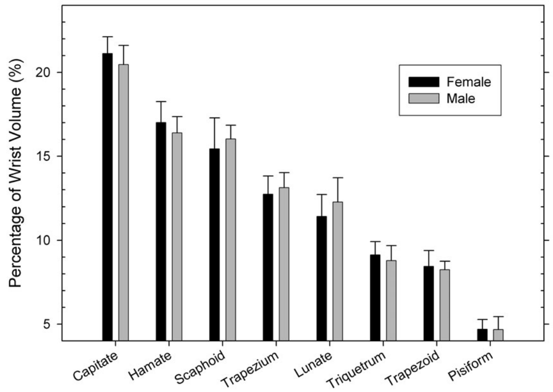

Fig. 2: Volume of each carpal bone as a percentage of the total wrist volume did not differ with gender.

Carpal bone dimensions increased as a function of volume, for each of the carpal bones (e.g. capitate, Fig. 3), and the relationship was similar in both men and women. The theoretical scaling curves had a slightly non-linear trend and closely followed the plots of the raw data from all subjects.

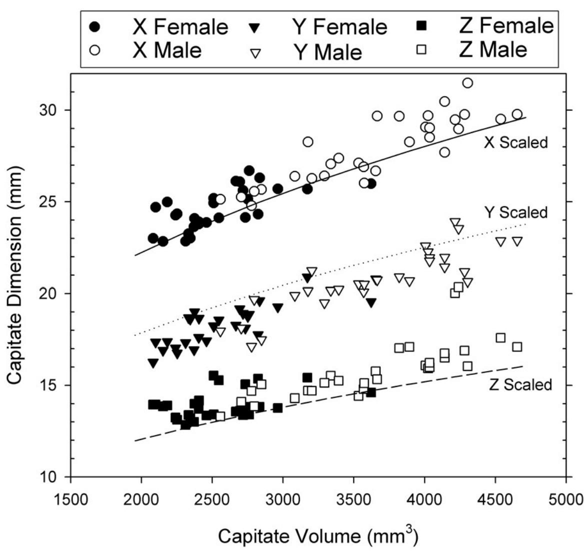

Fig. 3: The increase in each dimension of the capitate closely followed that predicted by the average capitate scaled isometrically, without any difference between male and females.

DISCUSSION

This study was performed to explore gender-related differences in carpal bone scaling. Our results suggest that the carpal bones in men and women scale similarly. While we found that the carpal bones in men are bigger than those in women, when comparisons were made of carpal bone volume as a percentage of overall wrist volume, we saw no significant differences. Our regressions revealed that the principal dimensions of the carpal bones (X, Y, and Z) in both men and women scaled on the same continuum and, most interestingly, despite their complex shapes, the three principal dimensions of the carpal bones scaled isometrically with volume (i.e. by the same factor in all three dimensions). There is little mention of this in the literature, though there are hints at such a trend in volume and inertial magnitude comparisons (Canovas, ’00).

Our results provide important insight into the scaling of carpal bones. However, our dimensioning studies do not address issues of shape, nor do they describe differences in the curvature of the articular surfaces or in the locations of the bony prominences associated with ligament insertions. These will be the subject of future studies.

REFERENCES

Brumfield, J., et al. (1966). *Southern Medical Journal*, **59**, 909-910.

Wolfe, S. W., et al. (2000). *J Hand Surg [Am]*, **25**, 860-869.

Neu, C. P., et al. (2001). *J Biomech*, **34**, 1429-1438.

Crisco, J. J., McGovern, R. D. (1998). *J. Biomechanics*, **31**, 97-101.

Canovas, F., et al. (2000). *Horm Res*, **54**, 6-13.

ACKNOWLEDGEMENTS

Funding for this work was provided by NIH AR44005, University Orthopedics, Inc. and the RIH Orthopaedic Foundation, Inc.

CAN A PENDULUM BE USED TO STUDY DYNAMIC PROPERTIES OF THE SPINE?

Lindsey Fujita[1], Joseph J. Crisco[1,2], David B. Spenciner[2]

[1]Department of Orthopaedics, Brown Medical School and Rhode Island Hospital, Providence, RI
[2]Division of Engineering, Brown University, Providence, RI
E-mail: Joseph_Crisco@brown.edu Web: www.BrownBiomechanics.org

INTRODUCTION

A pendulum with the interphalangeal joint as a fulcrum was first used to study synovial joint lubrication [2]. Charnley [1] used a pendulum to assist him in the design of his artificial hip joints, and Unsworth et al. [3] used a pendulum with the ability to apply sudden loads to demonstrate the various modes of joint lubrication.

While our joint of interest, the intervertebral joint, is not a synovial joint, the use of a pendulum system to examine its mechanical behavior is attractive from several perspectives. The spine is loaded dynamically during daily activities and the periodic loading of pendulum is a potential loading model. Mechanical testing of the spine is fraught with challenges when investigators consider constrained versus unconstrained control and application of large compressive loads. An unconstrained pendulum capable of carrying large compressive loads may address these issues.

The purpose of this work was to investigate the dynamic *in vitro* response of human lumbar functional spinal units (FSU) using an unconstrained three-dimensional pendulum system.

METHODS

A novel pendulum apparatus that placed the intervertbral disc of an FSU at approximately the fulcum was designed. The lower vertebral body was fixed and the pendulum was affixed to the upper vertebral body. The weight of the pendulum could be adjusted, as well as the direction of initial motion. Five human lumbar FSUs (ages ranging between 44-76 years) were potted and mounted within the pendulum apparatus. Specimens were tested with a total pendulum mass of 39, 89, 140, 191, and 242 N (the center of mass was calculated for each weight, but did not vary more than 10 cm). The pendulum was initially rotated 5° in flexion or in right lateral bending, then released, and its three-dimensional motion tracked using OptoTrak (Northern Digital, Ontario, Canada). The influence of pendulum mass (inertia) on amplitude decay, period, and natural frequency was analyzed.

RESULTS AND DISCUSSION

The dynamic motion of the FSU demonstrated damped vibration oscillations (Fig.1A and 2A), although it is unclear at this time if the decay behavior can be modeled as a classic linear system. The oscillations decayed to half of the initial values in 1.8 ± 0.3s and in 3.9 ± 1.1s, with 39N and 242 N, respectively. When the pendulum was initially rotated in flexion, the motion remained nearly in the sagittal plane, whereas initial lateral bending of the pendulum excited the coupled motion of flexion/extension (Fig. 2B). By studying these excited motions, this pendulum system could aid in the understanding of the complexities of coupled motions in the spine. The period of the oscillations increased significantly with increasing weights (e.g. from 0.59 ± 0.08s to 1.0 ± 0.06s, with 39N and 242 N, respectively), while the natural frequency correspondingly decreased (e.g. from 11 Hz to 6 Hz, with 39N and 242 N, respectively). We note that the dynamic response of a physical pendulum is dependent on both its length and weight. Accounting for these parameters through modeling would permit novel studies on the dynamic biomechanical properties of the spine and other joints that would not be possible with conventional testing apparatuses.

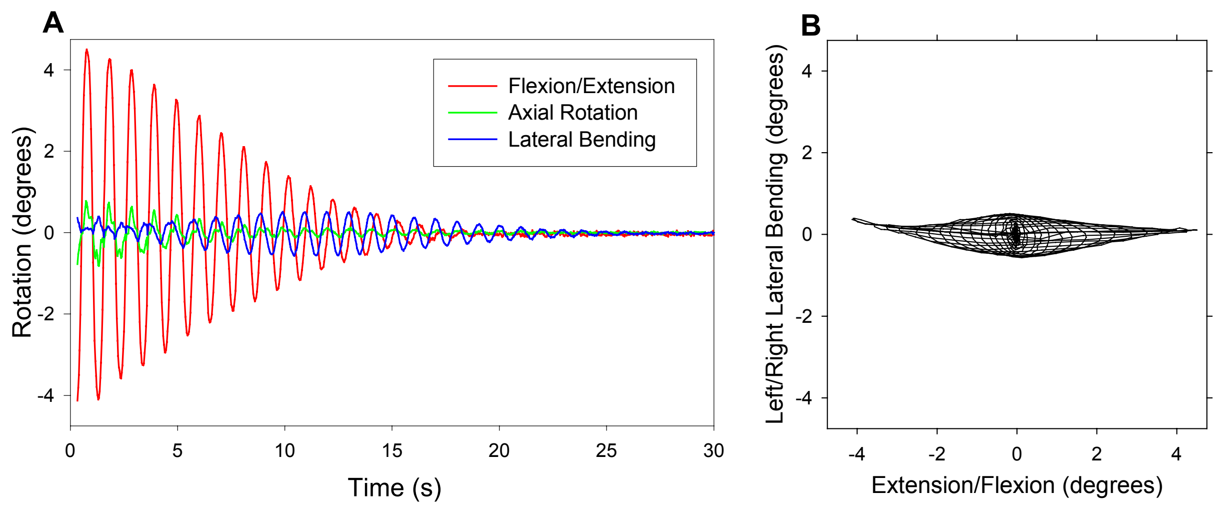

Figure 1. Flexion/extension rotation was the initial motion in this typical time series plot (**A**) and in the same data plotted as flexion/extension vs. lateral bending rotation (**B**).

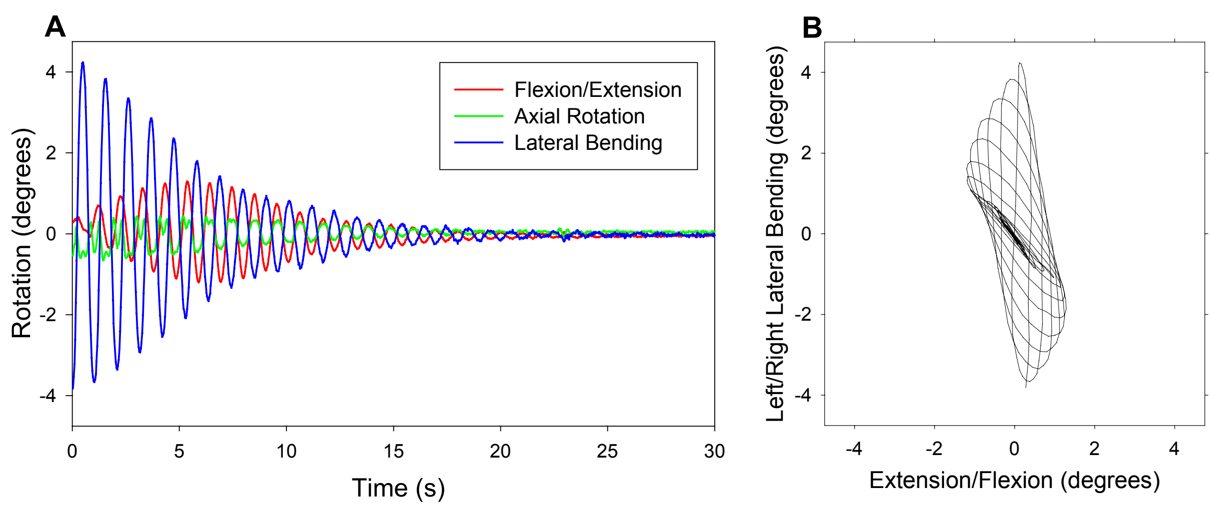

Figure 2. Lateral bending rotation was the initial motion in this typical time series plot (**A**) and in the same data plotted as flexion/extension vs. lateral bending rotation (**B**). Note the coupled motion of flexion/extension is excited as lateral bending decays.

REFERENCES

1. Charnley, J. Symp. on Biomechanics Institution of Mech. Eng., London, 1959, p.12.
2. Jones, E.S. Lancet 1, 1936, 1C43.
3. Unsworth, A. et al. J. Lubrication Tech., 1975, p 369

ACKNOWLEDGEMENTS

Funded in part by RIH Orthopaedic Foundation and University Orthopedics, Inc.

A FINITE ELEMENT MODEL FOR SIMULATING THE RESIDUAL LIMB SKIN TEMPERATURE DISTRIBUTION IN TRANSTIBIAL SOCKETS

Joanna J. Blevins [1], Jeffrey T. Peery [1], Glenn K. Klute [1,2] and William R. Ledoux [1,2,3]

[1] RR&D Center for Excellence in Limb Loss Prevention and
Prosthetic Engineering, VA Puget Sound, Seattle, WA, USA
Departments of [2] Mechanical Engineering, and
[3] Orthopaedics and Sports Medicine, University of Washington, Seattle, WA, USA
E-mail: jjb3@u.washington.edu Web: www.seattlerehabresearch.org

INTRODUCTION

In a recent survey, amputees ranked "avoidance of blisters or sores on the residual limb" as one of their top three prosthesis related concerns (Legro, 1999). Prostheses for amputated limbs are not well designed to accommodate the thermal loads that may cause discomfort to amputees during routine activities.

The purpose of this study was to develop a finite element (FE) model of a transtibial residual limb and prosthesis to predict the skin temperature distribution within suction and nonsuction socket systems. This model may help prosthetists and prosthesis manufacturers to better understand the thermal environment and lead to the development of improved prosthetic systems for amputees.

METHODS

Transverse CT images of a residual limb were used to obtain the FE model geometry (Camacho, 2002). The subject was scanned supine and approximately 300 transaxial slices were taken at 1 mm intervals between the tibial crest and the distal end of the residual limb. The tetrahedral mesh for the fat, skin, bone, muscle tissue and prosthesis was generated using 111,672 nodes and 33,146 elements (Cosmos 2003, SolidWorks Corp., Concord, MA).

To validate the FE model, the solution was compared to experimental results previously reported by our group. Skin temperatures were measured at the anterior, lateral, posterior and medial locations on five residual limbs within the suction socket and nonsuction socket prosthetic systems (Peery, 2004). Model predictions were obtained at locations comparable to the human subjects experimental results.

RESULTS AND DISCUSSION

In the model, muscle tissue generated a relatively large amount of thermal energy, due to its high rate of metabolism and

Table 1: Skin Temperatures (mean ± SD) for numerical and experimental data (Peery, 2004)

Section	Numerical Nonsuction Socket Temperature (˚C)	Numerical Suction Socket Temperature (˚C)	Experimental Nonsuction Socket Temperature (˚C)	Experimental Suction Socket Temperature (˚C)
Anterior	32.1 ± 0.6	30.6 ± 0.7	32.6 ± 0.4	30.8 ± 0.3
Lateral	33.5 ± 0.4	32.3 ± 0.5	33.5 ± 0.4	31.9 ± 0.3
Posterior	33.3 ± 0.5	32.1 ± 0.6	34.2 ± 0.5	31.4 ± 0.3
Medial	33.1 ± 0.4	31.8 ± 0.5	33.5 ± 1.0	30.7 ± 0.1
Overall	33.0 ± 0.6	31.7 ± 0.7	33.5 ± 0.4	31.4 ± 0.4

perfusion, resulting in elevated skin temperatures near muscle tissue. Lower temperatures were located anterior to the tibia and at the distal end where fat and bone provided increased thermal resistance between the muscle and the skin (Fig. 1). The suction and nonsuction models resulted in similarly shaped temperature contours. However, due to the lower conductivity of the liner used in the nonsuction socket which effectively insulated the limb, the mean skin temperature of the nonsuction socket was approximately 1.3 ˚C greater than that of the suction socket (Table 1).

Both numerical and experimental results demonstrated greater mean skin temperatures at lateral and posterior locations and lower mean skin temperatures at anterior and medial locations. Additionally, both numerical and experimental data generated warmer skin temperatures with the nonsuction socket.

SUMMARY

A thermal model of a transtibial residual limb was developed and used to predict the steady state skin temperature distribution inside suction and nonsuction socket systems. Model results, verified by experimental data, indicate that the type of prosthetic socket worn affects the temperature at the skin-prosthesis interface. High skin temperatures were predicted near muscle tissue and low temperatures were predicted anterior to the tibia and at the distal end of the residual limb. These results provide researchers with a better understanding of the thermal conditions at the skin-prosthesis interface that may relate to locality and severity of blister and sore occurrences.

REFERENCES

Camacho, D.L.A. et al. (2002). *J Rehabil Res Dev*, **39**, 401-410.
Legro, M.W. et al. (1999). *J Rehabil Res Dev*, **36**, 155-163.
Peery, J.T. et al. (2004). *J Rehabil Res Dev* (In review).

ACKNOWLEDGEMENTS

This study was funded by Dept. of Veterans Affairs No. A2878R. We would like to thank Jane Shofer for the statistical analysis.

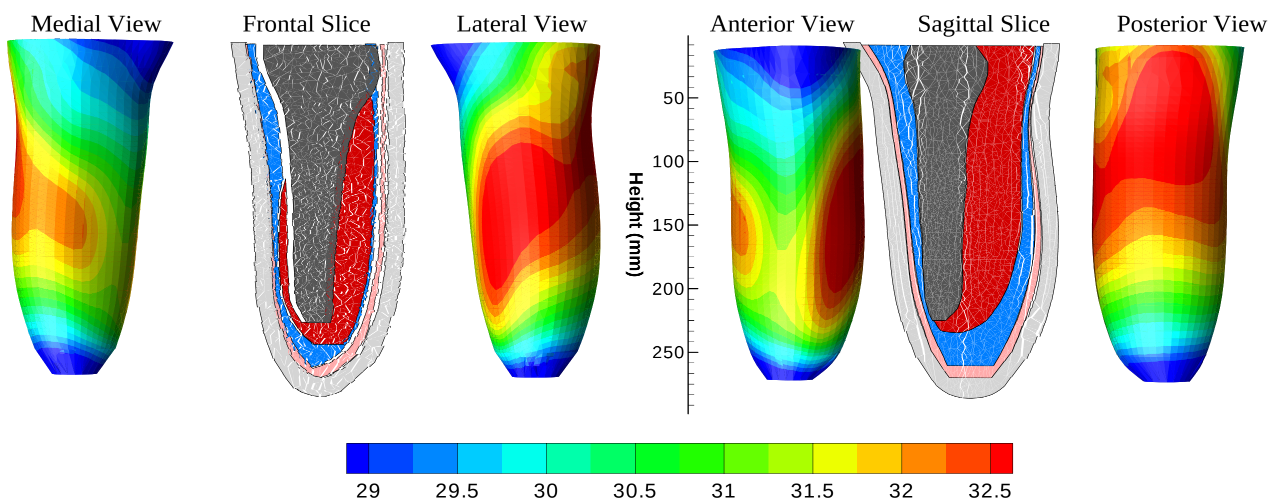

Figure 1: Frontal and sagittal slices illustrating the location of the tissues and medial, lateral, anterior and posterior views illustrating skin temperature contours (nonsuction socket shown).

MINIMAL FORWARD STEP LENGTH NEEDED FOR BALANCE RECOVERY OF HUMAN BODY AFTER PERTURBATIONS

Ming Wu[12] , Linhong Ji[3], Dewen Jin[3] and Yi-chung Pai [4]

[1] Sensory Motor Performance Program, Rehabilitation Institute of Chicago, Chicago, IL, USA
[2] Northwestern University Medical School, Chicago, IL, USA
[3] Department of Precision Instrument, Tsinghua Universigy, Beijing, PR China
[4] Department of Physical Therapy, University of Illinois at Chicago, Chicago, USA
E-mail: w-ming@northwestern.edu

INTRODUCTION

The stepping is a vital balance recover strategy when human upright standing or movement is disturbed (Pai, 2003). However, the factors determining balance recovery with a step remain uncertain. Although the boundary conditions necessary to trigger a step can be predicated (Pai & Patton, 1997), the stepping length needed for balance recovery is unclear. The purpose of this study was to predicate the minimal step length required for balance recovery with a work-energy approach.

METHODS

A simplified four-segment sagittal model of human body stepping for balance recovery was showed in Fig. 1.

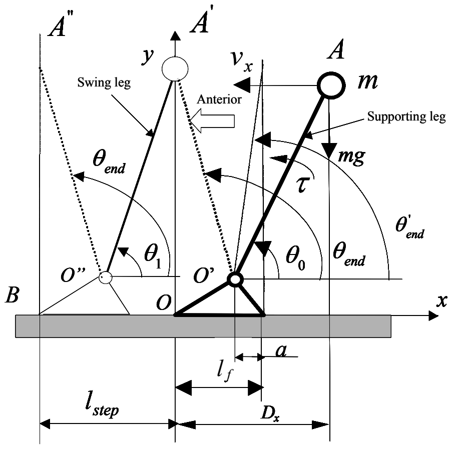

Figure 1. A 4-link stepping model.

At its initial state A, defined by D_x and v_x, the center of mass (COM) is rotating about the ankle at O', where v_x cannot be diminished at the leading edge, O, of the existing based of support (BOS). This new state A' requires a new BOS to be formed by a forward step with its leading at B. The body may require a second step, if forward velocity of COM at the leading edge of the new BOS, B, has not been reduced to zero. Our task objective is then to determine the boundary of the initial state A and the minimum step length, l_{step}, beyond which standing balance can be restored with only a single step.

During the process of balance recovery after perturbations, the kinetic energy of mass of body transforms into two parts: one of them is the increment of potential energy of mass when the human moves from its initial position A to the finial position A'; the other one is energy absorbed by ankle joints, including the ankle of supporting leg and swing leg after it touches with ground, when they generate plantar-flexion torques to prevent the forward rotation of the body. Thus, we define stability reserve of human body with a forward stepping after perturbations as

$$S_{stepant} = W_1 - (E - (P_{end} - P_0))\ (\mathrm{J}) \qquad (1)$$

where E is the kinetic energy of human body at initial position or after perturbations, P_0 and P_{end} are potential energy of mass at initial and finial position, W_1 is the energy absorbed by ankle joints of supporting leg and swing leg after touchdown.

With the increase of l_{step}, much more energy could be absorbed by ankle joint of swing leg after touchdown, e.g. W_1 would increase. Let $S_{stepant}=0$, for various values of initial displacements and velocities of COM, acceleration step-length searching optimization method was employed to search corresponding minimal stepping length l_{step} using equation (1). That is the minimal stepping length needed for balance recovery with single forward stepping matches with various initial states of COM after perturbations.

RESULTS AND DISCUSSIONS

The 3-D surface shown in Figure 2 indicates the minimal stepping length needed for balance recovery with one step for various initial displacements and velocities of COM.

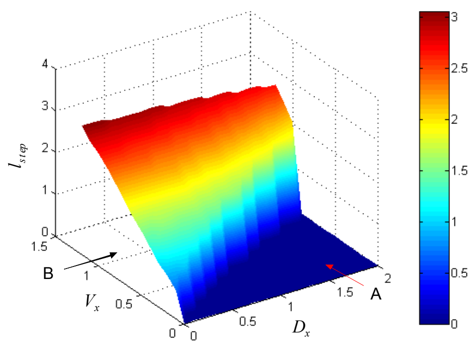

Figure 2. The minimal step length needed for balance recovery for various initial velocity and displacement

Balance can be recovered with one forward step if step length taken by subject is larger than the minimal step length after perturbations, otherwise, another forward steps are needed or a fall down may occur. With the increase of initial velocity and the decrease of initial displacement of COM the minimal step length needed for balance recovery increases.

REFERENCES

Pai, Y.-C. (2003) Movement termination and stability in standing. *Exercise and Sport Sciences Review*, **31:** 19-25.

Pai, Y. C., Patton, J. (1997) Center of mass velocity-position predictions for balance control. *Journal of Biomechanics*, **30,** 347-54.

ACKNOWLEDGEMENTS

This study was supported by National Science Foundation of China (30170242).

METHODS TO DETERMINE *IN VIVO* CARTILAGE STRESS IN THE PATELLOFEMORAL JOINT FROM WEIGHT-BEARING MRI

Thor Besier[1], Garry Gold[2], Christine Draper[1], Chris Powers[3], Scott Delp[1,4], and Gary Beaupré[4]

Departments of Mechanical Engineering[1], Bioengineering[1], and Radiology[2], Stanford University, Stanford. CA.
[3]Department of Biokinesiology and Physical Therapy, University of Southern California, LA.
[4]VA Palo Alto Rehabilitation R&D Center, Palo Alto, CA
besier@stanford.edu

INTRODUCTION

Elevated cartilage and subchondral bone stresses have been suggested as a possible cause of pain in subjects with patellofemoral (PF) syndrome (Powers, 1998). To test this hypothesis, *in vivo* cartilage stress needs to be estimated in subjects with and without patellofemoral pain. Given knowledge of joint loads, articulating geometries, cartilage thickness and tissue material properties, the finite element (FE) method provides a framework to calculate cartilage stress. Medical imaging techniques, such as magnetic resonance (MR) imaging, can provide subject-specific inputs to the FE model such as cartilage thickness and geometry. The purpose of this research was to estimate patellofemoral joint cartilage stress distribution and deformation using weight-bearing MR images as input to a FE model.

METHODS

We have developed a low-friction backrest for stabilizing subjects during upright, weight-bearing scans of the knee in a 0.5T open-configuration MR scanner (Gold et al., 2004). MR images were acquired from the right knee of a single healthy male subject using an open configuration scanner (0.5T GE SP/i MR GE Medical Systems, Milwaukee, WI). The subject had no previous history of patellofemoral pain and informed consent was gained prior to participation. The subject was asked to maintain a squatting posture with the knee at 60 deg (Fig. 1).

Figure 1: MR compatible back rest allows subject to assume ~0.45 body weight of load per knee.

A 3D fast spoiled gradient echo (SPGR) sequence was employed to obtain 2 mm contiguous sagittal plane images of the patellofemoral joint. The 0.5T scan took 2 min using the following parameters: TR = 33ms, TE = 9ms, Flip Angle = 45°, NEX = 1, FOV = 20x20cm, matrix dim = 256x160, interpolated to 256x256.

A separate, sagittal plane scan of the subject's knee was also taken in a standard 1.5T closed MR magnet to obtain images of the cartilage in its undeformed state (SPGR sequence, 1.5 mm slices, scan time 10:25 min). The MR images were manually segmented to obtain point cloud representations of the femur and patella bone and articular cartilage. The point clouds were then converted into triangulated surfaces using a commercial software package (Raindrop Geomagic, Research Triangle Park, NC). The bone surfaces from the 1.5T scan were then registered to the bone surfaces in the 0.5T weight-bearing scan. This transformation was used as a boundary condition in the FE model to place the undeformed cartilage

into the same position and same flexion angle as the deformed, weight-bearing state. Distance maps could then be calculated to compare the undeformed and deformed cartilage contact surfaces, as well as the cartilage thickness (Fig. 2a).
NURBS surface representations of the undeformed patella and femoral cartilage were then created and hexahedral meshes of the cartilage were generated using Patran (MSC.Software Corp., Santa Ana, CA) (Fig. 2b).

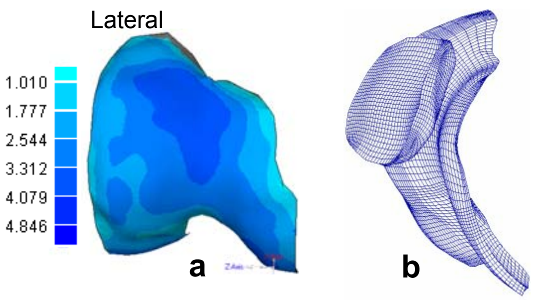

Figure 2: a) Femur cartilage thickness map. b) FE mesh of patella and femoral cartilage with a total of 11,550 elements. Typical element size ~1.5 mm^3.

FE analyses were performed using ABAQUS (ABAQUS Inc., Pawtucket, RI) and included surface to surface contact (friction coefficient of 0.001) Cartilage was modelled as a linear elastic solid with Young's modulus of 6 MPa and Poisson's ratio of 0.47. The subchondral surface of the patella and femur were both treated as rigid and the back of the femoral cartilage fixed. A displacement was then applied to the patella cartilage to reproduce the position of the patella in the weight-bearing scan. The hydrostatic pressure distribution on the subchondral cartilage surface was determined.

RESULTS AND DISCUSSION

For this subject, hydrostatic pressure was highest on the lateral condyle of the femur (Fig. 3a). Shear stresses were highest at the subchondral bone surface, at the periphery of PF contact (not shown).

A deformation map of the patella cartilage showed a band of higher deformation across the width of the patella with the greatest deformation centered on each facet (Fig. 3b).

This study demonstrates a technique for calculating in vivo stresses based on MR images obtained during an upright, weight-bearing activity representing bilateral squatting. This activity is often used during the clinical evaluation of subjects with PF pain. Future studies will examine age and activity-matched subjects with and without PF pain to determine if subjects with PF pain have elevated cartilage stresses.

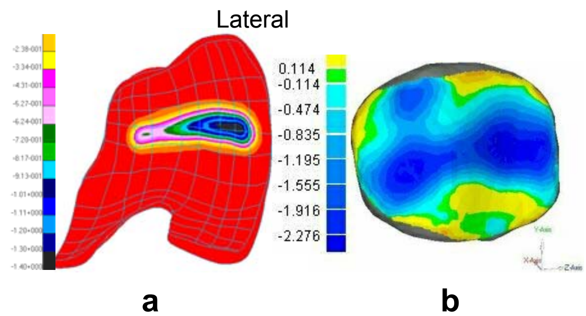

Figure 3. a) Hydrostatic pressure distribution on the subchondral cartilage surface. Peak pressure clearly indicated on the lateral femoral condyle. b) Patella cartilage deformation map.

REFERENCES

Gold, G. et al. (2004). *J Magn Reson Imaging*. Accepted.
Powers, C. M. (1998) *J Orthop Sports Phys Ther*, **28**, 345-354.

ACKNOWLEDGEMENTS

Dept. of Veterans Affairs (grant # A2592R). NIH EB 002524-01. Thanks to Brian Bradke for his helpful comments.

STRAIN DISTRIBUTION IN *IN-VIVO* HUMAN TRICEPS SURAE DURING PASSIVE AND ACTIVE DYNAMIC MOVEMENTS

Hae-Dong Lee[1,2], Taija Finni[3], John A. Hodgson[2], V. Reggie Edgerton[2], and Shantanu Sinha[1]

Departments of [1]Radiological and [2]Physiological Sciences, UCLA, CA 90095, USA and [3]Department of Health Sciences, University of Jyväskylä, 40014 Jyväskylän, Finland
E-mail: haedong@ucla.edu Web: www.ucla.edu

INTRODUCTION

It has been well recognized that understanding the mechanical behaviors of a skeletal muscle tendon-complex requires knowing the contractile properties of the force-generating (muscle fibers) component and the mechanical properties of the force-transmitting (tendon and aponeurosis) component. Although the contractile properties (instantaneous length and contraction velocity) have been well characterized, there is no consensus of the mechanical properties of tendon and aponeurosis in a muscle-tendon complex (Bavel et al., 1996; Zuurbier et al, 1994). The purpose of this study is to investigate the mechanical behaviors of the tendon and aponeurosis of human triceps surae muscles in vivo during passive and active dynamic movements.

METHODS

The strain distribution of tendinous tissues was investigated for in vivo human triceps surae muscles (n =4) during a cyclic movement of plantarflexion-dorsiflexion over the constant joint range. The movements were performed either passively or actively with resistance. A detailed description of the imaging technique is given elsewhere (Finni et al., 2003). Briefly, before the experiments, a set of detailed anatomical images were taken from axial, coronal and sagittal planes of the relaxed muscles. A sagittal slice was then chosen to visualize the lower leg from the calcaneus to the origin of the soleus muscle for testing. During the movements, anatomical images and velocity images in a superior/inferior (S/I; or proximal distal) direction were simultaneously obtained using a cine phase contrast magnetic resonance image (cine PC-MRI) technique. From the anatomical images, seventeen regions of interest (ROI) along the posterior aponeurosis of soleus and eight ROIs each along the anterior and posterior aponeuroses of gastrocnemius were defined. Using the velocity images and the initial locations of the ROIs, the displacement of each ROI during the movement was estimated. Then, the strain was assessed by estimating distance between adjacent ROIs.

RESULTS AND DISCUSSION

We observed that the maximum S/I velocities during the active movement with resistance were higher than those during the passive movement (Fig. 1). Regardless of loading condition, the S/I velocities of each ROI followed a similar pathway throughout the movements but were different in absolute value. The maximum displacements were larger for the active movement with resistance compared with the passive movement (Fig. 2).
The maximum strains along the posterior aponeurosis of soleus and the anterior and posterior aponeuroses of gastrocnemius were found to be heterogeneous regardless of loading condition (Fig. 3). Regarding the negative strains observed during static

isometric contractions in previous studies (in the proximal gastrocnemius for <60% MVC shown in the Figure 6 of Muramatsu et al., 2001; in the distal soleus for 20 and 40% MVC shown in the Figure 6 of Taija et al., 2003), this study also observed negative strain suggesting that for some reasons different regions of aponeuroses probably deform in different extent. The extent and pattern of heterogeneity were altered, over the whole region of the muscle during the active compared with the passive dynamic movements (Fig. 3), indicating that loading condition would be another factor influencing mechanical behaviors of tendon and aponeurosis.

Differences in experimental conditions between this study and previous studies made it difficult to directly compare the results of this study to those found in previous studies (Muramatsu et al., 2001; Taija et al., 2003). Nevertheless, the results of this study and our previous study (Finni et al., 2003) provided evidence that tendinous tissues behave in non-uniform pattern. Moreover, heterogeneity of the mechanical behaviors of tendinous tissues was probably altered depending on the contraction type and loading condition.

REFERENCES

Van Bavel, H. et al. (1996). *J. Biomech.*, **29 (8)**, 1069-1074.

Muramatsu, T. et al. (2001). *J. Appl. Physiol.*, **90**, 1671-1678.

Finni, T. et al. (2003). *J. Appl. Physiol.*, **95**, 829-837.

Zuurbier, C.J. et al. (1994). *J. Biomech.*, **27**, 445-453.

ACKNOWLEDGEMENTS

This work was supported by National Space Biomedical Research Institute Grant NCC9-58.

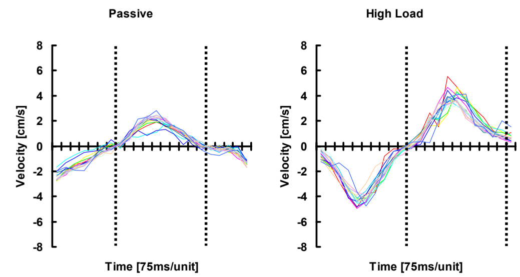

Figure 1: Superior/Inferior velocities of ROIs over time during the passive and active dynamic movements

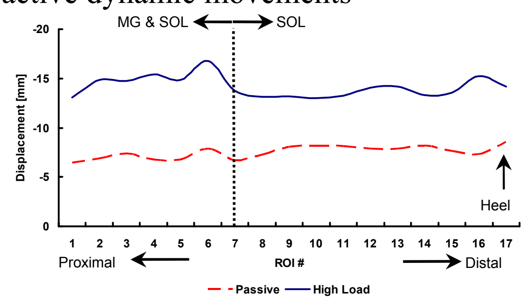

Figure 2: Maximum displacements of ROIs along the posterior aponeurosis of the soleus muscle during the passive and active dynamic movements

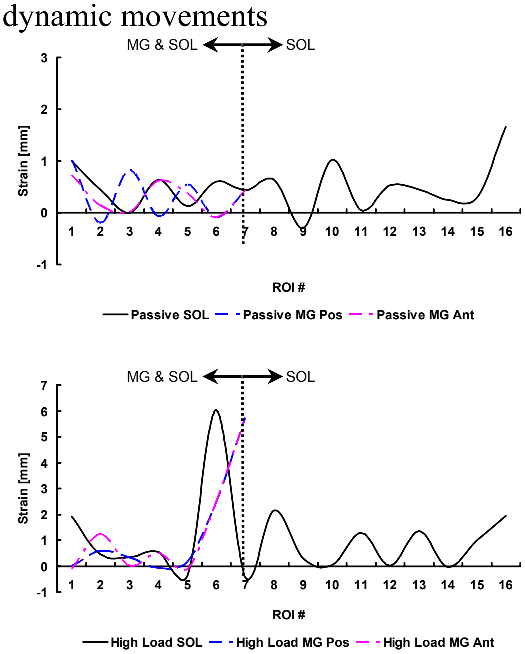

Figure 3. Maximum strain of the soleus posterior aponeurosis and the gastrocnemius anterior and posterior aponeuroses during the passive and active movements

THE THREE-DIMENSIONAL LUMBAR SPINE KINEMATICS OF TRANSFEMORAL AMPUTEES WITH AND WITHOUT BACK PAIN WHILE WALKING

Joseph M. Czerniecki [1,2], Ava D. Segal [1], Ali Shakir [3], Michael S. Orendurff [1]

[1] Rehab Research and Development, Department of Veterans Affairs, Seattle, WA USA.
[2] Dept. of Rehabilitation Medicine, University of Washington, Seattle, WA USA
[3] Buffalo Spine and Sports Medicine, PC, Buffalo, NY USA.
Email: jczern@u.washington.edu Web: www.seattlerehabresearch.org

INTRODUCTION

Low back pain (LBP) has long been recognized as a major health problem in the general population. Recent work suggests that it is an even greater problem for transfemoral amputees (TF). It is an important cause of secondary disability in as many as 71% of TF amputees (Edhe 2001, Smith 1999). Further, more than half of those TF amputees suffering from LBP rate it as either moderately or severely bothersome. Despite the magnitude of the problem, little is known about the kinematic alterations of the lumbar spine during amputee ambulation.

Increased lumbar lordosis (Steinberg 2003) and excessive and variable lumbar spine motion (Vogt 2001) are frequently cited causes of LBP in the general population. Each of these conditions is present to some degree in TF amputees as a result of prosthetic use, although their extent has yet to be fully documented. Because of their dual association with LBP in the general population and with prosthetic use in the TF population, we propose that these postural abnormalities underlie the development and continuation of LBP in the TF amputee. This study was carried out to determine the kinematic differences in lumbar spine motion between TF amputees and intact subjects, as well as to identify specific kinematic patterns that were associated with LBP in this population.

METHODS

Five intact subjects free from any known gait pathology and LBP and ten TF amputees gave informed consent to participate in this IRB approved study. Five of the amputees experienced LBP of 5 or greater on a 10 point scale for at least 15 of the past 30 days and comprised the Amputee Pain (AP) group (n=5). The remaining five amputees were without pain and comprised the Amputee No Pain (ANP) group. Thirty-eight reflective markers were placed on each subject for full body gait analysis according to Vicon's Plug In Gait model (Oxford Metrics, England). Lumbar spine motion was defined by a triad of markers (2 placed at level T8 and 1 at T10). 3-D Euler angles were calculated relative to the pelvis defined by 4 markers (2 at the ASIS and 2 at the PSIS). Subjects walked at a controlled walking speed of 1.0 ± 0.1 m/s and kinematic data were collected with a 10-camera Vicon 612 motion system at 120 Hz. Statistically significant differences in lumbar motion were detected with an ANOVA and Fishers tests post hoc ($p < 0.05$).

RESULTS AND DISCUSSION

The ranges of lumbar motion (deg) for the three subject groups across the gait cycle for each plane are compared in table 1. Ranges that were significantly different are denoted with an asterisk (*) in bold italics ($p < 0.05$). Intact subjects had significantly less sagittal plane lumbar excursion during sound limb stance compared to TF amputees; no difference was detected between AP and ANP. However, AP demonstrated significantly less sagittal plane lumbar excursion during prosthetic limb stance as compared to ANP and intact subjects.

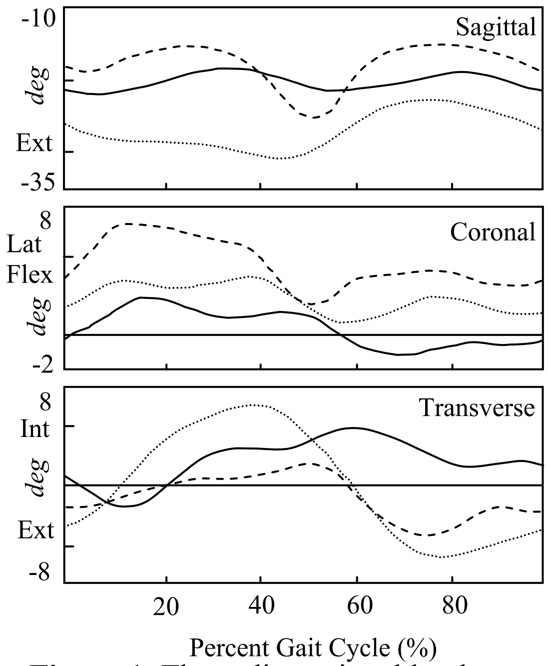

Figure 1: Three-dimensional lumbar angles during gait of intact subjects (——), TF amputees with LBP (········) and TF amputees without LBP (- - - -). Each graph begins at heel strike on the prosthetic limb and ends with the subsequent prosthetic heel strike.

In the coronal plane, ANP exhibited significantly larger lumbar range compared to both intact subjects and AP. In the transverse plane, AP had a two-fold increase in lumbar rotation compared to intact subjects and ANP. 3-D lumbar motion is shown across the gait cycle in figure 1. The lumbar spine kinematics of the intact subjects was similar to previous research (Callaghan 1999, Vogt 2001). The TF amputees without LBP exhibited significantly different spinal kinematics in the sagittal and coronal planes, but not in the transverse plane compared to the intact subjects. These are likely the result of neuromuscular adaptations related to prosthetic replacement of the lower extremity. The greatest differences in spinal kinematics of AP were that they exhibited a nearly two-fold increase in transverse plane rotation with a significant decrease in sagittal plane motion compared to ANP.

SUMMARY

TF amputees face significant physical challenges even without the additional burden of low back pain. Identifying differences in AP lumbar motion may lead to potential therapeutic interventions, which help to minimize these discrepancies and alleviate chronic back pain.

REFERENCES

Callaghan JP. et al. (1999) *Clinical Biomechanics*. 14, 203-16.
Ehde DM. et al. (2001) *Arch Phys Med Rehabil*. **82**, 731-4.
Smith DG. et al. (1999) *Clin Orthop*. 361, 29-38.
Steinberg EL. et al. (2003) *Clin Radiol*. **58**(12), 985-9.
Vogt L. et al. (2001) *Spine*. **26**, 1910-9.

ACKNOWLEDGEMENTS

Dept of Veterans Affairs project # A2661C

Table 1: Lumbar spine kinematic ranges (deg ± standard deviation) in three planes of motion.

Subject	Sagittal (Prosthetic Limb)	Sagittal (Sound Limb)	Coronal	Transverse
Intact	4.1 ± 1.6	***4.1 ± 1.6****	4.1 ± 1.4	7.9 ± 2.0
ANP	5.8 ± 4.0	11.7 ± 9.1	***9.0 ± 2.5****	7.1 ± 3.1
AP	***0.7 ± 0.9****	9.2 ± 5.2	4.8 ± 2.2	***14.5 ± 3.8****

ANKLE BIOMECHANICS DURING A SPIN TURN

Ava D. Segal [1,2], Michael S. Orendurff [1], Kevin C. Flick [1], Jocelyn S. Berge [1], Glenn K. Klute [1,2]

[1] Rehab. Research and Development Center, Department of Veteran Affairs, Seattle, WA USA
[2] Dept. of Mechanical Engineering, University of Washington, Seattle, WA USA
E-mail: avasegal@hotmail.com Web: www.seattlerehabresearch.org

INTRODUCTION

The biomechanics of human turning has been largely overlooked despite its frequent occurrence during community ambulation. A turn requires a combination of kinematic and kinetic adjustments that mediolaterally shift the center of mass (COM) and result in a change in orientation and heading. Turning also requires specific control mechanisms in order to maintain dynamic stability. Patients with mobility challenges (e.g., elderly and amputees) often have difficulty maneuvering, which may result in an increase in falls. Falls that occur while turning are nearly eight times more likely to result in a hip fracture compared to falls that occur while walking along a straight trajectory (Cumming 1994). This study explores the biomechanics one common turning strategy, the spin turn (Hase 1999). An increased comprehension of turning biomechanics may lead to the development of rehabilitation programs and prosthetic devices that address deficiencies and decrease the risk of falling.

METHODS

Seven subjects free from any known gait pathology gave informed consent to participate in this IRB approved study. Thirty-six markers were placed on each subject for full-body gait analysis according to the Vicon Plug-In-Gait model (Oxford Metrics, Oxford, England). Kinematic and kinetic data were collected with the Vicon 612 motion system at 120 Hz and embedded forceplate (Kistler, Wintethur, CH) at 600 Hz. All subjects completed three trials at their self-selected walking speeds under three different conditions: straight walking (ST), outside limb spin turn (OSP), and inside limb spin turn (ISP); where a spin turn consisted of the body spinning around on the ball of one foot resulting in a change of direction of 90˚. Pelvic rotation angle in the transverse plane was plotted across the gait cycle to demonstrate timing of the spin turn. Ankle transverse moment and power were also examined. In addition, sagittal plane ankle kinematics for the spin turn, as well as for the step on the opposite limb prior to the turn (inside prior to OSP: preOSP; outside prior to ISP: preISP) were explored. Significant differences ($p < 0.05$) between the means of the three walking conditions were tested using a repeated measures ANOVA with Scheffes' tests post hoc.

RESULTS AND DISCUSSION

Ankle transverse moment and power for ISP significantly increased compared to OSP and ST. From mid to late stance, the average ISP transverse moment was more than twice the magnitude of OSP and ST (figure 1A). The average peak ISP internal transverse power occurred at approximately midstance (~30% of the gait cycle), but quickly dropped back to zero just after 40% of the gait cycle (figure 1B). The transverse moment, however, remained at its peak until the end of stance. The graph of pelvic rotation angle in the transverse plane (figure

1C) demonstrates when the end of rotation occurred which corresponded to the sudden drop in ankle transverse power. Therefore, in order to stop rotation, the transverse moment remained high for the remainder of stance.

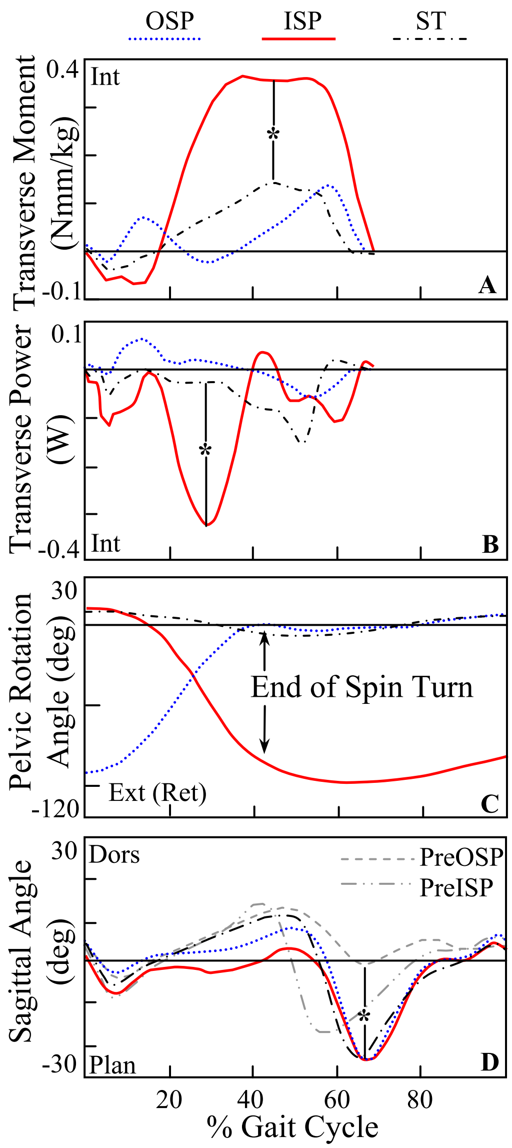

Figure 1: Average *ankle* transverse plane moment (A) and power (B), *pelvic* rotation angle (C) and sagittal plane *ankle* angle (D) across the gait cycle for all subjects. Regions marked with an asterisk (*) denote significant differences ($p < 0.05$).

The large difference in transverse moment and power was expected between ISP and ST, but rather unexpected between ISP and OSP. Since the peak internal rotation moment for OSP is almost identical to ST, it does not appear to be the biomechanical variable largely responsible for OSP. However, analysis of sagittal ankle angle may serve to elucidate the OSP turning mechanism. Peak plantarflexion of the inside limb step prior to OSP (preOSP) was significantly less than ST, OSP, ISP, and preISP (figure 1D). This difference in sagittal plane angle may signify that preOSP had a significant role in the outside spin turn. All graphs are presented across the gait cycle in order to highlight the differences between each curve. However, if plotted by time, preOSP and preISP would occur before the spin turn. Therefore, peak plantarflexion of preOSP occurred at about toe off, which was about the same moment in time as the increased ISP transverse power. Perhaps preOSP was responsible for the kinetic adjustments seen in ISP, thereby compensating for the lack of power demonstrated by OSP. Future research is planned to examine kinetic data of preOSP and preISP since the step prior to the turn may significantly affect the actual turn.

SUMMARY

ISP, OSP, and ST ankle biomechanics were shown to have significant differences in the transverse and sagittal planes.

REFERENCES

Cumming RG, Klineberg RJ. (1994). *J Am Geriatr Soc.* **42**(7)**,** 777-8.

Hase K, Stein RB. (1999). *J Neurophysiol.* **81**, 2914-22.

ACKNOWLEDGEMENTS

This study was funded by the Department of Veterans Affairs project # A2661C.

LONGITUDINAL TENSILE PROPERTIES OF ELASTIN, CURED ELASTIN, AND NATIVE CAROTID ARTERY

Ping-Cheng Wu, Ann Bazar, Carmen Campbell, and Kenton W. Gregory

Oregon Medical Laser Center, Providence St. Vincent Medical Center, Portland, OR
E-mail: ping-cheng.wu@providence.org

INTRODUCTION

Elastin is potentially a less thrombogenic blood-contacting surface than other biological or synthetic materials. This and other properties (Karnik et al., 2003) make elastin an ideal substrate material for the development of a small diameter vascular graft. Common studies have used bursting techniques and ring tests to study the circumferential mechanical properties of native carotid arteries (Cox, 1975; Roeder et al., 1999, 2000; Lillie and Gosline, 2002) but few have examined the longitudinal mechanical properties. Elastin, cured elastin, and native carotid vessels were tested longitudinally to quantify mechanical properties including ultimate strain, ultimate tensile strength, and elastic modulus.

METHODS

Twelve porcine carotid arterial vessels were trimmed of adherent fat. Eight vessels were treated with 80% ethanol and a hot alkali digestion and rinsed in 0.05 M HEPES buffer to produce a pure elastin matrix. The remaining four vessels were left untreated. Half of the purified elastin vessels were cured in a heated humidified environment resulting in three groups (elastin, cured elastin, and native) of four vessels. The vessels were cut into dumbbell shaped specimens in the longitudinal direction as shown in Figure 1. The specimens' gage length was 5 mm with 3 mm grips. The thickness and cross-sectional gage length were recorded.

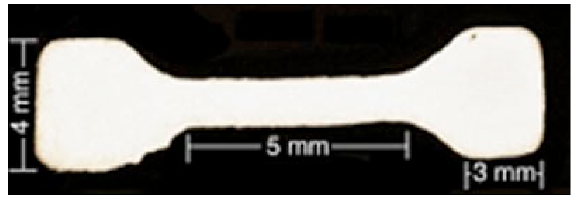

Figure 1: Typical dumbbell specimen representation.

All specimens were mounted on a MTS servo-hydraulic testing system and tested in tension at a crosshead speed of 5 mm/s until failure. All specimens were kept hydrated with saline during the test in ambient temperature. Force (N) and displacement (mm) were acquired. Stress (force/cross-sectional area) and strain ($L-L_i/L_i$) were calculated and plotted. The linear slope region of the stress-strain plots was used to calculate the elastic modulus (stress/strain).

Ultimate strain, ultimate tensile strength and elastic modulus data were analyzed by using a two-tailed unpaired t-test to determine any statistically significant differences between the groups.

RESULTS

No significant ultimate strain differences ($p>0.05$) were found between the three groups shown in Figure 2, which may be due to a small sample size. The average ultimate strain values for elastin, cured elastin, and native vessels were 112±1%, 114±13%, and 163±48%, respectively. Significant differences ($p<0.01$) were found with the average ultimate tensile strength and elastic modulus shown in Figures 3 and 4, respectively. Elastin demonstrated the lowest ultimate tensile strength (0.65±0.1 MPa) and elastic modulus (0.45±0.1 MPa). Native carotid averaged the highest ultimate tensile strength (3.2±0.7 MPa) and elastic modulus (4.6±0.7 MPa). Average ultimate tensile strength and elastic modulus values for cured elastin were 1.3±0.3 and 1.1±0.2, respectively.

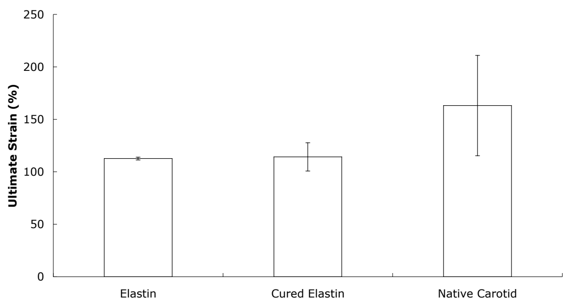

Figure 2: There were no significant ultimate strain differences ($p>0.05$).

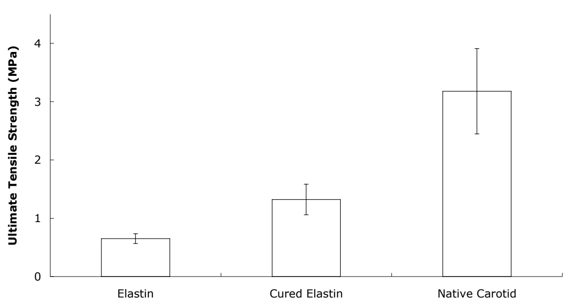

Figure 3: There were significant ultimate tensile strength differences ($p<0.01$).

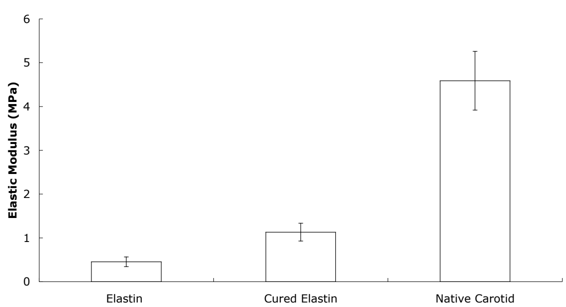

Figure 4: There were significant differences ($p<0.01$) between with elastic modulus.

DISCUSSION

Longitudinal tensile tests added another dimension to the requirements for a tissue engineered arterial graft. While the curing process increased the elastin's strength, the result is still significantly weaker than composite native carotid artery, consisting of elastin and collagen (Shadwick, 1999). Collagen is a major contributing factor to the ultimate tensile stress and strain properties of native arterial tissue (Roach and Burton, 1957). Various approaches to increase the longitudinal strength of the elastin graft will be investigated, including the incorporation of collagen.

REFERENCES

Cox, R.M. (1975). *Am J Physiology.* **229**, 807-812.

Karnik, S.K. et al. (2003). *Development.* **130**, 411-423.

Lillie, M.A. and Gosline, J.M. (2002). *Int. J. Biol Macromolecules.* **30**, 119-127.

Roach, M.R. and Burton, A.C. (1957). *Can. J. Biochem Physio.* **35**, 181-190.

Roeder, R. et al. (1999). *J. Biomed Mater Res.* **47**, 65-70.

Roeder, R. et al. (2000). *Australas Phys Eng Sci Med.* **23**, 66-67.

Shadwick, R.E. (1999). *J. Exp Biol.* **202**, 3305-3313.

ACKNOWLEDGEMENTS

Special thanks to Samuel Jensen-Segal for his assistance. This project was sponsored by the Department of the Army Grant No. DAMD-17-98-1-8654 and does not necessarily reflect the position or policy of the government. No official endorsement should be inferred.

MICROMOTION OF MULTI-STRAND FREE TENDON GRAFTS SECURED WITH INTERFERENCE FIXATION

Douglas J. Adams, Matthew W. Wheeler, and Carl W. Nissen

Department of Orthopaedic Surgery, University of Connecticut Health Center, Farmington, CT
E-mail: dadams@nso.uchc.edu Web: skeletalbiology.uchc.edu

INTRODUCTION

Surgical reconstruction of the cruciate ligaments of the knee (ACL and PCL) frequently involves fixing multiple free tendon strands within tunnels drilled at the femoral and tibial insertion sites of the native ligament. One common example of this surgical strategy employs a doubled, or four-strand, semitendinosus and gracilis (hamstring) tendon graft.

Because free tendon grafts do not preserve native insertions to bone, direct fixation of the soft tissue within bone tunnels does not provide initial fixation equal in strength to that achieved for bone-tendon-bone grafts. Free tendon grafts also rely on the integrity of initial fixation for a longer period of time prior to tendon-bone incorporation. Thus, adequate initial fixation of free tendon grafts is critical toward maintaining joint stability post-operatively, particularly since early rehabilitation and loading of the joint is beneficial to clinical outcome.

A primary outcome measure of stability following ACL reconstruction is a side-to-side difference in anterior laxity of less than 3 mm. Knee anatomy dictates that 3 mm anterior displacement of the tibia with respect to the femur is associated with less than 1 mm of lengthening between ACL insertion sites (Hollis et al., 1991). This corresponds to just 0.5 mm of tendon slip within each tunnel, such that cyclic slip on the order of tenths of millimeters (100 µm) should be elucidated at the tendon-tunnel interface when comparing fixation devices.

METHODS

This study compared the cyclic and static strength of three hamstring tendon graft fixation techniques (n = 9/group) commonly used in the United States (Figure 1): a single 35 mm long bioresorbable PLLA delta-shaped interference screw, a single 28 mm long PLLA bioresorbable screw augmented with a peripheral button anchor, and a central expansion sheath/screw device that separates the four individual strands within the tunnel (Mitek Intra-fix™).

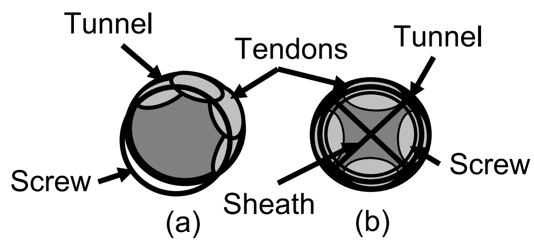

Figure 1: Interference fixation of free tendon strands typically employs (a) screws or (b) sheath and screw devices.

Bovine digital extensor tendons demonstrate static and dynamic mechanical properties similar to human semitendinosus and gracilis tendons (Haut-Donahue et al., 2001), and were configured as doubled four-strand grafts in identical fashion to human hamstring tendon grafts. Bone-analog polyurethane foam (ASTM F1839-97) was used to ensure a uniform testbed for comparing fixation strategies, without the complication of differences in donor bone density and quality. Tibial cancellous bone was modeled at a density of 0.24 g/cm^3 (Last-A-Foam FR-6715).

A custom apparatus was constructed to allow independent control of load applied cyclically to each of four tendon strands, ensuring equal distribution of force at the fixation site. The dynamic compliances of all fixturing, bone, and tendon tissue were measured and subtracted from combined creep-slip data collected for each construct to isolate progressive cyclic slip of fixation.

Tendon grafts were fixed within tunnels drilled in blocks of bone-analog polymer according to clinical guidelines for each technique. Importantly, maximal oversizing of screw versus tunnel diameter was exploited. The four tendon ends were held individually with serpentine clamps connected via ball joints, low-stretch cables, and 250 N load cells to four electromagnetic actuators (EnduraTec 3230).

Each strand was preloaded to 10 N and cycled 2000 times at 1 Hz between 10-50 N (40-200 N entire construct). Peak and valley displacement data were recorded at a resolution of 10 µm. The constructs then were pulled in tension to failure at a rate of 1 mm/sec using a servohydraulic actuator (MTS 858). ANOVA and unpaired t-tests were performed to compare cyclic and static fixation strengths, with statistical significance set at a level of $p = 0.05$.

RESULTS AND DISCUSSION

After subtracting average cyclic elongation associated with fixture compliance and tendon creep after 2000 cycles (0.3 mm and 1.1 mm, respectively), total fixation slip was 0.3 ± 0.4 mm, 0.5 ± 0.3 mm, and 0.3 ± 0.2 mm for the screw, screw + button, and sheath/screw, respectively (Figure 2). These are clinically acceptable magnitudes of slip using the aforementioned strict criteria. No construct failures occurred during cyclic loading tests to 200 N.

Post-cycling static failure loads were 997 ± 230 N, 1020 ± 200 N, and 1223 ± 131 N for the screw, screw + button, and sheath/screw, respectively. Interference screw constructs failed by pulling all four tendon strands past the screw, whereas the sheath/screw constructs failed by pulling the entire device from bone without tendon slip. Given the differences in maintaining tunnel aperture (Figure 1), bone compliance and strength may differentially affect fixation strength afforded by screws versus sheath/screw.

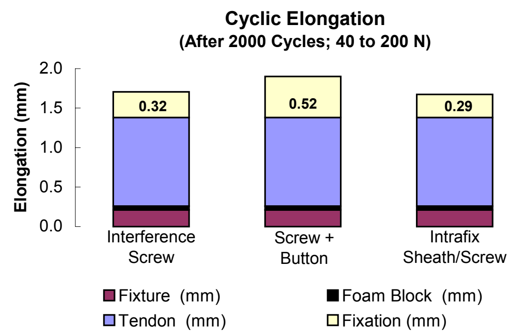

Figure 2: Fixation slip throughout 2000 cycles totaled 300 to 500 micrometers.

SUMMARY

Sub-millimeter slip of four-strand hamstring tendon grafts is clinically relevant and measurable. When maximally (over)sized to bone tunnel diameter, interference fixation can satisfactorily secure free tendons.

REFERENCES

Haut-Donahue, TL, Gregersen, C, Hull, ML (2001). *J Biomechanics,* **123**, 162-169.

Hollis, JM, Takai, S, Adams, DJ, Horibe, S, Woo, SL-Y (1991). *J Biomech Engrg*, **113**, 208-214.

ACKNOWLEDGEMENTS

Financial assistance was provided by the University of Connecticut and a MRI grant from the National Science Foundation.

A Concentric and Eccentric Loading Regime for Shoulder Rehabilitation

Karen P. Norton[1] and Sean S. Kohles[2],
[1] U.S. Army Natick Soldier Center, Natick, MA;
[2] Kohles Bioengineering, Portland State University, and Oregon Health & Science University, Portland, OR
E-mail: Karen.Norton@natick.army.mil Web: www.kohlesbioengineering.com

INTRODUCTION

The application of linear impulse and momentum as a means for exercise, rehabilitation and physical therapy has been previously demonstrated (Phillips et al., 2000). This technique uses inertial forces generated as actions and reactions to a weighted shuttle traveling on a horizontal rail system. The objectives of this study were to: 1) quantify the net shoulder joint forces and moments while using an impulse-momentum exercise system; and 2) test the influence of gender and muscle loading type (concentric or eccentric) on kinetic parameters.

METHODS

Exercise Regimen

Fourteen healthy adults (8 males, 6 females) were selected as subjects (mean age, 35 years). Each subject was tested utilizing a 10 cycle protocol repeated for 2 to 6 trials. Test subjects were seated (Biodex, Shirley, NY) with their dominant arm supported in 90^o of abduction (Figure 1). The subjects' flexed arm was placed in a neutral position (corresponding to 0^o) by positioning the forearm parallel to the floor and extended toward the impulse exercise system (**A**). While maintaining 90^o of shoulder abduction, the subjects externally rotated their upper arm from neutral to 90^o (perpendicular to the floor) causing the shuttle (22.2 N) to move from one end of the track to the central position (**B**). The subject then internally rotated their arm from 90^o to the initial position while maintaining a braking force in the rope as the momentum of the shuttle carried it to the opposite end of the track, completing a cycle (**C**). Tension was maintained in the cabled shuttle system at all times during the exercise. The outcome of this activity is a transition from concentric to eccentric loading during external and internal rotation, respectively. The data were collected at a sampling rate of 100 Hz and cycles 2 through 9 were analyzed.

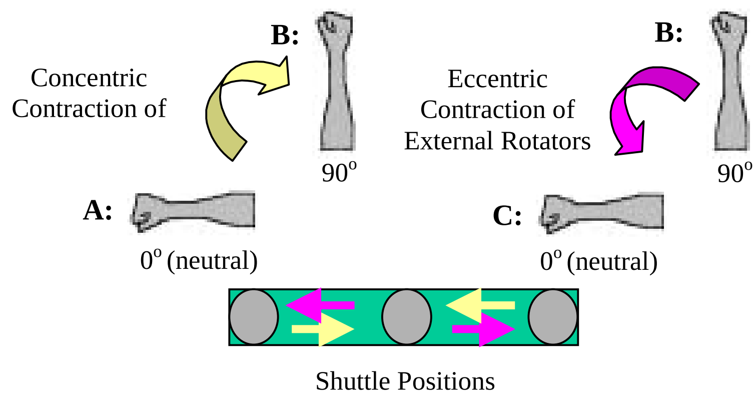

Figure 1: Schematic of arm position (side view) with respect to shuttle position (top view). See Methods for description.

Shoulder Calculations

The limb dimensions and masses of the 14 subjects were not available. Therefore, the anthropometric data used for the following calculations consisted of limb center of mass (Winter, 1990) and the 50th percentile limb dimensions and weights of U.S. adult civilians (Kroemer, 1989). The net shoulder joint reaction forces were calculated by applying Newton's Second Law of motion due to limb mass m and acceleration **a**. The net shoulder moments were calculated by applying the rotational analogue of Newton's second law of motion due to the moment of

Inertia I about the axis of rotation and the angular acceleration α relative to that axis.

The work done by the shoulder was incrementally calculated from the resultant moment and rotational data. Work was defined as:

$$W = \int \mathbf{m}\cdot d\theta, \quad (1)$$

where **m** is the average moment of two consecutive samples and $d\theta$ is the angular distance the forearm traveled in the 0.01-s period between samples. The power delivered by the shoulder during the concentric and eccentric phase of the exercise was then calculated by the expression:

$$P = dW/dt = \mathbf{m}\cdot(d\theta/dt). \quad (2)$$

Data Analysis

In order to identify peak net forces and moments at the beginning and end of each phase (concentric 0º-90º and eccentric 90º-0º) of motion, each phase was further subdivided into concentric (0º-45º and 45º-90º) and eccentric (90º-45º and 45º-0º) segments. A repeated measures ANOVA was conducted to assess the effects between factors (gender and subject) and within factors (muscle loading, loading phase, trial, cycle). A P-value ($P \leq 0.05$) indicates statistical significance.

RESULTS AND DISCUSSION

Overall concentric peak forces and moments were greater than eccentric peak forces and moments ($P<0.0001$, Table 1). Joint forces and moments reached a maximum during the initial phase of concentric loading (0º to 45º) compared with any other rotational position in the loading cycle (concentric 45º-90º or eccentric 90º-0º). The results also indicate that males experienced higher ($P<0.0001$) average resultant peak joint reaction forces than females. Moreover, males experienced higher ($P < 0.0001$) average resultant peak joint reaction moments than females.

The repeated measures analysis revealed that work and power performed by males was statistically similar to work and power performed by females ($P=0.0665$). However, the difference between concentric and eccentric work and power for all subjects was statistically different ($P<0.0001$).

SUMMARY

The shoulder joint mechanics of the impulse inertial exercise have been successfully quantified. The results of this study will aid therapists in the monitoring of patient rehabilitation by providing them with the essential force and moment information.

REFERENCES

Phillips, T.C. et al. (2000). *J Appl Biomech*,16: 60-67.

Tracy, J. et al. (1995). *J Ath Training*, 30(1): 277-286.

Winter, D.A. (1990). *Biomechanics and Motor Control of Human Movement.* 2nd edition, John Wiley & Sons, Inc.

Kroemer. (1989). *Eng Anthrop Ergo* 32(7): 767-784.

ACKNOWLEDGMENTS

Data for this work was collected at the University of Wisconsin and analyzed at Worcester Polytechnic Institute. The authors thank the technical contributions of co-authors TC Phillips, CE Bayirli, LT Brody, JF Orwin, and R Vanderby Jr.

Table 1:

		Resultant Average Peak Shoulder Joint Forces (N)				Resultant Average Peak Shoulder Joint Moments (N m)			
	Cycles	Concentric Phase		Eccentric Phase		Concentric Phase		Eccentric Phase	
		0º-45º	45º-90º	90º-45º	45º-0º	0º-45º	45º-90º	90º-45º	45º-0º
Males	208	302.1 ± 84.3	267.2 ± 91.5	261.8 ± 96.0	236.5 ± 77.1	84.4 ± 23.5	76.6 ± 24.2	64.8 ± 32.5	66.1 ± 20.6
Females	176	186.6 ± 52.2	136.3 ± 32.4	149.7 ± 50.1	150.5 ± 46.4	45.6 ± 10.2	40.5 ± 16.9	32.2 ± 13.8	37.6 ± 11.4
All subjects	384	249.2 ± 91.7	207.2 ± 96.3	210.4 ± 96.2	197.1 ± 77.7	66.6 ± 26.9	60.1 ± 27.8	49.9 ± 30.4	53.0 ± 22.1

FOOT ORTHOSES ALTER MUSCLE ACTIVITY PATTERNS IN RUNNERS DIAGNOSED WITH PATELLOFEMORAL PAIN SYNDROME

Yukiko Toyoda[1], Benno Nigg[1], Preston Wiley[2] and Neil Humble[3]
[1]Human Performance Lab, Faculty of Kinesiology, University of Calgary, Calgary, Canada,
[2]Sport Medicine Center, Faculty of Kinesiology,University of Calgary, Calgary, Canada,
[3]Department Surgery, University of Calgary, Canada
E-mail: yukiko@kin.ucalgary.ca

INTRODUCTION

Patellofemoral pain syndrome (PFPS) is one of the most common lower extremity injuries runners sustain (Taunton et al., 2002). Foot orthoses have been used successfully in reducing overuse pain including PFPS. In a review paper, Nigg et al. (1999) proposed a new concept suggesting that a main effects of foot orthoses may be to change muscle activity rather than rearfoot kinematics as traditionally proposed.
It has been shown that PFPS is related to imbalances between vastus lateralis (VL) and vastus medialis oblique (VMO) muscles. In addition, PFPS treatments which aim to alter the function of VL and VMO have reduced pain successfully. Therefore, it is possible that foot orthoses may alter muscle activity patterns and reduce overuse pain. However, few studies have tested the effects of foot orthoses on muscle activity. Therefore, the purpose of this study was to investigate the effects of custom-made foot orthoses on knee pain and muscle activity patterns in runners diagnosed with PFPS.

METHODS

Six runners (171.5±4.4cm, 67.4±5.6kg) who were diagnosed with PFPS by a physician have been initially recruited for this study. A podiatrist confirmed that all subjects exhibited abnormal foot pronation which contributed to their symptoms. They were otherwise healthy with no history of traumatic lower limb injuries or surgeries, and had never used orthoses before.

Custom-made foot orthoses were prescribed for each subject. Foot orthoses consisted of a semirigid polypropylene shell (custom molding at non-weight bearing subtalar neutral position) with thickness adjusted for patients' weight and a neoprene cover. Subject specific postings were added to both the rear- and forefoot as needed.

Data were collected over 6 weeks in prospective study design. EMG data were collected (2000 Hz) from VL and VMO while the subjects were running at a self-selected speed for 30 minutes. Pain during and after the run was assessed using a 10 cm VAS. Baseline data were collected from 4 days during the first 2 weeks without using foot orthoses. Then, all subjects received their foot orthoses and underwent a gradual 2-week adaptation followed by a 2-week treatment period. Treatment data were collected from 4 days during the last 2 weeks using foot orthoses.

EMG intensity was resolved into time-frequency space using wavelet technique. (Von Tscharner, 2000). EMG intensity (150ms before to 200 ms after heel strike) was calculated for both VL and VMO. VL/VMO intensity ratio and relative onset timing of VMO to VL for 10 % and 100 % of maximum intensity were calculated. Baseline data (without orthoses) and treatment data (with orthoses) were compared subjectively.

RESULTS AND DISCUSSION

Table 1 summarizes the results for both baseline and treatment for all the subjects. Five of 6 subjects showed reductions in pain and one subject showed no change in pain after being treated by custom-made orthoses.

It was shown that PFPS had weaker VMO relative to VL (Tang et al.2001) and delayed onset timing of VMO relative to VL (Cowan et al. 2001). These imbalances could cause abnormal lateral tracking of patella which is related to the onset of PFPS. In this study, VMO intensity and VL/VMO intensity ratio showed strong trends as 4 of 6 subjects exhibited increases in VMO intensity and decreases in VL/VMO intensity ratio. These results indicate that the VMO became more active after treatment with custom-made orthoses. Relative onset timing for 100% of maximum intensity was decreased in 3 of 6 subjects. This result indicates that earlier activation timing of VMO relative to VL after being treated by custom-made orthoses. However, relative onset timing for 100% maximum intensity was increased for one subject and did not change in 2 subjects. No trends were observed for relative onset timing for 10% of maximum intensity. VL intensity did not change in 4 subjects and increased in 2 subjects.

SUMMARY

Custom-made orthoses reduced pain in runners diagnosed with PFPS. Pain reduction may be related to increases in VMO intensity, decreases in VL/VMO intensity ratio and relative onset timing of VMO to VL.

REFERENCES

Cowan et a (2001). *Arch Phys Med Rehabil,* ***82,****183-189.*
Nigg et al (1999). *Med. Sci. Sports. Exerc.* ***31,*** *421-428.*
Tang et a (2001). *Arch Phys Med Rehabil,* ***82****,1441-1445.*
Taunton, J.E. et al (2002). *Brit J Sport Med,* **36,** 95-101.
Von Tscharner (2000). J. Electromyogr. Kinesiol. ***10,*** *433-445*

ACKNOWLEDGEMENTS

The project was supported by American Academy of Podiatric Sport Medicine, Paris Orthotics Ltd. and Alberta Ingenuity Fund.

Table 1: Individual results for pain and EMG variables. Values are mean(standard error).

subject		1	2	3	4	5	6
pain	baseline	3.1(0.7)	7.7(0.4)	5.1(0.4)	3.1(0.2)	1.2(0.4)	2.3(0.6)
	treatment	1.8(0.6)	3.4(0.2)	2.0(0.3)	0.5(0.1)	0.8(0.2)	1.5(0.3)
relative onset 10% [ms]	baseline	10.8(3.2)	-22.2(3.5)	-18.0(3.6)	-0.2(0.6)	3.7(1.7)	7.7(6.9)
	treatment	13.7(0.4)	-14.2(4.5)	-27.1(1.5)	5.7(1.4)	-3.1(4.9)	9.8(4.6)
relative onset 100% [ms]	baseline	4.4(1.4)	6.0(1.5)	-15.4(3.1)	-6.2(2.1)	4.7(1.3)	2.1(1.3)
	treatment	0.1(0.3)	4.2(2.0)	-33.0(2.5)	-13.5(1.6)	3.8(9.2)	4.2(2.6)
VL intensity [mv^2]	baseline	91.1(10.1)	30.0(3.3)	16.5(1.9)	72.0(7.8)	35.8(4.3)	19.1(0.5)
	treatment	94.1(7.0)	48.0(5.6)	16.9(1.7)	73.9(7.5)	75.3(20.3)	21.6(1.5)
VMO intensity [mv^2]	baseline	70.3(6.4)	8.2(0.3)	4.4(0.5)	39.3(1.3)	82.0(12.4)	23.2(0.6)
	treatment	81.1(5.4)	14.9(1.7)	10.4(6.3)	64.9(3.5)	52.4(10.8)	42.9(5.7)
VL/VMO ratio	baseline	1.4(0.3)	4.7(0.6)	3.3(0.3)	1.9(0.2)	0.4(0.1)	0.9(0.0)
	treatment	1.3(0.1)	3.9(0.7)	3.4(0.3)	1.2(0.1)	1.7(0.5)	0.6(0.1)

SOFT TISSUE MODELING AND MECHANICS

Amy E. Kerdok[1, 2], Simona Socrate[1, 3], Robert D. Howe[1, 2]

[1]Harvard/MIT Division of Health Sciences and Technology, Cambridge, MA
[2]Biorobotics Laboratory, Harvard University Division of Engineering and Applied Sciences, Cambridge, MA
[3] Massachusetts Institute of Technology Dept. of Mechanical Engineering, Cambridge, MA
E-mail: kerdok@fas.harvard.edu

INTRODUCTION

Although most soft tissues do not have load-bearing functions, understanding their mechanical behavior is of great interest to the medical simulation, diagnostic, and tissue engineering fields. Obtaining these properties is a formidable challenge due to soft tissue's mechanical and geometric nonlinearities, multi constituent heterogeneity, viscoelastic nature and poorly defined boundary conditions.

It has been shown that the mechanical response of soft tissues drastically change when removed from their natural environment (Brown et al. 2003; Ottensmeyer et al. 2004, accepted). It is necessary to measure the tissue's mechanical response under *in vivo* conditions. Several groups have made measurements *in vivo* (Brown et al. 2003; Ottensmeyer 2001), but the interpretation of these results remain to be understood because of the inability to control boundary conditions and other testing parameters.

Using a method to maintain a nearly *in vivo* environment for *ex vivo* tests, we have measured the force-displacement characteristics of whole porcine liver using a motorized indenter. The results of these tests are to be interpreted using inverse finite element modeling. The material parameters will be determined from a constitutive model developed for cervical tissue (Febvay 2003) and adapted for the liver.

METHODS

To obtain nearly *in vivo* conditions in an *ex vivo* state, a perfusion apparatus developed by Ottensmeyer et al. (2004) was used. Pigs used were systemically heparinized, their livers were harvested and flushed of blood, placed on ice for transport to the lab, and connected via the portal vein and the hepatic artery to a perfusion apparatus within 90 minutes post sacrifice that maintained nonpulsatile physiologic pressure (9 mmHg and 100 mmHg respectively) and temperature (39°C).

Tests were performed to capture the viscoelastic nature of the tissue using the motorized "ViscoElastic Soft tissue Property Indenter" (VESPI). As a preliminary step to guide the device development large strain (~50%) creep tests were performed. The thickness of the tissue was measured prior to each load (to determine nominal strain), and the tissue was allowed to recover to its initial state before repeating the test in each location. Future tests will be performed to capture the complete viscoelastic tissue response including large strain stress relaxation tests and cyclic loading/unloading tests at varied strain rates.

An axisymmetric finite element model to analyze the indentation of soft tissue is being developed using commercial finite-element software (ABAQUS 6.4, HKS, Rhode Island). This model will incorporate the constitutive model for liver tissue. The constitutive model reflects the tissue structure, as the global tissue response is controlled by the cooperative contributions of its major constituents. The response is modeled by the association in parallel of a nonlinear elastic 8-chain model network, accounting for the role of the interlobular septa, and a viscoelastic component, representing the hydrated ground substance. The transient effects associated with fluid flow are accounted for in terms of a linear Darcy's law. The complete three-dimensional model resulting from these components is implemented as a user material subroutine for ABAQUS 6.4.

The results of the VESPI tests and testing conditions will be used as inputs to the FEM containing the adapted constitutive model for liver tissue. An iterative process will ensue to determine the material parameters that uniquely identify the mechanical characteristics of the liver.

RESULTS AND DISCUSSION

Results from the preliminary large strain creep indentation tests using perfused *ex vivo* whole porcine livers are shown in Figure 1. These tests qualitatively reveal repeatable results within location over time, and a clear creep response where a steady state was achieved within 5 minutes.

The VESPI is currently being modified to operate under position control so that stress relaxation and ramp tests can be performed.

SUMMARY

This work presents preliminary results from large strain creep tests performed on *ex vivo* whole liver tissue using a perfusion system that mimics *in vivo* conditions. A description of the proposed constitutive model was also given. Future tests will obtain stress relaxation and hysteresis results as inputs for a finite element model that will be used to identify the mechanical parameters of the liver.

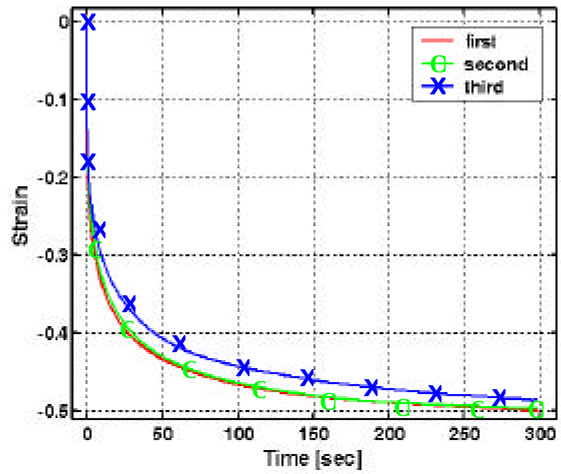

Figure 1: VESPI 100g-creep response on a 27kg perfused pig liver at the same location. The second and third indentations were taken 20 and 48 minutes after the first.

REFERENCES

Brown, J. D., Rosen, J., et al. (2003). *Proceedings of Medicine Meets Virtual Reality.*

Febvay, S. (2003). Massachusetts Institute of Technology. Master of Science.

Ottensmeyer, M. P. (2001). *Proceedings of Medical Image Computing and Computer-Assisted Intervention - MICCAI.*

Ottensmeyer, M. P., Kerdok, A. E., et al. (2004, accepted). *Proceedings of Second International Symposium on Medical Simulation.*

ACKNOWLEDGEMENTS

Support has been provided by a grant from the US Army, under contract number DAMD 17-01-1-0677. The ideas and opinions presented in this paper represent the views of the authors and do not, necessarily, represent the views of the Department of Defense.

CLINICIAN-FRIENDLY SOFTWARE FOR BIOMECHANICAL MODELING AND CONTROL OF MOVEMENT

Rahman Davoodi, Chet Urata, Emanuel Todorov, and Gerald E. Loeb

A.E. Mann Institute and Biomedical Engineering Department, University of Southern California
Los Angeles, CA 90089, USA

Email: davoodi@usc.edu Web: http://ami.usc.edu

INTRODUCTION

Research in biomechanics of movement and its applications to rehabilitation and restoration of movement require sophisticated musculoskeletal modeling software (MSMS). The currently available software packages have limited functionality, their use requires high-level programming expertise, and they are expensive (Davoodi *et al.* 2003). We have formed a core software development team to lead a collective effort by the biomechanics community to develop free and open-source software for musculoskeletal modeling that will satisfy the requirements of both researchers and clinicians. The effort is directed from our laboratory at Alfred Mann Institute (AMI) for Biomedical Engineering. We are motivated to lead this effort because AMI has pioneered the development and clinical application of BIONs™ (Loeb *et al.* 2001). This technology platform of wireless, injectable stimulators and sensors can be applied to a wide range of sensorimotor disabilities, but only if clinicians have accessible and reliable software tools to fit them systematically to individual patients.

METHODS

The statement of requirements is the first step in MSMS development in which all the features of MSMS are discussed and documented before writing a single line of code. A series of meetings between the software developers and researchers from different fields have produced documents that detail the requirements for MSMS.

The *vision document* identified the main users and their key requirements, provided a high-level analysis of the key features, and justified the decision to develop MSMS as open source software to promote its adoption by the research community and ensure its continuing evolution and growth. Various usage scenarios such as "building a model" or "forward dynamic simulation" were analyzed in *use case analysis.* Each use case analysis identified the primary users (actors), the goals, and the step-by-step sequence of actions to complete the task. Finally, based on the above requirement analyses, *software architecture* was designed that includes three top-level blocks: graphic user interface (GUI), Modeling and Simulation, and Database.

Development and testing of the MSMS were started after the completion of the requirements specification. We are using a method known as *iterative development,* in which consecutive three-week iteration cycles add more functionality to the MSMS until all the requirements are met. Each iteration produces an executable code that enables us to test the developed components for functionality and integration. As a result, we can discover the integration problems early in the process, which are then easier to remedy. We are using Java as the main programming language for development of the GUI, modeling, and database units. But computationally intensive dynamic simulation unit will use more efficient C programming language and Simulink simulation environment. We have performed a comprehensive test to select dynamic engines for dynamic simulations in MSMS. The details are described in a companion paper in this proceedings (Montazemi et al. 2004). The eXtensible Markup Language (XML) is used to define the standard model file formats.

RESULTS AND DISCUSSION

The implementation effort to date has resulted in a basic graphical user interface that could load, visualize, and animate the musculoskeletal models developed in SIMM (Fig. 1). We have implemented cylindrical wrapping objects and we are adding more to accurately model muscle wrappings around bony surfaces (Garner & Pandy 2000).

As a collective effort, the success of MSMS depends on active participation by the research community. The core development team at AMI is currently consulting with a group of thirteen prominent researchers in different musculoskeletal modeling fields in their area of expertise. They are helping to define the requirements for MSMS, define standards for musculoskeletal models, and test the alpha releases of the MSMS in their own applications. The larger community will be involved in the development through a central web page. They will provide feedback on the standards for musculoskeletal modeling drafted by the development team and consultants and test the beta releases of the MSMS.

Once developed, the MSMS will be distributed freely to the public. Procedures will be provided to enable end users to expand the MSMS with new features as new methods and data become available. We think this is essential because rapid advances in movement science and software algorithms produce new models and data that must be incorporated into pre-existing models with minimal effort. For the latest developments visit http://ami.usc.edu/msms/

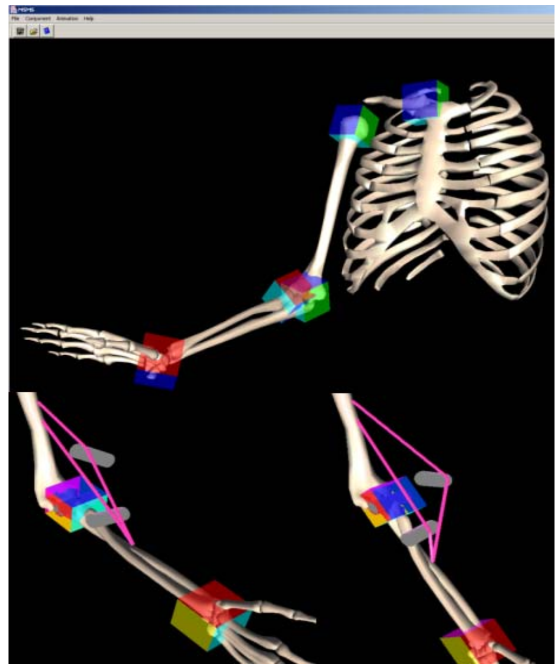

Fig. 1. The graphic user interface of MSMS under development. Muscle wrappings around cylindrical surfaces are shown.

REFERENCES

Davoodi, R. et al. (2003). *Med Eng Phys*, **25**,3-9.
Garner, B.A. and Pandy M.G. (2000). *Comput Methods Biomech Biomed Engin* **3,** 1-30.
Loeb, G.E. et al. (2001). *Med Eng Phys*,**23**,9-18.
Montazemi, P.T. et al. (2004). This proceedings.

ACKNOWLEDGEMENTS

We acknowledge the enthusiastic advice and support from the MSMS consulting team: Behzad Dariush, Francisco Valero, Garry Yamaguchi, Ian Brown, Marcus Pandy, Robert Kirsch, Scott Delp, Stefan Schaal, Steven Arms, Scott Selbie, and Victor Ng-Thow-Hing. Funded by Alfred E. Mann Institute for Biomedical Engineering, University of Southern California.

COMPARISON OF THREE DIFFERENT HYDROXYAPATITE COATINGS IN AN UNLOADED IMPLANT MODEL - EXPERIMENTAL CANINE STUDY

*Daugaard, H; *Elmengaard, B; **Bechtold, J E, *Jensen T B, *Søballe, K
*Orthopaedic Research Laboratory, Aarhus University Hospital, Denmark.
**Midwest Orthopaedic and Minneapolis Medical Research Foundations
E-mail: kohda@sc.aaa.dk

INTRODUCTION

Treatment of osteoarthritis and rheumatoid arthritis by total joint replacement generally shows a high success rate, however challenges (e.g. revision joint replacement) remain. Clinically and experimentally, plasma sprayed hydroxyapatite (HA) coating on porous implant surfaces has been shown to enhance mechanical implant fixation and bone ongrowth in the primary and revision settings. In this study we compare the well-documented plasma sprayed HA coating to two alternative thinner HA coatings: electrochemical deposition of HA and electrochemical deposition of HA mixed with mineralized collagen. Uncoated plasma sprayed Titanium (Ti) was the negative control. We hypothesize that the electrodeposited HA's (HA alone, and collagen mixed with HA) will achieve the same fixation as traditional plasma sprayed HA, with Ti being inferior to all three HA's.

METHODS

A paired and controlled experimental canine study was carried out following approval of our institution´s Animal Care and Use Committee. Cylindrical plasma sprayed titanium (Ti-6Al-4V) implants 10 mm long x 6 mm were used (Fig.1). Four different implant surfaces were investigated in each of 7 skeletally mature animals: (1) plasma spray titanium, (2) HA-plasma spray, (3) electrochemical HA-deposition (36C and pH 6.4) and (4) HA-mineralized collagen coating. Two implants surrounded by a 1 mm gap were inserted alternately in two unloaded extraarticular cancellous bone sites bilaterally in the proximal humeri. Specimens were obtained at 4 weeks and were frozen until testing. Sections (3.5 mm thickness) were cut perpendicular to the implant axis, using a diamond saw (Exact) and implant-based alignment post.

Figure 1: Implant placement (bilateral; 4/animal)

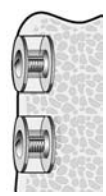

Mechanical testing
Mechanical pushout testing was performed on transverse sections, using an Instron test machine UK (5 mm/minute). Load versus displacement was recorded and ultimate shear strength (MPa), apparent shear stiffness (MPa/mm) and energy absorption to failure (J/mm^2) were derived. Histomorphometry Using stereological methods, vertical sections were obtained after random rotation of the 6.5 mm blocks. Computer assisted histomorphometry was performed blindly using a CAST-grid system (Olympus Denmark). Tissue ongrowth was defined as tissue directly at the implant surface, and was determined using the linear intercept technique and tissue volumes were obtained using point counting. Statistics: Non-parametric analysis was applied since differences between pairs did not follow a normal distribution. After Kruskal-Wallis on Ranks, the Wilcoxon sign ranks test was used to compare specimens pairwise. P-values < 0.05 are considered statistically significant. Data are accordingly presented as median and interquartile ranges.

RESULTS AND DISCUSSION

Table 1. Mechanical pushout properties

Median and interquartile range	Ultimate shear strength (MPa)	Apparent stiffness (MPa/mm)	Energy absorption (J/m^2)
Titanium	0.0 (0.0-0.3)	0.0 (0.0-1.3)	0 (0-45)
HA plasma	2.1 (1.5-3.2) ab	7.8 (4.2-17.9) ab	535 (213-574) ab
HA elec.depos.	1.97 (0.7-3.4) a	9.0 (2.7-16.6) a	339 (92-618) a
HA / Collagen	0.51 (0.1-2.1)	2.5 (0.6-8.9)	73 (7-456)

a: $p<0.05$ compared to Titanium.
b: $p<0.05$ compared to HA/collagen

Mechanical fixation of the electrochemically deposited HA was not statistically different than the plasma sprayed HA or the electrochemically deposited HA-collagen, and was significantly increased compared to the titanium control. The traditional HA-plasma sprayed implants achieved better mechanical fixation compared to electrodeposited HA-collagen and titanium controls (significant). In the histomorphometric analysis, significant differences were only seen directly at the implant interface (ongrowth). All HA coated implants demonstrated significantly higher bone ongrowth compared to the titanium control. The traditional plasma sprayed HA showed 2-fold higher bone ongrowth fraction (not significant, p=0.06) compared to the electrodeposited HA´s. There was a tendency for more marrow at the surface of the electrodeposited HA’s, (not significant).

Electrochemical deposition of HA does not require high temperature for application, can be thinner than plasma sprayed (retaining the macro roughness of the titanium plasma spray surface), and can achieve full three-dimensional coverage not possible with the line-of sight plasma spraying process. Conceptually, adding collagen to the HA could present a more “bone-like” surface.

Some of the findings could be related to differences in coating thickness, surface

Fig 2. Fraction of implant tissue ongrowth

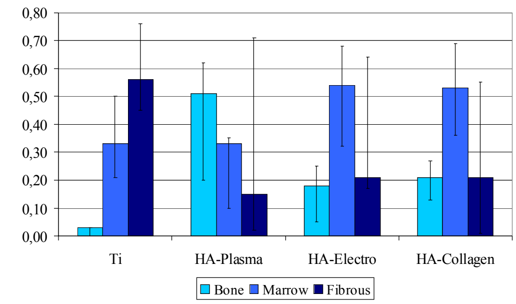

Bone ongrowth: $p<0.05$ for all coatings compared to titanium

morphology, composition, and dissolution rate of the mineral phase, with the electrodeposited HA’s having a thinner coating and smaller crystallites, and the high temperature plasma sprayed HA having a thicker coating and larger crystallites. From our previous experience, the low fixation for the titanium surface is not unexpected in a 1 mm gap at 4 weeks.

These results are limited to the plasma spray implant surface and unloaded gap setting, in a 4-week observation period. The potential for electro-deposited HA to be as good as (or to improve upon) plasma sprayed HA warrants further experimental study.

SUMMARY

Mechanical fixation of electrodeposited HA was not different than the traditional plasma spray method of HA coating, although there was a tendency for bone ongrowth to be less. Adding collagen to the mineral phase of the coating to create a surface that more closely imitated the natural bone setting did not improve fixation in this model.

REFERENCES

i Roessler S et al. J Biomed Mater Res 64A:655-663, 2002. ii Roessler S et al, J.Mat Sci, 12:871-877, 2001.

ACKNOWLEDGEMENTS

Biomet-Merck BioMaterials GmbH (Germany) & Biomet, Inc. (Warsaw, IN)

A DYNAMIC MODEL FOR ASSESSMENT OF MICROMOTION AND MIGRATION IN KNEE ARTHROPLASTIES

Marcus Mohr[1], Mark B. Sommers[1], Patrick Dawson[2], Scott Steffensmeier[3], and Michael Bottlang[1]

[1]Biomechanics Laboratory, Legacy Research & Technology Center, Portland, OR
[2]Oregon Health & Science University, Portland, OR; [3]Zimmer, Inc., Warsaw, IN
E-mail: mbottlang@biomechresearch.org

INTRODUCTION

Each year over 300,000 total knee arthroplasties (TKA) are preformed in the USA. Excessive motion at the bone-implant interface during the early post-operative phase is an essential contributor to early construct failure (Ryd, 1986).

Several studies have been conducted to quantify this relative motion *in vivo* (Vrooman, 1998), but the accuracy of radiographic and clinical evaluation methods is limited. This limitation has been eliminated in cadaveric studies (Kraemer, 1995), but inherent inter-specimen variability reduces the sensitivity in comparative testing.

This study introduces a dynamic surrogate model that allows quantitative assessment of micromotion and migration at the bone-implant interface during dynamic gait cycle simulation.

METHODS

To simulate dynamic loading as observed in level walking, a custom loading apparatus was designed for use in a bi-axial servo-hydraulic testing machine (Instron 8874, Canton, MA). The apparatus (Fig. 1) is symmetrical about its vertical center axis to enable simultaneous testing of two specimens, while avoiding bending moments on the top-mounted load cell. A pair of independently moving aluminum rollers mounted on double-row precision ball bearings simulated condylar rolling motion on both sides of the setup. The rollers closely approximated condylar geometry with a radius of 22 mm in both the sagittal and coronal plane. Intercondylar distance was set to 44 mm. Hinge joints in the center of each condylar unit, as well as in the center line of the apparatus, ensured symmetric load distribution between the left and right condyles and between the two test specimens.

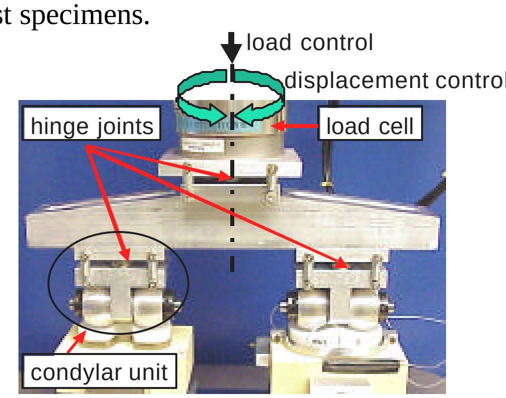

Figure 1: Dynamic knee test apparatus

Gait simulation was achieved through bi-axial dynamic loading in accordance with ISO-standard 14243 for wear testing in knee prostheses.

Rotation of the Instron actuator in displacement control induced antero-posterior (a-p) condylar translation of $\pm$ 5 mm (medially) and $\pm$ 6 mm (laterally) from the center of the implant.

The a-p translation was superimposed by dynamic axial loading. Peak load magnitude was at 2 kN (3 x bodyweight) per condylar unit, with the machine operating under load control.

Five screwless, non-cemented, cruciate retaining TKA tibial components were inserted into custom machined blocks of 7-pcf, closed cell, solid rigid polyurethane foam (General Plastics, Tacoma, WA). Insertion technique and instruments were used in accordance with manufacturer guidelines.

Axial motion between the implant and the upper surface of the foam block was measured with three sensors (M-DVRT-3, MicroStrain, Inc., Williston, VT). Sensors were fixed anteriorly, postero-medially (p-m), and postero-laterally (p-l) to an aluminum clamp, which in turn was rigidly mounted to the tibial tray (Fig. 2a). The clamp allowed reproducible and rigid positioning of the DVRTs at 2-mm distance from the implant's circumference (Fig. 2b). The DVRTs' plungers were fixed to the foam surface using cold-curing 2-component cement.

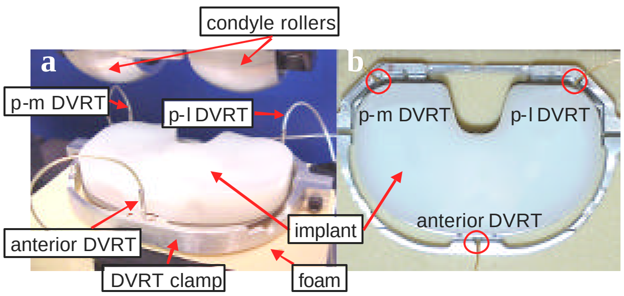

Figure 2: Tibial component, instrumentation

Outcome parameters were micromotion (difference between maximum and minimum DVRT reading within each load cycle) and migration (difference between minimum DVRT readings at 10 cycles and at the current cycle). The first nine cycles were considered as initial implant settling and excluded from analysis.

RESULTS

Results showed a continuous increase in micromotion over the number of load cycles (Fig. 3). The largest amount of micromotion was seen anteriorly with 370 ± 40 µm at 10 cycles. It increased to 460 ± 60 µm at 10,000 cycles. Posterior micromotion was similar between lateral and medial locations and reached a maximum of 340 ± 30 µm at the postero-lateral location after 10,000 cycles.

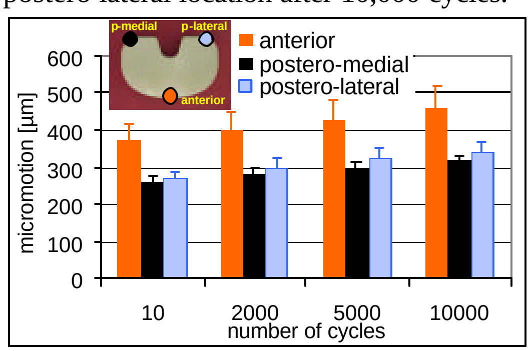

Figure 3: Average micromotion, n=5

Migration also increased continuously in magnitude over the number of cycles (Fig. 4).

Maximum migration was observed postero-medially, ranging from –140 ± 20 µm at 2,000 cycles to –240 ± 20 µm at 10,000 cycles. Minimal migration was measured postero-laterally, reaching –40 ± 20 µm after 10,000 cycles.

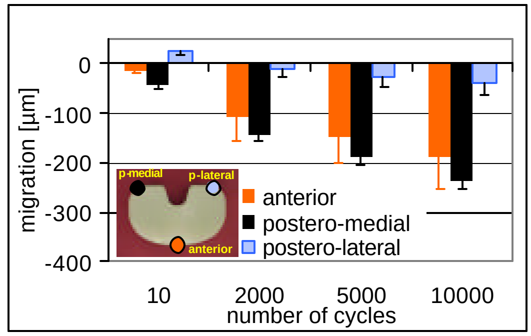

Figure 4: Average migration, n=5

DISCUSSION

The presented model provides a sensitive and reproducible tool to quantify micromotion and migration of knee arthroplasties during dynamic gait cycle simulation. The chosen foam type resembles highly osteoporotic bone, constituting a worst-case scenario of joint replacement. Since the magnitude of micromotion depends on the foam properties, it cannot be directly correlated to clinically observed micromotion magnitudes, but is a valuable indicator for comparative implant evaluation.

Notably low standard deviations indicate the model's potential to determine the benefits of the ever increasing number of implant design features aimed at reducing micromotion, such as pegs, screws, and structural backings.

REFERENCES

Ryd L. (1986). *Acta Orthop Scand Suppl.*, **220**, 1-80.

Vrooman H.A. et al. (1998). *J Biomech.*, **31**(5), 491-8.

Kraemer W.J. et al. (1995). *J Arthroplasty*, **10**, 227-35.

ACKNOWLEDGEMENT

Supported by Zimmer, Inc., Warsaw, IN, USA

EFFECT OF GENDER ON LANDING STRATEGY IN PREADOLESCENT CHILDREN

Michelle Sabick, Ph.D., Jeanie Sutter, M.S., Ronald Pfeiffer, Ed.D. A.T.C., Kevin Shea, M.D.

Center for Orthopaedic and Biomechanics Research, Boise State University,
Boise, Idaho, USA
E-mail: MSabick@boisestate.edu Web: http://coen.boisestate.edu/cobr

INTRODUCTION:

The effects of gender on lower extremity kinematics and kinetics during landing have been studied extensively in adults. Females tend to land in a more upright posture, with the hips and knees more extended than their male counterparts (Decker, 2003). Males tend to generate higher peak impact forces acting over shorter times.

Male and female preadolescents are quite similar morphologically as neither group has undergone the physical changes associated with pubescence. By studying landing strategies in preadolescent children, body morphology differences between the genders are essentially eliminated. Little is known about landing mechanics in preadolescent populations. Hass et al (2003) found that prepubescent females landed with more flexed hips and knees than post-pubescent females. These results hint that age related morphology changes play a role in landing strategies, at least within female subjects.

The purpose of this study was to determine whether gender affects landing strategies in preadolescent male and female soccer players. To our knowledge, this is the first study examining the effects of gender on landing mechanics in preadolescents.

METHODS:

Twelve females and 11 males (10 - 12 years of age) were recruited from a local youth soccer league. Subjects dropped from a horizontal bar (net drop 30.5cm) landing barefoot on one leg onto a force platform sampling at 1250 Hz. The test leg was randomized. Each subject performed 5 to 10 trials. The first five successful trials were analyzed.

Pelvis and lower extremity kinematic data were collected at 250 Hz. The 3-D marker coordinates were smoothed using a 4^{th} order Butterworth filter with a cutoff frequency of 17 Hz. Kinematics of the pelvis, hip, knee, and ankle were calculated using Euler angles (Fioretti, 1997).

Internal resultant joint forces and moments for the instrumented lower extremity were calculated using an inverse dynamics technique. Body segment parameters for all subjects were computed using data from de Leva (1996) specifically for male and female subjects. Comparisons of ground reaction force components, joint angles, and joint kinetic variables between the two groups were made using two tailed Student's t-tests with an α level of 0.05.

RESULTS and DISCUSSION:

Subjects: Body weight, height, and age were not significantly different between the two groups (Table 1).

Kinematics: None of the pelvis or lower extremity joint angles at initial ground contact was significantly different between the groups (Figure 1, $0.13 \leq p \leq 0.99$).

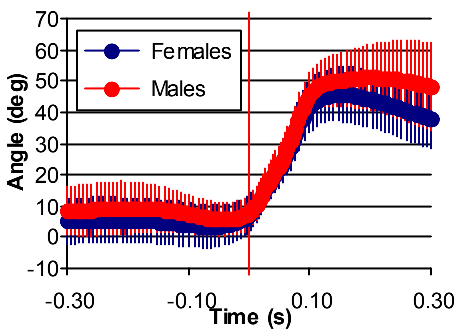

Figure 1. Mean (±SD) knee flexion (+) angle for the two groups. Vertical line indicates initial ground contact.

Kinetics: Although there was a trend for peak vertical impact force (Fz) to be greater in males, the difference between the groups was not statistically significant ($p = 0.17$). The time interval between initial ground contact and peak Fz (Δt Fz), and the peak anterior shear on the tibia also were not significantly different (Table 1).

There were no statistically significant differences in the magnitude or timing of landing forces between male and female preadolescent soccer players. These findings are in agreement with those of Decker et al (2003) who studied adult subjects. However, in our study peak Fz ranged from 3.0 to 8.0 BW. Ground reaction force values reported in adult cohorts range from approximately 2.4 to 3.7 body weights (BW). Our higher values may be due to differences in jump-landing task, age, or absence of footwear.

Investigators have noted increased anterior shear on the proximal tibia in adult females when compared to adult males (Chappell, 2002). In our cohort, the differences were not significant. Taken together, our lack of significant findings may indicate that differences in landing mechanics seen in adults are due to body mass distribution changes occurring at maturity.

SUMMARY:

The differences between genders in landing mechanics often observed in adult cohorts were not seen in this group of preadolescent soccer players. The magnitude and timing of landing forces were not significantly different between groups, nor were the joint kinematics at impact. Our ongoing analysis will focus on additional aspects of landing mechanics that may still be subtly different between the genders, even in preadolescents.

REFERENCES:

Chappell, J.D. et al. (2002). *Am. J. Sports Med.,* **30**, 261-267.

Decker, M.J. et al. (2003). *Clin. Biomechanics,* **18**, 662-669.

deLeva, P. (1996). *J. Biomechanics*, **29**, 1223-1230.

Fioretti, S. et al. (1997). *Three-dimensional Analysis of Human Locomotion.* John Wiley & Sons.

Hass, C.J. et al. (2003). *J. Applied Biomechanics,* **19**, 139-152.

ACKNOWLEDGEMENTS:

The authors would like to express their appreciation to Kristi Unholz and Kristof Kipp for their help with data analysis.

Table 1: Summary of subject characteristics and kinetic data for the two groups.

Group	Age (yr)	Height (m)	Weight (N)	Peak Fz (BW)	Δt Fz (ms)	Anterior Shear (BW)
Females	11.3 ± 0.7	1.48 ± 0.07	357 ± 75	4.71 ± 1.25	58.8 ± 14	1.21 ± 0.18
Males	11.4 ± 0.8	1.51 ± 0.06	379 ± 35	5.50 ± 1.39	53.3 ± 13	1.14 ± 0.15
p-value	0.92	0.31	0.46	0.17	0.35	0.15

TAI CHI AND STANCE WIDTH EFFECTS ON POSTURAL SWAY AND KNEE FLEXION

Arun K. Ramachandran[1], Yang Yang[2], Karl S. Rosengren[2], and Elizabeth T. Hsiao-Wecksler[1]

[1] Department of Mechanical and Industrial Engineering, [2] Department of Kinesiology
University of Illinois at Urbana-Champaign, Urbana, IL
E-mail: ethw@uiuc.edu Web: http://netfiles.uiuc.edu/ethw/www/hdcl/hdcl.html

INTRODUCTION

Previous studies on Tai Chi (TC) experience and its effect on balance and postural sway have been inconclusive. Some studies of quiet, unperturbed stance have found significant differences in certain measures of standing balance, while others have found none (Wu 2002). A recent study suggests that stance width and knee flexion may increase as a result of TC experience (Rosengren, in review). Stance width has been shown to influence postural sway (Maki 1997); however balance studies on TC practitioners have not controlled for stance width. Therefore, this study investigated whether stance width influences postural sway behavior and knee flexion in persons with and without TC experience.

METHODS

Fifteen Tai Chi practitioners (7 females; mean age 45.7 ± 10.6 yrs, range 25 – 66 yrs; mean TC experience 6.46 ± 4.32 yrs, range 1.5 -15 yrs) and fifteen control subjects matched by age, sex, and physical activity level were tested in quiet stance. TC practitioners were students of a local TC master. Subjects were asked to stand barefoot with their hands at their sides, eyes open, and feet in one of three different positions on a force platform (AMTI, Woburn, MA, model BP600900). The three positions were: *Constrained Stance* - heels separated by a distance (stance width) of 6 cm and feet abducted (abduction) 10 deg; Average *Normal Stance* – stance width of 17 cm and abduction of 15 deg; *Tai Chi Stance* - normal comfortable stance for each TC practitioner (control subjects matched their respective TC mate). Subjects completed ten 30 s trials in each stance.

Postural sway was analyzed based on center of pressure (COP) displacement as a function of time. Time-domain analysis yielding 'traditional' measures of COP (TRAD) and Stabilogram Diffusion Analysis (SDA) measures (Collins 1993) were used. TRAD parameters were: maximum absolute excursion from the mean (*Max*), standard deviation about the mean (*SD*), range between maximum and minimum excursions (*Range*), swept area (*SweptA*), path length (*PathL*), and sway speed (*SwaySpd*). SDA parameters included: short term and long term diffusion coefficients (D_S, D_L), short term and long term scaling exponents (H_S, H_L), critical time (t_c), and critical displacement (d_c). Parameters were calculated in the anterior-posterior, medial-lateral and radial directions (AP, ML, and R, respectively).

Knee flexion was calculated from motion analysis data (VICON, Oxford Metrics, UK). Knee flexion was defined by line segments joining the estimated hip, knee and ankle joint centers, such that full (collinear) extension was equal to 0 deg. Average knee flexion for both legs was reported.

Two-way repeated measures ANOVA were used to test for significant differences in these parameters based on group (TC, control) and stance width (*Tai Chi Stance*, *Normal Stance*, *Contrained Stance*). LSD test was used to test post-hoc comparisons.

RESULTS AND DISCUSSION

Postural sway behavior was found to be significantly affected by stance width, but not TC experience. No differences were found between TC practitioners and controls in quiet stance parameters, which is consistent with some studies (e.g., Wolf 1997). Stance width significantly affected balance measures, especially in the ML direction (Table 1). Constrained Stance parameters were significantly different from Tai Chi and Normal stance. There were no significant differences between Tai Chi and Normal stance. The average width during the *Tai Chi Stance* condition (25.3 cm) was substantially greater than *Normal Stance.*

Knee flexion was affected by both stance width (p = 0.003) and TC experience (p = 0.02); there was no interaction. TC practitioners used significantly greater knee flexion than control subjects (Table 1). Interestingly, knee flexion increased as stance width decreased; however, only knee flexion during the Tai Chi Stance was significantly different than the other stance widths.

SUMMARY

No difference in quiet-stance postural sway behavior was detected due to TC experience, when controlling for stance width; however, we did find that constrained stance increased postural sway. Our results support that TC practitioners use greater knee flexion and a wider stance. We also found that knee flexion appears to increase as stance width decreases.

REFERENCES

Collins, J.J., et al. Exp Brain Res, 1993. 95(2): 308-318.

Maki, B., et al. Phys Ther, 1997. 77(5): 455-507.

Rosengren, K.S., et al. Gait Posture, in review.

Wolf, S.L., et al. Phys Ther, 1997. 77(4): 371-384.

Wu, G. J Am Ger Soc, 2002. 50(4): 746-54.

Table 1: Statistically significant balance parameters for all subjects combined (p < 0.001 for all parameters), and knee flexion values by test group.

Description	Mean ± SD		
	Tai Chi stance	***Normal stance***	***Constrained stance***
Stance width (cm)	25.3 ± 31.7	17	6
Abduction (deg)	20.1 ± 5.9	15	10
SDA $D_{S, ML}$	2.0 ± 1.0	2.2 ± 1.2	9.5 ± 4.8
$D_{L, ML}$	0.16 ± 0.2	0.2 ± 0.2	0.85 ± 0.7
$D_{R, ML}$	11.8 ± 5.2	12.1 ± 6.8	20.7 ± 9.0
$H_{S, ML}$	0.7 ± 0.05	0.7 ± 0.04	0.8 ± 0.04
$t_{c,ML}$ (sec)	0.9 ± 0.1	1.0 ± 0.1	1.3 ± 0.4
$d_{c,ML}$ (mm)	1.9 ± 1.2	3.0 ± 1.8	20.1 ± 12.9
$d_{c,R}$ (mm)	20.5 ± 15.3	22.0 ± 12.9	37.7 ± 21.3
$H_{S, R}$	0.7 ± 0.04	0.7 ± 0.0	0.81 ± 0.0
TRAD ML_Max(mm)	4 ± 1	4 ± 1	10 ± 3
ML_SD (mm)	1 ± 0	1 ± 0	3 ± 1
ML_Range (mm)	7 ± 2	8 ± 2	18 ± 5
SweptA (mm^2)	728 ± 232	760 ± 282	1070 ± 281
SwaySpd (mm/sec)	19 ± 2	19 ± 2	20 ± 2
R_Max (mm)	12 ± 3	12 ± 3	14 ± 2
PathL (mm)	575 ± 80	574 ± 84	613 ± 80
Knee Flexion			
TaiChi subjects (deg)	14.9 ± 3.6	15.8 ± 3.8	16.2 ± 4.1
Control subjects (deg)	11.9 ± 3.5	12.5 ± 3.6	12.6 ± 3.6

OBLIQUE IMPACT TESTING OF BICYCLE HELMETS

Steven M. Madey, Larry W. Ehmke, Mark B. Sommers, and Michael Bottlang

Biomechanics Laboratory, Legacy Research & Technology Center, Portland, OR
E-mail: mbottlang@biomechresearch.org

INTRODUCTION

Of the 1,300 persons that die each year from bicycle accidents, 90% are due to head trauma (Waters, 1986). The most common injury mechanism is angular head acceleration caused by oblique impacts (Otte, 1999).

In stark contrast, contemporary test standards for bicycle helmets simulate perfectly radial impacts and assess linear acceleration only. Albeit oblique head impacts scenarios have been simulated, experimental setups were too complex for adaptation in test standards (Aare, 2003).

This research introduces a modification of a standard drop tester for bicycle helmets to enable oblique impact simulation and angular acceleration assessment. Furthermore the dependence of friction in oblique impacts was evaluated.

METHODS

Four aspects of a monorail guided drop tester, compliant to bicycle helmet test standards CPSC §1203.17, were modified (Figure 1): 1) to simulate oblique impacts, the standard flat anvil was replaced by a 30° oblique anvil; 2) to allow for unconstrained motion during the oblique impact, the head-form was connected to the drop follower with three highly flexible steel cables; 3) to measure linear acceleration in oblique impacts, the standard uniaxial accelerometer mounted at the headform center of mass was replaced by a biaxial accelerometer (PCB Piezotronics 356B21, Depew, NY); and 4) to measure angular acceleration in oblique tests a second uniaxial accelerometer (ACC103, Omega, Stamford, CT) was mounted at 90mm horizontal distance to the center of mass. Acceleration differences between the two accelerometers were used to estimate the angular acceleration pulse during helmet impact under the assumption of headform rotation around a transverse axis.

Three impact scenarios were investigated:
1) Perpendicular,
2) 30° oblique, high friction interface (HF),
3) 30° oblique, low friction interface (LF).

All drop tests were performed with a drop-height of 1.2 m, equivalent to CPSC §1203.17 curbstone impact testing, to approach an impact velocity of 4.9 m/s.

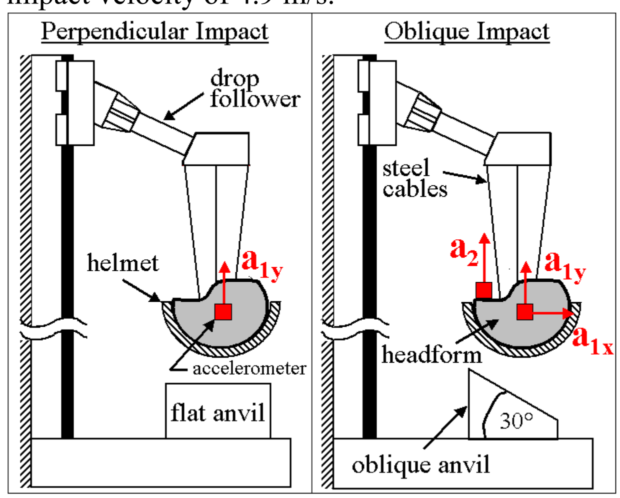

Figure 1: a) perpendicular and b) oblique impact test setup.

Perpendicular impacts were conducted for comparison to conventional helmet drop-testing. Oblique impacts were conducted with either a LF interface by means of a lightly greased anvil surface, or with a HF interface, for which a 60-grit sandpaper was glued on the anvil.

In each of the three scenarios, three contemporary microshell helmets (Bell Reflex, Rantoul, IL) were impacted. Results were presented in terms of linear acceleration and angular acceleration for all test scenarios.

RESULTS

Perpendicular impacts yielded an average linear acceleration of 187.5 ± 18.6 g. 30° LF and 30° HF yielded a significantly lower linear acceleration ($p<0.05$) of 151.3 ± 1.8 g and 150.11 ± 13.28 g, respectively (Figure 2). No significant differences in linear acceleration were noted between 30° LF and 30° HF oblique impacts ($p=0.88$). The angle between the drop trajectory and the acceleration vector was 31.2°±0.2° and 29.2°±1.3° for 30° LF and 30° HF, respectively.

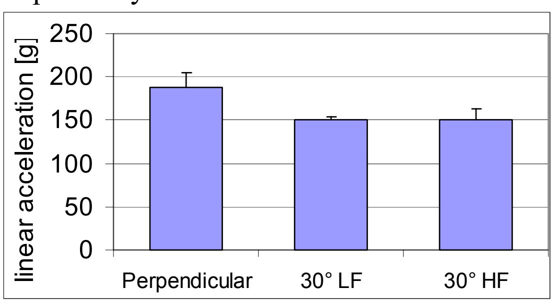

Figure 2: linear acceleration for three impact scenarios

Perpendicular impacts yielded an average angular acceleration of –506 ± 419 rad/s^2, with the negative value denoting counterclockwise acceleration. 30° LF and 30° HF yielded a significantly higher (clockwise) angular acceleration ($p<0.01$) of 5844 ± 265 rad/s^2 and 8846 ± 422 rad/s^2, respectively (Figure 3).

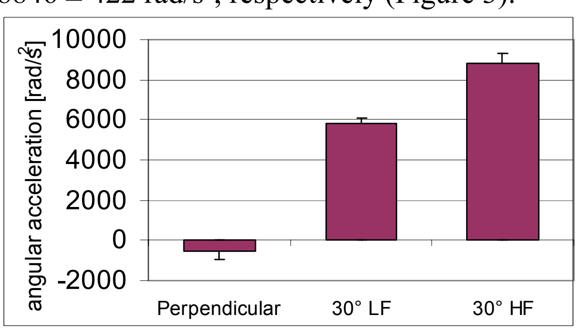

Figure 3: angular acceleration for three impact scenarios

Furthermore, oblique impacts on the LF surface induced significantly less rotational acceleration as oblique impacts on the HF surface ($p<0.01$).

DISCUSSION

Oblique impact tests can be conducted with relatively simple modifications of a standard drop tester to account for both, linear and angular acceleration during head impact simulation. At a later time we will implement two biaxial accelerometers, which are necessary to acquire the absolute angular acceleration independent of headform rotation.

The significant decrease in linear acceleration for oblique impacts may be attributed to energy transfer from linear to angular acceleration. This oblique impact test did not account for neck constraints and is therefore not intended to explore complex head/neck kinetics following the initial impact. However, it effectively captured the angular acceleration pulse generated during the initial impact. As such, this test addresses the consistent request for consideration of oblique impacts in helmet testing (Mills, 1997) in a simplicity that may be amendable for implementation into existing test standards. Such an advanced test standard is a likely prerequisite to trigger advances in helmet design aimed to protect the head from both, linear *and* angular acceleration.

REFERENCES

Waters, E.A., (1986). *Injury*, **17**(6), 372-375

Otte et al., (1999). *Contribution to Final Report COST 327*

Aare, M. and P. Halldin, (2003).*Traffic Inj Prev*, **4**(3), 240-248.

Mills, N.J., Gilchrist, A. (1997). *Int J Crashworthiness*, **2**, 7-23

ACKNOWLEDGMENTS

Funding provided by Legacy Foundation

OPTIMAL CONTROL SIMULATIONS OF STANDING LONG JUMPS WITH FREE AND RESTRICTED ARM MOVEMENT

Blake M. Ashby[1] and Scott L. Delp[1,2]

[1] Neuromuscular Biomechanics Laboratory, Mechanical Engineering Department, Stanford University, Stanford, CA, USA
[2] Bioengineering Department, Stanford University, Stanford, CA, USA
E-mail: bmashby@stanford.edu

Keywords: jumping, arms, optimization, computer simulation, modeling

INTRODUCTION

Using the arms during standing long jumps allows subjects to jump farther. Ashby and Heegaard (2002) showed that subjects were able to jump 37 cm (21%) farther with free arm motion than when arm motion was restricted. Two mechanisms have been hypothesized to account for this improvement. First, studies of the standing high jump have shown that arm swing generates a downward force on the body during the propulsion phase, which slows the shortening velocities of hip and knee extensors and allows for greater muscle torque production (Feltner et al., 1999; Harman et al., 1990). Second, studies of the standing long jump have suggested that when the arms are restrained the jumper must limit activation of the lower-limb extensors during the propulsive phase to eliminate excessive forward rotation that would preclude proper landing (Ashby and Heegaard, 2002). By contrast, swinging the arms during the jump can help alleviate excessive forward rotation about the center of gravity (CG) to better position the body segments for landing.

To clarify the role of arms in the standing long jump, we used optimal control theory to create simulations of maximum length standing jumps for free and restricted arm movement. The optimal control solutions with free and restricted arm movement were analyzed to explore the two hypothesized means for the improvement in standing long jump performance.

METHODS

The standing long jump was simulated with a 2-D five-segment (foot, shank, thigh, head-neck-trunk, arm) link model. The ankle, knee, hip, and shoulder joints were modeled as revolute joints and were actuated by joint torques. The magnitude of torque generated by the joint actuators was a function of the activation, the joint angle, and the joint angular velocity. The model for restricted arm movement was the same as that for free arm movement except that no shoulder torque was applied and the shoulder angle was fixed throughout the jump.

The optimal activations to generate maximum length jumps were found using a simulated annealing algorithm. The maximal jumps were determined for two different cases for jumps with both free and restricted arm movement. The objective for Case 1 was to maximize the horizontal position of the body's CG at landing without consideration for the landing configuration of the segments. The objective for Case 2 was to maximize the position of the toe at landing while maintaining an acceptable landing configuration (i.e., one that would allow subjects to land without falling down).

RESULTS AND DISCUSSION

Consistent with previous experimental findings, the simulated jump distances were greater with unrestricted use of the arms (compare upper and lower rows of Table 1).

Table 1: Horizontal CG Displacement

	Case 1	Case 2
Free arm motion	1.67 m	1.66 m
Restricted arm motion	1.37 m	1.29 m

The arm swing in jumps with free arm motion slowed the rate of hip extension during the propulsive phase, which allowed the joint actuator to generate more torque (Figure 1). The hip actuator was maximally activated between 0.12 s and 0.02 s before take-off in jumps with free and restricted arm motion, yet the torque generated was 60-80 N·m greater for the jumps with free arm movement over this time period. These results support the hypothesis that arm motion allows for greater torque production.

With free use of the arms, the CG displacement was 1.67 m when there were no requirements on the landing configuration (Case 1). The CG displacement was essentially equivalent (1.66 m) when an acceptable landing configuration was required (Case 2). This demonstrates that the landing requirement did not reduce activations during the propulsive phase of the jump because the arms were able to compensate for the excessive forward rotation of the trunk. When arm motion was restricted, the CG displacement was 1.37 m for Case 1 and 1.29 m for Case 2. This supports the hypothesis that to position the body segments properly for landing, the jumper must hold back during the propulsive phase in jumps with restricted arm movement.

Thus, our analysis of simulated standing long jumps suggests that both of the proposed mechanisms contribute to the greater jump distances with free arm motion.

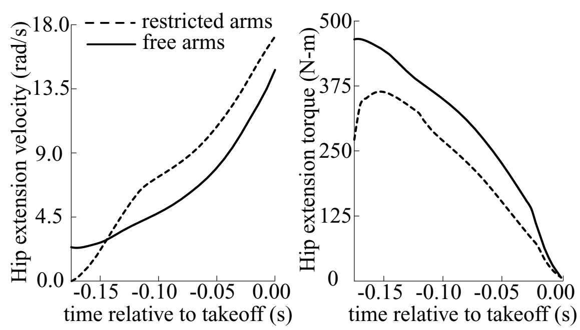

Figure 1: Hip extension velocities (left) and torques (right) just before take-off

REFERENCES

Ashby, B.M., Heegaard, J.H. (2002). *J. Biomechanics*, **35**, 1631-1637.

Feltner, M.E. et. al (1999). *J. Sports Sciences*, **17**, 449-466.

Harman, E.A. et. al (1990). *Med. Sci. Sports Exer.*, **22**, 825-833.

ACKNOWLEDGEMENTS

Blake M. Ashby has been supported by a William R. and Sara Hart Kimball Stanford Graduate Fellowship and a Veterans Affairs Rehabilitation Research & Development Fellowship.

3-D SCAPULAR-HUMERAL GEOMETRY IN SEATED DRIVER BRACED POSTURE

Vivek Khurana, Tim Nicklas, David Raymond, David Dainty, and Jeffrey Wheeler

Vector Scientific Inc., Los Angeles, CA, U.S.A.
E-mail: vkhurana@vectorscientific.com Web: www.vectorscientific.com

INTRODUCTION
Although clinical reports exist regarding shoulder injuries resulting from motor vehicle collisions, the anecdotal nature of these reports has not established the injury mechanics associated with specific shoulder pathologies. Seated driver braced posture, that is, firmly holding the steering wheel during various collision scenarios, has been hypothesized as creating a scapular-humeral geometry consistent with other known injury mechanism postures. To date, shoulder joint geometry for a driver braced posture or even the other established shoulder injury mechanisms, such as a fall onto an outstretched hand, have not been quantified. In order to proceed with scientific investigations of seated driver shoulder dynamics and specific shoulder injury mechanism potential, relative geometry in a seated braced posture need to be measured. The purpose of this study was to establish a measurement technique and to present preliminary results for scapular-humeral three-dimensional geometry in anatomical and seated driver static postures.

METHODS
Five male subjects participated (median age 27 years, height 1.79 m, and weight 82.8 kg). The top, right corner section of a standard driver seat back from a 1990 Mercury Topaz was cut away to allow access to the scapula. Seated driver position was standardized across subjects by placing third metacarpal heads on the steering wheel at 10 and 2 o'clock positions, initializing elbow angle at 65 degrees, and establishing a level plane between the acromion and lateral edge of the first metacarpal. Braced posture instructions included full extension of the elbows and co-contraction of applicable muscles. This created static equilibrium and stiffening across the wrist, elbow, and shoulder joints.

Bony landmarks and local coordinate systems were established based on the protocol set forth by the International Shoulder Group (Van der Helm, 1997). Palpation and demarcation of 14 bony landmarks were performed for all testing postures, and then digitized using a Faro Arm (*FARO Technologies, Inc.).* The 3-D location of the glenohumeral joint-rotation center was calculated using regression equations based on spatial orientations of the humeral epicondyles and 5 scapular bony landmarks (Meskers, 1998). BodyBuilder software (*Vicon Motion Systems, Inc.*) was used to process the digitized coordinate data.

Humeral line-of-action vectors originate at the midpoint of the lateral and medial epicondyles, terminate at the glenohumeral joint-rotation center, are normalized to humeral length and are computed in the scapular local coordinate system (millimeters) with the acromion (AC) serving as the origin. Euler rotation angles of the humerus were calculated using the scapular local coordinate system and the "x,y,z" rotation order convention. Data were averaged across all subjects for the two designated postures.

RESULTS AND DISCUSSION
Figure 1 shows the acquired bony landmark results and relative scapular-humeral geometry from two perspectives in the

scapular local coordinate system for the two designated postures. Table 1 lists the glenohumeral joint position (GH), humeral line-of-action vector (X,Y,Z), and Euler angle results for the two designated postures.

Figure 1

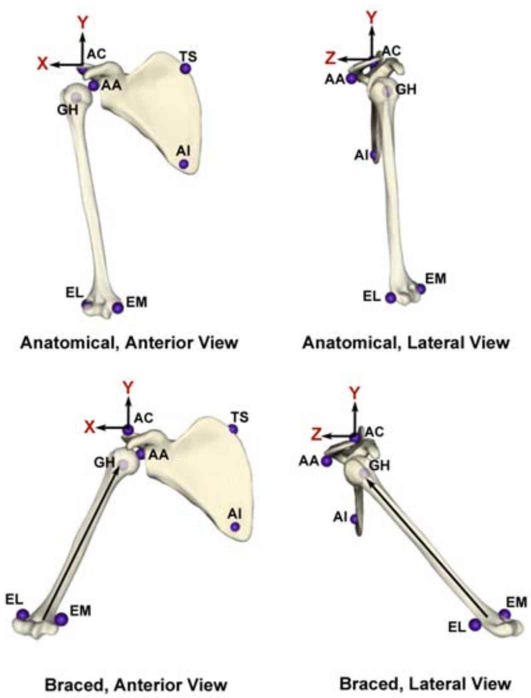

Forces and relative motion between the humeral head and glenoid cavity can result in trauma to various structures including the rotator cuff, sub-acromial bursa, glenoid labrum, or associated ligaments. The glenohumeral position and humeral line-of-action in a seated driver braced posture provides insight into the presence/ absence of injury mechanisms when loads might be transmitted axially through the humerus. Measurement limitations exist not in the instrumentation, but primarily during palpation and identification of bony landmarks.

Variations may also exist between genders, individual anthropometry, and vehicle and seat specific geometry. Therefore, it is recommended that these potential effects be considered during further testing. However, these techniques and preliminary geometry results can be utilized to establish initial physical and/or mathematical model parameters when incorporating applied shoulder dynamics to evaluate various injury mechanisms.

SUMMARY

A technique was described for quantifying scapular-humeral geometry and preliminary results were presented for seated driver bracing posture. Static glenohumeral joint rotation center position and the humeral line-of-action vector relative to the scapula will facilitate further investigation into shoulder injury biomechanics in motor-vehicle collisions when considering shoulder dynamics related to steering wheel loading.

REFERENCES

Van der Helm, Frans, *A standardized protocol for motion recordings of the shoulder*. Proceedings of the First Conference of the ISG. 1997.

Meskers, C. et al., *In vivo estimation of the glenohumeral joint rotation center from scapular bony landmarks by linear regression.* J. of Biomech. **31 (1998) 93-98.**

ACKNOWLEDGEMENTS

We would like to thank Jeff Squibbs of Faro Technologies, Inc. and Kristen Reed, of Vector Scientific, Inc., for their contributions to this study.

Table 1: GH joint rotation center (mm). Humerus line-of-action vector. Euler angles (degrees). Standard deviation in parenthesis.

Posture	**GH:x**	**GH:y**	**GH:z**	**X**	**Y**	**Z**	**Euler:X**	**Euler:Y**	**Euler:Z**
Anatomical	10(4)	-43(5)	-21(19)	-8(12)	-98(1)	-14(5)	-172(8)	-43(13)	-13(13)
Seated Braced	7(4)	-51(4)	-14(14)	33(16)	-74(7)	-56(5)	-131(11)	-35(8)	-7(20)

ESTIMATION OF FALLS RISK USING A NEURAL NETWORK MODEL BASED ON MEASURES OF GAIT AND BALANCE CONTROL

Michael E. Hahn [1,2] and Li-Shan Chou [1]

[1] Dept. of Exercise and Movement Science, University of Oregon, Eugene, OR, USA
[2] Movement Science Laboratory, Dept. of Health and Human Development, Montana State University, Bozeman, MT, USA
E-mail: chou@uoregon.edu

INTRODUCTION

Traumatic falls in the elderly are prevalent, debilitating and costly. Many studies have attempted falls prediction, with mixed results. Predictive models have included self-reports of imbalance, a history of previous falls, and clinical measures of daily living function, with prediction accuracy reaching 79% (Stalenhoef et al., 2002).

Of those models involving balance control, selection of predictive variables was restricted to static measures of posture (Maki et al., 1994), rather than dynamic measures of musculoskeletal function during activities where balance is challenged. A model that uses measures of muscular challenge, gait function and balance control as input may allow more accurate estimation of falls risk in the elderly.

For this study, neural network theory was selected to develop a model for mapping dynamic measures of gait and balance control onto estimates of falls risk in the individual. The purpose of this study was to test the application of this model in tasks of group categorization and risk estimation.

METHODS

The model consisted of two systems which used in tandem provide a relative distance measure from normal distribution, providing a scaled estimate of risk.

The first system, an artificial neural network (ANN) model, estimated the category of faller / non-faller, based on normalized electromyography (EMG) data from lower extremity muscles (gluteus medius, vastus lateralis, medial gastrocnemius), temporal distance (T-D) measures of gait (gait velocity, stride length, stride time, step width), and medio-lateral motion of the whole body center of mass (COM) during a low-level obstacle crossing condition (2.5% of body height). These measures were previously determined to have some association with balance impairment (Chou et al., 2003).

The ANN was a supervised, 3-layer, feed-forward design with Levenberg-Marquardt error-correction algorithm. Training set proportion was 0.7, randomly selected from a mixed sample of healthy elderly (n=19) and elderly with imbalance (n=10). The output resulted in categorization values between 0 (faller) and 1 (non-faller). The relative operating characteristic (ROC) was used to assess group categorization accuracy (Swets, 1988).

The second system discriminately classified relative risk that an individual would experience falls, based upon output from the first system. The ANN output for each individual case (X_1) was compared against a decision line (X_0; median value of the healthy sample). If X_1 was below X_0, it was inferred to be normal. If above X_0, the case was examined for its relative distance from the healthy group. Relative distance (D_r) was used as an index for risk estimation:

$$D_r = \frac{1 - x_1}{1 - x_0}$$

Higher values of D_r indicated lower risk of falls, lower values indicated higher risk of experiencing falls.

RESULTS AND DISCUSSION

Group categorization accuracy ranged from ROC values of 0.702 to 0.890. T-D input resulted in higher ROC values (0.848) than EMG (0.733) or COM (0.702). Categorization accuracy improved with the combination of input data types. Best overall accuracy was achieved with a combination of EMG and T-D data (Table 1).

Relative risk estimation using the distance metric D_r, produced varied results across the elderly subjects with imbalance, depending upon what types of input data were used to train the ANN. The distance metric values ranged between -1.50 and 1.50, with any values less than -1.00 indicating extremely high risk. When EMG and T-D were combined as input (best ROC value in group categorization), 90% of the individuals with imbalance were estimated to be at high risk of falls ($D_r < 0.20$) and 10% estimated to be at extremely high risk ($D_r < -1.00$).

Group categorization results confirmed the strength of using ANN models to map diverse inputs onto individual-specific outcomes. Accuracy achieved by this model surpassed that of previous studies (89% compared to 79%) which did not use dynamic measures of gait or musculoskeletal function (Stalenhoef et al., 2002). Results from the test of relative risk estimation revealed acceptable delineations of risk level across a variety of subjects with balance impairment.

SUMMARY

In combination, the two tasks evaluated in this study indicate the potential for accurately assessing individuals who may be at risk for experiencing falls; further estimating the severity of that risk, given the current gait function of each individual. If level of impairment is well estimated, many elderly individuals at greater risk of falls might be identified prior to traumatic fall events, thereby reducing the incidence and severity of falls in the elderly population.

REFERENCES

Chou, L-S. et al. (2003). *Gait Posture*, **18**, 125-133.

Maki, B.E. et al. (1994). *J. Gerontology*, **49**, M72-84.

Stalenhoef, P.A. et al. (2002). *J. Clinical Epidemiology*, **55**, 1088-1094.

Swets, J.A. (1988). *Science*, **240**, 1285-1293.

ACKNOWLEDGEMENTS

This study was supported in part by the NIH (AG 022204-01; HD 042039-01A1), the Oregon Medical Research Foundation, and the International Society of Biomechanics Dissertation Matching Grant.

Table 1. Accuracy results of the group categorization test.

Input Data Type	Training Goal	# Hidden Units	ROC
EMG	0.0001	20	0.733
T-D	0.001	5	0.848
COM	0.0001	5	0.702
EMG, T-D	0.001	5	0.890
EMG, T-D, COM	0.001	5	0.884

TRACKING NON-UNIFORM STRAIN OF THE AORTIC VALVE

Todd C. Doehring[1] and Ivan Vesely[2]

[1] Department of Biomedical Engineering, Lerner Research Institute, Cleveland Clinic Foundation, Cleveland, OH, USA, email: tcdoe@bme.ri.ccf.org
[2] Saban Research Institute, Los Angeles, CA, USA

INTRODUCTION

Understanding the response of soft tissues to applied loads is fundamental to developing accurate models of tissue behavior and for quantifying the effects of disease and surgical/pharmaceutical intervention. Historically, soft-tissue material properties have been estimated by assuming some form of constitutive relationship, and subjecting a specimen to uniaxial or biaxial tests. Strain data from these tests has generally been limited to clamp-to-clamp displacement, or at best, surface markers (dye, or particle based) arranged in a pattern, such as the 9-dot pattern used by Sacks [Sacks, 1993]. Surface-dot markers may be adequate for strain measurement in relatively homogenous materials, but for more complex soft tissue structures (i.e. the aortic valve) the possibility of local non-homogeneity can confound strain measurement, possibly leading to erroneous conclusions about the tissue response.

The purpose of this research was to determine the local strain patterns of aortic valve specimens under controlled applied loads using optical tracking methods. To achieve this, a novel marker-less feature-based tracking algorithm was applied to image data acquired using a custom-designed testing system. Marker-less feature tracking has previously been used to quantify deformations from MRI images [Bey, 2002].

METHODS

Five porcine aortic valve cusps were obtained from the abattoir, frozen, and thawed immediately prior to testing. Rectangular, circumferentially oriented, 5x15 mm coupons were cut from the center of the specimen using a guide. Specimens were mounted into a custom-designed mesostructural testing system (MSTS). The MSTS (Fig.1) consists of a biaxial loading frame, two computer controlled stepper motors (2 µm per step), and two load-cells accurate to 2 g. The entire system fits on a microscope stage. Testing is automated and controlled by custom software (Visual basic and C++) providing displacement control and synchronized measurement of loads and digital images (10 Hz frame rate). For this study, specimens were subjected to uniaxial extension in three stages, first to 100 g, then to 500 g, and finally to failure.

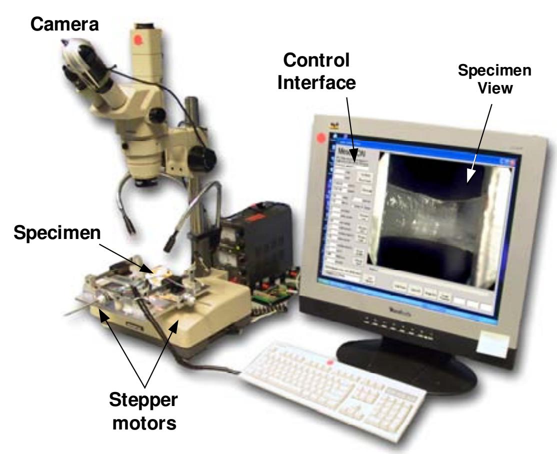

Figure 1: Mesostructural Testing System.

Sequential images were analyzed with a feature-tracking algorithm programmed in Matlab (Mathworks.com). The algorithm is based on a patch-matching method [Lucas-Kanade 1981]. First, initial points are computed using a Direchelet triangulation within the boundary of the specimen in the first image of a sequence (Fig. 2a). The nodes and triangular element connectivity are stored in arrays. The algorithm then analyzes the RGB intensity of a rectangular patch (typically 12x12 pixels) surrounding each node, computing the least-square fit of patches in subsequent images. If a "good" match (typical tolerance is 0.01) is *not* found, then the feature point is "lost". If a tracking point is lost (which rarely happens) then the current location is estimated using a cubic spline fit to the path of motion from the previous images. If any point is lost in two subsequent images, it is flagged and deleted. The current Matlab program requires approximately 2 minutes to track 100 points in a 30-image sequence using a personal computer with a 1.8 GHz processor. Accuracy of the tracking algorithm was validated using specimens inscribed with known grid/dot patterns. Validation results will be presented. From the measured local displacements, quantities such as Green's strain and strain energy density were computed.

RESULTS AND DISCUSSION

All five specimens exhibited highly non-uniform strain patterns under uniaxial load. Examining the strain energy for a typical specimen (Fig. 2), strain was localized to the lower middle and left areas of the specimen. Some areas of the tissue experienced almost no strain, despite the best efforts to achieve uniform loading. In 4 of 5 specimens, the area of highest local strain was coincident with the observed initiation of failure.

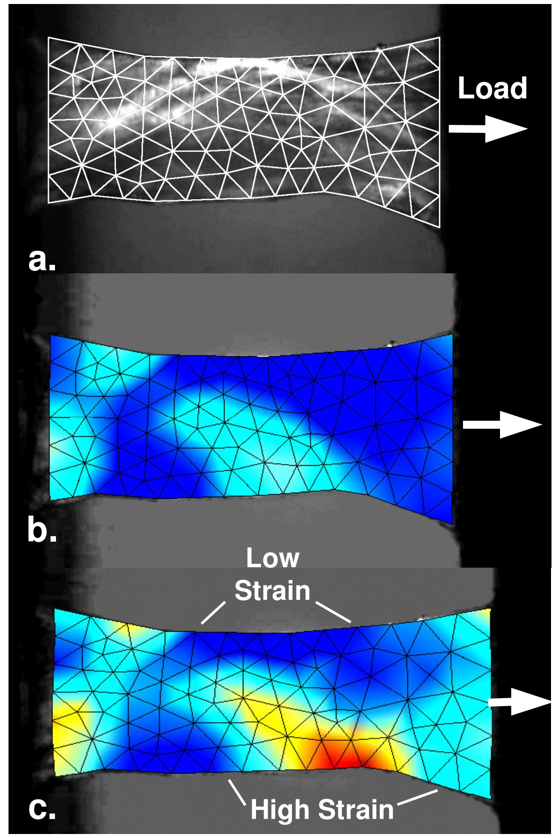

Figure 2: (a.) initial tracking mesh, (b.) local strain energy at 100g load, and (c.) at 500g load. Strain was highly non-uniform.

These results show the potential for highly non-uniform strains during uniaxial loading. If markers were used to measure strain in the specimen shown above, the results could strongly depend on the location of the markers.

REFERENCES

Sacks, M. S. and C. J. Chuong (1993). *J Biomech Eng* 115(2): 202-5.

Bey, M.J., Song, H.K., Wehrli F.W., Soslowski, L.J. (2002) *J Biomech Eng* 124(2): 253-8

Lucas, B.D. et al. (1981) Proc. DARPA Img. Understng. Wkshp. p121-30

ACKNOWLEDGEMENTS

We thank Michael Kahelin for MSTS design work. This study was funded by the DOD (# DA 170110673) and NIH (#HL57236).

EFFECT OF INTERNAL AND EXTERNAL KNEE ROTATION ON HOOP STRAIN IN THE MEDIAL MENISCUS

Kurt Bormann[1], Oliver Kessler[2], Savas E. Lacatusu[3], Tanja Augustin[3], Mark B. Sommers[3], and Michael Bottlang[3]

[1] University of Iowa, Iowa City, IA, USA; [2] Stryker Europe, Thalwil, Switzerland
[3] Legacy Biomechanics Laboratory, Portland, OR, USA, email: mbottlan@lhs.org

INTRODUCTION

Menisci contribute to load distribution, damping and stabilization of the knee. Meniscal tears are a common injury in the young and active population and can lead to posttraumatic osteoarthritis. Despite the high incidence and debilitating potential of meniscal tears, surprisingly few studies have addressed meniscus function and injury mechanisms. Meniscal tears are believed to occur during combined axial loading and twisting of the knee, and are most prevalent in the medial meniscus (Nielson, 1991). However, no study to date measured the effect of such combined axial and rotational loading on meniscus strain *in situ*.
This research examined the effect of combined axial loading and internal / external knee rotation on hoop strain in the medial meniscus of human cadaveric specimens with intact ligamentous and capsular constraints. Results of this study describe functional aspects of the intact meniscus, and hold implications for meniscal repair strategies.

METHODS

Four fresh-frozen human lower extremities (average age 74 years) were osteotomized 120 mm above and below the tibial plateau. Muscle tissue was removed, and the joint capsule and ligamentous structures were preserved. The diaphyses of each specimen were rigidly potted in base fixtures. Two arthrotomies of 1.5 cm length were made 1cm anterior and posterior to the middle of the medial collateral ligament in height of the joint line. Through these incisions, differential variable reluctance transducers (M-DVRT-3, MicroStrain Inc., Williston, VT) were placed in the peripheral border into the mid-substance of the medial meniscus. These DVRTs captured circumferential hoop strain ε_{AM} and ε_{PM} in the anteromedial and posteromedial medial meniscus, respectively. Each specimen was mounted in a knee loading simulator, driven by a bi-axial material test system (Instron 7800, Canton, MA) (Fig. 1).

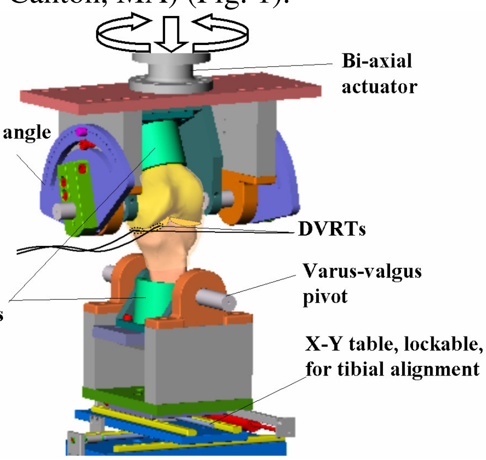

Fig. 1: Axial + rotational knee loading setup.

To ensure physiological loading, this setup accounted for anteroposterior and mediolateral tibial alignment, neutral varus/valgus alignment, and 60% medial / 40% lateral load distribution on the tibial plateau. Knee flexion angles could be fixed between 10° and 60° in 10° intervals. Each specimen was subjected to a loading sequence, starting with purely axial loading of 1,4 KN (2 x Bodyweight (BW)) at 140N/s under load control. While maintaining this axial load, 10° tibial internal rotation and 10° external tibial rotation were subsequently applied at 1°/s in displacement control. After testing at 30° knee flexion, the entire loading sequence was repeated from 10° to 60° flexion in 10° intervals. For each test, strain reports were extracted at 1,4 KN axial loading, and after 10° internal and 10° external tibial rotation. Effects of axial and rotation loading on meniscal strain were statistically analyzed with paired, two-tailed Student's t-tests at α=0.05.

RESULTS

Both, ε_{AM} and ε_{PM} yielded similar strain histories during the loading sequence (Fig. 2). No significant differences between ε_{AM} and ε_{PM} magnitudes were observed for any loading condition. Therefore, DVRT reports ε_{AM} and ε_{PM} were averaged as ε_{AVG}.

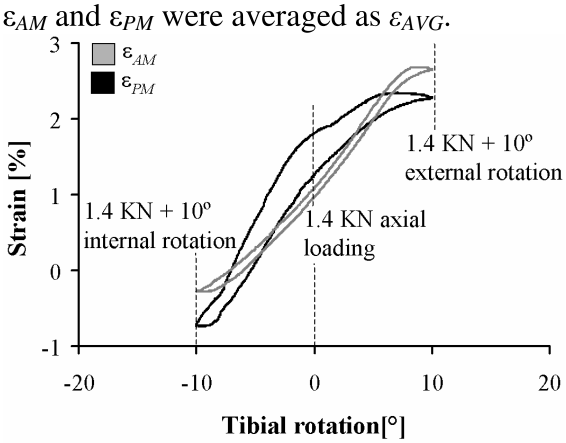

Fig. 2: Exemplary strain history of ε_{AM} and ε_{PM} for one load sequence at 30° flexion.

At 30° flexion, 1.4 KN axial loading induced meniscal hoop strain of ε_{AVG} = 0.9%±0.4%. External rotation resulted in a significant strain increase to ε_{AVG} = 2.1%±0.8% (p= 0.003). Internal rotation caused a decrease in ε_{AVG} to 0.2%±0.7%, however, this decrease was not significant. Knee flexion significantly affected meniscal hoop strain (Figure 3). At 10° knee flexion, 10° external rotation yielded ε_{AVG}=2.8%±1.3%. At 60° knee flexion, 10° external rotation induced significantly less strain, with ε_{AVG}= 1.3%±0.9%. This decrease of ε_{AVG} for increasing flexion angles was not significant for axial loading alone, or for axial loading and internal rotation. For knee flexion from 10° to 50°, combined external rotation and axial loading caused significantly higher strain as compared to axial loading alone.

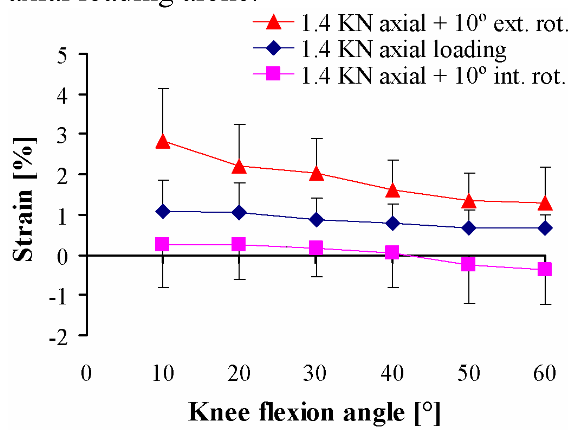

Fig. 3: Effect of knee flexion on ε_{AVG}.

DISCUSSION

This study documented for the first time strain in the medial meniscus under combined axial and torsional loading. Strain results for axial loading alone correlate with Jones et al. (1996), reporting medial meniscus strain in the range of 1.5% to 2.9% in response to axial loads of 3x body weight. The finding that meniscal strain can increase over two-fold during 10° external rotation holds implications for injury biomechanics and meniscal repair strategies.

REFERENCES

Nielson, A.B., et al. (1991). *J Trauma*, **31**, 1644-48.

Jones R.S. (1996). *Clin Biomech*, **5**, 295-00.

ACKNOWLEDGEMENTS

Supported by Stryker Europe

BIOMECHANICAL EXAMINATION OF INTERVERTEBRAL DISCS SUBSEQUENT TO BURST FRACTURE

Suneil R. Ramchandani[1], Manohar M. Panjabi[1], Peter A. Cripton[1], and Tyler J. VanderWeele[2]

[1]Biomechanics Research Laboratory, Yale Univ. School of Medicine, New Haven, CT, USA
[2] Department of Biostatistics, Harvard School of Public Health, Boston, MA, USA
E-mail: suneil.ramchandani@yale.edu Web: http://info.med.yale.edu/ortho/research.html

INTRODUCTION

Burst fractures are serious spinal injuries, as approximately 50-60% of burst fractures result in some type of neurological deficit. Although numerous studies have been conducted on injured vertebral bodies, there have been few investigations of intervertebral disc integrity following injury. The objectives of this study were to compare the biomechanical integrity of intervertebral discs immediately adjacent and next-adjacent to burst fractured vertebra, determine whether there were any localized differences within each disc, and if so, to determine whether localized differences within discs were similar in adjacent and next-adjacent discs.

METHODS

Ten fresh-frozen T11-L3 human cadaveric spines were used. Specimens were subjected to an axial impact (using a previously published protocol) to create a burst fracture at L1 (Wang et al., 2001). Post burst fracture, posterior elements were removed by a frontal plane cut through the pedicles. Four endplate-disc-endplate (T11-T12, T12-L1, L1-L2, L2-L3) units were prepared from each spine by two transverse cuts through the vertebral bodies (4mm above and below the endplates). Epoxy resin casts were subsequently molded onto each endplate. Twenty-five points were marked on casts for bending flexibility testing in 8 different planes (0°, 45°, 90°, 135°, 180°, 225°, 270°, and 315°) and at three radii (1cm, 2cm, and 3cm, **Figure 1**). A custom materials testing machine was used to measure the disc flexibility at these 25 points. A load was applied at a rate of 2 mm/sec to a maximum of 50 N. Three load cycles were completed, and the third cycle was used to calculate the flexibility of the disc at each specific point.

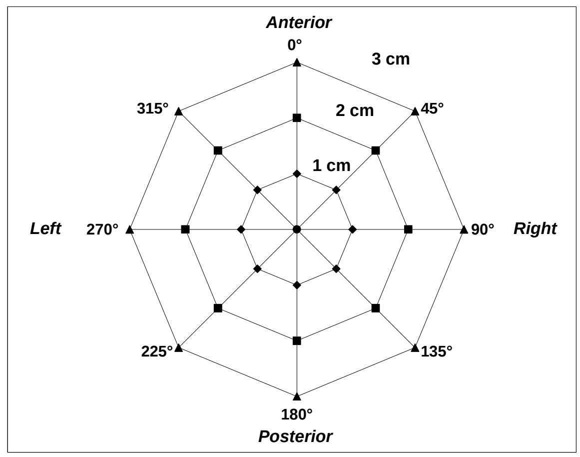

Figure 1: Radar Plot of Axial Compression Points on Intervertebral Discs

<u>Statistical Analysis:</u> A linear mixed model was used to examine the biomechanical integrity of intervertebral discs that were adjacent and next-adjacent to burst fractured vertebrae. Averages over eight different directional measurements (0°, 45°, 90°, 135°, 180°, 225°, 270°, and 315°) were taken for each disc and each radius (1cm, 2cm, and 3cm). Two sets of flexibility measurements for three different angles were averaged to give a localized comparison of the flexibilities of the anterior and posterior portions of the disc respectively (315°, 0°, 45° for the anterior and 135°, 180°, 225° for the posterior). Linear mixed models were

again used to assess localized differences within each disc across radii with fixed effects for location, radius, disc, and all two-way interactions.

RESULTS

Across all radii, the T11-T12 disc was significantly less flexible ($p<0.001$) than the other three discs (**Table 1**).

Effect	*Value*	*Flexiblity (µm/N)*	*Estimate*	*P-Value* *** (p<0.05)**
Disc	T11 - T12	24.08	-6.6866	**0.0034***
Disc	T12 - L1	31.20	0.1108	0.9608
Disc	L1 - L2	31.73	0.9687	0.6437
Disc	L2 - L3	30.76	0	-
Radius	1cm	19.94	-20.178	**<.0001***
Radius	2cm	28.04	-12.0624	**<.0001***
Radius	3cm	40.07	0	-

Table 1: Mean Flexibility Stratified by Radii and Disc

Further, the flexibility of each disc increased with the radius. The mean flexibility of each disc was higher at the anterior region of the discs (32.00 µm/N) when compared to the posterior region of the discs (27.94 µm/N). The differences between the anterior and posterior regions increased with the increase in radius (2.20 µm/N at 1cm, 4.24 µm/N at 2cm, 5.54 µm/N at 3cm), and most were statistically significant at larger radii (**Figure 2**).

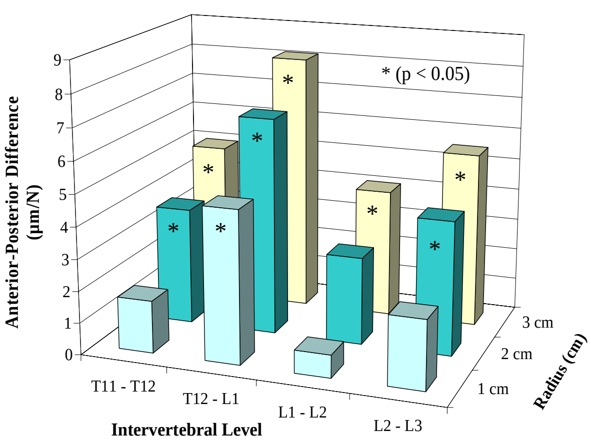

Figure 2: Comparing Anterior-Posterior Differences within Discs

Further, the average flexibility difference between the anterior and posterior portions was significantly greater in the T12-L1 disc than in any other disc.

DISCUSSION AND SUMMARY

Although compressive disc testing has been performed in the past, bending flexibility in multiple oblique planes has rarely been studied. This technique demonstrated localized differences both within and between discs. The most important finding of this study was that the flexibility of the T11-T12 disc was significantly less than the other three discs. As one may expect, there was also an increase in flexibility on the outer edges of the disc (radius = 3 cm) when compared to the innermost radius (1cm).

There were localized differences within each disc, showing that the anterior portion of each disc was more flexible when compared to the posterior portion. One finding suggests that the anterior portion of the upper adjacent disc (T12-L1) may be more susceptible to injury during burst fracture. The fact that the upper adjacent disc (T12-L1) had a higher flexibility difference between the anterior and posterior portions when compared to the other three discs suggests that not only were adjacent discs injured during high impact trauma, but also that the upper adjacent disc was injured to a greater extent. Clinicians should not only be aware of injuries to the vertebral body during burst fracture, but also of the potential damage done to the intervertebral discs.

REFERENCES

Wang, J.L. et al. (2002) *Spine*, **27**, 235-40

ACKNOWLEDGEMENTS

Funding was provided by the Yale University School of Medicine, Office of Research.

TIME-LAG RADIOGRAPHIC ASSESSMENT OF BRAIN DISTORTION DURING HEAD IMPACT SIMULATION

Jan F. Schöbel, Mark B. Sommers, and Michael Bottlang

Biomechanics Laboratory, Legacy Research & Technology Center, Portland, OR. mbottlang@lhs.org

INTRODUCTION

Assessment of brain deformation and shear during head impacts is of central interest to understand traumatic brain injury (TBI) and to investigate head protective technology. Over the past decade, high-speed photography has been employed to directly capture deformation in skull hemi-spheres filled with brain-surrogate. More recently, Hardy et al. (2001) were the first to measure spatial brain distortion inside a complete human cadaveric skull by use of high-speed stereoradiography. We proposed a time-lag radiography approach to directly capture brain motion relative to the skull during head impact simulation. Compare to high-speed stereoradiography, this approach may allow capturing brain motion with standard radiography equipment, and does not require subtraction of superimposed skull kinematics from brain motion. This study investigated the feasibility of time-lag radiography on a surrogate model of the skull and brain.

METHODS

Time-lag radiography captures motion of radiodense tracer particles on an X-ray sensitive medium in form of time-lag streaks. These streaks reflect the magnitude and direction of tracer particle motion during the duration of time-lag exposure. To simulate brain distortion relative to the skull, a surrogate model based on the design and materials of Ivarsson et al. (2000) was fabricated (Figure 1). This model reflects a 100mm thick parasagittal cross-section of the human skull made of aluminum, which accounts for prominent anatomical structures. Brain was substituted with a silicone gel (Sylgard 527, Dow Corning, Midland, MI), which was confined in the skull between Plexiglas caps. Radiodense tracer particles, consisting of 1.5mm Ø lead spheres enclosed in PE foam were placed in a 2cm grid in the mid-section of the brain surrogate. The density of the composite tracers (0.82g/cm^3) was less than that of the silicon gel (0.97g/cm^3) to trace region-specific brain deformation without influencing deformation. An 8x10inch imaging plate (ST-VI, Fuji-film, Burbank, CA) with 0.1mm pixel size was rigidly connected to the skull to capture brain distortion in absence of superimposed skull motion. The head model was confined to rotation around a transverse axis. Rapid angular acceleration of the head around this axis was induced with an impact pendulum.

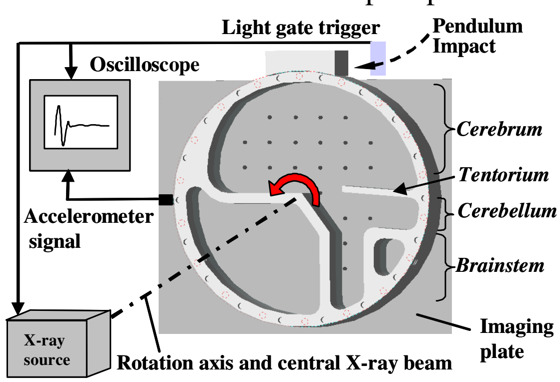

Figure 1: Time-lag radiography setup.

An X-ray source (GE AMX II, SOMA Tech., Cheshire, CT) was placed at 2m distance from the head model with its X-ray beam aligned with the rotation axis. The X-ray source was triggered by the pendulum by a light gate 10ms prior to impact. Time-lag exposure of 100ms duration at 110kVp and 10mAs during head acceleration projected time-lag streaks of tracer displacements relative to the skull on the imaging plate. Time-lag radiographs were enhanced by regional histogram equalization and analyzed with digital image analysis software (Matlab, MathWorks, Natick, MA) to quantify the magnitude and direction of time-lag streaks. Head acceleration was measured with an accelerometer (ACC103, Instrument Lab Inc., Oberlin, OH) and recorded with an oscilloscope (54603B HP, Palo Alto, CA) at 60kHz. Reproducibility of the technique was assessed on three time-lag radiographs, obtained at acceleration levels which did not yield irreversible deformation of the brain surrogate.

RESULTS

Pendulum impacts caused a head surrogate acceleration of 2380 ± 150rad/s^2 magnitude and 6.9 ± 0.6ms duration. Static projection of a reference lead sphere of 4mm Ø ensured that no relative motion between the imaging film and the skull surrogate occurred (Figure 2). Brain surrogate deformation relative to the skull was apparent by time-lag tracings with pronounced visibility of the initial position and reversal point of the makers. The smallest displacement magnitude was observed in the frontal lobe (C1, 0.5±0.2mm) (Table 1). The largest displacement occurred in the parietal lobe region (A4, 2.6±0.2mm). The direction of displacement was inhomogeneous and depicted a quasi-circular pattern. Deep layers (C1-6) translated in anterior and superior direction, while outer layers (A2-5, B4-6) translated in posterior and inferior direction.

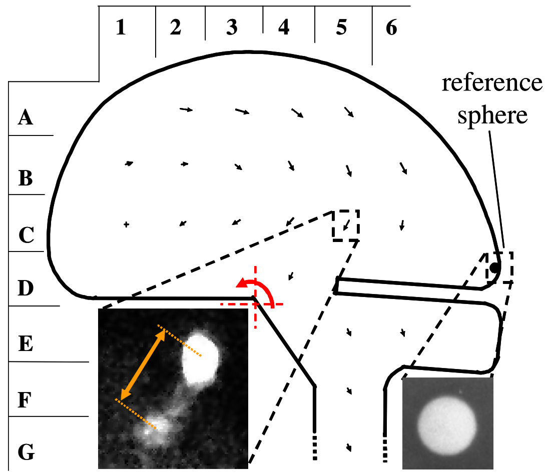

Fig. 2: Time-lag streaks and reference bead.

DISCUSSION

This study demonstrated feasibility and reproducibility of time-lag radiography for assessment of brain deformation during head acceleration. Results correlate to Ivarsson et al. (2002), who also noted opposing displacement patterns in outer brain layers compared to deep layers under rotational head acceleration. The present study was limited to 2.4 Krad/s^2 acceleration to preserve the surrogate brain for reproducibility testing. Due to absence of sampling rate limitations, this approach may be capable to capture brain deformation during injurious levels of rotational head acceleration in the range of 7-10 Krad/s^2.

REFERENCES

Ivarsson, J., et al., (2000), *J Biomech*, **33**, 181-189.

Hardy et al., (2001), *Stapp Car Crash J.*, **45**, 337-368.

ACKNOWLEDGMENTS

Supported by Legacy Foundation

Table 1: Region-specific displacement magnitudes

	1	2	3	4	5	6
A		1.8±0.1mm	1.8±0.2mm	2.6±0.2mm	2.2±0.1mm	
B	1.1±0.2mm	0.9±0.2mm	0.9±0.3mm	1.7±0.1mm	2.1±0.1mm	1.8±0.2mm
C	0.5±0.2mm	0.6±0.1mm	1.4±0.1mm	1.9±0.3mm	1.8±0.3mm	1.3±0.1mm
D				1.0±0.2mm		

THE ROLE OF HEAD STABILIZATION IN NECK AND TRUNK MOVEMENT DURING FOUR DIFFERENT LOCOMOTION TASKS

Gail F Forrest [1]and Ronita Cromwell[2]

[1]Kessler Medical Rehabilitation Research and Education Corporation, West Orange, NJ, USA
gforrest@ kmrrec.org
[2]Department of Physical Therapy, Center for Rehabilitation Sciences, and Sealy Center on Aging, The University of Texas, Medical Branch Galveston.

INTRODUCTION

Researchers have been investigating movement profiles of the head, neck, trunk, and lower limbs and the role of head stabilization during various activities since the 1960s (Murray, 1964). Previously, researchers have established that when the body moves, head position can be adjusted by: (a) the vestibulo-collic reflex (VCR), (b) the cervico-collic reflex (CCR), (c) vision, (d) higher order mechanisms, and (e) head in space movement.

Suggested strategies for head stabilization include:

1. The head remains stable in space as the body moves beneath it. (Di Fabio & Emasithi, 1997) Head displacements occur in anticipation of a change in the body's center of gravity. Head movement is independent of trunk movement.
2. The control of head stability is the cooperative interaction between linked body segments. There is a strong dependence between body segment coordination in the control of head stability (Cromwell, Newton, and Carlton, in press).

Investigators have also illustrated that intersegmental and gravitational torques (i.e., passive torques) can significantly contribute to the control of movement of the non weight-bearing, unrestrained limb segment (Schneider & Zernicke, 1991).

The purpose of this study was to determine if head stability (or control of head movement) was directly related to coordination of linked body segments during 4 different locomotion tasks.

METHODS

Fifteen participants (mean age 26.0 ± 2.0 years) participated in this study. Testing involved 4 repeated trials of different walking tasks where participants walked at their preferred velocity and cadence. The four walking conditions were: walking along a 10 meter walkway, walking down a 10-m platform declined at 10 degrees, walking up a 10-m platform inclined at 10 degrees and walking the length of a 10-m walkway wearing a weighted vest. The vest was weighted to represent 20% of total body and weights on the vest were placed at the center of mass of the trunk. Eight reflective markers were placed at the apex of the skull, the junction of the first cervical vertebrae and occiput (C1/occiput), the junction of the sixth and seventh cervical (C6/C7) vertebrae, and the junction of the fifth lumbar and first sacral (L5/S1) vertebrae. Sagittal plane kinematic data were collected at 60Hz using a Qualysis AB, 3-D motion tracking system.

The head, neck, and trunk linked system was modeled an unrestrained limb segment with three interconnected-planar segments where the head was most distal. The trunk was allowed to move freely to ensure that the resulting torques due to linear accelerations of the trunk were included in the equations of motion. At each joint, torques were partitioned into four categories: net joint, gravitational, intersegmental, and generalized muscle torques. Limb dynamics were calculated in the local moving plane, with calculation of orientation angles for each segment relative to the right horizontal. Inverse dynamic modeling (Schneider and Zernicke, 1991) was used to quantify the net, gravitational and intersegmental and the residual term (muscle torque) for the distal joints of the trunk neck and head segments. Net joint torque describes the joint motion. All torque data were inverted and appended to original torque data in order to filter the original data. These appended data sets were filtered using a low pass Butterworth filter with a cutoff frequency of 6 Hz (Winter, 1990).

Cross correlation functions (CCF) were also performed and provided analyses of time series data for head, neck, and trunk multi-segment movement. CCF were computed to statistically correlate trunk torques and head angular acceleration, neck torques and head angular acceleration, and head torques and head angular acceleration.

RESULTS AND DISCUSSION

For all walking tasks the analyses of the data indicated that the torques for head and trunk (an example shown in Figure 1) demonstrated there was an increase in extensor muscle torque at heel strike to counteract the increase in the gravitational and intersegmental torques. This pattern was bimodal for 100% of stride length.

Also the analyses showed that there was a significant difference for incline, decline and weighted vest walking compared to level walking for peak net, muscle and gravitational trunk torques (Table 1). Peak intersegmental torque for inclined walking was significantly less compared to level walking. Peak head net torque and peak head gravitational torque were significantly differently among four tasks ($\underline{F}$= 12.81, $\underline{F}$ = 4.28, $\underline{p}$< .05).

For all walking conditions the CCFs for trunk gravitational (and head angular acceleration) and neck gravitational torque (and head angular acceleration) were greater than all other CCFs (level: 0.89 ±0.11; 1.03 ±0.29; incline 0.87 ±0.11; 1.23±0.21; decline: 0.91±0.19; 1.03±0.21 weighted vest: 0.90±0.17; 1.15±0.21), and different from each other ($\underline{p}$ < .05). Changes in trunk and neck orientation generated changes in trunk and neck gravitational torque, and produced changes in trunk and neck motion. In summary, the analyses of the gravitational effects during the walking tasks indicates that it was through head intersegmental torque (i.e. mechanic interactions of connecting segments), and intrinsic motor control mechanisms that the trunk and neck segments were able to contribute to the control of head stability.

Table 1: Peak Trunk Torque Means

Segmental Torque	Level Walking	Decline Walking	Incline Walking	Weighted Vest
Net	0.14 ±0.06	0.20* ±0.07	0.18* ±0.10	0.22* ±0.14
Muscle	0.69 ±0.16	0.91* ±0.25	0.51* ±0.19	0.77* ±0.16
Gravitation-al	0.09 ±0.04	0.07* ±0.02	0.14* ±0.05	0.08 ±0.24
Interseg-mental	0.54 ±0.21	0.56 ±0.17	0.40* ±0.17	0.55 ±0.14

* ($\underline{p}$< .05): Normalized for body weight and segment length

SUMMARY

Results demonstrate that it is possible to model the head, neck, and trunk linked segment as three interconnected-planar segments to examine the coordination of linked body segments for the control of head stability. This study suggests that muscle, gravitational, and intersegmental torques at each of the three segments did integrate to determine segmental joint net torque and coordinate to control movement at the head, neck, and trunk.

REFERENCES

Murray, M. P., et al., (1967) *Physical Therapy,* **47**, 273-284.
Di Fabio, R. P., & Emasithi, A. (1997*),Physical Therapy*, **77**, 458-475.
Berthoz, A., & Pozzo, T. (1988). In B. Amblard, A. Berthoz, & F. Clarac. (Eds.), *Development, adaptation and modulation of posture and gait* (pp. **189-99**). Amsterdam:Elsevier Science
Schneider , K., Zernicke, R.F. (1991). *Advances in Engineeering Software*, **12**,123-128
Winter, D. A. (1984). *Human Movement Science*, **3**, 51-76.

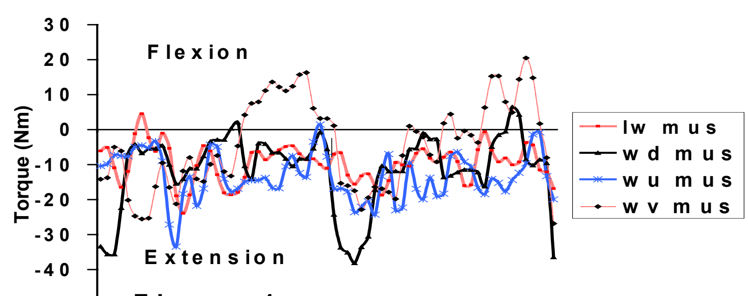

Figure 1: Muscle Torque Profiles

Cerebral Mechanics during traumatic brain injury

Binu Oommen [a], David Nicholson [a], Ted Conway [a], Alexandra Schönning [b], Irina Ionescu [c]

[a] *Mechanical Engineering, University of Central Florida, Orlando, FL, USA*

[b] *Mechanical Engineering, University of North Florida, Jacksonville, FL, USA*

[c] *Super Computing Institute, University of Utah, Salt Lake City, UT*

Introduction

Traumatic Brain injury (TBI) is a leading cause of death and disability among children and young adults in United States, with an estimated 1.5 million Americans sustaining TBI per year [1]. Pressure variations with respect to space and time cause brain tissue to deform beyond the level of recovery which is the elastic limit. The Cranio-Cerebral Complex is subjected to frontal impact. The shock wave propagating through the skull-brain complex as result of the external impact, causing coup and contre-coup lesions on the brain, are investigated in greater detail.

Modeling Methodology

The three dimensional model of the Cranio-cerebral complex is developed using MRI and CT data of a 20 year old male. The contours representing the individual slices of the skull, brain and Cerebro Spinal Fluid (CSF) are stacked together to form three-dimensional volumes, using packages MIMICS from Materialise, Geomagic from Raindrop and IDEAS from EDS. These surfaces are exported as International Graphics Exchange Standard (IGES) format to the mesh generation software, TRUEGRID, to build hexahedral meshes. The concept used for creating hexahedral meshes is to project simple block structures onto surfaces of interest such that the projected blocks conform to the shape of the actual geometry [2]. The final mesh of the brain generated from the basic block structure is shown in Figure 1.

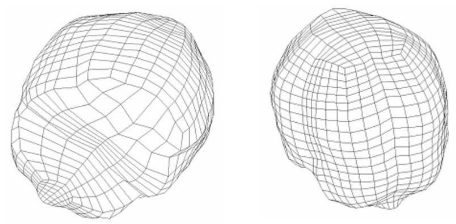

Fig. 1. Different views of the final mesh for the brain.

Boundary Conditions

The cranio-cerebral complex is subjected to impacts from the frontal direction as shown in Figure 2.

Tied and sliding contact conditions are used to define the skull - CSF interface and the CSF - brain in-

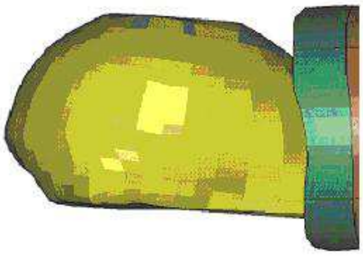

Fig. 2. Cranio-Cerebral complex subjected to frontal impact.

terface. A value of 0.2 is used to define the coefficient of friction between the sliding interfaces [3]. The velocity of 5.5 m/sec is imparted to the cranio-cerebral complex which impacts the stationary padded material.

Results and Discussion

The skull-brain complex is subjected to frontal impact and the simulated results compared with existing experimental results [4]. Figure 3 shows the coup stress contours at 6 mSec during the frontal impact.

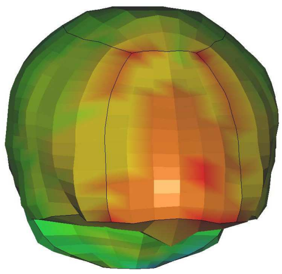

Fig. 3. Cranio-Cerebral complex subjected to frontal impact.

The contre coup stresses are concentrated on the occipital lobe of the cerebrum. This result is in accordance with the clinical studies, which shows the major portions of damage to the brain during a frontal impact to be the frontal and occipital regions of the cerebrum.

Conclusions

A hexahedral finite element model of the cranio-cerebral complex was developed. The intracranial pressure variations during frontal impact were analyzed the using explicit nonlinear finite element code, LS-DYNA. The coup and contre-coup pressure responses during the impacts were concentrated over a small region of the brain tissue which confirmed the clinical studies about the presence of focal lesions that were present on the brain tissue over a small region. It was also concluded that the location of maximum shear strain was always at the inferior portion of the brain stem. The developed finite element model of the cranio-cerebral complex can be used to understand the cerebral mechanics during various degenerative diseases such as hydrocephalus, edema etc. affecting brain.

References

[1] CDC, Traumatic Brain Injury In the United States, A Report to Congress, December (1999).

[2] TRUEGRID User's Manual Version 2.1.0, *XYZ Scientific Applications, Inc.*, (2001).

[3] Miller, R. T. et al, Finite Element Modeling approaches for predicting Injury in an Experimental Model of Severe Diffuse Axonal Injury, *SAE Paper no. 983154* (1998) 155–166.

[4] Nahum et al, Intracranial Pressure dynamics during head impact, *SAE paper number 770922* (1977)

COMPUTATIONAL MODEL OF A DYNAMIC ANKLE/FOOT SIMULATOR WITH ROUGH TERRAIN IMPEMENTATION

Loletta Wong and Lorin P. Maletsky

[1] Mechanical Engineering Department, University of Kansas, Lawrence, KS, USA
E-mail: chinger@ku.edu, maletsky@ku.edu

INTRODUCTION

One objective of this study was to create a computational model of a novel ankle/foot simulator to duplicate the loads and motions of daily human activities, specifically gait maneuvering over rough terrain. A second objective was to examine feedback from different foot-ankle-tibia (FAT) models. The types of FAT specimens that can be examined in the machine include below knee prostheses, robotic feet, and cadaver FAT.

Below-knee amputees can wear many types of prostheses during their daily activities. If a prosthetic could help them travel through rough terrain with the same ease as healthy people, they might be able to return to a similar activity level as before their injury. This study would aid in the development of lower limb prostheses to improve amputees' quality of life. Existing dynamic ankle/foot simulators have duplicated gait but have not studied feedback of the FAT on rough terrain, (Kim et al., 2001; Michelson et al., 2002; Monckton and Chrystall, 2002).

METHODS

A 6 degree-of-freedom (DOF) dynamic computational model was created in ADAMS (MSC Software Corporation, Santa Ana, CA) (Fig. 1). The degrees of freedom were required to simulate the different types of rough terrain and allow the FAT to respond appropriately. The design philosophy was that by controlling the motion and loads of the tibia and the floor, the appropriate loads and motions could be generated on the FAT. Joint at the tibia allowed medial-lateral translation and flexion-extension rotation. The floor contacts the foot to provide other desired motions and loads with anterior-posterior and vertical translations and internal-external inversion-eversion rotations.

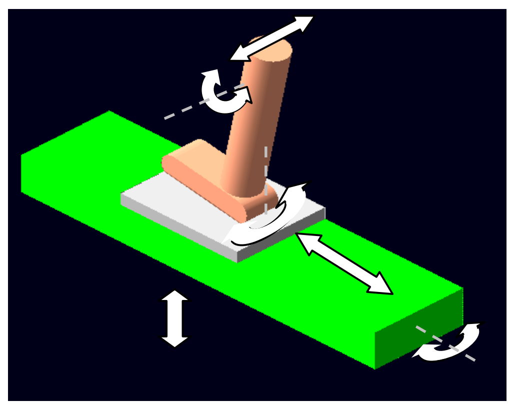

Figure 1 – Model of dynamic ankle/foot simulator. Arrows show DOF the machine.

To simulate stance, the tibia rotated according to a human gait flexion-extension angle profile measured in a gait lab. A ground reaction force profile was applied vertically through the floor. Friction between the foot and the floor allowed the floor to translate posteriorly with the foot during the stance phase. Two FAT were developed in this primarily study. They both had a rigid tibia and were symmetric about the sagittal plane with only compliance at the ankle in the three rotations. The ankle had three torsion springs with corresponding human ankle stiffness values. The models differed in the number of links for the foot. The 1-link foot had a single rigid link as the foot while the 2-links foot had two rigid links and torsion springs at mid-foot.

Preliminary rough terrain simulation was created by a 2.3cm diameter half sphere on the floor. Neutral position of the obstacle was at the center point under the foot. Forward was 3cm anterior to the neutral position while backward position is 3cm posterior. Two side positions were 1.25 and 2.5cm medially from the neutral position. Since the FAT were symmetric, lateral side would have the same magnitude of result.

Torques at the floor for the different cases during stance was measured to investigate the feedback of the effect of rough terrain and the ability of the machine to distinguish different FAT designs.

RESULTS AND DISCUSSION

The dorsiflexion-plantarflexion torque profile varied as the position of the obstacle changed (Fig. 2). Horizontal regions occurred when the foot was in contact with the obstacle alone. When the sphere was on the side, the foot had partial contact with the obstacle and the floor since no horizontal region occurred but had lower torque at mid-stance.

With the 2-links foot, the floor experienced a lower torque in dorsiflexion-plantarflexion during mid-stance and had a lower peak inversion-eversion torque (Fig. 3).

The results of this study successfully demonstrated that the ankle simulator was able to recognize the different position of the obstacle and distinguish between the two FAT designs as the measured torque in dorsi-plantarflex and inver-eversion direction varied during stance. Further investigations of different feedback with different designs of FAT and on other rough terrain are desired.

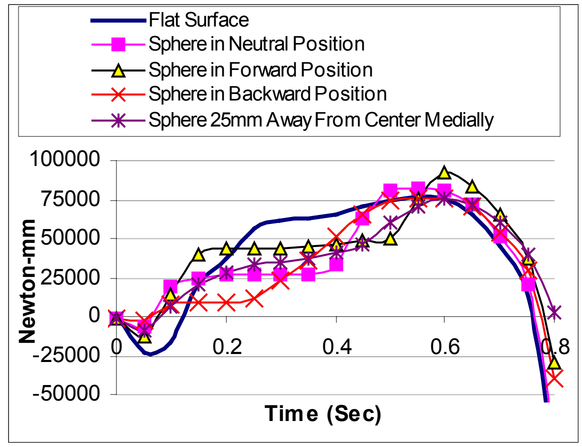

Figure 2 – dorsiflexion-plantarflexion torque measured at floor joint with different placement of obstacle. (One stance is about 0.78sec)

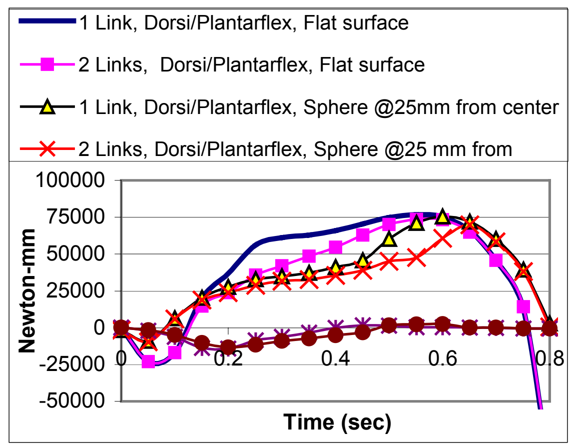

Figure 3 – Comparing torque measured at floor for 2 different leg-specimens on flat and rough terrain.

REFERENCES

Kim, K.J. et al., (2001). *Invitro Simulation Of The Stance Phase In Human Gait,* **5(2)**, 113-121.

Michelson, J.D. et al., (2002). *Kinematic Behavior of The Ankle Following Malleolar J. Motor Behavior Fracture Repair In A High-Fidelity Cadaver Model,* J of Bone and Joint Surgery, **84-A(11)**, 2029-38.

Monckton, S.P. and Chrystall, K., (2002). *Design and Development of An Automated Footwear Testing System,* IEEE, **4**, 3684-89

AGE INDUCED MECHANICAL PLASTICITY IN LOCOMOTION

Paul DeVita, Joe Helseth, Brandon Noyes, Michelle Pullen, Doug Powell & Tibor Hortobagyi

Biomechanics Laboratory, Dept. of Exercise and Sport Science, East Carolina University, Greenville, NC, USA; Email: DeVitaP@mail.ecu.edu

INTRODUCTION

While all muscles lose strength through the lifespan, lower vs. upper extremity (5) and distal vs. proximal muscles (4) have greater losses. Physiological and neurological changes underlie these patterns of force loss with age. Old vs. young skeletal muscle has a greater proportion of Type I vs. Type II muscle fibers and this reorganization is more pronounced in leg muscles (2,4) and distal vs. proximal muscles (3,6). Motor neuron apoptosis with age is followed by collateral sprouting in surviving neurons to re-innervate muscle fibers. Sprouting capacity however is inversely related to axon length such that more distal muscles have reduced re-innervation capability (7). These adaptations provide a physiological basis for our previous observation that old vs. young adults generate more torque and power with hip extensors and less with knee and ankle extensors when walking at the same speed (1). Based on these data we hypothesize that human aging involves a mechanical plasticity in locomotion that produces a distal to proximal shift in muscle function. Mechanical plasticity with age favoring proximal muscles may enable old adults to perform gait tasks with a control strategy better suited to their physiological and neurological traits. We investigate this hypothesis with the current study and purpose which is to compare lower limb joint torques and powers during ramp ascent and stair ascent in young and old adults.

METHODS

We measured ground forces and sagittal plane kinematics during ramp and stair ascent in 31 young and 26 old adults with mean ages of 21 +/- 3 and 74 +/- 5 years. All subjects were ostensibly healthy and were able to perform both tasks without difficulty. The ramp had a 10? slope and the stairs had a standard size of 19 cm and 27 cm height and depth. Walking speed was controlled in both tasks. Subjects ascended the ramp at 1.5 m/s the ascended the stairs at a pace 90 steps per minute. A timing system and a metronome were used to control speed. Inverse dynamics were used to compute lower extremity torques and powers. Torques were normalized to (%body weight x height) and powers to body mass. Areas under the extensor portions of the torque curves (extensor angular impulse) and the positive phases of the power curves (work) were derived and compared between age groups with separate t-tests for each task ($p<.05$).

RESULTS AND DISCUSSION

Young and old adults used joint torques and powers at all three lower extremity joints to perform stair and ramp ascent. The relative contributions of the individual torques and powers varied with age however. Old adults generated 30% more angular impulse and work with their hip extensors compared to young adults (both $p<.05$) to compensate for a 40% reduction in knee angular impulse and work during ramp ascent (fig 1). Identical relationships were observed in stair ascent. Older adults generated 85% more hip angular impulse and work and 76% less knee angular impulse and work compared to young adults (fig 2).

Age related adaptations were not as definitive at the ankle joint. Ankle angular impulses were not statistically different between age groups in the ramp task but old adults produced 15% less work with this angular impulse compared to young ($p<.05$). Ankle torques and powers were statistically identical between ages in stair ascent. It is possible that the action of making initial step contact with the forefoot and maintaining the center of pressure under the forefoot throughout stance may eliminate the possibility of altering the control strategy in this task.

These results supported the hypothesis and suggest a generalized mechanical plasticity in locomotion with age. Combined with our previous work on level walking, we have now observed in three distinct locomotion tasks that old adults use a distal to proximal shift in muscle function. They produce greater torque and power with hip extensors as a compensation for reduced knee and possibly ankle muscle kinetics.

REFERENCES

1. DeVita et al, (2000) *J Appl Physiol* 88: 1804-1811.
2. Grimby et al, (1982) *Acta Physiol Scand* 115: 125-134.
3. Jennekens et al, (1971) *J Neurol Sci* 14: 259-276.
4. Kirkeby et al, (2000) *Histol Histopathol* 15: 61-71.
5. Lynch et al, (1999) *J Appl Physiol* 86: 188-194.
6. Monemi et al, (1999) *Acta Physiol Scand* 167: 339-345.
7. Pestronk et al, (1980) *Exp Neurol* 70:65-82.

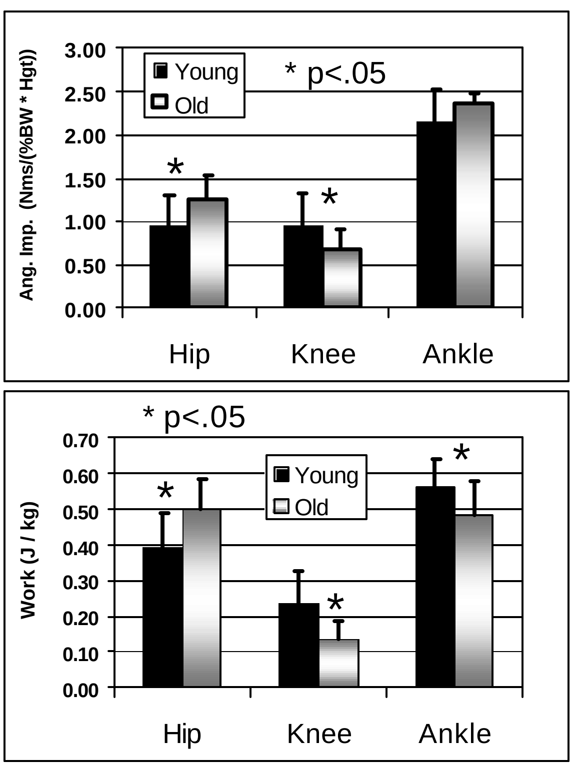

Fig 1. Angular impulse and work in ramp ascent.

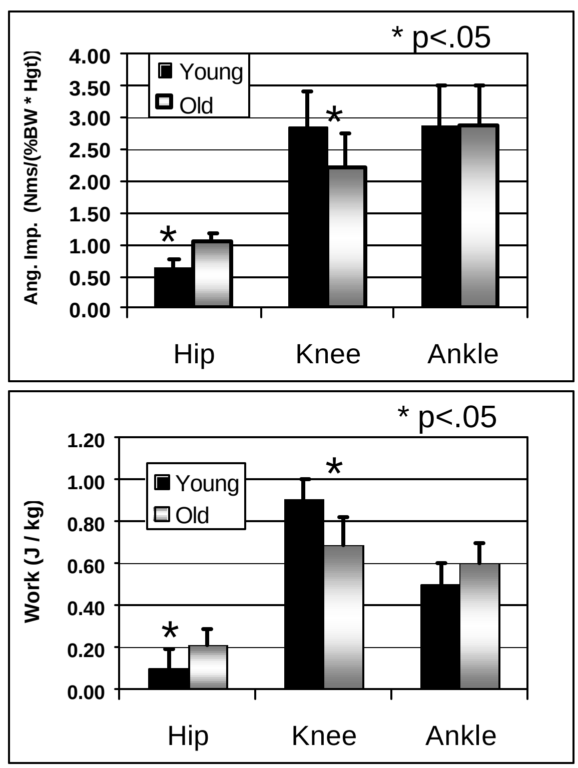

Fig 2. Angular impulse and work in stair ascent.

AUDIO BIOFEEDBACK OF TRUNK ACCELERATIONS IMPROVES BALANCE IN SUBJECTS WITH BILATERAL VESTIBULAR LOSS

Marco Dozza [1 2], Fay Horak [2], and Lorenzo Chiari[1]

[1] DEIS - Dept. of Electronics, Computer Science, and Systems – University of Bologna, Italy
[2] Neurological Science Institute – Oregon Health and Sciences University, Portland, OR, USA
E-mail: horakf@ohsu.edu Web: http://www.ohsu.edu/nsi/faculty/horakf/

INTRODUCTION

Humans maintain balance based on the information provided by the visual, vestibular and somatosensory systems. When one or more of these sensory systems is not available, balance is affected. Subjects who have lost vestibular function lack linear and angular head acceleration which provides information correlated with body sway and orientation with respect to gravity. Visual biofeedback of standing subjects' center of pressure (CoP) has been used successfully to reduce postural sway in stroke patients [Shumway-Cook et al, 1988]. Technological advances in the last few years provide new low-cost, portable sensors able to acquire kinematic data. In particular, data from accelerometers have been validated by comparing them with force plate and motion analysis data [Mayagoitia et al. 2002]. We developed an audio biofeedback device that encodes trunk biaxial accelerations into stereo sound. Our hypothesis is that audio information can improve balance in patients with profound bilateral loss of vestibular function (BVL).

METHODS

The ABF system we developed is comprised of a biaxial accelerometer, a laptop PC equipped with an acquisition card, and earphones. The accelerometer was mounted on the subject's back (L5) to sense the trunk accelerations. The laptop acquired the trunk accelerations and encoded those signals into

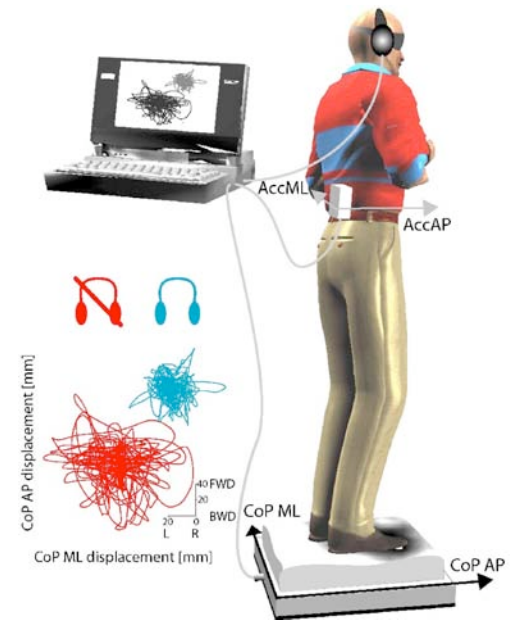

Figure 1 – Experimental set-up for ABF

a stereo sound. Anterior-posterior (AP) trunk acceleration was coded by changing the pitch of the sound. Medial-lateral (ML) trunk acceleration was coded by changing the balance of the volume between the stereo channels. The volume of both stereo channels increased whenever the subjects moved away from their initial stance position. While the subjects were within ±1 degree sway displacement from the initial position a low volume, pure, 400-Hz tone was provided through the earphones.
Nine BVL and 9 healthy subjects performed 6, 60-second trials in quiet standing. Subjects stood on 10-cm thick Tempur Foam with eyes closed to increase the importance of vestibular information for postural control. Trunk accelerations were

recorded as well as CoP displacement with a 100-Hz sample rate. From the CoP displacement we extracted 2 parameters: (1) root mean square distance RMS and (2) frequency containing the 95% of the spectrum power (F95%). We also divided the CoP spectrum into low (0.02 Hz - 0.5 Hz) and high (0.5 Hz – 5 Hz) frequencies. We computed the power for both frequencies bands. ANOVA was used to compare trials with and without ABF. We also determined correlation and coherence between CoP displacement and acceleration.

RESULTS AND DISCUSSION

ABF reduced CoP displacement and increased CoP bandwidth. RMS was reduced by ABF ($p<0.05$). RMS was reduced more in BVL (23%) than in control (16%) subjects. ABF increased F95% by 9% in BVL and by 8% in control subjects ($p<0.05$). ABF reduced both high and low frequencies power in BVL subjects ($p<0.05$). ABF reduced only low frequencies power in control subjects ($p<0.05$). The correlation between AP-trunk acceleration and AP-CoP displacement was highly significant ($r=0.88$, $p<0.01$). The coherence between AP-trunk accelerations and AP-CoP is shown in Fig. 2.

The larger RMS reduction for BVL than control subjects while using ABF supports our hypothesis that ABF effectively substitutes for the lack of vestibular information. The increasing F95% while using ABF suggests that ABF induced more postural corrections, i.e. augmented the postural control. Healthy subjects use ABF to control slow drift of their postural set point whereas BVL subjects also use ABF to improve high frequency postural corrections. The high correlation and coherence between trunk acceleration and CoP displacement, especially at the low frequencies, suggests trunk acceleration is a

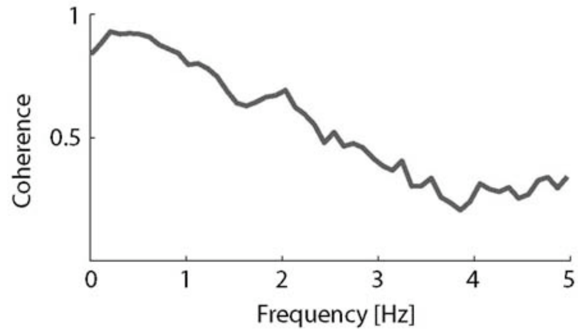

Figure 2 – Coherence between trunk accelerations and COP displacement.

good substitute for CoP displacement for development of biofeedback devices.

SUMMARY

An accelerometry-based ABF system was tested on BVL subjects during quiet stance on foam with eyes closed. Analysis of CoP showed that: (1) ABF reduces sway of BVL subjects more than controls; (2) BVL subjects reduced both high and low frequencies power. These results support our hypothesis that accelerometry-based ABF information can substitute for lack of vestibular information in BVL subjects.

REFERENCES

Shumway-Cook A, Anson D, Haller S. (1988). *Postural sway biofeedback: its effect on reestablishing stance stability in hemiplegic patients*. Arch Phys Med Rehabil, **69(6)**, 395-400.

Mayagoitia R. E., Nene A. V., and Veltink P. H. (2002). *Accelerometer and rate gyroscope measurement of kinematics: an inexpensive alternative to optical motion analysis systems* J. Biomech., **35**, 537-542.

ACKNOWLEDGEMENTS

Funding sources comes from NIH DC01849.

Constitutive Modeling of Vascular Constructs: A Modified Burst Pressure Method

Kathryn A. Lagerquist[1,2] , Samuel Jensen-Segal[1], Sean J. Kirkpatrick[2], Monica T. Hinds[2], and Kenton W. Gregory[1]

[1] Oregon Medical Laser Center, Portland, OR, USA
[2] Dept. of Biomedical Engineering, Oregon Health & Science University, Portland, OR, USA
E-mail: Kathryn.Lagerquist@providence.org

INTRODUCTION

Many small diameter vascular grafts are currently under development. A method of analyzing their mechanical properties must be instituted as a standard to enable meaningful comparisons between vascular grafts and native vessels. Constructs take many forms such as amorphous and fibrous protein conformations, and composite materials [Niklason, 1999, L'Heureux, 1998]. Native vessels are incompressible, due to the high water content, and heterogeneous materials comprised of a complex orientation of cells, elastin, and collagen. This proposed testing scheme is reasonable, because the final proposed configuration, i.e. tubes, is constant between constructs.

Burst pressure testing, a standard method used to evaluate vascular constructs, provides ultimate failure stress, but not the elastic modulus. Matching moduli of the graft to the native vessel influences the ultimate success of a graft [Kidson, 1978].

MODEL DEVELOPMENT

Cylindrical vascular constructs are modeled as a two dimensional continuum that behaves as a pseudoelastic material. Analysis must be made sufficiently far from the ends to negate the edge effects created by cannulating ends of the vessel. Bulging of the cylinder occurs, but the region analyzed will be sufficiently far from the ends to assume negligible bulging. The wall volume of the material is conserved during loading, therefore the determinant of the deformation matrix **F** (Equation 1) is equal to 1. X refers to the deformed state and x refers to reference state.

$$\mathbf{F} = \begin{bmatrix} \frac{\partial x_1}{\partial X_1} & \frac{\partial x_1}{\partial X_2} & \frac{\partial x_1}{\partial X_3} \\ \frac{\partial x_2}{\partial X_1} & \frac{\partial x_2}{\partial X_2} & \frac{\partial x_2}{\partial X_3} \\ \frac{\partial x_3}{\partial X_1} & \frac{\partial x_3}{\partial X_2} & \frac{\partial x_3}{\partial X_3} \end{bmatrix} \qquad [1]$$

The stretch ratios (λ_i) are defined by Equation 2.

$$\lambda_z = \frac{L_z}{L_{zo}}; \lambda_\theta = \frac{r_i}{r_{io}} \qquad [2]$$

Strains are derived in terms of Green's Strain (Equation 3).

$$E_{zz} = \frac{1}{2}(\lambda_z^2 - 1); E_{\theta\theta} = \frac{1}{2}(\lambda_\theta^2 - 1) \qquad [3]$$

Average Cauchy stress values (Equation 4) can be derived directly from the pressure diameter values acquired during the burst test. P_o is the pressure outside the vessel, P_i is the internal pressure, r_i is the inner radius, r_o is the outer radius, and t is the wall thickness.

$$\sigma_{\theta\theta} = \frac{P_o r_o - P_i r_i}{t} = -\frac{P_i r_i}{t}$$
$$\sigma_{zz} = \frac{P_i r_i}{2t} \qquad [4]$$

Kirchhoff stresses, related to Cauchy stresses by the stretch ratio, are conjugate to Green strains and can therefore be used to develop the constitutive model formulation. The strain energy density function is defined in Equation 5. This is simply an example of one possible fitting regimen. A nonlinear least squares fitting algorithm such as a modified Marquarts's algorithm should be used to attain the strain energy density function constants [Fung, 1993]

$$\rho_o W = \frac{C}{2}(e^Q - 1)$$
$$Q = a_1 E^2{}_{\theta\theta} + a_2 E^2{}_{zz} + 2a_4 E_{\theta\theta} E_{zz} \qquad [5]$$

MODEL VERIFICATION

The test setup uses a mandrel to hold the test specimen. The mandrel is equipped with a linear displacement control, which enables fine control and measurement of axial displacement. A transducer mounted at the fixed end of the mandrel measures axial force. A pressure transducer is located inline with the flow loop to measure internal construct pressure. A syringe pump is used to control internal hydraulic pressure. P_o is zero in all test conditions. Circumferential strains are dynamically measured non-invasively with a video dimension analyzer (VDA). Arterial constructs are modeled as cylinders with z, θ, and r, correlating to the longitudinal, circumferential and radial directions, respectively.

Two testing methods are proposed. First, the longitudinal stretch ratio is fixed at physiologic values, between 1.4 and 1.6, for native vessels. Once this value is set the transmural pressure of the vessel will be increased until failure occurs. The second testing scheme holds transmural pressure at zero, relative to atmospheric/gage pressure, while varying the longitudinal displacement.

DISCUSSION

This model can be expanded to three dimensions when shear and bending forces are assumed to be zero. This application is easily employed and can be built inexpensively in most laboratories.

The strain energy density functions derived from these experiments describe the behavior of the material along a single line of a more complex surface. Several lines will be determined and plotted to define a strain energy density surface.

SUMMARY

A method was developed to use a modified burst pressure testing system to derive a strain energy density function for vascular constructs. The method uses two basic testing schemes. To fully understand the material in the physiological ranges several conditions should be tested to attain a map or surface strain energy density function for the material. This scheme gives researchers an affordable unified tool for the testing of vascular grafts.

REFERENCES

Niklason LE, et al. Science.1999. 284(5413). 489–93.
L'Heureux N, Paquet S, Labbe R, Germain L, Auger FA. FASEB 1998. 12. 47-56.
Kidson, I.G., and Abbott, W.M. Circulation, 1978. 58, 1-4.
Fung, Y.C. New York, NY, Springer-Verlag, 1993. 321-384.

ACKNOWLEDGEMENTS

This work was supported by a grant from the Department of the Army, Grant No. 17-98-1-8654 and does not necessarily reflect the position or policy of the government. No official endorsement should be inferred.

Role of Skin Material Properties in Determining the Sensitivity of Stretch-Sensitive Cutaneous Mechanoreceptors

Peter Grigg

Department of Physiology University of Massachusetts Medical School Worcester MA 01609 USA E-mail: Peter.Grigg@umassmed.edu

Rotating a joint stretches the soft tissues on one side of the joint and relaxes them on the other side. All the soft tissues around joints contain mechanoreceptor neurons that are activated by stretch. Thus stretch responses of mechanoreceptors potentially contain information about joint displacements or movements, and are therefore of interest in studies of motor control. In this presentation I shall describe properties of mechanoreceptor (in particular cutaneous) afferent neurons from skin overlying the knee, that are activated by stretch. The results are all derived from in vitro studies of isolated, innervated, hairy skin from rats and mice.

Skin is a biaxial material, and stretching it creates biaxial states of tensile, compressive, and shear stresses and strains. A key question is, which of these states causes activation of neuronal mechanoreceptors? This is a point of some interest, since it is widely accepted that at a molecular level, displacements (i.e., strains) must be the key variable. After all, molecules have to change shape in order for their function to be altered, implying a dependence on strain. Yet many macroscopic experiments have shown that mechanoreceptor responses are more closely associated with stress variables than strain variables [1]. I shall present data that shows that many macroscopic variables are associated with spike responses, but that spike responses are most strongly associated with stress variables. In order to determine if stress or strain variables are more strongly associated with spikes, the experimental design has to decouple stress and strain. Stress and strain have been decoupled by using dynamic stimuli, which causes a phase shift between stress and strain in viscoelastic materials. Using dynamic stimuli also allows for studying rapidly adapting (RA) mechanoreceptors, which are the most abundant type found in hairy skin. The strength of associations between stochastic spikes and continuous stimulus variables has been determined using logistic regression analysis [2].

As in previous studies, neuronal responses have been found to be most strongly associated with stress rather than strain variables. Spike responses were strongly associated with the rate of change of tensile stress, and more weakly associated with tensile stress. Spikes were weakly associated with the rate of change of tensile strain, and there was no association between spikes and tensile strain. There was only a weak association at all between spikes and incremental strain energy. There were significant memory effects associated with these variables [2].

It is widely believed that the viscoelastic material properties of soft tissues influence the dynamic response of mechanoreceptor neurons that innervate them. In order to test this hypothesis, experiments were done using mutant mice whose skin had different viscoelastic mechanical properties. We stretched the skin and measured both skin viscoelasticity (characterized using the complex compliance) and the association between spike responses and various mechanical variables. The hypothesis predicted that mechanoreceptor neurons in the skin with the biggest viscous response would have the biggest dynamic response. However the results only weakly confirmed this hypothesis. Neurons recorded in more viscous skin had greater associations with some dynamic components of stimuli, but not with others [3].

Another way of testing whether soft tissue properties influence a mechanoreceptor's response properties is to use biaxial stretch stimuli. The skin samples we used were orthotropic, and it might be hypothesized that mechanoreceptors would be differentially sensitive to stretch along the skin's principal axes. However, applying identical stress stimuli along the 2 directions revealed that neuronal responses did not differ according to the direction of stretch [4].

Finally we wished to determine whether spike responses from mechanoreceptors were associated with shear stress in the skin. Not having a method to directly manipulate shear stress, we relied on the fact that the maximal level of shear stress along planes other than those actuated is proportional to the difference between the tensile stresses along the two directions of stretch. According to this model, shear stress would be minimal when a biaxial stretch stimulus is symmetrical (ie., when stresses of equal magnitude are applied along both directions). Conversely, the model predicts that shear stress would be maximal when biaxial stretch is asymmetrical (ie., when stresses of different magnitude are applied along the 2 directions). We confirmed this hypothesis although some aspects of the findings did not fit a shear stress model.

It is necessary to be rather careful in extrapolating results from rats and mice to humans. On the one hand, mechanoreceptor neurons in hairy skin are similar between rats and mice and other species. On the other hand, rodents have very loose, soft skin on their hindlimbs. Since mechanoreceptors are driven mainly by stress-related stimuli, this means that by definition rather large displacements will be required before stresses are high enough to activate neurons. In fact, rat cutaneous afferents are activated by stretch stimuli only at stresses that would be observed when the hindlimb was at or near its limit of movement.

Summary.

Stretch sensitive rapidly adapting mechanoreceptor neurons from the skin overlying the knee joint in rodents respond primarily to tensile stresses caused by stretch, although there may be a role for shear stress in causing spike responses. The material properties of the skin itself appear to contribute rather minimally in determining the response properties of neurons. Dynamic responses of neurons are quite similar when recorded in skin of differing viscosity. The skin is orthotropic but the response of rapidly adapting mechanoreceptor neurons is not. At least in rodents, the types of stimuli required to activate rapidly adapting afferents would seem to occur rather infrequently.

Acknowledgements. This work was supported by NIH grant NS-10783.

References.

1.Grigg, P.. J Neurophysiol, 1996. **76**: p. 2886-95.
2.Del Prete, Z., S.P. Baker, and P. Grigg. J Neurophysiol, 2003. **89**: p. 1649-59.
3. Grigg, P., D.I. Robichaud, and Z. Del Prete, Z. J Neurophysiol, In PresS 10.1152. /jn.01033.2003.
4. Grigg, P. and D.I. Robichaud. J Neurophysiol, In presS 10.1152 /jn.01045.2003.

THUMB KINEMATICS WITH NON-ORTHOGONAL AND NON-INTERSECTING AXES OF ROTATION MAY BE NECESSARY TO PREDICT REALISTIC ISOMETRIC THUMBTIP FORCES IN MULTIPLE DIRECTIONS

Veronica J. Santos [1] and Francisco J. Valero-Cuevas [1,2]

[1] Neuromuscular Biomechanics Laboratory, Cornell University, Ithaca, NY, U.S.A.
[2] The Hospital for Special Surgery, New York, NY, U.S.A.
E-mail: vjl4@cornell.edu   Web: www.mae.cornell.edu/nmbl

INTRODUCTION

Manipulation depends on the thumb's ability to produce well-directed forces of sufficient magnitude. We currently lack a model of the thumb that can realistically predict thumbtip forces in 3D, and the coordination patterns that produce them (Valero-Cuevas, et al., 2003). This may be because the assumed *model structure* is not able to reproduce functional outputs, and/or because the search for adequate *model parameter values* has been unsuccessful. Understanding the inherent biomechanical abilities of a chosen *model structure* is a necessary first step to modeling the thumb for clinical use and studies of neural control of the hand.

METHODS

We investigated whether: (1) adjusting the 50 musculoskeletal parameters (e.g., moment arms, hinge location and orientation) of a five-hinge serial linkage *model structure* (Fig. 1) can predict maximal, voluntary, isometric thumbtip forces measured experimentally; and (2) inputting the measured fine-wire electromyogram (EMG) data into these models produces well-directed forces (within 16° of the desired direction). Using a Bayesian approach that considers model parameters as random quantities instead of single unique values, we found the range of all possible functional outcomes for a specific *model structure* resulting from the natural anatomical variability of the thumb.

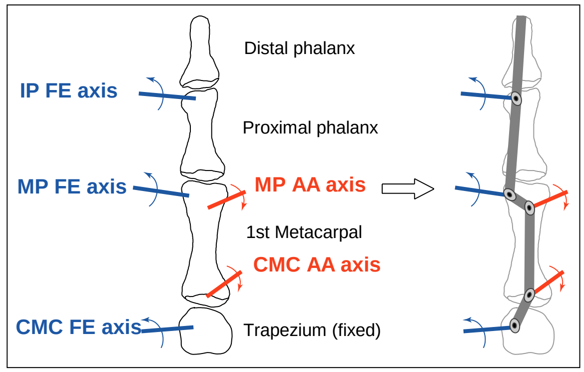

Figure 1: Thumb kinematics modeled as a serial chain of five hinges (Giurintano, et al., 1995). (*CMC=carpometacarpal, MP=metacarpo-phalangeal, IP=interphalangeal*)

We used a Markov Chain Monte Carlo (MCMC) algorithm to explore this 50-D parameter space (Gilks, et al., 1996). We represented each parameter by a statistical distribution based on published or measured data (Santos, et al., 2003). The MCMC algorithm stochastically explored the *model parameter space* using 10 independent Markov chains to find the model parameter distributions that drove input/output predictions towards a least-squares fit to thumbtip force/torque measurements. Chain convergence was determined by the Gelman-Rubin statistic (Gilks, et al., 1996), which indicates when all chains can be pooled for drawing inferences. Converged chains were extended such that 20,000 pooled iterations were achieved.

The exploration was driven by an "inverse" linear programming (LP) solution predicting maximal biomechanically feasible thumbtip forces. For a given thumb posture, static force production reduces to a matrix multiplication (Valero-Cuevas, et al., 2003), making LP appropriate for predicting the limits of performance. We then performed "forward" simulations using fine-wire EMG measurements, instead of inverse LP solutions, to evaluate the input-to-output behavior of the models.

RESULTS AND DISCUSSION

The distributions of parameter values to which all chains converged are those that can produce well-directed thumbtip forces in 3D for this robotics-based model structure. Since MCMC methods perform an exhaustive search of the *parameter* space (Gilks, et al., 1996) there is *no other* sub-region in the 50-D parameter space that would fit the measured force data better. Our MCMC approach has the important benefit of rigorously predicting the functional consequences of natural anatomical variability of the thumb.

We found model-predicted maximal thumbtip forces to be lower than those measured (Table 1), but closer to the measurements compared to the predictions of a simpler kinematic model with mutually orthogonal and intersecting axes of rotation at the CMC and MP joints (Valero-Cuevas, et al., 2003). The five-hinge serial linkage model predicted maximal palmar forces comparable to those predicted by the simpler model and improved upon predictions in the dorsal and distal directions for both pinch postures.

Table 1: Comparison of thumbtip force magnitudes between experimental measurements (n=4) and model predictions (20,080 pooled iterations). We observe improvements in model predictions over those from a simpler kinematic model (Valero-Cuevas, et al., 2003) in the dorsal and distal force directions for both pinch postures.

Pinch-type	Force dir.	Expt.		Model		Expt:Model Mean ratio
		Mean	Std	Mean	Std	
Key	Palmar	54.4	26.0	14.0	7.4	3.9
	Dorsal	10.7	3.0	9.0	1.9	1.2
	Distal	58.2	32.3	96.1	10.7	0.6
	Radial	21.5	9.7	5.7	3.1	3.8
	Ulnar	16.9	2.9	2.2	1.2	7.7
Opposition	Palmar	46.3	34.9	11.1	4.7	4.2
	Dorsal	10.8	3.2	7.2	2.6	1.5
	Distal	54.3	43.5	25.2	13.6	2.2
	Radial	22.2	8.3	8.1	2.8	2.8
	Ulnar	25.8	13.5	1.8	1.4	14.0

However, it is reasonable to consider increasing the PCSA values (collected from elderly cadavers) to better approximate the forces produced by the young subjects. For the forward simulations, we inputted the measured EMGs into the models resulting from the inverse MCMC simulations and found that thumbtip forces were not well directed. We will now pursue the question of whether EMG-based MCMC simulations can lead to more realistic models, or if non-hinged kinematic model structures of articular surface mechanics must be considered for future modeling.

REFERENCES

Gilks, W.R. et al. (1996). *Markov Chain Monte Carlo in Practice*. Chapman & Hall/CRC.

Giurintano, D.J. et al. (1995). *Med. Eng. Phys.*, **17**, 297-303.

Santos, V.J. et al. (2003). *Proc. IEEE EMBS'03*.

Valero-Cuevas, F.J. et al. (2003). *J. Biomech.* **36** (7), 1019-1030.

ACKNOWLEDGMENTS

We thank Prof. Carlos Bustamante from Cornell University for his guidance in Markov Chain Monte Carlo techniques, and Prof. Mark Campbell for his simulation advice. This material is based upon work supported under a National Science Foundation (NSF) Graduate Research Fellowship (to V. J. Santos); and from ITR-0312271 grant from NSF's Robotics and Computer Vision Program and CAREER Award BES-0237258 from NSF's Biomedical Engineering/Research to Aid Persons with Disabilities Program (to F. J. Valero-Cuevas).

THUMB KINEMATICS WITH NON-ORTHOGONAL AND NON-INTERSECTING AXES OF ROTATION MAY BE NECESSARY TO PREDICT REALISTIC ISOMETRIC THUMBTIP FORCES IN MULTIPLE DIRECTIONS

Veronica J. Santos [1] and Francisco J. Valero-Cuevas [1,2]

[1] Neuromuscular Biomechanics Laboratory, Cornell University, Ithaca, NY, U.S.A.
[2] The Hospital for Special Surgery, New York, NY, U.S.A.
E-mail: vjl4@cornell.edu Web: www.mae.cornell.edu/nmbl

INTRODUCTION

Manipulation depends on the thumb's ability to produce well-directed forces of sufficient magnitude. We currently lack a model of the thumb that can realistically predict thumbtip forces in 3D, and the coordination patterns that produce them (Valero-Cuevas, et al., 2003). This may be because the assumed *model structure* is not able to reproduce functional outputs, and/or because the search for adequate *model parameter values* has been unsuccessful. Understanding the inherent biomechanical abilities of a chosen *model structure* is a necessary first step to modeling the thumb for clinical use and studies of neural control of the hand.

METHODS

We investigated whether: (1) adjusting the 50 musculoskeletal parameters (e.g., moment arms, hinge location and orientation) of a five-hinge serial linkage *model structure* (Fig. 1) can predict maximal, voluntary, isometric thumbtip forces measured experimentally; and (2) inputting the measured fine-wire electromyogram (EMG) data into these models produces well-directed forces (within 16° of the desired direction). Using a Bayesian approach that considers model parameters as random quantities instead of single unique values, we found the range of all possible functional outcomes for a specific *model structure* resulting from the natural anatomical variability of the thumb.

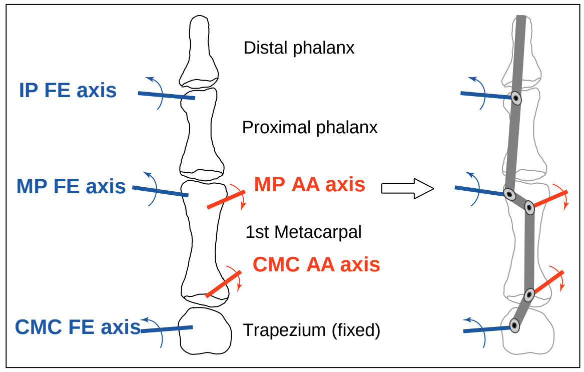

Figure 1: Thumb kinematics modeled as a serial chain of five hinges (Giurintano, et al., 1995). (*CMC=carpometacarpal, MP=metacarpo-phalangeal, IP=interphalangeal*)

We used a Markov Chain Monte Carlo (MCMC) algorithm to explore this 50-D parameter space (Gilks, et al., 1996). We represented each parameter by a statistical distribution based on published or measured data (Santos, et al., 2003). The MCMC algorithm stochastically explored the *model parameter space* using 10 independent Markov chains to find the model parameter distributions that drove input/output predictions towards a least-squares fit to thumbtip force/torque measurements. Chain convergence was determined by the Gelman-Rubin statistic (Gilks, et al., 1996), which indicates when all chains can be pooled for drawing inferences. Converged chains were extended such that 20,000 pooled iterations were achieved.

The exploration was driven by an "inverse" linear programming (LP) solution predicting maximal biomechanically feasible thumbtip forces. For a given thumb posture, static force production reduces to a matrix multiplication (Valero-Cuevas, et al., 2003), making LP appropriate for predicting the limits of performance. We then performed "forward" simulations using fine-wire EMG measurements, instead of inverse LP solutions, to evaluate the input-to-output behavior of the models.

RESULTS AND DISCUSSION

The distributions of parameter values to which all chains converged are those that can produce well-directed thumbtip forces in 3D for this robotics-based model structure. Since MCMC methods perform an exhaustive search of the *parameter* space (Gilks, et al., 1996) there is *no other* sub-region in the 50-D parameter space that would fit the measured force data better. Our MCMC approach has the important benefit of rigorously predicting the functional consequences of natural anatomical variability of the thumb.

We found model-predicted maximal thumbtip forces to be lower than those measured (Table 1), but closer to the measurements compared to the predictions of a simpler kinematic model with mutually orthogonal and intersecting axes of rotation at the CMC and MP joints (Valero-Cuevas, et al., 2003). The five-hinge serial linkage model predicted maximal palmar forces comparable to those predicted by the simpler model and improved upon predictions in the dorsal and distal directions for both pinch postures.

Table 1: Comparison of thumbtip force magnitudes between experimental measurements (n=4) and model predictions (20,080 pooled iterations). We observe improvements in model predictions over those from a simpler kinematic model (Valero-Cuevas, et al., 2003) in the dorsal and distal force directions for both pinch postures.

Pinch-type	Force dir.	Expt.		Model		Expt:Model Mean ratio
		Mean	Std	Mean	Std	
Key	Palmar	54.4	26.0	14.0	7.4	3.9
	Dorsal	10.7	3.0	9.0	1.9	1.2
	Distal	58.2	32.3	96.1	10.7	0.6
	Radial	21.5	9.7	5.7	3.1	3.8
	Ulnar	16.9	2.9	2.2	1.2	7.7
Opposition	Palmar	46.3	34.9	11.1	4.7	4.2
	Dorsal	10.8	3.2	7.2	2.6	1.5
	Distal	54.3	43.5	25.2	13.6	2.2
	Radial	22.2	8.3	8.1	2.8	2.8
	Ulnar	25.8	13.5	1.8	1.4	14.0

However, it is reasonable to consider increasing the PCSA values (collected from elderly cadavers) to better approximate the forces produced by the young subjects. For the forward simulations, we inputted the measured EMGs into the models resulting from the inverse MCMC simulations and found that thumbtip forces were not well directed. We will now pursue the question of whether EMG-based MCMC simulations can lead to more realistic models, or if non-hinged kinematic model structures of articular surface mechanics must be considered for future modeling.

REFERENCES

Gilks, W.R. et al. (1996). *Markov Chain Monte Carlo in Practice*. Chapman & Hall/CRC.

Giurintano, D.J. et al. (1995). *Med. Eng. Phys.*, **17**, 297-303.

Santos, V.J. et al. (2003). *Proc. IEEE EMBS'03*.

Valero-Cuevas, F.J. et al. (2003). *J. Biomech.* **36** (7), 1019-1030.

ACKNOWLEDGMENTS

We thank Prof. Carlos Bustamante from Cornell University for his guidance in Markov Chain Monte Carlo techniques, and Prof. Mark Campbell for his simulation advice. This material is based upon work supported under a National Science Foundation (NSF) Graduate Research Fellowship (to V. J. Santos); and from ITR-0312271 grant from NSF's Robotics and Computer Vision Program and CAREER Award BES-0237258 from NSF's Biomedical Engineering/Research to Aid Persons with Disabilities Program (to F. J. Valero-Cuevas).

THE ROLE OF RECIPROCAL EXCITATION IN THE REGULATION OF STIFFNESS OF THE FELINE ANKLE

T. Richard Nichols

Department of Physiology, Emory University, Atlanta, GA 30322
E-mail: trn@physio.emory.edu

INTRODUCTION

Evidence has accumulated that proprioceptive circuits in the spinal cord are organized to represent the architecture of the associated musculoskeletal system, and that these circuits promote interjoint coordination and regulate the stiffness of the limb measured at the endpoint (Nichols et al., 2002). Closely synergistic muscles are linked by excitatory length feedback (stretch reflexes) and muscles that cross different joints or axes of rotation are linked by force-dependent inhibition. Reciprocal inhibition links mutually antagonistic muscles. These results suggest that that the stretch reflex and reciprocal inhibition combine to regulate joint stiffness, while length and inhibitory force feedback work in opposition to regulate endpoint stiffness of the limb. Muscular, and presumably endpoint stiffness, increase during locomotion (Ross et al., 2003). This increase may be due to autogenic positive force feedback, which under these conditions coexists with inhibitory intermuscular feedback.

Preliminary evidence also suggests that a force-dependent excitatory pathway extends from the antigravity muscles of the ankle onto the pretibial flexors (Nichols, 1994). This reciprocal excitation is observed even when locomotion is not present. Further evidence for this pathway and its possible mechanical functions are described here.

METHODS

Experiments were performed on 7 adult cats. Animals were decerebrated at the intercollicular level under deep surgical anesthesia and all brain tissue rostral to the transaction was removed. Tendons of muscles crossing the ankle were freed and connected two at a time to two servo-controlled torque motors. The muscles were activated using electrical stimulation of either the ipsilateral or contralateral posterior tibial nerves. Force increased rapidly and then slowly declined, providing a range of initial forces on which responses to ramp-and-hold stretches were obtained. The ramps were 4 mm in amplitude and 100 ms in duration. During the even-numbered trials, the donor muscle was also stretched. Inhibitory or excitatory influences from the donor to the recipient were detected as increases or decreases in force response of the recipient during the even trials compared to the odd trials. The responses in both groups were plotted as functions of the initial force.

RESULTS

Evidence of force-dependent excitation from the gastrocnemius muscles (G) to tibialis anterior (TA) and extensor digitorum longus muscles was found. There was no evidence of positive feedback from the soleus muscle to the pretibial flexors. The inhibition was detectable at the termination of the ramp (100 ms following the initiation of stretch), but was fully developed at the end of the 300 ms hold period. Increases in the stiffness of TA of up to 100% due to excitation from G were observed at higher forces.

DISCUSSION

Electrophysiological evidence for excitatory feedback from agonists to antagonists has been available for several decades (Laporte & Lloyd, 1952), but the intermuscular distribution, magnitude, and functions are still unknown. The present results show that this pathway is powerful and suggest that the pathway arises predominantly from multijoint antigravity muscles and influences flexors. These effects are observed in the intercollicular decerebrate preparation, unlike autogenic positive force feedback (Ross et al., 2003), and so are not necessarily associated with locomotion. The force dependence of the reflex suggests that the reflex arises from Golgi tendon organs.

Reciprocal inhibition tends to increase the stiffness of joints, so it might seem that reciprocal excitation would tend to decrease joint stiffness in opposition to the reciprocal inhibition from flexors to ankle extensors. However, if this excitation arises from Golgi tendon organs, then it would be evoked by muscular contraction as well as muscle stretch. Its effect then might be to reinforce or provoke cocontraction, in which intrinsic muscular stiffness is increased. Therefore, the stiffness of the ankle joint would be increased by two mechanisms. First, in anticipation of foot contact, activation of the triceps surae would provoke a parallel activation of the flexors through reciprocal excitation with the associated increase in intrinsic stiffness. Second, stiffness would increase reflexly through reciprocal inhibition onto ankle extensors upon foot contact in the yield phase of stance.

During walking, the triceps surae muscles and the pretibial flexors are activated reciprocally. During trotting, however, a small burst in TA appears during the activation of the triceps surae (Abraham & Loeb, 1985). During landing from a fall, there is considerable cocontraction of the triceps surae muscles and TA. That is, the magnitude of the cocontraction increases with muscular force. It is possible that this cocontraction is a manifestation of force-dependent excitation.

SUMMARY

Evidence is provided for reciprocal excitation from the gastrocnemius muscles to the pretibial flexors in the cat. The reflex is force dependent, suggesting that it arises from Golgi tendon organs in the muscles of origin. A possible function is to increase the activation and intrinsic stiffness of the flexors in advance of landing in order to increase total joint stiffness. This increased joint stiffness might be important during higher speeds of locomotion or landing from a fall.

REFERENCES

Abraham, L.D. Loeb, G.E. (1985). *Exp. Brain Res.*, **58**, 580-593.
Laporte, Y., Lloyd, D.P.C. (1952). *Am. J. Physiol.* **169**, 609-621.
Nichols, T.R. (1994). *Acta Anat.* **151,** 1-13.
Nichols, T.R., Wilmink, R.J.H., Burkholder, T.J. (2002). *Progress in Motor Control*, Human Kinetics.
Ross, K.T., Huyghues-Despointes, C.M.J., T.R Nichols (2003). *Soc Neurosci Abstr,* 29.

ACKNOWLEDGEMENTS

NIH: NS20855

FIXATION STRENGTH EVALUATION OF HIP IMPLANTS UNDER BIAXIAL ROCKING MOTION

Larry W. Ehmke[1], James C. Krieg[1], Daniel C. Fitzpatrick[2], and Michael Bottlang[1]

[1]Biomechanics Laboratory, Legacy Clinical Research & Technology Center, Portland, OR;
[2]Orthopedic Healthcare Northwest, Springfield, OR; E-mail: mbottlang@biomechresearch.org

INTRODUCTION

Dynamic lag screws are the most frequently used implants for hip fracture fixation. Up to 23% of the time, these implants exhibit fixation failure leading to varus collapse and cutout of the lag screw through the femoral head (Baumgaertner, 1995). Lag screw fixation failure has been studied *in situ* under static or dynamic uni-directional loading (Haynes, 1997). Although these studies replicate implant migration and cutout failure, they fall short of replicating the characteristic rocking motion seen by the hip during walking, which is believed to be responsible for implant migration.

In this study we developed a model for fixation strength evaluation of hip fracture fixation hardware, which employs biaxial rocking motion (BRM). This study tested the hypothesis, that BRM induces implant migration kinematics, which differs significantly from implant migration under uniaxial dynamic loading alone.

METHODS

Specimens: Ten surrogate femoral head and neck specimens with defined geometry (50 mm ∅ head) were custom-manufactured from 12.5-pcf cellular polyurethane foam (1522-11, Pacific Research Inc., Vashon, WA) to simulate mildly osteoporotic cancellous bone with reproducible material properties.

Implants: Dynamic lag screws (Gamma, Stryker, Rutherford, NJ) were inserted centrally into surrogate specimens after reaming, yielding a 10-mm distance between the implant tip and the femoral head apex. The lag screw shafts were suspended in a stainless steel base, which replicated the constraints of the lag screw in the corresponding Gamma nail, allowing for axial sliding but no rotation.

Surrogate specimens were confined in a polished stainless steel shell for dynamic loading. The back plate of this steel shell rested against a polyethylene support to provide constraints characteristic for a reduced unstable pertrochanteric fracture (Figure 1a).

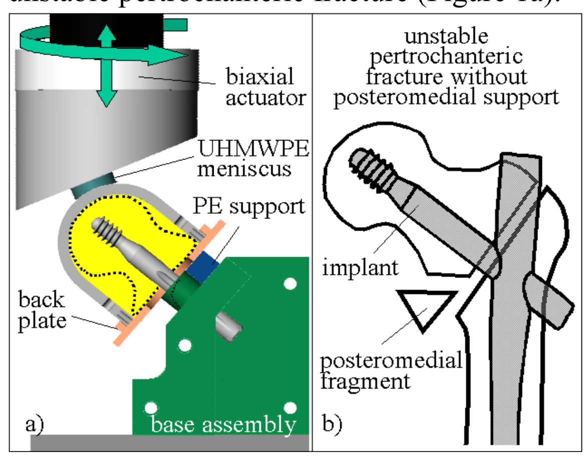

Figure 1: a) cross-sectional view of simulator; b) unstable pertrochanteric fracture, reduced.

Specifically, this support simulated abutment of the fracture surfaces after completion of lag screw sliding, and allowed for femoral head varus collapse and rotation, as clinically observed in the case of an unstable comminuted fracture with deficient posteromedial neck support (Figure 1b).

Biaxial Rocking Motion (BRM): BRM was induced in an approach comparable to contemporary hip arthroplasty wear simulators. Axial and rotary motion under concurrent load and rotation control was induced with a biaxial servo-hydraulic test system (Instron 8874)

(Figure 2a). Compressive load cycles were applied to the steel shell over a polyethylene meniscus (UHMWPE), which traced a consistent path across the superior aspect of the femoral head. A dynamic, double-peak loading regimen of 1.45 kN load was applied at 1 Hz (Bergmann, 2001). Flexion/extension (FE) and ab/adduction (AA) motion were simulated by rotation of a 23° inclined block affixed to the actuator. Exaggerated walking with 45° FE and 17° AA were simulated by ± 75° actuator rotation.

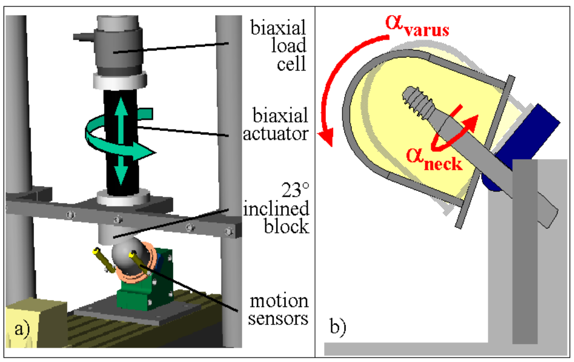

Figure 2: a) BRM implant migration simulator; b) outcome parameters α_{neck} , α_{varus}.

All 10 specimens were tested in the BRM setup for 20,000 load cycles. However, five specimens were subjected to dynamic axial loading only. The remaining five specimens were tested under combined axial and rotational loading. The spatial migration of the femoral head-neck complex in respect to the implant was continuously recorded with an electromagnetic motion tracking system (PcBird, Ascension Tech., Burlington, VT). Femoral head migration as a function of loading cycles was analyzed in terms of varus collapse (α_{varus}) and rotation around the femoral neck axis (α_{neck}) (Figure 2b).

RESULTS

BRM and uniaxial loading resulted in different implant migration mechanisms and magnitudes. Implant migration under BRM simulation was dominated by rotation α_{neck} (Figure 3). Uniaxial loading primarily caused varus collapse α_{varus}. BRM simulation yielded significantly higher migration magnitudes for both α_{neck} and α_{varus} as compared to uniaxial loading. After 20,000 cycles, BRM yielded 4 times more varus collapse ($p=0.02$) and over 40 times more neck rotation ($p<0.01$) as compared to uniaxial loading alone.

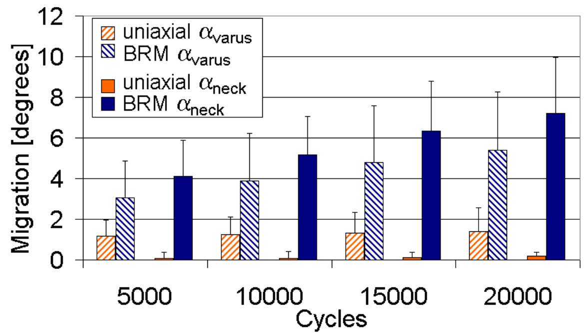

Figure 3: Implant migration α_{neck} and α_{varus}.

DISCUSSION

Clinical studies document that lag screw cutout failure is a consequence of both femoral head rotation and varus collapse (Lustenberger, 1995). The presented model reproduced for the first time both components of clinically observed lag screw migration. These results suggest that accounting for biaxial rocking motion is crucial to simulate and predict lag screw migration. As such, the BRM lag screw migration simulator provides a clinically relevant tool for comparative evaluation and systematic optimization of migration resistance of implant for hip fracture fixation.

REFERENCES

Baumgaertner, M.R. et al. (1995). *JBJS*, **77-A, 7**: 1058-1064.

Haynes, R.C., Miles A.W. (1997). *Proc Inst Mech Eng*, **211**(5), 411-417.

Bergmann, G. et al. (2001). *J Biomech*, **34**, 859-871.

Lustenberger, A. et al. (1995). *Unfallchirurg*, **98**(10), 514-517.

ACKNOWLEDGMENTS

Funding provided by the Legacy Foundation

LONGITUDINAL TENSILE PROPERTIES OF ELASTIN, CURED ELASTIN, AND NATIVE CAROTID ARTERY

Ping-Cheng Wu, Ann Bazar, Carmen Campbell, and Kenton W. Gregory

Oregon Medical Laser Center, Providence St. Vincent Medical Center, Portland, OR
E-mail: ping-cheng.wu@providence.org

INTRODUCTION

Elastin is potentially a less thrombogenic blood-contacting surface than other biological or synthetic materials. This and other properties (Karnik et al., 2003) make elastin an ideal substrate material for the development of a small diameter vascular graft. Common studies have used bursting techniques and ring tests to study the circumferential mechanical properties of native carotid arteries (Cox, 1975; Roeder et al., 1999, 2000; Lillie and Gosline, 2002) but few have examined the longitudinal mechanical properties. Elastin, cured elastin, and native carotid vessels were tested longitudinally to quantify mechanical properties including ultimate strain, ultimate tensile strength, and elastic modulus.

METHODS

Twelve porcine carotid arterial vessels were trimmed of adherent fat. Eight vessels were treated with 80% ethanol and a hot alkali digestion and rinsed in 0.05 M HEPES buffer to produce a pure elastin matrix. The remaining four vessels were left untreated. Half of the purified elastin vessels were cured in a heated humidified environment resulting in three groups (elastin, cured elastin, and native) of four vessels. The vessels were cut into dumbbell shaped specimens in the longitudinal direction as shown in Figure 1. The specimens' gage length was 5 mm with 3 mm grips. The thickness and cross-sectional gage length were recorded.

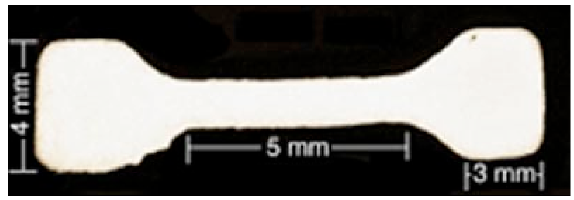

Figure 1: Typical dumbbell specimen representation.

All specimens were mounted on a MTS servo-hydraulic testing system and tested in tension at a crosshead speed of 5 mm/s until failure. All specimens were kept hydrated with saline during the test in ambient temperature. Force (N) and displacement (mm) were acquired. Stress (force/cross-sectional area) and strain ($L-L_i/L_i$) were calculated and plotted. The linear slope region of the stress-strain plots was used to calculate the elastic modulus (stress/strain).

Ultimate strain, ultimate tensile strength and elastic modulus data were analyzed by using a two-tailed unpaired t-test to determine any statistically significant differences between the groups.

RESULTS

No significant ultimate strain differences ($p>0.05$) were found between the three groups shown in Figure 2, which may be due to a small sample size. The average ultimate strain values for elastin, cured elastin, and native vessels were 112±1%, 114±13%, and 163±48%, respectively. Significant differences ($p<0.01$) were found with the average ultimate tensile strength and elastic modulus shown in Figures 3 and 4, respectively. Elastin demonstrated the lowest ultimate tensile strength (0.65±0.1 MPa) and elastic modulus (0.45±0.1 MPa). Native carotid averaged the highest ultimate tensile strength (3.2±0.7 MPa) and elastic modulus (4.6±0.7 MPa). Average ultimate tensile strength and elastic modulus values for cured elastin were 1.3±0.3 and 1.1±0.2, respectively.

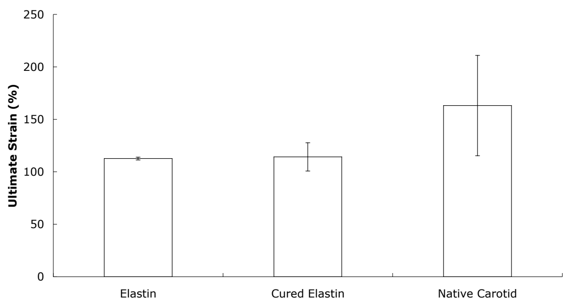

Figure 2: There were no significant ultimate strain differences ($p>0.05$).

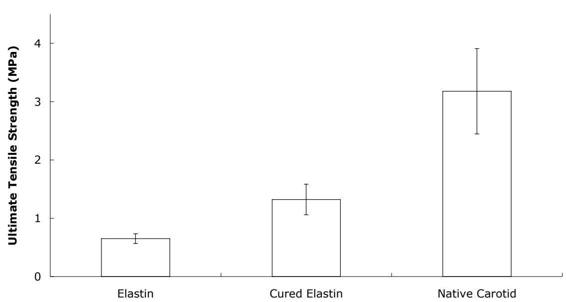

Figure 3: There were significant ultimate tensile strength differences ($p<0.01$).

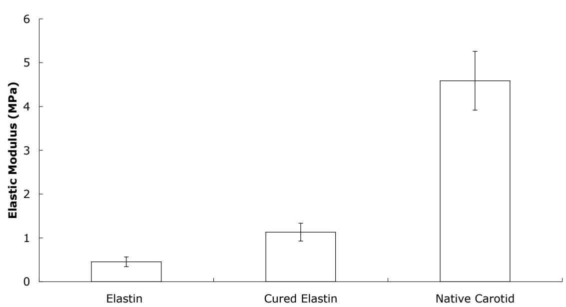

Figure 4: There were significant differences ($p<0.01$) between with elastic modulus.

DISCUSSION

Longitudinal tensile tests added another dimension to the requirements for a tissue engineered arterial graft. While the curing process increased the elastin's strength, the result is still significantly weaker than composite native carotid artery, consisting of elastin and collagen (Shadwick, 1999). Collagen is a major contributing factor to the ultimate tensile stress and strain properties of native arterial tissue (Roach and Burton, 1957). Various approaches to increase the longitudinal strength of the elastin graft will be investigated, including the incorporation of collagen.

REFERENCES

Cox, R.M. (1975). *Am J Physiology.* **229**, 807-812.

Karnik, S.K. et al. (2003). *Development.* **130**, 411-423.

Lillie, M.A. and Gosline, J.M. (2002). *Int. J. Biol Macromolecules.* **30**, 119-127.

Roach, M.R. and Burton, A.C. (1957). *Can. J. Biochem Physio.* **35**, 181-190.

Roeder, R. et al. (1999). *J. Biomed Mater Res.* **47**, 65-70.

Roeder, R. et al. (2000). *Australas Phys Eng Sci Med.* **23**, 66-67.

Shadwick, R.E. (1999). *J. Exp Biol.* **202**, 3305-3313.

ACKNOWLEDGEMENTS

Special thanks to Samuel Jensen-Segal for his assistance. This project was sponsored by the Department of the Army Grant No. DAMD-17-98-1-8654 and does not necessarily reflect the position or policy of the government. No official endorsement should be inferred.

EFFECT OF FLOOR STIFFNESS ON IMPACT FORCES DURING FALLS ON THE HIP

Andrew C.T. Laing, Iman Tootoonchi, Stephen N. Robinovitch
Injury Prevention and Mobility Laboratory, School of Kinesiology, Simon Fraser University, Burnaby, BC, Canada E-mail: aclaing@sfu.ca Website: www.sfu.ca/ipml/

INTRODUCTION

Over 90% of hip fractures are due to falls (Spaite et al., 1990), and fracture risk during a fall depends on the impact force applied to the proximal femur (Cummings and Nevitt, 1989). Accordingly, interventions that attenuate impact forces have considerable potential for reducing hip fracture incidence. One possible strategy for achieving this (especially relevant to high-risk environments such as nursing homes or senior centres) is to reduce the stiffness of the floor (Maki and Fernie, 1990; Gardner et al., 1998; Casalena et al., 1998a,b). However, previous studies have not quantified the relationship between floor stiffness and peak force. Our goal in the current study was to determine this relationship for safe fall heights, and test the hypothesis that peak force during impact to the hip associates with fall height and floor stiffness.

METHODS

Seven adult females (of mean age 22.7 ± 2.4 yrs and mean body mass 57.4 ± 5.8 kg) provided informed consent and completed the study protocol. During the trials, the subject rested her lower limbs and upper body on rigid platforms (Figure 1), and her pelvis on a linear-stiffness springboard that (in the undeflected condition) was flush to the surface of the platforms. A nylon sling and electromagnet was then used to lift and instantly release the pelvis from heights of 1.25 cm and 5 cm above the springboard (Robinovitch et al., 1997). The springboards had stiffness values (k_f) of 7.6, 17.6, 31.0,

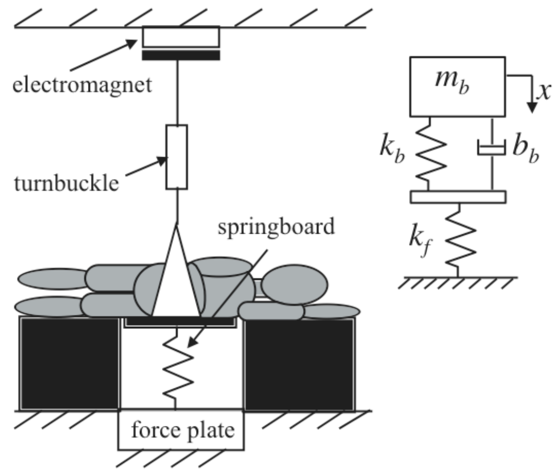

Figure 1: Experimental setup and mathematical model

86.4, and 733 kN/m (measured by impulse response). Impact forces were recorded from a forceplate under the springboard (Bertec, model 4060H), which we sampled at 960Hz. We acquired four trials for each combination of fall height and floor stiffness.

In each trial, contact force rose to a peak value and then decayed to a final resting force, reflecting single-degree-of-freedom behaviour (Figure 2). We used a 2-factor repeated measures ANOVA to determine whether peak impact force (normalized by body mass) was affected by floor stiffness and fall height. We also compared experimental trends to those predicted by a four-parameter mathematical (vibratory) model (inset to Figure 1). Model parameters were characterized using curve-fitting routines to determine the natural frequency and damping ratio, and corresponding values of m_b, k_b, and b_b.

RESULTS AND DISCUSSION

Peak impact force associated with both floor stiffness and fall height ($p<0.001$). At the 5cm fall height, average values of peak force were 54% lower in the 7.6 kN/m floor than the 733 kN/m floor. However, in the 1.25 cm fall, the same reduction in floor stiffness caused only 32% attenuation in impact force. Model predictions mimicked these experimental trends.

These trends reflect the complex effect that floor stiffness (k_f) has on the system's energy absorption and dissipation characteristics. Reducing k_f causes a reduction in system stiffness, and a decrease in energy dissipation (since the velocity across the damper is decreased). At higher fall heights (including any fall from standing height), the former effect dominates, and reductions in k_f lead to a substantial attenuation in peak force. At low fall heights, the two effects tend to cancel each other, and peak force is nearly constant.

An important consideration for future studies is determining the threshold in k_f, below which balance maintenance and recovery is substantially impaired.

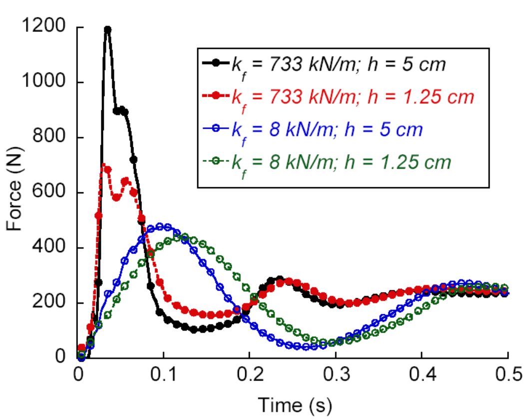

Figure 2: Typical force vs. time traces

SUMMARY

This study investigated the relationship between floor stiffness and peak impact forces during falls on the hip. We found that peak force was reduced by 54% by reducing the floor stiffness from 733 to 7.6 kN/m. These trends are supported by predictions from a four-parameter vibratory model. These data support the notion that low stiffness floors may significantly reduce hip fracture risk during a fall.

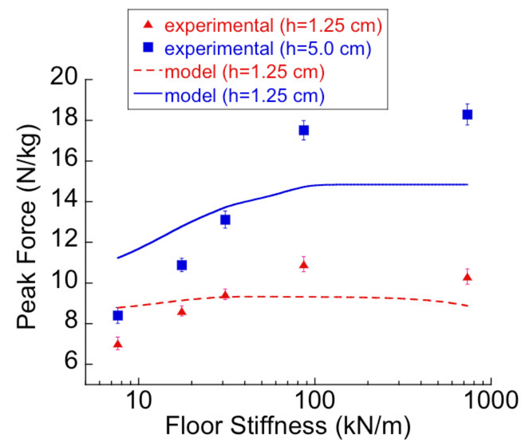

Figure 3: Model output and experimental peak force vs. floor stiffness results (mean across subjects +/- 1 SE) at 1.25 and 5cm fall heights.

REFERENCES

Cummings SR, Nevitt, MC (1989). *J. Gerontol.* **44**: M107-M111.

Maki BE, Fernie GR (1990). *Appl. Ergon.* **21**: 107-114.

Casalena JA et al., 1998a). *J Biomech Eng.* **120**:518-26.

Casalena JA et al.(1998b). *J Biomech Eng.* **120**: 527-32.

Robinovitch SN et al. (1997) *Ann Biomed Eng.* **25**: 499-50.

Spaite DW et al. (1990). *Ann Emerg Med.* **19**: 1418-21.

ACKNOWLEDGEMENTS

Mr. Laing was supported by fellowships from SFU, MSFHR, and NSERC. Dr. Robinovitch was supported by salary awards from MSFHR and CIHR.

EFFECTS OF PREPARATION ON POSTURAL STABILITY WHILE ACCEPTING A WEIGHT IN THE OUTSTRETCHED HANDS

[1]Jennifer Rattenbury, [2]Ted Milner, [1]Stephen N. Robinovitch,

[1]Injury Prevention and Mobility Laboratory, [2]Biomechanics Laboratory; School of Kinesiology, Simon Fraser University, Burnaby, British Columbia, Canada
Email: jrattenb@sfu.ca

INTRODUCTION

An essential aspect of postural stability is the ability to lift or catch objects with minimal corresponding displacement of the whole-body centre-of-gravity (COG). Our ability to achieve this depends in part on the use of anticipatory postural responses (APAs), in the form of muscle contractions and corresponding centre-of-pressure movements and limb dynamics, to offset the destabilizing effect of weight acceptance (Toussaint et al., 1997, Kaminski and Simpkins, 2001; Commissaris and Toussaint, 1997, Shiratori and Latash, 2001). When APAs are absent or ineffective, we must rely upon balance recovery responses (stretch reflexes and longer-loop responses) to limit COG displacement and maintain stability.

Our goal in the current study was to compare the effectiveness of APAs versus balance recovery responses in limiting whole-body COG movement when a weight is accepted in the outstretched hands. We hypothesized that COG and COP displacements would be less when weight acceptance is pre-planned and involves APAs (i.e., voluntary lifting) as opposed to being sudden and/or unexpected (involuntary or voluntary catching), thereby eliciting balance recovery responses.

METHODS

Eight young women participated as experimental subjects (mean age=23.4 ± 3.2 (SD) yrs). During the trials, we instructed the subject to reach forward into a position of impending weight acceptance, lightly grasping with both hands but not yet lifting a 1” diameter dowel of mass 1.9 kg suspended on a rope (Figure 1). The object weight was then transferred to the hands in one of three ways: (1) voluntary lifting (VOL_LIFT); (2) having the subject press a button to voluntarily release the tension in the suspending rope (VOL_REL); and (3) having the investigator unexpectedly release the tension in the rope (INVOL_REL). In all trials, the subject’s instructed goal was to minimize hand and body movement during weight acceptance. We acquired three repeated measures at two dowel heights (80% and 100% body height (BH)). In all cases, the horizontal distance from the ankles to the dowel was 45%BH.

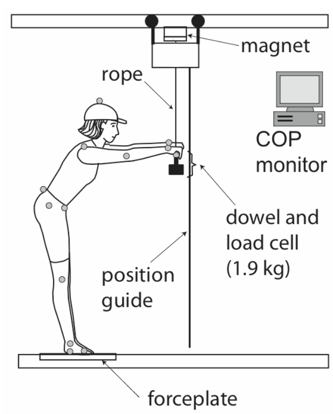

Figure 1. Experimental set up.

We measured body segment movements with an 8-camera, 120 Hz motion capture system (Motion Analysis Corp., Eagle model). Horizontal displacements of the whole-body COG were calculated from motion data. We used a forceplate (Bertec 6090-15) to measure foot contact forces and COP location, and load cells (Sensotec) to measure hand force. Hypothesis testing was based on repeated measures ANOVA and Bonferroni's post hoc tests (α = 0.05).

RESULTS AND DISCUSSION

The method of weight acceptance affected horizontal displacements of both the COG and COP (p<0.001; Figure 2). COG displacement was greater in VOL_REL than VOL_LIFT (mean diff=0.27 cm, SE=0.08, p=0.02), but not different between INVOL_REL and VOL_REL (mean diff=0.27 cm, SE=0.12, p=0.13). COP displacement was greater in INVOL_REL than VOL_REL (mean diff=0.77 cm; SE=0.12; p<0.001), and greater in VOL_REL than VOL_LIFT (mean diff=0.44 cm; SE=0.13; p=0.01). These trends persisted for the two dowel heights, although COG and COP displacements were greater in 80%BH than 100%BH trials (Figure 2).

These results indicate that APAs are generally more effective than balance recovery responses in minimizing COG displacement during weight acceptance. When compared to VOL_REL, COG displacements were smaller in VOL_LIFT, with smaller corresponding displacements of COP. However, the difference in COG displacement was remarkably small (in all cases well under 1 cm). This reflects the efficiency of balance recovery responses in our young subjects, especially when subjects had knowledge of the impending perturbation.

SUMMARY

We found that APAs were more effective than balance recovery responses in limiting COG displacement when accepting a weight in the outstretched hands. In future work, we plan to use this model to compare age-related changes in postural stability under voluntary and unexpected perturbations.

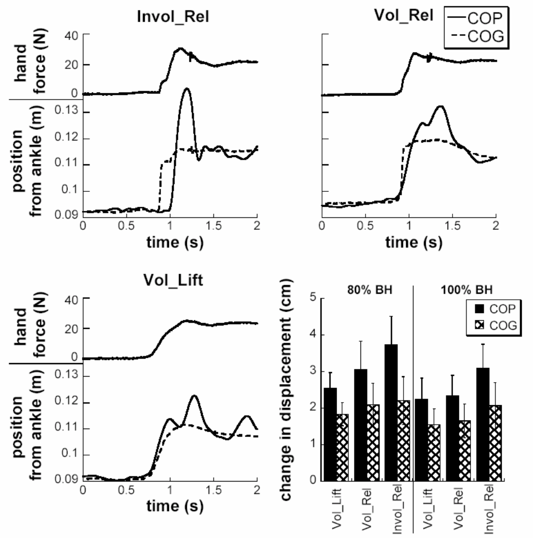

Figure 2. Typical variations in horizontal position of the COP and COG, and hand contact force, for the three weight acceptance conditions. Bar graph in the lower right shows mean COP and COG displacements for all conditions.

REFERENCES

(1) Cummings, S.R. and Klineberg, R.J.(1994). *JAGS*, **42**, 774-8.
(2) Commissaris D.A.C.M. and Toussaint H.M. (1997). *Ergonomics*, **40**(5), 559-75.
(3) Kaminiski and Simpkins (2001). *Exp Brain Res*, **136**(4), 439-46.
(4) Shiratori and Latash (2001). *Clin Neurophysiol*, **112**(7), 1250-65.
(5) Toussaint H.M.et al.(1997). *Med Sci Sports Exerc*, **29**(9), 1216-24.

ACKNOWLEDGEMENTS

Supported by a CIHR operating grant. SNR was supported by salary support awards from CIHR and MSFHR.

HOW DOES ABILITY TO RECOVER BALANCE DEPEND ON THE TIME REQUIRED TO EXECUTE A STEP?

Elmine H. Postma, Dawn C. Mackey and Stephen N. Robinovitch.

Injury Prevention and Mobility Laboratory, School of Kinesiology, Simon Fraser University, Burnaby, BC, Canada
E-mail: epostma@sfu.ca Web: www.sfu.ca/ipml

INTRODUCTION

Stepping represents a common balance recovery strategy. A better understanding of the variables that govern ability to recover balance by stepping should therefore lead to improved fall prevention programs for the elderly. Previous research has shown that step length and step execution time are important determinants of balance recovery ability. For example, subjects respond to larger perturbations by taking larger and faster steps (Do et al., 1982; Hsiao and Robinovitch, 1999). However, elderly individuals take smaller and slower steps than young (Medell & Alexander, 2000).

In the present study, we sought to determine how recovery ability depends on the time required to initiate and execute the swing and stance stages of the step, when step length is held constant. We considered that balance recovery by stepping involves three stages: step initiation, swing, and stance (Figure 1). We then conducted experiments to test the hypothesis that recovery ability would increase with reductions in time required to execute each stage. Our results indicate how postural stability would be enhanced by interventions to quicken step execution.

METHODS

Balance recovery experiments were conducted with 15 healthy young women (mean age = 22.1 ± 3.4 (SD) yrs). During the trials, subjects were supported by a tether in an inclined standing position, and instructed to recover balance by taking a single step of length 25% body height (Figure 2). Measures were acquired of body segment movements at 60 Hz (Qualysis, ProReflex model) and foot contact forces and lower extremity EMG at 960 Hz (Bertec, 6090H model).

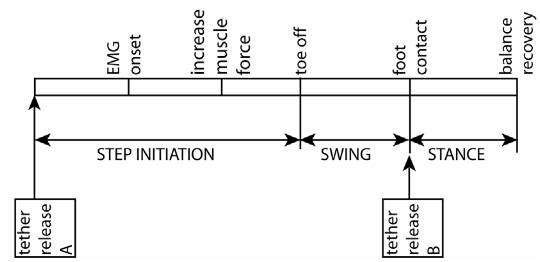

Figure 1: Stages of step initiation and execution. We conducted trials at tether release times A and B.

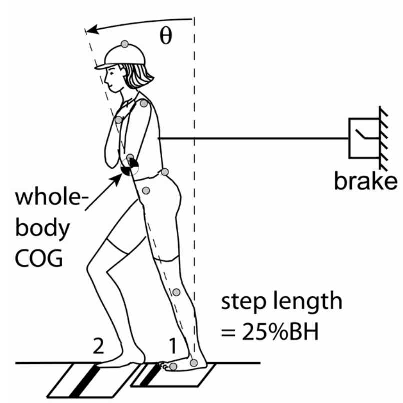

Figure 2: Experimental set-up.

For each subject, we gradually increased the initial lean angle to determine the maximum value (θ_{max}) where the subject could recover a stable upright stance in 3 out of 5 repeated trials. Furthermore, we measured recovery ability under three conditions. In the "*static"* condition, the subject stood with her dominant foot in the step contact position (position 2 in Figure 2) and recovered an upright stance when the tether was not released. In the "*dynamic no swing*" condition, the subject stood with her dominant foot barely contacting the ground in position 2, and recovered upright stance after sudden release of the tether (indicated as "tether release B" in Figure 1). In the "*dynamic swing*" condition, the subject stood with the dominant foot aligned with the stance foot (position 1 in Figure 2), bearing approximately one half body weight prior to tether release (indicated as "tether release A" in Figure 1).

These conditions provided measures of θ_{max} when: (a) there is the requirement to execute step initiation, swing, and stance (*dynamic swing* condition); (b) there is only the requirement to execute the foot contact and force development phases of stance (*dynamic no swing*); and (c) all of the step initiation, stance, and foot contact phase of stance are eliminated (*static*).

RESULTS AND DISCUSSION

We found that recovery ability was affected by the time required for step initiation and swing. $\theta_{\max}$ was 39% smaller in *dynamic swing* than in *dynamic no swing* conditions (11.4 ± 2.5 (SD) deg versus 18.6 ± 3.2 deg, $p< 0.001$). We also found that θ_{max} depended on the time required for force development and braking during stance. θ_{max} was 46% smaller in *dynamic no swing* than in *static* conditions (18.6 ± 3.2 deg vs. 34.2 ± 1.9 deg, $p < 0.001$). Thus, θ_{max} was reduced 67% by cumulative delays in step initiation and execution.

In dynamic conditions, faster response times led to increased recovery ability. A decrease of 10 ms in step contact time (the sum of step initiation and swing times) resulted in a 0.38 deg increase in θ_{max} (Figure 3). In the *dynamic swing* condition, θ_{max} correlated with the interval between tether release and EMG onset ($r = -0.557$, $p = 0.015$), and the interval between increase in muscle force and toe off ($r = -0.637$, $p = 0.005$).

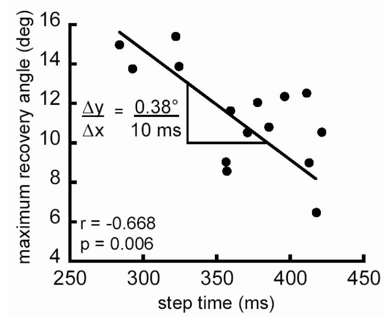

Figure 3: Recovery angle vs. step contact time.

SUMMARY

We examined how ability to recover balance by stepping depends on the time required to execute the step. We found that recovery ability is reduced by 67% due to the cumulative effect of "response delays," and that a linear relation exists between step contact time and recovery ability.

REFERENCES

Do M.C. et al. (1982) *J Biomech*, **15**(12): 933-9.

Hsiao E.T. & Robinovitch S.N. (1999) *J Biomech.* **32**:1099-106.

Medell J.L. & Alexander N.B. (2000) *J Gerontol A Biol Sci Med Sci.* **55**:M429-33.

ACKNOWLEDGEMENTS

This research was supported by a CIHR operating grant. DCM received graduate student fellowships from MSFHR and NSERC. SNR received salary support awards from MSFHR and CIHR.

POSTURAL STEADINESS DURING QUIET STANCE DOES NOT ASSOCIATE WITH ABILITY TO RECOVER BALANCE IN OLDER WOMEN

Dawn C. Mackey [1] and Stephen N. Robinovitch [1]

[1] Injury Prevention and Mobility Laboratory, School of Kinesiology, Simon Fraser University, Burnaby, BC, Canada
E-mail: dcmackey@sfu.ca Web: www.sfu.ca/ipml/

INTRODUCTION

Falls cause substantial death and morbidity in the elderly. Risk for falls associates with a wide variety of neuromuscular, behavioural, and environmental variables, but it depends ultimately on an individual's ability to maintain and recover balance. It is unclear whether, among elderly individuals, these two domains of postural stability are governed by similar neuromuscular variables. This is an important issue for the design of clinical balance assessment tools and exercise-based fall prevention programs. To improve our understanding of this relationship, we examined whether steadiness during quiet stance associated with ability to recover balance using a feet-in-place strategy, and whether these two measures of postural stability associated with similar neuromuscular variables.

METHODS

We conducted experiments with 24 community-dwelling elderly women (mean age = 78 ± 7(SD) yrs). All subjects reported at least one fall in the 18 months prior to testing and were free of substantial orthopaedic or neurological impairment. All subjects provided written informed consent.

In balance recovery trials, we used a tether and chest harness to position the subject in an inclined standing position (Figure 1A), and measured the maximum release angle $(\theta_{\max})$ where she could recover balance by contracting her ankle muscles after the tether was suddenly released. We also measured three neuromuscular variables during the recovery response: reaction time (Δt), rate of ankle torque generation (C), and peak ankle torque $(T_{\max})$ (Figure 1B).

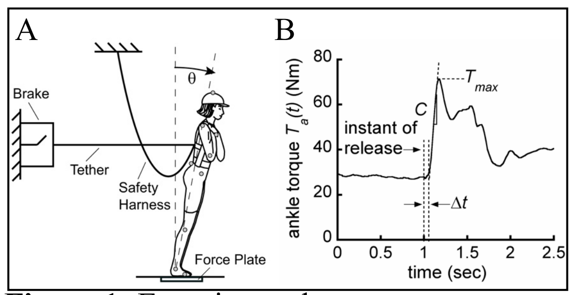

Figure 1: Experimental set-up.

In balance maintenance trials, we instructed the subject to stand still for 15 seconds with her feet on the rigid ground (R) or on foam (F), with her eyes open (EO) or closed (EC). We calculated 4 measures of postural sway of the centre of pressure (COP) of the feet in the anterior-posterior (AP), medial-lateral (ML), and resultant directions. These were range of sway (RANGE), root mean square distance of sway (RMS), mean velocity of sway (MVEL), and mean frequency of sway (MFREQ) (Prieto et al., 1996).

In all trials, we used a force plate (Bertec) to measure (at 540 Hz in balance maintenance trials, and 960 Hz in balance recovery trials) the position of the COP between the feet and the ground, and a seven-camera motion measurement system (Qualisys) to measure (at 60 Hz) the position of 16 skin surface markers (Figure 1A).

RESULTS AND DISCUSSION

We found no significant correlations between θ_{max} and any of the postural sway variables for the EOR, ECR, and EOF conditions of balance maintenance. For the ECF condition, MVEL-ML was the only sway variable that was significantly correlated with θ_{max} (r = 0.487, p = 0.029).

θ_{max} was associated with peak ankle torque and reaction time (Table 1). In contrast, postural sway variables were not associated strongly or consistently with the neuromuscular variables across different conditions of quiet stance.

Our results show that among healthy elderly, who nevertheless had a history of falls, steadiness during quiet stance and ability to recover balance are not well correlated, and furthermore, not associated with similar neuromuscular variables. This suggests that deficits (or exercise-based enhancements) in one measure are not predictive of performance in the other.

The one significant correlation between θ_{max} and MVEL-ML during the ECF condition indicates that ability to rapidly generate corrective postural actions under conditions of sensory deprivation is associated with improved ability to recover balance following a perturbation. This may relate to the higher sway and elicitation of balance recovery responses in the challenging ECF condition.

While previous studies have shown that postural sway during quiet stance is a significant predictor of fall risk, the association is moderate at best (Lord et al., 1994). It is likely that ability to recover balance may provide additional information about fall risk.

SUMMARY

We found that, among elderly women, ability to maintain and recover balance were not highly associated. Therefore, clinical balance assessments and fall prevention programs should target both components of postural stability.

REFERENCES

Lord SR et al. (1994) *JAGS.* **42**(10), 1110-7.
Prieto TE et al. (1996) *IEEE Trans Biomed Eng.* **43**(9), 956-66.

ACKNOWLEDGEMENTS

Operating grants from CIHR, NIH, & CDC. DCM had NSERC & MSFHR fellowships. SNR had a CIHR New Investigator Award & a MSFHR Scholar Award.

Table 1: Correlations between postural sway, balance recovery, and neuromuscular variables.

	Postural Sway				Balance Recovery
	RANGE	**RMS**	**MVEL**	**MFREQ**	θ_{max}
Peak Ankle Torque, T_{max}	ECR: -0.44* ECF: +0.10	ECR: -0.39* ECF: +0.16	ECR: -0.43* ECF: +0.27	ECR: -0.04 ECF: +0.17	+0.61**
Rate of Torque Generation, C	ECR: -0.29 ECF: +0.45*	ECR: -0.24 ECF: +0.56**	ECR: -0.39* ECF: +0.69**	ECR: -0.24 ECF: +0.32	+0.25
Reaction Time, Δt	ECR: +0.27 ECF: +0.05	ECR: +0.14 ECF: +0.07	ECR: +0.18 ECF: -0.04	ECR: -0.05 ECF: -0.04	-0.48**
θ_{max}	ECR: -0.25 ECF: +0.33	ECR: -0.18 ECF: +0.36	ECR: -0.23 ECF: +0.38	ECR: -0.12 ECF: +0.11	

* p<0.05, ** p<0.01

SAFE LANDING DURING A FALL: EFFECT OF RESPONSE TIME ON ABILITY TO AVOID HIP IMPACT DURING SIDEWAYS FALLS

Fabio Feldman and Stephen N. Robinovitch

Injury Prevention and Mobility Laboratory, School of Kinesiology, Simon Fraser University, Burnaby, BC, Canada
E-mail: ffeldman@sfu.ca Web: www.sfu.ca/ipml

INTRODUCTION

Ninety percent of hip fractures in the elderly are due to falls (Grisso et al., 1991), and there is considerable evidence that fall severity, as defined by the configuration and velocity of the body at impact, is a stronger predictor of hip fracture risk than bone density (Greenspan et al., 1994). Of particular importance is whether impact occurs to the hip region, which increases fracture risk 30-fold (Schwartz et al., 1998).

We previously found that young women can avoid hip impact during a sideways fall by rotating forward or backward during descent, when instructed to do so before fall initiation (Robinovitch et al., 2003). However, during real-life falls, individuals rarely have the ability to plan their descent strategy before fall initiation. Under these circumstances, the effectiveness of a specific safe landing strategy may depend on time delays in initiating the response.

Our goal in the current study was to test whether the ability of young women to avoid hip impact during a sideways fall depends on the time instant during descent when the instruction (to rotate forward or backward) is provided. We hypothesized that a critical time window exists following the onset of the fall, beyond which pelvis rotation is ineffective in allowing for avoidance of hip impact.

METHODS

Participants consisted of 15 women ranging in age from 20 to 32 years (mean = 23 ± 4 (SD) yrs). In all trials, a sideways fall onto a gymnasium mat was initiated by suddenly releasing a tether, which supported the subject at a 10 deg lean angle (Figure 1).

Subjects were instructed to respond to a

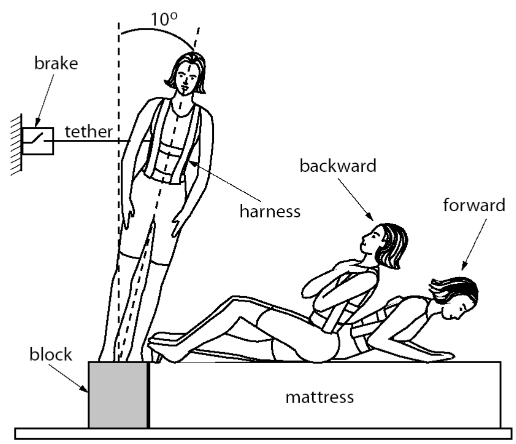

Figure 1: Experimental setup.

visual cue (110 x 160 cm) projected on a wall in front of them, and first displayed either before tether release (by 300, 200, or 100 ms), at the exact instant of release, or after tether release (by 100, 200, or 300 ms). If an image appeared of a person landing on her front side, the subject was to rotate forward to land on her hands. If an image appeared of a person landing on her back side, the subject was to rotate backward to land on her buttocks. If no image was displayed, the subject was to fall sideways with no rotation and land on her hip (control trial). Each subject participated in a total of

53 trials presented in a random order: 15 practice trials, followed by two trials in each of the 14 combinations of rotation direction and cue delivery time, with 10 interspersed control trials.

In each trial, we acquired the 3D positions of 22 skin surface markers with a 60 Hz motion measurement system (Qualisys, ProReflex). From these data, we determined the pelvis impact angle. A value of zero deg in this parameter indicated direct impact to the hip, and 90 deg indicated impact to the anterior or posterior aspects of the pelvis. We used a 2-way repeated measure ANOVA to test whether the absolute value of pelvis impact angle was affected by direction of rotation and time of cue delivery.

RESULTS AND DISCUSSION

We observed significant main effects for time of cue delivery ($p<0.001$) and direction of rotation ($p=0.003$). Earlier cue delivery led to increased pelvis impact angles (Figure 2). Furthermore, pelvis impact angles were greater for backward than forward rotation. In addition, a significant interaction existed, with pelvis impact angles being greater in backward than forward rotation trials, for cue delays of 200 and 300 ms after release.

These results indicate that young women can avoid direct impact to the hip during unexpected sideways falls. However, rotation must be initiated within 200 ms after release in order for it to be effective. Our results also show that, when there is a substantial delay in initiating the response, backward rotation is more effective than forward rotation.

Our findings suggest that fall severity and risk for hip fracture during a fall may depend strongly on reaction time and cognitive factors, such as attention (Nevitt et al., 1991). These data may help to guide the design and evaluation of exercise programs to enhance safe landing responses in elderly participants.

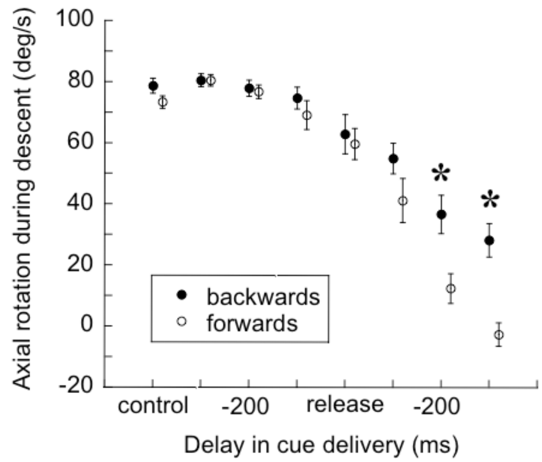

Figure 2: Mean ± S.E. values of pelvis impact angle. Asterisks (*) show where impact angles were greater for backward

SUMMARY

We found that individuals can avoid hip impact during a sideways fall by rotating during descent. However, to be effective the response must be initiated within 200 ms after fall initiation.

REFERENCES

Greenspan, SL et al.(1994). *J Am Med Assoc*, **271**, 128-33.
Grisso, JA et al.(1991). *N Engl J Med*, **324**, 1326-31.
Robinovitch, SN et al.(2003). *J Bone Mineral Res*, **31**:1-9.
Schwartz, AV et al.(1998). *Osteoporos Int*, **8**, 240-46.
Nevitt, MC et al.(1991) *J Gerontol*, **46(5)**, 164-70.

ACKNOWLEDGEMENTS

Supported by operating grants from the NIH (RO1 AR46890) and CIHR. SNR received salary support awards from the Canadian Institutes of Health Research (CIHR) and the Michael Smith Foundation for Health Research (MSFHR).

INTERNAL AND EXTERNAL ROTATION OF THE SHOULDER: EFFECTS OF PLANE, END RANGE DETERMINATION, AND SCAPULAR MOTION

Sean P. McCully [1], Naveen Kumar [2], Mark D. Lazarus [3], and Andrew R. Karduna[1]

[1] Orthopaedic Biomechanics Laboratory, Department of Exercise and Movement Science, University of Oregon, Eugene, OR, USA
[2] Drexel University School of Medicine, Philadelphia, PA, USA
[3] Department of Orthopaedic Surgery, Thomas Jefferson University, Philadelphia, PA, USA
E-mail: karduna@uoregon.edu

INTRODUCTION

Although many of the traditional studies of shoulder motion have primarily focused on shoulder elevation (Poppen et al., 1976), there has been considerable interest of late in measuring internal and external rotation along the long axis of the humerus (Reagan et al., 2002). Study of this motion is important for two main reasons. First, the available range of internal and external rotation impacts shoulder function, from simple activities of daily living, such as hair combing, to more complex tasks required by athletes and occupational workers. Secondly, measurement of internal and external rotations can be used as indicators of capsular tightness. The purpose of this study was to assess the effects of (1) end range determination (active vs. passive), (2) scapular motion, and (3) testing plane on internal and external rotation.

METHODS

Sixteen healthy subjects (mean age, 23.3 years) were recruited and instrumented with a six-degrees-of-freedom magnetic tracking device (Polhemus 3Space Fastrak Colchester, VT). Humerothoracic and glenohumeral motion were measured during active and passive humeral rotations in four clinically significant positions (arm at side and 90 degrees of elevation in the coronal, scapular, and sagittal plane). The first receiver was placed on the spinous process of the third thoracic vertebra. The second receiver was mounted on the distal forearm portion of a custom made Orthoplast splint positioned on the elbow with elastic straps. The final receiver was positioned over the scapula after mounting it on a custom made and previously validated (Karduna et al., 2001) scapular-tracking device machined from plastic. The dominant arm of each subject was supported by a jig, inserted into the Orthoplast splint, which was affixed to a wooden stand (*Figure 1*).

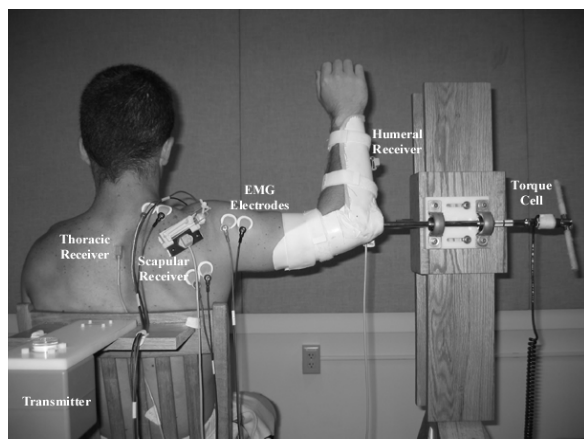

Figure 1: Experimental setup.

For passive motion, investigator applied torque and EMG activity (Myopac Jr. Run Technologies, Mission Viejo, CA) were measured. EMG was recorded from the pectoralis major (sternal head), trapezius (upper fibers), middle deltoid and infraspinatus. The chief purpose of these muscle recordings was to ensure that there was minimal muscle activity during passive positioning of the arm.

RESULTS

Passive humerothoracic motion was significantly greater than active humerothoracic motion for internal ($p<0.006$) and external rotations ($p<0.01$) in all planes (*Figure 2*).

A significant effect of motion type was found between passive humerothoracic and passive glenohumeral motion in six of seven conditions ($p<0.002$) (*Figure 3*).

Passive humerothoracic motion showed a significant effect of plane for internal rotation ($p<0.001$) but not for external rotation ($p=0.584$) (*Figure 4*).

DISCUSSION

End range determination and scapular motion had a significant effect on both internal and external rotation, while plane only had an effect on internal rotation. The least effect of scapular motion was observed for motion in the scapular plane. Measurements of internal and external rotation are dependent on the plane tested and how end range is determined. Additionally, if the scapula is not stabilized, a significant amount of motion may be occurring at the scapulothoracic articulation.

REFERENCES

Karduna AR, et al. (2001). *J Biomech Eng* **123**:184-90.

Poppen NK, et al. (1976). *J Bone Joint Surg Am* **58A**:195-201.

Reagan KM, et al. (2002). *Am J Sports Med* **30**:354-60.

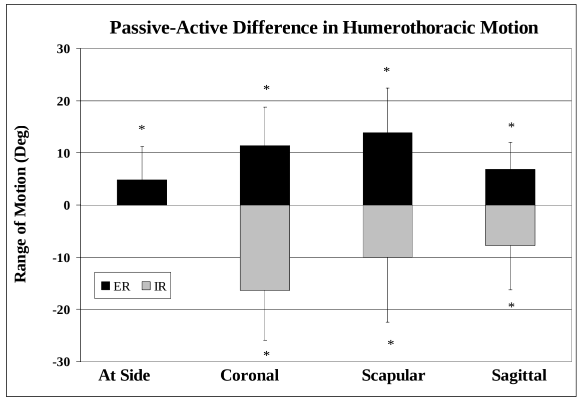

Figure 2: Mean (+/- sd) differences between passive and active humerothoracic motion. *****$p<0.05$

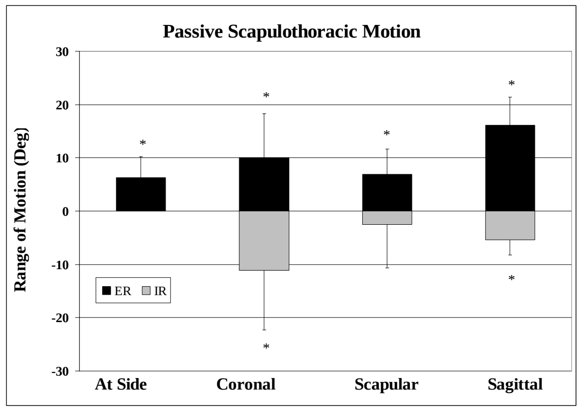

Figure 3: Mean (+/- sd) differences between passive humerothoracic and passive glenohumeral motion. *****$p<0.05$

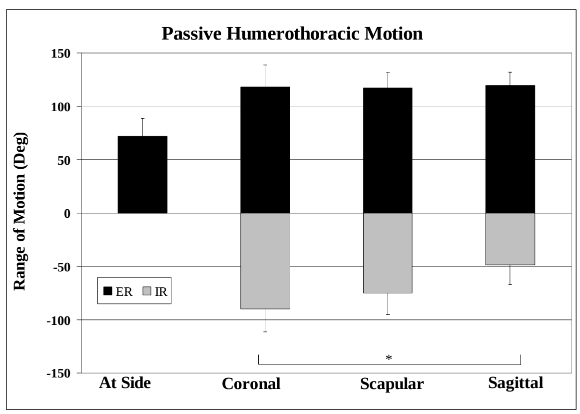

Figure 4: Mean (+/- sd) for passive humerothoracic motion across all seven conditions tested. *****$p<0.05$

MINIMAL ACTUATION REQUIREMENTS FOR POWERING THE PASSIVE WALKING MODEL WITH KNEES

Jesse C. Dean[1] and Arthur D. Kuo[1, 2]
[1]Dept. of Biomedical Engineering, [2]Dept. of Mechanical Engineering
University of Michigan, Ann Arbor, MI. E-mail: jcdean@umich.edu

INTRODUCTION

In passive dynamic walking, an unactuated pair of legs can descend a gentle slope with no need for control. We previously demonstrated powered walking on level ground for a straight-legged model, actuated by a combination of pushing off with the trailing leg, and moving the hips in a spring-like manner. Here we examine how the addition of knees affects the necessary actuation. We show that a kneed model can be stably powered solely through push-off. Adding springs to the swing hip and knee enables adjustment of step frequency, and it appears advantageous to actuate the knee by a minimal amount needed to achieve knee lock.

Passive walking has been described both with straight legs and with knees (McGeer, 1990a & b). We previously developed a powered straight-legged model that walks on level ground by pushing off with the trailing leg, to efficiently restore energy mechanical energy lost at heel strike (Kuo, 2002). A torsional spring acting on the legs, modeling hip muscles, allows step frequency to be tuned by speeding the pendular motion of the legs. Assigning a metabolic cost to each of these inputs, the model was able to predict the preferred speed–step length relationship seen in humans (Kuo, 2001). However, it is unclear how these results are affected by the addition of knees.

There are potential differences to a kneed model. Knees are obviously more anthropometrically realistic, resulting in a more human-like motion and greater toe clearance during the swing phase. But knees can also potentially alter the effects of push-off and the hip spring. Our approach was to use dynamical simulations to determine how the addition of knees to a powered model will affect the kinematics, energetic costs, and stability of walking.

METHODS

Our planar kneed walking model was similar to McGeer's (1990b), consisting of four segments with anthropomorphically distributed mass (Figure 1), and curved feet offset forward from the legs. Hyperextension of each knee was prevented by a passive mechanical stop. We added a push-off impulse applied at the ground contact point of the stance leg and directed toward the hip, and variable-stiffness torsional springs at the hips and knees. The model was made nondimensional by normalizing by body mass (M), leg length (L) and gravity (g).

The periodic gait was powered solely by push-off. During a gait cycle, knee lock and heel strike, modeled as impulsive, inelastic collisions, produced instantaneous changes in segment speeds with accompanying energy losses.

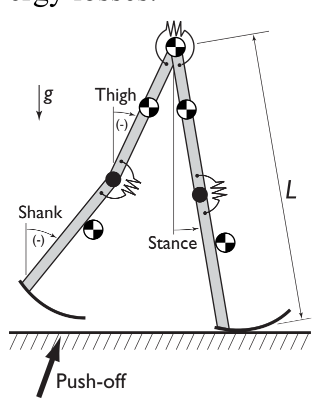

Figure 1: Side view of the walking model. The stance leg is actuated by an impulsive push applied along the leg prior to heel strike, and the joints are actuated by torsional springs. Stance, swing thigh, and swing shank angles are measured counter-clockwise with respect to vertical.

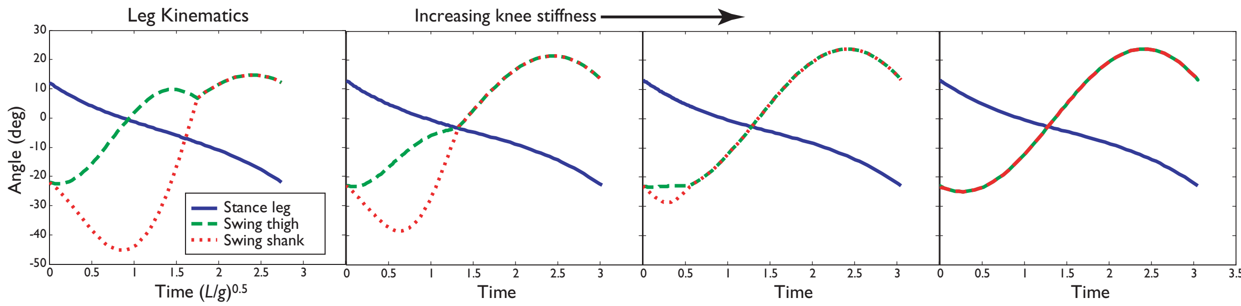

Figure 2: Kinematics of one full gait step, for models with successively stiffer knee springs, walking with a constant push-off impulse. A model with a fully passive knee (far left) has the greatest shank motion and reaches knee lock late in the step. As knee stiffness increases (left to right), knee lock occurs earlier and finally the gait resembles straight-legged walking (far right). Leg angles are defined in Figure 1.

RESULTS AND DISCUSSION

We found that with push-off alone, there is a wide range of stable gait cycles, just as in straight-legged walking. As reported by McGeer (1990b), the forward offset of the stance foot relative to the shank generates a passive knee extension moment that keeps the stance leg at full extension.

By varying the knee torsional stiffness, a continuum of gaits can be produced ranging from a fully free knee to a rigid leg. We found that the stiffer the knee, the earlier the occurrence of knee lock and the smaller the knee excursion (Figure 2). Some mechanical energy is lost when the knee locks, but interestingly, this is offset by a greater decrease in the energy lost at the heelstrike collision (associated with step-to-step transitions; Kuo, 2001). Here, the model with fully unactuated knees walks slightly faster than the straight legged model for the same push-off (Figure 3), but practically speaking, the difference is insignificant.

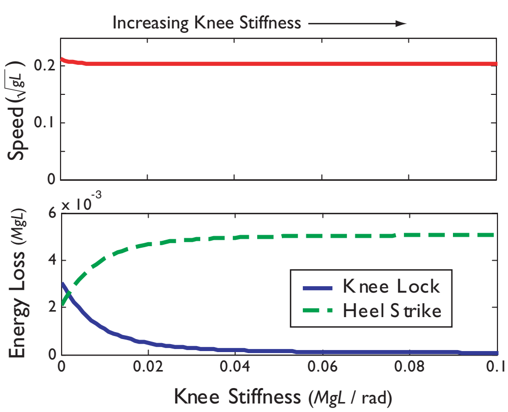

Figure 3: Speed (top) and energy losses at knee lock and heel strike, as a function of increasing knee torsional stiffness. For the same push-off, a slightly higher speed is achieved with a fully unactuated knee, where the energy lost at heel strike is minimized and that lost at knee lock is maximized.

We also found that step length is largely governed by push-off, and step frequency by hip spring stiffness. Stable gaits similar to the preferred human speed and step frequency (1.2 m/s, 1.8 Hz) were only possible if joint springs were included. For such a gait, a minimum knee stiffness was necessary for knee lock to occur by the end of the step. This stiffness also corresponded to minimum hip stiffness and lower collisional energy losses. To minimize muscle forces, it might be advantageous to actuate the knee only enough to achieve knee lock. In other respects, powering the kneed model follows the same principles as for straight legs.

ACKNOWLEDGEMENTS
Supported by the UM Institute of Gerontology, and NIH grant R21DC6466.

REFERENCES

Kuo A.D. (2001) *JBME* **123**, 264-269.
Kuo A.D. (2002) *JBME* **124**, 113-120.
McGeer T. (1990a) *Int J Rob Res*, **9**, 68-82.
McGeer T. (1990b) *IEEE Conf Rob Auto,* **2**, 1640-1645.

TRADE-OFFS IN THE DETERMINATION OF OPTIMUM STEP LENGTH IN HUMAN WALKING

Arthur D. Kuo[1], Jiro Doke[1], and J. Maxwell Donelan[2]

[1]Dept. of Mechanical Engineering, University of Michigan, Ann Arbor, MI
[2]University of Alberta, Edmonton, Canada   E-mail: artkuo@umich.edu

INTRODUCTION

Humans prefer to walk at the combination of step length and frequency that minimizes metabolic cost for a given speed (Elftman, 1966). We previously hypothesized that the optimum combination is largely determined by trade-offs between two costs. The first cost is for *step-to-step transitions*, associated with work needed to redirect the body center of mass (COM) from the pendular arc described by the stance leg. The second cost, for *forced leg motion*, is associated with work and force necessary to move the legs back and forth relative to the torso. Step-to-step transitions were shown to increase sharply with step length. Here we show that the cost of leg motion increases sharply with step frequency. Trade-offs between the two hypothesized costs determine optimum step length and the corresponding metabolic cost.

The optimum step length hypothesis is based on a simple model of passive dynamic walking, modified to walk on level ground (Kuo, 2001). In the passive model, energy dissipation only occurs when the COM is redirected from one pendular arc to the next. We powered this model by applying a push-off impulse, and found that step-to-step transition work was minimized by pushing off just prior to heelstrike (Fig. 1A). We also found that forcing the legs with spring-like actuation can reduce step-to-step transition costs. However, there is presumably a metabolic cost to forcing leg motion, even if no net work is performed over the step (Fig. 1B). We proposed metabolic rates $\dot{E}$ for step-to-step transitions and leg motion, roughly proportional to $l^4 \cdot f^3$ and $l \cdot f^4$, respectively, where l is step length and f is step frequency. The minimum of the summed costs yields optimum l and $\dot{E}$.

Each of these hypothesized costs can be tested by measuring $\dot{E}$ under conditions that highlight particular contributions. For example, we previously evaluated step-to-step transitions by asking subjects to walk with increasing l but constant f. We found that rate of work performed on the COM increased with l^4, and $\dot{E}$ also increased proportionally (Donelan et al., 2003). Below we describe an experiment to measure the cost of leg motion by increasing f with constant l.

METHODS

Eleven healthy subjects (7 male, 4 female; mass 67.2 ± 7.0 kg; leg length 0.93 ± 0.07

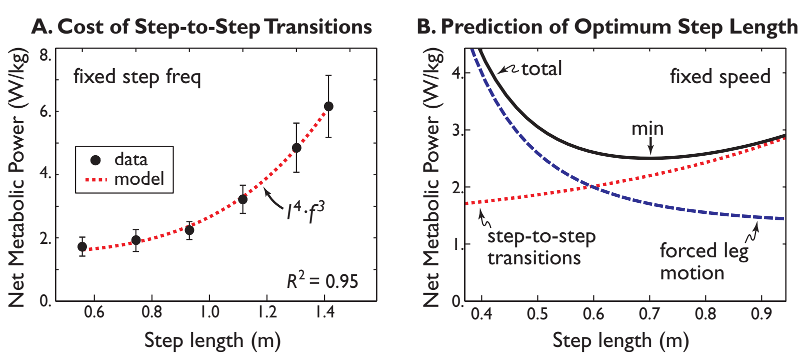

Figure 1: Trade-offs in metabolic cost of walking. (A) Net metabolic rate increases sharply with step length l, keeping step frequency f fixed (Donelan et al., 2001). (B) Minimum metabolic rate (min) at a given speed is observed to occur at intermediate step length, implying that another cost increases sharply with f. We hypothesize that a cost of forced leg motion produces the appropriate trade-off (Kuo, 2001).

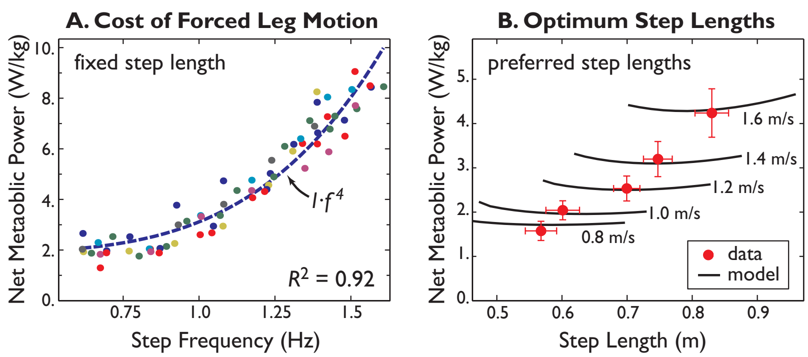

Figure 2: Net metabolic rate for walking at (A) fixed step length and (B) freely selected (preferred) step length. In (A), metabolic rate data increased sharply with step frequency, consistent with hypothesis. (B) Combining the relationships for step-to-step transitions (Fig. 1A) and forced leg motion yields combined costs (solid lines) whose minima agree well with recorded metabolic rate and preferred step length.

m; mean ± s.d.) provided informed consent and then familiarized themselves for 10 min. walking on a treadmill at 1.0 m/s, after which we measured their preferred step length l^* and step frequency f^* at that speed. We then measured their net metabolic rate (subtracting the cost of quiet standing) at seven speeds v ranging from 0.8 to 1.8 m/s, with constant l^* and increasing f^* ($v = l \cdot f$). The constraint was enforced with a metronome. At constant step length, the cost of forced leg motion is hypothesized to dominate step-to-step transitions, with metabolic rate $\dot{E}$ proportional to l^4. We also recorded net metabolic rate and preferred step length at the same speeds, allowing subjects to freely select gait. Both sets of conditions were applied in random order.

RESULTS AND DISCUSSION

We found that metabolic rate increased sharply with f when l was kept fixed. Consistent with the forced leg motion hypothesis, $l \cdot f^4$ fit these data well (Fig. 2A; R^2 = 0.92. Adding together the predicted costs of step-to-step transitions and forced leg motion yielded a curve for each speed, whose minimum was designed to roughly match the preferred step lengths we observed (Fig. 2B). A more significant test is whether $\dot{E}$ at those step lengths was also predicted. We found good agreement, $R^2 = 0.94$, but only with the addition of a relatively constant offset of about 1.4 W/kg (seen in Fig. 1B and 2B). At a speed of 1.2 m/s, the proportions of overall cost were 32% for step-to-step transitions, 12% for forced leg motion, and 56% for the offset.

Trade-offs between step-to-step transitions and forced leg motion offer a plausible explanation for the optimum step length in human walking. The metabolic cost of step-to-step transitions is explained by the work needed to redirect the COM, predicted by a simple walking model. However, what governs the cost of walking at increasing step frequencies (Fig. 2A) is less clear. Given that metabolic rate also increases sharply in isolated leg swinging without walking (Doke et al. 2003), it appears that the cost of increasing step frequencies is indeed for forcing the leg to move quickly. This cost might not only be for work but also for generation of force (yielding the f^4 relationship); series elasticity might also reduce the muscle fiber work needed to move the legs (Kuo, 2001). These latter predictions have yet to be addressed experimentally. Finally, we do not explain the relatively constant offset, which might be for supporting body weight or for controlling the limbs.

ACKNOWLEDGEMENTS

Supported by NIH grant R29DC0231201A1.

REFERENCES

Doke J. (2003) *Proc. ASB Ann. Mtg.*
Donelan J.M. (2002) *JEB* **205**, 3717-3727.
Elftman H. (1966) *JBJS* **48A**, 363-377.
Kuo A.D. (2001) *JBME* **123**, 264-269.

UPPER EXTREMITY JOINT STRESSES ASSOCIATED WITH WALKER-ASSISTED AMBULATION IN POST- SURGICAL PATIENTS

Margaret A. Finley[1,2] and Kevin J. McQuade[1,2]

[1] Rehabilitation Research and Development Service,
Baltimore Veterans Administration Medical Center, Baltimore, MD, USA
[2] University of Maryland School of Medicine,
Dept of Physical Therapy and Rehabilitation Science, Baltimore, MD, USA
Email: mfinley@som.umaryland.edu

INTRODUCTION

Whether on a temporary basis or permanently, individuals are prescribed walkers to assist with balance and/or to reduce lower extremity weight bearing. Over 77% of those reporting the use of a walker in 1997 were over 65 years of age (Russell, 1994). In order to understand the possible mechanisms of secondary conditions that may develop due the increased loading demands imposed by using walkers it is first necessary to obtain some baseline information on the actual joint forces and moments through biomechanical analysis of actual patients as they ambulate with their required walker. The purpose of this study was to describe the joint forces and moments of the wrist, elbow and shoulder in a sample of patients that are using a walker as a result of total joint surgery of the hips and knees.

METHODS

Twenty individuals (age = 66.6±8.2 years, M =11,F=9, height = 1.7±1.2m, weight = 89.6 ±14.0kg) post-surgical hip (n=8)or knee (n=12) joint replacement participated in the study. Three-dimensional kinematics of both upper extremities were collected at 100 Hz using infra-red light emitting diodes (Optotrack? , Northern Digital Inc., Waterloo, Ontario). Local coordinate reference frames defined by digitization of anatomical landmarks using specialized software (Innovative Sports Training, Chicago, IL). Kinematics were synchronized with forces transmitted through walkers obtained with transducers integrated into the handles of a walker (AMTI, Watertown, MA, USA). Inverse dynamics approach was used to calculate joint forces and moments at the wrist, elbow and shoulder.

Following subject set up, subjects ambulated approximately ten feet, two to three trials resulting in approximately 10-16 complete walker steps Walker steps were normalized from initial walker loading , to initial walker loading representing one walker cycle. Cycles were ensemble averaged and peak values calculated. Descriptive statistics were calculated and paired t-tests ($p \leq 0.05$) determined if differences existed in the surgical compared with non-surgical side upper extremity.

RESULTS AND DISCUSSION

Subjects were found to ambulate with 46.1% ± 13.9% weight on their upper extremities (r=-0.24), 25.7±7.0% and 20.4±8.5%, non-surgical and surgical side, respectively. No difference was found between the surgical and non-surgical side upper extremity joint kinematics. The wrist was found to be near neutral at contact and due to the progression of the forearm over the hand, the radial deviation angle increased until near peak hand force, then ulnar deviation was seen throughout the remainder of the cycle. The elbows were in flexion at initial contact, extended until peak hand loading, following which the elbows moved into flexion until the end of the cycle. Shoulder angles began in slight flexion and as the body progressed over the walker the shoulders moved into extension until after the swing phase started.

Peak forces at the hand transducer were greater in the non-surgical side, however, no difference was found in the total area during contact for the non-surgical limb (surgical = 241.2$\pm$143.0 N/kg BW, non-surgical = 273.2$\pm$108.8N/kg BW). Anterior shear forces were larger ($p=0.02$) for the non-surgical wrist as compared with the surgical side. The compressive (vertical) forces in the wrist ($p \leq 0.01$) and elbow ($p \leq 0.01$) were found to be greater in the uninvolved upper extremity (Figure 1). Larger sagittal plane moments were found in wrist ($p=0.01$) and elbow ($p \leq 0.01$) for the uninvolved limb as compared with the surgical side upper extremity (Figure 2).

Vertical, or compressive forces were found to be greater than body weight at each of the upper extremity joints, both surgical and non-surgical sides, greatest at the wrist and decreasing proximally. Because the upper extremity joints are functionally and structurally designed as non-weight bearing joints, the use of these types of mobility devices places increased demands on the user's upper extremities often resulting in and pain and pathology. Although the current subjects were post-surgical patients, they were in good health with normal upper extremity strength and function and utilized the walker for a reduction of lower extremity weight-bearing of less than 50% BW. However, many walker users are frail, elderly individuals following a sudden trauma such as a hip fracture and may have difficulty meeting the high demands of this task, especially if lower extremity weight bearing status is further limited.

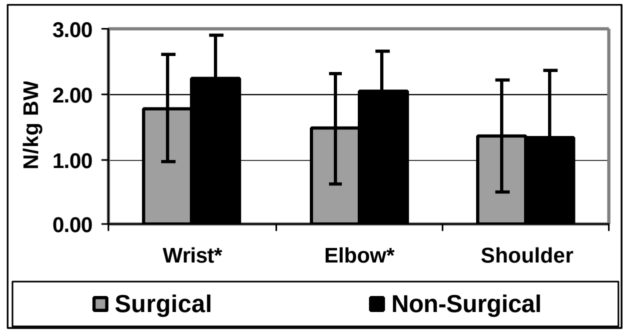

Figure 1: Vertical/compressive Joint Forces (*= significant difference between sides)

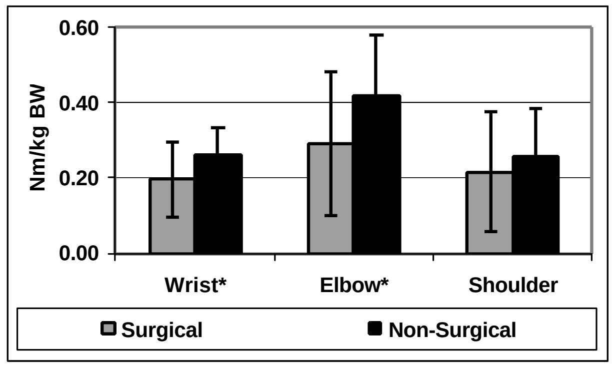

Figure 2: Sagittal Plane Moments (*= significant difference between sides)

SUMMARY

Results of this study indicate that demands on upper extremity joints associated with the use of a walker for assisted ambulation can reach as much as 2.5X body weight. The torque on the elbow joint tends to be the greatest suggesting high muscular demands of the elbow extensors and shoulder extensors. Further studies are needed to address the cause-effect relationship between the actual joint loading and the development of secondary musculoskeletal upper extremity complaints in more frail assistive device users.

REFERENCES

Russell JN, et al (1994) *Vital Health Stat Adv Data 1997*(292):1-12

COMPARISON OF HUMAN TURNING GAIT WITH THE MECHANICAL PERFORMANCE OF LOWER LIMB PROSTHETIC TRANSVERSE ROTATION ADAPTORS

Kevin C. Flick [1], Michael S. Orendurff [1], Jocelyn S. Berge [1], Ava D. Segal [1,2], Glenn K. Klute [1,2]

[1] Rehabilitation R&D, Center of Excellence for Limb Loss Prevention and Prosthetic Engineering, Seattle, WA USA. Web: www.seattlerehabresearch.org
[2] Dept. of Mechanical Engineering, University of Washington, Seattle, WA USA
Email: kflick@u.washington.edu

INTRODUCTION

Given that discomfort and injury are major complaints of amputees, it is important to minimize the forces (transverse and otherwise) arising from the prosthetic socket acting on the residual limb. While several Transverse Rotation Adaptors (TRAs) are available to reduce tissue loading in the transverse plane, little objective data exists documenting the effects of these devices. Two studies explored lower limb prosthesis rotation during straight-ahead walking (Lamoureux and Radcliffe 1977; Van der Linden, Twiste, et al. 2002). However, except for manufacturers' claims, there are no published reports on the influence of TRAs during more complex gait activities. Additionally, without again depending on the manufacturers' literature, there is no way to ascertain the differences between TRAs or between different setups on the same TRA.

METHODS

Three subjects with no gait pathologies consented to this IRB approved study. Each subject performed five trials walking straight and turning right around a 1m-radius circle at their self-selected speeds. Thirty-six reflective markers were placed on each subject according to the Plug In Gait model (Oxford Metrics). A ten-camera Vicon 612 system recorded the 3D coordinates of the markers. A Kistler force plate (Winterhur, CH) mounted flush with the laboratory floor recorded kinetic data. Torque is reported as moments generated by the subjects to counter environmental moments. The data include two conditions: right footstrikes during straight walking, and right turns on the right (inside) foot. The data were analyzed with Vicon's Workstation and Polygon software.

Five TRAs (Endolite TT and Demountable adaptors, Otto Bock Delta Twist and 4R39, and the Century XXII Total Shock) were purchased and tested in a servo-hydraulic material testing system (MTS, MTS System Corporation). Each elastomer for each TRA was tested over the full rotational range at 0.5 ^{0}/s, and 60 ^{0}/s. For all tests, the MTS rotated under displacement control from center to one end, back through the full range, then back to the center.

RESULTS AND DISCUSSION

The physiological torque vs. displacement curves were highly asymmetrical (figure 1). The greatest torques were applied during stance in the direction of internal rotation. The general pattern is external rotation under small external torque post heel-strike to mid-stance. At mid-stance, the foot is relatively immobile in the transverse plane but the torque reaches its maximum internal value. From mid-stance to toe-off, the torque declines, again with minimum angular displacement. During the swing phase, the foot rotates internally back to its neutral position under no torque. The notable exception to this pattern is the inside-right foot during right turns (red dashed line, fig. 1). In this condition, the foot angle changes at a more constant rate over the whole gait cycle.

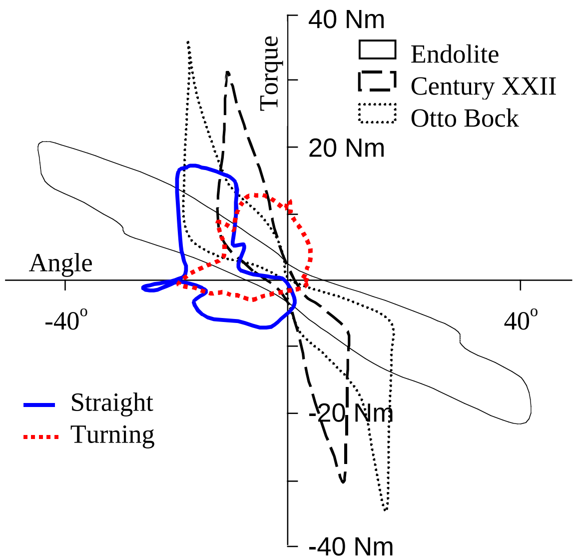

Figure 1: Torque vs. Angle for human subjects (n=3, 5 trials each, angle is foot relative to tibia) and TRA material testing (1 trial per TRA). Outlines are envelopes of actual data. Pos./neg. torques and angles are internal/external. Physiological data are from the right leg, which is on the inside during turning gait. Heel-strikes are positioned at the origin and time increases in the clockwise direction.

The main difference between human performance and TRA mechanical performance lies in the asymmetry of the physiological data. While walking straight-ahead and turning, nearly all of the rotation occurs externally relative to the angle at heel strike (figure 1). Also, internal torque is 6.6 times greater than external torque for the (inside) right leg during right turns. During straight-ahead walking, this asymmetry persists, with internal torque 2.2 times higher than external torque (figure 1). Despite this asymmetry, all the adaptors tested were capable of encompassing the maximum physiological torques.

All the adaptors tested have equal rotation, both internal and external, relative to their resting position (where the device would be at heel-strike). Given this, the necessary full range for the maneuvers tested in this study would be 52° (twice the maximum external rotation of 26°). If matching the physiological range of rotation is the critical performance measure, then only the Endolite adaptors in this study meet the needs indicated.

SUMMARY

These data allow the prosthetist to interpret qualitative issues raised by the amputee and direct him/her to the correct rotation adaptor and/or elastomer setup. The data from this study will also be useful in modeling a controllable TRA that can respond appropriately to minimize transverse tissue loading as the amputee maneuvers in the environment.

REFERENCES

Lamoureux, L.W., Radcliffe, C.W. (1977). *Prosthet Orthot Int*, **1**(2), 114-8.

Van der Linden, M.L., Twiste, N., et al. (2002). *Prosthet Orthot Int*, **26**(1), 35-43.

ACKNOWLEDGEMENTS

This study was funded by the Department of Veterans Affairs project # A2661C

Gastroc-Soleus Muscle Activation and its Association to Ankle and Knee Moments during Expected and Unexpected Side Step Cut Tasks

Jeff R. Houck[1], Sara Bigham[1], Patty Cruz[1], Megan Vanderhoof[1], Luke McCann[1], Cheri Ward[1], Kenneth De Haven[2], Andrew Duncan[2]

[1]Ithaca College- Rochester, 300 East River Road, Rochester, NY
[2]University of Rochester Medical Center, Rochester, NY

INTRODUCTION

The importance of understanding the role of the gastrocsoleus muscle at the knee is underscored by studies that suggest anterior cruciate ligament deficient subjects classified as copers utilize these muscles for stability(Rudolph et al, 1999). Besier et al (Besier, 2003) examined the knee moments during unexpected running tasks and identified a decrease in the knee abduction moment as a response. Houck (Houck, 2003) observed a differential response of the medial (MG) and lateral gastrocnemius (LG) EMG during contrasting cut styles. It was hypothesized that a differential response in the gastrocnemius muscle may partially explain control of the knee abduction moment during an unexpected side step cut task. The purpose of this study was to compare the ankle and knee moments and muscle activations of the gastrocsoleus during early stance (0 – 50 %) expected and unexpected walking straight and 45 ° side step cutting tasks.

METHODS

Eight young healthy subjects (22 ± 1.2 years) participated in this study. During a practice session the minimum time needed for subjects to side step cut 45 ° in response to a light cue was determined. Subsequently subjects were asked to perform walking straight ahead (ST), walking and side step cutting 45° (SS), both with no light cue (expected tasks). Then in a random sequence subjects responded to a light cue to proceed straight (STU) or side step cut 45 ° (SSU) (unexpected tasks). Feedback to maintain a target speed of 2.0 m/s was given using a infrared timing system (Brower Timing Systems) for 12 trials of each task. Data were collected using an Optotrak Motion Analysis System (Northern Digital, Inc.), force plates (Kistler) and 16 channel EMG system (Delsys, Inc.) integrated with Motion Monitor Software (Innsport Training, Inc.) to generate joint angles, moments and EMG patterns. Position data were sampled at 60 Hz, force and EMG data 1000 Hz. EMG data were RMS processed with a time constant of 11 ms, then binned in 5 % increments from 100 ms before heel strike to the end of stance. EMG was normalized to peak activation during a hop task. A 2 way ANOVA was used to test for an interaction between Muscle (Soleus, LG, MG) and Task (ST, STU, SS, SSU). Separate one way ANOVA's were used to test for differences across tasks (ST, STU, SS, SS) for the peak ankle and knee moments.

RESULTS AND DISCUSSION

Figure 1 shows a representative pattern of increased activation of the MG relative to the Soleus (SOL) and LG muscles. A significant interaction between muscle and task ($p = 0.031$) suggested a differential response between muscles across tasks (Table 1). Pairwise comparisons suggested the MG and LG showed a different response during the SS and SSU tasks. The ankle moments however were consistent for both the SS and SSU tasks (Table 2), suggesting the contribution to the ankle moment was similar between the SS and SSU tasks and therefore may not explain the difference in EMG between the LG and MG during the SSU task. However, the frontal plane moments were unique during the SSU task, and therefore are associated with the higher MG activation. The MG/LG differential response may also be influenced by the medial and lateral hamstrings muscles to balance the joint moments.

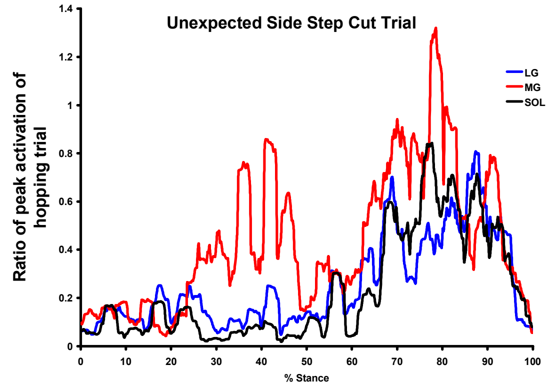

Figure 1. Representative subject trial (RMS) showing strong activation of MG relative to soleus and LG.

Table 1. Percent peak during hopping trial (Mean ± SD) of each task.

	Sol	MG.	LG	p-value*
ST	**15.5 ± 6.7**$^{\#,\&}$	9.5 ± 4.2	7.5 ± 2.7	**0.015**
STU	10.0 ± 3.4	10.6 ± 4.3	9.7 ± 3.6	0.794
SS	18.1 ± 8.4	**14.3 ± 4.4**$^{!}$	9.8 ± 4.4	**0.031**
SSU	**27.0 ± 14.9**$^{\&}$	**24.2 ± 12.4**$^{!}$	14.8 ± 6.5	**0.038**

significance Sol versus MG. $^{\&}$ significance Sol versus LG and **!** significance MG versus LG.

Table 2. Peak (Mean ± SD) internal joint moments (Nm/kg) across tasks.

	ST	STU	SS	SSU	p-value
Ankle PF	0.36 ± 0.13	0.27 ± 0.11	**0.53 ± 0.21**$^{\&}$	**0.68 ± 0.18**$^{\&}$	**0.001**
Knee Ext	0.82 ± 0.19	0.92 ± 0.26	**1.11 ± 0.27**$^{\&}$	**1.09 ± 0.22**$^{\&}$	**0.001**
Knee Abd.	0.57 ± 0.24	062 ± 0.27	0.55 ± 0.33	**0.30 ± 0.34**$^{!}$	**0.014**

*P-values represent result of One Way ANOVA. $^{\&}$ indicate ST/STU are significantly different than SS/SSU; **!** indicates SSU is significantly different than all other tasks.

SUMMARY

The new findings of this study suggest there is a differential response of the gastroc-soleus muscles during early stance of a unexpected side step cut task. The EMG activation is associated with the knee moment patterns suggesting a differential EMG pattern in response to altered loads at the knee and not the ankle. Distinguishing the role of the gastroc-soleus actions at the knee may impact injury prevention and rehabilitation.

REFERENCES

Besier et al. (2003)Med. Sci. Sports Exerc. **35**, 119-127.
Houck, J.R. (2003) J. Electromyogr. Kinesiol. **13**, 545-554.
Rudolph et al, (2001) Knee Surg., Sports Traumatol., Arthrosc **9**, 62-71.

ACKNOWLEDGEMENTS

Whitaker Foundation Grant #RG-02-0645.

FLUOROSCOPIC ASSESSMENT OF THE EFFECTS OF ROTATOR CUFF FATIGUE ON GLENOHUMERAL KINEMATICS IN SHOULDER IMPINGEMENT SYNDROME

Philip J. Royer[1], Edward J. Kane[1], Kyle E. Parks[1], Jacob C. Morrow[1],
Richard R. Moravec[1], Douglas S. Christie[1], Deydre S. Teyhen[1,2]
[1]Physical Therapy Research Center, U.S. Army-Baylor University Graduate Program in Physical Therapy, Fort Sam Houston, TX, USA
[2]Department of Kinesiology & Health Education, The University of Texas, Austin, TX, USA
E-mail: deydre.teyhen@us.army.mil

INTRODUCTION

Subacromial outlet impingement is the most common cause of shoulder pain. Rotator cuff (RTC) dysfunction has been postulated to contribute to shoulder impingement syndrome (SIS). Fatigue of the muscles of the RTC may result in increased superior glenohumeral migration, decreasing the subacromial space (Chen *et al.* 1998 & Deutsch *et al.* 1996). Gaining a better understanding of the effects of RTC fatigue on glenohumeral kinematics during dynamic motion, both in normal subjects and patients diagnosed with SIS, may provide improved insight into the etiology of SIS, more accurate and timely diagnostic techniques, and more focused treatments for patients suffering from shoulder pathologies such as SIS. The purposes of this study were to: 1) describe superior-inferior glenohumeral migration during arm elevation in individuals with SIS, 2) analyze the effect of RTC fatigue on glenohumeral migration and 3) determine interrater reliability for analyzing dynamic glenohumeral migration using digital fluoroscopic videos (DFV).

METHODS

Prior to subject recruitment, interrater reliability was established using DFV from 10 subjects in the lab database. An ICC (2,3) was utilized to determine reliability between raters.

Twenty male volunteers (27.70 ± 7.25 years) with right SIS completed this study. Three DFV of arm elevation in the plane of the scapula were collected for each subject at 30 Hz using a Dynamic Motion X-Ray (DMX-Works Inc., Palm Harbor, FL). DFV were obtained both pre- and post-fatigue of the RTC.

Fatigue of the RTC was achieved utilizing a protocol adapted from Chen *et al.* (1998). Fatigue was confirmed by at least a 40% strength decrement as measured by a hand held dynamometer. The DFV were analyzed according to the methods described by Chen *et al.* (1998) from 0-135°. The pre- and post-fatigue DFV were compared to assess the difference in humeral head migration due to RTC fatigue.

This study utilized a 2×4 repeated measures ANOVA in order to contrast humeral head migration at 0, 45, 90, and 135° pre- and post-fatigue ($\alpha = .05$). *Post hoc* analysis utilized paired t-tests with a Bonferroni correction.

RESULTS AND DISCUSSION

The ICC (2,3) values ranged from 0.70-0.92 with a SEM ranging from 0.534 to 0.644 mm (approximately 1.6 pixels). The repeated measures ANOVA revealed a main effect for fatigue state ($p = 0.025$) and arm angle ($p = 0.017$). *Post hoc* paired t-tests, with a Bonferroni Correction, revealed significant superior migration between 45° and 135° prior to fatigue of the RTC ($p = 0.040$). Post-fatigue, the position of the humeral head was more superior at the arm at side position ($p = 0.035$). There was no interaction effect between angle and fatigue state ($p = 0.093$) (Figure 1).

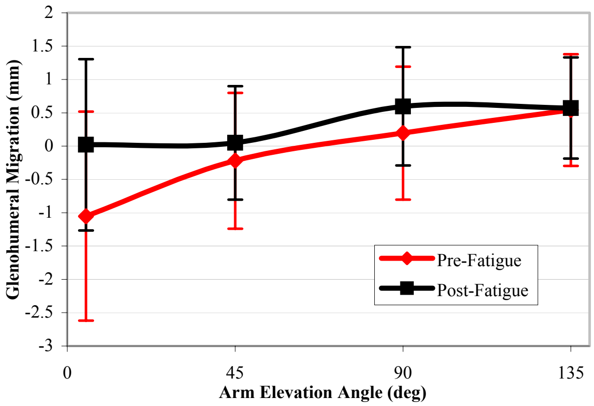

Figure 1: Glenohumeral migration during arm elevation, pre- and post- RTC fatigue.

The amount of superior migration during arm elevation pre-fatigue is consistent with prior reports (Deutsch *et al.* 1996 & Ludewig & Cook 2002) when analyzing subjects with SIS, and normal subjects during dynamic motion of the arm (Ludewig & Cook 2002 & Miller *et al.* 2003). However, the position of the humeral head in SIS subjects was more superior on the glenoid fossa when compared to normal subjects studied by Miller *et al.* (2003). Our results differ from previous studies (Chen *et al.* 1998 & Deutsch *et al.* 1996), which found no significant glenohumeral migration prior to RTC fatigue in non-pathologic shoulders. These differences may be attributable to the type of contraction utilized in the studies (dynamic versus isometric), or due to the subject's condition (non-pathologic versus SIS).

Following the RTC fatigue protocol, the humerus was positioned more superiorly on the glenoid fossa at the arm at side position, when compared to the pre-fatigue state. No significant differences were found at higher angles of elevation. Prior studies (Chen *et al.* 1998 & Miller *et al.* 2003) of normal subjects have found significant differences in humeral head position between fatigue states at higher angles of elevation. A possible explanation for these differences could be that the humeral head began more superiorly on the glenoid fossa following fatigue in our SIS subjects. This could potentially narrow the subacromial space and create a "ceiling effect" thereby limiting additional superior glenohumeral migration.

SUMMARY

DFV analysis is a reliable tool for studying glenohumeral kinematics during arm elevation. Prior to fatigue of the rotator cuff, superior migration of the humeral head was consistent with previous studies analyzing both normal and pathological shoulders. The more superior position of the humeral head following RTC fatigue may indicate the importance of the dynamic stabilizers of the shoulder at angles below 45° of arm elevation.

REFERENCES

Chen, S.K. *et al*. (1998). *J Shoulder Elbow Surgery,* **7**(2), 164-7.

Deutsch, A. *et al*. (1996). *J Shoulder Elbow Surgery*, **5**, 186-93.

Ludewig, P. M., Cook, T. M. (2002). *J Orthop Sports Phys Ther*, **32**, 248-59.

Miller, J. *et al*. (2003). Unpublished Research.

The opinions and assertions contained herein are the private views of the authors and are not to be construed as official or as reflecting the views of the Departments of the Army, Navy, or Defense.

DIGITAL FLUOROSCOPIC VIDEO ASSESSMENT OF SAGITTAL PLANE LUMBAR SPINE FLEXION

Deydre S. Teyhen,[1,2] Lawrence D. Abraham,[1] and Timothy W. Flynn[3]

[1] Department of Kinesiology & Health Education, The University of Texas, Austin, TX, USA
[2]U.S. Army-Baylor Graduate Program in Physical Therapy, Fort Sam Houston, TX, USA
[3]Department of Physical Therapy, Regis University, Denver, Colorado, USA
E-mail: Deydre.Teyhen@amedd.army.mil Web: utexas.edu/education/kinesiology/

INTRODUCTION

Despite the exponential rise in surgical rates of lumbar spinal fusion, there remains no clear consensus on what constitutes lumbar instability. The clinical diagnosis of lumbar instability is still largely based on patient history and certain inconclusive findings (Lund, 2002). To date, no definitive relationship exists between intervertebral motion and the clinical symptoms attributed to lumbar instability. This is in part due to a lack of a non-invasive measurement tool to assess lumbar kinematics.

Errors in measurement have limited the use of radiographic techniques to analyze lumbar kinematics. Frobin *et al.* (1996) and Brinckmann *et al.* (1994) developed a distortion compensated roentgen analysis (DCRA) technique that improves landmark verification while minimizing the effects of distortion and patient positioning in the field of view. Their technique uses a computer-assisted algorithm to determine segmental angle and displacement values from static images of vertebral body outlines. The purpose of this study was to assess the reliability of the DCRA technique using digitally enhanced images from digital fluoroscopic videos (DFV) captured during the eccentric phase of lumbar flexion.

METHODS

A convenience sample of 20 males, 11 with and 9 without LBP, 19-45 years of age, completed this study. Two lateral DFV of L3-S1 during eccentric lumbar flexion were obtained at 30 Hz. A Philips Diagnost 76 (Philips Medical Systems, Andover, MA) and an I-75 frame grabber (Foresight Imaging, Lowell, MA) were used.

Intra-image reliability was assessed from the upright and flexed single images of each subject from a single movement (40 images, 3,360 point placements). Inter-image reliability was assessed during two separate flexion trials separated by a 2-minute rest and 2-minute walk break (40 DFV, an average 2.27 $\pm$ .67 seconds per motion, 38,346 total point placements). To ensure dynamic motion throughout the range, the third of four consecutive movement patterns was captured. Hip and knee restraints minimized motion of the lower extremity during lumbar flexion.

The DFV were processed by four image processing techniques designed to accentuate the vertebral edges: band-passed filter, edge detection filter, median filter, and a subtraction of the BP-MF DFV (Fig. 1), using Image Pro-Plus (Media-Cybernetics, Silver Springs, MD) software.

A computer-assisted DCRA algorithm was developed to analyze intersegmental angle and displacement between L3-S1. The algorithm was altered to allow for direct location of the vertebral corners on the DFV. For the sacrum, only the cephalad border of S1 was located.

Two ICCs were calculated to determine a reliability coefficient for the intra- and inter-image reliability, respectively. Intra-image reliability was calculated from a mean of three cycles of the algorithm on single images of the upright and flexed postures, each representing the mean of four anatomical landmark locations. The inter-image reliability represented only one cycle of the algorithm for each frame over the entire trial. The SEM was calculated to determine response stability.

RESULTS AND DISCUSSION:

Analysis of the point placement technique and the computer algorithm using the intra-image reliability resulted in an average ICC (2, 12) value of 0.986 (0.966-0.999) across all levels for angle and displacement. This is interpreted as good (Portney & Watkins, 2000).

Analysis of inter-image reliability, including variability of motion over trials and errors associated with repositioning in the field of view, yielded an average ICC (2,4) value of 0.913 (0.816-0.945) for angle and 0.842 (.637-.933) for displacement. These were classified as moderate for displacement of L3/4 and good for all other segments.

The SEM for intra-image reliability ranged from 0.4-0.7° and 0.2-0.3 mm. For inter-image reliability the SEM averaged 1° (0.7-1.4°) and 0.6mm (0.4-0.7 mm), with a 95% CI of measurements within 2° and 1.2 mm. Frobin *et al.* (1996) reported *in vitro* error (SD) of a similar measurement technique ranging from 0.8-1.6° and 0.5-0.8 mm.

SUMMARY:

The use of DCRA on DFV is a reliable method with acceptably low measurement error. This technique can be used as a non-invasive tool to analyze lumbar movement patterns. On-going research is attempting to assess the validity of diagnosing patients with suspected lumbar segmental instability using this method.

REFERENCES:

Brinckmann, P. *et al.* (1994). *Clin. Biomech.*, **9**, S1-S83.
Frobin, W. *et al.* (1996). *Clin Biomech.*, **11**, 457-65.
Lund, T. *et al*. (2002) *Spine*., **27**, 2726-2733.
Portney L.G., Watkins M.P. (2000). *Foundations of Clinical Research.* Appleton & Lange.

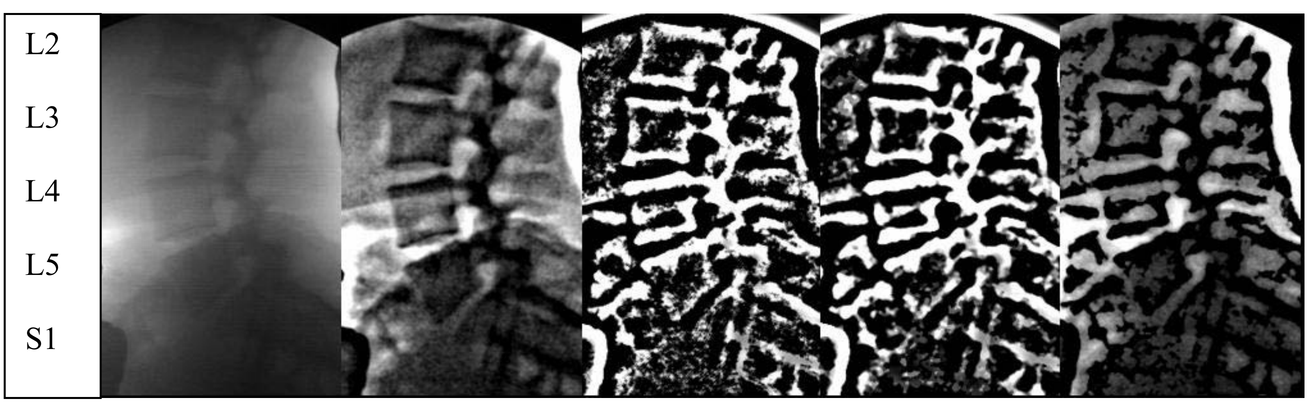

A B C D E

Figure 1: Image Processing Techniques: A: Original DFV, B: Band-Passed DFV, C: Edge-Detection DFV, Median Filter DFV, E: Final Version (B-D).

ON THE ANATOMY OF THE EXTENSOR MECHANISM AND WHY CO-CONTRACTION IS NECESSARY FOR VERSATILE STATIC FINGERTIP FORCES

Francisco J. Valero-Cuevas

Neuromuscular Biomechanics Laboratory, Cornell University, Ithaca, NY, USA
E-mail: fv24@cornell.edu Web: www.mae.cornell.edu/valero

INTRODUCTION

The so-called multi-articular musculo-tendons couple torque production across joints because they cross several degrees-of-freedom (DOFs) of a limb. There is much debate on whether the function and control differs for mono- and bi-articular musculotendons [4]. To expand this dialogue, I highlight some biomechanical aspects of multi-articular finger musclotendons. I conclude it is useful to consider these aspects before drawing conclusions about the neural selection of coordination patterns.

A SIMPLE FINGER MODEL

Consider a simple 2-joint, 5-musculotendon planar finger. Tendon routing produces moment arms $r_{i,j}$ at DOF i for musculotendon j (Fig. A), which combined with the level of muscle force determine the contribution of each musculotendon force to joint (i.e., DOF) torques τ_1 and τ_2. This contribution leads to a vector in "torque space," Fig. B [2, 5, 7]. The net joint torques are the resultant vector from the addition of the torque vectors from active musculotendons, Fig. D.

RESULTS AND DISCUSSION

I. For this model to be versatile at nonsingular finger postures, it should be able to produce static fingertip force vectors in every direction in the plane, Fig. A [2, 5, 7]. Given that fingertip force vectors are obtained by mapping net joint torque vectors through the Jacobian^{-T} of the model, *versatility is only possible if the musculature can produce net joint torque vectors in all quadrants of the torque space*. That is, the feasible torque set (FTS) of the finger must span portions of all quadrants (Fig. C). The FTS defines all possible net joint torque vectors that could be produced by a group of musculotendons. The FTS is obtained by finding all possible positive linear combinations in torque space. E.g., FTS1,2 includes all possible torque vectors m1 and m2 can produce; and FTS1,2,3,4,5 is the *total* FTS for all muscles (Fig. C).

II. *Every* musculotendon, no matter how weak, contributes uniquely to the size and shape of the fingertip feasible force set. Thus, the impairment or rehabilitation of any musculotendon will change the *size and shape* of the feasible force set [7]. This challenges notions of musculotendon "redundancy" by making it difficult to decide which musculotendon we would rather do without—and suggests means to quantify and counteract impairment in partial paralyses [1].

III. *Multi-articular musculotendons efficiently enlarge the total FTS*. For example, m4 can by itself span large sections of quadrant IV, which would otherwise need 2 dedicated musculotendons (Figs. C&D). Interestingly, this tendon cross-over (flexor first and then extensor) is a defining anatomical feature of the extensor mechanism. Greater coverage of quadrant IV can only enlarge the feasible force set of the fingertip. Interestingly, these cross-over musculotendons (lumbrical and palmar interosseous) produce index fingertip force in directions useful to oppose the thumb during grasp [6]. This begins to explain the known finger impairment when the extensor mechanism is disrupted [3]. While the alternative cross-over tendon route is possible, the associated fingertip forces would be directed roughly opposite to those needed for grasp, which I speculate may not have as strong an evolutionary advantage.

And **IV**. Co-contraction (i.e., simultaneous activation of agonists and antagonists) at some finger DOFs is often not an option, but a consequence of multiarticular tendon routing. Co-contraction is seen graphically as a reversal along a DOF in the vector addition needed for net joint torque production. For example, producing the net joint *torque vector 1* using m3, m4 and m5 must reverse direction one DOFs (wide bars on coordinate axes, Fig. D). Fig. E shows how only in FTS 1,2, FTS 3,4 and FTS 3,5 is it possible to achieve a net joint torque vector without reversing direction, e.g., *torque vector 2*. Redundancy is seen graphically as the possibility to reach any point inside FTS 1,2,3,4,5 via multiple vector additions. While points inside FTS 1,2, FTS 3,4 and FTS 3,5 can be reached both with and without co-contraction, co-contraction is unavoidable anywhere else in FTS 1,2,3,4,5. Thus versatile static fingertip force production requires co-contraction.

The FTS approach is only a linear approximation to the finger's torque capabilities, and its results are sensitive to tension-dependent nonlinearities in moment arms and/or possible neural synergies. Nevertheless, it provides insight into the attributes of multi-articular musculotendons. I suggest that our understanding "bi-articular" musculotendons can extended by also considering the "tri-" and "tetra-" articular musculotendons of the fingers.

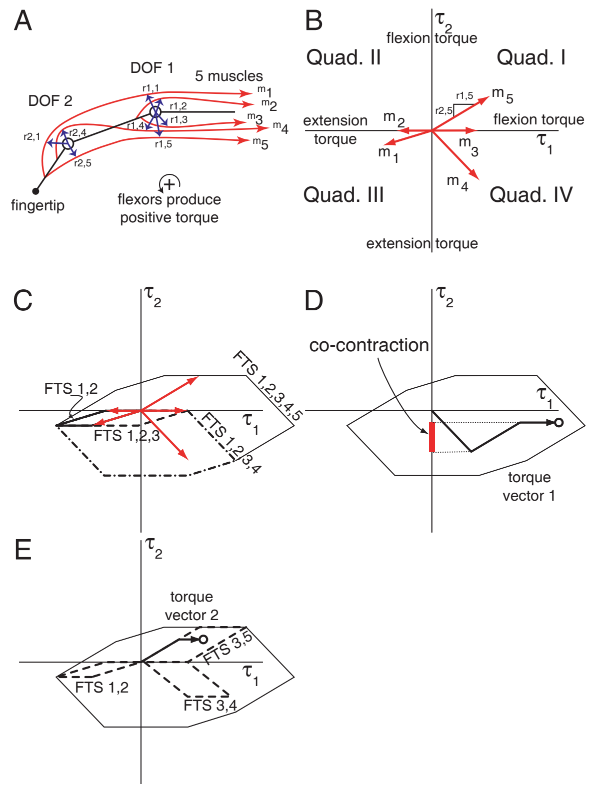

REFERENCES

[1] Kuxhaus, L.C. et al. Quantifying deficits in the 3D force capabilities of a digit caused by selective paralysis. J Biomech, In Rev.. **[2]** Leijnse, J.N., A graphic analysis of the biomechanics of the massless bi-articular chain. application to the proximal bi-articular chain of the human finger. J Biomech, 1996. 29(3): p. 355-66. **[3]** Malaviya, G.N., Correction of claw fingers in leprosy. Acta Leprol, 1991. 7(5): p. 389-95. **[4]** Prilutsky, B.I., Coordination of two- and one-joint muscles. Motor Control, 2000. 4(1): p. 1-44. **[5]** Spoor, C.W., Balancing a force on the fingertip of a two dimensional finger model without intrinsic muscles. J Biomech, 1983. 16(7): p. 497-504. **[6]** Valero-Cuevas, F.J. et al. Quantification of fingertip force reduction in the forefinger following simulated paralysis of extensor and intrinsic muscles. J Biomech, 2000. 33(12): p. 1601-09. **[7]** Valero-Cuevas, F.J. and V.R. Hentz, Releasing the A3 pulley and leaving flexor superficialis intact increase palmar force following the Zancolli lasso procedures to prevent claw deformity in the intrinsic minus hand. J Orthop Res, 2002. 20(5): p. 902-9.

ACKNOWLEDGEMENTS

This material is based upon work supported by NSF under CAREER Grant No. 0237258 and ITR Project No. 0312271, and the Whitaker Foundation.

FORCE TRANSMISSION VIA MYOFASCIAL PATHWAYS IN DYNAMIC CONDITIONS OF A SINGLE HEAD OF MULTI-TENDONED RAT EDL MUSCLE

Huub Maas [1], and Peter A. Huijing [2, 3]

[1] School of Applied Physiology, Georgia Institute of Technology, Atlanta, GA, USA
[2] Faculty of Human Movement Sciences, Vrije Universiteit Amsterdam, The Netherlands
[3] Institute for Biomedical Technology, Universiteit Twente, Enschede, The Netherlands
E-mail: huub.endemaas@ap.gatech.edu

INTRODUCTION

Movements of digits are caused by multi-tendoned muscles, which are characterized by multiple muscle heads connected proximally to one origin and connected distally to multiple aponeuroses and tendons. Experiments on fully dissected rat extensor digitorum longus muscle (EDL), a multi-tendoned muscle, clearly indicated intramuscular myofascial force transmission: force transmission between muscle heads via their shared connective tissue (Huijing et al., 1998). Force transmission from head III of EDL muscle (EDL III) via inter- and extramuscular connective tissues has also been shown (Maas et al., 2003). All previous experiments on myofascial force transmission involved isometric contractions exclusively. The purpose of the present study was to investigate the contribution of myofascial force transmission in dynamic muscle conditions. Therefore, effects of dynamic shortening of EDL III in rat, operating within an in vivo context of connective tissue, were studied.

METHODS

The distal tendon of EDL III and the proximal tendon of whole EDL were exposed, and connected to force transducers. The distal tendons of EDL head II, IV, and V were left attached to their insertions in the foot. The distal tendons of tibialis anterior (TA) and extensor hallucis longus (EHL) muscles were dissected, tied together and connected to a force transducer (TA+EHL). Connective tissue of the anterior crural compartment was left intact.

Muscle-tendon complex lengths (l_{m+t}) of TA+EHL as well as the position of the proximal tendon of EDL muscle were kept constant. Supramaximal stimulation of the peroneal nerve excited all muscles maximally and simultaneously. Forces of distal EDL III, proximal EDL and distal TA+EHL were measured while EDL III was shortened from optimum length (l_o) to l_o – 2 mm, following a sinusoidal trajectory in time (Fig. 1C).

RESULTS AND DISCUSSION

The force trace of TA+EHL, kept at constant length, resembled that of an isometric contraction (data not shown). This suggests that intermuscular interactions between EDL III and TA+EHL were negligible.

After the onset of nerve stimulation and the start of EDL III shortening, proximal EDL force built up to a maximum of 1.61 ± 0.08 N (Fig. 1A). Despite the fact that the muscle fibers of EDL III have the capability to transmit force onto the proximal aponeurosis of EDL, length changes of EDL III hardly affected proximal EDL force.

EDL III force (Fig. 1B) built up to a maximum of 0.58 ± 0.04 N and decreased progressively during active shortening (to 0.26 ± 0.02 N). The substantial difference

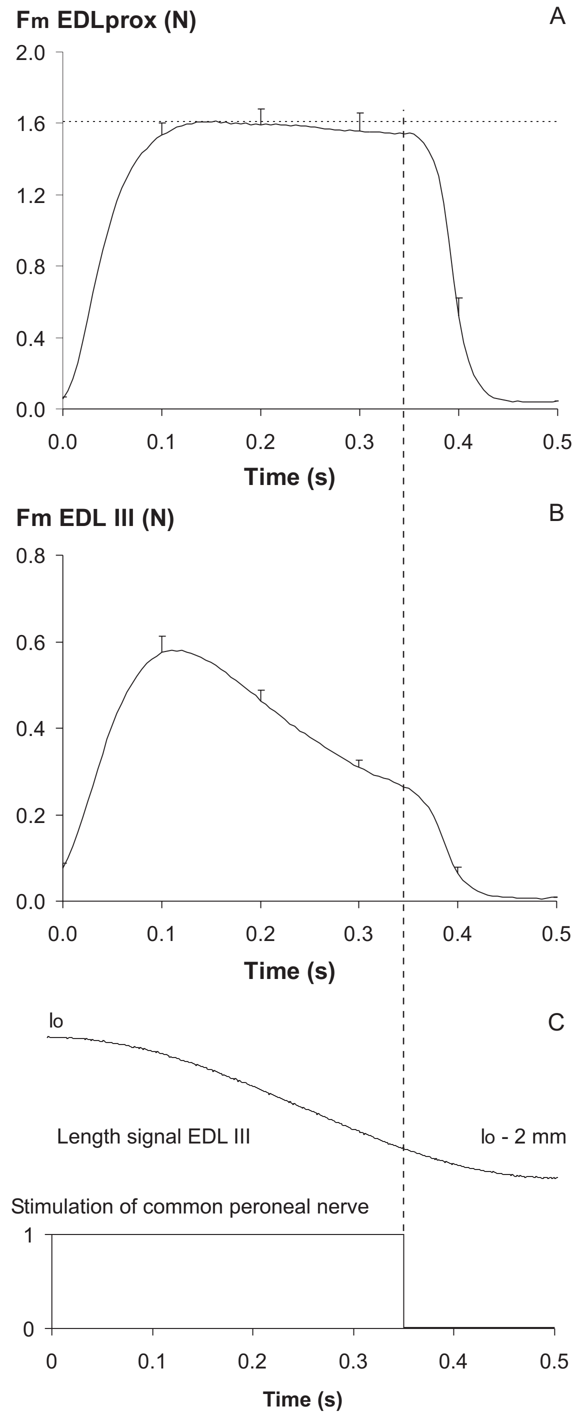

Figure 1: EDL total forces (F_m) during sinusoidal shortening of EDL III. (A) Proximal EDL, (B) distal EDL III, (C) l_{m+t} of EDL III and stimulation of the common peroneal nerve.

between changes of proximal EDL force and changes of EDL III force indicates effects of myofascial force transmission.

Despite effects of shortening velocity, maximal concentric force of EDL III was higher than maximal isometric force of EDL III muscle fibers (0.42 N). The latter was estimated on the basis of optimal isometric force of whole EDL muscle (2.60 N) and the relative mass of EDL III (16 %). This indicates that part of the force exerted at the distal EDL III tendon originated from other sources than from muscle fibers of EDL III.

It is concluded that also for concentric muscle conditions, force is transmitted via myofascial pathways between a single head of multi-tendoned muscle and adjacent tissues.

SUMMARY

Effects of dynamic shortening of EDL III were investigated. Substantial differences between force changes exerted at the proximal tendon of EDL and the distal tendon of EDL III were found. No effects of EDL III shortening on TA+EHL force could be shown. These results are explained in terms of intra- and extramuscular myofascial force transmission.

REFERENCES

Huijing, P. A. Et al. (1998). *J. Exp. Biol.*, **201**, 683-691.

Maas, H. et al. (2003). *J. Appl. Physiol.*, **95**, 2004-2013.

ACKNOWLEDGEMENTS

The School of Applied Physiology at the Georgia Institute of Technology is acknowledged for funding the costs of attending the ASB 2004 congress.

EFFECTS OF BLURRING VISION ON M/L BALANCE DURING STEPPING UP OR DOWN TO A NEW LEVEL IN THE ELDERLY

[1]John G Buckley, [1]Karen Heasley, [2]Andy Scally and [1]David B Elliott.
[1]Vision and Mobility Research Laboratory, Department of Optometry, [2]Institute of Health Research, School of Health, University of Bradford, Bradford, UK.
Email: j.buckley@bradford.ac.uk
Web: Brad.ac.uk/acad/lifesci/optometry/research/VisionMobilityLab.htm

BACKGROUND
Visual impairment has been found to be associated with an increased risk of falling in the elderly (e.g. Ivers et al. 1998, Jack et al. 1995). In the study by Jack et al. half of the elderly patients admitted to an acute geriatric clinic were reported to have impaired vision, with a high prevalence (76%) of visual impairment in patients admitted due to falls. Stair and kerb negotiation seems to be a particular problem for the elderly with falls on stairs being the leading cause of accidental death (Dowswell et al., 1999). It is widely accepted that the elderly have an increased susceptibility to falling due to age-related deterioration in postural control mechanisms, and it has been demonstrated that deficits in medio-lateral (ML) postural stability are able to distinguish fallers from non-fallers (Maki et al., 1994). It therefore seems pertinent to investigate how impaired vision in the elderly affects ML balance when negotiating stairs and/or steps.

The present study determined how ML balance parameters when stepping up or down to a new level were affected by blurring the vision of healthy elderly subjects.

METHODS.
Twelve elderly subjects (72.3 ± 4.2 yr) were analysed performing single steps up and single steps down to a new level (7.2cm, 14.4cm, 21.6cm) with vision optimally corrected or blurred by cataract simulation lenses. The order of measurement was randomised, and each stepping trial was completed twice. Subjects started with each foot placed on a separate (AMTI OR6-7) force platform (stepping up) or on a step positioned on top of each of the force platforms (stepping down). A five-camera motion analysis system (Vicon 250, Oxford Metrics Ltd) was used to determine whole body CM displacements and these along with GRF and centre of pressure data (at 50Hz) were exported in ASCII format for further analysis. Force and centre of pressure data from each platform were combined to provide global centre of pressure coordinates (CP). Differences between the ML GRF impulse (~to ML CM momentum) developed by the intended swing limb during double support, ML dynamic stability (RMS fluctuation in ML position of CP during single support), lateral position of the CM relative to the supporting foot (average horizontal ML distance between the CM and CP during single support) and movement phase times under optimal and blurred visual conditions were analysed using a random effects model. The terms in the model were vision (normal, blurred), step height (high, medium, low), direction (up, down) and repetition (trial 1, trial 2). Significance of the two-level factors were determined by the 'Z'-statistic, while the significance of the three-level factor was tested using a likelihood ratio (Chi-squared) test after first dropping the factor from the model.

RESULTS AND DISCUSSION.

Duration of double and single support and the ML GRF impulse were significantly greater when vision was blurred ($p<0.001$), while ML dynamic stability ($p<0.001$) and the average CM-CP ML distance ($p=0.04$) was significantly reduced. Interactions terms and the effect of repetition were not significant ($p>>0.05$). These findings suggest that with blur the visual system was unable to provide accurate exteroceptive information and the stepping movement thus became uncertain. This uncertainty may explain why duration of double support was found to significantly increase by 16.7%, because it is during this time that anticipatory postural adjustments initiate forward progression of the CM and a shift from bipedal to unilateral stance. The finding that *ML GRFi* also increased with blurred vision during this phase by about 11.4% indicates that subjects developed greater lateral impulse so their CM would be 'shifted' closer towards the stance limb during the subsequent single support phase (indeed CM-CP ML distance reduced with blur from 83 ± 23 to 78 ± 22 mm). The increase in single support time when vision was blurred suggests that subjects were more tentative placing their lead limb on the ground or step. These adaptations, which are in keeping with our earlier study (Buckley et al., In Press) suggesting that with blurred vision the elderly become more cautious and attempt to 'feel' their way to the ground with their lead limb when stepping down, may have all contributed to the substantial (~26%) reduction in ML dynamic stability during single support ($p<0.001$). Such reductions are likely to be crucial because of the narrow base of support during this time. In addition, ML dynamic stability decreased with increasing step height and was worse when stepping down than when stepping up ($p<0.001$). Alterations in swing limb kinematics with step height increases, e.g. greater toe clearance when stepping up (Heasley et al., In Press), increased ankle plantar-flexion ('reaching') when stepping down (Buckley et al., In Press), may explain why ML dynamic stability decreased with increases in step height and this might explain why stair riser heights of greater than 18cm have been associated with increased incidence of stairwell falls (Templer et al., 1985). The greater ML instability when stepping down compared to when stepping up was most likely due to the fact that stepping down includes a period (during single support) when body weight is supported on just the ball of the foot. This finding could explain why the incidence of falling is higher during stair descent than ascent (Tinetti et al., 1988).

In conclusion, findings of the present study indicate that ML balance parameters during the single support of stepping up and down are affected by blurred vision. Correcting common visual problems such as uncorrected refractive errors and cataract may thus be an important intervention strategy in improving how the elderly negotiate stairs.

REFERENCES

Buckley JG. et al. (In Press). *Gait Posture* http://www.sciencedirect.com/science/journal/09666362

Dowswell T. et al. (1999) UK:Department Trade & Industry.

Heasley K. et al. (In Press). *Invest Ophthalmol Vis Sci*.

Ivers RQ. et al. (1999). *J Am Geriatr Soc* **46**; 58-64.

Jack CIA. et al. (1995) *Gerontology* **41**; 280-5.

Maki BE. et al. (1994). *J Gerontol* **49**; M72-84.

Templer J. et al. (1985). *J Safety Res* **16**; 183-196.

Tinetti ME. et al. (1988). *N Engl J Med* **319**; 1701-7.

ACKNOWLEGEMENTS

This study was supported by a grant from The Health Foundation UK (Ref: 3991/882).

GAIT DEVIATIONS IN A VIRTUAL REALITY ENVIRONMENT

John H. Hollman,[1] Robert H. Brey,[2] Richard A. Robb,[3] Tami Bang,[4] and Kenton R. Kaufman [4]

[1]Program in Physical Therapy, Mayo Clinic College of Medicine, Rochester, MN
[2]Department of Otorhinolaryngology, Mayo Clinic College of Medicine, Rochester, MN
[3]Biomedical Imaging Resource, Mayo Clinic College of Medicine, Rochester, MN
[4]Department of Orthopedics, Mayo Clinic College of Medicine, Rochester, MN
E-mail: hollman.john@mayo.edu

INTRODUCTION

Integration of the visual, vestibular, and proprioceptive systems contributes to the maintenance of postural stability. In recent years, postural stability has been examined in virtual reality (VR) environments in which visual and/or vestibular conflicts can be induced. Akiduki et al. (2003) report that visual-vestibular conflicts induced by VR produce increased postural sway and symptoms of motion sickness in healthy subjects. Jasko et al. (2003) report that influences on peripheral and central visual fields result in increased postural sway when proprioceptive inputs are unreliable. These studies, however, were performed while subjects were standing. It is not clear whether instability is also reflected while walking in a VR setting. Therefore, the purpose of this study was to examine gait deviations and subjective responses of dizziness associated with walking in a VR environment.

METHODS

Ten healthy subjects (7 female, 3 male; mean age = 24 ± 3 years) participated in this study after providing informed consent. The experiment was a repeated measures design consisting of two factors: environment (VR and non-VR) and treadmill velocity (0.9, 1.1 and 1.3 m/sec).

A VisionStation 1024 (Elumens) consisting of a hemispherical screen that encompasses 160^o of a person's visual field and a projection system that disperses light in an arc of 180^o was used to create the VR environment. The image projected onto the screen was designed specifically for this study and was projected as an endless corridor with colored, vertical stripes on the wall (Figure 1). The corridor veered to the left as though it was a circular tunnel. The speed of the moving image was matched to the speed of the treadmill to create an illusion that subjects were walking through the endless corridor.

Figure 1: The virtual reality environment.

Spatiotemporal and kinetic data during gait were collected with a Gaitway® Instrumented Treadmill. As subjects walked on the treadmill, force platforms measured force and location of the center of pressure

(COP) for each footfall. Subjects walked for three minutes in each of the six conditions, and data were sampled at 100 Hz for 20 seconds during each trial. The order of testing was counterbalanced to minimize threats to the study's internal validity. Spatiotemporal gait parameters including stride length, base of support, and stride-to-stride variability in stride velocity were analyzed. In addition, subjects completed a questionnaire before testing and after each trial that assessed their symptoms of dizziness. The questionnaire consisted of six questions such as "Do you feel like you are spinning?" to which subjects provided responses to a 5-point scale ranging from "none" to "severe." Subjects' responses were summed after each trial to form a composite dizziness index.

Spatiotemporal gait data were analyzed with either a repeated measures ANOVA or a Wilcoxon Signed Ranks test if parametric assumptions were not met (α=.05). Subjective dizziness data were analyzed with the Wilcoxon Signed Ranks test.

RESULTS AND DISCUSSION

Subjects walked in the VR environment with a reduced stride length (p=.001), a wider base of support (p=.001), and with increased variability in stride velocity (p<.016) at each walking speed (Table 1). Walking in the VR environment induced mild feelings of dizziness at 1.1 and 1.3 m/sec (p=.046).

Of the various parameters that reflect gait instability, stride-to-stride variability appears to best represent instability and predict one's risk of falling (Maki, 1997). The increase in stride variability observed in this study therefore implies that people walk with reduced stability in a VR environment.

SUMMARY

The deviations observed during treadmill walking in a VR environment suggest that a VR environment may induce decreased gait stability in healthy subjects.

REFERENCES

Akiduki, H. et al. (2003). *Neurosci Lett*, **340**, 197-200.
Jasko, J.G. et al. (2003). *Proceedings of the 2003 ASB Annual Conference*.
Maki, B.E. (1997). *J Am Geriatr Soc*, **45**, 313-320.

ACKNOWLEDGMENTS

This research was supported by a grant from the Donald M. Kendall Foundation.

Table 1: Stride length, base of support, stride variability, and dizziness index (Mean ± SD).

Parameter		0.9 m/sec	1.1 m/sec	1.3 m/sec
Stride Length	VR	104.8 ± 11.6 cm	118.7 ± 8.0 cm	129.7 ± 6.0 cm
	Non-VR	112.6 ± 7.2 cm	122.6 ± 6.6 cm	133.5 ± 6.4 cm
Base of Support	VR	7.3 ± 2.5 cm	7.5 ± 2.2 cm	7.0 ± 2.2 cm
	Non-VR	6.2 ± 2.5 cm	6.1 ± 2.2 cm	6.3 ± 1.6 cm
Variability in Stride Velocity	VR	5.9 ± 5.3 %CV	3.5 ± 3.3 %CV	2.8 ± 1.2 %CV
	Non-VR	1.6 ± 0.3 %CV	1.6 ± 0.3 %CV	1.3 ± 0.4 %CV
Dizziness Index	VR	6.5 ± 1.1	6.9 ± 1.1	7.0 ± 1.2
	Non-VR	6.0 ± 0.0	6.5 ± 0.8	6.6 ± 0.8

A THREE-DIMENSIONAL MODEL OF VOCAL FOLD ABDUCTION/ADDUCTION

Eric J. Hunter[1] and Ingo R. Titze[1,2]

[1]National Center for Voice and Speech, A division of Denver Center for the Performing Arts, Denver, CO, USA
[2]Department of Speech Pathology and Audiology, The University of Iowa, Iowa City, IA, USA
E-mail: ehunter@dcpa.org Web: www.ncvs.org

INTRODUCTION

This report demonstrates a three-dimensional, biomechanical model of vocal fold posturing and the assumptions used in its creation (Hunter, et al. 2004). Vocal posturing affects the pitch, quality, and timbre of the sound produced (Titze & Sunberg, 1992) by defining the shape, strain, and stiffness of the vocal folds (Hirano, et al., 1970; Honda, 1983; Titze, 1990). Posturing is not only necessary for voice production but also for airway protection. Thus, models of slow-moving posturing can advance for more complete studies of neuromuscular speech disorders and pathologic tissue effects on vocal onset. Furthermore, a successful model of laryngeal posturing may lead to a better understanding of how laryngeal muscles coordinate their efforts to begin phonation and to sustain and manipulate oscillation.

METHODS

The model (Fig. 1) was based on a three-dimensional representation of the vocal fold anatomy from reported laryngeal specimens. (Kim, et al. 2003).

Two assumptions were made concerning the tissue properties: 1) all tissue was nearly incompressible; and 2) all tissue was initially isotropic, with fibrous nonisotripic tissue defined as a gel-fiber compound (superimposed fibrous characteristics). Six

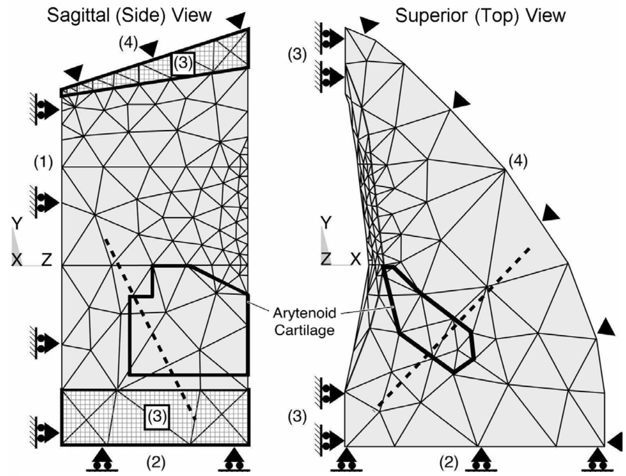

Figure 1. Vocal fold model divided into 1721 elements with only surface element faces shown. Four surface constraints and CAJ axis (dotted line) shown (CAJ axis passes though the arytenoid cartilage- represented by the dark outline).

types of fibrous tissue, the vocal ligament and the five intrinsic muscles, were included in the model. Muscles were simulated as nonlinear Kelvin-type models with nonlinear passive properties and damping. The nonlinear aspect of these passive properties are especially crucial to the laryngeal system, which often operates in the highly nonlinear region (e.g., 50 percent elongation is common for the vocal ligament).

Results from the model were shown in terms of the glottal angle to allow for comparisons to clinical endoscopic data. Dynamic glottal angle-based contours, their maximum angles, and timing measures were reported from the model. Maximum glottal angle and maximum angle velocity were then used to quantify the range and speed of motion.

RESULTS AND DISCUSSION

Each of the muscles was individually contracted 100 percent. The posture model simulated a maximum opening of over 34 degrees. Using the posterior-cricoarytenoid muscle, the model produced an abduction speed of 417 degrees per second (Figure 2.a). The model showed that laryngeal system mechanics seemed to favor abduction motion (used in inhalation) over adduction (used in vocal onset or airway protection) in terms of speed (Figure 2.b) even though the mechanical properties (not geometric properties) of the muscles were identical. These results were substantiated by endoscopic observations (e.g., Cooke *et al.* 1997).

The model also showed that the vocalis portion and the muscularis portion of the thyroarytenoid muscle have significantly different roles in posturing, the thyro-muscularis having the more important role. This finding substantiates and provides mechanical insight into the observation of Woodson *et al.* (1998) that the cricothyroid muscle does not abduct or adduct the vocal folds.

ACKNOWLEDGEMENTS

This work was supported by NIDCD grant No DC04347-03 from National Institutes of Health.

REFERENCES

Cooke A., Ludlow, C. L., Hallett, N., and Selbie, W. S. (1997), J. Voice.

Hirano, M., Vennard, W., and Ohala, J. (1970), Folia Phoniatr.

Honda, K. (1983), in Vocal Fold Physiology: Biomechanics, Acoustics and Phonatory Control, edited by I. Titze and R. Scherer.

Kim, M.J., Hunter, E.J. and Titze, I.R. (2004) Ann.Otol.Rhinol.Laryngol.

Titze, I. R., and Sundberg, J. (1992), J. Acoust. Soc. Am.

Titze, I. R. (1990), Journal of Voice.

Hunter, E.J., Titze, I. R., and Alipour, F. (In Press). J. Acoust. Soc. Am.

Sanders, I., Rau, F., and Biller, H.F. (1994), Laryngoscope.

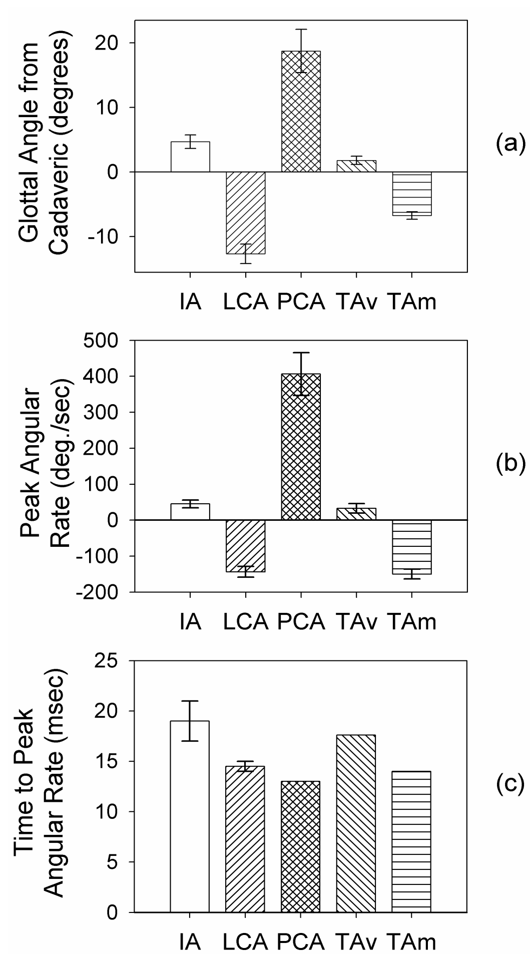

Figure 2. Average of all four possible glottal angles variants depict the results of individual 100% muscle contraction for 0.1 second): (a) change in glottal angle from cadaveric (initial) position, (b) peak glottal angle rate, and (c) time from contraction start to peak glottal angle rate.

SMALL CHANGES IN THE TIMING OF ACTIVATION AFFECTS FIBER LENGTHS AND SERIAL SARCOMERE NUMBER ADAPTATIONS IN RABBIT TIBIALIS ANTERIOR EXPOSED TO ECCENTRIC EXERCISE

Timothy A Butterfield, Walter Herzog

Human Performance Laboratory, University of Calgary, Calgary, Alberta, Canada
E-mail: timb@kin.ucalgary.ca Web: www.kin.ucalgary.ca

INTRODUCTION

Eccentric exercise has been shown to increase serial sarcomere number (Koh and Herzog, 1998). These adaptations have often been associated with the amount of strain in the muscle-tendon unit (MTU). However, MTU strains may not relate well to fiber strains (Griffiths, 1991), and the timing of activation may greatly affect fiber strain for a given MTU strain. Fiber strain has not been systematically studied in adaptive models of skeletal muscle. The purpose of this study was to measure fiber adaptations for a given cyclic MTU strain in the rabbit tibialis anterior (TA) that was activated exactly at the onset of the eccentric phase, or 100 ms offset to the eccentric phase. We hypothesized that the100ms offset would result in different fiber strains, and that fiber length and serial sarcomere number adaptations would be different for contractions of identical MTU strain, but different timing of activation.

METHODS

Nerve cuff electrodes were implanted bilaterally on the peroneal nerves of 13 adult New Zealand white rabbits. The left nerve cuff electrode was attached to a custom made subcutaneous electrical interface that allowed for temporary connections to an external stimulator (Koh and Leonard, 1996). The anesthetized rabbits were placed supine in a sling with their left foot attached to a plate connected to the cam of a servo motor. Supra-maximal stimulation was determined (voltage 3x α-motoneuron threshold, 150Hz). An eccentric exercise bout of 5 sets of 10 repetitions was performed (stimulus train duration = 500 ms) from a tibiotarsal joint angle of 70^o-105^o at 70^o sec^{-1}. ***Protocol 1*** (n=7) consisted of plantar flexion (eccentric TA action) beginning at the onset of activation, through a range of motion of 35^o from 70^o-105^o at $70^o \cdot sec^{-1}$. Afterwards, the foot was returned to the start angle passively. The entire eccentric protocol consisted of five sets of ten repetitions with a two minute rest between sets. ***Protocol 2*** (n=6) was identical to the first, however the timing of activation was offset by 100 ms. This resulted in a 100ms isometric contraction prior to stretch, and deactivation of the TA 100 ms prior to the end of plantar flexion.

For each protocol, the eccentric exercise was repeated 3 times per week for 6 weeks, with at least 48 hours rest between bouts. Nine days after the last exercise bout, the rabbits were euthanized. Left and right hind-limbs were fixed at 90^o. TA were excised, weighed and processed. Six fascicles were teased from the superficial layers of the central third, and placed on glass slides. Fascicle and sarcomere lengths were measured using digitization and laser diffraction, respectively.

RESULTS

Although the mechanical strain of the MTU was the same for both groups (~5.0%), the adaptive cellular response varied between protocols. Fiber lengths increased significantly more in the superficial central region of the TA (p=0.006) for protocol 2 compared to protocol 1 (9.1% compared to 3.3%, Fig. 1). These increases in fiber lengths were associated with increases in serial sarcomere number, however, these increases were not significantly different between protocols (p<0.15, table 1).

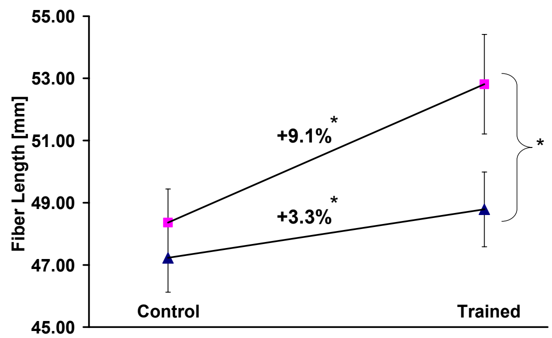

Figure 1: Central-superficial fiber lengths for control and trained TA for protocol 1 (▲) and protocol 2 (■). Means ±SE.

DISCUSSION

We have previously sown that a small shift in the timing of activation (i.e.100ms) affects fiber strain dramatically, even for identical MTU strain protocol (Butterfield and Herzog, 2004). For example, total fiber strain was shown to increase by 50% when activation was adjusted by 100ms from the start of the eccentric phase. Thus, we conclude that the changes in fiber strain resulted in the differential adaptation in fiber lengths and the observed trend in increased serial sarcomere number in the superficial central portion of the TA, and that fiber strain is a more potent factor in dictating the adaptive response of skeletal muscle than the MTU strain.

SUMMARY

Timing of activation appears to be a potent factor influencing muscle adaptation. Here we have shown that a shift in the activation of the muscle by 100ms resulted in significant sarcomere number and/or fiber length adaptations in the superficial and deep regions of the central TA. We believe that this increased adaptive response is due to the increased fiber strains achieved through the alteration of activation timing, while keeping MTU strain constant. Thus, fiber dynamics may be more valuable than MTU strain in understanding potential muscle injury and subsequent adaptation.

REFERENCES

Butterfield, T.A., Herzog, W. (2004) in: *XI Conf Can Soc Biomech, Halifax.* 2004.

Griffiths, R.I. (1991) *J Physiol*, **436**, 219-236

Koh, T.J., Herzog, W. (1998) *J Biomech*, **31**, 499-501.

Koh, T.J., Leonard, T.R. (1996) *J Neurosci Methods*, **70**, 27-32.

ACKNOWLEDGEMENTS

NSERC of Canada, CIHR training program in Bone and Joint Health, and Tim Leonard

Table 1. Serial sarcomere numbers. Values are Mean ± SD

	Protocol 1	**Protocol 2**
	TA Superficial	TA Superficial
trained	23084 ± 2732	23939 ± 2547
control	22377 ± 2599	22394 ± 2486
difference	+3.2%	+6.9%
P- value	.015*	.000*

MUSCULOSKELETAL PARAMETER VARIABILITY EXPLAINS VARIABILITY IN ELBOW FLEXION STRENGTH DEFICIT DUE TO LONG HEAD BICEPS TEAR: A STOCHASTIC MODEL

Joseph Langenderfer[1], James E. Carpenter[2], Richard E. Hughes[1,2]

[1]Department of Biomedical Engineering, [2]Department of Orthopaedic Surgery,
University of Michigan, Ann Arbor, MI USA
E-mail: rehughes@umich.edu

INTRODUCTION

Rupture of the Long Head of Biceps tendon (LHB) results in varying elbow flexion strength deficit (mean deficit: 8%, S.D. 12% of mean) (Mariani et al. 1988). This variability in strength is interesting because it is previously unexplained. Observations of musculoskeletal parameters also exhibit variability (Murray et al. 2000). We hypothesize that the variation in elbow flexion strength in healthy normals and in subjects with LHB rupture is explainable via variability in musculoskeletal parameters, specifically muscle physiologic cross sectional areas (PCSA), moment arms and optimal muscle lengths (OML) of elbow flexors. The purpose of this research was to use a stochastic model to predict the median and distribution of maximum isometric elbow flexor muscle forces when modeling PCSAs, moment arms, and OMLs as random variates.

METHODS

A Monte Carlo model was used to stochastically simulate the effects of variability in PCSAs, moment arms, and OMLs on elbow flexion strength. Data in the literature was used to construct gamma distributions (Law and Kelton, 2000) for the following parameters: measured elbow flexion torque (Askew et al. 1987, Mariani et al. 1988), PCSAs and moment arms (Murray et al. 2000), and OMLs (Chang et al. 1999). Parameters sampled from these distributions were input to a biomechanical model to predict muscle forces and flexion torque. The simulation was conducted for the healthy normal (No-tear) case and the LHB rupture (Tear) case. The work consisted of three phases; model validation, muscle specific tension prediction, and muscle force prediction.

As is commonly done in discrete event simulation (Law and Kelton, 2000), model validation consisted of adjusting model parameters to match model predictions to empirical measurements. One hundred distributions, each consisting of 10000 samples, of predicted and measured torque were constructed. For each case predicted and measured torque distributions were compared by forming 95% confidence intervals (C.I.) for the difference in means, and ratio of standard deviations. Standard deviations for PCSA and OML were iteratively increased (No-tear) and decreased (Tear) until the C.I. for the difference in means included 0 N-m and the C.I. for the ratio of standard deviations included unity. This process also drastically reduced RMS error between the measured and predicted torque distributions. With these parameter sets, predicted and measured torque distributions were equivalent.

Next, for the No-Tear case, 5000 samples were made from each parameter distribution to construct a predicted flexion torque distribution. Specific tension was determined by minimizing RMS error between the predicted torque distribution and a distribution of 5000 measured flexion torques. Specific tension was assumed equal between the two cases.

Specific tension was then used to predict muscle force distributions for another 5000 iterations of the simulation for the No Tear and Tear cases (Chang et al. 2000), respectively.

RESULTS AND DISCUSSION

The validation and specific tension phases resulted in RMS error between measured and predicted torques of 50 N-cm (Fig 1) for both the Tear and No-Tear cases. Specific tension was 140 MPa. Predicted muscle forces are shown in Table 1.

This model is not deterministic and therefore affords an examination of how variability in parameters affecting muscle force and torque can predict variance in strength in LHB rupture subjects and healthy normals. Limitations include a lack of an EMG-Activation model, i.e. assuming 100% muscle activation for maximum isometric contractions, and the assumption of equal specific tension for the two cases. Additionally there is no consideration of parameter covariance.

SUMMARY

This study furthers our understanding of effects of parameter variability on variability in muscle force and elbow flexion strength. Variability in elbow flexion strength is explainable via variability in musculoskeletal parameters. Differences in the variability of the measured torque between the two cases are explained by differences in PCSA and OML variability.

REFERENCES

Mariani, E.M. et al. (1988). *Clin. Orthop.*, **228**, 233-239.
Murray, W.M. et al. (2000). *J. Biomech.,* **33**, 943-952.
Law, A.M., and Kelton, W.D. (2000). *Sim. modeling and analysis*, McGraw-Hill.
Askew, L.J. et al. (1987). *Clin. Orthop.*, **222**, 261-266.
Chang Y.W. et al. (1999). *Clin. Biomech.*,**14**, 537-542.
Chang Y.W. et al. (2000). *JSES.*, **9**, 188-95.

ACKNOWLEDGEMENTS

This research was supported by grants from the Whitaker Foundation and the Rackham Graduate School of the University of Michigan.

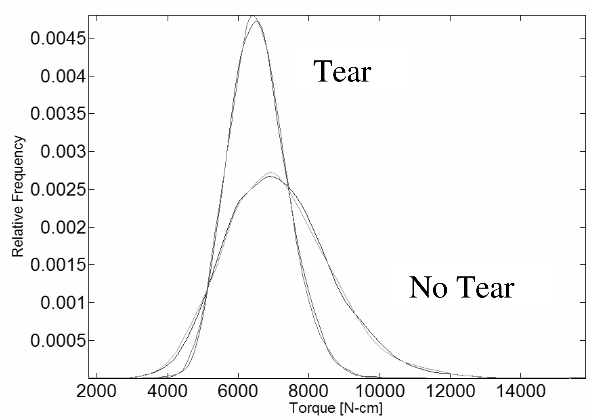

Figure 1: Probability distribution of measured and predicted flexion torque.

Table 1: Predicted elbow flexor muscle forces [Newtons] (median and S.D.)

	Biceps LH	**Biceps SH**	**Brachialis**	**Brachioradialis**
No Tear	406.1 (195.0)	353.9 (106.6)	928.4 (240.4)	86.1 (100.5)
Tear		474.4 (63.8)	1220.0 (140.8)	140.9 (71.4)

VISCOELASTIC CHARACTERIZATION OF CERVICAL SPINAL LIGAMENTS

Scott R. Lucas[1], Cameron R. Bass[1], Robert S. Salzar[1], James B. Folk[1], Lucy E. Donnellan[1], Glenn Paskoff[2], and Barry S. Shender[2]

[1]Center for Applied Biomechanics, University of Virginia
[2]NAVAIR, Patuxent River
E-mail: slucas@virginia.edu

INTRODUCTION

The neck is vulnerable to injury in automotive and military crash scenarios. To investigate these injuries and develop countermeasures, computational models of neck response may be used. In these models, however it is imperative to have accurate material properties of the internal ligamentous structures derived using appropriate loading rates. Previous studies have investigated the response of the cervical spinal ligaments in tension (1) and at quasistatic rates. The purpose of this study is to develop a viscoelastic characterization of the anterior longitudinal ligament (ALL), posterior longitudinal ligament (PLL), and ligamentum flavum (LF) in human male cervical spines under high-rate loading conditions.

METHODS

Six fresh frozen then thawed male cervical spines were used in this study. The average subject age was 59.5 ± 8.5. The average stature and mass were 1749 ± 40 mm and 77.3 ± 16.9 kg, respectively. The ALL, PLL, and LF were isolated from each cervical spine at C3-C4, C5-C6, and C7-T1, resulting in a total of 54 ligaments; 47 of which were used in the testing. The intervertebral disc and surrounding connective tissues were left intact until the specimen was ready to be mounted in the test fixture to preserve hydration. The ligaments were mounted in an Instron force test machine (Instron, Inc. # 8874) for uniaxial tests in an orientation that is representative of physiological conditions. The fixture was enclosed in an environmental chamber to maintain physiological temperature (99 ± 1 ˚F) and humidity (>90%). After application of a nominal preload (4 N), the initial length of each ligament was measured. After preconditioning at 10% strain, each ligament was subjected to a 25% strain step, 50% strain step, and a 50% strain oscillatory test. The typical strain rate in the step tests was 30-150 s^{-1}.

The force response was characterized for each ligament using a hereditary integral based on Quasi-Linear Viscoelasticity (QLV) (2):

$$F(\varepsilon,t) = \int_0^t G(t-\tau)\frac{dFe(\varepsilon(\tau))}{d\tau}d\tau \qquad (1)$$

The hereditary integral can be directly integrated numerically for arbitrary strain histories (3) in terms of instantaneous elastic coefficients, A and B, and relaxation coefficients, G_n:

Elastic Stress: $F_e(\varepsilon) = A[e^{B\varepsilon} - 1]$ (2a)

Relaxation: $G(t) = G_\infty + \sum G_n e^{-\beta_n t}$ (2b)

where G_∞ is the steady-state relaxation coefficient, and β_n are the inverse of the time constants corresponding to each relaxation coefficient, G_n, as shown in Table 1. These time constants were selected to represent a range of relaxation behavior in the tests (c.f. 4).

Table 1. Summary of G_n and β_n.

G_n	G_1	G_2	G_3	G_4	G_∞
β_n	1	10	100	1000	----

A generalized reduced gradient technique was used to find an optimal solution for the elastic and relaxation coefficients from

Equation 1. For each ligament, the relaxation coefficients were determined from the 50% step experimental data. These coefficients were used to predict response for the 25% step and 50% oscillatory tests.

RESULTS AND DISCUSSION

The agreement between measured (50% step) and predicted response (25% step, 25% oscillatory) was very good with averaged R^2 values for the ALL, PLL, and LF were 0.97 ± 0.02, 0.95 ± 0.03, and 0.89 ± 0.06, respectively. Figures 1 and 2 are representative comparisons between the actual force response for an ALL and the corresponding model fit for a 25% strain step and 50% strain oscillatory input using the 50% strain step coefficients.

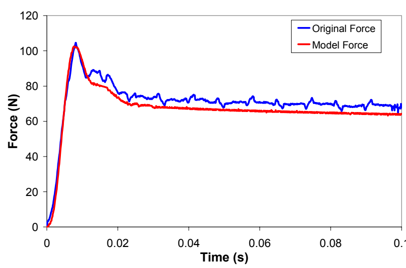

Figure 1. 25% strain response using 50% coefficients

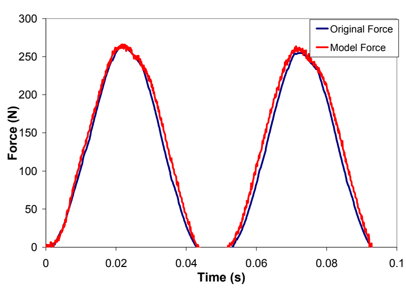

Figure 2. 50% oscillatory response using 50% coefficients

This indicates that the assumption that the QLV model provides an accurate representation for both strain level and strain rate over the subfailure strain levels and rates used in this test series.

The averaged viscoelastic coefficients used for the viscoelastic model are summarized in Table 2. The relaxation coefficients for the ALL, PLL and LF were dominated by G_4, which suggests that there is a large amount of relaxation occurring during the loading phase. G_∞ is the next highest weighted coefficient. G_3 is larger for the LF, indicating that the LF is not as stiff as the ALL and PLL. The peak force for the LF (142 ± 87 N) is lower than the ALL (190 ± 62 N) and PLL (205 ± 77 N), resulting in a flatter force curve and a higher G_3 contribution.

SUMMARY

The primary objective of this study is to determine a viscoelastic characterization of the ALL, PLL, and LF in the male cervical spine. It has been shown that these spinal ligaments exhibit large relaxation corresponding to small time constants.

REFERENCES

1. Yoganandan N. et al. (2001). *Biomechanics of the Cervical Spine Part 2.* Clinical Biomechanics, **16**, 1-27.
2. Fung, Y.C. (1981). *Biomechanics: Mechanical Properties of Living Tissues.* Springer-Verlag, New York.
3. Darvish, K.K. et al. (1999). *A Nonlinear Viscoelastic Model for Polyurethane Foams.* Journal of Materials and Manufacturing, **108**, 209-215.
4. Kent, R. et al. (2003). *Muscle Tetanus and Loading Condition Effects on the Elastic and Viscous Characteristics of the Thorax*. Traffic Injury Prevention, **4**, 297-314.

Table 2: Averaged Model Coefficients

	G_1	G_2	G_3	G_4	G_∞	A	B
ALL	0.028±0.022	0.026±0.008	0.046±0.050	0.663±0.102	0.237±0.046	24762±14661	0.011±0.005
PLL	0.024±0.017	0.034±0.016	0.040±0.030	0.694±0.062	0.208±0.042	34453±29149	0.011±0.008
LF	0.039±0.023	0.010±0.013	0.151±0.110	0.610±0.208	0.190±0.113	1075±653	0.086±0.006

SPEED EFFECTS ON KNEE ADDUCTION MOMENTS USING INTERVENTION FOOTWEAR: IMPLICATION FOR THE TREATMENT OF KNEE OSTEOARTHRITIS

David Fisher[1], Anne Mündermann[1,2], and Thomas Andriacchi[1,2]

[1] Stanford Biomotion Laboratory, Biomechanical Engineering Division,
Mechanical Engineering Department, Stanford, CA, USA
[2] Department of Veterans Affairs, VA Palo Alto Health Care System
Rehabilitation R&D Center, Palo Alto, CA, USA
E-mail: fisherds@stanford.edu Web: biomotion.stanford.edu

INTRODUCTION

During daily activities, people walk at a range of speeds. This change in speed has an effect on the external knee adduction moment, which is directly related to the load on the medial compartment of the knee. (Andriacchi 1994) Shoe interventions have been used to encourage alignments which produce lower knee adduction moments, (Crenshaw 2000, Fisher 2002) and, thus, may slow the rate of progression of knee osteoarthritis. The magnitude of the knee adduction moment, however, increases with increased walking speed for most subjects (Mündermann 2004), meaning that at higher speeds there is increased risk of higher knee adduction moments and cartilage damage.

The purpose of this study was to determine how walking speed affects the knee adduction moment using intervention shoes. The hypothesis was that the intervention shoes would be more effective in reducing the adduction moment at higher walking speeds.

METHODS

Eleven physically active subjects were tested in this study, (five females/six males, 29 ± 9 years, 169 ± 6 cm, 655 ± 77 N) with Institutional Review Board approval and signed consent obtained for all subjects. Subjects were tested in a pair of control and intervention walking shoes at three self selected speeds: slow (1.0m/s ± .1m/s), normal (1.3m/s ± .2m/s), and fast (1.7m/s ± .2m/s). The control shoes had a typical, flat, uniform stiffness sole. In the intervention shoes, the medial-side shoe sole had a stiffness and thickness that was the same as the control shoe, but the lateral side, while the same thickness, had an increased material stiffness (Figure 1).

Figure 1: Intervention shoe with medial side stiffness (orange) same as control and increased lateral side stiffness (green)

The external joint moments were measured by gathering motion and force plate data. A three-dimensional optoelectronic system collected the motion data, while a multi-component force plate measured the ground reaction force. External inter-segmental forces and moments were calculated for the lower limb using previously described methods (Andriacchi 1997).

The peak external knee adduction moment for each trial was calculated and a repeated measures ANOVA was performed with shoe type and walking speed as factors ($\alpha < 0.05$).

RESULTS AND DISCUSSION

Consistent with other literature (Mündermann 2004), there was an increase in the peak knee adduction moment in both the control and intervention shoes with increasing speed (Figure 2).

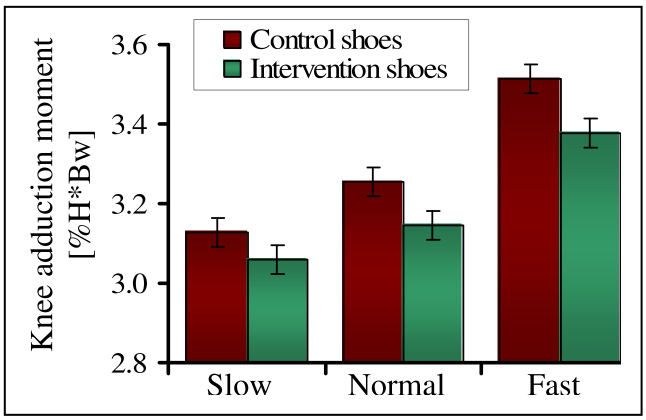

Figure 2: Average peak knee adduction moment in control and intervention shoes

The intervention shoes were also more successful at reducing the knee adduction moment at higher speeds (Figure 3). There was a statistically significant greater reduction in the peak knee adduction moment at the higher speeds, hereby, proving the test hypothesis.

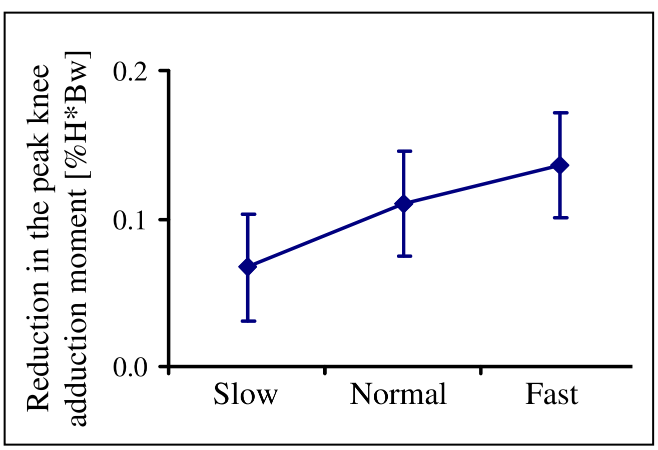

Figure 3: Reduction in the peak knee adduction moment using intervention shoes compared to control shoes at different speeds

SUMMARY

Since the peak external knee adduction moment is higher at greater walking speeds it is a useful finding that variable stiffness shoes are most effective at these times. This is believed to be the result of increased force in the sole of the shoe at higher speeds. This greater force increases the amount of medial compartment compression in the intervention shoe, resulting in more significant alignment changes.

Another study with related findings, showed that there was an increased reduction in the peak adduction moment for subjects with initially higher knee adduction moments. (Fisher 2002) This was a useful finding because the high adduction moment group most needed a benificial knee adduction moment reduction. These two finding show the advantage of this type of intervention shoe design, in that it benefits those who most need intervention and that it is most beneficial at the time it is most needed.

REFERENCES

Andriacchi, TP et al. (1994). *Orthop Clin North Am* 1994; 25 395-403.
Andriacchi, TP et al. (1997). *Basic Orthopaedic Biomechanics* 2nd ed., 37-68.
Crenshaw, SJ et al. (2000). *Clin Orthop*, 375, 185-192.
Fisher, DS et al. (2002) *48th Meeting of the ORS*, 27, 0700.
Mündermann, A et al. (2004) *Arthritis and Rehabilitation* (in print).

ACKNOWLEDGEMENTS

This study was supported in part by the Nike Sport Research Laboratory, Beaverton, OR

THE EFFECTS OF ADDED LEG MASS ON THE BIOMECHANICS AND ENERGETICS OF WALKING

Raymond C. Browning[1], Jesse Modica[1], Rodger Kram[1] and Ambarish Goswami[2]

[1] Locomotion Laboratory, Department of Integrative Physiology, University of Colorado, Boulder, CO, USA. Email: browning@colorado.edu
[2]Honda Research and Development, San Jose, CA, USA.

INTRODUCTION

During normal locomotion, humans select a movement pattern that minimizes the rate of metabolic energy consumption (Margaria, 1976). Do stance or swing phase mechanics predominately drive this energetic optimization? Adding leg mass does not change the inverted pendulum mechanics of the stance phase of walking. Thus, if the energetically optimal gait pattern is driven by stance phase mechanics, adding leg mass should have no effect. If the pendular swing phase mechanics drive the optimization, adding leg mass should alter the gait pattern. Adding mass to the feet has been shown to increase the energy cost (Ralston, et al., 1969) and alter the kinematics of walking (Inman, et al., 1981), but there are little data on the effects of thigh and shank loading.

Understanding the effects of added leg mass has practical importance in the design of powered exoskeletons (Yang, 2004), i.e. the effects of location and mass of motors/actuators on the energy cost and muscle control strategies of walking.

We hypothesized that with leg and trunk loading:
1. Kinematics would be conserved.
2. Net muscle moment magnitudes during swing would increase.
3. EMG of leg muscles would increase.
4. Metabolic cost would increase and the increase would be greater with more distal load location.

METHODS

Five healthy male volunteers, (74.16 kg $\pm$ 5.18 kg, mean $\pm$ s.d.) walked on a motorized treadmill at 1.25 m/sec. Subjects completed a series of 7-minute trials with at least 5 minute rest between trials. Trials included unloaded, foot, shank, thigh and waist load trials in random order. Foot and shank loads were 2 kg and 4 kg per foot/shank. Thigh loads were 4 kg and 8 kg per leg. Waist loads were 4, 8, and 16 kg. Loads did not change segment center of mass location. Footswitches and 200Hz video recorded kinematics. We calculated net muscle moments about the ankle, knee and hip during the swing phase using an inverse dynamics solution. Surface electrodes recorded the electrical activity of: medial gastrocnemius (MG), soleus (SOL), tibialis anterior (TA), vastus medialis (VM), rectus femoris (RF), and semitendinosus (ST). We determined the rate of metabolic energy consumption from expired gas analysis and subtracted the standing metabolic rate to yield net metabolic rate.

RESULTS AND DISCUSSION

Stride kinematics and net muscle moments were similar to the normal unloaded condition except for the foot loads. For the 2 kg and 4 kg/foot trials, stride frequency decreased by 6 and 10% respectively. Greater magnitude muscle moments were needed for swinging the 2 and 4 kg/foot loads (Figure 1).

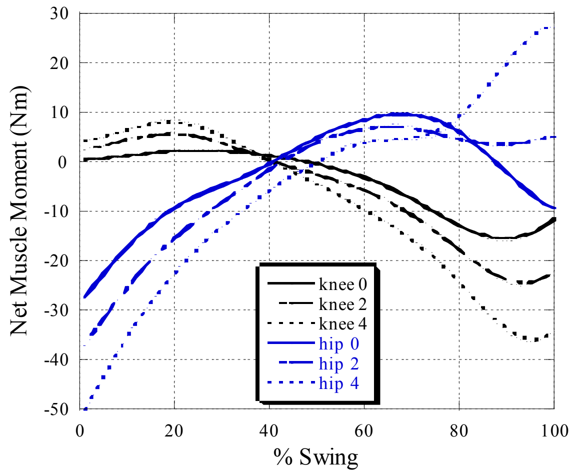

Figure 1. Net muscle moments during swing vs. foot load (0, 2, 4 kg).

EMG increased during swing initiation. During the second half of the stance phase MG mEMG increased by 23 and 32% for the 2 and 4 kg/foot loads and 9% for the 4 kg/shank load. MG mEMG increased by 22% with the 8 kg/thigh load and 16% with the 16 kg waist load. The RF mEMG during the second half of stance increased by 33 and 60% for the 2 and 4 kg/foot loads. During the first half of the swing phase, the mean RF EMG increased by 25 and 54% with the 2 and 4 kg/foot loads. These EMG results suggest that the ankle plantarflexors are important swing initiators and provide forward propulsion, while the RF acts to initiate and propagate leg swing as load increases.

As expected, leg loading increased the metabolic cost of walking, and more distal loads were more expensive (Figure 2). Carrying 4 and 16 kg at the waist increased metabolic rate by 6 and 27% respectively. Foot loads increased metabolic rate 36 and 68% for 2 and 4 kg per foot. Carrying 8 kg on the waist increased metabolic rate by 11%, whereas carrying 4 kg on each thigh, shank and foot increased metabolic rate by 29, 25 and 68%.

Foot loads elicit a disproportionately higher metabolic cost because of the increase in

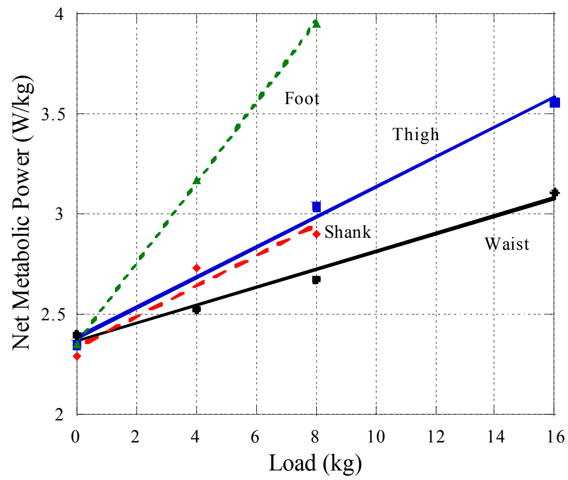

Figure 2. Net metabolic power vs. load

muscle activity required to swing the leg. The disproportionate increase in the cost of thigh loads was likely due to the wide steps required, which has been shown to increase metabolic cost (Donelan, et al., 2001).

Gait patterns were largely conserved despite dramatic leg loads suggesting that stance-phase mechanics dominate the gait optimization process. Powered exoskeleton mass should be concentrated proximally to minimize energy cost and alterations to gait patterns.

REFERENCES

Donelan, J. M., et al. (2001). *Proc R Soc Lond B Biol Sci*, **268**(1480), 1985-92.

Inman, V. T., et al. (1981). *Human Walking*, Williams and Wilkins**:** 62-77.

Margaria, R. (1976). *Biomechanics and Energetics of Muscular Exercise.* Oxford, Clarendon Press.

Ralston, H. J. and L. Lukin (1969). *Ergonomics*, **12**, 39-46.

Yang, S. (2004). *UC Berkeley News.* March 3, 2004. www.berkeley.edu/news.

ACKNOWLEDGEMENTS

This work was supported by a gift from Honda Research and Development.

Behavioral/Systems/Cognitive

Mechanical Characteristics of Rat Vibrissae: Resonant Frequencies and Damping in Isolated Whiskers and in the Awake Behaving Animal

Mitra J. Hartmann, Nicholas J. Johnson, R. Blythe Towal, and Christopher Assad
Jet Propulsion Laboratory, California Institute of Technology, Pasadena, California 91109

We investigated the natural resonance properties and damping characteristics of rat macrovibrissae (whiskers). Isolated whiskers rigidly fixed at the base showed first-mode resonance peaks between 27 and 260 Hz, principally depending on whisker length. These experimentally measured resonant frequencies were matched using a theoretical model of the whisker as a conical cantilever beam, with Young's modulus as the only free parameter. The best estimate for Young's modulus was ~3–4 GPa. Results of both vibration and impulse experiments showed that the whiskers are strongly damped, with damping ratios between 0.11 and 0.17. In the behaving animal, whiskers that deflected past an object were observed to resonate but were damped significantly more than isolated whiskers. The time course of damping varied depending on the individual whisker and the phase of the whisking cycle, which suggests that the rat may modulate biomechanical parameters that affect damping. No resonances were observed for whiskers that did not contact the object or during free whisking in air. Finally, whiskers on the same side of the face were sometimes observed to move in opposite directions over the full duration of a whisk. We discuss the potential roles of resonance during natural exploratory behavior and specifically suggest that resonant oscillations may be important in the rat's tactile detection of object boundaries.

Key words: **vibrissae; whiskers; rat; tactile; tactual; resonance; vibration; exploratory behavior; exploration; whisking; edge detection**

Introduction

Rats use active movements of their vibrissae (whisking) to extract information about the spatial properties of objects, including size, shape, and texture (Vincent, 1913; Welker, 1964; Carvell and Simons, 1990, 1995). Because whisking typically occurs at frequencies between 5 and 15 Hz (Welker, 1964; Berg and Kleinfeld, 2003), many studies have characterized neuronal responses to whisker stimulation or active movement in this frequency range (Zucker and Welker, 1969; Shipley, 1974; Simons, 1985; Hartings and Simons, 1998; Hartmann and Bower, 1998; Ahissar et al., 2000; Sosnik et al., 2001; Castro-Alamancos, 2002; Kleinfeld et al., 2002; O'Connor et al., 2002).

Several studies have additionally suggested that neurons in the trigeminal pathway may respond to whisker deflections at frequencies much higher than 15 Hz. Specifically, mechanoreceptors in the sinus hair follicle respond at frequencies up to 1500 Hz (Gottschaldt and Vahle-Hinz, 1981), and cells in the trigeminal ganglion respond to high frequency vibration up to 1000 Hz (Gibson and Welker, 1983a,b). More central levels of the trigeminal system show robust responses at least to 40 Hz (trigeminal nuclei) (Shipley, 1974) (thalamus) (Castro-Alamancos, 2002) (somatosensory cortex) (Simons, 1978; Kleinfeld et al., 2002), but generally have not been tested at higher frequencies. Thus, there are hints that cells at many levels of the trigeminal system may be responsive to frequencies far above typical whisking ranges.

One problem in identifying the frequency ranges of relevance to the vibrissal system is that the mechanics of whisker transduction have not yet been characterized; we do not have a quantitative description of how mechanical stimuli are generated during natural whisking behaviors, transmitted to sensory cells in the whisker follicle, and coupled to the rat's nervous system. Recently, Neimark proposed that high-frequency whisker resonances may aid in texture discrimination (Neimark, 2001; Neimark et al., 2003). In the current study, we performed vibration and impulse experiments on isolated whiskers and compared the results with whisker oscillations observed during exploratory behaviors in the awake animal. The whiskers exhibited natural resonance frequencies and damping that were well matched using a model of the whisker as a conical cantilever beam. Our results suggest that natural resonance properties of the whiskers contribute to vibrational stimuli during the initial transient responses that occur immediately after a whisker deflects past an object, which may be particularly important for the detection of object boundaries. Increases in damping seen under particular behavioral conditions also suggest that the rat may be able to actively modulate the resonant frequencies. This work represents our first step toward modeling whisker movements and predicting the

Received March 4, 2003; revised May 29, 2003; accepted May 30, 2003.

This work was supported by NASA's Information Technology Strategic Research Program. We are grateful to Terry Scharton, whose expertise on mechanical vibrations helped guide this work. We also thank Steve Lewis in the Jet Propulsion Laboratory standards laboratory for training and assistance on the use of the vibration table and Maria Neimark for useful discussions.

Correspondence should be addressed to Dr. Mitra J. Hartmann, Jet Propulsion Laboratory, Mail Stop 303-300, California Institute of Technology, 4800 Oak Grove Drive, Pasadena, CA 91109. E-mail: mitra.hartmann@jpl.nasa.gov.

 0270-6474/03/236510-10$15.00/0

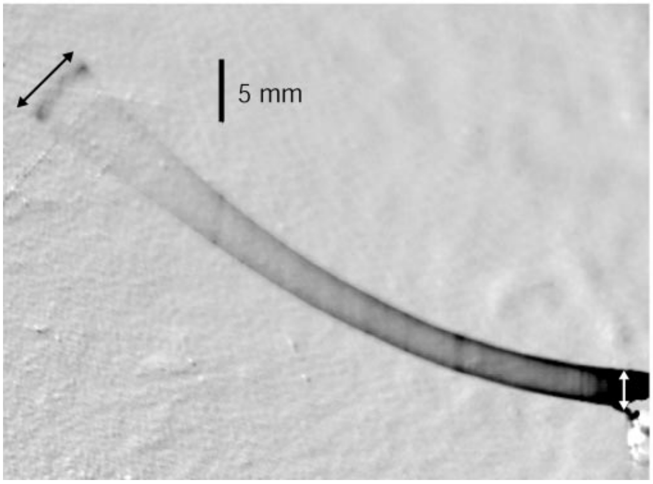

Figure 1. Measurement of tip displacement in a vibrating whisker. The displacement of the tip is indicated by the black arrow, and the displacement of the base by the white arrow. The picture is black-and-white reversed. The tip is illuminated by a laser line, and the amplitude of tip motion is measured between the two dark extrema.

pattern of peripheral input generated during the rat's active sensing behaviors.

Materials and Methods

Whisker measurements. Whiskers were obtained from an adult, female Sprague Dawley rat that had been killed in an unrelated experiment. We examined a total of 24 whiskers: α, β, γ, and δ, and the first four whiskers of each of rows A through E. Each whisker was grasped firmly at its base with fine forceps and plucked out of its follicle.

The mass of each whisker was measured on a Cahn-35 microbalance (Orion Research, Beverly, MA). The length of each whisker was measured with a ruler under a standard fluorescent magnifying lamp. The base and tip radii of each whisker were measured under a Leitz (Wetzlar, Germany) microscope. These measurements allowed us to calculate the whisker volume, assuming a truncated cone, and the density for each whisker was then determined by dividing its mass by its volume. This method of calculating whisker density is very sensitive to small errors in measurement of the radius of the base. We therefore used the average density over all of the whiskers (1.14 mg/mm^3) to predict the theoretical resonance frequencies (see Results). All of the procedures were approved in advance by the Animal Care and Use Committee of the California Institute of Technology.

Resonance measurements. A small drop of superglue was used to fix each whisker, in turn, to a computer-controlled vibration table in the standards laboratory at the Jet Propulsion Laboratory. Because the whiskers had an inherent curvature, each whisker was always mounted concave up (Fig. 1). Whiskers were illuminated with ambient light, and a linear laser beam was oriented along the direction of whisker motion at its tip. We videotaped the movement of each whisker on the vibration table using two high-speed digital video cameras (Photron Fastcams; Photron, San Diego, CA). One camera was mounted directly above the whisker (obtaining a bird's-eye view), while the second camera was mounted to view the vertical motion of the length of the whisker (longitudinal view). The vibration table moved only along the vertical axis, and, therefore, the longitudinal camera captured the whisker motion in the vertical plane.

Because we first wanted to evaluate the motion blur of the whisker (indicating the fullest extent of whisker displacement), the cameras were not used in high-speed mode in initial experiments but rather were set to take data at 30 frames/sec. During initial data analysis, we found that the motion of the whisker in the overhead camera view was negligible in comparison with its motion in the longitudinal camera view, and we therefore considered only the motion in the vertical plane.

A resonance curve for each whisker was obtained by driving the whisker at a wide range of different frequencies (f) using constant acceleration. Constant acceleration is standard engineering practice and means that the amplitude of vibration at the base is inversely proportional to $(2\pi f)^2$. In practice, constant acceleration ($\pm$0.5%) proved feasible down to 25 Hz.

All of the whiskers studied had first-mode resonant frequencies of $\geq$27 Hz. For particularly long whiskers, we constructed resonance curves that included frequencies as low as 10 Hz (see Fig. 4). At frequencies of $<$25 Hz, we measured the acceleration of the table, and then scaled the data appropriately (using Eq. 1) to match the constant acceleration obtainable at frequencies of $\geq$25 Hz.

The peak acceleration of the table (α) was measured in units of g, the acceleration of gravity (9.8 m/sec^2). At each frequency (f), the amplitude of the base displacement was thus calculated as follows:

$$A_{\text{base}} = (\alpha)(9.8)/(2\pi f)^2 \tag{1}$$

By using a wide range of frequencies, we were prepared to observe multiple resonance modes of the whisker. We generally began by increasing frequency of the vibration table in 10–20 Hz intervals and then narrowed in to 2 Hz intervals once the approximate resonances had been found. Between 100 and 500 frames of video data were recorded at each frequency, and each frame was saved as a TIFF file (640 $\times$ 480 pixels). At a frame rate of 30 frames/sec (shutter open), the whisker appears as a blur, and the image indicates the full range of motion. Extreme positions of whisker motion appear darker, because the whisker spends a longer time in these positions (the whisker velocity is zero). At the end of each run (covering the full frequency range), we calibrated the image by taking videos while a ruler was held parallel to and then perpendicular to the whisker. The whisker was then removed from the vibration table, and 500 frames of video data were taken of the background.

The frames of video data taken at each frequency were next imported into Matlab (The MathWorks, Nattick, MA) and averaged. The frames of the background image were also imported into Matlab and averaged. We then subtracted the average background image from the average image of the (blurred) whisker motion at each frequency. For each frequency, we then directly measured the tip displacement, as shown in Figure 1.

Dividing the tip displacement by the base displacement at each measured frequency yields a magnification ratio curve, which is useful in characterizing resonances. In principle, the base displacement could have been directly measured from an image such as Figure 1. However, it is difficult to obtain an accurate measure of base amplitude by this technique at higher frequencies (see Fig. 3, middle row). Therefore, base peak-to-peak displacement (2^*A_{base}) was directly calculated from Equation 1.

Damping measurements. To confirm our values for the first-mode resonance frequencies and also to investigate the damping characteristics of the whiskers, we performed impulse experiments on the four whiskers of row D. For these experiments, the whisker remained superglued to the vibration table, but the acceleration was turned off. The vibration table was isolated from the external vibrations in the environment.

We used a pair of fine forceps held by hand to deflect the whisker near its base. The forceps were initially placed above the whisker and then rapidly moved in a straight downward direction past the whisker to achieve an initial displacement with minimum initial velocity (plucking). Care was taken to deflect the whisker in only one direction and to ensure that the forceps were not in contact with the whisker after the initial displacement.

We again used the Photron Fastcams to monitor the displacement of the whisker in two dimensions. This time, however, video was taken at 1000 frames/sec with a shutter speed of 200 μsec. Again, motion of the whisker in the overhead camera view was found to be negligible. The video images were imported into Matlab, and the position of the whisker was manually tracked. For each frame, we determined the angle that the whisker tip made with respect to the horizontal axis as the whisker oscillated (in its first-mode resonance) back to its static position. These angle measurements were low-pass filtered at more than two times the fundamental resonance frequency for smoothness, and the peaks and troughs of the oscillations were then located.

Table 1. l_n values used in the theoretical model to predict resonant frequencies for the fixed-free conical beam

$(A_t/A_b)^{1/2}$	Mode 1	Mode 2	Mode 3
1.00	3.516	22.034	61.701
0.500	4.625	19.55	48.50
0.333	5.289	18.76	43.78
0.250	5.850	18.51	41.34
0.100	7.201	18.71	37.10
0	8.718	21.146	38.45

Values are from Table 1 by Georgian (1965). Our values were interpolated from this table to adjust for measured tip and base diameter. A_t is the area of the tip of the conical cantilever beam, and A_b is the area of the base.

To find the damping ratio, we plotted the log of the amplitudes of the peaks and troughs of the oscillation versus the number of oscillation cycles. The slope of this line is the logarithmic decrement Δ. The logarithmic decrement is then related to the damping ratio ζ as follows (Tongue, 2002):

$$\Delta = 2\pi\zeta/(1 - \zeta^2)^{1/2} \tag{2}$$

so that in the underdamped case,

$$\zeta = \Delta/(\Delta^2 + 4\pi^2)^{1/2} \tag{3}$$

A second value for ζ was calculated by dividing the bandwidth of the resonance curve at the half-power (−3 dB) point by twice the resonance frequency (Tongue, 2002). These resonance curves were those obtained in the previous experiment and provide an independent measurement of ζ. Finally, the quality factor (Q) is defined as $1/2\zeta$ (Tongue, 2002).

Theoretical prediction of natural frequencies. Neimark first proposed using a cylindrical cantilever beam to model the vibrations of the whiskers (Neimark, 2001). Here, we extend the model to a truncated conical cantilever beam. According to theory (Conway et al., 1964), a tapered conical beam fixed at one end and free to vibrate at the other end will have resonant frequencies f_n equal to

$$f_n = (\lambda_n/L^2)(EI/\rho A_b)^{1/2} \tag{4}$$

where λ_n are tabulated constants determined by boundary conditions, L is the length of the cone, E is Young's modulus, A_b is the cross-sectional area at the base of the cone, I is the cross-section moment of inertia at the base of the cone ($A_b{}^2/4\pi$), and ρ is the density of the material. The constants λ_n are determined by fixed–free boundary conditions and by the amount of tapering from base to tip. The numerical model of Conway et al. (1964) was verified experimentally by Georgian (1965), who tabulates λ_n in terms of $(A_t/A_b)^{1/2}$, where A_t is the area at the tip of the cone. We used these values for λ_n in our model to account for tip diameter, as shown in Table 1. As described above, we used an average value of ρ calculated over all of the whiskers in our theoretical prediction of resonant frequencies. We did not measure Young's modulus of the whiskers. Instead, E was left as a free parameter, and its value was estimated on the basis of the best fit between measured and predicted values (see Results).

Video quantification of natural exploratory behaviors. An adult (~6 months) female Sprague Dawley rat was placed in an 11 × 11 inch square cage with a sliding door that could be manually opened and closed. At the onset of each trial (indicated by door opening), the rat poked its head and upper body out of the cage and searched for a liquid reward in a pipette. The trial was terminated after the rat located and consumed the reward, and retracted its head back into the cage. All of the procedures were approved in advance by the Animal Care and Use Committee of the California Institute of Technology.

A flat fluorescent light source was positioned under the door, and the Photron Fastcams were used to monitor the head and whisker movements of the rat at either 250 or 1000 frames/sec. One camera was placed directly above the door, obtaining a bird's-eye view, silhouetted image of the rat's head and whiskers (Fig. 2). The second camera was positioned to the side of the animal to monitor head tilt. For the results presented in this paper, we analyzed only those trials in which head tilt was determined to be negligible.

On some trials, a metal "C" was placed in the rat's search space. The "C" consisted of a vertical bar ~12 inches tall and two horizontal bars positioned well above and below the search space of the rat (Fig. 2*A*). The "C" thus effectively appeared as a vertical post to the rat. Consistent with exploration strategies described previously (Brecht et al., 1997; Hartmann, 2001), the rat detected the vertical post with its macrovibrissae and then explored it more closely with its snout and microvibrissae. During the initial detection phase, we were able to examine the macrovibrissal deflections that occurred as the rat brushed its whiskers past the post.

Figure 2 shows representative video frames illustrating our tracking methods for determining angular whisker position during natural exploratory behaviors. For each video segment, we first determined which whiskers could be accurately tracked throughout the entire behavioral sequence. In each video frame, we then tracked the base of these whiskers and also a point further out along the whisker. For videos taken of free whisking behavior, we additionally traced out the entire whisker shape, as shown in Figure 2*B*.

Head and whisker positions were tracked semiautomatically using image-processing scripts written in Matlab. Whisker angles were measured relative to the rat's head angle, with 180° representing rostral and 0° representing caudal. When fully protracted, whiskers could attain angles close to 180° (e.g., see the most rostral whiskers of Fig. 2*B*). When fully retracted, the minimum angle a whisker could attain was the angle it formed when lying flat back against the head, or ~30°.

Results

Resonance modes

We first measured the resonance modes of isolated whiskers by applying a sinusoidal displacement at the whisker base over a range of frequencies (see Materials and Methods). The base of the whisker was superglued to the vibration table, so it was displaced directly with the table. The tip of the whisker was then free to move based on whisker dynamics. At some vibration frequencies, the displacement of the whisker tip was disproportionately large relative to the displacement of the whisker base, indicating that the whisker had entered a resonance mode. Figure 3 shows first-, second-, and third-mode vibrations for the C1 whisker, at frequencies of 40, 94, and 188 Hz, respectively. The C1 whisker was ~53 mm long and had a base radius of 105 μm and a tip radius of 5.5 μm. Note that the spatial position of the node of the second mode is not at the midpoint of the whisker, as would be expected for a cylindrical beam. Instead, the node is much further out along the length of the whisker, consistent with the expected effect of the whisker taper.

Figure 4 illustrates the resonance curve for whisker C1. The top graph shows the displacement of the tip (solid line) and the base (dashed line) as a function of frequency. The magnification ratio was calculated by dividing the tip displacement by the base displacement and is shown in the bottom graph of Figure 4. Two features of the ratio curve are particularly noteworthy. First, all of the modes are strongly damped, as shown by the fact that the peaks are very broad. In fact, the first mode is so highly damped that it appears only as a cusp on the resonance ratio curve.

Second, the amplitude of the resonance peaks increases with mode. This is a surprising result, because the amplitude of the resonance peaks in typical engineering applications decreases with mode number (Gorman, 1975). We suggest that this result is due at least in part to nonlinear effects of viscous and/or hysteretic damping. Viscous damping, arising from the motion of a body through a fluid, varies with velocity; hysteretic damping, resulting from the stresses placed on an imperfectly elastic material, varies with displacement (Tongue, 2002). Standard engineering analyses of beam vibrations, in which the amplitude of the resonance peaks typically decreases with mode number, usu-

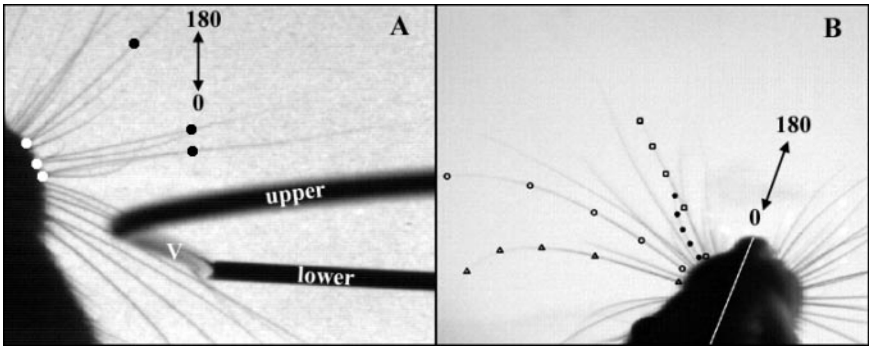

Figure 2. Method for tracking the angular position of whiskers during deflection past an object and during free whisking in air. Whisker angles are measured relative to head angle, with 180° representing rostral and 0° caudal. *A*, A single frame from a video of the rat driving its macrovibrissae past a metallic "C." The vertical portion of the "C" (labeled "V") is ~12 inches in height and appears foreshortened in the image. The horizontal bar labeled "upper" is well above the rat's head. The horizontal bar labeled "lower" is well below the rat's head. The more caudal whiskers are clearly stuck behind the vertical bar, while the more rostral whiskers are free to move in front of the bar. Whisker angles were defined as the angle formed by the base of the whisker (white circles) and a point some length out along the whisker (black circles), relative to the angle of the head. *B*, The full shape of each whisker was tracked during free whisking behavior. Whisker angles were determined from the angle between the base point and the last point out along the whisker, relative to the head angle. Triangles, filled and open circles, and squares exemplify the tracking of four separate whiskers.

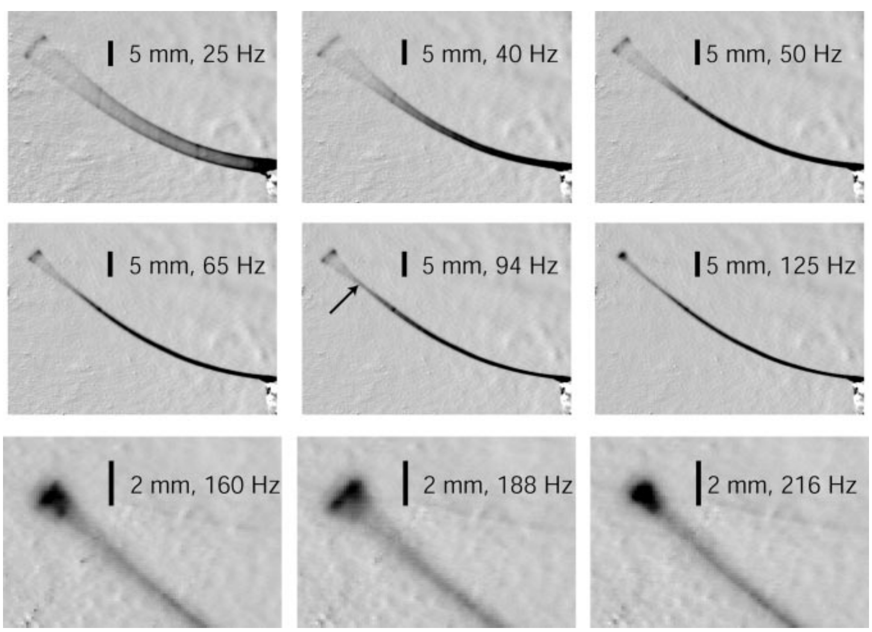

Figure 3. First, second, and third resonant modes for whisker C1. The top row shows the first mode near 40 Hz and vibration at surrounding frequencies of 25 and 50 Hz. Note that, although the tip displacement does not appear much larger in the 40 Hz image than in the 25 Hz image, the base amplitude is much smaller in the 40 Hz image. The middle row shows the second mode at 94 Hz and the vibration at nearby frequencies of 65 and 125 Hz. Note the narrow neck (arrow) at resonance indicating the node of the second mode. The bottom row shows the third mode at 188 Hz and the vibration at the surrounding values of 160 and 216 Hz.

ally assume small-amplitude deflections and linear viscous damping. These conditions were unlikely to hold during our experiments. If damping was nonlinear, in either velocity or displacement, then the lower modes would be more strongly damped, because these quantities are greater at lower frequencies for constant acceleration input.

In the behaving animal, the magnification ratio, as shown in Figure 4, is unlikely to be the most relevant parameter for sensory perception. More useful measures may be the ratio of whisker displacement to the force exerted by interactions with external objects, or the fraction of force transmitted to the base from a particular whisker displacement. However, these two measures require determining the forces exerted on a distributed mass, which is difficult even in the isolated whisker preparation and requires a more elaborate experimental apparatus.

Resonance frequencies: experiment versus theory

Using Equation 4 (Conway et al., 1964; Georgian, 1965), we were able to calculate natural resonances on the basis of measured values of length, density, moment of inertia, and known values of λ_1. The average whisker density over all 24 whiskers was found to be 1.14 ± 0.27 mg/mm^3, and this was therefore the value used to predict the resonant values for the whiskers. Young's modulus was taken to be a free parameter for all 24 whiskers. A comparison between theoretical calculations and measured first resonance frequency is shown in Figure 5. Figure 5*A* illustrates that, over all of the whiskers, the best match between predicted and measured values was found for a value of $E = 3.02$ GPa.

Careful inspection of Figure 5*A*, however, suggests that a lone outlier at high frequency (+) may have unduly influenced the curve fit between measured and predicted values. This whisker was the E4 whisker, the shortest one in our analysis. We therefore reanalyzed our data after removing the single highest-frequency value (Fig. 5*B*). The remaining 23 whiskers gave a much better fit between measured and predicted values, with $E = 3.68$ GPa. This range of values for E (~3–4 GPa) is close to E for keratin material (2.5 GPa) (Bonser and Purslow, 1995) (1.33–1.84 GPa) (Bonser, 2000). In biological materials, Young's modulus is likely to be anisotropic (Bonser, 2000), and thus, the value is at best an approximation. For comparison, E for rubber is 0.0028 GPa, E for nylon is between 2 and 3 GPa, and E for stainless steel is between 190 and 200 GPa.

Having determined a range of values for E, we can now compare the measured values of the resonant frequencies for whisker C1 above with predicted values. As shown in Figure 4, the measured values for the three first resonant frequencies for the C1 whisker were 40, 94, and 188 Hz. Assuming $E = 3.68$ GPa, our model of the whisker as a conical beam predicts that the first three resonant modes would occur at 47, 115, and 213 Hz. The measured values for the first three resonant modes of this whisker are thus lower, but within 20%, of the predicted values.

The measured natural frequencies of the whiskers varied inversely with whisker length (Fig. 6*A*). We next compared these experimental data with the theoretical model relating frequency to length (L). Equation 4 predicts explicitly that the resonant frequencies should decrease inversely as L^{-2}. However, a log–log plot of the measured data as a function of length has a slope of

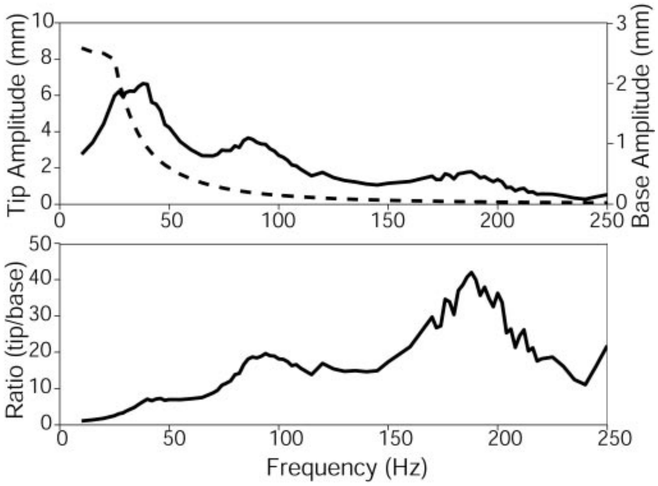

Figure 4. Resonance curve for whisker C1. The top graph shows the absolute displacement of the tip (solid line) and the absolute displacement of the base (dashed line). The vertical scale on the left applies to the tip, whereas the vertical scale on the right applies to the base. The bottom plot shows the magnification ratio curve for the whisker, calculated by dividing the displacement of the tip by the displacement of the base. Resonance peaks are seen near 40, 94, and 188 Hz. All of the peaks are broad because of damping.

-1.5 (Fig. 6*B*), indicating that the measured frequencies decrease as $L^{-1.5}$, instead of L^{-2}. This is because Equation 4 also has an implicit linear dependence on the base radius (R_b) of the whisker. Substituting for I and A_b, Equation 4 can be restated as:

$$f_n = (\lambda_n R_b / 2L^2)(E/\rho)^{1/2} \tag{5}$$

A log–log plot of measured base radii versus whisker length (Fig. 6*C*) showed that the radius increases approximately as the square root of the length (the slope of the plot is 0.49). Inserting this relationship into Equation 5 yields a frequency dependence of $L^{0.5}/L^2$, which corresponds to the $L^{-1.5}$ observed in Figure 6*B*.

Damping measurements

We next investigated the damping characteristics of the whiskers by performing impulse experiments on the four whiskers of the D row (see Materials and Methods). This serves as an independent check for the first-mode resonant frequencies and also permits a more detailed analysis of damping coefficients.

In our initial analysis of the impulse experiments, we observed that each whisker oscillated around a position different from its initial static position. In many cases, the whisker did not even return to its original static position after the oscillations ended. We therefore calculated the zero line for the oscillation based on the physical constraint that the amplitude of the oscillation must decrease with each half-cycle (i.e., energy must never be added into the oscillation). In practice, there was only one such line for each impulse trial (to within 0.2°), and its value corresponded directly to the midpoint of the last observable cycle in the oscillation.

We analyzed three impulse trials for each of the four whiskers in the D row. For each whisker, the impulse trials gave first-mode resonance values that agreed to within 5 Hz of each other, and also within 5 Hz of the first-mode resonance value as measured in the vibration table experiment. Figure 7 shows the damping results for the full D row of whiskers.

Table 2 shows the natural resonances and the damping ratios for the D row of whiskers as calculated from the vibration experiment and the impulse experiment. Resonant frequencies agreed within 2%, and damping ratios agreed within 30%. Note that these are relatively large values for ζ, meaning that the whiskers are very damped compared with many familiar resonant objects; typical values of ζ for musical instruments are on the order of $2–5 \times 10^{-5}$. This strong damping has significant implications for resonant oscillations during natural behavior. Most significantly, it suggests that whiskers are unlikely to bounce off of an object after contact (see case 3 below).

In all of our experiments, both on isolated whiskers and in the awake animal, the frequencies obtained are actually damped natural frequency. The damped natural frequency is related to the undamped natural frequency by the equation:

$$f_{\mathrm{damped}} = f_{\mathrm{undamped}}(1 - \zeta^2)^{1/2} \tag{6}$$

where ζ is the damping ratio. Our whiskers typically had values of ζ between 0.11 and 0.17 (Table 2), so this will nominally lower the actual undamped natural frequencies (<2%).

Resonances during active behavior

In the impulse experiments described previously, the base of the whisker was held rigidly fixed, and a pair of fine forceps was used to deflect the whisker. In the awake animal, however, the whiskers are actively moved back and forth near the base, and deflections occur when the whiskers make contact with objects in the environment. We wanted to determine whether resonances could be produced by interactions with objects during natural whisking behavior, and if so, how the resonant characteristics compared with those observed in the isolated whiskers. We considered five cases in which resonances might play a role in the interaction of the whiskers with the environment.

Case 1: the whisker bumps into an object and drives past it

We looked for resonant oscillations as the whiskers were actively deflected past a vertical bar, as described in Materials and Methods. A total of 19 trials were analyzed. Figure 8 shows four examples of typical whisker movement patterns that occurred as the rat drove its whiskers past the bar. In these behavioral sequences, some whiskers (those that had already passed the bar) moved freely in air, whereas other whiskers directly contacted and then deflected past the bar. This allowed us to directly compare whisker movements with and without object contact. In 10 of 19 trials, the deflected whisker exhibited one-half to one cycle of resonance before resuming the normal whisking pattern. In four cases, no clear resonance distinct from the normal whisking pattern was observable, despite clear deflection past the bar. In three trials, the whisker underwent more than two cycles of oscillation before the resonance damped out. Two trials gave ambiguous results and were not analyzed further.

Figure 8, *A* and *B*, shows two examples of the most commonly observed whisker movement pattern after deflection, in which the whisker exhibited one-half to one cycle of oscillation before resuming the normal whisking motion. The top and bottom traces of Figure 8*A* show the angular position of two whiskers that did not make contact with the bar at any point in time during the behavioral sequence. These two whiskers show a fundamental whisking frequency of ~9 Hz. The middle trace of Figure 8*A* shows the angular position of a third whisker (~29 mm long) that did make contact with the vertical bar. The whisker remained stuck behind the bar from 0 to 17 msec, at which time it suddenly deflected past the bar (vertical arrow). It reached peak protraction at ~25 msec, rebounded backwards until 32 msec, and appears to be reincorporated into the normal whisking pattern near

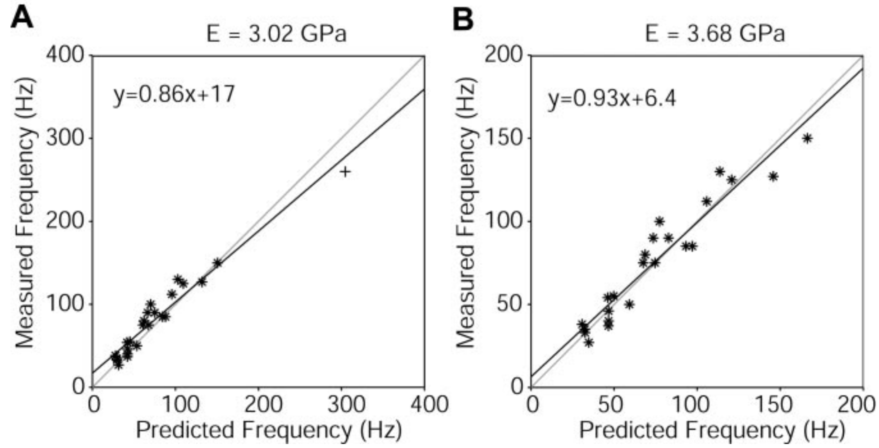

Figure 5. Experimental versus theoretical values for first-mode resonant frequencies. *A*, The best fit between predicted and measured values for the first-mode resonant frequency for all of the whiskers was found for a value of Young's modulus equal to 3.02 GPa. The line $y = x$ is shown in gray for comparison with the curve fit. An outlier at high frequency is indicated (+). *B*, Omitting the highest frequency from the plot in *A* yields an even better fit between predicted and measured values. In this case, the best fit was found for a value of $E = 3.68$ GPa. The line $y = x$ is again shown in gray for comparison with the curve fit.

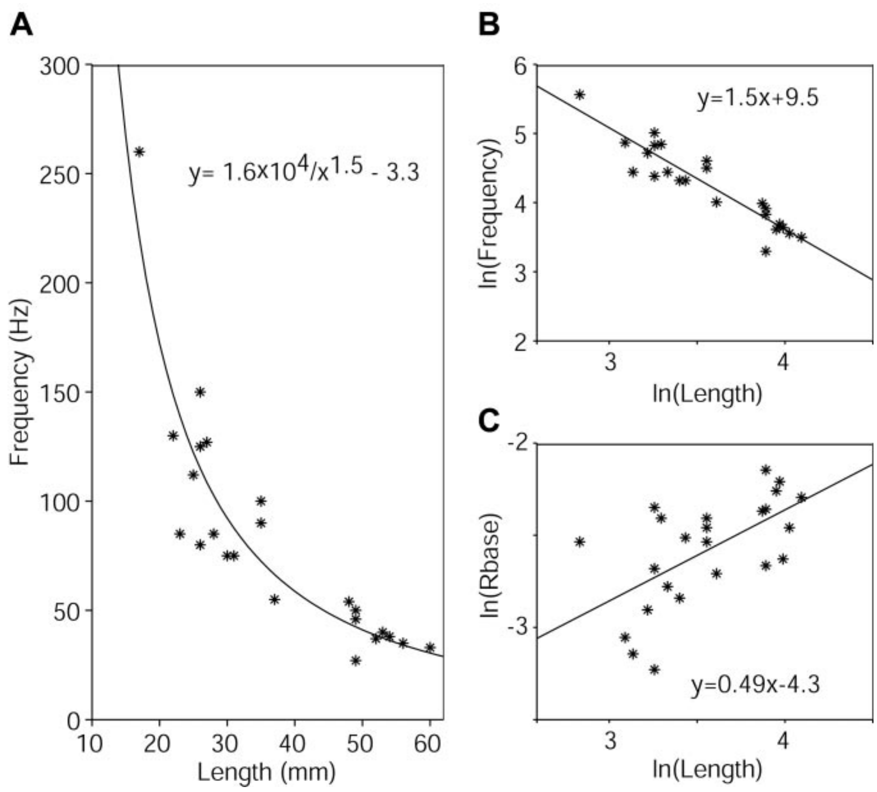

Figure 6. Resonant-frequency dependence on whisker length and base diameter. *A*, As predicted by Equation 4, the resonance frequencies are well fitted by a function that decreases inversely with the whisker length (L). *B*, A log–log plot of frequency versus length reveals a relationship of $L^{-1.5}$. *C*, The radius of the whisker base scales as the square root of whisker length, adding an extra 0.5 to the expected exponent of L^{-2} in Equation 4.

40 msec. The half-cycle of oscillation between 25 and 32 msec (duration, 7 ± 1 msec; horizontal arrow) was easy to identify as a first-mode resonance in the video, and represents a resonant frequency for this whisker between 62 and 83 Hz. To compare this experimentally measured value with theory, we used a base radius (averaged over 10 whiskers of similar length) of 0.072 ± 0.019 mm, a tip radius of 0.0029 ± 0.001 mm, an average density of 1.14 mg/mm^3, and the value for Young's modulus obtained from Figure 5*B* (3.68 GPa). Inserting these values into Equation 4 predicts a resonant-frequency value for this whisker between 68 and 131 Hz, centered at 107 Hz. Some of the discrepancy between predicted and measured values is almost certainly attributable to differences in boundary conditions at the base of the whisker (see Discussion).

Figure 8*B*, middle trace, shows a second example of a whisker deflecting past the bar. In this case, the whisker was ~37 mm long and passed by the bar after 21 msec (vertical arrow). This whisker showed one-half cycle of oscillation between 34 and 43 msec (duration, 9 ± 1 msec; horizontal arrow), representing a resonant frequency between 50 and 62 Hz. Again using the average values for base and tip radius calculated over 10 whiskers of comparable length, theory predicts a resonant frequency for this whisker between 51 and 89 Hz, centered at 62 Hz. The top and bottom traces in this figure show the smooth whisking trajectory achieved by whiskers that did not hit the bar.

Figure 8*C* illustrates the variability present in the resonant responses during natural behavior. In this example, two whiskers deflected past by the bar in quick succession (14 and 16 msec, vertical arrows). Trace 1 shows the angular position of a whisker (28 mm long) that underwent up to three cycles of oscillation before the resonant response damped out (lowest three horizontal arrows). Importantly, the cycles appeared to have different periods, with frequencies ranging between 41 and 55 Hz. This suggests that the rat may be changing boundary conditions at the base of the whisker during whisker resonance. Note also that these measured values are much lower than the predicted resonant frequency, between 73 and 140 Hz, for a whisker of this length. This large discrepancy is likely attributable to underestimation of the whisker length from foreshortening in the image, because this particular whisker appeared to be oriented at some angle extending below the image plane. In contrast to trace 1, trace 2 shows the angular position of a whisker (40 mm long) that did not resonate in a manner distinct from smooth whisker retraction. The resonant oscillation, if it occurs, appears to be dominated by the retraction phase of the normal whisking cycle (topmost horizontal arrow). The top two traces (traces 3 and 4) of Figure 8*C* again illustrate the smooth whisking trajectory achieved by whiskers that did not hit the bar.

Finally, Figure 8*D* shows an example of one of the most caudal whiskers (identifiable as belonging to the Greek row) deflecting past the bar near 10 msec (vertical arrow). This whisker was over 40 mm in length, and shows between one-half and one full cycle

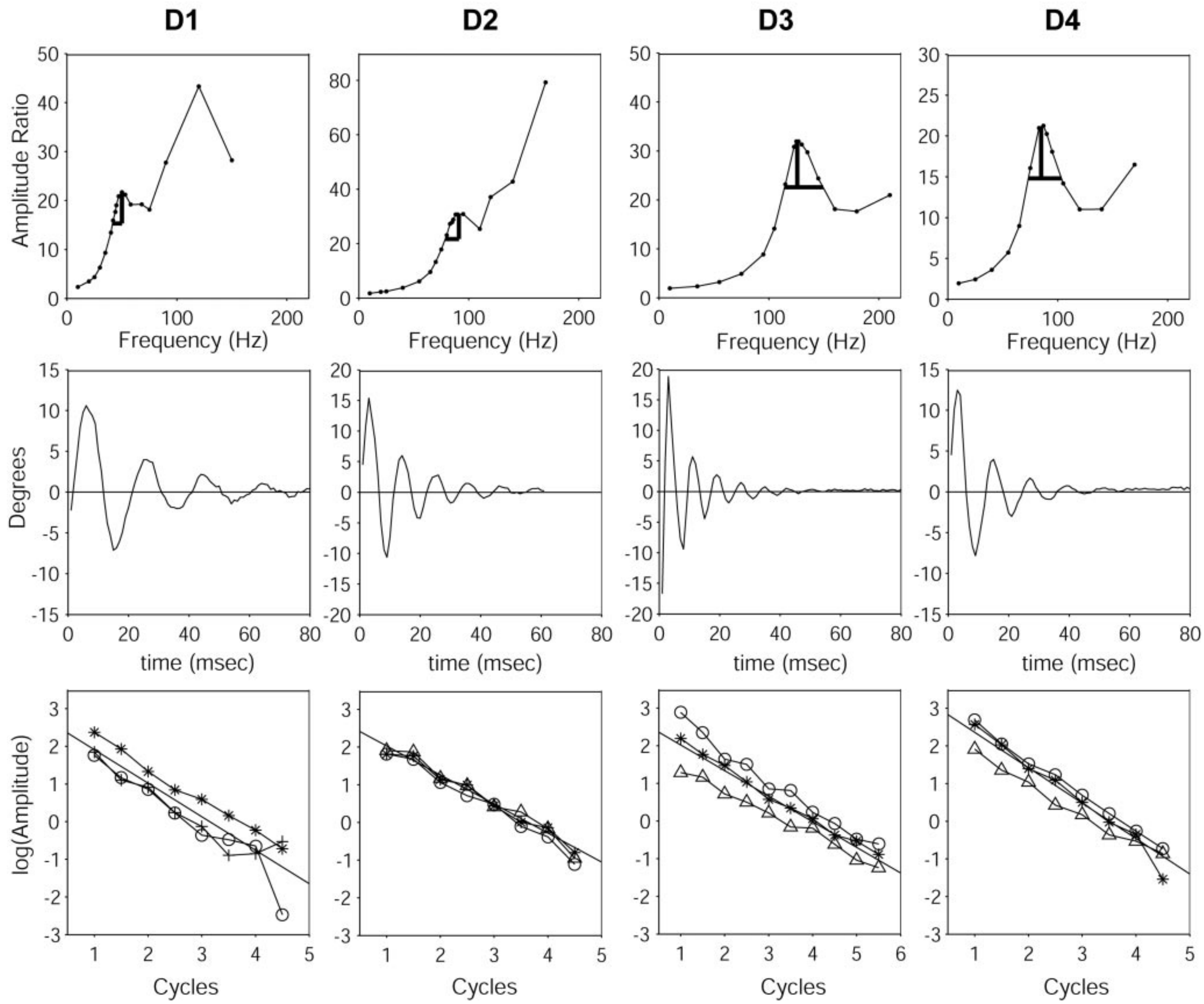

Figure 7. Damping characteristics for the D row of whiskers. Each column represents results for a different whisker (D1, D2, D3, and D4). The top row presents the resonance curve for each whisker. Damping characteristics were calculated from the width of the resonance peaks, as indicated by the gray lines. The middle row presents the results of one impulse trial for each whisker. Note that all of the whiskers are strongly damped, undergoing at most five full cycles of oscillation. The bottom row presents three log decrement curves (obtained from three impulse trials) for each whisker. Each of the three trials is indicated by a different symbol (triangles, circles, asterisks). In each graph, the *y*-axis is the log of the amplitude of the peaks and troughs of the oscillation (shown in the second row), and the *x*-axis is cycle number. The slope of the lines on these graphs is the log decrement Δ.

Table 2. Measured first-mode resonant frequencies (f_1), damping ratios (z), and quality factors (Q) for the whiskers of the D row

Whisker	Length (mm)	f_1 vib.	f_1 imp.	ζ vib.	ζ imp.	Q vib.	Q imp.
D1	49	50	50.5	0.17	0.14	5.9	7.1
D2	35	91	89	0.13	0.12	7.7	8.3
D3	27	126	128	0.14	0.11	7.1	9.0
D4	28	85	85	0.17	0.15	5.9	6.7

First-mode resonant frequencies (f_1) are given in Hertz. Vib. indicates that the data were obtained from the vibration experiment. Imp. indicates that the data were obtained from the impulse experiment. Q values were calculated as $Q = 1/2z$.

of resonance, at frequencies between 25 and 33 Hz (horizontal arrows). Again, the two half-cycles appear to have different periods. The top two traces show the movements of more rostral whiskers freely moving in air. Note that the caudal and rostral whiskers are moving in opposite directions over the entire duration of the whisk (100 msec).

Case 2: free whisking in air

Figure 8 shows examples of the movements of whiskers that both did and did not hit the vertical bar. As an additional control, we also tracked whisker movements during free whisking in air with no objects present, over ~0.5 sec. By tracking over a longer time period, we hoped to examine the relative variation between whisks, compared with the single whisk cycles and associated resonances shown in Figure 8. This controlled for the possibility of seeing high-frequency resonances at sharp stops at the extremes of each whisking cycle. Each of the four traces in Figure 9 shows the angular position of one of the whiskers in Figure 2*B* over time. The smooth cycles achieved by all four whiskers over

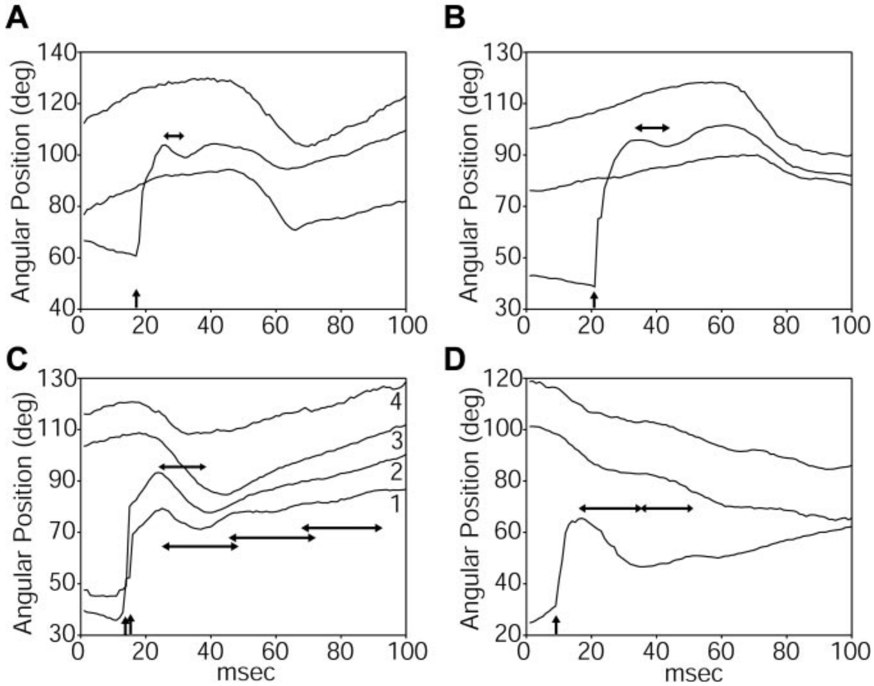

Figure 8. Resonant oscillations of the whiskers in response to deflection past a vertical bar. *A*, *B*, Examples of two whiskers of different lengths (29 mm in *A*; 37 mm in *B*) deflecting past the bar. The top and bottom traces in both figures show the angular position of two whiskers that did not make contact with the bar. The middle trace in each figure shows the angular position of a whisker that was stuck behind the bar and then deflected past it. Deflection times are indicated by vertical arrows. The horizontal arrows indicate the approximate half-cycle of the resonance. In *A*, the lowest trace has been offset by −5°, and in *B*, the top and bottom traces have been offset by +10° and −10°, respectively, for visual clarity. *C*, Whisker deflection did not always result in clear resonances. Traces 1 and 2 show the angular position of two whiskers that deflected past the bar at 14 and 16 msec (vertical arrows). In trace 2, any potential resonance exhibited immediately after deflection (top horizontal arrow) is synchronized with the fundamental whisking periodicity (compare with traces 3 and 4). In trace 1, the whisker undergoes up to three complete resonant oscillations (bottom three horizontal arrows) before damping out. Traces 3 and 4 show the angular position of two whiskers that did not make contact with the bar. Traces 3 and 1 have been offset by +5° and −5°, respectively, for visual clarity. *D*, In this example, one of the most caudal whiskers deflects past the bar, and one-half to one cycle of resonance is shown. Two half-cycles of resonance are indicated by the horizontal arrows, but it is difficult to determine whether the second half-cycle constitutes resonance, active protraction, or a combination of both. Note that the caudal and rostral whiskers move in opposite directions over the duration of the whisk.

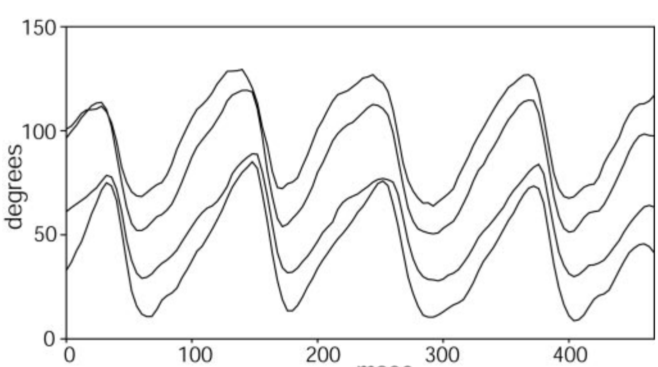

Figure 9. Whisker motion during free whisking. No resonant oscillations were observed during free whisking in air. Each trace shows the angular position of a single whisker over time. The top and bottom trace have been offset by +10° and −10°, respectively, for visual clarity.

the entire duration of whisking look very similar to those shown in Figure 8 and exhibit no discernable resonant oscillations.

Thus, as expected, when the whiskers are being driven in a (relatively) steady state, at a frequency well below resonance, no resonant oscillations are present. It has also been shown that the whisking cycle has a significant dorsoventral component, so that the whisking movement actually forms a loop (Bermejo et al., 2002). It is possible that this loop helps the rat avoid the resonances that would otherwise be associated with a hard (high acceleration) stop at the end points of the whisking cycle.

Case 3: the whisker bumps into an object, and the whisker either bounces off or remains in contact with the object

In none of the 19 trials did we observe the whisker to vibrate or bounce upon its initial contact with the metal bar. Instead, after its initial contact with the bar, each whisker appeared to remain in constant direct contact with the bar as the rat drove its whiskers even further forward. As the rat protracted its whiskers more, whiskers that were stuck behind the bar deformed more and slid along the bar, until they finally deflected past the bar at their tip (Fig. 2A). Although we think it unlikely, it is conceivable that, under some behavioral conditions (e.g., very high whisking velocity), the whiskers could bounce off of an object. In this case, different modes will be excited, depending on where along its length the whisker strikes the object. Specifically, striking at different places along its length will preferentially excite modes that have amplitude maxima at the striking points.

We suggest that the high damping of the whiskers, combined with any tendency by the rat to continue to protract its whiskers after initial object contact, will in general ensure that the whiskers will stick to, instead of bounce off of, objects under exploration. Assuming that this condition approximates a fixed–fixed or fixed–pinned boundary condition (see Discussion), the whisker may still resonate, but its effective length will be changed, thus altering the resonant frequency. The rat could potentially use these resonances to help determine how far away an object is. Although we never observed any resonances upon initial contact with the bar, the experiments presented here were not designed to look closely for this possibility.

Case 4: texture discrimination

The current study confirms that resonances exist in the awake, behaving animal and may enable the rat to perform fine texture discriminations as hypothesized by Neimark (2001) (for additional discussion, see Neimark et al., 2003).

Case 5: whiskers held erect during head movements

During several behaviors, including drinking and object exploration, the whiskers are often held stationary and erect while the head moves. In our behavioral videos, the tips of the whiskers were often observed to oscillate under these conditions, but these frequencies were not quantified. It is thus possible that sharp head movements may superimpose a resonance on top of the smooth whisking cycle.

Discussion

Resonances and trigeminal processing

The main finding of this paper is that whiskers exhibit natural resonances and strong damping, both in vibration tests on isolated whiskers and in the awake, behaving animal. In the awake animal, the whiskers clearly resonate after being driven past an object (Fig. 8). We suggest below that this may be particularly important for the detection of object boundaries: high-frequency vibrational information will arise from whiskers that have deflected past an edge. The observed resonant frequencies, ranging between 27 and 260 Hz depending on whisker length, were well above normal whisking frequencies. These resonant properties should facilitate the transduction of high-frequency mechanical stimuli to the sensors in the whisker follicles during natural exploratory behaviors. Peripheral neurons (e.g., those in the trigeminal ganglion) might follow this high-frequency information in a one-to-one manner up to frequencies as high as 1 kHz. More central neurons are unlikely to follow one-to-one up to such high frequencies, because they will be limited by longer refractory periods. However, at higher frequencies, central neurons may track the changes in amplitude of the resonances; in other words, they may follow the envelope of the resonant signal. These two mechanisms may drive the types of high-frequency responses found in previous electrophysiological experiments (Shipley, 1974; Simons, 1978; Castro-Alamancos, 2002; Kleinfeld et al., 2002).

Boundary conditions for isolated whiskers and for the behaving animal

In the experiments on isolated whiskers, each whisker was held fixed at the base and otherwise allowed to vibrate freely, replicating the type of seismic excitation that would occur during natural whisker movement. This represents a fixed–free boundary condition and compares reasonably well with the conditions that occur as the rat moves its whiskers freely in air and makes initial contact with an object.

That the isolated whiskers were held rigidly at the base has two implications for our results. First, it means that measured values for resonant frequencies presented in this paper represent upper bounds on these frequencies, for fixed–free boundary conditions. Second, the rigid base means that damping effects were minimized, and our values of ζ thus represent lower bounds. Any decrease in how rigidly the whiskers are held at the base will decrease the natural frequencies and is likely to increase damping.

The whiskers are almost certainly held much less stiffly in the behaving animal because of compliance in the facial tissue and musculature at the whisker base. This difference in boundary conditions is likely to account for the differences observed between the isolated-whisker and awake-animal experiments: lower resonant frequencies and higher damping were observed in the awake animal than in the isolated whiskers (Figs. 7 and 8). In addition, the rat may control the compliance at the base of the whisker to actively modulate boundary conditions, thus changing both damping and resonant frequencies (see below).

Modeling the whisker base with a torsional-spring boundary condition, instead of a fixed boundary condition, might be an even better approximation to boundary whisking in air and initial object contact because of the compliance of the follicle and associated musculature. In the torsional-spring case, the boundary conditions are a mix between fixed–free and pinned–free, and to find the natural resonances, we can, to first order, interpolate between those two conditions (Gorman, 1975). In the interpolated model, the predicted fundamental frequencies would decrease by ~30% (Gorman, 1975) to match our data. It may be possible to infer properties of the follicle base by using an equivalent torsional-spring constant.

Under some behavioral conditions involving object contact, such as the whisker bumping into an object and sticking against it (case 3b), the boundary conditions might be better modeled with a fixed–pinned or fixed–fixed beam. Under fixed–pinned or fixed–fixed conditions, the resonant frequencies will be higher than in the fixed–free condition, by factors of 4.39 and 6.36, respectively. The point of contact also shortens the effective length of the whisker, further increasing the resonant frequencies. In contrast, under fixed–free boundary conditions (cases 1, 2, 3a, and 5 in Results), the point at which the whisker contacts an object has no effect on the resonant frequencies (Morse, 1936), only on the relative amplitudes of the different spatial modes. Point of contact is also likely to be important during texture exploration (case 4) (Neimark et al., 2003).

Implications for natural exploratory behavior

Experimental limitations and general observations

In this study, we were concerned only with tracking the angular position of the whisker and examining the smoothness of the resulting trajectory for resonant frequencies. We were not concerned with tracking a particular point on the whisker, and we did not examine the dorsal–ventral component of whisker movement or resonance (Bermejo et al., 2002). Ideally, whisker movements would have been monitored in three dimensions, but we were concerned that placing any markers on the vibrissae would disrupt the natural frequencies. Instead, we were careful to examine resonances under natural conditions, with all of the whiskers intact and unaltered in any way.

In our initial analysis of the behavioral video data we observed a feature of whisking behavior that is yet undescribed in the freely behaving animal: whiskers on the same side of the face can move in opposite directions over the duration of an entire whisk. As shown in Figure 9*D*, the caudal whiskers can protract while the more rostral whiskers are retracting, over a time course of 100 msec. We also observed that, in general, whisking tended to be more synchronous (i.e., whiskers on the same side of the face tended to move in unison) when no obstacle was present (data not shown).

These results are consistent with, but differ slightly from, those found for rats performing a texture discrimination task (Carvell and Simons, 1990), and for rats in a head-fixed conditioned-whisking preparation (Sachdev et al., 2002). In the texture discrimination study, whiskers on the same side of the face were observed to move in opposite directions only 3% of the time, over a total of ~60 whisks (Carvell and Simons, 1990). The conditioned-whisking study reported that whiskers could move in opposite directions for durations ranging from 12 to 24 msec, most often when whiskers changed direction rapidly (Sachdev et al., 2002). Both studies reported that some whiskers could remain stationary, in continuous contact with an object, while other whiskers moved freely for several cycles (Carvell and Simons, 1990; Sachdev et al., 2002). In the present study, we found that the rostral and caudal whiskers could move in opposite directions for an entire whisk cycle (100 msec), even when only transient contact with an object occurred. The degree of independence of individual whisker movements in the freely behaving animal clearly warrants additional study.

Active modulation of whisker resonances

One of the most intriguing suggestions of our data is the possibility that the rat can actively modulate the resonant frequencies and damping. If the rat is able to actively change the boundary conditions at the base of the whisker, then the resonant frequencies and damping will change dramatically. In the awake animal, we observed shifts in the natural resonances over one or more cycles and also large variability in the time course of damping, dependent on the individual whisker and the phase of the whisking cycle. Both of these observations suggest that the rat may be actively changing biomechanical parameters that alter the resonances of whiskers. For example, the rat may be able to alter the resonances and time course of damping by changing muscle tension or blood flow to the follicle (Scott, 1955a,b).

Modulations of resonance are illustrated in trace 1 of Figure 8*C* and the lowest trace of *D*, which show that the frequencies can vary over the course of one or more cycles of resonance. In addition, the time course of damping appeared to depend not only on the individual whisker but also on the phase of the whisking cycle. For example, Figure 8, *A*, *B*, and *D*, shows that, if deflection past the bar occurs relatively early in the protraction cycle, at least one-half cycle of resonance will be present. In contrast, traces 1 and 2 of Figure 8*C* illustrate that, if the deflection occurs later in the protraction cycle, the rat can—but does not always—incorporate the resonance into the normal retraction phase of the whisking cycle. These results suggest that the rat may at times be able to actively suppress or enhance resonant frequencies by changing the time of retraction onset.

References

Ahissar E, Sosnik R, Haidarliu S (2000) Transformation from temporal to rate coding in a somatosensory thalamocortical pathway. Nature 406:302–306.

Berg RW, Kleinfeld D (2003) Rhythmic whisking by rat: retraction as well as protraction of the vibrissae is under active muscular control. J Neurophysiol 89:104–117.

Bermejo R, Vyas A, Zeigler HP (2002) Topography of whisking. I. Monitoring of whisking movements in two dimensions. Somatosens Mot Res 19:341–346.

Bonser RHC (2000) The Young's modulus of ostrich claw keratin. J Mater Sci Lett 19:1039–1040.

Bonser RHC, Purslow PP (1995) The Young's modulus of feather keratin. J Exp Biol 198:1029–1033.

Brecht M, Preilowski B, Merzenich MM (1997) Functional architecture of the mystacial vibrissae. Behav Brain Res 84:81–97.

Carvell GE, Simons DJ (1990) Biometric analyses of vibrissal tactile discrimination in the rat. J Neurosci 10:2638–2648.

Carvell GE, Simons DJ (1995) Task- and subject-related differences in sensorimotor behavior during active touch. Somatosens Mot Res 12:1–9.

Castro-Alamancos M (2002) Different temporal processing of sensory inputs in the rat thalamus during quiescent and information processing states in vivo. J Physiol (Lond) 539:567–578.

Conway HD, Becker ECH, Dubil JF (1964) Vibration frequencies of tapered bars and circular plates. J Appl Mech 31:329–331.

Georgian J (1965) Vibration frequencies of tapered bars and circular plates. J Appl Mech 32:234–235.

Gibson JM, Welker WI (1983a) Quantitative studies of stimulus coding in first-order vibrissa afferents of rats. 1. Receptive field properties and threshold distributions. Somatosens Res 1:51–67.

Gibson JM, Welker WI (1983b) Quantitative studies of stimulus coding in first-order vibrissa afferents of rats. 2. Adaptation and coding of stimulus parameters. Somatosens Res 1:95–117.

Gorman D (1975) Free vibration analysis of beams and shafts. New York: Wiley.

Gottschaldt K, Vahle-Hinz C (1981) Merkel cell receptors: structure and transducer function. Science 214:183–186.

Hartings JA, Simons DJ (1998) Thalamic relay of afferent responses to 1- to 12-Hz whisker stimulation in the rat. J Neurophysiol 80:1016–1019.

Hartmann MJ (2001) Active sensing capabilities of the rat whisker system. Auton Robots 11:249–254.

Hartmann MJ, Bower JM (1998) Oscillatory activity in the cerebellar hemispheres of unrestrained rats. J Neurophysiol 80:1598–1604.

Kleinfeld D, Sachdev R, Merchant L, Jarvis M, Ebner F (2002) Adaptive filtering of vibrissa input in motor cortex of rat. Neuron 34:1021–1034.

Morse PM (1936) Vibration and sound. New York: McGraw-Hill.

Neimark MA (2001) The mechanics of whisking: the first stage in the transduction of surface textures into neural signals. Undergraduate Senior thesis, Princeton University.

Neimark MA, Andermann ML, Hopfield JJ, Moore CI (2003) Vibrissa resonance as a transduction mechanism for tactile encoding. J Neurosci 23:6499–6509.

O'Connor S, Berg R, Kleinfeld D (2002) Coherent electrical activity between vibrissa sensory areas of cerebellum and neocortex is enhanced during free whisking. J Neurophysiol 87:2137–2148.

Sachdev RNS, Sato T, Ebner FF (2002) Divergent movement of adjacent whiskers. J Neurophysiol 87:1440–1448.

Scott M (1955a) Blood supply of mystacial vibrissae. Nature 175:395–396.

Scott M (1955b) Blood supply of mystacial vibrissae of the rat and cat. J Anat 89:556.

Shipley MT (1974) Response characteristics of single units in the rat's trigeminal nuclei to vibrissa displacements. J Neurophysiol 37:73–90.

Simons DJ (1978) Response properties of vibrissa units in rat S1 somatosensory neocortex. J Neurophysiol 41:798–820.

Simons DJ (1985) Temporal and spatial integration in rat S1 vibrissa cortex. J Neurophysiol 54:615–635.

Sosnik R, Haidarliu S, Ahissar E (2001) Temporal frequency of whisker movement. I. Representations in brain stem and thalamus. J Neurophysiol 86:339–353.

Tongue BH (2002) Principles of vibration. New York: Oxford UP.

Vincent SB (1913) The function of the vibrissae in the behaviour of the white rat. Behav Monogr 1:1–85.

Welker WI (1964) Analysis of sniffing of the albino rat. Behaviour 22:223–244.

Zucker E, Welker WI (1969) Coding of somatic sensory input by vibrissae neurons in the rat's trigeminal ganglion. Brain Res 12:138–156.

Estimation of Stress-Strength Ratio of Bone by Image-Based Finite-Element Analysis Considering Material Inhomogeneousness

Daisuke TAWARA[1], Jiro SAKAMOTO[1], and Juhachi ODA[1]

[1]Graduate School of Natural Science, Kanazawa University, Ishikawa, JAPAN
E-mail: daisuke_tawara@ybb.ne.jp Web: http://www.hm.t.kanazawa-u.ac.jp/bionic/

INTRODUCTION

Mechanical property of bone is inhomogeneous especially between cortical and cancellous bone. Range of mechanical property variation of a bone depends on individual, and it influences on the total stiffness and stress condition of the bone. Therefore, mechanical analysis considering inhomogeneous property is necessary for patients oriented evaluation of bone in clinic. While the finite element method is used, mechanical analysis considering the bone inhomogeneity is possible by giving a material property to an element one by one. Extreme fine meshing is required for precise analysis of bone with inhomogeneous property. Handling of material property data, element by element, is impracticable by general finite-element codes. In this study, we used "ADVENTURE system" which had developed as a large-scale finite element analysis system by Japan Society Promotion Science (JSPS). We improved it to be applicable to stress analysis of inhomogeneous bone problems. We applied it to proximal femur models and calculated their stress-strength ratio. Its distribution obtained by analysis considering bone inhomogeneity was compared to analysis assuming homogeneous bone. Then, efficiency of the system was discussed.

METHODS

We improved ADVENTURE system to be able to give a material property to an element one by one using element-property table based on CT image data. Because Young's modulus of each element is obtained from X-ray CT images, the system is applicable to stress analysis of inhomogeneous bone problems. Flow of calculating stress-strength ratio of bone using the system shows in figure 1. In this paper, stress-strength ratio is given by:

$$k = \frac{\sigma}{\sigma_r} \tag{1}$$

where k is stress-strength ratio, σ is major principal stress, and σ_r is yield stress. In equation (1), we assume yield stress is equal between tensile and compressive direction and σ_r is also given as:

$$\sigma_r = \begin{cases} 1.0\times10^{20} & (\rho \le 0.2) \\ 51.6\rho^2 & (0.2 < \rho) \end{cases} \tag{2}$$

provided by Carter (1997). ρ is local mass density of bone.

RESULTS AND DISCUSSION

Improved system was applied to estimation of stress-strength ratio of a femur. We prepared CAD model of 24-year-old male femur from based on CT images at 2mm intervals. Its boundary condition was assumed as standing still by one leg. We used 6 FE models: 2 types that were inhomogeneous type and homogeneous type, average mesh length were 10mm, 5mm, or 3mm respectively. CAD model with boundary condition and FE models meshed by tetrahedral elements are shown in figure 2, and number of nodes and elements are shown as table 1. Proportion of mass density of the femur model is shown in figure 3. In inhomogeneous models, Young's modulus E of each element was calculated due to mass density (E=2875ρ^3). On the other hand, in homogeneous models, constant Young's modulus were defined for cortical and cancellous region respectively as shown in figure 3. Stress-strength ratio contour are shown in figure 4. Principal stresses were overestimated in the homogeneous models, so stress-strength ratio overed 1.0 in wide area. On the contrary, level of stress-strength ratio was moderate in inhomogeneous models, and the location of high stress-strength ratio region was specified especially at the neck as FE mesh of the model was finer. Bone fracture of stumbling down in advanced age occurs at a neck region of femur continually. The improved system can solve the problem with very fine mesh considering bone inhomogeneity, so it is effective to evaluate the bone fracture analysis more precisely.

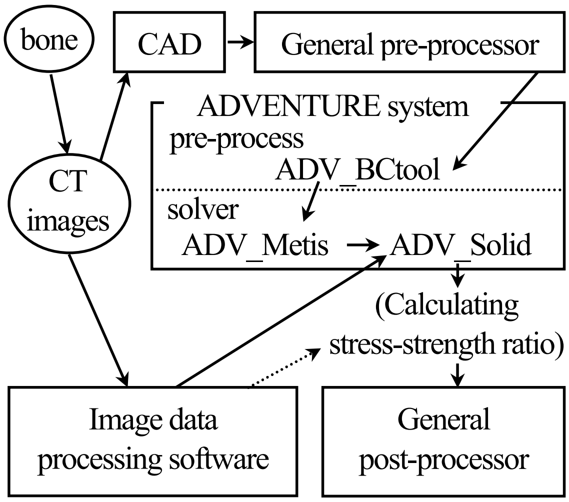

Figure 1: This figure illustrates the flow of calculating stress-strength ratio

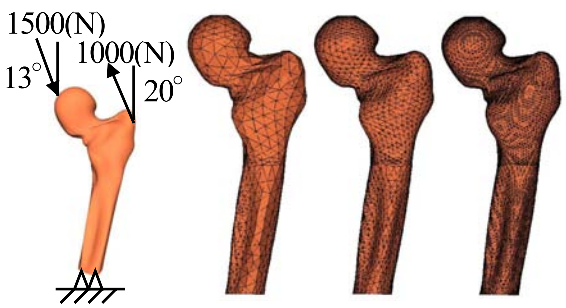

Figure 2: This figure illustrates femur CAD model with boundary condition and FE models meshed by tetrahedral elements (length are 10mm: left, 5mm: middle, and 3mm: right)

Table 1: Number of nodes and elements

Length	10mm	5mm	3mm
Nodes	1972	7636	26088
Elements	8856	36910	135537

SUMMARY

This paper proved that mechanical analysis considering bone inhomogeneity with fine FE mesh was necessary and the improved ADVENTURE system was efficient. The estimation of proximal femur also suggested availability of the system on a clinical analysis.

REFFERENCES

Dennis R.Carter, Wilson C.Hayes (1997). *The Compressive Behavior of Bone as a Two-Phase Porous Structure, Journal of bone and joint surgery*, **59A No.7**, 954-962

T.Nishii et al. (1996). *Analysis of mechanical property on an instability model of cementless femur stem –consideration of comparison for measurement of bone density*, Japanese Society for Clinical Biomechanics, **17**, 11-15

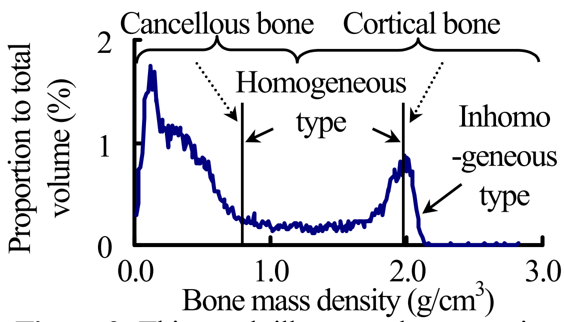

Figure 3: This graph illustrates the proportion of mass density of the femur model

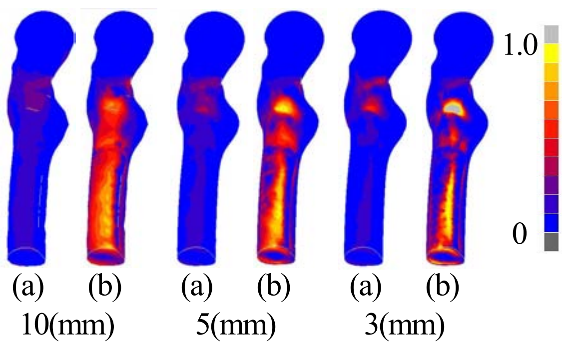

Figure 4: This figure illustrates stress-strength ratio contour of medial side (a: inhomogeneous type, b: homogeneous type)

NONLINEAR ANALYSIS OF POSTURAL CONTROL IN DIFFERENT POSITIONS

Georgios Korellis, Clinton J. Wutzke, Max J. Kurz, and Nicholas Stergiou

HPER Biomechanics Lab, University of Nebraska at Omaha, Omaha, NE, USA
Email: nstergiou@mail.unomaha.edu
Web: http://www.unocoe.unomaha.edu/hper/bio/home.htm

INTRODUCTION

Nonlinear measures have been used to quantify complex biological behaviors such as variability in heart rate (Buchman et al, 2001) and blood pressure control (Wagner et al, 1996). Recently, nonlinear analysis techniques have also been applied to the evaluation of postural control (Yamada, 1995; Harbourne & Stergiou, 2003). Nonlinear analysis has the advantage of examining the entire time series of the center of pressure in a continuous fashion. This is not possible using the traditional averaging methods (i.e., length of path), which are limited in their ability to detect true differences in postural sway (Palmieri et al., 2002). In addition, limited research has been conducted to evaluate the effect of different positions on postural sway (Shumway-Cook & Woollacott, 2001). Therefore, in the present study we utilized nonlinear analysis to examine the effect of position on the fluctuations present during postural sway. Specifically, we hypothesized that different positions such as sitting on the ground, and sitting on a stool, will produce different fluctuations in postural sway.

METHODS

Five subjects performed three trials with their eyes open in three different positions. In the first position, the subjects had to stand on a Kistler force platform quietly facing forward. In the second position, the subjects had to sit directly on the force platform with their legs folded in front of them in a yoga-like position and with their hands placed comfortably in their laps. In the third position, the subjects had to sit on a stool with their feet not supported by the ground or the stool. The stool was placed in the middle of the force platform. The coordinates of the center of pressure (COP) were collected (10 Hz) for a duration of five minutes for each trial. The time series from the unfiltered COP coordinates were analyzed using the Chaos Data Analyzer Professional software (Sprott & Rowlands, 1995). The Lyapunov Exponent (LyE) and the Hurst Exponent (HE) were calculated for each trial-condition. Before calculating the HE, all data were first integrated. A dynamical system is a system that continuously changes over time such as the swaying body during posture. HE is a measure of persistence, in other words, for how long a given fluctuation in a time series will be replicated in the future values of the series. To correctly calculate LyE, it is necessary to first reconstruct the state space by estimating the embedding dimensions (ED) and the time lag (TL). The ED is a measure of the number of dimensions needed to unfold a given attractor, while the TL determines how many of the data points will be used in the analysis. These two parameters were calculated with the tools for dynamics software. Mean group values for each nonlinear tool were analyzed using a repeated measures ANOVA ($p<0.05$) with a Tukey test as post-hoc.

RESULTS AND DISCUSSION

The group analysis indicated significant differences between the mean group values for the TL for both the anterior-posterior (AP) and medial-lateral (ML) COP time series. The post-hoc analysis for the TL for the AP direction revealed statistical differences between standing and both sitting conditions. The post hoc analysis for ML data series showed that significant differences existed only between the standing and the stool conditions. These results indicated that when sitting posture is evaluated it is necessary to examine the data in a more compound fashion. No other significant differences were found. However, it is interesting to notice that the LyE for the AP direction decreased from standing to sitting indicating more stability in the later position. We plan to increase the number of subjects of this pilot work and that may eventually achieve significance for the LyE values. In addition, all LyE values were found to be positive, suggesting the existence of chaotic dynamics within the data. This result is enhanced by the fact that the values for the HE revealed a black noise (0.9) supporting the existence of a deterministic nature within the data. Lastly, the number of ED was found to be approximately five in all time series which is in agreement with Harbourne & Stergiou (2003).

SUMMARY

Variability in postural sway at different positions found to be deterministic. In this pilot work we also found that position does not affect the nature of the fluctuations. However, the HE values observed, suggested that a given fluctuation in the postural sway time series will affect future values of the series. The larger the HE is, the longer the persistence (memory).

REFERENCES

Abarbanel, H.D.I. (1996). *Analysis of Observed Chaotic Data*, Springer-Verlag.
Buchman, T.G., Cobb, J.P., Lapedes, A.S., Kepler, T.B. (2001). Shock, 16, 248-251.
Palmieri, M.R., Ingersoll, D.C., Stone, B.M., Krause, A.B. (2002). *J. Sport Reh.,* **11,** 51-66
Harbourne, R.T., Stergiou, N. (2003). *Developmental Psychology*, **26**, 51-64.
Shumway-Cook, A., Woollacott, H.M. (2001). *Control theory and practical applications*. Lippincot Williams & Wilkins.

Sprott, J., Rowlands, G. (1995). *Chaos Data Analyzer*. American Institute of Physics.
Wagner, C.D. et al., (1996). *Cardiovascular Res.*, **31**, 380-387.
Yamada, N. (1995). Human Mov. Sc., **14**, 711-726.

Table 1: Group means of the nonlinear tools used. Significance is indicated in bold.

COPy (AP)	Stand	Sit	Stool
Time Lag	**3.720 ±1.200**	**2.064± 0.493**	**1.332 ± 0.470**
Embedding Dimensions	5.000 ± 0.212	5.196 ± 0.445	5.198 ± 0.295
Lyapunov Exponent	0.302 ± 0.030	0.257 ± 0.058	0.247 ± 0.027
Hurst Exponent	0.944 ± 0.037	0.986 ± 0.022	0.976 ± 0.027
COPx (ML)	Stand	Sit	Stool
Time Lag	**3.820 ± 1.031**	**3.390 ± 0.598**	**2.000 ± 0.000**
Embedded Dimension	5.360 ± 0.260	5.132 ± 0.180	5.132 ± 0.295
Lyapunov Exponent	0.221± 0.027	0.221± 0.023	0.220 ± 0.030
Hurst Exponent	0.987 ± 0.012	0.997 ± 0.002	0.975 ± 0.018

NONLINEAR ANALYSIS OF POSTURAL CONTROL IN HEALTHY ADULTS STANDING WITH EYES OPEN AND EYES CLOSED

Melissa M. Scott-Pandorf, Clinton J. Wutzke, Georgios Korellis, Max J. Kurz, and Nicholas Stergiou
HPER Biomechanics Laboratory, University of Nebraska at Omaha, Omaha, Nebraska, USA
Email: mmscott@mail.unomaha.edu
Web: http://www.unocoe.unomaha.edu/hper/bio/home.htm

INTRODUCTION

Therapy programs to improve standing postural control have been developed using the Center of Pressure (COP) obtained from a force platform. The basis for such programs is that the COP at the base of support in standing is a reflection of the organization of posture (Massion, 1992). Thus, COP has been utilized in various studies of postural control. Specifically, the sensory effect of vision on postural control has been examined. It has been found that lack of vision increases postural sway in the elderly (Patla *et al*., 1990; Wolfson, 1992; Shultz *et al*., 1993). However, the use of traditional linear averaging techniques to evaluate COP has been questioned (Palmieri, 2002). Thus, other researchers (Yamada, 1995; Harbourne & Stergiou, 2003) have used nonlinear dynamics to examine postural control. Analysis of postural stability using nonlinear dynamics has the potential to provide new insights in the ways that the nervous system controls the complexities of a dynamical system such as the swaying body during posture. Thus, the structure of the time series of the COP can provide information regarding the behavior of the moving body over time. The purpose of this study is to use nonlinear dynamics tools to investigate standing posture of healthy adults with eyes open and eyes closed.

METHODS

Five healthy adults (3 females, 2 males) between the ages of 19 and 35 performed three trials with their eyes open and eyes closed while standing on a force platform. Each subject was asked to stand quietly with arms resting comfortably at the sides, facing forward. Tape was placed at the edges of the subject's feet, ensuring that the participant will be in the same position for all standing trials. The anterior-posterior (AP) and medial-lateral (ML) displacement of the center of pressure (COP) were collected (10 Hz) for a duration of five minutes for each trial. The time series from the unfiltered COP coordinates were analyzed using the Chaos Data Analyzer Professional Software (Sprott & Rowlands, 1995), where we calculated Lyapunov Exponent (LyE) and the Hurst Exponent (HE) for each trial-condition. Before calculating the HE, all data were integrated. HE is a measure of persistence. In other words, for how long a given fluctuation in a time series will be replicated in the future values of the series. To correctly calculate LyE, it is necessary to first reconstruct the state space by estimating the embedding dimensions (ED) and the time lag (TL). The ED is a measure of the number of dimensions needed to unfold a given attractor, while the TL determines how many of the data points will be used in the analysis. These two parameters were calculated with the Tools for Dynamics Software (Abarbanel, 1996). Mean group values were analyzed using paired t-tests ($p<0.05$).

RESULTS

Our statistical analysis showed no significant differences. This is likely due to lack of statistical power as this investigation is pilot work and only five subjects were included. We plan to increase the number of our subjects and that may eventually achieve significance for several of the parameters examined (i.e. LyE for AP direction). However, there was no real separation in values for the LyE for ML so even with increased statistical power it is unlikely that significance would be achieved. All LyE values were found to be positive, suggesting the existence of chaotic dynamics within our data. This result is enhanced by the fact that the values for the HE revealed a black noise (0.9) supporting the existence of deterministic nature within the data. The number of ED was found to be approximately five in all time series which is in agreement with Harbourne & Stergiou (2003). Lastly, by inspection of the results (Table 1) it is interesting to note that the ML time series produced higher values for ED, TL, and HE for both conditions.

SUMMARY

Fluctuations in postural sway with and without vision were found to have a deterministic origin. In this pilot work it is found that lack of vision does not affect the nature of the COP fluctuations. This observation concurs with the rest of the literature that just removal of visual input does not elicit significant differences in healthy young adults during standing.

REFERENCES

Abarbanel, H.D.I. (1996). *Analysis of Observed Chaotic Data*, Springer-Verlag.
Harbourne, R.T., Stergiou, N. (2003). *Developmental Psychology*, **26**, 51-64.
Palmieri, M.R., Ingersoll, D.C., Stone, B.M., Krause, A.B. (2002). *J. Sport Reh.,* **11,** 51-66
Patla, A.E., Winter, D.A., Frank, J.S., et al. (1990). *Proceedings of APTA Forum*, 43-55.
Schultz, A., Alexander, N.B., Gu, J.J., Boismier, T. (1993). *Ann Otol Rhinol Laryngol*, **102**, 508-517.
Massion, J. (1992). *Progress in Neurobiology*, **38**, 35-56.
Sprott, J., Rowlands, G. (1995). *Chaos Data Analyzer*. American Institute of Physics.
Wolfson, L. et al. (1992). *Neurology*, **42**, 2069-2075.
Yamada, N. (1995). Human Mov. Sc., **14**, 711-726.

Table 1. Anterior-Posterior (AP) and Medial-Lateral (ML) COP group means and standard deviations for TL, ED, LyE, and HE.

	Variable	TL	ED	LyE	HE
AP	**Vision**	3.72±1.20	4.94±0.21	0.302±0.04	0.944±0.04
	Non-Vision	3.52±1.36	5.06±0.13	0.287±0.09	0.913±0.08
ML	**Vision**	3.82±1.03	5.36±0.26	0.221±0.02	0.987±0.01
	Non-Vision	5.54±1.13	5.34±0.31	0.220±0.03	0.989±0.01

AN INVESTIGATION OF THE DETERMINISTIC ORIGIN OF POSTURAL CONTROL DATA

Clinton J. Wutzke, Georgios Korellis, Max J. Kurz, and Nick Stergiou

HPER Biomechanics Lab, University of Nebraska at Omaha, Omaha, NE, USA
Email: nstergiou@mail.unomaha.edu
Web: www.unocoe.unomaha.edu/hper/bio/home.htm

INTRODUCTION

The center of pressure (COP) at the base of support is a reflection of the organization of posture (Massion, 1992). Although postural sway has been utilized to identify physiological and neurological pathologies, discrepancies exist regarding the nature of these fluctuations present in postural sway. Collins and DeLuca (1994) have suggested that postural sway is just random noise. This contradicts with other studies that have suggested that the nature of these fluctuations is actually deterministic (Yamada, 1995; Boker *et al., 1998*); Harbourne & Stergiou, 2003). In the present study we explored this contradiction. We examined postural data using a surrogation method (Theiler *et al., 1992*). To increase the generalizability of our results, we examined postural data collected from three different positions each with eyes open and eyes closed.

METHODS

Four healthy young adults (mean age = 25.5 yrs), free from any neurological disorders performed trials for three positions: 1) a standing position where subjects stood quietly with their arms at their sides and their feet placed at approximately shoulder length apart. 2) A sitting position where the subjects sat directly on the force platform (Kistler, dimensions 40 cm X 60 cm) in a yoga-like position with their hands comfortably resting on their lap. 3) A sitting position where the subjects sat on a stool (base 32x34 cm, height 75 cm) with their hands at their sides. The stool was placed in the geometrical center of the force platform. All subjects performed three trials per condition with their eyes open and closed. The duration of each trial was five minutes and our sampling frequency was set at 10 Hz. The time series from the COP coordinates (anterior/posterior (AP) and medial/lateral (ML)) were exported and analyzed via the surrogation method. This technique compares the original data and a random equivalent data set that has a similar structure to the original data set in question. Surrogation practically removes the deterministic structure from the original time series, generating essentially a time series of random data that has the same mean, variance, and power spectra as the original time series. This is accomplished via a phase randomization technique developed by Theiler *et al*. (1992) and implemented in the Chaos Data Analyzer software (Sprott & Rowlands, 1995). The same software was used to calculate Lyapunov exponents (LyE) from both the original and their surrogate counterparts. The LyE estimates the average logarithmic divergence from the time series trajectories in state space (Stergiou *et al; 2004*). The LyE from the original and the surrogated counterparts were compared for all trials and for each conditions using Student T-tests ($p<0.01$).

RESULTS AND DISCUSSION

Surrogated LyE values were larger than the LyE values of the original data sets in all positions with both eyes open and eyes closed (Table 1). All three positions with eyes closed were found to exhibit significant differences in both the AP and ML time series. Sitting on a stool with eyes open was also significantly different for both coordinates. For standing and sitting with eyes open, we obtained significance only for the ML time series. Although, the AP time series for sitting and standing with eyes open did not demonstrate significant differences, this may be due to the small number of data sets (i.e. four subjects and three trials per condition). This is based on the fact that in these conditions surrogated LyE values were still larger than the original data. This suggests that with a greater number of data sets significant differences may arise. Overall, our results clearly indicated that the fluctuations in postural sway are not random noise but they are deterministic in nature. This was demonstrated for three different positions with both eyes closed and eyes open.
Our results contradict Collins & DeLuca (1994). Differences may be related to the sampling frequency used to analyze postural sway. Collins and DeLuca used a much higher sampling frequency (100 Hz) which may have introduced measurement error and it is not justified based on our power spectrum analysis.

SUMMARY

Postural sway data was collected for three positions with eyes open and eyes closed and was analyzed using a surrogation method to determine if the fluctuations present in these data have deterministic origin. Results demonstrate large differences between surrogated and original data sets. This demonstrated that fluctuations in postural sway are deterministic in nature and not random noise. Past notions that posture is random noise may be related to measurement error.

REFERENCES

Boker, S. M. et al, (1998). Nonlinear analysis of perceptual-motor coupling in the development of postural control In: *Nonlinear Analysis of Physiological data*, Springer-Verlag.
Collins, J. J. & DeLuca, C. J., (1994). *Physical Review Letters,* **73**(5), 764-767.
Harbourne R. T., Stergiou, N. (2003). Nonlinear analysis of the development of sitting postural control, *Develop. Psych.,* **26**, 51-64.
Massion, J. (1992). *Progress in Neurobiology,* **38**, 35-36.
Sprott, J., Rowlands, G. (1995). *Chaos Data Analyzer*. American Institute of Physics.
Stergiou, N. et al (2004). Nonlinear Tools in Human Movement In: *Innovative Analysis for Human Movement*, Human Kinetics.
Theiler, J. et al. (1992). *Phys. D*, **58**, 77-94.

Table 1: LyE group mean values for all positions with eyes open (EO) and closed (EC). S = surrogated data. * = significant differences between LyE and S-LyE, $p<0.01$

	Stand EO	Sit EO	Stool EO	Stand EC	Sit EC	Stool EC
Anterior/Posterior						
LyE	0.3014	0.2483	0.2409*	0.2875*	0.2300*	0.2608*
S-LyE	0.3504	0.3082	0.3053*	0.3095*	0.3038*	0.3393*
Medial/Lateral						
LyE	0.2156*	0.2144*	0.2204*	0.2067*	0.2078*	0.2421*
S-LyE	0.3921*	0.3428*	0.3584*	0.3980*	0.3210*	0.3573*

THE ASSESSMENT OF THE VALIDITY OF A FOOTSWITCH SYSTEM USED FOR IDENTIFYING TEMPORAL VARIABLES IN CONTINUOUS WALKING

Kenji Narazaki[1], Bungo Hirata[2] and Nick Stergiou[1]

[1]HPER Biomechanics Lab, University of Nebraska at Omaha, Omaha, NE, USA
[2]College of Engineering and Technology, University of Nebraska at Lincoln, Lincoln, NE, USA
Email: knarazaki@mail.unomaha.edu
Web: http://www.unocoe.unomaha.edu/hper/bio/home.htm

INTRODUCTION

In recent years, biomechanists have focused on the stride-to-stride variability during continuous walking. Kinetic and kinematic variables are used to explore this variability and to quantify pathological disabilities with objective signatures (Stergiou et al., 2004; Dingwell et al., 2000). In such studies, accurate measurement of temporal variables is considered essential to conduct sound analyses. A footswitch system is one of the solutions used to identify with precision the timings of the start and the end of the foot contact during continuous walking (Hausdorff et al., 1995). Previous published footswitch systems are difficult to be replicated and their methodology is usually unclear. We have developed such a system and accompanying algorithm that is designed to be easily replicated by other researchers. The purpose of this study is to assess the validity of our footswitch system and the accompanying algorithm on estimating temporal variables during continuous walking.

METHODS

Our footswitch system roughly consists of: 1) two force sensing resistors (Tekscan, Inc.) that are placed on a subject-specific cut polyurethane insole at the anterior and posterior surface of the right foot, 2) an electric circuit box that is placed inside a pouch attaching to the subject's waist, and 3) shielded copper cables and connectors which join the sensors, the circuit and a data collection computer. The footswitch system is designed to output analog signals from each resistor ranged from 0 V (with no loading) to 3.2 V (with high loading). Three healthy subjects were asked to walk over□ground for ten times each at their perceived slow, normal and fast speed wearing the footswitch system and their own jogging shoes. In each trial, they were requested to step naturally on a Kistler force platform with their right foot. Data were collected simultaneously from both the footswitch and the force platform at 500 Hz using the data collection computer. The vertical ground reaction force was calculated from the force platform data and the heel-strike (HS) and the toe-off (TO) timings along with the stance phase duration (STA) were identified using a 10 N criterion/threshold (Hreljac et al., 2000). From the footswitch data, HS, TO and STA were also identified with a 2.5 V threshold (fHS, fTO and fSTA) and intervals between HS and fHS and between TO and fTO were calculated (IHS and ITO). Next, the data sets from all the trials of one arbitrarily selected subject were used to develop simple linear regression equations (i.e., intercept and slope) to estimate STA, IHS, and ITO, from fSTA. These equations were applied to all the data sets from the other two subjects to predict STA, IHS and ITO. Finally, the relationships between the actual and the predicted data were evaluated statistically using Pearson correlations for STA, IHS and ITO. The timing errors between the actual and the predicted data were also evaluated with descriptive statistics.

RESULTS AND DISCUSSION

The STA values obtained for all 90 trials were well distributed (640±71 ms, ranged from 504 to 788 ms). This allows us to conduct a regression analysis. The simple linear regression equations developed with the data sets from one selected subject were as follows:

$STA_{estimate} = 0.038 + 1.074*fSTA$
$IHS_{estimate} = –0.015 – 0.026*fSTA$
$ITO_{estimate} = 0.023 + 0.048*fSTA$

The results of the correlation analysis revealed that there was a significant strong correlation between actual and predicted STA ($r = 0.993$, $p<0.05$). It is assumed that fSTA and thus, $STA_{estimate}$ share sufficient variance with STA (98.6%). In fact, STA correlations for the other two combinations (i.e., using two other regression equations from the trials of the other two subjects) were also very high (0.995 and 0.988). Significant correlations were also found between the actual and the predicted IHS

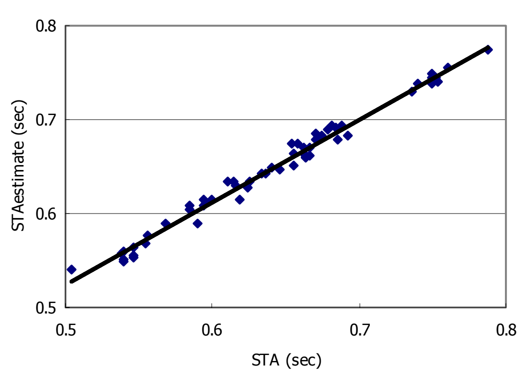

Figure 1. The relationship between STA and $STA_{estimate}$ for 60 trials and the line of best fit ($STA_{estimate} = 0.0882 + 0.8738*STA$)

and ITO ($r = 0.698$ and $r = 0.572$, respectively, $p<0.05$). However, these values are not as high as for STA and thus the validity of the estimation of these temporal variables may not be sufficient. It is possible that other factors, such as small differences in sensor placements between subjects, may influence these values. We may be able to obtain better results by manipulating such factors. Regarding the timing errors, although the ranges were relatively small, their distributions seem to be somewhat shifted to the right (ΔSTA = 7±11 ms, –13 to 37 ms, ΔHS = 9±10 ms, –9 to 30 ms and ΔTO = 16±6 ms, 1 to 40 ms). It is possible that the small sample size utilized in the present pilot work is a contributing factor for these shifts. A larger sample size may allow more accurate estimations.

SUMMARY

The footswitch system and accompanying algorithm that we have developed can be much easier replicated than other existing in the literature. They can also estimate the stance period as accurately as the force platform. We have also found that our algorithm is not hardware specific and can be used with any type of curve configurations derived from different systems.

REFERENCES

Dingwell, J.B., Cusumano, J.P. (2000). *Chaos*, **10**, 848-863.
Hausdorff, J.M. et al. (1995). *J Biomech*, **28**, 347-51.
Hreljac, A., Marshall, R.N. (2000). *J Biomech*, **33**, 783-6.
Stergiou, N. et al. (2004). Nonlinear Tools in Human Movement, *Innovative Analyses of Human Movement*, Human Kinetics, Champaign, IL.

AGING, REGULARITY AND VARIABILITY IN MAXIMUM ISOMETRIC MOMENTS

John H. Challis

Biomechanics Laboratory, Department of Kinesiology, The Pennsylvania State University, University Park, PA 16802, USA
E-mail: jhc10@psu.edu

INTRODUCTION

In old age there are various changes in the properties of human muscle, for example muscle cross-sectional area is reduced (e.g., Kent-Braun & Ng, 1999), and fiber type distribution changes (e.g., Lexell, 1995). These changes have implications for the ways in which movements are executed. There is also evidence that in older age there is a reduction in the number of motor units comprising a muscle (e.g., Sica et al., 1976).

Given a reduced number of motor units to coordinate it may be that in the development of maximum isometric force there is reduced variability, or increased regularity, in the force profile for older subjects compared with the young. This study examined the variability and regularity of maximum isometric moment production of the plantar flexors in the young and elderly.

METHOD

Two groups of subjects, one young and the other elderly, gave informed consent to participate in this study. Subject details and group sample sizes are presented in table 1.

Table 1: The means (standard deviations) of the subject characteristics for the three groups.

Group (n)	**Age (years)**	**Mass (kg)**	**Height (cm)**
I (10)	23.8 (2.8)	82.1 (11.5)	178 (5)
II (12)	73.7 (3.2)	76.2 (10.8)	172 (5)

After appropriate warm-up the subjects performed three maximum isometric plantar flexions using a Biodex dynamometer. Subjects were tested with an ankle angle of 90 degrees, and a knee angle of 180 degrees (fully extended). The dynamometer position was manipulated so the axis of rotation of the ankle joint was aligned with the axis of rotation of the dynamometer. For each trial data collection lasted 10 seconds, with two minutes rest between trials.

For each subject the trial producing the maximum moment under each condition was selected for additional analysis. From these trials only the plateau regions of the curves were analyzed.

The time-moment curves were assessed using the approximate entropy (***ApEn***) algorithm described by Pincus (1991). ***ApEn*** is a measure of the regularity of a data set. It takes sequences of $\boldsymbol{m}$ data points and determines the logarithmic likelihood that this sequence is similar to other sequences of data points. If the data set is regular then ***ApEn*** has a small value; conversely ***ApEn*** increases in value with increasing irregularity of the data set. A parameter $\boldsymbol{r}$ is used to determine the closeness of data sequences, which effectively filters out sequences which are not close. For the comparisons made in this study $\boldsymbol{m}$ was set to 2, and $\boldsymbol{r}$ was set at the measurement precision of the Biodex dynamometer.

Comparisons were made of the peak

moment, signal coefficient of variation (Coef. Var.), and ***ApEn*** for the two subject groups using analysis of variance. Bartlett's test was used to confirm homogeneity of variance before all analyses. A 0.05 significance level was used.

RESULTS

The young subjects produced a statistically greater peak moment than the elderly subjects (table 2). This pattern persisted when these data were normalized with respect to subject mass. The coefficient of variation was not statistically different between the two subject groups indicating similar variability. In contrast there was a statistically significant difference between the two groups in ***ApEn***, that is the older group demonstrated greater regularity.

ApEn does not distinguish between signal components due to the subject (deterministic), and that due to random noise in the measurement process. Therefore a surrogate data test was used, which confirmed that the results were reflecting the properties of subject signal not measurement system noise (Theiler et al., 1992).

DISCUSSION

As would be expected with increasing age the subjects demonstrated reduced plantar flexion strength, such decrements have previously been reported in the literature (e.g. Overend et al., 1992). Variability in the time-moment curves was the same for the two groups, but there was a difference in signal regularity. Surrogate analysis confirmed this result was due to signal properties not measurement noise.

With increasing age many physiological processes have been described as having reduced complexity (Lipsitz, 2002). While ***ApEn*** tests for regularity not complexity, the two are related (Gell-Mann, 1995); these results lend support to the hypothesis of reduced complexity with aging. The increased regularity in older age can be explained by the anticipated reduction in the number of motor units comprising the muscles used to produce the maximum moments. This reduction in the number of motor units means fewer units need to be coordinated to produce the moments.

Table 2: The means (standard deviations) of the analysis of the plateau of the time-moment curves.

Group	Peak Moment (N.m)	Coef. Var. (%)	***ApEn***
I	111.5 (33.5)	5.7 (1.4)	0.253 (0.075)
II	78.1 (29.6)	5.8 (1.4)	0.352 (0.072)

REFERENCES

Gell-Mann, M. (1995) *Complexity*, **1**, 16-19.

Lipsitz, L. A. (2002). *J Gerontol*, **57**, B115-125.

Kent-Braun, J.A., & Ng, A.V. (1999) *J Appl Physiol*, **87**, 22-29.

Lexell, J. (1995) *J Gerontol*, 50, 11-16.

Overend, T.J., et al. (1992). *J Gerontol*, *47*(6), M204-210.

Pincus, S.M. (1991). *Proc Natl Acad Sci.*, **88,** 2297-2301.

Sica, R.E, Sanz, O.P., & Colombi, A. (1976) *Medicina*, **36,** 443-446.

Theiler, J., et al. (1992). *Physica D*, **58**, 77-94.

EFFECT OF DYNAMIC ANKLE JOINT STIFFNESS ON JOINT MECHANICS DURING GAIT

Prism S. Schneider[1], James M. Wakeling[2] and Ronald F. Zernicke[1]
[1] Human Performance Laboratory, University of Calgary, Calgary, Canada
[2] Department of Basic Veterinary Sciences, Royal Veterinary College, London, United Kingdom
E-mail: prism@kin.ucalgary.ca Web: www.kin.uclagary.ca

INTRODUCTION

Ankle-foot orthotics (AFO) are externally applied orthopaedic devices that provide support for foot-drop or ankle instability associated with neuromuscular disorders. Currently, AFOs are either articulated (moveable) or rigid (ankle locked at a specific ankle joint angle).

Dynamic joint stiffness (JS) is calculated as the slope of the joint angle vs. moment plot and is an important constraint on the motor control system as it affects the generation of voluntary movements and the displacement resulting from an external perturbation (Hunter & Kearney, 1982). Understanding JS is essential to design of orthoses and the quantitative evaluation of neuromuscular diseases (Davis & DeLuca, 1995). In the past, ankle JS was varied by external stimuli and applied external moments (Gottlieb & Agarwal, 1978), but JS has not been examined experimentally or dynamically with the use of AFOs in human static or dynamic balance. The effects of dynamic AFO stiffness on ankle and knee joint kinematics and kinetics, muscular co-contraction, and the changes in mechanical JS were the focus of this study.

METHODS

Bilateral AFOs were instrumented with hydraulic disc brakes to allow for adjustable AFO stiffness, which permitted varied external resistance of ankle motion, graded from fixed to freely moving. The study design was prospective, randomized, and comprised six adult normal males.

3D kinematics were acquired using bilateral lower-extremity reflective marker placement (3/segment) and an 8-camera, high-speed motion analysis system (Motion Analysis Corp, Santa Rosa, CA; EVA© software). Force plate (Kistler, 9286; 2400 Hz), electromyographic (Biovision, Germany; 2400 Hz), and video (240 Hz) data were collected during 3 successful walking trials per subject for 3 AFO stiffness conditions: shod with rigid AFOs (Rigid), shod with articulated AFOs (Art), and shod with intermediate AFO stiffness (Inter).

3D knee and ankle joint kinematics and kinetics (Kintrak© software, Motion Analysis Corp, Santa Rosa, CA) were calculated. Knee joint moments were calculated at 3 time points to measure the difference in peak knee flexor and extensor moments throughout the stance phase. Dynamic ankle and knee JS were calculated for the heel rocker (0-10% gait cycle), ankle rocker (10-30% gait cycle) and forefoot rocker (30-55% gait cycle). Multivariate analysis of variance with a *post-hoc* test ($\alpha = 0.05$) revealed significant differences.

RESULTS AND DISCUSSION

During gait, the mean maximal ankle plantarflexion angle decreased at toe-off (TO) from Art to Inter and from Inter to Rigid AFO conditions. The decrease was statistically significant between the Art and Rigid conditions for 4 of 6 subjects. There was also a decrease in the maximal plantarflexion ankle angle between the Art and Rigid conditions following heel-strike (HS) in 5 of 6 subjects, with a significant difference observed in 2 subjects. Maximal knee flexion angle decreased between the Art and Rigid AFO conditions at TO for all 6 subjects, with a statistically significant difference for 2 subjects.

Negligible change occurred across all AFO conditions in the peak ankle plantarflexor joint moment for 5 subjects, while a significant increase occurred in 1 subject. Peak knee extensor moment during 10-30% stance phase increased in the Rigid condition compared to the Art condition for 4 of 6 subjects, with a significant difference observed in 3 subjects. That increased knee extensor moment was supported by increased quadriceps activity. Maximal knee flexor moment during 60-80% stance phase also increased in 4 subjects between the Rigid and Art condition, with significant differences occurring for 3, while the remaining 2 subjects showed negligible change. That change was supported by gastrocnemius recruitment and decreased quadriceps activity. Peak knee extensor moment for 80-100% stance decreased in the Rigid condition compared to the Art condition for 5 subjects.

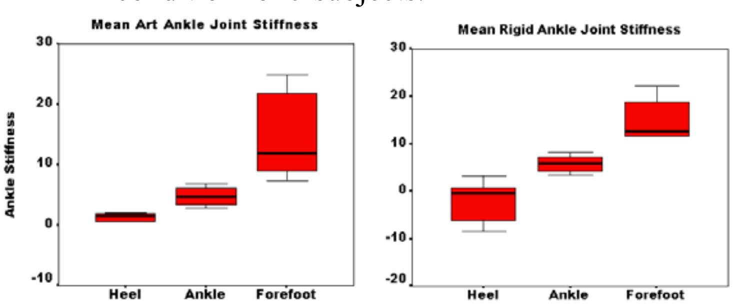

Figure 1: Mean (±sd) ankle JS for each rocker for Art (left) and Rigid (right) AFOs.

Ankle JS (Fig. 1) significantly increased from the heel to ankle rocker and from the ankle to forefoot rocker in the Art condition. In the Rigid condition, ankle JS increased from heel to ankle rocker and from ankle to forefoot rocker, with a significant increase between the heel and forefoot rockers.

Knee JS (Fig. 2) increased during the ankle rocker phase when compared to the other rockers for all AFO conditions, however that difference was only statistically significant in the Inter AFO condition. As AFO stiffness increased, mean knee JS increased for 5 of 6 subjects.

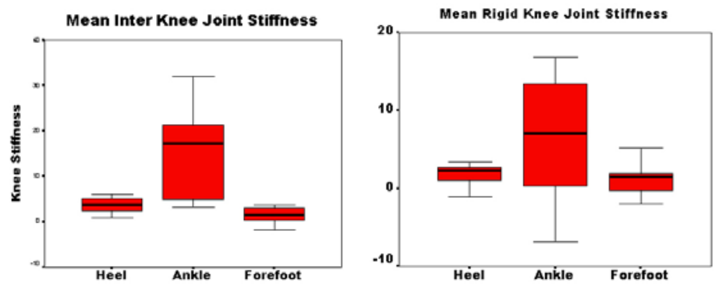

Figure 2: Mean (±sd) right knee JS for each rocker for Inter (left) and Rigid (right) AFOs.

SUMMARY

Results from this study provide data to help in our understanding of how AFO prescription may affect joint mechanics. Ankle JS increased during the forefoot rocker while knee JS increased during the ankle rocker, indicating a shift in the joint responsible for dynamic stability. Ankle plantarflexion angle and knee extensor moment decreased as the stiffness of the AFO was increased, which may indicate the need for greater joint stability and quadriceps recruitment for propulsion with rigid AFOs. As the AFO stiffness increased, knee JS also increased, indicating an increased demand on the knee joint for dynamic stability in the Rigid condition.

REFERENCES

Hunter, I. & Kearney, R. (1982). *J Biomech,* **15**, 747-52.

Davis, R. & DeLuca, P. (1995). *Gait & Posture,* **3**, 79-80.

Gottlieb, G. & Agarwal, G. (1978). *J Biomech,* **11**, 177-81.

ACKNOWLEDGEMENTS

NSERC, AHFMR, Wood Professorship in Joint Injury Research, Colman Prosthetics and Orthotics, Patrick Irwin

DEVELOPMENT OF LIGHT-WEIGHT POWERED WHEELCHAIR IN SNOWFALL CONDITIONS

Eiichi Uchiyama[1], Shigeo Nishimura[2], Kazutoshi Yokogushi[1], Hiroshi Narita[1], Gen Murakami[1], Ken-ichi Yamakoshi[3]

[1]Biomechanics Laboratory, Dept. of Anatomy, Sapporo Medical Univ., Sapporo, Japan,
[2]Hokkaido Rehab. Consult. Center [3]Faculty of Eng, Kanazawa Univ.
E-mail: uchiyama@sapmed.ac.jp

INTRODUCTION

Various types of motorized wheelchair have been commercially available, however, we cannot find any good qualified light-weight powered wheelchairs for snowfall conditions. From 1994 to 1996, we developed 6-wheel motorized wheelchair best for snowfall conditions [1,2,3]. This prototype had good driving performance and cleared a 100 [mm] step without difficulty, however, this wheelchair was very heavy (88kg) as it was used lead batteries. It is not easy for transportation by automobiles. The purpose of this study was to design a light-weight motorized wheelchair (6W-NProto) having good driving performances in uneven terrain.

CONCEPT OF WHEELCHAIR DESIGN

First, to get the light-weight wheelchair, instead of conventional lead batteries but nickel-hydrogen batteries were applied. Second, to get the good traction in snowfall conditions, 6-wheel mechanism was applied. This structure could possible to concentrate of weight to the main center wheels. Third, to get the high power, which is definitely required for snowfall conditions, part-time 4-wheel drive mechanism was applied. Rear wheels are powered only when running in the snowed road or clearing the step.

SPECIFICATIONS OF 6W-NProto:

Weight of wheelchair is 48.5 [kg]. Size of wheelchair in length, width, height is 970,610

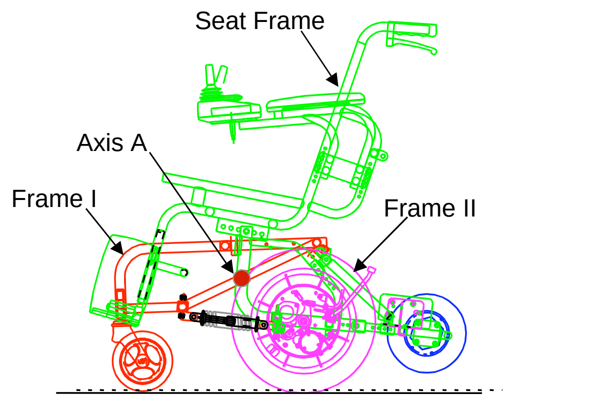

Fig. 1 A drawing of 6W-NProto: Caster wheels attached to the front frame I, center main- and rear sub-powered wheels are attached to the main frame II, seat frame is attached to the frame II by link. Frame I and II are linked by axis A

940[mm], respectively (Fig. 1). Driving mechanism is front caster wheels, center build-in main motors (90W x 2), rear build-in sub motors (70W x 2). Total power is 320[W]. Size of tires in front, center, rear wheels are 150, 350, 200 [mm] in diameter, respectively. Design of frame applied flexible link mechanism, i.e., frame I and II bend following the terrain and wheelbase is changed. For example, if front casters touch a step, distance between casters and center main wheels becomes shorter, seat frame shifts to posterior and gravity center shifts to backward, front casters lift up, rear wheels touch to the ground, sub motors start up, and the wheelchair clears the step (Fig. 2).

COMPARED TEST WITH YAMAHA JW3™

JW3 mounts the same main power-unit as that of 6W-NProto. JW3 has 6-wheel and has 90[W] motor in each center-wheel. Total weight of JW3 is 51[kg]. Power weight ratio of JW3 is 3.53[W/kg] and that of 6W-NProto is 6.60[W/kg].

RESULTS OF RUNNING TEST

Terrain condition is 3 to 5 cm thick slushy snow on the ice. This is the most difficult surface condition for wheelchairs.

With special netted tires: (Table 1)

On level road JW3 and 6W-NProto showed good driving performance, either dry or snow road. On 4.1° ramp both 6W-NProto and JW3 could run, however, JW3 was unstable to run on 6.6° ramp. 6W-NProto cleared 120mm step, but JW3 could not (Fig.2).

SUMMERY

Light-weight 6-wheel motorized wheelchair 6W-NProto was designed, mounting build-in motors in the center main wheels and rear wheels and having part time four-wheel drive mechanism. This proto-type is applicable for development of indoor-type motorized wheelchair able to clear small steps in the house, for development of off-road-type wheelchair good for uneven terrain or snowfall conditions.

REFERENCES

1. Uchiyama E. et al. Proceedings of the 10th International Conference on Biomedical Engineering, p251-252, 2000

2. Uchiyama E. et al. Critical Reviews™ in Biomedical Engineering, 26, p434, 1998

3. Uchiyama E. et al. J. Jap. Soc. for Clinical Biomechanics and Related Research, 18, p81-85, 1997 (in Japanese)

ACKNOWLEDGEMENTS

This work was partly supported by Grant-in-Aid for Scientific Research B(1)12470311 and SECOM Foundation.

Table 1. Comparison of running performance of two different types of powered wheelchairs JW3 and 6W-NProto. Four categories: (★★★★) quick and stable running; (★★★) good running; (★★) running with difficulty; (★) could not run.

Model	Level (dry)	Level (snow)	Ramp (4.1°)	Ramp (6.6°)	Step (dry)	Step (snow)
6W-Nproto	★★★★	★★★★	★★★★	★★★★	★★★	★★
JW-3	★★★★	★★★	★★★	★★	★	★

Fig. 2. A sequence of photographs when 6W-NProto cleared the 120mm step.

STEPPING UP TO A NEW LEVEL. EFFECTS OF BLURRING VISION IN THE ELDERLY

[1]Karen Heasley, [1]John G Buckley, [2]Andy Scally, [3]Pete Twigg, [1]David B. Elliott

[1] Vision and Mobility Research Laboratory, Department of Optometry, [2]Institute of Health Research, School of Health, and [3]School of Engineering, Design and Technology, University of Bradford.
E-mail: k.j.heasley1@bradford.ac.uk

INTRODUCTION

Falls within the elderly population are a major cause of injury-related admissions to emergency departments worldwide. In the UK for example 57% of all injury-related admissions into hospital were attributed to falls during 1995/6 (Dowsell 1999). Studies have sought to determine the causes of such falls and have revealed that fall location is very significant, with stairs and steps being the most frequently cited areas in which falls occur (Startzell 2000).

Research groups striving to highlight universal factors to falls have commonly agreed that visual impairment is a critical factor in increased fall risk (Ivers 1998). The deterioration of vision with age is an inevitable process, which may or may not be coupled with additional pathological conditions, such as cataract, a common condition experienced in the elderly, which has also been linked to falls (McCarty 2002).

Although links have been made between increased falls and stairs/steps negotiation and between increased falls and visual impairment little has been done to determine what effects visual impairment has on step negotiation in the elderly. Therefore the aim of this study was to look at the effects of blurring vision, using cataract simulation, on the step negotiation strategy of healthy elderly, through analysis of whole body centre of mass (CM) dynamics and foot clearance parameters.

METHODS

Subjects were initially screened to ensure no history of falls, mobility impairment and or visual impairment. Twelve subjects, 7 male and 5 female, (mean age 72.3 ± 4.17 years), volunteered to participate in this study. A battery of visual tests were undertaken to assess the visual functions of binocular visual acuity (VA), using the ETDRS logMAR chart, and binocular contrast sensitivity (CS), using the Pelli-Robson chart. Measurements were then repeated with the presence of the cataract simulation lenses.

A five-camera 3-D motion analysis system (Vicon 250, Oxford Metric Ltd) was used to record (at 50Hz) each subject stepping up to a new level, (heights of 73mm and 146mm). Two force platforms (AMTI OR6-7-1000) were used to collect centre of pressure (CP) data under each foot at 100Hz.

Trials began with subjects standing stationary with feet positioned half their foot length away from the step edge. They were instructed to take a single step-up onto the new level and resume a stationary position on the top of the step. Trials were performed twice and repeated with the addition of the cataract simulation lenses.

Using the Plug-in Gait software (Vicon Oxford Metrics Systems Ltd), whole body CM was calculated, as was joint ankle angle of the swing limb. Global CP was achieved by combining centre of pressure data from each force platform. The minimum distances between the step edge

and the tip of the subject's shoe in horizontal and vertical directions (toe clearance) were also exported for analysis in both horizontal and vertical directions. The stepping movement was divided into; anticipatory, initial swing, terminal swing and weight transfer.
Statistical analysis was performed using a random effects population averaged model (Stat Corp., College Station, USA)

RESULTS AND DISCUSSION

In the blurred condition subjects took 11% longer across all stepping phases ($p<0.05$), reduced the mediolateral (but not anterioposterior) displacement of their centre of pressure from 37.6% stance width to 28.3% during the anticipatory phase ($p<0.01$). Peak mediolateral divergence between the CM and CP also decreased whilst in the anticipatory phase by 9.8mm ($p<0.01$). Toe clearance was found to increase during the blurred trials in both horizontal (28%) and vertical (19%) directions ($p<0.05$).

Maximal CM-CP divergence has been said to denote positional instability (Zachazewski 1993). In the present study mediolateral CM-CP divergence during anticipatory phase decreased with blurred vision, and was a direct consequence of a decrease in mediolateral displacement of the CP with blur. This reduction in CP movement indicates that subjects were cautious with regard to mediolateral instability and thus ensured the horizontal position of their CM was close to the centre of the base of support.
The increase in step duration with blur was found to be similar across all phases of the stepping task. Increases in phase duration can be attributed to the visual system requiring more time to extrapolate appropriate exteroceptive information about the step itself, (anticipatory phase), and exproprioceptive information regarding accurate foot placement, (terminal swing and weight transfer phases). Additionally, the increase in toe clearance would result in longer step execution duration, due to the greater distance travelled by the foot to produce the higher trajectory over the step edge. As there was no change in ankle angle the increase in both vertical and horizontal toe clearance was postulated to be a change in hip kinematics. Vertical toe clearance decreased upon repetition indicating a learning effect that may have been due to energy conservation.

SUMMARY

This study has highlighted that a two-fold safety driven adaptation occurs when under the influence of visual disturbance such as cataract. Firstly CM excursion within the base of support was reduced, to increase dynamic stability, and secondly toe clearance in both horizontal and vertical directions, was increased to reduce the risk of tripping by providing greater room for error.
Since this study looked at the temporary effects of blurring vision future work is needed to compare the chronic effects of cataractous blur.

REFERENCES

Dowsell, T. et al. (1999).
UK Department of Trade and Industry:**68**.
Ivers, R.Q. et al. (1998).
J Am Geriatr Soc **46**(1): 58-64.
McCarty, C.A. et al. (2002).
Aust N Z J Public Health **26**(2): 116-9.
Startzell, J.K. et al. (2000).
J Am Geriatr Soc **48**(5): 567-80.
Zachazewski, J. E. et al. (1993).
J Rehabil Res Dev **30**(4): 412-22.

ACKNOWLEDGEMENT

This study was supported by a grant from The Health Foundation, UK. (Reference 3991/882)

AN ARTIFICIAL NEURAL NETWORK THAT UTILIZES A CHAOTIC CONTROL SCHEME FOR STABLE LOCOMOTION

Max J. Kurz and Nicholas Stergiou

HPER Biomechanics Laboratory, University of Nebraska at Omaha, Omaha, NE

E-mail: mkurz@mail.unomaha.edu Web: http://www.unocoe.unomaha.edu/hper.htm

INTRODUCTION

Although it is well known that chaos is a central feature of human locomotion, it is not clear what advantage it offers to the nervous system. Recently, we have used a passive dynamic bipedal model that has a chaotic locomotive pattern as our foundation to explore this question (Kurz and Stergiou, 2003). Our simulations have demonstrated that a locomotive system built upon the principles of chaos can utilize joint actuations to rapidly transition to any stable locomotive pattern embedded in the chaotic attractor. We have found that such flexibility cannot be demonstrated in a strictly periodic system. Based on these experiments, we propose that the nervous system may use well-timed joint actuations to switch to stable gaits embedded in the chaotic attractor. This type of control scheme may reduce the degrees of freedom problem and may allow the locomotive system to rapidly switch to a stable locomotive pattern when unforeseen perturbations are encountered. Here we show that a robust chaotic control scheme can be facilitated by an artificial neural network (ANN) that selects a proper hip actuation for a stable locomotive pattern.

METHODS

We utilized a passive dynamic bipedal model that consisted of two rigid legs connected by a frictionless hinge at the hip (Figure 1; Eq 1). Joint actuations were supplied by the ANN by adjusting the stiffness of a torsional spring (K) located between the swing leg and the torso. Locomotive energy was supplied to the model via a sloped walking surface (γ).

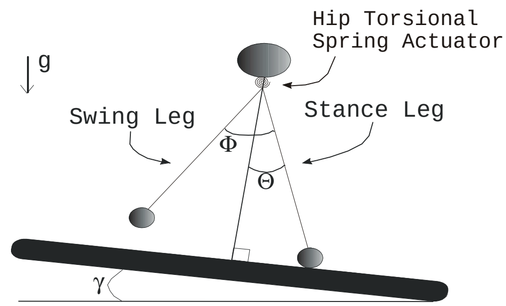

Figure 1. Passive dynamic walking model that has a chaotic gait pattern.

Simulating the model consisted of integrating the equations of motion and applying a transition rule at heel-contact. We modeled heel-contact as instantaneous and perfectly inelastic (Eq. 2 where P=0).

$$\begin{pmatrix} 1+2\beta(1-\cos\phi) & -\beta(1-\cos\phi) \\ \beta(1-\cos\phi) & -\beta \end{pmatrix}\begin{pmatrix} \ddot{\theta} \\ \ddot{\phi} \end{pmatrix}+\begin{pmatrix} -\beta\sin\phi(\dot{\phi}^2-2\dot{\theta}\dot{\phi}) \\ \beta\dot{\theta}^2\sin\phi \end{pmatrix}+ \qquad \text{Eq (1).}$$
$$\begin{pmatrix} (\beta g/l)[\sin(\theta-\phi-\gamma)-\sin(\theta-\gamma)]-g/l\sin(\theta-\gamma) \\ (\beta g/l)\sin(\theta-\phi-\gamma) \end{pmatrix}=\begin{pmatrix} 0 \\ k(\phi) \end{pmatrix}$$

$$\begin{pmatrix} \theta \\ \dot{\theta} \\ \phi \\ \dot{\phi} \end{pmatrix}^{+}=\begin{pmatrix} -1 & 0 & 00 \\ 0 & \cos 2\theta & 00 \\ 0 & \cos 2\theta(1-\cos 2\theta) & 00 \end{pmatrix}\begin{pmatrix} \theta \\ \dot{\theta} \\ \phi \\ \dot{\phi} \end{pmatrix}^{-}+\begin{pmatrix} 0 \\ \sin 2\theta \\ 0 \\ (1-\cos 2\theta)\sin 2\theta \end{pmatrix}P \qquad \text{Eq (2).}$$

A feed-forward ANN was developed that had sixteen input neurons, four hidden neurons and one output neuron (Figure 2). Neurons between each layer were connected via a series of weighted edges (w_{ij}). Each *i*th neuron had an input value x_i and an output value $y_i = g(x)$. A sigmoid function $g(x) = (1+ e^{x})^{-1}$ was used to determine the excitation of the neuron where the value of x was given by $x_i = \sum w_{ij}y_j$. The input to the ANN consisted of eight time delays of the model's initial right leg angle and angular velocity for a given step (X_{n-1}, X_{n-2}, … X_{n-8}).

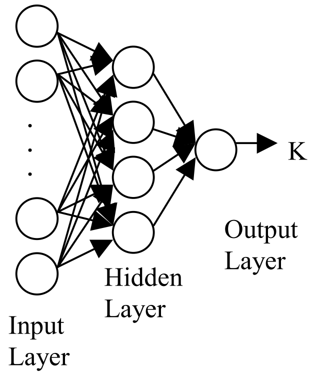

Figure 2. Schematic for the ANN that determines a stiffness value (K in Eq 1.) for modulating hip actuation.

These time delays served as a cognitive memory for the past states of the locomotive system. The assignment of edge weights in the final neural network were determined with a backpropogation algorithm where the output of the ANN was compared with the training data (Rumelhart *et al*., 1986).

We trained the ANN to select a hip stiffness (K in Eq 1.) that would transition a period-n gait to a period-2 gait. Although it is unlikely that humans walk with a period-2 gait, we selected period-2 because it is feasible to visually inspect the performance of the model with Poincarè sections. The same control scheme can apply to higher order gaits (Kurz and Stergiou, 2003). The training data utilized was from 0.0182 rad > γ > 0.0183 rad. Following this, we tested the ANN performance at γ that it had not been trained (e.g. 0.0183 rad > γ > 0.0191 rad). Additionally, the robustness of the ANN was tested by supplying an impulse directed toward the model's center of mass at the 150th step (Eq. 2 where P > 0). This impulse provided an unforeseen perturbation.

RESULTS AND DISCUSSION

Our simulations support the notion that the principles of chaos can be used as a robust control scheme. The ANN was capable of selecting a proper hip actuation that transitioned any period-n gait at a respective γ to a period-2 gait. When the ANN was not implemented for control, the model would fall down at γ > 0.019 rad. However, when the ANN was used it was able to capitalize on the properties of the chaotic attractor and select a hip actuation that transitioned the locomotive pattern to a stable gait that prevented falling. The results from the perturbation analysis demonstrated the robustness of the ANN. When the ANN was not used for control, the model was able to use passive dynamics alone to stabilize a perturbation of P = .0007. However, with the use of the ANN, unforeseen perturbations that were 73% larger were stabilized by rapidly transitioning to a stable gait embedded in the chaotic attractor.

SUMMARY

Human locomotion may use the principles of chaos as a robust control scheme for stable locomotion. The nervous system could implement chaotic principles to exhibit multiple stable locomotive patterns. Hence, when an unforeseen perturbation is encountered, the nervous system may use well-timed joint actuations to rapidly transition to a stable gait embedded in the chaotic attractor.

ACKNOWLEDGEMENT

This investigation was funded in part by the NASA Columbia Memorial Scholarship granted to MJK.

REFERENCES

Kurz M.J., N. Stergiou (2003). *Proc. ASB*, Toledo, OH.
Rumelhart D.E. et al. (1986). *Parallel Distributed Processing: Explorations in the Microstructure of Cognition*, Cambridge, MA, MIT Press.

DOES FOOTWEAR INFLUENCE THE STRUCTURE OF CHAOTIC GAIT PATTERNS?

Max J. Kurz, Nicholas Stergiou and Daniel Blanke
HPER Biomechanics Laboratory, University of Nebraska at Omaha, Omaha, NE
E-mail: mkurz@mail.unomaha.edu Web: http://www.unocoe.unomaha.edu/hper.htm

INTRODUCTION

It is well known that chaos is a central feature of human locomotion (Buzzi *et al.*, 2003; Dingwell *et al*., 2000). A chaotic gait pattern means that the lower extremity kinematics fluctuate from one step to the next with a deterministic pattern. Historically, fluctuations in the gait pattern were considered to be random noise or error in the output of the nervous system. However, recent investigations have suggested the contrary and have indicated that the chaotic structure present in the lower extremity kinematics may be related to the health of the neuromuscular system (Buzzi *et al*., 2003; Dingwell *et al*., 2000).

The Lyapunov exponent (LyE) is a mathematical tool that is used to quantify the chaotic structure present in a gait pattern (Buzzi *et al*., 2003; Dingwell *et al*., 2000). LyE classifies the exponential separation of nearby trajectories in a reconstructed state space from a given time series (Figure 1). The LyE for a periodic signal (e.g. sine wave) is zero, which indicates no separation in the attractor's trajectories. Alternatively, the LyE for Gaussian noise is positive (+0.469) and indicates large divergence in the attractor's trajectories. LyE values for human locomotion time series lie some where between these two extremes. It has been proposed that stability of human locomotion can be examined using LyE (Buzzi *et al*., 2003; Dingwell *et al*., 2000). Shifts of the LyE towards randomness indicate instability, while shifts towards periodicity are associated with stability or even rigidity. Therefore, the degree of stability of a locomotive pattern can be explored from a chaotic perspective by investigating if the LyE value shift toward one of the two extremes as the dependent variable is scaled.

No investigations have determined the influence of footwear on the chaotic structure present in gait patterns. Hence, the purpose of this investigation was to determine how the LyE value changes as humans run with and without footwear.

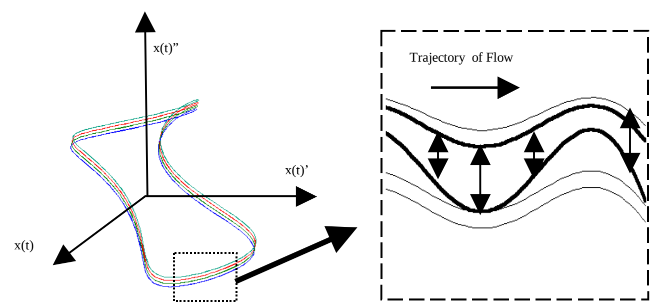

Figure 1. LyE measures the exponential separation of nearby trajectories. Conceptually, the larger the arrows between trajectories, the larger the LyE value.

METHODS

Ten subjects (Age = 27.1 $\pm$ 4.9 yrs., Mass = 71.9 $\pm$ 9.1 kg; Height = 1.76 $\pm$ 0.07 m) who were free from any neuromuscular injuries ran on a treadmill while wearing footwear and while barefoot. Conditions were presented in a random order. ASTM impact testing results indicated the peak acceleration for the footwear condition used in this investigation was 15 $\pm$ 0.3g. Subjects ran at a self-selected pace for two minutes while lower extremity sagittal kinematic data were collected with a high speed camera (180 Hz). The self-selected pace was used for both conditions (Average pace =

3.24 $\pm$ 0.85 ms^{-1}). Joint angles were calculated for the hip, knee and ankle. LyE were calculated for respective joint angle time series with an embedding dimension of five. Correlated t-tests were used to determine statistical differences between the LyE for the respective conditions.

RESULTS AND DISCUSSION

Footwear significantly affected the chaotic structure of the ankle movement pattern (P = 0.02; Table 1). Inspection of the LyE values indicate that while wearing footwear, the chaotic structure of the ankle kinematics had less divergence. This suggested that footwear tended to increase the stability of the ankle movement pattern. Alternatively, the LyE for the barefoot conditions indicated that the chaotic structure of the ankle kinematics tended to be more random. Footwear had no significant effects (P > 0.05) on the chaotic structure present in the knee and hip movement patterns (Table 1).

During the investigation we noted that the subjects ran with a forefoot posture while barefoot. It is possible that the surrounding musculature of the ankle may play a different mechanical role while barefoot. Such mechanical changes may have influenced the ankle's chaotic structure. Alternatively, De Clercq *et al.* (1994) have suggested that the human body makes kinematic adjustments according to the severity of perceived impact forces. Hence, it is possible that the observed changes in the chaotic structure may also be related to the nervous system's perception of impact forces. A recent investigation has suggested that increased joint variability may be necessary to spread forces across various tissues (Kurz and Stergiou, 2003). Based on this notion, it is possible that the nervous system may have utilized a more random pattern while barefoot to prevent various tissues from being overloaded by repetitive forces. However, this speculation needs to be further explored.

Table 1. LyE means and standard deviations for the respective lower extremity joints and conditions. * indicates a significant difference at the 0.05 alpha level.

Joint	Barefoot	Footwear
Ankle	0.114 (.01)*	0.092 (.02)
Knee	0.052 (.01)	0.050 (.01)
Hip	0.052 (.01)	0.053 (.01)

SUMMARY

Footwear influences the chaotic structure of the ankle kinematics. Our results indicate that footwear tends to increase stability. Chaotic tools are advantageous because they provide information about joint stability that is not possible with traditional time series averaging procedures. Further investigations may reveal how footwear modalities can be used to restore lower extremity function, stability and health.

ACKNOWLEDGEMENT

This investigation was funded in part by the NASA Columbia Memorial Scholarship granted to MJK.

REFERENCES

Buzzi U.H. *et al*. (2003). *Clin. Biomech*. **18**, 435-43.
De Clercq D.L. *et al.* (1994). *J. Biomech*. **27**, 1213-22.
Dingwell, J.B., et al. (2000). *J. Biomech.* **33**, 1269-77.
Kurz M.J., N. Stergiou (2003). *Gait and Posture* **17(2)**, 132-135.

EFFECTS OF SUPPORT SURFACE ML COMPLIANCE ON STEPPING BEHAVIOR OF HEALTHY ADULTS: AGE AND GENDER DIFFERENCES

Bing-Shiang Yang [1] and James A. Ashton-Miller

Biomechanics Research Laboratory, Department of Mechanical Engineering,
University of Michigan, Ann Arbor, Michigan
[1] E-mail: bsyang@umich.edu

INTRODUCTION

Falls from raised surfaces such as stepladders, chairs and stools cause injuries across the age spectrum, but especially in the elderly. In the case of a stepladder, a lateral fall is the most common type of accident (Björnstig and Johnsson, 1992). One reason may be that stepladders, chairs, and stools share a similar attribute in having structural compliance in the mediolateral (ML) direction. How humans adapt to the presence of ML structural compliance has not been quantified. In this study, therefore, we examined how humans alter their behavior while stepping up onto a structure with different ML compliances. We tested the hypotheses that the presence or absence of ML structural compliance does not (a) change stepping behavior, or (b) cause age or gender differences in stepping behavior.

METHODS

Thirty healthy subjects were equally divided into three subgroups: 10 young females (YF: 25.2 ± 2.0 yrs, 160 ± 5 cm, 53.2 ± 5.5 Kg), 10 young males (YM: 26.0 ± 2.5 yrs, 169 ± 2 cm, 71.4 ± 11.6 Kg), and 10 older males (OM: 72.2 ± 2.6 yrs, 169 ± 4 cm, 69.1 ± 8.1 Kg). Subjects were asked to stand on firm ground and step forward and up onto a seven-inch high structure at a self-selected comfortable speed. The ML compliance of the structure could be covertly assigned one of three different values: low compliance ($C_1=1\times10^{-3}$ m/N measured at the structure top surface), high compliance ($C_2=2\times10^{-3}$ m/N), and rigid ($C_0<10^{-4}$ m/N). Six trials were performed with each compliance. Trial order was C_0, C_1, and C_2 interspersed by different numbers of blocks of six C_0 trials to prevent subjects knowing when a change occurred. No practice trials were allowed. Ground reaction forces, body segment and structure kinematics were recorded at 100 Hz. The whole-body center of mass (COM) location was calculated using a three body segment model (head-arm-torso and two legs) and published segmental properties.

Phases of stepping movement. The stepping movement was divided into four phases (Figure 1):

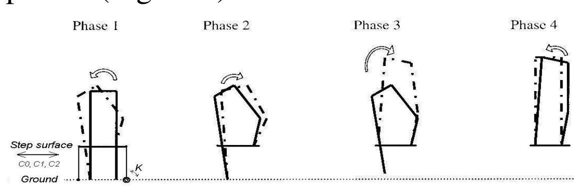

Figure 1. The four movement phases (Ph1-4) of stepping up and onto a raised structure. Solid lines illustrate initial leg states; broken lines illustrate final states of phases. Arrows indicate the directions of the weight transfer

Data and statistical analyses: Kinematic and kinetic parameters in each trial were compared. Only data from the first trial of each structural compliance are reported here. A two-way analysis of variance (ANOVA) was used to examine the main effects of age and ML structural compliance in the males. Similarly, a two-way ANOVA examined the effects of gender and ML structural compliance in the young subjects. $P< 0.05$ was considered statistically significant.

RESULTS AND DISCUSSION

The first hypothesis was rejected in that lateral structural compliance significantly lengthened the time (DT) that subjects used to execute the step-up movement (Figure 2). For YF and OM, DT increased 33-45% when stepping onto the compliant structure (C_1 or C_2) compared with stepping onto a rigid structure (C_0). YM used about 15% more time when stepping onto C_2 than onto C_0 or C_1. In general, subjects spent longer time in Ph2 and significantly shorter time in Ph3 when stepping onto the compliant structure than onto the rigid structure. Subjects developed lower lateral COM velocity (10-26% less with C_1 and 43-63% less with C_2 than with C_0) when switching from bipedal (Ph2) to unipedal (Ph3) support on the compliant structure. To regain balance after transferring weight onto the raised structure, YF needed 82-112% more time and OM used 73-80% more time on C_1 or C_2 than on C_0. YM only spent 34% longer time to recover their frontal plane balance on C_2 than on C_0 and C_1.

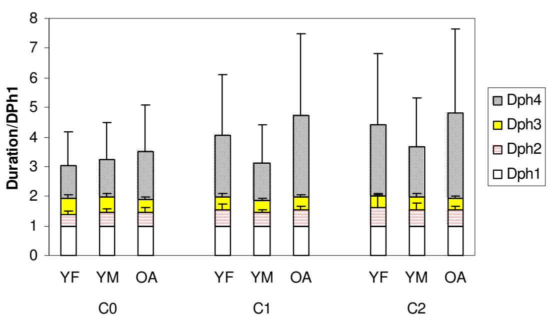

Figure 2. Mean (SD) duration of each stepping movement phase expressed as a ration of Ph1 duration (group effect: $p<0.05$) under three structural compliances (C0-2: $p<0.01$).

During the balance-recovery phase (Ph4) on the compliant structure, two alternative movement sub-phases were identified. The first sub-phase (Ph 4a) was that subjects tried to employ a hip load/unload mechanism (Winter et al., 1993) to attenuate ML COM movement propagating from the moving support structure. In this sub-phase, the human COM traveled through a larger amplitude on the phase plane (Figure 3) until COM was stabilized (D_{Ph4a}). Subjects (except for YF on C_1) needed longer time to control COM with increasing structural compliance (D_{Ph4a} increased 14-37% on C_1 and 56-59% on C_2 than on C_0); this was especially true of OM (84-125% longer than YM).

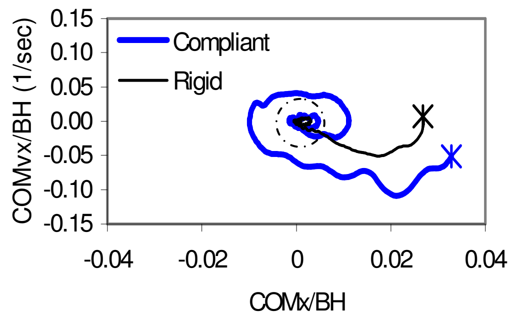

Figure 3. Phase plane of COM in Phase 4.

SUMMARY

Healthy adults adapted in the first trial to the presence of unexpected ML structural compliance as they stepped up and onto the structure. They did this by identifying its compliance, moving their COM more laterally in bipedal support, slowing their lateral velocity, and shortening the unipedal support phase. Of interventional interest, the older males needed more time than did young adults to step up and balance on laterally-compliant structures.

REFERENCES

Björnstig, U. and Johnsson, J. (1992). *J. Safety Research*, **23**, 9-18.
Winter, D.A. et al. (1993). *Neuroscience Res. Comm*, **12**, 141-148.

Supported by PHS grant P50 AG08808.

VISCOELASTIC EFFECTS AT THE BONE-SCREW INTERFACE

Serkan İnceoğlu[1], Atilla Akbay[1], and Robert F. McLain[2]
[1] Spine Research Laboratory, Spine Institute, The Cleveland Clinic Foundation, Cleveland, OH, USA
[2] Dept. of Orthopeadic Surgery, Spine Institute, The Cleveland Clinic Foundation, Cleveland, OH, USA
E-mail: inceogls@bme.ri.ccf.org

INTRODUCTION

Bone exhibits time-dependent behavior under external loading. The viscoelastic properties of cortical and trabecular bone have been well studied. It has been shown that the time-dependent effects can reduce mechanical performance of bone as drastically as do cycle-dependent effects via micro-fractures (Carter and Caler, 1985). In addition, there are very limited information towards the viscoelastic properties of cadaveric bone and specially bone-screw interface. Pedicle screw fixation system is one the most commonly used stabilization methods in spinal surgery. Despite of its success, the failure of pedicle screw fixation through loosening has been, however, reported. Loss of fixation strength in screws prior to successful arthrodesis was believed to be due to micro-fractures via fatique or bone loss in the proximity of the implant. However, there is no data available to assess the effects of viscoelastic properties of bone on its mechanical behavior. This study was designed to investigate the effects of stress relaxation phenomenon on the pullout performance of pedicle screw in human vertebra.

METHODS

For the study fourteen cadaveric thoracolumbar vertebral levels (T12-L4) were retrieved from three different donors. After DEXA-scanning for collecting bone mineral content (BMC) data, each specimen was instrumented with 6.5x40mm pedicle screws (Xia, Stryker Spine, New Jersey) according to the standard surgical procedure using appropriate surgical tools and instrumentation. After embedding, the specimens were secured into a material testing machine (MTS Alliance RT/10, MTS Corp., Eden Prairie, MN) using customized gripping fixtures. One of each screws at each specimen was withdrawn according to one of two pullout models, i.e., stress relaxation(SR) model and standard(S) model. In S-model pullout, screws were continuously pulled at a rate of 5mm/min whereas in SR-model pullout, screws were pulled stepwise manner, i.e., 0.5 mm actuator advancements and 1000 seconds rest period in between, until failure. The failure was defined as the highest load that the bone-screw interface could bear. Peak load, stiffness, displacement-to-failure(DtF), and energy-to-failure(EtF) data were calculated. The last two were calculated between 150N and failure point to exclude "toe-region". The stiffness for SR-model was calculated using the peaks of the load-displacement curve in pre-failure region as shown in Figure 1b. Correlation and regression analysis were done between the BMC and parameters of interest. Normalization was, then, carried out when correlation coefficient (R^2) was greater than 0.5. Two pullout models were compared using paired t-test in 95% confidence interval.

RESULTS

In the study, 28 pedicle screws were pulled. Statistical analysis showed correlations between BMC and peak load (R^2=0.66, R^2=0.63), DtF (R^2=0.34, R^2=0.51), EtF (R^2=0.61, R^2=0.65) in both SR-model and S-model, respectively. Due to lack of bone quality of the one of the donors, the stiffness calculations could not be done properly in SR-model. Therefore only nine specimens were used for stiffness calculations. No normalization was done on stiffness data due to lack of correlation (R^2=0.32 for SR-model, R^2=0.17 for S-model).

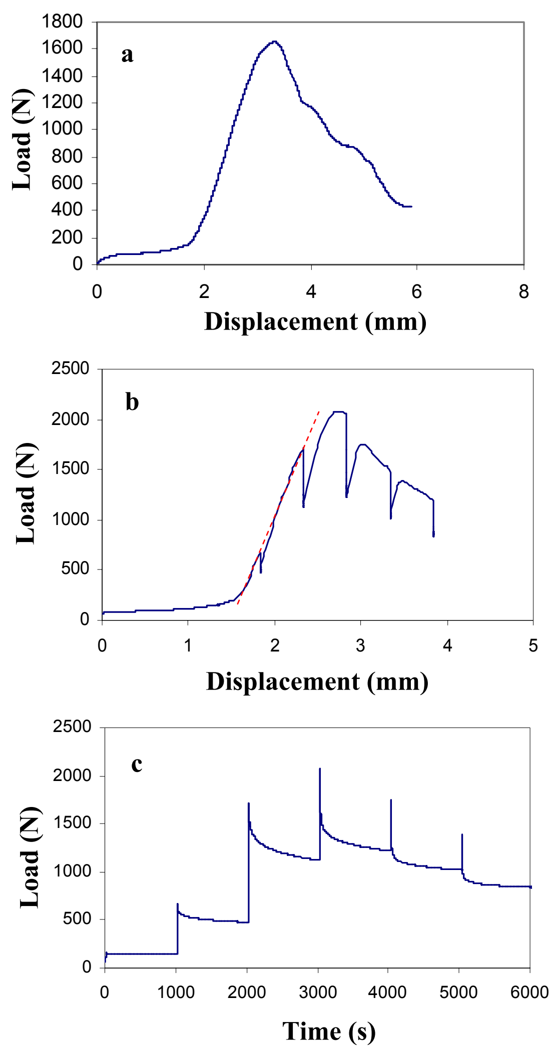

Figure 1: Represantative pullout curves from standard pullout **(a)** and stress relaxation pullout **(b,c)** models. Dashed-line depicted the line that was used for stiffness calculations in stress relaxation model.

Statistical analysis showed that the peak loads ($p<0.0001$) and stiffnesses ($p=0.04$) in SR-model were lower than those in S-model. EtF was higher in SR-model than that in S-model ($p=0.0004$). There was no significant difference in DtF data between the groups ($p=0.054$).

Table 1: Results of pullout tests from both pullout models (stress relaxation and standard models) were presented (mean±SD). Except for the stiffness, all the data were normalized with bone mineral content (g).

	SR-model	S-model
Peak Load (N/g)	305.7±51.5	387.1±64.9
Stiffness (N/mm)	1186.9±508.7	1650.5±597.7
DtF (mm/g)	0.136±0.046	0.179±0.043
EtF (Nmm/g)	537.3±88.7	477.2±74.9

SUMMARY

It is important to know the mechanical properties of the interface to prevent loss of implant purchase. The present results showed that stress relaxation phenomenon at the bone-pedicle screw interface altered mechanical behavior of the screw in cadaveric specimens by yielding lower ultimate strength and stiffness. These results coincided with previous studies conducted by using bovine model (İnceoğlu, 2004). This study provides information about the mechanics of the interface when a patient remains steady, i.e., sitting, sleeping, etc., during daily activities.

REFERENCES

Carter DR, Caler.1985. *J. of Ortho. Res.*, **3**:84-89.

İnceoğlu S, McLain RF *et al*. 2004. *J. of Ortho. Res.* (in press).

DENSITY AND HYDRATION OF FIXED HUMAN MUSCLE TISSUE

Samuel R. Ward and Richard L. Lieber

Departments of Bioengineering and Orthopaedic Surgery, University of California San Diego and VA Medical Center San Diego, CA, USA
E-mail: srward@ucsd.edu Web: http://muscle.ucsd.edu/

INTRODUCTION

The maximum force a muscle can produce is related to its physiological cross-sectional area (PCSA). PCSA is calculated using the equation (Sacks and Roy, 1982):

$$\text{PCSA (cm}^2\text{)} = \frac{\text{Muscle mass (g)} \bullet \cos(\theta)}{\rho\ (\text{g/cm}^3) \bullet \text{fiber length (cm)}}$$

where the density of muscle (ρ) has been determined to be 1.056 g/cm^3 in living rabbit and canine muscle tissue (Mendez and Keys, 1960) and θ is the pennation angle of the muscle. Since this time, most investigators have used this value to compute PCSA in fixed human muscles in an effort to estimate their maximum force producing capacities (Lieber *et al*, 1992; Wickiewicz *et al*, 1983).

Given the fact that human muscle density may differ from rabbit or canine muscle and the fact that fixation may alter muscle water content and its density, the aforementioned value may be inaccurate. If this were true, estimates of muscle PCSA would be inaccurate. Based on the importance of these values in determining the force producing capacity of human muscle, the purpose of this study was to measure muscle density as a function of hydration time in fixed human muscle tissue.

METHODS

Muscle samples (n=36) were obtained from one perfusion-fixed male cadaver specimen (age 73 years, height 181.6 cm). Whole vastus lateralis and psoas major muscles were dissected and harvested followed by division into small samples. Muscle samples were then divided into 6 groups and placed in 1X phosphate based saline (PBS) for 0, 6, 12, 18, 24, or 30 hours (n = 6/ time point).

Muscle volume was measured by obtaining MR images of each sample using a 1.5T GE Signa scanner (GE Medical Systems, Milwaukee, WI). Axial 3D FSPGR images were acquired using the following parameters; TR: 7.7 msec, TE: 2.2 msec, flip angle: 30°, NEX 2, FOV 12 x 12 cm, matrix 256 x 256, and slice thickness 1 mm. These parameters yielded a voxel resolution of 0.47 x 0.47 x 1 mm. Muscle volumes were then calculated using a semi-automated segmentation and reconstruction routine (Analyze 5.0, Analyze Direct, Lenexa, KS).

After scanning, samples were weighed, snap frozen in liquid nitrogen (-196º C), and stored at -80° C. Following this procedure, samples were lyophilized (freeze-dried) for 12 hours and reweighed. Hydration (% water) was calculated based on the difference between wet and dry weights.

Statistical comparisons of hydration and density over time were made with a one-way analysis of variance ($\alpha = 0.05$). Pairwise comparisons of each time point were made with *post-hoc* Tukey's tests.

RESULTS AND DISCUSSION

There was a significant difference in muscle hydration between time points ($p < 0.001$; Fig. 1). *Post-hoc* testing revealed that all time intervals were different from one another except for 6, 12, and 18 hours. These data indicate a general trend towards increasing hydration over time with the largest difference (12%) being between 0 hours (66.6 $\pm$ 0.9%) and 24 hours (79.4 $\pm$ 0.8%).

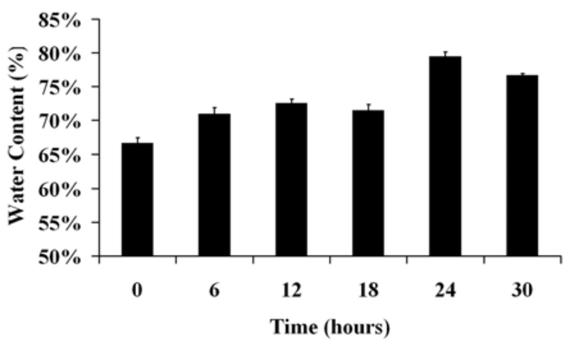

Figure 1: Bar graph (mean $\pm$ SE) of muscle hydration versus time.

There was no significant difference in muscle density between time points ($p = 0.29$). Given the lack of differences between time points, average density was calculated for all 36 samples. Wet-weights were then plotted against volumes to determine how well these samples fit the calculated average muscle density (1.067 $\pm$ 0.018 g/cm^3; Fig.2).

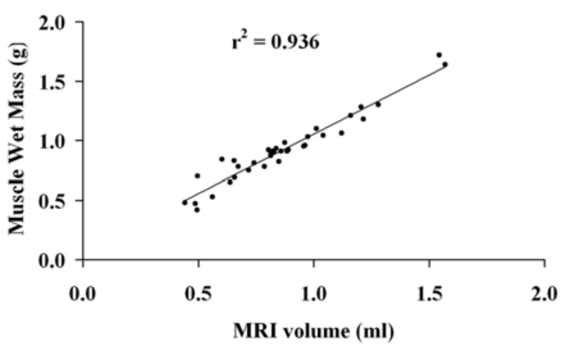

Figure 2: Scatter plot of wet-weight versus volume ($n = 36$). The association between these variables was excellent ($r^2 = 0.936$).

SUMMARY

Water content increases over time in fixed human muscle tissue when it is immersed in 1X PBS. This suggests that fixed tissue may be relatively dehydrated. However, the change in hydration does not appear to influence muscle density, which averages 1.067 g/cm^3. Given that the density of water is 1.0 g/cm^3, any change in muscle mass appears to be linearly related to changes in muscle volume with hydration, therefore, density is not affected. The difference between human muscle density (1.067 g/cm^3) and the value reported by Mendez and Keys (1.056 g/cm^3) is 1%. Therefore, previous studies characterizing muscle PCSA by weighing a muscle and dividing by this value are very accurate. However, future efforts should be aimed at determining the water content and density of living human muscle, thus elucidating the relation between fixed and living muscle hydration and density.

REFERENCES

Lieber, R.L., *et al*, (1992). *J Hand Surg [Am]*, **17A**, 787-798.

Mendez, J. and Keys, A. (1960). *Metabolism*, **9**, 184-188.

Sacks, R.D. and Roy, R.R. (1982). *J Morphology*, **173**, 185-195.

Wickiewicz, T.L., *et al*, (1983). *Clin. Orthop*, **179**, 275-283.

ACKNOWLEDGEMENTS

The authors gratefully acknowledge Dr. Lawrence Frank for his contributions of time and expertise with MR imaging.

IS THERE A GAIT TRANSITION BETWEEN RUN AND SPRINT?

Chris P. Hurt[1], Alan Hreljac[2], Max J. Kurz[1], and Nick Stergiou[1]

[1]HPER Biomechanics Lab, University of Nebraska at Omaha, Omaha, NE
[2]Kinesiology and Health Science Dept, California State University, Sacramento, CA
E-mail: nstergiou@mail.unomaha.edu Web: www.unocoe.unomaha.edu/hper/bio/home.htm

INTRODUCTION

The walk-to-run behavioral transition has been widely examined in the literature. It has been found that the preferred transition speed from walk to run is approximately 2.0 ms^{-1} (e.g. Hreljac, 1995). However, the corresponding speed for the behavioral transition from run-to-sprint is unknown. Although, previous studies have reported differences between run and sprint (Mann & Hagy, 1980; Stefanyshyn & Nigg, 1997), it is not clear if run and sprint are two different modes of locomotion or if sprint is actually a fast run (Hreljac et al., 2003). Hreljac et al. (2003), after analyzing data from seven different speeds, found that joint kinetics increased from run-to-sprint over a continuum; without any abrupt change at some discrete speed. However, they suggested that an analysis of intralimb coordination might be more sensitive in distinguishing a specific behavioral transition point. The purpose of this study was to examine the intralimb coordination of the interacting segments of the lower extremity, in an attempt to identify if there is a specific behavioral transition point. We hypothesized that intralimb coordination will change abruptly as speed increases, thus distinguishing between run and sprint.

METHODS

Seven male subjects, all of whom exhibited a heel strike landing pattern at their preferred running speed, ran down a 25 m runway at seven different speeds, including their preferred speed (0%), and speeds that were 15%, 30%, 45%, 60%, 75%, and 90% greater than this speed. Sagittal plane kinematics were collected (240 Hz) from four relevant markers (greater trochanter, knee joint center, lateral malleolus, and head of the fifth metatarsal). To examine segmental interactions, the phase portraits from segmental angular position and velocities were used to calculate phase angles (Kurz & Stergiou, 2004). Relative phase curves were calculated for two segmental relationships (foot-shank [F-S] and shank-thigh [S-T]) by subtracting the phase angle of the proximal segment from the distal. Mean relative phase (MRP) was calculated from the relative phase curves of each subject and for each condition. This was done by averaging the absolute values of all points of the curve for the braking and the propulsive periods of stance. A single factor repeated ANOVA was performed on the MRP group means for each segmental relationship and for each stance period. A Tukey test was performed in comparisons that resulted in a significant F-ratio ($p<0.05$).

RESULTS AND DISCUSSION

Statistical significance for both segmental relationships was found only during the braking period of the gait cycle but not for the propulsion period (Table 1). Based on the post-hoc analysis, statistical significance was achieved at the 30% greater speed. This was the same for both segmental relationships. This may indicate that there is a specific speed where the runner transitions from run to sprint. Graphically, we can also identify a transition speed. In Figure 1, we can observe that the transition speed for this specific subject occurred at 45% of the preferred speed, since the curve from this condition starts actually in-phase (values close to zero) rather than out-of-phase (values close to 180). We can also observe that for conditions 0, 15, 30, the segmental relationship began out-of-phase and then moved towards in-phase as the segment progressed toward the rest of the stance period.

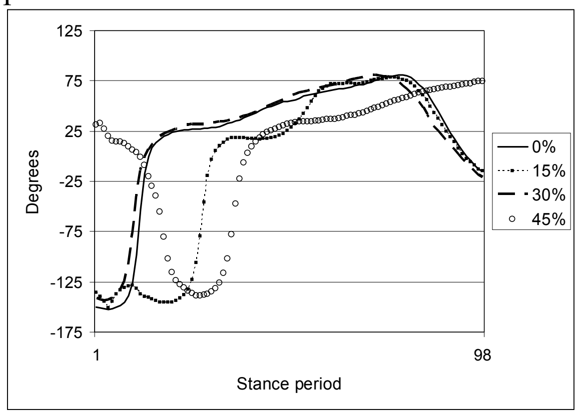

Figure 1: Relative phase curves of the foot-shank for all conditions from a representative subject. Conditions higher than 45% were omitted for clarity.

SUMMARY

In the present study, we attempted to identify if the transition from run to sprint occurs abruptly or in a continuum. Our results indicated that this change does not occur in a continuum and contradicts the findings from Hreljac et al. (2003). This is probably due to the fact that their analysis was based on joint moments and powers which may not be as sensitive in detecting differences as our present analysis of intralimb coordination. The transition speed for the group of runners examined seemed to be at 30% of their self-selected run speed. However, individual differences do exist (Figure 1).

REFERENCES

Hreljac, A. et al. (2003). *Proceedings of ASB* '03.

Hreljac, A. (1995). *J. Biomech*, 28, 669-677.

Kurz, M.J., Stergiou, N. (2004). *J. Am. Podiat. Med. Assoc.*, 94, 53-58.

Mann, R.A., Hagy, J. (1980). *Am. J. Sports Med.*, 8, 345-350.

Stefanyshyn, D.J., Nigg,B.M. (1997). *J. Biomech*, 30, 1081-1086.

Table 1: Group means for the parameters evaluated. Superscripts indicate post-hoc significance ($p<0.05$). All values are in degrees.

Variables	0%	15%	30%	45%	60%	75%	90%
Braking							
MRP F-S	80.7 $^{30\%\text{-}90\%}$	64.1$^{60\%\text{-}90\%}$	53.8$^{90\%}$	44.7	38.8	37.3	26.9
	±14.4	±19.9	±24.1	±15.7	±24.9	±13.2	±9.4
MRP S-T	68.0 $^{30\%\text{-}90\%}$	53.2$^{60\%,90\%}$	45.3$^{90\%}$	42.2	32.8	35.3	25.4
	±15.5	±12.2	±16.6	±11.2	±19.7	±9.4	±7.4
Propulsion							
MRP F-S	53.8	51.0	53.0	51.1	50.7	49.6	46.4
	±10.0	±4.1	±4.4	±10.6	±10.6	±4.2	±4.7
MRP S-T	46.6	44.4	45.2	43.9	43.3	43.3	41.5
	±7.2	±5.8	±5.8	±6.2	±8.4	±4.9	±4.2

STRESS-DEPENDENT AND STRESS-INDEPENDENT GENE EXPRESSION IN RAT SKELETAL MUSCLE AFTER A SINGLE BOUT OF "EXERCISE"

Eric Hentzen[1], Michelle Lahey[1], Liby Mathew[1], David Peters[1], Ilona A. Barash[1], Jan Fridén[2] and Richard L. Lieber[1]

[1]Departments of Orthopaedic Surgery and Bioengineering, University of California, San Diego, Veterans Affairs Medical Center, San Diego

[2]Department of Hand Surgery, Sahlgrenska University Hospital, Göteborg, Sweden

E-mail: rlieber@ucsd.edu Web: muscle.ucsd.edu

INTRODUCTION

The mechanical factors that affect skeletal muscle gene expression are largely unknown. Skeletal muscle tissue affords the unique opportunity to investigate the role of mechanical events on signaling and gene expression. Because muscle has well-defined contractile properties during isometric (IC) or eccentric (EC) modes (Close, 1972) and because muscle stress increases as a function of frequency (Rack & Westbury, 1969), it is possible to combine frequency and contraction mode in such a way as to vary the levels of stress and injury on the muscles. This approach permits investigation of the relationship between muscle mechanics during exercise, injury (if any), and gene expression.

METHODS

Experimental subjects were adult male Sprague-Dawley rats (n=40). All procedures were approved by the local Committees on the Use of Animal Subjects in Research. Five experimental groups were studied composed of rats exposed to ECs at either 40 Hz, 100 Hz or 150 Hz (EC40, EC100 and EC150) and those exposed to isometric contractions at either 40 Hz or 150 Hz (IC40 and IC150). Exercise consisted of 30 isometric or eccentric contractions of ankle dorsiflexors, with maximal isometric torque recorded before, immediately after and 24 hours after the exercise bout. For muscle stimulation, the peroneal nerve was stimulated for 650 ms once every two minutes. For the isometric group the foot was held stationary. For the eccentric group the foot was plantarflexed ~40° 200 ms after nerve stimulation commenced. During treatment (isometric or eccentric) dorsiflexion torque was measured on-line to infer tissue stress.

Twenty-four hours after the exercise bout, isometric torque was again measured, and the tibialis anterior muscle was harvested and immediately frozen. The quantitative polymerase chain reaction (QPCR) was used to quantify transcript levels of two isoforms of the muscle ankryn repeat protein (MARP) family. This gene family was our focus based on a recent gene profiling study that revealed tremendous upregulation of these genes after a single EC bout (Barash *et al*. 2004).

Analysis of variance (ANOVA; Statview, SAS Institute, NC) was used to compare transcript levels and functional measurements between groups. Statistical significance level (□) was set to 0.05, statistical power (1-□) exceeded 85%. and all values are presented as mean ± SEM.

RESULTS AND DISCUSSION

As expected based on well-known muscle mechanics, peak torque measured during exercise was highest for the EC150 group, intermediate for the EC40 and IC150 groups, and lowest for the IC40 group (Fig. 1A). The EC40 and ISO150 groups were "exercised" at the same torque levels. Similarly, muscle injury, as indicated by the torque change 24 hours after the exercise bout (Fig. 1B) was highly correlated with peak torque, independent of stimulation frequency and contraction type (Fig. 1B; $r^2=0.72$, $p<0.001$).

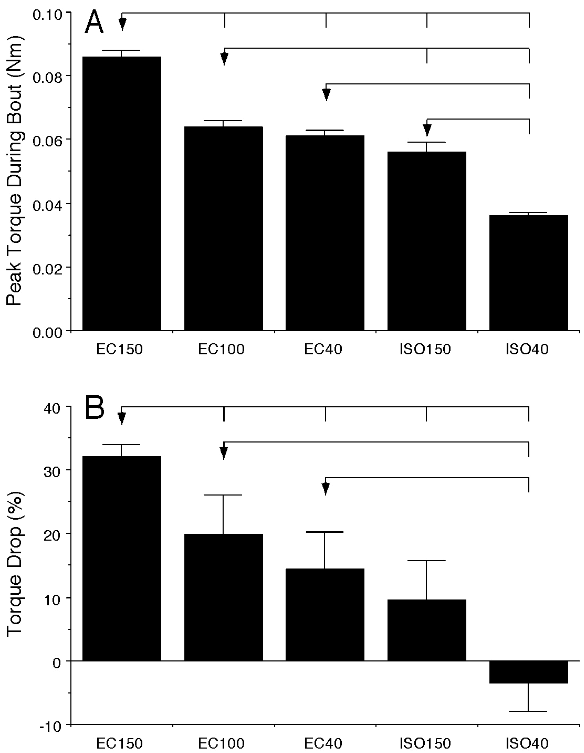

FIGURE 1: Functional changes of rat dorsiflexors muscles "exercised" under one of the conditions shown **(A)** Peak torque measured on-line during exercise. **(B)** Torque change measured 24 hours after exercise. Bars connected by vertical lines are significantly different ($p<0.05$).

In contrast to the consistent effects of peak stress on injury, the MARPs examined showed a distinct pattern of gene expression (Fig. 2). For example, MARP1 was highly correlated with torque, independent of contraction mode (Fig. 2A; $r^2=0.81$, $p<0.001$).

MARP2, on the other hand, was highly elevated in all EC groups and significantly lower in both IC groups, independent of stress (Fig. 2B).

These data demonstrate the rapid and gene-specific response of muscle to stress and/or contraction mode. Thus, skeletal muscle sensors can transduce not only tissue stress, but the nature of the contraction itself. Further studies are required to identify the structures and processes involved in this signal transduction.

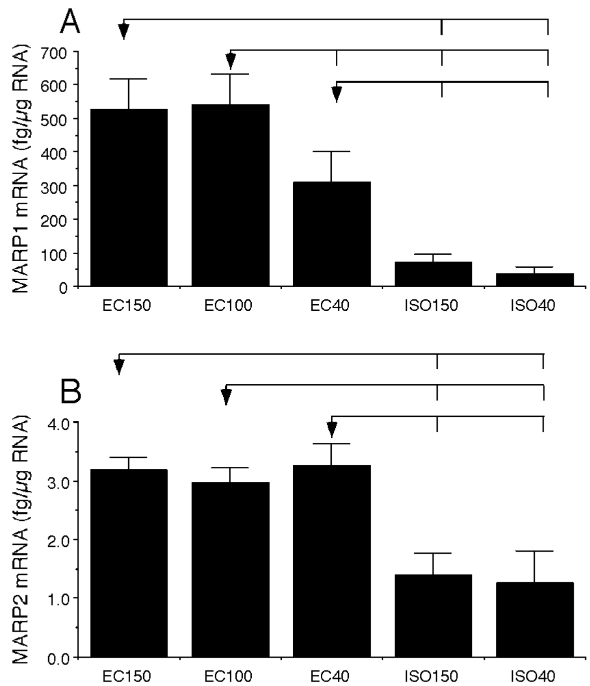

FIGURE 2: Expression levels of the MARP genes measured by QPCR. **(A)** MARP1 gene **(B)** MARP2 genes. Note that MARP1 expression levels are highly correlated to tissue stress (Fig. 1A) while MARP2 levels depend only on contraction mode (*i.e.,* isometric or eccentric contraction).

REFERENCES

Close, R. I. (1972). *Physiological Reviews* **52**, 129-197.

Barash, I.A. *et al*. (2004). *Amer. J. Physiol. Cell Physiol*. **286**, C355-C364.

Rack, P. M. H. & Westbury, D. R. (1969). *J. Physiol. (Lond.)* **204**, 443-460.

ACKNOWLEDGEMENTS

This work was supported by NIH grant AR40050 and the V.A.S.D.H.S.

FURTHER EVIDENCE THAT BONE MINERAL DENSITY AND SOFT TISSUES INFLUENCE PELVIC FRACTURE IN OLDER WOMEN DURING LATERAL IMPACT

Brandon S. Etheridge[1], David P. Beason[1], Jorge E. Alonso[2], Robert Lopez[3], *Alan W. Eberhardt[1]

[1]Dept. of Biomedical Engineering, [2]Division of Orthopaedic Surgery, [3]Department of Radiology
University of Alabama at Birmingham, Birmingham, Alabama, USA
*Email: aeberhar@uab.edu

INTRODUCTION

Pelvic fractures occur commonly in side impact automotive crashes (Gokcen et al., 1994). Women are more frequently injured (Lewis et al., 1996), leading automotive researchers to re-focus on women's safety in side impacts. There is, however, a paucity of biomechanical data for the human female pelvis with the currently accepted fracture tolerance of 4.26 kN based upon extrapolations from impacts on male and female cadavers (Cesari & Ramet, 1982).

Previously, we observed a linear correlation between fracture load and total hip bone mineral density (BMD) in drop tower tests of isolated bone-ligament pelvic structures (Beason et al., 2003). The purpose of the present study was to investigate the influence of trochanteric soft tissues on pelvic fracture measures in more realistic lateral impact experiments. It was hypothesized that intact specimens would fracture at increased force and compression levels as compared to isolated pelvic bones, but would display a similar linear correlation with BMD.

METHODS

Sixteen lateral impacts were conducted on eight fresh-frozen lower torsos (L4 to proximal femurs, hereafter referred to as "pelves") from female cadavers (age 76 ± 10 years). Total hip BMD of the left hip was assessed via dual-energy X-ray absorptiometry (QDR 4500, Hologic Inc., Waltham, MA).

Lateral impacts, centered at the left greater trochanter, were performed using a linear impactor (VIA Systems, Brighton, MI), which employed a pneumatic cylinder to accelerate a 22.1-kg impact mass to the desired impact velocity. The thawed pelves were placed in a custom seat with contralateral support, which allowed lateral translation. An axial preload (~60% body weight) was applied to the vertebral column to simulate upper body weight. The weight of the seat was adjusted to account for the absent body mass.

The first six specimens were impacted at a velocity of 3.33 ± 0.04 m/s. No fractures were observed in subsequent x-rays, so the pelves were struck again at a higher velocity (6.44 ± 0.22 m/s), which induced fracture in each case. Two additional pelves were impacted at an intermediate velocity, 5.01 ± 0.02 m/s to achieve overlapping fracture/no fracture outcomes in order to perform logistic regression analysis. One pelvis fractured at this impact speed. The second pelvis was impacted at 6.4 m/s, and then again at 8.3 m/s, at which point it also fractured. Computed tomography (CT) scans (LightSpeed QX/i, GE Medical Systems, Milwaukee, WI) were examined to classify pelvic ring and/or acetabular fractures.

Force data, $F(t)$, were obtained through using a uniaxial load cell in series with the impacting mass and striker. The inertially compensated force (Bouquet et al., 1994) was filtered according to SAE J211 (SAE, 2000). The impulse, I, defined as the integral of $F(t)*dt$ was also computed. A 1-kHz infrared camera (MCU1000, Qualisys Inc., Glastonbury, CT) captured motion of reflective markers attached to the impactor and seat to calculate pelvic compression, $C(t)$, and the maximum viscous response, $(VC)_{max}$, where $V(t)$ = velocity of the impact mass.

F_{max}, I, C_{max} and $(VC)_{max}$ were analyzed using linear regression to test for correlation with BMD. Logistic regression was used to determine a 25% probability of pelvic fracture for each parameter.

RESULTS

Fractures were located predominantly in the areas of the pubic rami and acetabulum, consistent with those observed in automotive side impacts (e.g., Lewis et al., 1996). The average force to fracture was 4.4 ± 0.95 kN, a 89% increase over the 2.33 ± 0.90 kN average calculated using female data only from Beason et al. (2003). Linear regression showed that as total hip BMD increased, the force to fracture also increased. The regression is shown, along with female data from Beason et al. (2003), in Figure 1. Main effects ANCOVA revealed that the slopes were similar and the intercepts were significantly different ($p < 0.005$). C_{max} and $(VC)_{max}$ each demonstrated a negative relationship with BMD, which were not significant ($p > 0.1$). Impulse displayed no correlation with BMD.

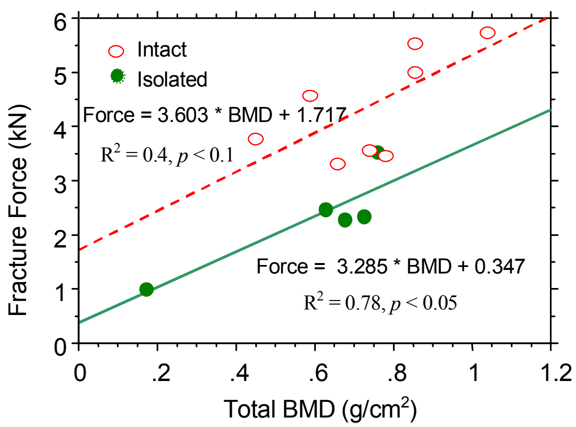

Figure 1: Fracture load-BMD correlation between impacts of isolated (solid) and intact (open circle) female cadaver pelves.

Logistic regression analysis (Figure 2) revealed fracture tolerances (at 25% probability) of 2.99 kN and 90.7 N-s for peak load and impulse, respectively. The 25% tolerance values for $C(t)$ and $(VC)_{max}$ were 12.54% and 0.27 m/s, respectively.

DISCUSSION

The results of this study indicated that fracture force best correlated with total hip BMD of intact cadaver pelves. As hypothesized, the inclusion of soft tissues around the bony pelvis resulted in increased fracture loads as compared to those found for isolated pelvic bones. The current force

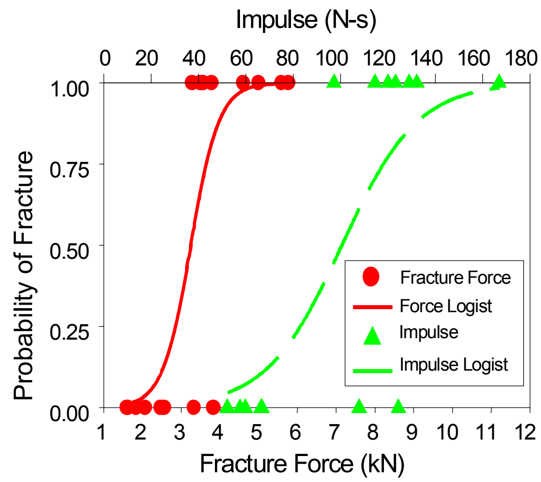

Figure 2: Logistic regression plots for fracture force (red) and impulse (green).

tolerance of 2.99 kN is lower than the 4.26 kN value extrapolated by Cesari and Ramet (1982) for the 5th percentile female. Our impulse tolerance of 90.7 N-s is within 10% of the 100 N-s tolerance suggested by Cesari et al. (1980). Discrepancies between our results and those of Cesari and co-workers may be attributed to differences in test procedures. While they used full cadavers, both male and female, we used only the lower torso of the female cadaver, inertially compensated by adding mass to the seat. Nevertheless, the present results suggest that older women, especially those with decreased BMD, may be at higher risk for pelvic fracture in automotive side impacts.

REFERENCES

Beason, D.P. et al. (2003). *J. of Biomechanics*, **36,** 219-227.

Bouquet, R. et al. (1994). *Proc. 14th Internat. Tech. Conf. ESV*, 1100-1110.

Cesari, D., et al. (1980). *Proc. 24th Stapp Conference*, 231-253.

Cesari, D., Ramet, M. (1982). *Proc. 26th Stapp Conference,* 145-154.

Gokcen, E.C. et al. (1994). *J. of Trauma*, **36**, 789-796.

Lewis P.R. et al. (1996). *Proc. 40th Stapp Conference*, 1-7.

SAE (2000). *2000 SAE Handbook*. 34.356-34.635.

ACKNOWLEDGMENTS

This research was funded by the UAB Center for Aging and the UAB Center for Injury Sciences.

A METHOD FOR DETERMINING ANGULAR HEAD ACCELERATIONS FOR VOLUNTEER SUBJECTS WEARING AN ARRAY OF LINEAR ACCELEROMETERS

James K. Sprague, Ph.D., P.E. and Laura A. Wojcik, Ph.D., P.E.
Packer Engineering, Inc., Ann Arbor, MI, USA

E-mail: jks@packereng.com and law@packereng.com Web: www.packereng.com

INTRODUCTION

There are many situations in which human head accelerations are of significant interest. Safety research has, to date, largely focused on injury tolerance levels for linear head accelerations during short-duration impacts. These linear accelerations from impact are characterized with HIC (Head Impact Criterion) values and injury tolerance curves. For longer-duration tasks not involving impact, but including both linear and angular acceleration, methods of analysis have been less explicitly defined. Linear accelerations can be recorded directly using single- or multi-axial accelerometers affixed to a person's head, but determination of rotational accelerations has generally been performed in conjunction with data from a roll rate sensor held on a bite plate in the test subject's mouth. More simplified rigid-body approximations of angular accelerations are easy to calculate, but do not capture the full three-dimensional dynamics of a moving person (Smith and Meany, 2002).

Extension of a nine-accelerometer array first suggested for use in crash test surrogates by Padgaonkar et al. (1975) allows for the explicit calculation of rotational head accelerations from linear accelerometers without the need for a bite plate and without the potential errors introduced by numerical differentiation of other sensor data.

RESULTS AND DISCUSSION

Given a rigid body both translating and rotating in space, the acceleration of a given point P on that body can be written

$$\mathbf{A}_P = \ddot{\mathbf{R}} + \overline{w} \times \overline{w} \times \overline{r}_P + \dot{\overline{w}} \times \overline{r}_P \qquad (1)$$

where

$\ddot{\mathbf{R}}$ = acceleration of the body-fixed reference frame with respect to ground;
$\overline{w}$ = angular velocity of the body;
$\dot{\overline{w}}$ = angular acceleration of the body;
$\overline{r}_P$ = position of the point P relative to the origin of the body-fixed reference frame.

In Padgaonkar et al. (1975), a set of nine linear accelerometers is aligned in an array around a crash surrogate's head and at its center of mass. Placement of a triaxial accelerometer at the head's CM is clearly not feasible, however, in human volunteers. Our modified array of four accelerometer positions is shown in Figure 1. In order to simplify the equations of motion, Position 4 is defined directly over the glabella, Positions 2 and 3 are on the glabella-occiput plane approximately 40-50% forward of the occiput (Chaffin and

Andersson, 1991), and Position 1 is at the top of the head, also at the same relative position forward on the glabella-occiput line. Assuming that the head is symmetrical about its mid-sagittal plane and that accelerometers at Positions 2 and 3 are rigidly linked, then the linear acceleration of the head's center of mass

$$\ddot{\mathbf{R}} = A_{CMx}\hat{i} + A_{CMy}\hat{j} + A_{CMz}\hat{k} \qquad (2)$$

can be approximated as the mean of the linear accelerations at 2 and 3.

Expanding Equation (1) for the accelerometer at Position 1 at the top of the head yields two useful equations:

$$\dot{w}_x = \frac{A_{1y} - A_{CMy}}{r_1} + w_y w_z \qquad (3)$$

$$\dot{w}_y = \frac{A_{CMx} - A_{1x}}{r_1} - w_x w_z \qquad (4)$$

Similar expansion of the equations for acceleration at Positions 4 and 2 and substitution including Equations (3) and (4) allows for the elimination of cross terms. The triaxial angular accelerations can then be solved directly:

$$\dot{w}_x = \frac{A_{1y} - A_{CMy}}{2r_1} + \frac{A_{2z} - A_{CMz}}{2r_2} \qquad (5)$$

$$\dot{w}_y = \frac{A_{CMx} - A_{1x}}{2r_1} + \frac{A_{CMz} - A_{4z}}{2r_4} \qquad (6)$$

$$\dot{w}_z = \frac{A_{CMx} - A_{2x}}{2r_2} - \frac{A_{CMy} - A_{4y}}{2r_4} \qquad (7)$$

If instrumentation constraints only allow for the use of three triaxial accelerometers, then the sensor at Position 1 can be eliminated. This reduced array allows for the direct calculation of $\dot{w}_z$ as above and solution for the greatest possible magnitudes of $\dot{w}_x$ and $\dot{w}_y$.

SUMMARY

The use of three or four triaxial linear accelerometers placed at prescribed locations on a volunteer's head allows for the direct calculation of angular accelerations without the need for roll rate sensors or extensive data processing that can result in the exacerbation of noise artifacts. This method of calculating rotational accelerations can be used effectively in any application in which both linear and angular head accelerations are of interest.

REFERENCES

Chaffin DB and Andersson GBJ. (1991) *Occupational Biomechanics*. Wiley-Interscience.

Padgaonkar AJ, Krieger KW, and King AI. (1975). *ASME Journal of Applied Mechanics*, September 1975, 552-556.

Smith DH and Meany DF. (2002). *J Neurotrauma*, **19**(10), 1117-1120.

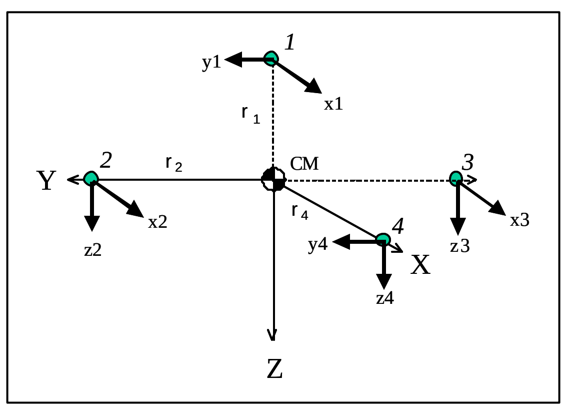

Figure 1. Notation and accelerometer signals required to generate Equations (5), (6), and (7).

PREDICTION OF RELAXATION FROM CREEP IN LIGAMENTS

Ashish L. Oza [1], Roderic S. Lakes [2,3] and Ray Vanderby [1,2,3]

[1] Orthopedic Research Laboratories, Department of Orthopedics and Rehabilitation
University of Wisconsin, Madison, Wisconsin
[2] Department of Biomedical Engineering, University of Wisconsin, Madison, Wisconsin
[3] Department of Engineering Physics, University of Wisconsin, Madison, Wisconsin
E-mail: vanderby@surgery.wisc.edu Web: http://www.engr.wisc.edu/bme/

INTRODUCTION

To robustly model the nonlinearly viscoelastic behavior of ligament is challenging. Stiffness increases with strain, relaxation proceeds faster than creep, rate of creep is a function of stress and rate of relaxation is a function of strain. Testing both creep and relaxation behaviors is time consuming. We show herein a robust model for the above complexities that predicts relaxation from creep, thus reducing the number of experiments it takes to characterize ligament. Using the principle of nonlinear superposition in a single-integral constitutive equation, we develop an interrelation between creep and relaxation for nonlinearly viscoelastic materials. Ligament creep data obtained from rabbit medial collateral ligament are fit to our model. We then use our interrelationship to predict nonlinear, stress relaxation.

CONSTITUTIVE EQUATIONS

We use a single integral nonlinear superposition where relaxation function depends on strain and creep depends on stress (Lakes and Vanderby, 1999; Oza et al. 2003). The creep kernel in Eq. 1 is non-separable in stress and time and the relaxation kernel in the Eq. 2 is non-separable in strain and time.

$$\varepsilon(\sigma,t)=\int_0^t J(t-\tau,\sigma(\tau))\frac{d\sigma(\tau)}{d\tau}d\tau. \qquad (1)$$

$$\sigma(\varepsilon,t)=\int_0^t E(t-\tau,\varepsilon(\tau))\frac{d\varepsilon(\tau)}{d\tau}d\tau. \qquad (2)$$

Separable forms of creep compliance and relaxation modulus known as quasilinear viscoelasticity (QLV) as shown in Eq. 3-4 have been widely used in the biomechanics literature for modeling of soft tissues.

$$\varepsilon(\sigma,t)=\int_0^t J(t-\tau)\frac{d\varepsilon}{d\sigma}\frac{d\sigma(\tau)}{d\tau}d\tau \qquad (3)$$

$$\sigma(\varepsilon,t)=\int_0^t E(t-\tau)\frac{d\sigma}{d\varepsilon}\frac{d\varepsilon(\tau)}{d\tau}d\tau \qquad (4)$$

Since time dependence is separated from the strain dependence in QLV relaxation and time dependence is separated from stress dependence in QLV creep, creep and relaxation proceed at rates independent of loading (Provenzano et al. (2001)). Lakes and Vanderby (1999) used a separable form of creep and the interrelation gave rise to a non-separable form of relaxation. This showed it is inconsistent to simultaneously assume both creep and relaxation functions as separable.

METHODS

To obtain explicit interrelations, we assume explicit time dependent functions (power laws in time) of creep compliance (J) and relaxation modulus (E).

$$J(t,\sigma) = g_1 t^n + g_2 \sigma t^m \quad (5)$$

$$E(t,\varepsilon) = f_1 t^{-n} + f_2 \varepsilon t^{-(3n-m)} \quad (6)$$

Using the formulation developed for interrelation based on the principle of nonlinear superposition, the parameters are interrelated as follows:

$$f_1 = \frac{1}{g_1} \frac{Sin(n\pi)}{n\pi} \quad (7)$$

$$f_2 = \frac{-f_1 g_2}{{g_1}^2} \frac{m}{n} \frac{\Gamma(-n+1)\Gamma(m)}{\Gamma(-2n+m+1)\Gamma(n)} \quad (8)$$

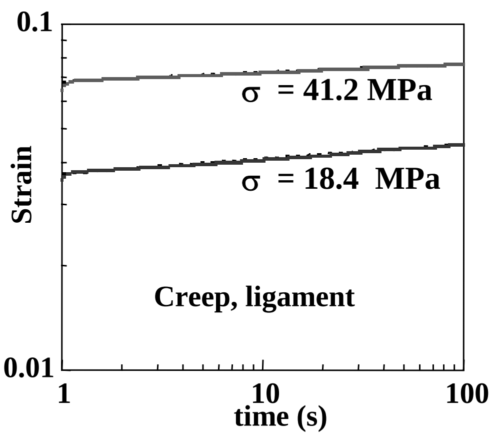

Figure 1. Curve fitting of creep of ligament. Data from rabbit medial collateral ligament at 18.4 MPa and 41.2 MPa. Dense points: experiment. Dash line: Curve fit

RESULTS

Figure 1 shows two different creep tests done at 18 MPa and 41 MPa and Figure 2 shows two different relaxation tests done at 3.5 % and 6.6% strain respectively. Creep curves are fit using Eq. 5 and relaxation with interrelated parameters is predicted using Eq. 6.

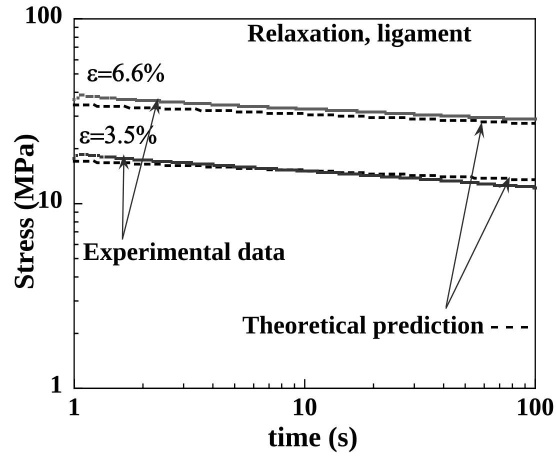

Figure 2. Prediction of relaxation from creep. Experimental data at 3.5% and 6.6% strain. Dense points: experiment. Dash line: theoretical prediction

DISCUSSION

This study shows that relaxation can be accurately predicted from creep using our interrelation formulation. The complexity of the model increases as number of terms increases for *J* and *E*, but that limitation is well balanced by experimental saving. The single integral constitutive equation proposed herein still needs testing through more complex load regimes.

REFERENCES

Lakes, R. S., Vanderby, R. (1999). *ASME J. of Biomech. Eng.*, 121(6), 612-615.
Oza, A. L., Vanderby, R., Lakes, R. S. (2003). *Rheol. Acta*, 42, 557-568.
Provenzano, P., Lakes, R. S., Keenan, T., Vanderby, R. (2001). *Ann. Biomed. Eng.*, 28, 908-914.

ACKNOWLEDGEMENTS

National Science Foundation (Grant no. CMS-9907977).

BIOMECHANICAL EVALUATION OF VERTEBRAL AUGMENTATION WITH CALCIUM SULFATE CEMENT IN CADAVERIC OSTEOPOROTIC VERTEBRAL COMPRESSION FRACTURES

Andrew Mahar[1,2], Andrew Perry[1], Noemi Arrieta[1], Steven Garfin[1], Jennifer Massie[1], Choll Kim[1]
amahar@chsd.org

[1] Department of Orthopaedics
University of California, San Diego
San Diego, CA
[2] Department of Orthopedics
Children's Hospital, San Diego
San Diego, CA

INTRODUCTION

Vertebral compression fractures cause pain, disability and deformity. Treatment with kyphoplasty utilizes an inflatable balloon tamp followed by the percutaneous injection of polymethylmethacrylate (PMMA) cement into the fractured vertebral body (Figures 1-4, from www.kyphon.com).

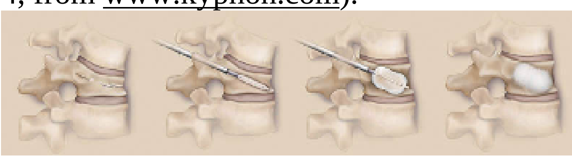

Figures 1-4: (fracture, insert, expand, fill).

This procedure restores vertebral body height and may spontaneously resolve debilitating pain. However, PMMA kyphoplasty has disadvantages such as thermal necrosis, lack of biocompatibility and potentially fatal toxicity. Calcium sulfate cement is less toxic, biocompatible, osteoconductive and bioabsorbable. The purpose of this study was to evaluate the biomechanical performance of calcium sulfate for kyphoplasty compared to the clinical standard.

METHODS

Thirty-three vertebral bodies (T9 to L4) were harvested from cadaveric spines without tumors or deformity. After obtaining T-scores to determine the level of osteoporosis/osteopenia, the vertebral bodies were disarticulated, stripped of soft tissue and measured for height and volume. The posterior elements were then removed. Each vertebral body was compressed at 0.5 mm/sec using a hinged plating system on a materials testing machine (MTS, Eden Prairie, MN) to create an anterior wedge fracture and reduce anterior height by 25%. (Figure 5)

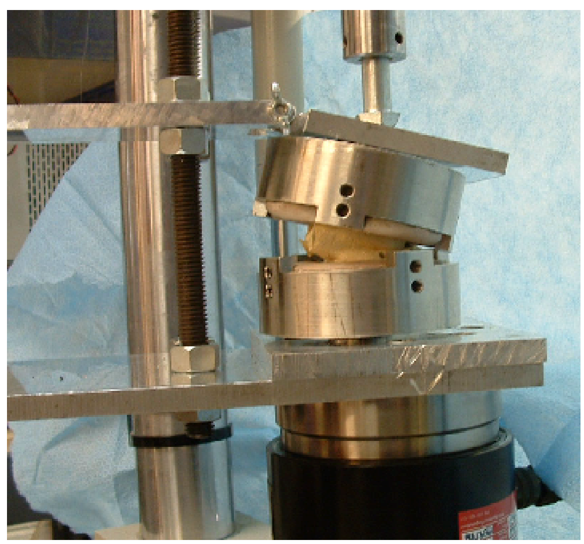

Figure 5: Test setup.

Failure strength (N) and stiffness (N/mm) were measured. Two KyphX inflatable balloon tamps were used to expand each vertebral body to within 10% of original vertebral height. After randomization three groups were created: Group A- no cement; Group B- Calcium Sulfate; Group C- PMMA. Groups B and C were filled to 25% of intact vertebral volume. All vertebral bodies were then retested to obtain post-treatment stiffness and failure load. Data between treatments and across repairs were compared using a two-way ANOVA ($p<0.05$) using a Tukey's *post-hoc* correction test for multiple comparisons.

RESULTS

Treatment with PMMA restored vertebral strength to 127% of intact (4168N±2288) and stiffness to 70% of intact (810N/mm±380). Treatment with calcium sulfate restored strength to 108% of intact (3429N±2440) and stiffness to 46% of intact (598N/mm±318). For strength (Figure 6), PMMA and calcium sulfate were not significantly different ($p=0.3$). Calcium sulfate approached, but did not achieve, statistical significance when compared to control ($p=0.06$). PMMA had significantly greater strength than control ($p=0.007$).

Figure 6: Failure Strength

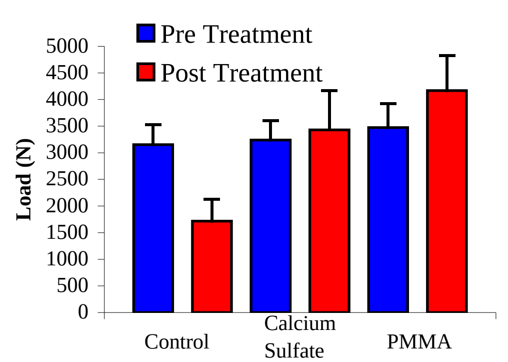

For stiffness (Figure 7), there was no difference between PMMA and calcium sulfate ($p=0.2$) while both were statistically greater than control ($p<0.05$). No statistically significant difference in T-scores or pre-treatment strength and stiffness values were found among the three groups.

Figure 7: Failure Stiffness

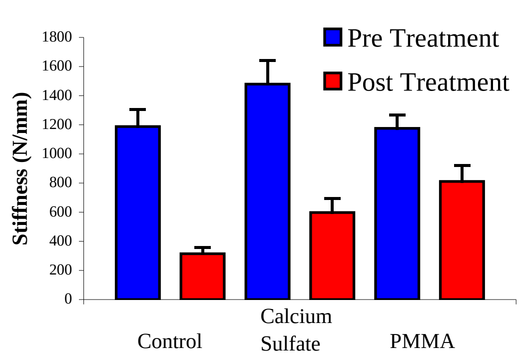

DISCUSSION

Use of calcium sulfate for kyphoplasty yields lower vertebral body strength and stiffness than PMMA kyphoplasty. This was not surprising given the much higher ex-vivo strength and stiffness profile of PMMA cement. The degree of restoration of strength with calcium sulfate was greater than expected, being slightly above pre-treatment intact bone which may reflect other properties of the cements such as filling differences. After kyphoplasty, high cement stiffness may be associated with increased adjacent level fractures in patients. The lower stiffness of calcium sulfate may potentially decrease this complication. Furthermore, calcium sulfate is non toxic, bio-absorbable, ostoeconductive and euthermic. These properties may lessen the likelihood of adverse tissue reactions and may make it a suitable agent for the incorporation of growth factors that increase bone density. Further studies are required to assess in-vivo degradation of calcium sulfate after kyphoplasty prior to clinical use.

ACKNOWLEDGEMENTS

The study was funded in part by Wright Medical, Inc.

BIOMECHANICAL EVALUATION OF A NEW FACET SCREW DESIGN FOR POSTERIOR SPINAL FIXATION

Andrew Mahar[1,2], Mike Rimlawi[2], Richard Oka[1], Michelle Wedemeyer[1], Andrew Perry[2], Steve Garfin[2], Choll Kim[2]

[1] Department of Orthopedics
Children's Hospital, San Diego
San Diego, CA
[2] Department of Orthopaedics
University of California, San Diego
San Diego, CA

INTRODUCTION

Posterior spinal fusions are indicated for spinal disorders such as degenerative disc disease, trauma and tumor. Adjunctive goals for spinal fusion are to limit fusion length without compromising stability and minimize tissue trauma. Despite positive reports, the use of facet screws for lumbar fusion has not gained significant popularity due in part to technical difficulties in screw placement. A new device has been designed to conquer some placement problems. The Triage Bone-LOK facet screw utilizes a variable length design that can be shortened in situ to the precise length needed. This variable length design achieves compression secondary to insertion across the joint. The combination of a self-tapping helical thread, cannulated design, and variable length make the device simple to apply. The current study biomechanically compared the new Triage facet screw to the standard cortical screw for posterior fusion through facet fixation.

METHODS

Five cadaveric lumbar spines were harvested retaining only ligamentous structures. Motion segments from L2-L3 and L4-L5 were randomly assigned to one of two repair groups for direct facet fixation using the Boucher technique. (Figure 1)

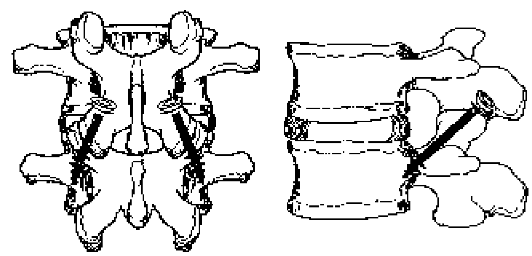

Figure 1: Facet screw fixation [1]

A 3.5mm cortical screw (Synthes) was used as the current clinical standard. The 3.5mm Triage Bone-LOK facet screw was inserted in an analogous technique over a guide wire. Physiologic moments of ± 5Nm were applied for flexion/extension and lateral bending. Torsion tests applied a 100N axial load and physiologic moments of ± 2Nm. All tests involved eight preconditioning cycles and data for displacement (mm), force (N), angle (degrees) and torque (Nm) were sampled at 10Hz for the duration of the test. Stiffness (Nm/deg) for each test condition was calculated during the final two cycles. Intact motion segments were tested first to establish intact stiffness measures. Three different fixation methods were evaluated. The first tested intact spines with facet screw fixation. The second tested spines with facet screws and discectomy without anterior column support. The third tested spines with facet screws and discectomy with anterior column support containing a compression-only load cell. Force data (N) from the device was collected at 10Hz. All data were normalized to the intact condition. The normalized data were then compared between fixation constructs using a one-way ANOVA ($p<0.05$) for each test.

RESULTS

The Triage facet screw was 65% more stiff than standard cortical screws for flexion tests with and without anterior structural support. This difference was not statistically significant ($p=0.4$). (Figure 2)

Figure 2: % Flexion Stiffness

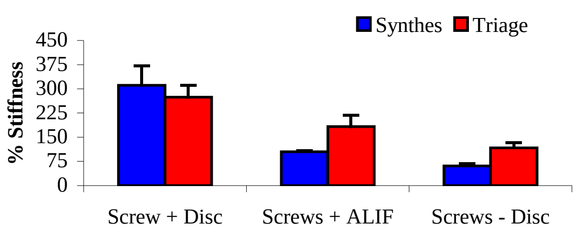

There was no difference for any test between devices for extension stiffness or lateral bending. For torsion tests with and without anterior structural support, the Triage facet screw was 50% more stiff compared to standard cortical screws. This difference approached, but did not achieve, statistical significance ($p=0.1$). (Figure 3)

Figure 3: % Torsional Stiffness

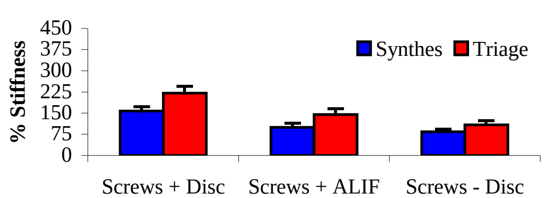

The compression only load cell for anterior structural support demonstrated magnitude and phasic responses similar to the input load. (Figure 4)

Figure 4: Compression Output

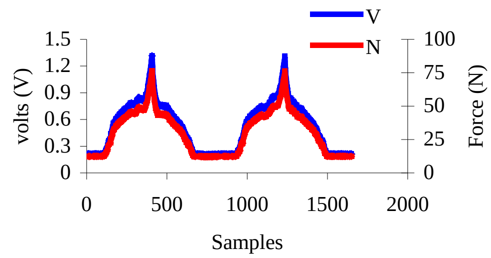

The Synthes facet screw had 4X greater fluctuations in load across the anterior column during flexion/extension testing.

DISCUSSION

When compared to the current clinical standard (3.5mm cortical screws), the Triage facet screw provided statistically equivalent fixation in all modes tested. In fact, these data indicate a generalized increase in motion segment stiffness associated with the Triage facet screw. The global stiffness data may indicate a greater likelihood of fusion or earlier fusion incorporation with the Triage device. This is also supported with the lower fluctuations in anterior column load demonstrated during flexion/extension testing with the Triage device.

REFERENCES

Ferrara, L.A. (2004). *Spine*, 28,1226-1234.

ACKNOWLEDGEMENTS

This study was funded in part by Triage Medical Inc.

Response Surface Analysis of Flexural and Membrane Stresses to Characterize Flexible Biologic Materials

Sean S. Kohles[1]
[1] Kohles Bioengineering, Portland State University, and Oregon Health & Science University, Portland, OR.
Email: ssk@kohlesbioengineering.com Web: www.kohlesbioengineering.com

INTRODUCTION

Three-point bending is a common experimental technique for determining the mechanical properties of hard tissues. However, the use of the governing equation for this method of evaluation is fraught with material and geometric assumptions, including: uniform cross-sections along the specimen length; a neutral axis about which flexural stresses exist; dominant flexural conditions without membrane stresses; and structural deflections that are sufficiently small (much less than the specimen thickness). The reality is that for many biomechanical bending tests, deflections are often measured beyond the thickness distance and yet still used for calculations of material properties. This is particularly true when tissues are tested to failure. Additionally, many soft connective tissues (ear cartilage, heart valves) experience large-deflection bending *in vivo* and bending experiments have provided functional insight [Vesely and Boeghner, 1989; Yu et al., 1993; Gloeckner et al., 1999; Roy et al., 2004].

In the following paper, the use of large-deflection plate theory is posed as a means to: 1) more accurately assess the results generated from standard three-point bending experiments which apply flexural and membrane stresses; and 2) determine distinct tensile and compressive moduli and Poisson's ratio through control of the bending stress state. The results are compared with that of the elastic curve equation. Although the plate equations are applicable to both hard and soft tissues, the intent here is to highlight the value of this theory as a tool for determining elastic moduli for highly flexible, cardiovascular and connective tissues. This type of mechanical analysis is also appropriate for functional engineered tissues in the early (fragile) states of development [Wilson et al., 2002; Saha et al., 2004]. In tissue engineering, extracellular matrix and scaffold content are being synthesized and degraded, respectively, according to synchronized time constants which may compromise mechanical integrity. Experimental data from published native cartilage is presented as a validation of this analytical approach.

METHODOLOGY

Deflection (z) of beams by integration, reduces the governing equation for beam curvature to two typical loading scenarios used during three-point bending analysis:

Point: $z_{max} = \dfrac{PL^3}{48EI}$; Distributed: $z_{max} = \dfrac{5P_0L^4}{384EI}$

applied to a beam of length (L), elastic modulus (E), and moment of inertia (I).

Deflection (w) from plate theory, solves the governing elasticity equation in which membrane and flexural stresses dominate a plate of length (a), width (b), and thickness (t), such that:

$$\frac{\sigma_z a^4}{E_x t^4} = K_1\left(\frac{w}{t}\right) + K_2\left(\frac{w}{t}\right)^3$$

for an applied transverse stress (σ_z), elastic modulus (E_x), and Poisson's ratios (ν_{ij}). If the flexible plate is assumed to have a large lateral dimension (y = b) and $\left(\dfrac{a^2}{b^2}\right),\left(\dfrac{a^4}{b^4}\right) \approx 0$, the coefficients K_1 and K_2 reduce to:

$$K_1 = \frac{\pi^4}{12(1-\nu_{xy}\nu_{yx})}, K_2 = \frac{\pi^4}{16} \text{ and}$$

$$K_1 = \frac{\pi^4}{12(1-\nu_{xy}\nu_{yx})}, K_2 = \frac{\pi^4}{16}\left(\frac{3-\nu_{xy}\nu_{yx}}{1-\nu_{xy}\nu_{yx}}\right)$$

for roller or hinge constrained, respectively. Thus the deflection of a central segment of width (Δb) and length ($x = 0$ to a), sufficiently far from the influence of the y-direction lateral edges ($y \approx b/2$), is equivalent to a dual-edge supported, narrow beam [Donnell, 1976].

Statistical response surface analysis of load versus deflection data, optimizes the fit of the appropriate bending equation in order to determine tensile and compression moduli as well as Poisson's ratios during small to large bending regimes.

RESULTS AND DISCUSSION

A comparison of analysis techniques applied to a published data set from bovine ear cartilage [Roy et al., 2004], indicated a variety of curve fits (Figure 1).

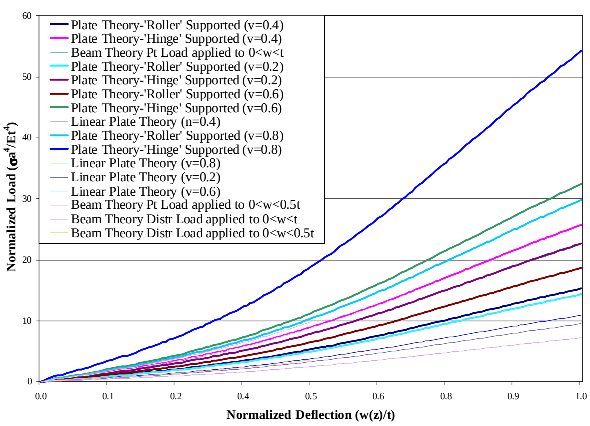

Figure 1: Variability in normalized curves for a single cartilage bending test.

Surface response modeling determined the optimal value of tensile elastic modulus (E) and Poisson ratio (ν) for this particular sample (Table 1).

Table 1: Optimization results.

Model	Modulus (MPa)	Poisson ratio	%RMS
Plate Theory 'Roller' Supported	4.872	0.2	5.71% b
	4.570	*0.4*	*4.86%* *
	3.738	0.6	6.49%
	2.344	0.8	10.08%
Plate Theory 'Hinge' Supported	3.080	0.2	15.00% c
	2.713	0.4	14.26% a
	2.154	0.6	13.27%
	1.288	0.8	11.77%
Linear Portion of Plate Theory	7.349	0.2	16.51%
	6.418	0.4	16.50%
	4.893	0.6	16.50% b
	2.751	0.8	16.50% a
Beam Theory Point Load 0<w<t	3.100	NA	16.50% c
0<w<0.5t	2.460	NA	17.33%
Beam Theory Distr Load 0<w<t	9.699	NA	16.50%
0<w<0.5t	6.771	NA	10.43%

*Root Mean Square error (%RMS) minimized for modulus and Poisson ra
a,b,c: Indicate similar curve fits

SUMMARY

The utility of plate theory is in the determination of tensile moduli and Poisson's ratios from experiments dominated by membrane stresses. During small-deflection bending of thick, more rigid materials, the measured elastic modulus is derived from tensile and compressive stresses culminating about a neutral axis. Ongoing analysis will determine both tensile and compressive moduli, which are often not equivalent in biologic materials or engineered tissues.

REFERENCES

Donnell, L.H.(1976) *Beams, Plates, and Shells*. McGraw-Hill.

Gloeckner, D.C. et al.(1999) *ASAIO*, **45**:59-63.

Roy, R. et al. (2004) *Biomed Mat Res*, **68A(4)**:597-602.

Saha, A.K. et al.(2004) *Ann Biomed Eng*, **32(6)**:650-660.

Vesely, I., Boughner, D.(1989) *J Biomech*, **22(6/7):**655-671.

Wilson, C.G. et al. (2002) *Arch Biochem Biophys*, **408(2):**246-254.

Yu, Q. et al.(1993) *Am J Physiol*, **265**:H52-H60.

ACKNOWLEDGMENT

This work was supported by the National Institutes of Health (NIDCR grant DE14288).

STABILIZATION OF INTERVERTEBRAL DISCS BY TISSUE ENGINEERED NUCLEUS REPLACEMENT: A BIOMECHANICAL FEASIBILITY STUDY

Frank Heuer, Cornelia Neidlinger-Wilke, Lutz Claes and Hans-Joachim Wilke

Institute of Orthopaedic Research and Biomechanics
University of Ulm, Germany

E-mail: hans-joachim.wilke@medizin.uni-ulm.de Web: www.biomechanics.de

INTRODUCTION

Intervertebral disc (IVD) prolapse has been reported to be most frequent in young adults [Jonsson et al., 1995]. Spinal fusion and discectomy are two common surgical procedures of treatment [Bao et al., 2000]. Rigid spinal fixation has several limitations due to the loss of segmental mobility and the potential progress of degeneration in adjacent segments. In contrast, discectomy benefits good short-term effects of pain relieve, but it reduces disc height and increases segmental instability. Restoring disc height and mobility would require a replacement of the morbid nucleus pulposus by an artificial compound. Recently, it has been shown that rebuilding the nucleus by seeding autologous cells inside the IVD is capable to enhance anatomical integrity, which also preserves vital structures maintaining nutrition transport and metabolism [Ganey et al., 2002].

In this study, we investigated whether implantation of the new tissue engineered nucleus implant into a spinal segment after a nucleotomy is able to restore disc height and flexibility.

METHODS

The implant basically consists of condensed collagen type-I matrix (Figure 1a). For clinical use, this matrix will be used for reinforcing and supporting the culturing of nucleus cells. In experiments, matrixes were concentrated with barium sulfate for x-ray purposes and cell seeding was disclaimed in order to evaluate the biomechanical performance of the collagen material.

The in vitro testing was performed on six lumbar functional spinal units (FSU), which have been taken from calves. Specimens were carefully stripped off soft tissue and muscle layers preserving all bony structures and ligaments. The cranial and caudal ends of the specimens were embedded into polymethylmethacrylate. In each specimen, an oblique incision was performed from a right lateral approach. Dissecting one annulus fibrosus fiber orientation preserves fibers of the other orientation achieving a minimal invasive access to the interior of the disc. Through this fissure an IVD defect was created by means of complete removal of the nucleus pulposus. Subsequently, the remaining cavity of the intervertebral disc was filled with the implant (Figure 1b). Proper application of the implant was controlled by radiographic visualization.

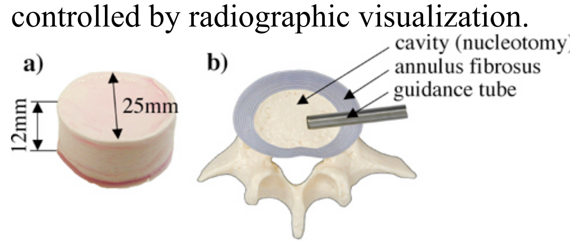

Figure 1: a) condensed collagen matrix, b) schematic implantation.

Spinal segment flexibility was assessed using a custom-built spine tester [Wilke et al., 1994]. Specimens were affixed in the spine tester, and subsequently forced by unconstrained pure moments of 7.5Nm to move towards spinal axial rotation, flexion/ extension and lateral bending in sequence (Figure 2d). For each tested stage (intact, nucleotomy, and implanted stage) flexibility and height measurements were obtained. Motion data were evaluated for range of motion (ROM) and neutral zone (NZ).

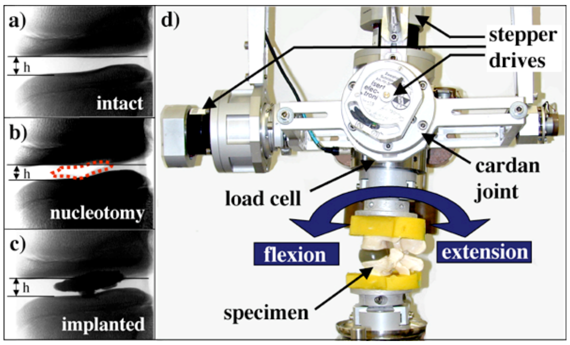

Figure 2: X-rays of a) intact, b) nucleotomy, and c) implanted stage. d) Spine tester.

RESULTS AND DISCUSSION

Removal of the nucleus reduced disc height by 0.9±0.5mm in respect to intact stage (Figure 2a-c). In contrast, implantation of the vital nucleus replacement increased the disc height by 0.6±1.0mm compared to intact stage. Averaged flexibility of intact specimens was in order of 7.9±4.3° ROM and 3.0±2.3° NZ towards spinal flexion/ extension (Figure 3). Nucleotomy caused a significant loss of stability resulted in 10.0±4.7° ROM and a NZ of 3.5±2.2° ($p<0.05$). Application of the implant significantly stabilized FSUs to a ROM and NZ of 7.6±2.0° and 1.4±0.3°, respectively ($p<0.05$). There was no statistical difference between the stability provided by the implant and intact stage. Results of movements in lateral bending and axial rotation show the same trend compared to flexion/extension, as previously described. However, during flexibility measurements, implant extrusions have been observed in three of six cases while loaded in right lateral bending.

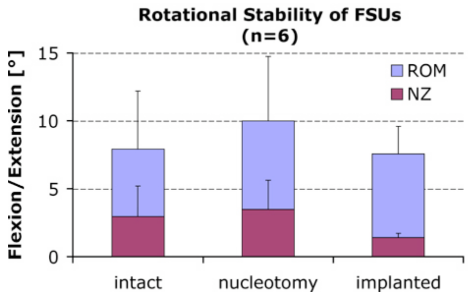

Figure 3: Stability in flexion/extension.

Artificial and tissue engineered nucleus replacement has been of great interest for orthopaedics and neurosurgeons in past five years. Early diagnostic and treatment of disc degeneration or even IVD prolapse are intended to be the main field for the new tissue engineered nucleus replacement.

The results of this study directly reflect the efficacy of vital nucleus replacement to restore disc height and to provide stability to intervertebral discs. However, from a biomechanical point of view the challenge is to employ an appropriate annulus fibrosus sealing method, which is capable to keep the nucleus implant in place over a long-time period. Securing the nucleus implant inside the IVD will be considered as an objective for future biomechanical studies.

REFERENCES

Bao, Q.-B., Yuan, H.A., (2000), *Neurosurg Focus,* **9**, 1-7.

Ganey, T.M., Meisel, H.J., (2002), *Eur Spine J,* **11**, 206-14.

Jonsson, B., Stromqvist, B., (1995), *Eur Spine J*, **4(4)**, 202-5.

Wilke, H.-J., Claes, L., et al., (1994). *Eur Spine J*, **3**, 91-7.

ACKNOWLEDGEMENTS

Supported by ARS-Arthro, Esslingen, Germany.

A COMPARISON OF VERTICAL GROUND REACTION FORCES BETWEEN ONE AND TWO-LEG DROP LANDINGS

Steven T. McCaw, Saori Hanaki, Meredith A. Olson, and Joshua J. Kauten

School of Kinesiology and Recreation, Normal, IL, USA
E-mail: smccaw@ilstu.edu Web: cast.ilstu.edu/mccaw

INTRODUCTION

Both the propulsion phase and landing phase of vertical jumps have been analyzed to quantify loads and understand performance. In addition to affecting performance, mechanical loading affects the osteogenic process and presents an injury risk. Measuring the vertical ground reaction force (vGRF)-time pattern to quantify force magnitude and timing, and the rate of force application (loading rate) provides an initial basis to better understand the loading associated with an activity. Research comparing one and two leg rope jumping (Pittenger et al, 2002) indicated that although the vGRF was higher for one leg landings, magnitude and loading rate values were not double those in two leg landings. Comparisons of the propulsive phase of one versus two leg vertical jumps have suggested that both the bilateral deficit (van Soest et al, 1985) and/or biomechanical factors (Vint & Hinrichs, 1998) affect performance. The purpose of this study was to compare vGRF parameters between one and two leg drop landings in a controlled landing situation.

METHODS

Nineteen healthy college age females (height 167.3 ± 6.1 cm; mass 58.2 ± 5.3 kg; age 20.5±1.2 y) provided informed consent. All participated in athletic activities involving landing. The study was conducted using a repeated measures design. Each participant completed ten trials of one-leg and ten trials of two-leg landing, a total of 20 landings. Participants were allowed to rest at their request. To eliminate order effects, landings were performed in random order. To control landing speed at 2.73 m/s, participants stepped off of a 38 cm take-off box aligned next to the force platform; the only instructions provided in both leg conditions were to "land comfortably".

Instrumentation: vGRF data were collected from a force platform installed flush with the floor. Landing stability was visually assessed. A typical vGRF-time curve in landing (Figure 1) is characterized by the presence of F1 and F2, peak vGRF values corresponding to the instances of complete forefoot contact and lowest vertical position of the heel, respectively. vGRF data were initially scaled to the participant's mass. Subsequently, for each trial in each of the different leg conditions, custom software was used to quantify the magnitude of and the time to both F1 and F2, in addition to quantifying loading rate (calculated twice, once as the slope of the vGRF time curve from initial contact to F1, and once from initial contact to F2, units of Body Weights per second (BW/s)).

For each dependent variable, the 10-trial mean value for each participant was calculated in each leg condition and entered into paired t-tests (α =.05) to test the significance of the observed difference between the mean values for the one and two leg landings.

RESULTS AND DISCUSSION

Although mean magnitude values for both F1 and F2 were significantly different, neither value was twice as high in one leg landings compared to two leg landings (F1 values 13.2 ± 3.4 vs 11.7 ± 2.7 N/kg; F2 values 43.0 ± 6.8 vs 29.9 ± 8.7 N/kg, one vs two leg landings respectively). Temporally, in one leg landings both F1 and F2 occurred later after initial contact, although only F1 was significantly different (F1 values 13 ± 3 vs 11 ± 3 ms, F2 values 48 ± 7 vs 47 ± 10 ms, one vs two leg landings respectively). Loading rate (LR) to F1 was not significantly different between the one and two leg landings (110.5 ± 30.6 vs 118.9 ± 44.8 BW/s, respectively), reflecting the inverse effect of the magnitude and temporal changes in F1. However, LR to F2 was significantly higher in one leg compared to two leg landings (97.9 ± 24.3 vs 72.5 ± 33.8 BW/s, respectively). The 135% higher value for LR to F1 in one leg landings reflects the higher force magnitude, since there were no temporal differences in F2 between the two leg conditions.

Since the vGRF reflects the net external force applied to the body, these results suggest that in a controlled situation, a participant must make neuromuscular adjustments during one leg landings to reduce the impulsive load applied to the body to a level similar to that imposed during a two leg landing. Since the adjustments must occur at the ankle, knee and hip joints, quantifying the joint kinetics and energetics would provide insight to the mechanism of neuromuscular control utilized to reduce the impulsive load.

Figure 1. Typical vertical ground reaction force – time curve.

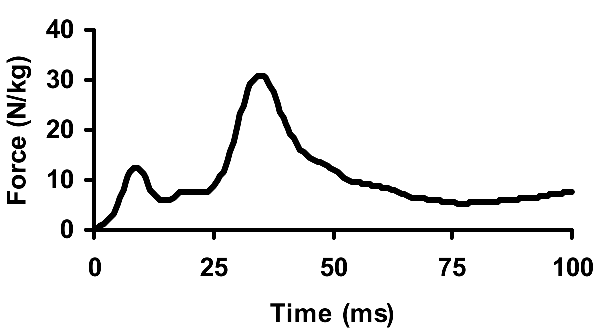

CONCLUSION

Vertical ground reaction force descriptors when landing on one leg are less than double the values exhibited when landing on two legs.

REFERENCES

Pittenger et al, (2002). *RQES*, **73**:445-449.
Vint & Hinrichs, *Proc. NACOB.,* 1998.
Van Soest et al, *MSSE*, **17**:635-639.

ACKNOWLEDGEMENTS

This project was funded by a *Jump Rope for Heart* grant from the Illinois Association for Health, Physical Education, Recreation and Dance, and a Research Grant from Illinois State University.

NORMAL VIBRATION FREQUENCIES OF THE VOCAL LIGAMENT

Ingo R. Titze[1,2] and Eric J. Hunter[1]

[1]National Center for Voice and Speech, A division of Denver Center for the Performing Arts, Denver, CO, USA
[2]Department of Speech Pathology and Audiology, The University of Iowa, Iowa City, IA, USA
E-mail: ehunter@dcpa.org Web: www.ncvs.org

INTRODUCTION

In previous studies of pitch control, it has usually been assumed that the ligament vibrates as a string with fixed boundary conditions, a uniform cross section, uniform tension, and negligible bending stiffness. The result of these assumptions are normal mode frequencies which were easy to predict using the ideal string law (e.g., Titze, Luschei and Hirano, 1989). However, recent attempts to reconcile human phonation frequencies with biomechanical data on vocal fold length and stress-strain characteristics of the ligament suggest that the ideal string law may underestimate the normal mode frequencies.

The purpose of this paper is to re-analyze the normal mode frequencies of the vocal ligament with the inclusion of bending stiffness and variable cross-section (at the macula flavae) in addition to tensile restoring forces. Both analytical and finite-element computational methods will be employed. The result will be based on actual measurements performed previously on human vocal ligaments (Min et al., 1995).

METHODS

A theoretical analysis of vibration of beams with longitudinal tension and bending stiffness was given by Morse (1936). Starting with his fourth-order differential equation, we assumed clamped boundary conditions at the posterior and the anterior endpoints. From this, an exact analytical solution was found for the vibrating bending ligament of uniform cross section (see complete steps in Titze and Hunter, 2004). Using constants selected from Min et al. (1995), the difference between the modal shapes and modal frequencies of the ideal string equation compared to the exact solution with bending was shown.

The effects of the macula flavae, gradual widenings of the cross sectional areas at the anterior and posterior endpoints, could not be solved using the analytical solution. Therefore, a second step was completed to investigate the modal frequencies of the vocal ligament. This was implemented with 100 finite elements using ANSYS for a structural beam (elements LINK10 for uniform beam with no bending and BEAM54 uniform with bending and non-uniform with bending).

For 20% elongation, the first several natural modes were found for the above analytical and finite element solutions. Also, for 1-50% elongation, mode 1 was found for the above models.

RESULTS AND DISCUSSION

For mode 1, neglect of bending stiffness lowers the frequency from 170 Hz to 130 Hz. For mode 4, neglect of bending stiffness lowers the frequency from 1030 Hz to 500 Hz. For 1% elongation, the contribution of bending stiffness and macula flavae raises the frequency from about 10 Hz to 100 Hz, a profound difference. At 50% elongation, the inclusion of bending stiffness and macula flavae raises the mode 1 frequency from 680 Hz to 770 Hz. The addition of the macula flavae raises the frequency by another 110 Hz. On a percentage basis, the bending stiffness reduces with increasing strain, whereas the macula flavae contribution remains roughly constant (about 20-30%).

The bending stiffness and non-uniform cross-sectional area of the vocal ligament appear to have an impact on the normal mode frequencies of the vocal ligament. With the mode shapes appearing visually similar to those of a simple string, it is understandable that the ideal string law has been the standard model. At low strains, the ideal string law underestimates the lowest mode frequency by an order of magnitude if bending stiffness is excluded.

Asymptotically, as strain goes to zero, bending moments alone can account for the restoring force of the tissue. In previous modeling (e.g., Titze and Story, 2002), a ground substance Young's modulus was used to account for this restoring force. At higher strains, bending moments become less significant as tension takes over. Macula flavae contributions remain relatively constant at about 30% increase in mode 1 frequency. Implementing the full mathematical complexity of bending stiffness and non-uniform area may not be suitable for simple models of vocal fold vibration. A rule is therefore adopted for the lowest string mode frequency between 10-50% elongation:

$$f = \frac{1}{2L} \left(\frac{\sigma}{\rho}\right)^{1/2} \left(1 - 0.45\ln(\varepsilon)\right)$$

which corrects for bending stiffness and the macula flavae.

For low pitches and in modal voice productions, the vocal fold length is mostly below the cadaveric resting length. Ligament tension does not play much of a role. The stiffness of the thyroarytenoid muscle fibers then dominate in F_0 control, rather than the ligament. It is not yet clear if bending stiffness plays a significant role in thyroarytenoid muscle vibration.

ACKNOWLEDGEMENTS

This work was supported by grant No DC04347-03 from NIH.

REFERENCES

Descout, R., Auloge, J.Y. and Guérin, B. (1980). I.C.A.S.S.P.

Perrier, P. Guérin, B. and Auloge, J.Y. (1982). F.A.S.E./D.A.G.A.

Min, Y. B., Titze, I. R., and Alipour-Haghighi, F. (1995). Ann. Oto. Rhinol. Laryngol.

Morse, P.M. (1936, reprinted 1976). Vibration and Sound. The Acoustical Society of America, New York, NY. Also published by McGraw-Hill, New York, 1948

Titze, I. R., Luschei, E. S., and Hirano, M. (1989). J. Voice

Titze, I. R., Story, B. H. (2002). J Acoust Soc Am.

Titze, I. R., Hunter, E. J. (2004). J Acoust Soc Am.

SHEAR-STRESS-INDUCED CHONDROCYTE DEATH IS REDUCED BY ANTIOXIDANT TREATMENT

James A. Martin, Anneliese D. Heiner, Benjamin R. Beecher, and Thomas D. Brown

Department of Orthopaedics and Rehabilitation, The University of Iowa, Iowa City, Iowa
Email: james-martin@uiowa.edu

INTRODUCTION

A history of joint injury is among the most significant risk factors for osteoarthritis (OA). Injury-induced, or post-traumatic, OA often develops within five to ten years of the injury, and the process depends in part on mechanical stress conditions in the healing joint (Beaupre et al., 2000; Stevens et al., 2001). The mechanisms linking joint trauma with post-traumatic OA are poorly understood. However, surface incongruities arising from incompletely-reduced joint fractures can lead to excessive mechanical stress at and around step-offs. Excessive shear stress appears to promote cartilage destruction and arthritis (Wilkins et al., 2000). Preliminary studies in our laboratory suggested that elevated shear stress leads to the release of reactive oxygen species (ROS) by chondrocytes. Oxidative damage resulting from chronically elevated ROS can accelerate cell senescence and induce apoptosis, suggesting a link between chondrocyte damage and subsequent cartilage degeneration (Toussaint, 2000).

Based on these findings, we hypothesized that excessive mechanical shear stress causes chondrocyte death *via* an oxidative mechanism. To test this, we cultured human cartilage explants in a mechanically active bioreactor, the Triaxial Compression Vessel (TCV), which is capable of modulating shear stress levels (Heiner and Martin, 2004). This device was used to test the effects of shear stress on chondrocyte viability. We also tested the effect of adding an antioxidant, n-acetyl cysteine (NAC), to determine the role of oxidants in mediating shear stress effects.

METHODS

Human cartilage explants (4 mm diameter) were harvested from non-osteoarthritic ankle joints from four donors. A subset of the explants was pretreated overnight with 2.5 mM NAC, and all explants were placed in the TCV for mechanical stress treatment. The TCV is a novel culture device capable of imposing variable shear stress states at quasi-physiologic levels. A water chamber applies transverse compression, and a piston applies axial compression. The interplay between axial and transverse compression determines shear stress levels. In this study, four different treatments (900 cycles at 1 Hz) were applied: 1) non-stressed control, 2) 5 MPa axial compression only (maximum shear stress), 3) 5 MPa axial plus 5 MPa transverse compression (minimal shear stress), and 4) 5 MPa axial plus 2.5 MPa transverse compression (intermediate shear stress). At least six explants were used for each treatment group. Following mechanical stress treatment in the TCV, explants were removed from the device and incubated overnight in calcein AM to stain viable cells. After cryosectioning, slides were mounted with DAPI to stain cell nuclei. Micrographs of the superficial, middle, and deep zones of the cartilage sections were taken under UV light (to image DAPI-stained nuclei) and under 488 nm light (to image calcein-stained cells). Total cells (DAPI-stained) and live cells (calcein-stained) were counted to determine percent viability. One-way

ANOVA and Tukey's test were used to evaluate the statistical significance of differences between treatment groups.

RESULTS AND DISCUSSION

Chondrocyte viability in all zones was high (>95% of unstressed controls) when explants were treated with low or moderate shear stress (5 MPa axial compression with either 5 MPa or 2.5 MPa transverse compression), but there was loss of viability when explants were treated with high shear stress (5 MPa axial compression alone). The highest loss of chondrocyte viability occurred in the superficial zone, where viability was reduced to less than 75% of unstressed controls (Figure 1).

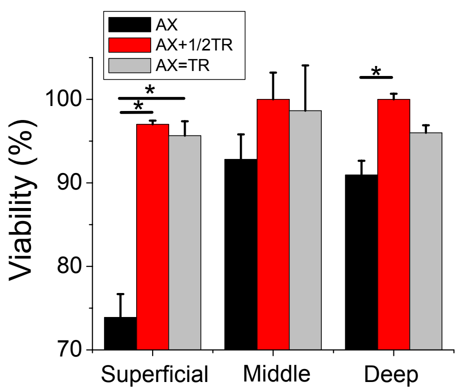

Figure 1. Effects of shear stress on chondrocyte viability (vs. unstressed controls). Explants were exposed to 5 MPa axial compression alone (AX), or 5 MPa axial compression plus either 2.5 MPa transverse compression (AX+1/2TR) or 5 MPa transverse compression (AX=TR). Bars and asterisks indicate significant differences ($p < 0.05$).

Pre-incubation of explants with the antioxidant NAC significantly reduced shear-stress-induced chondrocyte death in the superficial zone. NAC-treated explants exposed to high shear stress showed >85% viability in the superficial zone, which was not significantly different from the value for unstressed controls (93% viable) and significantly greater than in explants without NAC (<75% viable) (Figure 2).

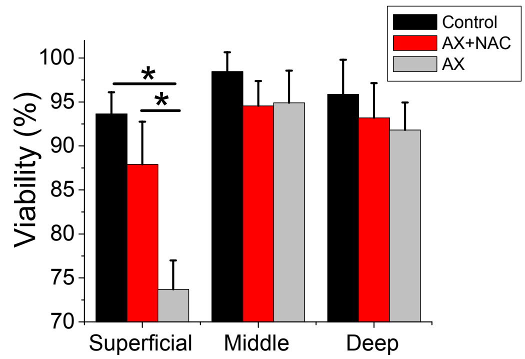

Figure 2. Effect of an antioxidant (NAC) on responses to high shear stress. Explants were unstressed (Control) or exposed to axial compression with NAC (AX+NAC) or without NAC (AX). Bars and asterisks indicate significant differences ($p < 0.05$).

SUMMARY

High shear stress induces chondrocyte death in the superficial zone of cartilage explants, and an antioxidant reduces this effect. These findings support the hypothesis that the harmful effects of shear stress on chondrocytes are mediated by oxidative stress. Also, antioxidant use may represent a possible preventative or treatment for post-traumatic OA.

REFERENCES

Beaupre G.S. et al. (2000). *J Rehabil Res Dev*, **37**, 145–151.

Heiner A.D. and Martin J.A. (2004). *J Biomech* **37**, 689–695.

Stevens D.G. et al. (2001). *J Orthop Trauma*, **15**, 312–320.

Toussaint O. et al. (2000). *Exp Gerontol*, **35**, 927–945.

Wilkins R.J. et al. (2000). *Biorheology*, **37**, 67–74.

ACKNOWLEDGEMENT

Supported by award 5 P50 AR048939, National Institutes of Health Specialized Center of Research for Osteoarthritis.

THE EFFECT OF HIGH INTENSITY STRENGTH TRAINING ON ANKLE INVERSE DYNAMICS IN BALANCE IMPAIRED OLDER ADULTS

Jennifer A. Hess

Department of Exercise and Movement Science, University of Oregon, Eugene, OR
E-mail: jhessdc@earthlink.net

INTRODUCTION

Fifty percent of all people over the age of 80 fall each year and the most common cause of accidental death in people over age 65 results from the impact associated with falling (Gehlsen 1990). Declines in the ability to respond to balance threats places older adults at risk for falling. Diminished balance capacity in the elderly may be due in part to loss of muscle strength. Leg muscle weakness, especially in ankle musculature, is a common factor in elderly fallers (Whipple 1987). Rovinovitch (2002) demonstrated that balance recovery limits increase as ankle torque increases and as the rate of ankle torque generation increases. It was hypothesized that 10-weeks of high intensity resistance training, focused on key postural muscles, would result in increased ankle joint moments, power and the rate of torque production and enhanced balance ability in balance impaired older adults.

METHODS

Participants were community dwelling balance impaired men and women aged 74-96 years. Thirteen subjects and fourteen controls completed the study. Participants were chosen based on having 2 of 5 balance impairment criteria: a low score on the Berg Balance Scale and TUG, plus either a history of balance impairment, gait abnormalities or poor tandem walking ability. Subjects participated in a 10-week high intensity exercise program while controls maintained their normal daily routine. Subjects trained 3 days a week, performing 3 sets of 8 repetitions at 80% of their 1 repetition maximum. Four key postural muscles quadriceps, hamstrings, tibialis anterior and gastrocnemius were trained on Maxicam and Hammerstrength training equipment.

Data were collect in the University of Oregon Motor Control Laboratory. Ankle joint kinematic data were collected using the Peak Performance Motion Analysis System, a 3-dimensional system using 6 cameras, positioned around the subject. A 2-dimensional, 4-segment, model of body motion (foot, shank, thigh and head-arms-trunk) was used to evaluate kinematics and kinetics. A 6-degree of freedom custom-built platform system with the ability to simulate slips and trips during quiet stance measured the ground reaction forces used to quantify reactive postural responses. Two conditions were evaluated, backwards sway in which the force platform translated anteriorly and forward sway in which the platform translated posteriorly.

RESULTS AND DISCUSSION

Following 10-weeks of strength training subjects were significantly stronger in all 4 posture control muscles, especially in ankle plantarflexors and dorsiflexors. Subjects also improved significantly on clinical measures of balance ability (BERG, TUG).

For the backward sway condition mean ankle moments increased significantly in subjects (Right: F =5.434, p=0.031, Left: F=4.058, p=0.058), following strength training (Figure 1).

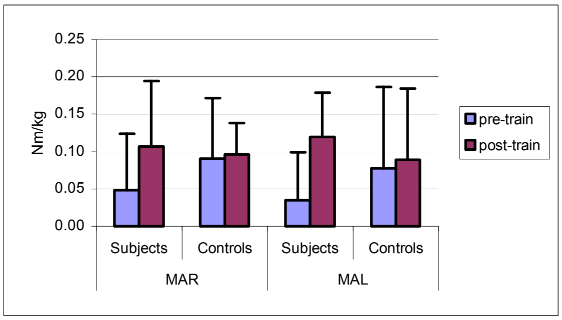

Figure 1. Mean Ankle Moments

Ankle rate of torque production also increased significantly in subjects (Right: F=6.951, p=.016, Left: F = 5.448, p=.031) following strength training (Figure 2). For the forward sway condition mean left ankle moment increased significantly in subjects (F=8.155, p=.009) while the right mean ankle moment approached significance (F=3.716, p=.067).

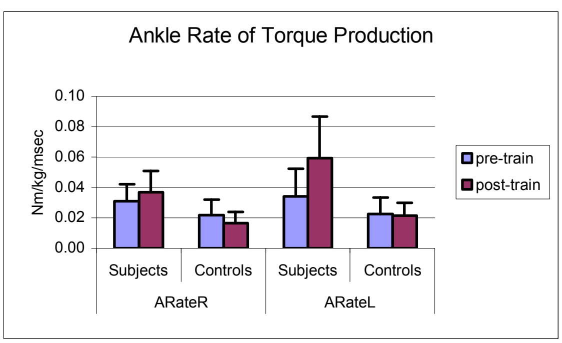

Figure 2. Ankle Rate of Torque Production

Ankle rates of torque production did not change significantly in subjects after training for the forward sway condition. However, maximum ankle joint powers increased significantly in subjects (Right: F = 11.049, p=.003, Left: F= 9.227, p=.006) after 10 weeks of strength training. Ankle ranges of motion (ROM) also improved in subjects following training.

Diminished lower extremity strength and slower reaction times have been associated with trip related falls in the elderly. Recovery from a balance threat depends in part upon ones ability to produce sufficient force in posture control muscles and more importantly, to do so rapidly enough to maintain the body's center of mass over the base of support. Reduced ankle ROM may contribute to smaller ankle moments and power. The biomechanical changes noted in this group of subjects suggest that balance improvements may be associated with a shift from a hip or stepping strategy common in balance impaired older adults, to a more ankle dominated strategy common in healthy older adults and young adults.

SUMMARY

This study demonstrated that high intensity strength training results in improved balance control in balance impaired older adults, as measured using validated clinical tools, and that balance improvements resulted from increased muscle force and power, and the ability to generate that force more rapidly.

REFERENCES

Gehlsen, GM, Whaley MH. (1990). *Arch Phys Med Rehabil*, 71:739-41.
Robinovitch SN, Heller B, Lui A, Cortez J. (2002). *J Neurophysiol*, 88:613-620.
Whipple RH, Wolfson LI, Amerman P. (1987). *J Am Geriatr Soc*, 35:329-332.

ACKNOWLEDGEMENTS

This study was supported by the Northwest Health Foundation Grant (#441791), The Center for Study of Women in Society Stanton Scholarship, and the Chiropractic Foundation for Education and Research.

Acute effect of vibration training with a portable muscle-tendon vibrator on muscle power

Jin Luo[1,2] Brian McNamara[2] Kieran Moran[1]

[1] School of Sport Science and Health, Dublin City University, Dublin, Ireland
[2] School of Mechanical and Manufacturing engineering, Dublin City University, Dublin, Ireland
Email: luo.jin2@mail.dcu.ie

INTRODUCTION

Vibration training has gained in popularity in recent years as a method of enhancing strength training (Cardinale and Bosco, 2003). We have developed a portable muscle-tendon vibrator which can be strapped to muscle tendon during strength training exercise. The aim of this study is to investigate the acute neuromuscular response to a bout of vibration training using this muscle-tendon vibrator.

METHODS

Fourteen healthy male volunteers took part in this study. Subjects were exposed to 4 experimental conditions in random order: 1) exercise with vibration (E+V); 2) exercise with sham-vibration (E+SV); 3) no exercise with vibration (NE+V); 4) no exercise with sham-vibration (NE+SV). The exercise was three sets of dynamic bicep curl (70% 1RM load) with the dominant arm. The vibrator was strapped on the bicep tendon and the vibration amplitude and frequency were 1.2mm and 65 Hz respectively. The power output of bicep curl was tested 5 min before the training and 1.5 min and 10 min after the training. Elbow joint angle and EMG of biceps brachii were measured. Mean angular power of concentric phase (P_{mean}) and this power at 100ms of the concentric phase (P_{100}) were calculated from the joint angle data. Average value of EMG ($EMG_{average}$) and mean power frequency of EMG (EMG_{mpf}) of the concentric phase were also analyzed.

RESULTS AND DISCUSSION

The inter-day reliability of P_{mean} and P_{100} were found to be 0.91 and 0.74 respectively. During vibration training, P_{100} was enhanced significantly by vibration in set1. P_{100} in set2 and set3 were significantly less than set1, but not significantly differ from the sham vibration group. With vibration, $EMG_{average}$ decreased significantly from set1 to set3. These results suggest that vibration does enhance the power output of muscle during training, and may also induce more muscle fatigue. The significant increase of EMG_{mpf} during vibration exercise suggests that more large motor units were recruited by vibration training (Rittweger et al., 2003). However, P_{mean} was not enhanced by vibration. It is suggested that in this kind of training (bicep curl with free weight), although the initial power (P_{100}) could be enhanced by vibration, subjects had to decelerate the weights in later part of concentric phase, and this may inhibit the mean power enhancement by vibration in the whole concentric phase. When there was no exercise during training, vibration seems to have a facilitatory residual effect on muscle power. This was shown by the significantly higher power (P_{mean} and P_{100}) in vibration group compared with sham-vibration group tested 1.5 min after vibration. It was also found that although power performance was enhanced after vibration, $EMG_{average}$ did not have any significant change. An increased neuromuscular efficiency that results from the increased temperature by vibration may be the underlying mechanism (Bosco et al., 1999).

Table 1: Percentage change of power (P_{mean} and P_{100}) during and after training (mean±SD)

Power	**Condition**	**Set1**	**Set2**	**Set3**	**Post-1.5min**	**Post-10min**
P_{mean}	E+V	-3.8±7.1	-2.9±12.5	-1.3±13.5	-1.3±15.4	3.2±12.2
	E+SV	2.3±9.8	2.4±9.0	-0.4±10.6	3.1±17.7	5.5±15.9
	NE+V	*Note*: ξ=significant difference compared with sham-vibration			2.8±10.7 ξ	-1.4±6.9
	NE+SV				-10.0±10.7	0.4±9.8
P_{100}	E+V	22.5±28.6 ξ	4.3±26.8 *	-2.9±28.3 *	4.3±40.0	16.1±47.1
	E+SV	5.0±22.7	2.8±22.3	4.6±27.2	-1.3±31.2	2.9±23.2
	NE+V	*Note*: *=significant difference compared with set1			29.6±39.0 ξ	7.8±26.8
	NE+SV				-15.8±33.5	6.9±35.6

Table 2: Percentage change of $EMG_{average}$ and EMG_{mpf} during and after training (mean±SD)

EMG	**Condition**	**Set1**	**Set2**	**Set3**	**Post-1.5min**	**Post-10min**
$EMG_{average}$	E+V	11.2±22.8	8.2±26.0	-0.5±15.7*	-1.8±17.8	-5.1±19.2
	E+SV	0.6±12.6	-3.0±12.4	-4.2±10.8	-6.9±8.9	-8.2±13.1
	NE+V				-7.2±10.8	-2.4±15.7
	NE+SV				-7.4±9.9	-1.7±12.8
EMG_{mpf}	E+V	-0.9±12.8	7.9±14.4 *	6.5±11.7 *	11.9±13.9	7.7±10.6
	E+SV	1.6±6.0	4.8±5.3	5.6±6.6	8.9±5.9	6.2±8.1
	NE+V	*Note*: *=significant difference compared with set1			-2.3±9.5	2.1±8.4
	NE+SV				0.0±13.1	-2.3±11.6

SUMMARY

The muscle-tendon vibrator developed in our study could stimulate muscle to exert greater power during strength training. More muscle fatigue was elicited by the strength training exercise with added vibration. There was a facilitatory effect on power performance immediately after vibration with no exercise.

REFERENCES

Bosco et al. (1999). *Eur J Appl Physiol*, **79**, 306-311

Cardinale and Bosco (2003). *Exerc Sport Sci Rev*, **31**(1), 3-7

Rittweger et al. (2003). *Clin Physiol Funct Imaging*, **23**, 81-86

ANGULAR MOMENTUM TRANSFER DURING A POWER TENNIS SERVE

Brian J. Gordon and Jesús Dapena

Biomechanics Laboratory, Dept. of Kinesiology, Indiana University,
Bloomington, IN, USA
E-mail: bgordon@indiana.edu

INTRODUCTION

The racquet speed needed for a power tennis serve requires a large amount of angular momentum in the hand+racquet segment just before impact. This angular momentum is a function of the angular momentum acquired by the legs from the ground, and its transfer through the body to the hand+ racquet segment. The purpose of this study was to measure the transfer of angular momentum to the hand+racquet segment in a power tennis serve.

METHODS

Eight NCAA Division I players were filmed with three motion-picture cameras. The DLT method was used to compute three-dimensional (3D) coordinates of body and racquet landmarks. The 3D coordinates were expressed in an orthogonal reference frame in which the X axis pointed to the right, the Y axis forward, and the Z axis up. Instantaneous angular momentum values were calculated for the individual body segments and for the racquet, relative to the body+racquet system center of mass (c.m.), from the instant of maximum knee flexion (MKF) to ball contact at 0.01 s intervals. Calculations were based on Dapena (1978). To simplify the analysis, the angular momentum terms for the segments and racquet were combined into six sub-systems: legs, trunk+head, left arm, hitting upper arm, hitting forearm, and hand+racquet. Transfers of angular momentum were expressed by the angular impulses exerted on each sub-system at its endpoints. These terms did not include the angular impulses of the sub-system weights about the system c.m. All values were averaged across subjects, and analyzed over three periods defined by: (1) MKF to racquet horizontal (HOR) in the backswing; (2) HOR to racquet head low point (RLP) at the end of the backswing; (3) RLP to contact.

RESULTS AND DISCUSSION

The Z components of angular momentum were small, and the Y components served mainly to position the system. The generation of racquet speed was driven primarily by the X components of angular momentum. Thus, the analysis focused on the acquisition and transfer of the X component of angular momentum, described as clockwise (CW) or counterclockwise (CCW) in relation to the view from the right side. To facilitate interpretations, CW values were considered positive.

The transfer of angular momentum between MKF and HOR is illustrated in Figure 1a. The legs received a large CW angular impulse from the ground. Most of it was transmitted to the trunk, where it accumulated. Only a small fraction was passed on to the hitting arm segments.

The transfer of angular momentum between HOR and RLP is illustrated in Figure 1b. The angular impulse to the system was much smaller. The trunk received angular momentum from the left arm and from the legs. Most of it was transmitted to the hitting upper arm, and half of this was passed on to the hitting forearm.

The transfer of angular momentum between RLP and contact is illustrated in Figure 1c. The legs lost angular momentum to the ground. Transfer of angular momentum into the trunk from the left arm was mostly negated by a small transfer from the trunk to the legs. The angular momentum stored in the trunk during the previous periods was transmitted through the hitting upper arm and forearm to the hand+racquet segment.

It has been speculated (Bahamonde, 2000) that the angular momentum transfer from the trunk to the hitting arm in the late part of the period between RLP and contact might be the result of torques exerted by the trunk extensor muscles. However, this would require the large transfer of CW angular momentum to the hitting arm to be coupled with a large transfer of CW angular momentum to the legs. In the present study, the transfer of CW angular momentum to the legs was very small. This suggests that the flow of CW angular momentum from the trunk to the hitting arm is due primarily to direct interaction of the trunk with the arm, and not a function of trunk extensor torque.

SUMMARY

Large amounts of angular momentum are first accumulated in the trunk during the backswing, and then transmitted to the racquet during the upward swing. Trunk extensor torques do not seem to play an important role in the final transmission of angular momentum to the hitting arm.

REFERENCES

Bahamonde, R.E. (2000). *J. Sport Sciences*, **18**, 579-592.

Dapena, J. (1978). *J. Biomechanics*, **11**, 251-256.

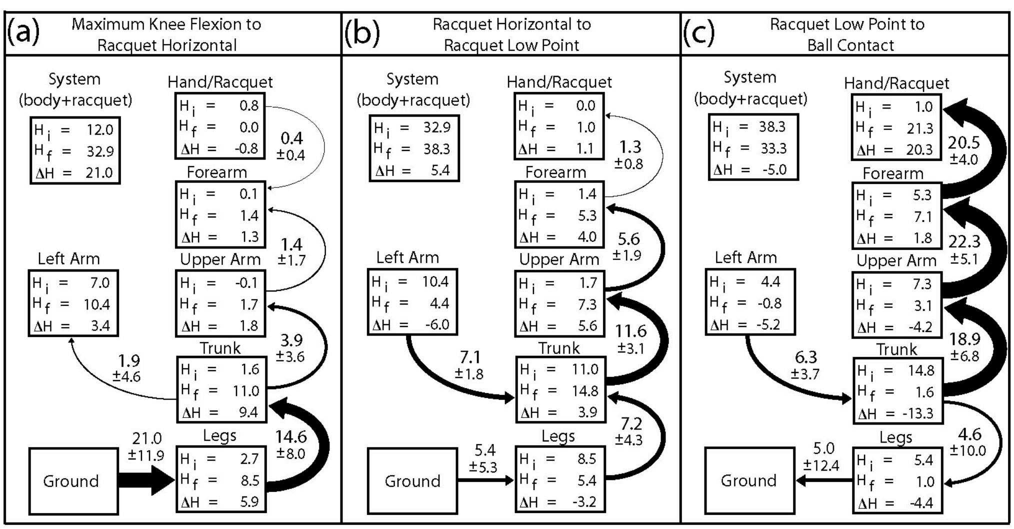

Figure 1: Angular momentum flow diagrams for the three periods: (a) MKF to HOR; (b) HOR to RLP; (c) RLP to contact. Boxes represent the six segment sub-systems, the body+racquet system, and the ground. Initial (H_i) and final (H_f) angular momentum (kg·m^2/s) about the X axis, and its change (ΔH), are given for each sub-system. The arrows and the values next to them show the directions and sizes of the angular momentum transfers (N·m·s).

MUSCLE WEAKNESS AND FORCE SHARING IN THE CAT HINDLIMB

Karyn M.A. Weiss-Bundy[1], Tim R. Leonard[2] and Walter Herzog[2]

[1] Human Performance Laboratory, Dept. of Mechanical Engineering, University of Calgary, Calgary, AB, Canada Email: karyn@kin.ucalgary.ca
[2] Human Performance Laboratory, Dept. of Kinesiology, University of Calgary, Calgary, AB, Canada

INTRODUCTION

One of the most basic problems in biomechanics is the so-called distribution (Crowninshield and Brand, 1981) or force sharing problem. Due to the redundant nature of musculoskeletal systems, the force sharing problem is concerned with determining the force contributions and the coordination of muscles to voluntary movement, stability, and control of joints. However, the properties of muscle can change over time due to use, injury, or illness, leading to the weakening of the muscle; which in turn affects the ability of the muscle to produce force and to control movements in an appropriate way.

It is desired to determine if the weakening of the force production capacity in one muscle of a functional group will alter the normal force sharing patterns observed between synergistic muscles. Misiaszek and Pearson (2002) conducted an initial study into this problem using a botulinum toxin type-A injection into the ankle extensor muscles of cats. Botulinum toxin type-A (BTX-A) is a neuromuscular blocking agent, which inhibits the fusion of acetylcholine with the motor nerve ending (Brin, 1997). Without the release of acetylcholine, the muscle fibres cannot be physiologically activated.

To examine the implications of muscle weakness on force sharing, this study investigated two synergistic muscles in the cat hindlimb: soleus and medial gastrocnemius. It was hypothesized that when the force production capability if soleus is reduced via an injection of BTX-A, a corresponding increase in the force production of the other synergistic muscles, represented by the medial gastrocnemius, would be seen.

METHODS

A skeletally mature, male cat (5.75 kg) was anesthetised using halothane. The soleus (SOL) and medial gastrocnemius (MG) muscles in the left hindlimb were surgically implanted with buckle-type muscle force transducers (Walmsley et al., 1978) and indwelling bipolar fine wire electrodes (Herzog et al., 1993) for the measurement of muscle forces and muscle activations, respectively.

At 6 days following the implantation surgery, kinematics, ground reaction forces, muscle forces and EMG recordings were taken. Kinematics and three-dimensional ground reaction forces of the cat during locomotion on a walkway were recorded using a high-speed video system and a set of walkway-embedded, animal size force platforms (AMTI). Four reflective, circular skin markers (diameter: 8mm) were placed over the hip, knee, ankle, and metatarsophalangeal joint of both hindlimbs to allow joint position identification in the subsequent digitization of the video.

Seven days following the implant surgery, the SOL muscle in the left hindlimb was surgically exposed and BTX-A was injected into the muscle belly of SOL to weaken it. A 100-unit vial of vacuum-dried Clostridium botulinum type-A (BOTOX, Allergan, Inc., Toronto, Ontario, Canada) was rehydrated with 0.9% preservative free saline to a concentration of 50 units/ml. The muscle belly was injected at multiple sites with a total dose of 40 units of BTX-A to increase toxin diffusion. The exposed muscle was irrigated with sterile saline solution prior to closing the incision site to remove any BTX-A, which may have seeped from the injection site. Following a 24-hour recovery period, data recordings of cat locomotion on the walkway were made over the next 13 days.

RESULTS AND DISCUSSION

The muscle force recordings from SOL show that the injection of botulinum toxin type-A into the muscle belly resulted in a loss of force production during locomotion (Fig. 1). Within 24 hours following the injection, the force had decreased by approximately 52%, and after 48 hours the loss of force was near complete (97%). Over the course of the remaining 12 days following the injection, the muscle force in SOL began gradually increasing from 3% of the pre-injection force level to 8%.

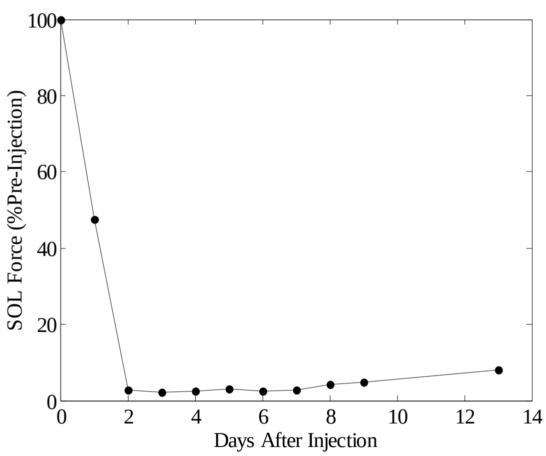

Figure 1: Soleus muscle forces as a percentage of pre-injection level (day 0).

However, a corresponding rise in the MG muscle force was not detected. The overall trend of the MG force, following the BTX-A injection of SOL, was observed to decrease slowly over the testing period. Therefore the original stated hypothesis of this study was not supported. In addition, throughout the post injection test period, the ground reaction forces exerted by the left hindlimb remained approximately constant, indicating that the left hindlimb was not being unloaded to a large extent.

One possibility for the lack of increase in the MG force production is simply that some diffusion of the botulinum toxin occurred from SOL into the neighbouring muscles. At the conclusion of testing, when the implantation site was surgically exposed, the buckle transducer was encapsulated in new tissue growth. This may have created an alternate force transmission route in the tendon, decreasing the MG force sensed by the transducer. Finally, it is possible that when the SOL muscle is weakened, the corresponding increase in force is occurring in synergist muscles other than MG, such as lateral gastrocnemius or plantaris, or that the ankle moments are reduced by small changes in walking kinematics despite similar ground reaction forces. Further research into the force sharing of the ankle extensor muscle of the cat hindlimb must be performed before more definitive conclusions can be made.

REFERENCES

Brin, MF (1997). *Muscle and Nerve*, **6**, S146-159.

Crowninshield, RD, and Brand, RA (1981). *J. Biomechanics*, **14**, 793-801.

Herzog, W, et al. (1993). *J. Biomechanics*, **26**, 945-953.

Misiaszek, JE, and Pearson, KG (2002). *J. Neurophysiology*, **87**, 229-239.

Walmsley, B, et al. (1978). *J. Neurophys.*, **41**, 1203-1216.

ACKNOWLEDGEMENTS

Natural Sciences and Engineering Research Council of Canada

AN ERGONOMICS INTERVENTION WITH CONSTRUCTION CONCRETE LABORERS TO DECREASE LOW BACK INJURY RISK

Jennifer A Hess[1] Steven Hecker[1] Marc Weinstein[2] and Mindy Lunger[3]
[1]Labor Education and Research Center, University of Oregon
[2] Lillis Business College, University of Oregon
[3]Student Health Center, University of Oregon
E-mail: jhessdc@earthlink.net

INTRODUCTION

Construction workers run a significant risk of musculoskeletal injury. Laborers have the highest risk occupation for work related back pain (Guo 1995). The placement of concrete in construction poses risks of musculoskeletal injury to laborers due to the weight of materials, frequent awkward postures, schedule pressures, and harsh environmental conditions. Ergonomic tools could decrease the risk of injury. Past studies of injury risk among construction workers have focused on observational or survey data. The goals of this study were to 1) evaluate the effectiveness of an ergonomic tool called a skid plate, for decreasing exposure to low back injury among concrete laborers and 2) explore instruments that could quantify the dynamic aspects of the low back in relation to injury risk.

METHODS

This study focused on laborers manually moving the hose that delivers concrete from a pumper truck to a placement site, in a case where pouring from above was not possible. The hypothesis tested was that skid plates would prevent hose joints from catching on rebar matting and allow the hose to slide more easily, reducing the need for repetitive bending and excessive force to move the hose. Four laborers were evaluated using the Lumbar Motion Monitor (LMM) developed at Ohio State University. The LMM is a portable tri-axial electrogoniometer that records position, velocity and acceleration in three planes of movement. The force used by workers to move the hose was measured with a dynamometer, while lifting frequency was collected by timing workers in several 10-minute increments. Workers were measured during three different but comparable concrete pours: Time 1, baseline, before introducing the skid plates, Time 2, using unmodified skid plates, and Time 3, after workers modified skid plate use by tying the concrete hose to the skid plates.

RESULTS AND DISCUSSION

Results showed that at Time 2, when skid plates were not secured, lumbar flexion and right sided bending increased significantly (Figure 1), while velocity and acceleration did not change (Figure 2). At Time 3, after workers modified skid plate use by tying the concrete hose to the skid plates, kinematic factors, including average twisting velocity and maximum lateral velocity were significantly reduced ($p<.001$).

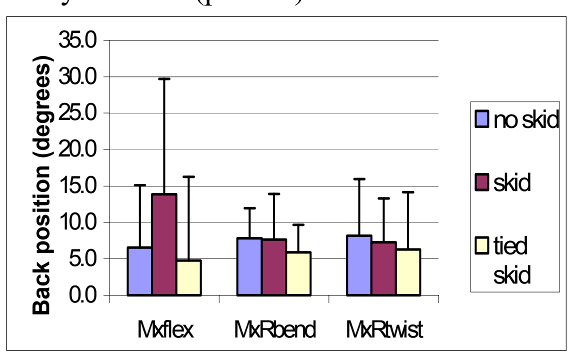

Figure 1: Low back position with skid plates

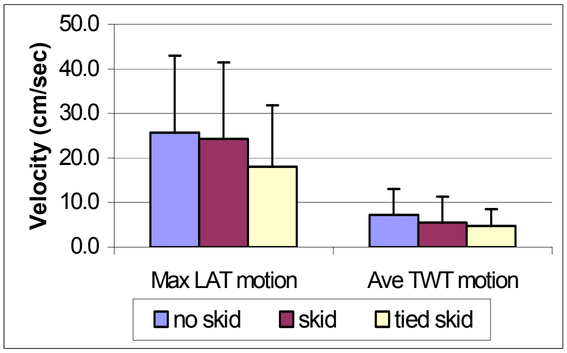

Figure 2: Low back velocity with skid plates

These are two of five factors found by Marras (1993) to be associated with risk of occupationally related low back disorder (LBD). Maximum frontal, sagittal and axial acceleration, in the lumbar region, were also significantly reduced after skid plates were secured ($p<.01$). Estimates of low back moments calculated using acceleration data, demonstrated that the maximum lumbar moment was significantly decreased in all three planes of motion when using secured skid plates ($p<.05$-$.001$) (Figure 3).

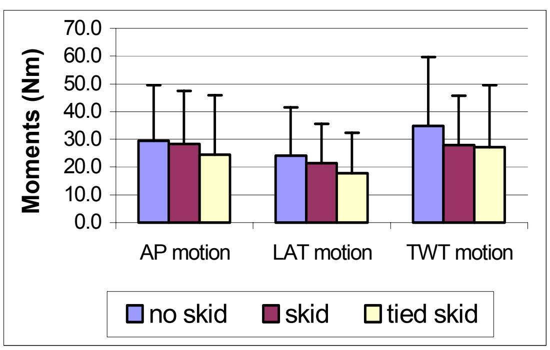

Figure 3: Low back moments

As results from biomechanical studies become available, it is evident that in addition to handling heavy loads and repetitive activities, asymmetry and kinematics such as trunk velocity and acceleration, and more importantly, the interactions among these factors are integral to understanding injury risk. Further, load moment has also been associated with the risk of LBD by Marras (1993). The findings of this study suggest that use of secured skid plates, during horizontal concrete hose movement, decreases factors associated with exposure to low back injury group membership (Figure 4). In concrete laborers the risk of low back injury group membership decreased from 46% to 67% when using secured skid plates.

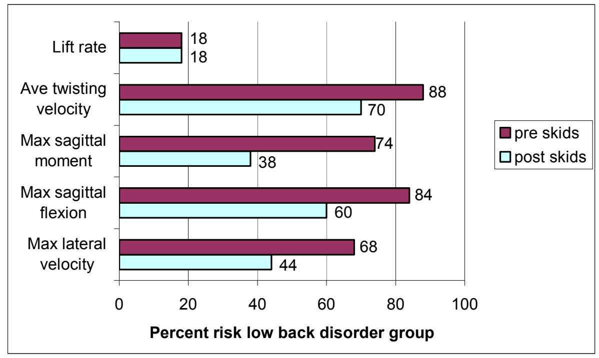

Figure 4: Risk of low back injury group risk.

SUMMARY

For laborers pulling concrete hoses, use of secured skid plates decreased awkward postures, velocity, acceleration and force in the lumbar region. Use of unsecured skid plates significantly increased flexion and right sided bending. These changes may play a part in reducing injury risk. For concrete laborers the LMM proved to be an effective field tool for evaluating dynamic lumbar spine movements during work activities.

REFERENCES

Gou, H.R. et al (1995). *Am J Ind Med,* **28**,591-602.

Marras, W.S. et al (1993). *Spine*, **18**, 617-628.

ACKNOWLDGEMENTS

National Institute for Occupational Safety (NIOSH) through the Center to Protect Workers Rights NIOSH grant no. U02/CCU317202

AN EMG DRIVEN OPTIMIZATION MODEL FOR ESTIMATING DYANAMIC KNEE MUSCLE FORCES WITHOUT MAXIMUM VOLUNTARY CONTRACTION TESTS

Bing Yu and Evan J.X. Tong

Center for Human Movement Science, Division of Physical Therapy, The University of North Carolina at Chapel Hill, Chapel Hill, NC, USA

INTRODUCTION

Anterior cruciate ligament (ACL) injuries are common in sports. Women are at a greater risk for ACL injuries than men. Neuromuscular control has been proposed as factor responsible to the elevated risk for ACL injuries in women. Previous studies show significant gender differences in lower extremity kinematics and kinetics when performing athletic tasks, but have not establish the relationship between the observed gender differences in motion patterns and the risk for ACL injuries. To further investigate the risk factors for ACL injuries, a musculoskeletal model is needed to estimate dynamic knee muscle forces in athletic tasks. The purpose of this study was to develop an EMG driven optimization model to estimate dynamic knee model forces in athletic tasks without maximum voluntary contraction tests.

METHODS

The muscle fiber force was expressed as the sum of forces generated by the contractile and parallel elastic elements. The force generated by the contractile element was expressed as a function of dynamic EMG, EMG-to-force gain, muscle physiological cross section area, muscle length-tension adjustment, and velocity-tension adjustment. The force generated by the parallel elastic element was expressed as a function of muscle specific stress, muscle physiological cross section area, and parallel elastic length-tension adjustment. The muscle origin and insertion coordinate, physiological cross section area, optimum fiber length, muscle tendon length, muscle maximum contraction velocity, and muscle pinnation angle data, and length-tension and velocity-tension relationships in the relevant literature were used in the model to determine muscle length, PCSA, length-tension adjustments and velocity adjustments. Force fiber force was converted to the muscle tendon force using the muscle pinnation angle. Vastus medialis, lateralis, and intermedius, rectus femoris, semimembranosus, semitendinosus, biceps femoris long and short heads, medial and lateral gastrocnemius were considered as the knee flexion-extension moment generators. EMG-to-force gains and muscle specific stresses were optimized to minimize the sum of squares of the differences between the muscle generated knee flexion-extension moment and knee resultant flexion-extension moment, subject to the constraints to the muscle EMG-to-force gains and muscle specific stresses.

Five male and five female recreational athletes were recruited as the subjects. Three-dimensional (3D) kinematics and kinetics, and EMG were collected for a stop-jump and a running task. Knee joint resultants were estimated using an inverse dynamic procedure. EMG signals were band-pass filtered (10 – 300 Hz) and then low-pass filtered (6 Hz) for linear enveloped

EMG. The stop-jump and running tasks were rotated as calibration and validation tasks to validate the estimated EMG-to-force gains and muscle specific stresses. Regression determinant (R^2) and mean error (e) between muscle generated knee flexion-extension moment and knee resultant flexion-extension moments were used to evaluate the quality of predicated knee flexion-extension moment.

RESULTS AND DISCUSSION

The proposed EMG driven optimization model predicted knee flexion-extension moment for calibration tasks with a good accuracy (Figures 1 and 2, and Table 1). The accuracy of the predicated knee flexion-extension moment was decreased for validation tasks (Table 1).

The ability of the proposed EMG driven optimization model to predict knee flexion-extension moment for the calibration task was comparable to the similar models in literature. The decreased ability to predict knee flexion-extension moment for the validation task might be due to (1) assumed linear EMG-to-force relationship, and (2) lack of consideration of the relationship between muscle activation level and muscle length-tension relationship. Adding a non-linear EMG-to-force relationship is most likely to improve the ability of the proposed model to predict the knee flexion-extension moment in validation tasks.

REFERENCES

Kaufman, K.R. et al. (1989). *J. Biomech*, **22**, 943-949.

Kaufman, K.R. et al. (1991). *Am. J. Sports Med.* **40**, 781-792.

Lloyd, D.G., Besier, T.F. (2003). *J. Biomech*, **36**, 765-776.

Table 1. Regression determinant between predicted knee flexion-extension moment and knee resultant flexion-extension moment.

Calibration Task	Gender	Jump	Run
Jump	M	0.8029	0.5327
	F	0.9282	0.7141
Run	M	0.6319	0.8368
	F	0.6498	0.8786
Jump and Run	M	0.7967	0.7894
	F	0.8879	0.8304

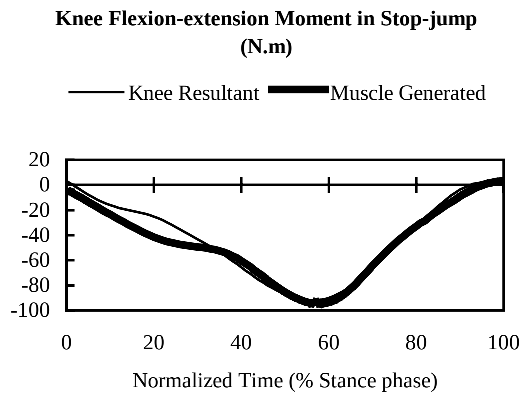

Figrue 1. Estimated muscle generated knee flexion-extension moment in the stop-jump task with the stop-jump task as the calibration task.

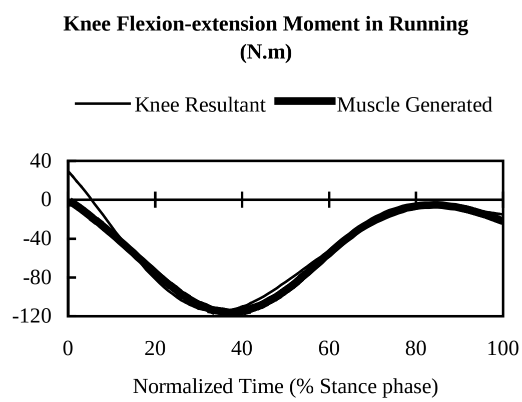

Figure 2. Estiamted muscle generated knee flexion-extension moment in running task with the running task as the calibration task.

TIBIOFEMORAL LOAD DISTRIBUTION DURING GAIT OF NORMAL SUBJECTS

Rose F. Riemer[1,2], Tammy Haut Donahue[2], and Kenton R. Kaufman[1]

[1]Motion Analysis Laboratory, Mayo Clinic, Rochester, MN, USA
[2]Mechanical Engineering, Michigan Technological University, Houghton, MI, USA
Email: Kaufman.Kenton@mayo.edu Web: http://researchweb.mayo.edu/biomechanics/

INTRODUCTION

Instrumented gait analysis has become a standard method of precisely analyzing movement. Current gait analysis methods report the intersegmental forces and moments at the joint center. However, the internal loading environment is only implied from the external forces. The purpose of this study was to analyze the knee force distributions during gait for normal individuals using a validated tibio-femoral model that includes subject-specific geometry and gait inputs.

METHODS

Seventeen subjects (age 29 ±8.8 years, 12 female, 5 male) were recruited on a volunteer basis to participate in the study. Knee radiographs were taken and gait analysis was completed for each subject. The radiographs were inspected by a radiologist for evidence of osteoarthritis, in which case the subject was excluded. All subjects were free of musculoskeletal impairments.

Knee geometry data inputs

The knee geometry for each individual was obtained from fluoroscopy-guided, weight-bearing radiographs that imaged the tibial plateau in a reproducible position (Buckland-Wright 1995). These radiographs were analyzed with an edge detection algorithm (Mathworks, Natick, MA) developed to measure the minimum joint space width (Schmidt, et al. 2004). The femoral condyle shape was approximated as a segment of a circle that fit the data points.

Motion analysis data collection

The gait parameters were calculated using a 10 digital camera motion analysis system sampled at 60 Hz (Eagle 1 EVa RT -Motion Analysis Corporation, Santa Rosa, CA). A set of 21 reflective markers was placed on each subject (Kadaba et al. 1989). The level walkway contained four force plates (Advanced Mechanical Technology, Inc., Watertown, MA; Kistler Instrument Corp, Amherst, NY). A set of stairs with six steps (16.5cm rise by 28cm run) was used for collecting stair gait data. The third and fourth steps had force plates (Advanced Mechanical Technology, Inc., Watertown, MA). The 3D marker coordinates and force plate data were used as input to a commercial software program, OrthoTrak 5.0 (Motion Analysis Corp., Santa Rosa, CA), to calculate the intersegmental joint kinematics and kinetics which were then input into the analytical model.

Analytical model

A validated, mathematical model was used to calculate the load distribution across the tibial plateaus, using subject-specific loads and geometry (Riemer, et al. 2003). The tibia and femur were modeled as rigid bodies, the cartilage as linear springs and collateral ligaments as piece-wise linear springs. Intersegmental forces and moments at the knee joint were used as inputs to the analytical model. The quadriceps, hamstrings, and gastrocnemius forces were calculated from the joint moments and angles collected with the gait analysis system (Morrison 1970). The muscle activation pattern matched the normal EMG pattern (Perry 1992).

RESULTS AND DISCUSSION

An average peak load of 2.4±0.2 times body weight (xBW) was found for level walking, 3.7±0.6 xBW for ascending stairs, and 3.4±0.4 xBW for descending stairs (Figure 1). Previous models have calculated slightly higher peak loads at the knee. (Morrison 1968; Morrison 1970; Mikosz, et al. 1988; Schipplein and Andriacchi 1991) None of these studies used subject-specific geometry in their computations as the present study does.

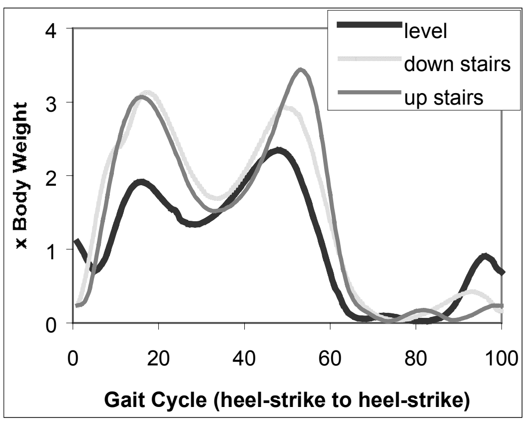

Figure 1: Average total loads experienced at the knee for stair and level gait.

The medial-lateral distribution was calculated and a higher medial load was found for level walking than for the stair walking (Table 1).

Table 1: Force distribution (% total load) on the medial plateau at the maximum load for level and stair walking (n=17)	
Level	68 ±16 %
Up stairs	58 ±13 %
Down stairs	58 ±17 %

Hsu et al (1990) used a similar mathematical technique and reported medial loads of 75% during static stance. Schipplein and Andriacchi (1991) found an average 71% of the load transferred through the medial plateau at the peak load during gait. This compares with the current study's average medial load of 68%. Medial-lateral distributions during stair gait have not been calculated before.

SUMMARY

A subject-specific tibiofemoral knee model was used to calculate peak loads and medial-lateral force distribution during level and stair gait. Gathering specific information about internal knee loads during gait may lead to improved understanding and treatment of the degenerative diseases such as osteoarthritis.

ACKNOWLEDGEMENTS

This study is funded by NIH grant # R01 AR048768

REFERENCES

Buckland-Wright, C. (1995) *Osteoarthr. Cartil.* **3**(Suppl A): 71-80.
Hsu, R.W., et al. (1990). *Clin. Orthop.* **255**: 215-227.
Kadaba, M, et al. (1989). *J. Orthop. Res.* **7**(6): 849-60.
Mikosz, R., et al. (1988). *J. Orthop. Res.* **6**(2): 205-214.
Morrison, J.B. (1970). *J Biomech.* **3**: 51-61.
Morrison, J.B. (1968). *Biomed Eng* April 1968:164-170.
Perry, J. (1992). *Gait analysis: normal and pathological function*. Thorofare, NJ, Slack Inc.
Riemer, R.F., et al. (2003). *Proceedings of ASB*, Toledo, OH.
Schipplein, O., Andriacchi, T. (1991). *J. Orthop. Res*. **9**: 113-119.
Schmidt, J.E., et al. (2004). *Transactions of ORS* Vol.**29**. Poster #1000.

EFFECTS OF AGE GROUP ON LANDING MECHANICS IN THE ADOLESCENT FEMALE BASKETBALL PLAYER

Thomas Kernozek[1], Hanni Cowley[1], and David Carney[1]

[1]Biomechanics Laboratory, Department of Health Professions, University of Wisconsin – La Crosse, La Crosse, WI, USA
E-mail:kernozek.thom@uwlax.edu

INTRODUCTION

Female athletes may be 2.4 to 9.7 times more likely to sustain an anterior cruciate ligament (ACL) injury than males (Arendt et al., 1995; Gwinn et al., 2000). The majority of ACL injuries (78%) are from non-contact injuries such as planting, cutting, or landing from a jump (Noyes et al.,1983). In a retrospective survey on female basketball players, 58% reported landing from a jump when the injury occurred (Gray et al., 1985). The ACL is most susceptible to injury when the body is in forward flexion, hip adduction, internal rotation, 20-30° of knee flexion, external rotation of the tibia, and foot pronation (Ireland et al., 1997). Females are more likely than males to land with these risky characteristics, especially increased knee valgus (Chappell et al., 2002; Ford et al., 2003) and decreased knee flexion (Chappell et al., 2002). A combination of biomechanical, neuromuscular, hormonal, and anatomical differences may contribute to gender differences in ACL injury and landing mechanics.

Jump-training programs that include stretching, plyometrics, and weight lifting have been shown to not only decrease varus and valgus moments at the knee, but also decrease the rate of non-contact ACL injuries (Hewett et al., 1996; Hewett et al., 1999).

Research studies have yet to evaluate athletes of different age groups. Identifying when these landing differences occur during age may indicate when training programs should be implemented to have the greatest impact on decreasing the risk of ACL injury.

METHODS

Forty-two female basketball players (14 sixth graders, 17 ninth graders, and 11 twelfth graders) without history of knee injury participated in this study. Athletes completed a five-minute warm-up on a stationary bike prior to testing. Static measurements obtained were height, weight, hip width, femur length, tibial femoral angle, and navicular drop. Knee extension and flexion strength was measured using a Cybex isokinetic dynamometer at 180°/s. Abductor hip strength was measured using a hand-held dynamometer affixed to an anchoring station.

Three-dimensional motion analysis system (Motion Analysis, Santa Rosa, CA) recorded the movement of the hip, knee, and ankle, as defined by the Helen Hayes marker set, while performing a drop-landing from a height of .40m. Signals from the Bertec force platform were collected at 1200 Hz and synchronized with kinematic data (Wilson et al., 2000).

Statistics were calculated using ANOVA.

RESULTS AND DISCUSSION

All athletes performed forefoot-to-rearfoot landings and the group mean landing phase times were not different between groups ($p>0.05$). At initial contact 6th grade athletes landed with significantly more knee valgus than 9th grade ($p<0.05$). (Figure 1)

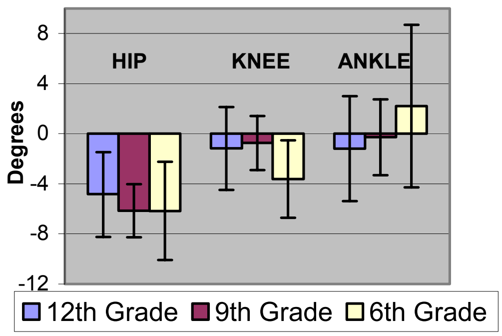

Figure 1: Frontal Plane Motion at Initial Contact (Positive values indicate hip and knee varus, and ankle supination. Negative values indicate hip and knee valgus, and foot pronation.)

The maximum range of motion in the frontal plane was not different among the three groups ($p>0.05$). All three age groups landed in a more extended position at initial contact comparable to results of Decker et al. (2003) and Huston et al. (2001). The peak joint moments were not different in the frontal plane ($p>0.05$), but were different in the sagittal plane at the knee between participants in 6th and 12th grade ($p<0.05$). (Figure 2)

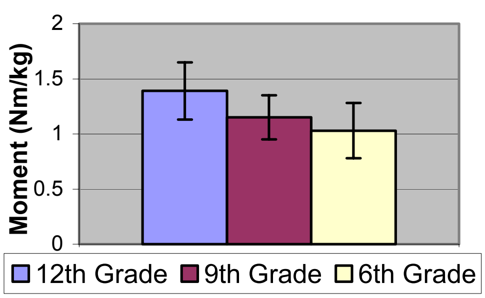

Figure 2: Peak Sagittal Knee Moments

Hip abduction strength, q-angle, navicular drop, and quadriceps/hamstring strength were not different among the three groups ($p>0.05$). The peak braking force was also less in 6th grade than 9th grade participants ($p<0.05$).

SUMMARY

All three age groups tended to demonstrate landing mechanics that may place them at risk for injury: knee valgus on contact with a more erect position. These results suggest that implementation of jump-training programs may benefit female athletes as young as 6th grade if the goal is specifically to alter these kinematic factors. Younger participants may be already demonstrating mechanics that may be a risk factor for ACL injury.

REFERENCES

Arendt, E. et al. (1995). *Am J Sports Med,* **23**,694-701.

Chappell, J.D. et al. (2002). *Am J Sports Med,* **30(2)**, 261-7.

Decker, M.J. et al. (2003). *Clin Biomech,* **18(7)**, 662-9

Ford, K.R. et al. (2003). *MSSE*, **35(10)**1745-1750

Gray, J. et al. (1985). *Int J Sports Med* **6**: 314-6.

Gwinn, D.E. et al. (2000). *Am J Sports Med,* **28(1),**98-102.

Hewett, T.E. et al. (1996). *Am J Sports Med,* **24(6)**, 765-773.

Hewett, T.E. et al. (1999). *Am J Sports Med,* **27(6)**, 699-705.

Huston, L.J. et al. (2001). *Am J Knee Surg,* **14**, 219-220.

Ireland, M.L. (1997). *J Sport Rehab,* **34(2)**, 97-110.

Noyes, F.R. et al. (1983). *J Bone Joint Surg*, **65A**, 154-174.

Wilson, J. et al. (2000). *MSSE,* ***33(1),***142-7.

ACKNOWLEDGEMENTS
This study was funded by a UW-La Crosse Graduate Student Research Grant and NATA Research Foundation Grant (Osternig Masters Grant).

VARIATION IN MUSCLE MOMENT ARMS WITH INDEX FINGER POSTURE

Derek G. Kamper[1,2], Erik Cruz[2], Heidi Waldinger[2]

[1] Department of Physical Medicine and Rehabilitation, Northwestern University Feinberg School of Medicine, Chicago, IL, USA
[2] Sensory Motor Performance Program, Rehabilitation Institute of Chicago, Chicago, IL, USA
E-mail: d-kamper@northwestern.edu Web: www.smpp.nwu.edu/hand%20lab/index.htm

INTRODUCTION

Determining the effects of the finger muscles on torque generation at the joints is complicated by the intricate anatomy of the fingers. For the index finger alone, 7 muscles, each spanning at least two of the three finger joints - metacarpophalangeal (MCP), proximal interphalangeal (PIP), and distal interphalangeal (DIP) - coordinate finger movement. On the palmar side of the finger, the flexor digitorum superficialis (FDS) and profundus (FDP) travel through anatomical pulleys. On the dorsal side of the finger, the tendons of the extensor indicis (EI) and digitorum communis (EDC) merge with those of the first doral interosseous (FDI), first palmar interosseous (FPI), and first lumbrical (LUM) to form the extensor hood.

While efforts have been made to estimate the moment arms for these muscles for specific sets of joint angles (An et al., 1983; Fowler et al., 2001), their alteration with different joint angles has not been systematically described. The goal of this study is to elucidate these relationships using in vivo methods in human subjects.

METHODS

Intramuscular electrical stimulation was performed on the muscles of the index finger in two subjects. Two stainless steel fine-wire electrodes (55 µm in diameter) were inserted into each of the 7 muscles of the index finger. A series of stimulation pulses, (280µs pulse-width, 35 Hz) was delivered for one-half second across the pair of wires to each muscle, in turn, by triggering an electrical stimulator (Compex Technologies, Inc.). Tetanic muscle contraction was thereby induced.

The resulting forces and moments produced at the fingertip were measured with a 6 degree-of-freedom load cell (JR3, Inc.). The fingertip was affixed to this load cell by set screws contacting a fiberglass cast placed on the fingertip. The wrist and forearm were also placed within a fiberglass cast which was clamped to a table to prevent any alteration in hand orientation or position.

Twelve postures were tested, chosen randomly from the possible combinations of MCP flexion ({-20°, 0°, 30°, 60°}, negative value denotes extension) with (PIP, DIP) flexion ({(0°, 0°), (30°, 0°), (60°, 30°)}). For a given muscle, stimulation amplitude was kept constant across all 12 postures to maintain a given level of activation.

Joint torques for DIP flexion/extension, PIP flexion/extension, MCP flexion/extension, and MCP abduction/adduction were calculated from the recorded forces and moments using the transpose of the Jacobian matrix.

RESULTS AND DISCUSSION

Finger posture had a substantial effect on joint torque magnitude. For example, MCP flexion torque for certain postures was only 30% of the value recorded for other postures during stimulation of FDS and FDP. This disparity is much greater than the difference attributable to changes in muscle length-tension properties and greater than what has been reported in the literature (Fowler et al., 2001).

For FDI, FPI, and LUM, the abduction/ adduction torques recorded when the MCP joint was flexed 60° were only 10-30% of those recorded when the MCP joint was in the other, more extended, positions, irrespective of PIP and DIP posture (Fig. 1).

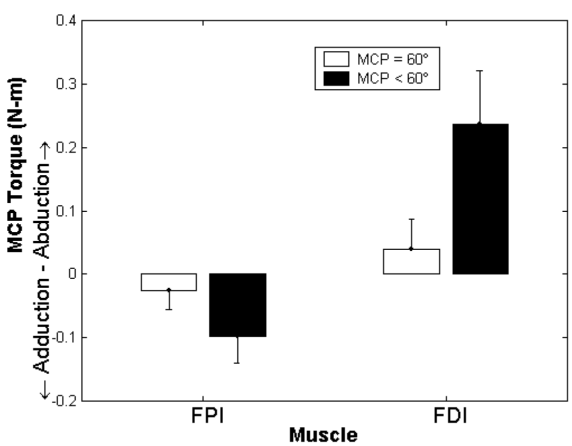

Figure 1: Mean and SD (error bars) for MCP torque for FPI and FDI in response to stimulation when MCP angle = 60° of flexion (white bars) and MCP angle < 60° (black bars).

For the extrinsic extensors, EDC and EI, DIP extension torque was only present when the PIP and DIP joints were in the most flexed posture (60°, 30°). PIP and MCP extension torques were present at all postures. Conversely, the intrinsic finger muscles produced greater DIP than PIP extension.

Torque distribution about the different joints was also highly dependent upon finger posture. For FDS, the ratio of PIP:MCP torque varied considerably depending on the joint angles, ranging from 0.3 to 0.8. FDP ratios also varied, from 0.5 to 1.2. Ratios were largest for the most flexed posture of PIP and DIP (60°, 30°) and smallest for the most extended posture (0°, 0°). The ratio between MCP adduction: MCP flexion was also dependent upon posture, ranging from 0 to 0.25 for FDS and 0 to 0.5 for FDP.

The range for the PIP:MCP ratios for EI and EDC across all postures were much smaller (0.2 to 0.4) than for the extrinsic flexors.

SUMMARY

Finger posture clearly impacts the net effect of contraction of the muscles controlling it. Since the observed variations in torque cannot be predominantly ascribed to force alterations, moment arms must change significantly, to a greater extent than previously described. In support of this view of moment arm changes, the distribution of joint torques varied considerably with finger posture for some muscles, such as FDS and FDP. The effect of posture on moment arms needs to be addressed when modeling finger mechanics.

REFERENCES

An, K.N. et al. (1983). *J. Biomech*, **16**, 419-425.

Fowler, N.K. et al. (2001). *J. Biomech*, **34**, 791-797.

ACKNOWLEDGMENTS

This work was supported by a Biomedical Engineering Research Grant from the Whitaker Foundation and by the Department of Veteran Affairs.

A MUSCULOSKELETAL MODEL OF THE UPPER EXTREMITY FOR SURGICAL SIMULATION AND NEUROCONTROL APPLICATIONS

Katherine R. S. Holzbaur, MS[1], Wendy M. Murray, PhD[2], Scott L. Delp, PhD[1,2,3]
[1]Mechanical Engineering Department, Stanford University, Stanford, CA
[2] VA Palo Alto HCS Bone and Joint Center, Palo Alto, CA
[3]Bioengineering Department, Stanford University, Stanford, CA
Email: kholzbaur@stanford.edu Web: nmbl.stanford.edu

INTRODUCTION

Biomechanical models of the musculoskeletal system provide a framework for investigating neural control of movement and simulating surgical reconstructions. The purpose of this study was to develop a model of the upper limb that includes joints from the shoulder to the fingers and represents the muscles that surround these joints. Previous models have generally represented an individual joint, such as the shoulder (van der Helm 1994) or wrist (Gonzalez, et al. 1997), and are most often used to analyze these joints in isolation. However, many muscles of the upper extremity cross multiple joints, and an integrated model is needed to better understand the coupling between joints. A recent model of the shoulder, elbow, and wrist provides an excellent foundation for such an approach (Garner and Pandy 2001), but excludes the hand and several important muscles of the forearm. This abstract describes an integrated upper extremity model, compares the model to selected experimental data, and tests the ability of the model to represent joint coupling.

METHODS

The model we developed includes 15 degrees of freedom, incorporating kinematics of the shoulder (including clavicle and scapula motion), elbow, forearm, wrist, thumb, and index finger. Fifty muscles and muscle compartments were represented, including shoulder muscles crossing the glenohumeral joint and all the muscles of the arm and forearm. Muscle architecture was obtained from the literature (An, et al. 1981, Garner and Pandy 2001, Jacobson, et al. 1992, Lieber, et al. 1990, Lieber, et al. 1992, Murray, et al. 2000). Model-estimated moment arms were tested by comparison with published data (Brand 1993, Liu, et al. 1997, Loren, et al. 1996, Murray, et al. 1995, Otis, et al. 1994). The isometric moment-generating capacity predicted by the model was also compared to experimentally measured maximum isometric joint moments (Buchanan, et al. 1998, Delp, et al. 1996, Garner and Pandy 2001, Otis, et al. 1990).

To illustrate the ability of the model to represent coupling between joints, we simulated the relationship between passive finger flexion moment and wrist flexion angle. The increase in passive flexion of the fingers with wrist extension, a phenomenon known as the tenodesis effect, is an important mechanism that permits patients with a paralyzed hand to grasp objects by extending their wrist.

RESULTS

The maximum isometric joint moments estimated using the model represent many features observed in experimental data. For example, the model reproduces both the decrease in shoulder abduction strength and increase in shoulder adduction strength with increasing shoulder abduction angle that has been observed experimentally (Fig. 1). In addition to accurate representation of the active moments produced during maximum effort at individual joints, the model reflects

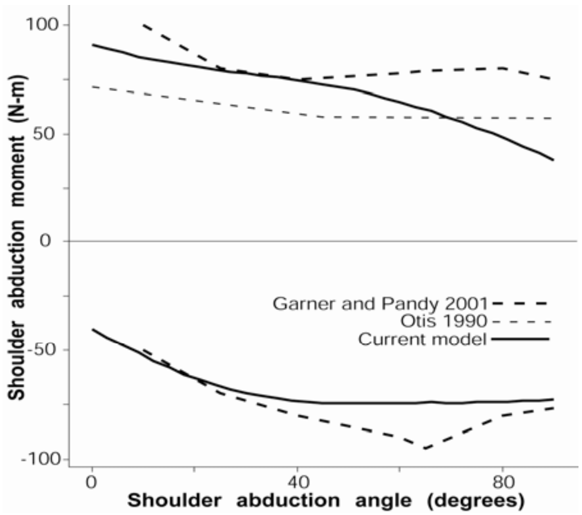

Figure 1. Maximum isometric shoulder abduction and adduction moment vs. shoulder abduction. Abduction moments are positive and adduction moments are negative.

interactions between joints that affect muscle function. In particular, the model estimates a marked increase in the passive flexion moment at the second metacarpophalangeal joint with extension of the wrist (Fig. 2), which is consistent with the tenodesis effect.

DISCUSSION

The model we have described represents an adult of average size with average muscle properties. Subject-specific models using an individual's muscle parameters and muscle paths would be useful for designing subject-specific surgical plans. However, such models can be time-consuming to create. Generic models are useful for a broad range of studies, including simulations of upper limb surgery, calculation of limb impedance, and calculation of end-point forces at a fingertip generated by individual muscles. Future directions in the development of this model will focus on defining scaling rules to tailor the model to more accurately represent individual subjects.

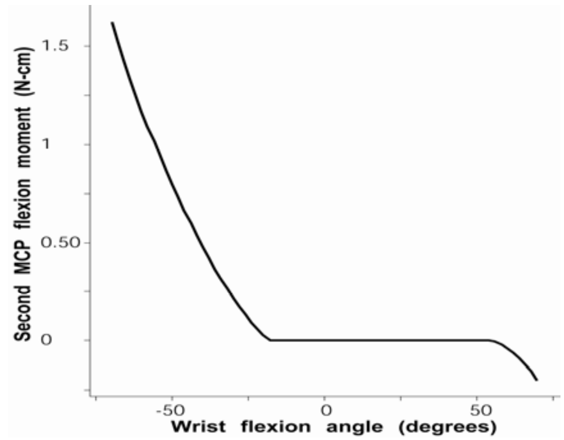

Figure 2. Passive moment about the second metacarpophalangeal (MCP) joint vs. wrist flexion. The wrist is flexed in positive angles and extended for negative angles. Finger flexion moment is positive and finger extension moment is negative.

REFERENCES

An, K.N., et al. (1981). *J Biomech*, **14**, 659-69.
Brand, P.W., Hollister, A. (1993). *Clinical Mechanics of the Hand: Second Edition*. Mosby-Year Book, Inc.
Buchanan, T.S., et al. (1998). *J Biomech Eng*, **120**, 634-9.
Delp, S.L., et al. (1996). *J Biomech*, **29**, 1371-5.
Garner, B.A., Pandy, M.G. (2001). *Comput Methods Biomech Biomed Engin*, **4**, 93-126.
Gonzalez, R.V., et al. (1997). *J Biomech*, **30**, 705-12.
Jacobson, M.D., et al. (1992). *J Hand Surg [Am]*, **17**, 804-9.
Lieber, R.L., et al. (1990). *J Hand Surg [Am]*, **15**, 244-50.
Lieber, R.L., et al. (1992). *J Hand Surg [Am]*, **17**, 787-98.
Liu, J., et al. (1997). *Clin Biomech (Bristol, Avon)*, **12**, 32-38.
Loren, G.J., et al. (1996). *J Biomech*, **29**, 331-42.
Murray, W.M., et al. (2000). *J Biomech*, **33**, 943-52.
Murray, W.M., et al. (1995). *J Biomech*, **28**, 513-25.
Otis, J.C., et al. (1994). *J Bone Joint Surg Am*, **76**, 667-76.
Otis, J.C., et al. (1990). *Am J Sports Med*, **18**, 119-23.
van der Helm, F.C. (1994). *J Biomech*, **27**, 551-69.

ACKNOWLEDGEMENTS

The Whitaker Foundation, Medtronic Foundation Stanford Graduate Fellowship, and the Rehabilitation R&D Service of the Department of Veterans Affairs (#B2785R).

THREE-DIMENSIONAL FINITE ELEMENT BONE DAMAGE SIMULATIONS USING QUASI-CONTINUUM DAMAGE MECHANICS

Victor Kosmopoulos[1] and Tony S. Keller[2]

[1]Department of Mechanical Engineering, School of Engineering, The College of New Jersey, Ewing, NJ, United States
[2]Department of Mechanical Engineering, College of Engineering and Mathematics, The University of Vermont, Burlington, VT, United States
E-mail: kosmopou@tcnj.edu

INTRODUCTION

Load bearing bone structures such as spinal vertebrae may be damaged at relatively low loads such as experienced during upright weight bearing posture [Kosmopoulos and Keller 2003]. When damaged, bone exhibits reduced modulus and strength. Understanding the mechanics of bone damage is important for predicting and providing early treatment of fractures. Microdamage, or loss of material continuity at the micro scale, has also been hypothesized to be a precursor for bone remodeling [Martin et al 1982].

Continuum damage mechanics (CDM) is a rapidly developing area in the study of bone damage and fracture. In the simple case of isotropic damage, the presence of cracks or damage (D) has been expressed as a loss of load carrying area:

$$D = A_D/A \qquad \text{(eq. 1)}$$

where A is the undamaged area, A_D is the reduced damaged area (area of the cracks), and 0 (undamaged) $\leq D \leq$ 1 (damaged) [Kachanov 1986]. Modulus reduction (MR) can be characterized as [Davy et al 2001]:

$$MR = (1 - D) \qquad \text{(eq. 2)}$$

Finite element modeling (FEM) is well suited for analyses of complex geometric structures like bone, and yields important information about internal tissue stresses and strains that are not easily determined. The objective of this study is to use a quasi-continuum damage FEM approach to study trabecular bone damage evolution.

METHODS

The apparent elastic modulus (E) of porous bone structures is closely related to apparent density (ρ) [Carter et al 1977, Keller 1994]:

$$E \propto \rho^3 \qquad \text{(eq. 3)}$$

Assuming that damage can be equated to modulus, then we have the following damage-density relationship:

$$D = E_D/E_U = \rho_D^3/\rho_U^3 \qquad \text{(eq. 4)}$$

where ρ_D and ρ_U are the damaged and undamaged material densities, respectively. Damage accumulation can be defined using an elasto-plastic modulus reduction (EPMR) method [Kosmopoulos and Keller 2003]:

$$\frac{d\sigma_{EFF}}{d\varepsilon_{EFF}} = -\sigma_y\, \beta\left[\left(-\tanh\beta^{-(m-1)/m}\right)+\left(\tanh\beta^{m+1/m}\right)\right]\varepsilon_{EFF}^{-1}$$

where: (eq.5)

$$\beta = \left[\frac{E_{NEW}\,\varepsilon_{EFF}}{\sigma_y}\right] \text{ and } E_{NEW} = \left[(1-D)E_0\right]$$

The exponent (m) is adjusted to control the elasto-plastic transition. As $m\to\infty$, the mechanical damaging behavior becomes elastic-perfectly plastic, and if no damage is present, becomes fully elastic as $m\to 0$.

To illustrate the quasi-continuum MR method, a 1.9x1.9x3.0 mm sub-region of trabecular bone from an L5 vertebral mechanical test specimen was analyzed (Figure 1A). Trabecular bone was modeled as an isotropic material, with an initial elastic modulus E_0 = 10 GPa. Marrow was assumed to be a low modulus solid (10 kPa). A Poisson's ratio of 0.3 was assumed for all

8-node isoparametric elements. The 37200 DOF model had a spatial resolution of 100 μm and an element aspect ratio of 1.

Compressive loads, ranging from 0 N to 25 N (in 1 N increments), were uniformly applied to a rigid, laterally constrained top plate (mimicking test conditions). The model was incrementally unloaded resulting in a total of 49 load-unload iterations. Following each load-unload iteration, the bone element strain intensity (ε_{EFF}) was used with eq. 5 (m= 4, σ_y=159 MPa) to determine the element-by-element *MR* (if any).

RESULTS AND DISCUSSION

Damage evolution following the 49 load-unload increments is illustrated in Figures 1B, 2A and 2B. The apparent elastic modulus (E_z) decreased from 385 MPa (iteration 1) to 276 MPa (iteration 25) to 210 MPa (iteration 49). Damage initiated at an apparent stress of 1.94 MPa, and at the maximum stress (6.93 MPa), the apparent *MR* was 0.283 (28.3%). The damage simulation predicted a yield stress σ_y = 4.1 MPa and yield strain ε_y = 1.1% (0.2% strain offset). Numerical findings agree qualitatively with the experimental findings for the original 9x9x9 mm compression test sample (σ_y = 3.3 MPa, E = 296 MPa).

SUMMARY

The quasi-CDM formulation presented is unique in that it uses material properties (density reductions) to model the elasto-plastic damage of bone. As illustrated, "q-CDM" is easily adapted into finite element analyses and can be used to study the damage evolution and microstructural mechanical behavior of complex material geometries, including trabecular bone. Damage simulation predictions can be improved by calibrating E_0 to the experimental apparent modulus [Kosmopoulos and Keller, 2003].

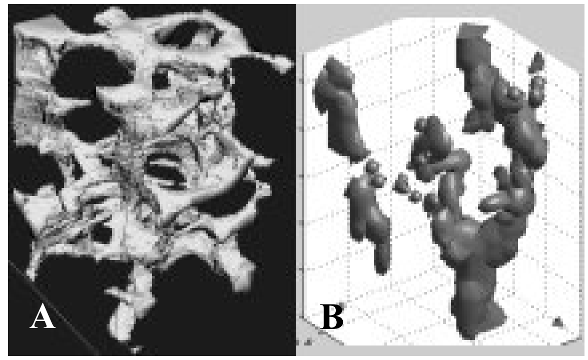

Figure 1. (A) Original sub-region of bone; (B) regions of damage after 49 iterations.

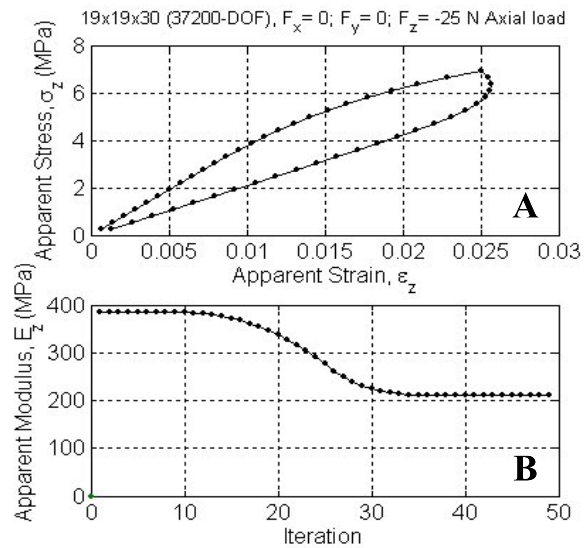

Figure 2. (A) q-CDM apparent stress-strain simulation; (B) apparent modulus change.

REFERENCES

Davy, DT, Jepsen, KJ (2001). *Bone Mechanics Handbook*. CRC Press.

Carter, DR, Hayes, WC (1977) *J. Bone Joint Surg*, **59A**, 954-62.

Kachanov, LM (1986) *Intro. to Continuum Damage Mechanics*, Martinus Nijhoff.

Keller, TS (1994) *J. Biomech.*, **27**, 1159-68.

Kosmopoulos, V, Keller, TS (2003) *Comp. Meth. Biomech. Biomed. Eng.*, **6**, 209-16.

Martin, RB, Burr, DB (1982) *J. Biomech.*, **15**, 137-9.

ACKNOWLEDGEMENTS

DOE EPSCoR, NASA EPSCoR, The Whitaker Foundation

SERUM COMP CONCENTRATION IS RELATED TO LOAD DISTRIBUTION AT THE KNEE DURING WALKING IN HEALTHY ADULTS

Anne Mündermann[1,2], Karen B. King[3], Chris O. Dyrby[1,2], Thomas P. Andriacchi[1,2,4]

[1]Division of Biomechanical Engineering, Stanford University, Stanford, CA
[2]Bone and Joint Center, Palo Alto VA, Palo Alto, CA
[3]Department of Medicine, University of California San Francisco, San Francisco, CA
[4]Department of Orthopedic Surgery, Stanford University Medical Center, Stanford, CA
amuender@stanford.edu

INTRODUCTION

Cartilage oligomeric matrix protein (COMP) is a proposed biomarker for cartilage degradation. The loss of COMP from the cartilage (indicated by increased serum levels) seems especially important since it has been suggested that COMP molecules transfer forces from the cartilage matrix to the cell, and thus are involved in the regulation of cartilage synthesis and degradation (Wong et al. 1999). The load distribution between the medial and lateral compartment of the knee during walking measured in terms of the external knee adduction moment has been related to the progression of knee osteoarthritis (OA) (Miyazaki et al. 2002). Yet, a link between cartilage degradation and load distribution at the knee during walking has not been established. The purpose of this study was to test the hypothesis that the change in serum COMP concentration in healthy adults following a 30-minute walking exercise correlates with the knee adduction moment times the number of loading cycles.

METHODS

Ten physically active adults (5 male, 5 female; Table 1) with no history of lower extremity injuries or pain gave informed consent prior to their participation. Subjects self-limited their physical activity 36 h prior to the experiment. Tests began at least 3 h after waking. Blood samples (5 ml) were drawn from the same antecubital vein immediately before and after, and 0.5, 1.5, 3.5, and 5.5 h after a 30-min. walking exercise on a level outdoor walking track at self-selected normal speed. An activity monitor (AMP331, Dynastream Innovations Inc., Cochrance, Alberta) was attached to the right ankle to record basic time-distance measurements of gait including total step count, total distance and average walking speed, cadence and stride length. Serum COMP concentrations were determined using a commercial enzyme immunoassay (COMP® ELISA, AnaMar Medical AB, Uppsala, Sweden). Each subject's gait was analyzed within one week of the walking exercise experiment. Each subject was instructed to walk at three speeds: slow, self-selected normal, and fast. Kinematic and kinetic data were collected (Andriacchi 1998). One trial per subject and side representing a best match to the time-distance characteristics of the walking exercise was selected. The total load at the knee was defined as the peak external knee adduction moment

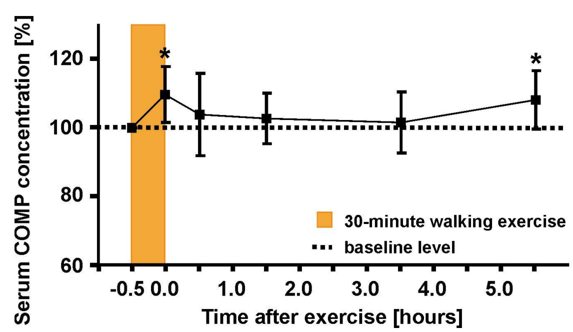

Figure 1: Mean (SD) serum COMP concentration before (-0.5 h) and up to 5.5 h after a 30-min. walking exercise (n = 10 subjects). * significant at $\alpha = .05$.

multiplied by the number of steps taken during the 30-min. walking exercise for each subject. Repeated measures ANOVA was used to detect differences in COMP concentration between the six time points. Linear regression analysis was used to relate the increase in serum COMP concentration to the total load at the knee ($\alpha = 0.05$).

RESULTS AND DISCUSSION

This study is the first study to quantify and correlate changes in serum COMP concentration and *in vivo* loading at the knee during activities of daily living.

Two peaks in serum COMP concentration followed the exercise regimen (Figure 1). The first peak was immediately after the walking exercise and likely represents diffusion of present COMP fragments from the cartilage via synovial fluid into the blood. This immediate increase in serum COMP concentration (9.7%) did not correlate with any basic time-distance measures (Table 1) of gait or the total load placed upon the knee during the walking exercise.

The second peak in serum COMP concentration (7.0%) was 5.5 h after the walking exercise and correlated negatively with the maximum external adduction moment times the number of steps taken during the waking exercise (Figure 2; R^2 = 0.692, P = 0.003). This peak likely reflects a metabolic response of cartilage to cyclic loading during the walking exercise. The increase in COMP concentration in response to the walking exercise was smaller in subjects with greater loads on the medial compartment of the knee, suggesting less degradation of COMP molecules. Such protective effects of higher loads on the medial compartment at the healthy knee are in agreement with earlier reports (Andriacchi et al. 2003; Koo et al. 2002) of relative thicker cartilage in the medial compartment of the knee in subjects with greater knee adduction moments during walking. The results of our study suggest that the load distribution at the knee during activities of daily living may influence cartilage metabolism.

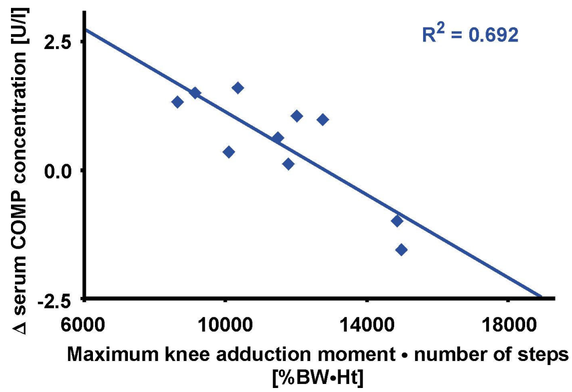

Figure 2: Increase in serum COMP concentration from 3.5 to 5.5 h after 30-min. walking exercise dependent on maximum external adduction moment multiplied by number of steps taken during the 30-min. walking exercise (P = 0.003).

REFERENCES

Andriacchi, T.P. et al. (2003) *Ann Biomed Eng*, **32**, 447-457.

Andriacchi, T.P. et al. (1998) *J Biomech Eng*, **120**, 743-749.

Koo, S. et al. (2003) *ORS Meeting*, New Orleans.

Miyazaki, T. et al. (2002) *Ann Rheum Dis*, **61**, 617-622.

Wong, M. et al. (1999) *Matrix Biol*, **18**, 391-399.

ACKNOWLEDGEMENTS

Louise McManus; AnaMar Medical AB; Dynastream Innovations Inc.

Table 1: Demographic data and basic time-distance measurements of the 30-min. walking exercise for all subjects (n = 10).

	Age [yrs]	Mass [kg]	Height [cm]	Number of Steps	Distance [m]	Speed [m/s]	Cadence [steps/min]	Stride Length [m]
Mean	31.9	70.7	173.9	3507.0	2748.9	1.49	114.3	0.78
St.Dev.	5.9	15.9	9.8	216.9	196.1	0.11	7.0	0.05

MUSCLE-TENDON LENGTHS AND VELOCITIES OF THE HAMSTRINGS AFTER SURGICAL LENGTHENING TO CORRECT CROUCH GAIT

Allison Arnold[1], May Liu[1], Michael Schwartz[3], Sylvia Õunpuu[4], Luciano Dias[5], Scott Delp[1,2]

[1]Depts. of Mechanical Engineering and [2]Bioengineering, Stanford University, Stanford, CA
[3]Motion Analysis Laboratory, Gillette Children's Specialty Healthcare, St. Paul, MN
[4]Center for Motion Analysis, Connecticut Children's Medical Center, Hartford, CT
[5]Motion Analysis Center, Children's Memorial Medical Center, Chicago, IL

E-mail: asarnold@stanford.edu Web: www.stanford.edu/group/nmbl/

INTRODUCTION

Crouch gait, one of the most prevalent and troublesome movement abnormalities among children with cerebral palsy, is characterized by excessive knee flexion during the terminal swing and stance phases. The reputed cause of the excessive knee flexion is abnormally "short" or "spastic" hamstrings that restrict knee extension; thus, crouch gait is commonly treated by hamstrings lengthening surgery. Unfortunately, it is difficult to predict which patients will benefit from these procedures, in part, because the biomechanical factors that contribute to crouch gait and the mechanisms responsible for patients' postoperative improvements are unclear. Many individuals achieve dramatic improvements in knee extension and stride length after surgery, while others show little improvement or get worse. We believe that treatments for crouch gait could be designed more effectively if the mechanisms responsible for patients' postsurgical improvements were better understood.

This study tested the hypothesis that surgical lengthening enables the hamstrings of persons with crouch gait to operate at longer muscle-tendon lengths or lengthen at faster muscle-tendon velocities during walking. We reasoned that the surgery may improve knee extension by *(i)* decreasing the passive forces generated by hamstrings with abnormally short muscle fiber lengths, thereby enabling "short" hamstrings to operate at longer muscle-tendon lengths, or by *(ii)* attenuating the exaggerated, velocity-dependent resistance of the hamstrings to stretch, thereby enabling "spastic" hamstrings to lengthen at greater muscle-tendon velocities. Previous studies have confirmed that some children with crouch gait walk with hamstrings that are shorter than normal (e.g., Delp et al. 1996), while others walk with hamstrings that are activated at lengthening velocities slower than normal (Crenna 1998). However, no study has examined whether surgical lengthening allows patients' hamstrings to operate at greater muscle-tendon velocities or longer muscle-tendon lengths. The aim of this study was to investigate this issue.

METHODS

The muscle-tendon lengths and velocities of the semimembranosus were determined for 69 subjects with favorable surgical outcomes by combining kinematic data from gait analysis with a 3D computer model of the lower extremity (Arnold et al., 2001). The subjects' "peak" lengths and velocities during walking were identified, since these measures correspond to times in the gait cycle when abnormally short or spastic hamstrings may restrict knee extension. Log-linear analyses were performed to assess whether the subjects' hamstrings operated at increased muscle-tendon lengths and/or velocities after surgery. A test statistic was considered to be significant for p-values less than 0.05.

RESULTS AND DISCUSSION

The subjects who walked with abnormally short semimembranosus muscle-tendon lengths preoperatively tended to walk with longer peak lengths following hamstrings lengthening surgery (21 of 29 subjects, $p < 0.01$, Table 1), suggesting that surgical lengthening may have slackened these subjects' tight hamstrings. The subjects who walked with abnormally slow muscle-tendon velocities preoperatively tended to walk with faster peak semimembranosus velocities postoperatively (30 of 40 subjects, $p < 0.01$, Table 2), suggesting that, in most of these cases, surgical lengthening may have diminished the spastic response of the subjects' hamstrings to stretch. Approximately one third of the subjects walked with muscle-tendon lengths and velocities that were neither abnormally short nor slow preoperatively (22 of 69 subjects), and the hamstrings of most of these subjects did *not* operate at longer peak lengths or faster peak velocities postoperatively. In these subjects, spasticity or contracture of the hamstrings may not have been the source of the excessive knee flexion, and the improvements in knee extension exhibited by the subjects after treatment may not have been related to the hamstrings surgery.

SUMMARY

Analyses of muscle-tendon lengths and velocities during crouch gait may help to distinguish individuals who have abnormally "short" or "spastic" hamstrings from those who do not, and thus may augment conventional methods used to describe patients' neuromusculoskeletal impairments and gait abnormalities.

REFERENCES

Arnold et al. (2001). *Ann. Biomed. Eng.,* **29**, 263-274.

Crenna (1998). *Neurosci. Biobehav. Rev.,* **22**, 571-578.

Delp et al. (1996). *J. Orthop. Res.,* **14**, 144-151.

ACKNOWLEDGMENTS

NIH, The Whitaker Foundation, and the United Cerebral Palsy Foundation.

Table 1: Subjects who walked with longer semimembranosus muscle-tendon lengths after surgical lengthening, cross-classified by their preoperative muscle-tendon lengths and velocities

		Change in Muscle-Tendon Length	
Preoperative Length	*Preoperative Velocity*	Longer	Not Longer
Short	Slow	15	7
	Not Slow	6	1
Not Short	Slow	7	11
	Not Slow	8	14

Likelihood ratio χ^2 (3 degrees of freedom) for 2-way interactions = 16.15, $p < 0.01$

Table 2: Subjects who walked with faster semimembranosus muscle-tendon velocities after surgical lengthening, cross-classified by their preoperative muscle-tendon lengths and velocities

		Change in Muscle-Tendon Velocity	
Preoperative Length	*Preoperative Velocity*	Faster	Not Faster
Short	Slow	16	6
	Not Slow	2	5
Not Short	Slow	14	4
	Not Slow	8	14

Likelihood ratio χ^2 (3 degrees of freedom) for 2-way interactions = 18.61, $p < 0.01$

PREDICTING THE ANTERIOR-POSTERIOR COMPONENT OF GROUND REACTION FORCE FROM WEARABLE INSTRUMENTATION

Dan C. Billing [1,2], Jason P. Hayes [1,2], John Baker [3], Romesh C. Nagarajah [1]

[1] IRIS, Swinburne University of Technology, Hawthorn, Melbourne, Australia
[2] CRC for microTechnology, Hawthorn, Melbourne, Australia
[3] Australian Institute of Sport, Belconnen, Canberra, Australia
E-mail: dbilling@swin.edu.au

INTRODUCTION

Force platforms, embedded in the surface of a runway, are the 'gold standard' contact measurement technique for the collection of ground reaction force (GRF) data during running. However, this technique requires that data is collected in a laboratory environment and factors such as targeting and limited successive foot contacts restrict the knowledge that can be gained by this form of instrumentation.

In recent years the availability of miniature electromechanical transducers suitable for the construction of wearable instrumentation have become available. Such transducers have been used to measure the distributed GRF at the foot-shoe interface (in-shoe pressure) and measure acceleration in three orthogonal components from a site approximating the subject's centre of mass (CoM acceleration). However, there are a number of difficulties in relating measurements from these transducers to anterior-posterior (AP) GRF as their output is not directly related to this component of GRF and the transducers themselves are mediated by the subjective conditions in which they are applied.

To circumvent the individual disadvantages of both GRF and wearable instrumentation a method based on the application of artificial neural networks (ANN) in conjunction with both forms of instrumentation has been proposed (Savelberg, & de Lange, 1999). An ANN can be likened to a flexible mathematical function, which has many configurable internal parameters (Chau, 2001). To accurately represent complicated relationships between wearable instrumentation and the AP component of GRF, these internal parameters are adjusted through an optimization or learning algorithm.

The purpose of this research is to investigate the accuracy of this proposed method using different forms of wearable instrumentation: In-shoe pressure (4 inputs), CoM acceleration (3 inputs) and a combination of the two (In-shoe pressure & CoM acceleration). The development of such a technique would enable the assessment of braking and propulsive forces from wearable instrumentation in a training and competition environment, which is currently not possible.

METHODS

Data was collected from four elite middle distance runners, running at an average velocity of 6.13ms^{-1} along a runway with embedded Kistler force plates. Running velocity was measured instantaneously as the subject crossed the force plates using a laser system. Force plates where separated by an appropriate distance in order to obtain consecutive foot-falls from each foot.

Custom microprocessor based wearable instrumentation has been developed to sample eight channels of in-shoe pressure and three channels of CoM acceleration simultaneously at 500Hz per channel. Discrete in-shoe pressure sensors were positioned at the heel, first metatarsal head, third metatarsal head and hallux of the subjects left and right foot. A three orthogonal component CoM acceleration system was incorporated into a semi-elastic belt and fastened around the subject's waist so that the sensor system is pressed onto the medial lumbar region.

Matching AP GRF and wearable instrumentation data sets were aligned and trained by an optimized three layer feed-forward back propagation ANN. Upon completion of the training process the network is presented with new data from the wearable instrumentation with which it attempts to predict (testing) AP GRF. The application of the ANN technique described herein has been tested on an intra-subject level only. That is training and testing files were from the same subject.
To evaluate the accuracy of the ANN predicted AP GRF by each form of wearable instrumentation and the actual GRF measured by a force plate a correlation coefficient (CC) was calculated. Correlation coefficients above 0.90 were considered to be good.

RESULTS AND DISCUSSION

Figure 1 illustrates the correlation coefficients achieved in training and testing using different forms of wearable instrumentation. In-shoe pressure & CoM acceleration provided the most accurate prediction of AP GRF (CC 0.94). The correlation coefficients for in-shoe pressure (CC 0.91) and CoM acceleration (CC 0.90) alone were above 0.90.

The results from this study indicate that AP GRF can be predicted from wearable instrumentation. The improved prediction accuracy seen for In-shoe pressure & CoM acceleration is likely to be due to the increase in input parameters to the ANN.

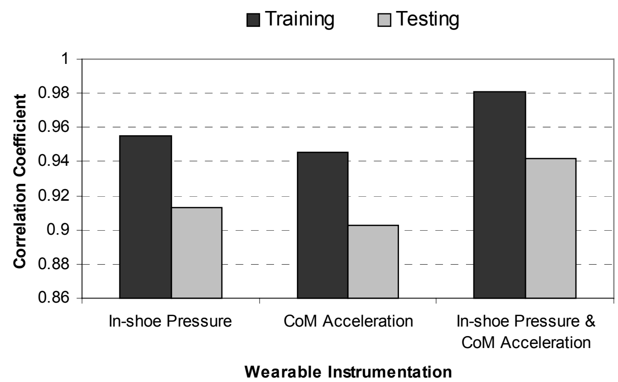

Figure 1: Wearable instrumentation correlation coefficient for the prediction of AP GRF

SUMMARY

These findings indicate that the AP component of GRF can be predicted from wearable instrumentation and provides the possibility of determining braking and propulsive forces in a competition and training environment, which is currently not possible.

REFERENCES

Savelberg, H.H.C.M. & de Lange, A.L.H. (1999). *Clinical Biomechanics*, **14**, 585-592.

Chau, T. (2001). *Gait and Posture*, **13**, 102-120.

ACKNOWLEDGEMENTS

The authors would like to thank the Cooperative Research Centre for microTechnology and the Australian Institute of Sport for funding this research.

A Multivariate Logistical Model Describing Compressive Sensitivity of Tactile Receptors

Sean S. Kohles[1], Sam Bradshaw [2], and Fred J. Looft [3]
[1] Kohles Bioengineering, Portland State University, and Oregon Health & Science University, Portland, OR;
[2] Azul Systems, Inc., Sacramento, CA;
[3] Department of Electrical & Computer Engineering, Worcester Polytechnic Institute, Worcester, MA.
Email: ssk@kohlesbioengineering.com Web: www.kohlesbioengineering.com

INTRODUCTION

Tactile skin mechanoreceptors transduce mechanical stimuli into a binary action potential. It is often difficult to correlate mechanical stimuli with observed nerve responses due to interactive effects, with no clear input to output relationship [Looft, 1994; DelPrete et al., 2003]. As a means to clarify mechanoreception, multivariate logistical regression (MLR) offers a mathematical technique in which multiple continuous explanatory variables, or covariates, are correlated to a dichotomous response variable [Hosmer and Lemeshow, 2000]. For this study, the explanatory variables were controlled, time-sampled compressive stimuli expressed as stress (σ), strain (ε), their respective time-derivatives, and interaction terms:

$$Y = \frac{e^{\beta_0+\sigma\beta_1+\varepsilon\beta_2+\frac{d\sigma}{dt}\beta_3+\frac{d\varepsilon}{dt}\beta_4+\sigma\varepsilon\beta_5+\sigma\frac{d\sigma}{dt}\beta_6+\varepsilon\frac{d\varepsilon}{dt}\beta_7+\frac{d\sigma}{dt}\frac{d\varepsilon}{dt}\beta_8}}{1+e^{\beta_0+\sigma\beta_1+\varepsilon\beta_2+\frac{d\sigma}{dt}\beta_3+\frac{d\varepsilon}{dt}\beta_4+\sigma\varepsilon\beta_5+\sigma\frac{d\sigma}{dt}\beta_6+\varepsilon\frac{d\varepsilon}{dt}\beta_7+\frac{d\sigma}{dt}\frac{d\varepsilon}{dt}\beta_8}}$$

where the influence of the input variables is determined by the coefficients (β_i). The binary response variable (probability, Y) was the presence or absence of a nerve action potential. The objective of this study was to apply a multivariate logistical model to characterize the *in vitro* behavior of isolated rapidly adapting mechanoreceptor afferents (Meissner corpuscles) in rat hairy skin.

METHODOLOGY

Single afferent nerve fibers were isolated within excised skin patches (n = 10, Sprague Dawley rats). Each skin patch was positioned on a rigid platen, stretched to its original dimensions, and bathed in Hepes solution. The afferent nerve-skin sample was stimulated at its most sensitive point with an actuator-controlled indenting tip of known dimensions. The indent position and applied force of the tip were controlled using non-repeating, pseudorandom noise inputs (0.5 – 80 Hz bandwidth) [Hoffman and Grigg, 2002]. Up to three trials of load-controlled and eight trials of deformation-controlled stimulation were applied to each afferent-skin sample (k = 110 total trials). The output signals were recorded using an electrode submersed in a non-conductive bath and sampled at 2 kHz for ~1 minute. Stimulus magnitude was varied from 2x to 8x the nerve threshold. The force and deformation data were then normalized into stress, strain, and their time derivatives.

MLR was performed and odds ratios (OR) were calculated for each explanatory variable and interaction term in the regression model using a maximum likelihood estimation technique (SPSS, Chicago). The OR is a quantitative measure of the degree to which the outcome variable changes for a single-unit change in a covariate [Hosmer and Lemeshow, 2000]. The OR can be interpreted as a unitless measure of the strength of association between the explanatory variable and the response relative to all other explanatory variables included in the model [strong association when OR >> 1.0]. The OR was used to compare afferent behavior under dynamic compressive loads of varying magnitudes. Since an evoked action potential may correspond to a stimulus before the action potential is recorded, ORs were also calculated for explanatory variables that occurred up to 100 ms before the observed action potential. This approach effectively decoupled the stimulus variables across samples, ensuring independency among explanatory variables that had been confounded in time by discrete sampling. Nerve responses are also typically followed by a refractory period, during which no magnitude of stimuli can elicit an action potential. In order to break this cross-sample dependency, post-spike sample points were assigned binary 1 outcomes. This technique determined which samples were protective against spikes, i.e., which samples fell in the refractory period. The samples were culled from the data sets and the regression rerun.

RESULTS AND DISCUSSION

Based on preliminary investigations using linear cross-correlation and stimulus-response plots [Looft, 1994], it was expected that the nerve responses would correlate strongly with compressive stress, strain, and the strain energy conveyed to the skin, rather than their time derivatives.

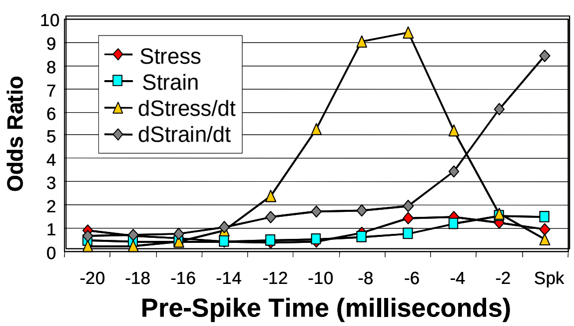

Figure 1: A representative pre-spike correlation during low intensity loading.

However, for this MLR analysis of afferent sensitivity at low intensity compressive loading (2x threshold), the dσ/dt and dε/dt stimuli were highly correlated to the neural firings up to 10 ms prior to the observed action potential (Figure 1). At higher intensity compressive loading (8x threshold), σ, ε and dε/dt were correlated with a neural response. During tensile stretch experiments, spike responses were also strongly associated with dσ/dt and weakly associated with the dε/dt and with σ [DelPrete et al., 2003]. The statistical influence of the model coefficients were consistently significant for dε/dt sensitivity (large Wald statistic) while interaction terms were consistently insignificant. The accuracy of the logistical model can be seen in a plot (Figure 2) comparing the probability of an observed impulse versus a predicted coefficient (8.6% maximum error).

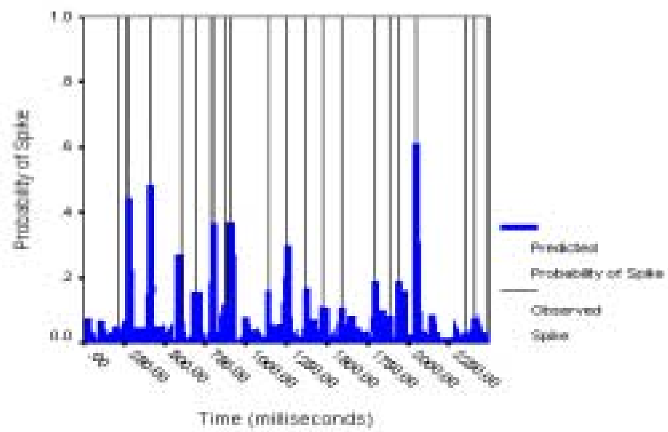

Figure 2: Predicted probability peaks with and without observed spikes, indicating high and low model efficiencies, respectively.

SUMMARY

MLR proved to be a powerful tool in characterizing afferent mechanotransduction.

REFERENCES

DelPrete, Z. et al. (2003) *J Neurophysiol*, **89(3)**:1649-1659.

Hoffman, A.H. and Grigg, P. (2002) *Ann Biomed Eng.* **30(1)**:44-53.

Hosmer, D.W. and Lemeshow, S. (2000) *Applied Logistic Regression*, Wiley.

Looft, F.J. (1994) *Somatosens Mot Res*, **11**:327-344.

ACKNOWLEDGMENTS

This work was supported by the National Science Foundation (grant IBN-9800116). The authors thank Dr. P. Grigg.

THE EFFECTS OF SKELETAL METASTASIS ON BONE TISSUE PROPERTIES

Ara Nazarian[1, 5], Jae Y Rho[3], Marc Grynpas[4], David Zurakowski[2], Ralph Müller[5] and Brian D. Snyder[1, 2]

[1]Orthopedic Biomechanics Laboratory, Beth Israel Deaconess Medical Center and Harvard Medical School, Boston, MA
[2]Department of Orthopaedic Surgery, The Children's Hospital, Boston, MA
bsnyder@bidmc.harvard.edu
[3]Department of Biomedical Engineering, University of Memphis, Memphis, TN
[4]Institute for Biomaterials and Biomedical Engineering, University of Toronto, Toronto, Canada
[5]Institute for Biomedical Engineering, Swiss Federal Institute of Technology, Zürich, Switzerland

INTRODUCTION

We have previously shown that at continuum level metastatic cancer bone tissue, much like non-pathologic cancellous bone, behaves mechanically as a rigid porous foam, where the modulus varies as the product of the tissue density (ρ_{tiss}) and the square of the bone volume fraction (BV/TV) [von Stechow, 2003]. The BV/TV accounts for changes in trabecular morphology, and the ρ_{tiss} accounts for changes in mineralization [Gibson, 1997].

The contribution of ρ_{tiss} to this relationship is small, but significant. This suggests that bone tissue material properties at the microscopic level may be different for metastatic bone tissue compared to non-pathologic bone tissue. We hypothesize that skeletal metastasis adversely affects bone tissue material properties at the microscopic level; however, the contribution of the bone tissue properties is subsidiary to the changes in the cancellous bone morphology induced by the cancer, and it will not affect the continuum level structure-property relationships for metastatic and non-pathologic cancellous bone.

Therefore our goal was to measure the microscopic bone tissue material properties using nano-indentation, and back-scattering emission (BSE) imaging for both metastatic and non-pathologic bone and determine the relative influence of the microscopic bone tissue material properties relative to the microscopic structural morphology.

METHODS

After obtaining IRB approval and informed consent, 11 patients (7 male, 4 females, 70 ±15 years) underwent excisional biopsy of metastatic prostate, breast, lung, ovarian or colon cancer at surgery or necropsy (CA). Lytic or osteoblastic metastases were identified from biplanar radiographs. In addition, 2 site and age matched cadaveric spines (1 male, 1 female, 63 ± 2 years) were obtained for non-cancerous (NC) bone specimens.

After freezing, specimens were cored along the principal trabecular orientation to form 36 (26 cancer, 10 non-cancer) cylindrical cores with a 2:1 aspect ratio (CA: ∅ 4.57 mm ±0.15, H 9.85 mm ±0.80, NC: ∅ 7.85 mm ±0.21, H 11.69 mm ±1.10). The ρ_{tiss} of each specimen was measured using a pycnometer (Quantachrome). The average BV/TV for each specimen was determined from thresholded micro-computed tomographic (μCT) images (Scanco Medical). Progressive step-wise compressive strains of 0%, 2%, 4%, 8% and 12% were applied to each specimen at a strain rate of $0.01 s^{-1}$.

A pathologist confirmed the presence of metastatic cancer in each cancer specimen histologically. After mechanical testing, the specimens were dehydrated in air, sectioned in half (along the height of the cylinder) and embedded in epoxy resin without infiltration at room temperature.

Indentation testing was conducted using a Triboindenter system (Hysitron, Inc. Minneapolis, MN) with a Berkovich indenter. The Oliver-Pharr method was used to determine the indentation modulus [Pharr, 1992]. The

hardness (H) and the Modulus of Elasticity (E_{Nano}) (derived from the hardness data) were determined.
BSE imaging was performed using a XL30 SEM (Philips/FEI, Eindhoven, The Netherlands) with a BSE detector (Philips/FEI) and a beam intensity of 20 kV. The mean, weighted average (BSE-WA), standard deviation, median, mode, skewness and kurtosis were determined for each specimen gray level distribution.
Student's T-test was performed to determine differences in tissue properties between the CA and NC groups. In addition, multiple logistic regression analysis was applied to determine which bone material properties differentiated the CA and NC groups.

RESULTS

The ρ_{tiss} for the CA and NC specimens were not significantly different. However, there were significant differences between the CA and NC groups for all other parameters (Table1).

Table 1. Comparison between Cancer and Control Specimens

Variable	**CA Group**	**NC Group**	***P* value**
ρ_{tiss} [g/cm^3]	1.59 ± 0.28	1.58 ± 0.26	0.87
BV/TV [mm^2/mm^3]	26.53 ± 17.60	7.08 ± 1.71	<0.001
BSE-WA [-]	114.82 ± 15.75	138.86 ± 14.26	<0.001
Er [GPa]	10.85 ± 1.49	15.39 ± 2.21	<0.001
H [GPa]	0.24 ± 0.03	0.49 ± 0.07	<0.001
E_{Nano} [GPa]	0.22 ± 0.03	0.44 ± 0.06	<0.001
Y_S [MPa]	4.58 ± 2.16	0.87 ± 0.40	<0.001
E [MPa]	0.19 ± 0.15	0.06 ± 0.02	<0.001

The coefficients of variation for measured tissue properties were within 4%-10% of one for CA and NC specimens.
A multivariate regression model revealed that H and E_{Nano} were the only significant nano-indentation variables that differentiated CA from NC specimens (likelihood ratio test = 42.54, $p < 0.0001$). CA specimens had significantly lower values of H and E_{Nano} compared to NC specimens (0.24 ± 0.03 vs. 0.49 ± 0.07). Using a mean cutoff value of >0.30 for H, diagnostic performance was excellent having a sensitivity of 26/26 = 1.00 (95% confidence interval = 0.87-1.00) and a specificity of 10/10 = 1.00 (95% confidence interval = 0.70-1.00).

DISCUSSION

The results of this study suggest that bone microscopic tissue properties are adversely affected by skeletal metastasis. However, the cancellous bone morphology, represented by BV/TV, is the primary factor accounting for the continuum level mechanical behavior of both CA and NC specimens. The higher BV/TV, E and Y_S values for the CA specimens reflect the predominance of osteoblastic and mixed osteolytic/osteoblastic metastases observed in the prostate, breast and lung cancer metastases. The lower BV/TV value in NC specimens reflects the osteopenic nature of the bones in this age matched group.
The significantly lower E_{Nano}, H and BSE-WA values for the CA specimens, suggest that the metastatic bone tissue is less rigid and less mineralized at the microscopic level compared to NC bone tissue, likely reflecting an unbalanced state of bone turnover, and perhaps a larger proportion of woven bone. Finally, H and E_{Nano} appear to differentiate metastatic bone tissue from normal bone. μCT volumetric data and continuum level mechanical testing parameters were insensitive to changes in microscopic bone tissue properties induced by metastatic cancer.
We conclude that cancellous bone morphology accounts for most of the continuum level mechanical properties for both metastatic cancer bone tissue and non-cancerous cancellous bone tissue. The effects of metastatic cancer on bone tissue material properties are only evident at the microscopic level and are not apparent at the continuum level. Therefore all bone, metastatic and non-cancerous can be modeled mechanically as rigid porous foam.

REFERENCES

von Stechow D, Nazarian A, et al. (2003). *Trans. Orthop. Res. Soc.*, **28**:995.
Gibson LJ, Ashby MF (1997). *Cellular Solids*, Cambridge University Press.
Oliver WC, Pharr GM (1992). *Journal of Material Research*, **7**:1564-1583.

ACKNOWLEDGMENT

NIH CA40211

CONTROL OF FINGER FORCE VECTOR IN THE FLEXION-EXTENSION PLANE

Fan Gao[1], Vladimir M. Zatsiorsky[1] and Mark L. Latash[2]

[1] Biomechanics Laboratory, Department of Kinesiology, the Pennsylvania State University, UP, State College, PA, USA
[2] Motor Control Laboratory, Department of Kinesiology, the Pennsylvania State University, UP, State College, PA, USA
E-mail: fug101@psu.edu

INTRODUCTION

To manipulate hand-held objects— such as a glass, a utensil, or a tool—humans exert forces on them. For accurate manipulation, both the force magnitude and the force direction have to be specified precisely and stabilized against possible internal and external perturbations. The control of force magnitude has been an object of vigorous research while the control of force direction has been addressed to a much lesser degree.

The present study has four main goals: (a) To determine the accuracy and precision of the force direction control in maximal voluntary contraction (MVC) tasks; (b) To test the dependence of the direction accuracy on the target force direction; (c) To explore the dependence of the direction of forces produced by fingers that are not required to produce force (enslaved forces, Zatsiorsky et al. 1998) on the direction of the force by a finger(s) that is instructed to produce force (master finger); and (d) To establish whether there is a multi-finger synergy stabilizing the direction of the total force.

METHODS

Nine subjects produced fingertip forces in a prescribed direction with a MVC effort and held the peak force for two seconds. Six finger combinations were tested, including Index (*I*), Middle (*M*), Ring (*R*) and Little (*L*), one two-digit task (*IM*) and one four-digit task (*IMRL*). Two directions, 0° (perpendicular to the surface of the transducer) and 15° toward the palm were tested. In all task conditions, there were two experimental sessions, with and without visual feedback on the task force vector.

Raw data were low-pass filtered by the fourth-order Butterworth filter with the cutoff frequency set at 5 *Hz*. Moving average values were calculated using a 100-ms wide window over the whole trial duration. Maximum window value was chosen and treated as MVC. Constant Error (*CE*)—an average deviation from a target—and Variable Error (*VE*)—the standard deviation from the average—were used to characterize the performance. Wilcoxon Signed Rank test was used for *CE* and *VE*. The level of significance was set at $P < 0.05$.

RESULTS AND DISCUSSION

The subjects did not usually exert the maximal force precisely at the target direction but the deviation was relatively small (Figure 1). The target direction significantly affected the *CE* but not *VE*. There was a systematical offset in the force direction with target set at 15°.

Removal of feedback resulted in an increase in *VE* in 11 of 12 cases. The enslaving effect was always observed. Enslaved finger forces

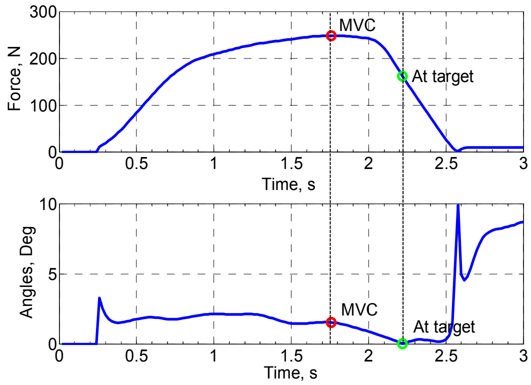

Figure 1: Force magnitude and direction during a trial (*IMRL*, 0° target, with feedback). A representative example, subject 01 (Trial 1). The deviation of the maximal force vector from the target direction is 1.8° while the magnitude of force exerted precisely in the target direction is only 65% of the MVC.

significantly deviated from the target direction. Directions of the enslaved finger forces depended on the target directions in only 11 of 24 cases. The force vectors in the *IM* task are shown in Figure 2. Note that while the IM vector points almost exactly at the target the two contributing force vectors, I and M, point in dissimilar directions.

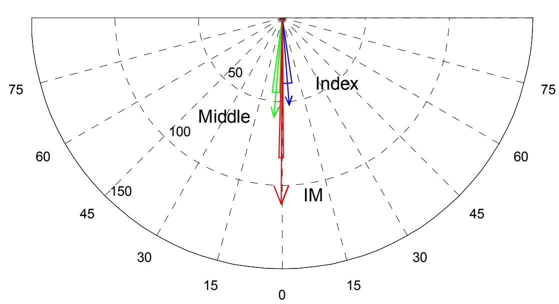

Figure 2: Force vectors, group average (*IM*-task, 0°, with feedback).

In general, the *CE* and *VE* were smaller for the task forces than for the individual master finger forces. In multi-finger tasks, the inter-trial variability of of the total (task) force was smaller than the variability of the individual finger forces (Figure 3).

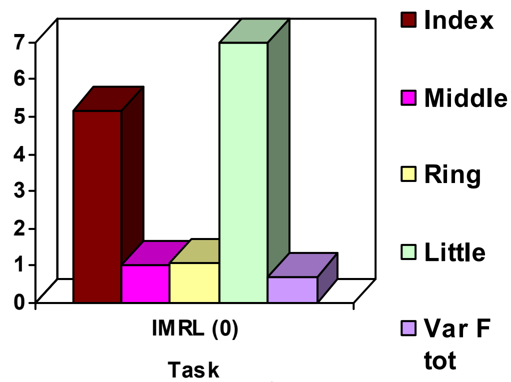

Figure 3: Variance (deg^2) of the total force and the individual finger forces in the IMRL task (0° target).

SUMMARY

The target direction significantly affected *CE* but not *VE*. The direction of the enslaved finger forces may or may not depend on the target direction. Multi-finger tasks are performed with better accuracy and precision than single-finger tasks. This is achieved due to inter-compensation (negative correlation) among the individual finger forces. Such an inter-compensation is a notable mark of a synergy (Bernstein 1967)

REFERENCES

Bernstein NA (1967) *The co-ordination and regulation of movements*. Pergamon Press, Oxford

Zatsiorsky VM, Li ZM, Latash ML (1998) *Biol Cybern* 79: 139-150

ACKNOWLEDGEMENTS

Supported in part by NIH AG-018751, NS-35032 and AR- 048563

MEASUREMENT FORCES DURING MANIPULATION IN NON-HUMAN PRIMATES

Warren G. Darling[1], James Herrick[2], David McNeal[2], Kimberly Stilwell-Morecraft[2] ,Robert J. Morecraft[2]

[1]Department of Exercise Science, The University of Iowa, Iowa City, IA 52242
[2]Division of Basic Biomedical Sciences, The University of South Dakota, Vermillion, SD 57069
Email: warren-darling@uiowa.edu

INTRODUCTION

Dexterous manipulation of objects is most highly developed in primates and requires precise control of the forces applied to objects held between two or more digits. Scientific study of control of these digit forces has been limited by measurement difficulties. Most studies involve simple gripping and lifting of an object instrumented with load cells that require placement of the digits in specific locations to permit accurate force measurements (e.g., (Flanagan et al. 1999, Brochier et al. 1999). Training monkeys to perform such a task requires considerable time and effort. We aimed to develop a method to record forces applied by the hand and digits during a behaviourally relevant task that requires precise control. Such a method should provide a very sensitive measure of hand motor coordination because skilled movements would result in low applied forces while clumsiness would be reflected in high force application, even when the object is successfully acquired.

PROCEDURES

We modified the automated monkey movement assessment panel developed by Gash and colleagues (Gash et al. 1999) to permit measurement of forces applied by the digits and hand during complex food acquisition tasks. This device (Fig. 1) attaches to the monkey's cage and requires the monkey to place one hand (depending on which port is open) into a food acquisition chamber. There are three levels of difficulty in the task as the monkey lifts food from a flat plate or threads a lifesaver (or other suitable food) over a straight or curved bar (Fig. 1B). We modified the original design (see Gash et al. 1999) to incorporate a 6 degree of freedom load cell (JR3, Inc. model 30E12A 25L) below the food acquisition chamber (Fig. 1A) that supported circular Plexiglas plates on which the food was placed (Fig. 1B). The plates are interchangeable and are rigidly attached to the load cell with a central screw. Thus, the system recorded forces and torques applied to the Plexiglas plate and the bar as the food was acquired.

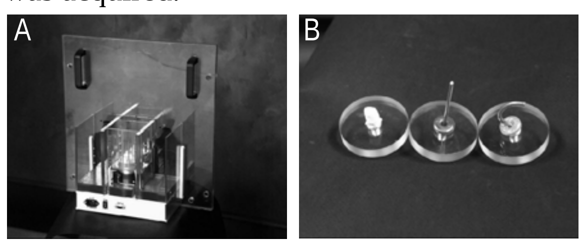

Figure 1: A – modified monkey movement assessment panel with JR3 load cell. B - 3 Plexiglas plates (one flat and two with embedded bars) with treats to be lifted.

Three adult rhesus monkeys performed the food acquisition tasks with both hands. During early testing we found that the monkeys were quickly satiated by the lifesavers and were not highly motivated to perform despite 24 hours of food deprivation before the experiment. Thus, we used carrot chips (a preferred food of these monkeys) prepared using a punch device that created chips from whole carrots that were of the same thickness and diameter with equal sized central holes. Forces recorded while acquiring the carrot chips were similar to those recorded from lifesavers. The monkeys attempted to perform the food acquisition six times for each of the three levels of difficulty and with each hand for a total of 36 trials. They were allowed up to one minute to acquire the food on each attempt. Order of performing with the left and right hand and the different levels of difficulty was varied on different testing days for each monkey.

Forces and torques from the load cell were recorded at 100 samples/s (16 bits resolution). Duration of force application, peak forces and number of force peaks exerted in each of the six directions (+/- X – left/right,Y – forward/backward,Z – up/down) were recorded along with success (food acquired or not) on each trial. These data were used to assess progress of learning the task and quality of performance by the left and right hands.

RESULTS & DISCUSSION

During initial attempts the monkeys were usually successful when acquiring the food from the flat surface with low forces (1 N or less) applied for less than 1 s. They were also usually successful in the straight bar task, but much higher forces (over 5 N) were often applied for several seconds with multiple force peaks. With additional training the peak forces were typically less than 5 N applied for 2 s or less with fewer force peaks. In the curved bar task the monkeys were usually unsuccessful on initial attempts on the first training day and applied very large forces (up to20 N) with many force peaks. Within a few sessions these forces decreased to about 5 N or less and were applied for only 1-3 s. Fig. 2B shows force patterns recorded from a monkey who was experienced with the task but had not performed it for several months. She was unsuccessful in acquiring the food with the right hand on all attempts with peak forces of about 4 N (e.g., Fig. 2B). With her left hand she was always successful within a few seconds and applied forces lower than 4 N (fig. 2A). Similar results were obtained from other monkeys.

In conclusion, the task appears quite sensitive to motor skill and hand preference in monkeys. Clearly, the force records provide a highly sensitive measure of hand coordination during food acquisition. Such measures could be used to examine cerebral dominance of motor skill and the effects of brain trauma on hand/digit coordination.

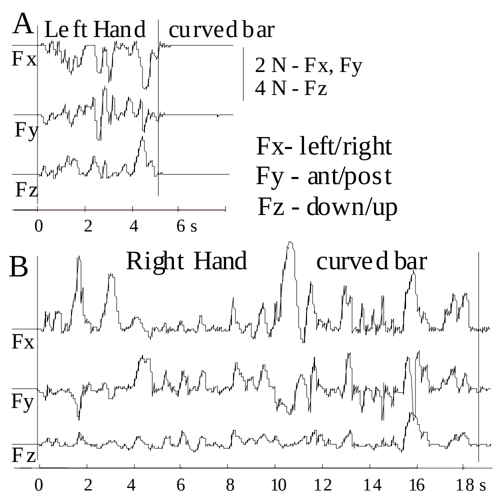

Fig. 2: Forces exerted while threading a lifesaver over the curved bar.

References

Brochier, T.. et al. (1999). Exp Brain Res. **128**(1-2): 31-40.
Flanagan, J.R. et al. (1999). J. Neurophys. **81**(4): 1706-17.
Gash, D. M. et al. (1999). " J. Neurosci. Meth. **89**(2): 111-7.

Acknowledgements

Partially supported by US PHS grants NS36397, NS33003, RR15567 (RJM), NS046367 (WGD & RJM), and a seed grant from the Center for Advanced Research on Neurorehabilitation (NIH R24) (WGD & RJM).

SARCOMERE NON-UNIFORMITY ASSOCIATED WITH STABILITY OF SKELETAL MUSCLE MYOFIBRILS

Dilson E. Rassier, Timothy Leonard and Walter Herzog

Human Performance Laboratory, Faculty of Kinesiology
University of Calgary (AB), Canada - Email: rassier@kin.ucalgary.ca

INTRODUCTION

Studies conducted with single fibers show a linear association between force and sarcomere length (SL), and consequently the degree of filament overlap (Gordon et al., 1966). On the descending limb of the force-SL relation, filament overlap is decreased when muscle length is increased, and force is thus assumed to decrease proportionally. However, in a previous study with myofibrils, a preparation in which each sarcomere length can be tracked during experiments, we observed that sarcomeres of vastly different lengths produce the same force (Rassier et al., 2003). This result challenges the traditional relationship between force and degree of filament overlap, and therefore the sliding filament theory (Huxley and Hansen, 1954).

There is evidence that A-bands shift from the sarcomere centre position during activation (Horowits et al., 1989). Previously, we measured the SL as the distance between the centroids of adjacent A-bands (Rassier et al., 2003). Therefore our previously observed SL non-uniformity might have been a consequence of shifts in A-bands, which would change the degree of filament overlap in a half-sarcomere. The purpose of this study was to re-evaluate the relationship between SL and force, and carefully investigate the position of each sarcomere in a given myofibril to check if shifts in A-band could explain our previous results.

METHODS

Myofibrils were isolated from rabbit psoas muscle and attached to a glass needle at one end and to a pair of nanolevers at the other end. The glass needle was attached to a motor arm, allowing for length changes, and the displacement of one of the nanolevers provided force measurements. The image of the myofibrils was projected onto a linear 1024-element photodiode array, which was scanned to produce tracings of light intensity vs. position along the myofibril. Due to the contrast between the A-bands and I-bands, the photodiode array output gave a striation pattern, and the SL could be calculated as the span between A-band centroids by a minimum average risk algorithm method. Myofibrils were activated by exchanging the surrounding solution from low to high Ca^{2+} concentrations (pCa^{2+} 8.0 and pCa^{2+} 4.0, respectively). Once full activation was achieved, stretches ranging from 5-17% of the mean SL, starting at a mean SL of 2.55 µm (descending limb of FL relationship) were applied (nominal speed: 119 nm·sec^{-1}). Myofibrils were held isometrically for about 8 s after stretch. Only results from six myofibrils which presented stable SL throughout testing are reported.

RESULTS AND DISCUSSION

When myofibrils were fully activated, individual SLs differed vastly within a myofibril before and after stretch (Fig 1). This result was consistent across the all tested myofibrils. Furthermore, sarcomeres did not change in length during the isometric period after stretch, i.e., they were stable.

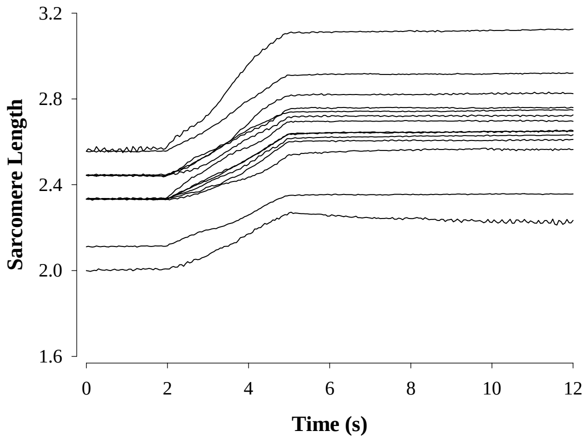

Figure 1: The behavior of individual sarcomeres during stretch of an activated myofibril

It has been shown that A-bands shift during activation (Horowits et al., 1989). Figure 2 shows conceptual shifts in the A-bands within a myofibril. The magnitude of this shift is denoted as "x", and has to be the same for each sarcomere, based on the cross-bridge and filament overlap theories. A shift of two consecutive A-bands to the left or the right of the sarcomere (1st and 2nd sarcomere from the left, and 5th and 6th sarcomere from the left, respectively) give a SL measurement identical to the SL measured from z-line to z-line.

A shift of one A-band to the left (2nd sarcomere from left) and one to the right (3rd sarcomere from left) for two consecutive sarcomeres results in a measurement of the actual SL, plus twice the distance of the A-band shift (i.e., SL + 2x). A shift of the A-band to the right (3rd sarcomere from left) and one to the left (4th sarcomere from left) of two consecutive sarcomeres results in a measured SL of SL-2x. Therefore, A-band shifts would produce three distinct clusters of SLs; one corresponding to the actual SL (z-line to z-line), the others corresponding to SL + 2x and SL – 2x. Such clustering of SLs was not observed experimentally (Figure 1). Furthermore, three or more adjacent sarcomeres displayed similar lengths on several occasions, and such a result is not compatible with shifts in the A-bands as shown in Figure 2. Therefore, we concluded that our previously observed SL non-uniformities are likely not explained by shifts in A-bands, and that sarcomeres of distinctively different lengths can support the same force.

REFERENCES

Gordon,A.M. et al. (1966). *J. Physiol.* **184,** 170-192.
Horowits,R. et al. (1989). *J. Cell Biol.* **109**, 2169-2176.
Huxley,H.E.,Hansen,J. (1954). *Nature* **173**, 973-976.
Rassier,D.E. et al. (2003). *Proc. Royal Soc. Lon B* **270**, 1735-7450.

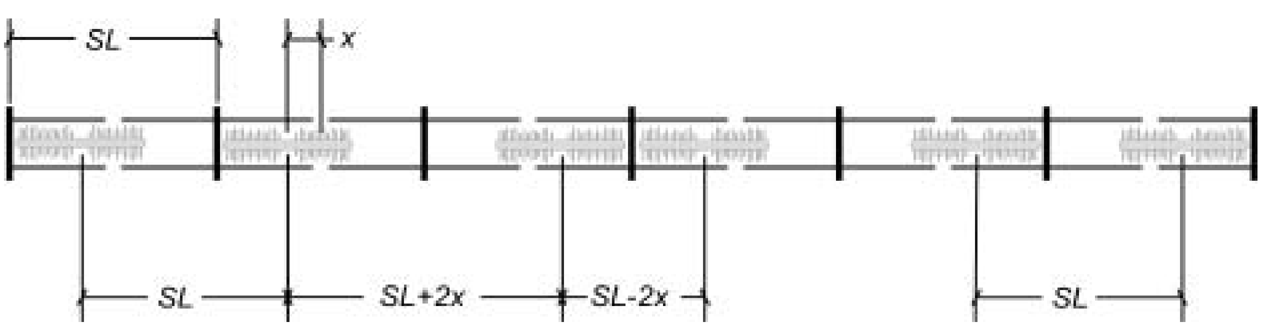

Figure 2: Schematic illustration of six sarcomeres aligned in series with shifts of their A-bands to the left or the right from the centre sarcomere position.

LUMBAR FACET JOINT CAPSULE CREEP DURING STATIC FLEXION

Jesse S. Little [1] and Partap S. Khalsa [1]

[1] Dept. of Biomedical Engineering, State University of New York at Stony Brook, Stony Brook, NY, USA; E-mail: partap.khalsa@sunysb.edu

INTRODUCTION

There is a high incidence of low back pain (LBP) disorders associated with occupations requiring sustained lumbar flexion (SLF) (NIOSH, 1997). Although paraspinal muscles are primary contributors to lumbar stiffness, the reflexive activation of the muscles is significantly decreased after creep of the surrounding ligaments (Solomonow et al., 2003), which is believed to result in laxity developed across the facet joint. However, it is still unclear which viscoelastic tissues contribute to intact lumbar spine creep and what effect creep has on subsequent lumbar biomechanics.

The purpose of this study was to determine if SLF resulted in creep of the facet joint capsule (FJC) and to determine what effect FJC creep has on lumbar biomechanics.

METHODS

Unembalmed, human lumbar spine specimens (T_{12}-Sacrum; n = 4) were procured using a university approved protocol. Specimens were dissected free of superficial soft tissues and intrinsic paraspinal muscles, while leaving the FJC and ligaments intact. The sacrum of the specimen was potted, such that the L_3 endplate was horizontal to the testing surface and full range of motion of the L_5-S_1 joint was maintained. The T_{12} body was connected to a rod via a rigid U-shaped coupling with a pin through the middle of the vertebra allowing a single degree of freedom. The coupling was in series with a force transducer mounted to a linear actuator by a low friction u-joint (Ianuzzi et al., 2004).

Specimens were actuated at T_{12} in 10 cycles of flexion, reaching a 10 Nm moment at L_5-S_1 (Pre-SLF). After the 10^{th} cycle, the 10 Nm moment was maintained for 20 min (i.e. SLF). Immediately following SLF, another 10 flexion cycles to 10 Nm at L_5-S_1 was performed (Post-SLF). The specimen was then allowed to recover for 20 min before performing another 10 cycles (20Post-SLF).

FJC plane strains (Exx, Eyy, Exy; Lagrangian large strain formulation) were measured optically using two CCD cameras, by tracking the displacements of infrared reflective markers (1 mm rad.) glued to capsule surfaces, relative to the neutral vertical position of the spine (Ianuzzi et al., 2004).

RESULTS

The flexion displacement of the specimens at the T_{12} level necessary to maintain a 10 Nm moment at L_5-S_1 significantly increased during SLF ($p < 0.05$, RM ANOVA), indicating that the lumbar spine creeped (Fig. 1).

FJC strains also increased in magnitude during SLF and remained increased even after 20 minutes of rest (Fig. 2). The increase in Exx strain during and after the 20 minutes of SLF was significant at $L_{3\text{-}4}$ compared to Pre-SLF capsule strain ($p < 0.05$, RM ANOVA w/ Dunnett's). $L_{3\text{-}4}$ Eyy and L_5-S_1 Exx and Eyy strains also exhibited a trend of increasing strain, but the data was more variable and statistical significance

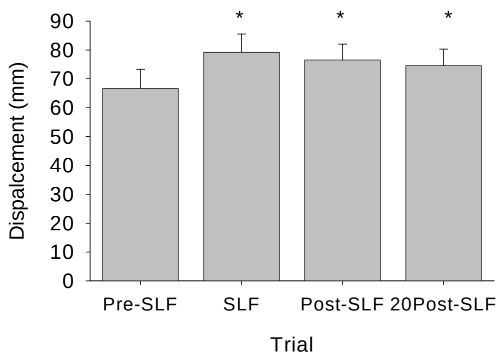

Figure 1. The displacement of the spine at T_{12} needed to create a 10 Nm moment at L_5-S_1 significantly increased during and after SLF compared to Pre-SLF (*).

was not found. Additional testing is being performed to increase statistical power.

DISCUSSION

The increase in capsule strain indicates that the FJC contributes to lumbar creep during SLF. The increased FJC strain after 20 min of rest demonstrates that the re-covery time of the FJC is longer and that residual strain may still exist creating the potential for abnormally large strains during normal physicologic motions. Although the stimulus threshold for human FJC mechano-nociceptors is not yet known, data from other species & other tissues suggests that it's likely to be ~ 20 – 40 kPa (Khalsa et al. 1996; Khalsa & Ge 2004). The nonlinear FJC elasticity modulus implies that at greater strains, stresses will be increasingly greater. Hence, the increased FJC loading developed during SLF is likely to stimulate FJC mechano-nociceptors and contribute to subsequent LBP. Given the biomechanical similarities in spinal ligaments, it is likely that all the posterior spinal ligaments during SLF would have their respective mechano-nociceptors stimulated.

REFERENCES

Ianuzzi A. et al. (2004). *Spine J*, **4**, 141-152.
NIOSH. (1997). *Pub. No*. 97-141.
Khalsa P.S. et al. (1996). *J Neurophysiol*., **76**, 175-187.
Khalsa P.S. & Ge W. (2004). *Muscle Nerve*, in press.
Little J.S. and Khalsa P.S. (2004) *J Biomech. Eng.*, submitted Feb. 2004
Solomonow M. et al. (2003). *Clin Biomech*, **18**, 273-279.

ACKNOWLEDGEMENTS

Sigma-Xi Grant, (Little, 2003)

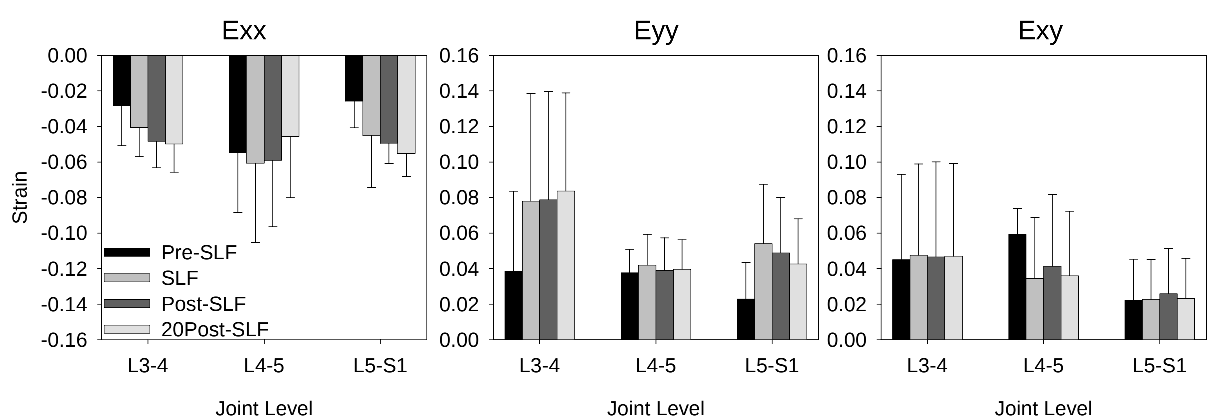

Figure 2. Facet joint capsule planar strains (Exx and Eyy) increased in magnitude during 20 minutes of static lumbar flexion (SLF). Strain measurements were made before (Pre-), during (SLF), immediately after (Post-) and 20 minutes after (20Post-) SLF.

A COMPARISON OF VERTICAL GROUND REACTION FORCES BETWEEN ONE AND TWO-LEG DROP LANDINGS

Steven T. McCaw, Saori Hanaki, Meredith A. Olson, and Joshua J. Kauten

School of Kinesiology and Recreation, Normal, IL, USA
E-mail: smccaw@ilstu.edu Web: cast.ilstu.edu/mccaw

INTRODUCTION

Both the propulsion phase and landing phase of vertical jumps have been analyzed to quantify loads and understand performance. In addition to affecting performance, mechanical loading affects the osteogenic process and presents an injury risk. Measuring the vertical ground reaction force (vGRF)-time pattern to quantify force magnitude and timing, and the rate of force application (loading rate) provides an initial basis to better understand the loading associated with an activity. Research comparing one and two leg rope jumping (Pittenger et al, 2002) indicated that although the vGRF was higher for one leg landings, magnitude and loading rate values were not double those in two leg landings. Comparisons of the propulsive phase of one versus two leg vertical jumps have suggested that both the bilateral deficit (van Soest et al, 1985) and/or biomechanical factors (Vint & Hinrichs, 1998) affect performance. The purpose of this study was to compare vGRF parameters between one and two leg drop landings in a controlled landing situation.

METHODS

Nineteen healthy college age females (height 167.3 ± 6.1 cm; mass 58.2 ± 5.3 kg; age 20.5±1.2 y) provided informed consent. All participated in athletic activities involving landing. The study was conducted using a repeated measures design. Each participant completed ten trials of one-leg and ten trials of two-leg landing, a total of 20 landings. Participants were allowed to rest at their request. To eliminate order effects, landings were performed in random order. To control landing speed at 2.73 m/s, participants stepped off of a 38 cm take-off box aligned next to the force platform; the only instructions provided in both leg conditions were to "land comfortably".

Instrumentation: vGRF data were collected from a force platform installed flush with the floor. Landing stability was visually assessed. A typical vGRF-time curve in landing (Figure 1) is characterized by the presence of F1 and F2, peak vGRF values corresponding to the instances of complete forefoot contact and lowest vertical position of the heel, respectively. vGRF data were initially scaled to the participant's mass. Subsequently, for each trial in each of the different leg conditions, custom software was used to quantify the magnitude of and the time to both F1 and F2, in addition to quantifying loading rate (calculated twice, once as the slope of the vGRF time curve from initial contact to F1, and once from initial contact to F2, units of Body Weights per second (BW/s)).

For each dependent variable, the 10-trial mean value for each participant was calculated in each leg condition and entered into paired t-tests (α =.05) to test the significance of the observed difference between the mean values for the one and two leg landings.

RESULTS AND DISCUSSION

Although mean magnitude values for both F1 and F2 were significantly different, neither value was twice as high in one leg landings compared to two leg landings (F1 values 13.2 ± 3.4 vs 11.7 ± 2.7 N/kg; F2 values 43.0 ± 6.8 vs 29.9 ± 8.7 N/kg, one vs two leg landings respectively). Temporally, in one leg landings both F1 and F2 occurred later after initial contact, although only F1 was significantly different (F1 values 13 ± 3 vs 11 ± 3 ms, F2 values 48 ± 7 vs 47 ± 10 ms, one vs two leg landings respectively). Loading rate (LR) to F1 was not significantly different between the one and two leg landings (110.5 ± 30.6 vs 118.9 ± 44.8 BW/s, respectively), reflecting the inverse effect of the magnitude and temporal changes in F1. However, LR to F2 was significantly higher in one leg compared to two leg landings (97.9 ± 24.3 vs 72.5 ± 33.8 BW/s, respectively). The 135% higher value for LR to F1 in one leg landings reflects the higher force magnitude, since there were no temporal differences in F2 between the two leg conditions.

Since the vGRF reflects the net external force applied to the body, these results suggest that in a controlled situation, a participant must make neuromuscular adjustments during one leg landings to reduce the impulsive load applied to the body to a level similar to that imposed during a two leg landing. Since the adjustments must occur at the ankle, knee and hip joints, quantifying the joint kinetics and energetics would provide insight to the mechanism of neuromuscular control utilized to reduce the impulsive load.

Figure 1. Typical vertical ground reaction force – time curve.

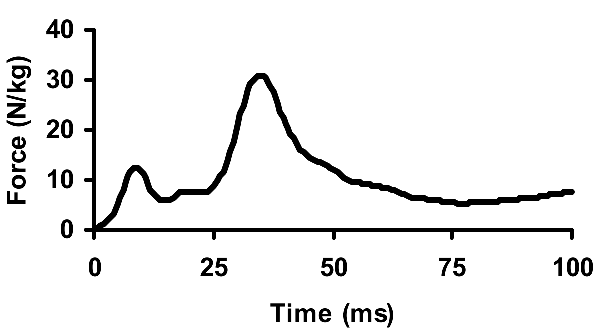

CONCLUSION

Vertical ground reaction force descriptors when landing on one leg are less than double the values exhibited when landing on two legs.

REFERENCES

Pittenger et al, (2002). *RQES*, **73**:445-449.
Vint & Hinrichs, *Proc. NACOB.,* 1998.
Van Soest et al, *MSSE*, **17**:635-639.

ACKNOWLEDGEMENTS

This project was funded by a *Jump Rope for Heart* grant from the Illinois Association for Health, Physical Education, Recreation and Dance, and a Research Grant from Illinois State University.

Are Neurologic Factors Important in Degenerative Arthritis?

Paul T. Salo

Department of Surgery, University of Calgary, Calgary, AB, Canada

E-mail: salo@ucalgary.ca

INTRODUCTION

Charcot arthropathy is a severe degenerative arthritis that occurs in patients with sensory neuropathy. Although Charcot believed the disease was caused by a loss of trophic substances derived from the nerves, leading to atrophy of the joint tissues, Volkmann and Virchow subsequently developed the consensus argument that the loss of limb sensation compromises muscular function in the limb leading to mechanical damage of the joint (Resnick 1988). Acceptance of this hypothesis has, in turn, has led to more recent speculations that a subtle, subclinical form of neuromuscular or sensory deficit may be a cause or contributing factor in the development of idiopathic osteoarthritis (OA).

Age is the highest risk factor for OA and 27%, 34% and 44% of persons exhibit radiographic osteoarthritis of the knee in the 7th, 8th and 9th decades of life respectively (Felson et al. 1987). Age-related loss of neurons from the central nervous system is a well-established phenomenon, but has not been widely documented in the peripheral nervous system.

Experiments in our laboratory revealed that in mice (and rats), innervation of the knee joint can be accurately and consistently quantified by retrograde tracing with the fluorescent dye Fluoro-Gold (FG). Using this technique in C57BL/6 mice of different ages, we found a 60% loss of joint afferents over the life span of the mouse (Salo and Tatton 1993).

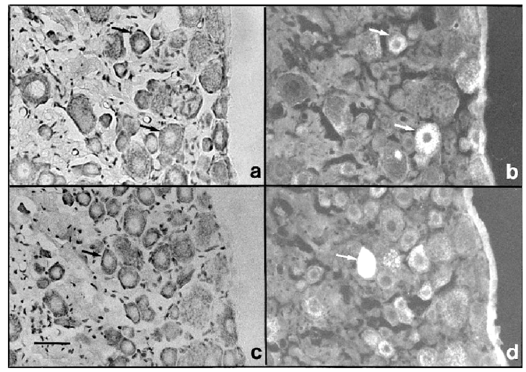

Fig. 1 Sections of dorsal root ganglion showing FG-labeling of knee-joint innervating neurons. Brightfield (a,c) and UV illumination (b,d).

Most of the loss occurs in the first six months of the mouse's 2-yr mean lifespan and appeared to be relatively selective for mechanoreceptors. We later found it correlated with the development of OA in this strain of mice (Fig.2).

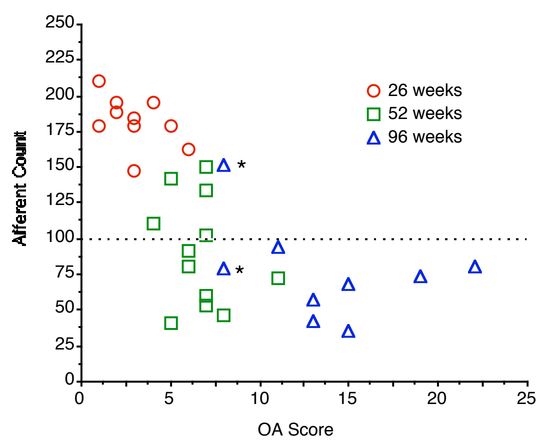

Fig. 2 Scatterplot of OA score (x-axis) vs afferent count (y-axis) for mice in three age groups. Dotted line is an arbitrary threshold of 100 afferents, below which the severity of OA is increased.

Further denervating the limb by excising the L3 dorsal root ganglion (which contains 80% of the knee joint afferents in this species) significantly worsened the degenerative changes (Salo et al. 2002).

This led us to examine the effect of selective joint denervation in an animal model less prone to spontaneous OA (the rat). Selective joint denervation can be done by injection of the joint with an immunotoxin such as OX7-saporin, which selectively destroys rat sensory neurons. Up to 88% of knee joint afferents can be ablated with this technique (Salo et al. 1997).

We subsequently followed a group of rats that had been denervated in this way for up to 24 months. The rats were exercised on a treadmill for 30 minutes, 3 times a week. Interestingly, in control rats we found on average, a spontaneous loss of 42% of joint afferents. In the denervated group we documented a reduction by 69%. Careful histologic examination and grading of the knee joints of control and denervated rats revealed some degenerative change in almost all joints, but on average these changes were significantly worse in the denervated joints (Salo et al. 2002)(Fig. 3).

SUMMARY

Age-related loss of joint innervation occurs in both mice and rats. Surgical or chemical denervation of the knee joint promotes the development and progression of OA changes in these animals.

REFERENCES

Felson DT, et al. (1987). *Arthritis Rheum.* **30**(8): 914-918.

Resnick D (1988). *Diagnosis of Bone and Joint Disorders.* W. B. Saunders.

Salo PT, et al. (2002). *J Orthop Res* **20**(6): 1256-64.

Salo PT, et al. (2002). *Acta Orthop Scand* **73**(1): 77-84.

Salo PT, Tatton WG (1993). *J Neurosci Res* **35**: 664-677.

Salo PT, et al. (1997). *J Ortho Res* **15**(4): 622-628.

ACKNOWLEDGEMENTS

Funded by the Alberta Heritage Foundation For Medical Research, The Arthritis Society of Canada and the Canadian Institute Of Health Research

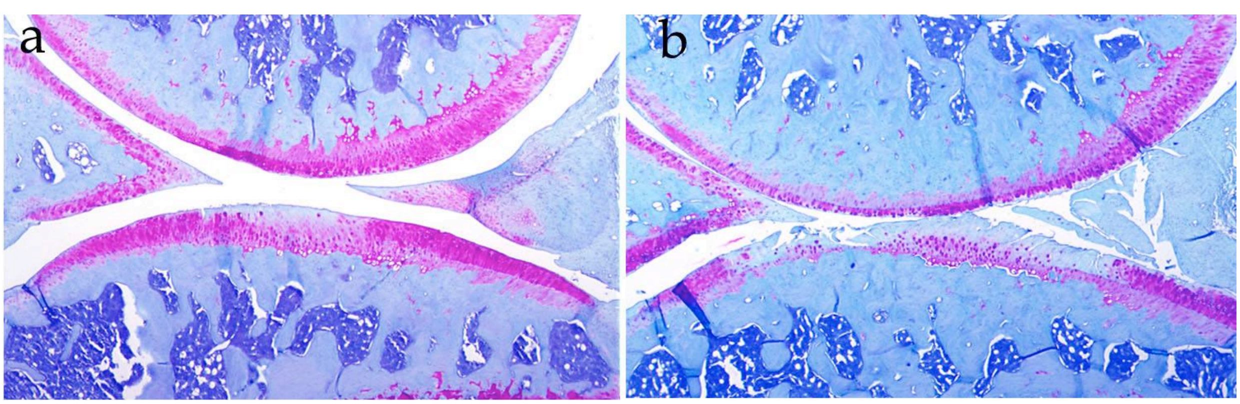

Fig. 3 Sagittal sections through the medial compartment of rat tibiofemoral joints. (a) control rat, showing mild central loss of cartilage matrix staining and superficial fibrillation. (b) denervated rat, showing major loss of cartilage matrix staining, disruption and loss of matrix down to tidemark, torn meniscus.